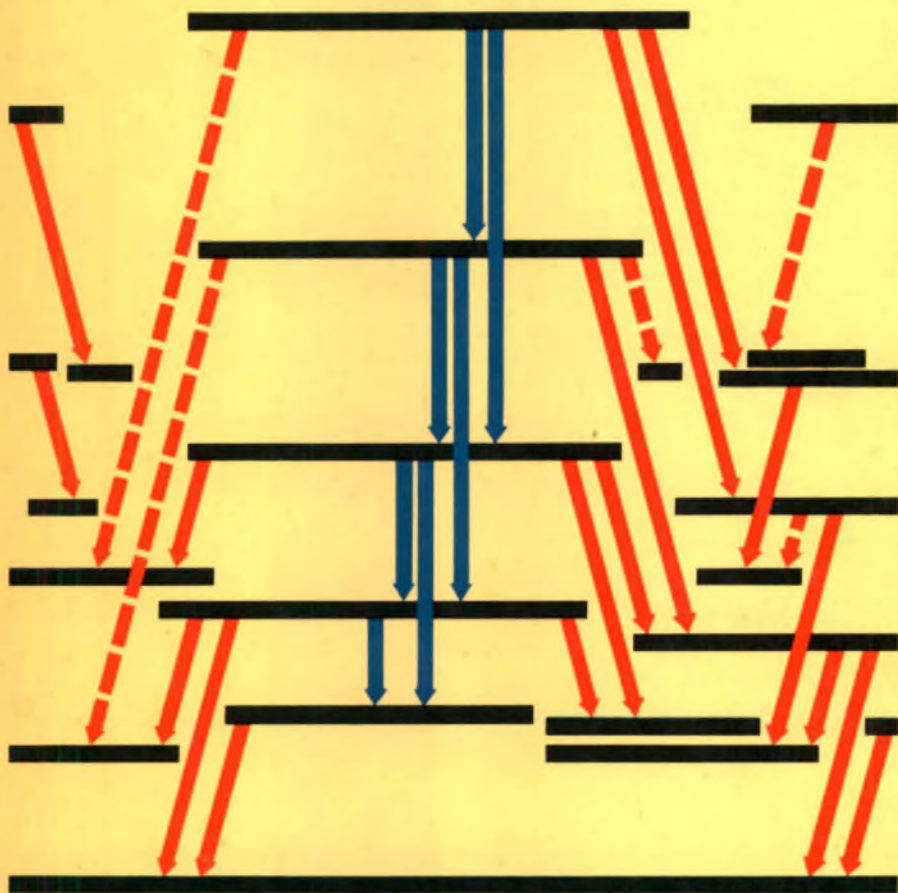


Neutron Capture Gamma-Ray Spectroscopy

Proceedings of the
International Symposium on Neutron Capture Gamma-Ray Spectroscopy,
Studsvik, 11-15 August 1969
organized by
Chalmers University of Technology and the University of Gothenburg



INTERNATIONAL ATOMIC ENERGY AGENCY, VIENNA, 1969

NEUTRON CAPTURE GAMMA-RAY SPECTROSCOPY

PROCEEDINGS SERIES

NEUTRON CAPTURE GAMMA-RAY SPECTROSCOPY

PROCEEDINGS OF THE INTERNATIONAL SYMPOSIUM ON
NEUTRON CAPTURE GAMMA-RAY SPECTROSCOPY
ORGANIZED BY
CHALMERS UNIVERSITY OF TECHNOLOGY
AND THE UNIVERSITY OF GOTHENBURG
AND HELD IN STUDSVIK, 11-15 AUGUST 1969

Supported by:
The International Atomic Energy Agency,
The Swedish Atomic Research Council,
The Swedish Research Institute of National Defence
and AB Atomenergi

INTERNATIONAL ATOMIC ENERGY AGENCY
VIENNA, 1969

NEUTRON CAPTURE GAMMA-RAY SPECTROSCOPY
IAEA, VIENNA, 1969
STI/PUB/235

Printed by the IAEA in Austria
November 1969

FOREWORD

Experimental capabilities in the field of neutron capture gamma-ray spectroscopy have expanded greatly in the last few years; this has been due in large part to the advent of high-quality Ge(Li) detectors, improvements in electronic data processing, and improvements in bent-crystal spectrometers. Previously unsuspected phenomena, such as the '5.5-MeV' anomaly, have appeared and new research tools, such as neutron guide tubes, have been brought into use. Equally exciting developments have occurred in the theory of neutron capture. Complex spectra have yielded to analysis after account had been taken of such effects as vibration, rotation and Coriolis forces, and the theoretical prediction of capture spectra seems to be a future possibility.

In view of the International Atomic Energy Agency's close interest in this subject and the need for an international exchange of ideas to analyse and study the latest developments, the Agency was very pleased to accede to the request of the Institute of Physics, Chalmers University of Technology and the University of Gothenburg, to support the Studsvik international meeting of 11-15 August and to publish the proceedings.

INTRODUCTION BY THE CHAIRMAN OF THE SYMPOSIUM

The International Symposium on Neutron Capture Gamma-Ray Spectroscopy was held on 11-15 August 1969 at the Swedish Nuclear Reactor Centre, Studsvik, organized by Chalmers University of Technology and the University of Gothenburg and supported by the International Atomic Energy Agency and AB Atomenergi. The holding of the Symposium was made possible by the financial support of the International Atomic Energy Agency, The Swedish Atomic Research Council, AB Atomenergi and the town of Nyköping. The excellent facilities provided by AB Atomenergi were of great benefit to the smooth running of the Symposium.

The organizers of the Symposium felt that work on neutron capture gamma-ray spectroscopy had achieved such valuable and significant results that the time had come for this information to be presented, examined and discussed internationally. This kind of spectroscopy has permitted the study of nuclear level systems up to very high excitation energies. An important aspect of the work is the rapidly advancing study of the de-excitation of resonance states, which promises to become a most valuable method for elucidating the nature of higher excited states. Investigations of neutron

resonance capture have also proved very effective in, and convenient for, the understanding of the slow-neutron capture mechanism itself. The lines of research on these and other aspects of neutron capture gamma-ray spectroscopy which were revealed by the participants at the meeting will doubtless stimulate many ideas for future studies leading to a deeper comprehension of the nuclear processes involved.

The Advisory Committee consisted of Dr. G.A. Bartholomew, Chalk River; Dr. H.H. Bolotin, Argonne; Prof. L.V. Groshev, Moscow; Prof. H. Maier-Leibnitz, Grenoble; Dr. H.T. Motz, Los Alamos; Prof. N. Ryde (Chairman), Gothenburg; Dr. O.W.B. Schult, Munich; and Dr. J. Vervier, Héveillé-Louvain. The Organizing Committee responsible for the running of the Symposium and the scientific program consisted of Dr. S.E. Arnell, Dr. I. Bergqvist, Dr. P.H. Blichert-Toft, Dr. L. Broman, Dr. A. Bäcklin, Dr. R. Hardell, Dr. L. Jonsson (Secretary), Dr. S. Nilsson, Dr. R. Pauli, Prof. N. Ryde (Chairman), Dr. E. Selin, Dr. Ö. Skepstedt (Assistant Secretary), Dr. N. Starfelt and Dr. T. Wiedling. I am grateful to the members of both committees for their helpful suggestions and efforts. On behalf of the Organizing Committee, I wish to thank all the participants, the session chairmen and the service staff for helping to make the Symposium a success.

The Organizing Committee is also very grateful to Prof. Maier-Leibnitz for his willingness to act as President of the Symposium; the participants will especially remember his excellent summing-up of the Symposium with valuable pointers to future developments.

The Symposium, being the first international meeting on this important topic, aroused great interest: a total of 117 invited scientists from 21 countries attended the meeting and 77 papers were contributed. These Proceedings contain the papers presented, together with seven invited talks; papers published or intended for publication elsewhere have been presented by abstract only. The publication of the Proceedings has been made possible through financial support from the International Atomic Energy Agency and the Swedish Research Institute of National Defence, and the Organizing Committee wishes to acknowledge the effective help of the Agency in editing the Proceedings.

Nils Ryde

CONTENTS

INTRODUCTORY SESSION

- Vibrational fields and nuclear dipole modes (Invited talk) 3
A. Bohr and B.R. Mottelson

EXPERIMENTAL TECHNIQUES

- Thermal-neutron capture gamma-gamma coincidence studies and techniques (Invited talk) 15
H.H. Bolotin
- High-precision neutron capture gamma-ray spectroscopy using germanium detectors in Compton-suppression technique 35
W. Michaelis and F. Horsch
- Radiative neutron capture in fissionable nuclei 51
W. Michaelis, H. Leuschner and P. Matussek
- Recent improvements in the Argonne 7.7-m bent-crystal spectrometer 55
R.K. Smither and D.J. Buss
- The automation of the curved crystal spectrometer at Risø 65
H.R. Koch, H.A. Baader, D. Breitig,
K. Mühlbauer, U. Gruber, B.P.K. Maier and
O.W.B. Schult
- Feasibility study of an internal pair formation spectrometer for neutron capture spectroscopy 75
W. Michaelis, D. Lange and G. Wilhelmi
- Plans for high-resolution (n, γ) studies at the RILL 89
O.W.B. Schult, H.R. Koch and B.P.K. Maier
- Neutron conducting tubes (Invited talk) 93
H. Maier-Leibnitz
- Studies of the (n, γ) reaction with a neutron monochromator 105
W. Kane, D. Gardner, T. Brown, A. Kevey,
E. der Mateosian, G.T. Emery, W. Gelletly,
M.A.J. Mariscotti and I. Schröder
- Simple and accurate calibration technique for measuring gamma-ray energies and Ge(Li) detector linearity (Abstract only) 113
M.G. Strauss, F.R. Lenkszus and J.J. Eichholz
- Experience with a three-crystal pair and anti-Compton spectrometer for (n, γ) spectroscopy (Abstract only) 115
J.D. Jafar, A.A. Abdulla, N.H. Al-Quraishi,
M.S. Alwash, J. Kajfusz, I.Y. Khadduri,
M.A. Khalil and Z. Kosina
- Measurement of resonance neutron capture gamma rays using a Ge(Li)-NaI spectrometer and an electron Linac (Abstract only) 117
V.J. Orphan, C.G. Hoot, A.D. Carlson, J. John
and J.R. Beyster

Spectrometry of photons emitted by reactions induced by fast neutrons on various elements	119
G. Haouat, J. Lachkar, Y. Patin and J. Sigaud	
Gaussian product functions applied to automatic analysis of gamma-ray spectra (Abstract only)	123
I.A. Slavić	

CONVERSION ELECTRON STUDIES OF (n, γ) REACTIONS

Recent experiments for neutron capture conversion electrons	127
T. von Egidy	
Conversion electrons and gamma rays from neutron capture in ^{235}U ..	141
A. Bäcklin, B. Fogelberg and Eva Falkström-Lund	
Energy levels in ^{156}Gd	147
A. Bäcklin, B. Fogelberg, G. Hedin, M. Saraceno, R.C. Greenwood, C.W. Reich, H.R. Koch, H.A. Baader, H.D. Breitig and O.W.B. Schult	
A K=2 band in ^{178}Hf	155
B. Fogelberg and A. Bäcklin	
(n, γ) and (n, e^-) investigation of the ^{177}Lu level structure (Short communication)	161
P. Manfrass, H. Prade, F. Stary, M. Beitins, N. Kramer and P. Prokoviev	

THERMAL NEUTRON CAPTURE

Gamma calibration energies in the $^{23}\text{Na}(n, \gamma)^{24}\text{Na}$ and $^{14}\text{N}(n, \gamma)^{15}\text{N}$ reactions	165
P.H.M. van Assche	
Gamma rays from thermal neutron capture in natural and ^{28}Si -enriched silicon (Abstract only)	171
A.M.J. Spits, A.M.F. Op den Kamp and H. Gruppelaar	
Neutron capture gamma-ray studies of silicon isotopes	173
P.H. Blichert-Toft and K.C. Tripathi	
Thermal neutron capture gamma-ray studies of natural titanium	183
K.C. Tripathi, P.H. Blichert-Toft and S. Boreving	
Energies and intensities of gamma rays from slow neutron capture in nitrogen	199
L. Jonsson and R. Hardell	
Gamma rays from thermal neutron capture in ^{24}Mg	209
R. Hardell	
Thermal neutron capture gamma rays from ^{39}K and ^{41}K	217
Ö. Skeppstedt	
Gamma rays from thermal neutron capture in ^{40}Ca , ^{42}Ca , ^{43}Ca , ^{44}Ca and ^{48}Ca	231
S.E. Arnell, R. Hardell, Ö. Skeppstedt and E. Wallander	
Gamma-gamma angular-correlation measurements in the $^{44}\text{Ca}(n, \gamma)^{45}\text{Ca}$ reaction (Abstract only)	257
H. Gruppelaar, A.M.F. Op den Kamp and A.M.J. Spits	

The level scheme of ^{48}Ti and ^{49}Ti as studied by the neutron capture gamma-ray spectra (Abstract only)	259
P. Fettweis and M. Saidane	
Circulation polarization of gamma radiation following capture of polarized thermal neutrons in ^{59}Co	261
F. Stecher-Rasmussen, J. Kopecký and K. Abrahams	
Thermal neutron capture gamma rays from ^{61}Ni	267
R. Samama, J. Girard, R. Babinet; A. Audias and J.J. Gardien	
Shell model configurations in even spherical nuclei	273
U. Fanger, R. Gaeta, W. Michaelis, H. Ottmar and H. Schmidt	
Radiative neutron capture studies of nuclear excitations in ^{68}Zn	289
H. Ottmar, N.M. Ahmed, U. Fanger, D. Heck, W. Michaelis and H. Schmidt	
The level structure of ^{71}Ge	301
C. Hofmeyr, B.C. Winkler, J.A.M. de Villiers, J.G. Malan and J.W. Tepel	
High-energy gamma rays of ^{76}As and ^{197}Au following thermal and epithermal neutron capture (Abstract only)	307
P. Gryska, P. Riehs and K. Rumpold	
Gamma decay of ^{96}Mo and ^{98}Mo after thermal neutron capture in ^{95}Mo and ^{97}Mo	309
D. Heck, W. Michaelis, H. Ottmar and H. Schmidt	
The level structure of ^{116}In from the $^{115}\text{In}(n, \gamma)$ reaction	317
A. Fubini, M. Giannini, E. Ivanov, M. Popa, D. Prospero and V. Rado	
Excited levels in ^{139}Ba , ^{140}La and ^{141}Ce through thermal neutron capture	337
J.L. Irigaray, M. Asghar, G.Y. Petit, A. Audias, J. Girard and R. Samama	
Gamma rays from thermal neutron capture in lanthanum (Abstract only)	349
J. Simić, I. Slavić, V. Ajdačić and B. Lalović	
Study of the reaction $^{167}\text{Er}(n, \gamma)^{168}\text{Er}$	351
Eva Falkström-Lund and A. Bäcklin	
Low-lying rotational bands in ^{158}Sm	355
R.K. Smither and T. von Egidy	
Directional anisotropy of capture gamma rays from aligned ^{149}Sm nuclei	359
E.R. Reddingius and H. Postma	
Investigation of the ^{158}Gd level scheme by thermal neutron capture ..	363
H.A. Baader, H.R. Koch, D. Breitig, O.W.B. Schult, R.C. Greenwood, C.W. Reich, A. Bäcklin and B. Fogelberg	
Angular correlation measurements on gamma-ray cascades following thermal neutron capture	371
H. Schmidt and D. Heck	
Level structure of low-lying excited states of ^{187}W	389
H.H. Bolotin and D.A. McClure	

Thermal neutron capture investigation of the ^{190}Os level structure ...	403
E. Böhm and K. Stelzer	
Neutron capture investigation of the ^{192}Ir and ^{194}Ir level structures ..	411
H. Krüger, K. Stelzer, H. Hanle and M. Koriath	
Low-lying excited states of ^{204}Tl and ^{206}Tl populated in thermal neutron capture	421
C. Weitkamp, J.A. Harvey, G.G. Slaughter and E.C. Campbell	
Excitation of levels in ^{235}U by the $^{234}\text{U}(n, \gamma)^{235}\text{U}$ reaction	431
E.T. Journey	

COLLECTIVE DESCRIPTION OF NUCLEAR STATES

Analysis and description of nuclear rotational spectra (Invited talk) ..	443
B. Elbek	
Calculation of rotational states in deformed nuclei	463
P. Holmberg	
Band mixing in deformed odd-mass nuclei	469
W. Michaelis, F. Weller, H. Ottmar, U. Fanger, R. Gaeta and H. Schmidt	

SCATTERING OF GAMMA RAYS FROM (n, γ) REACTIONS

The use of a new high-resolution gamma monochromator (Abstract only)	481
R. Moreh and A. Wolf	
Gamma-ray intensity anomaly in the (γ, γ') reaction	483
R. Moreh and A. Wolf	
Study of the energy levels of ^{139}La using nuclear photoexcitation	487
R. Moreh and A. Nof	
Recent results on (γ, γ) and (γ, γ') reactions from neutron capture gamma rays	491
R. Cesareo, M. Giannini, P. Oliva, D. Prospero and M.C. Ramorino	
(γ, γ') spectroscopy of even-even nuclei using the (n, γ) reaction	507
Y. Schlesinger, H. Szichman, M. Hass and G. Ben-David	

THEORY OF CAPTURE

The present theory of capture (Invited talk)	513
A.M. Lane	
Search for simple configurations in the capture state of (n, γ) reactions	527
H.-U. Gersch and W. Rudolph	
Statistical calculations of neutron capture radiation	541
T. von Egidy	

FAST NEUTRON CAPTURE

The 5.5-MeV gamma-ray anomaly, recent studies (Invited talk)	553
G.A. Bartholomew	
High-energy gamma-ray transitions from MeV neutron capture in ^{206}Pb	569
I. Bergqvist, B. Lundberg and L. Nilsson	
Radiative capture of nucleons in the giant resonance region	575
G. Longo and F. Saporetti	
Some statistical properties of partial radiation widths in tungsten	579
J. Murray, B.W. Thomas and E.R. Rae	
keV neutron capture in the mass region $A = 40-70$	587
J.R. Bird, B.J. Allen and M.J. Kenny	
Gamma decay, including intense M1's, in $^{115}\text{In}(n, \gamma)^{116}\text{In}$	595
E.D. Earle, M.A. Lone and G.A. Bartholomew	
Use of average resonance capture measurements for nuclear spectroscopy	601
R.K. Smither and L.M. Bollinger	
Neutron capture gamma-ray measurements with a reactor-produced 2-keV neutron beam	607
R.C. Greenwood, R.A. Harlan, R.G. Helmer and C.W. Reich	
Levels in ^{182}Ta	615
R.G. Helmer, R.C. Greenwood and C.W. Reich	

NEUTRON RESONANCE CAPTURE

Experimental studies of resonance neutron capture gamma rays (Invited talk)	627
R.E. Chrien	
Fluctuation of partial widths from resonance neutron capture in the ^{141}Pr nucleus	651
F. Bečvář, J. Pospíšil, S.A. Telezhnikov, J. Urbanec and J. Vrzal	
Gamma-ray spectra from radiative capture of resonance neutrons in antimony	657
D. Paya and A. Lottin	
Study of gamma-ray spectra from the $^{163}\text{Dy}(n, \gamma)^{164}\text{Dy}$ reaction on neutron resonance capture	663
L.S. Danelyan, B.V. Efimov, S.K. Sotnikov, B. Kardon, D. Kiss, Z. Seres and L. Szabo	
Gamma rays from neutron resonance capture in Mg, Si, P and S	667
B. Lundberg, G. Nyström and I. Bergqvist	
Radiative transitions from neutron resonances of ^{105}Pd	675
C. Coceva, F. Corvi, P. Giacobbe, M. Stefanon and G. Carraro	
Measurements of prompt gamma rays from neutron interaction in ^{235}U resonances	687
H. Weigmann and J. Winter	

OFFICERS OF THE SYMPOSIUM	693
LIST OF PARTICIPANTS	695
AUTHOR INDEX	707

INTRODUCTORY SESSION

Chairman: H. MAIER-LEIBNITZ

Invited talk

VIBRATIONAL FIELDS AND NUCLEAR DIPOLE MODES*

A. BOHR

The Niels Bohr Institute,
University of Copenhagen,
and

B.R. MOTTELSON

NORDITA,

Copenhagen, Denmark

Abstract

VIBRATIONAL FIELDS AND NUCLEAR DIPOLE MODES. The vibrational field in isovector modes is estimated on the basis of the symmetry potential. The estimate yields a frequency for the dipole mode in agreement with the observed photoresonance frequency in heavy nuclei. The effect of the neutron excess on the dipole modes with and without charge-exchange is also discussed.

VIBRATIONAL FIELDS

A basic property of a vibrational mode in a system with independent-particle motion is the field it generates. The vibration involves a coherent motion of particles giving rise to variations in the nucleonic density with respect to the equilibrium distribution and these density variations generate corresponding variations in the average potential.

To leading order in the vibrational amplitude, α , the variations in the nuclear potential can be expressed in the form

$$\delta V = \kappa F(x)\alpha \quad (1)$$

where $F(x)$ describes the dependence of the potential on the nucleonic variables (space, spin, isospin), while the coupling constant κ is a measure of the strength of the coupling between density and field.

The field (1) acts on the individual particles in the nucleus and can be observed in inelastic scattering of nucleons (Fig.1a), in the decay of a quantum into a particle-hole pair (Fig.1b), and in many other processes involving particle-vibration coupling (see, for example, the interaction between a particle and a quantum and the polarization charge, represented by diagrams such as those in Fig.1c and Fig.1d, respectively). One also expects the field coupling (1) to play a decisive role in the structure of the quanta, by organizing the collective motion of the particles (see Fig.1e).

* A more detailed discussion of the topics considered in the present article, as well as references to the earlier developments of the subject, will be given in the forthcoming Vol.II of the monograph "Nuclear Structure" (W. Benjamin Inc., New York) by the present authors.

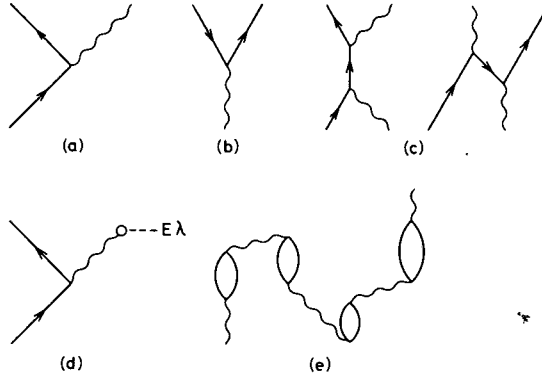


FIG. 1. Examples of processes associated with the field coupling.

The vibrational field is a result of the nucleonic (and mesonic) interactions. The relationship is similar to that of the static nuclear potential to the two-body forces, which is known to be a subtle one and in which many correlation effects are involved.

The point to be emphasized is that the vibrational field is a quantity with which we deal very directly in a variety of phenomena associated with vibrational excitations. It is thus of significance to explore this quantity by the various tools available including direct experimental study, the application of general theoretical relationships and deductions based on the underlying nucleonic interactions.

SHAPE OSCILLATIONS

Among the best studied nuclear vibrations are the quadrupole and octupole modes that are a prominent feature of low-energy nuclear spectra. These excitations can be approximately described as shape vibrations, by which the variations in the nucleonic density and field are obtained by deforming the known static density and field

$$r \rightarrow r \left(1 + \sum_{\mu} Y_{\lambda\mu}^* (\vartheta, \varphi) \alpha_{\lambda\mu} \right)$$

(2)

$$\delta V \approx -r \frac{\partial V}{\partial r} \sum_{\mu} Y_{\lambda\mu}^* \alpha_{\lambda\mu}$$

The central static potential is denoted by V ; an additional, smaller term in δV arises from the deformation of the spin-orbit potential. (In a more detailed description it may be necessary to consider the variation of α with r .)

Evidence in favour of the field coupling (2) comes from the observed cross-sections for inelastic nucleon scattering exciting the collective 2+ and 3- levels. In particular, these experiments yield values of the deformation parameter α in approximate agreement with those obtained from determinations of the multipole moments of the charge distribution.

A favourable opportunity for a quantitative study of the particle-vibration coupling is provided by the octupole excitations in the nuclei adjacent to ^{208}Pb . The evidence appears to be consistent with the coupling (2) and detailed tests may soon be expected.

The coupling (2) also appears to account qualitatively for the structure of the quadrupole and octupole quanta (frequencies and transition amplitudes). Quantitative analysis is beset with the difficulty that, for many nuclei, the nuclear shape is near instability with respect to quadrupole deformations and that the vibrational spectra therefore exhibit large anharmonicity effects.

ISOVECTOR MODES

The shape oscillations involve a symmetric motion of neutrons and protons and are thus isoscalar. In the isovector modes, neutrons and protons move with opposite phase. A variety of such modes may occur, but at present the only isovector mode that has been systematically identified in nuclear spectra is dipole oscillation, known as giant resonance in photo-absorption.

The relation between the density and field oscillations in isovector modes may be estimated from the nuclear symmetry potential. The dependence of the nuclear potential on the isospin variable t_z ($=+\frac{1}{2}$ for neutrons, $-\frac{1}{2}$ for protons) is usually expressed in the form

$$\begin{aligned} V &= V_0 + \frac{1}{2} V_1 t_z \frac{N-Z}{A} \\ &= V_0 + \frac{1}{2} V_1 t_z \frac{\rho_1}{\rho_0} \end{aligned} \quad (3)$$

The last term is the isovector potential which describes the potential produced by a small isovector density $\rho_1 = \rho_n - \rho_p$ superposed on the isoscalar density $\rho_0 = \rho_n + \rho_p$. The empirically determined value of V_1 is ≈ 100 MeV. Thus, if the density variation in an isovector vibrational mode is of the form

$$\delta \rho_1 = f(\vec{r}) \alpha \quad (4)$$

we may expect the associated potential to be

$$\delta V \approx \frac{V_1}{2\rho_0} f(\vec{r}) t_z \alpha \quad (5)$$

DIPOLE MODE

For the dipole mode we shall assume that $f(\vec{r})$ is approximately proportional to \vec{r} , as indicated by the fact that the mode is known to approximately exhaust the classical dipole sum rule. If we normalize the vibrational amplitude, such that

$$\alpha = \frac{2}{A} \sum_{k=1}^A (x t_z)_k \quad (6)$$

$$= \frac{1}{A} \int \delta \rho_1 x d^3 r$$

for the motion in the x-direction, it follows that

$$\begin{aligned} f(\vec{r}) &= \frac{\rho_0}{\langle x^2 \rangle} x \\ &= \frac{5\rho_0}{R^2} x \end{aligned} \quad (7)$$

where $\langle x^2 \rangle$ is the mean value of x^2 for a particle in the nucleus, which has been expressed in terms of the radius parameter R . The potential (5) can thus be written

$$\delta V = \kappa \frac{2}{A} x t_z \alpha \quad (8)$$

with the coupling constant

$$\kappa = \frac{5 V_1 A}{4 R^2} \quad (9)$$

In terms of this coupling one can determine the eigenfrequency of the collective mode by the standard methods of the microscopic theory of vibrations (Fig. 1d). In the present case the problem is especially simple since the one-particle excitations produced by a field proportional to x have frequencies clustering around the frequency ω_0 of the representative oscillator potential ($\hbar\omega_0 \approx 41 A^{-\frac{1}{3}}$ MeV). The coupling between the one-particle excitations produced by the field (5) is large compared with the separation between the one-particle frequencies, and one may therefore treat these as degenerate. In such a situation the collective frequency ω can be obtained by an elementary calculation yielding (with $V_1 = 100$ MeV and $R = 1.2 A^{\frac{1}{3}}$ fm)

$$\hbar\omega = \hbar\omega_0 \left(1 + \frac{\kappa}{AM\omega_0^2} \right)^{\frac{1}{2}} \approx 73 A^{-\frac{1}{3}} \text{ MeV} \quad (10)$$

in rather good agreement with the observed giant resonance frequencies in heavy nuclei ($A > 40$). (A more detailed estimate of ω , based on the available information of the one-particle dipole excitation spectrum and the coupling constant (9), yields values very close to (10); see Ref. [1].)

The isovector modes are basically of volume type, as distinct from the shape oscillations, which may be characterized as surface modes, but the role of the surface region in the isovector modes needs further investigation. This uncertainty, however, hardly alters the conclusion that the observed properties of the dipole mode are consistent with the empirical evidence on the symmetry potential. Estimates of the dipole resonance frequency on the basis of effective interactions derived from nucleonic two-body forces have tended to underestimate the value of ω (see Ref. [2]); it appears likely that these effective interactions would also fail to reproduce the observed strength of the symmetry potential.

The essential element in the above description of the dipole mode is the strong isovector field. This field can be probed by various phenomena involving the particle-vibration coupling. Thus, the field is directly involved in the excitation of the dipole mode by inelastic nucleon scattering (see Fig. 1a), but the evidence so far is very limited. The decay of the dipole state with the emission of fast nucleons (see Fig. 1b) may also be a valuable source of information. Furthermore, the field coupling gives rise to a renormalization of the effective charge for E1 transitions, which is estimated to be

$$e_{\text{eff}}(\text{E1}; \Delta E) = -et_z \frac{(\hbar\omega_0)^2 - (\Delta E)^2}{(\hbar\omega)^2 - (\Delta E)^2} \quad (11)$$

$$= -et_z \left(1 - 0.7 \frac{(\hbar\omega)^2}{(\hbar\omega)^2 - (\Delta E)^2} \right)$$

where ΔE is the transition energy. For $\Delta E \ll \hbar\omega$, estimate (11) implies a reduction of the effective charge by a factor of about 0.3, as a consequence of the coupling to the dipole mode.

Expression (11) applies to nuclei with $N = Z$. In nuclei with a neutron excess the effective charge receives the additional contribution

$$\delta e_{\text{eff}}(\text{E1}) = e \frac{N - Z}{2A} \left(1 - p \cdot 0.7 \frac{(\hbar\omega)^2}{(\hbar\omega)^2 - (\Delta E)^2} \right) \quad (11a)$$

The first term is the isovector part of the centre-of-mass correction, while the second term arises from the isoscalar component in the field produced by the dipole mode. This field is expressed in the form of expression (8) with t_z replaced by $(t_z - [(N - Z)/2A] p)$. The value of the parameter p is not known empirically; for $p = 1$ the coupling is such that a probe with a charge-to-mass ratio equal to that of the target does not excite the dipole mode. (For the analysis of low-energy E1 transitions in ^{209}Bi an effective charge for protons of 0.2 to 0.25 units has been deduced [3], which may suggest a rather small value of p . A sensitive

test of p would be provided by a measurement of the effective charge for a neutron in the region around Pb.)

For high-energy transitions, $\Delta E \geq \hbar\omega$, one obtains from expression (11) an enhancement of the E1 strength, for which there is evidence from the direct capture of fast neutrons ([4, 5]; the direct capture with the inclusion of the polarization effect has been referred to as 'semi-direct' capture).

In lighter nuclei ($A < 40$) the resonance energies observed in photo-absorption are smaller than estimate (10), but the oscillator strength is found to be appreciably less than the classical sum rule value. It appears possible that a significant dipole strength may lead to excitations in the energy region beyond that so far studied.

ISOSPIN OF DIPOLE EXCITATIONS. CHARGE EXCHANGE MODES

For an isovector mode each quantum of excitation carries unit isospin, $\tau = 1$. The classical dipole mode has isospin component $\mu_\tau = 0$, but further opportunities to explore nuclear dipole motion are provided by a study of the charge-exchange components ($\mu_\tau = \pm 1$). In a nucleus with isospin $T_0 = 0$ the charge exchange modes excite the isobaric analogues of the photonuclear resonance, while in a nucleus with neutron excess ($T_0 \neq 0$), the excitation of an isovector quantum leads to states with $T = T_0 - 1, T_0, T_0 + 1$, as illustrated schematically in Fig. 2. (The dipole modes in a nucleus with neutron excess have been considered in Refs [1, 6-8].)

If we neglect the effect of the excess neutrons on the dipole modes, the matrix elements of an isovector dipole operator for exciting the different dipole states in Fig. 2 are proportional to the vector addition coefficient $\langle T_0 T_0 1 \mu_\tau | T M_T \rangle$. Thus, for $T_0 \gg 1$, the dominant transitions are those leading to the fully aligned states with $M_T = T$ (indicated by arrows in Fig. 2). The excitations to the isobaric analogue states, with $M_T < T$, are weaker by inverse powers of T_0 . The strong transitions can be approximately described in terms of particle-hole excitations of the type illustrated in Fig. 3.

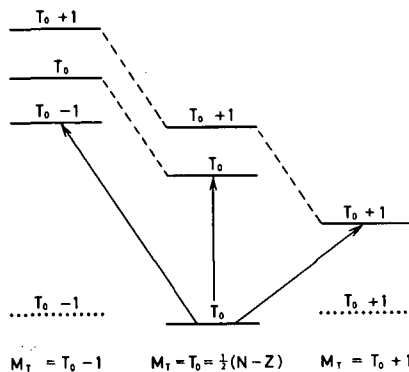


FIG. 2. Schematic illustration of pattern of states involving the excitation of an isovector quantum. The dashed lines connect isobaric analogue states; the dotted lines represent ground states of neighbouring nuclei with same value of A .

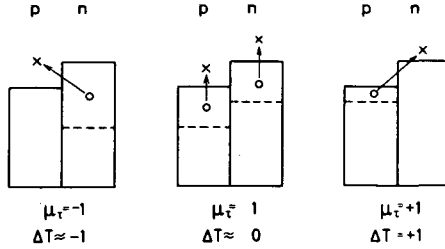


FIG. 3. Single-particle excitations associated with dipole modes with different ΔT in a nucleus with large neutron excess.

The interaction between the excess neutrons and the dipole motion gives rise to a splitting between the excitations with different T . For not too large values of the neutron excess the interaction energy is proportional to T_0 and of the form

$$\begin{aligned} H' &= a(\vec{\tau} \cdot \vec{T}_0) \\ &= \frac{1}{2} a (T(T+1) - T_0(T_0+1) - 2) \end{aligned} \quad (12)$$

The coefficient a receives contributions partly from the monopole part of the symmetry potential, which favours states of low T , and partly from the coupling between the excess neutrons and the dipole mode (as in the diagrams in Fig. 1c); this coupling is given by expression (8) generalized to form a charge-independent expression by inclusion of the charge-exchange components. These two contributions give the estimate

$$a \approx \frac{V_1}{A} - 2 \frac{\kappa \langle x^2 \rangle}{A^2} \approx 40 A^{-1} \text{ MeV} \quad (13)$$

where $\langle x^2 \rangle$ refers to the excess neutrons.

In a similar manner the matrix elements of the multipole moment for the excitation of a quantum, with the inclusion of terms linear in T_0 , have the form

$$\begin{aligned} &\langle (\tau T_0) T M_T \mid \sum_k (x t_{\mu_\tau})_k \mid T_0, M_T = T_0 \rangle \\ &= \langle T_0 T_0 1 \mu_\tau \mid T M_T \rangle F_0 [1 + \beta (T(T+1) - T_0(T_0+1) - 2)] \end{aligned} \quad (14)$$

as follows from arguments of invariance in isospace. The microscopic analysis leads to the parameters

$$\begin{aligned} F_0 &= \frac{1}{2} \left(\frac{\hbar A}{2M\omega} \right)^{\frac{1}{2}} \\ \beta &= - \frac{\langle x^2 \rangle}{8F_0^2} \approx -0.6 A^{-\frac{2}{3}} \end{aligned} \quad (15)$$

The term proportional to β in expression (14) - which implies a reduction of the transition strength for $\Delta T = T - T_0 = +1$ and a corresponding increase for $\Delta T = -1$ - reflects the fact that the presence of the excess neutrons blocks p-n transitions and leads to new n-p transitions (see Fig. 3).

The total number of single-particle transitions contributing to the dipole mode corresponds to the number of particles, S , in a major shell. The effect of the neutron excess on the dipole modes may therefore be characterized by the parameter [7, 9]

$$\nu = \frac{N - Z}{S} \approx (3N)^{\frac{1}{3}} - (3Z)^{\frac{1}{3}} \approx 0.76 \frac{N - Z}{A^{\frac{2}{3}}} \quad (16)$$

Expressions (12) and (14) are valid for $\nu \ll 1$. For larger values of ν one can determine the three eigenmodes with $\Delta T = -1, 0$ and $+1$ in terms of the single-particle excitations in Fig. 3 and the coupling (8) in the charge-independent form. The frequencies as a function of ν are illustrated in Fig. 4, and the transition amplitudes exhibit a similar behaviour. The frequencies represent excitation energies in the final nuclei with $M_T = T$; for beta-stable nuclei this energy corresponds approximately to the difference in binding energy. For $\nu > 1$ there is no mode in Fig. 4 with $\Delta T = +1$, but two modes with $\Delta T = -1$. However, in the determination of the eigenmodes in Fig. 4 the finite spread in the dipole excitation frequencies has been ignored. Thus, for example, for ^{208}Pb , with $\nu \approx 1$, there remains a weak $\Delta T = +1$ mode, mainly associated with the transition $(h_{11/2})_p \rightarrow (g_{9/2})_n$. (For a more detailed analysis of the spectrum of dipole excitations with different ΔT see Ref. [1].)

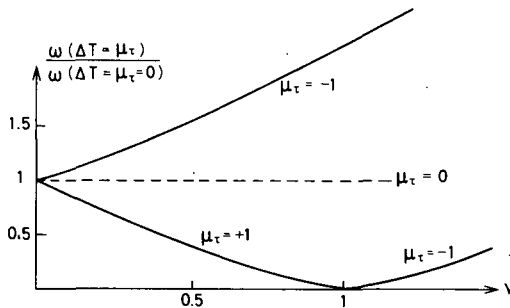


FIG. 4. Frequencies of dipole excitations with different ΔT . For $\Delta T = 0$, $\mu_T = 0$, the frequency is given by expression (10).

At present the evidence for the expected $\Delta T = \pm 1$ dipole modes is meagre. Search for the $T = +1$ mode has been made in the study of the nuclear photo-effect where it is expected as a weak satellite; thus, for example, tentative evidence has been reported for such a satellite in the E1 strength function of ^{90}Zr [10], and the energy separation from the main photo-absorption peak ($\Delta T = 0$) corresponds rather well to estimate (13). A test of the field coupling in the $\Delta T = +1$ channel can also be obtained by the study of E1 gamma radiation from isobaric analogue

states. These E1 transitions are expected to be retarded by polarization effects similar to those leading to the effective charge (11). Recent evidence on the proton capture in $^{140}_{58}\text{Ce}_{82}$ [11] indicates such a reduction of the E1 matrix element by a factor of about 0.3, corresponding to the magnitude of the expected effect.

The strongest transitions exciting the $\Delta T = \pm 1$ modes are the charge-exchange processes, such as (p, n), (^3He , t) and their inverse, but there appears at present to be no evidence on dipole excitations in these processes. The $\Delta T = +1$, $\mu_\tau = +1$ mode may also play a role in the capture of μ -mesons as well as in the beta-decay of neutron-deficient nuclei with large Q_β values. In the study of these various charge-exchange processes it is usually necessary to consider additional couplings to spin-dependent excitation modes, which may also exhibit collective properties. Rather little is known at the present time about the spin-dependent fields, but the exploration of these modes represents an important problem in the future study of nuclear dynamics.

REFERENCES

- [1] PETERSEN, D.F., VEJE, C.J., to be published.
- [2] BROWN, G.E., to be published.
- [3] HAMAMOTO, I., Contribution 7.37 to the Int. Conf. Properties of Nuclear States, Montreal, August 1969.
- [4] BROWN, G.E., Nucl. Phys. 57 (1964) 339.
- [5] CLEMENT, C.F., LANE, A.M., ROOK, J.R., Nucl. Phys. 66 (1965) 273.
- [6] FALLIEROS, S., GOULARD, B., VENTER, R.H., Physics Lett. 19 (1965) 398.
- [7] GOULARD, B., FALLIEROS, S., Can. J. Phys. 45 (1967) 3221.
- [8] PETERSEN, D.F., VEJE, C.J., Physics Lett. 24B (1967) 449.
- [9] NOVIKOV, N.M., URIN, M.G., Jaderná Fiz. 3 (1966) 419.
- [10] AXEL, P., DRAKE, D.M., WHETSTONE, S., HANNA, S.S., Phys. Rev. Lett. 19 (1967) 1343.
- [11] EJRI, H., RICHARD, P., FERGUSON, S., HEFFNER, R., PERRY, D., Nucl. Phys. A128 (1969) 388.

EXPERIMENTAL TECHNIQUES

Chairmen: G.A. BARTHOLOMEW
J. VERVIER

Invited talk

THERMAL-NEUTRON CAPTURE GAMMA-GAMMA COINCIDENCE STUDIES AND TECHNIQUES*

H.H. BOLOTIN

Argonne National Laboratory,
Argonne, Ill., United States of America

Abstract

THERMAL-NEUTRON CAPTURE GAMMA-GAMMA COINCIDENCE STUDIES AND TECHNIQUES.

The advantageous use of gamma-gamma coincidence techniques in slow-neutron capture gamma-ray spectroscopic investigations is examined and the unique information derived from such studies is compared with that obtained by more conventional spectroscopic methods. The feasibility, practicality, and value of gamma-gamma coincidence studies performed with the exclusive use of Ge(Li) detectors are clearly demonstrated. It is shown that the clarity of the data and the unequivocal information gleaned from the use of this technique are clearly superior to previously employed NaI(Tl)-Ge(Li) coincidence systems. Salient details of the method are described. Several examples of data obtained with the use of the Ge(Li)-Ge(Li) coincidence method are presented. It is concluded that widespread use of these coincidence techniques should provide a significant contribution to the understanding of the level structure of nuclides studied in slow-neutron capture gamma-ray reaction experiments.

1. INTRODUCTION

The field of slow-neutron capture gamma-ray spectroscopy has developed and matured enormously over the past four or five years due to significant developments and improvements in experimental techniques. The most outstanding technical advance has been brought about by the use of solid-state high-resolution detectors — principally the Ge(Li) gamma-ray spectrometer. This, of course, is well known to all of you, but particularly for those who had been working in this field prior to the Ge(Li) detector age (i. e. in the NaI(Tl) scintillator and magnetic Compton spectrometer era) it is abundantly clear that the Ge(Li) detector has not only enlarged the scope, accuracy and quantitative significance of studies in the (n, γ) field but has effectively resurrected to full vigour a potentially vital area of investigation that appeared to have one foot in the grave.

The use of high resolution Ge(Li) detectors has supplanted virtually all gamma-ray spectroscopic instruments previously used for the investigation of neutron-capture gamma-ray spectra above a gamma-ray energy of $\sim 500 - 600$ keV. Even in the earliest stages of the development of these detectors the high-resolution properties of these devices allowed the detection and separation of individual high-energy gamma-ray transitions to a degree not achieved earlier, and in many cases even the relatively low detection efficiency of the earlier versions of these detectors was superior to many of the highest-resolution spectrometers in use at the time these

* Work performed under the auspices of the US Atomic Energy Commission.

solid-state devices were initially developed. Significant subsequent improvements in resolution, detection efficiency (detector volume) and associated electronics have made the use of Ge(Li) gamma-ray spectrometers the standard in virtually all (n, γ) investigations for the study of gamma-ray transitions more energetic than ~ 500 keV, to the extent that I cannot recall a single experimental paper on the programme of this Symposium that does not make use of solid-state detection devices for high-energy gamma-ray studies.

Despite parallel improvements in bent-crystal spectrometers, whose energy resolution is superior to that of Ge(Li) detectors, the fine resolution capabilities of the latter devices, coupled with their superior gamma-ray detection efficiency, has led to their widespread use in studies of low-energy gamma-ray spectra. Thus, many investigations, of which we shall hear several at this Symposium, have employed Ge(Li) devices in singles- and pair-spectrometer investigations of high-energy gamma-ray spectra, as well as in singles and Compton-suppression spectrometers for low-energy gamma-ray work below an energy of ~ 1 MeV. Recent improvements in these instruments will be described in several papers presented here and I need not touch upon them in this presentation. Instead, I will concentrate upon the use of Ge(Li) detectors in another area of investigation that has not received universal adoption and recognition, but has been brought to a state of significant sophistication and usefulness that merits serious consideration for widespread utilization in the field of slow-neutron capture gamma-ray spectroscopy - i.e. the use of Ge(Li)-Ge(Li) spectrometer systems in γ - γ coincidence studies.

2. RATIONALE FOR GAMMA-GAMMA COINCIDENCE STUDIES

Singles high-energy Ge(Li) studies usually permit the delineation of individual primary transitions associated with the gamma-ray decay of the capture state populated in thermal- or resonance-neutron capture. Except in the cases of the lighter nuclides, gamma-ray transitions following slow-neutron capture that have energies $\geq 70\%$ of the neutron-binding energy can be reliably attributed to primary events proceeding from the capture state to individual low-lying excited states in the product nucleus. Thus, the determination of the energies of these transitions (often to a precision of ~ 0.5 - 2.0 keV when viewed with a Ge(Li) spectrometer), coupled with the previously known or simultaneously determined neutron-binding energy, leads to the definition of the excitation energies of many of the low-lying excited states. However, since these primary transitions are predominantly of dipole character, only those excited states whose spin differences from that of the capture state allow dipole transitions to proceed, are likely to be populated directly from the capture state. In addition, the bulk statistical character of the capture states is such that at any particular incident neutron energy the Porter-Thomas fluctuations governing the decay of each capture state favour primary transitions of relatively small partial widths, and many 'allowed' primary dipole transitions may be so weak as to elude observation. Thus, many low-lying excited states of spins differing by more than one unit of angular momentum from that of the capture state may not be represented in the primary gamma-ray spectrum and in addition the presence of some low-lying states of spins conducive to primary dipole

population may not be observed in the high-energy spectrum due to statistical effects. Further, if primary gamma-ray population of the ground state is not observed, and/or the neutron-binding energy is not known to sufficient precision, the excitation energies of the low-lying states directly populated may be ambiguous.

Despite the somewhat limited direct population of low-lying excited states, the multiplicity of the gamma-ray decay pattern from the capture-to-ground states endows the (n, γ) process with a catholic nature — i. e. subsequent low-energy gamma-ray decay of levels populated directly from the capture level can be expected to proceed to low-energy states of either parity having spins significantly different from that of the capture state, without regard to their detailed microscopic structural configurations. This feature not only affords the opportunity for population of levels not serving as terminal states of primary events and/or not seen in (d, p) or other charged-particle reactions because of restrictions based on angular momentum, spin etc., but also allows population of virtually all levels that are observed in these other studies. Therefore, the combined study of both low- and high-energy gamma-ray transitions following slow-neutron capture can provide a valuable complement and extension of the information gleaned from studies of other reactions.

The outstanding precision and wide dynamic range of bent-crystal spectrometers provides a most valuable tool for the study of the low-energy secondary transitions. It allows the observation of more, and weaker, low-energy gamma-rays than does the Ge(Li) detector. However, many instances arise in which, despite the precise high-resolution determination of a wealth of low-energy gamma-ray information, the data obtained with this instrument, even when combined with those of the less precise high-energy primary gamma-ray information of Ge(Li) spectrometers, are still not sufficient to determine the level structure and decay pattern of the low-lying excited states as completely and unambiguously as could be hoped. As is unavoidable, the use of these instruments in the construction of the level scheme of the low-lying states often must depend upon confidence that the statistical expectation for accidental energy balances is extremely small. However, since the (n, γ) process populates a myriad of low-lying excited states, there are often several pairs of levels between which a given low-energy transition might be placed. This is not a fault of the bent-crystal spectrometer, since the high-resolution of this device is supreme in the ability to minimize such accidental energy balances. Indeed, it is the plethora of excited states and low-energy gamma-rays that is at fault. In other words, the nucleus itself is the guilty party.

Although not blessed with the energy resolution necessary to resolve all of the transitions observable by bent-crystal spectroscopy, Ge(Li) detectors do possess energy resolution characteristics that are otherwise unrivalled. Some material advantages possessed by Ge(Li) detectors that are not shared by bent-crystal spectrometers are: (a) superior gamma-ray detection efficiency; (b) multichannel characteristics (i. e. detection of effectively all gamma-ray spectral energy ranges simultaneously); (c) ability to view gamma rays from samples placed in external neutron beams; (d) mobility and ease of operation; (e) monetarily less costly; and (f) the ability to be used in γ - γ and γ -electron coincidence studies and lifetime measurements of excited states.

Indeed, the sole shortcomings of the use of Ge(Li) detectors for low-energy gamma-ray spectra compared to bent-crystal spectrometers lie in poorer energy resolution and dynamic range. However, these detectors are capable of defining many of the stronger low-energy transitions which often carry the bulk of the low-energy transition intensity present in the decay. In many cases, though by no means all, these transitions form the majority of those low-energy events successfully placed into a level and decay scheme even when bent-crystal data are available. Let me, however, point out that it is an extremely rare situation when the bent-crystal does not supply more precisely measured low-energy transition data. Thus, except in the case of relatively low-cross-section targets not available in sufficient quantity (principally separated isotopes), the low-energy data obtained by means of Ge(Li) spectrometers is primarily of a complementary nature and serves as an extension of the information gleaned from the high-resolution bent-crystal spectra.

However, this is just the main point of the present discussion and as you will hear in later papers, as well as in the present talk, much new, complementary, and at times otherwise previously unreported data have been obtained from the use of Ge(Li) detectors viewing low-energy secondary transitions.

If the above considerations appear overstressed, it is due to the fact that, in my opinion, there has been a decided lack of such an exposition presented in the literature or at symposia such as this one.

The coincidence technique can provide unequivocal data concerning the sequential time ordering of transitions, information on the lifetime of some excited states, γ - γ and γ -electron angular correlations and directional polarization correlations. Gamma-gamma coincidence studies between high-energy primary and low-energy secondary transitions permit a relatively simple study of the depopulation of particular states populated by the high-energy event and the subsequent population of states at lower excitation not populated by direct transitions from the capture state. As such, in certain cases, these studies can establish the neutron-binding energy and thus provide the necessary energy calibration required to interpret the high-energy data. Coincidence studies among the low-energy secondary transitions can complement and extend our knowledge of the low-lying level structure provided by the 'high-low' coincidence data. At times, and I shall present such an example later, coincidence data have provided the missing link in the interpretation of the combined data of bent-crystal spectrometers, conversion-electron studies, high-energy primary transition investigations, and charged-particle data that allows all of the previously recorded information to fall quickly into place to establish a rather complete understanding of the level scheme.

Presumably the above is not unfamiliar to any of you. In fact, NaI-Ge(Li) coincidence studies of the (n, γ) reaction have been reported in the literature by several groups around the world, some of whom are present at this Symposium. The main aim of this talk is not only to present data that show the feasibility of Ge(Li)-Ge(Li) γ - γ coincidence studies, but further to demonstrate that the use of a two Ge(Li) detector coincidence system can provide fruitful information of such high quality that NaI-Ge(Li) coincidence studies are obsolete.

3. GAMMA-GAMMA COINCIDENCE TECHNIQUES

I am aware of only two groups involved in slow-neutron capture gamma-ray spectroscopy studies that have developed and are utilizing γ - γ coincidence systems that exclusively employ Ge(Li) detectors. These groups are at Argonne National Laboratory and Los Alamos Scientific Laboratory. If any other workers in this field are using such a system at present, I have not been informed. Therefore, in the balance of this presentation I will draw exclusively upon the work of E. B. Shera at Los Alamos and my own work at Argonne. Both coincidence systems are similar and I shall present illustrations of these systems and data obtained with their use in an interchangeable manner. All examples will be drawn from thermal-neutron capture gamma-ray studies.

An external neutron beam, necessary for coincidences studies, is employed. Figure 1. shows a schematic representation of the thermal-neutron beam extracted from a modified thermal-column at the Argonne National Laboratory CP-5 reactor and is typical of many external beam arrangements. A highly collimated external beam of thermal-neutrons, effectively free of fast neutrons (Cd ratio ≈ 570) and pile gamma rays, impinges on a target positioned between two Ge(Li) detectors. The neutron beam at the target has a flux of $\sim 2 \times 10^7$ n cm⁻²sec⁻¹, a height of ~ 2 cm and a width of ~ 0.5 cm and is defined by apertures of ⁶Li F enriched to 95.5% in ⁶Li. This beam is more than ample to allow γ - γ coincidence studies using as little as 100 millibarn-moles of isotopically separated target material.

A block diagram of the electronic components of the Argonne Ge(Li)-Ge(Li) coincidence system is shown in Fig. 2. The data are stored on a two-parameter magnetic-tape storage unit in a 1024 \times 1024-channel pulse-height array. A 4096-channel ADC is employed in each arm of the coincidence system in order to obtain the pulse-height resolution of the large ADC's while any desired 1024-channel segment of each 4096-channel spectrum is selected for storage. The storage capacity of each magnetic tape is $\sim 2.75 \times 10^6$ event-address pairs. This system is presently being modified to store $\sim 7 \times 10^6$ coincidence events in a 2048 \times 2048-channel representation on a single reel of computer-compatible magnetic tape.

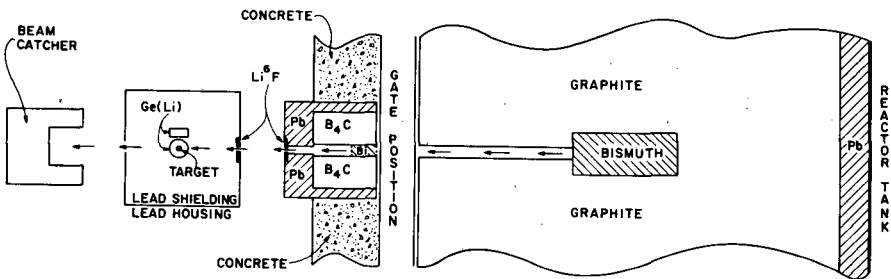


FIG. 1. Schematic representation of Argonne external thermal-neutron beam facility.

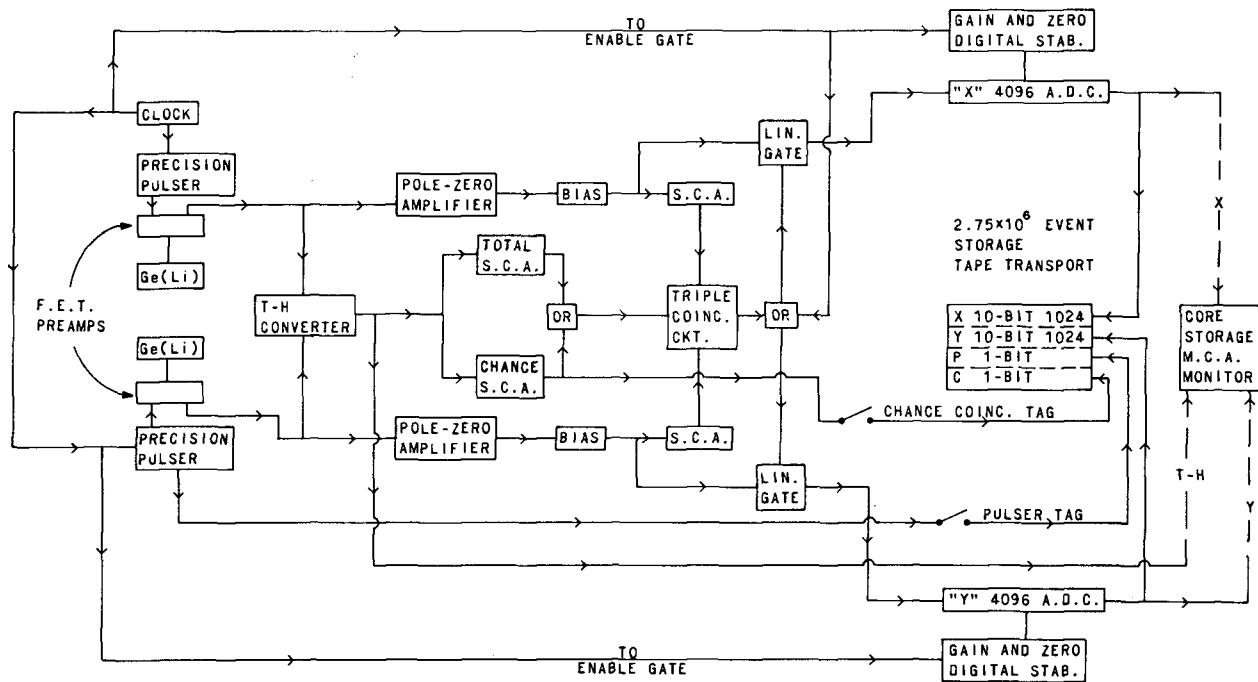


FIG. 2. Block schematic diagram of Argonne Ge(Li)-Ge(Li) coincidence system.

A time-to-pulse-height converter [1], serves as the basis of the fast coincidence timing unit. The outputs of two highly stable single-channel pulse-height analysers — one set on the prompt time pulse-height distribution and the other set on the chance portion of the distribution — are recorded on the magnetic tape as fast-coincidence 'total' and 'chance' labels for each recorded event which satisfies the triple fast-slow coincidence requirement. Thus, the total and chance coincidence spectra are simultaneously registered and are separately scanned during the tape-searching process with the aid of these tag bits. (This system is being modified to allow the time-to-pulse-height information corresponding to each coincidence event to be stored on tape together with the two normal pulse-height addresses of the linear signals.)

Digital zero and gain shift stabilization is employed in each arm of the coincidence system with the aid of two highly stable dual pulse-generators [2]. Coincidence studies lasting several weeks have been made with no noticeable line shift or broadening.

High count-rate electronics is used throughout this system and permits a detection rate in each detector of $\sim 50\,000$ events/sec with little or no line broadening. A fast-slow coincidence resolving time of from 60 to 100 nsec is employed, depending upon the gamma-ray energy range selected. Usually, total singles counting rates of $\sim 12\,000$ events/sec are employed with an overall attendant true-to-chance coincidence ratio of between 5 and 10.

4. EXAMPLES OF GAMMA-GAMMA COINCIDENCE DATA

Let us regress and present some old NaI-Ge(Li) coincidence work that resulted from an earlier collaborative investigation of the low-lying excited states of the odd-odd Cu isotopes performed by Shera and myself [3] at Los Alamos. This will provide an adequate starting point from

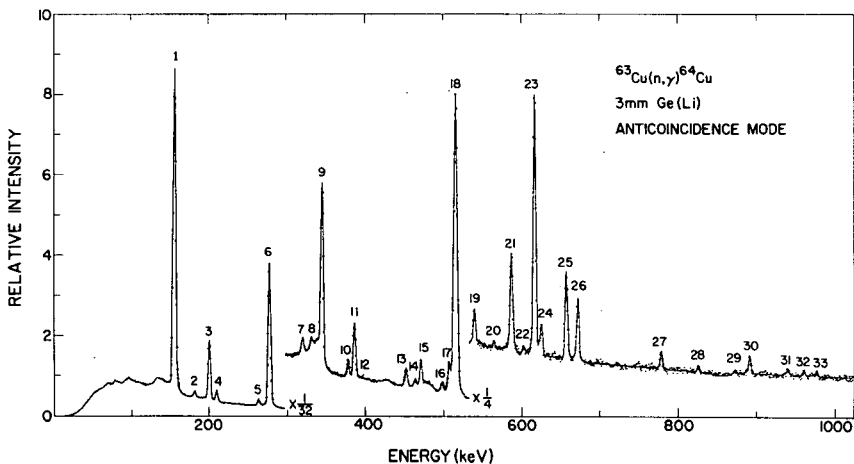


FIG. 3. Low-energy portion of the gamma-ray spectrum from the $^{63}\text{Cu}(n,\gamma)^{64}\text{Cu}$ reaction obtained with a Ge(Li) detector. The detector was operated inside a large anti-coincidence NaI(Tl) annulus.

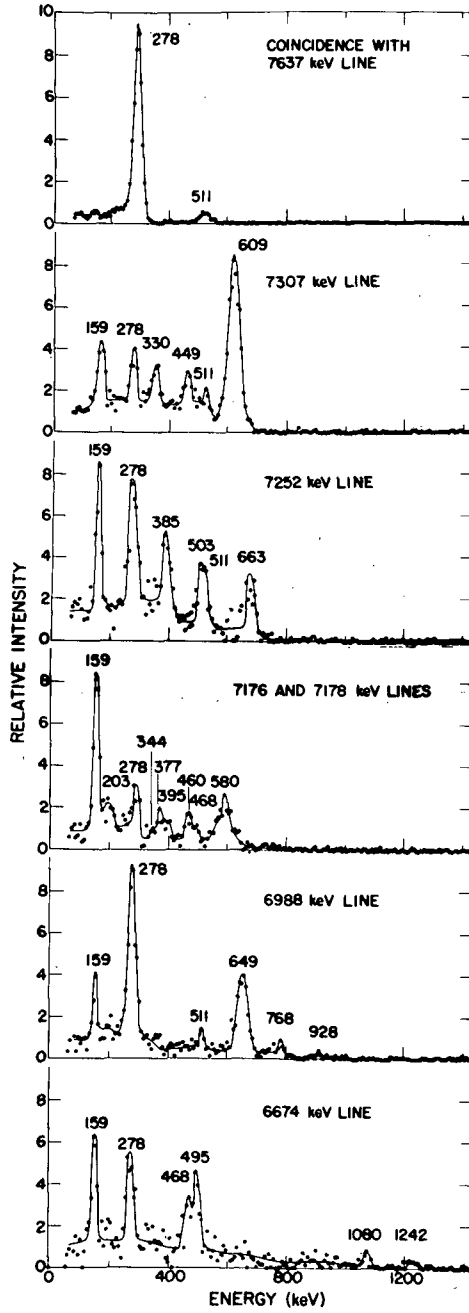


FIG. 4. Representative low-energy spectra from the $^{63}\text{Cu}(n,\gamma)^{64}\text{Cu}$ reaction, as recorded by the NaI scintillator in coincidence with particular high-energy gamma rays viewed by the Ge(Li) detector.

analysis allowed a fairly complete level scheme (Fig. 5) of the low-lying states to be constructed. Similar high-low NaI-Ge(Li) coincidence data recorded for other nuclides have not yielded spectra of this quality and have not always contributed as much in the way of new or additional information — principally because of the poor NaI resolution and the complexity of the low-energy gamma-ray spectrum. Even for the Cu isotopes the low-low NaI-Ge(Li) coincidence data were only of limited aid.

At about this time it became evident that if (n, γ) coincidence spectroscopy was to be of more general utility and significance, the severe limitation imposed upon these data by the use of NaI(Tl) would have to be removed. This requirement stimulated the first (n, γ) Ge(Li)-Ge(Li) coincidence system to be developed at Argonne. At that time, only small ($\sim 4 \text{ cm}^3$) Ge(Li) detectors were available and the first investigation suffered from the lack of larger, more efficient detectors. Nevertheless, the initial study of the $^{45}\text{Sc}(n, \gamma)^{46}\text{Sc}$ [5] reaction was an unqualified success and demonstrated not only the feasibility of the technique but its practicality even with small Ge(Li) detectors. Figure 6 displays a portion of the high-energy singles spectrum. The cross-hatched peaks are those that served as coincidence gates for the low-energy spectra viewed by the second Ge(Li) detector. Typical high-low coincidence spectra so obtained are shown in Fig. 7. Although the low-energy spectrum is not quite as complex as was

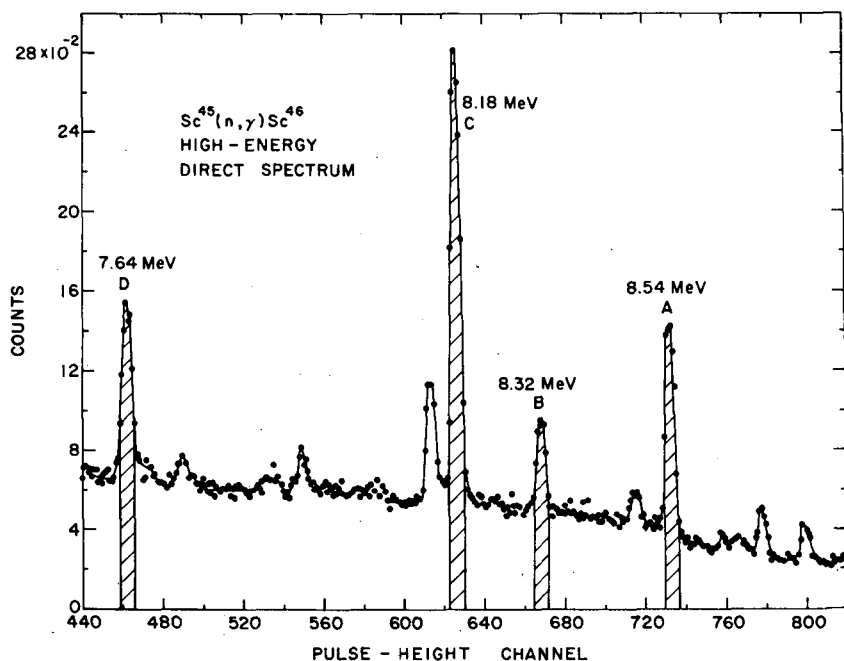


FIG. 6. Representative high-energy Ge(Li) singles pulse-height spectrum obtained in the external beam arrangement for the reaction $^{45}\text{Sc}(n, \gamma)^{46}\text{Sc}$. The lettered and cross-hatched double-escape peaks are the ones that served as coincidence gates in the two-parameter magnetic-tape-searching procedure for the low-energy coincidence spectra shown in Fig. 7. The double-escape peaks are labelled with their respective gamma-ray energies.

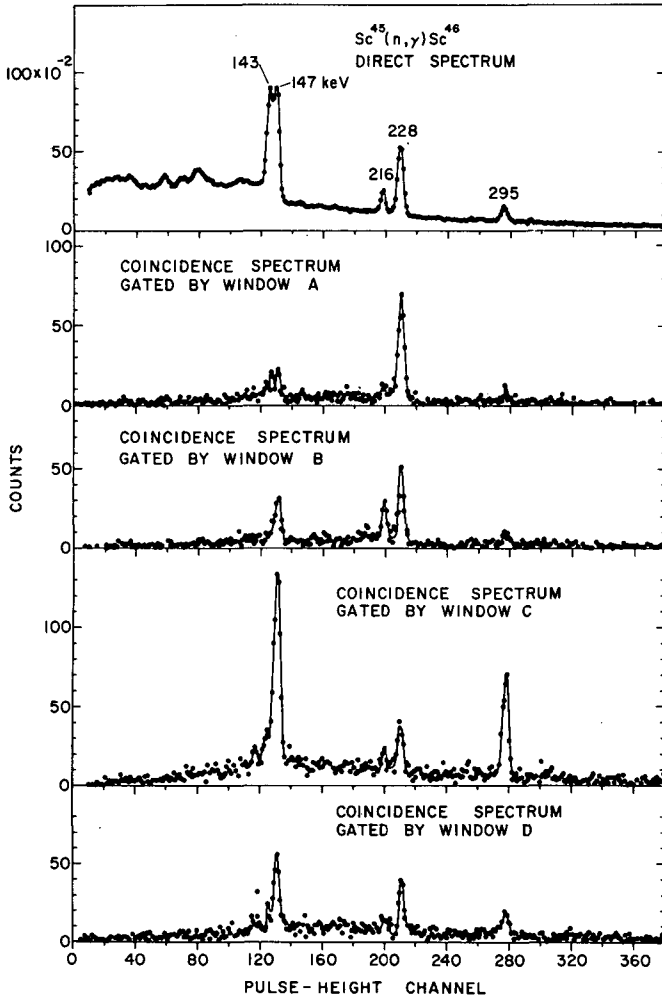


FIG. 7. Representative portions of the low-energy spectra in coincidence with the correspondingly labelled high-energy transitions shown in Fig. 6. The upper curve is the singles spectrum recorded under the same experimental conditions as the four lower coincidence spectra. In this figure no corrections have been made for the presence of chance coincidences or of coincidences with transitions of higher pulse heights whose continua underlie the particular high-energy coincidence gates employed. The contribution from chance coincidences can be assessed by comparing the magnitude of the 142-keV transition (which follows the decay of the 142-keV 19-sec isomeric level and for which no prompt coincidences are recorded) in the coincidence spectra with that of same transition in the singles spectrum (upper portion of figure) whose shape the chance coincidence spectrum follows.

the case in the Cu isotopes, still several clumps of low-energy transitions are present that could not have been resolved nor successfully analysed had NaI(Tl) been used in the low-energy arm of the spectrometer. Although the total number of recorded coincidence events is not large, the high-resolution of these detectors presents spectra with high peak-to-Compton ratios and the coincident lines are readily evident and easily recognizable. Figure 8 shows some representative low-low coincidence obtained in this investigation. Had a NaI scintillator been used in either arm of the system, individual peaks could not have been selected as gates and/or resolved in these coincidence spectra. In this case, the use of two Ge(Li) detectors in these low-low coincidence studies provided new and indispensable information on the coincident relationships among the low-energy transitions, as opposed to similar studies using a NaI-Ge(Li) system that rarely provide significant new data in most low-low coincidence studies.

The total experimental running time of these two sets of coincidence investigations was ~ 140 hours. The high quality of these data, taken months after the NaI-Ge(Li) study of the Cu isotopes, allowed analysis and construction of a detailed level scheme of ^{46}Sc to be completed (Fig. 9) somewhat earlier than that of the $^{64,66}\text{Cu}$ study. This was due principally to the clarity and simplicity of the Ge(Li)-Ge(Li) coincidence spectra.

As apparently successful as this initial Ge(Li)-Ge(Li) study appeared, it was evident that larger, more efficient detectors were needed to improve the quality of these data further and reveal the coincident relationships of some of the weaker transitions. Immediately upon the acquisition of larger detectors, the Argonne system was up-dated and the Los Alamos Ge(Li)-Ge(Li) system was put into operation, both yielding (n, γ) coincidence data on particular nuclides.

The Argonne system now employs a 20 and a 30 cm^3 detector combination, while the Los Alamos arrangement utilizes a 15 and 30 cm^3 pair of Ge(Li) detectors for the high-low studies and a 45 and 30 cm^3 pair for low-low work.

Before I present some examples of the more recent Ge(Li)-Ge(Li) coincidence data obtained at these laboratories, it must be stated that, just as in any other experimental investigation, some nuclides present themselves as better or worse candidates for these coincidence studies. No experimental facility provides data that is universally of the most superior quality. In the present case the greater number of strong transitions the better. However, even if an exceptionally poor case for coincidence studies presents itself and the sole contribution of the spectra so obtained is merely corroborative of the sequences of transitions inferred from other data, the coincidence information is of great value in that it removes some uncertainties and/or ambiguities that might otherwise be present. That is, coincidence data can at least provide positive unequivocal results on which one can hang one's hat.

The next illustration concerns coincidence data obtained from a study of the reaction $^{186}\text{W}(n, \gamma)^{187}\text{W}$ by D. A. McClure and myself at Argonne taken with the larger set of Ge(Li) detectors. At first sight these data do not appear to be quite as revealing as was the case for ^{46}Sc . However, these data were crucial in the establishment of the level scheme of ^{187}W (to be discussed in detail in a later paper at this Symposium¹).

¹ H. H. Bolotin and D. A. McClure, "Level structure of low-lying excited states of ^{187}W ", these Proceedings.

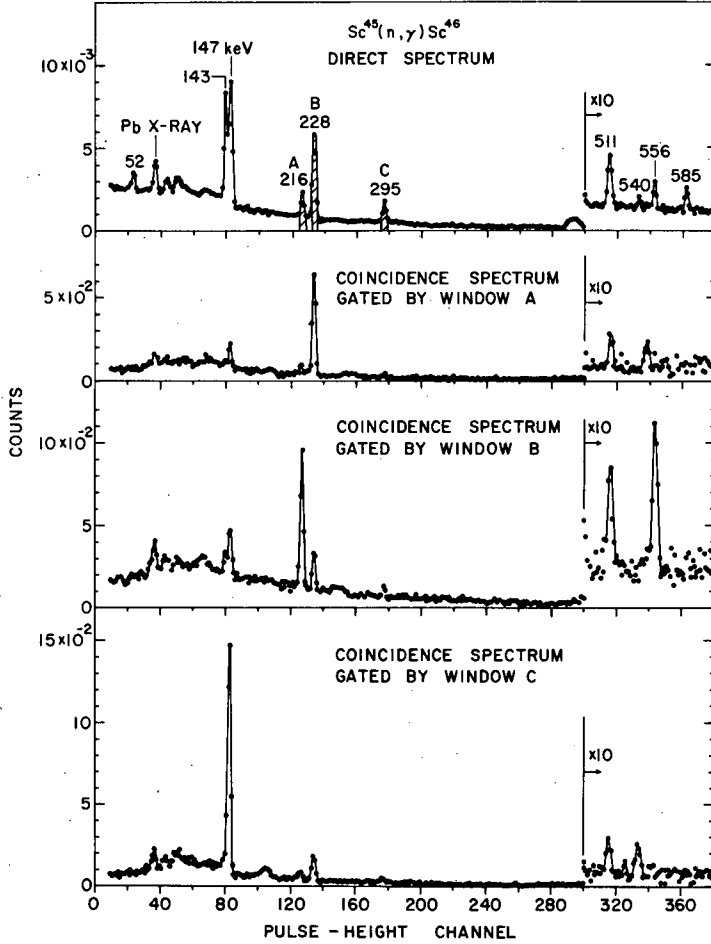


FIG. 8. Typical portions of the low-energy spectra in coincidence with the particular low-energy coincidence gates specified by the cross-hatched peaks of the singles spectrum shown in the upper portion of this figure. The three lower coincidence spectra shown have not been corrected for chance coincidences or for coincidence contributions due to those portions of the Compton distributions of higher energy transitions which underlie the respective coincidence gates used. The chance contribution can be estimated from a comparison of the singles spectrum (whose shape the chance coincidence spectrum follows) and the magnitude of the 142-keV peak (which follows the decay of the non-coincident 19-sec isomeric level) in the coincidence spectra.

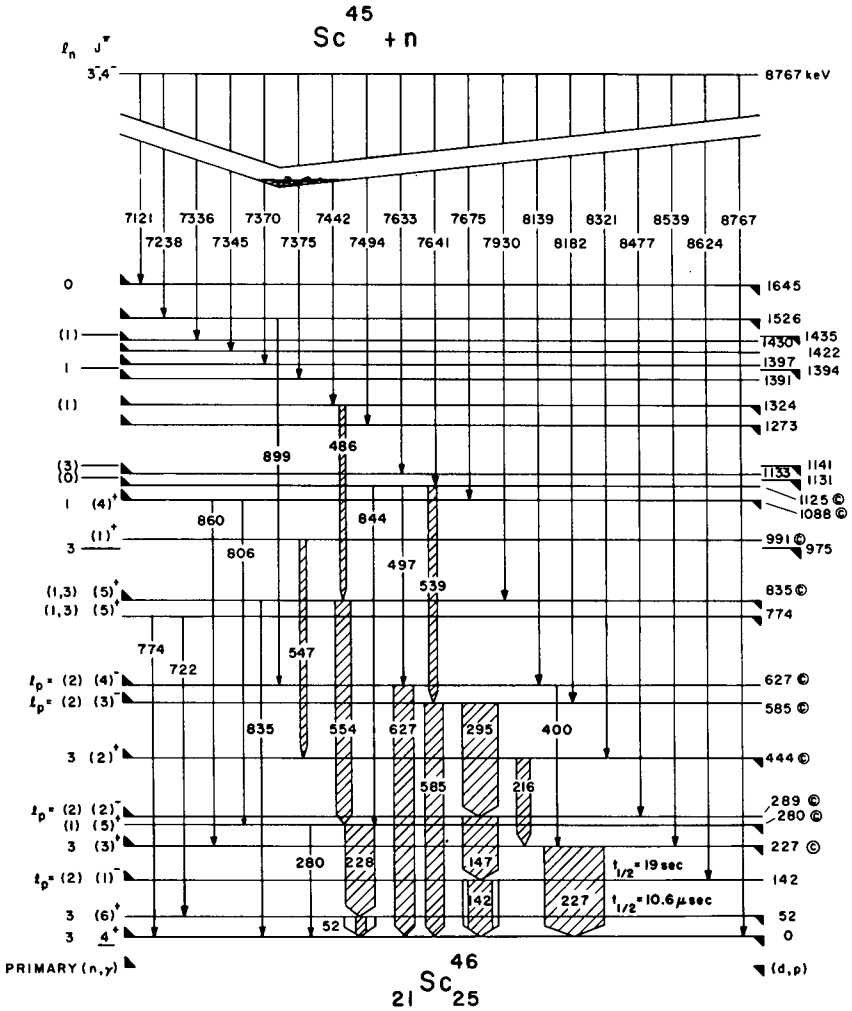


FIG. 9. Proposed level scheme of ^{46}Sc deduced from the various coincidence and singles gamma-ray investigations of the present work. The excitation energies are expressed in keV. Those levels marked on the left by upward-pointing flags are those that were observed to be populated by primary transitions from the capture state. Those levels marked on the right by downward-pointing flags are levels associated with reported (d, p) population. The levels observed to be populated in the present work are designated by full horizontal lines across the level scheme. The (d, p) states whose identification with the (n, γ) levels is somewhat doubtful because their energies do not quite agree are shown as short lines at the right and again at the left, with no connection across the diagram. The states designated by (C) are those that were established in the present work on the basis of the presently reported coincidence studies. The 774-keV state is the only level presented which is based solely upon the energy balance of low-energy transitions. Consequently, it is not proposed as confidently as are the states assigned on the basis of the coincidence results. The proposed spins and parities of the levels are shown immediately to the left of the levels.

Typical high-low and low-low γ - γ coincidence data on ^{187}W are shown in Figs 2 and 3 of our later paper¹. The complexity of the low-energy spectrum is more severe than in earlier examples, but these data definitely establish many particular coincident relationships that, together with the high- and low-energy singles data, lead to the final detailed level scheme shown in Fig. 4 of the later paper.

The next set of figures represents a true tour-de-force of the coincidence method and is representative of the excellent work of Shera of Los Alamos. The reaction studied was that of $^{209}\text{Bi}(n, \gamma)^{210}\text{Bi}$. Bismuth has a thermal-neutron capture cross-section of only ~ 32 millibarns, much smaller than the usual cross-sections encountered in thermal-capture work, and is the smallest cross-section of any nuclide studied with the coincidence technique. The high Z of bismuth and its small cross-section severely limit the size of the target sample used, as self-absorption of the low-energy gamma rays prevents use of arbitrarily large quantities of target material. Thus these coincidence studies required 30 days of experimental running time. The digital zero and gain stabilization employed prevented line broadening over the duration of this investigation. Figure 10 is a portion of the total coincidence high-energy primary spectrum obtained during this run and displays rather weak, but well-resolved transitions. Figure 11 shows a portion of the low-energy spectra in coincidence with each of four high-energy γ -rays and is impressive in its quality. Figure 12 is the new level scheme of ^{210}Bi deduced from these studies and is an enormous contribution to the elucidation of the level scheme and the properties of the low-lying states of this nuclide.

The final examples also come from the work of Shera and are concerned with his work on the $^{175}\text{Lu}(n, \gamma)^{176}\text{Lu}$ reaction. Prior to these coincidence studies, high-resolution (n, γ) singles data (both high-energy Ge(Li) and low-energy bent-crystal work) and (d, p) data were available, but a level scheme that united these data could not be established. The coincidence work of Shera quickly resolved the difficulties and a comprehensive level scheme of the ^{176}Lu nuclide was established that incorporated all of the existing data. Much of the low-low coincidence data that served to clarify the situation are shown in Figs 13-15. These spectra speak for themselves and clearly demonstrate the success, virtuosity, and indispensability of the Ge(Li)-Ge(Li) γ - γ coincidence technique.

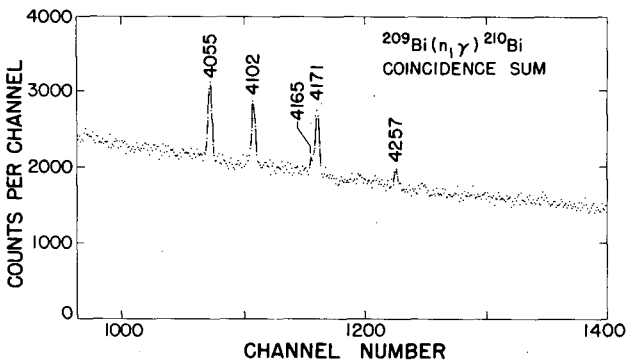


FIG. 10. Portion of the total Ge(Li)-Ge(Li) coincidence high-energy primary spectrum obtained in the Los Alamos study of Shera of the $^{209}\text{Bi}(n, \gamma)^{210}\text{Bi}$ reaction. The energies of the transitions are in keV.

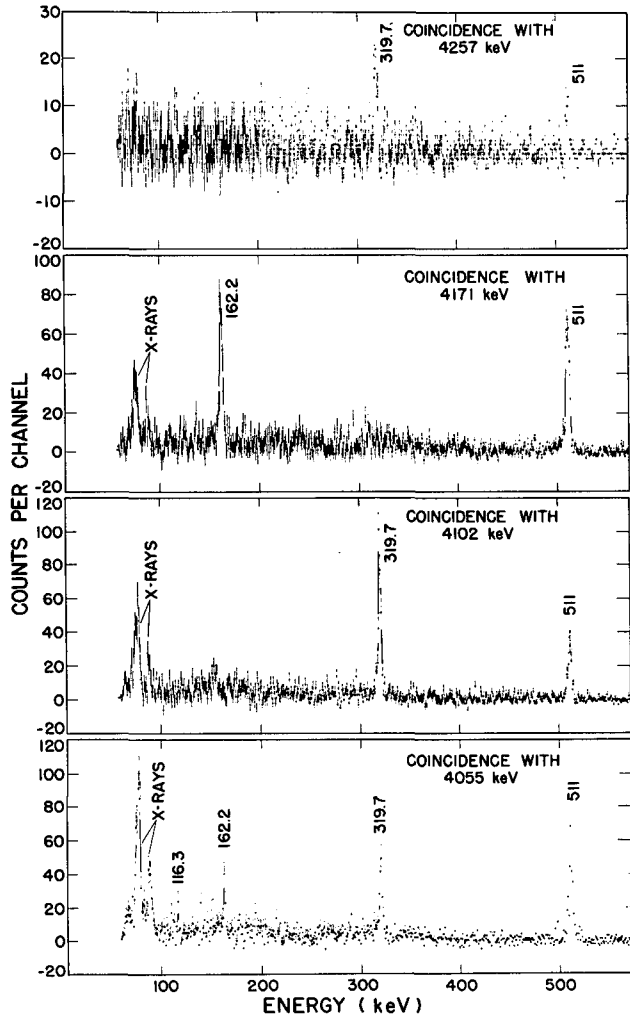


FIG. 11. Representative portions of the low-energy spectra in coincidence with each of four designated high-energy gamma rays from the all-Ge(Li) study of the $^{209}\text{Bi}(n,\gamma)^{210}\text{Bi}$ reaction by Shera.

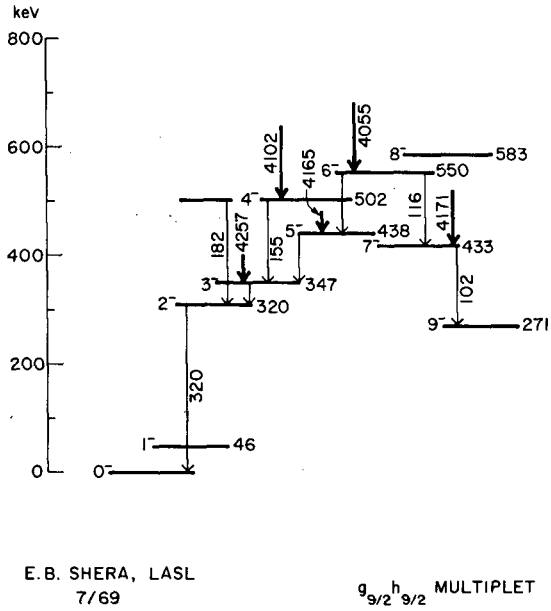


FIG. 12. The low-energy level scheme of ^{210}Bi proposed by Shera. All energies are in keV.

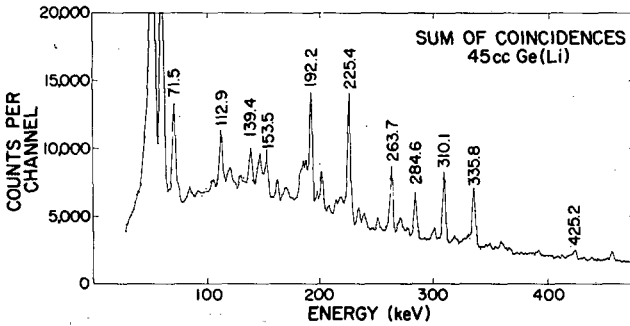


FIG. 13. Sum of low-energy Ge(Li)-Ge(Li) coincidence spectrum of Shera for the $^{176}\text{Lu}(n, \gamma)^{176}\text{Lu}$ reaction.

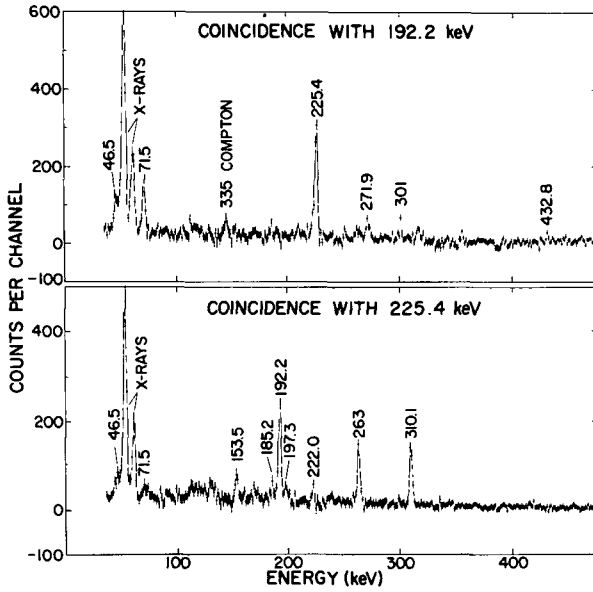


FIG.14. Representative low-energy spectra in coincidence with designated low-energy transitions for the $^{175}\text{Lu}(n,\gamma)^{176}\text{Lu}$ reaction by Shera.

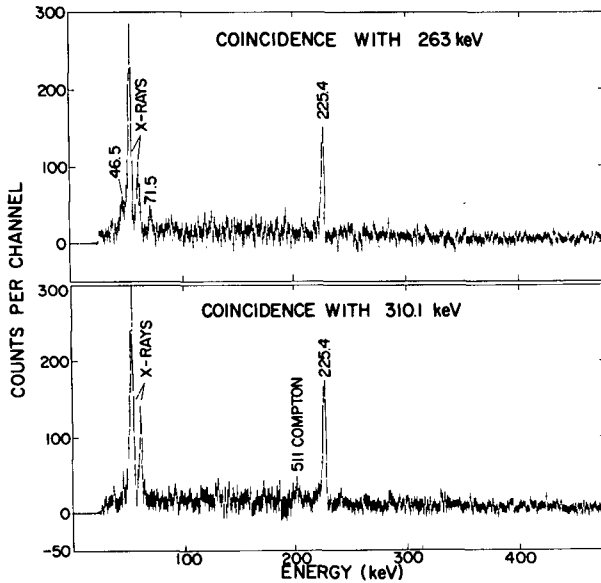


FIG.15. Additional representative low-energy spectra in coincidence with designated low-energy transitions for the $^{175}\text{Lu}(n,\gamma)^{176}\text{Lu}$ reaction (after Shera, Los Alamos Scientific Laboratory).

5. SUMMARY

The above examples of the new Ge(Li)-Ge(Li) gamma-gamma coincidence systems and spectra were presented to demonstrate the quality and usefulness of the data obtained with their use. The more widespread availability of the larger Ge(Li) detectors has endowed these coincidence studies with greater selectivity and resultant data of unrivalled quality and clarity. Despite the higher detection efficiency of a NaI(Tl)-Ge(Li) coincidence system, the inherently poor resolution of the scintillator so seriously minimizes its value that the all-Ge(Li) system is still immeasurably superior. The high peak-to-Compton ratio of the Ge(Li) spectra affords clear-cut interpretation of data recorded over an experimental time that is of much shorter duration than would be suggested from a comparison of the relative detection efficiencies of NaI(Tl) and Ge(Li) alone. In fact, as was shown in the ^{46}Sc study, the use of even relatively small Ge(Li) detectors provided data of easily interpretable quality in a relatively short time that could not be obtained in a much longer experimental running time had a NaI(Tl) scintillator been employed. The relative simplicity of the Ge(Li)-Ge(Li) coincidence system, the unrivalled character of the data obtainable with its use and the reasonable running times required lead to the conclusion that, by comparison, the use of a NaI(Tl)-Ge(Li) system is a waste of valuable experimental time and presents an unrewarding burden of data analysis to the experimenter. Thus, it is hoped that the preceding exposition has not only gone far to convince you of the unquestioned value of the coincidence technique, but has stimulated an early burial of NaI(Tl)-Ge(Li) coincidence systems.

The present Ge(Li)-Ge(Li) coincidence method has now reached the stage at which it is not limited to only the valuable γ - γ coincidence experiments designed to provide data used in the establishment of (n, γ) level schemes. Indeed, γ - γ angular correlation experiments, γ - γ polarization-directional correlation studies [6], γ -conversion electron coincidence work [using a Ge(Li)-Si(Li) combination], etc. are now practical. Some of these studies, now being planned, should open a new era of more detailed parameterization of the level structure of nuclides populated by the (n, γ) reaction that rival the sophistication of experimental work of less complex nuclear spectroscopic investigations.

The ^{210}Bi work of Shera clearly demonstrated that within reason the available external-beam neutron flux and/or the neutron capture cross-section of the target nuclide under investigation do not necessarily preclude (n, γ) all-Ge(Li) γ - γ coincidence studies at resonance. I particularly have in mind neutron-diffraction spectrometers of the Brookhaven type that can concentrate all of the available diffracted flux into a single low-energy resonance in which the capture cross-section can be quite sizeable.

The feasibility and practicality of the use of a Ge(Li)-Ge(Li) coincidence system in other particular (n, γ) studies is best judged by the experimenter and the experimental situation. However, it is hoped that the above exposition will stimulate workers in this field to seriously consider its use in a variety of other possible (n, γ) experimental studies that may not have been touched upon in this paper.

ACKNOWLEDGEMENTS

The author wishes to express his appreciation of the efforts of M. G. Strauss and co-workers at Argonne National Laboratory for the design and construction of the electronic systems employed, and he is indebted to E. B. Shera of Los Alamos Scientific Laboratory for providing examples of his excellent results for inclusion in this talk prior to their publication.

REFERENCES

- [1] RODDICK, R., LYNCH, F.J., IEEE Trans. Nucl. Sci. 11 (1964) 399.
- [2] STRAUSS, M.G., SIFTER, L.L., LENKSZUS, F.R., BRENNER, R., IEEE Trans. Nucl. Sci. 15 (1968) 518.
- [3] SHERA, E.B., BOLOTIN, H.H., Phys. Rev. 169 (1968) 940.
- [4] De FIGUEIREDO, R.P., MAZARI, M., BUECHNER, W.W., Phys. Rev. 112 (1958) 873.
- [5] BOLOTIN, H.H., Phys. Rev. 168 (1968) 1317.
- [6] A Ge(Li) linear polarimeter of the type developed by LITHERLAND, R.E., EWAN, G.T., BARTHOLOMEW, G.A., Bull. Am. Phys. Soc. 13 (1968) 1405, although of relatively small volume, appears feasible to be used in conjunction with a larger Ge(Li) detector in γ - γ linear polarization coincidence experiments.

HIGH-PRECISION NEUTRON CAPTURE GAMMA-RAY SPECTROSCOPY USING GERMANIUM DETECTORS IN COMPTON-SUPPRESSION TECHNIQUE

W. MICHAELIS, F. HORSCH
Institut für angewandte Kernphysik,
Kernforschungszentrum Karlsruhe,
Karlsruhe, Federal Republic of Germany

Abstract

HIGH-PRECISION NEUTRON CAPTURE GAMMA-RAY SPECTROSCOPY USING GERMANIUM DETECTORS IN COMPTON-SUPPRESSION TECHNIQUE. The use of lithium-drifted germanium detectors in Compton-suppression technique will play a very important role in future neutron capture gamma-ray spectroscopy. Over a broad range of energy these devices are superior to all other instruments. High-precision measurements require a favourable peak-to-background ratio and reliable methods in spectrum stabilization, spectrum analysis, calibration and non-linearity correction. The paper reports the procedures that are applied at Karlsruhe and gives some results to demonstrate the efficiency of this technique. Conclusions are drawn on the future potential in neutron capture spectroscopy.

1. INTRODUCTION

Over the last years in gamma-ray spectroscopy increasing attention has been given to the application of lithium-drifted germanium counters since the energy resolution of these devices considerably exceeds that of conventional scintillation detectors. It is understandable that very soon germanium diodes were also being applied to studies of the radiative neutron capture process where spectra with several hundreds of gamma-ray lines have to be analysed and in fact a notable amount of the available data has been accumulated with these instruments. The potential was further increased by operating the detectors in the Compton-suppression mode. In this technique the germanium counter is surrounded by a NaI(Tl), a plastic or a liquid scintillator and Compton events are eliminated to a large extent by means of an anticoincidence circuit. Usually the range of application is between 100 keV and 3 MeV.

In the upper part of this energy range the anti-Compton spectrometer is superior to all other sophisticated instruments both in resolution, precision and sensitivity. For low energies (≤ 500 keV) a competitive instrument is provided by the coherent scattering spectrometers which possess uncontested characteristics at very low energies. The boundary in the optimum resolution between crystal diffraction and anti-Compton spectrometer is not fixed. Due to the very different sensitivity, it greatly depends on the cross-section of the material under study. For targets with very high cross-sections (> 1000 b) the boundary may be at energies above 500 keV, while for materials with low cross-sections (< 100 b) the semiconductor system provides the superior instrument over nearly the whole range of application. In this connection it is useful to realize that about

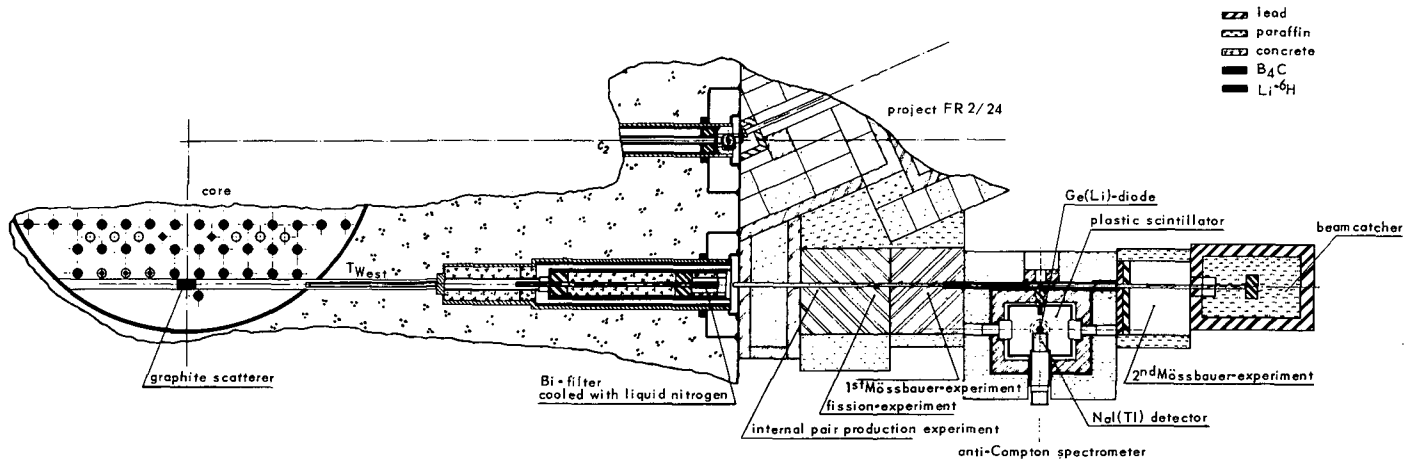


FIG. 1. Schematic diagram of the experimental arrangement at the reactor.

60% of the natural elements have capture cross-sections below 10 b. The correlation between energy resolution expressed in FWHM and precision in energy determination may be quite different for the two devices. In the coherent scattering instrument the energy precision is limited by the optimum resolution in scattering angle, while for the semiconductor spectrometer, in principle, the peak position can be determined to an infinitely small fraction of the line width. Gamma-ray intensities are obtained in a more direct way from semiconductor measurements.

These considerations lead to the conclusion that in spite of the excellent characteristics of the diffraction instruments, the use of germanium detectors in Compton-suppression technique will play a very important role in future neutron capture spectroscopy. However, for obtaining optimum precision with these devices several essential requirements must be fulfilled:

- (1) The noise performance should ensure a line width close to the statistical limit; counting-rate effects must be negligible
- (2) The peak-to-Compton ratio should be as high as possible or, in other words, the background under the full energy peaks should be low and smooth
- (3) The instrument must have a high stability and linearity
- (4) The peak positions have to be determined very accurately
- (5) The spectra must be carefully calibrated and a suitable non-linearity correction has to be applied to the channel-energy relationship.

The first topic is a general problem in semiconductor spectroscopy and is treated extensively in the literature. Thus we need not discuss it here in detail. The purpose of this presentation is to provide a brief summary of the procedures applied at Karlsruhe on topics (2) to (5) and to draw conclusions from this work on the future potential of anti-Compton devices in neutron capture spectroscopy.

2. PEAK-TO-BACKGROUND RATIO

The anti-Compton instrument, installed in 1966 at the Karlsruhe reactor FR-2, at present consists of an unencapsulated 5-cm³ Ge(Li) diode, a 50-cm diam. × 40 cm plastic scintillator (NE 102 A) with the germanium counter in its centre, and a 4 in. diam. × 6 in. NaI(Tl) detector placed within a well directly behind the vacuum chamber of the semiconductor diode (for a detailed description see Ref. [1]). The spectrometer is used in external target geometry and is one of five instruments installed at one output of a tangential beam hole which passes through the heavy water of the reflector. A schematic drawing of the arrangement is shown in Fig. 1.

The design of the spectrometer offers the following advantages:

- (1) The NaI(Tl) counter ensures a strong absorption of gamma rays scattered in the forward direction. This reduces very effectively the contribution of the ever present intense high-energy radiation to the background under the peaks.

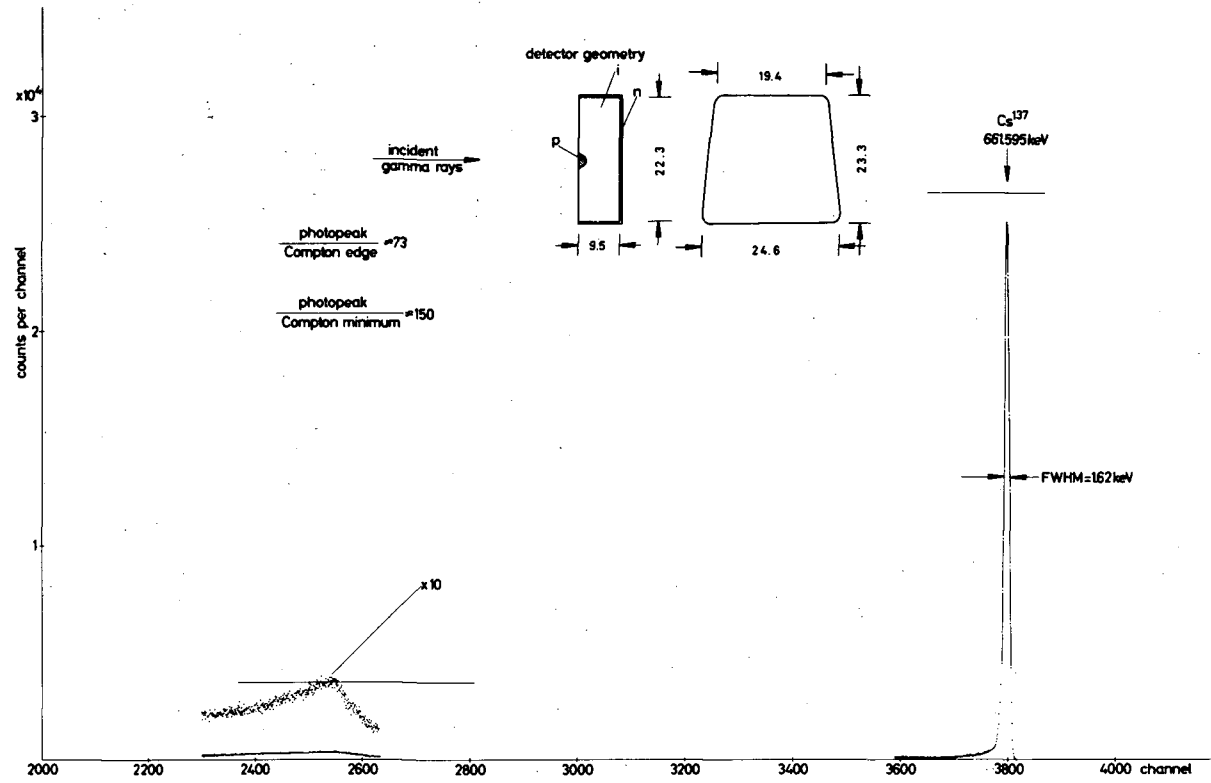


FIG. 2. Sectional display of the pulse-height spectrum of ^{137}Cs taken with the anti-Compton spectrometer.

(2) The plastic scintillator can be used unencapsulated and the reflector, in the form of a water-based emulsion paint, can be kept very thin. Thus the harmful absorption of backscattered soft gamma rays between germanium detector and anti-Compton shield can be minimized. The solid angle for photons escaping out of the anticoincidence shield is very small and is certainly negligible.

(3) The spectrometer is less expensive than other devices which use large NaI(Tl) shields.

A disadvantage of the plastic scintillator is the lower light output compared to NaI(Tl) and the necessarily larger volume of the detector.

The present performance of the system is illustrated in Fig. 2. For the ^{137}Cs 661.595-keV gamma ray the ratio of photopeak to total height of the background is 73:1 at the Compton edge and about 150:1 in the minimum of the Compton distribution. The energy resolution including long-term instabilities is 1.62-keV FWHM. In the inset of Fig. 2 the drift geometry of the diode is shown. The absence of a dead layer on the detector front face minimizes the amount of absorbing material for the backscattered soft gamma rays.

The performance of an anti-Compton spectrometer for neutron capture spectroscopy is not only determined by the peak-to-Compton ratio for gamma rays possessing energies within the range being measured (100 keV to 3 MeV), but also by the effectiveness in suppressing the background caused by the high-energy transitions above 3 MeV. Here we have to deal mainly with events from photons scattered in the forward direction and high-energy electrons which deposit only part of their energy in the sensitive volume of the detector. The first component is strongly suppressed by the NaI(Tl) detector, while for reduction of the second component it was found useful to apply a pulse-shape discrimination method to the pre-amplifier signals of the germanium detector. A detailed description of this circuit has been given elsewhere [2]. To demonstrate the actual performance of the spectrometer a sectional display of a typical capture spectrum is shown in Fig. 3. The spectrum was obtained from a sample of natural erbium (capture cross-section 160 b). Above the energy interval displayed in Fig. 3 more than 300 gamma-ray lines have been detected in the total spectrum. All these lines contribute to the background under the peaks in Fig. 3. The yet excellent peak-to-background ratio clearly illustrates the efficiency of the applied method. Another example is given in the paper on ^{68}Zn presented at this Symposium [3].

Several decisive improvements of the system are still feasible. In single mode the present diode exhibits a peak-to-Compton ratio of approximately 10:1 for ^{137}Cs . When the detector was installed, planar diodes were superior to coaxially drifted devices with respect to energy resolution. Thus postulate (1) in section 1 was the dominant criterion. Meanwhile large-volume coaxial detectors with comparable resolving power have appeared on the market. The peak-to-Compton ratio of these devices is considerably higher; values up to 30:1 for ^{137}Cs are obtainable.

Other possible improvements concern the detection threshold of the plastic scintillator. The present photomultipliers (EMI 9618B) may be replaced by tubes with photocathodes of higher sensitivity. Furthermore, it would be useful to mount additional tubes on the scintillator, in particular

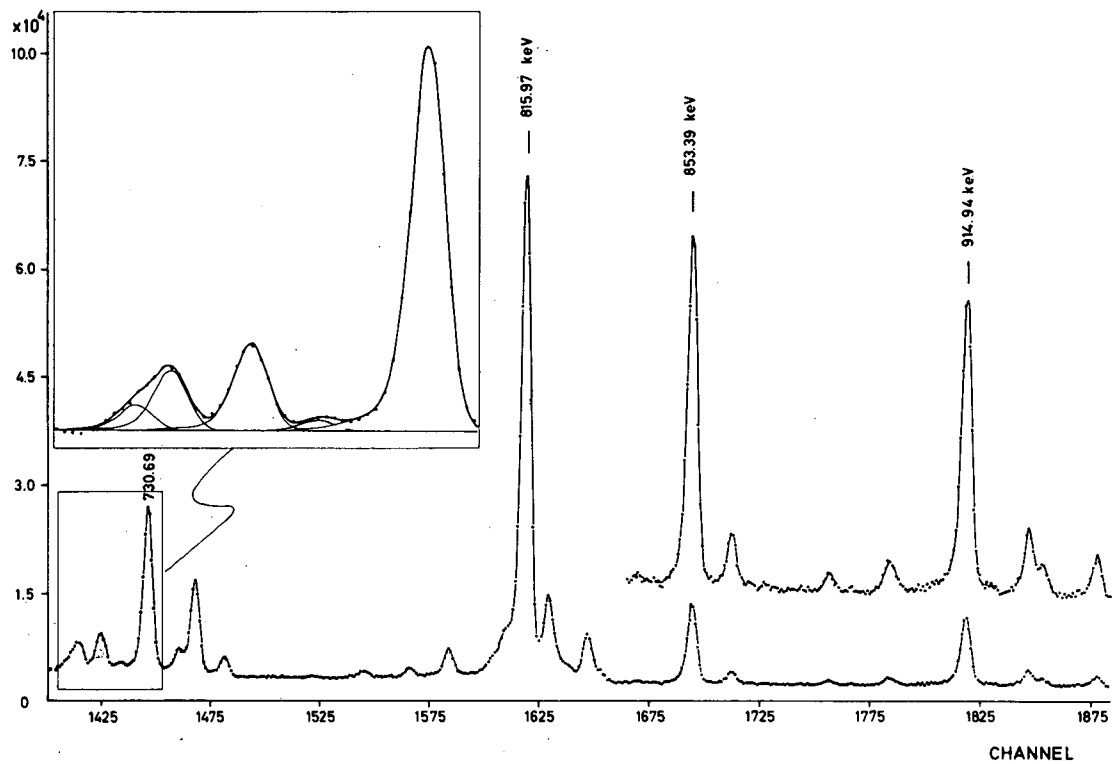


FIG. 3. Sectional display of the capture spectrum from a natural erbium sample.

in the backward direction. Finally, coincidence techniques and cooling of the tubes may improve the signal-to-noise ratio.

We thus can conclude that without sacrifice in energy resolution peak-to-Compton ratios of 250:1 for ^{137}Cs are now quite realistic. Suitable modifications of the system will be tackled in the near future.

3. SPECTRUM STABILIZATION

Depending on the cross-section of the sample under study, the measurement of a capture spectrum may cover a period of days or even weeks. Therefore digital stabilization of the amplifier chain and the analog-to-digital converter is a basic requirement for obtaining high precision. This includes both zero drift and gain stabilization. In neutron capture spectra the intensity is distributed over a large number of gamma rays. Thus in most cases no well-isolated natural line with sufficient peak counting rate is available. The presence of an isolated and intense line, however, is very important, if all instabilities independent of their time behaviour are to be eliminated. An alternative procedure is to use an ultra-high precision pulse generator. Here an adequate peak counting rate is attained without producing any additional background outside the full-energy line. Storage of the pulses can easily be prevented by means of an inhibit circuit.

Exceeding demands are made on such a pulser. Since advanced techniques aim at a precision of about 50 eV at 2 MeV (see below), the accuracy of the pulser should be of the order of 10^{-5} . Figure 4 presents an outline of the basic instrument which is now used at Karlsruhe both for gain stabilization and non-linearity correction. The pulser has an instability of < 10 ppm per degC and a non-linearity of $\leq \pm 10$ ppm. The main components of the circuit are a Zener diode network, a Kelvin Varley precision voltage divider, a chopper stabilized operational amplifier for impedance conversion and a mercury relay with pulse shaper. The reference voltage circuit with the carefully aged Zener diode is placed in a temperature-regulated oven and is compensated against variations in temperature and line voltage. Optimum stability is achieved at 65°C where the temperature coefficient of the diode is zero. The impedance matching amplifier ensures the excellent linearity characteristics of the pulser. As regards long-term instabilities this component proved to be the most frequent source of failures¹. Therefore it is useful to check carefully the warranted performance of the amplifier and to repeat this test at time intervals not longer than a few months. Design and wiring of the pulser output ensure that the influence of the following factors on the output pulse amplitude is kept sufficiently small: the normal amplifier drift rate ($1 \mu\text{V}$ per week), the instability of the pulse shaping capacitor (0.1% per year) and the variation of the mercury relay contact resistance ($\pm 1 \text{ m}\Omega$). A detailed description of the circuit is given in Refs [4, 5].

If the pulser is only applied for gain stabilization, the impedance matching amplifier can be omitted and the Kelvin Varley voltage divider can be replaced by a simple and less expensive resistance network. For zero-drift stabilization it is convenient to use a natural gamma emitter, e.g. ^{57}Co , with appropriate source strength. The source should not emit any gamma rays within the measuring interval.

¹ "Failure" means in this connection that the pulser output varies by clearly more than 10 ppm.

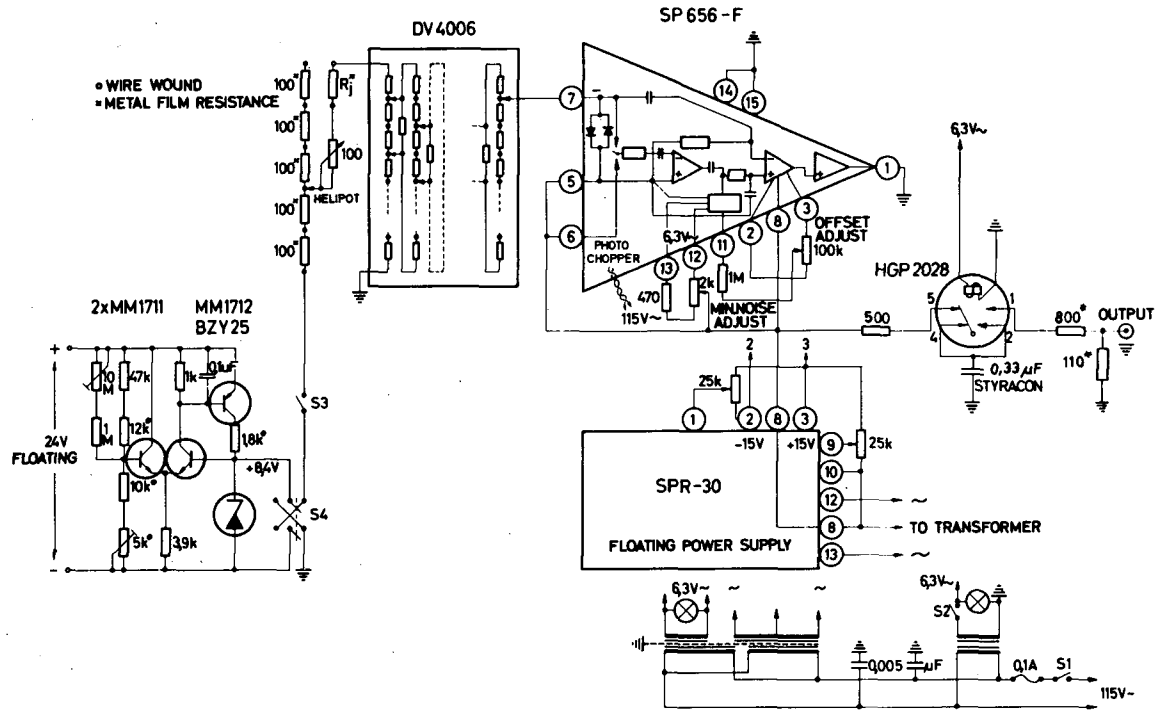


FIG. 4. Outline of the precision pulser.

4. SPECTRUM ANALYSIS

High precision in the energy determination requires utmost accuracy in the evaluation of the peak position. In a computer programme for spectrum analysis reasonable assumptions have to be made on the line shape. An analytical expression should fulfil two requirements: The application to complex spectra must not involve intolerably long computer times and the evaluated curve should fit to the experimental points as well as possible. Very promising results have been obtained by means of the following line shape representation:

$$y = A \exp \{-\lambda (x - x_0)^2\} \quad \text{for } x \geq x_0 - b$$

$$y = A [\exp \{-\lambda (x - x_0)^2\} - B x_{\text{cor}} \exp (x_{\text{cor}})] \quad \text{for } x < x_0 - b$$

where $b = (\lambda^{-1} \ln 2)^{\frac{1}{2}}$ and $x_{\text{cor}} = (x - x_0 + b)/b$.

In the case of efficient charge carrier collection in the diode the use of these expressions gives excellent fits for the whole energy range of the spectrometer. This can be seen from Fig. 5 which shows experimental and fitted line shapes for gamma rays at 296, 1173 and 1836 keV. Complex structures are resolved with much success. An example is given in the inset of Fig. 3.

The following procedure is used for the analysis. The spectra are divided into groups each containing at most six gamma lines. Since the background under the peaks is very smooth and only a slowly varying function of energy (cf. Fig. 3), within such an interval the background can be well approximated by a straight line or an exponential function. Energies and intensities are calculated, taking into account a non-linearity correction (section 5) and the response function of the spectrometer. The results are listed by means of a fast printer and each group is plotted in a figure that shows the experimental points together with the fitted background, the fitted gamma lines and the total sum of these curves. Each fit is accomplished with a given number of lines which is chosen to be as low as possible on the basis of a coarse examination of the spectrum. In those cases where the results are insufficient the calculation is repeated, conceding one or more additional lines. This procedure, which guarantees a reliable control by the experimentalist, is clearly preferred to a fully automatic analysis. A detailed description of the programme is given in Ref. [6].

5. CALIBRATION AND NON-LINEARITY CORRECTION

The most suitable gamma sources for energy calibration are the following beta-unstable isotopes: ^{57}Co , ^{192}Ir , ^{137}Cs , ^{95}Zr , ^{95}Nb , ^{54}Mn , ^{88}Y , ^{60}Co , ^{22}Na and ^{24}Na . The gamma-ray energies are known very accurately and may be found in Refs [7-10]. Considerable aid in the calibration procedure is provided by the precision pulser described in section 3. A narrow sequence of calibration points can be created with this instrument, even in those energy regions where only few or no natural lines of sufficient accuracy are available.

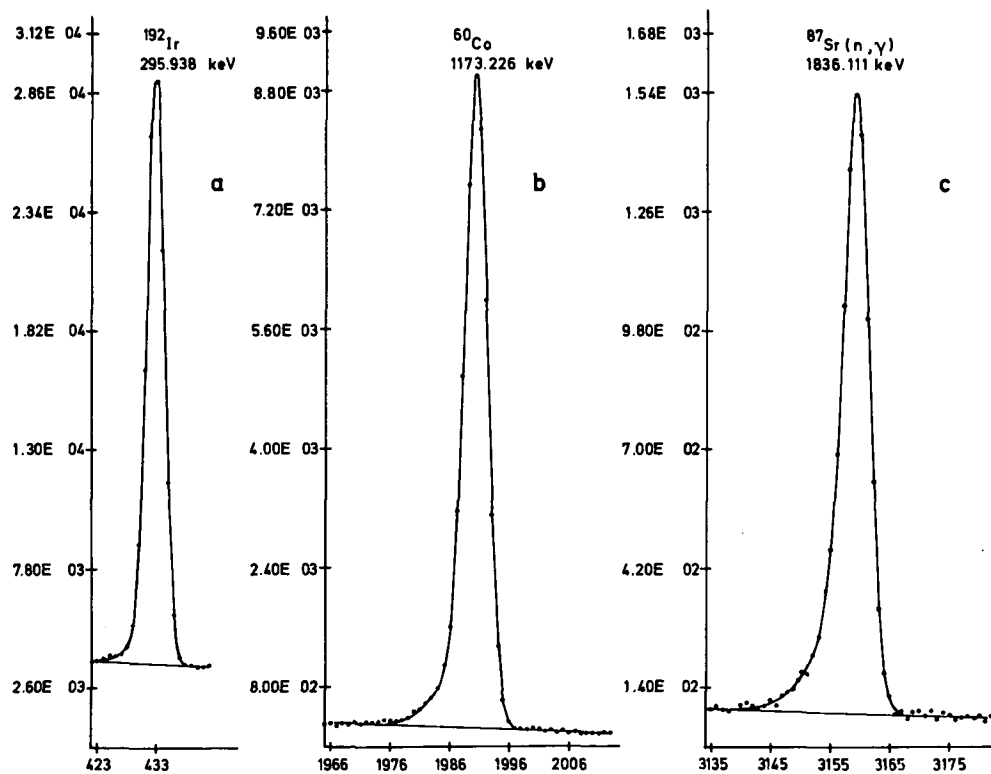


FIG. 5. Experimental and fitted line shape.

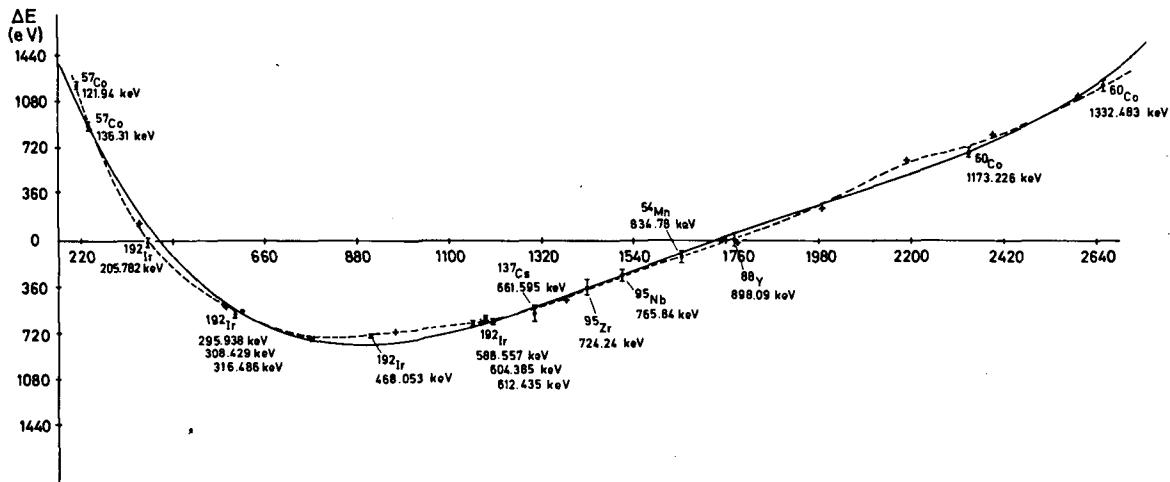


FIG. 6. Typical deviation of the channel-energy relationship from a straight line in eV. The crosses represent calibration points obtained with the precision pulser.

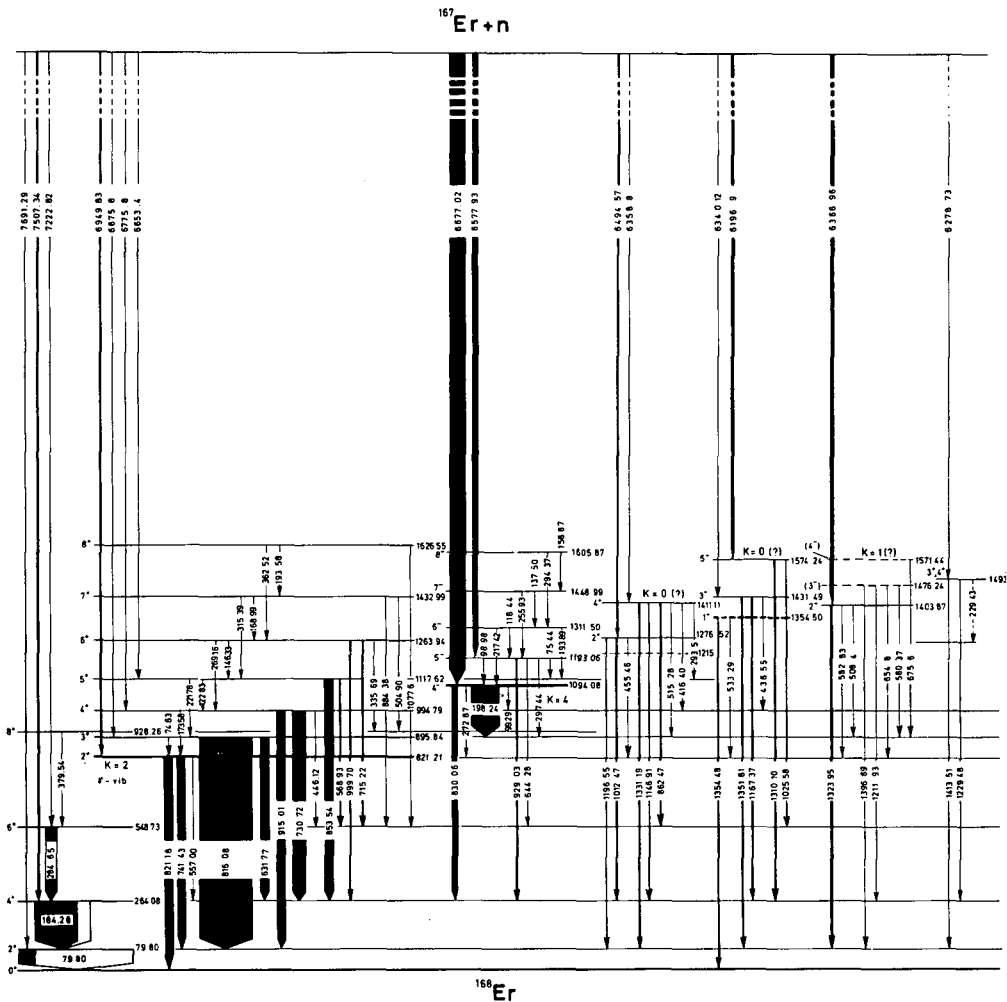


FIG. 7. Transition diagram for ¹⁶⁸Er: (a) bandhead energies below 1.5 MeV;

The non-linearity of most commercial amplifiers is of the order of $\pm 0.05 - 0.1\%$. Similar values are specified for analog-to-digital converters. Thus for the total system non-linearities of $\pm 0.1\%$ or more are expected. A typical example for the deviation of the channel-energy relationship from a straight line is shown in Fig. 6. In this measurement the amplifier chain consisted of a cooled FET preamplifier [11] and a main amplifier of type Ortec 410. The pulses were analysed with a 4096-channel ND-160F ADC. The points obtained with the pulser coincide very well with those based on natural gamma lines. The dashed curve represents the 'exact' non-linearity which can be determined with an accuracy of about 50 eV. The full curve shows the result of a fit to the experimental points as obtained with a polynomial of fourth degree. The maximum deviation of this curve from the 'exact' function is 90 eV. In most regions the deviation is much less. We see, however, that a large number of calibration points and a high degree of the fit polynomial are required.

The non-linearity correction discussed here does not account for 'short-range' fluctuations of the differential non-linearity such as the so-called odd-even effect. To minimize the influence of these sources of error, it is convenient to use as small a channel width as possible (≈ 200 eV).

6. EXPERIMENTAL PROCEDURE AND RESULTS

The following procedure is applied for precision measurements of capture spectra: Before the (n, γ) spectrum is taken, a spectrum of the calibration lines is accumulated. The result of this measurement is later compared with that from a similar run performed at the end of the experi-

TABLE I. GAMMA-RAY CASCADES IN ^{68}Zn AND ^{88}Sr

Target nucleus	Cross-section (b)	Gamma-ray energy (keV)			Recoil correction (keV)	Level energy (keV)
		E_{γ_1}	E_{γ_2}	E_{γ_3}		
^{67}Zn	6.9	805.75	1077.35	-	0.014	1883.12
		1883.09	-	-	0.028	1883.12
		670.89	1261.00	1077.35	0.026	3009.27
		1126.07	1883.09	-	0.038	3009.20
^{87}Sr	~ 17	898.05	1836.08	-	0.025	2734.16
		2733.97	-	-	0.046	2734.02
		1493.41	2733.97	-	0.060	4227.44
		2391.20	1836.08	-	0.055	4227.34

ment. It provides a reliable control that during the experiment no failure (cf. footnote 1) has occurred in the critical electronic components (pre-amplifier, main amplifier, precision pulser, ADC, zero drift and gain stabilizers). In the second run the capture spectrum is taken. After read-out the calibration lines are accumulated on the capture spectrum without memory reset. This ensures that all lines are analysed under the same background conditions. Finally the first run is repeated and the result is used for determining and interpolating the parameters in the line shape representation.

Measurements have been performed on a large number of nuclei. Results on ^{58}Fe (target cross-section 2.5 b), ^{62}Ni (2.0 b), ^{68}Zn (6.9 b), ^{96}Mo (14.5 b), ^{98}Mo (2.2 b) and ^{167}Er (650 b) are briefly discussed in other contributions to this Symposium. Up to 300 gamma rays have been detected in a single spectrum. Because of the heavy shielding of the spectrometer no problems from background lines arise, even for very low target cross-sections. Gamma rays differing in intensity by a factor of 5×10^{-5} have been observed for cross-sections below 10 b. Table I gives an impression on the accuracy that can be obtained for pronounced peaks in the spectra. The absolute errors for the quoted gamma-ray energies are about 50 eV. The errors arising from the fitting procedure and the non-linearity correction are between 5 and 100 eV. The high accuracy permits a reliable application of Ritz' combination principle to excitation energies of several MeV. The accuracy for weak lines is limited by the pure counting statistics. As an example of the efficiency of the method, Fig. 7 presents a considerably extended transition diagram for the nucleus ^{168}Er .

7. CONCLUSIONS

Anti-Compton spectrometers with peak-to-Compton ratios of 250 : 1 for ^{137}Cs are now feasible. By effectively suppressing background events from high-energy gamma rays, a smooth background can be achieved which shows only a slight increase with decreasing energy. The instruments allow energy determinations with an accuracy in the order of 50 eV. For weak lines the precision can be improved by using internal target geometry and thus improved counting statistics. With only a few exceptions precision measurements will be possible over the whole range of cross-sections. Even below 10 b gamma-ray lines that differ in intensity from the most intense peaks by five orders of magnitude should be detectable. Several hundreds of lines can be observed in a single spectrum.

In summary, the application of lithium-drifted germanium detectors in Compton-suppression technique will bring about a considerable improvement in the quality and detail of data that can be attained from neutron capture spectroscopy.

REFERENCES

- [1] MICHAELIS, W., KÜPFER, H., Nucl. Instrum. Meth. 56 (1967) 181.
- [2] TAMM, U., MICHAELIS, W., COUSSIEU, P., Nucl. Instrum. Meth. 48 (1967) 301.
- [3] OTTMAR, H. et al., "Radiative neutron capture studies of nuclear excitations in ^{68}Zn ", these Proceedings.

- [4] HORSCH, F., MEYER, O., MICHAELIS, W., Rep. KFK 778 (1968); Proc. Symp. Nuclear Electronics, Versailles, 1968.
- [5] HORSCH, F., Rep. KFK 558 (1968).
- [6] HAASE, V., Rep. KFK 730 (1968).
- [7] LEGRAND, J., BOULANGER, J.P., BRETHON, J.P., Nucl. Phys. A107 (1968) 177.
- [8] BLACK, W.W., HEATH, R.L., Nucl. Phys. A90 (1967) 650.
- [9] BELLICARD, J.B., MOUSSA, A., Compt. Rend. 241 (1955) 1202.
- [10] MARION, J.B., Nuclear Data A4 (1968) 301.
- [11] TAMM, U., Rep. KFK 509 (1967).

RADIATIVE NEUTRON CAPTURE IN FISSIONABLE NUCLEI

W. MICHAELIS, H. LEUSCHNER, P. MATUSSEK
Institut für angewandte Kernphysik,
Kernforschungszentrum Karlsruhe,
Karlsruhe, Federal Republic of Germany

Abstract

RADIATIVE NEUTRON CAPTURE IN FISSIONABLE NUCLEI. Because of the great success of the (n, γ) method in nuclear structure studies, it is desirable to extend such measurements to fissionable target nuclei. A suitable spectrometer for investigating the high-energy radiative capture spectrum without significant interference from the fission process has been installed at the Karlsruhe research reactor FR-2. The instrument is briefly discussed. First preliminary results are presented.

Studies of the radiative neutron capture process have revealed detailed information on nuclear structure. As yet, however, the application of this method has been restricted to compound nuclei which are stable against nuclear fission. With fissile target material the capture spectrum is masked by the prompt gamma-ray spectrum from fission and — to a lesser extent — by the delayed gamma rays arising from the beta decay of the fission products. The target nucleus ^{235}U , for instance, has a thermal neutron fission cross-section of 578 b while the capture cross-section is only 101 b. Thus the thermal neutron capture reaction accounts for 14.9% of the neutron absorption in ^{235}U , with the fission process accounting for the remaining 85.1%. For the total energy released in prompt photon emission from fission values of 7.2 and 8 MeV are given [1]. This energy is distributed between 9 ± 2 photons per fission. The multiplicity for the radiative capture process is probably less than 5 photons per capture. Thus it is evident that the prompt gamma rays emitted in the fission process provide the dominant structure in the ^{235}U spectrum. As further confirmation of this conclusion, a comparison of the spectra from uranium and plutonium shows that these spectra are essentially identical; only very minor, and probably not significant, differences occur [2].

Because of the great success of the (n, γ) method in nuclear structure studies, it is desirable to extend these measurements on fissionable nuclei. Moreover, such an extension will reveal new possibilities for the non-destructive assay of nuclear fuel. Preliminary attempts should be directed to the high-energy spectrum, since at high energies the most favourable intensity distribution between capture gamma rays, prompt radiation from fission and delayed photons from fission products is expected. As has been proposed by one of us [3], the interfering component from fission may be suppressed by detecting the fast fission neutrons in anticoincidence and in 4π geometry. Since the average number of neutrons emitted per fission is 2.5 or even 3.0, a detection efficiency of about 70% for the single neutron is sufficient to obtain 95% total efficiency. The proposed principle can be sketched as follows: The sample is surrounded by a plastic or a liquid scintillator of appropriate thickness. Neutrons scattered in the target are

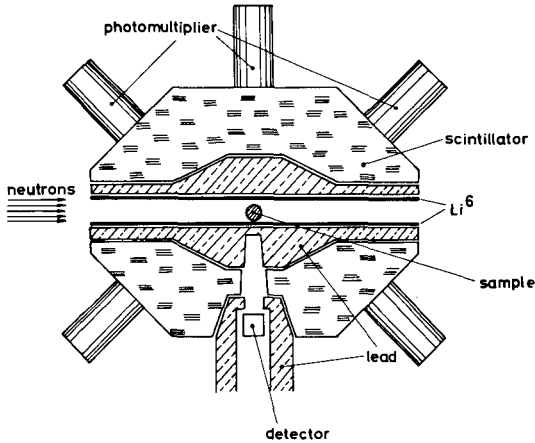


FIG. 1. Schematic outline of the neutron-anticoincidence spectrometer.

kept off the detectors by a shield of ${}^6\text{Li}$. The gamma rays are filtered by a few millimetres of lead to reduce the count rate from soft fission gamma rays. The photons are detected in a Ge(Li) counter which is used as a double-escape spectrometer. A lead shield of about 5 cm thickness between sample material and neutron detector prevents suppression of the capture gamma rays by coincident low-energy photons. A detailed analysis of the system may be found in Ref. [3].

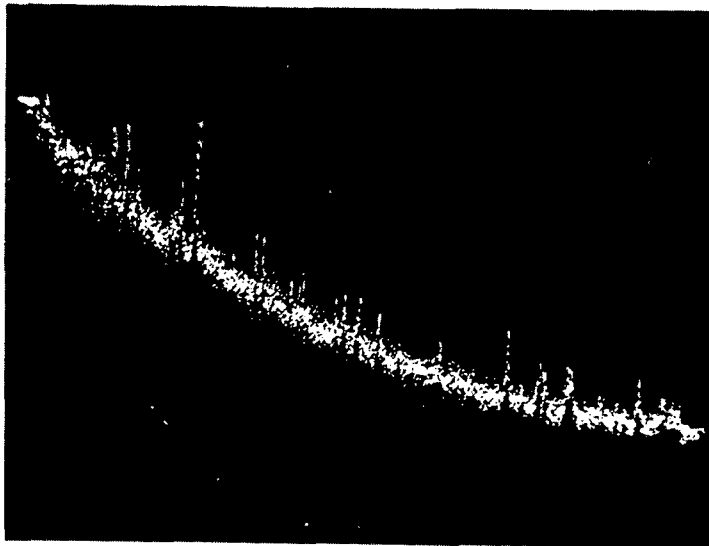
Gamma rays arising from beta decay of the fission products are no severe obstacle in the case of short measuring intervals. If all half-lives between 350 msec and 1 h are included, the intensity ratio for the prompt and delayed spectrum is about 2 : 1 at 4 MeV and about 10 : 1 at 6 MeV. This was calculated in Ref. [3] from the experimental data reported in Refs [4-7].

To demonstrate the feasibility of the neutron-anticoincidence spectrometer, an experimental set-up has been installed at the reactor FR-2 consisting of a Ge(Li) counter and a 44 cm diam. \times 60 cm plastic scintillator. The scintillator is provided with appropriate wells for the neutron beam and the gamma detector. A schematic drawing of this instrument is shown in Fig. 1. To obtain a maximum signal-to-background ratio the scintillator was bevelled on both ends.

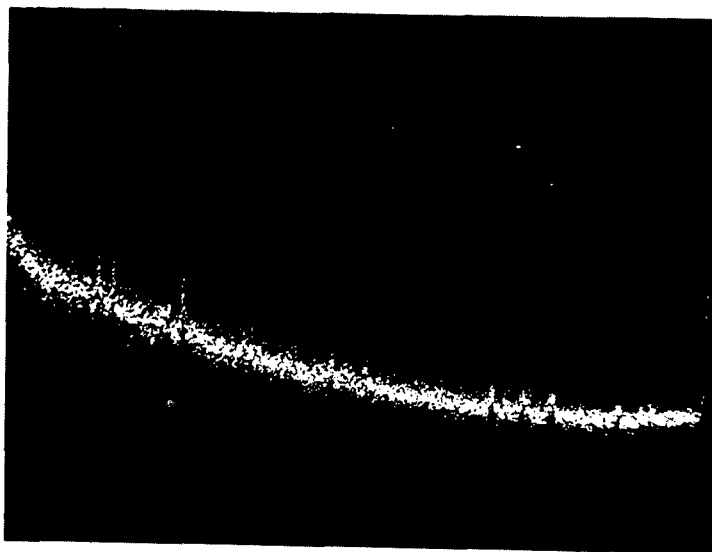
Delayed gamma rays occurring in the measured spectra will be identified by means of a combined fast/slow chopper system which has been installed at the reactor to study the delayed radiation from fission [8].

A preliminary test spectrum obtained with the neutron-anticoincidence spectrometer and a spectrum taken in single mode are presented in Fig. 2. The energy interval ranges from about 3.4 to 6.4 MeV. The sample was uranium oxide enriched to 20% in ${}^{235}\text{U}$. The spectra were measured using a provisional electronic system. Only a coarse adjustment of the various components had been performed. The spectra are therefore considered as preliminary. Nevertheless, a clear structure already appears in the anticoincidence result. The suppression of the fission gamma rays can certainly be improved further and probably the spectrum still contains

some contamination from delayed fission gamma rays and from neutron capture in germanium caused by fission neutrons. By placing the detector in a proper geometry relative to the plastic scintillator interference from capture in germanium can be eliminated. In this case the scintillator serves at the same time as an anticoincidence shield for capture events occurring in the detector.



a)



b)

FIG. 2. Preliminary results from a sample of uranium enriched to 20% in ^{235}U : (a) spectrum taken in anticoincidence; (b) spectrum observed in single mode.

It should be pointed out that ^{235}U is one of the most unfavourable target materials [3]. For other samples the capture-to-fission ratio is much higher. It is, for instance, 0.358 for ^{239}Pu and about 0.39 for ^{241}Pu .

In summary, we can conclude that it will be possible to extend (n, γ) investigations also to fissionable nuclei.

REFERENCES

- [1] MAIER-LEIBNITZ, H., ARMBRUSTER, P., SPECHT, H.J., *Physics and Chemistry of Fission* (Proc. Symp. Salzburg, 1965) 2, IAEA, Vienna (1965) 113.
- [2] GREENWOOD, R.C., REED, J.H., IITRI - 1193 - 53 (Vols 1 and 2).
- [3] MICHAELIS, W., *Atomkernenergie* (in press).
- [4] MAIENSCHNIG, F.C., PEELE, R.W., ZOBEL, W., LOVE, T.A., *Int. Conf. peaceful Uses atom. Energy* (Proc. Conf. Geneva, 1958) 15, UN, New York (1958) 366.
- [5] RAU, F.E.W., *Ann. Phys.*, Paris 10 (1963) 252.
- [6] PEELE, R.W., ZOBEL, W., LOVE, T.A., *Rep. ORNL-2081* (1956) 91.
- [7] ZOBEL, W., LOVE, T.A., *Rep. ORNL-2081* (1956) 95.
- [8] MICHAELIS, W., HORSCH, F., LEUSCHNER, H., WEITKAMP, C., *Trans. Am. nucl. Soc.* 11 (1968) 663.

RECENT IMPROVEMENTS IN THE ARGONNE 7.7-m BENT-CRYSTAL SPECTROMETER

R.K. SMITHER, D.J. BUSS
Argonne National Laboratory,
Argonne, Ill., United States of America

Abstract

RECENT IMPROVEMENTS IN THE ARGONNE 7.7-m BENT-CRYSTAL SPECTROMETER. Recent improvements to the Argonne 7.7-m bent-crystal spectrometer have led to a doubling of its resolving power and to at least a 4-fold improvement in its sensitivity (ratio of diffraction peak to background) over the whole range of the spectrometer, and an improvement of 20-fold or more above 2 MeV. The energy range of the spectrometer was extended to cover the full (n, γ) spectrum from 20 keV to 6 MeV.

In 1964 I gave a talk in Athens at the Symposium for the Diffraction of Nuclear Gamma Rays [1] on a set of proposed improvements for the Argonne 7.7-m bent-crystal spectrometer. All of these modifications and a few more have now been completed. Usually the results of these modifications were as predicted, but occasionally they were much better than expected.

The configuration of the spectrometer as it was in 1964 is shown in Fig. 1. The neutron-capturing source is located in the center of a through hole which is tangent to the reactor core. The gamma beam emerges from the reactor through a series of apertures and is diffracted by the bent crystal. The diffracted beam is then separated from the undiffracted beam by a multislit collimator and detected in a bank of NaI crystals. The source is loaded and aligned from the far side of the hole.

The first major modification to the system completely revised the method of changing samples and reduced the pile down-time for the whole operation from 2 days to 20 min. This made it possible to change samples during the short pile-down periods which occurred about twice a week. Incorporated in this new system is a heavily shielded storage facility which can handle seven separate samples. This storage facility removed any previous restriction on sample size related to induced radioactivity since the old sample could be left in one of the storage spaces to cool after being removed from the reactor. It also made provision for reinserting an old sample into the reactor system without handling it manually. The ability to re-examine an old sample for a few days to check an energy or intensity value or to look for a missing gamma ray has proved to be the most valuable asset of the new system. The improved control over the source alignment is also appreciated. After primary insertion of the sample into the system, all further sample handling is done remotely. A number of "bugs" developed in this remote-handling system and had to be corrected through later modifications.

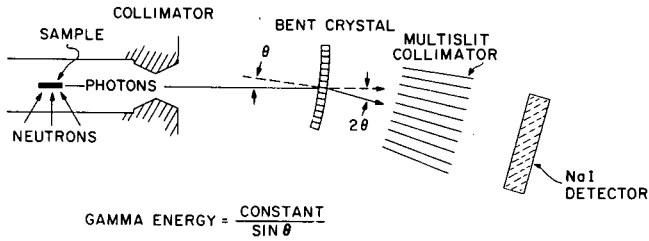


FIG. 1. Schematic drawing of the Argonne 7.7-m bent-crystal spectrometer located at the research reactor CP-5 as it existed in 1964. The neutron-capture gamma-ray source, shown at the left, is located in a through hole in the reactor. The gamma beam emerges through two circular apertures (one not shown) and a narrow energy increment of this beam is then diffracted by the (310) planes of the bent quartz crystal. The diffracted beam is separated from the undiffracted beam by the multislit post-collimator and detected by a bank of ten NaI crystals.

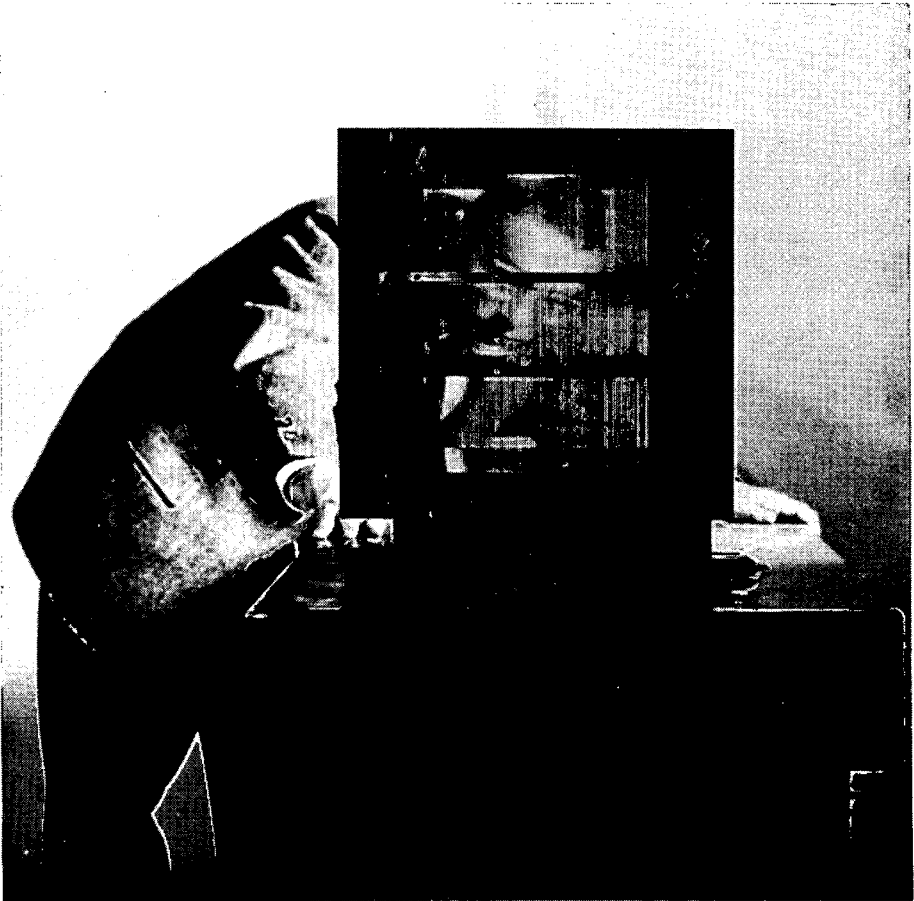


FIG. 2. Photograph of the new multislit post-collimator taken at the point of convergence of the tapered slots. Each tier contains 106 lead plates 1 m long and 1 mm thick. The full width is 25 cm. The quality of the image attests to the uniform spacing of the Pb plates.

The second improvement was the replacement of the old multislit post-collimator (Fig. 1) which consisted of 106 lead plates 33 cm high, 100 cm long, and 1 mm thick and spaced 1 mm apart. The old collimator used five vertical Mg spacers to keep the 33-cm-high Pb plates from bowing in the vertical direction. These Mg spacers, each 0.63 cm thick, resulted in serious absorption of the diffracted beam at low gamma energies. (The transmission through the 3.2 cm of Mg was 0.05 for a 30-keV gamma ray.) The absence of vertical spacers in the new post-collimator eliminates this low-energy absorption. The vertical bowing problem is greatly reduced by dividing the collimator into three separate vertical sections. Figure 2 is a photograph of the new collimator, taken from the source position (the point of convergence of the tapered multislits of the collimator). The Pb plates are slid into slots in the top and bottom of each section. The thin cross supports that bear the weight of the first and second rows of plates are in the shadow of the horizontal ribs of the crystal-clamping block, so their presence causes no appreciable reduction in transmission.

A new quartz crystal, 30 cm \times 28 cm \times 0.2 cm, was bent and installed in the spectrometer. In Fig. 3 the line width (FWHM) of this 2-mm-thick bent crystal is compared with the 4-mm- and 6-mm-thick crystals previously used in the spectrometer. The full width at half maximum of the diffraction peak using the (310) planes of the crystal are plotted as a function of the thickness τ of the crystal. This is equivalent to plotting the width as a function of the stress in the crystal when the radius of curvature R is held constant. Stress = constant \times τ/R . All crystals were cut from the same piece of quartz. The experimental widths of 13.5, 9.0, and 4.5 sec of arc for the 6-mm, 4-mm, and 2-mm crystals, respectively, strongly suggest that the width of the diffraction peak is a linear function of the stress. This is consistent with the theory of Sumbaev [2], which

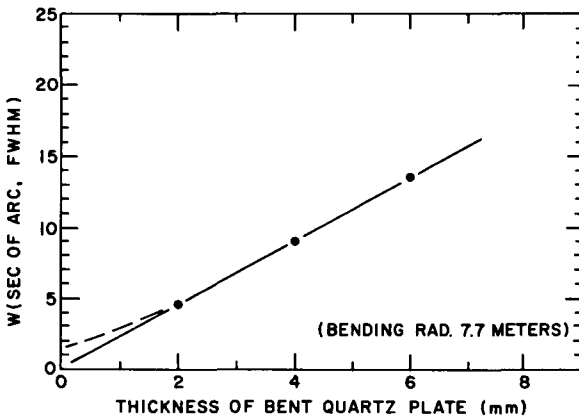


FIG. 3. A plot of the full width at half maximum W of the diffraction peak of the (310) planes of quartz bent to a 7.7-m radius as a function of crystal thickness for the 2 mm, 4 mm and 6 mm crystals at present in use with the Argonne bent-crystal spectrometer. The stress introduced into the crystal through bending is proportional to the thickness τ if the radius R is kept constant (stress = constant \times τ/R). All crystal plates were cut from the same single crystal. The solid line is a straight line through the experimental points. The dashed line is the upper limit allowed by the error in the points.

predicts a bowing of the (310) crystalline planes when the quartz crystal is bent. This bowing is related to the asymmetry of the elastic constants of the crystal and should be proportional to the applied stress. The fact that the straight line through the experimental points passes through zero width at zero stress suggests that the width of the rocking curve of the unstressed crystal is much smaller than the 4.5-sec width obtained with the 2-mm-thick crystal bent to a 7.7-m radius. The width of the diffraction peak W should follow the relationship

$$W = [W_0^2 + (A \tau/R)^2]^{1/2},$$

where W_0 is the width of the rocking curve of the unbent crystal, τ is the thickness, R is the radius of curvature, and A is a constant related to the theory and the units used for τ , R , and W_0 . The experimental data predicts zero for W_0 but the error on the points allow $W_0 \leq 1.5$ sec of arc. It is obvious from this graph that one should try a thinner crystal (~ 1 mm) or use a different set of crystalline planes to take advantage of the near-perfect quality of the quartz crystal. We hope to do just this in the near future. The remarkable thing about the use of thinner and thinner crystals is that it has not appreciably reduced the peak intensity of the diffraction peak. This is consistent with the assumption that the integral reflectivity (area under the diffraction peak) is proportional to the thickness while the height is proportional to the area divided by the width. If this is true, then the diffraction-peak intensity should remain the same as long as the experimental points in Fig. 3 remain close to the straight line. A very interesting question that as yet remains unanswered concerns the dependence of the width and peak height on stress if the radius of curvature is varied instead of the thickness. Figure 4 compares these two cases. The shaded area is the region of the crystal that contributes to the diffraction process when the spectrometer is set at the center of the diffraction peak. This region is defined by the angle $\Delta\Theta$ in each case. If this picture is correct, then the maximum intensity of the diffraction peak will double if R is doubled, provided each usable part of the crystal acts independently. If adjacent regions act coherently so that the amplitudes rather than the intensities of the waves are added, then the dependence would go as R^2 rather than as R and doubling the radius would quadruple the peak intensity. In this case the choice of R would not affect the peak intensity since the loss in solid angle would be made up by the increase in reflectivity. The undiffracted background would, of course, go down with increasing R . In either case an improvement in both the resolution and the signal-to-background ratio would result from increasing the radius of curvature R .

The alternative approach to this problem of distortion of the crystalline plane when stressed is to use a low-order plane, such as the (110), that is symmetric with respect to the elastic constants. In this case no distortion occurs and one can take full advantage of the near-perfect crystal structure. The lower dispersion of the (110) plane can be overcome by using a higher order of diffraction, e.g., the second or third order.

The most recent modification of the spectrometer was the addition of the multislit pre-collimator to collimate the gamma ray beam before it strikes the bent quartz crystal. The new configuration is shown

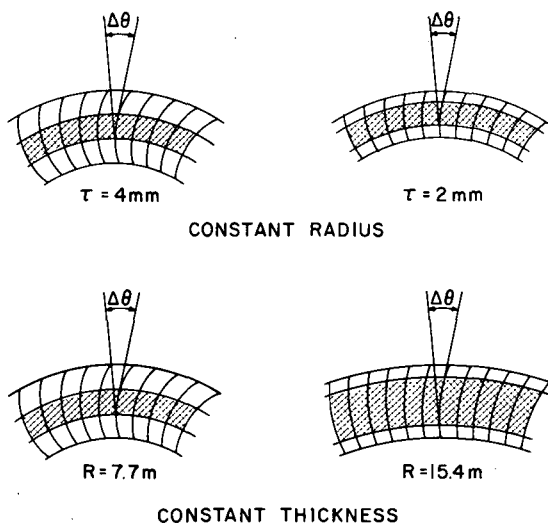
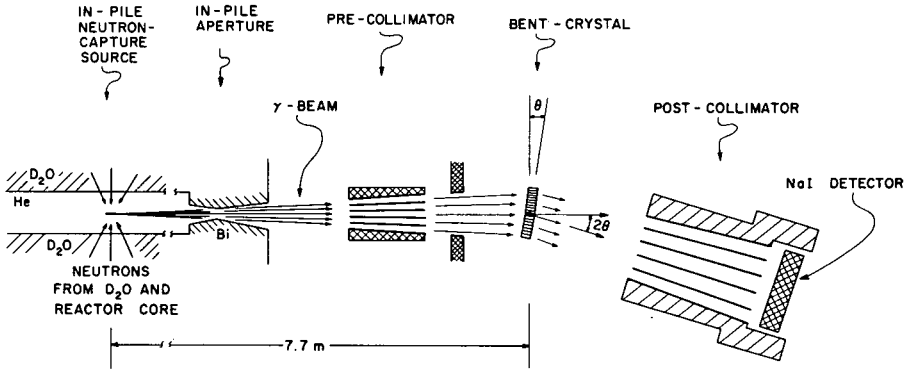


FIG. 4. Schematic diagrams in which the shaded areas show what portion of a bent crystal is able to contribute to the diffraction process when the crystal is set at the Bragg angle for peak diffraction intensity. The upper pair of drawings explains why very little intensity is lost in going to a much smaller thickness τ if the radius of curvature R is kept constant. The lower pair indicates that the intensity could be increased appreciably by increasing the radius of curvature without changing the thickness.

in Fig. 5. The pre-collimator is located just outside the reactor face and is about halfway from the source to the bent crystal. This collimator consists of 106 lead plates 15 cm high and 60 cm long. The thickness of each plate is 0.046 cm. The space between them is 0.055 cm at the front of the collimator and opens out to 0.061 cm at the back. This collimator must be matched to the post-collimator so that the diffracted beam will pass through the post-collimator. Any bowing or misalignment of the plates in either collimator can cause serious loss in the intensity of the diffracted gamma beam. The plates slide into grooves cut into the top and bottom members of the collimator frame, just as they did in the post-collimator. These precision-cut grooves ensure the proper one-to-one correspondence between the pre- and post-collimator. The bowing in the vertical direction was reduced by cementing the plates top and bottom and applying tension to the whole set. This was done slowly so that the cold flow of the lead could even out the tension on the individual lead plates.

The effect of this pre-collimator on the recorded background was rather spectacular. Figure 6 compares the backgrounds with precollimation (lower solid line) and without it (upper solid line). The reduction is at least an order of magnitude over the whole spectrum and approaches 3 or 4 orders of magnitude at the higher energies. The dashed line indicates the improvement we expect to achieve by increasing the shield around the NaI detectors to reduce the contribution related to the general room background. The double collimator system is much like having a single collimator 4. m long, except that the detectors cannot view the front of the collimator directly.



$$\text{GAMMA ENERGY} = \frac{\text{CONSTANT}}{\text{sine } \theta}$$

FIG. 5. Diagram of the bent-crystal spectrometer with the multislit pre-collimator in place. The gamma rays result from neutron capture in a small sample at the left, near the core of the reactor. They emerge from the reactor through a Bi aperture and pass through the pre-collimator and a second aperture. A narrow energy increment of this gamma beam is then diffracted by the (310) planes of the bent crystal, separated from the undiffracted beam by the post-collimator, and finally detected by a band of ten NaI crystals.

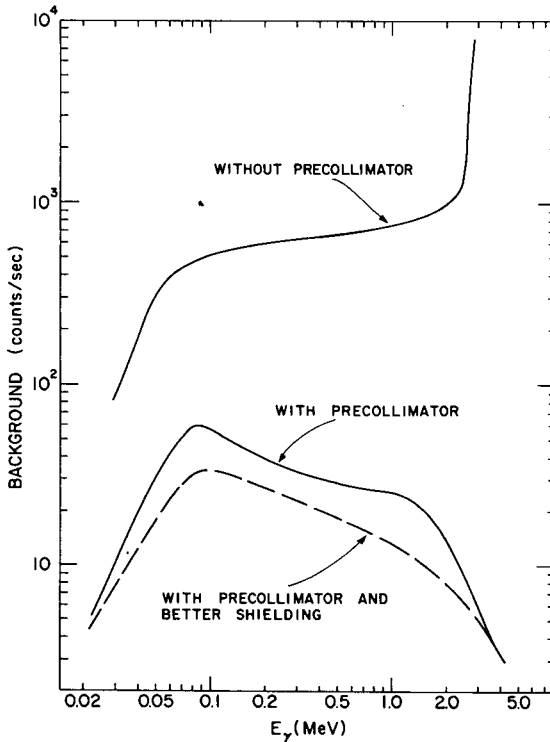


FIG. 6. Graph of the background counting rate before and after installation of the multislit pre-collimator and thinner crystal. The dashed line is the background associated exclusively with the γ -ray beam when the pre-collimator is in place. The source used in this comparison was the $^{152}\text{Sm}(n, \gamma)^{153}\text{Sm}$ reaction. The counting rate plotted is that in 10% of the aperture of the bent crystal.

The pre-collimator absorbs or scatters a great many of the fast neutrons and gamma rays scattered in the in-pile aperture. This doubly-scattered radiation is absorbed in a heavy shield around the pre-collimator and does not contribute to the room background or to the detector background. In addition, the intensity of the primary beam of γ rays from the source—and therefore the intensity of the undiffracted beam which must be stopped in the post-collimator—is cut in half by the precollimator. This is an important improvement since it is this undiffracted beam that accounts for most of the background at the higher gamma energies. Some bowing or "oil canning" still exists in the very thin Pb plates of the precollimator. This reduces the transmitted beam to 60% of that measured without the pre-collimator in place.

Figure 7 compares data taken before and after the new 2-mm bent crystal and the pre-collimator were installed in the spectrometer. The improvement in resolution and sensitivity in this part of the $^{152}\text{Sm}(n, \gamma)^{153}\text{Sm}$

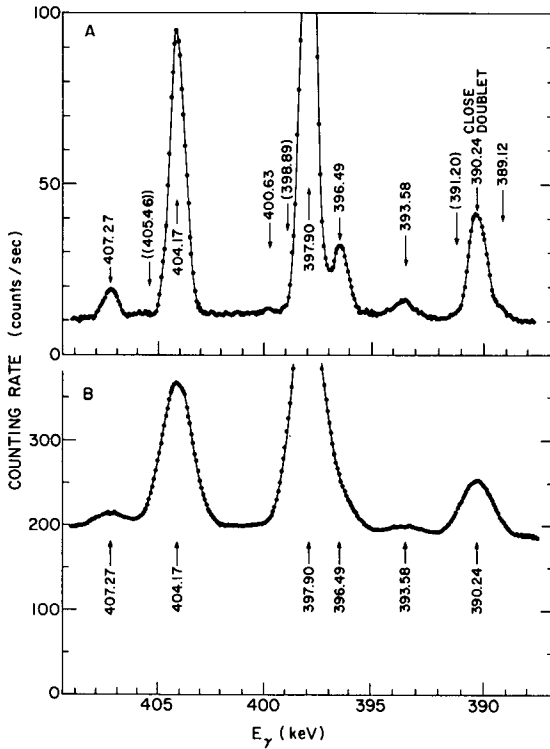


FIG. 7. A comparison between data obtained with the bent-crystal spectrometer after the installation of the thinner bent crystal and the multislit pre-collimator (curve A) and before the installation (curve B). Both curves represent the 390-410-keV region of the $^{152}\text{Sm}(n, \gamma)^{153}\text{Sm}$ spectrum; the counting rate plotted is that in 10% of the aperture of the bent crystal — i. e. in one of the ten NaI crystals in the detector bank. In an attempt to obtain statistics good enough that the doublet at 397.90 and 396.49 keV could be resolved by line-shape analysis, a long counting time was used for each point of the "before" spectrum. Although the counting time per point was only 1/25 as large for the "after" spectrum as for the "before", the "after" spectrum obviously is far superior for this purpose.

spectrum as well as the need for this improvement is obvious. This need is particularly imperative when one is trying to detect weak lines in the spectrum (such as the 400.63-keV line) or resolving close doublets (such as the 397.90- and 396.49- keV set or the unresolved 390.24-keV doublet). It is also very useful in setting upper limits on missing transitions (such as the one at 405.46 keV, indicated by the double parenthesis in Fig. 7).

The drastic reduction in the background above 2 MeV has made it possible to make meaningful measurements up to 6 MeV by using the first-order diffraction of the (310) planes in quartz. The energy resolution (FWHM) is much poorer than that achieved with Ge(Li) detectors at 6 MeV, but it is still possible to identify the stronger members of the (n, γ) spectrum. Figure 8 shows a bent-crystal spectrometer run over the strong 5.8-MeV line in the $^{113}\text{Cd}(n, \gamma)^{114}\text{Cd}$ spectrum. The run was made with the spectrometer beam stopped down to a fifth of its normal area and with a source only one-tenth as strong as is normally used for the investigation of the (n, γ) spectrum above 500 keV. The run was part of a series designed to calibrate the relative efficiency of the new system for gamma energies from 20 keV to 6 MeV. Both the restriction of the aperture and the use of the smaller sample were necessary to keep the corrections for self-absorption of the gamma rays in the source and the distortion of the line shape for low gamma energies from adding too much uncertainty to the efficiency calculation. The counting rate for a normal sample would

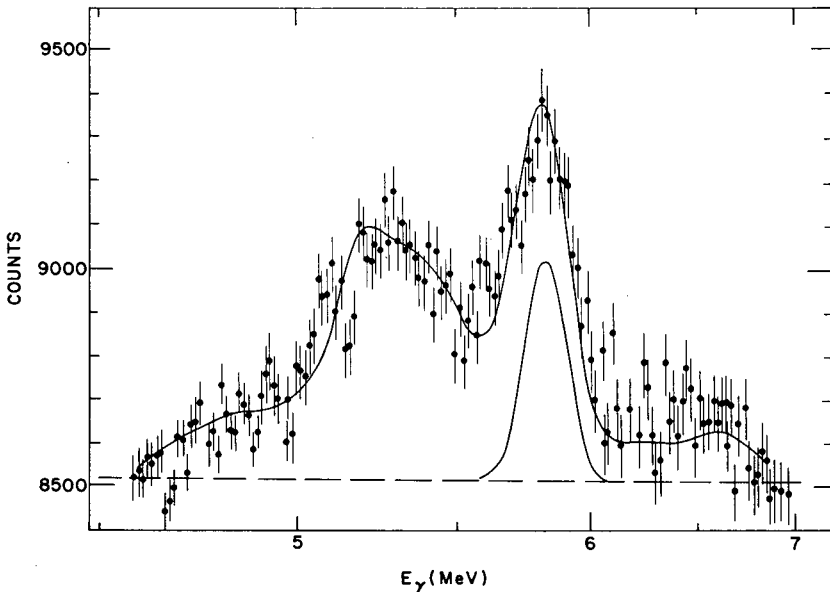


FIG. 8. A bent-crystal spectrometer run over the strong 5.8-MeV line in the $^{113}\text{Cd}(n, \gamma)^{114}\text{Cd}$ spectrum. It was obtained with the first-order diffraction of the (310) planes in quartz. The solid line is the envelope of the known spectral components in this energy region; it is based on Ge(Li) data normalized to the experimental counting rate. A single line shape of appropriate height for the 5.8-MeV line is also shown. The dashed line is the undiffracted background.

be an order of magnitude higher. Nevertheless the strong line at 5.8 MeV stands out in the spectrum. The solid line through the data points is the envelope of the expected response function of the bent-crystal spectrometer for the known (n, γ) spectrum in this energy region; relative energies and intensities were taken from the Ge(Li) work and the height of the envelope was normalized to the data. The background is determined by rotating the bent crystal to destroy the diffraction condition. The intensity of the individual line is proportional to the height of the full response function and can be calculated in a straightforward manner. A similar procedure was used on other strong lines to give a detailed description of the relative intensities of the (n, γ) spectrum for the intermediate energies. The major uncertainty in this method was the response function of the NaI detector (a 5 × 5-in. right cylinder). This was measured directly by recording the NaI pulse-height spectrum in a multichannel analyzer with the bent crystal set on the diffraction peak, then rotating the bent crystal to remove the diffracted peak and subtracting off the undiffracted background. The new values obtained for the relative intensities of the strong lines in the spectrum were then used to recalibrate the rest of the spectrum and to check the efficiency curve of the Ge(Li) detector.

References

- [1] R. K. Smither, in Symposium on Crystal Diffraction of Nuclear Gamma Rays, National Technical University, Athens, 1964, edited by Felix Boehm, (California Institute of Technology, Pasadena, California, 1964), p. 9.
- [2] O. I. Sumbaev, Soviet Phys. JETP 5, 1046 (1957); O. I. Sumbaev and A. I. Smirnov, Nucl. Instr. Methods 22, 125 (1963).

THE AUTOMATION OF THE CURVED CRYSTAL SPECTROMETER AT RISØ

H. R. KOCH, H. A. BAADER, D. BREITIG, K. MÜHLBAUER,
U. GRUBER, B. P. K. MAIER, O. W. B. SCHULT

Physics Department,
Technische Hochschule, Munich,
Federal Republic of Germany
and
Risø Research Establishment,
Roskilde, Denmark

Abstract

THE AUTOMATION OF THE CURVED CRYSTAL SPECTROMETER AT RISØ. The automated curved crystal gamma-spectrometer at Risø is described and new essential attributes are presented. An angular reflection width of $1.2''$ can be obtained. The optimal energy resolution and the energy error of a single gamma-reflection are given by $\Delta E(\text{keV}) = A \times E^2 \times 10^{-6} \times 1/n$, where E is the gamma energy in keV and n the order of reflection. A is 2.5 if ΔE stands for the resolution, and 0.4 for the energy error. Strong transitions over 200 keV are measured in the 5th order. Results for the nuclei ^{152}Eu and ^{153}Eu are reported.

1. INTRODUCTION

A great number of neutron-capture gamma-ray spectra [1] have been studied with the curved crystal spectrometer at the reactor DR 3 at Risø, Denmark. This instrument and its basic principles have been described previously [2]. The measurements were performed in the following way.

- (a) The total spectrum was recorded automatically on paper tape with an angular accuracy of $1-2''$.
- (b) The angles of reflection of strong lines were then measured manually with an accuracy of $0.2-0.3''$ by means of a very good theodolite. Because of unavoidable displacements of the source it was necessary to measure the reflections of these gamma lines consecutively several times on both sides of the zero point (Bragg angle = 0).
- (c) The energies of weak gamma transitions were finally obtained from the automatically plotted spectrum, using the energies of the intense lines as references.

The manual measurements were very time-consuming. In fact, about 10 000 points had to be measured during the study of a complex (n, γ) spectrum.

Obviously one would wish to record automatically the whole low-energy (n, γ) -spectrum with an angular accuracy of $0.2''$ or less. Such an automatic operation has the following advantages: (1) the total measuring time is used exclusively for precision measurements; (2) the energy of each gamma transition is obtained from all orders of reflection, and not only from one order as was the case during the manual measurements; and

(3) the automation of the spectrometer enables the experimenter to measure the whole spectrum in a fairly short time. Such fast runs cannot be performed by manual measurements. They are necessary if double neutron-capture occurs (e. g. target: ^{151}Eu) and if targets (e. g. ^{155}Gd , ^{157}Gd) with high neutron capture cross-section are studied, because of the burn-out of the sources.

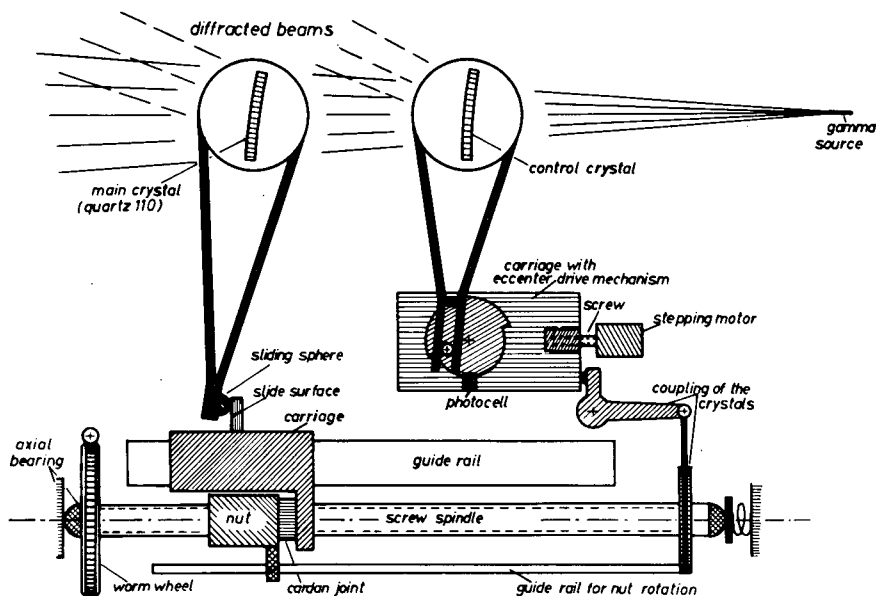


FIG.1. Principle of the driving mechanism and the control system.

2. THE COMPENSATION OF THE SOURCE DISPLACEMENTS

The accuracy of the determination of Bragg angles is limited by the uncontrolled displacements of the source that is suspended inside the tangential channel of the reactor at a distance of 6 m from the spectrometer. Because of temperature variations the gamma reflections shift irregularly by about 3" in the course of three weeks. This is 15 times the error of the angle measurement. The automatization of the Risø spectrometer must, therefore, include a device that continuously measures the source position. This is achieved by means of a control crystal (Fig. 1) that is set to reflect a certain very strong gamma line.

The control crystal is bent like the main crystal and it is focused on the source. It is driven by a cranking mechanism (Fig. 1) and oscillates about the Bragg angle of a strong gamma line with an amplitude equal to the line width. The counting rates for the positive and negative part of the oscillator movement are compared with each other. A number of pulses proportional to the difference between these two counting rates are fed into a stepping motor, which moves the carriage with the crank mechanism to

such an extent that the centre of the crystal oscillations follows the centre of the reference gamma reflection. The rotation of the control crystal is fed back to the main crystal to compensate the source displacement.

3. THE DRIVING MECHANISM OF THE CRYSTAL

A very accurate rotation and a precise measurement of the angular orientation of the main spectrometer crystal is achieved with the use of a crystal arm which is 2 m long and which is moved by a high precision screw. As seen in Fig. 1, the screw spindle is rotated by a worm gear and moves a carriage by means of a very precise nut whose rotational position is defined by a guide rail. The end of the crystal arm slides on a well-ground plate fastened to the carriage. A displacement of $1 \mu\text{m}$ causes a crystal rotation of $0.1''$. By this system the sine of the crystal angle or the wavelength of the reflected radiation is proportional to the number of revolutions of the screw spindle. The guide rail for the nut rotation is moved about the screw axis by amounts proportional to the source displacement. The proportionality factor is adjusted in the feed back system in such a way that a source movement is compensated to better than $0.1''$. The total accuracy of the determination of the Bragg angles is $0.15\text{--}0.2''$.

Another screw spindle, nut and guide system is used for the movement of the NaI detector and the lead-plate collimator, which have to follow the angle of the diffracted gamma radiation. Together with the automation the old 0.4-m long collimator has been replaced by a 1.4-m long one causing a reduction of the background by a factor 3 for energies above 400 keV.

4. THE RESOLUTION

The most valuable property of the Risø spectrometer is its high resolution, which is determined by the quality of the crystal and its curvature, and by the width of the source in the direction perpendicular to the beam.

4.1. The source

An improvement of the technique for the source preparation caused a great reduction of the line width. We now use small, carefully ground U-profiles made of 0.2 mm thick Al-foil to keep the source material plane to 0.01 mm or less (see Fig. 1 of Ref. [3]). Such source holders must be built as light as possible because any material near the source increases the background for energies below about 200 keV.

The dimensions of the source are $25 \times 5 \times (0.03 \text{ to } 0.1)$ mm; it contains from 10 to 80 mg of target material. The thinnest source we have used was a 25 to $30\text{-}\mu\text{m}$ thick gold foil.

4.2. The diffraction crystal

We use a 4-mm thick quartz sheet of extremely small mosaic spread, reflecting at the 110-planes and bent to a radius of 5.80 m. The diameter of the crystal window is 42 mm. For high-resolution measurements only one half of it can be used.

The angular line width of the spectrometer is in a wide energy range independent of the energy and the reflection order. For energies below about 200 keV the reflection power of the first and second order is so big that the crystal appears no longer thin. Then the saturation of the reflectivity of mosaic crystallites in the centre of the angular distribution introduces a broadening of the gamma-ray reflections. This contribution to the line width amounts at 100 keV to $1''$ for the first order of reflection.

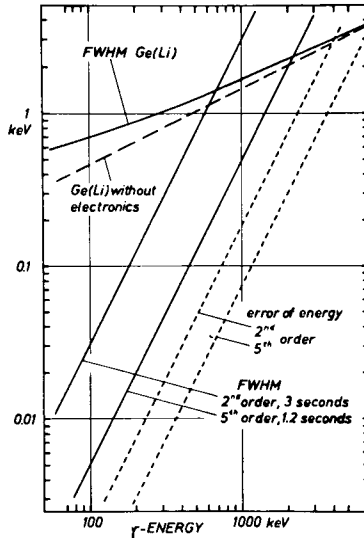


FIG. 2. Resolution and energy error.

We have observed a total width of $1.2''$ at half maximum for the ^{197}Au (n, γ) lines. At least $1''$ must be attributed to the source. If we assume Gaussian distributions for the contributions to the line width, there remains at most $0.7''$ for the sum of the mosaic spread and the non-ideal curvature of the crystal. This shows that the mosaic spread does not necessarily increase when a quartz crystal is bent. The smallest values for the mosaic spread that have been found in selected regions of flat quartz crystals are also of the order of $0.7''$. Most of the other curved crystal spectrometers produce a line width from 10 to $20''$. This is due to a distortion of the reflection planes in the bent state of a quartz crystal. The anisotropy of quartz normally causes a plane perpendicular to the surface of the flat crystal plate to be curved when the plate is bent cylindrically, the cylinder axis being parallel to the plane. The 110-plane, which we use at Risø, is not distorted by such a procedure. This is a result of the symmetry properties of the elastic constants. However, Sumbaev [4] has shown that the distortion of any reflection plane can be avoided if an appropriate orientation of the crystal sheet with respect to the crystal axes is chosen.

Another extraordinary property of the 110-plane is the strong reflection power of higher reflection orders. The geometrical structure factor of the 5th order is nearly ideal. The reflection power of this order is $1/25$ of that of the first order. Because of the low background in the 5th order,

which is 1/40 of the background of the first order, 20 to 40% of the total number of lines of a (n, γ) -spectrum can be measured with an accuracy and a resolution corresponding to a grating constant of 0.49 Å. Very strong transitions are observed even in the 7th order of reflection.

In Fig. 2 the resolution of a very good Ge(Li) gamma-spectrometer [5] is compared with the resolution of the Risø diffractometer. The two parallel solid lines show the best attainable resolution and the line width obtained under the poorest conditions. The lower line corresponds to 5th-order reflections of 1.2" angular width, the upper line gives the resolution for a 3" source in the second order. This order of reflection is the most useful one for weak lines. For sources consisting of oxide powder we have usually obtained a line width between 2" and 3" for the last eighteen months. The FWHM is 0.5 to 3 keV for gamma energies of 1 MeV. In the energy scale the line width is proportional to the square of the energy. So we have for 200 keV an optimal resolution of 20 eV, and for weak lines in broad sources we have a line width of 120 eV.

The resolution of the best Ge(Li) detectors and that of a diffraction spectrometer overlap in the region between 700 keV and 2 MeV. Therefore the main field of activity of a curved crystal spectrometer must lie below 1.5 MeV.

5. ENERGY ACCURACY

The great number of reflection orders provides an excellent method of determining deviations from the linearity of the driving mechanism of the spectrometer. In the ideal case the reflection positions of one gamma transition in different orders must have equal distances. The largest deviations amounted to 1". They are mostly due to the non-linearity of the driving mechanism and could be eliminated with the use of a correction function consisting of a sine function of a period equal to one revolution of the screw and of a polynomial. The remaining error is about 0.18".

For a single gamma reflection the band of normal energy errors caused by the spectrometer itself is given in Fig. 2 by the dashed lines. The statistical error of the determination of the centre of a line is not included. The final error of the energy of a line is usually around one half of the value shown in Fig. 2. This is due to the fact that the weighted average is taken of the results in the different reflection orders. Thus an error of 40 eV for a strong 1-MeV transition is attainable.

6. EFFICIENCY

The probability that a gamma quantum emitted from the source will be detected in the photo peak of a 2×2-in. NaI detector after diffraction in the maximum of the 2nd-order reflection is about 10^{-7} for $40 \text{ keV} \leq E \leq 200 \text{ keV}$ and it decreases proportional to E_γ^{-2} for $E_\gamma \geq 200 \text{ keV}$. The full-energy peak detection efficiency of a reasonable size (10 cm³) Ge(Li) detector viewing an internal target is roughly 10 - 50 times that of the curved-crystal spectrometer. However, the resolution of such a Ge(Li) spectrometer is usually more than a factor 1.5 poorer than that of the very small (0.2 cm³) high-resolution diode the line width of which has been in-

cluded in Fig. 2. Besides the lower detection efficiency of the curved crystal spectrometer there remains another disadvantage of the diffractometer: the spectrum must be measured in about 20 000 angular steps. Nevertheless, for neutron-capture cross-sections larger than about 100 b and gamma energies up to 1 MeV, the curved-crystal spectrometer can compete with solid-state detectors, if one compares the actual sensitivity for the detection of lines. This is due to the following properties of the diffraction spectrometer:

- (a) Counting rates of any magnitude are allowed. They do not affect the resolution.
- (b) The ratio of peak height to background is bigger than in Ge(Li)-detector spectra, where the Compton distribution is responsible for the high background. For instance for the strong 89-keV line of our ^{152}Eu measurement (Fig. 5) this ratio is as high as 1000.

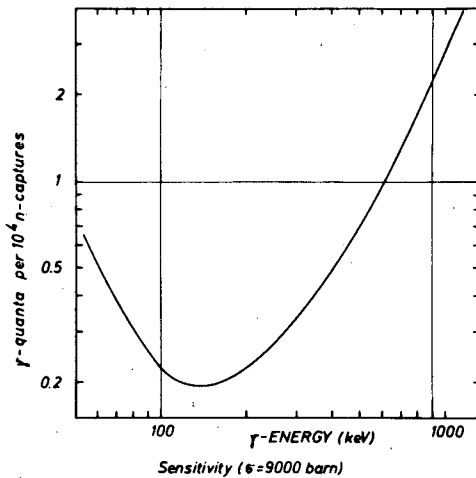


FIG. 3. Sensitivity of the Risø spectrometer for the detection of gamma transitions in a source of 9000 b neutron-capture cross-section.

Figure 3 shows the weakest gamma lines that may be detected in a source of 9000 b (^{151}Eu) in the case of a total measuring time of 10 days. The values are approximately proportional to $1/\sqrt{\sigma}$ where σ means the neutron capture cross-section. However, the sensitivity may be increased in small energy regions by a factor up to 4 without the total time of measurement being increased significantly. An example of this procedure is given in Fig. 3 of Ref. [3].

7. MEASUREMENTS

In a normal run the crystal is rotated once from 6° to 4° in a period of 3 weeks, while 6 orders of reflection are recorded (the 1st to the 5th and the 7th order).

Figure 4 gives an example taken from our measurement on ^{169}Yb . The small bump on the left side of the 760-keV line is only resolved in the 5th order, which is shown in the upper-right corner of the figure.

The counting rates of the different orders are registered for each angle step on punched paper tape. Thus the spectra can be evaluated by computer. We have made a program which calculates the background, finds the lines of the spectrum and performs a least-squares fit of Gauss functions to the lines. Up to 12 lines can be fitted to a complex structure.

The following nuclei have been investigated with the automated spectrometer: ^{156}Gd , ^{158}Gd , ^{152}Eu , the Yb isotopes 169, 172, 174 and 175, ^{198}Au , ^{76}As , ^{110}Ag and ^{160}Tb . The Gd isotopes and ^{169}Yb have been examined in co-operation with A. Bäcklin from Studsvik, who has measured the conversion electrons, and with R. C. Greenwood and C. W. Reich from the Idaho Nuclear Corporation, who made very good high and low-energy measurements with a Ge(Li) detector. Some results for these nuclei are discussed in separate contributions to this Symposium.

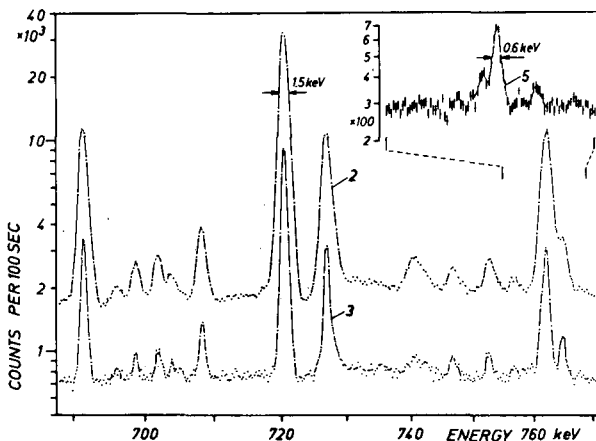


FIG. 4. Part of the $^{168}\text{Yb}(n, \gamma)^{169}\text{Yb}$ spectrum. The second, third and fifth order of reflection are shown.

Europium-152

The evaluation of the ^{152}Eu data, which is being done by K. Mühlbauer, is almost finished. The measurement of the (n, γ) spectrum of this odd-odd nucleus at the beginning of the region of deformed nuclei has disclosed a tremendous number of lines. At a neutron capture cross-section of 8800 b, 2600 gamma lines were measured between 20 and 600 keV. In the energy region between 100 and 200 keV the line density reaches the value of 10 lines per 1 keV. Figure 5 shows a part of the 3rd-order spectrum. Although the resolution is 17 eV, it is obvious that a still smaller line-width is needed. The difficulty of obtaining valuable information from γ - γ coincidence experiments with Ge(Li) detectors is obvious. The energy region presented in Fig. 5 covers only 1 keV.

Some new features of the level scheme have been disclosed already. Figure 6 shows the level scheme of ^{152}Eu , constructed by Borovikov and

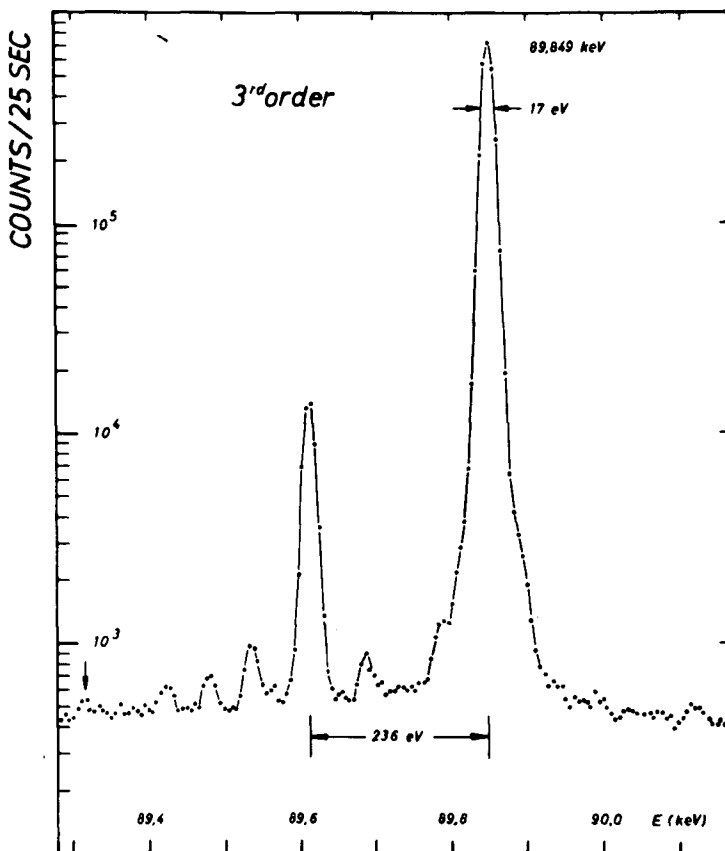


FIG.5. Part of the $^{151}\text{Eu}(n, \gamma)^{152}\text{Eu}$ spectrum.

co-workers [6]. The levels of the cascade leading to the 9.2-h state have been fixed by the combination of the 89.9, 109.3 and 199.2-keV transitions. The energies were known from an older crystal spectrometer measurement. Our new data contain three lines around 199.2 keV. None of them fulfils the energy combination. Thus the above-mentioned cascade may not be placed as shown in Fig. 5. The combination of the 77.3, 73.4 and 150.7 keV lines is confirmed by our energies.

We have not yet made an attempt to establish the level scheme of this nucleus from energy combinations alone. The number of cases, in which the sum of the energies of two lines is by chance equal to the energy of a third line may be estimated from $n^3 \cdot \Delta E/E$, where n is the total number of lines, ΔE a mean energy error and E the total energy range of the lines. For $\Delta E = 10$ eV one obtains for our ^{152}Eu results about 300 000 chance combinations. The work on the level scheme will be continued when in addition to the very high quality (n, γ) data, taken by the Los Alamos group, other additional information is available, such as the results of conversion electron measurements carried out by von Egidy's group at the Munich research reactor.

Europium-153

During the ^{152}Eu measurement transitions in ^{153}Eu could also be observed. They result from neutron capture in the 13-year isomer of ^{152}Eu at a cross-section of 6000 b. They were attributed to ^{153}Eu because their intensity increased during the irradiation.

The ground-state rotational band of ^{153}Eu , already known from Coulomb-excitation experiments up to $I = 15/2$, is confirmed by our data. All intra-band transitions between levels of the spin difference 1 or 2 have been observed.

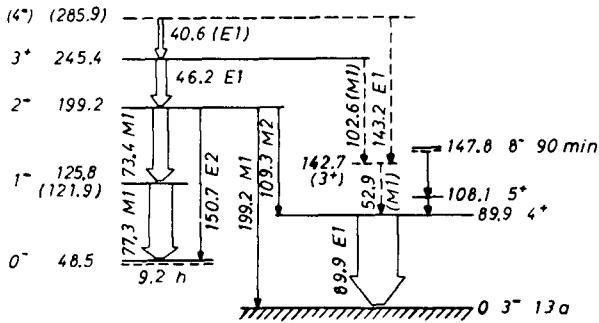


FIG.6. Level scheme of ^{152}Eu as proposed by Borovikov et al. [6].

The $9/2$, $11/2$ and $13/2$ members of the $K = 5/2^- [532]$ band were disclosed. The $K = 3/2^+ [411]$ band was extended by the $I = 9/2$ and $11/2$ members. The intensities of the intraband transitions of these bands yield the ratio of $|g_K - g_R|$ to the intrinsic quadrupole moment. A detailed presentation and discussion of the results has been given elsewhere [7].

The data of the other nuclei investigated with the Risø spectrometer are being evaluated at the present time.

ACKNOWLEDGEMENTS

We wish to thank Professor Maier-Leibnitz for his support of this work. The generous hospitality of the Danish Atomic Energy Commission is gratefully acknowledged. We are especially indebted to the staff of DR 3 and to the Computer group of Risø.

REFERENCES

- [1] Nuclear Data, 3 4-6 (1967); 5 1-2 (1968); 5 3-4 (1969).
- [2] GRUBER, U., MAIER, B.P., SCHULT, O.W.B., Kerntechnik 5 (1963) 17; MAIER, B.P., GRUBER, U., SCHULT, O.W.B., Kerntechnik 5 (1963) 19.
- [3] BAADER, H.A. et al., "Investigation of the ^{158}Gd level scheme by thermal neutron capture", these Proceedings.

- [4] SUMBAEV, O.I., Soviet Physics JETP 5 (1957) 1042; SUMBAEV, O.I., SMIRNOV, A.I., Nucl. Instrum. Meth. 22 (1963) 125.
- [5] PALMS, J.M., VENUGOPALA RAO, P., WOOD, R.E., Nucl. Instrum. Meth. 64 (1968) 310.
- [6] BOROVIKOV, A.V., GROZDEV, V.S., PORSEV, G.D., 18th Conf. Nuclear Spectroscopy and Nuclear Structure, Riga, (1968) 73.
- [7] MÜHLBAUER, K., accepted for publication in Z. Physik.

FEASIBILITY STUDY OF AN INTERNAL PAIR FORMATION SPECTROMETER FOR NEUTRON CAPTURE SPECTROSCOPY

W. MICHAELIS, D. LANGE*
Institut für angewandte Kernphysik
and
G. WILHELMI
Datenverarbeitungszentrale,
Kernforschungszentrum Karlsruhe,
Karlsruhe, Federal Republic of Germany

Abstract

FEASIBILITY STUDY OF AN INTERNAL PAIR FORMATION SPECTROMETER FOR NEUTRON CAPTURE SPECTROSCOPY. The internal pair formation process may be utilized to investigate the multipolarity of high-energy transitions in neutron capture spectroscopy. For such measurements an instrument is needed that is based on the energy summing principle and that exhibits high resolution and sensitivity. The paper discusses the properties of a spectrometer which consists of a silicon detector telescope, two NaI(Tl) scintillation detectors and a superconducting magnet. The detection efficiency and the multipolarity discrimination power are calculated using the Born approximation. The sensitivity to background radiation is investigated. A system of suitable design is proposed. The spectrometer may also be used for measurements of internal conversion electrons.

1. Introduction

Investigations of the radiative neutron capture process have proved to be a useful means for the study of nuclear structure. Considerable aid in interpreting the transition diagram is provided by a knowledge of the primary transition multiplicities. Information about these high-energy transitions can be derived from measurements of the internal conversion and, in fact, magnetic electron spectrometers have been applied in neutron capture spectroscopy up to several MeV [1]. An alternative process which can be utilized is the internal pair formation process, i.e. the emission of a positron-electron pair instead of a gamma ray. As yet studies of this process have not attracted much effort, mainly because of the continuous character of the single radiation. The pair production coefficient is fairly high, being about 10^{-3} in an average case. While the internal conversion coefficient is small for low atomic numbers and decreases with increasing transition energy, the dependence of pair formation upon atomic number is only slight and the coefficient increases with increase of gamma-ray energy. A comparison of both processes is given in Table I. Over a wide range of energy and atomic number utilization of pair formation may be preferable to internal conversion.

* Present address: Strahlenklinik, University of Heidelberg, Heidelberg,
Federal Republic of Germany.

Table I

Comparison of internal pair formation and internal conversion
Coefficient ($\times 10^4$)

	Z = 33; k = 5 ^a			Z = 84; k = 5			Z = 84; k = 7		
	E1	E2	M1	E1	E2	M1	E1	E2	M1
Conversion ^b	0.32	0.53	0.52	4.72	10.8	15.4	2.8 ^c	6.0 ^c	6.7 ^c
Pair formation ^d	9.6	5.3	4.1	8.8	4.5	3.5	13.9	8.0 ^c	

^a The energy, k, is given in units of mc^2

^b From tables of Sliv and Band [2]

^c Extrapolated values

^d Interpolated values from exact calculations performed by Jaeger and Hulme [3]

Most of the presently available data on internal pair production have been accumulated by means of lens type or semi-circular focussing magnetic spectrometers [2]. Other techniques are the detection by annihilation radiation and the use of two double coincidence Geiger or scintillation counter telescopes. The sources were mainly beta-unstable isotopes or proton-induced reactions on light nuclei. From the standpoint of resolution and/or sensitivity the hitherto known spectroscopic methods are hardly applicable to the complex neutron capture process. In this field a high-resolution system is needed that makes use of the energy summing principle and that collects the positron-electron pairs with high efficiency. Two of us [4] therefore proposed a new instrument which is based on the resolution, sensitivity and coincidence capabilities of semiconductor detectors. It is the purpose of this study to investigate the properties of such a system in more detail.

2. General Considerations

The main components of the proposed spectrometer are two silicon detectors and two NaI(Tl) scintillation counters operated in a fourfold coincidence. The semiconductor diodes are stacked to form a $dE/dE + E$ telescope. They determine the total kinetic energy of the positron-electron pair when both particles are emitted into the solid angle subtended by the detectors. The annihilation quanta arising from the positrons stopped in the E-detector are selected by the scintillation counters which are placed on an axis perpendicular to the axis of the telescope.

The dE/dx -detector should be very thin (100 - 200 μm). The electrons then suffer only a small energy loss and reach the E-counter with high counting probability. Another important feature is that more than 99.84 % of the gamma rays emitted into the solid angle of the telescope pass through a 150 μm detector without undergoing any interaction, if the photon energy is higher than 2 MeV. For electrons with energies ≥ 500 keV the specific energy loss is nearly independent of energy and amounts to 0.35 - 0.40 keV per μm silicon. Thus the internal pair formation events which involve the simultaneous passage of two particles through the counter can be pulse-height selected.

The solid angle defined by the telescope should be as large as possible for two reasons. The first requirement is simply the postulate of an adequate detection efficiency. The second reason is the necessity to minimize the influence of the positron-electron angular correlation on the response characteristics. When utilizing the total coefficient or any other quantity correlated with it one has to take into account that the differential cross section for production of pairs with a small angular separation is almost independent of multipole order, whereas the differential cross section for production of pairs with a large angular separation depends critically upon multipole order. In a neutron beam experiment the solid angle is limited not only by the obtainable detector size, but also by shielding problems and the maximum total counting rate in the detectors. A very powerful and favourable method for arriving at a large solid angle is provided by the use of a superconducting magnet, if the axis of the solenoid coincides with the axis of the telescope. With this system the silicon counters can be remote enough from the target that the total counting rate is significantly attenuated while at the same time the magnetic field insures the collection of positron-electron pairs emitted into a large solid angle. Both particles describe helical paths about the magnetic field lines the sense of rotation being of opposite sign. In the case of a homogeneous field of sufficient strength 50 % of all pairs leaving the target will reach the telescope, if the detectors are only a little wider than the target. Thus with regard to intensity considerations the external target geometry, i.e. the extraction of a neutron beam from the reactor, implies no disadvantage compared to internal target geometry while at the same time the energy summing principle can be applied. A loss by a factor of 2 can easily be overcompensated by using a neutron beam with large radiating area. Because of these interesting features it is worthwhile to study the response characteristics of the proposed system in more detail.

3. Response Characteristics

When considering the detection efficiency and multipolarity discrimination power we have to deal with the problem to calculate the probability that for a given energy and multipolarity both the electron and the positron are emitted into a given solid angle Ω . It is convenient to take the Born approximation as a basis of such calculations. This approximation assumes that $Z\alpha/(v/c) \ll 1$, where v is the velocity of either the electron or the positron and $\alpha = 1/137$. In addition, we shall neglect the influence of the atomic number on the formation process. These simplifications are justified for the following reasons. Exact calculations [3] on pair production have been made using the exact Coulomb wave function solutions of the Dirac equation. The numerical computation is very tedious and only a few values of atomic number and transition energy were treated. However, the results show that the change in the total coefficient is small between $Z = 0$ and $Z = 84$ (less than 15 %) and that for sufficiently high energies agreement is found with the Born approximation to within 15 %⁺⁾ . Unsatisfactory results are obtained from the Born approximation, if the energy distribution of positrons or electrons is considered, but in our case we shall integrate over the energy division and concentrate on the angular distribution in which even in the exact treatment the atomic number does not enter.

⁺⁾ An exhaustive compilation of the literature is given in Ref. [5].

We start with the differential internal pair formation coefficient for production of pairs with a definite energy division and a definite angular separation ϑ , as obtained by Rose [6, 7] from the Born approximation:

$$F(k, W_+, \vartheta) = \frac{2\alpha}{\pi(1+1)} \frac{p_+ p_-}{q} \frac{(q/k)^2}{(k^2 - q^2)^2} {}^{1-1}$$

$$\times \left\{ (2 \ 1+1)(W_+ W_- + 1 - 1/3 p_+ p_- \cos \vartheta) \right.$$

$$+ 1 \left[(q^2/k^2) - 2 \right] (W_+ W_- - 1 + p_+ p_- \cos \vartheta)$$

$$+ 1/3 (1-1) p_+ p_- \left[(3/q^2)(p_- + p_+ \cos \vartheta)(p_+ + p_- \cos \vartheta) \right.$$

$$\left. \left. - \cos \vartheta \right] \right\}$$

for electric multipole transitions of order 2^1 and

$$F(k, W_+, \vartheta) = \frac{2\alpha}{\pi} \frac{p_+ p_-}{q} \frac{(q/k)^2}{(k^2 - q^2)^2} {}^{1+1}$$

$$\times \left\{ 1 + W_+ W_- - \frac{p_+ p_-}{q} (p_- + p_+ \cos \vartheta)(p_+ + p_- \cos \vartheta) \right\}$$

for magnetic multipole transitions.

Here the energy, k , is given in units of mc^2 and

$$W_+ + W_- = k \quad ; \quad p_+ = \sqrt{W_+^2 - 1} ;$$

$$p_- = \sqrt{W_-^2 - 1} \quad ; \quad q^2 = p_+^2 + p_-^2 + 2p_+ p_- \cos \vartheta$$

W_+ and ϑ cover the intervals $1 \leq W_+ \leq k - 1$ and $0 \leq \vartheta \leq \pi$, respectively.

The probability for emission of an internal pair with angular separation ϑ irrespective of the energy division is readily obtained from

$$G(k, \vartheta) = \int_1^{k-1} F(k, W_+, \vartheta) dW_+$$

and the total coefficient is given by

$$\alpha(k) = \int_0^\pi G(k, \vartheta) \sin \vartheta d\vartheta$$

Let us assume that the given solid angle Ω is defined by the aperture angle 2Φ . If ψ denotes the angle between detector axis and direction of a particle emitted into Ω , then the probability for emission of both particles into the telescope referred to gamma emission into 4π follows from

$$H(k, \Omega) = \int_{\psi=0}^{\text{Min}[\pi, 2\Phi]} \int_{\varphi=0}^{\Phi} \sin \varphi d\varphi g^*(\psi, \phi, \varphi) G(k, \psi) \sin \psi d\psi$$

where $g^*(\psi, \phi, \varphi)$ represents a suitable weighting function. Since G is independent of φ , the integration over φ can be included into the weighting function and we get

$$H(k, \Omega) = \int_0^{\text{Min}[\pi, 2\Phi]} g(\psi, \phi) G(k, \psi) \sin \psi d\psi$$

Thus the problem reduces to calculate $g(\psi, \phi)$. It is convenient to determine also the function $f(\psi, \phi)$ which refers to the case that at least one particle is emitted into Ω .

If $0 < \phi \leq \frac{\pi}{2}$, we obtain using the abbreviation

$$x(\psi, \phi, \varphi) = \text{Arc cos} \left(\frac{\cos \phi - \cos \varphi \cos \psi}{\sin \varphi \sin \psi} \right)$$

$$g(\psi, \phi) = \begin{cases} \frac{1}{2} [1 - \cos(\phi - \psi)] + \frac{1}{2\pi} \int_{\phi - \psi}^{\phi} x(\psi, \phi, \varphi) \sin \varphi d\varphi; & 0 \leq \psi \leq \phi \\ \frac{1}{2\pi} \int_{\psi - \phi}^{\phi} x(\psi, \phi, \varphi) \sin \varphi d\varphi; & \phi \leq \psi \leq 2\phi \\ 0; & 2\phi \leq \psi \leq \pi \end{cases}$$

The function $f(\psi, \phi)$ is calculated to be

a) $0 < \phi \leq \frac{\pi}{2}$; $0 \leq \psi \leq 2\phi$:

$$f(\psi, \phi) = \begin{cases} \frac{1}{2} [1 - \cos \phi] + \frac{1}{2\pi} \int_{\psi + \phi}^{\phi + \psi} x(\psi, \phi, \varphi) \sin \varphi d\varphi; & \psi + \phi \leq \pi \\ \frac{1}{2} [\cos(\phi + \psi) - \cos \phi] + \frac{1}{2\pi} \int_{\phi}^{2\pi - (\phi + \psi)} x(\psi, \phi, \varphi) \sin \varphi d\varphi; & \psi + \phi \geq \pi \end{cases}$$

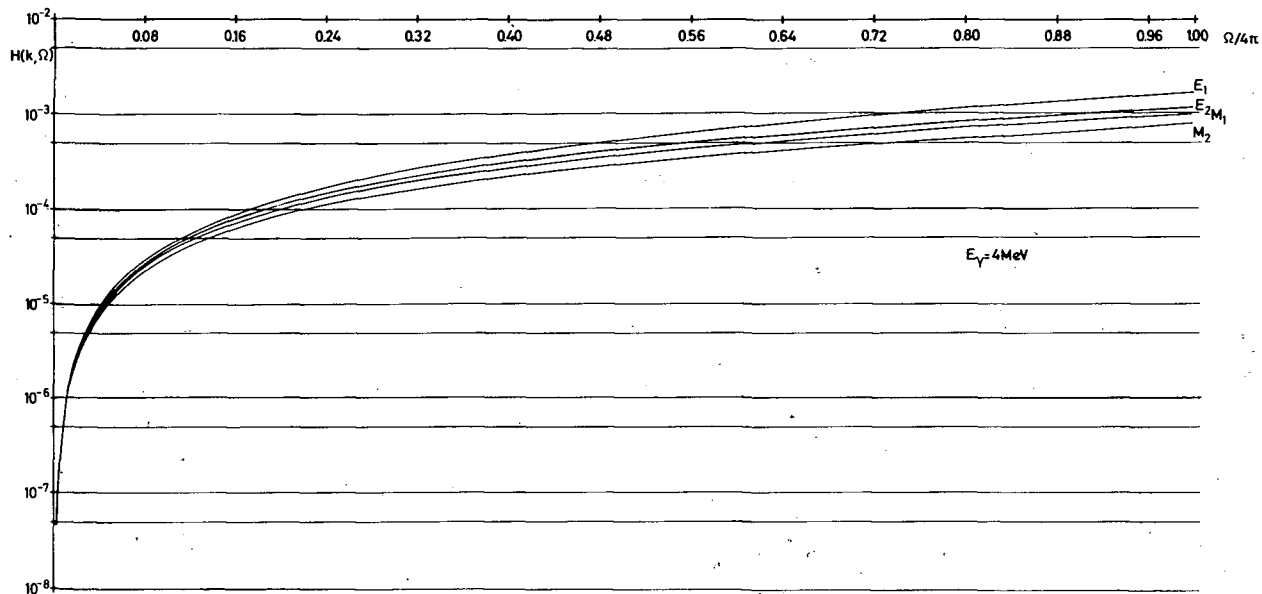


FIG.1. Response characteristics. Logarithmic plot for $E_\gamma = 4 \text{ MeV}$.

$$b) \quad 0 < \phi \leq \frac{\pi}{2}; \quad 2\phi \leq \vartheta \leq \pi:$$

$$f(\vartheta, \phi) = \begin{cases} \frac{1}{2} [1 - \cos \phi] + \frac{1}{2\pi} \int_{\vartheta-\phi}^{\vartheta+\phi} x(\vartheta, \phi, \gamma) \sin \gamma d\gamma; & \vartheta + \phi \leq \pi \\ \frac{1}{2} [\cos(\phi + \vartheta) - \cos \phi] + \frac{1}{2\pi} \int_{\vartheta-\phi}^{2\pi - (\phi + \vartheta)} x(\vartheta, \phi, \gamma) \sin \gamma d\gamma; & \vartheta + \phi \geq \pi \end{cases}$$

In the case $\frac{\pi}{2} \leq \phi \leq \pi$ the corresponding formulae are readily obtained from the relationships

$$g(\vartheta, \phi) = 1 - f(\vartheta, \pi - \phi)$$

$$f(\vartheta, \phi) = 1 - g(\vartheta, \pi - \phi)$$

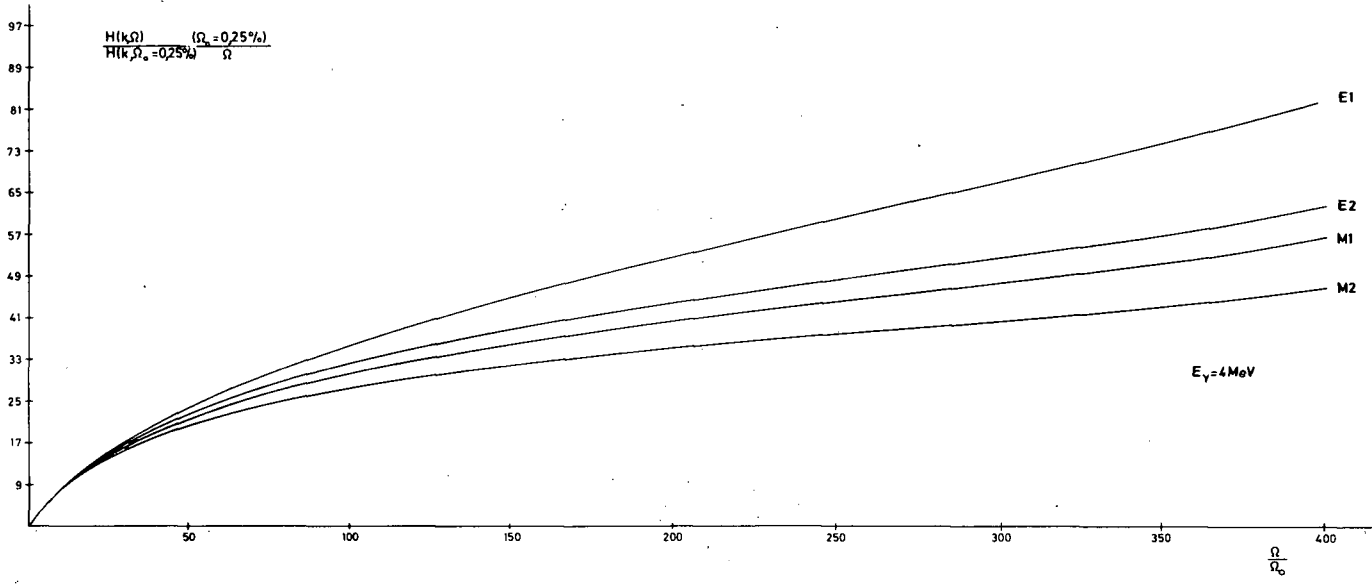
With the above expressions numerical computations have been performed for the multiplicities E1, M1, E2, M2 and the transition energies 4, 5 and 6 MeV. In Fig. 1 the ratio of the number of internal pairs emitted into Ω to the number of gamma rays emitted into 4π is plotted as a function of Ω for $E_\gamma = 4$ MeV. The results show that the detection efficiency is strongly dependent on solid angle. Increasing Ω from 1 % to 50 % yields nearly three orders of magnitude in the counting rate. In addition, the multipolarity discrimination power is improving with increasing solid angle. Since without magnet Ω is limited to at best 10 % of 4π , the collecting action of a magnetic field provides a considerable improvement in the performance of the system. The relative differences in the detection efficiency for the most important multipoles are sufficiently large to allow an experimental determination of the multipole character. They are about 50 % for 4 MeV E1 and M1 radiation observed in 2π geometry. The corresponding values at 5 and 6 MeV are 40 % and 30 %, respectively. The ratios for $\Omega/4\pi = 1$ in Fig. 1 are identical with the total pair formation coefficient.

In Fig. 2 the function

$$\frac{H(k, \Omega)}{H(k, \Omega_0)} \cdot \frac{\Omega_0}{\Omega}$$

with $\Omega_0 = 0.25\%$ is plotted. This expression is a slowly varying function of Ω and allows a linear scale.

The calculations described here are only approximately valid, if a lower limit is set on the energy of either the positron or the electron by the pulse-height selection in the dE/dx -counter. For sufficiently high transition energies the fraction of pairs which is excluded in this way is small. Thus we can expect that more sophisticated calculations will not considerably alter the results. Studies which allow for the pulse-height selection will be performed in the near future. These calculations will also include a proper correction to the shape of the positron energy spectrum. Such a correction is suggested from the exact solutions of the Dirac equation.

FIG. 2. Response characteristics. Linear plot in a relative scale. $E_\gamma = 4 \text{ MeV}$.

4. Discrimination Against Interfering Radiation

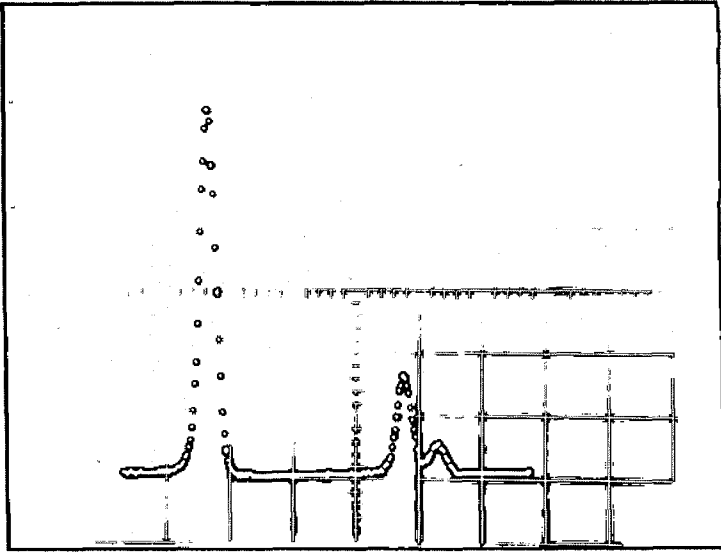
Since the values for $H(k, \Omega)$ range between 10^{-4} and 10^{-3} , it must be insured that the coincidence counting rate due to gamma rays emitted from the target is suppressed with high effectiveness. This problem was investigated experimentally. A telescope consisting of a 170 μm dE/dx-detector and a 2 mm E-counter was irradiated with conversion electrons from a ^{207}Bi source (without magnet). No distortion of the electron spectrum occurred when a gamma-ray source of ^{60}Co was added which had a source strength more than three orders of magnitude higher than that of the electron source. This is demonstrated in Fig. 3 where the spectra taken without and with Co source are shown. By using a superconducting magnet and thus a remote position of the telescope the sensitivity to gamma radiation can be further attenuated by more than an order of magnitude while the charged particle intensity is increased. Finally, the requirement of a fourfold coincidence relationship considerably reduces the gamma induced background. Thus we can conclude that interference from gamma radiation presents no severe problem.

Another source of interfering radiation is the internal conversion process. Such an event alone is not capable to trigger the coincidence circuit since there is no source of positrons. The same is true for events occurring in cascade. Another obvious possibility is the emission of a low-energy internal conversion electron into the dE/dx-counter with simultaneous production of a positron in the E-detector via external pair formation. The probability for such an event is very small because of the unfavourable geometry for gamma rays, the low atomic number of silicon and the pulse-height selection in the dE/dx-counter. Only in those cases where the energy of intense conversion electrons is such that the energy loss in the thin detector equals that of two high-energy electrons interference may occur with measurable intensity. However, the internal pair lines remain undisturbed. The background has either a continuous character or satellite peaks appear. Moreover, the possibility for this interference can easily be controlled.

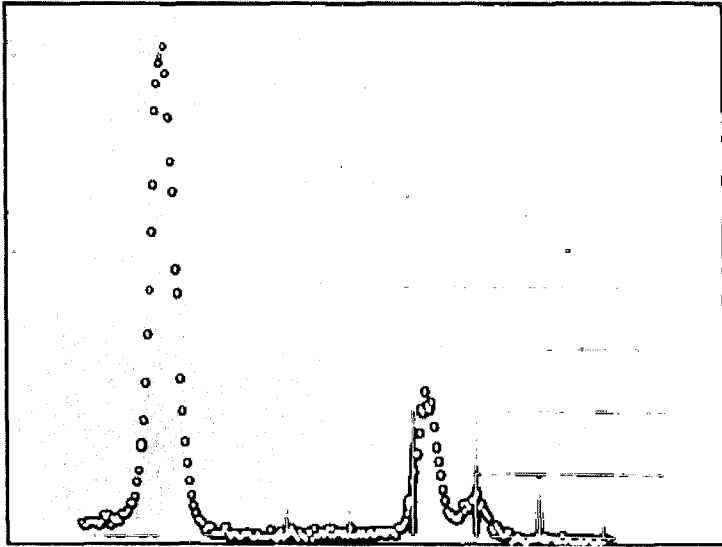
Summing with low-energy conversion electrons can also occur in the case of internal pair events, if there are highly converted coincident transitions and if a large solid angle is used. This interference results in a reduction of the pair lines and thus may falsify the measurement. A direct way to eliminate such summing effects is a reduction of the solid angle. This may be accomplished by placing the target in a diverging magnetic field. Then the efficiency is reduced by the magnetic mirror effect. As the electrons or positrons move towards the detector, the radius of the helical orbits will decrease due to the increase in magnetic field strength. Since the angular momentum of the particles remains constant, the velocity component perpendicular to the direction of the field will increase. As a result particles emitted from the target at an angle θ relative to the field vector will be totally reflected, if θ exceeds the angle θ_0 given by

$$\sin^2 \theta_0 = \frac{B}{B_{\text{max}}}$$

Here B is the field strength at the target position and B_{max} is the maximum magnetic field strength on the path to the telescope. By varying B the collection efficiency and thus the magnitude of the



a)



b)

FIG. 3. K, L, M conversion electron spectrum from ^{207}Bi : (a) without ^{60}Co source; (b) with ^{60}Co source. See text.

summing effects can be controlled. A proper method to vary the field at the target position without changing the maximum field strength is discussed in section 6.

Another procedure for eliminating the influence of summing with conversion electrons might be to correct the pair lines for the intensity distributed over the sum peaks. This intensity may be obtained from a (simultaneous) measurement where an energy loss greater than that of two fast electrons is admitted in the dE/dx -counter.

5. Timing

Due to the remote position of the telescope and the collecting action of the magnetic field part of the electrons or positrons have to travel a long flight path before they reach the detector system. Therefore we have to study the time behaviour for unfavourable emission angles and energy divisions. In a homogeneous magnetic field the time of flight is given by

$$t = \frac{d}{c \cos \theta \sqrt{1 - \left(\frac{m_0 c^2}{m_0 c^2 + E_{kin}} \right)^2}}$$

where d is the target - detector distance. Let us consider a total kinetic energy of 7 MeV. If one particle is emitted with 6.5 MeV at $\theta = 0^\circ$ and the other particle with 0.5 MeV at $\theta = 80^\circ$, then the difference in time of flight for $d = 20$ cm is calculated to be 3.8 nsec. Thus no problems arise both for the time and the energy resolution.

6. Design

A schematic lay-out of a proper spectrometer design is shown in Fig. 4. A beam of thermal neutrons enters an evacuated target chamber and impinges upon a thin target located on the symmetry axis of a superconducting solenoid system. The inside diameter of the magnet is 5 cm. The central field is approximately 50 kOe. Thus 9 MeV electrons describe helical paths with at most 0.64 cm radius and can reach a 3 cm dia. detector without striking the wall. The telescope is placed 19 cm above the target and is mounted on the end of a cold finger connected to a liquid-nitrogen cryostat. A liquid-helium cryostat shielded by liquid nitrogen houses the superconducting magnet. Target and detector system can be removed without disassembling the helium cryostat.

The main problem in designing a superconducting magnet with constant field strength over the whole distance between target and telescope arises from the requirement that the solenoid be divided for the passage of the neutron beam and the emergence of the annihilation quanta. A proper solution is indicated in Fig. 4. A suitable geometric arrangement of several coils insures a practically homogeneous magnetic field. The local dependence of the field strength as calculated for the spectrometer axis with a current

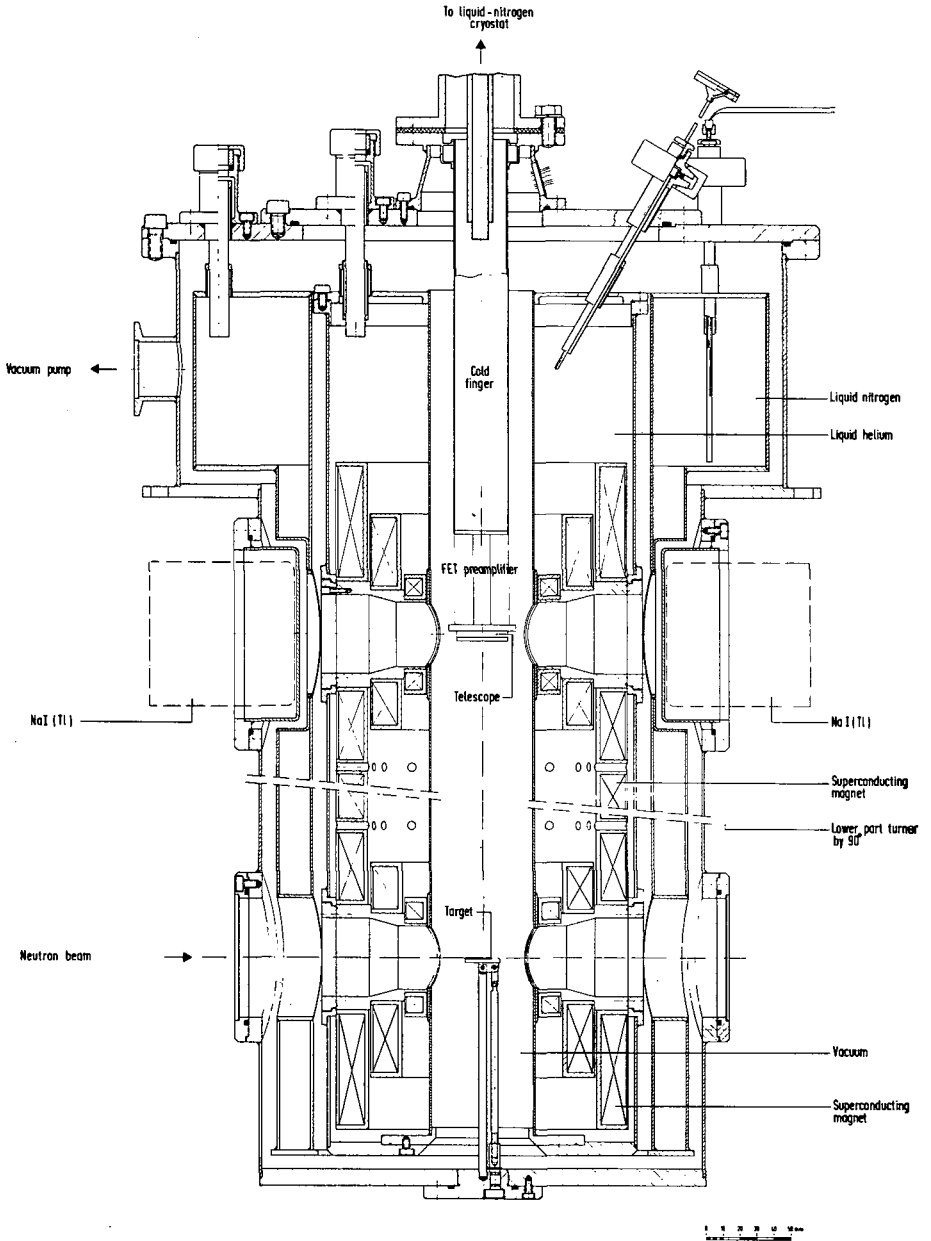


FIG. 4. Design of the spectrometer.

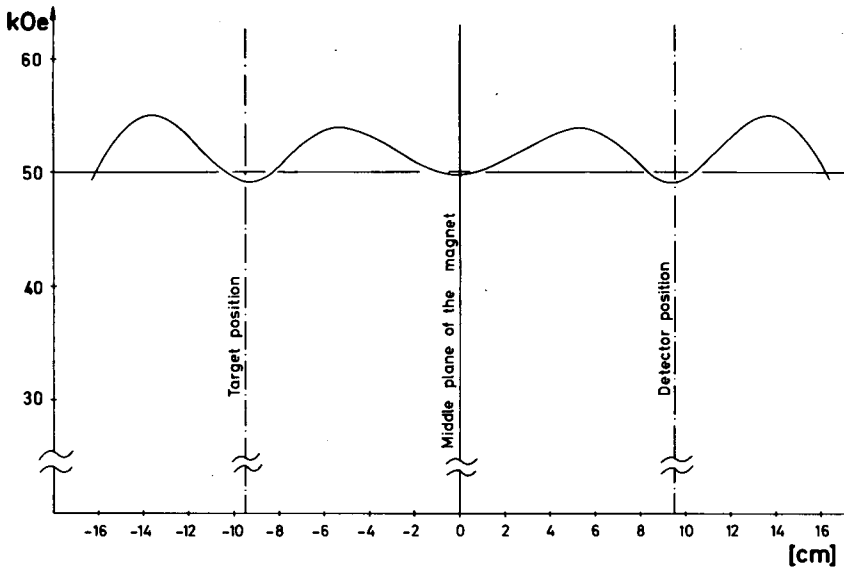


FIG. 5. Magnetic field strength on the spectrometer axis.

of 55 A is shown in ^{+) Fig. 5. By changing the current through the auxiliary coils placed beyond the target position a diverging field can be produced at the target and the effective solid angle can be controlled by means of the magnetic mirror effect. In this way a very versatile instrument is obtainable.}

The E-counter should be as thick as possible. Fully depleted detectors produced by ion implantation are very well suited for stacking a thick counter. The energy resolution of the telescope is essentially determined by the dE/dx -counter because of the large capacitance of this detector. With present techniques an optimum resolution of 0.07 % at 10 MeV can be attained.

It is worthwhile to remark that the principle discussed here may also be successfully applied for measurements of the internal conversion electron spectrum from neutron capture.

References

- [1] T. v.Egidy, Ann. Physik VII, 9 (1962) 221
- [2] See, e.g. Alpha-, Beta- and Gamma-Ray Spectroscopy (ed. K. Siegbahn; North Holland Publishing Company, Amsterdam, 1965)
- [3] J.C. Jaeger and H.R. Hulme, Proc. Roy. Soc. 148 (1935) 708
- [4] W. Michaelis and D. Lange, Nuclear Instr. and Meth. 58 (1968) 349

^{+) The field was calculated by Siemens AG, Erlangen}

- [5] H.P. Kennedy, Thesis University of Virginia 1964,
University Microfilms, Inc., Ann Arbor, Michigan
- [6] M.E. Rose, Phys. Rev. 76 (1949) 678
- [7] M.E. Rose, Phys. Rev. 78 (1950) 184

PLANS FOR HIGH-RESOLUTION (n, γ) STUDIES AT THE RILL

O. W. B. SCHULT, H. R. KOCH, B. P. K. MAIER
Department of Physics,
Technische Hochschule,
Munich, Federal Republic of Germany

Abstract

PLANS FOR HIGH-RESOLUTION (n, γ) STUDIES AT THE RILL. The measurement of slow neutron capture gamma-ray spectra at the RILL will be carried out with different instruments located at both ends of a tangential through hole. The low-energy spectrum will be measured with four curved-crystal spectrometers with focal lengths from 5.8 to 24 m. The high-energy spectrum will be recorded with a Ge(Li) spectrometer. Medium-energy gamma rays will be detected with a Ge(Li) diode combined with a curved crystal monochromator and operated in the anti-Compton mode.

High-resolution (n, γ) studies have been performed at many laboratories during the past decades. The data obtained in these experiments have helped to extend our knowledge of the structure of a great number of nuclei, in particular where the experimenters have measured rather complete and detailed (n, γ) spectra [1]. This has been possible predominantly when the slow neutron capture cross-section has been fairly large.

A good Ge (Li) spectrometer is well suited for the measurement of the whole (n, γ) spectrum of a probe even when this has a very small cross-section if it is located properly at a medium strength reactor. However, such a solid-state counter shows drawbacks in the low-energy region: its resolving power $E/\Delta E$ decreases with decreasing energy E , the full width at half maximum ΔE is seldom less than 0.7 keV for $E = 100$ keV and 1.6 keV for $E = 1$ MeV [2], and its dynamic range is reduced at lower energies because of the Compton events of radiation with higher energy. The latter disadvantage has been overcome to a great extent with anti-Compton spectrometers [3, 4].

Curved-crystal spectrometers have a resolution up to $E/\Delta E = 2$ GeV/E [5] and a large dynamic range at low energies. However, the extremely small detection efficiency of these diffractometers requires very strong sources, which can be produced only in regions of sufficiently high neutron flux. The quality of the curved-crystal spectrometer data decreases more strongly with decreasing source strength than does that of the Ge(Li) data. At the present time a fairly small curved-crystal spectrometer for the measurement of (n, γ) spectra from a 20-mg source with $\sigma = 2000$ b in a thermal neutron flux of about $6 \times 10^{13} \text{ n cm}^{-2} \text{ sec}^{-1}$ yields data which are more detailed for $E < 800$ keV than the low-energy (n, γ) spectrum from the same target material recorded with one of the best anti-Compton spectrometers [4].

A curved-crystal spectrometer at a high flux reactor is the most powerful instrument for the spectroscopy of low-energy gamma radiation from targets with capture cross-sections $\sigma > 0.1$ b. The Ge(Li) diode is the best spectrometer for medium- and high-energy gamma rays and the

universal detector for (n, γ) spectra from nuclei with $\sigma < 0.1$ b. For these reasons we have planned to use both types of instruments for one-dimensional high-resolution (n, γ) studies at the Reactor of the Institute Laue-Langevin (RILL).

The RILL has been designed as a heavy-water-moderated high-flux reactor mainly for solid-state physics work. Several special beam holes are under construction for nuclear physics experiments. One of these is a horizontal through hole with 10 cm internal diameter. Its axis passes the reactor core at a distance of 55 cm. This will guarantee a relatively low epithermal and fast neutron flux while the slow neutron flux is expected to be around $5 \times 10^{14} \text{ n cm}^{-2} \text{ sec}^{-1}$ in the centre of the tube, which should make it ideal for (n, γ) studies.

The cost of construction and operation of a high-flux reactor demands that each beam tube be used very efficiently. We intend to install and operate in parallel five gamma spectrometers at the (n, γ) liner.

(1) The Risø spectrometer will be transferred to Grenoble and located at one end of the beam hole. A few constructional changes will be necessary to fit the instrument to the face of the huge reactor. The length of the multi-slit collimator should be increased from 1.4 m to about 2.4 m so that the collimator and the detector, together with the present shielding, will remain outside the intense undiffracted beam for an angle of reflection $\varphi > 4^\circ$. The spectrometer will be used mainly for measurements of gamma-ray reflections with $4^\circ < \varphi < 12^\circ$ corresponding to $20 \text{ keV} < E < 180 \text{ keV}$. High resolution is maintained if the focussing condition is satisfied, which implies that the distance between the source and the spectrometer must be reduced by 11 cm if φ is increased from 4° to 12° . This should be accomplished by mounting the instrument on a movable frame.

A small servo diffractometer will be installed in front of the Risø spectrometer. The instrument will record only the reflection of a single, very strong low-energy line and thereby measure continuously the exact position of the source which cannot be mounted rigidly inside the channel. The angles of reflection of (n, γ) lines recorded with any spectrometer viewing the source can then be determined with an accuracy which is given essentially by the precision of the angular setting of the curved crystal. The planned servo diffractometer should resemble the present system used in feedback operation at the Risø spectrometer. However, it should operate independently of a special spectrometer at Grenoble. This will simplify the design considerably.

(2) A second spectrometer has been planned with a focal length of 24 m. Recent measurements at Risø have shown that reflection widths as small as 1.2 seconds of arc can be obtained from a sufficiently small source [5]. Therefore, it is reasonable to design the RILL curved crystal spectrometers in such a way that the source contribution to the reflection width is around 1 in. for average sources. These will be about 40 mm high, 2 - 10 mm deep (along the axis of the beam tube) and ~ 0.1 mm thick, so that they appear to be 1 in. broad from a distance of 20 m. The 24-m spectrometer will consist of two independent units on top of each other. These systems can be operated in different ways: (a) one unit measures the (n, γ) spectrum from $+\varphi$ to $+\varphi_{\text{min}} \sim 2^\circ$ and the other unit from $-\varphi$ to $-\varphi_{\text{min}}$. This mode of operation provides an independent automatic control of the source fluctuations. (b) One system is used for the measurement from $\sim 2^\circ$ to φ_{min} and the other system for recording the spectrum between

-2° and -4° . In this case the 24-m spectrometer yields the (n, γ) spectrum with $E_\gamma > 180$ keV (for fifth-order reflection from the 110 planes of quartz) or $E_\gamma > 72$ keV (for second-order reflection).

(3) A third spectrometer with a focal length of 18 m could be located in front of the 24-m spectrometer. The 18-m instrument will be used for measurements at reflection angles greater than 2° since the collimator and the detector and its gamma shield must be kept outside the direct beam to the 24-m spectrometer. The 18-m spectrometer would enable the experimenter to restrict the angular range of the 24-m diffractometer to $\varphi < 2^\circ$ ($E_\gamma > 360$ keV or 144 keV for the fifth or second order of reflection). The angular range of the 18-m apparatus would then be $2^\circ - 4^\circ$. The reduction of the angular range is directly proportional to the reduction of the number of measuring steps and inversely proportional to the counting time per step. Thus, the counting time per point at the 24-m spectrometer would be about 400 sec if the reflection width is 2 in. and if the total measuring period is about 1 month. Such counting times allow spectra with very good statistics to be recorded, as shown by Baader in another contribution to this Symposium [6].

(4) A fourth, very simple spectrometer will be used for the study of gamma rays with energies less than 30 keV. The instrument will be equipped with a bent LiF crystal or with a very thin curved quartz crystal. The maximum resolution will be obtained with the quartz crystal if the distance between the source and the spectrometer crystal satisfies the focussing condition $l(\varphi) = l_0(1 - \cos\varphi)$. The spectrometer should therefore be mounted on a suitable carriage between the 18-m spectrometer and the source changer, whose length puts a lower limit on the focal length ($l_0 \gtrsim 11$ m).

The defocussing effects at the 18-m and 24-m spectrometers are negligible so that these instruments can be located stationary.

(5) Gamma radiation that is not diffracted by the crystal of the modified Risø spectrometer can be analysed further with an additional spectrometer. This spectrometer would be useful for measuring the whole (n, γ) spectrum of an isotope with very small cross-section and for studying medium- and high-energy neutron capture gamma rays from strong sources. The most flexible instrument for this purpose is a Ge(Li) detector surrounded by a split scintillator. Such a spectrometer can be operated in both the pair and the anti-Compton modes. It would be placed in the direct beam for the measurement of high-energy (n, γ) rays or of the total capture gamma-ray spectrum of weak sources. Intense (n, γ) lines with medium energy can be studied very well if one uses the geometry chosen successfully by Smither [7]. He used a Ge(Li) detector to analyse the gamma beam diffracted from a curved crystal. The anti-Compton arrangement will reduce the background considerably so that one can hope to find even weak transitions in the spectral region which is diffracted into the germanium diode.

The Ge(Li) spectrometer would therefore complement the curved-crystal diffractometers. The instruments described should make it possible to measure the whole (n, γ) spectrum from a single source, while occupying only one channel at the high-flux reactor.

ACKNOWLEDGEMENTS

The authors are very grateful to Professor H. Maier-Leibnitz, the director of the Institute Laue-Langevin, for his support and continuous interest in the (n, γ) project and for valuable discussion.

REFERENCES

- [1] Nuclear Data, Academic Press, New York, 3 4-6 (1967); 5 1-2 (1968); 5 3-4 (1969).
- [2] PALMS, J. M., VENUGOPALA RAO, P., WOOD, R. E., Nucl. Instrum. Meth. 64 (1968) 310.
- [3] MOTZ, H. T. et al., Phys. Rev. 155 (1967) 1265.
- [4] MICHAELIS, W., KÜPFER, H., Nucl. Instrum. Meth. 56 (1967) 181.
- [5] KOCH, H. R. et al., "The automation of the curved crystal spectrometer at Risø", these Proceedings.
- [6] BAADER, H. A. et al., "Investigation of the ^{158}Gd level scheme by thermal neutron capture", these Proceedings.
- [7] SMITHER, R. K., private communication; Proc. Conf. The Study of Nuclear Structure with Neutrons, Antwerp, 1965, North Holland Publ. Co. (1965) 519.

Invited talk

NEUTRON CONDUCTING TUBES

H. MAIER-LEIBNITZ

Institut Max von Laue - Paul Langevin,
Grenoble, France

Abstract

NEUTRON CONDUCTING TUBES. The relationships characterizing neutron reflection along ideal straight neutron guide tubes are summarized and extended to the cases of curved tubes and real guide tubes with imperfections. Practical aspects on the construction and use of real guide tubes are presented, including data on neutron reflectivity, associated radiation levels and neutron polarization.

From the work of Fermi's group [1, 2] soon after the war it is known that the refractive index of most substances for thermal neutrons is slightly smaller than one. Thus total reflection from mirrors is possible with critical angles of the order of one degree (the critical angle is proportional to the wavelength; for nickel, the angle is one degree for 10-Å neutrons).

Neutron mirrors have been used by several authors [3] to measure critical angles; to deflect neutron beams; and to produce polarized neutrons, using the fact that the refraction index of magnetized substances is different for the two possible spin orientations of the neutron.

Christ and Springer [4] were the first to guide slow neutrons by multiple total reflection in a polished copper tube. In a straight tube, after a first reflection all subsequent reflections occur under the same angle. This means that except for reflection losses, the specific brightness (neutrons per cm^2 -sec, per solid angle, and per wavelength interval) will be the same at the exit of the tube as at the entrance, for the angular range of neutrons that is transmitted at each wavelength.

This situation is not fundamentally changed if a long tube is slightly bent so as to forbid the passage of fast neutrons and gamma rays. With these properties, neutron guides may serve the following purposes:

Production of a pure beam of slow neutrons at a distance from the reactor

Production of beams of very slow neutrons ($\lambda > 10 \text{ \AA}$) with angular width larger than can be obtained with normal beam tubes at a reactor

Provision of long beam paths for time-of-flight experiments without loss of angular divergence

Separation of experiments, by using several neutron guide tubes at a distance from the reactor

Production of intense polarized beams.

Neutron guide tubes are in use now at various places (Munich [5, 6], Saclay [7], Brookhaven [8], Oak Ridge [9]). Experiments have been done to improve them, mainly by trying (with moderate success) to use

laminated guide tubes in the shape of a bent Soller collimator (Risø [10, 11], Brookhaven [8], Bucharest [12], Vienna [13]); polarized neutrons have been produced by such systems, too. An attempt has been made [14] (without success so far) to make very short bent guides by evaporating alternate layers of nickel and aluminium on a curved surface; the nickel surfaces are the neutron mirrors and the aluminium replaces the vacuum of a normal guide.

At the high-flux reactor for thermal neutron beams which is under construction at Grenoble, ten neutron guide tubes are foreseen, five for thermal neutrons and five from the cold source, with a rectangular cross-section of 3×20 cm each.

'IDEAL' NEUTRON GUIDE TUBES

The critical angle of total reflection is

$$\gamma_c = \sqrt{1 - n^2} = \sqrt{\frac{Na}{\pi}} \lambda \quad (1)$$

n = refractive index, N = number of atoms/cm³, a = coherent scattering length, λ = neutron wavelength. To good approximation even for absorbing substances, it may be assumed that the reflectivity r is one for all angles $\gamma < \gamma_c$, and zero for all $\gamma > \gamma_c$ (the reflectivity r decreases to $r = 0.3$ for $\gamma = 1.1 \gamma_c$). Since Eq. (1) may be written in terms of $k = 2\pi/\lambda$

$$\gamma_c = \frac{\Delta k}{k} \quad (1a)$$

This means that all neutrons with wave vector component normal to the surface smaller than Δk are reflected, independent of wave number.

A straight, rectangular neutron guide tube in the z direction with ideally reflecting walls parallel to x and y therefore reflects all neutrons with

$$-\Delta k < k_x < \Delta k; \quad -\Delta k < k_y < \Delta k \quad (2)$$

Out of a Maxwell spectrum of thermal neutrons with momentum space density ρ_r

$$\rho_r \hbar^3 dk_x dk_y dk_z = \frac{\phi}{4\pi v_T} \frac{e^{-k^2/k_T^2}}{k_T^3} dk_x dk_y dk_z \quad (3)$$

$$\frac{\hbar^2}{2m} k_T^2 = k_B T = \frac{m}{2} v_T^2$$

k_B = Boltzmann constant, T = temperature of the Maxwell spectrum, the neutron guide transports a current

$$\begin{aligned} J &= F \iiint v \rho_p dk_x dk_y dk_z \\ &= F \frac{\phi}{4\pi} 4 \left(\frac{\Delta k}{k_T} \right)^2 \int_0^\infty \frac{v}{v_T} e^{-k^2/k_T^2} \frac{dk_z}{k_T} = F \frac{\phi}{2\pi} \left(\frac{\Delta k}{k_T} \right)^2 \end{aligned} \quad (4)$$

F = cross-section of the neutron guide.

For nickel which is the best material for neutron guides (usually evaporated on glass) $\Delta k = 0.0107 \text{ \AA}^{-1}$.

For $T = 300^\circ\text{K}$, $k_T = 3.25 \text{ \AA}^{-1}$, $V_T = 2200 \text{ m/sec}$.

In this case

$$J = F \frac{\phi}{4\pi} 2.2 \times 10^{-5}$$

For a cold source with $T = 30^\circ\text{K}$

$$J = F \frac{\phi}{4\pi} \cdot 2.2 \times 10^{-4}$$

Thus, a cold source Maxwellian flux density of $10^{15} \text{ n cm}^{-2} \text{ sec}^{-1}$ at the guide-tube entrance would yield a cold neutron flux density of $2 \times 10^{11} \text{ n cm}^{-2} \text{ sec}^{-1}$ at the guide-tube exit.

We now consider an 'ideal' bent guide consisting of two concentric cylinders, with radius R for the outer cylinder and distance d between them, with neutrons travelling normal to the cylinder axis. A neutron passing through a point whose distance from the outer wall is x , and at an angle $(\pi/2) + \gamma_x$ with the radius vector, will hit the outer wall at an angle γ_a . Assuming $x/R \ll 1$

$$\gamma_x^2 = \gamma_a^2 - \frac{2x}{R} \quad (5)$$

and, since

$$\gamma_a^2 \leq \left(\frac{\Delta k}{k}\right)^2$$

$$\gamma_x^2 \leq \left(\frac{\Delta k}{k}\right)^2 - \frac{2x}{R}$$

or, with $\Delta k_x/k = \gamma_x \text{ max}$

$$\left(\frac{\Delta k_x}{\Delta k}\right)^2 = 1 - \frac{2x}{R} \left(\frac{k}{\Delta k}\right)^2 \quad (6)$$

Thus, near the outer wall neutrons of all moments are reflected within the angular range $\Delta k/k$. At a distance x the angular range is more limited, and above

$$k_{\text{max}} = \Delta k \sqrt{\frac{R}{2x}} \quad (7)$$

neutrons cannot pass. This holds if the guide is long enough (length L) to prevent the passage of neutrons without reflection

$$L \geq L_1 = \sqrt{8 d R} \quad (8)$$

The angular range as a function of $k/\Delta k$ and of x/R is shown in Fig.1 for a certain range of $k/\Delta k$ and of x/R . By applying a transformation parameter α as indicated, the figure may be adapted to other ranges

of the two variables. The intensity of the faster neutrons is concentrated near the outer wall, while for slow neutrons the distribution is nearly uniform. A 'design value, k_{des} ' of k for a guide tube for nearly uniform transmission may be defined by asking (rather arbitrarily) that

$$k_{des} = 2/3 k_{max}(d) \tag{9}$$

which gives

$$\frac{\Delta kd}{\Delta k} = 0.75 \tag{10}$$

For calculations of total neutrons intensity at x a cut-off value

$$k_c = \frac{\pi}{4} k_{max} = \frac{\pi}{4} \Delta k \sqrt{\frac{R}{2x}} \tag{11}$$

may be introduced as an upper limit in the integral (4).

REAL GUIDE TUBES WITH IMPERFECTIONS

Neutron beams from real guide tubes are different in geometry and intensity as compared to the 'ideal' case for three reasons:

- (1) Imperfect reflectivity due to microscopic roughness of the surface

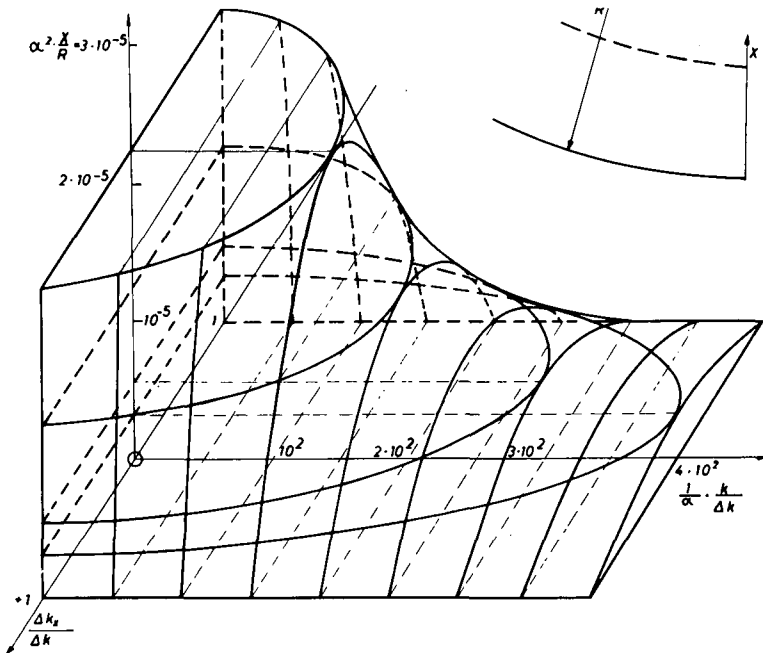


FIG. 1. Wave number range Δk_x for neutrons of wave number k emerging at a distance x from the outer wall of a curved neutron guide (radius R). $\Delta k/k$ is the critical angle of total reflection of the surface, α is a parameter that may be chosen to vary the range of k or of x/R .

- (2) Deviations of the reflecting surfaces from the 'ideal' geometry ('waviness')
- (3) Imperfect joints between the parts that make up a long neutron guide.

The roughness of a surface will cause a loss of specular reflectivity, and will create a diffuse reflectivity which may be concentrated at small angles around the regular reflection. This is well known from measurements on mirrors for X-rays and for neutrons [15].

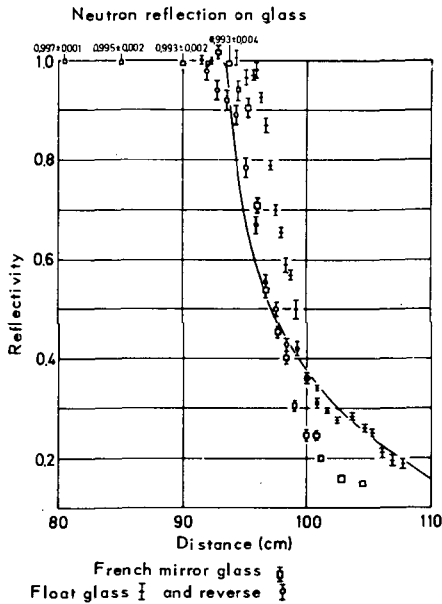


FIG.2. Reflectivity of ground mirror glass (Saint Gobain) and float glass, measured in the gravity refractometer.

The requirements of surface smoothness for good reflectivity are about one order of magnitude higher for neutrons (near the critical angle for all energies) than for optical light. However, normal optical polishing yields surfaces that are quite satisfactory. Quite a number of measurements have been made on single or multiple reflection from glass surfaces with or without evaporated coatings; they all give reflectivities around 0.99. Figure 2 shows a recent example on commercial mirror-glass plates.

The average number $\bar{n}(k)$ of reflections in a straight guide tube of width d , height h and length L is

$$\bar{n}(k) = \frac{1}{2} \gamma_c(k) \left(\frac{L}{d} + \frac{L}{h} \right) \quad (12)$$

and the maximum number of reflections is twice as high.

In a quadratic bent tube of length $L = L_1$ (length of direct sight, see Eq.(8)) \bar{n} has a minimum value $\bar{n}_{des} \approx 3$ for $k = k_{des}$ (k_{des} see Eq.(9)). For smaller k values

$$\bar{n}(k) = \bar{n}_{des} \frac{k_{des}}{k} \approx 3 \frac{k_{des}}{k} \quad (13)$$

For larger k values, \bar{n} will increase again because a neutron may move in 'garland' reflections near the outer surface.

Angular deviations ϵ from the desired flat or cylindrical shape of the neutron guide surface will cause losses of about $\epsilon/\gamma_c(k)$ per reflection. The total loss will be proportional to the square root of \bar{n}

$$\Delta J/J = \frac{\epsilon}{\gamma_c(k)} \sqrt{\bar{n}(k)} \quad (14)$$

For large k values where γ_c is small and \bar{n} may become large due to garland reflections, the angular surface deviations will greatly reduce the neutron intensity. This is clearly shown in the results of the Saclay group [7] who have made a most careful investigation of the intensity as a function of x and of angle. For instance, there is an intensity minimum for fast neutrons that emerge near the outer guide tube surface in the tangential direction.

Deviations ϵ may be caused by the natural waviness of commercial glass surfaces. For a neutron guide tube designed in Munich for 1-Å neutrons ($\gamma_c = 0.0017$), glass with $\epsilon \leq 10^{-4}$ was selected (mirror glass from Saint Gobain) with a rejection rate of 30%. Since neutron guides are not expected to be used for wavelengths smaller than 1 Å, the usefulness of commercial glass is now proven generally.

However, deviations ϵ are also expected by involuntary bending of neutron guide glass plates. In Saclay this problem has been solved (down to 2 Å) by using thick plates (2 cm). These plates were specially ground and polished and cemented into a self-sustaining, vacuum-tight guide tube. In Munich frames, 1 m in length by 2.5 cm and 14 cm wide, were cemented together, using a large flat table to support the lower plate, steel spheres to define the distance between the plates, and appropriate weighting to compensate for their natural curvature.

Another deviation ϵ will be caused if a curved neutrons guide is approximated by straight sections. This will not usually be serious. If necessary, the tube section may be slightly bent during the process of cementing.

Angular adjustment of neutron guide sections is easy. Flush surface adjustment can be obtained using washers, with an accuracy of $\delta = 0.02$ mm. The intensity losses due to this are for m sections

$$\Delta J/J \approx m \frac{\delta}{d} \quad (15)$$

In Munich the guide tube sections are mounted in long (up to 10 m) rectangular steel tubes which are then adjusted on pillars, sealed and evacuated. The mechanical stability appears to be satisfactory if large temperature variations (e.g. by solar irradiation) are avoided.

From the glass or plated glass guides that are in operation or that have been tested, the following conclusions may be drawn:

Neutron guide tubes are feasible for all wavelengths down to 1 Å. They operate according to theoretical expectations; the neutron losses that are observed may be described by assuming an effective reflectivity [7] between 0.98 and 0.97 (instead of the observed reflectivity which is better than 0.99). For neutrons that are several times faster than the design velocity the losses are higher (effective reflectivity 0.93 [7]).

Experience with reflectors other than glass seems to be less favourable. It is difficult to achieve the combination of good micro-smoothness and small waviness. Foils have always given inferior results. Attempts are being made to use electroplating but the results are not yet known.

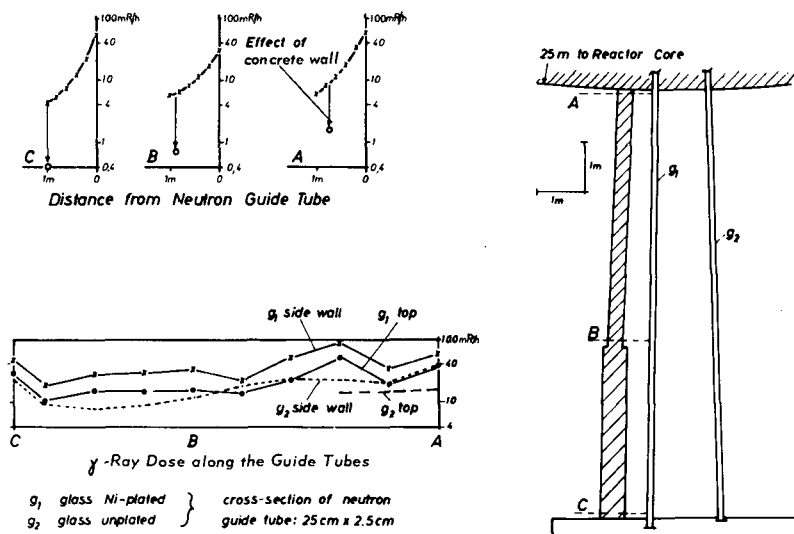


FIG. 3. Gamma-ray dose around neutron guide tubes at Munich.

SHIELDING; BACKGROUND RADIATION

A neutron guide tube, or a set of several tubes, makes a large opening in the reactor shield. Fast neutrons and core gammas will mostly penetrate the guide tube walls. Therefore, in Munich where a set of three guide tubes 2.5 × 2.5 cm originates from one beam tube, a water basin, 2.50 m wide and 0.80 m high above the neutron guides with 0.3 m concrete walls, with borated water and with lead shields (5 cm) and 6 cm of concrete in the upward direction near the reactor wall, is used up to a distance of 15 m from the core and provides just about sufficient shielding. One tube, for 20-Å neutrons, passes into the hall after a total length of 12 m; two tubes, one with Ni for 4.5-Å neutrons, one with glass for 6 Å, with total length of 34 m ($L = 1.4 L_1$), pass through

several walls into the open and into a laboratory. The gamma dose around the outer parts of these guides is shown in Fig.3¹ (the fast neutron dose is small in this region).

Most of this gamma radiation does not come from the core. It is produced by thermal neutrons which are lost from the guide by one of the processes mentioned above. The average neutron flux is about $6 \times 10^6 \text{ n cm}^{-2} \text{ sec}^{-1}$ for the Ni guide. Assuming that one third of the neutrons have been lost by imperfect reflection along a path of 30 m, the neutron guide surface is a source of slow neutron capture radiation from $7500 \text{ n cm}^{-2} \text{ sec}^{-1}$ (both sides of the neutron guide together). A considerable fraction (somewhat more than Σ_a/Σ_s , the ratio of absorption to scattering cross-section, which for glass and 2200 m/sec neutrons is about 0.03) of the neutrons will be captured in the glass. The rest may be absorbed outside, by lithium if possible. Boron glass may be used for the neutron guide. In this case, all neutrons are absorbed, but low energy gammas (only) are emitted, against which gamma protection is easy.

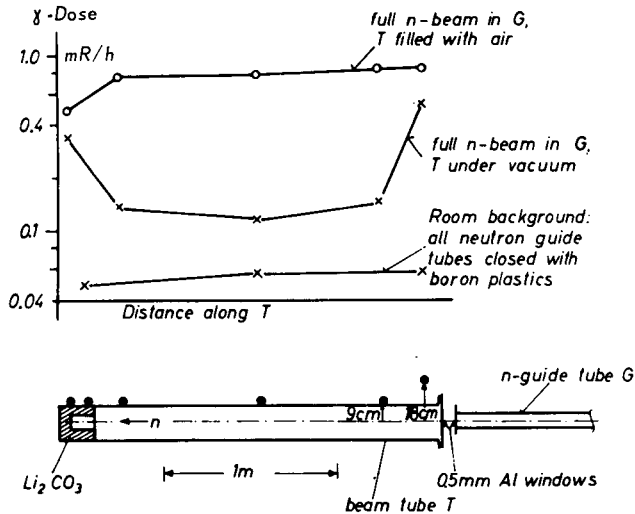


FIG. 4. Gamma-ray dose at the end of a neutron guide tube.

Of course, all matter in the neutron beam will produce capture radiation. Figure 4 shows the influence of windows and the difference between vacuum and air in the target tube. It also shows that far from windows and in vacuum the gamma level is quite low. At the High Flux Reactor at Grenoble slow neutron capture work on out-of-pile targets will be done mostly in subthermal beams from the cold source. Table I shows a comparison² between a thermal beam tube (10 cm diam., length 5 m) and a neutron guide tube (Ni, 3×20 cm, 33 mm long,

¹ Figures 3 and 4 are from O.W.B. Schult, unpublished.

² This comparison has been made by P. Ageron, unpublished.

TABLE I. FLUXES FROM NORMAL BEAM TUBE AND FROM BENT NEUTRON GUIDE TUBE

	Tangential Beam Tube 10 cm diameter length 5 m 10^{14} n cm ⁻² sec ⁻¹ sterad at the nose of the beam tube T = 300°K	Curved neutron guide tube length L = 33 m = 1.1 L _I cross section 3 × 20 cm 0.4×10^{14} n cm ⁻² sec ⁻¹ sterad at the wall of the cold source T = 30°K
Slow neutron flux (n cm ⁻² sec ⁻¹)	3.2×10^{10} (1.3×10^{10} at beam tube from cold source)	10^{10}
Slow neutron flux weighted with $\frac{2200 \text{ m/sec}}{v}$	2.8×10^{10} (3.6×10^{10} from cold source)	5×10^{10}
Gamma flux (mrem/h)	without filter and without collimator 7×10^8	at 10 cm from end of neutron guide 500 at 100 cm 50
Fast neutrons (n cm ⁻² sec ⁻¹)	3.2×10^7	≈ 10 < 6.7×10^5 for straight neutron guide of equal length

L_I = 30 m). It is seen that the advantage of the neutron guide tube is not so much in increased slow neutron intensity, but in decreased neutron and gamma background. There is, however, the possibility of gaining in flux by using a 'funnel', a tapered neutron guide with decreasing width, to illuminate small targets with increased solid angle. In this case, however, many neutrons are lost, and precautions must be taken to avoid excessive capture radiation from them.

GUIDE TUBE FOR POLARIZED NEUTRONS

Several authors [8, 10, 11] have used magnetized foils in the shape of a curved Soller collimator to polarize neutrons. This seems to work rather well but the optical imperfection of foil surfaces is a serious handicap. Recently Berndorfer [16] has completed a polarizing neutron guide with polished surfaces which has the following characteristics: Cross-section 0.5 × 5.7 cm, length 5 m = 1.2 L_I, radius of curvature 430 m. The guide is composed of 25-cm pieces of 0.55 mm foils of HYPERM Co 50 (50% Co, 48% Fe, 2% V). The foils were glued on brass and then ground and polished. The magnetic field was 850 Oe. The

material was chosen to give a large critical angle for one polarization ($\Delta k = 0.016 \text{ \AA}^{-1}$), and $n > 1$ for the opposite polarization. The guide transmits neutrons up to $k = 2.37 \text{ \AA}^{-1}$ near the inner wall. The total flux, averaged over the cross-section of the guide, was $3 \times 10^6 \text{ n cm}^{-2} \text{ sec}^{-1}$; the average polarization was better for faster than for slower neutrons, see Fig.5.

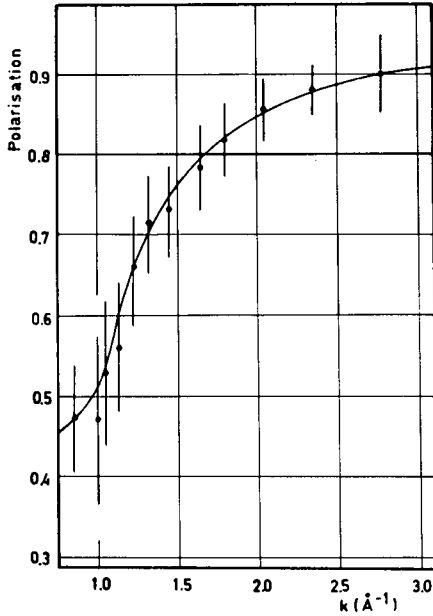


FIG.5. Polarization of neutrons from a guide tube with "HYPERM Co 50" walls in a magnetic field of 850 Oe.

The value for the total intensity shows that the reflectivity is good. The polarization is somewhat disappointing in view of the excellent polarization ($> 98\%$) obtained with Bragg reflection from magnetic crystals. It agrees, however, with other mirror results, but is a little less good than the careful work of the Leningrad group [17] who report polarizations around 85%. It would certainly seem worthwhile to continue this work with the aim of obtaining better polarization.

REFERENCES

- [1] FERMI, E., ZINN, W.H., Phys. Rev. 70 (1946) 103.
- [2] FERMI, E., MARSHALL, L., Phys. Rev. 71 (1947) 10.
- [3] See HIGES, D.J., Neutron Optics, Interscience Publ., New York (1954).
- [4] CHRIST, J., SPRINGER, T., Nukleonik 4 (1962) 23.
- [5] ALEFELD, B., CHRIST, J., KUKLA, D., SCHERM, R., SCHMATZ, W., Jülich Rep. 294-NP (1965).
- [6] ALEFELD, B., thesis, to be published.

- [7] FARNOUX, B., HENNIO, B., FAGOT, J., "Description et caractéristiques neutroniques du tube conducteur de neutrons installé près du réacteur EL3", Neutron Inelastic Scattering (Proc. Symp. Copenhagen, 1968) 2, IAEA, Vienna (1968) 353.
- [8] SCHRÖDER, I.G., MOORE, Z.A., POWELL, R.W., Bull. Am. phys. Soc. II 8 (1963) 512; see also SHULL, G., Phys. Rev. 179 (1969) 752.
- [9] MILLER, P.D., Rep. ORNL-TM-1149 (1965).
- [10] MOELLER, A.B., PASSEL, L., STECHER-RASMUSSEN, F., J. nucl. Energy A/B 17 (1963) 227.
- [11] ABRAHAMS, K., RATINSKY, W., STECHER-RASMUSSEN, F., WARMING, E., Nucl. Instrum. Meth. 45 (1966) 293.
- [12] BALLY, D., Roumain.Phys. 9 (1964) 245.
- [13] FIALA, W., RAUCH, H., Nucl. Instrum. Meth. 52 (1967) 15.
- [14] MARX, D., (Grenoble), unpublished.
- [15] See e.g. THOMAS, P., Z. Phys. 208 (1968) 338.
- [16] BERNDORFER, K., Thesis, Technische Hochschule München.
- [17] DRABKIN, S.M., ZABADIROW, E.I., KASMAN, Y.A., OKOROKOW, A.I., JETP Pisma 2 (1965) 54; the same authors plus TRUNOV, V.A., Rep. Institute "A.F. Ioffe" (1969).

STUDIES OF THE (n, γ) REACTION WITH A NEUTRON MONOCHROMATOR*

W.R. KANE, D. GARDNER, T. BROWN, A. KEVEY,
E. DER MATEOSIAN, G.T. EMERY**, W. GELLETLY,
M.A.J. MARISCOTTI
Brookhaven National Laboratory,
Upton, Long Island, N. Y.,
and
I. SCHRÖDER
National Bureau of Standards,
Washington, D. C.,
United States of America

Abstract

STUDIES OF THE (n, γ) REACTION WITH A NEUTRON MONOCHROMATOR. A crystal diffraction neutron monochromator has been constructed specifically for studies of the (n, γ) reaction. This equipment plays a complementary role to that of time-of-flight devices in providing a neutron beam with a full duty cycle at a given energy. This feature and the small target size, large geometrical efficiency for γ -ray detection, and negligible fast neutron background afford advantages for certain classes of experiments. The useful energy range extends from 0.01 to 20 eV. Novel features of the equipment include a complete reliance upon precision angle encoders for setting arm and crystal angles, the employment of a liquid shield to facilitate the extraction of the diffracted neutron beam, and the use of air bearings to provide for the motion of the target, detection devices, and associated shielding. Results obtained on low energy resonances of ^{139}La , ^{189}Os , and ^{235}U will be presented.

The time-of-flight method has been the traditional means for studying the interactions with matter of neutrons with higher than thermal energies. A necessary feature of this method is that the entire energy spectrum of the neutron source is available during each cycle of the equipment, with the experimental time available for a given energy interval determined by a fixed relationship between neutron energy and velocity. This is an evident advantage when a wide energy range is desired, as for example in cross section measurements or in studies of the statistical properties of resonances. It is clearly a disadvantage, however, when only certain neutron energies are of interest, or when neutrons within a small energy interval are required for long periods of time. A typical experiment of the latter type would be a coincidence or angular correlation experiment on the gamma rays emitted after neutron capture in a single resonance.

A neutron monochromator employing Bragg diffraction, on the other hand, provides a continuous beam of neutrons at a fixed energy. Although Bragg reflection is relatively inefficient above thermal energies, the elimination of the long flight path gives increased beam intensity, and the consequently smaller target size affords a greater geometrical efficiency for the detection of secondary radiations. The elimination of the burst of gamma rays and fast neutrons at the beginning of each cycle, inherent in the

* Work performed under the auspices of the US Atomic Energy Commission.

** Present address: Indiana University, Bloomington, Ind.

time-of-flight method, is also a decided advantage. Systems of this type have been employed by Spencer, Faler, and Harlan [1] in studies of the gamma rays emitted after resonance neutron capture by W and Hf, and by Vogt and Holloway [2] in similar studies of Te, Dy, Hf, and W. In both experiments the steady beam of neutrons at the resonance energy was used to advantage in coincidence measurements.

We have constructed a neutron monochromator intended specifically for capture gamma ray investigations. A schematic diagram of the equipment is shown in Fig. 1. The primary neutron beam proceeds through a Soller collimator 7 feet in length, one inch wide, and which has a vertical aperture which tapers outward, viewing the full 3-1/2 inch height of the beam thimble in the reactor and converging to a height of one inch at the target position. At present the collimator has 6 gaps, giving it an angular aperture of 13'. The second collimator, with a slightly greater angular aperture, is in an Al housing in the tank of liquid shielding. At the position of the monochromator crystal the primary beam intensity is 2×10^9 n/cm² sec and the beam current 2×10^{10} n/sec. At the target position the diffracted beam current is $\sim 2 \times 10^5$ /sec at 1 eV. The useful energy range is from 0.01 to 20 eV.

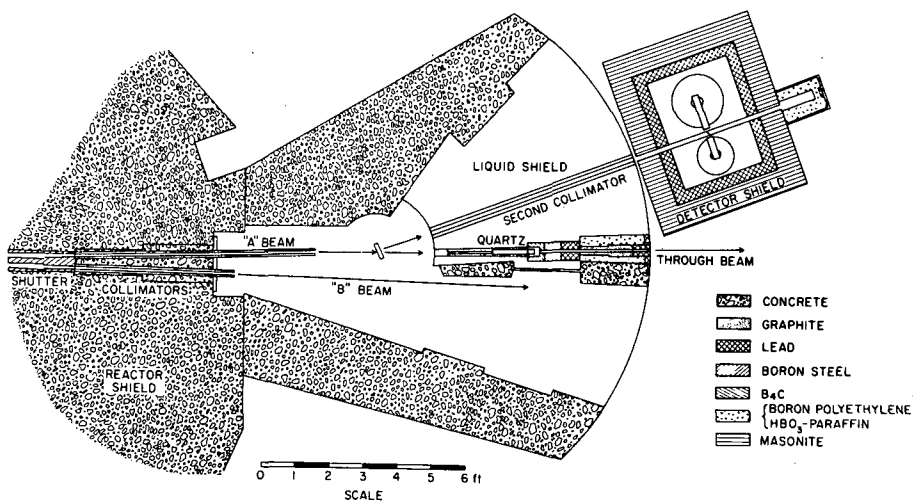


FIG. 1. Simplified diagram of the neutron monochromator and associated equipment. Two primary neutron beams are brought out from the reactor. The beam on the right (A beam) may be utilized either by the monochromator or brought directly out through a single-crystal quartz filter. The left-hand beam (B Beam) is available as needed for additional experiments.

The equipment has some novel features. Since our experiments involve secondary radiations (gamma rays) rather than neutrons, the shielding requirements are rather severe. It was therefore apparent that the conventional type of neutron spectrometer, in which the arm that supports the second collimator, detectors, and shielding must rotate on precision bearings to precisely determined angles, was not feasible here. The target, detectors, and associated shielding (seen on the right) were therefore divorced completely from the second collimator and arm. Furthermore, the conventional mechanical coupling between the crystal table and the second collimator usually employed to provide the 2:1 ratio between the Bragg

angle and arm angle was completely eliminated. Instead, complete reliance was placed upon two precision angle encoders. The encoder chosen, the "inductosyn" [3] is essentially a many-pole transformer in which a comparison of audio frequency signals on the primary and secondary windings gives their relative angular positions to a very high precision. Analog voltages from the inductosyn system are digitized and compared with the levels of digital registers set to the desired arm and crystal table angles. The error signal from this comparison is used to drive the arm and crystal table servos. A 2:1 ratio between the arm and crystal table angles may be maintained automatically, and the angle registers may be interfaced to a punched tape recorder or to a computer. The overall accuracy of the system exceeds 10". This permits the rocking of the crystal without the use of any additional precision angle measuring device.

It was further evident that customary methods of providing for the motion of the second collimator - a rotating shield, removable wedges, or counter-rotating cones, would be difficult. The motion of the collimator through a liquid was therefore chosen. The liquid shielding used is a commercial brake fluid additive [4] consisting of a 37% solution of anhydrous borax in ethylene glycol, with a small additional amount of ethylene glycol added by us to reduce the viscosity. The tank has 0.005 inch Al beam windows at each end. At each end of the collimator housing there is a flexible rubber diaphragm with a 0.005 inch mylar window cemented to it. The collimator housing is filled with He at a positive pressure of 10" H₂O, effectively forcing out any liquid trapped between the mylar collimator window and the Al tank window. The neutron transmission of each window combination is ~ 90%.

The "detector box" containing the target and detectors consists of 8 inches of high density masonite, 4 inches of lead, and two layers of boral. The use of iron in this shield was carefully avoided. The entire assembly moves on three air bearings on a large ground steel plate. Rollers clamped against a circular rail maintain the orientation of the assembly with respect to the beam. Tracking of the collimator is accomplished by a servo system which senses the position of a magnet attached to the end of the collimator.

In addition to the Bragg-diffracted beam, provision is made for bringing out a small (1 cm. dia.) direct beam. This beam is filtered through 15 inches of crystalline quartz at room temperature. The neutron intensity is 7×10^7 n/cm²sec and the Cd ratio 2×10^4 .

A second in-pile collimator has been installed at the facility to provide one or more additional neutron beams in the space at the left. This has been used by G. Scharff-Goldhaber, I. Schröder, and M. McKeown for studies of the (n, α) and (n,p) reactions. [5]

A number of experiments have already been carried out at the facility. For example, we are pursuing the study of the capture gamma rays from resonances of osmium. The primary purpose is to learn more about the collective levels of the even osmium isotopes, which lie in the transition region between spherical and deformed nuclei. In particular, we are interested in the two collective levels at 911 and 1115 keV recently discovered in thermal neutron capture. [6] Some of the results of a run on the 6.71 eV resonance of Os¹⁸⁹ are shown in Fig. 2. A number of transitions populating low-lying collective states in Os¹⁹⁰ have been indicated. In particular, we note the strong transitions from the capture state to the 0⁺ ground state and 2⁺ rotational state at 187 keV. Since strong primary transitions from

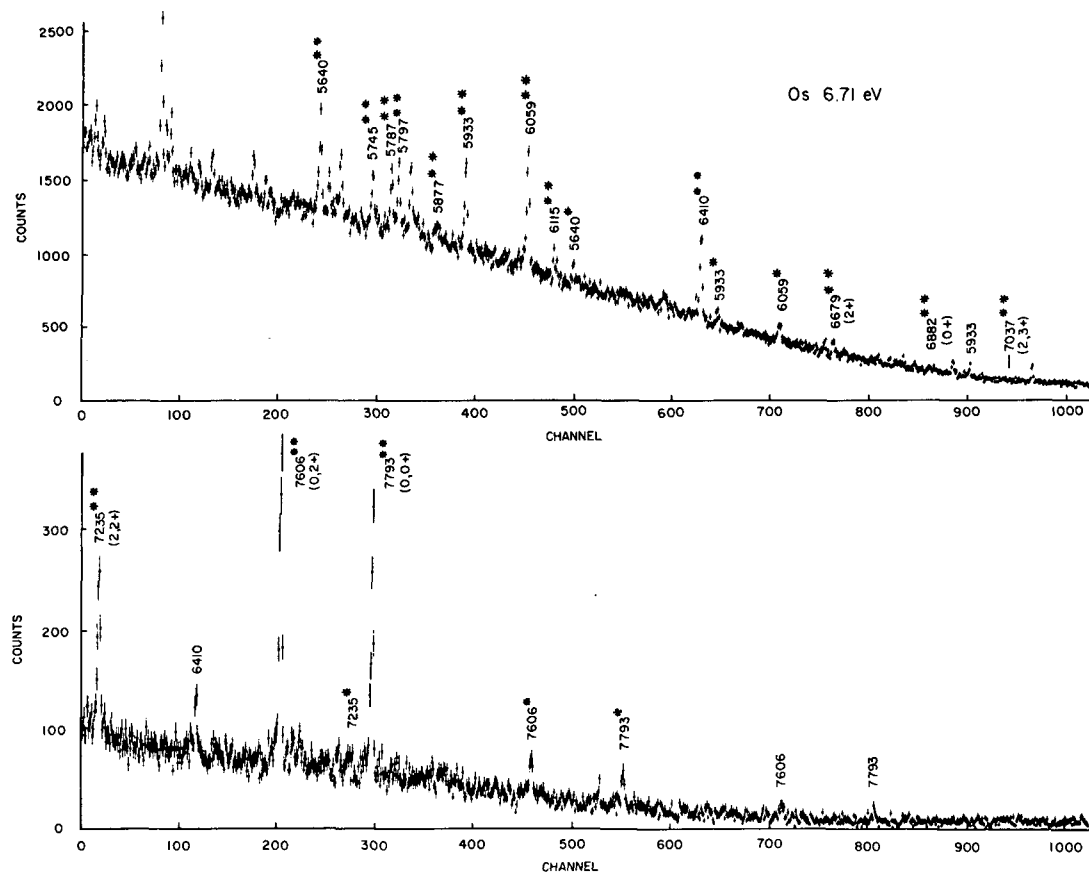


FIG.2. High-energy gamma rays from neutron capture in the 6.71-eV resonance of ^{189}Os . The full-energy and one and two-escape peaks from the Ge(Li) detector are designated by the transition energy and by the energy with one and two asterisks respectively.

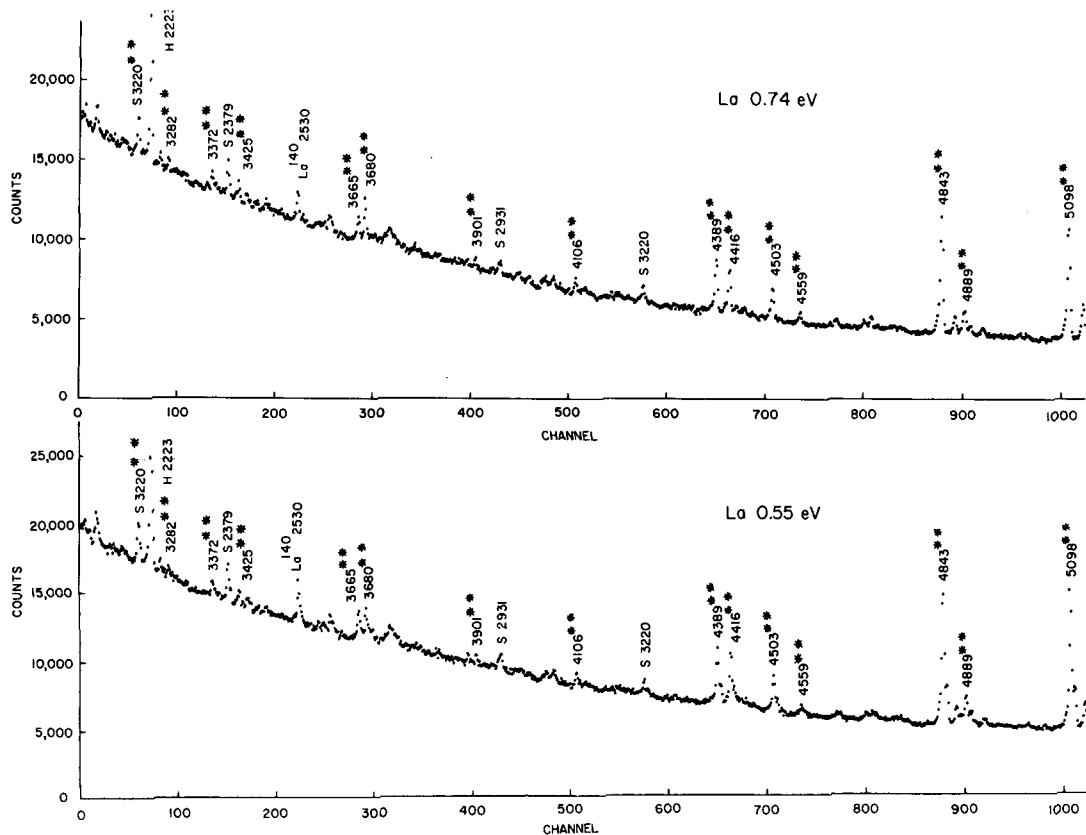


FIG. 3. High-energy gamma rays from neutron capture in ^{139}La . The upper and lower spectra correspond respectively to neutron energies on the 0.74 p-wave resonance and below it (0.55 eV). Full-energy and one and two-escape peaks are designated as in Fig. 2. In addition to lanthanum peaks the spectra contains also the hydrogen capture peak and a number of peaks from sulphur (a diluent in the target).

the capture state to lower-lying levels are known to be almost exclusively dipole transitions, it is evident that the 6.71 eV resonance has 1- spin and parity, since it populates directly both the 0+ and 2+ states. As a somewhat weaker argument for the same conclusion we note that the 7037 keV transition to the 3+ state in the gamma vibrational band at 755 keV does not appear, as it does in thermal capture. The 6882 and 6679 keV transitions to the collective levels at 911 and 1115 keV previously found in thermal neutron capture are present, but are very weak.

Another current experiment at our facility is the study of the 0.74 eV p-wave resonance in La^{139} , carried out in collaboration with the Brookhaven Chopper Group. Since this resonance has a neutron width $2g\Gamma_n = 8 \times 10^{-5}$ mV, the peak cross section is very small. The study of the capture gamma rays from this resonance should yield not only the spin of the resonance but information on even parity shell model states in La^{140} at 1 to 2 MeV excitation not populated strongly by s-wave capture. In Fig. 3 we show a portion of two gamma ray spectra, obtained on and below the 0.74 eV resonance respectively. In addition to the La peaks, a number of sulfur peaks (a diluent in the target) and the 2223 keV hydrogen line are seen. While the two spectra resemble each other closely, the intensities of a number of peaks with energies below 4 MeV differ by more than the statistical errors. In particular, we note the shift in relative intensities of the 3665 and 3680 keV peaks in the two runs. The 3680 keV transition is evidently strong in the 0.74 eV resonance capture spectrum.

Still another current experiment is the study of the $\text{U}^{235}(n,\gamma)$ reaction. The principal objective of this work is the determination of the spins of certain resonances by observing transitions from the 3- or 4- capture states to low-lying collective levels in U^{236} . A great deal of effort has been devoted to various attempts to determine the spins of U^{235} resonances at several laboratories with rather inconclusive results. Since the capture to fission ratio α fluctuates considerably from resonance to resonance in U^{235} , our equipment has a particular advantage in providing a beam at an energy where this ratio is most favorable. We have chosen the 4.845 eV resonance for an initial experiment, where $\Gamma_\gamma = 35$ mV and $\Gamma_f = 4$ mV, or a ratio ~ 20 times more favorable than at thermal energy. We find, for example, that with a 14 gm target of U^{235} the fast neutron background from fission events at our Ge(Li) detector is only $\sim 10/\text{cm}^2\text{-sec}$. Our initial results indicate that any high energy gamma rays present are extremely weak. Several peaks, however, were fitted by our computer program. In particular, peaks were found at 6400, 6928, and 5493 keV. The energy separation of these peaks matches closely that of known states in U^{236} at 45 keV (0,2+), 148 keV (0,4+), and 952 keV (0,2+'). This gives a neutron separation energy $S_n = 6445 \pm 2$ keV, to be compared with the least squares adjusted value of Mattauch, Thiele, and Wapstra [7] of $S_n = 6467 \pm 18$ keV. These results should be viewed as tentative, however, until we make further runs with improved statistics.

We have also investigated the low energy region. A careful search of the energy region below 500 keV at high resolution (~ 1 keV) failed to reveal any peaks attributable to neutron capture. At higher energies, however, a number of such peaks appear. For example, the 641.7 and 687.0 keV transitions from the 687 keV level in U^{236} are very strong. A number of other peaks correspond to internal conversion lines observed by Prokofiev, Balodis, and coworkers in Riga [8]. Finally, the 909 keV transition observed by Durham, Rester, and Class [9] in Coulomb excitation is also present.

References

- [1] K. T. Faler, R. R. Spencer, and R. A. Harlan, Nucl. Phys. A123, 616 (1969).
- [2] R. H. Vogt and G. E. Holloway, Bull. Am. Phys. Soc. 1, 433 (1964).
- [3] Del. Electronics Corp., Mt. Vernon, N.Y.
- [4] U.S. Borax Co. "Liquibor 524".
- [5] I. G. Schröder, M. McKeown, and G. Scharff-Goldhaber, Phys. Rev. 165, 1184 (1968).
- [6] M. A. Mariscotti, W. R. Kane, and G. T. Emery, Bull. Am. Phys. Soc. 12, 597 (1967).
- [7] J. H. E. Mattauch, W. Thiele, and A. H. Wapstra, Nucl. Phys. 67, 73 (1965).
- [8] P. T. Prokof'ev, M. K. Balodis, Ya. Ya. Berzin, V. A. Bondarenko, N. D. Kramer, E. Ya. Lure, G. L. Rezvaya, and L. I. Simonova, Atlas of Internal Conversion Electron Spectra Emitted Upon Capture of Thermal Neutrons by Nuclei with A=143 to 197 and Schemes of Radiative Transitions, pp. 125-126 (Zinatne, Riga, 1967).
- [9] F. E. Durham, D. H. Rester, and C. M. Class, Proc. Int. Conf. on Nuclear Structure, Kingston, Aug. 29 - Sept. 3, 1960, D. A. Bromley and E. W. Vogt, Editors, pp. 594-598 (University of Toronto Press, Toronto, and North-Holland Publishing Co., Amsterdam, 1960).

SIMPLE AND ACCURATE CALIBRATION TECHNIQUE FOR MEASURING GAMMA-RAY ENERGIES AND Ge(Li) DETECTOR LINEARITY *

(Abstract only)

M. G. STRAUSS, F. R. LENKSZUS, J. J. EICHHOLZ
Argonne National Laboratory,
Argonne, Ill., United States of America

(Presented by H.H. Bolotin)

Abstract

SIMPLE AND ACCURATE CALIBRATION TECHNIQUE FOR MEASURING GAMMA-RAY ENERGIES AND Ge(Li) DETECTOR LINEARITY. A technique for precise calibration of Ge(Li) gamma-ray spectrometers, which is particularly useful in studies of decay schemes, has been developed. The differential response of a multichannel analyser is measured with a sliding pulse generator whose incremental non-linearity is 0.005 - 0.01%. The integral of this response with respect to counts is a linear function of energy. With the use of two known gamma-ray lines the calibration constant in counts/keV and, in turn, the energies corresponding to unknown gamma-ray peaks can be determined. The technique is simple, fast and virtually automatic. The method was evaluated by measuring gamma-ray energies (0.27 - 2.75 MeV) from ten sources. The results obtained agree with published values to within the measurement uncertainty of 40 - 110 eV. The accuracy of the technique depends on the linearity of the sliding pulser and the Ge(Li) detector. From a spectrum of ^{66}Ga measured energy intervals of $2 m_0 c^2$ were examined as a function of gamma-ray energy. The standard deviation of the eight $2 m_0 c^2$ intervals was only 0.08 keV. It is therefore concluded that between 1 and 5 MeV the incremental non-linearity of the coaxial Ge(Li) detector is less than ± 0.1 keV. Measurement uncertainties due to errors in the calibration standards, peak location and the number of counts/channel in the differential response are discussed.

* Work performed under the auspices of the US Atomic Energy Commission. The full text of this paper will be published in Nuclear Instruments and Methods.

EXPERIENCE WITH A THREE-CRYSTAL PAIR AND ANTI-COMPTON SPECTROMETER FOR (n, γ) SPECTROSCOPY

(Abstract only)

J.D. JAFAR, A.A. ABDULLA, N.H. AL-QURAISHI, M.S. ALWASH,
J. KAJFOSZ*, I.Y. KHADDURI, M.A. KHALIL, Z. KOSINA*

Physics Division,
Nuclear Research Institute,
Atomic Energy Commission,
Baghdad, Iraq

Abstract

EXPERIENCE WITH A THREE-CRYSTAL PAIR AND ANTI-COMPTON SPECTROMETER FOR (n, γ) SPECTROSCOPY. The paper describes a spectrometer system that is useful in high-resolution gamma spectroscopy. The system consists of a 10-cm³ Ge(Li) central detector surrounded by a split-ring annular NaI(Tl) scintillation crystal. The spectrometer can be operated in the anti-Compton mode and/or as a three-crystal pair spectrometer. A computer program was developed for the automatic analysis of gamma-ray spectra and includes position finding, Gaussian-shape line fitting and plotting routines for the gamma peaks. The (n, γ) spectrum from natural chlorine was measured with this spectrometer and the energies and intensities of 190 resolved gamma-ray lines are reported. A bootstrap technique was used to generate a self-consistent energy calibration and a Q-value of 8580.7 \pm 1 keV was obtained for the ³⁵Cl(n, γ) reaction.

* Permanent address: Nuclear Research Institute, Řež near Prague, Czechoslovakia

MEASUREMENT OF RESONANCE NEUTRON CAPTURE GAMMA RAYS USING A Ge(Li)-NaI SPECTROMETER AND AN ELECTRON LINAC ^{*}

(Abstract only)

V.J. ORPHAN, C.G. HOOT, A.D. CARLSON,
J. JOHN, J.R. BEYSTER
Gulf General Atomic Incorporated,
San Diego, Calif.,
United States of America

Abstract

MEASUREMENT OF RESONANCE NEUTRON CAPTURE GAMMA RAYS USING A Ge(Li)-NaI SPECTROMETER AND AN ELECTRON LINAC. A study of resonance neutron capture gamma-ray spectra using a Ge(Li)-NaI spectrometer and a pulsed LINAC neutron source is described. The Ge(Li)-NaI spectrometer can be operated simultaneously in the Compton-suppression mode for gamma rays below about 3 MeV and in the three-crystal pair spectrometer mode for higher-energy gamma rays. The gamma-ray pulse height and the corresponding neutron time-of-flight are recorded using an on-line computer. The principal features of the capture gamma-ray facility are described and spectra resulting from the capture of neutrons in natural tungsten are shown.

^{*} Supported by the US Atomic Energy Commission and performed under subcontract No. 3032 with Union Carbide Corporation. The text and results of the paper have been accepted for publication by Nucl. Instrum. Meth. under the title "Neutron capture gamma-ray facility using an electron linear accelerator" by the same authors.

SPECTROMETRY OF PHOTONS EMITTED BY REACTIONS INDUCED BY FAST NEUTRONS ON VARIOUS ELEMENTS

G. HAOUAT, J. LACHKAR, Y. PATIN, J. SIGAUD

Commissariat à l'énergie atomique,
Centre d'études de Bruyères le Chatel,
France

Abstract

SPECTROMETRY OF PHOTONS EMITTED BY REACTIONS INDUCED BY FAST NEUTRONS ON VARIOUS ELEMENTS. The following paper describes briefly a spectrometer used for the study of photons emitted by fast neutron reactions and gives some experimental data on various elements.

We have investigated and realized a spectrometer for studying the photons emitted by fast neutron reactions.

The photons are detected by a spectrometer composed of a large-volume coaxial Ge(Li) detector surrounded by a $305 \times 305 \times 80$ mm NaI(Tl) crystal divided into 4 optically separated sectors [1]. Associated electronics perform the analog treatment of the information detected and permit the simultaneous recording of the gamma spectra in the 3 principal modes: (1) photoelectric and anti-Compton in the range 0.3 - 8 MeV; (2) pair effect above 1.022 MeV; and (3) total absorption in the range 60 - 300 keV.

The continuous Compton background is reduced by the anticoincidence selector by the following factors: 8 for photons of 663 keV; 6.5 for photons of 2.614 MeV; and 3 for photons of 6.14 MeV. The attenuation of the total absorption peak is less than 20%.

The stability of the spectrometer is of the order of ± 300 eV/d. The optimization of the large-volume coaxial Ge(Li) detector's time definition [2, 3] allows time discrimination of scattered neutrons and gamma rays by a time-of-flight method.

The production time of the neutrons is defined either by the associated particle method ($E_n = 2.5$ and 14.1 MeV for the 400-keV Van de Graaff) or by the pulsed-beam method of a tandem Van de Graaff accelerator.

The time information is selected either at the output of the charge preamplifier (charge pulse) or at the extremities of a low-value resistor in series with the charge resistance (current pulse). This last method reduced appreciably the influence of the position of photon detection. The time resolution of our detector is about 5 nsec for photons with energy above 500 keV.

We have studied the response of the Ge(Li) detector to an important background from scattered neutrons. In a coaxial diode the mean field is weak, and the recombination of the electron-hole pairs produced by highly ionizing particles is important. For the same energy the charge collected is different for a Ge recoil nucleus, an alpha particle and an

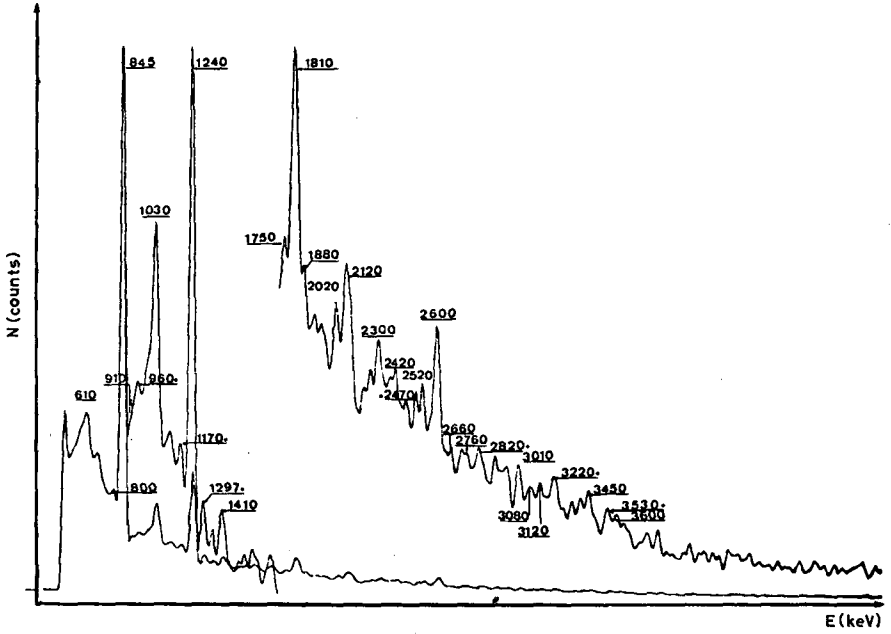


FIG. 1. (n-n' γ) reaction for natural iron; $E_n = 8.7$ MeV.

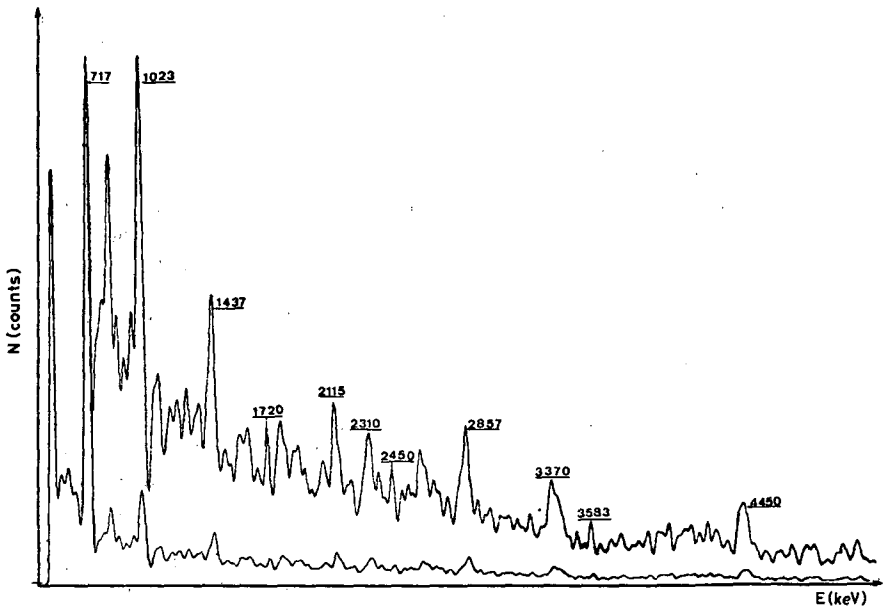


FIG. 2. (n-n' γ) reaction for ^{10}B .

electron and consequently the (n, α) reactions on Ge isotopes are difficult to identify. Moreover, in an elastic collision, the recoil energy of Ge is recorded with weak efficiency [4].

The most apparent aspect of the interaction of neutrons on Ge is the detection of a large peak corresponding to the de-excitation of a ^{72}Ge 0^+ level at 691 ± 1 keV energy [5]. This long life (300 nsec) has an internal conversion decay. According to our calibration, the energy of this peak is equal to 696 ± 0.5 keV.

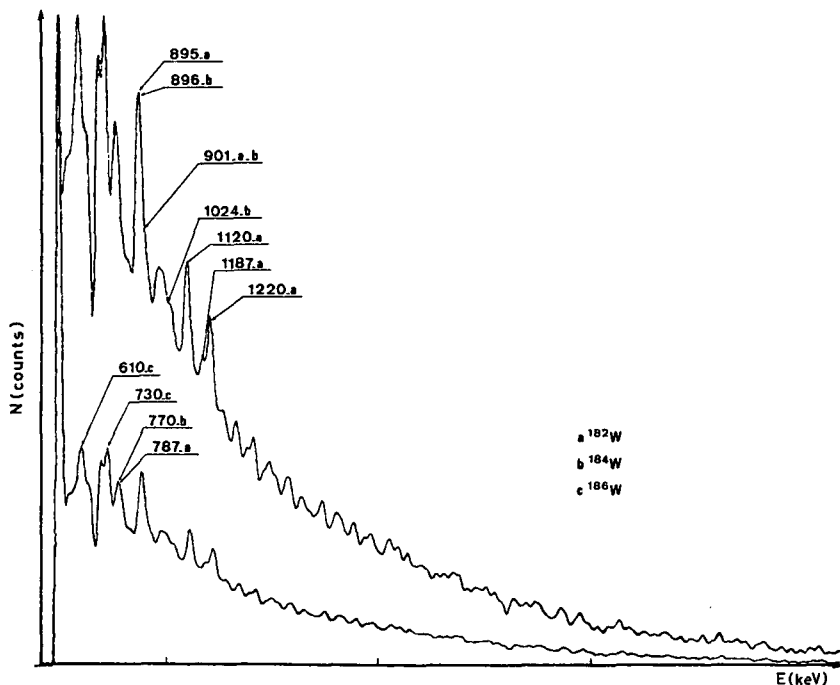


FIG. 3. $(n-n'\gamma)$ reaction for tungsten; $E_n = 8.7$ MeV, $\theta = 90^\circ$.

This energy does not depend on the incident neutron energy which suggests that the recoil ^{72}Ge energy contributes only a small part to the total energy detected. On the other hand, we have observed an increase in the FWHM and a symmetry of this peak when the energy of neutrons increased.

This spectrometer has been used to study the $(n-n'\gamma)$ reaction at 2.5, 8, 8.72 and 14.1 MeV; some typical spectra are shown in Figs 1-3. The cross-sections and angular distributions of the more intense transitions of natural Fe, ^{10}B , ^{182}W and ^{184}W have been recorded. They show that the various experimental techniques used here allow a fruitful study of the emitted photons by reaction of fast neutrons.

REFERENCES

- [1] LACHKAR, J., ROQUEFORT, H., CEA Rep. R 3747 (1969).
- [2] HAOUAT, G., LACHKAR, J., SIGAUD, J., Proc. Int. Symp. Nuclear Electronics, Versailles, 1969, Vol. 1.
- [3] SAKAI, E.J., IEEE Trans. nucl. Sci., 15 3 (1968) 310-320.
- [4] CHASMAN, C., Nucl. Instrum. Meth., 37 (1965) 1.
- [5] MacGOWAN, F.K., Rep. ORNL 952 (1951).

GAUSSIAN PRODUCT FUNCTIONS APPLIED TO AUTOMATIC ANALYSIS OF GAMMA-RAY SPECTRA *

(Abstract only)

I. A. SLAVIĆ

Boris Kidrič Institute of Nuclear Sciences,
Belgrade, Yugoslavia

Abstract

GAUSSIAN PRODUCT FUNCTIONS APPLIED TO AUTOMATIC ANALYSIS OF GAMMA-RAY SPECTRA. The paper presents some new functions deduced from the Gaussian function in a simple way. These functions, called Gaussian product functions, can be used for automatic analysis of gamma-ray spectra giving a real range of the peaks and their widths. Thus, it is possible to base the analysis very precisely on the observation of widths.

* A more detailed version of this paper will be published by I. A. Slavić and S. P. Bingulac in Nuclear Instruments and Methods.

CONVERSION ELECTRON STUDIES OF (n, γ) REACTIONS

Chairman: O.W.B. SCHULT

RECENT EXPERIMENTS FOR NEUTRON CAPTURE CONVERSION ELECTRONS

T. von EGIDY

Technische Hochschule,

Munich, Federal Republic of Germany

Abstract

RECENT EXPERIMENTS FOR NEUTRON CAPTURE CONVERSION ELECTRONS. The information on the structure of the nucleus which can be obtained by measuring conversion electrons following neutron capture is discussed. The electron spectrometers in operation at Munich, Studsvik, Riga, Moscow, Leningrad and Argonne and the one planned for the high flux reactor at Grenoble are described briefly and compared with the aid of different figures of merit.

1. INTRODUCTION

In 1938 Hoffman and Bacher [1] observed electrons following neutron capture for the first time. They put a cadmium sheet on a photographic plate in a neutron flux and found much more blackening without an absorber than with a thin absorber. In the same year Fleischmann [2] independently measured conversion electrons in Cd and determined a conversion coefficient. The first magnetic spectrometer for neutron capture conversion electrons was constructed by Hibdon and Muehlhause [3] in 1951. Several other groups installed spectrometers for this purpose [4-7] but could only investigate isotopes with very high capture cross-sections. At present there are instruments in operation in Munich, Studsvik, Riga, Moscow, Leningrad and Argonne. Spectrometers for coincidence measurements with neutron capture conversion electrons are used by two groups [8, 9].

The energies and intensities of conversion electron lines provide valuable information on transitions in nuclei. At energies between 1 and 3 MeV conversion electrons can sometimes give the most accurate energy values. Some transitions such as E0 and low-energy lines with high multipolarity can only be observed in the electron spectrum. The intensity enables one to calculate the multipolarity (and the mixing of the multipolarities) of the transitions by K:L-ratios, L-subshell ratios or conversion coefficients. At low energies the electron intensity contributes appreciably to the total intensity of transitions. With the multipolarity of the transitions one can determine the parity of the levels, set limits to the spin of the levels and give the Ritz combination principle more reliability for new levels.

2. CHARACTERISTICS OF THE SPECTROMETERS

A spectrometer for conversion electrons from neutron capture must have very good resolution, very good sensitivity and a low background to separate as many lines as possible in the electron spectra, which are

very complex in many cases (see Fig.10). The L-lines should at least be resolved for lines below 500 keV because their intensity ratio is very sensitive to the multipolarity. The dynamic range of a spectrometer has to have several orders of magnitude so that large (small) branching ratios, which are important checks of nuclear models, can be determined.

There are two possible arrangements for a conversion electron spectrometer at the reactor: the internal target geometry (target close to the reactor core, electrons being extracted through a collimator) and the external target geometry (target in an external neutron beam). The first has the advantage of higher intensity, while the second permits easier changes in the target and coincidence measurements. In most cases magnetic spectrometers have been used. At Argonne a semiconductor spectrometer arrangement was set up [10-12] and a similar experiment has been planned at Frankfurt [13].

It is difficult to compare different spectrometers because they differ not only in sensitivity and resolution, but also in measuring time, background (depending on energy), reactor arrangement, reactor type and relations between all parameters. It is, however, possible to define figures of merit to compare spectrometers. The line intensity is proportional to the target area A , the solid angle in the spectrometer Ω and the neutron flux at the target Φ :

$$I = A \cdot \Omega \cdot \Phi$$

The sensitivity depends on the line intensity and the background counting rate:

$$S = \frac{I}{\sqrt{I+B}}$$

and for small lines:

$$S = \frac{I}{\sqrt{B}}$$

Bieber [14] defined a figure of merit which relates the line intensity to the maximal thermal neutron flux of the reactor:

$$Q_1 = \frac{I}{\Phi_{\max}}$$

Since there is usually a relation between the line intensity of a spectrometer and the resolution $R = dp/p$, Demidov [15] gives another figure of merit:

$$Q_2 = \frac{I}{R}$$

One can combine these formulas, taking into consideration that the sensitivity of a spectrometer increases only with the square root of the reactor power ($\propto \Phi_{\max}$), because the background will also increase [16]:

$$Q_3 = \frac{I}{R \sqrt{B \Phi_{\max}}}$$

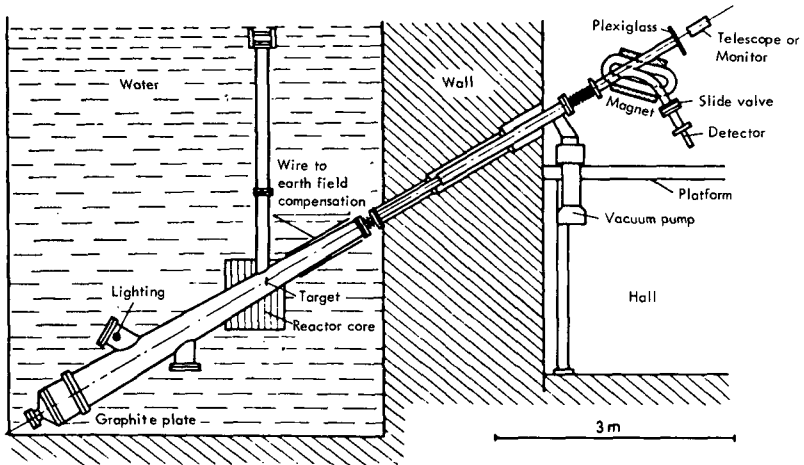


FIG. 1. Spectrometer at Munich.

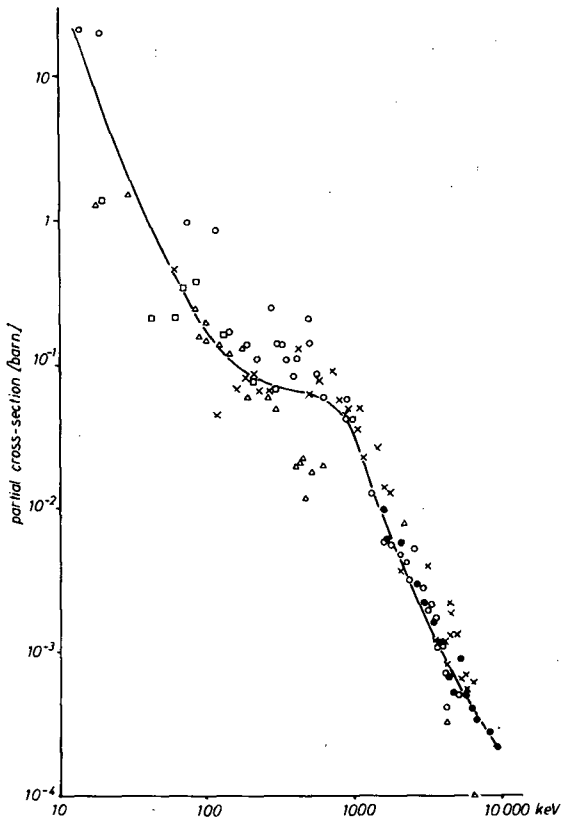


FIG. 2. Partial capture cross-section of the weakest conversion lines measured with the Munich spectrometer. ● ^{114}Cd , × ^{150}Sm , ○ ^{165}Dy , △ ^{198}Au , □ ^{188}Re . The curve corresponds roughly to the sensitivity of the spectrometer at 1-MW reactor power.

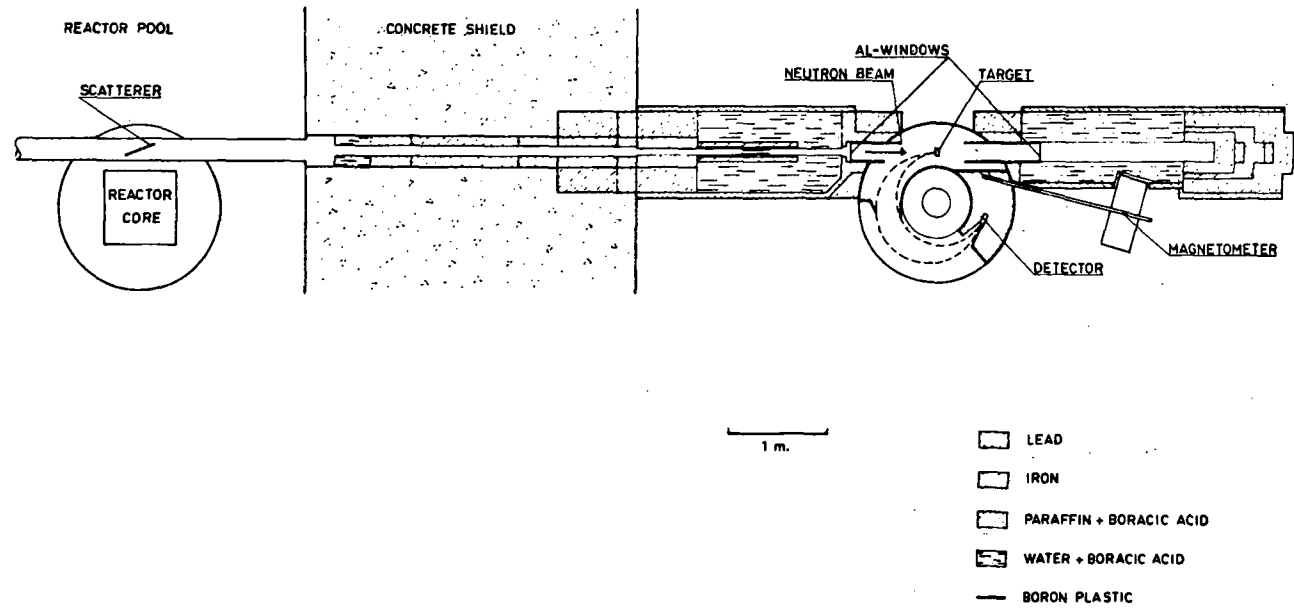


FIG. 3. Spectrometer at Studsvik.

3. THE SPECTROMETER AT MUNICH

The Munich spectrometer is shown in Fig.1 [17-20]. It has an internal target geometry. The spectrometer magnet is a combination of a homogeneous and a $1/r$ sector field which deflects the electrons by 90° and which is double focusing. With a biased target (15 kV) the electrons are preaccelerated and it is possible to measure electrons from zero energy upwards. The partial cross-sections (electron intensity per capture times capture cross-section) of the smallest detected lines of several isotopes are plotted in Fig.2. This gives the experimental curve for the sensitivity (at 1-MW reactor power) of the spectrometer in dependence on the energy. One can measure high-energy conversion electrons because the sensitivity improves at about the same rate as the conversion coefficient decreases. The reason for this is the lower background at higher energies. Therefore the Munich spectrometer was the first to measure conversion electrons up to 9 MeV, although the conversion coefficient is only 10^{-5} at these high energies.

4. THE SPECTROMETER AT STUDSVIK

The spectrometer at Studsvik (Fig.3 [21-23]) is of the $\pi\sqrt{2}$ type and has therefore a good resolution. The smaller intensity - because of the external target geometry - is compensated by the high neutron flux of the 30-MW reactor and by a multiple target arrangement. 20 target strips are biased up to 35 kV. This arrangement can only be used below 1.4 MeV. The efficiency for higher energies is much worse because of this reason.

5. THE SPECTROMETER AT RIGA

The spectrometer at Riga (Fig.4 [24-26]) uses the internal target geometry. The electrons are guided by a Mu-metal tube into a homogeneous magnetic field. The shape of the end of this tube causes double focussing. Electrons of different energies are registered simultaneously with a photographic plate. This permits the measurement of one spectrum within a few hours. But the intensity error is always rather large.

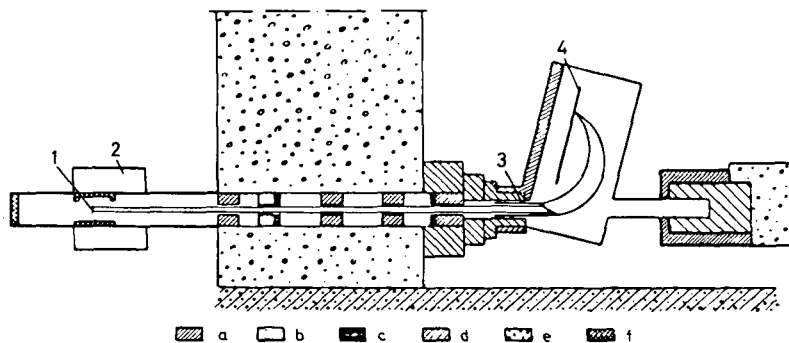


FIG.4. Spectrometer at Riga: 1. target; 2. reactor core; 3. magnetic shield; 4. photographic plate.

6. THE NEW SPECTROMETER AT MOSCOW

In 1968 a new spectrometer was installed in Moscow (Fig.5 [27]) which is similar to the old one [7], but has an average radius of 60 cm instead of 30 cm. The electrons from an external target pass through two $\pi\sqrt{2}$ spectrometers. Between the spectrometers is a transmission detector which is in coincidence with the final detector to reduce the background. The resolution and the target size have been increased compared to the old spectrometer. The neutron flux at the target is supposed to be $10^7 \text{ n cm}^{-2} \text{ sec}^{-1}$ [27]. With this flux and with the target area and the solid angle one calculates an intensity of the ^{150}Sm lines [27] which is about a factor of 10 too low. Therefore the neutron flux was assumed for the figures of merit in Table I to be about $10^8 \text{ n cm}^{-2} \text{ sec}^{-1}$. The spectrometer was adjusted to measure electrons with energies between 1.5 and 8 MeV.

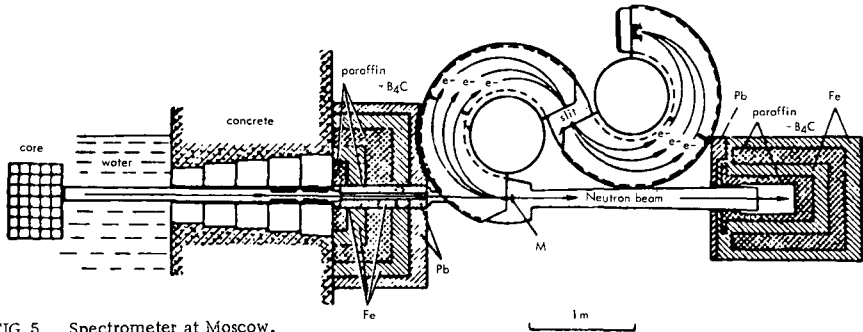


FIG.5. Spectrometer at Moscow.

7. THE SPECTROMETER IN LENINGRAD

A new type of an internal target geometry spectrometer has been constructed in Leningrad (Fig.6 [28]). A magnetic lens produces an image of the target outside the reactor shielding. This image is the source for a 180° inhomogeneous sector field spectrometer. This arrangement has good resolution and good sensitivity. Electrons with an energy up to 4 MeV can be measured. The distance between the target and the reactor core is larger than in the Munich and in the Riga spectrometers. This reduces the background from core gamma radiation.

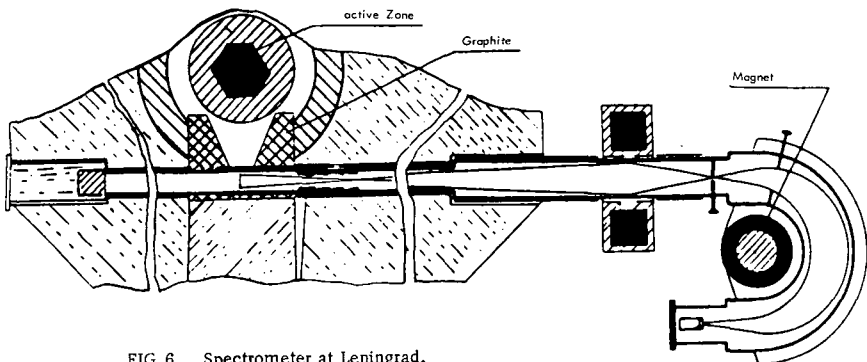


FIG.6. Spectrometer at Leningrad.

8 THE SEMICONDUCTOR SPECTROMETER IN ARGONNE

Burson and co-workers [10-12] were the first to measure neutron capture conversion electrons with a semiconductor detector (Fig.7). The main difficulty of such an arrangement is the sensitivity of these detectors to gamma radiation. The gamma background is nearly completely eliminated by extracting the electrons with the strong magnetic field of a superconducting coil. The electrons from an external target describe helical paths about the magnetic field lines to the detector which is 25 cm away. Four per cent of the electrons leaving the target reach the detector. This can be increased up to 50%. Since such a spectrometer permits the analysis of all energies simultaneously, the sensitivity is very good, especially for isotopes with low capture cross-sections. The resolution above 2 MeV might be better than that of a magnetic spectrometer. Till now this system has been used only for electrons with energies less than 2 MeV.

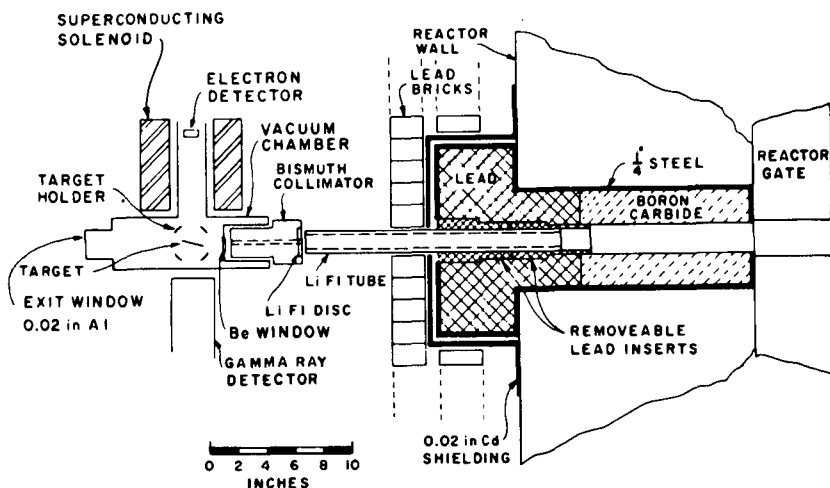


FIG.7. Spectrometer at Argonne.

9. THE PROJECTED SPECTROMETER AT GRENOBLE

A new spectrometer has been planned at the High Flux Reactor at Grenoble [29]. An improved spectrometer was calculated by Mahlein [30] in which the electrons of the internal target are first deflected and double focussed by a 60° sector field. The focus is the source for a 290° sector field spectrometer which consists of homogeneous fields and a 216° $1/r$ field (Fig.8). This gives a very good dispersion. Figure 9 shows the arrangement at the reactor [31]. The target is exchanged through a vertical tube. The tube for the electrons is slightly inclined. The ratio of the neutron flux to the gamma flux near the target is much better than in the Munich spectrometer because of the 80 cm of heavy water between

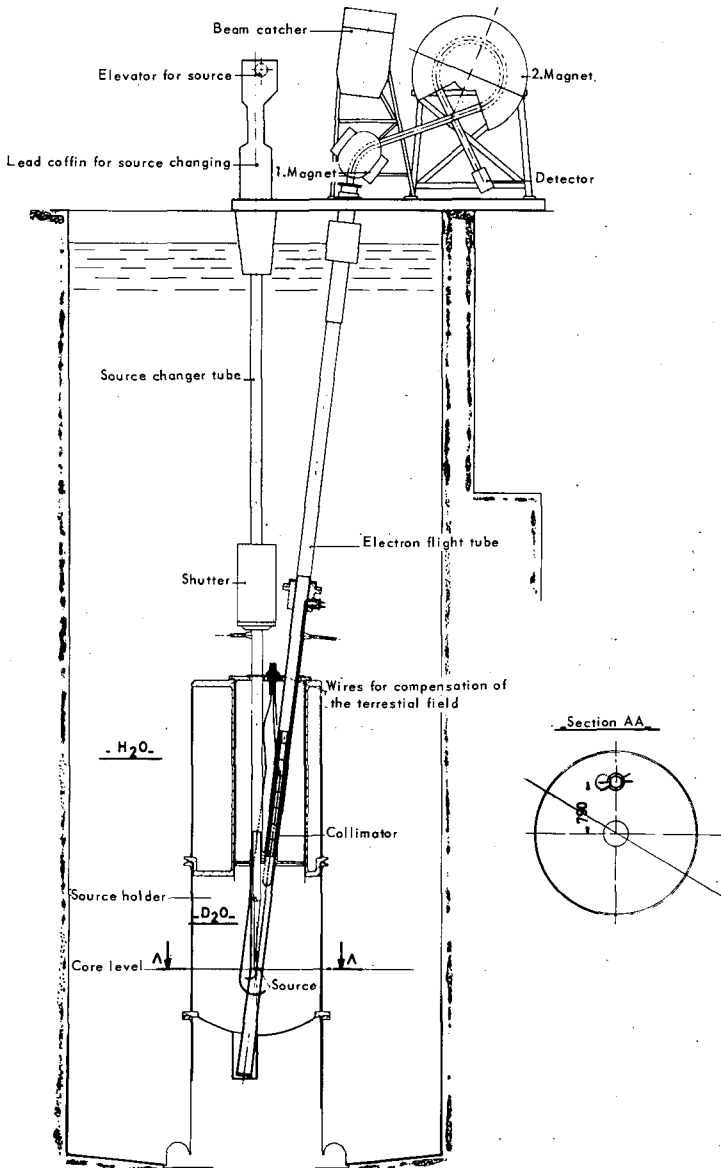


FIG. 9. Conversion electron spectrometer at the HFR Grenoble.

TABLE I. COMPARISON OF THE SPECTROMETERS

Data	Munich	Studsvik	Riga	Moscow	Leningrad	Argonne	Grenoble
Reactor	FRM	R2	IRT - C	IRT - M - IAE	WWR - M	CP - 5	HFR - ILL
Power (MW)	4	30	2	2	10	5	57
Φ_{\max} : max. therm. flux ($n \text{ cm}^{-2}\text{sec}^{-1}$)	5.5×10^{13}	3×10^{14}	3.2×10^{13}	3.2×10^{13}	10^{14}	10^{14}	1.5×10^{15}
Target geometry	internal	external	internal	external	internal	external	internal
Distance target - core (m)	0.1	8	0.1	4.2	0.8	5	0.7
Distance target - spectrometer (m)	5	0	5	0	5.5	0.25	13.5
Φ : n-flux at target ($n \text{ cm}^{-2}\text{sec}^{-1}$)	6×10^{12}	1.4×10^8	5×10^{12}	10^7 ; (10^8)	10^{12}	(10^7)	3×10^{14}
Type of spectrometer	inhom. sector field	$\pi\sqrt{2}$	hom. f. spectrograph	$2 \times \pi\sqrt{2}$	lens + inhom. sector field	semiconductor + supercond. solen.	2 inhom. sector field
Ω : solid angle (spectrom.) (of 4π)	10^{-5}	3×10^{-3}	2.5×10^{-5}	3×10^{-3}	2.5×10^{-5}	0.04	5×10^{-6}
A: target area (cm^2)	1.2×8	4×5	$3 \times 3 \times \pi$	1×5	2×8	$1.7 \times 1.7 \times \pi$	2.5×8
R: resolution (best-normal) (%)	0.08 - 0.3	0.18 - 0.3	0.07 - 0.4	0.19 - 0.38	0.13 - 0.21	(0.4)	0.04×0.15
Energy range (MeV)	0 - 10	0.01 - 4	0.03 - 3	1.5 - 10	- 4	0.03 - 2	0.03 - 10
B: background (cpm)	below 500 keV: 15 000 - 80 000 above 8 MeV: 500	below 150 keV: 40 - 120 above 150 keV: 20	about 80 000	about 10 at 5 MeV: 1	at 900 keV: 35 000	about 100	below 500 keV: 10 000 - 100 000
Line intensity $I = A \cdot \Omega \cdot \Phi$ (sec^{-1})	6×10^8	8×10^8	$3.5 \times 10^8 \times 100$	(1.5×10^5)	4×10^8	$4 \times 10^6 \times 1000$	3×10^{10}
Sensitivity $S = A \cdot \Omega \cdot \Phi / \sqrt{B}$ ($\text{sec}^{-1/2}$)	2×10^6	2×10^8	$1.3 \times 10^6 \times 10$	(5×10^5)	2×10^6	$4 \times 10^5 \times 30$	10^8
Figure of merit:							
Bieber: $Q_1 = 1/\Phi_{\max}$ (cm^2)	10^{-5}	3×10^{-3}	$10^5 \times 100$	(5×10^{-3})	4×10^{-6}	$4 \times 10^{-3} \times 1000$	2×10^{-5}
Demidov: $Q_2 = 1/R$ (sec^{-1})	3×10^{11}	4×10^9	$1.4 \times 10^{11} \times 100$	(5×10^8)	3×10^{11}	$10^9 \times 1000$	3×10^{13}
Egidy: $Q_3 = 1/(R\sqrt{B} \cdot \Phi_{\max})$ (cm)	140	50	90×10	(30)	160	10×30	3000

According to the values in Table I, the Munich, Studsvik, Riga, Moscow and Leningrad spectrometers have very similar resolution. The resolution of the Argonne semiconductor spectrometer is worse by more than a factor two, the resolution of the projected Grenoble spectrometer is expected to be better. The sensitivity of the Grenoble spectrometer is expected to be at least an order of magnitude better than any of the other spectrometers. The spectroscopes in Riga and Argonne have better sensitivity than the other existing ones because they collect different energies at the same time. The spectrometers in Munich, Studsvik and Leningrad have about the same sensitivity. The different figures of merit show again that the Grenoble spectrometer is expected to be superior to the others. The instruments in Riga and Argonne are better if one includes the factor for multichannel registration. The spectrometers in Leningrad and Munich have very similar figures of merit. The magnetic spectrometers with external target geometry have a smaller figure of merit.

The best way to compare the efficiency of the spectrometers is to look at the measurements, especially where the same isotope has been measured by different groups. The fastest spectrometer is certainly the one in Riga, because this group has measured 37 isotopes in the last 5 years, while 15 isotopes were measured in Munich and 10 in Studsvik. The sensitivity of the spectrometers which corresponds to the number of detected lines is very similar in Studsvik and Riga. The Munich spectrometer in several cases found more, or at least the same number of lines as the Riga spectrometer. The energy and intensity errors are usually smaller in the results of the Munich and Studsvik spectrometer than in the results from Riga.

In Fig. 10 spectra of ^{158}Gd near 900 keV measured in Studsvik [32], Leningrad [28] and Munich [33] are compared. The resolution of the Leningrad spectrum is slightly better than that of the Studsvik spectrum, while that of the Munich spectrum looks worse. This is caused by the thicker target installed for high-energy measurements. The high-energy slope of the lines which corresponds to the spectrometer resolution without influence of the target thickness is as steep as in the other spectra. The sensitivity is about the same in all three spectra. ^{158}Gd was measured in Riga too [34], but no graph was published and the table is not in good agreement with the other results.

The high-energy spectrum of ^{150}Sm was measured in Munich [35, 36] and Moscow [24]. The resolution was 0.35% in Munich and 0.38% in Moscow. With a measuring time of 45 min per point the sensitivity of the Moscow spectrometer was slightly better than the sensitivity of the Munich spectrometer with 6 min measuring time per point.

REFERENCES

- [1] HOFFMAN, J.G., BACHER, R.F., Phys. Rev. 54 (1938) 644.
- [2] FLEISCHMANN, R., Z. Physik 111 (1938) 281.
- [3] HIBDON, C.T., MUEHLHAUSE, C.O., Phys. Rev. 83 (1951) 235; 87 (1952) 222; 88 (1952) 943.
- [4] CHURCH, E.L., GOLDHABER, M., Phys. Rev. 95 (1954) 626.
- [5] MOTZ, H.T., Phys. Rev. 104 (1956) 1353.
- [6] GROSHEV, L.V., DEMIDOV, A.M., NAIDENOV, V.A., Bull. Acad. Sci. USSR, Phys. Ser. 21 (1957) 1606.

- [7] PELEKHOV, V.I., MALOV, A.F., Bull. Acad. Sci. USSR, Phys. Ser. 25 (1961) 1077.
- [8] GOVOR, L.I., IVANOV, V.A., Izv. Akad. Nauk SSSR, ser. fiz. 31 (1967) 277.
- [9] BOROVIKOV, A.V., GVOZDEV, V.S., PORSEV, G.D., Sov. J. nucl. Phys. 7 (1968) 694.
- [10] BURSON, S.B., Rep. ANL-7282 (1966) 297.
- [11] BURSON, S.B., DALY, P.J., GOUDSMIT, P.F.A., Bull. Am. phys. Soc. 13 (1968) 673.
- [12] GOUDSMIT, P.F.A., Thesis, University of Amsterdam (1969).
- [13] WALDSCHMIDT, M., Verhandlungen der Deutschen Phys. Ges. 4 (1968) 366.
- [14] BIEBER, E., Rep. ANL-6797 (1963) 148.
- [15] DEMIDOV, A.M., Metody issledovaniya izlucheniya yader pri radiacionnom zahvate teplovyh neutronov, Gosatomizdat, Moscow (1963).
- [16] von EGIDY, T., Habilitationsschrift, Technische Hochschule, Munich (1968).
- [17] von EGIDY, T., Ann. Physik 9 (1962) 221.
- [18] BIEBER, E., von EGIDY, T., SCHULT, O.W.B., Z. Physik 170 (1962) 465.
- [19] SCHULT, O.W.B. et al., "Experimental arrangements for the measurement of neutron capture radiation, in particular in-pile components", Research Reactor Experimental Techniques (Proc. Study-Group Meeting Bucharest, 1964), Editura Academiei Republicii Socialiste România, Bucharest (1966) 477.
- [20] NÖRENBERG, W., Z. angew. Phys. 17 (1964) 452.
- [21] BÄCKSTRÖM, G., BÄCKLIN, A., HOLMBERG, N.E., Nucl. Instrum. Meth. 16 (1962) 199.
- [22] BÄCKLIN, A., HOLMBERG, N.E., BÄCKSTRÖM, G., Nucl. Phys. 80 (1966) 154.
- [23] BÄCKLIN, A., Nucl. Instrum. Meth. 57 (1967) 261.
- [24] BALODIS, M.K., OSIS, N.L., PROKOF'EV, P.T., Radioaktivnye Izlucheniya i Metody ih issledovaniyach, Riga (1961) 135.
- [25] BALODIS, M., BONDARENKO, V., PROKOF'EV, P., SERMONS, G., Izv. Akad. Nauk latv. SSR 11 (1962) 41.
- [26] BALODIS, M.K., BONDARENKO, V.A., PROKOF'EV, P.T., Bull. Acad. Sci. USSR, Phys. Ser. 28 (1964) 179.
- [27] PANIN, Yu.N., PELEKHOV, V.I., TURGUNTAEV, T.I., Izv. Akad. Nauk SSSR, ser. fiz 33 (1969) 670.
- [28] GVOZDEV, V.S., EMEL'YANOV, B.A., KAMINKER, D.M., SAKHAROV, S.L., KHAZOV, Yu.L., Physico-Technical Institute A.F. Ioffe, Leningrad, 169 (1969).
- [29] von EGIDY, T., Beta spectrometer for internal conversion electrons following neutron capture, beam tube experiment at High Flux Reactor, Grenoble, ILL (1967).
- [30] MAHLEIN, H.F., Nucl. Instrum.Meth. 53 (1967) 229.
- [31] MAIER, B.P.K., private communication.
- [32] BAADER, H.A. et al., "Investigation of the ^{158}Gd level scheme by thermal neutron capture", these Proceedings.
- [33] MAMPE, W., private communication.
- [34] PROKOF'EV, P.T. et al., Atlas of Conversion Electron Spectra following Thermal Neutron Capture of Nuclei with $A = 143$ to $A = 197$ and Level Schemes, Izdatel'stvo "Zinatne", Riga (1967).
- [35] ELZE, Th., von EGIDY, T., BIEBER, E., Z. Physik 184 (1965) 229.
- [36] ELZE, Th., Z. Physik 194 (1966) 280.

CONVERSION ELECTRONS AND GAMMA RAYS FROM NEUTRON CAPTURE IN ^{235}U

A. BÄCKLIN, B. FOGELBERG

Institute of Physics,

Uppsala University, and

The Swedish Research Council's Laboratory,

Studsvik, and

Eva FALKSTRÖM-LUND

Chalmers University of Technology,

Gothenburg, and

The Swedish Research Council's Laboratory,

Studsvik, Nyköping, Sweden

Abstract

CONVERSION ELECTRONS AND GAMMA RAYS FROM NEUTRON CAPTURE IN ^{235}U . Conversion electrons and gamma rays following neutron capture in ^{235}U have been studied. Simple methods to distinguish between lines from ^{236}U and lines from the fission products are given. Preliminary results are given for conversion electrons in the range 0.5 - 1.2 MeV.

Introduction

The level structure of ^{236}U has so far to our knowledge been very little studied. Since the capture cross section of ^{235}U is as high as 100 barns the reaction $^{235}\text{U}(n,\gamma)^{236}\text{U}$ seems to offer good possibilities to study at least the lowest level structure of ^{236}U .

An experimental difficulty in registering the radiation from the (n,γ) process lies in the strong competition from the radiation from the fission process ($\sigma = 580$ b). For intensity reasons a uranium target thick enough to stop a considerable fraction of the fission fragments must be used. Then three types of radiation will compete with the (n,γ) radiation: 1) Prompt radiation from the fission fragments, 2) radiation following beta decay of the fragments, 3) radiation from the possible $(n,\gamma f)$ process.

In this report measurements of conversion electron and gamma-ray spectra are described, which are able to distinguish the (n,γ) and $(n,\gamma f)$ radiations from the radiations from the fragments. The $(n,\gamma f)$ radiation may be observed either by direct observation (1) or by comparison between the present experiment and experiments detecting the gamma-radiation coincident with the fission fragments (1, 2).

Conversion electron measurements

Provided an electron spectrometer with high enough resolving power is used, electron lines from the fission fragments can be distinguished from electrons from ^{236}U simply by using a target thickness definitely smaller than the range of the fission fragments in combination with a backing thick

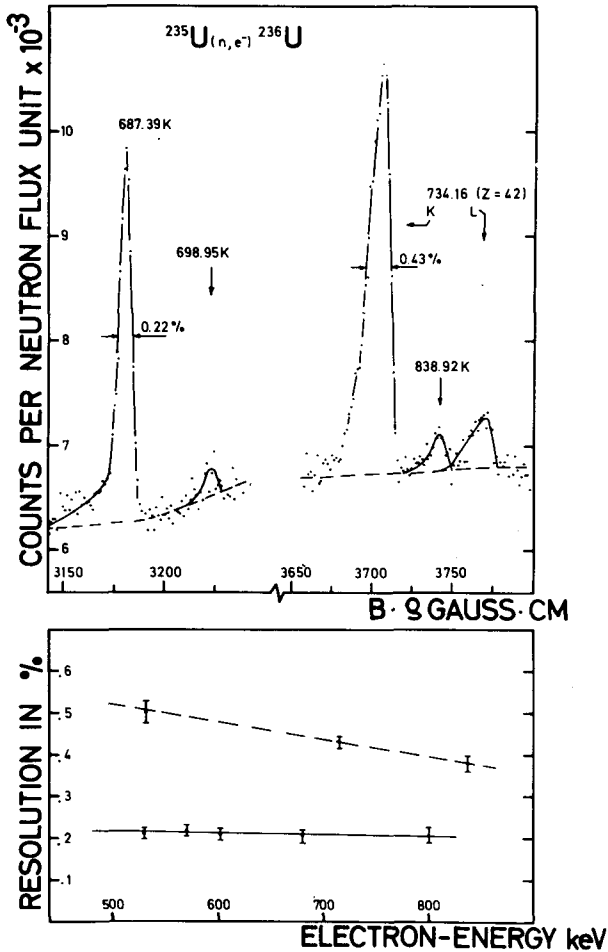


FIG. 1. Top: Parts of the internal conversion electron spectrum. To the left are shown lines assigned to ^{236}U . To the right are the much broader lines from the decay of fission fragments. Bottom: Graph of the relative half-width of conversion lines as a function of energy. Solid line: uranium, dashed line: fission fragments.

enough to stop a considerable amount of the fragments. All electrons lines following the beta decay of the fragments and those "prompt" fission electrons that are emitted after the fragment has stopped, will then give rise to electron lines which are definitely broader than electron lines from ^{236}U . Alternatively, a variation of the thickness of the backing will vary the intensity of the fission product lines relative the ^{236}U lines. The "prompt" fission electrons, which are emitted while the fragments are moving will only contribute to the continuous background or give rise to very broad lines. This is because the high velocity of the fragments which move in all directions will smear out the lines, cf. the shifts of up to 50 keV observed in ref. (2).

The Studsvik double focusing beta spectrometer was employed for the conversion electron measurements. The resolution was adjusted to 0.2 % FWHM.

TABLE I. THE STRONGEST CONVERSION LINES IN THE REGION 0.5 - 1.2 MeV ASSIGNED TO ^{236}U

Electron-energy keV	Error	Transition energy keV	Shell	Relative electron intensity	Error %
526.46	0.17	642.06	K	100	-
			L	26.3	7
540.22	0.17	655.82	K	5.8	15
571.79	0.17	687.39	K	55.0	7
			L	15.2	10
583.35	0.25	698.95	K	4.1	30
674.60	0.20	790.20	K	4.2	25
723.32	0.20	838.92	K	4.5	20
785.65	0.17	901.25	K	9.4	10
			L	(1.9) ^a	-
793.50	0.20	909.10	K	5.0	15
796.76	0.30	912.36	K	4.2	30
799.50	0.25	915.10	K	11.7	10
			L	<2.3	
803.30	0.30	918.90	K	3.6	20
850.20	0.25	965.80	K	4.2	30
879.34	0.25	994.94	K	7.8	15
906.73	0.25	1022.33	K	4.6	30
984.46	0.25	1100.06	K	2.3	30

a) Subtracted from 994.94 K

TABLE II. THE STRONGEST CONVERSION LINES ASSIGNED TO FISSION PRODUCTS

Electron-energy ^{a)} keV	Error	Suggested interpretation
302.2	-	^{133}Te , K 334.0
492.4	-	^{135}Xe , K 527
537.70	0.30	
601.48	0.60	
631.31	0.50	
714.16	0.20	} K- and L-lines of transition in Mo
731.22	0.30	
835.00	0.20	} K- and L-lines of transition in La
867.54	0.60	

a) The energy-values given have not been corrected for the energy-loss suffered by the electrons in the backing material.

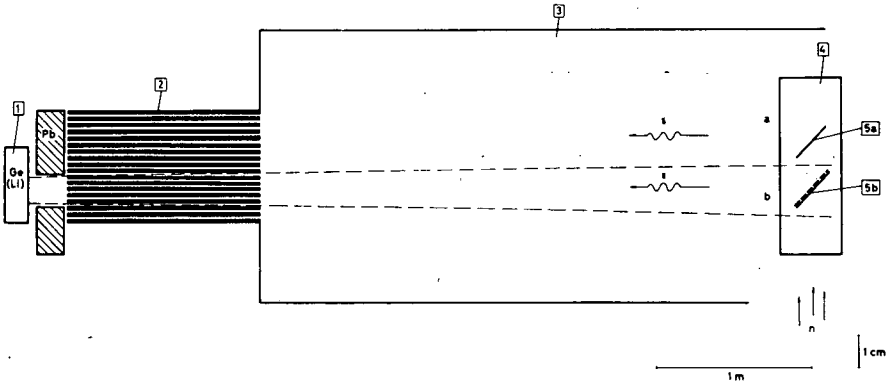


FIG. 2. Principle of the experimental arrangement for the study of $^{235}\text{U}(n, \gamma)^{236}\text{U}$: (1) Ge(Li) detector, (2) lead collimator, (3) reactor channel, (4) evacuated Al cylinder containing the Ni foils, (5a) Ni foil without and (5b) with uranium. The dashed line shows the target region (b) which exposes the detector in this arrangement.

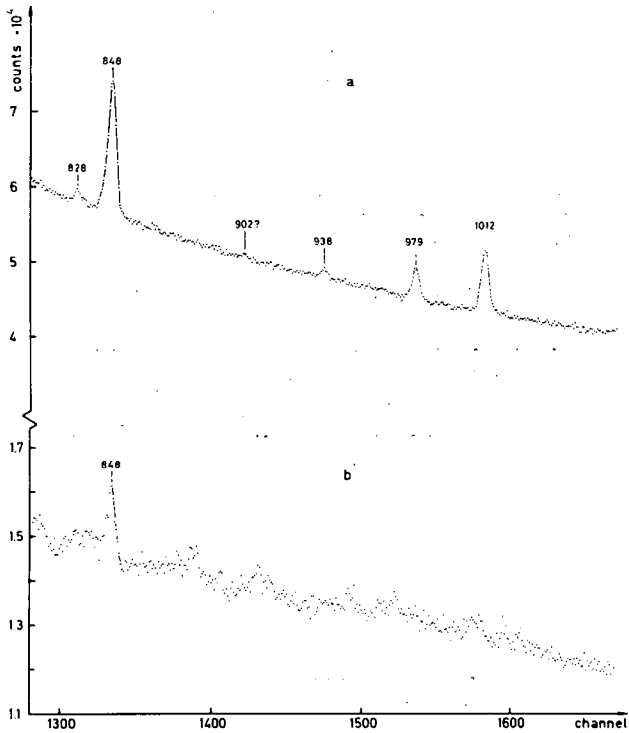


FIG. 3. Parts of the gamma spectrum: (a) the sum of all radiations from the U and Ni foil; (b) fission product radiation from the Ni foil.

The target consisted of a layer of about 1 mg/cm^2 ^{235}U enriched to 93 % on a backing of 3 mg/cm^2 Al. The multi-strip target technique (3) was used, the target area being $4 \times 4 \text{ cm}^2$. Since the target was inclined 45° to the direction of the electrons the effective thicknesses sensed by the electrons were 1.4 mg/cm^2 U and 4.2 mg/cm^2 Al.

The region from 0.5 to 1.1 MeV electron energy was scanned. In fig. 1 are shown two regions clearly demonstrating the difference in line-shape between electrons emitted in the Uranium layer and those emitted also in the backing. Further support for this interpretation was obtained from a separate experiment using the same uranium thickness on a backing of only 0.8 mg/cm^2 , in which the intensities of the broad lines decreased about a factor of 2, compared to the narrow lines. In table I a preliminary list of lines assigned to ^{236}U are given. Energy calibration was made relative to the 661.595 keV K-line in ^{137}Ba (4). The strongest lines found in the electron spectrum arise from the highly converted 642 and 687 keV transitions, which are known from radioactive decay to proceed in ^{236}U (5). In Table II are given the strongest of the lines arising from the fission products.

Gamma-ray measurements

In order to obtain the multipolarities of at least the strongest transitions in ^{236}U found in the conversion measurements, an attempt is made to measure the gamma-ray spectrum with a Ge(Li)-detector. In order to separate the ^{236}U -lines from fission product lines a special target arrangement is used, which is shown schematically in fig. 2. Approximately 1 mg/cm^2 ^{235}U (90 %) enriched is electroplated on 0.8 mg/cm^2 Ni-foil and covered with a similar foil. The target area is $6 \times 20 \text{ cm}$ and the target plane is inclined about 3° to the direction to the Ge(Li) detector. A 1.6 mg/cm^2 Ni foil is placed parallel to the target foil at a distance of 1 cm from it. About 25 % of the fission fragments are then stopped in this foil. Using the lead collimator at the end of the beam-hole the Ge(Li) detector could be adjusted either to measure the sum of all radiations from the U + Ni foil or only the fission product radiation from the Ni foil. Like in the conversion electron experiment the gamma lines emitted by the fragments in flight will be smeared out by the Doppler effect. Figure 3 shows preliminary spectra from the two foils. Only the 848 keV peak can be identified with certainty in both spectra indicating it as a fission product line. The 1012 and perhaps also the 979 keV lines are probably transitions in ^{236}U . A weak line corresponding to the 1012 keV line was observed also in the electron spectrum.

References:

1. F. Horsch, W. Michaelis and H.W. Schmitt, JÜL-CONF-1, Mai 1967
2. H.R. Bowman, S.G. Thompson, R.L. Watson, S.S. Kapoor and J.O. Rasmussen in Physics and Chemistry of Fission, IAEA, Vienna 1965
3. G. Bäckström, A. Bäcklin, N.E. Holmberg and K.E. Bergkvist, Nucl. Instr. and Meth. 16, 199 (1962)
A. Bäcklin, Nucl. Instr. and Meth. 57, 261 (1967)
4. J.S. Geiger, R.L. Graham and F. Brown, Can. J. Phys. 40, 1258 (1962)
5. C.M. Lederer, J.M. Hollander and I. Perlman, Table of Isotopes, John Wiley & Sons Inc., New York 1967.

ENERGY LEVELS IN ^{156}Gd *

A. BÄCKLIN, B. FOGELBERG, G. HEDIN, M. SARACENO

The Swedish Research Council's Laboratory,

Studsvik, Nyköping, and

Institute of Physics,

Uppsala University, Sweden

R. C. GREENWOOD, C. W. REICH

National Reactor Testing Station,

Idaho Nuclear Corporation,

Idaho Falls, Idaho, United States of America, and

H. R. KOCH, H. A. BAADER, H. D. BREITIG, O. W. B. SCHULT

Department of Physics,

Technische Hochschule, Munich,

Federal Republic of Germany, and

Risø Research Establishment,

Roskilde, Denmark

Abstract

ENERGY LEVELS IN ^{156}Gd . The reaction $^{155}\text{Gd}(n, \gamma)^{156}\text{Gd}$ has been studied at high resolution by measuring the internal conversion spectrum and the gamma-ray spectrum. In a preliminary analysis members were found of 4 positive parity bands and 7 negative parity states belonging to at least two bands. Some characteristics of these bands are discussed.

Introduction

Several studies on the level scheme of ^{156}Gd have been made through the years (1). Recent work of general character include investigations of the beta-decay of ^{156}Tb (2) and of ^{156}Eu (3). Several levels have been excited in the (d, d') reaction (4). In the reaction $^{155}\text{Gd}(n, \gamma)^{156}\text{Gd}$ levels with excitation energies between 1 and 2 MeV may be expected to be populated more completely than in the processes mentioned above. Since the capture cross-section of ^{155}Gd is as high as $6 \cdot 10^4$ b, the situation is favorable for high-resolution spectroscopy. We have undertaken an investigation of the radiation from the $^{155}\text{Gd}(n, \gamma)^{156}\text{Gd}$ reaction using crystal diffraction, high-resolution Ge-detectors and internal conversion spectroscopy. Earlier investigations of this reaction have been performed by Knowles et al. (5) and by Groshev et al. (6).

Crystal diffraction measurements

The gamma-ray spectrum from $^{155}\text{Gd}(n, \gamma)^{156}\text{Gd}$ was measured from 0.07 to 2.5 MeV with the Risø curved crystal spectrometer (7). The source consisted of 18 mg $^{155}\text{Gd}_2\text{O}_3$ enriched to 98.9%. The line width was 2.7 seconds of arc, which corresponds to the energy resolution of ΔE (keV) = $1.1 \cdot 10^{-6} E^2$ for strong transitions above 200 keV. E stands for the gamma-

* Part of this work was performed under the auspices of the US Atomic Energy Commission.

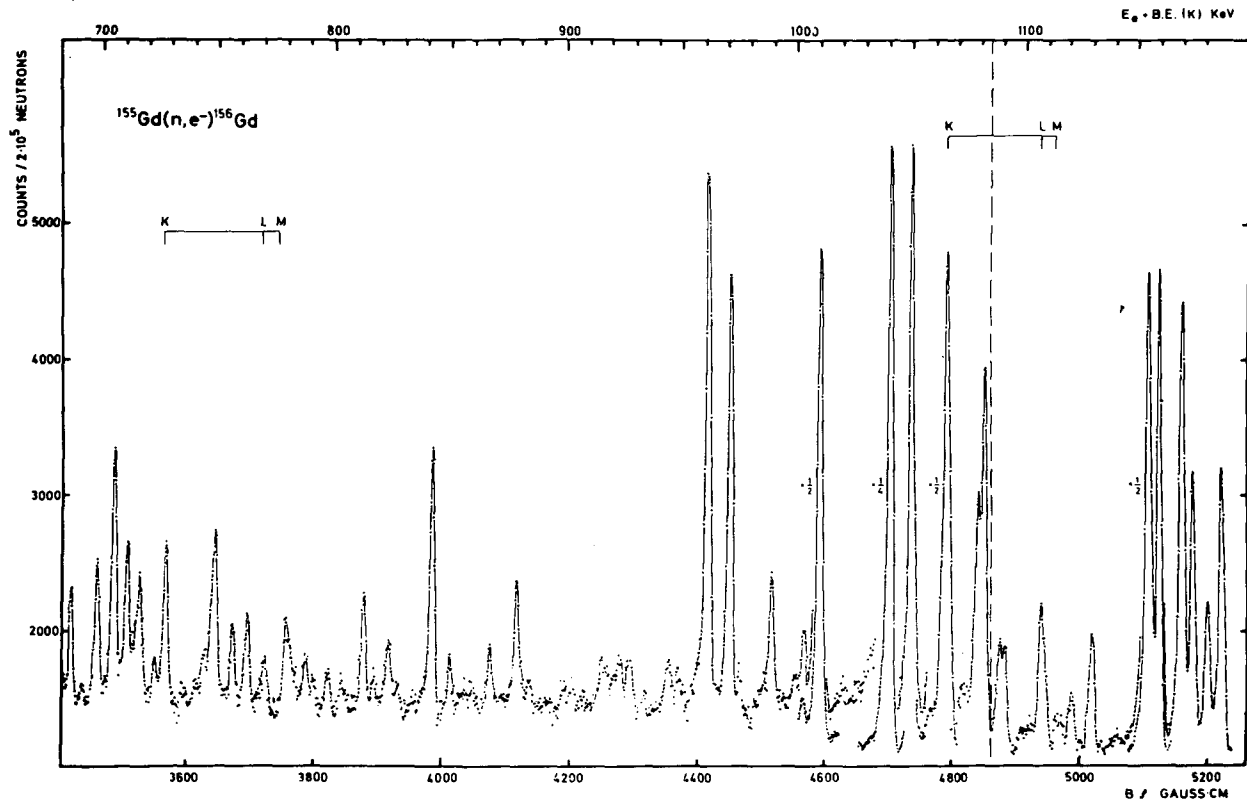


FIG. 1. Part of the internal conversion spectrum from $^{155}\text{Gd}(n, \gamma)^{156}\text{Gd}$. The transition energies of K-lines are given in the upper scale. The separations between the K, L and M lines are indicated in the upper and lower parts of the region. The dashed line indicates parts measured with different sources.

ray energy in keV. About 500 lines were detected. Details of the instrumentation and procedure of the measurements are given elsewhere at this conference (7, 8).

Ge(Li) detector measurements

The gamma-ray spectrum up to the neutron binding energy was measured at Idaho Falls using a high resolution Ge(Li) detector in an external neutron beam geometry. Details on the apparatus and experimental procedure are reported elsewhere at this conference (9). 130 lines were detected in the region 0.08-2.4 MeV and about 100 lines were observed in the region 4-8.5 MeV.

Primary gamma-rays were also measured from capture of 2 keV neutrons obtained from a scandium filter with an energy spread FWHM of 0.7 keV (10, 11). About 60 primary gamma-rays were observed above 5 MeV, many of them feeding states not observed in the thermal neutron capture reaction.

Internal conversion measurements

The internal conversion spectrum was scanned from 0.04 to 2 MeV electron energy with the Studsvik beta-spectrometer (12). Multi-strip targets 2 with an area of about 15 cm^2 and thicknesses ranging from 0.02 to 1.4 mg/cm^2 were made from 98.7 % enriched ^{155}Gd . At energies above 100 keV the source thickness was chosen so that the resolution FWHM never exceeded 0.2 %. Above 1 MeV the resolution FWHM was 0.16 ‰. The spectrum obtained was extremely complex, especially in the region around 1 MeV, cf. fig. 1. To make possible the resolution of weak lines from close strong lines a special computer program was developed, in which the line shape is described numerically as a table of co-ordinates. This had to be done since no simple mathematical function could be found that described the line shape accurately enough. The spectrum contained several strong single lines suitable for defining the line shape. Conversion lines belonging to about 300 transitions have been resolved so far.

Level scheme

Although the evaluation of the experimental data is not yet complete, the available data are sufficient for a beginning of the construction of the level scheme in the 1 MeV region. The accuracy of the relative energy measurements for the stronger lines in this region was for the internal conversion lines about 1 in 10^4 and for the Ge(Li) data 0.5 parts in 10^4 , which forms a good basis for work with energy combinations. The final transition energies have not yet been calculated, so all energy values given below have been truncated to show their preliminary character. Conversion coefficients were calculated with $\sim 10\%$ accuracy and multipolarities obtained using the tables of Hager and Selzer (13).

As a start the levels observed under the "cleaner" conditions of refs. (2-4) were looked for. With one possible exception all levels below 1.6 MeV reported in refs. (2-4) have been identified and some additional members of the bands have been found. Furthermore a new $K=0^+$ band has been observed. The preliminary level scheme is shown in fig. 2 and was arrived at independently using the Idaho and Risø + Studsvik data. To give an idea of the reliability of the level scheme one may mention that the probability of finding an accidental combination of 2 transitions to levels in the ground state band within 5 keV from an anticipated position is only a few percent

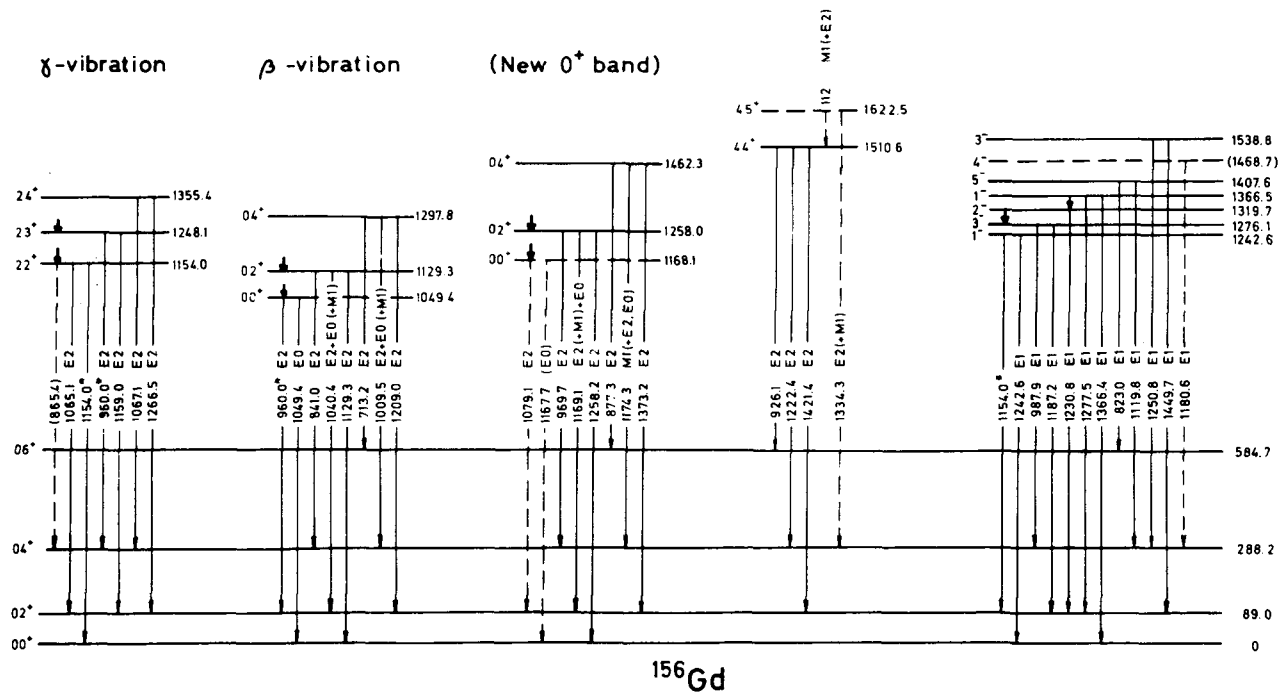


FIG. 2. Preliminary level scheme of ^{156}Gd . Only approximate energies are given. A short, thick arrow indicates population by a primary gamma ray.

The gamma vibrational band The first three members have been identified both in β -decay (2, 3) and in the (d, d') reaction. We found strong E2 transitions to combine according to fig. 2. The 2^+ and 3^+ levels are fed by primary gamma-rays. The $22^+ \rightarrow 00^+$ and $23^+ \rightarrow 04^+$ transitions were resolved from the $00^+ \rightarrow 02^+$ and $(0)1^- \rightarrow 02^+$ transitions, respectively in 5:th order crystal diffraction. The conversion coefficients of the 1065, 1159 and 1067 keV transitions are compatible with pure E2 with less than 25 % M1, in agreement with ref. (2). Using the branching ratios from the $I = 3^+$ and $I = 4^+$ levels we obtain a value of the mixing parameter Z_2 of 0.041 ± 0.009 and 0.049 ± 0.008 , respectively, which is definitely larger than the predicted values of 0.020 (14), 0.021 (15) and 0.027 (16).

The beta vibrational band The 0^+ and 2^+ members of this band were found in the (d, d') reaction (4) and the 2^+ member is also populated in the decay of ¹⁵⁶Tb. We have identified the 0^+ , 2^+ and 4^+ members according to fig. 2. The I-I transitions are all very highly converted indicating E0-admixture. In table I are given ratios of reduced E2 transition probabilities. Mixing with the ground state rotational band as expressed in terms of the mixing parameter Z_0 evidently does not describe the situation in a consistent way

Table I

Ratios of reduced E2 transition probabilities for E2 transitions from the $K^\pi = 0^+$ bands

Ratio	Experimental value		Theoretical value		$Z_0 \times 10^3$
	a)	b)	No mixing	$Z_0 = 0.018^c)$	
A. Beta vibrational band					
(2→0)/(2→2)	0.22(2) ^{d)}	0.55(5)	0.70	0.56	74(4)
(2→4)/(2→2)	1.12(9)	2.80(25)	1.80	2.80	-15(2)
(2→0)/(2→4)	0.19(2)	0.19(2)	0.39	0.20	19(2)
(4→2)/(4→4)	0.35(4)	0.62(8)	1.10	0.61	31(2)
(4→6)/(4→4)	0.65(26)	1.15(45)	1.75	3.4	-21(7)
(4→2)/(4→6)	0.55(22)	0.55(22)	0.63	0.18	2(7)
B. New 0^+ band					
$Z_0 = 0.039^c)$					
(2→0)/(2→2)	0.21(3)	0.37(5)	0.70	0.41	76(6)
(2→4)/(2→2)	2.8(2)	4.9(4)	1.80	4.3	18(2)
(2→0)/(2→4)	0.07(1)	0.07(1)	0.39	0.095	48(4)
(4→2)/(4→4)	0.06(1)	0.27(5)	1.10	0.23	55(2)
(4→6)/(4→4)	1.15(18)	5.2(8)	1.75	6	-10(3)
(4→2)/(4→6)	0.050(9)	0.050(9)	0.63	0.037	36(2)

a) The I-I transition assumed to be pure E2

b) Assuming M1 admixture in I-I transitions: Beta vib. band: 2→2: 60 %, 4→4: 44 %. New $K=0^+$ band: 2→2: 43 %, 4→4: 78 %

c) Weighted average of Z_0 for the ratios not containing the I-I transition

d) Number in parenthesis gives the error of the last digit

unless strong M1 admixture is assumed for the 2-2 (60 %) and 4-4 (44 %) transitions. This is possible but does not seem to be very likely, since in ^{154}Gd , where a similar situation occurs, the 2-2 transition has been found to be E2 + < 2 % M1 (17).

In table II are given the strengths of the I-I E0 transitions. These are expressed in units of (see ref. (18)) $\chi = e^2 R^2 \rho^2 / B(E2; 0 \rightarrow 2)$ where ρ^2 is the E0 "strength parameter" (19). From the present data χ can be correctly obtained only for the $0^+ \rightarrow 0^+$ transition for the $2^+ \rightarrow 2^+$ and $4^+ \rightarrow 4^+$ transitions approximate values of χ were calculated assuming the Z_0 correction to be valid for the E2 transition probabilities using $Z_0 = 0.018$.

Table II

Values of $\chi = e^2 R^2 \rho^2 / B(E2; 0 \rightarrow 2)$ for the two excited $K=0^+$ bands

Transition	χ	
	Beta vibrational band	New 0^+ band
0-0	0.10	< 0.018
2-2	~0.16	\lesssim 0.011
4-4	~0.25	\lesssim 0.024

Negative parity states Strong E1 transitions corresponding to the 1^- , 3^- and 5^- states observed in the (d, d') reaction (4) were observed. On basis of their strong (d, d') cross-sections and the systematic behaviour of these levels they have been assigned as members of the $K = 0^-$ octupole band (4). Additional 1^- and 3^- levels were found by combining strong E1 transitions at 1366 and 1538 keV. Only two strong E1 transitions were then left in the spectrum of which the 1230 keV transition may define a 2^- state at 1319 keV as suggested by a primary transition and from the decay of ^{156}Tb (3), and the 1180 keV transition possibly defines a 4^- level at 1468 keV as suggested in fig. 2. Since energies and branching ratios suggest strong mixing no definite conclusions regarding the K-quantum numbers of the negative parity states can be made at this stage.

A new $K=0^+$ band Six of the remaining strong positive parity transitions in the region around 1 MeV were found to combine to a 2^+ level at 1258 keV and a 4^+ level at 1462 keV. The 1258 keV level is supported by a primary γ -ray in 2 keV neutron capture. Using the simple rotational formula for the energies yielded 1081 keV for the transition from the expected 0^+ state to the 2^+ state in the ground state band. The only remaining E2 transition with an intensity of the expected order of magnitude has an energy of 1079 keV, and it is therefore reasonable to assume this transition deexcites the 0^+ state. A possible E0 transition from this state was found by resolving the broad K- line mainly arising from the 1169 keV transition. The E2 branching ratios show a trend fairly similar to those of the beta-vibrational band, cf table I. A rather good consistency is obtained with a value of the mixing parameter with the ground

Table III

Approximate rotational energy parameters for the three 0^+ bands

	Ground state band	Beta vib. band	New 0^+ band
A keV	15.0	13.7	15.2
B eV	-30	-64	-21

state band Z_0 of 0.037, assuming 43 % M1 for the 2-2 transition and 78 % M1 for the 4-4 transition. The α_K of the 4-4 transition is compatible with this mixture, while the α_K of the 2-2 transition is somewhat large, which may be explained by E0 admixture. The upper limits of the quantity X for the E0 part of the I-I transitions are given in table II assuming only E2 competition. The small values indicate a difference in character between this band and the beta vibrational band. In table III the rotational energy parameters are given for all three $K=0^+$ band.

References

1. Nuclear Data Sheets, National Academy of Sciences, Washington, D. C.
2. P F Kenealy, E. G. Funk and J. W. Mihelich, Nucl. Phys. A 105 (1967), 522.
3. N. F. Peek, J. A. Jungerman and C. G. Patten, Phys. Rev. 136 (1964) B 330.
4. R. Block, B Elbek and P. O. Tjøm, Nucl. Phys. A 91 (1967), 576.
5. J. W. Knowles, G. Manning, G. A. Bartholomew and P. J. Champion, Proc. Conf. Nucl. Structure, Kingston, Canada (1960), p. 579.
6. L. V. Groshev, A. M. Demidov, V. A. Ivanov, V. N. Lutsenko and V. I. Pelekhov, Izv. Acad Nauk SSSR 26 (1963) 1127.
7. H. R. Koch et al., "The automation of the curved-crystal spectrometer at Risø", these Proceedings.
8. H. A. Baader et al., "Investigation of the ^{158}Gd level scheme by thermal neutron capture", these Proceedings.
9. R. G. Helmer, R. C. Greenwood and C. W. Reich, "Levels in ^{182}Ta ", these Proceedings.
10. O. D. Simpson and L. G. Miller, Nucl. Instr. and Methods 61 (1968), 245.
11. R. C. Greenwood, Report at this conference on Neutron Capture Gamma-Ray Measurements with a Reactor Produced 2-keV Neutron Beam.
12. A. Bäcklin, Nucl. Instr. and Meth. 57 (1967), 261.

13. R.S. Hager and E. C. Selzer, CALT-63-60.
14. D.R. Bés et al., Nucl. Phys. 65 (1965), 1.
15. I. M. Pavlichenkov, Nucl. Phys. 55 (1964), 225.
16. E.R. Marshalek, Phys. Rev. 158 (1967), 993.
17. J.H. Hamilton, A.V. Ramayya and L. C. Whitlock, Phys. Rev. Lett. 22 (1969), 65.
18. J.O. Rasmussen, Nucl. Phys. 19 (1969), 85.
19. E. L. Church and J. Weneser, Phys. Rev. 103 (1956), 1035.

A $K = 2^+$ BAND IN ^{178}Hf

B. FOGELBERG, A. BÄCKLIN

Institute of Physics,

University of Uppsala, and

The Swedish Research Council's Laboratory,

Studsvik, Nyköping, Sweden

Abstract

A $K = 2^+$ BAND IN ^{178}Hf . The gamma-ray spectrum and the conversion electron spectrum in the 1-MeV region from $^{177}\text{Hf}(n, \gamma)^{178}\text{Hf}$ have been studied. From these data five members of a $K = 2^+$ band, which may be identified as the gamma-vibrational band, were found. Confirmation of the levels was obtained from a γ - γ coincidence measurement. From the measured branching ratios we have deduced a value of the band-mixing parameter Z_2 and this quantity is compared with different theoretical estimates.

INTRODUCTION

The band-mixing parameter Z_2 for the gamma-vibrational band in even deformed nuclei has been theoretically calculated in the microscopic approach by several authors [1 - 3]. In general these calculations show rather good agreement both with each other and with experiment, except for the region around $A \sim 180$ where Bés et al. [1] predict significantly higher values than those of Refs [2] and [3]. The deviation is most pronounced in the case of ^{178}Hf , in which the predictions differ by almost a factor of 10.

The experimental data for the gamma vibration in ^{178}Hf are very scanty, with suggestions for the band head (or the first $KI^\pi = 22^+$ state) ranging from 1175 to 1402 keV [4, 5]. Furthermore, no reliable gamma intensities are given for the de-excitation of this proposed band.

We therefore investigated the reaction $^{177}\text{Hf}(n, \gamma)^{178}\text{Hf}$ with the aim to locate the gamma-vibrational band and to determine the Z_2 parameter.

EXPERIMENTAL PROCEDURE

The energy region from 850 - 1420 keV of the internal conversion electron spectrum was measured with the double-focussing beta-spectrometer at the R2 reactor in Studsvik [6].

An extracted neutron beam passed through the spectrometer at the target position, where the beam cross-section is about $5 \times 5 \text{ cm}^2$ and the neutron flux is $10^8 \text{ n cm}^{-2} \text{ sec}^{-1}$.

To increase the luminosity of the spectrometer, the target was arranged in the voltage gradient system [6], which made it possible to use a target with 15 cm^2 area. Targets were prepared by electroplating 91.7% enriched ^{177}Hf onto thin aluminium backing. A thickness of about 2 mg/cm^2 was used in the present measurement. The measurements were made with a momentum resolution of 0.2% and the magnetic field of the spectrometer was regulated with a precision better than one part in 10^4 .

The gamma-ray spectrum was measured from 470 to 3000 keV with an ORTEC true coaxial Ge(Li) detector of 25 cm³ volume. Also in this experiment a neutron beam was extracted from the reactor. The beam passed through a tube made of ⁶LiCO₃ in which the target was placed. The target was made by filling 70 mg of 91.7% enriched ¹⁷⁷Hf into a small bag of 0.6 mg/cm² Melinex-foil which gave a negligible background. Some background due to capture in the various shielding materials was, however, present and a special run was made of these lines. The energy-resolution of the gamma-counting system was 3.5 keV in the 1-MeV region.

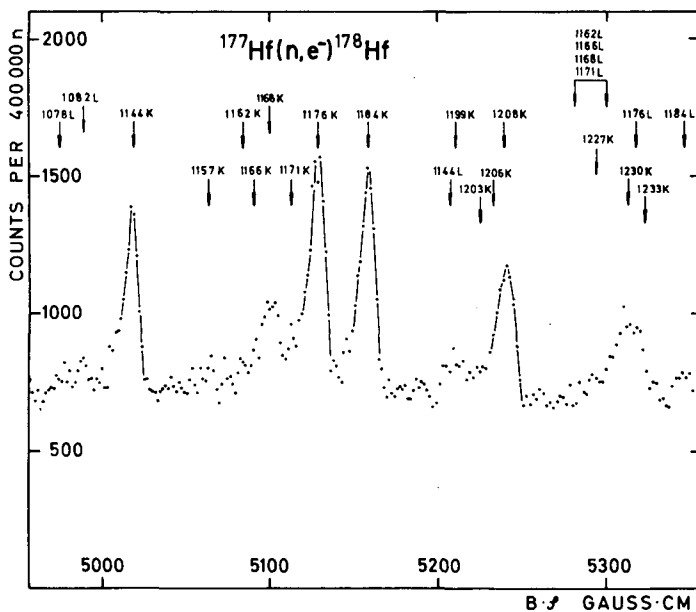


FIG. 1. A part of the conversion electron spectrum recorded with the double-focussing beta-spectrometer. Each line is labelled by the transition energy rounded off to the nearest keV, and by the electron-shell.

Parts of the internal conversion electron spectrum and the single gamma-ray spectrum are shown in Figs 1 and 2.

The conversion coefficients were normalized by assuming the 1175-keV transition to be pure E2. This assignment gives a good consistency with the conversion coefficients of the transitions that are also seen in the beta decay of ¹⁷⁸Ta [7], and with the conversion coefficients found for E1 transitions in the spectrum.

The large number of lines observed in the 1-MeV region implies a non-negligible probability of obtaining accidental combinations if the level scheme is constructed purely on the basis of energy-combinations. Because of this, we performed a γ - γ coincidence experiment as an extra check of combinations involving strong transitions. A 3 × 3 -in. NaI crystal was used in conjunction with the Ge(Li) counter. Four gates were placed in the pulse-height spectrum from the Na(I) detector, two at the intense transitions from the 4⁺ and 2⁺ level in the ground-state rotational band, and

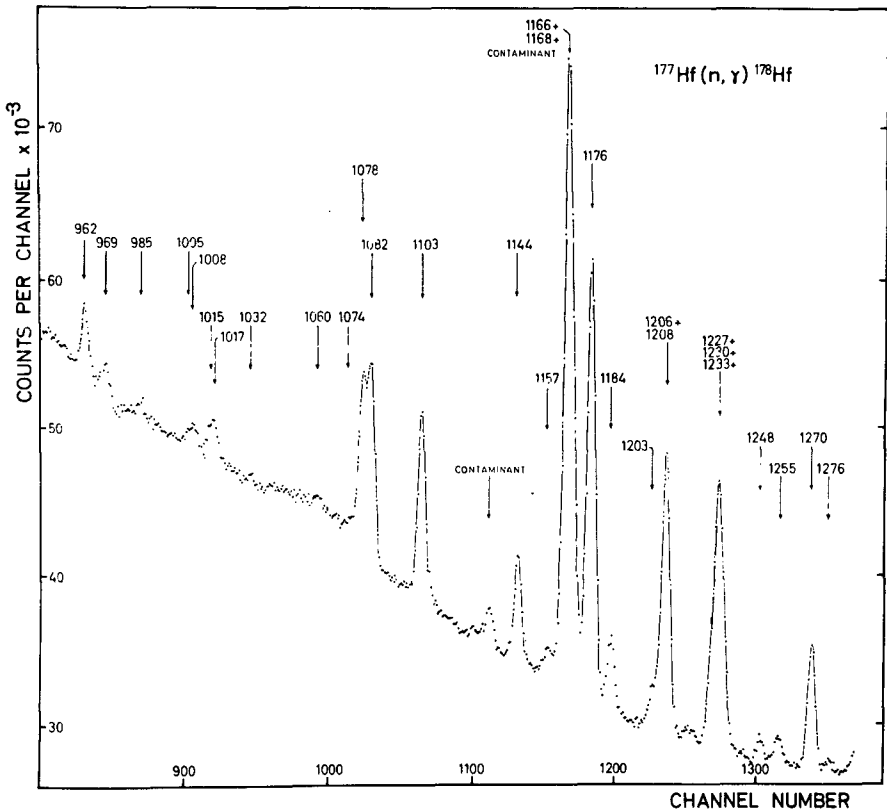


FIG. 2. Gamma rays in the 1-MeV region as measured with the Ge(Li) detector. Each line is labelled by the transition energy rounded off to the nearest keV. Total recording time was about 2 days with a 70-mg target.

the other two at the background slightly above each of the mentioned peaks. The coincident spectra from the Ge(Li) counter were stored in a multichannel analyser with the memory grouped in 4×1024 channels.

RESULTS AND DISCUSSION

From the results of the coincidence measurements and by the use of the conversion coefficients, positive parity levels could be established at 1174.70, 1268.70, 1384.48 and 1533.99 keV. The decay modes of these levels are consistent with $I^\pi = 2^+, 3^+, 4^+$ and 5^+ . The spacings of the level energies agree well with what can be expected for a rotational band and the lack of members with angular momentum less than 2 units indicates a K-quantum number of 2. Applying the energy formula [8] for K = 2⁺ bands,

$$E = E_0 + A I(I+1) + B I^2(I+1)^2 + D(-1)^I (I-1) I(I+1)(I+2)$$

one finds for the coefficients:

$$A = 15.91 \text{ keV} \quad B = -31.4 \text{ eV} \quad D = -5.6 \text{ eV}$$

TABLE I. PROPERTIES OF GAMMA RAYS CONNECTING THE $K = 2$ BAND AND THE GROUND-STATE BAND IN ^{178}Hf

In the first two columns the initial and final spins of the connected states are given. Columns 3 and 4 contain energies and intensities of the connecting gamma rays. The multipole assignments are based on conversion coefficients measured in this work. These conversion coefficients have been normalized on the pure E2 value of the 1175-keV transition. The next column gives the ratios of the reduced $B(E2)$ values, assuming all transitions to be pure E2. In the last two columns are shown the prediction of Alaga's rule, and the values of the band-mixing parameter Z_2 obtained from the deviations from Alaga's rule.

I_i	I_f	Transition energy (keV)	Relative gamma intensity	Multipole assignment	Ratios of reduced $B(E2)$ values	Alaga	$Z_2 \times 10^2$
2	0	1175.55	40 ± 10^a	E2	$\frac{2 \rightarrow 0}{2 \rightarrow 2} = 0.67 \pm 0.12$	0.70	0.8 ± 3.0
2	2	1081.55	36.5 ± 2.5	$E2 + < 25\% M1$	$\frac{2 \rightarrow 4}{2 \rightarrow 2} = 0.12 \pm 0.06$	0.05	9 ± 8
2	4	867.92	1.6 ± 0.8	-			
3	2	1175.55	60 ± 10^a	E2	$\frac{3 \rightarrow 4}{3 \rightarrow 2} = 0.46 \pm 0.08$	0.40	1.0 ± 1.3
3	4	962.11	12.2 ± 1.2	$E2 + < 15\% M1$	$\frac{3 \rightarrow 2}{3 \rightarrow 2} = 0.46 \pm 0.08$		
4	2	1291.71	$15. \pm 3.5$	$E2 + < 40\% M1$	$\frac{4 \rightarrow 2}{4 \rightarrow 4} = 0.18 \pm 0.04$	0.34	4.2 ± 1.2
4	4	1077.79	$33. \pm 2.5_b$	$E2 + < 25\% M1$	$\frac{4 \rightarrow 6}{4 \rightarrow 4} = 0.35 \pm 0.09$		
4	6	752.66	$2. \pm 0.5_b$	-	$\frac{4 \rightarrow 4}{4 \rightarrow 4} = 0.35 \pm 0.09$	0.086	$(11 \pm 4)^b$
5	4	1227.00	31.4 ± 4.5	$E2 + < 10\% M1$	$\frac{5 \rightarrow 6}{5 \rightarrow 4} = 0.57 \pm 0.14$		
5	6	902.16	3.7 ± 0.8	-	$\frac{6 \rightarrow 4}{6 \rightarrow 6} = 0.21 \pm 0.09$	0.27	1.0 ± 1.0
6	4	1385.40	2.5 ± 0.8	-			
6	6	1059.66	$3.1 \pm 1.$	E2 or M1	Weighted average:		1.3 ± 1

Theory: Bés et al. [1] 7.8; Pavlichenkov [2] 0.8; Marshalek [3] 1.7.

^a These transitions could not be resolved in the single spectrum. The intensities are obtained from the coincidence measurement.

^b This value can be caused by other transitions coinciding with the 752-keV line. The value of Z_2 has been omitted in the average.

Using these values the expected position of the 6⁺ member is at 1692 keV. Experimentally we find a combination of two transitions to the 4⁺ and 6⁺ members of the ground-state band at 1691.90 keV. This combination could, however, not be confirmed by further evidence and is thus only tentatively assigned as the 6⁺ member of the K = 2⁺ band.

Although we have no strong arguments to support us, we would like to suggest that this K^π = 2⁺ band is the gamma-vibrational band. The energy is higher than for the lowest 2-quasiparticle (K^π = 8⁻) band [9], but the energy is definitely lower than the lowest K^π = 2⁺ 2-quasiparticle band predicted by Gallagher and Soloviev [10] at 2.3 MeV.

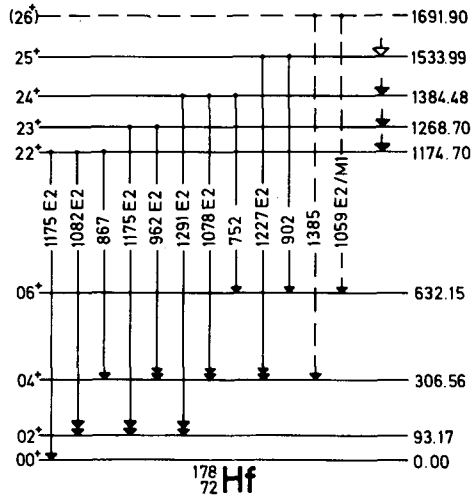


FIG. 3. Level scheme showing the de-excitation of the K = 2⁺ band. To the left of each level is the assignment in the quantum numbers K^π. The level energies are given to the right. The estimated energy uncertainty is 0.2 keV. Filled arrows which terminate on a level in the K = 2⁺ band indicate that the level has been observed in studies of direct capture gamma rays [12]. Transitions with double arrowheads have had their place in the level scheme established by the coincidence measurements.

In Table I preliminary values of the ratios of the reduced E2 transition probabilities from the suggested gamma-vibrational band to the ground-state band are given together with the Z₂ mixing parameters. All transitions were assumed to be pure E2, which may not necessarily be true. Angular correlation measurements are planned in order to deduce possible M1 admixtures. It can, however, be said already at this stage that the Z₂ value is low, thereby supporting the calculations by Pavlichenkov [2] and Marshalek [3].

The part of the ¹⁷⁸Hf level scheme containing the 2⁺ band is shown in Fig. 3. Very recently the three lowest members of the band have been identified by Faler et al. [11] from studies of resonance capture gamma rays. In this work, however, a definite assignment could only be given to the 3⁺ level.

R E F E R E N C E S

- [1] BÉS, D.R., FEDERMAN, P., MAQUEDA, E., ZUKER, A., Nucl. Phys. 65 (1965) 1.
- [2] PAVLICHENKOV, I.M., Nucl. Phys. 55 (1964) 225.
- [3] MARSHALEK, E.R., Phys. Rev. 158 (1967) 993.
- [4] GROSHEV, L.V., DEMIDOV, A.M., IVANOV, V.A., LUTSENKO, V.N., PELEKOV, V.I., Izv. Akad. Nauk SSSR, Ser. fiz. 28 (1964) 1142.
- [5] SMITHER, R.K., Phys. Rev. 129 (1963) 1691.
- [6] BÄCKLIN, A., Nucl. Instrum. Meth. 57 (1967) 261.
- [7] NIELSEN, H.L., WILSKY, K., ZYLICZ, J., Nucl. Phys. A93 (1967) 385.
- [8] BOHR, Å, MOTTELSON, B.R., Atomn. Energ. 14 (1963) 41.
- [9] GALLAGHER, C.J., Jr, NIELSEN, H.L., Phys. Rev. 126 (1962) 1520.
- [10] GALLAGHER, C.J., Jr, SOLOVIEV, V.G., Mat. Fys. Skr. Dan. Vid. Selsk. 2 (1962) 2.
- [11] FALER, K.T., SPENCER, R.R., HARLAN, R.A., Nucl. Phys. A 123 (1969) 616.
- [12] NAMENSON, A.I., BOLOTIN, H.H., Phys. Rev. 158 (1967) 1206.

(n, γ) AND (n, e^-) INVESTIGATION OF THE ^{177}Lu LEVEL STRUCTURE

(Short communication)

P. MANFRASS, H. PRADE, F. STARY

Central Institute for Nuclear Research,

Rosendorf Nr Dresden,

Democratic Republic of Germany, and

M. BEITINS, N. KRAMER, P. PROKOVIEV

Institute for Physics,

Riga, USSR

The measurements of the conversion electron spectrum previously carried out by some of the authors [1] have now been supplemented by the investigation of single and coincidence gamma-ray spectra. Especially from the high-energy parts many new levels of positive parity with spin values of $I = 11/2, 13/2$ and $15/2$ with excitation energies > 1 MeV could be deduced. Energy of the capture state ($13/2^-$ or $15/2^-$) amounts to 7071.3 keV. The different gamma-gamma coincidence measurements yielded probable spin values of the states directly excited from the capture state. These values are listed in Table I. So far, only the structure of some of the levels could be explained. Experimental confirmation was established of the excitation energy and the mode of deexcitation, of the three lowest rotational levels at 1350.4($9/2^+$), (1480.3($11/2^+$) and 1630.2 ($13/2^+$) of the known three-quasiparticle state [2] with $K = 7/2^+$ at 1241.0 keV.

Two rotational bands of the three-quasiparticle states $p\ 7/2^+$ [404] $n\ 7/2^-$ [514] $\pm 1/2^-$ [510] at 1357 and 1503 keV were derived from (d, p) and (d, t) investigations [3]. With our gamma measurements we could obtain more accurate level energy values (in keV): 1356.6($15/2^+$), 1544.0($17/2^+$), 1749.7($19/2^+$); 1502.5 ($13/2^+$), 1677.6($15/2^+$), 1872.2($17/2^+$).

The experimental (d, p) cross-sections for the $19/2$ ($K = 13/2$) level and the $17/2$ ($K = 13/2$) level are too high compared with theoretical values [3]. We assume an admixture of the neighbouring levels at 1752.1 and 1882.6 keV to be excited in the (n, γ) reaction by strong direct transitions from the capture state.

REFERENCES

- [1] BEITINS, M. et al., 19th Allunion Conference, Erewan, USSR.
- [2] JOHANSEN, H. S. et al., Physics Lett. **8** (1964) 61.
- [3] SHELINE, R. K. et al., private communication.

TABLE I. HIGH-ENERGY GAMMA-RAY SPECTRUM OF THE
 $^{176}\text{Lu}(n, \gamma)^{177}\text{Lu}$ REACTION

Gamma energy (keV)	Relative intensity	Level energy (keV)	Spin, parity
6802.5 ± 0.5	552 ± 16	268.8	11/2 ⁺
6434.5 ± 0.4	160 ± 5	636.8	15/2 ⁺
6254.7 ± 0.5	110 ± 6	816.6	11/2 ⁺
6112.1 ± 2.0	36 ± 12	959.2	(11/2 ⁺)
6082.5 ± 3.0	54 ± 25	988.8	13/2 ⁺
5893.7 ± 0.8	116 ± 14	1177.6	15/2 ⁺
5840.0 ± 0.9	57 ± 8	1231.3	11/2 ⁺
5768.2 ± 0.5	322 ± 25	1303.1	(11/2, 13/2) ⁺
5727.6 ± 0.5	394 ± 21	1343.7	11/2 ⁺
5600.1 ± 0.5	567 ± 29	1471.2	11/2 ⁺
5568.4 ± 0.5	577 ± 29	1502.9	13/2 ⁺
5463.7 ± 0.6	343 ± 27	1607.6	(11/2, 13/2) ⁺
5436.5 ± 1.4	97 ± 26	1634.8	13/2 ⁺
5394.2 ± 0.6	180 ± 16	1677.1	15/2 ⁺
5379.9 ± 0.8	140 ± 16	1691.4	(11/2, 13/2, 15/2) ⁺
5364.8 ± 0.7	163 ± 16	1706.5	(11/2, 13/2) ⁺
5341.6 ± 0.5	403 ± 18	1729.7	(11/2, 13/2, 15/2) ⁺
5319.2 ± 0.5	496 ± 18	1752.1	11/2 ⁺
5265.5 ± 0.7	155 ± 16	1805.8	(11/2, 13/2) ⁺
5211.4 ± 1.0	121 ± 20	1859.9	(11/2, 13/2) ⁺
5188.7 ± 0.6	241 ± 24	1882.6	15/2 ⁺
5163.9 ± 0.5	301 ± 24	1907.4	13/2 ⁺
5109.9 ± 0.7	221 ± 20	1961.4	(11/2, 13/2) ⁺
5092.9 ± 2.8	50 ± 20	1978.4	(11/2, 13/2, 15/2) ⁺
5080.8 ± 2.3	61 ± 20	1990.5	(11/2, 13/2, 15/2)
5046.2 ± 1.6	75 ± 19	2025.1	(11/2, 13/2, 15/2)
5016.5 ± 0.5	530 ± 21	2054.8	11/2 ⁺
4981.3 ± 0.8	198 ± 20	2090.0	(11/2, 13/2, 15/2) ⁺
4884.5 ± 1.0	152 ± 18	2186.8	15/2 ⁺
4866.2 ± 0.8	340 ± 19	2205.1	13/2 ⁺

THERMAL NEUTRON CAPTURE

Chairmen: L. V. GROSHEV
H. H. BOLOTIN
B. ELBEK
R. E. CHRIEN

GAMMA CALIBRATION ENERGIES IN THE $^{23}\text{Na}(n, \gamma)^{24}\text{Na}$ AND $^{14}\text{N}(n, \gamma)^{15}\text{N}$ REACTIONS

P. H. M. VAN ASSCHE

SCK - CEN,
Mol, Belgium

(Presented by P. Fettweis)

Abstract

GAMMA CALIBRATION ENERGIES IN THE $^{23}\text{Na}(n, \gamma)^{24}\text{Na}$ AND $^{14}\text{N}(n, \gamma)^{15}\text{N}$ REACTIONS. Starting from the $\text{H}(n, \gamma)\text{D}$ capture gamma line an energy of $6396,93 \pm 0,40$ keV is obtained for the intense gamma ray in the $^{23}\text{Na}(n, \gamma)^{24}\text{Na}$ reaction.

When using the $2223,29 \pm 0,07$ keV gamma energy from the $\text{H}(n, \gamma)\text{D}$ reaction as a reference value [1], a systematic deviation has been observed between the line at 2.75 MeV in the $^{23}\text{Na}(n, \gamma)^{24}\text{Na}$ reaction and the $2753,92 \pm 0,12$ keV decay line [2] of ^{24}Na .

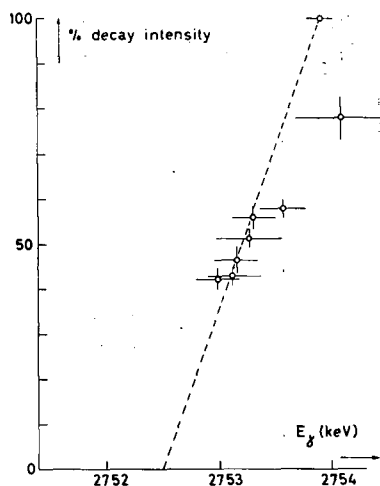


FIG. 1. Energy variation of the 2.75-MeV doublet as a function of the intensity of the decay line (given at the top).

Spectra are measured with a 25-cm^3 $\text{Ge}(\text{Li})$ coaxial detector. To avoid systematic errors, five different amplifications have been used. Consequently, each of them needed a different correction for the non-linearity in the electronic equipment.

It has been observed that the intensity of the 2.75-MeV line was too high with respect to the 100% decay line at 1.368 MeV. Therefore we concluded the presence of a (n, γ) line next to the decay line of 2753.92 keV.

TABLE I. CHARACTERISTICS OF THE DOUBLET AT 2.75-MeV GAMMA ENERGY IN THE $^{23}\text{Na}(n, \gamma)^{24}\text{Na}$ SPECTRUM

E_γ (keV)	σ_E (keV)	$R = \frac{\text{Decay intensity}}{\text{Total intensity}}$ (%)	σ_R (%)	Dispersion E (keV)/channel
2753.00	0.25	42.7	2.5	1.62
2753.14	0.25	42.7	2.1	1.70
2753.17	0.20	46.7	3.1	1.16
2753.28	0.30	51.5	2.3	1.62
2753.32	0.20	56.0	2.8	1.16
2753.59	0.20	58.0	2.0	0.68
2754.10	0.40	78	10	2.56

TABLE II. SOME GAMMA TRANSITIONS OBSERVED DURING THIS STUDY

All gamma energies are from the $^{23}\text{Na}(n, \gamma)^{24}\text{Na}$ spectrum, except those at a and c.

E_{γ} (keV)	σ_E (keV)	Remarks	E_{γ} (keV)	σ_E (keV)	Remarks
472.39	0.14		2505.67	0.35	DE/Ph
500.42	0.43		2752.50 ^b	0.30	
562.6	0.6		2808.7	0.5	DE/Ph
780.6	0.6		2862.8	0.4	DE/Ph
835.4	0.5		3097.33	0.13	DE/SE/Ph
868.81	0.18		3587.81	0.14	DE/SE/Ph
873.99	0.16		3644.3	0.7	DE
1093.5	1.0		3878.5	0.4	DE/Ph
1343.7	0.5		3981.69	0.22	DE/SE/Ph
1368.87 ^a	0.20		5270.03 ^c	0.23	DE/SE/Ph
2026.72	0.24	DE/Ph	5298.52 ^c	0.23	DE/SE
2210.00	0.4		5617.91	0.32	DE/SE/Ph
2414.36	0.14	DE/Ph	6396.93	0.40	DE

DE : double escape peak is well separated; SE: single escape peak is well separated; Ph : photopeak is well separated; if no remark, the gamma ray is observed at the photopeak.

^a Decay line of ^{24}Na .

^b Gamma energy deduced from Fig. 1.

^c Gamma ray from the $^{14}\text{N}(n, \gamma)^{15}\text{N}$ reaction.

TABLE III. PROMINENT GAMMA TRANSITIONS FROM ^{24}Na AND ^{15}N USED IN THE BOOT-STRAP APPROACH

Nucleus	Gamma-ray energies			
	Greenwood	Chasman et al. [4]	Marion [5]	This work
^{24}Na				3097.33 ± 0.13
^{24}Na	3587.24 [3]			3587.81 ± 0.14
^{24}Na	3981.30 [3]			3981.69 ± 0.22
^{15}N	5269.20 ± 0.35 [6]	5270.60 ± 0.46	5268.5 ± 0.2	5270.03 ± 0.30
^{15}N	5297.8 ± 0.35 [6]	5299.03 ± 0.43	5297.4 ± 0.3	5298.53 ± 0.30
^{24}Na				5617.91 ± 0.32
^{24}Na	6395.1 ± 0.4 [3]			6396.93 ± 0.40

The energy and the intensity distribution of this doublet are given in Table I. An extrapolation to zero decay intensity allows 2752.5 ± 0.3 keV to be deduced for the energy of the (n, γ) line (Fig. 1).

As a previous determination [3] of the intense 6.4-MeV gamma ray in ^{24}Na is based on the 2.75-MeV "decay" line of ^{24}Na , we decided to repeat this measurement. To avoid any dependence of the ^{24}Na level scheme, the boot-strap approach has been applied up to the desired value of 6.4 MeV. This has been achieved by including some intense gamma rays of the $^{14}\text{N}(n, \gamma)^{15}\text{N}$ reaction. The observed gamma energies are displayed in Table II.

Gamma rays that are essentially used in the boot-strap approach are compared with other results in Table III. Only the correspondence with Chasman et al. [4] is satisfactory.

As their results are equally obtained from careful energy-interpolations this correspondence increases the confidence in our method.

Note: After private discussion with R.C. Greenwood, it appears that the simple relation E (double escape) + 1022,012 keV = E (photopeak) - the base of the actual measurement - might have to be corrected because of different probe formation mechanisms in the detector. This fact could at least partly explain the anomaly observed.

The doublet at 2.75 MeV - observed in this work - was also observed previously by Greenwood. Unfortunately he did not mention it in the reference quoted, but elsewhere (e. g. the Argonne Conference, 1966).

REFERENCES

- [1] GREENWOOD, R.C., BLACK, W.W., *Physics Lett.* 21 (1966) 702.
- [2] MURRAY, G., GRAHAM, R.L., GEIGER, J.S., *Nucl. Phys.* 63 (1965) 353.
- [3] GREENWOOD, R.C., *Physics Lett.* 23 (1966) 482.
- [4] CHASMAN, C., JONES, K.W., RISTINEN, R.A., ALBURGER, D.E., *Phys. Rev.* 159 (1967) 830.
- [5] MARION, J.B., *Nuclear Data A4* (1968) 301.
- [6] GREENWOOD, R.C., private communication quoted in Ref. [5].

GAMMA RAYS FROM THERMAL NEUTRON CAPTURE IN NATURAL AND ^{28}Si -ENRICHED SILICON*

(Abstract only)

A. M. J. SPITS, A. M. F. OP DEN KAMP, H. GRUPPELAAR
Physics Laboratory,
Rijksuniversiteit,
Utrecht, The Netherlands

Abstract

GAMMA RAYS FROM THERMAL NEUTRON CAPTURE IN NATURAL AND ^{28}Si -ENRICHED SILICON.

The gamma radiation following thermal neutron capture in natural and in ^{28}Si -enriched silicon was investigated with a Ge(Li) detector. Altogether 43 gamma rays were found, most of which could be fitted into one of the level schemes of ^{29}Si , ^{30}Si or ^{31}Si . The determination of the excitation energies of ^{29}Si was improved. The Q values for the (n, γ) reactions in the three silicon isotopes have been determined as:

$^{28}\text{Si}(n, \gamma)^{29}\text{Si}$

Q = 8 473.7 \pm 0.5 keV

$^{29}\text{Si}(n, \gamma)^{30}\text{Si}$

Q = 10 609.8 \pm 1.0 keV

$^{30}\text{Si}(n, \gamma)^{31}\text{Si}$

Q = 6 587.9 \pm 1.5 keV.

* This paper will be published in full in Nuclear Physics under the same title.

NEUTRON CAPTURE GAMMA-RAY STUDIES OF SILICON ISOTOPES

P.H. BLICHERT-TOFT, K.C. TRIPATHI
Swedish Research Council's Laboratory,
Studsvik, Nyköping, Sweden

Abstract

NEUTRON CAPTURE GAMMA-RAY STUDIES OF SILICON ISOTOPES. Neutron capture gamma rays of silicon have been studied using a Ge(Li) solid-state detector. Eighteen previously observed transitions were identified and more than 25 previously unreported transitions were observed, but all of these are not as yet firmly assigned as emitted by silicon isotopes. The neutron separation energies were found to be 8475.2 ± 0.5 , 10612.3 ± 1.0 and 5591 ± 5 keV for ^{29}Si , ^{30}Si and ^{31}Si , respectively. A single-crystal spectrometer was used to reflect the gamma-ray beam in order to suppress the Compton background from intense higher-energy gamma rays.

INTRODUCTION

The neutron capture reaction in silicon is predominantly $^{28}\text{Si}(n, \gamma)^{29}\text{Si}$ and has been investigated previously. Kinsey et al. [1] used a magnetic pair spectrometer to study this reaction and, for the gamma-ray transitions observed, reported energies with accuracies ranging from 5 to 8 keV. Adyasevich et al. [2] were able to extend the energy range covered through the use of a Compton spectrometer. The accuracy of the reported gamma-ray energies ranged from 10 to 30 keV. The most accurate and extensive data at present on transition energies and intensities were obtained by Kennett [3] using a Ge(Li) counter and a Ge(Li)-Na(Tl) coincidence spectrometer. A considerable amount of information concerning the level structure of ^{29}Si has been deduced from the (d, p) results of van Patter and Buechner [4] and Browne and Radzysinski [5] and the (p, p') data of White [6]. A summary of spin, parity and neutron orbital momentum for several states in ^{29}Si has been given by Endt and van der Leun [7]. The most recent experimental value for the neutron separation energy for ^{29}Si has been measured by Lycklama et al. [8] and is 8473.8 ± 1.4 keV.

EXPERIMENTAL PROCEDURE AND RESULTS

This measurement has been made at the research reactor R2 at AB Atomenergi, Studsvik. A detailed account of the experimental equipment has been given by Broman [9]. A target consisting of a 30-cm^3 single crystal of silicon is placed close to the reactor core in a neutron flux of about 10^{13} $\text{n cm}^{-2} \text{ sec}^{-1}$. The capture gammas are collimated by a slit collimator in front of which is placed a 1-cm thick flat-type germanium crystal. The (400) planes are used for diffraction. After the passage of a second slit collimator the gammas are finally recorded by a 3.5-cm^3 Ge(Li) detector. The crystal arrangement along with the

mounting of the Ge(Li) detector. The crystal arrangement along with the mounting of the Ge(Li) detector is described by Broman et al. [10]. The energy of the diffracted beam is given by the well-known Bragg formula

$$E = K/\sin \theta$$

θ being the angle between the crystal planes and incident gammas and K a constant determined by the crystal grating parameters. The diffraction peak width is a measure of the energy interval which is possible to scan in a single run. Since the Compton background from higher-energy gammas is almost eliminated from the diffraction region it is possible to discern weak gamma-ray transitions by this method. The angle of incidence is successively set in line with the energy region to be studied. In this particular work we have carefully scanned the energy region between 400 and 2500 keV by this method.

The gamma-ray transition energies and intensities were determined using a Ge(Li) solid-state detector (Princeton-Gammatech) with a depletion depth of 5 mm and area of 7 cm². The overall resolution of the Ge(Li) detector plus amplification system was 3.5 keV at 1.33 MeV. The relative efficiency of the Ge(Li) detector was obtained in the energy range from 0.1 to 10 MeV using a calibrated set of standardized gamma-ray sources and the relative intensities of prominent neutron capture gamma-ray transitions in titanium isotopes as established by Tripathi et al. [11].

In Fig. 1 the Ge(Li) spectrum is shown for such energy regions between 500 - 2500 keV which reveal new information as compared to results reported by previous workers [1-3, 8]. Eighteen cm of borated paraffin was used as a standard absorber in all runs to reduce the background of fast neutrons and the sufficiently low level as required by the solid-state detector. The spectra displayed in Fig. 1 have all been taken in the diffraction mode [9, 10] with the diffraction peak position falling approximately in the middle of the energy range displayed on the multichannel analyser for each particular run. A large number of similar diffraction spectra were taken for the special purpose of a careful investigation of the energy region from 400 to about 2500 keV for weak gamma-ray transitions which are not seen in a direct spectrum due to the fact that the Compton distributions of higher-energy gammas would not be sorted out.

Figure 2 shows the Ge(Li) spectrum at a collimator angle very close to the central position for the energy range from 2500 to 4500 keV. In Fig. 3 is shown the Ge(Li) spectrum with the collimator at the central position for such energy regions only which yield new information as compared to previous work [1-3, 8] between 4500 and 10 000 keV. Since the collimator is at the central position in this special measurement the gamma-ray beam enters the detector without having suffered any deflection and becomes very intense. Therefore, in addition to 18 cm of borated paraffin, a 5-cm lead absorber is applied in a distance of 30 cm from the solid-state detector.

The experimental results for gamma-ray energies and intensities are summarized in Table I and compared with the results obtained by Kennett [3] from measurements on an external target of natural silicon. The energies and isotopic assignment of calibration lines used are designated

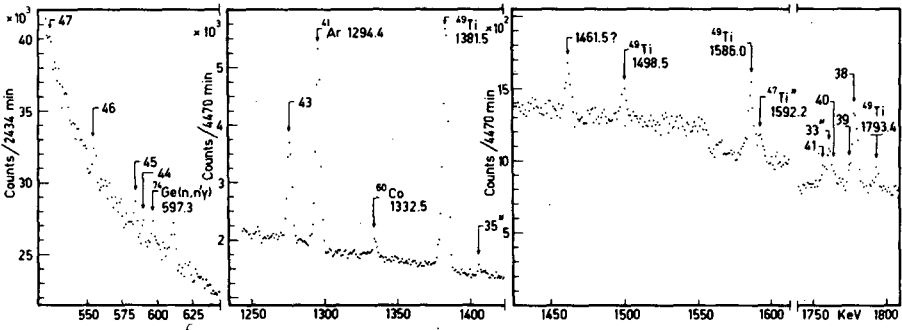


FIG. 1. Singles spectra obtained in different diffraction mode positions of neutron capture gammas from pure silicon in energy ranges of interest between 500 - 2500 keV with an 18 g/cm² borated paraffin absorber. The peaks assigned to the neutron capture gammas in silicon are labelled with a number in agreement with the conventions and those assigned to the background arising from capture in titanium are unmarked except when used for internal energy calibration. Energy transitions of unknown origin are indicated with a question mark.

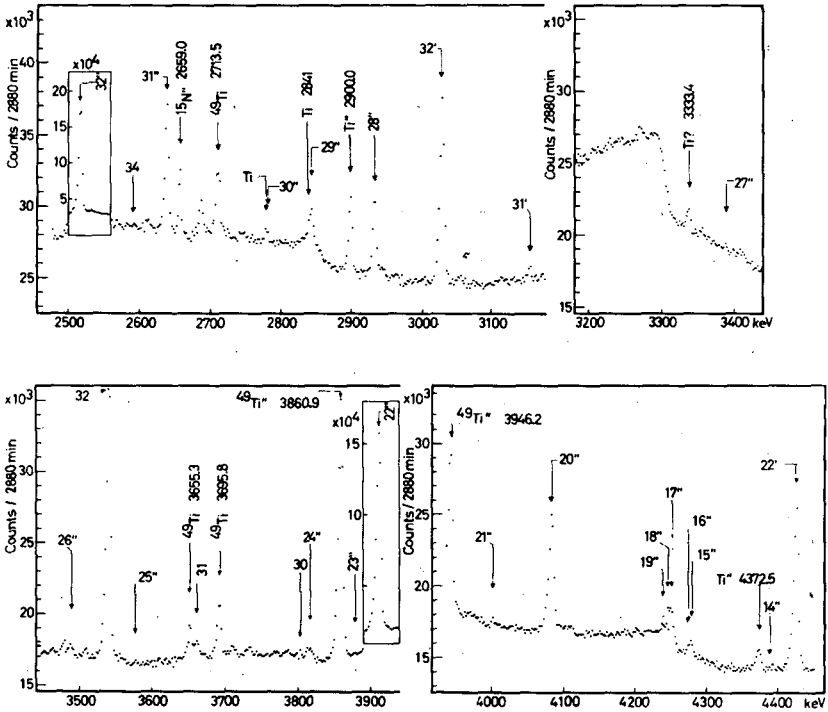


FIG. 2. Singles spectrum at a collimator angle close to the central position for the energy range 2500 to 4500 keV with an 18 g/cm² borated paraffin absorber. Peaks assigned to the neutron capture in silicon are labelled with a number and those belonging to the background due to capture in titanium are unmarked except when such lines have been used for internal energy calibration. Transitions of unknown origin are indicated by a question mark.

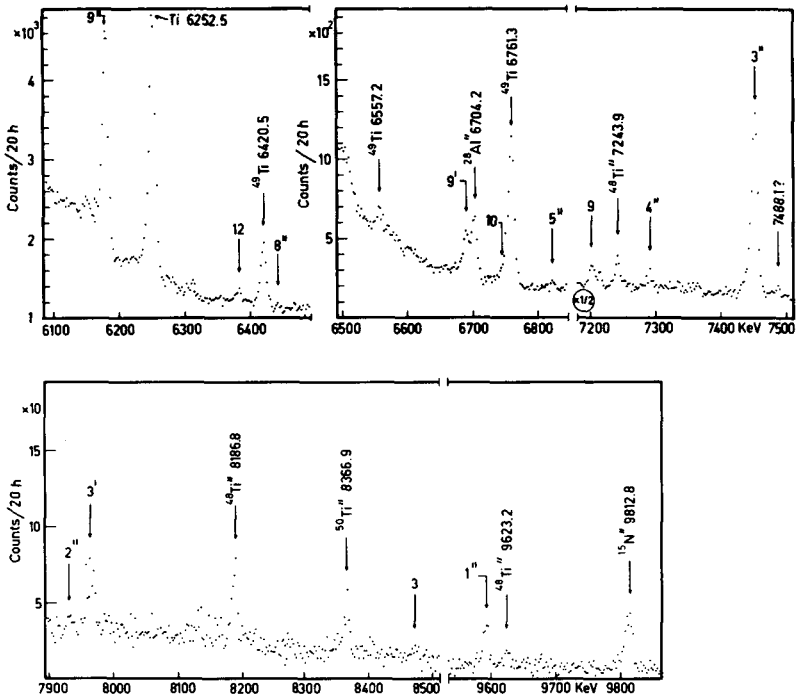


FIG. 3. Singles spectrum with the collimator at central position for energy ranges of interest between 4500-10000 keV with 18 g/cm² borated paraffin and 57 g/cm² lead absorbers. The peaks assigned to the neutron capture gammas in silicon are labelled with a number and those assigned to the background arising from neutron capture in titanium are unmarked except when used for internal energy calibration. Energies of unknown origin are labelled with a question mark.

on the spectra shown. The agreement in energy and photon intensity is in general within the experimental errors in cases where the corresponding transition has been seen by Kennett [3]. Pile-up effects due to excessive counting rates were minimized by choosing suitable absorbers and geometries.

The neutron capture decay schemes of ²⁹Si, ³⁰Si and ³¹Si are shown in Fig. 4 and are based essentially on accurate transition energies and photon intensity data (Table I) plus the coincidence data obtained by Lycklama et al. [8]. Since we have not found any experimental evidence to sustain the earlier assumption that the 3662.5-keV line is a double peak, we have not been able to place the 2783.0-keV transition. The conclusion is that previously proposed levels at 5690.7 and 4814.8 keV are not supported by this work. We have tentatively incorporated five previously unreported transitions to the ²⁹Si level scheme. These transitions are in agreement, as they should be, with the strong spin-parity rules for electromagnetic radiation. The mean value of the neutron separation energy for ²⁹Si has been found to be 8475.2 ± 0.5 keV.

The neutron capture decay scheme of ³⁰Si is rather simple, as appears from Fig. 4. Transitions considered tentatively placed are

TABLE I. LIST OF GAMMA RAYS EMITTED UPON NEUTRON CAPTURE IN SILICON AS LABELLED IN FIGS 1-3

Line No.	Emitting isotope	Transition energy ^a (keV)		Intensity (γ -rays per 100 captures)	
		Present work	[3]	Present work ^b	[3]
1	³⁰ Si	10612.5 \pm 1.5		0.2	
2		8952 \pm 3		w	
3	²⁹ Si	8474.5 \pm 0.8	8474.6	2.9	2.7
4		8314 \pm 4		w	
5		7846 \pm 3		\approx 0.15	
6		7815 \pm 4		w	
7		7696 \pm 4		w	
8		7465 \pm 3		\approx 0.3	
9	²⁹ Si	7202.0 \pm 0.5	7202.2	9	10
10	³⁰ Si	6748 \pm 2	6748.2	1.4	1.5
11	³¹ Si ?	6594 \pm 3		w	
12	²⁹ Si	6383.3 \pm 1.0	6383.2	14	14.5
13	²⁹ Si	6048 \pm 3	6048.9	0.7	0.7
14	²⁹ Si	5405 \pm 3		w	
15		5301 \pm 3		\approx 0.4	
16		5297 \pm 3		\approx 0.2	
17	³⁰ Si	5274 \pm 3		\approx 0.6	
18	³⁰ Si	5269 \pm 3		\approx 0.5	
19		5262 \pm 3		\approx 0.2	
20	²⁹ Si	5109.4 \pm 1.0	5110.3	4.1	4.5
21		5028 \pm 2		\approx 0.2	
22	²⁹ Si	4935.7 \pm 0.5	4935.8	61	61
23	³¹ Si ?	4902 \pm 3		\approx 0.07	
24	²⁹ Si	4842 \pm 3		\approx 0.3	
25		4600 \pm 2		\approx 0.1	
26		4508 \pm 2		\approx 0.4	
27		4408 \pm 2		\approx 0.2	
28	²⁹ Si	3956.2 \pm 0.5	3956.0	2.0	1.8
29	³⁰ Si	3864.0 \pm 1.0	3864.4	1.9	1.5
30	³¹ Si ?	3805 \pm 3		w	

TABLE I (cont.)

Line No.	Emitting isotope	Transition energy ^a (keV)		Intensity (γ -rays per 100 captures)	
		Present work	[3]	Present work ^b	[3]
31	²⁹ Si	3662.5 \pm 0.5	3662.6	3.6	3.6
32	²⁹ Si	3540.0 \pm 0.5	3539.7	65	64
33	²⁹ Si	2783.0 \pm 0.5	2783.1	3.2	3.0
34		2593 \pm 2		w	
35	²⁹ Si	2426.6 \pm 0.8	2427.0	2.5	2.7
36	²⁹ Si	2092.8 \pm 1.0	2092.0	20 ^b	20
37	²⁹ Si	2031.5 \pm 0.5	2031.7	4.0	3.7
38	²⁸ Si	1778.4 \pm 0.5	1779.0		
39	²⁹ Si	1775.1 \pm 0.6		4	
40	²⁹ Si	1764.5 \pm 0.6		3	
41		1757.7 \pm 0.6		4	
42	³¹ Si ?	1693 \pm 3		w	
43	²⁹ Si	1273.1 \pm 0.5	1273.0	19	20
44		589.5 \pm 1.0		w	
45		583.4 \pm 1.0		w	
46		553.8 \pm 1.0		w	
47		521.5 \pm 1.0		w	

^a All transition energies have been corrected for nuclear recoil.

^b The relative photon intensities obtained have been corrected for the various absorptions of the radiations emitted by the sample and have been normalized to the absolute intensities given by Kennett [3] in units of gamma rays per 100 captures for the 2092.8-keV transition. The accuracy of the measured intensities is about 10% except where otherwise stated. w indicates the intensity of a transition too weak for a reasonably exact intensity estimate.

shown as dashed lines. The neutron separation energy of ³⁰Si has been measured to be 10 612.3 \pm 1.0 keV by using the ground-state transition in ¹⁴N(n, γ)¹⁵N for calibration. No earlier neutron capture decay scheme of ³¹Si has ever been presented in the literature. The one shown in Fig. 4 is conjectured from transition energies and intensities and should be considered as uncertain. The tentative placements shown are the ones which should be expected on the basis of spin-parity arguments for transitions between levels known from other reaction data.

The fact that we have not been able to place consistently all the previously unknown transitions (Table I) in the level schemes of silicon isotopes indicates that these are not yet known as completely as we might

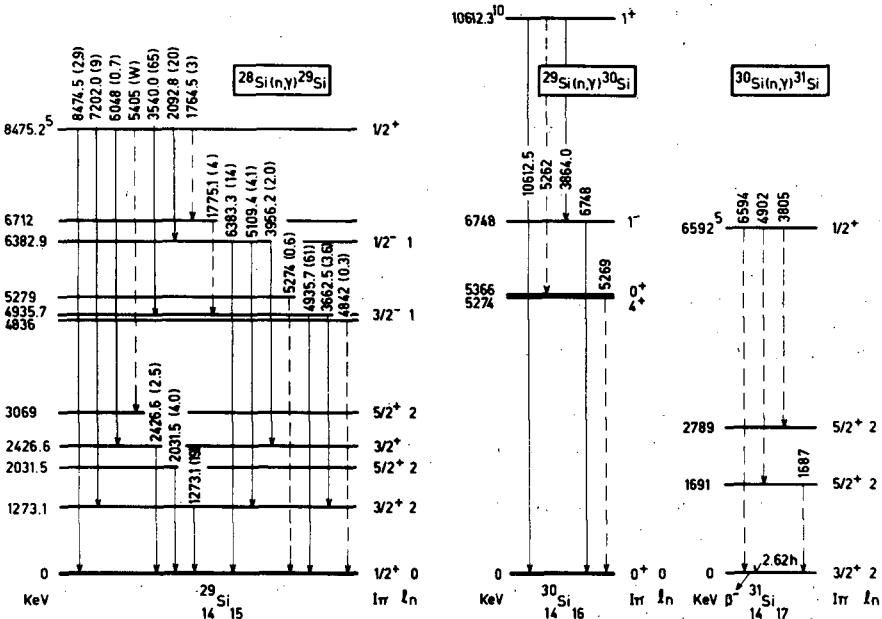


FIG.4. Levels in ^{29}Si , ^{30}Si and ^{31}Si populated in neutron capture reactions of silicon isotopes. Spin, parity and neutron orbital momentum of these levels are listed where known from other reactions as presented in the literature. Transitions shown by broken arrows have been conjectured on the basis of energies and intensities and should be considered as uncertain or ambiguous placements. Intensities in gamma rays per 100 captures for the case of $^{28}\text{Si}(n,\gamma)^{29}\text{Si}$ are given within parentheses.

desire from (d, p) or (p, p') reactions. It would also be very helpful if the existing level energies were known a little more accurately from these reactions. It may also indicate, however, that we have been unsuccessful in identifying one or the other of these transitions as belonging to the intense background radiation present, although we would emphasize that we have tried hard during the rather cumbersome and painstaking identification process.

To account for our endeavours on these aspects and to characterize the organization of the data obtained we have classified the lines which may belong to silicon isotopes into four categories:

(1) Lines which have been firmly determined on the basis of the spectra taken and which we have not been able to identify with any background radiation known at present. These lines are shown in Table I. Where it has been possible to associate the radiated line with a particular silicon isotope this has been indicated in column 2. Our assignments of gamma rays with number 14, 24, 39 and 40, however, are quite uncertain since these assignments have been based on an energy fit only. Whereas lines number 17 and 18 are clearly seen as a doublet we cannot be quite certain about the origin of these transitions.

(2) Lines of rather weak intensity which we have attributed to either silicon or titanium isotopes, partly on the basis of information given in

the work by Tripathi et al. [11]. Such lines, determined with an accuracy of 1 or 2 keV, are the following, in order of increasing energy:

725, 731, 752, 858, 1592,
2206, 2236, 3054, 3104 and 7057 keV

The upper limit of the intensity of these lines is 4 gamma rays per 100 captures.

(3) Transitions which have been poorly indicated by our experimental data, either due to overlapping with other radiations or a lack of sufficient statistics of the peaks. These transitions have been determined with an accuracy of 2 or 3 keV and are the following, in order of increasing energy:

1252, 1306, 1448, 1534, 1566, 1868,
2027, 3772, 6447 and 7112 keV

Since the existence of the above-listed lines is to some extent doubtful we have not attempted to place them.

(4) It is clear that weak lines emitted by silicon isotopes may exist which are hidden by prominent neutron capture gamma-ray transitions of titanium isotopes (our target holder consisted of titanium). To find out which line energies could come into focus the reader is referred to Figs 1, 2 and 3 and the extensive work by Tripathi et al. [11] on neutron capture studies of titanium isotopes. We are here, of course, limited in our efforts to see any of the weaker gamma rays emitted by silicon isotopes which belong to the above-mentioned category. This would require an experimental geometry which would allow the background radiation to be considerably reduced with regard to number of lines as well as in intensity.

An attempt will be made to give a further description of the level schemes presented in this paper in the light of existing theories of nuclear structure within the particular mass region to which silicon isotopes belong.

ACKNOWLEDGEMENTS

We wish to express our gratitude to Professor Nils Ryde for his valuable advice and confidence in our work. Financial support was furnished by Statens råd för atomforskning.

REFERENCES

- [1] KINSEY, B.B., BARTHOLOMEW, G.A., WALKER, W.H., *Phys. Rev.* 83 (1951) 519.
- [2] ADYASEVICH, B.P., GROSHEV, L.V., DEMIDOV, A.M., *Nucl. Energy* 3 (1956) 258.
- [3] KENNETT, T.J., private communication to *Nuclear Data A3* (1967) 420.
- [4] VAN PATTTER, D.M., BUECHNER, W.W., *Phys. Rev.* 87 (1952) 51.
- [5] BROWNE, C.P., RADZYMINSKI, J.T., *Nucl. Phys.* 14 (1960) 164.

- [6] WHITE, R.E., Phys. Rev. 119 (1960) 767.
- [7] ENDT, P.M., VAN DER LEUN, C., Nucl. Phys. A105 (1967) 154.
- [8] LYCKLAMA, H., HUGHES, L.B., KENNETT, T.J., Can. J. Phys. 45 (1967) 1871.
- [9] BROMAN, L., Studsvik Rep. LFF-22 (1966).
- [10] BROMAN, L., LILJENFORS, B., TRIPATHI, K.C., Studsvik Rep. LFF-23 (1967).
- [11] TRIPATHI, K.C., BLICHERT-TOFT, P.H., BOREVING, S., "Thermal neutron capture gamma-ray studies of natural titanium", these Proceedings.

THERMAL NEUTRON CAPTURE GAMMA-RAY STUDIES OF NATURAL TITANIUM

K. C. TRIPATHI, P. H. BLICHERT-TOFT, S. BOREVING

Department of Physics,

Chalmers University of Technology,

Gothenburg,

and

The Swedish Research Council's Laboratory,

Studsvik, Nyköping, Sweden

Abstract

THERMAL NEUTRON CAPTURE GAMMA-RAY STUDIES OF NATURAL TITANIUM. Detailed and precise measurements of the gamma rays following thermal neutron capture in natural titanium have been made by means of a single flat crystal diffraction spectrometer and Ge(Li) detectors below 3.5 MeV and as direct spectra above 1.6 MeV. Many previously unreported transition energies have been observed and fitted into the level schemes of ^{47}Ti , ^{48}Ti , ^{49}Ti , ^{50}Ti and ^{51}Ti . The neutron binding energies obtained for the titanium isotopes from the transition assignments are in agreement with the values calculated from mass measurements within the experimental errors (about 2 keV). More accurate values of a number of levels in the titanium isotopes have been determined as compared to earlier (d, p) measurements.

INTRODUCTION

Earlier measurements on capture gamma-rays from natural titanium have been done by Motz [1], Adyasevich, Groshev and Demidov [2], Kinsey and Bartholomew [3], and Knowles et al. [4]. These measurements were made by means of Compton or pair spectrometers or crystal diffraction spectrometers using NaI(Tl) scintillation spectrometers. Knowles et al. [4] and Carlos et al. [5] have performed coincidence measurements. Trumpy [6] and Vervier [7] have contributed with polarization measurements. Tenenbaum et al. [8] have used a Ge(Li) detector in their investigations. The present work reports on the measurements made by a single flat crystal diffraction spectrometer in combination with a large Ge(Li) detector. In this method the Compton background and double-escape peaks due to lines beyond the diffraction region are almost absent. This makes it a high resolution and an effective apparatus. The investigation has led to the detection of 146 gamma-rays, many of which were previously unreported.

EXPERIMENTAL ARRANGEMENT AND PROCEDURE

This work was performed at the Swedish Reactor R2 at AB Atomenergi, Studsvik. An internal target geometry was used where the reactor channel is tangential to the reactor core so as to avoid the detector from seeing the core and facilitate sample changing. The target was placed as close as possible to the core to obtain a maximum of neutron flux of approximately $10^{13} \text{ n cm}^{-2} \text{ sec}^{-1}$. The target used consisted of a rectangular slab of natural

metallic titanium of weight and purity 51 g and 99.9%, respectively. The spectra were recorded with a 1024-channel analyser exhibiting a small deviation from linearity which was taken into proper account by the experiment and energy calculation.

1. Measurements of direct spectra

For these measurements a 17-cm³ Ge(Li) detector was used with a resolution of 5.5 keV at 1.33 MeV. The detector was placed so as to see the direct incident beam of gamma rays. A 15.5-cm thick lead absorber was put at a distance of 50 cm from the detector, allowing the low-energy X-rays to be absorbed in the air before reaching the detector and thus reducing further the dead time of the multichannel analyser. This absorber also decreases the neutron background at the detector to the required level. The energy region between 1.6 and 10.0 MeV was well spread along the energy axis and divided into a number of parts, each of which successively overlapped the neighbouring one. Long-time measurements were made to obtain reasonable statistics for analysing even the weaker transitions emitted by the titanium isotopes.

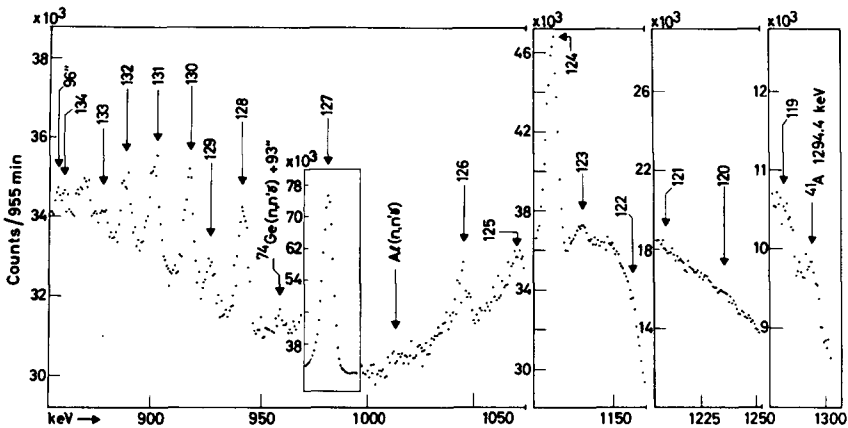


FIG.1. Spectrum of thermal neutron capture gamma-rays of natural titanium in the diffraction region of 800-1300 keV using the (400) diffraction plane of the flat crystal. A 5-mm lead absorber was put in front of the detector.

2. Single flat crystal diffraction measurements

The energy region below 3.5 MeV has been investigated using a single flat crystal diffraction spectrometer in combination with the above-mentioned Ge(Li) detector. This arrangement is described in more detail by Broman [9] and reviewed by Blichert-Toft et al. [10].

In most measurements the (400) planes of the germanium flat crystal have been used for diffraction of the gamma rays. In some cases, however, the information has been obtained by diffraction in the (200) and other planes. Below 200 keV the absorption in the germanium crystal starts to play a dominant role and results in a lower limit of about 100 keV.

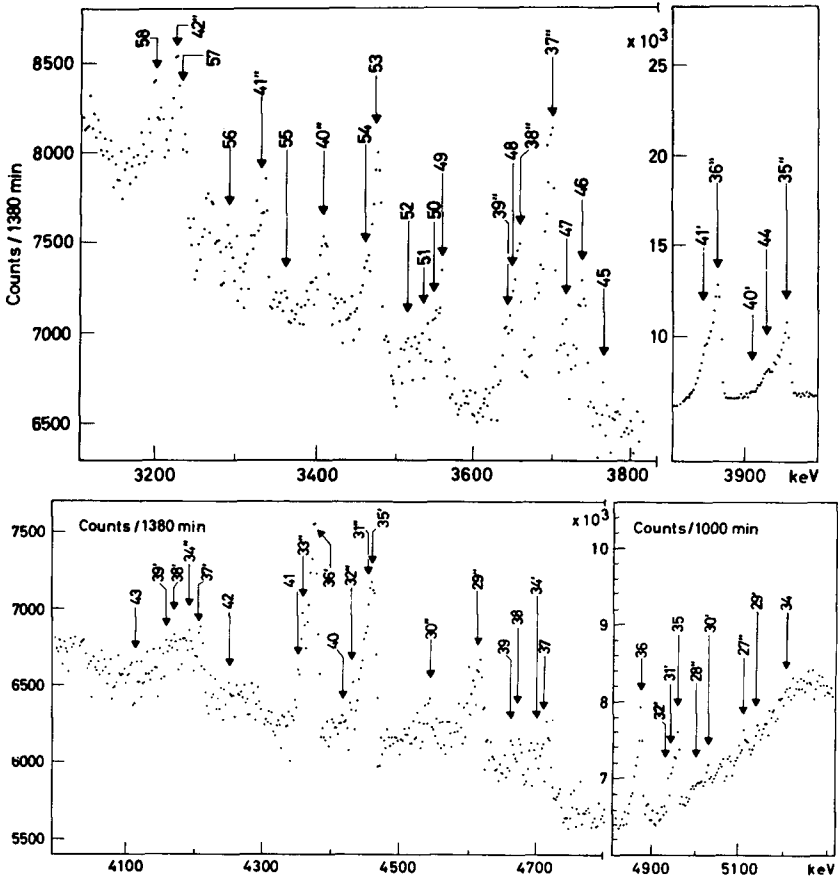


FIG.2. Observed direct spectrum of thermal neutron capture gamma-rays of natural titanium in the region of 3100-5300 keV taken with a 17-cm³ Ge(Li) detector. The information obtained is based on two different experimental runs. A 15.5-cm thick lead absorber was put in front of the detector.

3. Experimental data

A typical spectrum from the diffraction measurements which cover the energy region from 150-2900 keV is shown in Fig. 1 and a typical direct spectrum in Fig. 2. The direct spectra cover the energy region from 2200-9300 keV and have all been observed with a 17-cm³ Ge(Li) detector with an energy resolution of 5.5 keV at 1.33 MeV.

Figure 3 is part of a spectrum taken by Blichert-Toft et al. [10] during an investigation of thermal neutron capture gamma-rays from silicon isotopes. Since a target holder consisting of titanium has been used, strong titanium lines are observed as background because the neutron capture cross-section of titanium is much larger than that of the silicon isotopes.

For energy calibration IAEA standard sources were used up to about 3 MeV and precise energy values of these sources were adopted from the compilation of Legrand et al. [11]. For determination of the higher energies

the position of double and single-escape peaks of strong higher-energy titanium lines falling below 3 MeV were determined and the corresponding photolines were used for calibration above 3 MeV. This process was repeated to obtain successively higher calibration lines.

By means of a computer program the peaks were fitted to a Gaussian and the positions of the peaks and the areas below them were determined. By another computer program the energies corresponding to the peaks were computed by means of the known calibration lines. From various runs in the same energy region a mean value was adopted for the energy of each line. The non-linearity in the multichannel analyser was accounted for. The energies above 4 MeV were corrected for nuclear recoil. Later on these energy values were checked by using the well-known ^{15}N neutron separation energy and the neutron separation energies of silicon isotopes for calibration as shown in Fig. 3.

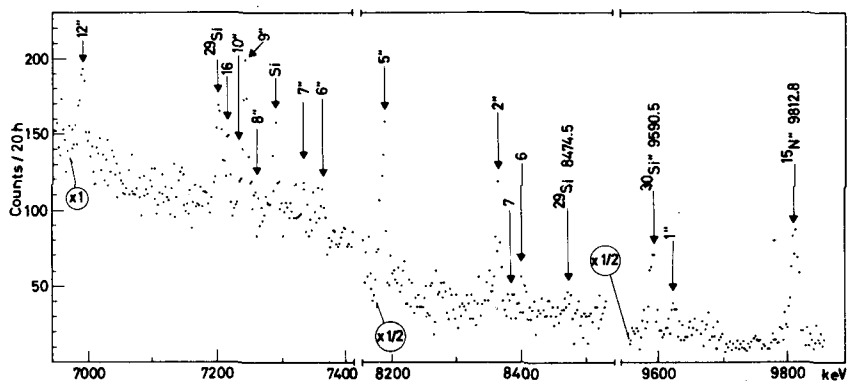


FIG. 3. A part of the direct spectrum observed by a 3.5-cm^3 Ge(Li) detector and a 4096-channel analyser in the energy region of 7000-9900 keV. Only the parts of general interest are shown in the figure.

To determine intensities the areas under the relatively strong peaks calculated by the computer were used, while a manual procedure was adopted for the weaker lines. In the case of a direct incident beam of gamma rays corrections were made to account for self-absorption, absorption due to air, crystal and lead between sample and detector and the efficiency of the detector itself. For diffraction measurements a correction for the crystal reflectivity was added.

4. Results

The gamma rays observed following thermal neutron capture in natural titanium originate from five isotopes. The relative abundances and thermal neutron capture cross-sections of these isotopes as taken from the Nuclear Data Sheets along with their relevant contributions to neutron capture have been given in Table I.

The calculated energies with errors and intensities have been tabulated in Table II. The accuracy of the intensities is about 20% unless otherwise noted. On the basis of the known relative contributions to neutron capture

TABLE I. RELATIVE ABUNDANCES AND THERMAL NEUTRON CAPTURE CROSS-SECTIONS OF TITANIUM ISOTOPES AND RELEVANT CONTRIBUTION OF TARGET IN NATURAL TITANIUM

Target	Abundance (%)	Isotopic σ_{nA}	Relevant contribution of target	Approximate contribution of target (%)
^{46}Ti	7.95	0.6	4.77	0.7
^{47}Ti	7.75	1.7	13.18	2.2
^{48}Ti	73.45	7.7	565.56	95.0
^{49}Ti	5.51	1.8	9.92	1.7
^{50}Ti	5.34	≈ 0.4	2.14	0.3

it is evident that the most intense gamma-ray lines are emitted by ^{49}Ti . The lines with energy larger than the neutron separation energy of ^{49}Ti are likely to be emitted by ^{47}Ti , ^{48}Ti , ^{50}Ti or ^{51}Ti . On the basis of a careful energy determination, most of the observed energies have been fitted in the respective level schemes of titanium isotopes. The neutron-binding energies based on the calculated energies of the observed lines and their placements in the relevant level schemes agree within 3 keV with the corresponding values obtained from mass data [12]. By using the Ritz combination principle it has thus been possible to determine the energy values of a number of levels belonging to above-mentioned isotopes with more accuracy than earlier measurements. A few previously unreported thermal neutron capture gamma-ray transitions have been given in Table II and in many cases of previously known transitions the transition energies have been determined more accurately than before.

In some cases where transition energies may fit in the level schemes of more than one isotope it may be possible to predict the origin of such lines on the basis of a comparison of the relevant intensities with the relative contributions to neutron capture by the various isotopes as presented in Table I. In other cases, however, in which a unique isotope assignment was not possible the transitions in question have been placed in the level schemes of the relevant isotopes. Table III presents the energy values of the levels and spins of ^{47}Ti , ^{48}Ti , ^{49}Ti , ^{50}Ti and ^{51}Ti as determined in the present work.

INTERPRETATION OF LEVEL SCHEMES

According to the simple shell model the titanium isotopes ^{47}Ti to ^{51}Ti consist of a doubly magic core of ^{40}Ca surrounded by two protons plus an appropriate number of neutrons in the $f_{7/2}$ and higher orbits. McCullen et al. [13] have made calculations based upon shell model theory and predict the energies and wave functions of states of pure $(f_{7/2})^n$ configurations for all of the nuclei in the shell. On this basis the neutron wave functions of the ground states of ^{47}Ti , ^{48}Ti and ^{49}Ti may be represented by $f_{7/2}^5$, $f_{7/2}^6$

TABLE II. OBSERVED ENERGIES AND INTENSITIES OF GAMMA RAYS EMITTED AFTER THERMAL NEUTRON CAPTURE IN NATURAL TITANIUM AND ASSIGNMENTS OF ISOTOPES TO WHICH THEY MAY BELONG, AND POSSIBLE TRANSITIONS

Line No.	Energy ^a (keV)	Intensity ^b	Isotope assignment	Probable transition	Line No.	Energy ^a (keV)	Intensity ^b	Isotope assignment	Probable transition
1	10647 ± 2.0	0.03	⁴⁸ Ti	C → 983.5	23	6557.2 ± 1.0	3.9	⁴⁹ Ti	C → 1586.0
2	9389.1 ± 2.0	0.09	⁵⁰ Ti	C → 1553.4	24	6532 ± 5	w	⁴⁹ Ti ⁵⁰ Ti	C → 1618 C → 4422
3	9326 ± 6	v w	⁴⁸ Ti	C → 2295.6	25	6419.6 ± 3.0	29	⁴⁹ Ti	C → 1722.9
4	9235 ± 8	v w	?		26	6378 ± 2	w	⁴⁷ Ti ⁵¹ Ti	C → 2500 C → g
5	9209 ± 3	0.13	⁴⁸ Ti	C → 2420.8	27	6146 ± 8	v w	⁵⁰ Ti	C → 4799
6	8410 ± 5	>0.06	⁴⁸ Ti	C → 3224.3	28	6011 ?	v w	⁴⁷ Ti	C → 2852
7	8390 ± 5	≤0.06	⁴⁸ Ti	C → 3239.5	29	5637.5 ± 2.0	≈1	⁴⁹ Ti	C → 2505
8	8281 ± 5	<0.01	⁴⁸ Ti	C → 3342	30	5561 ± 5	≈0.5	⁵⁰ Ti	C → 5394
9	8265 ± 3	0.17	⁴⁸ Ti	C → 3362	31	5472 ± 10	w	⁴⁹ Ti	C → 2662
10	8256 ± 2	0.02	⁵⁰ Ti ⁴⁸ Ti	C → 2688 C → 3377	32	5428 ± 10	w	⁴⁹ Ti	C → 2717
11	8114 ± 5	0.02	⁴⁸ Ti	C → 3514	33	5365 ± 10	v w	⁴⁷ Ti	5365 → g
12	8013 ± 2	0.15	⁴⁸ Ti	C → 3623	34	5214 ± 10	v w	⁵¹ Ti	C → 1159
13	7627 ± 2	0.2	⁴⁷ Ti	C → 1248	35	4969.5 ± 1.0	4.0	⁴⁹ Ti	C → 3174.9
14	7554 ± 10	v w	⁴⁸ Ti	C → 4087	36	4883.0 ± 1.0	5.6	⁴⁹ Ti	C → 3262
15	7334 ± 2	<0.1	⁴⁷ Ti	C → 1541	37	4716.0 ± 2.0	≈1	⁴⁹ Ti	C → 3429
16	7217 ± 5	0.03	⁴⁸ Ti	C → 4410	38	4675 ± 3	w	⁴⁹ Ti	C → 3470
17	7171 ± 4	0.12	⁴⁸ Ti ⁵⁰ Ti	C → 4465 C → 3770	39	4659 ± 5	w		
18	7083 ± 2	<0.1	⁴⁷ Ti	C → 1793.4	40	4418 ± 5	w	⁵⁰ Ti	4422 → g
19	7063 ± 4	0.45	⁴⁷ Ti ⁵⁰ Ti	C → 1818.4 C → 3879	41	4352 ± 5	w		
20	6819 ± 6	0.04	⁴⁸ Ti	C → 4809	42	4247 ± 2	w	⁵¹ Ti	C → 2132
21	6761.6 ± 2.0	41	⁴⁹ Ti ⁵⁰ Ti	C → 1381.5 C → 4184	43	4177 ± 8	v w	⁴⁸ Ti ?	
22	6604 ± 3	w	⁴⁹ Ti	C → 1540.1	44	3921.7 ± 2.0	2.1	⁴⁹ Ti	$\left\{ \begin{array}{l} C \rightarrow 4224.5 \\ 5310 \rightarrow 1381.5 \end{array} \right.$
					45	3762.6 ± 2.0	0.1	⁵¹ Ti	3762.6 → g

TABLE II. (cont.)

Line No.	Energy ^a (keV)	Intensity ^b	Isotope assignment	Probable transition	Line No.	Energy ^a (keV)	Intensity ^b	Isotope assignment	Probable transition
46	3734 ± 2	0.7	⁴⁹ Ti	{ C → 4410 5120 → 1381.5	70	2841.5 ± 1.5	0.8	⁴⁹ Ti	{ C → 5310 5310 → 2464 4224 → 1381.5
47	3713 ± 2	w			71	2728 ± 5		{ ⁵⁰ Ti ? ⁴⁸ Ti ?	
48	3642 ± 8	w	⁵⁰ Ti ?						
49	3556 ± 5				72	2712 ± 5			
50	3544 ± 3	0.44	⁴⁹ Ti	5800 → 2260	73	2692.5 ± 2.0			
51	3530 ± 10	<0.1	⁴⁷ Ti	C → 5365	74	2635 ± 2	≈0.3	⁴⁸ Ti	3623 → 983.5
52	3508 ± 10	w			75	2617 ± 2		{ ⁴⁷ Ti ⁵¹ Ti	2617 → g C → 3763
53	3476 ± 2	1.5	⁴⁹ Ti	C → 4668	76	2535 ± 5			
54	3462 ± 10	w	⁴⁸ Ti ?		77	2513 ± 5	w	⁴⁸ Ti	4809 → 2295.6
55	3380 ± 4	w	⁴⁸ Ti	3362 → g	78	2500 ± 5	w	{ ⁴⁷ Ti ⁴⁹ Ti ?	2500 → g
56	3284 ± 5	w			79	2475 ± 4	w	⁴⁹ Ti	4980 → 2505
57	3225.2 ± 0.5				80	2407 ± 5	w	⁴⁸ Ti	3377 → 983.5
58	3197 ± 4		⁴⁷ Ti ?		81	2378 ± 5	w	⁴⁸ Ti	3362 → 983.5
59	3099 ± 8		⁴⁸ Ti ?		82	2350 ± 5	w	⁴⁹ Ti	C → 5800
60	3083 ± 2	≈0.2	⁴⁹ Ti	5800 → 2717	fep (?)	2316 ± 10	w	⁵⁰ Ti	3879 → 1553.4
61	3069 ± 8				83	2260 ± 4	0.2	⁴⁸ Ti	3239.5 → 983.5
62	3048 ± 8	w	⁴⁹ Ti	5310 → 2260	84	2239 ± 2	0.08	⁴⁸ Ti	3224.3 → 983.5
63	3027.2 ± 1.0	2.1	⁴⁹ Ti	{ C → 5120 4410 → 1381.5 5135.5 → 2132	85	2216 ± 4	≈0.2	⁵⁰ Ti	3770 → 1553.4
64	3003.5 ± 3.0	w	⁵¹ Ti			86	2192 ± 4		{ ⁴⁸ Ti ? ⁵¹ Ti
65	2994.6 ?	v w			87	2158 ± 5		{ ⁴⁸ Ti ? ⁴⁹ Ti ?	
66	2967.4 ± 2.0	0.8							
67	2945.0 ± 1.0	0.8	⁴⁹ Ti	4668 → 1722.9					
68	2931 ?	v w							
69	2855 ± 5	w	{ ⁴⁷ Ti ⁵⁰ Ti	{ 2852 → g 4422 → 1553.4					

TABLE II. (cont.)

Line No.	Energy ^a (keV)	Intensity ^b	Isotope assignment	Probable transition	Line No.	Energy ^a (keV)	Intensity ^b	Isotope assignment	Probable transition
88	2132 ± 2	w	⁵¹ Ti	2132 → g	110	1586.0 ± 0.2	10.4	⁴⁹ Ti	1586.0 → g
89	2090.6 ± 3.0		⁴⁸ Ti ?		111	1553.4 ± 0.2	1.7	⁵⁰ Ti	1553.4 → g
90	2077 ± 5				112	1498.5 ± 0.5	4.9	{ ⁴⁹ Ti ⁵⁰ Ti	{3262 → 1761.9 4184 → 2688
91	2047.4 ± 2.0 ^c		{ ⁴⁸ Ti ⁴⁹ Ti	{4465 → 2420.8 3429 → 1381.5	113	1473.3 ± 1.0	0.2	{ ⁵⁰ Ti ? ⁴⁸ Ti ?	
92	2027.5 ± 2.0		⁴⁸ Ti	3010 → 983.5	114	1451 ± 2	0.2		
93	1984 ± 1	0.5	⁴⁸ Ti	4410 → 2420	115	1437.3 ± 0.5	0.7	⁴⁸ Ti	2420.8 → 983.5
94	1940.2 ± 1.0				116	1381.5 ± 0.5	82	{ ⁴⁹ Ti ⁴⁷ Ti	{1381.5 → g 1541 → 158.6
95	1915 ± 2		⁴⁸ Ti ?		117	1328.3 ± 0.5	0.36	⁴⁸ Ti	{3623 → 2295.6 3752 → 2420.8
96	1881 ± 1	≈ 0.5	⁴⁹ Ti	{3262 → 1381.5 3470 → 1586	118	1312.1 ± 0.3	0.77	⁴⁸ Ti	2295.6 → 983.5
97	1842.2 ± 0.5	≈ 1.2	⁴⁹ Ti	3429 → 1586	119	1282 ± 1	w		
98	1818.4 ± 1.0		{ ⁴⁷ Ti ⁴⁸ Ti	{1818 → g	120	1242 ± 1	w	⁵¹ Ti	C → 5136
99	1793.4 ± 0.4	2.0	{ ⁴⁹ Ti ⁴⁸ Ti	{3174.9 → 1381.5 4087 → 2295.6	121	1214 ± 3	w	⁴⁸ Ti	3514 → 2295.6
100	1761.9 ± 0.5	4.5	⁴⁹ Ti	1761.9 → g	122	1159 ± 2	w	⁵¹ Ti	1159 → g
101	1739 ± 1				123	1134.6 ± 0.5	0.14	⁵⁰ Ti	2688 → 1553.4
102	1718 ± 2				124	1121 ± 1	1.0	{ ⁴⁹ Ti ⁴⁸ Ti	{2505 → 1381.5 2662 → 1540.1
103	1675.2 ± 0.8	0.22	⁴⁸ Ti	3262 → 1586					4465 → 3342
104	1669 ± 1	w			125	1064 ± 3	w	{ ⁴⁹ Ti ? ⁴⁸ Ti	{3362 → 2295.6 ?
105	1650 ± 3	w	⁵⁰ Ti ?		126	1046.2 ± 1.0	0.07	{ ⁴⁹ Ti ⁴⁸ Ti	{2662 → 1618 3342 → 2295.6
106	1640 ± 3	w							4410 → 3362
107	1632 ± 3	w	⁴⁷ Ti	1793 → 158.6					
108	1622 ± 3	w	⁴⁸ Ti ?						
109	1618 ± 3	w	{ ⁵⁰ Ti ? ⁴⁹ Ti	{1618 → g					

TABLE II. (cont.)

Line No.	Energy ^a (keV)	Intensity ^b	Isotope assignment	Probable transition	Line No.	Energy ^a (keV)	Intensity ^b	Isotope assignment	Probable transition
127	983.5 ± 0.4	2.9	⁴⁸ Ti	983.5 → g	138	608 ± 1	w	⁴⁸ Ti ?	
128	943.7 ± 0.5	0.19	{ ⁴⁸ Ti ⁴⁸ Ti	3362 → 2420.8	139	602.3 ± 0.5	w	⁴⁸ Ti ?	
				3239.5 → 2295.6	140	482 ± 2			
129	928.7 ± 0.7	0.08	⁴⁸ Ti	3224.3 → 2295.6	141	454 ± 1 ^c	w	⁴⁹ Ti	2717 → 2260
130	918.2 ± 0.5	0.18	{ ⁵⁰ Ti ? ⁴⁹ Ti ?		142	351.5 ± 0.5		⁴⁸ Ti	3362 → 3010
					143	341.4 ± 0.5	29	⁴⁹ Ti	1722.9 → 1381.5
131	902.0 ± 0.6	0.19			144	328 ± 2			
132	889.1 ± 0.5	0.12	⁴⁸ Ti	2505 → 1618	145	251.5 ± 0.5	w	⁴⁹ Ti	2717 → 2464
133	878.5 ± 0.5	0.05	⁴⁹ Ti	2260 → 1381.5	146	158.6 ± 0.5		{ ⁴⁷ Ti ⁴⁹ Ti	158.6 → g
134	860.2 ± 0.5	0.04	⁴⁸ Ti	4087 → 3224.3					1540 → 1381.5
135	819 ± 1	w	⁴⁸ Ti	3239 → 2420.8					
136	793 ± 1	w	⁴⁸ Ti ?						
137	637.8 ± 0.5	w	⁴⁹ Ti	2260 → 1618					

^a The transition energies have been corrected for nuclear recoil.

^b The relative photon intensities obtained have been corrected for the various absorptions of the radiations emitted by the sample and have been normalized to the absolute intensities given by Knowles [4] in units of gamma rays per 100 captures for the 1381.5-keV transition. The accuracy of the measured intensities is about 20% except where otherwise stated. w and v w indicate the intensity of a transition too weak for a reasonably exact intensity estimate. Where no intensity has been given, an estimate of the proper intensity was not possible due to overlapping of radiations.

^c This peak appears to be a doublet line.

TABLE III. LEVEL ENERGIES AND SPIN VALUES AND CALCULATED MEAN VALUES OF NEUTRON BINDING ENERGIES OF TITANIUM ISOTOPES AS OBTAINED IN THE PRESENT WORK

⁴⁷ Ti		⁴⁹ Ti		⁵¹ Ti		⁴⁸ Ti		⁵⁰ Ti	
Energy (keV)	$I\pi^a$	Energy (keV)	$I\pi^a$	Energy (keV)	$I\pi^a$	Energy (keV)	$I\pi^a$	Energy (keV)	$I\pi^a$
0	5/2 ⁻	0	7/2 ⁻	0	3/2 ⁻	0	0 ⁺	0	0 ⁺
158.6 ± 0.5	7/2 ⁻	1381.5 ± 0.5	3/2 ⁻	1159 ± 2	1/2 ⁻	983.5 ± 0.4	2 ⁺	1553.4 ± 0.5	2 ⁺
1248 ± 2	1/2 ⁻	1540.1 ± 0.5		2132 ± 2	5/2 ⁻	2295.6 ± 0.5	4 ⁺	2688.0 ± 0.5	4 ⁺
1541 ± 2	3/2 ⁻	1586.0 ± 0.2	3/2 ⁻	3762.6 ± 2.0	5/2 ⁻ ?	2420.8 ± 0.5	2 ⁺	3770 ± 2	
1793.4 ± 2.0	1/2 ⁻	1618 ± 2		5136 ± 5	5/2 ⁻	3010 ± 1	0 ⁺	3879 ± 10	0 ⁺
						3224.3 ± 1.0	4 ⁺	4184 ± 10	2 ⁺
1818.4 ± 1.2	3/2 ⁺	1722.9 ± 1.0	1/2 ⁻	6378.7 ± 1.0 ^b	1/2 ⁺ ?	3239.5 ± 1.0 (4 ⁺)		4422 ± 8	3 ⁻
						3342.0 ± 0.5 =4 ^d		4799 ± 10	
2500 ± 3	1/2	1761.9 ± 0.5		6379 ± 5 ^c		3362 ± 1	3 ⁻ , 2 ⁺	5394 ± 8	
2617 ± 3		2260 ± 4							
2852 ± 5	(3/2 ⁻)	2464 ± 5	7/2 ⁻			3372 ± 5	4 ⁺ ?	10943.3 ± 2	^b 3, 4 ⁻
5365 ± 10		2505 ± 2	5/2 ⁻			3514 ± 5	=6 ⁺	10944.4 ± 3.5 ^c	
8873.2 ± 3.0 ^b	1/2 ⁺	2662 ± 3				3623 ± 8	=4 ⁺		
						3752 ± 5	=4 ⁺		
8875.4 ± 2.5 ^c		2717 ± 3				4087 ± 5			
		3174.9 ± 1.0	1/2 ⁻			4410 ± 5			
		3262.0 ± 1.6	3/2 ⁻			4465 ± 5			
		3429 ± 2				4809 ± 4			
		3470 ± 4							
		4224.5 ± 1.0							
		4410 ± 2				11628.7 ± 2.3 ^b			
		4668 ± 2				11628.0 ± 2.7 ^c	2, 3 ⁻		
		4980 ± 5							
		5120 ± 5							
		5310 ± 8							
		5800 ± 4							
		8143.3 ± 1.2 ^b	1/2 ⁺						
		8146.0 ± 2.2 ^c							

^a In cases of disagreement between spin values reported in the literature these values have been based upon the transition intensities obtained in this work.

^b The value of the neutron binding energy as calculated on the basis of transition intensities obtained in this work.

^c The value of the neutron binding energy as derived from mass data [12].

^d Our results, in agreement with Konijn et al. [23], do not support a spin value of 6⁺ as reported elsewhere.

and $f_{7/2}^7$ configurations or, in terms of holes in the closed $f_{7/2}$ shell, by $f_{7/2}^{-3}$, $f_{7/2}^{-2}$ and $f_{7/2}^{-1}$ configurations respectively. In ⁵⁰Ti the $f_{7/2}$ shell is full and in ⁵¹Ti the last neutron is in the $p_{3/2}$ state. For all these isotopes except one the experimental ground state spins are in agreement with these calculations. ⁴⁷Ti has spin 5/2 instead of the theoretically predicted value of 7/2. McCullen et al. [13] account for this discrepancy by assuming configuration mixing. Malik and Scholz [14], however, account for the anomaly by using the strong-coupling symmetric-rotator model including Coriolis coupling between bands.

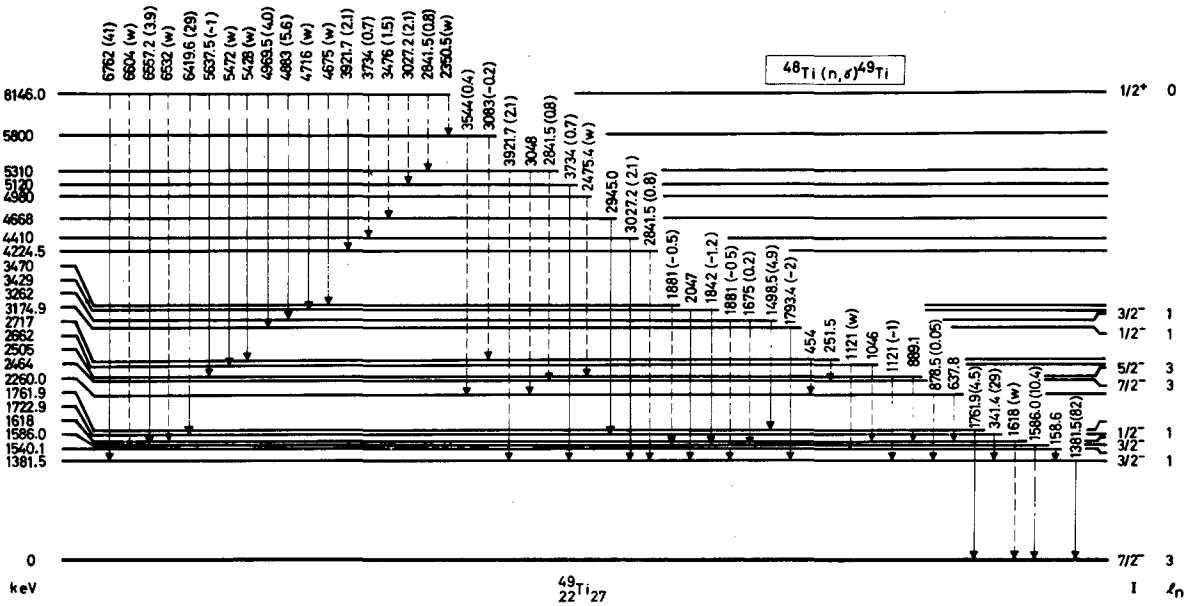


FIG.6. Levels in ^{49}Ti as decided on the basis of energy fit. Other information taken from the sources indicated in Fig.4.

that it may have a $(f_{7/2})^n$ configuration. It may, however, have a long half-life. The levels at 1818.4 and 2617 keV may be candidates for hole states, since Kashy and Conlon [16] do observe an $l_n = 2$ distribution with appreciable spectroscopic strength for the 1818.4 state in (p, d) reactions. But considering the intensity of the 7063-keV transition, $l_n = 3$ is favoured since

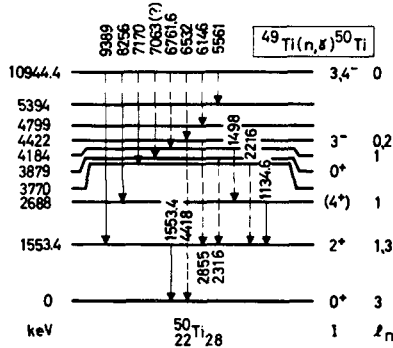


FIG.7. Levels in ^{50}Ti as decided on the basis of energy fit. Other information taken from the sources indicated in Fig.4.

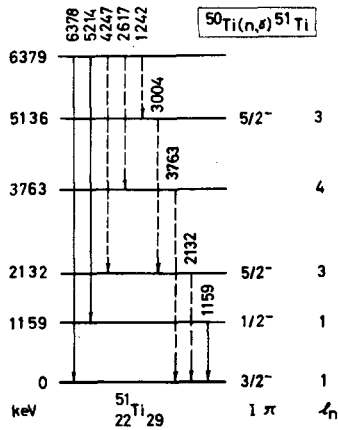


FIG.8. Levels in ^{51}Ti as decided on the basis of energy fit. Other information taken from the sources indicated in Fig.4.

this transition has a higher spectroscopic strength. The 1818-keV state may belong to the $(1f_{5/2})$ configuration. I_γ/E_γ^3 from (n, γ) reactions are in general proportional to reduced widths (spectroscopic factors) of (d, p) reactions. Moreover in the present (n, γ) measurements no feeding to the 2617-keV state from the capture state was observed. A comparison could be made with the (n, γ) coincidence measurements by Tenenbaum et al. [17].

The calculated neutron binding energy of ^{48}Ti is 11628.7 ± 2.3 keV. The level energies, shown in Table III, seem to agree well with the (d, p) measurements by Bjerregaard et al. [18], Barnes et al. [19] and Alty et al. [20].

More accurate energy values of the levels have been determined. The 983.5-keV level (which is a 2^+ state) is fed by a transition from the capture state, from the 2295.6-keV level (which is a well-established 4^+ state), and from the 2420.8-keV level (which is a 2^+ state). These feedings are in agreement with the shell model. A transition energy of 2027 keV, observed by us, seems to fit reasonably well with the transition from the 3010-keV 0^+ level to the 983.5-keV 2^+ level. This is in agreement with the collective model. The 3010-keV 0^+ state may be formed due to mixing of rotational and shell model states [21]. Theoretical calculations by Mukherjee et al. [22] on the collective behaviour in some $1f_{7/2}$ even-even nuclei on the basis of asymmetric rotor-vibrator predictions seem to agree with the experimental results of ^{48}Ti . The 2295.6-keV level is a well-established 4^+ state. Possible level feedings on the basis of energy fit are shown in the level scheme. No direct feeding to the level at 3010 keV (0^+ state) from the capture state has been observed. The 3342-keV level may not be a 6^+ state but its spin should probably be less than 4 as suggested by Konijn et al. [23]. The 6^+ state lies most probably at 3331.8 keV. We do not observe any direct feeding to the 6^+ state which is in agreement with theory.

Some ambiguity exists in the literature regarding the 3362-keV level. Bernstein et al. [24] have reported that this level is a doublet consisting of spin 3^- or 4^+ . Konijn et al. [23] have reported a level at 3361 keV with spin and parity 1^+ , 2^+ or 3^- . On the basis of energy fit 2^+ seems to be in agreement with the general theory. On the other hand, the 3^- state has unusual characteristics and generally the lowest 3^- state consists of most of the octopole strength. Horoshko et al. [25] indicate that $3^- \rightarrow 0^+$ could have an intensity up to 2%. On this consideration 3^- assignment cannot be completely ruled out.

The calculated neutron binding energy of ^{49}Ti from the present experiment is 8143.3 ± 1.2 . The levels agree well with the (d, p) measurements by Bjerregaard et al. [18], (d, d') measurement by Wilhjelm et al. [26] and (n, γ) work by Carlos et al. [5].

Kashy et al. [16] has assigned $l_n = 2$ for the 2.62-MeV level. This energy is actually at 2662 keV and the corresponding level is a candidate for a hole state.

Feeding is observed from this level to weakly fed levels at 1540 keV and 1618 keV. Both of them are very weakly fed from the capture state as well. At present it has not been possible to explain this. In the present measurements many new transitions are observed.

During an attempt to see if the energy at 1586 keV was a doublet no change in line width was observed as compared with the 1498.5-keV line (except for a tail on the higher-energy side) when using a Ge(Li) detector of 5.5-keV resolution at 1.33 MeV. This rules out the possibility of two lines of equal intensity at 1583 and 1586 keV as reported by Knowles et al. [4]. The present observation is in agreement with the work of Tenenbaum et al. [8]. During an investigation using a detector of resolution 3.5 keV at 1.33 MeV on capture radiations from isotopes of silicon by Blichert-Toft et al. [10] two lines with a large intensity ratio were observed, one at 1586 keV and the other at 1592 keV. The line at 1592 keV has been interpreted as a double-escape line on the basis of its intensity, considering the reflectivity variation of the crystal. Moreover, the 1586-keV level is

populated by transitions whose intensities are in agreement with that of the depopulating 1586-keV line.

On the whole the shell model ($f_{7/2}^2$) ($f_{7/2}^7$) configuration seems to agree rather well in the case of ^{49}Ti but it is generally considered that a nuclear deformation takes place in this mass region.

The calculated neutron binding energy of ^{50}Ti is 10942.2 ± 2.0 . Hinds and Middleton [27] have discussed the levels on the basis of particle-hole interactions. The transitions shown in Fig. 7 seem to agree well with this work. The energy observed at 2316 keV may belong to the cascade $0^+ \rightarrow 2^+ \rightarrow 0^+$ in ^{50}Ti . But due to the uncertainty in defining it as a full-energy peak it has not been shown in the level scheme. The energy at 7063 keV is rather well fitted as a transition from the capture state to the 3879-keV level. There is some doubt, however, about this transition. Since the proton core is unchanged, for an explanation the levels could to some extent be compared with the levels of ^{48}Ti .

The calculated neutron binding energy of ^{51}Ti has been determined to 6378.7 ± 2.0 keV. The lines with low intensity which have not been fitted in the other isotopes have been tried for a fit in ^{51}Ti . In cases where transition placements turned out to be possible these seemed to agree well with the (d, p) measurements by Barnes et al. [28]. The percentage abundance of ^{50}Ti is 5.34% and its neutron capture cross-section $\sigma_{\text{na}} = 0.4$ barns. On this consideration the observed intensities seem to agree well. The lines which have been fitted in ^{51}Ti depopulate levels which have been observed with strong strength functions in (d, p) measurements.

The gamma energy observed at 6378 ± 2 keV may be the transition energy from the capture state to the ground state of ^{51}Ti since the neutron separation energy of ^{51}Ti is 6379 ± 5 keV. As the ground-state spin of ^{51}Ti is $3/2^-$, a strong transition between the capturing state and the ground state should be expected to occur. The 5214 ± 10 -keV line may be a transition from the capturing state to a level at 1159 ± 2 keV. This level is supposed to have $J^\pi = \frac{1}{2}^-$ according to the literature and therefore should combine with the capturing state to give a relatively strong transition. We observe also a line at 1159 ± 2 keV. The occurrence of two $l_n = 3$ states with an energy of 3 MeV between them (at 2132 and 5135.5 keV) with relatively large and nearly equal strength functions are accounted for rather well by the nucleon-nucleon interaction theory by Vervier [29]. The sum of the energies observed at 2617.1 and 3762.6 keV is 6379.7 keV which fits well with the neutron separation energy of ^{51}Ti . The 2617.1-keV transition may therefore proceed from the capturing state to a level at 3759 keV observed by Barnes et al. [28] and reported to have $l_n = 4$ and $I^\pi = 9/2^+$. However, Vervier [29] did not give any evidence for a level having such a high l_n and spin value. The experimental data indicate the possibility of a transition from the capturing state to the $3/2^-$ level at 2189 keV, and a transition from this level to the ground state.

ACKNOWLEDGEMENTS

The authors wish to express gratitude to Professor Nils Ryde for his kind interest and valuable discussions. Sincere thanks are due to Mr. Leif Jacobsson for his help with the instrumentation. The important

assistance of the personnel at AFK and RFN as well as from the other divisions at AB Atomenergi is much appreciated. Financial support was furnished by Statens råd för atomforskning and Göteborg Universitets Fond för Ograduerade Forskares Vetenskapliga Verksamhet.

R E F E R E N C E S

- [1] MOTZ, H.T., Phys. Rev. 93 (1954) 925.
- [2] ADYASEVICH, B.P., GROSHEV, L.V., DEMIDOV, A.M., Atomn. Energ. 1 (1956) 40.
- [3] KINSEY, B.B., BARTHOLOMEW, G.A., Phys. Rev. 89 (1958) 37.
- [4] KNOWLES, J.W., MANNING, G., BARTHOLOMEW, G.A., CAMPION, P.J., Phys. Rev. 114 (1959) 4.
- [5] CARLOS, P. et al., Nucl. Phys. A107 (1968) 436.
- [6] TRUMPY, G., Nucl. Phys. 2 (1956) 664.
- [7] VERVIER, J., Nucl. Phys. 26 (1961) 10.
- [8] TENENBAUM, J., ARAD, B., BEN-DAVID, G., MOREH, R., Rep. I.A.-1102 (1967).
- [9] BROMAN, L., Nucl. Instrum. Meth. 50 (1967) 29.
- [10] Blichert-Toft, P.H., TRIPATHI, K.C., (to be published).
- [11] LEGRAND, J., BOULANGER, J.P., BRETHON, J.P., Nucl. Phys. A107 (1968) 177.
- [12] MATTAUCH, J.H.E., THIELE, W., WAPSTRA, A.H., Nucl. Phys. 67 (1965) 1.
- [13] McCULLEN, J.D., BAYMAN, B.F., ŽAMIK, L., Phys. Rev. 134 (1964) 515.
- [14] MALIK, F.B., SCHOLZ, W., Phys. Rev. 150 (1966) 919.
- [15] RAPAPORT, J., SPERDUTO, A., BUECHNER, W.W., Phys. Rev. 143 (1966) 808.
- [16] KASHY, E., CONLON, T.W., Phys. Rev. 135B (1964) 389.
- [17] TENENBAUM, J., MARCH, R., WAND, Y., Phys. Rev. 117 4 (1969) 1595.
- [18] BJERREGAARD, J.H., DAHL, P.F., HANSEN, O., SIDENIUS, G., Nucl. Phys. 51 (1964) 641.
- [19] BARNES, P.D., BOCKELMAN, C.K., HANSEN, O., SPERDUTO, A., Phys. Rev. 138B (1965) 597.
- [20] ALTY, J.L., GREEN, L.L., JONES, G.D., SHARPEY-SCHAFFER, J.F., Nucl. Phys. A100 (1967) 191.
- [21] KAVALOSKI, C.D., KOSSLER, W.J., Bull. Am. phys. Soc. 11 (1968) 1384.
- [22] MUKHERJEE, S.N., SHASTRY, S., RUSTGI, M.L., Nuovo Cim. LV II B (1968) 25.
- [23] KONIJN, J., LINGEMAN, E.W.A., DE WIT, S.A., Nucl. Phys. A90 (1967) 558.
- [24] BERNSTEIN, A.M., LIPPINCOTT, E.P., SAMPLE, G.T., THORN, C.B., Nucl. Phys. A115 (1968) 79.
- [25] HOROSHKO, R.N., SCOTT, H.L., VAN PATTEN, D.M., Bull. Am. phys. Soc. 11 (1968) 1425.
- [26] WILHELM, P. et al., Phys. Rev. 166 (1968) 1121.
- [27] HINDS, S., MIDDLETON, R., Nucl. Phys. A92 (1967) 422.
- [28] BARNES, P.D., BOCKELMAN, C.K., HANSEN, O., SPERDUTO, A., Phys. Rev. 136B (1964) 438.
- [29] VERVIER, J., Nucl. Phys. 78 (1966) 497.

ENERGIES AND INTENSITIES OF GAMMA RAYS FROM SLOW NEUTRON CAPTURE IN NITROGEN

L. JONSSON, R. HARDELL
Chalmers University of Technology,
Gothenburg, Sweden

Abstract

ENERGIES AND INTENSITIES OF GAMMA RAYS FROM SLOW NEUTRON CAPTURE IN NITROGEN. The $^{14}\text{N}(n, \gamma)^{15}\text{N}$ reaction has been studied using Ge(Li) spectrometers. The principal aim was to establish this reaction as a standard for energy and intensity calibration in (n, γ) spectroscopy.

1. INTRODUCTION

During the past few years Ge(Li) detectors have been taken into use very widely for the measurement of gamma-ray spectra in a broad energy region. The high resolution of these detectors has implicated requests for accurately determined calibration lines in the energy region 1 - 10 MeV. Recent measurements of calibration lines from radioactive sources have been tabulated by Marion [1]. These measurements have been done with magnetic and crystal spectrometers and refer to the annihilation radiation 511.006 keV or the 411.795-keV line following the decay of ^{198}Au . The primary gamma-ray calibration energies in the compilation of Marion [1] cover the energy region 26 - 2754 keV. In nuclear reaction experiments the gamma-ray spectrum may, however, be extended up to several MeV where calibration lines are very rare. For measurements of prompt gamma rays, following thermal neutron capture, calibration lines from the $^{14}\text{N}(n, \gamma)^{15}\text{N}$ reaction have been used as this reaction can easily be produced at reactors and even constitutes a background source in certain types of experimental arrangements. In Ref.[1] recent measurements of gamma rays from this reaction are tabulated and the adopted energy values are presented. It can be observed that the results of Greenwood quoted in this reference are not in agreement with other results [2, 3] also given by Greenwood. The need for an accurate determination of the gamma-ray energies in the $^{14}\text{N}(n, \gamma)^{15}\text{N}$ reaction motivated a new investigation. As pointed out by Marion it is also of interest to measure the intensities of the gamma lines as they cover a broad energy region and consequently are suitable for relative efficiency calibrations.

2. EXPERIMENTAL ARRANGEMENTS

The experiment has been performed at the 1-MW heavy-water reactor R1 in Stockholm. The target was natural nitrogen gas at the pressure of 4 atm which was passed into a through reactor channel. The capture gamma rays pass a 6-mm diam. by 1.5-m long collimator before reaching the detector which is situated about 4.5 m from the centre of the reactor.

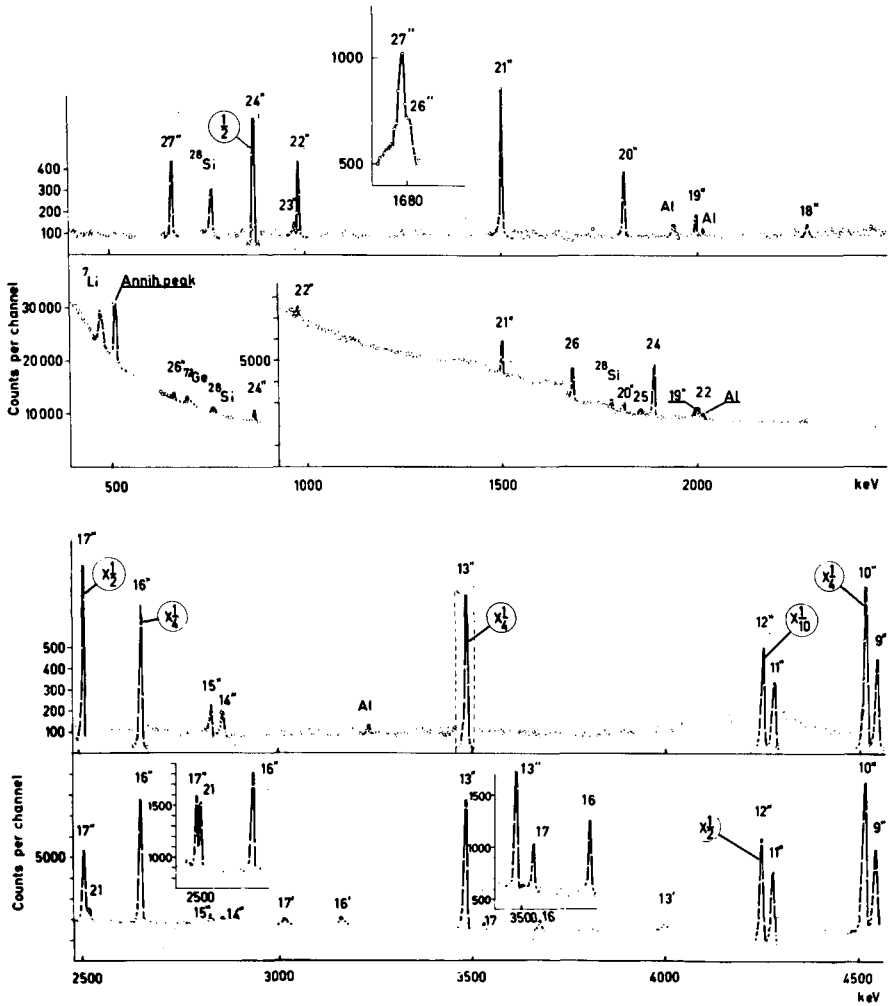


FIG. 1. Low-energy pair and direct spectra following thermal neutron capture by nitrogen. The insets are taken from anticoincidence spectra.

The effective target quantity can be estimated to be roughly 350 mg and the thermal neutron flux is about 3×10^{12} n cm⁻² sec⁻¹. A staff-shaped Ge(Li) detector, length 2.0 cm, volume 1.5 cm³, followed by a cooled FET preamplifier, both manufactured by AB Atomenergi, Studsvik, have been used for the detection of the gamma-ray spectra. The preamplifier is followed by a Tennelec TC 200 main amplifier and an Intertechnique 4096-channel pulse-height analyser. The energy resolution of the detector is about 3 keV at 1 MeV and 6 keV at 6 MeV. To simplify the response function above the pair-production threshold the Ge(Li) detector can be used in a pair spectrometer arrangement. The two side crystals are made in the form of a NaI annulus, 15 cm diam. by 10 cm

long and with a 4-cm diam. through hole. The annulus is bisected and the two segments are optically isolated. For the measurement of low-energy spectra the detector arrangement described can be used in the anticoincidence mode. It is then complemented with a NaI crystal, 12.5 cm diam. by 10 cm long and with a 1.8-cm through hole, placed in front of the bisected NaI annulus to detect backscattered radiation. Further experimental details can be found in Ref. [4].

The purpose of using pair or anticoincidence spectrometer arrangements is to remove possible ambiguities in the spectra. A high-energy line gives rise to three peaks in a direct spectrum, a full-energy peak, a single and a double-escape peak. Only double-escape peaks appear in a pair spectrum. In an anticoincidence spectrum the Compton distribution associated with every photopeak is reduced; anticoincidence spectra are often useful in the low-energy region. For the energy calibration of a high-energy spectrum it is obvious that the distance between the three peaks associated with one gamma line gives a measure of the energy scale in the direct spectrum. At gamma-ray energies higher than about 4 MeV the photopeak as well as the first-escape peak are quite small compared to the strong double-escape peak. In an anticoincidence spectrum, the escape peaks are depressed; for the 6.3-MeV line it is found that the ratio between the areas of the photopeak and the double-escape peak increases with a factor of 8. The depression of the Compton distribution and the secondary peaks associated with the photopeaks facilitates the determination of the channel number separation between photopeak and escape peaks. Previous experiences from the analysis of (n, γ) spectra with a small Ge(Li) detector have shown that direct spectra may be useful for the identification of weak lines in the energy region above 6 MeV, whereas pair spectra have their definite advantage in the energy region 2-6 MeV. Anticoincidence spectra are generally taken for energies below 2 MeV. In the present case direct spectra as well as pair and anticoincidence spectra have been used for the whole energy region as discussed below. The characteristics of the direct and pair spectra can be studied in Figs 1 and 2. The insets in Fig. 1 are taken from anticoincidence spectra. A high-energy direct spectrum is shown in Fig. 3.

3. RESULTS

To make an accurate energy determination possible it is necessary to know the response function of the detector and associated electronic equipment including the multi-channel analyser. The integral linearity was determined with a precision pulser and with radioactive sources. These measurements were in good agreement and could be used for the construction of an S-shaped calibration curve which showed a maximum deviation of 0.4 channels from linearity between channel number 50 and 4000. This curve was used to apply small corrections between calibration points in the ^{15}N spectrum. The determination of gamma-ray energies up to 5.3 MeV in the ^{15}N spectrum was made using other energy standards. The detector was irradiated with ^{137}Cs , ^{60}Co or ^{24}Na sources and ^{15}N capture gamma rays simultaneously and accurate values could be obtained from the composite spectra for the ^{15}N lines up to 3.8 MeV. A small graphite target was introduced in the reactor channel and a composite ^{15}N - ^{13}C spectrum was taken. The very accurate determination

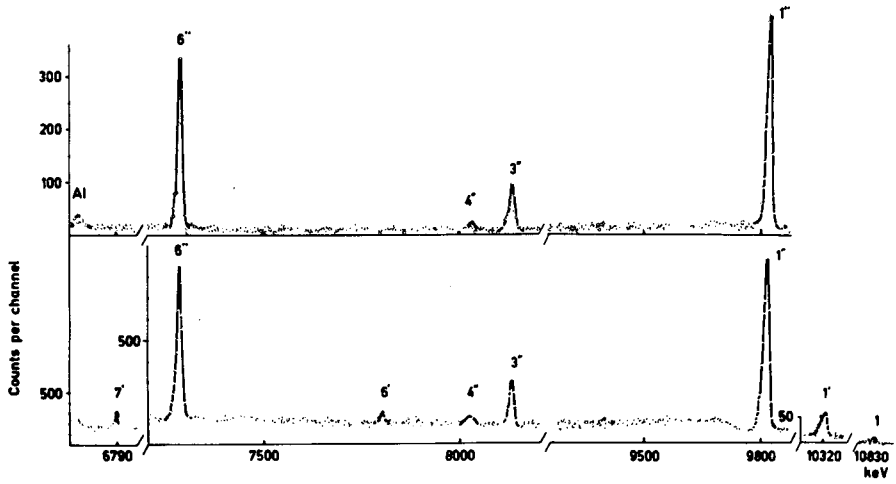
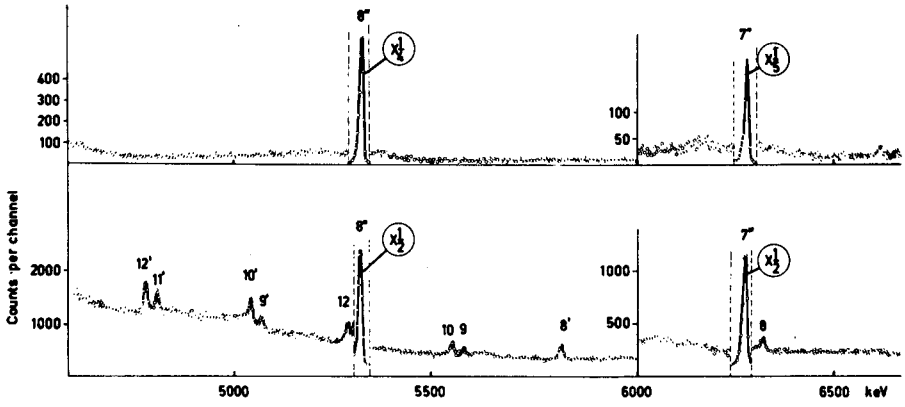


FIG. 2. High-energy pair and direct spectra following thermal neutron capture by nitrogen.

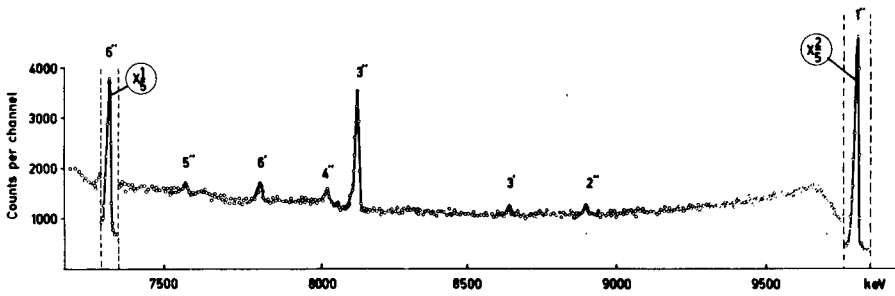


FIG. 3. High-energy direct spectrum following thermal neutron capture by nitrogen.

TABLE I. CALIBRATION ENERGIES USED IN THIS WORK

Energy	Source	Reference
511.006 ± 0.002	Annihilation radiation	[6]
661.635 ± 0.076	¹³⁷ Cs	[7]
1173.226 ± 0.040	⁶⁰ Co	[7]
1261.92 ± 0.06	¹² C(n, γ) ¹³ C	[5]
1332.483 ± 0.046	⁶⁰ Co	[7]
1368.526 ± 0.044	²⁴ Na	[7]
1778.70 ± 0.17	²⁸ Al	[8]
2753.92 ± 0.12	²⁴ Na	[7]
3683.94 ± 0.17	¹² C(n, γ) ¹³ C	[5]
4945.46 ± 0.17	¹² C(n, γ) ¹³ C	[5]

by Prestwich et al. [5] of the ¹³C capture gamma rays was used for the calibration of the ¹⁵N spectrum up to 5298 keV. The calibration lines used for the energy determinations in this investigation are given in Table I. The single-escape peaks and photopeaks of the 5270- and 5298-keV lines were used for the determination of the 5533, 5563 and 6323-keV gamma-ray energies. The 7300-keV line was easily determined as its double-escape peak is very close to the 6323-keV photopeak. As the 7300-keV photopeak is partly hidden in the 8311-keV double-escape peak, only the 7300-keV first escape peak could be used for the calculation of the 8311-keV line. From the ¹⁵N decay scheme it is seen that the 8313-keV state is also de-excited via the 3014 → 5298 and 1990 → 6323-keV gamma-ray cascades. The energy of the 8311-keV transition could thus be checked with the sums of these cascades. The energies of the 8568, 9047 and 9149-keV lines were determined using the escape peaks of the 8311-keV transition. The energy of the 9924-keV line was obtained from the escape peaks of the 9149-keV line, and the energy of the 10830-keV line has been estimated from the energy value of the 10834-keV capturing state, which is determined from several gamma-ray cascades. The energy values of the gamma lines with errors are given in Table II. The errors quoted are due to statistical uncertainties in peak positions, uncertainties in the deviations from linearity of the analyser and errors quoted for the calibration lines. The spectra used for the energy calculations have been taken in several different runs with varying amplifier gain to minimize the influence of errors in the differential and integral linearities of the analog-digital converter. In Table III the gamma transitions used for the Q-value determination are given. The average Q-value = 10834.0 ± 0.5 keV was calculated without weighting since systematic errors may be as large as statistical ones. The standard error in the average Q-value is calculated to be as low as ± 0.1 keV. An estimation of the influence of a possible systematic error in the gamma-ray energies above 5.3 MeV shows that the probable

TABLE II. GAMMA-RAY ENERGIES AND INTENSITIES FROM THE
 $^{14}\text{N}(n, \gamma)^{15}\text{N}$ REACTION

No.	Gamma-ray energy (keV)	Recoil energy (keV)	Transition energy (keV)	Intensity: γ -rays per 100 neutron captures
1	10829.8 \pm 0.6 ^a	4.2	10834.0	14 ^c
2	9924 \pm 3 ^b	3.5	9927.5	0.2 \pm 0.1
3	9149.3 \pm 1.0 ^b	3.0	9152.3	1.6 \pm 0.2
4	9046.6 \pm 2.0 ^b	2.9	9049.5	0.2 \pm 0.1
5	8568.0 \pm 3.0 ^b	2.6	8570.6	0.1 \pm 0.05
6	8310.8 \pm 0.9 ^a	2.5	8313.3	3.8 \pm 0.4
7	7299.5 \pm 0.8	1.9	7301.4	9.2 \pm 1.0
8	6322.7 \pm 0.6	1.4	6324.1	18.4 \pm 1.3
9	5562.5 \pm 0.6	1.1	5563.6	10.4 \pm 0.7
10	5533.8 \pm 0.6	1.1	5534.9	18.5 \pm 1.3
11	5298.1 \pm 0.6	1.0	5299.1	21.4 \pm 1.5
12	5269.5 \pm 0.6	1.0	5270.5	31.4 \pm 2.2
13	4509.1 \pm 0.6	0.7	4509.8	16.5 \pm 1.2
14	3884.2 \pm 0.6	0.5	3884.7	0.9 \pm 0.2
15	3855.2 \pm 0.6	0.5	3855.7	1.0 \pm 0.2
16	3678.0 \pm 0.4	0.5	3678.5	15.0 \pm 1.4
17	3532.0 \pm 0.4	0.4	3532.4	9.3 \pm 0.6
18	3299.7 \pm 1.5	0.3	3300.0	0.2 \pm 0.1
19	3013.7 \pm 0.6	0.3	3014.0	0.7 \pm 0.2
20	2831.1 \pm 0.6	0.3	2831.4	2.0 \pm 0.3
21	2520.6 \pm 0.3	0.2	2520.8	6.0 \pm 0.4
22	1999.6 \pm 0.6	0.1	1999.7	4.2 \pm 0.3
23	1989.5 \pm 1.0	0.1	1989.6	0.5 \pm 0.2
24	1884.9 \pm 0.3	0.1	1885.0	18.3 \pm 1.5
25	1853.6 \pm 1.5	0.1	1853.7	0.4 \pm 0.2
26	1681.3 \pm 0.3	0.1	1681.4	1.7 \pm 0.4
27	1678.2 \pm 0.3	0.1	1678.3	8.0 \pm 1.0

^a For the determination of this energy value both cross-over transition and cascades have been used.

^b This determination is made relative to the 8310.8-keV line.

^c This value is taken from Ref. [14].

TABLE IV. INTENSITY BALANCE FOR ^{15}N LEVELS

E_x (keV)	Intensity balance I_{in}/I_{out}	Energy sum for cascading gamma rays (keV)
0	100.3/-	
5270.5 \pm 0.6	29.8/31.4	10834.2 \pm 0.9
5299.1 \pm 0.6	20.2/21.4	10834.0 \pm 0.9
6324.1 \pm 0.6	19.0/18.4	10833.9 \pm 0.9
7155.5 \pm 0.6	19.2/18.3	10834.0 \pm 0.8
7301.4 \pm 0.8	9.7/ 9.2	10833.8 \pm 0.9
8313.2 \pm 0.6	6.0/ 5.0	10834.1 \pm 1.0
8570.5 \pm 1.5	- / 0.3	
9049.5 \pm 2.0	- / 0.2	
9152.4 \pm 1.0	1.7/ 1.6	10833.7 \pm 1.1
9155.3 \pm 0.7	8.0/ 8.5	10833.5 \pm 1.0
9927.5 \pm 3.0	- / 0.2	

error in the average Q-value is about ± 0.5 keV. The present value may be compared with previous values $Q = 10833.2 \pm 0.6$ keV and $Q_m = 10834.8 \pm 0.8$ keV in Refs [3, 9].

To obtain relative-intensity values for the ^{15}N lines the efficiency curve of the detector must be known. The pair peak efficiency curve was primarily constructed using the capture gamma rays from natural nickel as determined by Groshev et al. quoted in Ref. [10]. This efficiency curve was successively complemented to include the 1368 \rightarrow 2754-keV cascade in ^{24}Na decay, the 1262 \rightarrow 3684-keV cascade in ^{13}C , the 3532 \rightarrow 7300 keV cascade in ^{15}N and a few other simple intensity relations in the ^{15}N , ^{21}Ne and ^{41}Ar decay schemes as reported in Refs [11 - 13]. The extrapolation of the efficiency curve to energies higher than 9 MeV was made using the intensity value for the 10830-keV line determined by Motz et al. [14]. The relative intensity values obtained are adjusted to an absolute scale in accordance with the decay scheme in Fig.4. In Table II the intensities are thus given in gamma rays per 100 neutron captures. In Table IV energies are given for the ^{15}N states found to be excited in the (n, γ) reaction. The intensity balance for each level is fulfilled within the error limits for all states to which feeding is observed.

4. DISCUSSION

The intensities of the primary transitions from the capturing state in ^{15}N as shown in the decay scheme in Fig.4 are in very good agreement with the results found by Thomas et al. [11]. The 9.15-MeV state is, however, found to be a doublet [3] which was not observed in Ref. [11].

The decay modes of ^{15}N states excited in (d,p), (d,n) and (^3He ,p) reactions have been studied in Refs [15, 16] and most spin values in Fig.3 have been taken from Refs [15, 17]. The present results are mainly in good agreement with previous findings and a few more weak transitions are reported. The good energy resolution of the Ge(Li) detector allows one to detect the 1678 - 1681-keV doublet that feeds the two states at 9152 and 9155 keV (see inset in Fig.1). The de-excitation of these states is found to agree with the results of Greenwood [3]. From these results and the branchings from the capturing state one may propose that the 9155-keV level has spin ($5/2^-$) whereas the 9152-keV level has spin ($3/2^+$). Primary transitions to the 8571, 9050 and 9928-keV states have not been observed in this investigation. The decay of these states has, however, been studied in Refs [12, 13] and the de-excitation lines shown in Fig.4 are in agreement with previous results. The 9928-keV state has not previously been found to be excited in the (n, γ) reaction.

ACKNOWLEDGEMENTS

We are indebted to Ing. N. Berglund and the reactor staff at R1, Stockholm, for assistance during the measurements. We would also like to thank Professor N. Ryde and Dr. S.E. Arnell for their interest in this work.

REFERENCES

- [1] MARION, J.B., Nuclear Data A4 (1968) 301.
- [2] GREENWOOD, R.C., in Slow-neutron capture gamma-ray spectroscopy, Rep. ANL-7282 (1966).
- [3] GREENWOOD, R.C., Phys. Lett. 27B (1968) 274.
- [4] ARNELL, S.E., HARDELL, R., HASSELGREN, A., JONSSON, L., SKEPPSTEDT, O., Nucl. Instrum. 54 (1967) 165.
- [5] PRESTWICH, W.V., COTÉ, R.E., THOMAS, G.E., Phys. Rev. 161 (1967) 1080.
- [6] COHEN, E.R., DU MOND, J.W.M., Rev. mod. Phys. 37 (1965) 537.
- [7] MURRAY, G., GRAHAM, R.L., GEIGER, J.S., Nucl. Phys. 63 (1965) 353.
- [8] WHITE, D.H., GROVES, D.J., Nucl. Phys. A96 (1967) 453.
- [9] MATTAUCH, J.H.E., THIELE, W., WAPSTRA, A.H., Nucl. Phys. 67 (1965) 73.
- [10] BARTHOLOMEW, G.A., DOVEIKA, A., EASTWOOD, K.M., MONARO, S., GROSHEV, L.V., DEMIDOV, A.M., PELAKHOV, V.I., SOKOLOVSKII, L.L., Nuclear Data A3 (1967) 367.
- [11] THOMAS, G.E., BLATCHLEY, D.E., BOLLINGER, L.M., Nucl. Instrum. 56 (1967) 325.
- [12] JONSSON, L., HARDELL, R., ARNELL, S.E., Ark. Fys. 35 (1968) 423.
- [13] SKEPPSTEDT, Ö., HARDELL, R., ARNELL, S.E., Ark. Fys. 35 (1968) 527.
- [14] MOTZ, H.T., CARTER, R.E., BARFIELD, W.D., "Thermal-neutron capture gamma-rays from beryllium and nitrogen", Pile neutron Research in Physics (Proc. Symp. Vienna, 1960), IAEA, Vienna (1962) 225.
- [15] WARBURTON, E.K., OLNESS, J.W., ALBURGER, D.E., Phys. Rev. 140 (1965) B 1202.
- [16] PHILLIPS, G.W., YOUNG, F.C., MARION, J.B., Phys. Rev. 159 (1967) 891.
- [17] SIETKEN, H.E., COCKBURN, P.M., KRONE, R.W., Nucl. Phys. A128 (1969) 162.

GAMMA RAYS FROM THERMAL NEUTRON CAPTURE IN ^{24}Mg

R. HARDELL
Chalmers University of Technology,
Gothenburg, Sweden

Abstract

GAMMA RAYS FROM THERMAL NEUTRON CAPTURE IN ^{24}Mg . The energies and intensities of gamma rays following thermal neutron capture in ^{24}Mg have been determined with a Ge(Li) detector used in pair and anti-Compton arrangements. An internal target of enriched ^{24}Mg has been used. Excitation energies and branchings from ^{25}Mg levels have been determined. The reaction Q-value was found to be 7330.0 ± 1.0 keV.

1. INTRODUCTION

The close similarity of the structure of the low-lying levels in the mirror nuclei ^{25}Mg and ^{25}Al has been discussed by Litherland et al. [1]. A rotational description of the levels up to about 4 MeV has proved very successful and the decay modes of mirror levels in the two nuclei have been compared by several authors. For the classification of higher excited levels the present experimental data seem insufficient and additional studies of the level scheme will be required.

A recent study of the gamma rays following neutron capture in ^{24}Mg was made by Spilling et al. [2]. Targets of natural element and enriched ^{25}Mg were used and the measurements were performed with Ge(Li) detectors. The gamma branchings from a few states in ^{25}Mg excited in the (p,p') reaction were measured by McCallum and Sowerby [3]. Lifetimes and decay modes of energy levels in ^{25}Mg also excited in the (p,p') reaction were recently determined by Sharpey-Schafer et al. [4]. Other relevant references up to 1967 are compiled in the review article by Endt and van der Leun [5].

2. EXPERIMENTAL ARRANGEMENTS

The measurements were performed at the 1-MW heavy-water reactor R1 in Stockholm. The target consisted of 1 g of Mg enriched to 99.84% in ^{24}Mg , chemical form MgO, and was on loan from the Electromagnetic Separation Group at Harwell. The neutron capture cross-section for ^{24}Mg is about 52 mb [2]. The experimental equipment used for the present work is described elsewhere in these Proceedings and in detail in Ref. [6]. Energy and intensity values were obtained using accurately determined lines following neutron capture in nitrogen [7, 8] and nickel [9].

3. RESULTS

An anticoincidence spectrum from neutron capture in ^{24}Mg , recorded for 17 h, is shown in Fig. 1. The low-energy part of the spectrum shows a fairly strong background distribution which makes the identification of

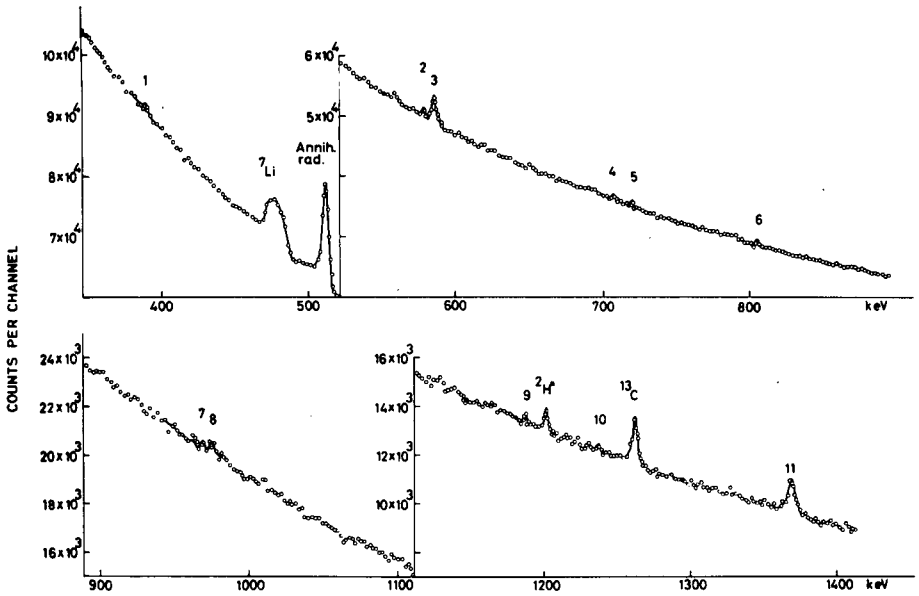


FIG. 1. Anticoincidence spectrum following neutron capture in ^{24}Mg . Accumulation time 17h.

weak gamma lines somewhat difficult. The pair spectrum is shown in Fig. 2. The background lines in the spectra are due to neutron capture and neutron inelastic scattering in the graphite container and in the impurities of the target. The dominant contaminant in the magnesium target is chlorine, whereas most other impurities have not been identified. Background lines were distinguished from magnesium lines by making a comparison between the gamma spectra from enriched targets of all stable Mg isotopes; the contaminants are supposed to be the same in the three different Mg samples studied. The 1369 and 2754-keV lines in the gamma-ray spectra probably result from neutron inelastic scattering in ^{24}Mg ; the 1809-keV line may be due to neutron capture in ^{25}Mg . According to the mass analysis for the magnesium target it should contain ^{25}Mg to 0.13% and ^{26}Mg to 0.04%. The 1809-keV line is the strongest line in the gamma-ray spectrum following neutron capture in ^{25}Mg [2].

The energies and intensities of the gamma rays from the $^{24}\text{Mg}(n, \gamma)$ reaction are listed in Table I. Energy values are corrected for recoil. The intensity of the 3917-keV transition has been set to 1000. The overlap between the relative intensities in the pair and anticoincidence spectra was conveniently achieved by the presence in both spectra of the 1368-keV line from inelastic neutron scattering in ^{24}Mg and the 2223.3-keV line from neutron capture in hydrogen. The errors in the intensity values are about 15% for strong lines and increase to about 100% for the weakest lines.

In the review article of Endt and van der Leun [5] 45 excited states in ^{25}Mg are reported up to the capturing state at 7330 keV. A computer was used to calculate and list in order of increasing energy the differences between all these energy values. The assignments for the gamma transitions obtained in this way are shown in Table I. Because of the uncertainty

TABLE I. GAMMA RAYS FROM NEUTRON INTERACTION WITH ^{24}Mg

No.	E_γ^a (keV)	I (rel. intensity)	Assignment ^b
1	389.7 ± 0.5	130	975 → 585, (C → 6940)
2	577.6 ± 0.8	140	(6038 → 5455, 3977 → 3397)
3	585.2 ± 0.4	1650	585 → 0
4	706.9 ± 0.5	160	(6561 → 5853)
5	718.7 ± 0.8	100	(7175 → 6460, 6460 → 5742)
6	805.6 ± 1.2	260	(4708 → 3903, 5515 → 4708)
7	968.4 ± 1.5	85	C → 6361, (5245 → 4277)
8	974.2 ± 1.5	208	975 → 0
9	1187.6 ± 1.0	83	(5465 → 4277)
10	1237.8 ± 1.5	88	(5515 → 4277)
11	1368.7 ± 1.0	1420	^{24}Mg
12	1396.8 ± 1.0	100	
13	1435.5 ± 1.0	150	(5786 → 4353, 3397 → 1960)
14	1606.0 ± 1.5	68	1606 → 0
15	1661.7 ± 2.0	97	(6772 → 5112)
16	1714.1 ± 3.0	61	4277 → 2564
17	1809.3 ± 1.0	74	^{24}Mg , (C → 5515)
18	1925.1 ± 1.5	32	(7175 → 5245)
19	1979.2 ± 1.5	26	2564 → 585
20	2264.4 ± 2.0	12	(5005 → 2738)
21	2438.6 ± 1.0	142	3414 → 975
22	2459.4 ± 2.5	23	6361 → 3903, (7175 → 4715)
23	2483.0 ± 3.0	24	(6460 → 3977)
24	2550.6 ± 2.0	14	5112 → 2564
25	2558.2 ± 2.0	15	(6460 → 3903, 5974 → 3414)
26	2565.0 ± 2.0	10	2564 → 0
27	2622.4 ± 2.0	19	6038 → 3414
28	2676.7 ± 2.5	22	(6075 → 3397)
29	2753.5 ± 2.0	20	^{24}Mg
30	2802.2 ± 2.0	12	2802 → 0
31	2828.7 ± 1.0	770	3414 → 585
32	2864.0 ± 1.5	15	(6772 → 3903, 7215 → 4353)
33	2918.0 ± 1.5	10	(7273 → 4353)
34	2930.7 ± 2.5	11	3903 → 975
35	3052.9 ± 1.0	250	C → 4277
36	3239.5 ± 2.0	12	6038 → 2802
37	3271.1 ± 2.0	7	(6667 → 3397, 7175 → 3903)
38	3301.9 ± 1.0	190	4277 → 975
39	3413.2 ± 1.0	113	3414 → 0
40	3506.9 ± 2.5	7	(5465 → 1960)
41	3525.5 ± 2.5	6	(6940 → 3414)
42	3559.8 ± 2.0	5	6361 → 2802, (5515 → 1960)
43	3818.1 ± 2.0	3	(7215 → 3397)
44	3823.7 ± 2.0	2	(6561 → 2738)
45	3917.0 ± 1.0	1000	C → 3414
46	3980.1 ± 2.5	8	(3977 → 0)
47	3997.9 ± 2.5	6	(6561 → 2564)
48	4016.5 ± 2.5	6	(5974 → 1960)
49	4248.9 ± 2.5	6	(5853 → 1606)
50	4526.7 ± 2.0	14	5112 → 585, (C → 2802)
51	4765.9 ± 2.0	11	C → 2564
52	4813.6 ± 2.5	4	(6772 → 1960, 5786 → 975)
53	5333.8 ± 3.0	3	(6940 → 1606)
54	5661.3 ± 2.5	3	(7273 → 1606)
55	5685.8 ± 2.5	6	(6667 → 975)
56	6037.4 ± 3.0	4	6038 → 0
57	6355.0 ± 1.5	24	C → 975
58	6575.5 ± 2.5	2	
59	6744.3 ± 2.5	5	C → 585
60	6750.6 ± 1.5	10	
61	6762.4 ± 2.5	2	

^a Energy values are corrected for recoil.

^b C-capturing state. The assignments given in parenthesis are mainly based on the gamma-ray energies; they are not confirmed by an intensity balance and have therefore been omitted in the decay scheme.

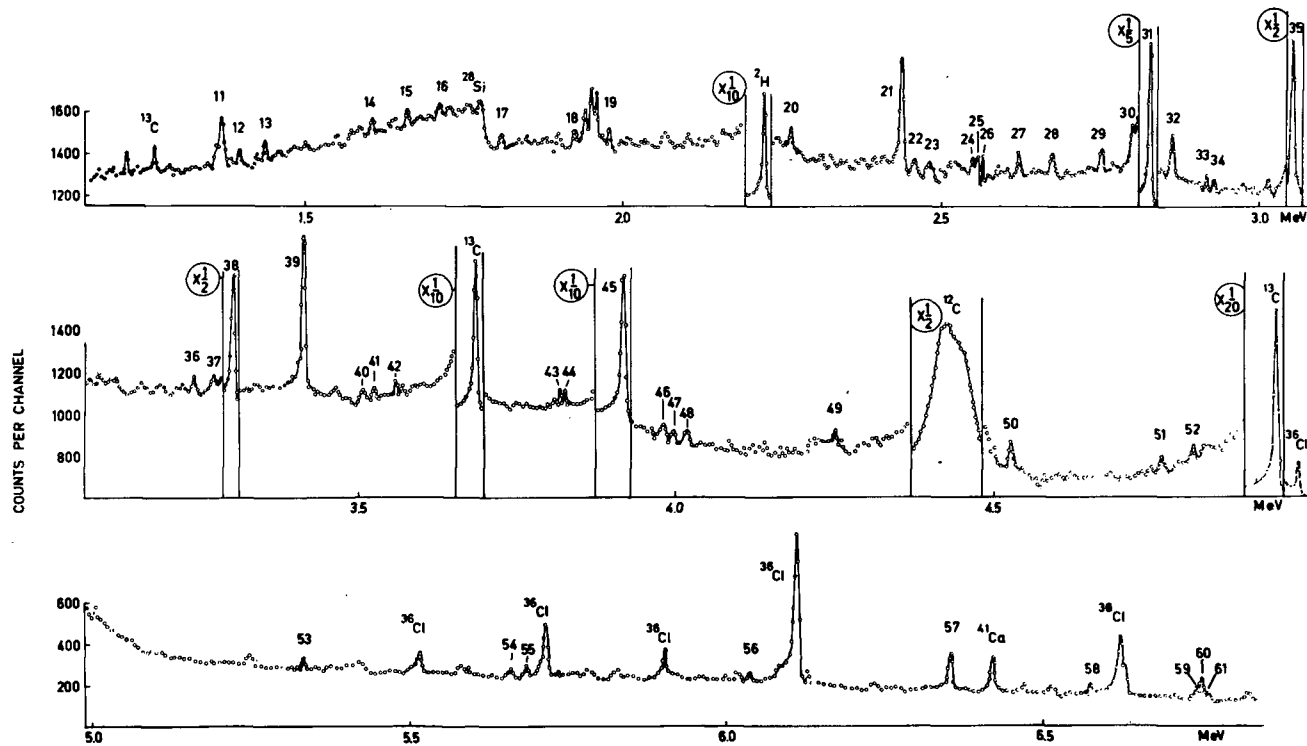


FIG. 2. Pair spectrum following neutron capture in ^{24}Mg . Accumulation time 48 h. Unlabelled peaks are due to unidentified impurities.

in previous determinations of the energy values of the ^{25}Mg states, the assignments should be regarded as more or less tentative. Assignments that are given in parenthesis are not shown in the decay scheme in Fig. 3. In Table II excitation energies with errors are given for some of the ^{25}Mg levels. The Q-value 7330.0 keV was calculated from sums of gamma-ray cascades. Previous determinations of the Q-value yield 7330.3 ± 1.0 keV [10] and 7332.8 ± 0.4 keV [2].

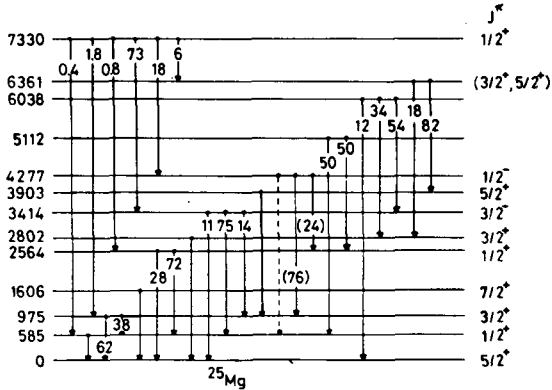


FIG. 3. Decay scheme of ^{25}Mg as obtained from the present work. Branchings are given in per cent.

4. DISCUSSION

All excited states in ^{25}Mg up to the 4277-keV level have been identified as members of four rotational bands [5]. The two principal bands have $K = 5/2$ and $K = 1/2$, which implies that the perturbations of the bands should be quite small and facilitates the identification of the rotational states. The comparison that can be made with the ^{25}Al level scheme has also been helpful for the deduction of spins and parities of ^{25}Mg levels. The spins and parities given in the level scheme in Fig. 3 have been taken from previous work [5]. The present results do not contradict any of these previous spin assignments. Other conclusions on the level scheme that can be made from the present investigation are summarized below.

The 585-keV level

A mismatch in the intensity balance for this level and a comparison with the results in Ref. [2] seem to indicate that the intensity value of the 585-keV transition is overestimated. No background lines are ex-

TABLE II. EXCITATION ENERGIES (keV) OF SOME ^{25}Mg LEVELS EXCITED IN THE NEUTRON CAPTURE REACTION

585.2 ± 0.4	974.8 ± 0.6	1606.0 ± 1.5	2564.4 ± 1.0
2802.2 ± 2.0	3413.4 ± 0.8	4276.8 ± 1.0	6037.8 ± 2.0

Q-value = 7330.0 ± 1.0

pected around 585 keV and the mismatch in the intensity balance remains unexplained.

The 975-keV level

The decay mode of this level as found from the present work is in good agreement with previous results [2, 4]. Considering the high background level in the low-energy region of our spectrum, it seems probable that the determinations of the branchings in Refs [2, 4] are more accurate than the present values.

The 1606-keV level

The energy value of the ground-state transition is in disagreement with the value 1613.7 ± 1.5 keV found by Spilling et al. [2]. In Ref. [4] the $7/2^+$ 1606-keV level is proposed to be fed from two $9/2^+$ states at 3399 and 4055 keV. As the spin of the capturing state at 7330 keV is $1/2^+$, high spin levels are not expected to be strongly populated which may explain that transitions from $9/2^+$ levels have not been observed. In Table I three gamma lines have tentatively been interpreted as transitions from the 7273, 6940 and 5853-keV states to the 1606-keV level.

The 2564-keV level

As the K-values of this state and the ground state differ by two units, a ground-state dipole transition should be forbidden. The de-excitation of the 2564-keV level has been found to proceed mainly via the 585 and 975-keV levels in (p, p') experiments [3, 4]. This result is in agreement with the decay mode found for the mirror level in ^{25}Al . In the (n, γ) experiment of Spilling et al. [2], however, a 2561-keV line has been interpreted as a ground-state transition from the 2564-keV state. In the present experiment a 2565-keV line was found, which has been given the same assignment. Another interpretation for this line would be that it represents a $7273 \rightarrow 4708$ -keV transition. As the spin value $9/2^+$ has been proposed for the 4708-keV level [4], this interpretation does not seem probable. The results from (n, γ) and (p, p') experiments are thus concluded to be in disagreement as far as the branching to the ground state is concerned. The tentative character of the present assignments must, however, be kept in mind. The discrepancy observed might be due to errors in the excitation energy values given for ^{25}Mg .

The 2803-keV level

In the present work only a ground-state transition was observed from this state. In Refs [3, 4] a 2219-keV transition to the 585-keV state was also reported. A gamma line of this energy may very well be hidden under the strong ^2H line at 2223 keV.

The 3414-keV level

This level is the lowest negative parity state in ^{25}Mg and is found to be very strongly populated in the (n, γ) reaction. The branchings to the three lowest states in ^{25}Mg were found to agree exactly with the values

reported in Ref. [2]. The mirror level in ^{25}Al shows a very similar decay mode [1]. The results of Sharpey-Schafer et al. [4], however, do not quite agree with the present findings.

The 3903-keV level

According to Ref. [4] a 19% ground-state de-excitation line from this level should be seen. In the present experiment a 3903-keV line will be hidden in the low-energy tail of the intense 3917-keV transition. The only de-excitation line observed is the 69% transition [4] to the 975-keV state.

The 4277-keV level

In Ref. [2] transitions from the $1/2^-$ 4277-keV state were observed to the 585, 975 and 2564-keV levels. In the present measurement the 3692-keV transition to the first excited state is hidden under the ^{13}C line at 3684 keV and has been indicated in the level scheme as a broken line.

The 5112-keV level

This level was found to be de-excited via the two $1/2^+$ levels at 2564 and 585 keV. If the 5112-keV state is fed from the capturing state, the corresponding 2218-keV transition would not be observed in the pair spectrum as it would be hidden by the 2223-keV line in ^2H .

Higher excited levels

Among the higher excited levels that may be populated in the neutron capture reaction only two have been included in the decay scheme, the 6038 and 6361-keV levels. As can be seen from the tentative assignments in Table I several more levels may be excited. The quality of the low-energy data is, however, not good enough to make the identification of weak transitions from the capturing state to high-lying excited states possible. Only a few of the assignments made have consequently been considered definite and are included in the decay scheme.

Acknowledgements

I would like to thank Dr. E. Selin for valuable discussions on the interpretation of the spectra. My thanks are also due to Ing. N. Bergland, Mr. C. Beer and the reactor staff at R1 for their support of my work.

R E F E R E N C E S

- [1] LITHERLAND, A.E., McMANUS, H., PAUL, E.B., BROMLEY, D.A., GOVE, H.E.,
Can. J. Phys. 36 (1958) 378.
- [2] SPILLING, P., GRUPPELAAR, H., OP DEN KAMP, A.M.F., Nucl. Phys. A102 (1967) 209.
- [3] McCALLUM, G.J., SOWERBY, B.D., Phys. Lett. 25B (1967) 109.
- [4] SHARPEY-SCHAFFER, J.F., OLLERHEAD, R.W., FERGUSON, A.J., LITHERLAND, A.E.,
Can. J. Phys. 46 (1968) 2039.

- [5] ENDT, P. M., van der LEUN, C., Nucl. Phys. A105(1967) 1.
- [6] ARNELL, S. E., HARDELL, R., HASSELGREN, A., JONSSON, L., SKEPPSTEDT, Ö., Nucl. Instrum. 54 (1967) 165.
- [7] GREENWOOD, R. C., in Slow-neutron capture gamma-ray spectroscopy, Rep. ANL-7282 (1966).
- [8] JONSSON, L., HARDELL, R., to be published.
- [9] BARTHOLOMEW, G. A., DOVEIKA, A., EASTWOOD, K. M., MONARO, S., GROSHEV, L. V., DEMIDOV, A. M., PELEKHOV, V. J., SOKOLOWSKII, L. L., Nucl. Data A3 (1967) 367.
- [10] JACKSON, H. E., NAMENSON, A. I., THOMAS, G. E., Physics Lett. 17 (1965) 324.

THERMAL NEUTRON CAPTURE GAMMA RAYS FROM ^{39}K AND ^{41}K

Ö. SKEPPSTEDT

Chalmers University of Technology,
Gothenburg, Sweden

Abstract

THERMAL NEUTRON CAPTURE GAMMA RAYS FROM ^{39}K AND ^{41}K . Energies and intensities of the gamma rays following thermal neutron capture in enriched samples of ^{39}K and ^{41}K have been measured using internal reactor targets and a three crystal Ge(Li) pair spectrometer and anti-Compton spectrometer. The reaction Q-values, excitation energies and decay schemes of ^{40}K and ^{42}K have been deduced.

1. Introduction.

The cross sections and abundances of the potassium isotopes indicate that studies performed with a target of natural composition essentially give information of the $^{39}\text{K}(n,\gamma)^{40}\text{K}$ reaction. The natural potassium composition is 93.1% ^{39}K , 0.012% ^{40}K and 6.9% ^{41}K and the thermal cross sections for ^{39}K , ^{40}K and ^{41}K are $1.94 \pm 0.15\text{b}$, $70 \pm 20\text{b}$ and $1.24 \pm 0.10\text{b}$ respectively (1).

The most detailed picture of the gamma spectrum resulting from thermal neutron capture in natural potassium has been given by Kennett et al. (2), who used a neutron beam impinging on a KOH sample and a conventional Ge(Li) spectrometer. There are also some measurements with lower resolution performed with magnetic pair spectrometers (3,4,5), magnetic Compton spectrometers (6,7,8) and with scintillation spectrometers (9,10). Recently, Harvey et al. (11) reported an investigation of the level structure of ^{42}K from thermal neutron capture in an enriched fluoride sample of ^{41}K . They used an external beam of thermal neutrons from a reactor and a 6 cm^3 Ge(Li) crystal. Up to now, no gamma rays, which definitely have their origins in the $^{40}\text{K}(n,\gamma)^{41}\text{K}$ reaction have been reported.

In this work thermal neutron capture in enriched samples of ^{39}K and ^{41}K has been investigated. The results from this experiment are in very good agreement with those published by Kennett et al. (2) and by Harvey et al. (11). The work by Kennett et al. gives a rather complete picture of the gamma rays resulting from capture in ^{39}K in the energy intervals 0-2.5 MeV and 3.9-7.8 MeV, but in the region 2.5-3.9 MeV the direct spectra from the Ge(Li) crystal seem to have been too complex to be interpreted. However, the gamma spectra from the two spectrometers used in this work are complete enough over the whole energy region to construct a tentative decay scheme of ^{40}K . Harvey et al. give a decay scheme of ^{42}K , in which gamma rays from the capturing state to low lying states and gamma rays deexciting these states are shown. This decay scheme is confirmed from the results of this work and furthermore it is extended to include levels up to 3.7 MeV.

Energy levels in ^{40}K are well known from the (d,p) work with magnetic spectrograph performed by Enge et al. (12), who also assigned l_n -values to most of the levels. The (d,p) data of ^{42}K are not

so complete as in the case of ^{40}K . Moore et al. (13) have determined the energies of the levels up to 4.8 MeV, but they only proposed l_n -values for four levels. However, in a recent work by Lynen et al. (14) the l_n -values of seven low lying levels are determined. Lynen et al. have also proposed spin for the five lowest levels in ^{42}K .

2. Experimental details

The experiments have been carried out at the 1 MW heavy water reactor R1 in Stockholm, where the high sensitive facility designed for measurements of thermal neutron capture gammas with Ge(Li) three crystal pair and anticoincidence spectrometers and internal targets (15,16) has been used. The potassium targets, which were separated in the form of KCl and then converted into K_2CO_3 , were encapsulated in graphite target holders and placed in the centre of a through channel of the reactor in a thermal flux of $3 \cdot 10^{12}$ n/cm²,s. The target quantities were 100 mg potassium enriched to 99.97 % in ^{39}K , 100 mg potassium enriched to 99.18 % in ^{41}K and 3.5 g potassium of natural composition.

3. Analysis of the measurements

For energy calibration of the pair spectra, nitrogen gas at a pressure of up to 3 atm was passed into the normally evacuated through channel. A mixed spectrum containing gamma lines following thermal neutron capture in nitrogen and potassium was then recorded. As gamma rays of well known energies (16) are properly distributed in the energy region 1.5-11 MeV in the gamma spectrum resulting from thermal neutron capture in nitrogen, this is a convenient method of getting a reliable energy calibration. Energy determination in the low energy region was performed by irradiating the Ge(Li) crystal with the radiation from radioactive sources of ^{60}Co , ^{137}Cs and ^{152}Eu at the same time as the capture spectra were taken.

The relative efficiency of the Ge(Li) pair spectrometer has been determined from the measurements mentioned above, when the spectra from nitrogen and potassium targets were recorded simultaneously. The nitrogen intensities were taken from ref. (16). The anticoincidence spectrometer efficiency was determined with radioactive sources. In the case of the ^{42}K spectra the relative intensities obtained were transferred to absolute values as the line at 1525 keV due to the β decay of ^{42}K appears both in the pair and in the anticoincidence spectra. An absolute intensity scale for the pair spectrum resulting from the $^{39}\text{K}(n,\gamma)^{40}\text{K}$ reaction was determined by setting the sum of the intensities of the gamma lines, which could be identified to deexcite the capturing state in ^{40}K to 100 photons per 100 captures. As several gamma lines from this reaction were found in both the pair spectrum and the anticoincidence spectrum, the intensities in the anticoincidence spectrum could be transferred to the same scale as was used for the pair spectrum.

4. Experimental results

The pair and anticoincidence spectra from the two reactions $^{39}\text{K}(n,\gamma)^{40}\text{K}$ and $^{41}\text{K}(n,\gamma)^{42}\text{K}$ are shown in figs. 1-4. The background lines are essentially the same in both reactions. The peaks labeled ^{28}Al , ^{28}Si , ^{57}Fe and $^{10}\text{B}(n,\gamma)^7\text{Li}$ originate from neutron interactions in aluminium, iron and boron construction parts. The graphite

target holder is the source for the ^{13}C lines and also for the broad distributions around 4.43 MeV resulting from inelastic neutron scattering in ^{12}C . As the samples are hygroscopic, a line at 2223 keV appears from the $\text{H}(n,\gamma)^2\text{D}$ reaction. The ^{36}Cl lines have probably their origins in the samples as they were originally separated as chlorides and then converted to carbonates.

The recoilcorrected energies and intensities in photons per 100 neutron captures for the gamma rays in the $^{39}\text{K}(n,\gamma)^{40}\text{K}$ reaction are given in table I. The errors in the intensities are estimated to about 20 % for strong lines and increase successively to about 100 % for the weakest lines. The ratio $\sum_i F_i I_i / 100 B$ ($B = 7799$ keV) is calculated to be 1.1, i.e. close to the theoretical value 1, which is an indication that most of the gamma rays in the decay are included in the table. However, one must bear in mind that, as the intensity scale was based upon setting the sum of the intensities deexciting the capturing state to 100 photons per 100 captures, one cannot exclude the possibility of a systematic error in the intensities. When the interpretations of the gamma lines were done, a computer program was used, where all the energy differences between levels in ^{40}K were calculated. The energy values of the levels were taken from table 40.3 in the review article Energy Levels of $Z = 11-21$ Nuclei (IV) by Endt and van der Leun (17). In table I, the interpretations are given in the last column. In this column, C denotes the capturing state. In three cases, cascades were found, where levels not reported earlier must be supposed to be involved. However, there is no possibility to pick out the primary gamma rays from the members of the cascades. In these cases the energies of the gamma rays in the cascades and their sum have been written in the interpretation column. All gamma lines which could be given an interpretation are inserted in the decay scheme shown in fig. 5. There is a doubtfulness concerning the 890 keV level. No gamma rays leading to this state could be identified, but the 890 keV line with the relatively low intensity 2.5 photons per 100 captures has been assigned the deexcitation of the 890 keV state and there are probably some gamma rays, which are too weak to be observed feeding this state. There are also some high energy levels, which are fed by weak primary rays, for which no deexcitation could be seen. The energy values of the levels shown in the decay scheme are determined from this experiment and are in very close agreement with the values given by Endt and van der Leun in their review article mentioned above.

From the cascades leading to the ground state and to the first excited state a determination of the Q-value for the $^{39}\text{K}(n,\gamma)^{40}\text{K}$ reaction has been done. The result is $Q = 7798.6 \pm 1.0$ keV, which is in agreement with the value 7797 ± 3 keV determined by Kennett et al. (2).

In table II, the energies and intensities for gamma rays observed in the $^{41}\text{K}(n,\gamma)^{42}\text{K}$ reaction are shown. The absolute intensity scale is supposed to be rather definite in this case as it was based upon the 1525 keV line from the β decay of ^{42}K , which appears in both the high and low energy spectra. The ratio $\sum_i F_i I_i / 100 B$ ($B = 7535$ keV) was for this reaction determined to 1.2, which is also close to the theoretical value. The computer program mentioned above for calculation of energy differences between energy levels was also used for identifying transitions between ^{42}K levels, but in this case, there is a systematic difference between the energy values determined in this work and those determined by Moore et al. (13) from the (d,p) reaction. The energy values of the ^{42}K levels used in the computer

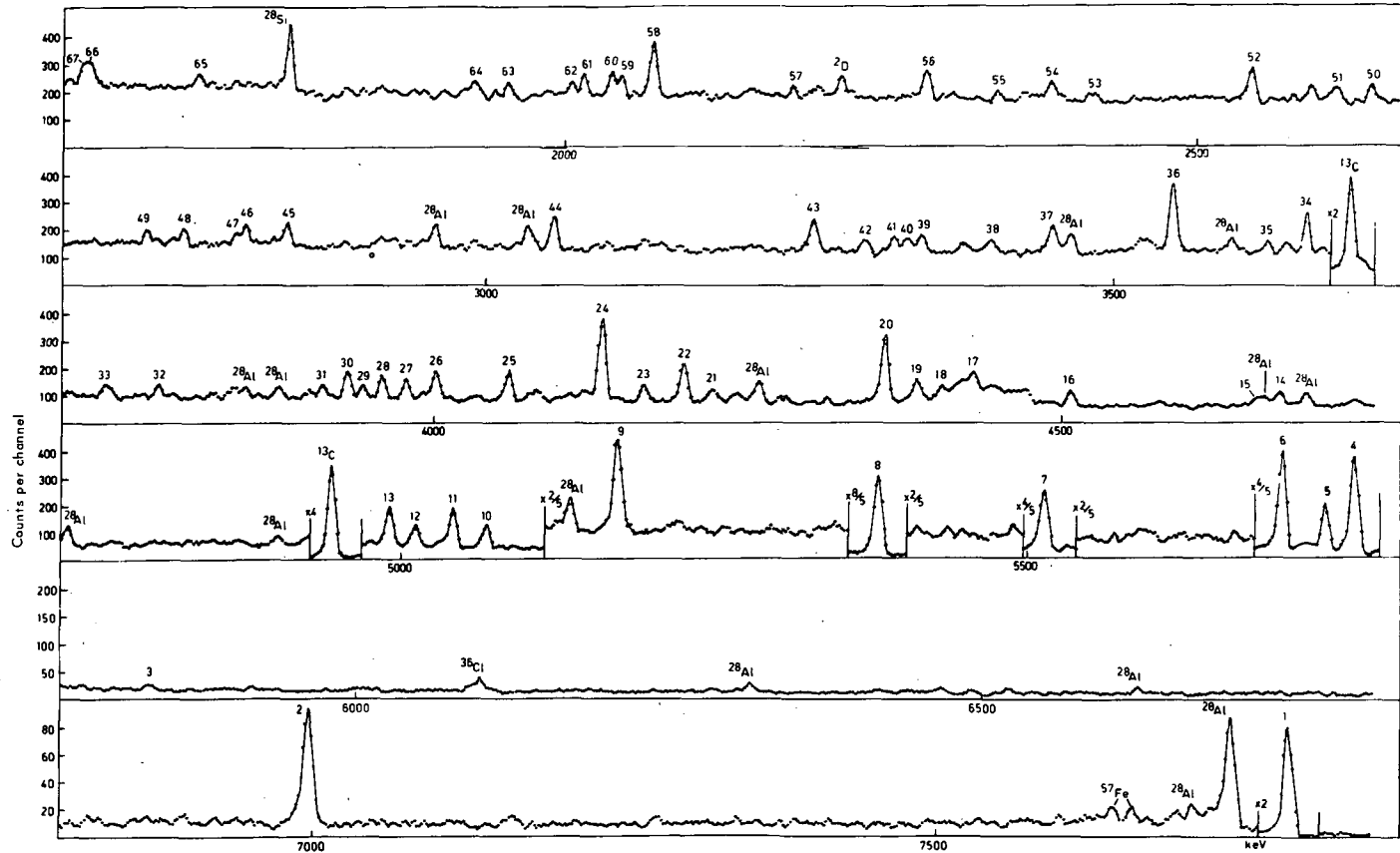


FIG.1. Three-crystal Ge(Li) pair spectrum following thermal neutron capture by ^{39}K . Accumulation time 42 h.

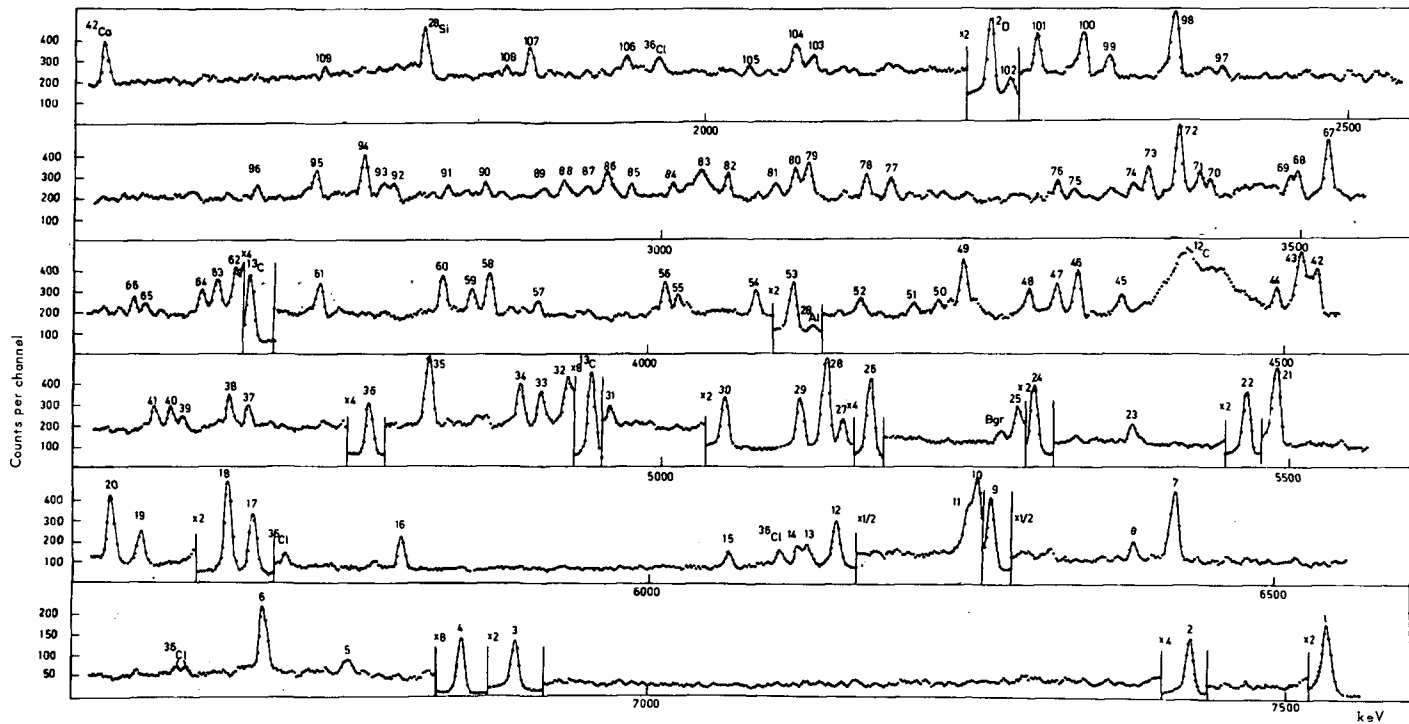


FIG.2. Three-crystal Ge(Li) pair spectrum following thermal neutron capture by ^{41}K . Accumulation time 45 h.

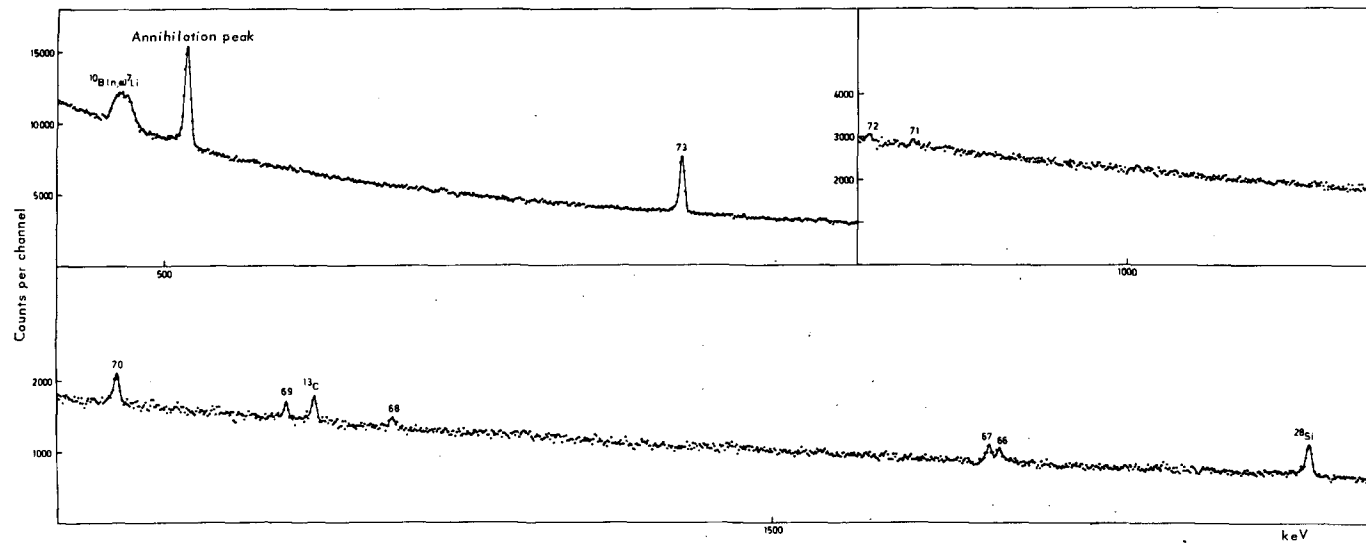


FIG. 3. Low-energy gamma-ray anticoincidence spectrum following thermal neutron capture by ^{39}K . Accumulation time 23 h.

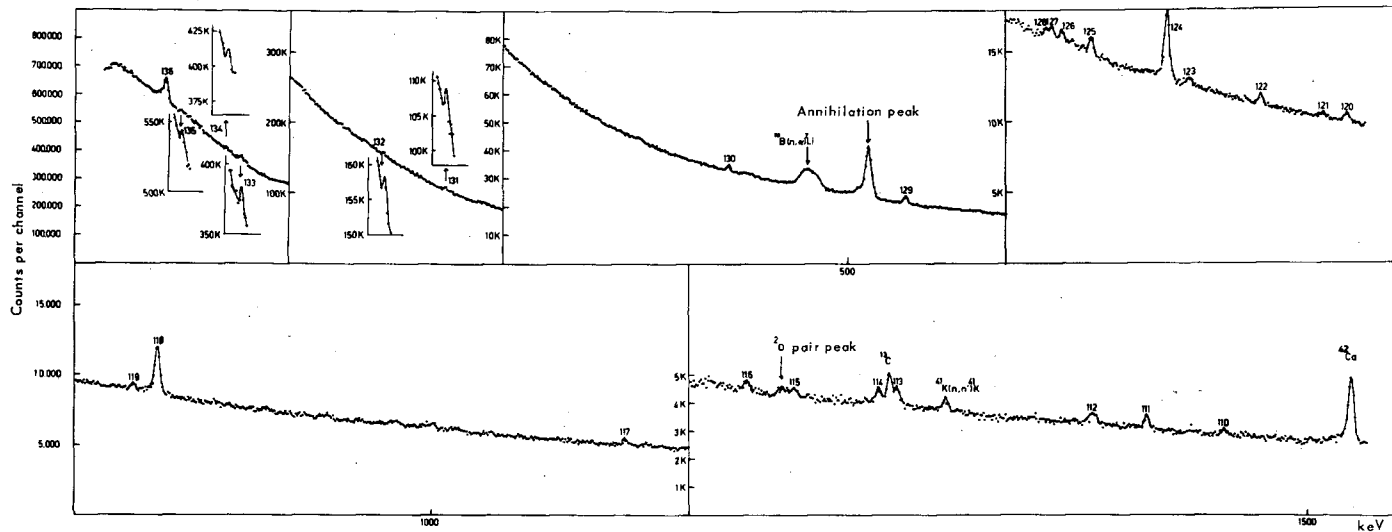


FIG. 4. Low-energy gamma-ray anticoincidence spectrum following thermal neutron capture by ^{41}K . Accumulation time 19 h.

Table I
Gamma rays observed in the $^{39}\text{K}(n,\gamma)^{40}\text{K}$ reaction

Peak number	E (keV)	Intensity (number of γ -rays per 100 captures)	Interpretation (keV)	Peak number	E (keV)	Intensity (number of γ -rays per 100 captures)	Interpretation (keV)
1	7770±1	7.6	C+ 30	37	3451±2	3.5	4253+ 800
2	6999±1	3.5	C- 800	38	3404±3	1.5	C-4396
3	5843±3	0.3	C-1958	39	3348±2	1.5	3650+3348+800=7798
4	5753±1	9.0	C-2047	40	3336±2	1.5	C-4462
5	5730±1	3.6	C-2069	41	3327±2	1.5	
6	5696±1	8.6	C-2103	42	3303±3	1.6	
7	5509±1	4.8	C-2290	43	3262±1	3.8	C-4537
8	5380±1	13	C-2419	44	3055±1	4.1	3943+3055+800=7798
9	5174±1	3.5	C-2625	45	2839±1	3.1	
10	5070±1	2.1		46	2805±2	2.8	2807+ 0
11	5043±1	3.4	C-2756	47	2798±3	1.3	3599+ 800
12	5013±1	1.4	C-2786	48	2756±2	2.1	2756+ 0
13	4491±1	3.2	C-2807	49	2726±2	1.5	2756+ 30
14	4671±1	1.3	C-3127	50	2637±2	1.0	4360+2637+800=7797
15	4653±1	0.7	C-3146	51	2610±3	1.9	3611+ 800
16	4507±1	1.2	4537+ 50	52	2544±1	4.8	2419+ 0
17	4431±2	0.7	4462+ 30	53	2419±3	2.1	2419+ 0
18	4406±2	0.9	C-3393	54	2387±2	2.5	2419+ 30
19	4386±1	1.9	C-3611	55	2346±2	1.5	3146+ 800
20	4360±1	5.5	4360+2637+800=7797	56	2289±1	4.5	2290+ 0
21	4223±3	0.7	4253+ 30	57	2184±2	1.8	4253+2069
22	4200±1	3.0	C-3590	58	2073±1	12	2103+ 30
23	4169±1	1.3	C-3630	59	2047±2	3.8	2047+ 0
24	4135±2	5.2	C-3664	60	2039±2	4.9	2069+ 30
25	4061±1	2.5	C-3739	61	2017±1	4.0	2047+ 30
26	4002±1	2.0	C-3797	62	2007±2	3.7	2807+ 800
27	3978±1	1.6	C-3821	63	1956±2	3.6	2756+ 800
28	3959±1	1.8	C-3840	64	1928±2	4.0	1958+ 30
29	3943±1	0.8	3943+3055+800=7798	65	1705±2	4.0	3664+1958
30	3931±1	2.2	C-3868	66	1619±1	4.4	2419+ 800
31	3911±2	1.0	C-3888	67	1614±1	6.2	
32	3779±2	0.9	C-4020	68	1302±2	3.5	2103+ 800
33	3739±3	1.1	3739+ 0	69	1246±1	3.9	2047+ 800
34	3650±1	3.0	3650+3348+800=7798	70	1159.3±0.5	8.3	1958+ 800
35	3620±2	0.6		71	890±2	2.6	890+ 0
36	3546±1	7.1	C-4253	72	868±2	0.9	
				73	769.5±0.5	62	800+ 30

calculation have consequently been adjusted to values resulting from this work. The values used are given in table III, where they are compared to the values determined by Moore et al. (13). The differences in excitation energy of the levels between the two measurements are given in the last column and they are also shown graphically in fig. 6.

In the interpretation column of table II, there are a number of assignments shown in brackets. These belong to transitions feeding or deexciting levels not reported in the work by Moore et al. or levels where the difference in excitation energy plotted in fig. 6 is far from the dashed line in the figure. These levels are listed in table III as tentative levels and they are shown as dashed lines in the decay scheme in fig. 7. There are in all cases transitions feeding and deexciting these tentative levels. Concerning these levels the gamma ray of highest energy has been chosen as the primary ray in the cascade. It cannot be excluded that this choice is wrong, and that some levels have been fitted at wrong places in the level diagram. However, in all of the cascades, where well established levels are intermediate states, the gamma ray of highest energy is the primary ray, so this somewhat dubious choice of the primary ray seems to have a rather high probability to be correct.

For the determination of the Q-value for the $^{41}\text{K}(n,\gamma)^{42}\text{K}$ reaction only cascades leading to the ground state were used. The result is $Q = 7535.2 \pm 0.5$ keV, which is to be compared to the value $Q = 7534.9$ keV given by Harvey et al. (11).

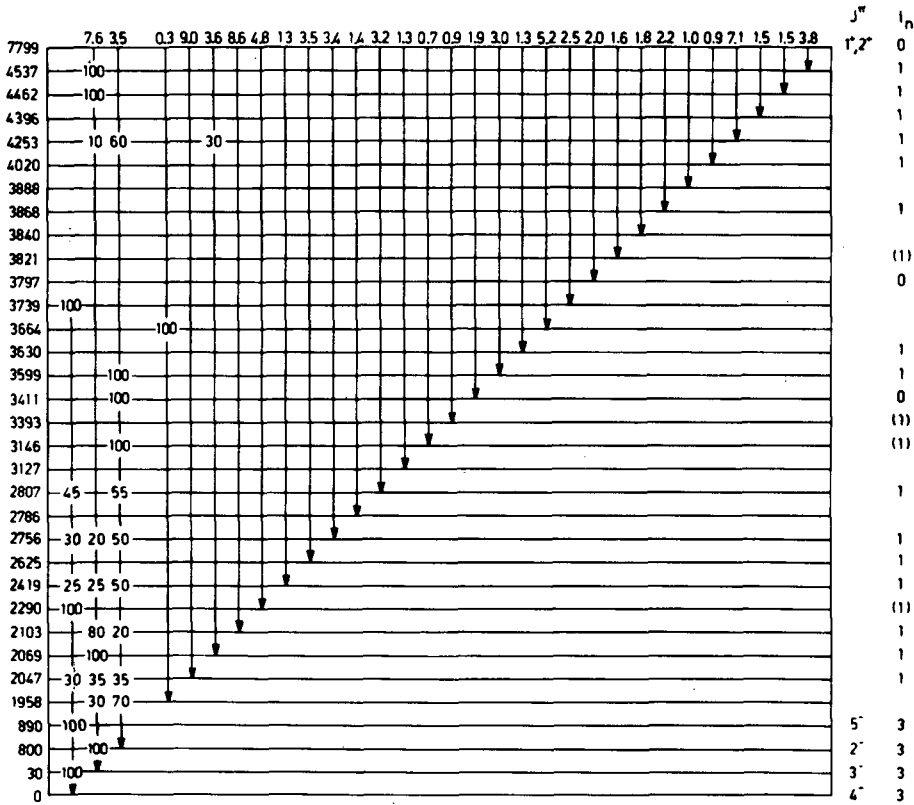


FIG.5. Decay of ^{40}K as deduced from this work. Branchings are given in per cent. The I_n values are taken from Ref.(12) and the spin values from Ref.(17). Only levels involved in the decay are shown.

The $^{39}\text{K}(n,\gamma)^{40}\text{K}$ reaction

The ground state of ^{39}K is found to have $J^\pi = 3/2^+$, so s-wave neutron capture in ^{39}K results in a 2^+ or 1^+ capturing state in ^{40}K . The ground state configuration of ^{40}K is $(1d_{3/2})^{-1}(1f_{7/2})$ from the shell model point of view. The spin values of levels arising from this configuration are 2^- , 3^- , 4^- and 5^- . This quadruplet has been identified as the four lowest levels in ^{40}K . The spins of these are, in order of increasing excitation energy from the ground state and up, 4, 3, 2 and 5. E1 transitions from the capturing state to levels belonging to this quadruplet are possible to the 30 keV, 3^- -state and the 800 keV, 2^- -state. Strong transitions to these two levels were also recorded in the high energy spectrum. Transitions to the 4^- ground state and the 890 keV 5^- state cannot proceed by dipole radiation and primary gamma rays to these two states could not either be found. The deexcitation of the three excited states belonging to the $(1d_{3/2})^{-1}(1f_{7/2})$ configuration, shown in the decay scheme in fig. 5, is in agreement with the assigned spin values.

Table II
Gamma rays observed in the $^{41}\text{K}(n,\gamma)^{42}\text{K}$ reaction

Peak number	E_γ (keV)	Intensity (number of γ -rays per 100 captures)	Interpretation (keV)	Peak number	E_γ (keV)	Intensity (number of γ -rays per 100 captures)	Interpretation (keV)
1	7535.1	3.4	C→ 0	69	3491±3	0.8	
2	7428.1	5.9	C→ 107	70	3429±2	0.7	
3	6896±2	1.6	C→ 639	71	3421±2	0.8	3419→ 0
4	6853.1	12	C→ 682	72	3406±1	3.5	
5	6761.3	0.2	(C→ 772)	73	3381±1	1.4	
6	6692±2	1.1	C→ 843	74	3370±2	0.5	3368→ 0
7	6424±2	1.2	C→ 1111	75	3323±3	0.4	
8	6392±3	0.3		76	3311±2	0.9	3419→ 107
9	6281.1	2.5	C→ 1255	77	3182±2	1.1	
10	6269±2	1.4	(C→ 1268)	78	3163±1	1.1	(3163→ 0)
11	6263±3	1.2		79	3118±2	2.8	
12	6158.1	1.6	C→ 1378	80	3106±2	1.6	(3212→ 107)
13	6135±3	0.5		81	3091±2	0.7	(3196→ 107)
14	6129±3	0.4	C→ 1408	82	3052±2	1.1	
15	6072±3	0.4	C→ 1463	83	3032±3	3.6	3674→ 639
16	5813±2	0.8		84	3009±2	0.8	(3009→ 0)
17	5692.1	3.8	(C→ 1842)	85	2977±2	0.7	
18	5673.1	5.7	C→ 1862	86	2958±2	1.1	
19	5621±2	0.9		87	2942±3	0.4	
20	5597.1	2.2	C→ 1938	88	2924±2	0.9	(2925→ 0)
21	5491.1	3.1	C→ 2044	89	2908±3	0.4	
22	5463.1	3.9	C→ 2072	90	2861±3	0.6	(2862→ 0)
23	5374±3	0.5		91	2832±3	0.4	2939→ 107
24	5296.1	4.3	C→ 2239	92	2788±2	1.3	
25	5284±2	1.1		93	2781±2	1.0	(3040→ 259)
26	5168.1	11	C→ 2367	94	2766±1	3.4	2766→ 0
27	5146.1	1.5		95	2728±1	1.9	3368→ 639
28	5133.1	5.8	C→ 2403	96	2680±2	0.9	
29	5114.1	2.8	(C→ 2421)	97	2403±2	1.0	2403→ 0
30	5052.1	3.1	C→ 2483	98	2366±1	6.3	2367→ 0
31	4961±3	0.5	C→ 2574	99	2316±1	1.6	(2421→ 107)
32	4928±2	0.7	C→ 2607	100	2295±1	5.3	2403→ 107
33	4907±2	1.0	C→ 2628	101	2260±1	3.3	2367→ 107
34	4890±2	1.3	C→ 2645	102	2239±1	3.3	2239→ 0
35	4816.1	2.4	C→ 2719	103	2084±2	2.0	2719→ 639
36	4769.1	6.5	C→ 2766	104	2072±1	2.9	2072→ 0
37	4672±2	0.5	(C→ 2862)	105	2035±2	1.0	(2878→ 843)
38	4657±2	1.0	(C→ 2878)	106	1937±1	1.2	1938→ 0
39	4618±3	0.3		107	1862±1	5.0	1862→ 0
40	4609±3	0.4	(C→ 2925)	108	1842±2	1.2	1842→ 0
41	4596±3	0.5	C→ 2939	109	1698±2	1.5	
42	4526±2	1.7	(C→ 3009)	110	1453±2	0.4	
43	4514±2	2.5		111	1408.3±1.0	1.0	1408→ 0
44	4495±2	0.5	(C→ 3040)	112	1377.9±1.0	1.0	1378→ 0
45	4373±2	0.7	(C→ 3163)	113	1269±2	1.3	(1268→ 0)
46	4339±1	1.6	(C→ 3196)	114	1256.3±1.0	1.4	1255→ 0
47	4323±2	1.0	(C→ 3212)	115	1210±2	0.6	
48	4301±2	0.6		116	1179.9±1.0	0.8	1862→ 682
49	4251.1	1.3	C→ 3284	117	1111.9±1.0	1.6	1111→ 0
50	4230±3	0.3		118	843.3±0.5	13	843→ 0
51	4211±3	0.5		119	829.6±1.2	1.1	
52	4169±2	0.6	C→ 3368	120	785.3±1.0	1.7	
53	4116±1	3.8	C→ 3419	121	771.7±1.0	0.8	(772→ 0)
54	4087±2	0.8		122	735.5±1.0	3.2	843→ 107
55	4025±2	0.5		123	694.7±1.0	1.2	
56	4015±2	0.8	(C→ 3520)	124	682.4±0.5	13	682→ 0
57	3914±3	0.4		125	638.8±1.0	3.3	639→ 0
58	3876±1	1.2	C→ 3659	126	620.4±1.0	1.5	1463→ 843
59	3861±2	0.8	C→ 3674	127	616±2	0.9	1255→ 639
60	3838±1	1.4	C→ 3697	128	612±2	0.8	
61	3739±2	1.5		129	532.3±0.5	6.2	639→ 107
62	3673±3	0.8	3674→ 0	130	431.5±1.0	2.7	1111→ 682
63	3658±2	1.1	3659→ 0	131	269.0±1.0	2.2	1111→ 843
64	3645±2	0.7		132	232.6±1.0	1.7	
65	3600±3	0.4		133	151.5±1.0	6.1	259→ 107
66	3590±2	0.6	3697→ 107	134	143.1±1.0	2.5	1255→ 1111
67	3520±1	2.9	(3520→ 0)	135	116.2±1.0	6.3	
68	3496±2	1.2		136	107.4±0.5	42	107→ 0

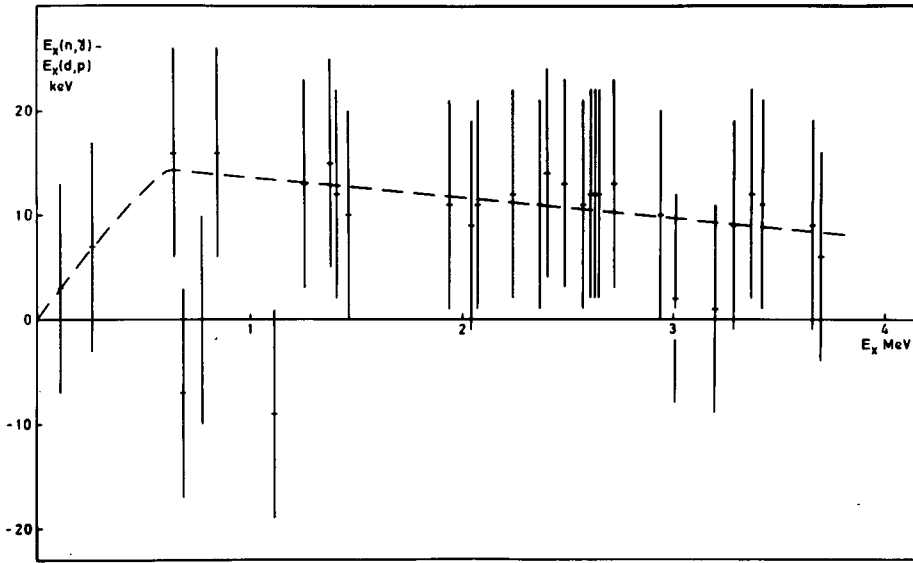


FIG. 6. The differences between the excitation energies in ⁴²K from the present (n, γ) work and the (d, p) work in Ref. (13) as a function of E_x.

Table III
Energy levels observed in the ⁴¹K(n,γ) ⁴²K reaction compared to levels observed in the ⁴¹K(d,p) ⁴²K reaction

I Levels observed in this work		II		I Levels observed in this work		II	
Strongly confirmed levels (keV)	Tentative levels (keV)	Previously reported levels (keV)	Difference in excitation energy (I-II) (keV)	Strongly confirmed levels (keV)	Tentative levels (keV)	Previously reported levels (keV)	Difference in excitation energy (I-II) (keV)
0		0	0	2483		2470	+13
107		104	+3			2542	
259		252	+7	2574		2563	+11
639		623	+16	2607		2595	+12
682		689	-7	2628		2616	+12
843	772	772	0	2645		2633	+12
		827	+16	2719		2706	+13
1111		1120	-9	2766		2740 - 2800	
		1179				2832	
1255		1242	+13		2862		
	1268				2878		
137 E		1363	+15			2906	
1408		1396	+12		2925		
1463		1453	+10	2939		2929	+10
		1472			3009	3007	+2
	1842	1776			3040		
1862						3076	
		1913			3163		
1938		1927	+11		3196	3195	+1
2044		2035	+9	3284	3212		
2072		2061	+11	3368		3275	+9
		2162		3419		3356	+12
		2189			3520	3408	+11
2239		2227	+12			3606	
2367		2356	+11	3659		3650	+9
2403		2389	+14	3674			
	2421			3697		3691	+6

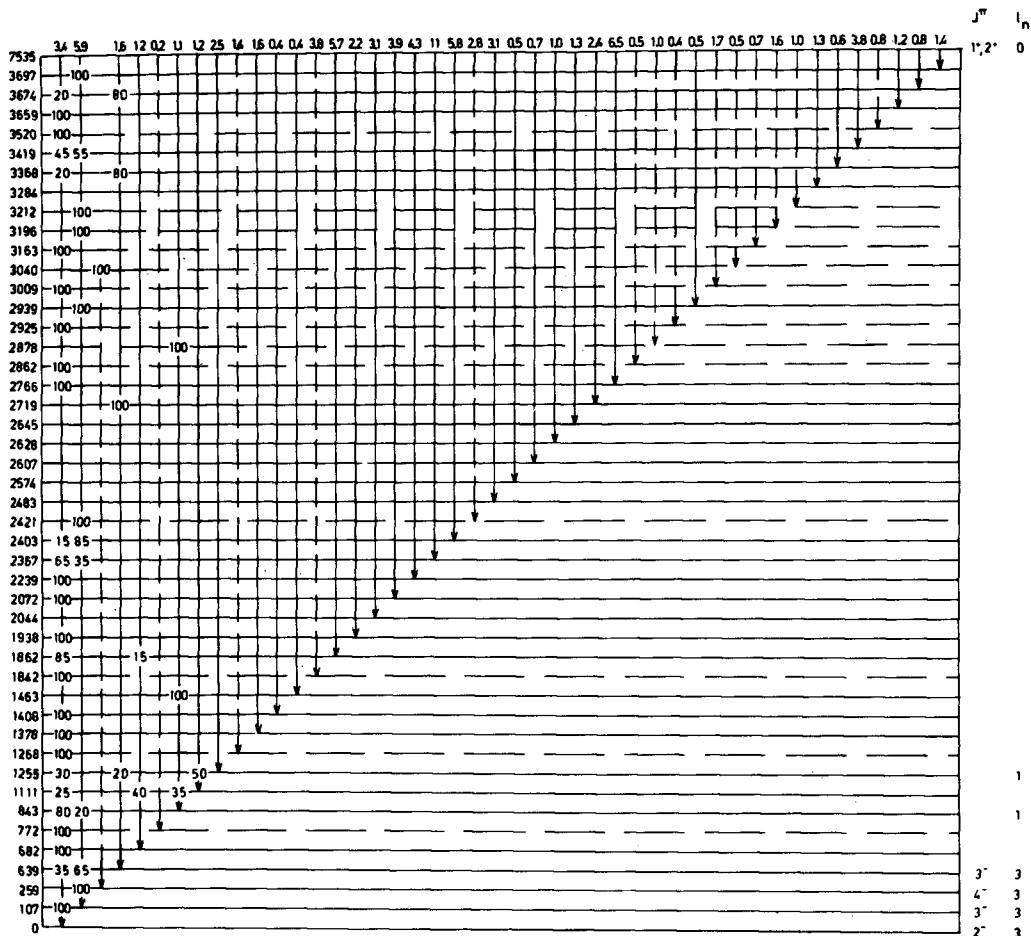


FIG. 7. Decay of ^{42}K as deduced from this work. Branchings are given in per cent. The I_n values are taken from Ref. (14) and the spin values from Ref. (13). Only levels involved in the decay are shown.

One of the reasons to study (n,γ) reactions is to search for correlation effects between the reduced widths for primary gamma rays in (n,γ) reactions and the reduced stripping widths for proton groups in (d,p) reactions leading to the same final state. As Bockelman (18) has pointed out, the correlation should be strong if direct capture in the neutron capture process is significant. In the work by Kennett et al. (2) such an investigation for the $^{39}\text{K}(n,\gamma)^{40}\text{K}$ reaction was performed, but the correlation between the (n,γ) and (d,p) reduced widths was found to be very weak. The data from this work confirm that no correlation exist and accordingly one can conclude that the capture of a neutron by ^{39}K predominantly proceeds via compound nucleus formation.

The $^{41}\text{K}(n,\gamma)^{42}\text{K}$ reaction

In similarity to the $^{39}\text{K}(n,\gamma)^{40}\text{K}$ reaction capture of s-wave neutrons in ^{41}K result in a 1^+ or 2^+ state as the ground state of ^{41}K is known to be a $3/2^+$ state. The shell model ground state configuration of ^{42}K is $(1d_{3/2})^{-1}(1f_{7/2})^3$. In the work by Lynen et al. (14) four levels of this configuration have been identified as the ground state and levels at 0.11 MeV, 0.26 MeV and 0.70 MeV on the basis of their $l=3$ character in the $^{41}\text{K}(d,p)^{42}\text{K}$ reaction and the $l=2$ character of their analog state in ^{42}Ca determined in the $^{43}\text{Ca}(^3\text{He},\alpha)^{42}\text{Ca}$ reaction. They suggest the spin sequence of 3^- , 4^- , and 5^- for the 0.11 MeV, 0.26 MeV and 0.70 MeV states. This is in accordance with the (d,p) work by Moore et al. (13), who give the energy values 104 keV, 252 keV and 689 keV for the excited states. Lynen et al. also propose the spin 3^- to the 0.64 MeV level. In a shell-model calculation on $(f_{7/2})^n$ and $(f_{7/2})^{n+1}(d_{3/2})^{-1}$ configurations, Dieperink and Brussaard (19) have calculated the level spectrum of ^{42}K . This theoretical spectrum is in very good agreement with the experimental results from the work by Lynen et al. mentioned above.

In this (n,γ) work the ground state and the levels at 107, 639 and 682 keV are fed by primary transitions which are supposed to be of E1 nature, but there is no gamma ray from the capturing state to the 259 keV state. These facts together with the deexcitation of the levels support the spin values proposed by Lynen et al. except for the 682 keV level which cannot be the 5^- state. The systematic difference between the excitation energies in ^{42}K from the present (n,γ) work and the (d,p) work by Moore et al. shown in fig. 6 also indicates that the level at 682 keV from this work is not the same level as the 689 keV, 5^- state measured in the (d,p) works. There should accordingly be two close levels around 0.68 MeV and fig. 6 indicates that the 5^- state should lie somewhat lower than the 682 keV level.

It would be of great interest to make a comparison between the $^{41}\text{K}(n,\gamma)^{42}\text{K}$ and the $^{41}\text{K}(d,p)^{42}\text{K}$ reactions, but the (d,p) information is unfortunately too scarce to make such an investigation possible.

Acknowledgements

The author wants to thank Tekn. lic. R. Hardell for assistance during the measurements, Dr. S.E. Arnell for valuable discussions and Professor N. Ryde for his interest in this work. I am also indebted to the reactor staff at R1 for good collaboration.

References

1. G.A. Bartholomew, A. Doveika, K.M. Eastwood, S. Monaro, L.V. Groshev, A.M. Demidov, V.I. Pelekhov and L.L. Sokolovskii, Nuclear Data A3(1967)367.
2. T.J. Kennett, L.B. Hughes and W.V. Prestwich, Nuclear Physics 89(1966)254.
3. B.B. Kinsey, G.A. Bartholomew and W. Walker, Phys. Rev. 85(1952)1012.
4. G.A. Bartholomew and B.B. Kinsey, Can. J. Phys. 31(1953)927.
5. G.A. Bartholomew and L.A. Higgs, Chalk River Report AECL No. 669(1958).
6. B.P. Adyasevich, L.V. Groshev, A.M. Demidov and V.N. Lutsenko, Atomnaya Energiya 1(1956)28; J. Nuclear Energy 3(1956)258.
7. L.V. Groshev, A.M. Demidov, V.N. Lutsenko and V.I. Pelekhov, Atlas of Gamma Ray Spectra from Radiative Capture of Thermal Neutrons (Moscow, 1958).
8. W. Rudolph and H.U. Gersch, Nuclear Physics 7(1965)221.
9. T.H. Braid, Phys. Rev. 102(1956)1109.
10. J. Urbanec, J. Kopecky and J. Kajfosz, Czechoslov. J. Phys. 9(1959)544.
11. J.A. Harvey, E.C. Campell, C.C. Weitkamp and G.G. Slaughter, ORNL-4230, UC-34-Physics (1968)42.
12. H.A. Enge, E.J. Irwin and D.H. Weaner, Phys. Rev. 115(1959)949.
13. W.H. Moore, J.W. Kelley and H.A. Enge, MIT, Lab. Nucl. Sci. Progr. Rept. May 1958, p 114.
14. U. Lynen, H. Oeschler, R. Santo and P. Stock, Max-Planck-Institut für Kernphysik, Heidelberg, rept, 1968, V 19.
15. S.E. Arnell, R. Hardell, A. Hasselgren, L. Jonsson and Ö. Skeppstedt, Nucl. Instr. 54(1967)165.
16. L. Jonsson and R. Hardell, these proceedings.
17. P.M. Endt and C. van der Leun, Nuclear Physics A 105(1967)1.
18. C.K. Bockelman, Nuclear Physics 13(1959)205.
19. A.E.L. Dieperink and P.J. Brussaard, Nuclear Physics A 106(1968)177.

GAMMA RAYS FROM THERMAL NEUTRON CAPTURE IN ^{40}Ca , ^{42}Ca , ^{43}Ca , ^{44}Ca AND ^{48}Ca

S. E. ARNELL, R. HARDELL, Ö. SKEPPSTEDT, E. WALLANDER
Chalmers University of Technology,
Gothenburg, Sweden

Abstract

GAMMA RAYS FROM THERMAL NEUTRON CAPTURE IN ^{40}Ca , ^{42}Ca , ^{43}Ca , ^{44}Ca AND ^{48}Ca . Energies and intensities of the gamma rays following thermal neutron capture in enriched samples of ^{40}Ca , ^{42}Ca , ^{43}Ca , ^{44}Ca and ^{48}Ca have been measured using internal reactor targets and a three-crystal Ge(Li) pair spectrometer and anti-Compton spectrometer. The reaction Q-values, excitation energies and absolute intensity values have been deduced. Decay schemes of ^{41}Ca , ^{43}Ca , ^{44}Ca and ^{49}Ca are given. The $^{42}\text{Ca}(n,\gamma)^{43}\text{Ca}$ and $^{42}\text{Ca}(d,p)^{43}\text{Ca}$ reactions are compared and found to give a good correlation between the strengths in the (d,p) and (n, γ) reactions.

1. Introduction

There are six stable isotopes of calcium. The spectrometer efficiency of our experimental arrangement (1), the availability of enriched isotopes and the costs make an experimental investigation of thermal neutron capture gamma rays with highly enriched isotopes possible in all the calcium isotopes except in ^{46}Ca .

Thermal neutron capture gamma rays from capture in natural and in enriched calcium isotopes are listed in Endt and van der Leun (2) and in Nuclear Data (3). Recently the $^{44}\text{Ca}(n,\gamma)^{45}\text{Ca}$ reaction has been studied by Gruppelaar et al. (4) with enriched isotopes and a Ge(Li)-spectrometer. It is hoped that the present investigation where the spectra from five highly enriched calcium isotopes are investigated under identical experimental conditions will facilitate the identification of contributions from various calcium isotopes as well as from impurities.

In a previous work (5) in this mass region a good correlation between the (n, γ) and (d,p) strengths was found. It is also the purpose of this investigation to find out if this correlation also can be found for all the calcium isotopes. For those two cases, ^{41}Ca and ^{45}Ca , which have been recently thoroughly investigated, only the high energy parts of the spectra were studied in this work with the purpose of possibly finding weak direct transitions from the capturing states of value for a detailed comparison with the (d,p) strengths.

2. Experimental details

The calcium targets were encapsulated in the centres of graphite target holders and positioned in an evacuated aluminium tube traversing the reactor vessel of the 1 MW heavy water reactor R1 in Stockholm. The thermal neutron flux in the target position is $3 \cdot 10^{12}$ n/cm².s. The calcium sample quantities, the isotopic compositions of the samples and the contributions from the various calcium isotopes are listed in Table I. The capture gamma rays pass a 6 mm diam. by 1.5 m

TABLE I. SAMPLE QUANTITY, ISOTOPIC COMPOSITION AND CONTRIBUTION OF THE VARIOUS CALCIUM ISOTOPES

Main contributing isotope in sample ^a	Cross-section ^b , σ (b), of main contributing isotopes	Sample quantity of calcium (mg) in the form of CaCO ₃	Isotopic composition of sample (P atomic abundance in %)						P x σ					
			⁴⁰ Ca	⁴² Ca	⁴³ Ca	⁴⁴ Ca	⁴⁶ Ca	⁴⁸ Ca	⁴⁰ Ca	⁴² Ca	⁴³ Ca	⁴⁴ Ca	⁴⁶ Ca	⁴⁸ Ca
⁴⁶ Ca	(0,44)	600	99.965	0.009	0.002	0.22	< 0.01	0.002	44	0.006	0.01	0.02	-	0.002
⁴² Ca	0.70	200	40.6	57.3	0.44	1.58	< 0.002	0.05	17.2	40	2.7	1.7	-	0.06
⁴³ Ca	6.2	50	23.58	2.49	49.34	15.78	< 0.01	< 0.01	10.4	1.7	306	17	-	-
⁴⁴ Ca	1.1	150	5.22	0.43	0.32	94.0	< 0.01	0.02	2.3	0.30	2	103	-	0.02
⁴⁸ Ca	1.1	100	29.8	0.5	0.4	2.2	0.1	67.1	13.1	0.35	2.5	2.4	0.03	74

^a The ⁴⁰Ca, ⁴²Ca, ⁴³Ca and ⁴⁴Ca samples were delivered from Oak Ridge, Tennessee. The ⁴⁶Ca sample was bought from V/K Technobexport, Moscow.

^b The thermal neutron capture cross-sections for ⁴²Ca, ⁴³Ca and ⁴⁴Ca are from ref.(9), the ⁴⁸Ca cross-section from ref.(10). The cross-section for ⁴⁶Ca is not known exactly. The value 0.22 b (10) is certainly too low as more than 90% of the thermal neutron absorption in natural calcium occurs in ⁴⁰Ca (abundance 96.97%) and the cross-section for natural calcium is 0.44 b(10). In ref.(12) the cross-section for ⁴⁰Ca is estimated as 0.43 b. In Table 1 the cross-section for natural calcium has been used for ⁴⁰Ca.

long collimating system before reaching the detector, situated about 4.5 m from the target. A lowering of the background was obtained by evacuating the tube thus avoiding neutron capture in nitrogen. A staff-shaped Ge(Li) crystal¹, length 2.0 cm, volume 1.5 cm³ and a cooled FET preamplifier¹ were used for the capture gamma detection. To simplify the response function of the detector above the pair production threshold a pair spectrometer arrangement has been used. Two side crystals form together an annulus of NaI, 15 cm in diameter and 10 cm long with a through hole, 4 cm in diameter. The annulus is bisected and the two segments are optically isolated. For the measurement of low energy gammas the same NaI side crystals are used as part of an anticoincidence mantle. Furthermore a NaI crystal of dimensions 12.5 cm diameter by 10 cm long with a through hole, diameter 1.8 cm, is placed in front of the NaI annulus to detect backscattered radiation. The pulses from the NaI crystals are summed and fed via a discriminator to the anticoincidence gate of the 4096 channel pulse height analyzer. A detailed description of the whole arrangement is given in ref. (1).

The background lines, common for all spectra, originate mainly from neutron capture and scattering in the carbon target holder. Some weak lines from neutron capture in construction details of aluminium are also visible as well as a hydrogen peak. Some chlorine contamination is also visible in most of the calcium spectra. In the low energy spectra background lines are caused by the annihilation radiation and from neutron capture in the boron compound shield giving the $^{10}\text{B}(n,\alpha\gamma)\text{Li}$ reaction.

To obtain energy calibration in the high energy region nitrogen gas was passed into the reactor channel and a composite spectrum was taken. Well-determined gamma lines from neutron capture in nitrogen and carbon are found in refs (6-8). In the low energy region radioactive sources were used for the energy calibration by irradiating the detector at the same time as the capture spectra were taken. The relative efficiency of the Ge(Li) pair spectrometer has been calculated using the composite spectrum. The nitrogen intensities have been taken from ref.(6). In the low energy region radioactive sources were used for intensity calibration. The absolute intensity values of the gamma lines in photons/100 neutron captures are obtained by normalizing the sum of the primary gamma rays equal to 100. The errors in the intensities are estimated to about 20 % for strong lines and increase successively to about 100 % for weak lines.

The experimental Q-value is found from the ground state transition, if present, and by summing the energies of obvious cascade transitions. The energy value of an excited level fed directly from the capturing state is obtained from the Q-value, the energy of the primary gamma ray and the gamma energies of the transitions from the excited state. The error in the energy level determination is about 1 keV using this method. The uncertainty in the (d,p) values of the energy levels on the other hand may be up to 10 keV. It is then necessary, especially when the level density is high, to find out if there exists a systematic deviation in the (d,p) measurements. A knowledge of the value of this deviation makes it possible to make a correction to the (d,p) energy levels at higher excitation and in this way make sure which (d,p) energy levels are fed by primary gamma rays in the (n, γ) reaction. The general process used for constructing the decay schemes

¹ Manufactured by AB Atomenergi, Studsvik, Sweden.

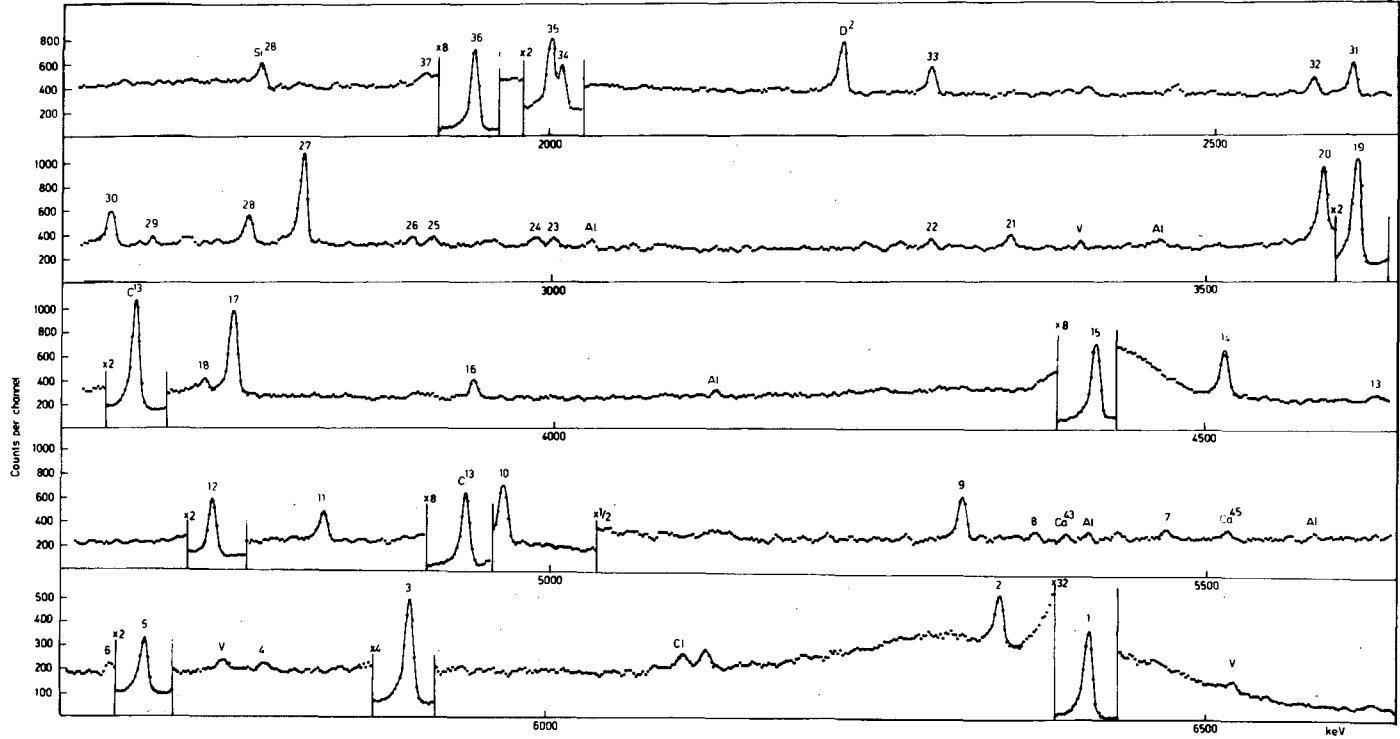


FIG.1. Three-crystal Ge(Li) pair spectrum following thermal neutron capture in ^{40}Ca . Accumulation time 25 h.

consists of using the energy values of the levels and employing a computer for the calculation and ordering of the differences between levels. It is in this way possible to find alternative positions for the gamma rays in the decay scheme.

3. The $^{40}\text{Ca}(n,\gamma)^{41}\text{Ca}$ reaction

Gamma rays from neutron capture in natural calcium where more than 90 % of the gamma rays result from capture in ^{40}Ca have been thoroughly studied by several workers (2,3,11). The recent study by Gruppelaar and Spilling (12), however, used calcium enriched in ^{40}Ca . As the contribution from neutron capture in ^{40}Ca is present to some extent in all the other measurements with enriched isotopes in the present work it is important for us to know the spectrum under our experimental conditions. This is one of the reasons for including the $^{40}\text{Ca}(n,\gamma)^{41}\text{Ca}$ reaction in our study.

The gamma ray pair spectrum is shown in Fig. 1. Traces from impurities of vanadium are observed in the spectrum besides the background lines mentioned in section 2. The gamma energy values and the absolute intensities for gamma rays from the $^{40}\text{Ca}(n,\gamma)^{41}\text{Ca}$ reaction in the pair spectrum are given in Table II. The table also includes a comparison with the results of Gruppelaar and Spilling (12). In the decay scheme shown in Fig. 2 the gamma lines are fitted as transitions between levels in ^{41}Ca . The experimental Q-value is 8364.3 ± 0.5 keV in good agreement with the value 8364.4 ± 0.4 keV obtained by Gruppelaar and Spilling (12). Their energy values of the excited states are also in good agreement with our values (see Table III) and about 10 keV lower than those found by Belote et al. (13). It can be remarked that the values found with the MIT broad range spectrograph and quoted in Braams' thesis (14) agree, up to an excitation energy of 3 MeV, within about 1 keV with the energy values found in the (n, γ) work. The intensity sum of gamma rays to a level and from a level must be in balance. Table III shows the intensity balance which is generally good.

In addition to the results obtained by previous workers (2,3,11,12) the decay scheme contains some new features. Weak gamma lines are fitted as transitions between the capturing $1/2^+$ state and levels around 5.5 MeV. Some of these levels have been given $l_n = 1$ assignments by Belote et al. (13). Three of these levels seem to deexcite directly to the ground state.

Gruppelaar and Spilling (12) remark from an analysis of the decay scheme of ^{41}Ca that the gamma transitions between two hole states and between two single particle states are favoured. They also observe that the $l_n=0$ state at 5012 keV does not deexcite to the 2010 keV hole state with $l_n=0$ but with a 3067 keV line to the $3/2^-$ state at 1943 keV which has single particle character. They interpret this as an indication that the 5012 keV state has a $3s_{1/2}$ single particle character instead of a hole configuration. The observation of a 3001 keV line fitted as a transition between the 5012 keV level and the 2010 keV level together with the absence or near absence of the 3067 keV line in our spectrum make their interpretation less probable. On the other hand, according to our interpretation, the 3846 keV level with $l_n=0$ deexcites to the 1943 keV level.

Table II. Thermal neutron capture gamma rays from the $^{40}\text{Ca}(n,\gamma)^{41}\text{Ca}$ reaction measured with the Ge(Li) pair spectrometer

Present work with Ge(Li) pair spectrometer				Gruppelaar and Spilling (12)	
No.	E_γ (keV) (corrected for recoil)	I_γ (photons/100 captures)	Assignment	E_γ (keV)	I_γ^{xx}
1	6421.4±1.0	38.2	C ^x -1943	6421.2±1.0	43.5
2	6353.6±1.0	1.0	C-2010	6352.5±3.0	0.2
3	5901.5±1.0	8.3	C-2463	5900.7±1.0	7.0
4	5787.0±1.5	0.1	C-2576	-	-
5	5693.7±1.0	2.2	C-2671	5692.9±2.0	1.1
6	5670.0±1.5	0.2	5671-0	-	-
7	5468.0±1.5	0.1	5469-0	-	-
8	5369.0±1.5	0.1	(5371-0)	-	-
9	5314.2±1.0	0.6	C-3050	5314.1±3.0	0.3
10	4963.1±1.0	1.7	C-3401	4962.7±2.0	1.8
	-	-	-	4944.7±3.0	0.8
11	4838.0±1.5	1.0	C-3526	4839.0±3.0	0.5
12	4749.8±1.0	1.7	C-3614	4749.6±1.5	2.6
13	4626.0±2.0	0.4	C-3738	-	-
14	-	-	-	4560.0±3.0	0.1
14	4516.2±1.0	1.9	C-3847	4518.0±3.0	0.7
15	4419.0±1.0	24.8	C-3944	4419.4±1.0	17.1
16	3944.1±1.5	0.9	-	3947.5±3.0	0.4
17	3759.8±1.0	3.2	C-4604	3760.0±0.8	3.1
18	3737.0±1.5 ^{xxx}	0.5	3738-0	-	-
19	3610.8±1.0	8.4	C-4753	3610.3±0.4	6.0
20	3586.0±1.5	3.9	C-4778	3585.4±0.6	1.6
21	3351.7±1.0	0.6	C-5012	3351.1±1.5	0.4
22	3290.0±2.0	0.3	C-5074	-	-
	-	-	-	3083.1±2.0	0.7
	-	-	-	3067.4±2.0	0.7
23	3001.0±2.0	0.4	5012-2010 (5671-2671)	-	-
24	2992.0±2.0	0.4	C-5371	-	-
25	2913.0±2.0	0.4	C-5451	-	-
26	2895.0±2.0	0.4	C-5469	-	-
27	2810.2±1.0	5.1	4753-1943	2811.2±1.5	3.8
28	2768.0±1.5	1.7	4778-2010	2768.9±2.0	2.8
29	2693.0±1.5	0.3	C-5671	-	-
30	2660.6±1.0	6.3	4604-1943	2660.4±2.0	1.3
31	2605.5±1.0	1.2	-	2606.6±0.5	1.6
32	2576.0±1.5	1.0	2576-0	-	-
33	2290.5±1.0	2.6	4753-2463	2290.3±0.8	1.6
34	2010.0±1.5	10.5	2010-0	2010.1±0.5	11.5
35	2001.4±1.0	18.5	3944-1943	2001.2±0.4	18.9
36	1942.7±1.0	81.0	1943-0	1942.7±0.3	88.5
37	1904.0±2.0	1.6	3847-1943	-	-

x) C denotes the capturing state.

xx) The sum of the intensities of the 1943 and 2010 keV gamma lines is 100.

xxx) Part of the intensity of this line may be due to the $^{40}\text{Ca}(n,n'\gamma)$ -reaction.

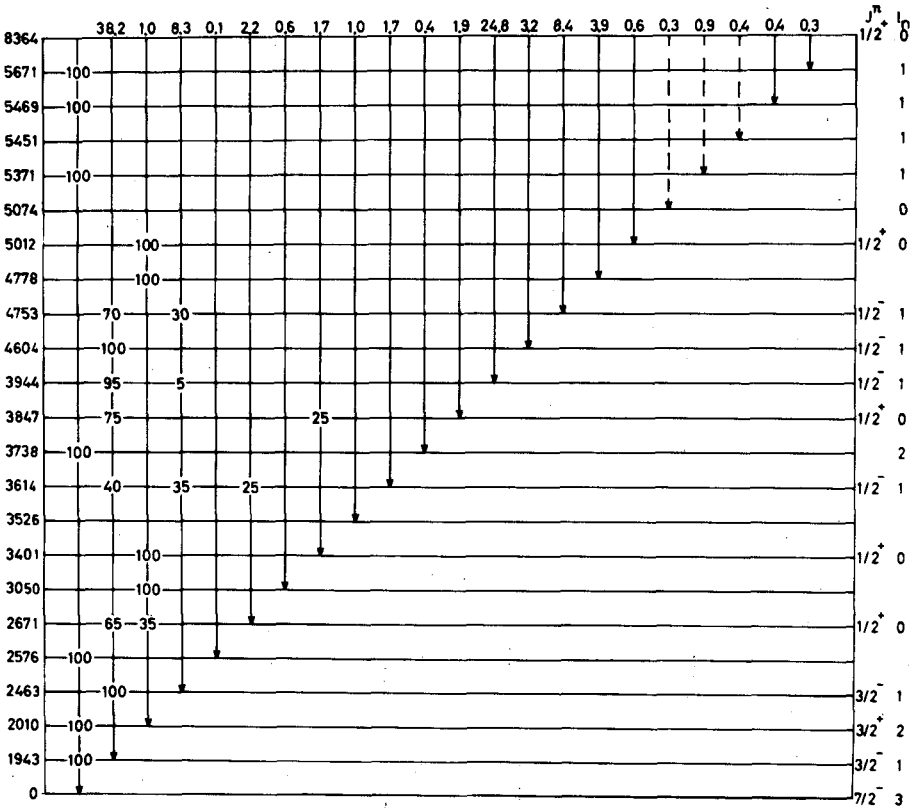


FIG.2. Decay scheme of ^{41}Ca . The low gamma energy branching is taken from ref.(12).

Table III. Excitation energies of ^{41}Ca levels and intensity balance

E_x (keV)	Intensity in/ Intensity out	E_x (keV)	Intensity in/ Intensity out
0	93.4/-	3847.0 \pm 1.5	1.9/2.1
1942.7 \pm 1.0	86.5/81.0	3944.1 \pm 1.0	24.8/18.5
2010.0 \pm 1.5	6.4/10.5	4604.0 \pm 1.5	3.2/6.3
2462.8 \pm 1.0	12.0/13.4	4753.0 \pm 1.0	8.4/7.7
2576.0 \pm 1.5	0.1/1.0	4778.0 \pm 1.5	3.9/1.7
2670.6 \pm 1.0	2.7/2.9	5011.8 \pm 1.5	0.6/0.4
3050.1 \pm 1.0	0.6/0.3	5074.3 \pm 2.0	0.3/-
3401.2 \pm 1.0	2.2/2.2	5371.0 \pm 2.0	0.4/0.1
3526.3 \pm 1.5	1.0/-	5451.3 \pm 2.0	0.4/-
3614.4 \pm 1.0	1.7/2.9	5468.5 \pm 1.5	0.4/0.1
3738.3 \pm 2.0	0.4/0.5	5670.5 \pm 1.5	0.3/0.2

The absolute intensity values for $E_\gamma < 1904.0$ keV are taken from ref. (12).

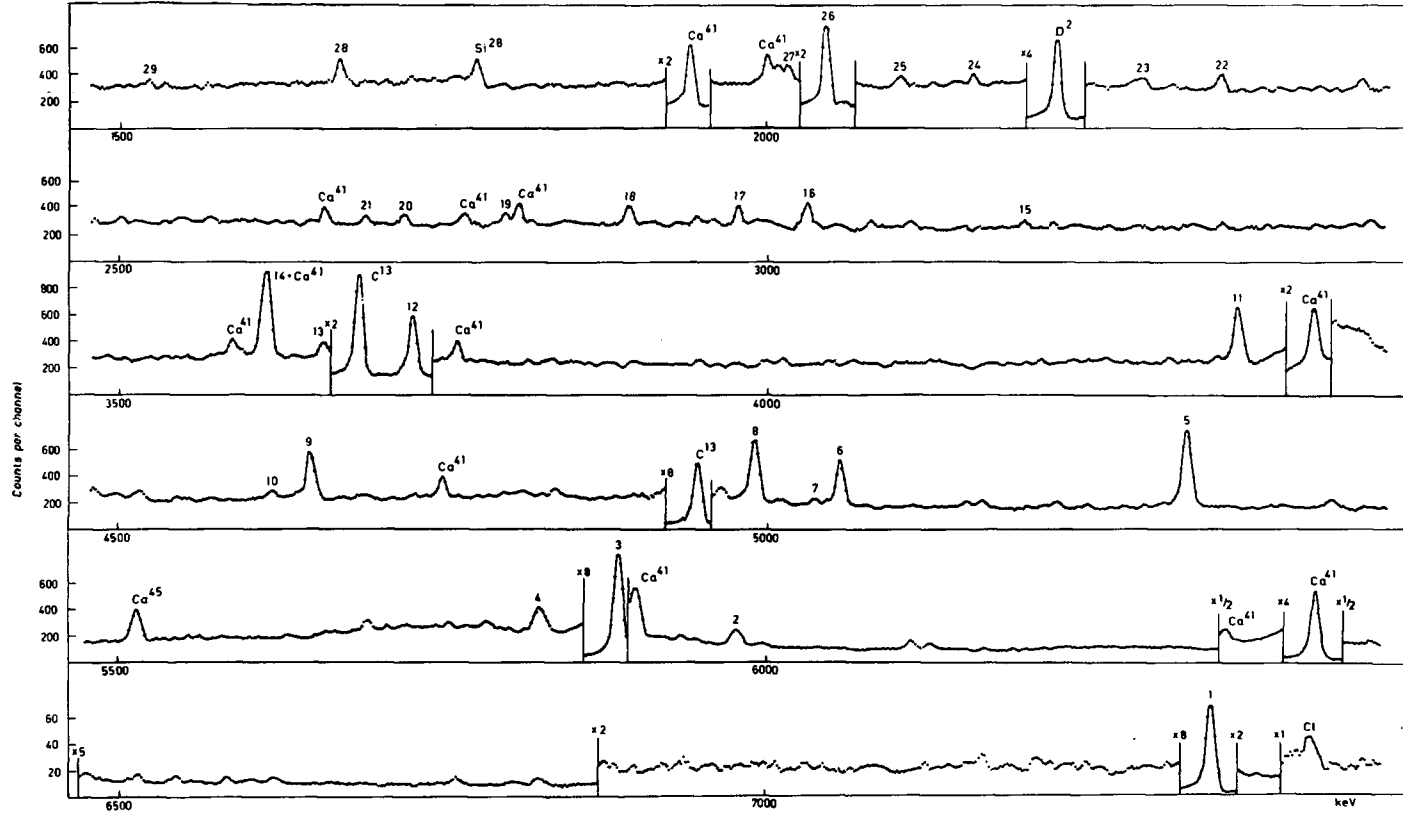


FIG.3. Three-crystal Ge(Li) pair spectrum following thermal neutron capture in ^{42}Ca . Accumulation time 43 h.

4. The $^{42}\text{Ca}(n,\gamma)^{43}\text{Ca}$ reaction

Gamma rays from thermal neutron capture in enriched ^{42}Ca are quoted in Endt and van der Leun (2) and in Nuclear Data (3)². The last reference also gives a decay scheme with some fifteen gamma lines.

The gamma ray pair spectrum is shown in Fig. 3 and the anticoincidence spectrum in Fig. 4. Besides the contaminations mentioned in sec. 2, some Cd peaks are visible in the low energy spectrum. As can be seen in Table I the main contributing calcium isotopes in the spectra besides ^{42}Ca are ^{40}Ca and ^{43}Ca . The energies and the absolute intensities of the gamma lines are listed in Table IV, where also the most probable interpretations based on energy differences between the ^{43}Ca levels are given. The decay scheme is shown in Fig. 5. The experimental Q-value 7932.9 ± 1.0 keV which can be compared to the value 7927.6 ± 3.9 keV from mass data (2). In Table V the energy values of the ^{43}Ca levels excited in the (n, γ) work are given. The excitation energies from the (d,p) work (15) differ in a systematic way from those found in the (n, γ) work, the former being generally too low. The differences between the excitation energies from the (n, γ) and (d,p) work are plotted in Fig. 6. The intensity balance for each level is also given in Table V. It is probable that the balance is affected by the reduced detection efficiency in the anticoincidence spectrum due to the high background in the low energy region. Weak gamma lines of low energy are consequently not detected.

The decay scheme shown in Nuclear Data (3) shows a cascade from the 2046 keV level through a level at 1676 ± 2 keV (16) to the ground state. The probable spin values of the 1676 keV level are $3/2^-$, $5/2^-$ or $7/2^-$ (16). The 373 keV line is, according to this interpretation, a close double line partly deexciting the 2046 keV level and partly the 373 keV level. Considering, however, the energy value of the 1676 keV level compared to the energy value of the deexciting gamma line, 1672.4 keV, this interpretation has not been adopted here. There is some evidence from the pair spectrum that the 5826 keV line is double. The high energy part of the line could then excite the 2103 keV level which deexcites directly to the ground state.

5. The $^{43}\text{Ca}(n,\gamma)^{44}\text{Ca}$ reaction

Cranston et al. (17) have observed forty gamma rays from thermal neutron capture in enriched ^{43}Ca , only sixteen of these have been fitted into the ^{44}Ca level scheme (2,3). Our gamma ray pair spectrum is shown in Fig. 7 and the anticoincidence spectrum in Fig. 8. Compared to the relatively simple spectra following capture in the even calcium isotopes, capture in ^{43}Ca gives rise to a complicated spectrum as can be seen by the large number of gamma transitions. The gamma energy values and the absolute intensity values are given in Table VI. The absolute intensity values are not obtained from the primary transitions in the usual way by normalizing their sum to 100, as the decay is too complicated to allow such a procedure to be used. Instead the 6421 keV (38 %) and 1943 keV (81 %) peaks in the $^{40}\text{Ca}(n,\gamma)^{41}\text{Ca}$ reaction are used in combination with the atomic percentage of ^{40}Ca and ^{43}Ca as well as their cross sections to give the absolute intensities of the nearby 6480 keV and 1887 keV lines in ^{44}Ca . This method, however, has the drawback that

² Note added in print. See also H. Gruppelaar, Nucl. Phys., to be published.

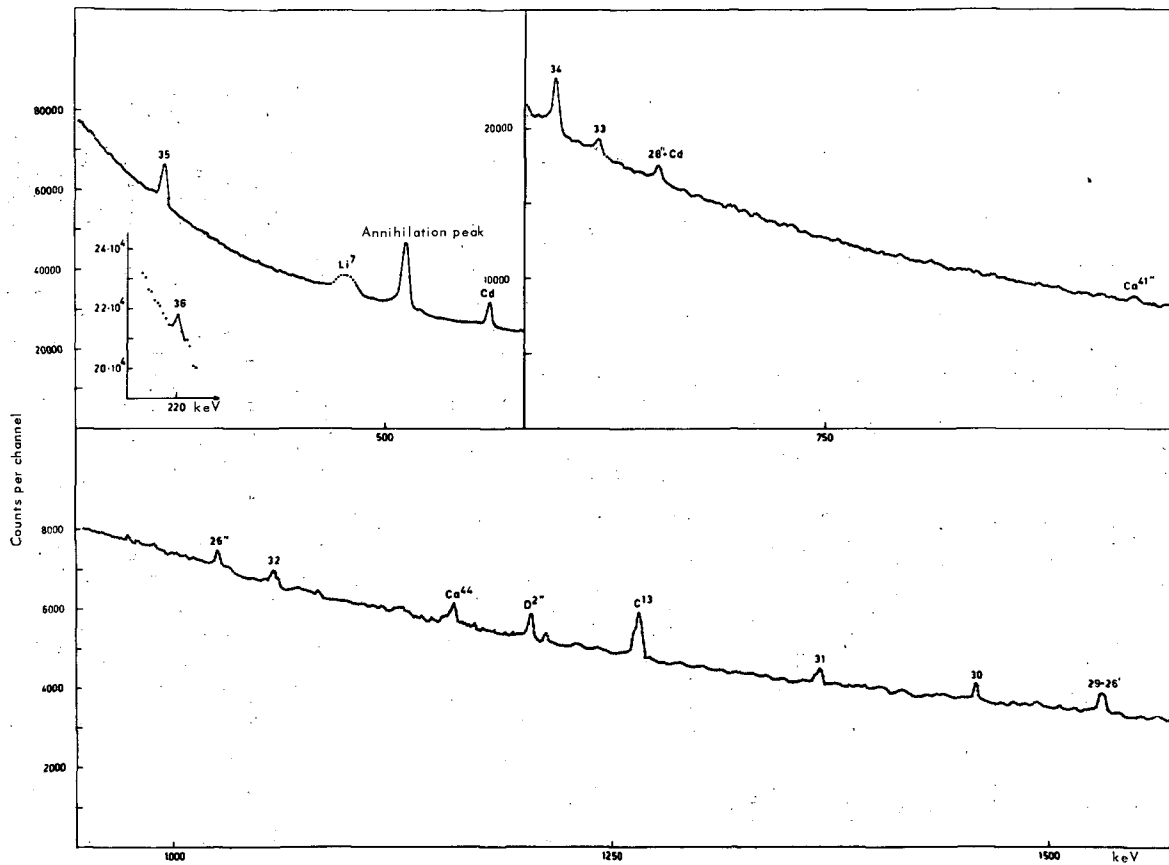


FIG. 4. Anticoincidence spectrum of gamma radiation from neutron capture in ^{42}Ca . Accumulation time 16 h. Double-escape peaks are labelled with double primes.

Table IV. Thermal neutron capture gamma rays from the $^{42}\text{Ca}(n,\gamma)^{43}\text{Ca}$ reaction

No.	E_γ (keV) (corrected for recoil)	I_γ (photons/100 captures)	Assignment	No.	E_γ (keV) (corrected for recoil)	I_γ (photons/100 captures)	Assignment	
1	7340.3±1.0	7.6	C- 594	19	2800.9	1.0	1.4	4902-2103
2	5976.8±1.5	1.0	C-1958	20	2722.5	1.0	1.2	3315- 594
3	5886.6±1.0	55.0	C-2046	21	2692.8	1.0	0.7	3286- 594
4	5826.2±1.0 ^x	1.5	(C-2107)	22	2351.0	1.0	2.6	2943- 594
5	5321.6±1.0	6.2	C-2611	23	2286.0	1.0	2.4	2878- 594
6	5054.9±1.0	2.5	C-2878	24	2159.1	1.0	2.0	4207-2046
7	5036.0±2.0	0.3	5037-0	25	2103.2	1.0	3.7	2103- 0
8	4989.5±1.0	4.0	C-2943	26	2046.0	1.0	45.0	2046- 0
9	4647.4±1.0	3.4	C-3286	27	2018.0	1.0	4.9	2611- 594
10	4617.9±1.0	0.5	C-3315	28	1672.4	1.0	15.0	2046- 373
11	4361.4±1.0	4.1	C-3572	29	1525.0	1.0	1.8 ^{xx}	3572-2046
12	3725.7±1.0	9.7	C-4207	30	1453.0	1.0	6.0	2046- 594
13	3655.9±1.0	0.8	C-4277	31	1364.7±1.0		3.0	1958- 594
14	3612.1±1.0	4.3	4207- 594	32	1055.0±1.0		4.0	2046- 991
15	3199.4±1.0	0.6	3572- 373	33	617.5±1.0		6.8	991- 373
16	3030.1 1.5	1.5	C-4902	34	593.5	0.5	25.0	594- 0
17	2979.1 1.0	1.7	3572- 594	35	373.1	0.5	33.0	373- 0
18	2895.7 1.0	2.3	C-5037	36	221.0	0.5	10.0	594- 373

^x There is some possibility that this line is double with the energy values 5824.5 keV and 5830.1 keV.

^{xx} Part of the intensity of the 1525 keV line may be due to the $^{42}\text{Ca}(n,n'\gamma)$ reaction.

the thermal neutron cross section of ^{40}Ca is not known exactly. The value 0.22 b (10) is certainly too low, as essentially all of the thermal neutron absorption in natural calcium occurs in ^{40}Ca (probably more than 90 %). Lacking a more reliable cross section for ^{40}Ca we used the value 0.44 b (10) for natural calcium. The procedure is dependent on the ratio of the $^{40}\text{Ca}/^{43}\text{Ca}$ cross sections, which adds some uncertainty to the quoted intensities. It seems to us as the intensities of the transitions come out too low as the ratio $\sum_i E_i I_{\gamma i} / 100 B$ ($B=11131$ keV) is only 0.6 and the sum of the primary transitions in the decay scheme (Fig. 9) is 35.5 %. The last figure probably also means that many more of the high energy gamma transitions go to excited states of ^{44}Ca .

The energy values of the excited states are quoted in Table VII. Up to an excitation energy of 3923 keV energy levels can be identified with those found from (d,p) and (t,p) measurements (18,19) although the deviations between the (n, γ) and (d,p) energies of the excited states are large. At higher energy a one-to-one correspondence between levels excited in the (n, γ) and (d,p) reactions is not possible to obtain. However, it seems that the levels with high values of the 2 p strength ($l_n=1$) in the (d,p) reaction also are excited with good intensity in the (n, γ) reaction, the (d,p) excitation energy being about 10 keV higher than the (n, γ) excitation energy. As an example the highest values obtained by Bjerregaard and Hansen (18) for the 2p spectroscopic strength in $^{43}\text{Ca}(d,p)^{44}\text{Ca}$ reaction are 0.75 to a level at 5743 keV and 0.54 to a level at 5243 keV. The highest intensity

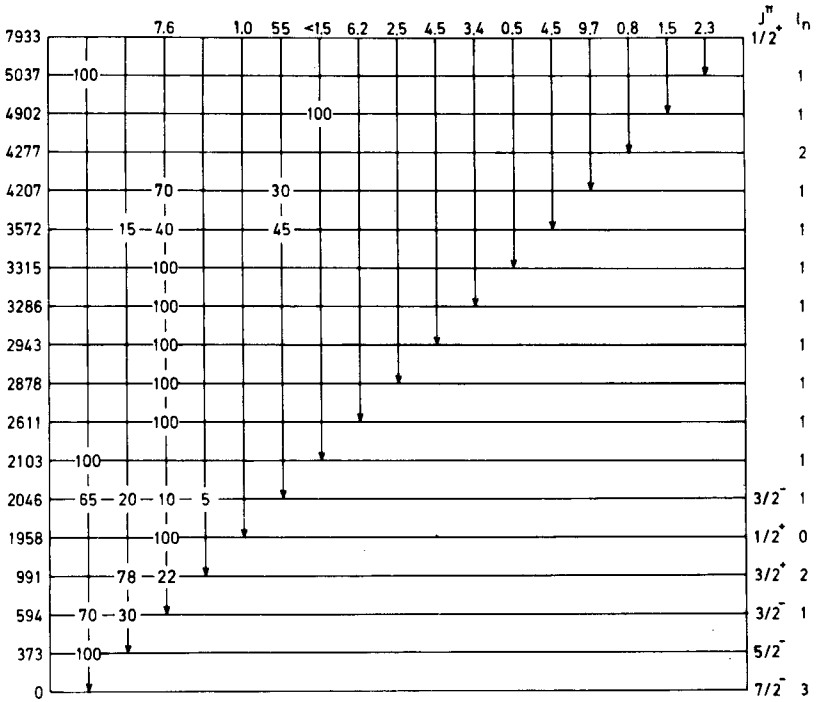


FIG.5. Decay scheme of ^{43}Ca . The percentage of the de-excitation of the 991-keV level is from ref.(16).

Table V. Excitation energies of ^{43}Ca levels and intensity balance

E_x (keV)	Intensity in/ Intensity out	E_x (keV)	Intensity in/ Intensity out
0	108/-	2943.4±1.0	4/2.6
373.1±0.5	33/33	3285.5±1.0	3.4/0.7
593.5±0.5	34/36	3315.0±1.0	0.5/1.2
990.6±0.5	4.0/6.8	3571.5±1.0	4.1/4.1
1958.2±1.0	1.0/3.0	4207.2±1.0	9.7/6.3
2046.0±1.0	59/70	4277.0±1.0	0.8/-
2103.2±1.0	≤ 2.9/3.7	4901.5±1.0	1.5/1.4
2611.3±1.0	6.2/4.9	5037.2±1.0	2.3/0.3
2878.0±1.0	2.5/2.4		

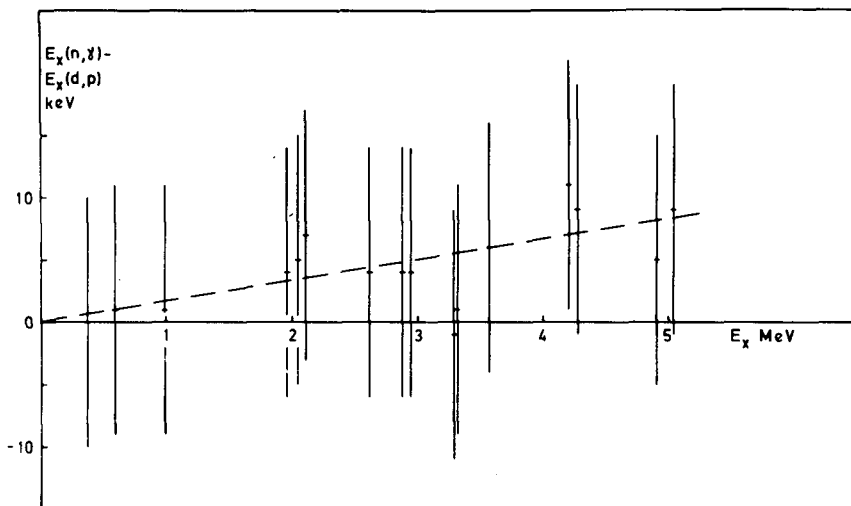


FIG. 6. The differences between the excitation energies of ^{43}Ca from the (n, γ) and (d, p) works plotted as function of E_x .

values of the transitions in the $^{43}\text{Ca}(n, \gamma)^{44}\text{Ca}$ reaction to excited states in ^{44}Ca are 3% to a level at 5734 keV and 4.7% to a level at 5232 keV. The correlation diagram shown in Fig. 9 supports this correspondence. In addition to transitions of the type just mentioned also some other gamma lines of high energy and reasonable intensity have been assumed being primary transitions. The Q-value determination gives 11131.3 ± 0.5 keV, which value can be compared to 11135 ± 5 keV quoted in Endt and van der Leun (2).

The capturing state in ^{44}Ca has a spin and parity of 3^- and 4^- and dipole transitions from the capturing state cover a wide range of spin and parity values of the excited states of ^{44}Ca . The majority of the transitions seem to go through the first excited 2^+ state at 1157 keV. (See the decay scheme in Fig. 10.) A few spin and parity assignments have been made for the low lying states of ^{44}Ca (2, 19-22).

Gamma radiation following the β -decay of ^{44}K has given information of gamma branching from some low lying levels of ^{44}Ca (23). For the 2656 keV level excited both in the (n, γ) -reaction and in the β -decay the branching figures agree satisfactorily but not for the 3307 keV level. Some of the lines involved in the decay of the latter level may, however, be close double lines in the (n, γ) -work. (See Table VI.)

In the energy region around 3.30 MeV the β -decay of ^{44}mSc has established a level at 3287 ± 2 keV with a tentative 6^+ assignment (21, 22). The β -decay of ^{44}K excites two levels at 3307 ± 2 keV and 3297 ± 3 keV (23). Particle reactions (18) give a 3^- state at 3302 ± 10 keV and a state at 3296 ± 10 keV with a tentative 6^+ assignment. In the present work three energy levels are found in the 3.30 MeV region. One level at 3306.3 ± 2.0 keV which we identify as the 3^- state, one level at 3301.7 ± 1.0 keV which is supposed to deexcite directly to the ground state indicating a low spin value of this level which also is supported by the direct transition from the capturing state to this level. The third level at 3283.7 ± 1.5 keV is found by adding the 1001.6 keV line to the 2282.1

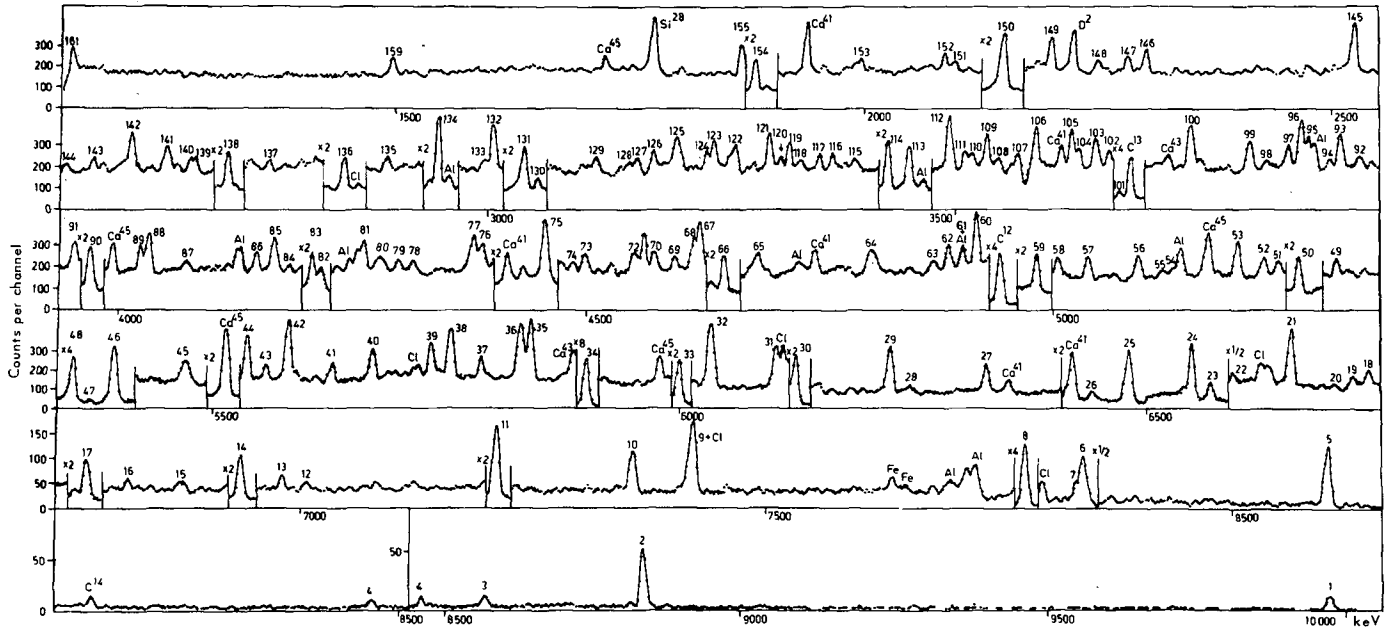


FIG. 7. Three-crystal Ge(Li) pair spectrum following thermal neutron capture in ⁴³Ca. Accumulation time 45 h.

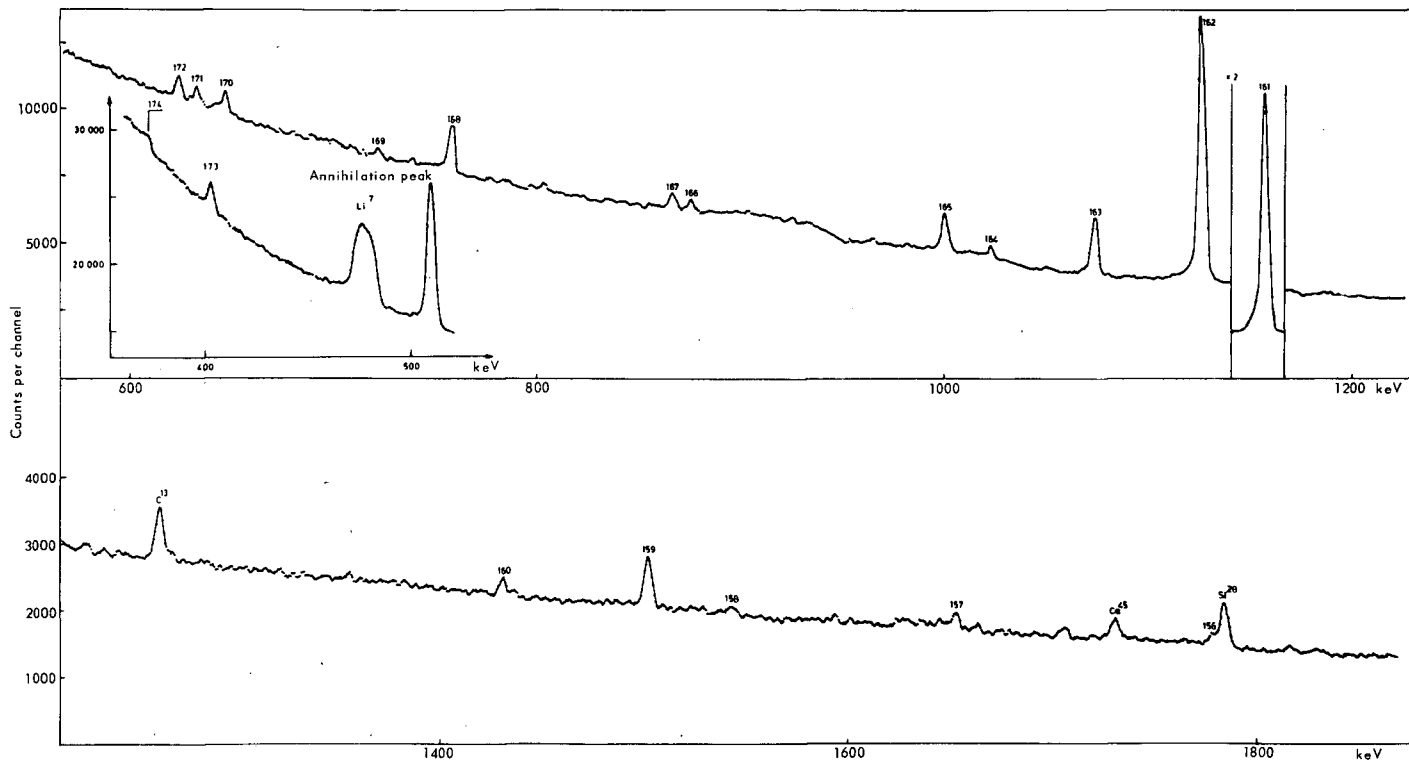


FIG.8. Anticoincidence spectrum of gamma radiation from neutron capture in ^{43}Ca . Accumulation time 24 h.

Table VI. Thermal neutron capture gamma rays from the $^{43}\text{Ca}(n,\gamma)^{44}\text{Ca}$ reaction

No.	E_γ (keV) (corrected for recoil)	I_γ (pho- tons/100 captures)	Tentative assignment	No.	E_γ (keV) (corrected for recoil)	I_γ (pho- tons/100 captures)	Tentative assignment
1	9973.0±1.0	0.2	C-1157	51	5238.0±1.5	0.3	
2	8849.2±1.0	0.1	C-2282	52	5227.0±1.5	0.3	
3	8580.5±1.0	0.07		53	5197.8±1.0	0.5	
4	8475.2±1.0	0.07	C-2656	54	5131.0±2.0	0.4	5131-0
5	8086.4±1.0	0.8	C-3045	55	5118.0±2.0	0.3	
6	7829.6±1.0	0.8	C-3302	56	5094.0±1.5	0.3	C-6037
7	7825.0±2.0	0.3	C-3306	57	5040.0±1.5	0.4	
8	7773.5±1.0	3.3	C-3358	58	5007.0±1.5	0.4	5007-0
9	7419.2±1.5	0.4	C-3712	59	4985.0±1.5	1.0	C-6146
10	7354.4±1.0	0.3	C-3777	60	4919.6±1.0	0.9	
11	7208.2±1.0	1.0	C-3923	61	4906.0±1.5	0.2	4906-0
12	7005.5±1.5	0.06		62	4891.0±1.5	0.4	
13	6978.4±1.5	0.07		63	4876.3±2.0	0.4	
14	6935.3±1.0	0.6	C-4196	64	4808.9±2.0	0.7	
15	6873.0±2.0	0.09		65	4692.0±2.0	0.4	4691-0
16	6816.0±1.0	0.06		66	4651.5±1.5	0.8	4651-0
17	6772.4±1.0	0.6	C-4359	67	4626.8±1.5	0.5	
18	6760.0±1.5	0.06		68	4619.0±1.5	0.4	5776-1157
19	6731.0±1.5	0.2	C-4400	69	4599.0±1.5	0.2	
20	6715.0±1.5	0.06		70	4577.0±1.5	0.4	5734-1157
21	6651.3±1.0	0.4	C-4480	71	4566.0±1.5	0.4	4565-0
22	6588.5±1.5	0.04		72	4554.0±2.0	0.3	
23	6566.0±1.0	0.4	C-4565	73	4502.0±2.0	0.2	
24	6546.4±1.0	1.7	C-4585	74	4488.0±2.0	0.1	
25	6480.0±1.0	1.8	C-4651	75	4458.0±1.0	2.0	
26	6440.1±1.5	0.3	C-4691	76	4392.0±1.5	0.6	
27	6327.0±1.5	0.6	C-4804	77	4383.0±1.5	0.7	
28	6247.0±1.5	0.09		78	4316.0±1.5	0.1	
29	6225.7±1.0	0.7	C-4906	79	4303.0±1.5	0.1	5459-1157
30	6124.6±1.0	2.4	C-5007	80	4283.2±2.0	0.3	
31	6100.0±1.5	0.6		81	4264.6±1.5	0.4	6146-1884
32	6034.4±1.0	1.1		82	4218.8±1.5	0.7	5375-1157
33	6000.5±1.0	2.6	C-5131	83	4209.7±1.5	0.9	
34	5900.6±1.0	4.7	C-5232	84	4186.9±2.0	0.09	
35	5842.0±1.0	1.0	C-5289	85	4168.7±1.5	0.5	5342-1157
36	5831.0±1.5	0.8		86	4151.0±1.5	0.3	6037-1884
37	5789.0±1.5	0.2	C-5342	87	4074.0±2.0	0.1	5232-1157
38	5756.0±1.0	0.7	C-5375	88	4034.1±1.5	0.6	
39	5734.8±1.0	0.4	5734-0	89	4026.4±1.5	0.4	
40	5672.5±1.5	0.4	C-5459	90	3973.8±1.0	1.4	5131-1157
41	5626.0±1.5	0.2		91	3958.0±1.5	0.5	
42	5578.3±1.0	0.8	C-5553	92	3924.0±1.5	0.2	3923-0
43	5559.1±1.5	0.1		93	3903.8±1.0	0.3	
44	5536.0±1.5	0.6		94	3891.0±1.5	0.3	5776-1884
45	5472.0±1.5	0.3		95	3870.3±2.0	0.2	
46	5397.5±1.0	3.0	C-5734	96	3863.0±1.5	0.7	6146-2282
47	5376.0±1.5	0.04	5375-0	97	3849.3±1.5	0.4	5007-1157
48	5355.0±1.0	2.8	C-5776				5734-1884
49	5301.0±1.5	0.3		98	3828.0±1.5	0.07	
50	5263.5±1.0	1.0	C-5868	99	3810.0±1.5	0.4	

No.	E_{γ} (keV) (corrected for recoil)	I_{γ} (pho- tons/100 captures)	Tentative assignment	No.	E_{γ} (keV) (corrected for recoil)	I_{γ} (pho- tons/100 captures)	Tentative assignment
100	3747.5±1.5	0.8	4906-1157	141	2657.0±1.0	0.8	2656-0
101	3673.9±1.5	0.7		142	2619.0±1.5	1.1	3777-1157
102	3662.2±1.5	0.3		143	2579.3±1.5	0.6	
103	3648.0±1.5	0.7	4804-1157	144	2551.0±2.0	0.3	
104	3626.0±2.0	0.5		145	2519.0±1.0	1.2	4400-1884
105	3622.4±1.5	0.6		146	2299.0±1.5	0.7	5342-3044
106	3584.5±1.5	0.8		147	2281.5±1.0	0.8	4565-2282 (2282-0)
107	3565.1±1.5	0.2					
108	3544.0±2.0	0.1					
109	3533.8±1.5	0.7	4691-1157	148	2249.0±2.0	0.6	4906-2656
110	3516.6±2.0	0.3					5553-3302
111	3508.0±1.5	0.4					5553-3306
112	3493.1±1.0	0.8	4651-1157	149	2200.1±1.0	1.2	4480-2282
			5375-1884				3358-1157
			5776-2282	150	2150.4±1.0	5.5	3306-1157
			5734-2282				4804-2656
113	3450.2±1.0	1.8	4585-1157	151	2100.0±1.5	0.3	5459-3358
114	3427.4±1.0	1.7		152	2088.1±1.5	0.6	5131-3045
115	3391.0±2.0	0.2		153	2000.0±2.0	1.1	5776-3777
116	3368.0±1.5	0.2		154	1887.0±0.5	3.7	3045-1157
117	3355.0±1.5	0.4		155	1872.3±1.0	1.9	5232-3358
118	3334.0±2.0	0.1		156	1772.8±1.0	0.6	5131-3358
119	3323.2±1.5	0.5	4480-1157	157	1648.7±1.0	1.0	4691-3045
120	3313.0±2.0	0.1					5007-3358
121	3302.0±1.5	0.8	3302-0				4196-2656
122	3265.4±2.0	0.7		158	1540.4±1.5	0.4	4585-3045
123	3242.0±1.5	0.7	4400-1157				2656-1157
124	3234.0±2.0	0.4		159	1499.5±1.0	3.3	3712-2282
125	3202.0±1.5	0.8	4359-1157	160	1428.9±1.0	1.0	1157-0
126	3176.5±1.5	0.5	5459-2282	161	1157.0±0.5	70	2282-1157
127	3159.0±2.0	0.3		162	1125.9±0.5	40	3358-2282
128	3150.3±2.0	0.4		163	1074.1±0.5	8.0	3306-2282
129	3116.2±2.0	0.3		164	1024.1±1.0	0.6	3284-2282
130	3052.3±1.5	0.4		165	1001.6±0.5	4.5	3923-3045
131	3038.3±1.0	1.6	4196-1157	166	878.0±1.0	1.0	5776-4906
132	3006.3±1.5	0.9	5289-2282	167	869.0±1.0	1.5	3045-2282
133	2998.0±2.0	0.3		168	761.5±0.5	4.7	1884-1157
134	2946.7±1.0	3.6		169	726.8±1.0	0.7	3306-2656
135	2892.4±1.5	0.3		170	651.3±0.5	1.7	5131-4480
136	2846.4±1.0	1.3	5131-2282				5342-4691
			6146-3302				5868-5232
137	2766.0±1.5	0.4	3923-1157	171	637.4±1.5	1.5	5289-4651
			4651-1884				3923-3284
138	2722.9±1.0	2.1	5007-2282				3284-2656
139	2687.0±1.5	0.4	5342-2656	172	629.0±0.5	1.6	3712-3306
			5734-3045	173	404.5±1.0	1.8	4804-4400
			4565-1884				2656-2282
140	2682.0±1.5	0.3	6037-3358	174	373.6±1.0	0.4	

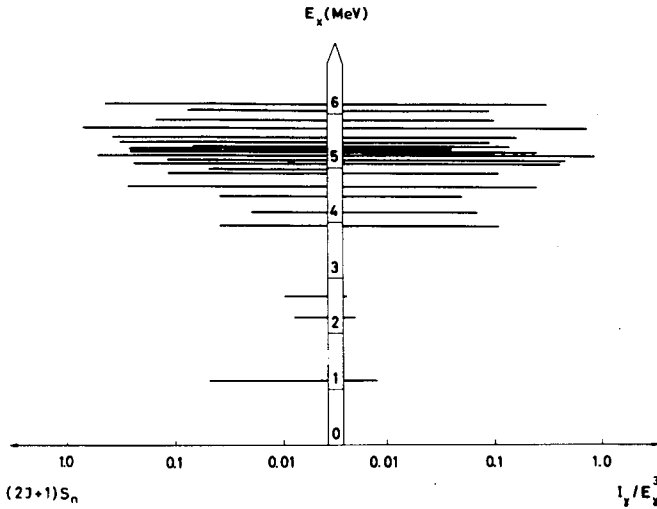


FIG.9. Comparison of reduced E1 probability with the 2p spectroscopic strength for ^{44}Ca .

Table VII. Excitation energies of ^{44}Ca levels

No.	E_x (keV)	No.	E_x (keV)	No.	E_x (keV)
1	1157.0±0.5	13	4196.0±1.0	25	5231.7±1.0
2	1883.8±1.0	14	4358.9±1.0	26	5289.3±1.0
3	2282.1±1.0	15	4400.3±1.5	27	5342.3±1.0
4	2656.1±1.0	16	4480.0±1.0	28	5375.3±1.0
5	3044.9±1.0	17	4565.3±1.0	29	5458.8±1.5
6	3283.7±1.5	18	4584.9±1.0	30	5553.0±1.0
7	3301.7±1.0	19	4651.3±1.0	31	5733.8±1.0
8	3306.3±2.0	20	4691.2±1.5	32	5776.3±1.0
9	3357.8±1.0	21	4804.3±1.5	33	5867.8±1.0
10	3712.1±1.5	22	4905.6±1.0	34	6037.3±1.5
11	3776.9±1.0	23	5006.7±1.0	35	6146.3±1.5
12	3923.1±1.0	24	5131.0±1.0		

keV level assuming that the 1001.6 keV line represents the 1002 keV transition found in the decay of ^{44m}Sc . As the energy values of Bjerregaard and Hansen (18) generally are 5-10 keV too high their 3296 keV level probably is the same as our 3284 keV level. Our 3302 keV level may be the same as the 3297 ± 3 keV level from the decay of ^{44m}K which is deexcited by a 643 ± 2 keV line not found with certainty in this work. There is, however, a low energy tail at the 651 keV line in our spectrum which could give a line at 646.7 ± 1.0 keV ($I_\gamma \approx 0.5\%$). The unresolved peaks look somewhat as the same peaks in the β -decay. If this interpretation is chosen it is astonishing that no 3302 keV line ($I_\gamma = 0.8\%$) is observed in the β -decay. No other assignment has been found for this line in the present work.

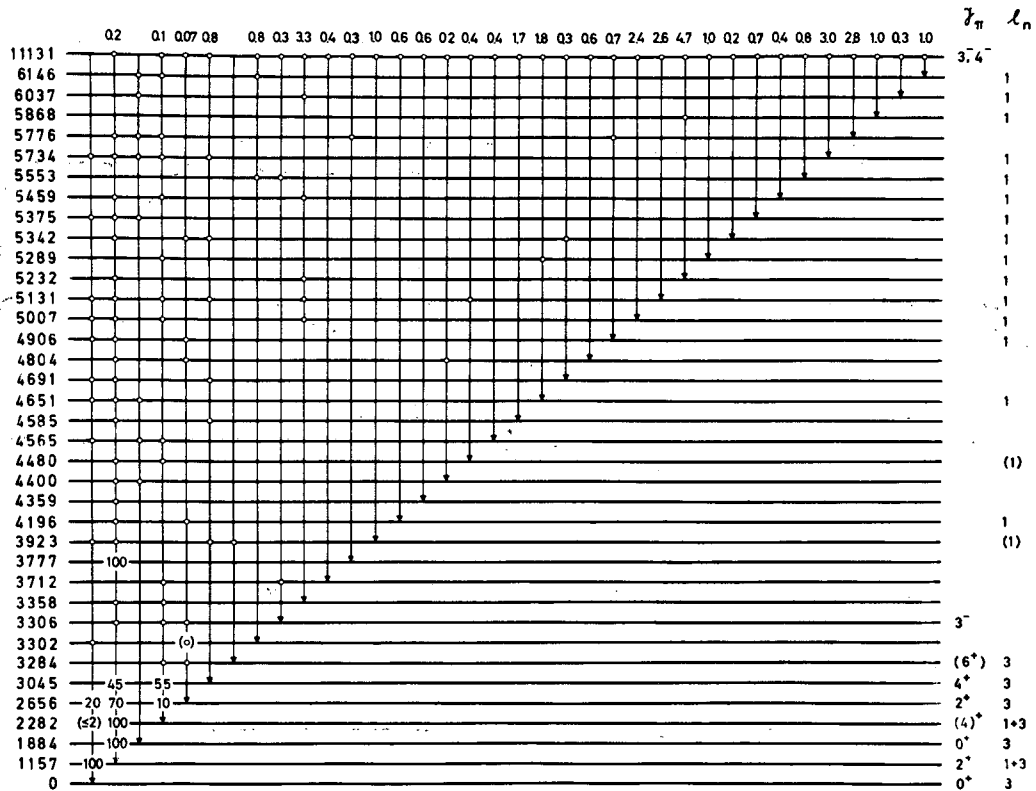


FIG.10. Tentative decay scheme of ^{44}Ca . The decay scheme shows alternative positions of gamma lines fitted as transitions between levels on the basis of energy considerations.

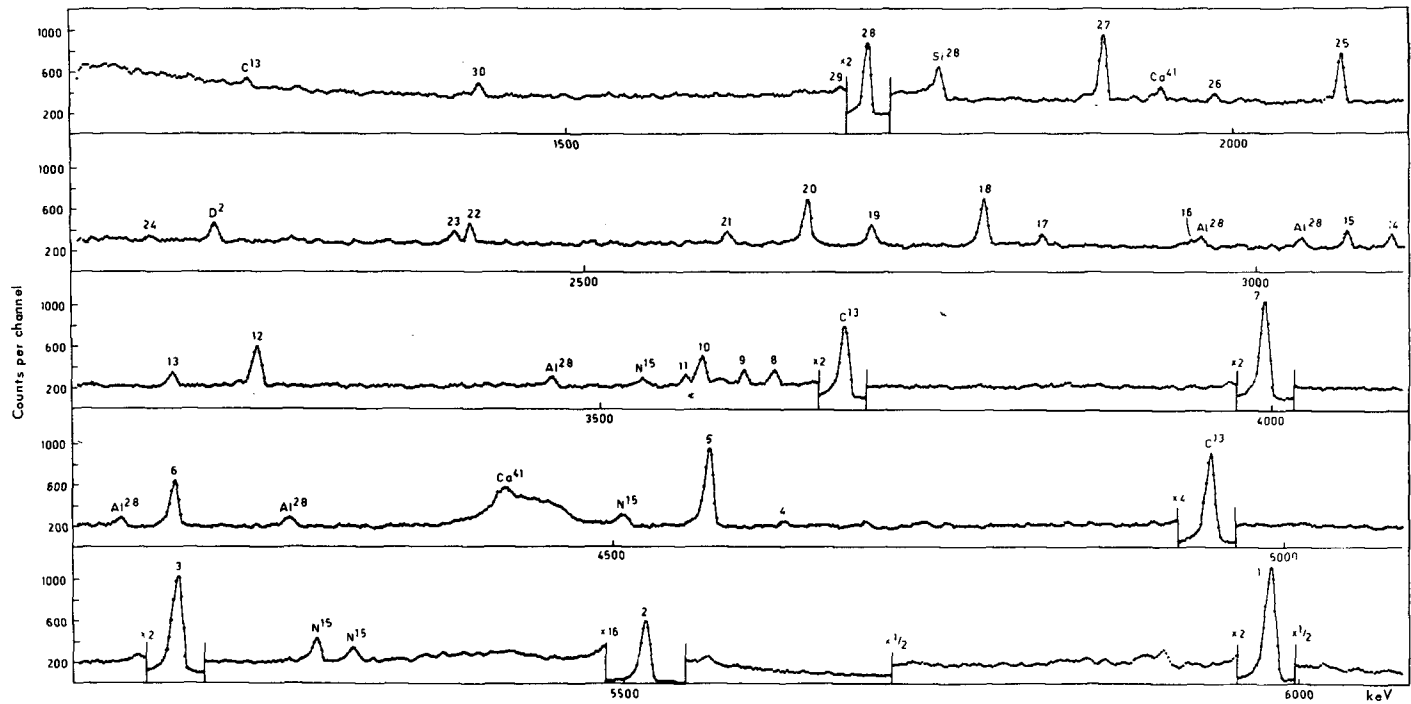


FIG. 11. Three-crystal Ge(Li) pair spectrum following thermal neutron capture in ^{44}Ca . Accumulation time 44 h.

6. The $^{44}\text{Ca}(n,\gamma)^{45}\text{Ca}$ reaction

Gamma rays from thermal neutron capture in enriched isotopes of ^{44}Ca have recently been thoroughly studied by Gruppelaar et al. (4). In order to get a comparison with their results a Ge(Li)-pair spectrum was taken. The spectrum is shown in Fig. 11. A contamination with nitrogen is seen in the spectrum besides those quoted in section 2. The nitrogen contamination was first thought to be caused by a leak in the vacuum system but later measurements made it probable that the sample contains some nitrogen compound. The gamma ray energy values and the absolute intensities of the ^{45}Ca lines in the pair spectrum are given in Table VIII. The table also includes comparison with the results of ref. 4. The general agreement is good as well as the Q-value determination, 7415.3±1.0 keV which can be compared to the

Table VIII. Thermal neutron capture gamma rays from the $^{44}\text{Ca}(n,\gamma)^{45}\text{Ca}$ reaction measured with Ge(Li) pair spectrometer

Present work with Ge(Li) pair spectrometer				Gruppelaar et al. (4)	
No.	E_γ (keV) (corrected for recoil)	I_γ (photons/100 captures)	Assignment (when differ- ring from that of ref.(4))	E_γ (keV)	I_γ
1	5980.6±1.0	11		5980.3±1.0	10.7
2	5515.5±1.0	50		5515.1±1.0	54.5
3	5166.2±1.0	9.6		5165.5±0.8	9.7
4	4630.0±2.0	0.2		4630.3±1.0	1.0
5	4573.1±1.0	3.8		4572.5±0.8	4.1
6	4173.4±1.0	2.4		4173.0±0.8	2.4
				4121.6±1.0	0.3
7	3996.3±1.0	11		3996.0±0.5	10.2
8	3630.9±1.0	0.8		3631.5±0.5	1.0
9	3609.0±1.0	0.4		3608.5±0.5	0.7
10	3576.8±1.0	1.8		3576.8±0.4	1.3
11	3566.1±1.5	0.7		3565.0±1.5	0.3
12	3243.6±1.0	2.6		3243.7±0.6	2.5
13	3181.1±1.0	1.0		3180.8±0.6	1.0
14	3101.1±1.0	1.6	C-4314		
15	3068.1±1.0	0.9		3067.6±0.6	1.1
16	2947.0±3.0	0.2		2947.1±1.0	0.3
17	2842.1±1.0	1.5		2841.6±0.8	0.7
18	2799.1±1.0	3.7		2799.3±0.4	3.4
19	2715.7±1.0	1.9		2716.1±0.4	1.4
20	2667.9±1.0	4.7		2668.1±0.3	3.3
21	2607.1±1.0	1.1	C-4808	2608.3±1.5	1.1
22	2415.9±1.0	1.5		2415.4±0.5	2.2
23	2404.1±1.0	0.8		2403.6±1.0	0.7
				2287.5±0.6	0.9
24	2176.0±2.0	0.8		2178.5±3.0	0.2
25	2074.9±1.0	8.1		2075.5±0.4	7.9
26	1983.0±1.0	1.9		1983.6±2.0	1.0
				1942.0±4.0	1.0
27	1900.1±1.0	12		1900.0±0.3	11.8
				1751.1±0.3	0.2
28	1725.7±1.0	40		1725.8±0.3	43.5
29	1710.0±2.0	1.0		1710.2±2.0	1.1
30	1434.8±1.0	9.8		1434.72±0.10	8.8

value 7414.7 ± 1.0 keV of Gruppelaar et al. (4). In a few cases, where the complex response function of the detector used by Gruppelaar et al. (4) made it uncertain whether a peak has full energy or double escape character, these ambiguities could be resolved. No feeding from the capturing state to the first $l_n=0$ level at 1884 keV was observed.

7. The $^{48}\text{Ca}(n,\gamma)^{49}\text{Ca}$ reaction

Measurements with NaI crystals of the gamma rays from thermal neutron capture in calcium enriched in ^{48}Ca are reported by Raboy and Trail (24). In the gamma decay a ground state transition and a cascade through the first excited state at 2022 keV were observed.

The gamma ray pair spectrum is shown in Fig. 12. Two gamma lines with the energies 4071.1 ± 0.5 keV (rel. int. 100) and 3084.3 ± 0.5 keV (rel. int. 8.9) from the 8.8 min. decay of ^{49}Ca to ^{49}Sc are also present in the spectra besides the background lines mentioned in section 2. The energies and absolute intensities of the few gamma lines attributed to the $^{48}\text{Ca}(n,\gamma)^{49}\text{Ca}$ reaction are listed in Table IX. The experimental Q-value is 5146.6 ± 1.0 keV and is in good agreement with the Q-value 5144 ± 6 keV obtained from particle reactions (25). The decay scheme of ^{49}Ca is shown in Fig. 13.

Table IX. Thermal neutron gamma rays from the $^{48}\text{Ca}(n,\gamma)^{49}\text{Ca}$ reaction

No.	E_γ (keV) (corrected for recoil)	I_γ (photons/100 captures)	Assignment
1	5146.7 1.0	75	C-0
2	3123.1 1.0	25	C-2023
3	2023.2 0.3	25	2023-0

8. Discussion

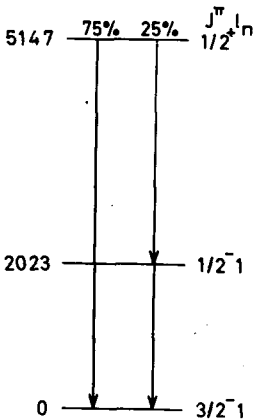
A common feature of the neutron capture in the calcium isotopes studied in this investigation is strong transitions to 2p states. In the odd calcium isotopes about half of the primary intensity from the capturing state is to a single $2p_{3/2}$ state, in the even calcium isotope studied the strongest primary transitions go to 2p levels at an excitation energy around 5 MeV.

It has previously been shown by Gruppelaar et al. (4) that a good correlation exists between the relative (n,γ) transition strengths I_γ/E_γ^3 and the (d,p) strengths $(2J+1)S_n$ for the same final states for two of the calcium isotopes. The correlation can be expressed with the coefficient

$$\rho = \frac{\sum_i (x_i - \bar{x})(y_i - \bar{y})}{\left[\sum_i (x_i - \bar{x})^2 \sum_i (y_i - \bar{y})^2 \right]^{1/2}}$$

FIG. 13. Decay scheme of ^{49}Ca .

where x_i and y_i are the (n,γ) and (d,p) strengths for the i th level.



The correlation coefficients $\rho = 0.59$ and 0.91 were found for ^{41}Ca and ^{45}Ca respectively (4). Our values for the same reactions are $\rho = 0.61$ and 0.89 in good agreement. The correlation for ^{43}Ca is shown in Fig. 14 and the correlation coefficient is found to be $\rho = 0.91$. The good correlation especially for ^{43}Ca and ^{45}Ca indicates that direct capture is of importance for these reactions.

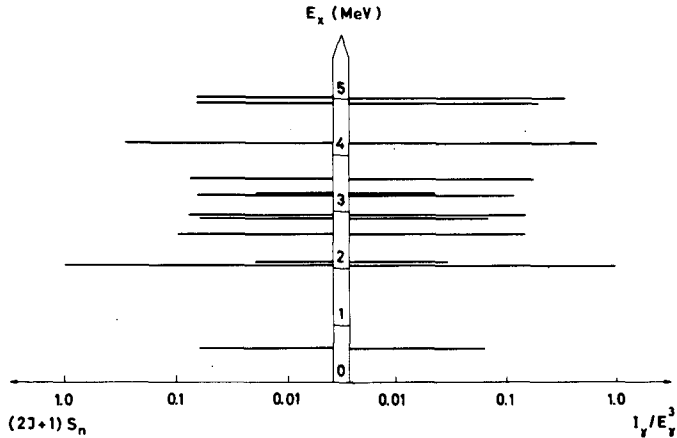


FIG.14. Comparison of the reduced E1 probability I_γ/E^3 from the (n, γ) reaction with the (d, p) reduced widths $(2J+1)S_n$ for levels in ^{43}Ca .

Acknowledgements

It is a pleasure to thank Ing. N. Berglund and the reactor staff of the reactor R1, Stockholm, for good collaboration and Fil. kand N.G. Alenius and L. Olsson for help with the publication of this work.

References

1. S.E. Arnell, R. Hardell, A. Hasselgren, L. Jonsson and Ö. Skeppstedt, Nucl. Instr. and Meth. 54 (1967) 165.
2. P.M. Endt and C. Van der Leun, Nuclear Physics A 105 (1967) 1.
3. Nuclear Data, Vol. 3, Numbers 4-6 (1967) 367.
4. H. Gruppelaar, P. Spilling and A.M.J. Spits, Nucl. Phys. A 114 (1968) 463.
5. Ö. Skeppstedt, R. Hardell and S.E. Arnell, Arkiv Fysik 35 (1968) 527.
6. L. Jonsson and R. Hardell, see elsewhere in the proceedings.
7. R.C. Greenwood, private communication.
8. W.V. Prestwick, T.J. Kennet, L.B. Hughes and Y. Fiedler, Can. J. Phys. 43 (1965) 2086.
9. F.P. Cranston, P.B. Snow and D.H. White, Bull Am. Phys. Soc. 11 (1966) 909.
10. D.J. Hughes and R.B. Schwartz, BNL Rep. 325 (1956) 6.

11. S. Boreving and E. Falkström, Thermal neutron capture in natural calcium, Report LF-22, Studsvik, Nyköping (1968).
12. H. Gruppelaar and P. Spilling, Nucl. Phys. A 102 (1967) 226.
13. T.A. Belote, A. Sperduto and W.W. Buechner, Phys. Rev. 139 (1965) B80.
14. C.M. Braams, thesis University of Utrecht, 1956 (unpublished).
15. W.E. Dorenbusch, T.A. Belote and O. Hansen, Phys. Rev. 146 (1966) 734.
16. C. Chasman, K.W. Jones and R.A. Ristinen, Phys. Rev. 169 (1968) 911.
17. F.P. Cranston, R.E. Birkett, D.H. White, Bull Am. Phys. Soc. 11, No. 3 (1966) 335.
18. J.H. Bjerregaard and O. Hansen, Phys. Rev. 155 (1967) 1229.
19. J.H. Bjerregaard, O. Hansen, O. Nathan, R. Chapman, S. Hinds and R. Middleton, Nucl. Phys. A 103 (1967) 33.
20. E.P. Lippincott and A.M. Bernstein, Phys. Rev. 163 (1967) 1170.
21. J.D. King, N. Neff and H.W. Taylor, Can. J. Phys. 45 (1967) 2446.
22. J.D. King, B. Lalovic and H.W. Taylor, Can. J. Phys. 46 (1968) 2119.
23. H.W. Taylor, J.D. King, H. Ing and R.J. Cox, Nucl. Phys. A 125 (1969) 358.
24. S. Raboy and C.C. Trail, Intern. Conf. Nucl. Phys. with Reactor Neutrons, Argonne Nat. Lab. Paper III - 7 (October 1963); ANL - 6797, p. 243 (1963).
25. A. Rytz, Nucl. Phys. 70 (1965) 369.

GAMMA-GAMMA ANGULAR-CORRELATION MEASUREMENTS IN THE $^{44}\text{Ca}(n, \gamma)^{45}\text{Ca}$ REACTION *

(Abstract only)

H. GRUPPELAAR, A. M. F. OP DEN KAMP, A. M. J. SPITS
Physics Laboratory,
Rijksuniversiteit,
Utrecht, The Netherlands

Abstract

GAMMA-GAMMA ANGULAR-CORRELATION MEASUREMENTS IN THE $^{44}\text{Ca}(n, \gamma)^{45}\text{Ca}$ REACTION.
Angular-correlation measurements of gamma radiation following thermal neutron capture in ^{44}Ca have been performed with a combination of Ge(Li) and NaI detectors. The following spin assignments of levels in ^{45}Ca were derived: $J^\pi(0.17) = (5/2, 7/2^+)$, $J^\pi(1.44) = 3/2^-$, $J^\pi(1.90) = 3/2^-$ and $J^\pi(2.25) = 1/2^-, (3/2)^-$. Some E2/M1 mixing ratios of transitions between bound states of ^{45}Ca have been determined.

* This paper has already been published in full in Nuclear Physics under the same title.

THE LEVEL SCHEME OF ^{48}Ti AND ^{49}Ti AS STUDIED BY THE NEUTRON CAPTURE GAMMA-RAY SPECTRA *

(Abstract only)

P. FETTWEIS, M. SAIDANE **
SCK-CEN,
Mol, Belgium

Abstract

THE LEVEL SCHEME OF ^{48}Ti AND ^{49}Ti AS STUDIED BY THE NEUTRON CAPTURE GAMMA-RAY SPECTRA. Using an enriched ^{47}Ti target and a natural titanium target, the neutron capture gamma-ray spectrum following the $^{47}\text{Ti}(n,\gamma)^{48}\text{Ti}$ reaction has been studied by straight spectroscopy using Ge(Li) detectors; a level scheme of ^{48}Ti has been established. Valuable information on the neutron capture gamma-ray spectrum following the $^{48}\text{Ti}(n,\gamma)^{49}\text{Ti}$ reaction and on the ^{49}Ti level scheme has also been extracted from the experimental data. The neutron-binding energies of ^{48}Ti and ^{49}Ti are found to be 11627.6 ± 1.3 keV and 8143.3 ± 1.2 keV, respectively.

* The full text of this paper has been accepted for publication in Nuclear Physics.

** OCD bursary, on leave from CEA, Tunis.

CIRCULAR POLARIZATION OF GAMMA RADIATION FOLLOWING CAPTURE OF POLARIZED THERMAL NEUTRONS IN ^{59}Co

F. STECHER-RASMUSSEN, J. KOPECKÝ*, K. ABRAHAMS
Reactor Centrum Nederland,
Petten, the Netherlands

Abstract

CIRCULAR POLARIZATION OF GAMMA RADIATION FOLLOWING CAPTURE OF POLARIZED THERMAL NEUTRONS IN ^{59}Co . The circular polarization of gamma radiation after capture of polarized thermal neutrons in ^{59}Co was studied with a Ge(Li) spectrometer. The results are in general agreement with previous measurements. The levels at 505 and 785 keV are discussed in some detail.

Some spin assignments of levels excited by the $^{59}\text{Co}(n, \gamma)^{60}\text{Co}$ reaction have been made recently [1, 2, 3]. In Refs [1] and [2] measurements of the circular polarization P_γ of gamma radiation following capture of polarized thermal neutrons are given, while Ref.[3] treats the measurement of the angular distribution after capture of unpolarized neutrons in aligned target nuclei. Although the conclusions of these papers are in general consistent with each other, one ambiguity remains: the 785-keV level in ^{60}Co is shown to have $J^\pi = 4^+$ by means of the alignment method, while the circular polarization method yields $J^\pi = 5^+$. The suggestion was made by Mellema et al.[3] that this could possibly be explained by an E1(M2) admixture in the primary capture gamma radiation to this level.

To check this suggestion the circular polarization was remeasured with an improved mirror system, allowing a data accumulation rate which was 27 times faster than that of the system described in Ref.[1]. The details of the experimental method and the assumptions made in the analysis are as described in Refs [1, 2]. The degree of neutron polarization P_n in the present experiment was about 90%.

Figure 1 shows the relevant part of the decay scheme of ^{60}Co , while Table I shows the new R values measured by means of the circular polarization method. These R values were obtained from the difference spectrum and single spectrum shown in Fig.2. The way in which R, defined by $P_\gamma = R P_n \cos \theta$, depends on the spin of the final state and on the mixing percentage of $J_0 = 4^-$ in the capturing state is given in Fig.3, together with the experimental R-values taken from Table I. It was assumed that all transitions were pure dipole transitions. Any inconsistency in spins assigned by this method might lead to the necessity of a quadrupole admixture.

The data given above are consistent with previous R values except maybe the primary transition to the 505-keV level which was in the

*On leave from Nuclear Research Institute, Prague.

previous measurements of Refs [1, 2] not properly corrected for the influence of the 6485' and the 5976-keV lines.

It should be noted that for the primary transition to the 785-keV level a pure $4^- \rightarrow 5^+$ E1 character is indeed improbable. So one should either accept a $4^- \rightarrow 4^+$ case with a multipole M2 admixture of at least 5% or assign a spin 3^+ to the 785-keV level with the pure E1 transition being mainly fed by the 3^- component in the capturing state (see Fig.2). This last conclusion is in disagreement with the measurements of Prestwich and Coté [5] and Wasson et al.[6] which showed that the 132-eV resonance, $J^\pi = 4^-$, contributes strongly to this transition.

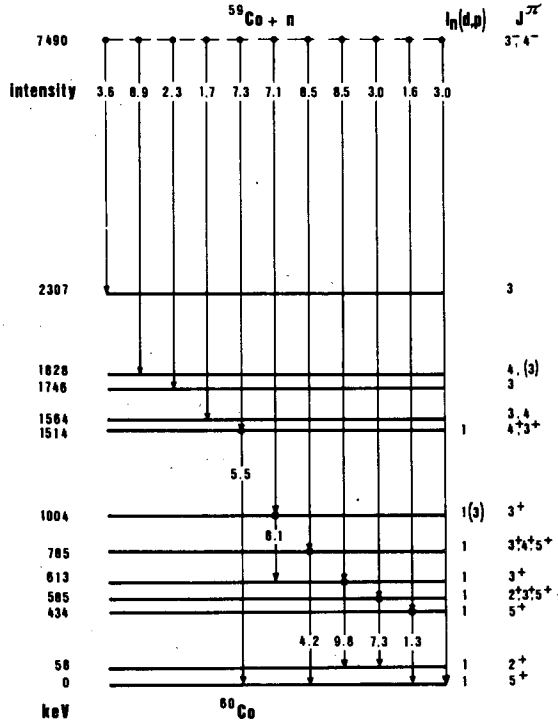


FIG.1. Simplified decay scheme of ^{60}Co .

Finally the R-value belonging to the primary transition to the 505-keV level seems somehow puzzling. It would easily lead to the conclusion that $J^\pi(505 \text{ keV})$ is 5^+ or, if the transition is mainly fed by the 3^- component of the capturing state, that J^π may be 3^+ or 2^+ . The first conclusion is improbable because the strong transition to the 58-keV 2^+ level would have M3 character. The last two conclusions are again in contradiction to the previously mentioned resonance (n, γ) measurements. Also in this case therefore an E1(M2) admixture in the primary transition may not be excluded.

TABLE I. $^{59}\text{Co}(n, \gamma)^{60}\text{Co}$ RESULTS

E_γ (keV)	Interpretation	Circular polarization		Nuclear orientation [3]	Present work $R_{\text{exp.}}$	J^π	Conclusion ^a
		[1]	[2]				
7489	C → 0		$2^+, 5^+$		-0.57 ± 0.09	$2^+, 5^+$	5^+
7213	C → 276			4^+	} $+0.82 \pm 0.05$		
7201	C → 288			3^+			
7055	C → 434		$2^+, 5^+, (3^+, 4^+)$	$3^+, 4^+, 5^+, (2^+)$	-0.97 ± 0.27	$2^+, 5^+$	5^+
6984	C → 505	$(2)^+, 3^+, 4^+, (5)^+$	$3^+, 4^+$	$2^+, 3^+$	-0.45 ± 0.18	$2^+, 3^+, 5^+$	$2^+, 3^+, 5^+?$
6876	C → 613	$3^+, (4)^+$	$3^+, 4^+$	$3^+, (2)^+$	$+0.80 \pm 0.04$	3^+	3^+
6705	C → 785	$2^+, 5^+$	$(2^+, 5^+)$	4^+	-0.20 ± 0.04	3^+	$3^+, 4^+, 5^+?$
6486	C → 1004	$(2)^+, 3^+, 4^+, (5)^+$	$3^+, 4^+$	$3^+, 4^+$	$+0.56 \pm 0.06$	$3^+, 4^+$	3^+
5976	C → 1514	$3^+, 4^+$	$3^+, 4^+$	$3^+, 4^+$	$+0.31 \pm 0.04$	$3^+, 4^+$	$4^+, 3^+$
5925	C → 1564		$3^+, 4^+, (2^+, 5^+)$		$+0.02 \pm 0.18$	$3, 4, (2, 5)$	$3, 4$
5743	C → 1746				$+1.36 \pm 0.26$	$3, (4)$	3
5662	C → 1828	$3, 4$			$+0.15 \pm 0.05$	$3, 4$	$4, (3)$
5617	C → 1873				} $+0.19 \pm 0.21$		
5605	C → 1885						
5183	C → 2307	$(2), 3, 4, (5)$			$+0.70 \pm 0.12$	$3, (4)$	3

^a If the data of Refs [4, 5, 6] are included.

) These transitions cannot be easily explained by means of pure E1 transitions from the 4^- component in the capturing state.

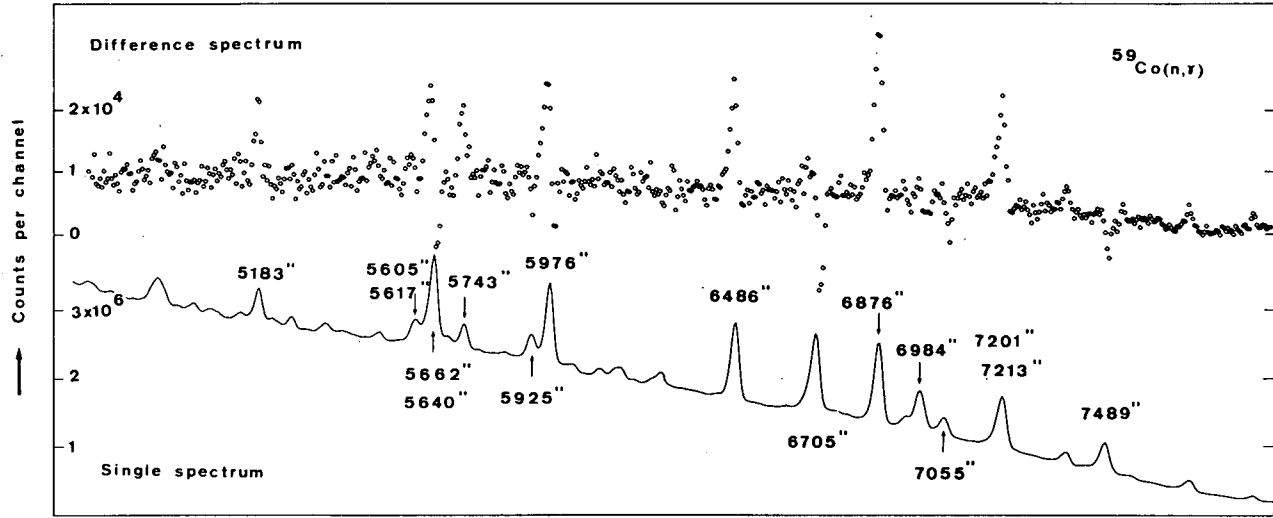


FIG. 2. Difference and single spectra of $^{59}\text{Co}(n, \gamma)$.

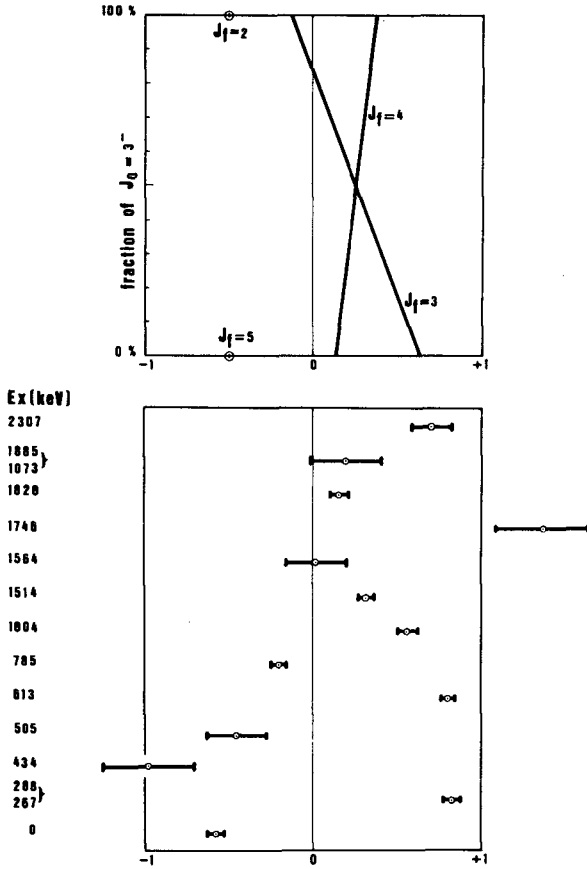


FIG. 3. The polarization function R as related to the $J_0 = 3^-$ mixing percentage and measured R -values for ^{60}Co .

REFERENCES

[1] ABRAHAMS, K., RATYNSKI W., Nucl. Phys. A124 (1969) 34.
 [2] KOPECKÝ, J., WARMING, E., Nucl. Phys. A127 (1969) 385.
 [3] MELLEMA, J., POSTMA, H., Nucl. Phys. (to be published).
 [4] SHERA, E. B., HAFEMEISTER, D. W., Phys. Rev. 150 (1966) 894.
 [5] PRESTWICH, W. V., COTÉ, R. E., Phys. Rev. 155 (1967) 1223.
 [6] WASSON, O. A., CHRIEN, R. E., BHAT, M. R., LONE, M. A., BEER, M., Phys. Rev. 176 (1968) 1314.

THERMAL NEUTRON CAPTURE GAMMA RAYS FROM ^{61}Ni

R. SAMAMA, J. GIRARD, R. BABINET,
A. AUDIAS, J. J. GARDIEN
Commissariat à l' énergie atomique,
CEN de Saclay,
91 Gif-sur- Yvette, France

Abstract

THERMAL NEUTRON CAPTURE GAMMA RAYS FROM ^{61}Ni . We have investigated the gamma rays following thermal neutron capture by ^{60}Ni with a pair and anti-Compton spectrometer using a coaxial-type Ge(Li) detector. We were especially interested in the region from 2 to 5 MeV in which we observed 15 transitions not reported previously.

The gamma-ray spectrum from the $^{60}\text{Ni}(n, \gamma)^{61}\text{Ni}$ reaction has been measured by Groshev et al.[1] with the aid of a magnetic Compton spectrometer, by Kinsey and Bartholomew [2] and by Treado and Chagnon [3]. Angular correlation measurements were made by Zamori et al.[4] and Coté et al.[5]. The (d, p), (d, t) and (d, α) reactions leading to levels in ^{61}Ni have been studied by Fulmer et al.[9], Cohen et al.[10] and Hjorth et al.[11]. Recently Vervier [12] compiled the data relative to ^{61}Ni . It appears from this compilation that below 2 MeV and above 5.5 MeV the gamma-ray energies are well known, whereas in the intermediate region not many transitions are given and their accuracy is frequently worse than 30 keV.

To investigate more thoroughly this part of the spectrum we measured gamma rays following thermal neutron capture in ^{60}Ni at the reactor EL3 in Saclay. The neutron beam used (flux = 3×10^6 n cm $^{-2}$ sec $^{-1}$) was obtained by Bragg diffraction on a lead single crystal. The target was 10 g of ^{60}Ni enriched to 99.8%. We used a pair and anti-Compton spectrometer consisting of a coaxial Ge(Li) detector surrounded by an annular crystal of NaI. Figure 1 compares part of the pair spectrum with the corresponding part of the direct spectrum. The 25-cm 3 semiconductor detector has a resolution of 4.2 keV at 1.3 MeV and 12 keV at 7 MeV. The gamma-ray spectrum from the Ge(Li) detector was stored in one of three memories according to whether the event was classified as a single, pair or anti-Compton event. This selection was done after the 4096-channel ADC. The spectra were also stabilized using two peaks in the spectrum itself. Our experimental set-up is described in Ref.[13].

The gamma energies of the $^{14}\text{N}(n, \gamma)^{15}\text{N}$ reaction given by Marion [14] enabled us to draw the correction curve for the linearity of the analysis system. The peaks in the spectra were fitted by the GRAP program¹ run on a CDC 6600 computer.

¹ This program was kindly sent to us by J. A. Harvey (Oak Ridge).

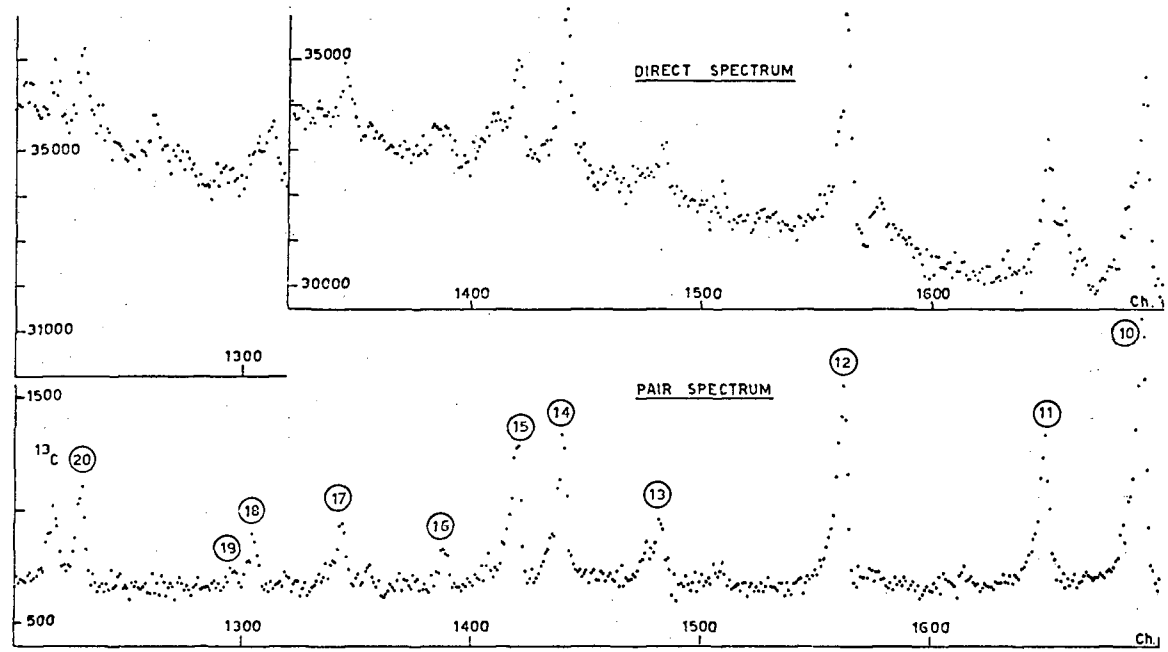


FIG. 1. Partial gamma-ray spectra from $^{60}\text{Ni}(n,\gamma)^{61}\text{Ni}$. Identification numbers correspond to those indicated in Table I.

TABLE I. HIGH-ENERGY GAMMA RAYS FROM THE $^{60}\text{Ni}(n_{\text{th}}, \gamma)^{61}\text{Ni}$ REACTION

No.	Present results E_{γ} (keV) ΔE_{γ} (keV)	L_{γ} per 100 captures	Groshev [1]	Bystrov [12]	Treado [3]
1	7819.7 \pm 1.	37.5	7814 \pm 5	7820 \pm 20	7810 \pm 20
2	7536.6 \pm 1.	22.9	7535 \pm 5	7530 \pm 20	7520 \pm 30 7180 \pm 50
3	6719.4 \pm 1.	2.4	6716 \pm 5		6720 \pm 100
4	6633.9 \pm 1.	1.2	6629	6670 \pm 30 6070 \pm 30	
5	5695.6 \pm 1.	8.4	5692 \pm 5	5690 \pm 20	5790 \pm 100 5550 \pm 50
6	5179.1 \pm 3.	0.2		5200	5280 \pm 80
7	5054.5 \pm 1.5	0.1			
8	4956.6 \pm 1.	< 0.1			
9	4756.7 \pm 2.	0.3			4700 \pm 100
10	4674.4 \pm 1.5	1.		4650 \pm 30	
11	4587.2 \pm 1.5	0.5			
12	4404.1 \pm 1.	0.7		4400 \pm 20	
13	4239.2 \pm 3.	0.3		4250 \pm 20	
14	4150.9 \pm 1.	0.4		4140 \pm 20	
15	4108.6 \pm 1.	0.4			
16	4042.1 \pm 2.	0.1			
17	3949.6 \pm 1.5	0.2			3940 \pm 100
18	3867.8 \pm 3.				
19	3847				
20	3710.3 \pm 1.5	0.3		3670 \pm 30	
21	3642.1 \pm 1.5	0.1			
22	3580.4 \pm 1.	0.1			
23	3414.6 \pm 1.	0.1		3400 \pm 30	
24	3385.5 \pm 1.	0.3			
25	3145.2 \pm 1.	0.1			3200 \pm 50
26	3132.3 \pm 1.	0.1			
27	2861.9 \pm 1.	0.1		2900	
28	2703 \pm 3.	0.1			
29	2640 \pm 3.	0.1			

TABLE II. LOW-ENERGY GAMMA RAYS FROM $^{60}\text{Ni}(n_{\text{th}}, \gamma)^{61}\text{Ni}$ REACTION

No.	Our results E γ (keV) Δ E γ (keV)	I γ per 100 captures	^{61}Cu decay			
			Bolotin [6]	Schöneberg [7]	Béraud [8]	Wapstra [12]
30	2124.0 \pm 1.	6.3	2119.8	2128.0	2124.	2122. 1977.
31	1730.6 \pm 1.	0.2	1730.2	1730.8	1729.9	1729.0
32	1686.5 \pm 1.5	<0.1				
33	1662.7 \pm 1.5	0.1	1663.2	1662.7	1662.7	1661.7
34	1661.7 \pm 1.5	0.2	1611.8	1610.6	1609.9	1609.8
35	1542.6 \pm 1.	0.2	1544.6	1542.3	1542.2	1542.7 1463
36	1446.9 \pm 1.5	0.1	1446.9	1446.6	1446.2	1446.8 1395
37	1184.7 \pm 0.3	2.7	1185.5	1186.8	1185.5	1185.7
38	1133.6 \pm 0.7	0.2	1132.4	1132.7	1132.	1132.8
39	1118.0 \pm 2.		1117.8	1116.8	1118.4	1118.0
40	1099.1 \pm 0.3	1.9	1100.2	1099.8	1100.6	1100.0
41	1073.2 \pm 0.5	0.1		1075.0	1075.4	1073.2
42	1065.1 \pm 0.5	0.2		1065.4	1064.8	1065.5
43	1031.6 \pm 0.3	3.1		1032.5	1033.0	1032.7
44	1022.1 \pm 1.	0.1				1019.
45	937.7 \pm 0.3	1.				
46	907.6 \pm 0.3	0.5	908.8	907.9	909.8	909.0 903.7
47	898.2 \pm 0.8	0.1				850
48	a		841.2	840.8	842.4	840.8
49	815.9 \pm 0.5	2.2	817.5	816.5	816.4	817.1
50	655.3 \pm 0.2	1.3	655.7	656.0	656.0	656.3 626
51	a		588.4	588.4	588.7	588.9
52	529.2 \pm 0.4	0.5	529.6	529.5	529.2	529.3
53	374.0 \pm 0.7	0.4	372.7	372.3	373.1	373.4
54	283.6 \pm 1.0		282.8	282.9	283.0	282.9
			67.3	67.7	67.4	67.35

^a Multiple peak ^{61}Ni and background.

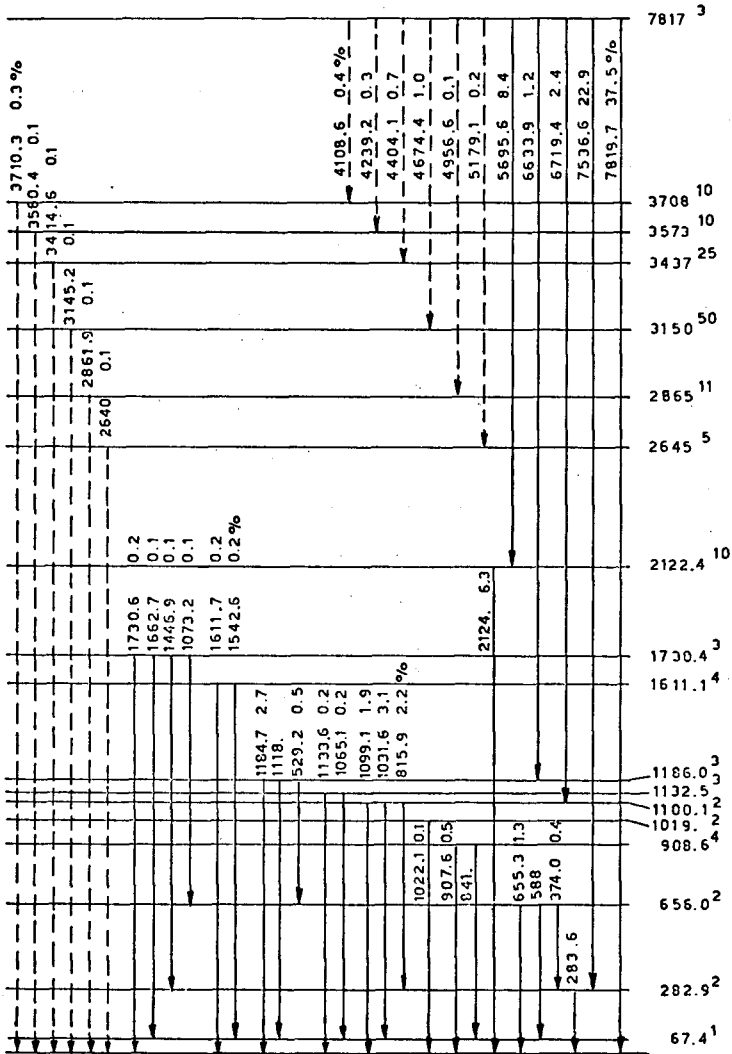


FIG. 2. Scheme of gamma transitions of ^{61}Ni . The energies mentioned for the levels are those of Ref. [12].

Energies and intensities of the gamma rays are given in Table I together with comparison with the results of other authors. Fifteen transitions have been found which have not been reported previously.

The 7.18 and 5.55-MeV lines mentioned by Treado and the 6.07-MeV line mentioned by Bystrov [12] were not observed. For the highest energies our results are in agreement with those of Groshev but consistently above them.

Table II shows our results and those obtained by Bolotin [6], Schöneberg [7], Béraud [8] and Wapstra [12] who investigated the decay of ^{61}Cu . Our energies are in good agreement with theirs.

The dashed lines indicated in the level diagram (Fig.2) are to be considered as tentative. They satisfy the Ritz combination principle and feed levels which have been identified in other nuclear reactions.

To confirm these cascades we are about to perform coincidence experiments with two Ge(Li) detectors.

REFERENCES

- [1] GROSHEV, L.V., DEMIDOV, A.M., SHADIEV, N., Sov. J. nucl. Phys. 3 (1966) 444.
- [2] KINSEY, B.B., BARTHOLOMEW, G.A., Phys. Rev. 89 (1953) 375.
- [3] TREADO, P.A., CHAGNON, P.R., Phys. Rev. 121 (1961) 1734.
- [4] ZAMORI, Z., Nucl. Phys. 52 (1964) 269.
- [5] COTÉ, R.E., JACKSON, H.E., Jr., LEE, L.L., Jr., SCHIFFER, J.P., Phys. Rev. 135 (1964) B52.
- [6] BOLOTIN, H.H., FISCHBECK, H.J., Phys. Rev. 158 (1967) 1069.
- [7] SCHÖNEBERG, R., FLAMMERSFELD, A., Z. Phys. 200 (1967) 205.
- [8] BERAUD, R. et al., Nucl. Phys. A99 (1967) 577.
- [9] FULMER, R.H., MCCARTHY, A.L., COHEN, B.L., Phys. Rev. 133 (1964) B955; FULMER, R.H., DAEHLNICK, W.W., Phys. Rev. 139 (1965) B579.
- [10] COHEN, B.L., FULMER, R.H., MCCARTHY, A.L., Phys. Rev. 126 (1962) 698.
- [11] HJORTH, S. A. et al., Ark. Fys. 33/11 (1966) 147.
- [12] VERVIER, J., Nuclear data sheets for A=61, Nuclear Data B2 5 (1968) 85-103.
- [13] GIRARD, J. et al., Colloque sur les méthodes expérimentales en physique nucléaire et physique des particules, Strasbourg, 1968, AED-CONF 1968-356.
- [14] MARION, J.B., Gamma ray calibration energies, Tech. Rep. 656 (Mar. 1968).

SHELL MODEL CONFIGURATIONS IN EVEN SPHERICAL NUCLEI

U. FANGER, R. GAETA*, W. MICHAELIS,
H. OTTMAR, H. SCHMIDT
Institut für angewandte Kernphysik,
Kernforschungszentrum Karlsruhe,
Karlsruhe, Federal Republic of Germany

Abstract

SHELL MODEL CONFIGURATIONS IN EVEN SPHERICAL NUCLEI. Latest results of thermal neutron capture gamma-ray investigations of ^{62}Ni are reported. Enriched samples of 92.11% ^{61}Ni were used as external targets at the Karlsruhe reactor FR-2. The gamma radiation has been studied with a Ge(Li) anti-Compton device, a 5-crystal Ge(Li) pair spectrometer, and both a Ge(Li)-NaI coincidence and a NaI-NaI angular correlation spectrometer coupled to an on-line computer. On the basis of these measurements a considerably extended level scheme of ^{62}Ni is proposed. Several new spins were assigned. The experimental levels and transition rates are compared with results of various shell-model calculations which reproduce the low-lying experimental ^{62}Ni states fairly well. The comparison is extended to the ^{58}Fe level scheme discussed in more detail elsewhere.

1. Introduction

The even nuclei not far away from a closed $1f7/2$ shell for neutrons and/or protons have generally been considered to be spherical and to tend to surface oscillations. Especially the nickel isotopes ^{60}Ni and ^{62}Ni have been cited by several authors [1, 2, 3] as good examples for collective quadrupole vibrations - at least with respect to the one- and two- phonon states. On the other hand, recent detailed shell-model calculations performed by Auerbach [4] and Cohen et al. [5] reproduce the low-lying energy levels of even and odd-neutron Ni isotopes quite well within about 200 keV. For nuclei with $20 \leq Z \leq 27$ and $N = 30, 32$ there exist also theoretical level schemes calculated by McGrory [6, 7] which can be compared with the results of our ^{58}Fe measurements [8]. In these papers no theoretical transition probabilities are given, whereas Cohen et al. and Auerbach have calculated some $B(E2)$ -transition rates. The prediction of transition rates is of great interest, also with respect to transition rules of vibrational models.

Experimentally the thermal neutron capture γ -ray method is a valuable tool for checking transition modes and rates up to high excitation states. The determination of level positions might be somewhat more complicated than in other reactions, but involves very precise values. The reaction $^{61}\text{Ni}(n,\gamma)^{62}\text{Ni}$ has not been studied before. The mechanism of deexcitation of ^{62}Ni states was therefore essentially unknown except for the first four levels which had been investigated by β^- decay of ^{62}Co [9, 10], β^+ decay of ^{62}Cu [11, 12], and the $(p,p'\gamma)$ reaction [13].

* Visiting scientist from Junta de Energía Nuclear, Ciudad Universitaria, Madrid, Spain.

Table I

Sample used for the $^{61}\text{Ni}(n,\gamma)^{62}\text{Ni}$ investigation

Isotope	Binding energy ^{a)} of the neutron in the product nucleus (MeV)	Capture cross section ^{b)} for thermal neutrons (b)	Ni^{nat}		^{62}Ni enriched sample	
			Content (%)	Capture contribution (%)	Content (%)	Capture contribution (%)
^{58}Ni	9.00	4.4	67.88	70	1.62	3
^{60}Ni	7.82	2.6	26.23	16	5.18	6
^{61}Ni	10.59	2.0	1.19	0.6	92.11	83.5
^{62}Ni	6.84	15	3.66	13	1.08	7.5
^{64}Ni	6.13	1.52	1.08	0.4	< 0.05	< 0.03

a) Ref. [26]

b) Ref. [14]

2. Experimental Procedure

The experimental procedure will only be mentioned briefly, as it is similar to that followed for the $^{57}\text{Fe}(n,\gamma)$ measurements and extensively described in Ref. [8].

The isotope ^{61}Ni has a thermal neutron cross section of 2 b [14] and is represented only to 1.2 % in the natural element, thus yielding a capture contribution of 0.6 % (cf. Table I). This contribution in our samples had been increased to 83.5 % by an enrichment in ^{61}Ni to 92.11 %. In spite of this relatively high enrichment care had to be taken in the isotope assignments of lines appearing in the γ -ray spectra. - The metallic powder samples in 0.5 mm thin polythene containers were used as external targets for thermalized neutrons at the Karlsruhe research reactor FR-2. The γ radiation following the capture of neutrons was detected with four devices: 1) an anti-Compton arrangement [15] with a 4.9 cm³ Ge(Li) diode for the low energy portion up to 2.8 MeV, 2) a 5-crystal pair spectrometer with a 2 mm x 2.7 cm² Ge(Li) detector [16], 3) a 34 cm³ Ge(Li)-7.6 x 7.6 cm NaI(Tl) coincidence system [17], and 4) an angular correlation spectrometer with two 10.2 x 12.7 cm NaI(Tl) crystals [18]. The latter two were coupled to an on-line computer [19]. The energy calibration is based on the decay lines of ^{57}Co [20], ^{192}Ir , ^{137}Cs , ^{88}Y , ^{60}Co [21] and capture γ -rays of the reaction $\text{H}(n,\gamma)$ [22] up to 2.8 MeV and on capture lines in ^{56}Fe [23], ^{164}Dy [24] and ^{14}N [25] in the higher energy region.

As an example for the γ -ray spectra taken with the pair spectrometer the portion from 6.4 to 8.6 MeV is shown in Fig. 1. As expected from the 16.5 % capture contribution of isotopes other than ^{61}Ni , strong lines of ^{59}Ni , ^{61}Ni and ^{63}Ni also do appear. These lines enable us to calculate absolute ^{62}Ni γ -ray intensities (per capture in ^{61}Ni) on the basis of the $\text{Ni}^{\text{nat}}(n,\gamma)$ reaction investigated by Groshev [26], if we take into account the different capture contributions in the samples. As can be seen from intensity ratios compared with the measurements of Groshev, only weak ^{62}Ni lines may be masked by γ -rays from other isotopes.

Fig. 2 represents Ge(Li) γ -ray spectra of ^{58}Fe as an example for the coincidence technique which has been applied for ^{62}Ni as well. The spectra shown are coincident with two unresolved lines at 810 keV and 864 keV in the NaI(Tl) spectrum, for which the window positions are marked in the inset. The first (upper) spectrum represents the coincidences with the full peak, the second one with the 810 keV line, the third one with the 864 keV line. The coincident background has been subtracted in all cases. The coincidences of the 810 keV and 864 keV lines could be separated by computing appropriate differences of the spectra.

As a last example for techniques of measurement and evaluation, Fig. 3 demonstrates a parametric plot of A_2 , A_4 coefficients of the angular correlation function $W(\theta) = \sum_k A_{2k} P_{2k}(\cos\theta)$ for some I - 2 - 0 spin sequences. The crosses correspond to values of measured cascades in ^{58}Fe [8], again.

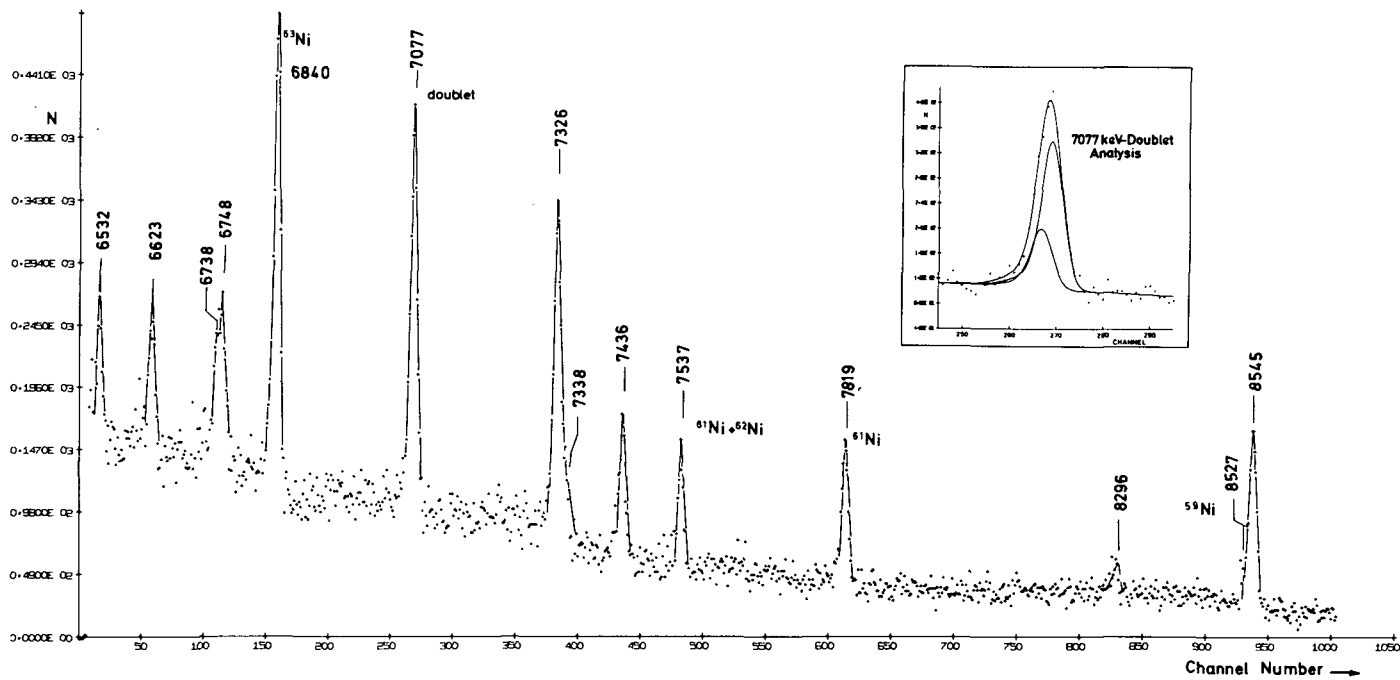


FIG.1. $^{61}\text{Ni}(n, \gamma)^{62}\text{Ni}$ portion of the pair spectrum, energy range 6.4 to 8.6 MeV.

3. Level Scheme of ^{62}Ni

The results of all our measurements on the reaction $^{61}\text{Ni}(n,\gamma)^{62}\text{Ni}$ suggest a level scheme as represented in Fig. 4. The intensities of the transitions are expressed by the line widths. Well established coincidences are indicated by full circles, probable ones by open circles. Five coincidence relations between primary and groundstate transitions have been established by the sum-coincidence technique with the sum window position at the binding energy. Only lines fitting well into the level scheme within their experimental error have been used. The energy values of transitions and levels are considered to be accurate within less than 500 eV when given to two decimal places. In spite of this precision there are two transitions - marked by asterisks - that fit the level energy differences twice in that scheme. In the case of the 968.16 keV transition this might be fortuitous; this is signified by a dashed line. But the second placement of the 1220.76 keV γ ray is postulated by coincidence relations, and both transitions should be of about the same intensity. Studying the line shape of the 1220 keV γ ray in the singles spectrum, one finds that peak wider than neighbouring peaks, but the energies of these two lines cannot differ by more than about 400 eV. - As could be seen in Fig. 1, the 7077 keV doublet can be resolved, thus revealing two primary transitions feeding the level doublet at 3520 keV. In the same spectrum there appear two lines at 7537 keV and 7819 keV which have to be assigned to ^{61}Ni . But comparing the intensity ratio to that measured by Groshev et al. [26] in natural Ni, one must conclude that the lower peak contains a weak ^{62}Ni line to a fraction of 13%. Such a transition fits excellently into the ^{62}Ni level scheme. Due to the weakness of this primary transition, the general rule that strong high-energy de-excitations from the capture level have E1 character cannot be applied. Therefore it is impossible to decide the parity of the level at 3058.63 keV. The same argument holds for the level at 4627 keV. - For a great part of levels fed by strong primary transitions, the possible spins can be restricted to $I^\pi = 0^+, 1^+, 2^+, 3^+$ due to the fact that the capture state in ^{62}Ni has $I^\pi = 1^-, 2^-$. From the de-excitations of these levels one can exclude either the spins 0^+ and 3^+ in the case of transitions to 0^+ states (e.g. to the ground state) or the spins 0^+ and 1^+ for transitions to a 4^+ state (e.g. to that known one at 2336 keV). That was the procedure for all levels designated by two spin values, except the level at 2891 keV. This state has to be discussed in more detail. First, a feeding primary transition was not found. Only one deexcitation of 1718 keV to the first 2^+ state, none to the ground or first excited 0^+ state could be observed. Therefore $I^\pi = 1^+$ doesn't seem likely, although the spin assignments $I^\pi = 0^+, 1^+, 2^+, 3^+$ for the level at 2891 keV are all compatible with the observed $l = 1$ value in the $^{61}\text{Ni}(d,p)$ reaction [27]. Our measured angular distribution of the 1718 keV - 1173 keV cascade revealing a rather strong positive anisotropy, is consistent with a $2 - 2 - 0$ spin sequence. Earlier not quite convincing investigations of the ^{62}Co decay [9] postulated a 3^+ level at 2.89 MeV which must be identified with our state at 2891 keV. Recently Mo et al. [10] repeated those measurements using Ge(Li) detectors and concluded that no 3^+ state is populated by ^{62}Co decay. The $^{61}\text{Ni}(n,\gamma)$ angular correlation analysis which is still in progress, yields unambiguous results for the strong 875 keV - 1173 keV and 2346 keV - 1173 keV cascades. Thus the spin 0^+ for the known level at 2048 keV is confirmed, and a new spin

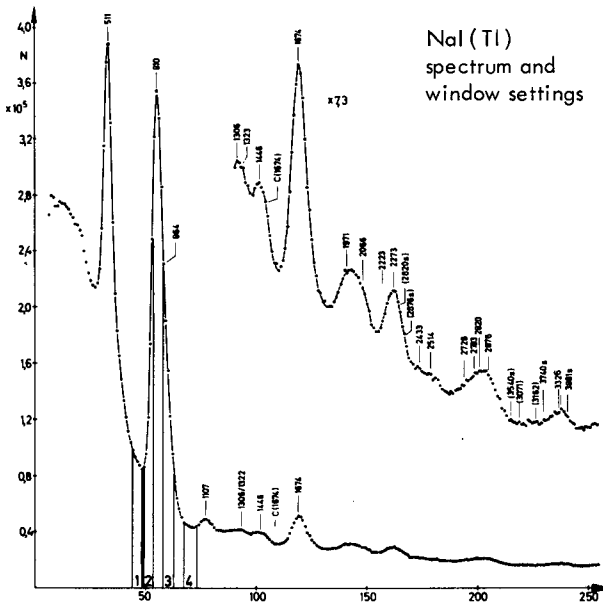


FIG. 2. Sections of the ^{58}Fe germanium spectra coincident to digital windows in the Na(I) spectrum.

assignment $I^{\pi} = 2^+$ for the state at 3519 keV has been established. Another result of a preliminary analysis in that in the unresolved 2097 keV/2084 keV - 1173 keV cascade at least a spin 0 for the level doublet 3257/70 keV can be excluded. Thus, from all 24 excited states established in this (n,γ) investigation, only six states could not be assigned spins.

If one compares the discussed (n,γ) level scheme with those found in inelastic scattering [2, 28 - 30] and stripping reactions [27, 29], as done in Fig. 5, an excellent agreement is revealed up to an excitation energy of about 4 MeV. There are significant, large level spacings from 1.2 to 2.0 MeV, from 2.3 to 2.9 MeV, and from 3.5 to 3.8 MeV (except a probably collective 3^- level at 3.7 MeV not observed in the (n,γ) reaction). For higher energies the comparison gets more difficult due to the increasing level density. In this region, of course, the (n,γ) scheme is not complete. Two levels (up to 3.5 MeV) are missing in our scheme compared with those of the (p,p') and (d,p) reactions, i.e. at 3175 keV^{*)} and 3467 keV^{*)}. Probably one has to assign spins higher than 3 to these states. Due to the $l = 3$ value measured by Fulmer and McCarthy [27] for the level at 3175 keV, the spin assignment of 4^+ , 5^+ seems to be consistent. According to the deexcitation of this level to the first 2^+ state, as observed in the decay of ^{62}Co [10], the spin 5^+ can be excluded. - For the sake of completeness it may be noted, that two additional levels at 3275 keV and 4051 keV have been proposed by

^{*)} Here the energy values of the MIT measurements [28] are cited, as they mostly agree best with our values.

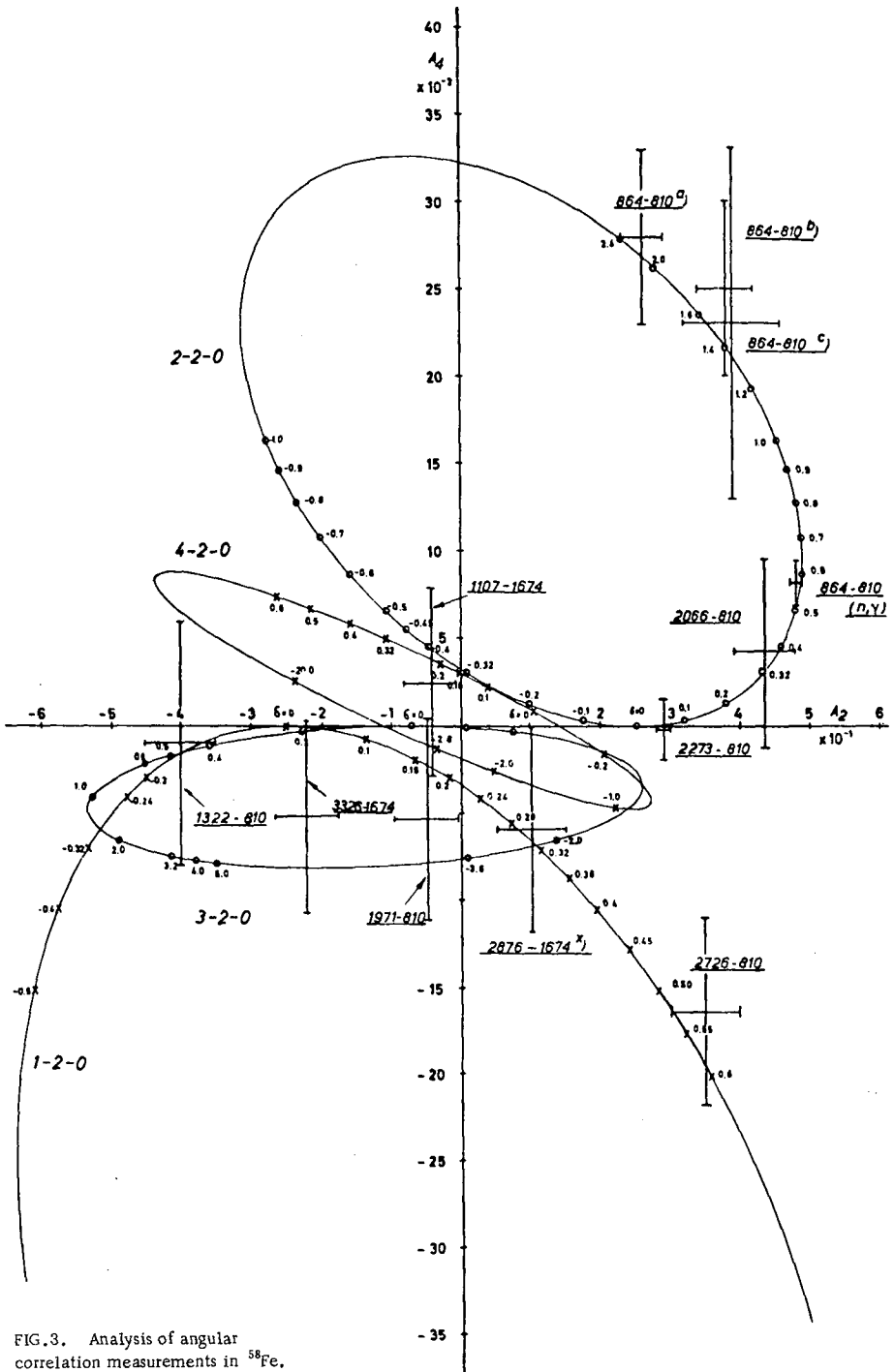


FIG.3. Analysis of angular correlation measurements in ^{58}Fe .

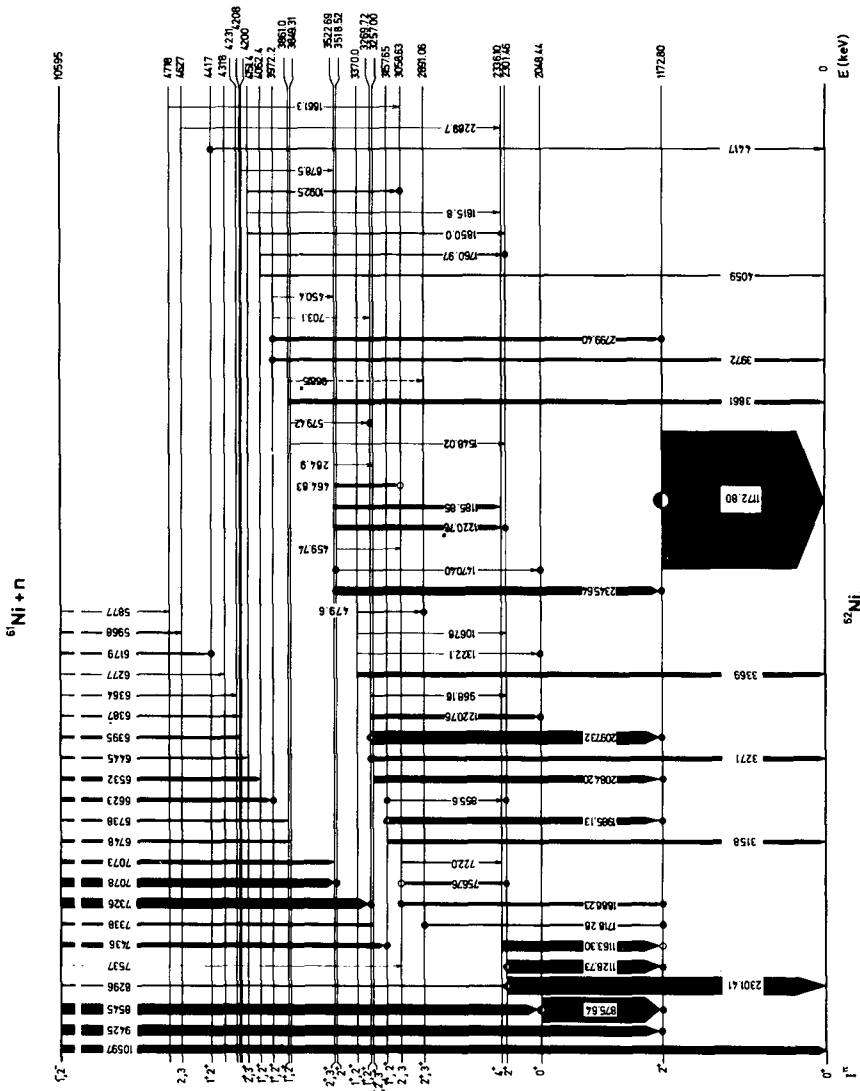


FIG. 4. Level scheme of ^{62}Ni .

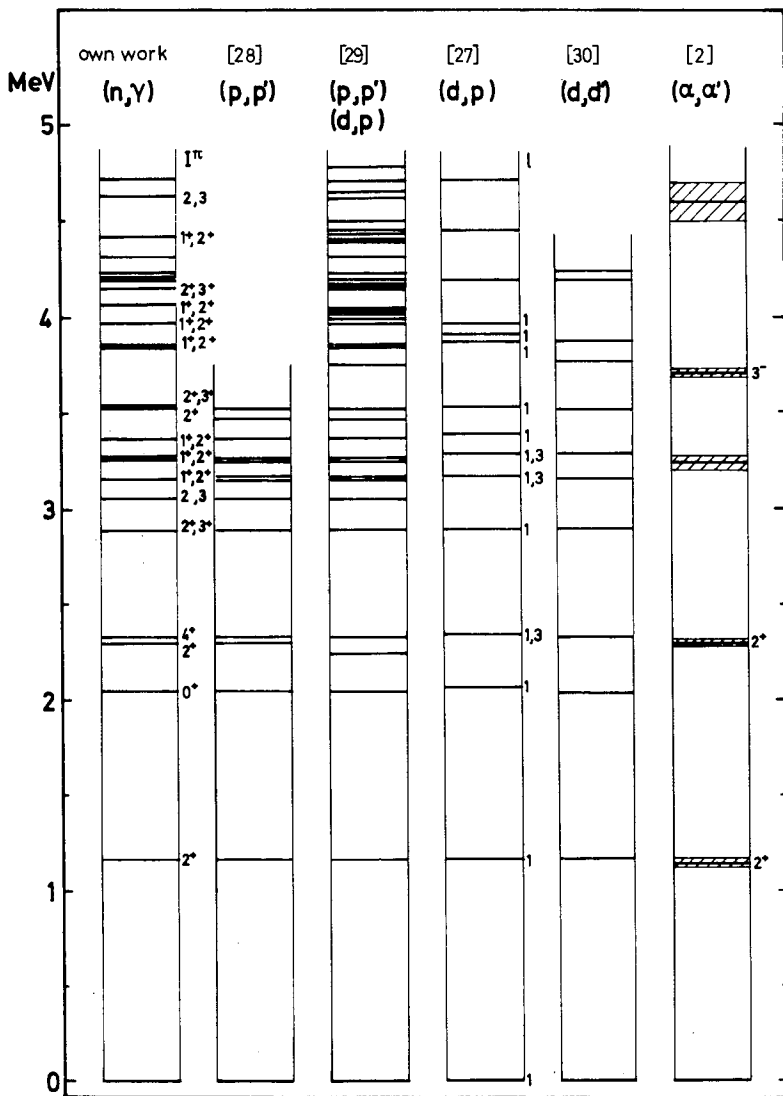


FIG. 5. Comparison of ^{62}Ni levels found by different reactions.

Mo et al. [10]. Because of the energy precision and of the spin assignment 4, the first of these cannot be identified with our 1^+ , 2^+ state at 3270 keV. For the level at 4051 keV, too, no analogue can be seen in the (n,γ) scheme.

4. Comparison of Experimental Schemes with Theory

Out of those available data an "experimental" ^{62}Ni level scheme has been constructed for comparison with calculated states in Fig. 6. A similar procedure was done with the ^{58}Fe scheme in Fig. 7, also including experiments other than the (n,γ) investigation. In Fig. 6 there are shown four theoretical level schemes resulting from shell-model calculations taking into account effective interactions. The common basic assumptions are the following: In all Ni isotopes a ^{56}Ni core is treated as being inert, i.e. excitations of neutrons or protons from the completely filled $1f\ 7/2$ shell ("core excitations") are neglected. The low-lying states are due to the motion of neutrons around a doubly closed-shell core. These active neutrons are restricted to the shells $2p\ 3/2$, $1f\ 5/2$, $2p\ 1/2$.

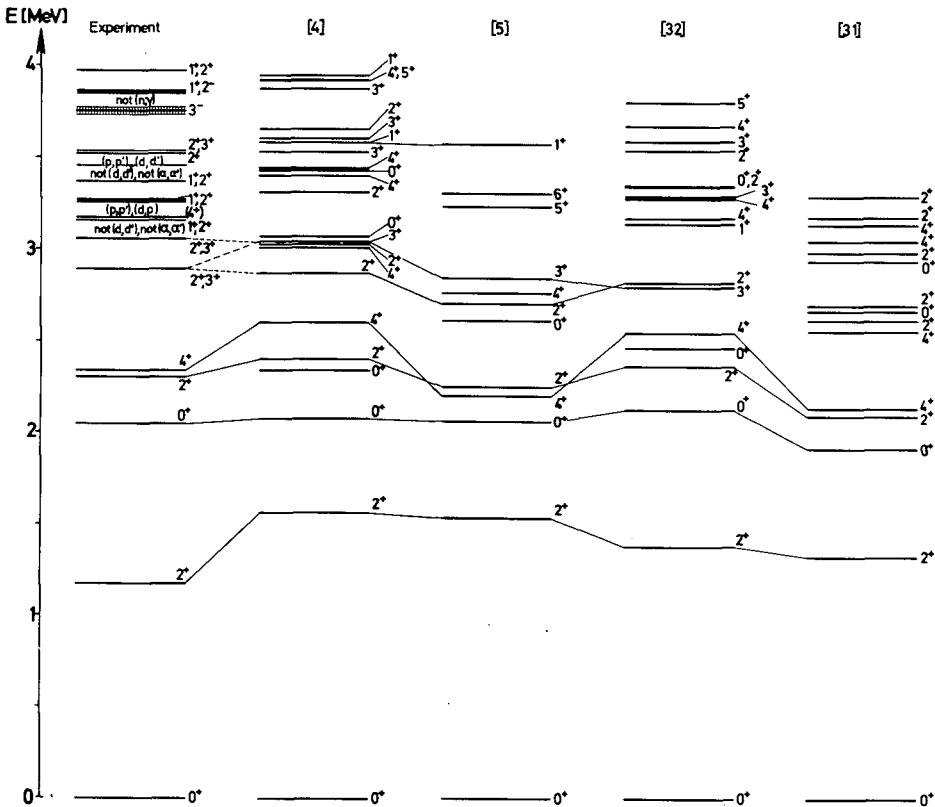


FIG. 6. Experimental and calculated energy levels in ^{62}Ni .

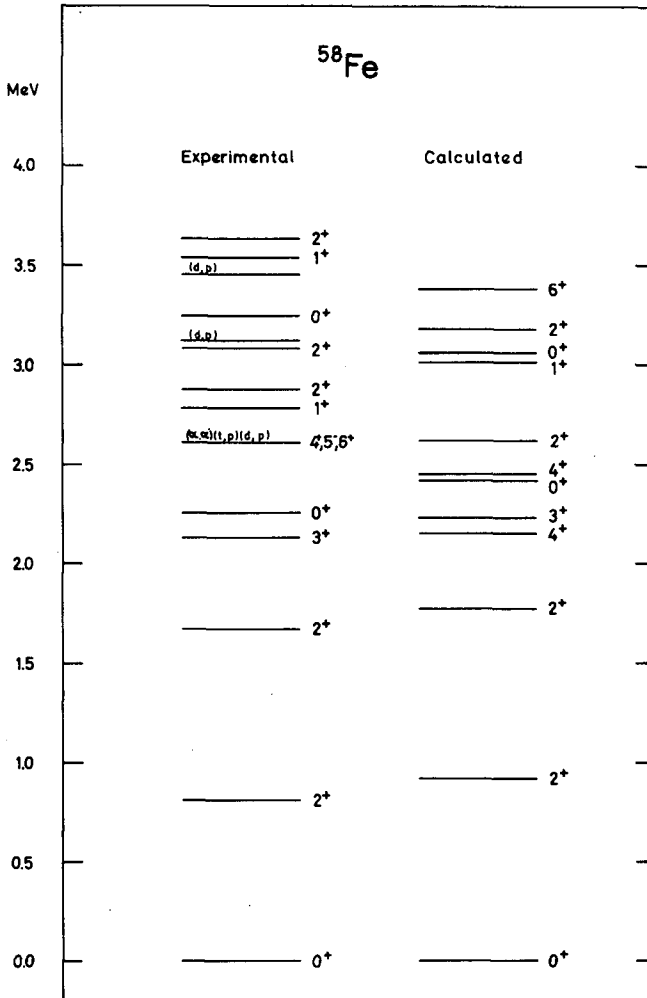


FIG. 7. Comparison of the experimental and theoretical ^{58}Fe level scheme.

Contributions of the $1g_{9/2}$ shell (estimated at least 3 MeV above the $2p_{3/2}$ level in ^{57}Ni) are not included. The single particle level spacings are taken from the experimental ^{57}Ni spectrum. Within the configurations chosen there exist 30 two-body matrix elements between the antisymmetric two-particle states. As the number of experimental data is too small for a direct parametrization, the number of parameters is cut down. The calculations differ - roughly spoken - in the procedure of restricting and fitting the parameters to the experimental data. Looking at Fig. 6 again, in the right hand level scheme surface delta interaction [31] was applied with an attractive strength constant fitted to the odd-even mass difference. The agreement of the low-lying levels with experiment is surprisingly good. In the scheme of Hsu et al. [32] the nucleon-nucleon potential

used was an s-state interaction with four radial matrix elements, as suggested by a least-squares fit to 27 experimental Ni-energy values. In one of the most refined calculations Cohen et al. [5] parametrized a two-body potential with central, tensor and two-body spin-orbit parts together with the four (already mentioned) radial matrix elements. This procedure yields 12 free parameters to be fitted to 24 experimental level energies in Ni. Finally Auerbach [4] fitted 17 of a total of 30 matrix elements to the body of available energy data, using the Kallio-Kolltveit potential for calculating the rest of them.

On the whole the agreement between calculations and experiment is quite satisfactory up to about 3.2 MeV. Generally the first 2^+ state is reproduced too high. There is a trend in these calculations to predict more 0^+ states than will probably ever be observed. Particularly 0^+ states should be fed strongly in the (n,γ) reaction, but there is no indication that such an experimental state exists between 2.1 and 3.8 MeV. The calculations would prefer the level at 3059 keV to be a 3^+ state, thus leaving the spin 2 for the level at 2891 keV. The experimental 3^- state, of course, cannot be reproduced within the configurations chosen. Taking another nucleus, ^{58}Fe , for a comparison between shell-model calculations and experimental states, the agreement seems to be even better (see Fig. 7). For each experimental level there exists a theoretical counterpart within about 250 keV (except one 4^+ level). The assumptions of these calculations performed by McGroary [7] had been (i) an inert ^{48}Ca core, (ii) the last six protons being restricted to the $1f_{7/2}$ shell and (iii) only $(2p_{3/2}, 1f_{5/2}, 2p_{1/2})^n$ configurations for the four active neutrons. The Hamiltonian included p-p, n-n, and n-p interactions, the parameters of which were fitted to spectroscopic data in ^{54}Fe , in the Ni isotopes (as done by Cohen et al.) and in the $N = 29$ isotones from ^{49}Ca to ^{57}Ni (as done by Vervier [33]), respectively.

In the case of ^{58}Fe a comparison between experimental and theoretical transition rates is impossible because of a lack of such calculations. But for ^{62}Ni there were given some theoretical $B(E2)$ ratios by Auerbach and by Cohen et al., presented in Table II. This table is a compilation of $B(E2)$ ratios as predicted by the simple vibrational model (Col. 1) (with the phonon selection rule $|\Delta v| = 1$), as deduced from our experimental data in ^{58}Fe (Col. 2) and in ^{62}Ni (Col. 3), and as calculated in the shell model with effective interactions (Col. 4). The first experimental value has to be considered as an upper limit, as the $2_2^+ \rightarrow 2_1^+$ transition was assumed to be pure E2 radiation which is most probably not true. The same assumption holds for the other experimental values; there the deduced ratios express limits only if one of the transitions is below the detection threshold. One interesting feature should be pointed out that can be seen in the first line: The experimental fact of a strong inhibition of the crossover transition $2_2^+ \rightarrow 0_1^+$ in ^{62}Ni - as postulated by vibrational models - is also reproduced by shell-model calculations. This inhibition had been thought to be a good argument for the vibrational character of ^{62}Ni . As the position of the first 3^+ state in ^{62}Ni has not yet been definitely established, the experimental $B(E2)$ value was calculated for both possible candidates, the levels at 2891 keV (c) and 3059 keV (d). The first one seems to agree better with the shell-model value. The corresponding ratio for ^{58}Fe is much

Table II
Comparison of reduced transition rates

Ratio	Vibrational model	^{58}Fe experiment	^{62}Ni experiment	^{62}Ni shell model
$\frac{B(E2; 2_2^+ \rightarrow 2_1^+)}{B(E2; 2_2^+ \rightarrow 0_1^+)}$	∞	10.5	≤ 23	1310 a) 33 b)
$\frac{B(E2; 3_1^+ \rightarrow 2_2^+)}{B(E2; 3_1^+ \rightarrow 2_1^+)}$	∞	≤ 350	≤ 10 c) 100 d)	1 b)
$\frac{B(E2; 2_2^+ \rightarrow 2_1^+)}{B(E2; 2_2^+ \rightarrow 0_2^+)}$	(∞)	-	≥ 0.1	29 a)

a) Ref. [4] b) Ref. [5] c), d) see text

higher (in the limit). - One cannot say that these few examples strongly support the shell-model calculations, but there are no serious discrepancies either. It is remarkable that the two shell-model values given for the cascade-crossover ratio of the second 2^+ state differ by a factor of 40. One would like to know how much the theoretical values for other transitions differ from each other. Finally, our decay scheme offers many more experimental γ -branching ratios waiting for a comparison with theory.

References

- [1] R.K. Mohindra and D.M. Van Patter, Phys. Rev. 139B (1965) 274
 [2] H.W. Broek, Phys. Rev. 130 (1963) 1914
 [3] A.K. Kerman and C.M. Shakin, Phys. Lett. 1 (1962) 151
 [4] N. Auerbach, Phys. Rev. 163 (1967) 1203
 [5] S. Cohen, R.D. Lawson, M.H. Macfarlane, S.P. Pandya, and Michitoshi Soga; Phys. Rev. 160 (1967) 903
 [6] J.B. McGrory, Phys. Rev. 160 (1967) 915
 [7] J.B. McGrory, Phys. Lett. 26B (1968) 604
 [8] U. Fanger, W. Michaelis, H. Schmidt, and H. Ottmar; Nucl. Phys. A128(1969)641
 [9] D.G. Gardner and W.W. Meinke, Phys. Rev. 107 (1957) 1628; Nucl. Data Sheets, compiled by K. Way et al.
 [10] J.N. Mo, S. Ray, and S.K. Mark, Nucl. Phys. A125 (1969) 440

- [11] E. Brun, W.E. Meyerhof, J.J. Kraushaar, and D.J. Horen;
Phys. Rev. 107 (1957) 1324
- [12] J.W. Butler and C.R. Gossett, Phys. Rev. 112 (1958) 1257
- [13] A.K. Sen Gupta and D.M. Van Patter, Phys. Rev. 131 (1963) 318
- [14] Nuklidkarte, 3rd edition,
Kernforschungszentrum Karlsruhe, Gersbach, München 1968
- [15] W. Michaelis and H. Küpfer, Nucl. Instr. and Meth. 56 (1967) 181
- [16] G. Markus, Dissertation Karlsruhe (1967)
- [17] U. Fanger, KFK 887 (1969)
- [18] H. Schmidt, KFK 877 (1969)
- [19] G. Krüger and G. Zipf, KFK 371 (1965)
- [20] G.D. Sprouse and S.S. Hanna, Nucl. Phys. 74 (1965) 177
- [21] J.B. Marion, Nucl. Data A4 (1968) 301
- [22] R.C. Greenwood and W.W. Black, Phys. Lett. 21 (1966) 702
- [23] H.E. Jackson, A.I. Namenson, and G.E. Thomas
Phys. Lett. 17 (1965) 324
- [24] R.K. Sheline and W.N. Shelton, H.T. Motz and R.E. Carter,
Phys. Rev. 136 (1964) 351
- [25] R.C. Greenwood, Paper F1 Slow Neutron Capture Conf.,
Argonne National Laboratory, Nov. 1966
- [26] L.V. Groshev, A.M. Demidov, and N. Shadiev,
Soviet J. of Nucl. Phys. 3 (1966) 319
- [27] R.H. Fulmer and A.L. McCarthy, Phys. Rev. 131 (1963) 2133
- [28] MIT, LNS Progress Report (28th Febr. 1958) ONR Generator
Group
- [29] R.G. Tee and A. Aspinall, Nucl. Phys. A98 (1967) 417
- [30] R.K. Jolly, E.K. Lin and B.L. Cohen,
Phys. Rev. 128 (1962) 2292
- [31] A. Plastino, R. Arvieu, and S.A. Moszkowski;
Phys. Rev. 145 (1966) 837
- [32] L.S. Hsu and J.B. French, Phys. Lett. 19 (1965) 135
- [33] J. Vervier, Nucl. Phys. 78 (1966) 497

RADIATIVE NEUTRON CAPTURE STUDIES OF NUCLEAR EXCITATIONS IN ^{68}Zn

H. OTTMAR, N. M. AHMED, U. FANGER, D. HECK,
W. MICHAELIS, H. SCHMIDT
Institut für angewandte Kernphysik,
Kernforschungszentrum Karlsruhe,
Karlsruhe, Federal Republic of Germany

Abstract

RADIATIVE NEUTRON CAPTURE STUDIES OF NUCLEAR EXCITATIONS IN ^{68}Zn . Nuclear excitations in ^{68}Zn were investigated via the (n, γ) reaction on a highly enriched ^{67}Zn sample. Four different spectrometers, a Ge(Li) anti-Compton spectrometer, a Ge(Li)-4 NaI(Tl) pair spectrometer, a Ge(Li)-NaI(Tl) coincidence device and an angular correlation system, were used to establish a reliable decay scheme.

1. INTRODUCTION

Even nuclei in the mass region around $A = 70$ reveal interesting features in their nuclear structure. The occurrence of low-lying 0^+ states is a puzzling problem and as yet not well understood. Therefore much experimental work has been done in this mass region during the last few years, most of it via particle reactions and radioactive decay. An additional helpful tool for nuclear structure studies is the (n, γ) reaction. At the present state of the art this allows not only a very precise energy determination of nuclear levels but also the measurement of transition probabilities and mixing ratios of gamma transitions, i.e. quantities very sensitive to nuclear models.

The only even nuclei in the above mass region accessible to study by the (n, γ) method are ^{68}Zn and ^{74}Ge . Results on ^{74}Ge were reported earlier [1]. In this paper we will present data which we obtained from the reaction $^{67}\text{Zn}(n, \gamma)^{68}\text{Zn}$ at the Karlsruhe research reactor FR-2.

2. SOME DATA ON ZINC ISOTOPES TARGET

The abundance of ^{67}Zn in natural zinc amounts only to 4.11%. We used, therefore, a target enriched to 89.55% in ^{67}Zn . Unfortunately the contribution of ^{67}Zn to the total contribution of this sample could not be calculated because the cross-sections for both ^{67}Zn and ^{66}Zn are not known. Our spectra reveal, however, only minute contributions from the other zinc isotopes. Nevertheless we tried to determine the previously unknown cross-sections of ^{66}Zn and ^{67}Zn from their intensity contributions in the natural mixture by assigning primary transitions [2] to the corresponding isotopes. We assumed thereby that for each of the participating isotopes, ^{64}Zn , ^{66}Zn , ^{67}Zn and ^{68}Zn , comparable portions of their total intensity have been detected. The contribution of ^{70}Zn can be neglected. The

TABLE I. DATA ON ZINC ISOTOPES

	^{64}Zn	^{66}Zn	^{67}Zn	^{68}Zn	^{70}Zn
Natural abundance (%)	48.89	27.81	4.11	18.56	0.62
σ (b) ^a	0.77 ± 0.03	?	?	1.07 ± 0.15	0.1 ± 0.02
Capture contribution (%)	34.2	?	?	18.1	0.6
Contribution derived from γ -intensity	36.7	20.5	25.1	17.7	
σ from γ -intensity (b)		0.85 ± 0.2	6.9 ± 1.4		
E_n of product nucleus (keV)	7979.2	7052.3	10 197.9	6482.6	5833 ^b
Contribution in 89.55% ^{67}Zn enriched sample	0.23	0.62	98.4	0.75	

^aRefs [3, 4]^bRef. [5]

assignment of gamma rays in the natural mixture was considerably facilitated by the knowledge of all ^{68}Zn gamma lines originating from the present measurements with the enriched target. The results of this procedure are listed in Table I.

The agreement of the contributions of ^{64}Zn and ^{68}Zn calculated from the known cross-sections with the contributions derived from the gamma intensities assigned gives confidence that the contributions of ^{66}Zn and ^{67}Zn and hence their cross-sections, determined from these contributions and the known cross-section for the natural mixture [4], are correct within 20%.

3. EXPERIMENTAL TECHNIQUES

3.1. Spectrometers

Four different spectrometers were used for the (n, γ) studies. Precise energy measurements of transition energies in the energy region up to 3 MeV were carried out in a Compton-suppressed system. The most significant feature of this system is the high suppression of the Compton distribution. This is demonstrated in Fig.1 which shows a portion of the (n, γ) spectrum of ^{68}Zn . Transitions with intensities 5×10^{-5} of the intensity of the 1077-keV transition can be detected. For a detailed description of the system see Ref.[6].

In the mean energy region from 2 to 6 MeV we recorded the gamma spectra in a 5-crystal pair spectrometer consisting of a 4-cm³ Ge(Li) detector with a cooled FET-preamplifier and four bevelled 3 × 3-in. NaI(Tl) detectors. The extrinsic detection probability of a double-escape event in the Ge(Li) detector via the selected photopeaks of the annihilation radiation amounts to 5%. In Fig.2 a part of the pair spectrum of ^{68}Zn is shown. To preserve the good resolution of 5.9 keV at 6 MeV over a long time, the spectrometer is digitally stabilized with a stable double-pulse generator against zero and gain shifts of the electronics including the 4096-channel ADC. In the energy region above 6 MeV the spectra were recorded as singles spectra.

To establish a reliable decay scheme much work was done in γ - γ coincidence and angular correlation measurements. For these investigations we have two spectrometers connected to an on-line computer, thus allowing the simultaneous measurements of all interesting coincidences and angular correlations with the aid of the double-window technique. The coincidence arrangement used for these measurements comprised a 34-cm³ Ge(Li) detector and a 3 × 3-in. NaI(Tl) detector. Later the NaI(Tl) detector was replaced by another large-volume Ge(Li) detector. The angular correlation spectrometer and the data processing therefrom are described in Ref.[7].

3.2. Calibration

To make full use of the high resolution of the anti-Compton and pair spectrometers with respect to precise energy determination, the gamma spectra were analysed with a computer fit program [6]. An example of the analysis of the spectra is given in the inset of Fig.2 showing a fitted

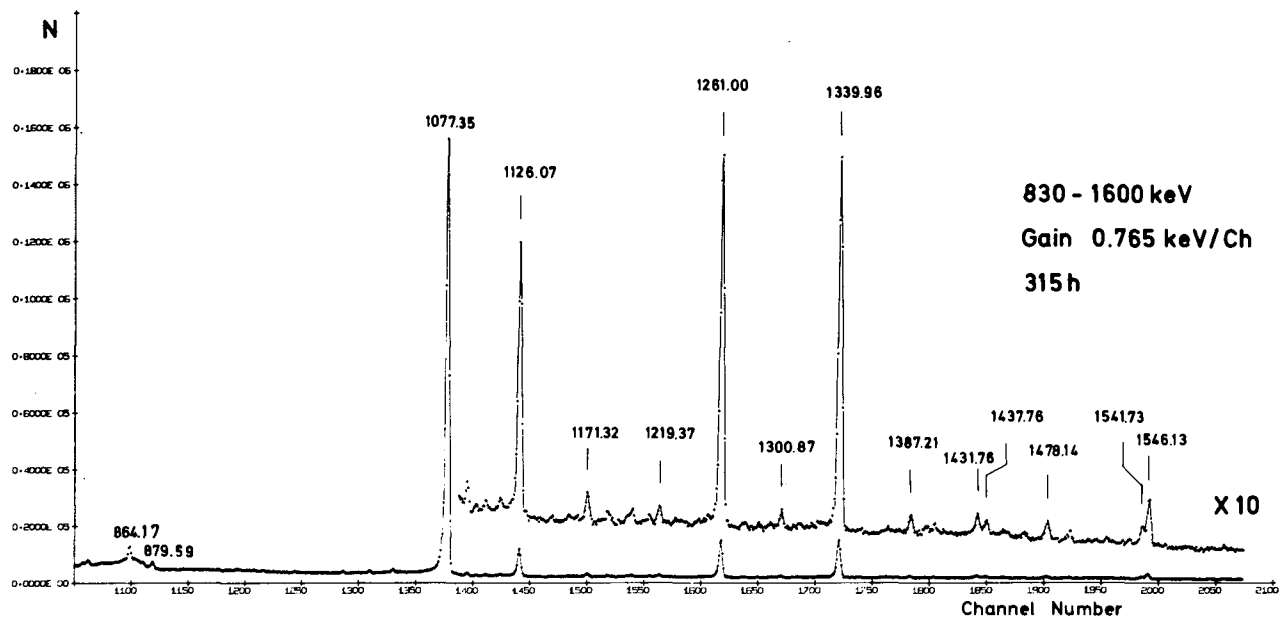


FIG. 1. Portion of the anti-Compton spectrum of $^{67}\text{Zn}(n, \gamma)^{68}\text{Zn}$.

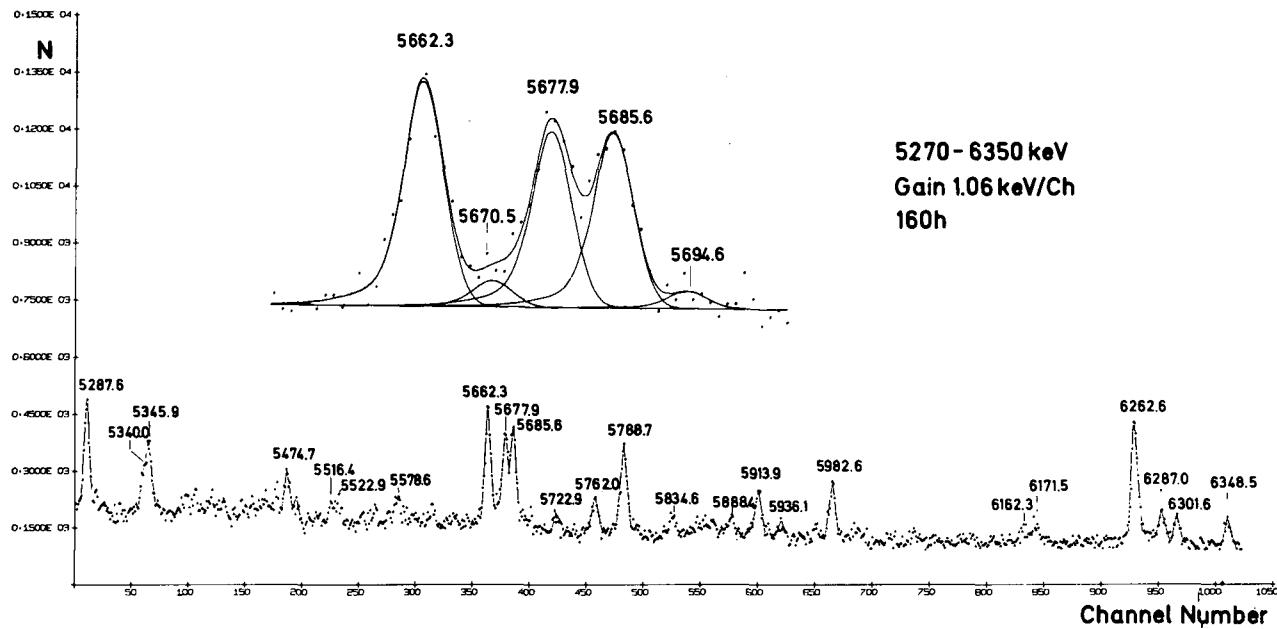


FIG. 2. Portion of the pair spectrum of $^{67}\text{Zn}(n, \gamma)^{68}\text{Zn}$.

TABLE II. POLYNOMIAL FIT OF NITROGEN CALIBRATION LINES

Input data (keV)	Output data (keV)			
Marion [10]	Measurement 1	Measurement 2	Measurement 3	Mean value
4508.8 ± 0.3	4508.81	4508.83	4508.82	4508.8
	4945.07	4945.14	4945.07	4945.1
5268.5 ± 0.2	5268.90	5268.92	5268.88	5268.9
5297.4 ± 0.3	5297.60	5297.46	5297.62	5297.6
5533.0 ± 0.3	5533.01	5533.01	5532.97	5533.0
5562.0 ± 0.3	5561.91	5561.69	5561.78	5561.7
6322.1 ± 0.4	6322.12	6322.10	6322.12	6322.1
Greenwood [11]				a
4508.8 ± 0.3	4508.88	4508.86	4508.88	4508.9 ± 0.3
	4945.42	4945.32	4945.32	4945.35 ^b
5269.2 ± 0.35	5269.26	5269.26	5269.21	5269.2 ± 0.3
5297.8 ± 0.35	5297.80	5297.96	5297.95	5297.9 ± 0.3
5533.2 ± 0.35	5533.29	5533.31	5533.33	5533.3 ± 0.3
5562.2 ± 0.35	5562.09	5561.98	5561.99	5562.0 ± 0.3
6322.0 ± 0.4	6322.0	6322.01	6322.01	6322.0 ± 0.4

^aUsed for calibrating the gamma rays in ⁶⁸Zn.

^bE_γ = 4945.46 ± 0.17 keV. Calibration standard from ¹³C [12].

line group in the pair spectrum. This fitting with modified Gaussian functions, i.e. Gaussian function plus exponential function taking into account the low-energy tailing of the peaks, allows the exact determination of peak locations. The system non-linearity was measured by feeding pulses from a highly stable pulse generator with a linearity better than 1 part in 10^5 and a resolution of 1 part in 10^6 [8] into the preamplifier. The pulser peak locations resulting from the fitting procedure were then fitted by the least-squares method to a polynomial of order up to four. For the calibration the peak positions of the calibration lines taken together with the spectrum were fitted with a polynomial of same order. The polynomial best describing the system non-linearity was then chosen for calibration. To obtain best results the polynomial sometimes had to be divided into two or three parts.

In the low-energy region the well-known calibration lines were used [9]. In the high-energy region, unfortunately, there is still a lack of precise calibration standards. Lately the capture lines of ^{15}N have been commonly used as energy as well as intensity standards. However, there remain some ambiguities because the data of different authors do not coincide within the errors indicated. This is especially true for the intense lines between 5 and 6 MeV. Recently Marion [10] has published a set of adopted values. While calibrating different independent measurements with different peak channel locations of the calibration lines we got indications that these values are not quite correct. Table II shows the results of the polynomial fit of two different sets of nitrogen calibration lines between 4.5 and 6.3 MeV: in one we used the adopted values of Marion and in the second the data of Greenwood [11]. One can see from the table that the calibration set of Greenwood reproduces the best known energy in this region – the 4945.46 ± 0.17 -keV capture line of ^{13}C [12] – much better than that of Marion. For calibrating our high-energy spectra we used, therefore, the values of Greenwood for calibration lines above 6 MeV together with our slightly different values from Table II.

4. EXPERIMENTAL RESULTS

The results of all measurements are summarized in the level scheme in Fig.3. All transition energies therein are corrected for recoil. Up to 3 MeV all levels with spins between 0 and 4, seen in different reactions [13-17], are excited in the (n, γ) process and are now precisely fixed. All levels in the decay scheme are fed by primary gamma rays from the capture state except the 0^+ level at 1655.90 keV and the 2821.54-keV level. A primary transition to the 3281.5-keV level could be masked by the intense transition to the close-lying 3286.93-keV level. Though the precise energy determination allows one to apply the Ritz combination principle with confidence, most of the transitions have been well established by coincidence measurements. Such well-established coincidences of transitions are marked with dots at their arrowheads in the level scheme. Only one ambiguity arises: thorough investigation of the spectrum coincident to the 1077.36-keV transition reveals a line at 1883 keV, although the coincident background and the contribution from the nearly 1126.08-keV transition have been subtracted appropriately with the double-window technique. A recent coincidence measurement on natural zinc with

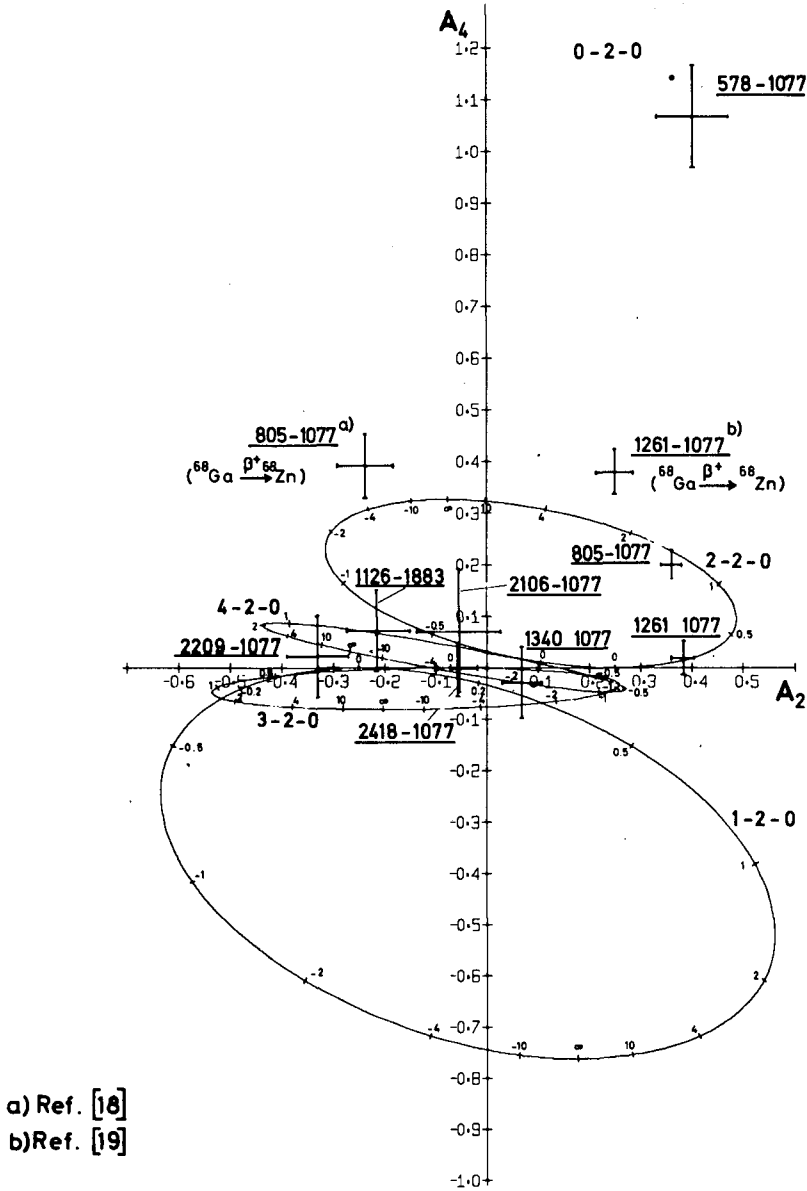


FIG. 4. Angular correlation coefficients for transitions in ^{68}Zn from the reaction $^{67}\text{Zn}(n, \gamma)^{68}\text{Zn}$.

The results of the studies in radioactive decay of ^{68}Ga , also shown in Fig.4, yield a $\delta = -(4 \pm \frac{3}{2})$ or 94% E2 contribution for the 805.76-keV transition [18] whereas the analysis of our (n, γ) measurement yields a $\delta = 1.45 \pm 0.15$ or 68% E2 contribution for the same transition. For the

1261.01-keV transition Taylor and McPherson [19] obtained from radioactive decay of ^{68}Ga a $\delta = 2.25 \pm 0.30$ or 84% E2 contribution, however, our

$$\delta = 0.21 \begin{matrix} +0.06 \\ -0.04 \end{matrix} \text{ yields only a small amount of 4\% E2 contribution to this}$$

transition. These discrepancies may have two reasons: first both transitions appear in the β^+ decay of ^{68}Ga with much less intensity than in the (n, γ) reaction, on the other hand the spectra obtained from the radioactive decay are characterized by a high background caused by annihilation radiation and bremsstrahlung. This requires a large background subtraction and therefore there remains some uncertainty as to what extent this was correctly done. A detailed description of our angular correlation analysis of the 1260.01 transition is given in Ref. [7].

The angular correlation analysis of the other cascades shown in Fig.4 yields, in conjunction with the excitation and de-excitation behaviour of the involved levels, spin and parity 2^+ or 3^+ for the 3009.27-keV level and 1^- or 2^- for the 3184.00-keV level. The negative parity assignment to this level was taken from (d, p) measurements [17] which reveal a negative parity level at 3180 keV. This is compatible with the very weak primary feeding of the 3184.00-keV level found in the present investigation. Spin and parity assignments for the 3286.93-keV level come out unambiguously to be 1^+ , while the 3495.74-keV level most probably has the assignment 3^+ . The 4^+ (3^+) assignment to the 3725.92-keV level, also taken from the (d, p) measurements [17] where a level with this spin was seen at 3730 keV, agrees with its feeding and de-excitation.

The spin 3^- for the 2750.68-keV and 2^+ for the 2821.54-keV levels seem to be well established from other measurements [14, 15, 20]. It is astonishing that the latter level is not excited by a possible primary E1 transition from the 2^- , 3^- capture state. Hudson et al. [14] assigned from (t, p) measurements an unambiguous spin 4^+ to a level at 2954 ± 8 keV. If, however, the 2959.9-keV transition represents a ground-state transition from the 2959.39-keV level found in our investigation and assumed to be identical with the level of Hudson, the spin of this level should be 2^+ . The assignments to the remaining levels in the level scheme represent most probable values with respect to their excitation and de-excitation behaviour.

5. CONCLUSIONS

Coulomb excitation and various inelastic scattering experiments leave no doubt that most of the low-lying excitations of the so-called 'spherical' nuclei have collective character. Discussing nuclear level patterns one enters, however, the problem as to what sort of collective motion one should ascribe to these excitations. It seems now to be rather certain that the model most applied to these nuclei – the vibrational model – does not give an adequate description of their excitations. Looking at the level scheme in Fig.4 with the phonon picture of this model in mind, one might consider the first excited 0^+ level, the second 2^+ and the first 4^+ level as two-phonon candidates though these three levels are relatively widely spaced. The 2^+ level at 2338 keV can be completely ruled out as a phonon-state because of the pure M1 character of its de-excitation transition.

A deeper insight in the level structure may be obtained by comparing the level patterns of neighbouring nuclei. This is done in Fig.5 for even nuclei between ^{64}Zn and ^{72}Ge . Included in the figure are all the data available in literature about the levels up to the 3rd octupole state. The comparison shows very nice analogies between different isotopes for the first and second 2⁺ levels and for the first 4⁺ level. While these levels vary only slowly in their energies from one nucleus to the other, the first 0⁺ level comes down very rapidly in its energy – more than 1.5 MeV. In ^{64}Zn the situation is complicated by the presence of two 0⁺ levels. Nevertheless, the quite different behaviour of these 0⁺ states implies that they represent another type of excitation than other states in this region.

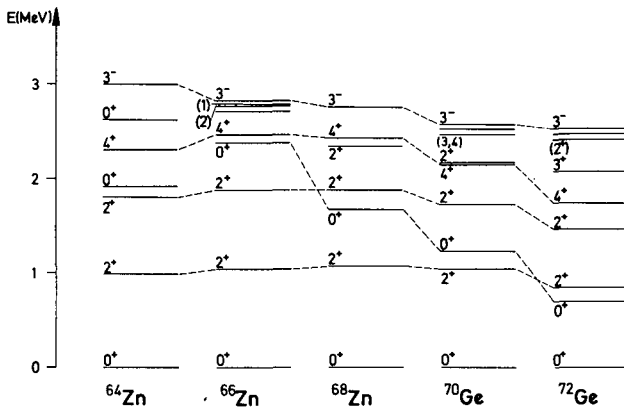


FIG. 5. Comparison between level schemes of even nuclei around $A = 68$ including all experimental data available in the literature.

The recently observed large quadrupole moments of the first excited 2⁺ states [21], also in nuclei commonly believed to be spherical, indicate that anharmonic effects probably play an important role. There have been empirical attempts to treat the vibrational spectra as quasi-rotational spectra [22] and to decompose them into quasi-rotational bands, beta-like bands and gamma-like bands. The first excited 0⁺ state is thus considered as a band head of a quasi-beta band. The numerical calculations recently started [23] involving the exactly treated coupling of these three motions yielded promising results for nuclei with masses around $A = 190$, i.e. in the transition region from deformed to spherical shapes. One may hope that this will also be true for the lighter nuclei.

REFERENCES

- [1] WEITKAMP, C., MICHAELIS, W., SCHMIDT, H., FANGER, U., Z. Phys. 192 (1966) 423.
- [2] Nuclear Data A3 (1967) 546.
- [3] KIM, J.I., ADAMS, I., Radiochim. Acta 9 (1968) 61.
- [4] Rep. BNL 325 No.2 (1966).

- [5] von EHRENSTEIN, D., SCHIFFER, J.P., Phys. Rev. 164 (1967) 1374.
- [6] MICHAELIS, W., HORSCH, F., "High-precision neutron capture gamma-ray spectroscopy using germanium detectors in Compton-suppression technique", these Proceedings.
- [7] SCHMIDT, H., HECK, D., "Angular correlation measurements on gamma-ray cascades following thermal neutron capture", these Proceedings.
- [8] HORSCH, F., Rep. KFK 558 (1968).
- [9] Nuclear Data A4 (1968) 310.
- [10] Nuclear Data A4 (1968) 316.
- [11] GREENWOOD, R.C., Physics Lett. 27B (1968) 274.
- [12] PRESTWICH, W.V., COTÉ, R.E., THOMAS, G.E., Phys. Rev. 161 (1967) 1080.
- [13] CARTER, H.K., HAMILTON, J.H., RAMAYYA, A.V., PINAJIAN, Phys. Rev. 174 (1968) 1329.
- [14] HUDSON, F.R., BAMPPTON, P.F., GLOVER, R.N., Physics Lett. 27B (1968) 84.
- [15] LIN, E.K., Nucl. Phys. 73 (1965) 613.
- [16] McINTYRE, L.C., Phys. Rev. 152 (1966) 1013.
- [17] LIN, E.K., COHEN, B.L., Phys. Rev. 132 (1963) 2632.
- [18] KONO, S., J. phys. Soc. Jap. 17 (1962) 907.
- [19] TAYLOR, H.W., McPHERSON, R., Can. J. Phys. 41 (1963) 554.
- [20] TAYLOR, H.W., Nucl. Phys. A91 (1967) 659.
- [21] See for instance de BOER, J., Proc. Int. Conf. Nuclear Structure, Tokyo (1967) 199 and other Refs cited there.
- [22] SHELINE, R.K., Rev. mod. Phys. 32 (1960) 1; SAKAI, M., Proc. Int. Conf. Nuclear Structure, Tokyo (1967) 576.
- [23] KUMAR, K., BARANGER, M., Phys. Rev. Lett. 17 (1966) 1146.

THE LEVEL STRUCTURE OF ^{71}Ge

C. HOFMEYR, B. C. WINKLER, J. A. M. DE VILLIERS,
J. G. MALAN, J. W. TEPEL
Atomic Energy Board,
Pelindaba, South Africa

Abstract

THE LEVEL STRUCTURE OF ^{71}Ge . The decay gamma rays of ^{71}Ge have been observed and the neutron binding energy deduced from neutron capture in ^{70}Ge . The levels which are directly populated from the capture state were determined. The level structure of ^{71}Ge below 1.8-MeV excitation energy has been investigated by means of the $^{71}\text{Ga}(p, n)^{71}\text{Ge}$ and the $^{71}\text{Ga}(p, n\gamma)^{71}\text{Ge}$ reactions.

Interest in the germanium isotopes has been stimulated by the widespread use of Ge(Li) detectors in nuclear physics. High-resolution studies, including (n, γ) measurements, have been made on several of the Ge isotopes, but the level structure of ^{71}Ge has previously been investigated only by means of the (d, p) reaction on ^{70}Ge , recently by Goldman [1]. The first two excited levels of ^{71}Ge are well known from beta-decay studies. In this experiment the level structure of ^{71}Ge was investigated by means of the $^{70}\text{Ge}(n, \gamma)^{71}\text{Ge}$, the $^{71}\text{Ga}(p, n\gamma)^{71}\text{Ge}$ and the $^{71}\text{Ga}(p, n)^{71}\text{Ge}$ reactions.

The (n, γ) experiment on ^{70}Ge was performed at the ORR-type reactor, SAFARI-1, of the Atomic Energy Board of South Africa. A beam of sub-thermal neutrons is extracted via a beam tube which extends tangentially outwards with respect to the core from a high flux region. This arrangement discriminates against fast neutrons and gamma rays from the core. In addition, a bismuth filter of 30 cm is used. The gamma rays from the sample were detected in a 30-cm³ Ge(Li) spectrometer and recorded on a 4096-channel analyser in the energy regions 0-8, 0-2.6 and 2.6-7.8 MeV with a system resolution of approximately 6 keV at 1.3 MeV. Background runs of equal live time were recorded under identical conditions. The detector calibration and relative efficiency determination were performed by means of chlorine (n, γ) runs over the full energy range, supplemented by runs with standard sources up to 2.6 MeV. The energies of the chlorine lines were taken from the work of Kennett et al., as published in Ref. [2], from which relative intensities were also obtained. An independent relative efficiency determination for this detector, using numerous simple cascades from (p, γ) experiments, is in agreement with our result. The 1-g ^{70}Ge sample, in oxide form, was enriched to 91.4%.

The $^{71}\text{Ga}(p, n)^{71}\text{Ge}$ experiment ($Q = -1017$ keV) was performed at the 3-MeV pulsed Van de Graaff accelerator of the South African Atomic Energy Board. Neutron spectra were recorded with a 4×2 -in. plastic scintillator and a conventional time-of-flight arrangement utilizing flight paths up to 3 m and various incident proton energies up to 3 MeV. The decay gamma rays were detected with a 30-cm³ Ge(Li) detector either directly or in coincidence with the neutrons. Direct gamma spectra were observed by irradiating a target, consisting of natural Ga_2O_3 evaporated to a thickness of 100 keV onto a 0.25-mm Ta backing, in energy intervals

of 100 keV from 1.5 to 3.0 MeV. Due to the extremely low cross-section for this reaction, the coincidence measurements mentioned were used only to identify gammas associated with the neutron flux. A 14-keV target (at $E_p = 2$ MeV) was used in the time-of-flight experiment.

Levels which are populated directly from the $\frac{1}{2}^+$ capture state of slow neutrons and decay directly to the ground state ($J^\pi = \frac{1}{2}^-$) are listed in Table I. A comprehensive list of gamma rays observed in the (n, γ) experiment is given in Table II. The intensities are relative and normalized to 100 for the 1097-keV transition.

In Fig. 1 the levels of ^{71}Ge as deduced from the (n, γ) study on ^{70}Ge are compared with the levels determined from the $(p, n\gamma)$ and (p, n) studies on ^{71}Ga . More levels are evident from the neutron time-of-flight spectra, although with lower precision. Levels which are not directly populated from the capture state in the (n, γ) work, but which can be inferred from the gamma-ray spectra when considering the $(p, n\gamma)$ results, are shown in dotted lines, whereas direct population is indicated by arrows. Figure 2 represents a proposed level and decay scheme for ^{71}Ge . The spin and parity values in brackets are those given by Goldman [1]. The decays

TABLE I. SIMPLE CASCADES FROM THE CAPTURE TO THE GROUND STATE IN ^{71}Ge

^{70}Ge (n, γ) ^{71}Ge	Direct Transition from Capture State	Sum
Level (G.S. Transition) keV	keV	keV
0	7420	7420
501	6920	7421
709	6712	7421
832	6588	7420
1097	6324	7421
1140	6281	7421
1300	6121	7421
1379	6041	7420
1599	5819	7418
(1740)	5680	(7420)
1965	5455	7420
2033	5388	7421
(2146)	5274	(7420)
2223	5197	7420
2351	5070	7421
2459	4959	7418
2534	4886	7420

Binding Energy = 7420.5 ± 0.6 keV (including recoil)

TABLE II. $^{70}\text{Ge}(n, \gamma)^{71}\text{Ge}$: RECORDED GAMMA-RAY TRANSITIONS

Precision: ± 0.7 keV for intense transitions $E \leq 2.6$ MeV
 ± 2.0 keV for intense transitions $E \geq 2.6$ MeV

Energy keV	Relative Intensity*	Energy keV	Relative Intensity*	Energy keV	Relative Intensity*
7420	35	(3377)		1015	6
6920	54	2534	weak	921.3	3
6711	68	2528	weak	869.5	25**
6588	16	2515	weak	852	weak
6324	37	2459	weak	831.9	70
6281	26	2351	13	808.6	25
6121	62	2223.0	15	798.6	1
6041	67	(2146)	weak	789.2	9
5819	45	2033.0	18	748.1	7
5680	1.5	1965.3	13	708.7	125
5455	43	1777.8	6	671	weak
5388	14	1740	weak	639	weak
5274	10	1598.6	5	633.1	10
5197	5	1441.3	weak	596.5	30***
5164	10	1424	weak	573	20
5070	19	1430	weak	528	weak
4990	11	1397	weak	(511.6)	200
4980	6	1379.0	20	500.7	240
4959	6	1300.2	45	392	40
4886	25	1205.3	25	350.5	7
4640	10	1139.6	50	327.2	105
4516	17	1096.7	100	308.0	13
4393	12	1032	6	284.0	25
4340	11	1038	6	247.4	20
4312	14	1020	8	175.8	310
4038	10				

* 1096.7 transition taken as 100. ** With contribution from ^{74}Ge [3] *** Mainly from ^{74}Ge [3]

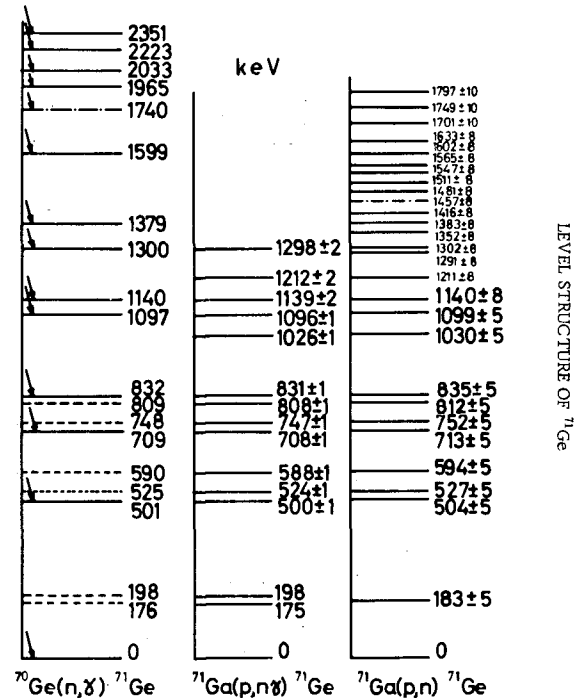


FIG.1. Comparison of the energy levels in ^{71}Ge as deduced from the three experiments.

LEVEL STRUCTURE OF ^{71}Ge

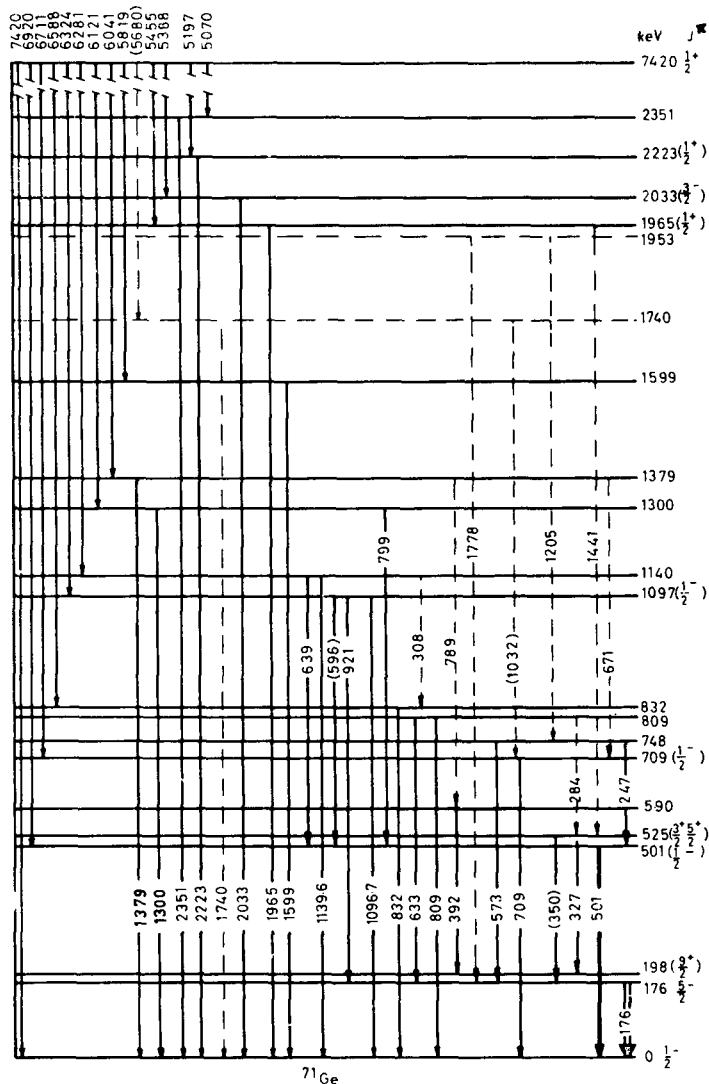


FIG. 2. Proposed level and decay scheme for ^{71}Ge , indicating gamma rays recorded in the $^{70}\text{Ge}(n, \gamma)^{71}\text{Ge}$ experiment (see text).

indicated by solid lines, with the exception of primary transitions from the slow neutron capture state, have been observed in both the (n, γ) and $(p, n\gamma)$ studies. Dotted decay lines between excited levels indicate transitions which were observed only in the (n, γ) work. These lines were fitted by considering energy differences between levels. Primary transitions and associated simple cascades to the ground state (energy sum equal to neutron binding energy) are indicated in full lines, except where these are uncertain.

In the $(p, n\gamma)$ work decay gammas have been identified from their threshold behaviour, the energy sum in the case of cascades and from a neutron-gamma coincidence experiment. These investigations are at present being extended and will be published in more detail elsewhere.

R E F E R E N C E S

- [1] GOLDMAN, L.H., Phys. Rev. 165 (1968) 1203.
- [2] BARTHOLOMEW, G.A. et al., Nuclear Data 3 (1967) 436.
- [3] WEITKAMP, C. et al., Z. Phys. 192 (1966) 423.

HIGH-ENERGY GAMMA RAYS OF ^{76}As AND ^{197}Au FOLLOWING THERMAL AND EPITHERMAL NEUTRON CAPTURE *

(Abstract only)

P. GRYSKA, P. RIEHS, K. RUMPOLD
Physics Institute,
Reactor Center Seibersdorf,
Austria

Abstract

HIGH-ENERGY GAMMA RAYS OF ^{76}As AND ^{197}Au FOLLOWING THERMAL AND EPITHERMAL NEUTRON CAPTURE. Using a Ge(Li) detector, the energies and intensities of the high-energy gamma transitions of the $^{75}\text{As}(n, \gamma)^{76}\text{As}$ and $^{197}\text{Au}(n, \gamma)^{198}\text{Au}$ reactions have been measured. By comparison between gamma-ray intensities in thermal and epithermal neutron capture of arsenic, 6 intense transitions are found to be due mainly to direct neutron capture. A classification of gamma-ray intensities after epithermal neutron capture indicated an E1 multipolarity for 8 gamma transitions. A determination of the binding energy relative to ^{36}Cl transitions yielded 7330 ± 4 keV. Contrary to measurement results with As, experiments carried out with gold yielded the same gamma-ray intensity ratios for epithermal and thermal neutron capture.

* The full text of this paper has been published by the same authors in Nuclear Physics (A132 (1969) 123) under the title "High energy gamma rays of ^{76}As following thermal and epithermal neutron capture".

GAMMA DECAY OF ^{96}Mo AND ^{98}Mo AFTER THERMAL NEUTRON CAPTURE IN ^{95}Mo AND ^{97}Mo

D. HECK, W. MICHAELIS, H. OTTMAR, H. SCHMIDT
Institut für angewandte Kernphysik,
Kernforschungszentrum Karlsruhe,
Karlsruhe, Federal Republic of Germany

Abstract

GAMMA DECAY OF ^{96}Mo AND ^{98}Mo AFTER THERMAL NEUTRON CAPTURE IN ^{95}Mo AND ^{97}Mo . The gamma-ray spectra following neutron capture in the odd-mass molybdenum isotopes have been studied with Ge(Li) and NaI(Tl) detectors. The analysis of measured angular distributions yields detailed information on the structure of some levels. The results are compared with theoretical predictions.

1. EXPERIMENTAL PROCEDURE

The measurements were performed at the FR-2 research reactor in Karlsruhe. The targets consisted of MoO_3 powder (enriched to 96.2% in ^{95}Mo , $\sigma_c = 14.5$ b) and metallic molybdenum powder (enriched to 92.8% in ^{97}Mo , $\sigma_c = 2.2$ b), enclosed in thin-walled polyethylene capsules. For the energy range up to 2.7 MeV a Ge(Li) diode with anti-Compton shield [1] has been used. Coincidences and angular correlations of some gamma-gamma cascades have been measured with two 4-in. diam. \times 5-in. NaI(Tl) crystals in a fast-slow coincidence set-up [2] coupled with the on-line computer system MIDAS [3].

2. RESULTS FROM $^{95}\text{Mo}(n, \gamma)^{96}\text{Mo}$

The decay scheme known from the radioactive beta decay of ^{96g}Tc , ^{96m}Tc and ^{96}Nb [4] could be extended considerably by the present investigation (Fig. 1). Noteworthy is a new level at 1625.93 keV. Because of the good resolution of the anti-Compton spectrometer [1], it could be established that the known 850-keV gamma-ray [6] de-exciting the 4^+ level at 1628 keV is really a triplet with two intense lines at 847.67 and 849.95 keV and a weak one at 853.03 keV (Fig. 2). Comparing the intensities of the gamma rays observed in the Ge(Li) spectrum with those observed in the NaI(Tl) spectrum coincident with the 778-keV transition, one must conclude that both intense gamma rays at 850 keV are in coincidence with the 778-keV transition. The intensity balance does not allow the strong 847.67-keV line to be fitted between higher energy levels. Another fact confirming this new level is the energy difference of 128 keV between the 7656 and 7528-keV primary transitions, which is too small to fit the energy difference between the known 1498 and 1628-keV levels. The 1625.7-keV line is probably a ground-state transition, in which case the spin of the new level is limited to 1 or 2. From the angular correlation measurement of the unresolved 848 to 778 and 850 to 778-keV cascades,

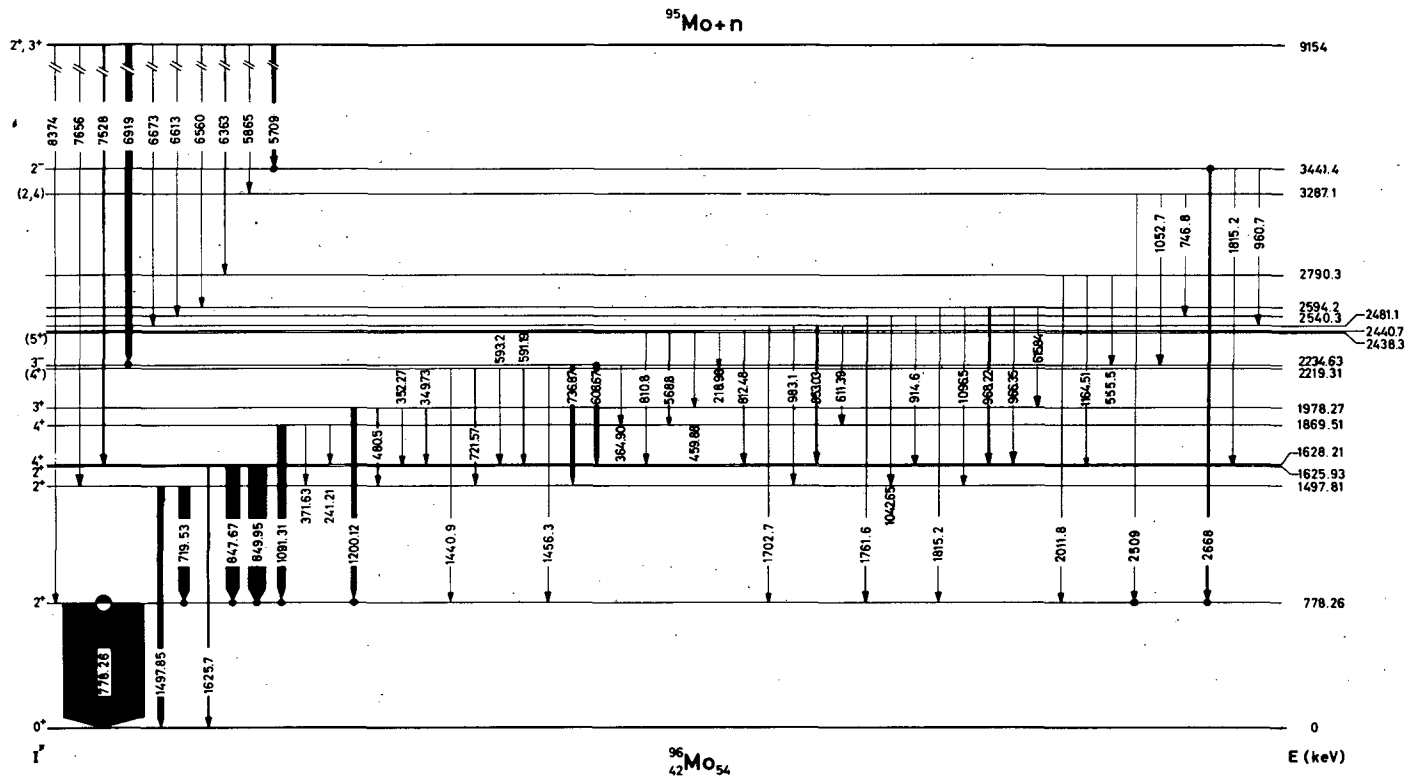


FIG. 1. Level scheme of ^{96}Mo observed in the reaction $^{95}\text{Mo}(n,\gamma)^{96}\text{Mo}$. Levels above 2.6 MeV found only by Ritz's combination principle are not shown.

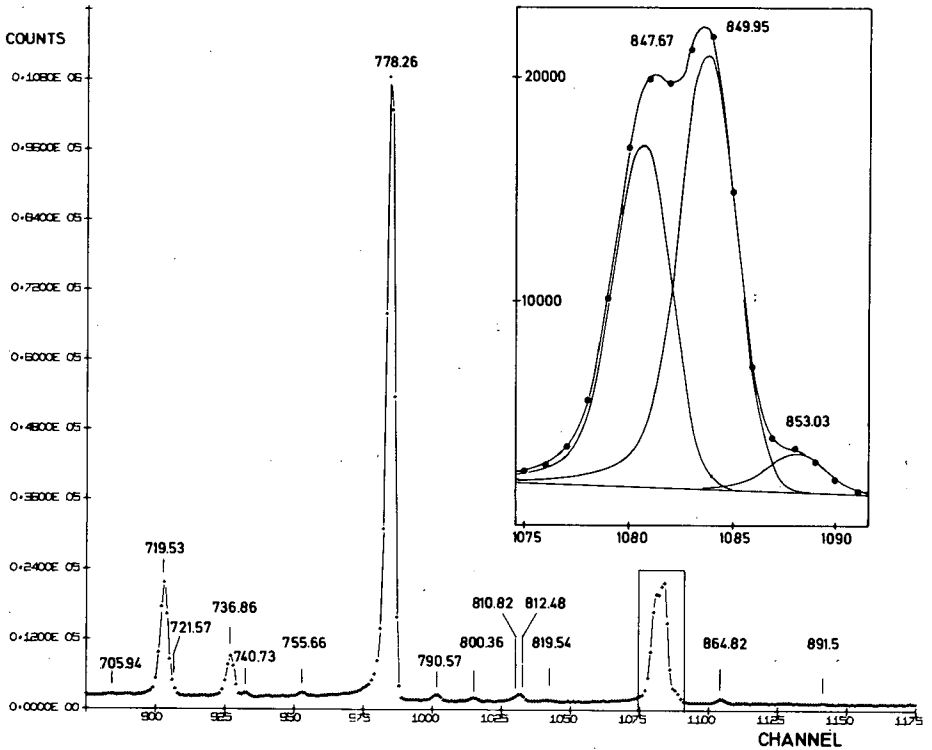


FIG. 2. Portion of the ^{96}Mo spectrum, measured with a Ge(Li) detector in the anti-Compton spectrometer [1]. The inset shows the triplet at 850 keV with computer fit analysis (solid line).

the spin 1 for the 1626-keV level is ruled out (Fig. 3). Assuming that the 850-keV transition de-exciting the 4^+ level is a pure quadrupole radiation, the mixing parameter of the 848-keV line is near 1. This value implies a positive parity for the 1626-keV level and should be compared with the quadrupole admixture of only 15% ($\delta \approx 0.45$) found for the 720-keV transition from the 1498-keV level. This shows that the new level has much more collective character than the second 2^+ state. The spin/parity values of 4^+ and 3^+ for the levels at 1869.51 and 1978.27 keV, respectively, found in beta decay [4, 5], could be confirmed by angular correlation measurements of the 1091 to 778 and 1200 to 778-keV gamma cascades. An additional transition of 352.27 keV from the 3^+ level to the 1626-keV level could be assigned. Probably this transition is identical with the 351.9-keV line observed in the decay of ^{96}Nb and ^{96m}Tc , but placed in a different position [4]. The energy of the 2234.63-keV level corresponds with the energy value of the 3^- octupole vibrational state at 2.25 MeV found in (d, d') measurements [7]. The negative parity of this level is confirmed by the assumption of multipolarity E1 for the strong primary 6919-keV transition feeding this level from the positive parity capture state. Between 2.6 and 3.6 MeV a large number of levels can easily be obtained by applying Ritz's combination principle. Only three levels,

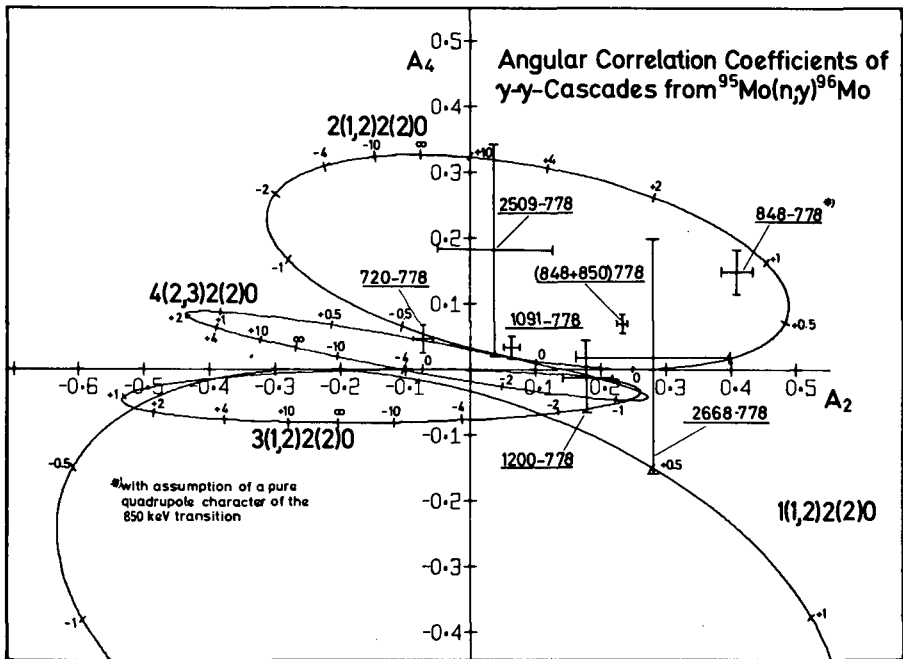


FIG. 3. Angular correlation measurements on ^{96}Mo cascades with the 2-0 transition 778 keV. The crosses show positions of the measured A_2 , A_4 coefficients with errors in the A_2 , A_4 plane; solid lines are theoretical values as functions of the mixing parameters δ .

namely those at 2790.3, 3287.1 and 3441.4 keV, have been taken over in the level scheme, whose existence was confirmed either by coincidence measurements or by the feeding with intense primary gamma rays. The spin determinations of the levels at 2790.3 and 3287.1 keV are not unique. For the latter, with the 2509 to 778-keV cascade, spin 2 seems very probable, but spin 4 may also be possible, as shown in Fig. 3. The 2668-keV transition is supposed to be a pure E1 transition because of its high intensity. This will give us spin and parity 1^- , 2^- or 3^- for the 3441.4-keV level. Because M2 admixtures to an E1 radiation are usually very weak, one would expect a δ -value near 0 for the 2668-keV radiation. With this assumption one can extract from the angular correlation measurement, despite the great errors, a spin sequence of 2-2-0 for the 2668 to 778-keV cascade. Further coincidence measurements with two Ge(Li) detectors are in progress and should be useful in adding to and confirming this level scheme.

3. RESULTS FROM $^{97}\text{Mo}(n,\gamma)^{98}\text{Mo}$

In the ^{98}Mo level scheme (Fig. 4) the first excited level at 734.77 keV has the spin/parity 0^+ [8]. The existence of this remarkable level is assured by the weak primary 7909.6-keV transition (the binding energy of

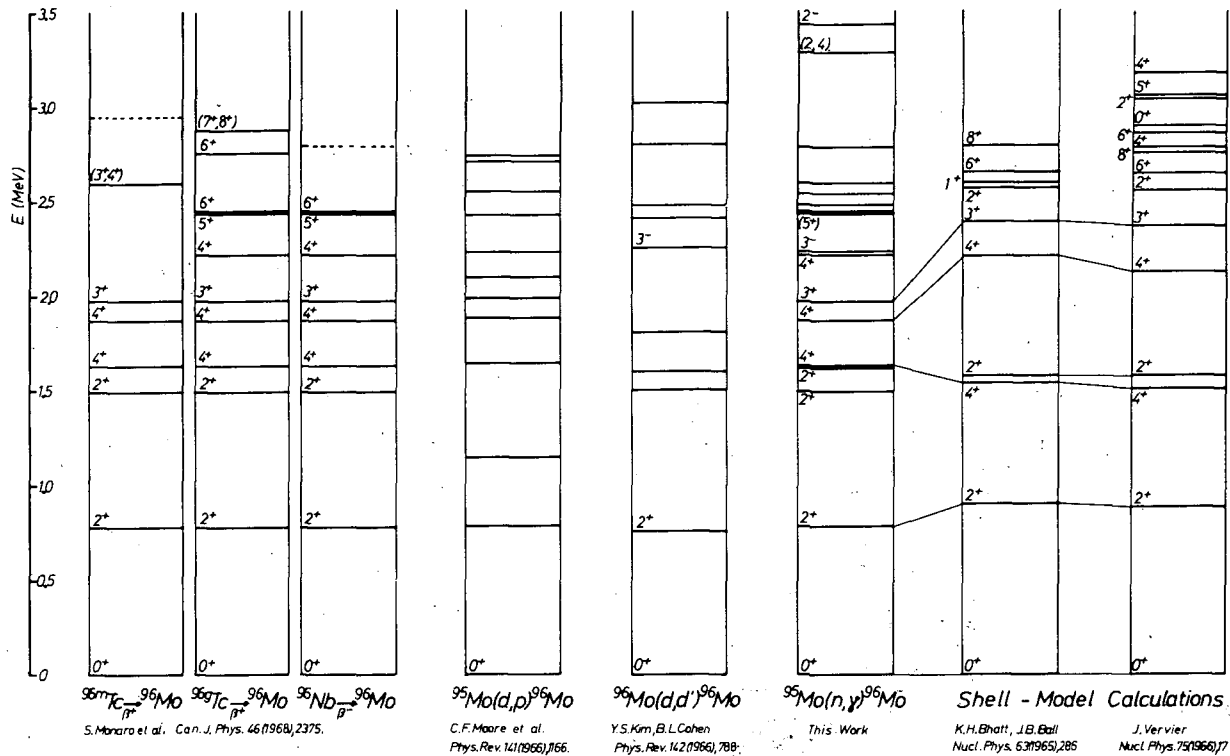


FIG. 5. ^{96}Mo level schemes found by different reactions [4, 7, 12] compared with shell-model calculations from Refs [10, 11].

4. COMPARISON WITH THEORETICAL CALCULATIONS

When looking at the level schemes of ^{96}Mo and ^{98}Mo one finds levels which cannot be explained by vibrational models, such as one of the two 2^+ states around 1.5 MeV in ^{96}Mo and the low-lying 0^+ state at 735 keV in ^{98}Mo . As these two nuclei are not too far off the closed neutron shell $N = 50$ and the semi-closed proton shell $Z = 40$, one would expect that the level scheme will be reproduced by the shell-model. Bhatt and Ball [10] and Vervier [11] have performed shell-model calculations, based on the $^{90}_{40}\text{Zr}_{50}$ core. For nucleons outside this core they use residual interactions empirically determined from the known level schemes of $^{92}_{42}\text{Mo}_{50}$, $^{92}_{41}\text{Nb}_{51}$, and $^{92}_{40}\text{Zr}_{52}$ for the protons and neutrons in the $\pi 1g_{9/2}$ and $\nu 2d_{5/2}$ orbits, respectively. For ^{96}Mo the results of these calculations are shown in Fig. 5, together with the level schemes observed in different reactions [4, 7, 12]. The agreement is not very good. Again there is only one 2^+ level in the region of 1.5 MeV. The second 4^+ and the 3^+ levels observed between 1.8 and 2.0 MeV are reproduced with too high energies. This disagreement is very likely due to the increasing number of neutrons outside the closed shell. For ^{98}Mo with the closed subshell $\nu 2d_{5/2}$ the theory expects a simple level scheme with a spin sequence 0^+ (ground state), 2^+ , 4^+ , 6^+ , 8^+ , according to a pure proton excitation to higher orbits. This is in complete contradiction to the experimental results and shows that the influence of the subshell closure cannot be very significant.

5. FINAL REMARKS

Further investigations of the (n, γ) reaction with the odd-mass molybdenum isotopes are in progress and will give reliable information of higher levels. In addition, attempts should be made to extend shell-model calculations by involving admixtures of further nucleon configurations to improve the reproduction of experimentally found levels.

REFERENCES

- [1] MICHAELIS, W., HORSCH, F., "High-precision neutron capture gamma-rays spectroscopy using germanium detectors in Compton-suppression technique", these Proceedings.
- [2] SCHMIDT, H., HECK, D., "Angular correlation measurements on gamma-ray cascades following thermal neutron capture", these Proceedings.
- [3] KRÜGER, G., ZIPF, G., Rep. KFK 371 (1965).
- [4] MONARO, S., BARETTE, J., BOUTARD, A., Can. J. Phys. **46** (1968) 2375.
- [5] SIMONS, L., HOLLARD, R.E., WENDT, G., SPRING, E., KÄLD, L., HAGEBØ, E., Nucl. Phys. **39** (1962) 130.
- [6] EARLE, E.D., MONARO, S., Rep. AECL 2639.
- [7] KIM, Y.S., COHEN, B.L., Phys. Rev. **142** (1966) 788.
- [8] HÜBENTHAL, K., BERTHIER, J., HOCQUENHEIM, J.C., MOUSSA, A., Compt. r. Acad. Sci. **265B** (1967) 162.
- [9] HÜBENTHAL, K., MONNAND, E., MOUSSA, A., to be published in Nucl. Phys.
- [10] BHATT, K.H., BALL, J.B., Nucl. Phys. **63** (1965) 286.
- [11] VERVIER, J., Nucl. Phys. **75** (1966) 17.
- [12] MOORE, C.F., RICHARD, P., WATSON, C.E., ROBSON, D., FOX, J.D., Phys. Rev. **141** (1966) 1166.

THE LEVEL STRUCTURE OF ^{116}In FROM THE $^{115}\text{In}(n, \gamma)$ REACTION

A. FUBINI, M. GIANNINI, E. IVANOV*, M. POPA*,
D. PROSPERI, V. RADO
Laboratorio di Fisica Nucleare Applicata,
Centro di Studi Nucleari della Casaccia,
Comitato Nazionale per l'Energia Nucleare,
Rome, Italy

Abstract

THE LEVEL STRUCTURE OF ^{116}In FROM THE $^{115}\text{In}(n, \gamma)$ REACTION. The gamma spectra resulting from thermal neutron capture in natural indium were measured with lithium-drifted germanium detectors. The energies and intensities of about 320 gamma lines in the ranges from 60 - 1300 and 2100 - 6700 keV were determined. The high-energy spectrum was used to identify 19 new levels below 1100 keV. A computer code which applies the Ritz combination method has been used to fit the energies of the low-lying excited levels.

The dependence on the excitation energy of the E1 and M1 reduced widths has been studied. A bump has been observed for M1 transitions leading to final levels with a neutron configuration of $1=2$ orbital angular momentum. This has been explained in terms of $g_{7/2} \rightarrow g_{9/2}$ spin-flip transitions.

1. INTRODUCTION

The present work reports the results of a study of the reaction $^{115}\text{In}(n, \gamma)^{116}\text{In}$ and is a part of a programme concerning odd-odd nuclei performed by the RC-1 reactor of CNEN.

Previous measurements of the $^{115}\text{In}(n, \gamma)$ capture gamma rays were performed by bent-crystals in the 50 to 450-keV region [1] and by Ge(Li) detectors in the 200 to 6500-keV region [2]. In the latter study, however, no M1 transitions to the low-lying levels were observed. The conversion-electron lines of the low-energy transitions ($E_{\gamma} \leq 400$ keV) were also measured [3].

Moreover, the complementary $^{115}\text{In}(d, p)$ reaction has been recently studied by means of a high-resolution magnetic spectrograph [4]. In this experiment a large number of excited levels in ^{116}In have been identified.

2. EXPERIMENTAL ARRANGEMENT AND PROCEDURE

A target 0.2 mm thick of natural In metal (99.999% pure), was placed in a cylindrical box containing ^6LiF enriched to 93% and B_4C . The box was then inserted in the neutron beam of the through tube facility shown in Fig. 1. With this geometry, we had a neutron flux of $\approx 4 \times 10^5$ n cm $^{-2}$ sec $^{-1}$ over an area of 4 cm 2 .

* IAEA fellowship, on leave of absence from the Institute of Atomic Physics, Bucharest, Romania.

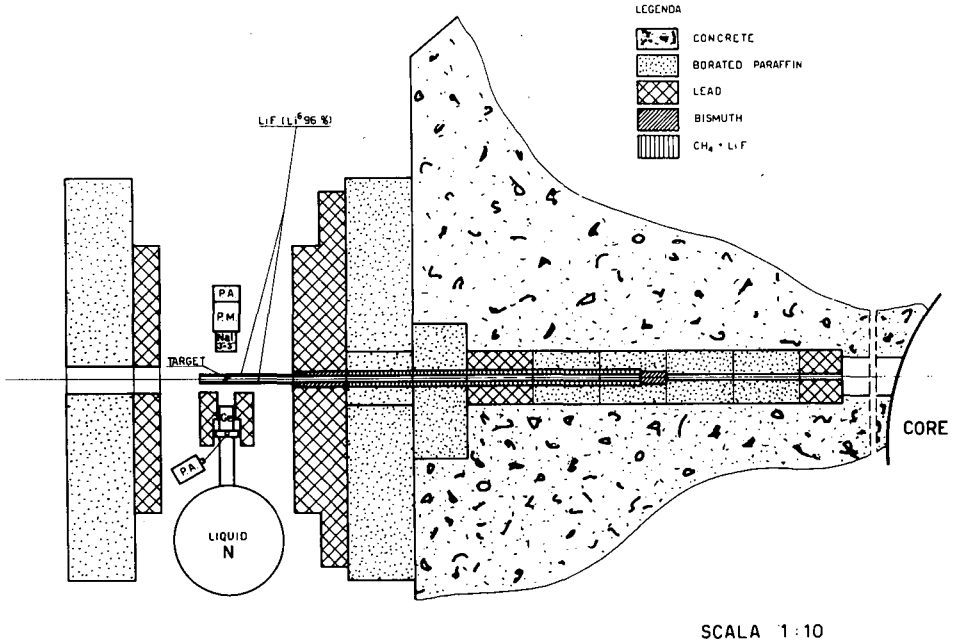


FIG. 1. Experimental arrangement for measuring neutron capture gamma rays with a Ge(Li) detector.

The gamma rays were detected with a 30-cm³ Ge(Li) coaxial diode. The pulses from the detector were amplified in a Tennelec electronic chain. The output of the biased amplifier was analysed by a 4096-channel system. The low-energy spectrum (60 - 1300 keV) was measured at a gain of ≈ 0.7 keV/channel. The high-energy spectrum (≥ 2100 keV) was analysed both by a single Ge(Li) detector and a pair spectrometer; in these measurements the gain was, respectively, 3.6 and 2 keV/channel. The resolution in the experimental condition was ≈ 10 keV at 6 MeV and ≈ 4 keV at 1 MeV.

All targets used for low-energy measurements have been irradiated for about 10 minutes; in this way the activation of the 54-min isomer is about 8% of its saturation value.

The energy of the transitions in the low-energy region has been obtained by using as calibration points the gamma lines of the isomer [5] and the capture gamma-lines observed in the bent-crystal experiment [1]; in the high-energy region the lines of the $^{35}\text{Cl}(n, \gamma)$ reaction and the highest lines of the isomer have been used; the comparison with the lines of the $^{35}\text{Cl}(n, \gamma)$ reaction was performed by using a sample consisting of Cl+In. The non-linearities of the system have been studied and the required corrections made. The accuracy in the energy scale is about 1 keV in the high-energy region, about 0.2 keV in the 50 to 200-keV region and, finally, about 0.3 keV in the 400 to 1300-keV region. The position of resolved peaks of high intensity has been determined to an accuracy of 0.2 channel. The position of the lines, obtained by means of a decomposition, is less determinate, the uncertainty being at most about

1 channel. Moreover, the total error in the energies ranges from 0.25 to 0.35 keV in the low-energy region and is about 1.5 keV in the high-energy region.

The absolute intensities of transitions have been obtained by a comparison with the lines of the isomer; the values 157 ± 4 b and 197 ± 5 b have been adopted for activation and capture cross-sections. Corrections for self-absorption of gamma lines have been introduced. The efficiency curve here employed in the 60 to 2600-keV region has been determined by standard radioactive sources; for the high-energy region the $^{35}\text{Cl}(n, \gamma)$ reaction has been used. The error in the absolute intensity of the resolved peaks has been estimated to be about 30%.

3. EXPERIMENTAL RESULTS

A part of the low-energy gamma-ray spectrum from the $^{115}\text{In}(n, \gamma)$ reaction is shown in Fig. 2; the results are summarized in Table I. For completeness previous results obtained with (n, γ) reactions [1, 2] are included in the table. The errors assigned to the energies and intensities have been discussed in the previous section.

In the region of 60-400 keV we have a good agreement with the results obtained with the bent-crystal technique [1].

A part of the high-energy spectrum is shown in Fig. 3 and the results are reported in Table II. Each of these spectra has been obtained by adding more different measurements of about 7 hours each; the sum of the single measurements has been performed with the aid of a computer program which introduces linear shifts in the channels, reducing the effect of the drift in the electronic bias. Previous results obtained by (n, γ) and (d, p) reactions are also included in Table II.

The energy of the levels in ^{116}In deduced from the energy of the primary gamma rays is reported in column 4 of Table II. Because of the large experimental uncertainty in the neutron separation energy, the level energies have been calculated by using the value $Q = 6779.5 \pm 1.5$ keV established in the present work (see next section). The standard deviation of our energies from those of Rasmussen et al. is about 2.3 keV.

We have studied also the intermediate energy region of 1300-2100 keV. No evident gamma-ray line has been observed in this energy range. The 1300 to 2100-keV spectrum is not shown here.

4. ANALYSIS OF RESULTS

By assuming as excitation energies the Moorhead values [4] and using the gamma-ray energies of Table II, a mean value $Q = 6779.5 \pm 1.5$ keV is obtained for the neutron separation energy, in agreement with the result $Q = 6805 \pm 30$ keV, obtained in a (d, p) experiment [6].

A simple inspection of the level spins and parities assigned by Moorhead et al. allows us to conclude that all the transitions of highest energy (6655, 6560, 6504, 6470 and 6351 keV) have M1 multipolarity; they were not previously observed because of their low intensities. The comparison with the (d, p) experiment allows us to identify the multipolarity of about 20 E1 and M1 transitions in the 6700 to 5300-keV energy range.

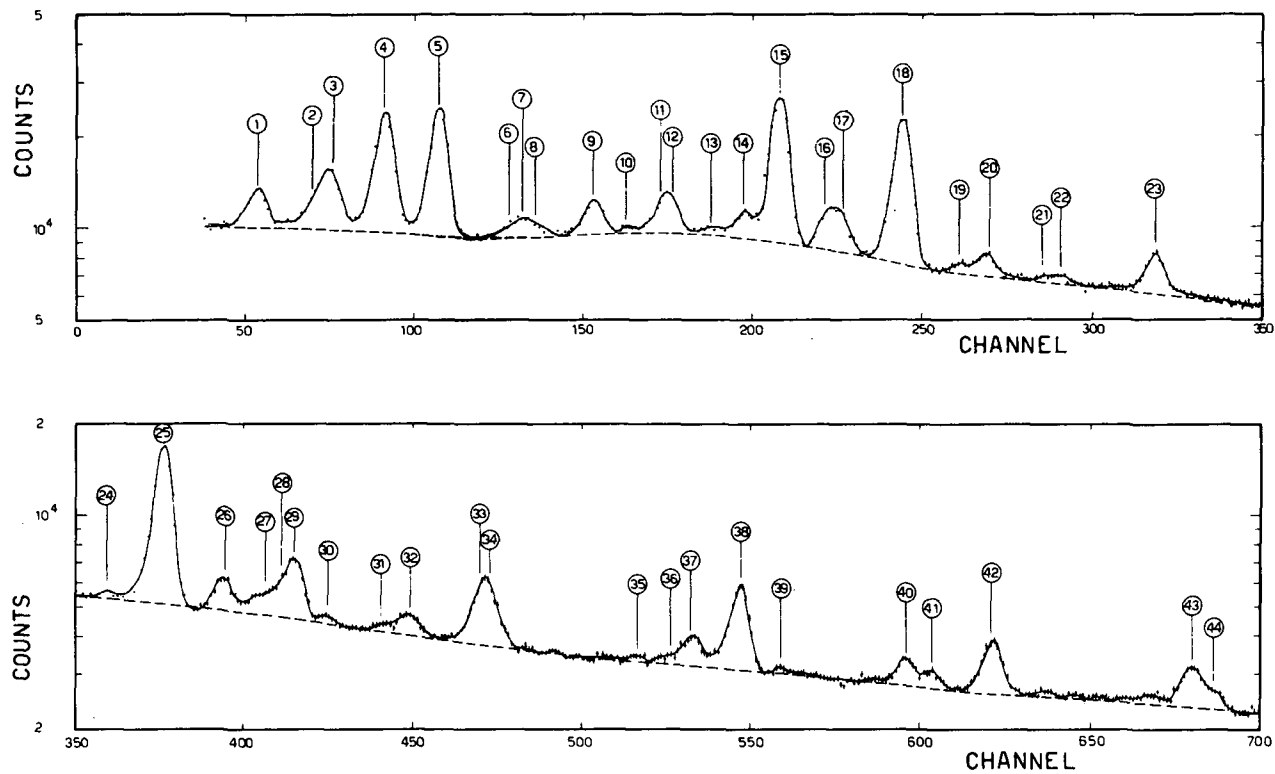


FIG. 2. Neutron capture gamma-ray spectrum from $^{115}\text{In}(n, \gamma)^{116}\text{In}$ in the range 60 - 480 keV.

The energies of the most intense E1 and M1 transitions agree with those of Rasmussen et al. Moreover, we observe an E2 transition to the 505-keV level.

Nineteen new levels not observed in the (d, p) experiment have been identified below 1100 keV; assuming the populating transitions to be E1 or M1 and the capturing state to be 5^+ , they are all (4, 5, 6) $^+$.

A tentative decay scheme has been constructed for the levels below 1 MeV using a computer program which applies the Ritz combination method and is a trivial modification of a previously published program [7]. Figure 4 shows the best values obtained for the levels directly observed in the (d, p) or (n, γ) experiments. The total error on the energy of these levels is about 0.8 keV.

Table III shows the assignment of configuration made on the basis of deuteron-stripping results [4]. We have essentially proton groups displaying stripping patterns with $l = 0$, $l = 2$, and $l = 5$, probably corresponding to $s_{1/2}$, $d_{3/2}$, $d_{5/2}$ and $h_{11/2}$ configurations.

The transitions leading to levels of neutron configurations with $l = 0, 2, 4$ are assumed to be M1, while mixtures of higher multipolarity (especially E2) are neglected. This assumption is based on the results of average resonance-capture experiments [8] which show that E2 transitions are much weaker than M1 transitions in ^{96}Mo , ^{98}Mo , ^{106}Pd , ^{136}Ba , ^{166}Ho and ^{168}Er . Further, the $l = 5$ transitions are assumed to be E1.

Let us now define the average reduced width for E1 and M1 transitions by the relationship

$$\bar{K}_{\sigma 1} = \langle \Gamma_{\gamma if} E_{\gamma}^{-\alpha} D_i^{-1} \rangle = \frac{1}{n_i \cdot n_f} \sum_i^{n_i} \sum_f^{n_f} \left(\frac{\Gamma_{\gamma if}}{E_{\gamma}^{\alpha}} \right) D_i^{-1} \quad (\sigma = E, M) \quad (1)$$

where D_i is the average spacing of the levels at the energy of the initial level i , $\Gamma_{\gamma if}$ is the radiation width (E1 or M1) for the transition connecting i and f levels; for E1 and M1 transitions we assume $\alpha = 5$ and $\alpha = 3$. In thermal neutron capture experiments the average on the initial states must be omitted so that we are confined to estimate

$$\bar{K}_{\sigma 1} = \frac{1}{n_f} \sum_f^{n_f} \left(\frac{\Gamma_{\gamma if}}{E_{\gamma}^{\alpha}} \right) D_i^{-1} \quad (2)$$

Two different kinds of information on the E1 and M1 reduced widths can be obtained by capture of thermal neutrons. The first is the ratio

$$R = \frac{\bar{K}(E1)}{\bar{K}(M1)} = \frac{\langle \Gamma_{\gamma if} / E_{\gamma}^5 \rangle_{E1}}{\langle \Gamma_{\gamma if} / E_{\gamma}^3 \rangle_{M1}} \quad (3)$$

and the second is the average absolute intensity of both M1 and E1 transitions. The current estimate for R , as given by Bollinger [8], is

$$R \approx 0.035 \left(\frac{A}{100} \right)^{8/3} \approx 0.052 \quad (4)$$

TABLE I. NEUTRON CAPTURE GAMMA RAYS
 IN THE 60 TO 1300-keV REGION

Gamma transition	E_γ (keV)			I_γ ($\gamma/100$ cap.)	
	Present work	Ref. [3]	Ref. [2]	Present work	Ref. [2]
1	60.7			6.31	
2	72.1			3.58	
3	75.9			6.50	
4	85.7	85.608 90.94		10.37	
5	96.3	96.05		8.86	
6	110.3	110.75 112.06		0.41	
7	113.0	112.45		0.41	
8	115.3	114.94 122.00		0.41	
9	126.3	126.37		1.44	
10	133.0			(0.18)	
11	139.9	140.44		0.88	
12	141.6	141.15		0.88	
13	149.1			(0.26)	
14	155.4	155.27		0.99	
15	162.2	162.39		7.84	
16	171.7	171.07 173.83		1.12	
17	174.7	175.09		1.11	
18	186.1	186.18		7.30	
19	197.0	196.60		0.26	
20	202.7	202.45	203.9	0.75	0.48
21	213.4		214.4	0.20	0.25
22	216.8		219.1 232.3	0.40	0.28 0.25
23	235.0		236.3	1.69	0.48
24	261.9			0.30	
25	273.0	272.97	273.3	10.60	7.07
26	285.3		285.8	1.35	0.22
27	291.9			0.59	
28	295.9			0.72	
29	298.5		298.4	2.40	1.85

TABLE I (cont.)

Gamma transition	E_γ (keV)			I_γ ($\gamma/100$ cap.)	
	Present work	Ref. [3]	Ref. [2]	Present work	Ref. [2]
30	305.1			0.32	
31	315.6			0.23	
32	321.2		320.4	0.75	0.16
33	334.8			1.02	
34	336.5	335.90	335.6 356.9	2.94	2.3 0.11
35	365.5			0.24	
36	372.0		368.2	0.28	0.16
37	375.7	376.30	374.3	1.35	0.16
38	385.3	385.27	385.3	5.06	1.94
39	393.3		401.8	0.25	0.06
40	411.3			0.27	
41	417.5 ^a		417.2	-	7.37
42	422.4			0.74	
43	434.0	434.17	434.0 445.1	2.83	1.03 0.09
44	465.3			0.39	
45	473.0		473.5	3.17	1.53
46	476.9			0.92	
47	491.4		491.3	1.14	0.62
48	493.4			0.77	
49	510.5 ^b			10.23	
50	513.4			4.60	
51	519.0			1.40	
52	522.9			0.91	
53	541.3			0.40	
54	547.1		547.2	0.49	0.34
55	550.0			0.54	
56	556.9		557.5	2.10	1.41
57	559.6			1.01	
58	568.0			1.01	
59	577.4		578.5	1.09	0.21
60	590.1			0.47	

TABLE I (cont.)

Gamma transition	E_γ (keV)			I_γ ($\gamma/100$ cap.)	
	Present work	Ref. [3]	Ref. [2]	Present work	Ref. [2]
61	595.7			1.01	
62	601.0			0.80	
63	603.3			1.48	
64	608.9		608.3	1.66	0.98
65	622.3		622.8	0.42	0.20
66	625.3			0.51	
67	633.0		634.2	0.78	0.51
68	635.4			0.80	
69	647.5		645.6	0.35	0.25
70	656.0			0.44	
71	658.7			0.33	
72	693.5			0.70	
73	696.5			0.47	
74	700.4			0.29	
75	707.7			0.42	
76	715.4			0.49	
77	718.9		717.8	0.61	0.23
78	729.0		727.7	0.43	0.13
79	744.1			0.25	
80	750.0			0.81	
81	759.9		761.6	0.54	0.12
82	764.9			0.59	
83	772.0			0.46	
84	782.4			0.34	
85	805.0			0.17	
86	819.1 ^a		819.5		2.77
87	845.8			0.52	
88	848.7		848.0	0.73	0.17
89	853.7			0.26	
90	875.9		875.6	0.35	0.12
91	885.8		886.0	0.44	0.59
92	926.7			0.27	
93	929.9			3.70	
94	934.1			0.29	

TABLE I (cont.)

Gamma transition	E_γ (keV)			I_γ ($\gamma/100$ cap.)	
	Present work	Ref. [3]	Ref. [2]	Present work	Ref. [2]
95	938.3			0.57	
96	943.7			0.70	
97	963.6			0.64	
98	966.0			0.50	
99	968.5			0.50	
100	973.0		973.6	0.47	0.14
101	990.2			0.42	
102	993.6			0.32	
103	1008.6		1007.9	0.39	0.14
104	1023.7			0.48	
105	1026.7			0.47	
106	1029.6			0.38	
			1067.8		0.16
107	1077.1		1077.2	0.29	0.54
108	1097.1 ^a			-	12.20
109	1173.5			1.20	
			1245.8		0.15
110	1293.4 ^a		1293.4		17.97

^a Decay of ^{116}Sn

^b Annihilation line

It should be pointed out that this relationship may be in error as much as a factor 3 for some nuclides. The experimental evaluation of R is $R = 0.035$, in reasonable agreement with the estimate of Eq. (4).

The most recent results on the absolute intensities can be summarized by the relationships

$$\bar{K}_{M1} = \langle \Gamma_{\gamma if} E_\gamma^3 D_i^{-1} \rangle = 2 \times 10^{-8}$$

$$\bar{K}_{E1} = \langle \Gamma_{\gamma if} E_\gamma^5 D_i^{-1} \rangle = \begin{cases} 6.1 \times 10^{-15} A^{8/3}, & \text{from photonuclear data} \\ 3.2 \times 10^{-15} A^{8/3}, & \text{from resonance capture data [8]} \end{cases} \quad (5)$$

where E_γ is in MeV and both D_i and $\Gamma_{\gamma if}$ are in eV. The present study allows us to conclude that in ^{115}In we have

$$\bar{K}_{M1} = 2.7 \times 10^{-8} \qquad \bar{K}_{E1} = 2.9 \times 10^{-15} A^{8/3}$$

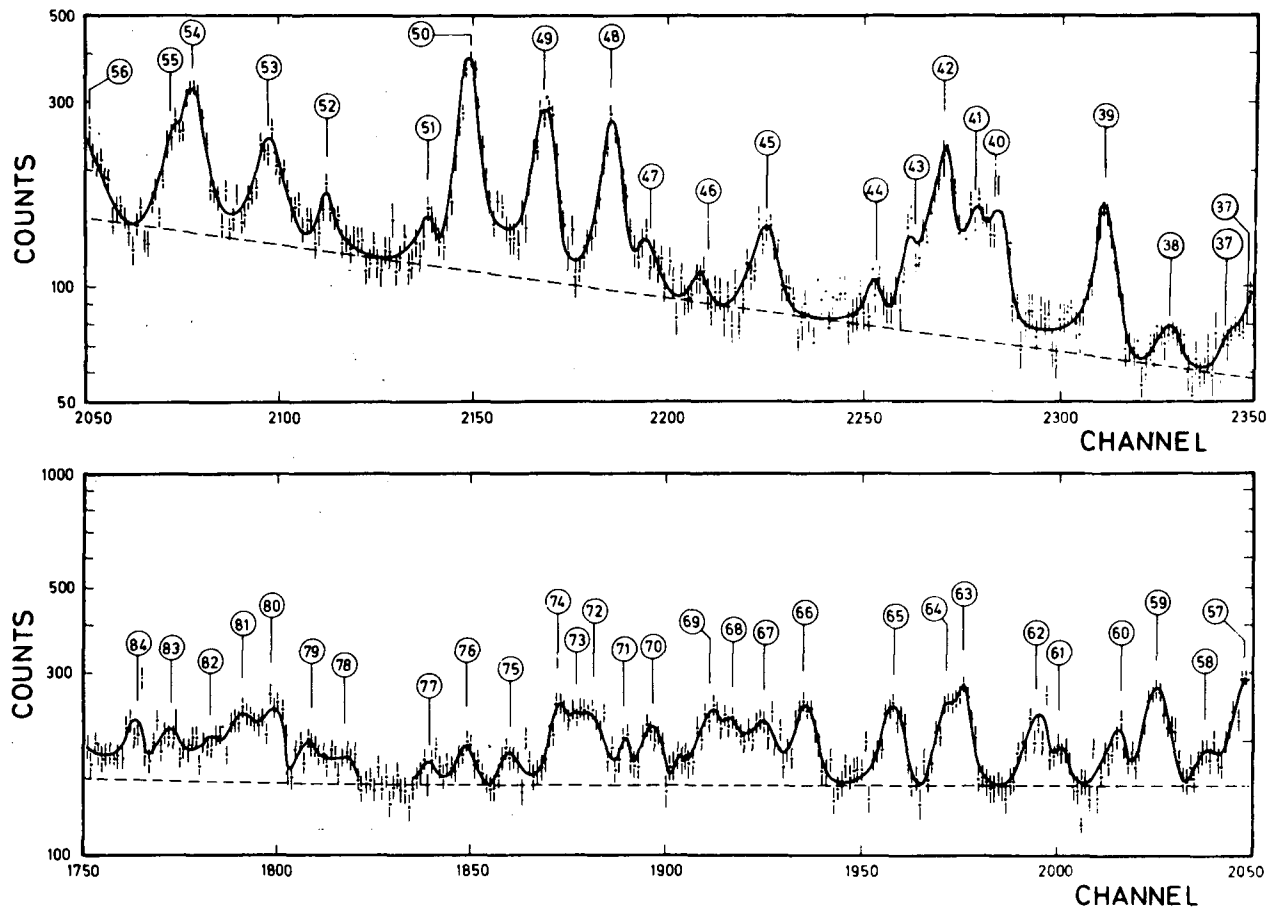


FIG. 3. Neutron capture gamma-ray spectrum from $^{115}\text{In}(n, \gamma)^{116}\text{In}$ in the range 4400 - 5500 keV obtained by a pair spectrometer.

TABLE II. NEUTRON CAPTURE GAMMA RAYS
IN THE 2100 TO 6700-keV REGION

Gamma transition	E_γ (MeV)	I_γ ($\gamma/100$ cap.)	Level energy (MeV)		Level spin	
			Present work	Ref. [4]	Ref. [4]	Present work
1	6.6555	0.04	0.124	0.125	5^+	
2	6.5597	0.03	0.220	0.221	4^+	
2 ^I	6.5370	0.02	0.242			
3	6.5037	0.02	0.276	0.273 0.288	$4^+ 5^+$ 8^-	
4	6.4696	0.03	0.310	0.313 0.349	5^+ $5^- 6^- 7^- 9^-$	
5	6.4107	0.18	0.369	0.366 0.373	$5^- 6^- 7^- 9^-$ $9^- 10^-$	$5^- 6^-$
6	6.3913	0.05	0.388			
6 ^I	6.3740	0.03	0.405			
6 ^{II}	6.3510	0.04	0.428	0.426	4^+	
7	6.3247	0.14	0.455	0.460	$5^- 6^- 7^- 9^-$	$5^- 6^-$
8	6.2754	0.04	0.504	0.508	3^+	
9	6.2524	0.02	0.527			
10	6.2281	0.13	0.552	0.556	$3^- 4^- 5^-$	$4^- 5^-$
11	6.1959	0.04	0.585			
12	6.1727	0.04	0.607			
13	6.1367	0.11	0.643			
14	6.1240	0.05	0.655	0.650 0.666	6^+ $5^- 6^- 7^- 9^-$	
15	6.1005	0.02	0.680			
16	6.0796	0.03	0.699			
17	6.0534	0.06	0.726	0.729	$3^- 4^- 5^-$	$4^- 5^-$
18	6.0438	0.05	0.736	0.761	$2^+ 7^+$	
18 ^I	6.0010	0.04	0.778			
18 ^{II}	5.9860	0.03	0.793	0.790	$2^+ 7^+$	$4^+ 5^+ 6^+$
19	5.9482	0.04	0.831			
20	5.9272	0.05	0.852			
21	5.8913	1.10	0.888			
22	5.8687	0.08	0.911	0.913	$2^+ 7^+$	$4^+ 5^+ 6^+$
23	5.8368	0.09	0.943	0.951	$3^- 6^-$	

TABLE II (cont.)

Gamma transition	E_γ (MeV)	I_γ ($\gamma/100$ cap.)	Level energy (MeV)		Level spin	
			Present work	Ref. [4]	Ref. [4]	Present work
24	5.8100	0.08	0.969			
25	5.7700	0.30	1.010	1.007	$3^- 6^-$	$4^- 5^- 6^-$
26	5.7529	0.03	1.026			
27	5.7312	0.09	1.048			
28	5.7114	0.02	1.068	1.062	$2^- 7^-$	$4^- 5^- 6^-$
28 ^I	5.7003	0.02	1.079	1.076		
29	5.6875	0.03	1.092			
29 ^I	5.6710	0.04	1.108	1.104	$2^+ 7^+$	$4^+ 5^+ 6^+$
29 ^{II}	5.6580	0.04	1.121			
29 ^{III}	5.6460	0.03	1.133	1.144	$2^+ 7^+$	
29 ^{IV}	5.6220	0.03	1.157			
30	5.6104	0.06	1.169			
31	5.5961	0.04	1.183	1.193	$2^+ 7^+$	
32	5.5818	0.16	1.198			
33	5.5719	0.15	1.207	1.208	$2^+ 7^+$	$4^+ 5^+ 6^+$
34	5.5505	0.04	1.229			
35	5.5274	0.08	1.252			
36	5.4988	0.25	1.281	1.279	$8^+ a$	
37	5.4822	0.13	1.297	1.292	$2^+ 7^+$	$4^+ 5^+ 6^+$
37 ^I	5.4740	0.04	1.305	1.323	$(2)^-$	
38	5.4411	0.05	1.339	1.347 1.364	$(1)^-$ $4^+ 5^+$	
39	5.4095	0.30	1.370	1.371	$4^+ 5^+$	
40	5.3574	0.21	1.422			
41	5.3476	0.18	1.432			
42	5.3337	0.42	1.446	1.444	$2^+ 7^+$	$4^+ 5^+ 6^+$
43	5.3186	0.20	1.461	1.458	$2^- 7^-$	$4^- 5^- 6^-$
44	5.2990	0.08	1.480	1.497	$2^+ 7^+$	$4^+ 5^+ 6^+$
45	5.2466	0.19	1.533	1.539	$2^+ 7^+$	$4^+ 5^+ 6^+$
46	5.2171	0.05	1.562			

TABLE II (cont.)

Gamma transition	E_γ (MeV)	I_γ ($\gamma/100$ cap.)	Level energy (MeV)		Level spin	
			Present work	Ref. [4]	Ref. [4]	Present work
47	5.1896	0.07	1.590	1.598	2^+ 7^+	4^+ 5^+ 6^+
48	5.1717	0.48	1.607			
49	5.1392	0.62	1.640			
50	5.1023	0.81	1.677			
51	5.0808	0.09	1.699			
52	5.0324	0.13	1.747			
53	5.0059	0.37	1.773			
54	4.9680	0.46	1.811			
55	4.9560	0.21	1.823			
56	4.9166	0.10	1.863			
57	4.9100	0.40	1.869			
58	4.8912	0.81	1.898			
59	4.8686	0.30	1.911			
60	4.8505	0.18				
61	4.8198	0.14				
62	4.8082	0.23				
63	4.7735	0.34				
64	4.7660	0.28				
65	4.7398	0.34				
66	4.6969	0.35				
67	4.6791	0.31				
68	4.6629	0.20				
69	4.5522	0.32				
70	4.6240	0.22				
71	4.6100	0.14				
72	4.5954	0.25				
73	4.5871	0.24				
74	4.5778	0.29				
75	4.5547	0.11				
76	4.5338	0.12				
77	4.5117	0.08				
78	4.4744	0.14				
79	4.4577	0.17				

TABLE II (cont.)

Gamma transition	E_γ (MeV)	I_γ ($\gamma/100$ cap.)	Gamma transition	E_γ (MeV)	I_γ ($\gamma/100$ cap.)
80	4.4402	0.32	114	3.8344	0.10
81	4.4246	0.30	115	3.8092	0.13
82	4.4079	0.12	116	3.7901	0.21
83	4.3891	0.18	117	3.7730	0.17
84	4.3730	0.29	118	3.7675	0.14
85	4.3219	0.31	119	3.7410	0.19
86	4.3122	0.31	120	3.7141	0.12
87	4.3018	0.14	121	3.6944	0.13
88	4.2927	0.09	122	3.6806	0.18
89	4.2645	0.10	123	3.6547	0.11
90	4.2531	0.21	124	3.6297	0.09
91	4.2400	0.13	125	3.6143	0.17
92	4.2237	0.55	126	3.6066	0.08
93	4.2059	0.14	127	3.5895	0.12
94	4.1969	0.12	128	3.5428	0.19
95	4.1887	0.06	129	3.5324	0.07
96	4.1681	0.10	130	3.5009	0.21
97	4.1497	0.10	131	3.4792	0.10
98	4.1340	0.20	132	3.4489	0.11
99	4.1169	0.20	133	3.4426	0.17
100	4.1054	0.15	134	3.4351	0.18
101	4.0866	0.15	135	3.4235	0.13
102	4.0715	0.33	136	3.4159	0.07
103	4.0554	0.26	137	3.4006	0.07
104	4.0406	0.29	138	3.3942	0.11
105	4.0139	0.13	139	3.3802	0.11
106	4.0050	0.17	140	3.3722	0.15
107	3.9845	0.09	141	3.3537	0.18
108	3.9749	0.18	142	3.3465	0.24
109	3.9455	0.16	143	3.3283	0.22
110	3.9249	0.23	144	3.3226	0.11
111	3.9150	0.11	144 I	3.3149	0.09
112	3.8736	0.20	145	3.3048	0.30
113	3.8548	0.10	146	3.2897	0.31

TABLE II (cont.)

Gamma transition	E_γ (MeV)	I_γ ($\gamma/100$ cap.)	Gamma transition	E_γ (MeV)	I_γ ($\gamma/100$ cap.)
147	3.2747	0.17	175	2.8202	0.14
148	3.2641	0.18	176	2.8151	0.16
149	3.2558	0.09	177	2.8056	0.22
150	3.2414	0.21	178	2.7943	0.22
151	3.2340	0.17	179	2.7786	0.28
152	3.2087	0.23	180	2.7742	0.30
153	3.1905	0.24	181	2.7653	0.28
154	3.1805	0.10	182	2.7532	0.30
155	3.1599	0.15	183	2.7326	0.17
156	3.1487	0.16	184	2.7269	0.22
157	3.1213	0.14	185	2.6802	0.26
158	3.1116	0.11	186	2.6705	0.19
159	3.1021	0.23	187	2.5979	0.30
159 ^I	3.0889	0.10	188	2.5883	0.30
160	3.0739	0.17	189	2.5805	0.29
161	3.0658	0.12	190	2.5605	0.17
161 ^I	3.0492	0.12	191	2.5548	0.30
162	3.0386	0.12	192	2.5264	0.23
163	3.0308	0.13	193	2.5207	0.20
164	3.0130	0.19	194	2.4786	0.16
165	3.0022	0.13	195	2.4074	0.19
166	2.9875	0.12	196	2.3414	0.23
167	2.9814	0.24	197	2.3346	0.18
168	2.9646	0.14	198	2.2526	0.34
169	2.9265	0.26	199 ^b	2.2232	-
170	2.9040	0.29	200	2.2161	0.18
171	2.8860	0.19	201	2.1966	0.90
172	2.8817	0.11	202	2.1595	0.23
173	2.8457	0.22	203	2.1489	0.22
174	2.8323	0.28	204 ^c	2.1116	-

^a The existence of the transition is not compatible with the spin assigned in Ref. [5].

^b Background from the H(n, γ) reaction.

^c Decay from ^{116}Sn .

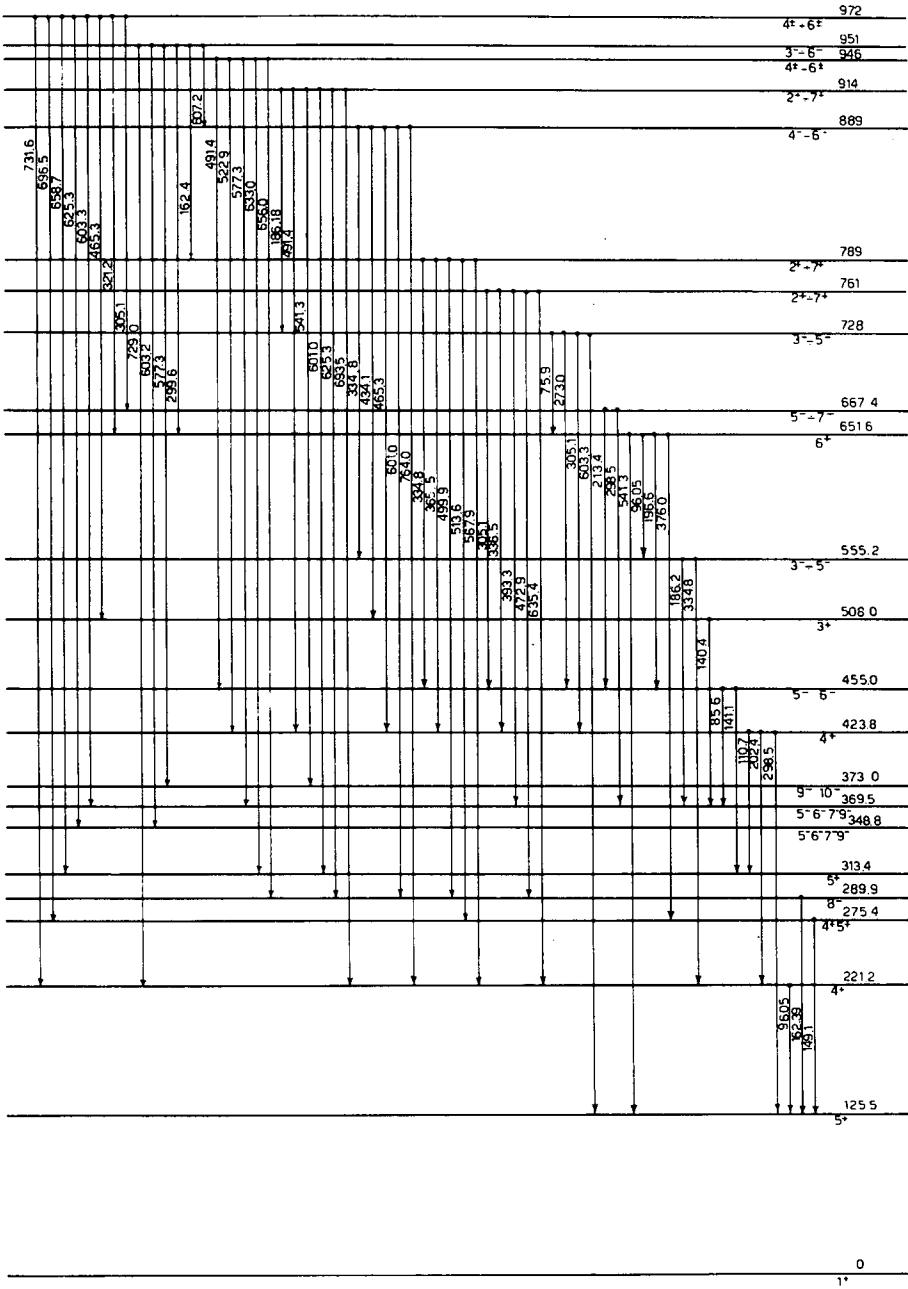


FIG. 4. Low-lying levels in ^{116}In .

TABLE III. NEUTRON ANGULAR MOMENTA [4] AND MULTIPARITIES OF GAMMA TRANSITIONS

Excitation energy (MeV)	ℓ of neutron	Type of transition
0	4	
0.125	0	M1
0.221	0; 2	M1
0.273	0	M1
0.313	2; 0	M1
0.366	5	E1
0.426	0; 2	M1
0.460	5	E1
0.508	2	E2
0.556	5	E1
0.650	2	M1
0.729	5	E1
0.790	2	M1
0.913	2	M1
1.007	1	E1
1.062	3	E1
1.104	2	M1
1.208	2	M1
1.292	2	M1
1.371	2	M1
1.444	2	M1
1.458	3	E1
1.539	2	M1
1.598	2	M1

these values have been obtained in an obvious way by using the experimental data $\Gamma_\gamma = 70$ meV and $D_1 = 16$ eV. Both our \bar{K}_{01} values are in agreement with the estimates (5). However, they depend on the absolute intensity normalization of the gamma transitions which is a possible source of large errors.

Figure 5 shows the \bar{K}_{01} values for transitions of fixed l . No clear dependence on l can be inferred from the analysis of this figure; however, the M1 transitions with $l = 2$ show an evident systematic increase with the excitation energy E up to about 1.5 MeV. In the range $E = 0.3 - 1.5$ MeV, \bar{K}_{M1} varies by a factor ≈ 30 . Moreover, around 1.5 MeV we observe several enhanced M1 transitions of intensity comparable to that of E1 transitions. A similar situation has been recently observed in several Sn isotopes [9].

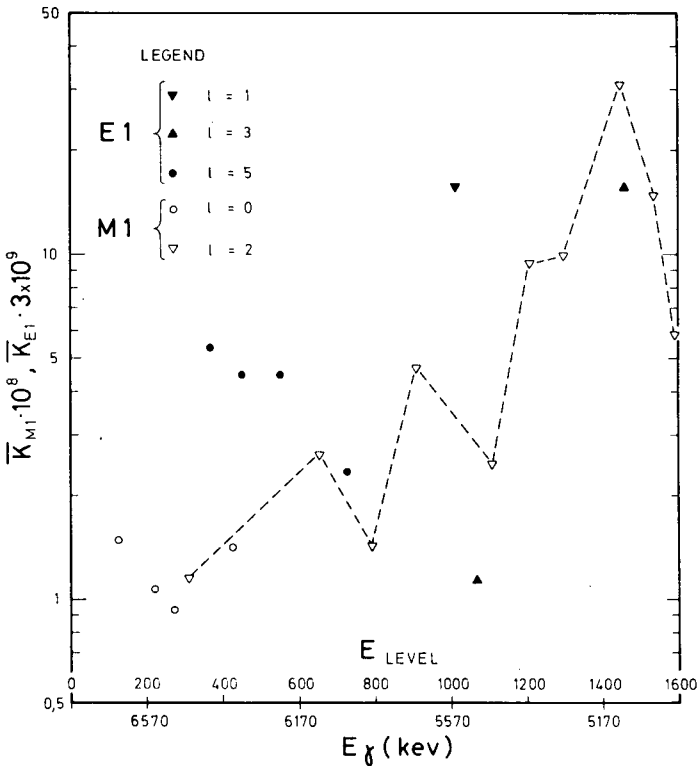


FIG. 5. Reduced width versus gamma-ray energy for E1 and M1 transitions of different l (Arbitrary units).

Let us finally note that the observed energy dependence is certainly real, because the random fluctuations cannot cause the data points to deviate from a constant value as much as they do. Unfortunately there are no published theoretical calculations concerning M1 radiation that, taking into account nuclear structure effects, can reproduce the observed energy dependence.

This behaviour is probably related to the bump observed at about $E_\gamma = 5.5$ MeV in the gamma-ray spectra of several nuclei in the same mass region ($110 \leq A \leq 140$). A possible explanation can be obtained by assuming that the incoming neutron excites a neutron particle-hole configuration of the type $(g\ 9/2)^{-1} (g\ 7/2)$; we then have spin-flip M1 neutron transitions, $g\ 7/2$ to $g\ 9/2$, for which the splitting is about 5 MeV. The increasing of the M1 reduced width observed in ^{116}In is finally connected to the increasing mixing of the configuration (^{115}In ground state) + $(s\ \frac{1}{2}$ neutron). Also more complex particle-hole excitations probably contribute to the observed behaviour.

REFERENCES

- [1] JOHN, W., JEWELL, R. W., Bull. Am. phys. Soc. 9 (1964) 175.
- [2] RASMUSSEN, N. C., HUKAI, Y., INOUE, T., ORPHAN, V. C., Rep. AFCRL-69-0071.
- [3] BALODIS, M. K., BONDARENKO, V. A., PROKOF'EV, P. T., SIMONOVA, L. I., Sov. J. nucl. Phys. 1 (1965) 175.
- [4] MOORHEAD, J. B., COHEN, B. L., MOYER, R. A., Phys. Rev. 165 (1967) 1287.
- [5] LEDERER, C. M., HOLLANDER, J. M., PERLMAN, I., Table of Isotopes, John Wiley & Sons, New York (1967).
- [6] HYORT, S. A., ALLEN, L. H., Ark. Fys. 33 (1966) 121.
- [7] BÄCKLIN, A., Nucl. Instrum. Meth. 53 (1967) 177.
- [8] BOLLINGER, L. M., "Radiative transitions from highly excited nuclear states", Nuclear Structure (Proc. Symp. Dubna, 1968), IAEA, Vienna (1968) 317.
- [9] HARVEY, J. A., SLAUGHTER, G. G., BIRDAUD, J. R., CHAPMAN, G. T., Rep. ANL 6797 (1963) 230; BATH, M. R., CHRIEN, R. E., WASSEN, O. H., BEER, M., LONE, M. A., Phys. Rev. 106 (1968) 1111.

EXCITED LEVELS IN ^{139}Ba , ^{140}La AND ^{141}Ce THROUGH THERMAL NEUTRON CAPTURE

J.L. IRIGARAY, M. ASGHAR, G.Y. PETIT
Laboratoire de Physique Nucléaire,
Faculté des Sciences de L'Université de Bordeaux,
Le Haut-Vigneau, 33 Gradignan, and
A. AUDIAS, J. GIRARD, R. SAMAMA
CEN de Saclay,
91 Gif-sur-Yvette, France

Abstract

EXCITED LEVELS IN ^{139}Ba , ^{140}La AND ^{141}Ce THROUGH THERMAL NEUTRON CAPTURE. Levels excited through thermal neutron capture in target nuclei of ^{138}Ba , ^{139}La and ^{140}Ce have been studied with a Ge(Li) diode of 120 cm³ sensitive volume. Decay schemes are presented in which 16, 17 and 10 gamma rays from totals of 20 seen in ^{139}Ba , 45 in ^{140}La and 37 in ^{141}Ce respectively have been fitted. These level schemes take account of all the primary gamma-ray transitions seen in each of these nuclei. The present results on the spin and parity values of various excited levels are compared with those obtained by other authors and by other methods. The values of the neutron separation energy S_n for these nuclei are determined with a high precision and their significance pointed out. An attempt has been made to explain the various excited levels in the nuclei studied here.

1. INTRODUCTION

This paper presents the results obtained on ^{139}Ba , ^{140}La and ^{141}Ce through the (n, γ) reaction with thermal neutrons studied with a Ge(Li) diode of 120 cm³ sensitive volume. Each of these nuclei has one neutron outside the magic number of $N = 82$. In ^{139}Ba and ^{141}Ce , where the number of protons is even, the radiative capture of neutrons should lead to some pertinent information on the neutron levels up to a fairly high excitation energy and whether there exist any complex excitations caused by, for instance, the coupling between the single-particle states and the collective excitations of the core. In addition to the excitation of neutron levels, one would expect excitations in ^{140}La due to the odd-neutron and odd-proton configurations.

Very little is known about the structure of these nuclei [1]. Some data exist on the levels of these nuclei obtained with the help of a Compton spectrometer and NaI(Tl) crystals [2, 3], but these can certainly be improved upon by using present-day high-resolution Ge(Li) systems. During the course of present studies Moragues et al. [4] reported their results on the $^{138}\text{Ba}(n, \gamma)^{139}\text{Ba}$ reaction with thermal neutrons using a Ge(Li) diode. These show that a strong correlation between the gamma-ray and the (d, p) reduced widths exists, implying a contribution from direct neutron capture.

A few studies of stripping reactions have been carried out on these nuclei [5-8] and some information on the orbital angular momentum and the spins and parities of some levels have been obtained, which is very useful in understanding the characteristics of various levels excited in the

(n, γ) reaction on these nuclei. Information on 5 levels up to an excitation energy of 580 keV on ^{140}La has been obtained from the study of the beta decay of ^{140}Ba [9, 10].

2. EXPERIMENTAL PROCEDURE

2.1. Targets

Both lanthanum and cerium were in the form of oxide, each having a purity of better than 99.9%. About 2 g of barium as BaCO_3 was available and was enriched to 99.8% in ^{138}Ba . Each of these materials was contained in a cylinder of graphite with a wall thickness of 0.8 mm.

2.2. Detector

These measurements were carried out at the thermal neutron facility of the reactor EL3 at Saclay with a thermal neutron flux of $2.5 \times 10^6 \text{ n cm}^{-2} \text{ sec}^{-1}$ incident on the capture target. The Ge(Li) diode used in these measurements had a sensitive volume of 120 cm^3 with a capacity of 88 pF, when polarized at 1200 V; its energy resolution varied from 6.8 keV for 1.3 MeV gamma rays to about 12 keV for 6.5 MeV gamma rays.

The gamma-ray energy calibration and gamma-ray detection efficiency curves as a function of gamma-ray energy for the full-energy and double-escape peaks were obtained using the well-known radiative-capture lines in Co [11, 12]; in addition, the lines in the background from neutron capture in argon and hydrogen proved useful for energy calibration and for checking the system linearity. To take into account any existing non-linearity in the system, the 4096 channels used were divided into three groups, each of which was shown to be linear in its own range.

The uncertainty in the gamma-ray energies varies from about 1 keV for $E_\gamma \leq 2 \text{ MeV}$ to about 2 keV for $E_\gamma > 2 \text{ MeV}$. The errors quoted on the values of gamma-ray intensities take into account the statistical error on the area of a gamma-ray peak and the corresponding error on the gamma-ray detection efficiency calibration.

3. EXPERIMENTAL RESULTS

Tables I, II and III give the various gamma-rays seen in the $^{138}\text{Ba}(n, \gamma)^{139}\text{Ba}$, $^{139}\text{La}(n, \gamma)^{140}\text{La}$ and $^{140}\text{Ce}(n, \gamma)^{141}\text{Ce}$ reactions. In the case of ^{139}Ba and ^{141}Ce the relative intensities were determined with respect to the strong gamma-ray transition seen (in each of them) between the first excited state and the ground state, but for ^{140}La , where such a transition does not exist, the values of relative intensities were evaluated in comparison with the intense primary transition of $E_\gamma = 5094 \text{ keV}$.

Figures 1, 2 and 3 give the decay schemes of ^{139}Ba , ^{140}La and ^{141}Ce as deduced from the present energy and intensity measurements. In building up these schemes, all the existing data of stripping reactions were taken into account.

Table IV gives the various gamma-ray cascades employed to determine the neutron separation energy, S_n , for the nuclei studied. These values of

TABLE I. GAMMA-RAY LINES IN $^{138}\text{Ba}(n, \gamma)^{139}\text{Ba}$

No.	$E_\gamma(\Delta E_\gamma)$ (keV)	I_γ	ΔI_γ	Values of Ref. [5]	
				E_γ (keV)	I_γ
1	4095 (2)	79	7	4096.1	60
2	3639 (2)	21.5	2	3641.4	20
3	2593 (2)	13.0	2	2594.1	8
4	2567 (3)	2.7	0.5	2567.0	3
5	2538 (3)	5.5	0.8	2537.0	3
6	2528 (3)	5.5	0.8	2522.5	8.5
7	2289 (3)	3.3	0.8		
8	2244 (2)	7.0	1.0	2242.0	5
9	1853 (1)	5.0	1.5	1854.0	3
10	1752 (1)	3.5	0.7		
11	1557 (1)	2.8	0.6	1558.0	2.5
12	1418 (1)	3.1	0.6	1420.1	5
13	1399 (1)	2.1	0.5		
14	1341 (1)	2.2	0.4		
15	1075 (1)	2.0	0.5	1076.0	< 1
16	1064 (1)	2.8	0.6		
17	1049 (1)	11.0	2.0	1047.4	3
18	627 (1)	100.0	7.0	627.26	100
19	456 (1)	26.0	3.0	454.67	27
20	296 (2)	1.6	0.8	295	< 1

S_n are given in Table V, where they are compared with the existing experimental values and values calculated using the mass tables of Mattauch et al. [13].

4. DISCUSSION

4.1. Levels in ^{139}Ba

The target nucleus ^{138}Ba has spin and parity $I^\pi = 0^+$ and the capture state in ^{139}Ba after capturing an s-wave neutron will have spin and parity $J^\pi = \frac{1}{2}^+$. Assuming that the high-energy primary gamma-ray transitions from the capturing state are E1 in nature, the levels to which these transitions decay should have spin and parity $J^\pi = \frac{1}{2}^-$ or $\frac{3}{2}^-$. As Fig.1 shows, there are six primary transitions going to six levels up to 2480 keV. The

TABLE II. GAMMA-RAY LINES IN $^{139}\text{La}(n, \gamma)^{140}\text{La}$

No.	$E_\gamma (\pm \Delta E_\gamma)$ (keV)	I_γ	ΔI_γ	Values of Ref. [4]	
				E_γ (keV)	I_γ
1	5157 (4)	1.5	0.5	5165	1.5
2	5126 (4)	1.8	0.4	5130	2.3
3	5094 (2)	12.5	2	5101	12.5
4	4885 (3)	4.4	0.8	4890	2.6
5	4838 (2)	10.8	1.5	4845	12.1
6	4501 (3)	3.5	0.5	4503	3.1
7	4411 (3)	2.6	0.4	4416	4.3
8	4387 (3)	3.6	0.5	4390	4.6
9	4045 (4)			4043	0.43
10	3900 (4)			3900	0.75
11	3817 (4)			3820	0.39
12	3726 (4)			3728	1.6
13	3715 (3)	2.0	0.4	3717	1.2
14	3662 (3)	3.5	0.5	3666	2.8
15	3603 (3)	1.7	0.3	3608	2.1
16	3436 (3)	0.5	0.1	3441	0.82
17	3421 (3)	0.5	0.1	3421	1.4
18	3329 (3)	0.5	0.1		
19	3313 (3)	0.8	0.1		
20	3281 (3)	0.5	0.1	3285	1.0
21	3260 (3)	0.8	0.1		
22	3078 (2)	1.9	0.2	3080	1.9
23	2347 (2)	0.8	0.1		
24	1970 (2)	0.7	0.09		
25	1749 (2)	0.6	0.08		
26	1697 (1)	1.1	0.1		
27	1615 (1)	0.6	0.07		
28	1493 (1)	0.9	0.09		
29	1444 (1)	1.1	0.1		
30	1326 (1)	0.8	0.06		
31	1258 (1)	1.0	0.3		
32	779 (1)	0.6	0.2		
33	747 (2)	0.2	0.08		
34	721 (1)	1.7	0.2	722	23
35	667 (2)	0.5	0.1		
36	655 (1)	1.4	0.2	659	21
37	605 (1)	2.2	0.4	609	17
38	566 (1)	3.2	0.5	567	32
39	498 (1)	1.4	0.3		
40	422 (1)	4.2	0.6	423	4
41	319 (2)			317	3
42	289 (1)	3.5	0.5	286	86
43	274 (1)	2.9	0.6	271	61
44	240 (1)	1.6	0.3	236	58
45	221 (1)	3.0	0.5	217	100

TABLE III. GAMMA-RAY LINES IN $^{140}\text{Ce}(n, \gamma)^{141}\text{Ce}$

No.	$E_\gamma(\pm \Delta E_\gamma)$ (keV)	I_γ	ΔI_γ
1	4764 (2)	78.0	7
2	4336 (2)	15.9	2
3	4319 (4)		
4	4289 (2)	32.5	4
5	3718 (4)		
6	3666 (3)	3.12	0.5
7	3615 (3)	4.0	0.4
8	3607 (3)	4.0	0.4
9	3366 (3)	2.6	0.5
10	3331 (4)		
11	3237 (3)	3.6	0.6
12	3107 (3)	3.9	1
13	3087 (3)	3.25	0.4
14	3016 (2)	6.9	0.8
15	2997 (2)	6.2	0.6
16	1809 (2)	2.7	0.3
17	1747 (2)	7.5	0.4
18	1675 (2)	2.0	0.3
19	1495 (2)	2.6	0.2
20	1347 (1)	5.4	0.5
21	1324 (1)	5.4	0.5
22	1229 (1)	6.2	0.7
23	1183 (1)	10.3	1.0
24	1169 (2)	3.0	0.6
25	1115 (1)	4.0	0.8
26	1089 (1)	17.0	3
27	1049 (1)	12.6	2
28	1035 (2)	6.3	1
29	994 (2)	4.0	1
30	975 (2)	4.5	0.9
31	942 (1)	10.3	2
32	661 (1)	100.0	10
33	605 (2)	6.6	0.7
34	582 (2)	5.9	1
35	475 (1)	26.0	3
36	440 (1)	61.1	5
37	339 (2)	93.0	6

characteristics of these levels have already been studied through the (d, p) reaction and the measurements of elastic and inelastic proton scattering and polarization of protons scattered from ^{138}Ba with a view to studying the analogue states and their spins and parities in ^{138}La [14-16]. As is clear from Fig. 1, the known characteristics of these 6 levels are consistent with the present spin and parity assignments. The 627-keV level decays to the $\frac{1}{2}^-$ ground state. The value $J^\pi = \frac{3}{2}^-$ is preferred for this level to $J^\pi = \frac{1}{2}^-$, because the latter would make this transition M3, which is very unlikely.

As expected, no primary transitions are seen to the $\frac{7}{2}^-$ ground state and the $\frac{5}{2}^-$ excited state at 1418 keV. They would have to be E3 and M2 in

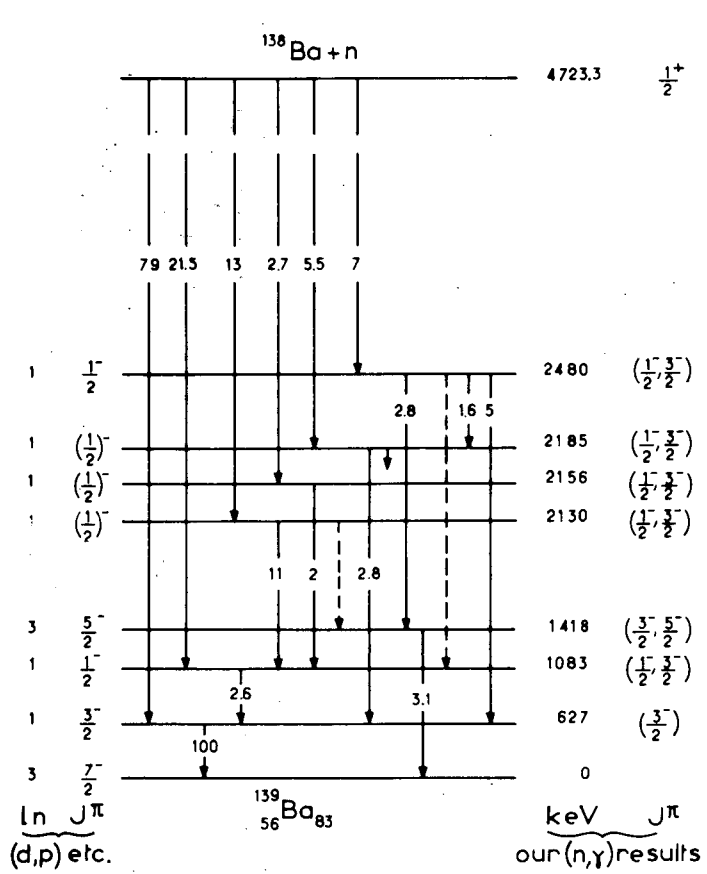


FIG. 1. The decay scheme of ¹³⁸Ba obtained from the present results.

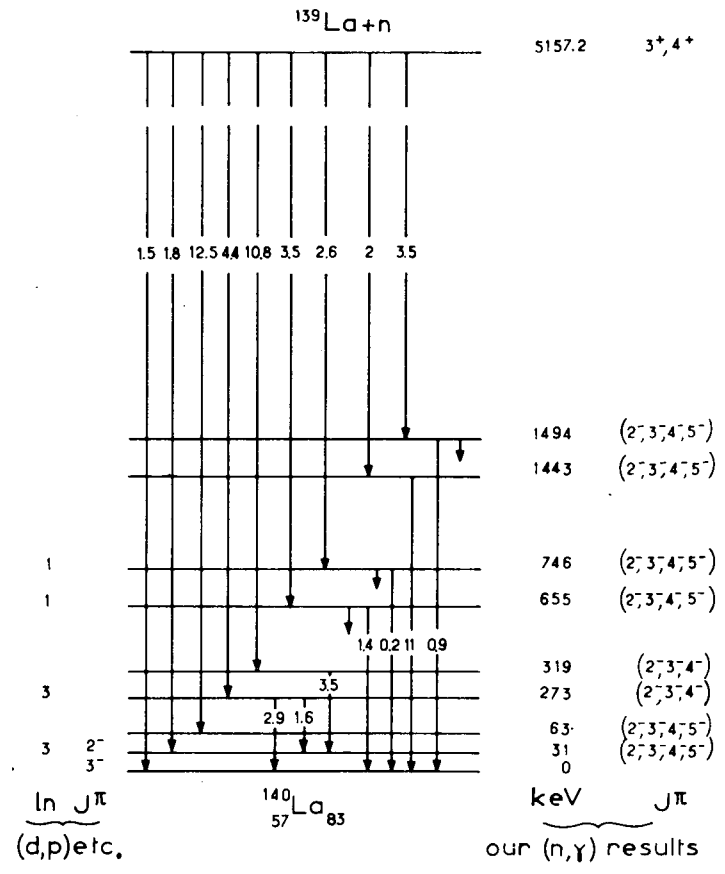


FIG. 2. The decay scheme of ¹⁴⁰La obtained from the present capture data.

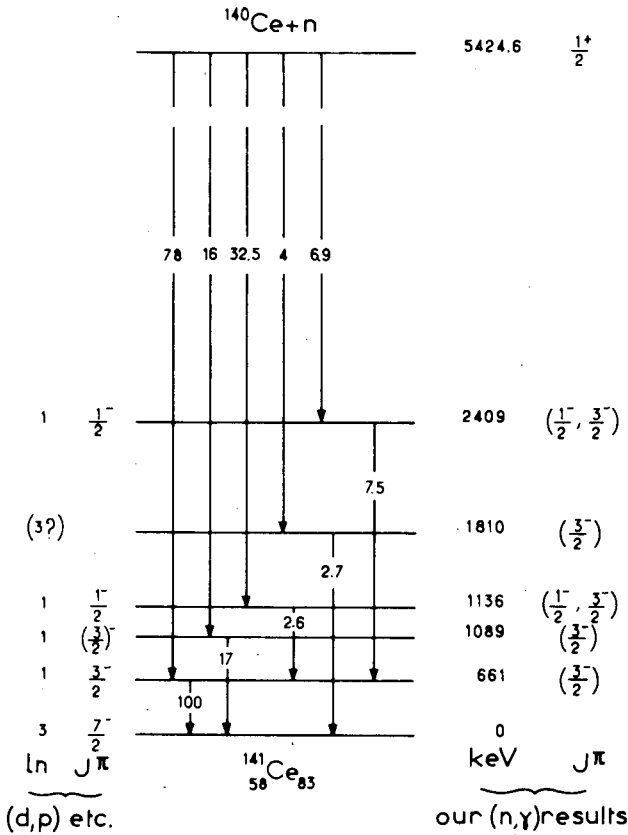


FIG. 3. The level scheme of ^{141}Ce deduced from the present capture data.

nature which is much less likely for these high-energy transitions. However, the level at 1418 keV decays to the $\frac{1}{2}^-$ ground state. If one assumes that this transition is either M1 or E2, then this level should have $J^\pi = \frac{3}{2}^-$ or $\frac{5}{2}^-$.

The ground state ($\frac{1}{2}^-$) and the levels at 627 keV ($\frac{3}{2}^-$), 1083 keV ($\frac{1}{2}^-$) and 1418 keV ($\frac{5}{2}^-$) are known to be due to the odd-neutron outside the magic core of $N=82$, which finds itself respectively in the $2f_{7/2}$, $3p_{3/2}$, $3p_{1/2}$ and $2f_{5/2}$ orbits [5-8]. The other p-states may have been caused by the excitation of complex configurations such as the coupling between the single-particle excitation and the collective excitation of the ^{138}Ba core, for example the triplet at 2130, 2156 and 2185 keV could arise from the coupling of single-particle states ($2f_{7/2}$, $3p_{1/2}$, $3p_{3/2}$) with the 2-phonon vibrational triplet that should exist around this energy of excitation. One hopes that detailed theoretical calculations will help to understand the way these additional levels are produced.

TABLE IV. CASCADES USED TO OBTAIN THE VALUE OF S_n IN ^{139}Ba , ^{140}La AND ^{141}Ce

^{139}Ba	^{140}La	^{141}Ce
4095 + 627 = 4722	5157 + 0 = 5157	4764 + 661 = 5425
3639 + 456 + 627 = 4722	4885 + 274 = 5159	4336 + 1089 = 5425
2593 + 1049 + 456 + 627 = 4725	4501 + 655 = 5156	4289 + 475 + 661 = 5425
2567 + 1075 + 456 + 627 = 4725	3715 + 1444 = 5159	3615 + 1809 = 5424
2538 + 1557 + 627 = 4722	3662 + 1493 = 5155	3016 + 1747 + 661 = 5424
2244 + 1853 + 627 = 4724		
Mean $S_n = 4723.3 \pm 1.5$ keV	Mean $S_n = 5157.2 \pm 1.5$ keV	Mean $S_n = 5424.6 \pm 1.5$ keV

TABLE V. NEUTRON SEPARATION ENERGY S_n FOR VARIOUS NUCLEI

Nucleus	S_n (keV)		
	Mass tables [14]	Other authors	Present values
$^{139}_{56}\text{Ba}_{83}$	4717 ± 10	4723 ± 0.7 [5]	4723.3 ± 1.5
$^{140}_{57}\text{La}_{83}$	5000 ± 48	5165 ± 5 [4]	5157.2 ± 1.5
$^{141}_{58}\text{Ce}_{83}$	5438 ± 9	-	5424.6 ± 1.5

4.2. Levels in ^{140}La

The odd nucleus ^{140}La should have a more complicated level structure than the two other nuclei studied here. This is due to the fact that it has a neutron outside the $N = 82$ neutron magic number and an unpaired proton. This comparatively complicated structure should give rise to a higher number of levels in this nucleus than in either of the other two nuclei.

The target nucleus ^{139}La has spin and parity $J^\pi = \frac{7}{2}^+$ which would lead to the capture state in ^{140}La having $J^\pi = 3^+$ or 4^+ .

Figure 2 shows the level scheme on ^{140}La obtained from the present capture data. Again, if we should assume that the primary transitions are of E1 nature, the levels populated through primary transitions should have $J^\pi = 2^-, 3^-, 4^-$ or 5^- .

The ground state and the first excited state at 31 keV are known to have $J^\pi = 3^-$ and 2^- respectively [1] and these are reached by the primary transitions. These two levels are presumed to be formed through the coupling of the $2f\frac{1}{2}$ odd neutron and the $1g\frac{7}{2}$ unpaired proton. This can give rise to states with spin values that lie between 0 and 7 and have a negative parity.

The decay of the 63-keV level towards the 3^- ground state is not observed. This is because the low gamma-ray energy threshold in the present measurements was higher than this energy. Hughes et al. [17] have seen this low-energy transition. It is not possible to pin down the spin of this level; the E1 or E2 transition leaves it open whether this level has $J^\pi = 2^-, 3^-, 4^-$ or 5^- .

As one can observe the decay of the two levels at 272 and 319 keV towards the 2^- level at 31 keV but not towards the 3^- ground state, this should exclude these two levels from being 5^- because this choice would demand that each of these quite intense transitions should be M3, which is not very likely. These transitions may be either M1 or E2 and under these conditions each of these levels could have $J^\pi = 2^-, 3^-$ or 4^- .

Stripping reaction studies [6] have suggested that the levels at 655 and 746 keV should belong to the configuration of $(1g\frac{7}{2})_p(3p\frac{3}{2})_n$, hence these levels can have spins and parities $J^\pi = 2^-, 3^-, 4^-$ and 5^- . Each of these two levels de-excites towards the 3^- ground state, but not towards the 2^- first excited state. However, the balance of intensities shows that these levels

decay towards other levels not populated by the direct primary transitions from the capturing state. Again it is not possible to narrow down the choice of the values of spins for these two levels; the M1 or E2 transitions leave a choice of $J^\pi = 2^-, 3^-, 4^-$ or 5^- for each of these two levels.

Under the present conditions it is not possible to say much about the other two levels at 1443 and 1494 keV because no supporting information exists. Since these levels are fed by the primary transitions, they can have $J^\pi = 2^-, 3^-, 4^-$ or 5^- .

Figure 2 shows that the gamma-ray transitions from the capture state to the known $l_n = 1$ levels do not seem to be preferred over the transitions to the known $l_n = 3$ levels; this lack of preference for the $l_n = 1$ levels should imply that in the $^{139}\text{La}(n, \gamma)^{140}\text{La}$ reaction with thermal neutrons the contribution from the compound nucleus reaction process is dominant over the process of direct capture, as already pointed out by Hughes et al. [17].

4.3. Levels in ^{141}Ce

The structure of this nucleus should be close to that of ^{139}Ba because the two differ only in a pair of protons. The spin and parity of the target nucleus are $I^\pi = 0^+$ and the capture of an s-wave neutron gives the capture state spin and parity $J^\pi = \frac{1}{2}^+$. Again, the high-energy E1 primary transitions should lead to levels with spin and parity $J^\pi = \frac{1}{2}^-$ or $\frac{3}{2}^-$. Figure 3 shows the level scheme of ^{141}Ce obtained from the present (n, γ) experiment. For the level at 1810 keV $l_n = (3)$ has been suggested [5] which would give this level spin and parity $J^\pi = \frac{5}{2}^-$ or $\frac{1}{2}^-$. The present results do not support this assignment. As Fig. 3 shows, this level decays to the $\frac{1}{2}^-$ ground state and it would be preferable to assign $J^\pi = \frac{3}{2}^-$ to this level because a value of $J^\pi = \frac{1}{2}^-$ would lead to this transition being a less likely M3 transition, while $\frac{3}{2}^-$ would make it an E2 transition. On similar grounds the assignment $\frac{3}{2}^-$ is preferable for the levels at 661 and 1089 keV.

As in ^{139}Ba , the $\frac{1}{2}^-$ ground state and the $\frac{3}{2}^-$ first excited state at 661 keV are due to the odd neutron outside the $N = 82$ magic number being in the $2f_{\frac{1}{2}}$ and $3p_{\frac{3}{2}}$ orbits respectively. There is a $\frac{1}{2}^-$ level at 1136 keV due to the $3p_{\frac{1}{2}}$ neutron; this state is, perhaps, similar to the $\frac{1}{2}^-$ state at 1083 keV in ^{139}Ba . The excitation of other $\frac{1}{2}^-$ or $\frac{3}{2}^-$ levels cannot be accounted for by a simple shell model; to explain them, it would perhaps be necessary to invoke some complex configurations such as the coupling between the single-particle states and the collective excitation of the core.

It is interesting to note that the triplet (2130, 2156 and 2185 keV) seen in ^{139}Ba (section 4.1) is absent in ^{141}Ce . It was suggested that this triplet in ^{139}Ba could arise from the coupling of the $2f_{\frac{1}{2}}$, $3p_{\frac{1}{2}}$ and $3p_{\frac{3}{2}}$ single-particle states with the 2-phonon vibrational triplet that may be present around this energy of excitation. The absence of this triplet in ^{141}Ce is not clear, even though one expects to find this 2-phonon vibrational triplet from the excitation of the ^{140}Ce core at about the same excitation energy.

4.4. The neutron separation energies S_n

Table V gives the neutron separation energies for the nuclei studied here obtained from the mass tables [13] measured in other laboratories and the values determined from the present measurements. As the table shows, the values of S_n obtained from the mass tables lack the precision of

the experimental results. The present values of S_n are in good agreement with the already existing values of S_n for ^{139}Ba and ^{140}La .

The values of S_n for the 83rd neutron are known with high precision and it would be interesting to see how this value of S_n behaves as the number of protons is increased. Table V shows that as the number of protons increases the value of S_n increases also; this increase is due to the decrease in the contribution to the nuclear mass from the mass asymmetry term $(N-Z)^2/A$. High-precision experimental results of this type should lead to a corresponding improvement of this term in the existing empirical mass formulae.

5. CONCLUSION

A comparison was made of the level schemes of ^{139}Ba and ^{141}Ce which differ only in a pair of protons: 56 and 58 respectively. The $\frac{1}{2}^-$ ground state, the $\frac{3}{2}^-$ first excited states at 627 keV (^{139}Ba) and 661 keV (^{141}Ce) and, perhaps, also the states at 1083 keV (^{139}Ba) and 1136 keV (^{141}Ce) have identical characteristics and are all produced by the odd neutron outside the $N = 82$ magic number. It is possible that the 2480-keV (^{139}Ba) and the 2409-keV (^{141}Ce) levels may be produced through identical configurations in these two nuclei. However, the levels at 1089 and 1810 keV in ^{141}Ce are not seen in ^{139}Ba and the triplet observed at 2130, 2156 and 2185 keV in ^{139}Ba is absent in ^{141}Ce . It was suggested that this triplet in ^{139}Ba may have been produced through the $2f \frac{1}{2}$, $3p \frac{1}{2}$ and $3p \frac{3}{2}$ single-particle states coupled to the 2-phonon vibrational triplet of the ^{138}Ba core which may be excited around this energy of excitation. The reason for its absence in ^{141}Ce is not clear even though one expects to find this 2-phonon vibrational triplet from the ^{140}Ce core at about the same excitation energy.

The neutron separation energies S_n for the nuclei studied here have been deduced and compared with values obtained from the mass tables. The significance of these high-precision experimental values of S_n to the mass asymmetry term in the empirical nuclear mass formulae is discussed.

REFERENCES

- [1] LEDERER, C. M., HOLLANDER, J. M., PERLMAN, I., Table of Isotopes, John Wiley and Sons, Inc., New York (1967).
- [2] GROSHEV, L. V., LUTSENKO, V. N., DEMIDOV, A. M., PELEKHOV, V. I., Atlas of Gamma-Ray Spectra from Radiative Capture of Thermal Neutrons, Pergamon Press, Oxford (1959).
- [3] GIANNINI, M., PINTO, G., PROSPERI, D., SCIUTI, S., Nuovo Cim. 29 (1963) 977.
- [4] MORAGUES, J. A., MARISCOTTI, M. A. J., GELLETTY, W., KANE, W. R., Rep. BNL 1280-R (1969).
- [5] FULMER, R. H., MCCARTHY, A. L., COHEN, B. L., Phys. Rev. 128 (1962) 1302.
- [6] BINGHAM, F. W., SAMPSON, M. B., Phys. Rev. 128 (1966) 1796.
- [7] RAPAPORT, J., BUECHNER, W. W., Physics Lett. 18 (1965) 299; RAPAPORT, J., KERMAN, A. K., Nucl. Phys. A119 (1968) 641.
- [8] WIEDNER, C. A., HEUSLER, A., SOLF, J., WURM, J. P., Nucl. Phys. A103 (1967) 433.
- [9] AGARWAL, Y. K., BABA, C. V. K., BHATTACHERJEE, S. K., Nucl. Phys. 58 (1964) 641.
- [10] BURDE, J., RAKAVY, M., ADAM, G., Nucl. Phys. 68 (1965) 561.
- [11] SHERA, E. B., HAFEMEISTER, D. W., Phys. Rev. 150 (1966) 894.
- [12] PRESTWICH, W. V., KENNETT, T. J., HUGHES, L. B., Nucl. Phys. 88 (1966) 548.

- [13] MATTAUCH, J.H.E., THIELE, W., WAPSTRA, A.H., Nucl.Phys. 67 (1965) 32.
- [14] VON BRENTANO, P., MARQUARDT, N., WURM, J.P., ZAIDI, S.A.A., Physics Lett. 17 (1965) 124.
- [15] MORRISON, G.C., WILLIAMS, N., NOLEN, J.A., Jr., VON EHRENSTEIN, D., Phys.Rev.Lett. 19 (1967) 592.
- [16] VEESER, L., ELLIS, J., HAEBERLI, W., Phys.Rev.Lett. 18 (1967) 1063; VEESER, L., HAEBERLI, W., Nucl.Phys. A115 (1968) 172.
- [17] HUGHES, L.B., KENNETT, T.J., PRESTWICH, W.V., Nucl.Phys. 89 (1966) 241.

GAMMA RAYS FROM THERMAL NEUTRON CAPTURE IN LANTHANUM *

(Abstract only)

J. SIMIĆ, I. SLAVIĆ, V. AJDAČIĆ, B. LALOVIĆ
Boris Kidrič Institute of Nuclear Sciences,
Belgrade, Yugoslavia

Abstract

GAMMA RAYS FROM THERMAL NEUTRON CAPTURE IN LANTHANUM. Gamma rays from the $\text{La}(n, \gamma)$ reaction have been measured with single and coincidence Ge(Li) spectrometers. The Ge(Li) diodes have effective volumes of 25 and 15 cm^3 with resolutions of 4 and 3 keV at 1.33 MeV and 6 and 5.5 keV at 5 MeV, respectively. The target was 1 g of spectroscopically pure lanthanum oxide bombarded with a filtered external beam with an intensity of $6 \times 10^6 \text{ n cm}^{-2} \text{ sec}^{-1}$. The electronic equipment consisted of ORTEC units and a 4096-channel Nuclear Data 2200 analyser. The data accumulated were punched on paper tape and computed on an IBM 360 by means of a program that automatically finds the peaks and fits them to Gaussian functions.

Energy and intensity measurements were carried out in the gamma-ray interval from 0-5200 keV. The energy calibration was carried out with ^{140}Ce gamma rays and the $\text{S}(n, \gamma)$ reaction. The background spectrum was taken with a graphite target in a Teflon capsule. The coincidence measurements were mainly carried out in such a way that the low-energy spectrum was gated with the stronger high-energy transitions.

From a total of 117 transitions found 23 were assigned as primaries populating low-lying levels in ^{140}La found from the $^{139}\text{La}(d, p)^{140}\text{La}$ reaction. A further 59 transitions could be placed in the level scheme of ^{140}La . The separation energy of the last neutron in ^{140}La has been calculated as $5160.4 \pm 1.5 \text{ keV}$ (based on $8641.2 \pm 1.0 \text{ keV}$, the separation energy in the reaction $^{32}\text{S}(n, \gamma)^{33}\text{S}$).

* A fuller description of this work will be published elsewhere.

STUDY OF THE REACTION $^{167}\text{Er}(n, \gamma)^{168}\text{Er}$

Eva FALKSTRÖM-LUND

Department of Physics,

Chalmers University of Technology,

Gothenburg and

The Swedish Research Council's Laboratory, and

A. BÄCKLIN

Institute of Physics,

Uppsala University, Uppsala and

The Swedish Research Council's Laboratory,

Studsvik, Nyköping, Sweden

Abstract

STUDY OF THE REACTION $^{167}\text{Er}(n, \gamma)^{168}\text{Er}$. Gamma rays from the reaction $^{167}\text{Er}(n, \gamma)^{168}\text{Er}$ have been measured between 0.5 and 2 MeV with a flat crystal diffraction monochromator combined with a Ge(Li) detector. In addition to transitions found in earlier investigations we have found evidence for transitions depopulating a $K = 1^-$ band.

INTRODUCTION

The reaction $^{167}\text{Er}(n, \gamma)^{168}\text{Er}$ was previously investigated by Koch [1] with a bent-crystal diffraction spectrometer. The transition energies and intensities were measured with high accuracy to about 1 MeV. The ground-state rotational band, the gamma-vibrational band and two bands with $K = 3^-$ and $K = 4^-$ were established. Measurements of gamma rays and internal conversion electrons from this reaction have also been performed by Groshev et al. [2]. Spin and parity of about 20 low-energy states were suggested by means of neutron resonance capture by Bollinger et al. [3].

In (d, p) measurements by Harlan et al. [4] the bands mentioned above have been observed, together with a number of unassigned states above 1300 keV. Tjøm et al. [5] have observed some of those levels mentioned above in the $^{168}\text{Er}(dd')$ reaction but leave about 10 states unassigned or with very uncertain assignments. Some of the ^{168}Er levels have also been studied from the decay of ^{168}Tm [6, 7]. One may expect more bands in the region around 1.5 MeV than those mentioned above to be populated in the (n, γ) reaction. We have therefore studied the gamma-ray spectrum in the region 0.5-2 MeV using Ge(Li) detectors.

EXPERIMENTAL PROCEDURE

The target material was Er_2O_3 enriched to 90% in ^{168}Er . The gamma spectra were measured with Ge(Li) detectors using two different experimental arrangements. Direct measurements were made with 100 mg of the target material placed in an external neutron beam with a flux of about

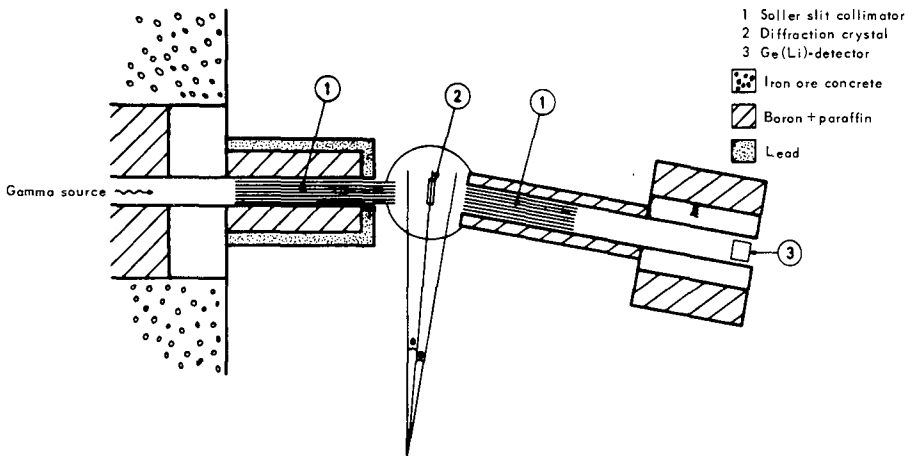


FIG. 1. Principle of the combination of a diffraction monochromator and a Ge(Li) detector.

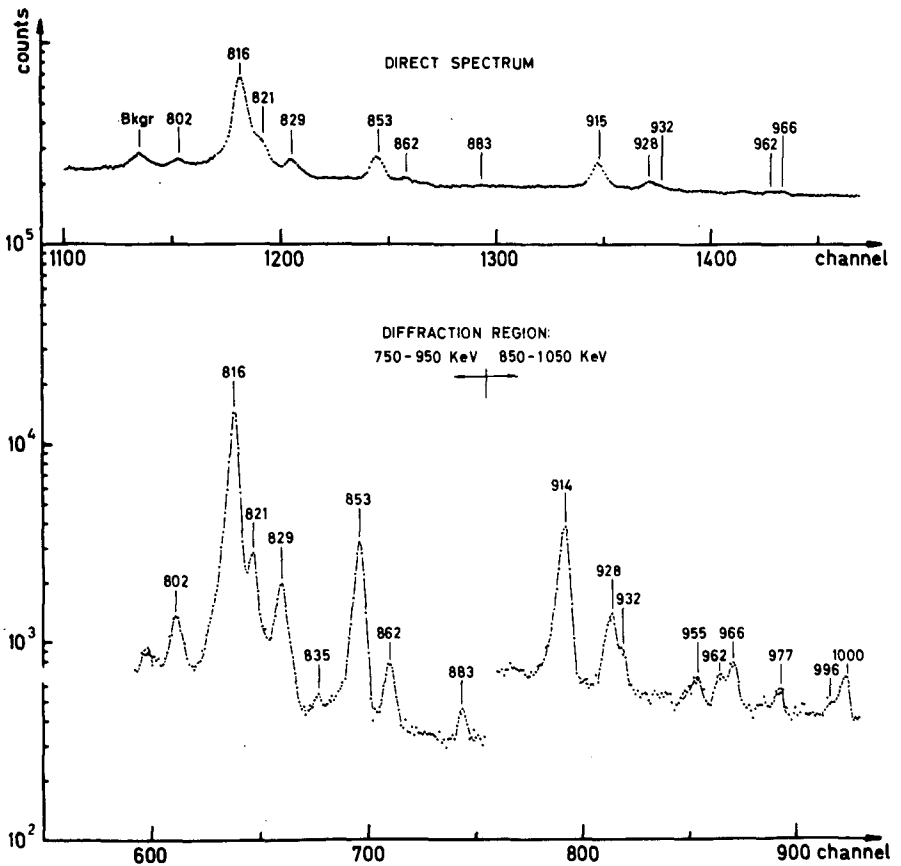


FIG. 2. Part of the gamma spectrum. Top: direct spectrum, bottom: two spectra measured with the combined arrangement together covering the same energy region as above. Energies in keV.

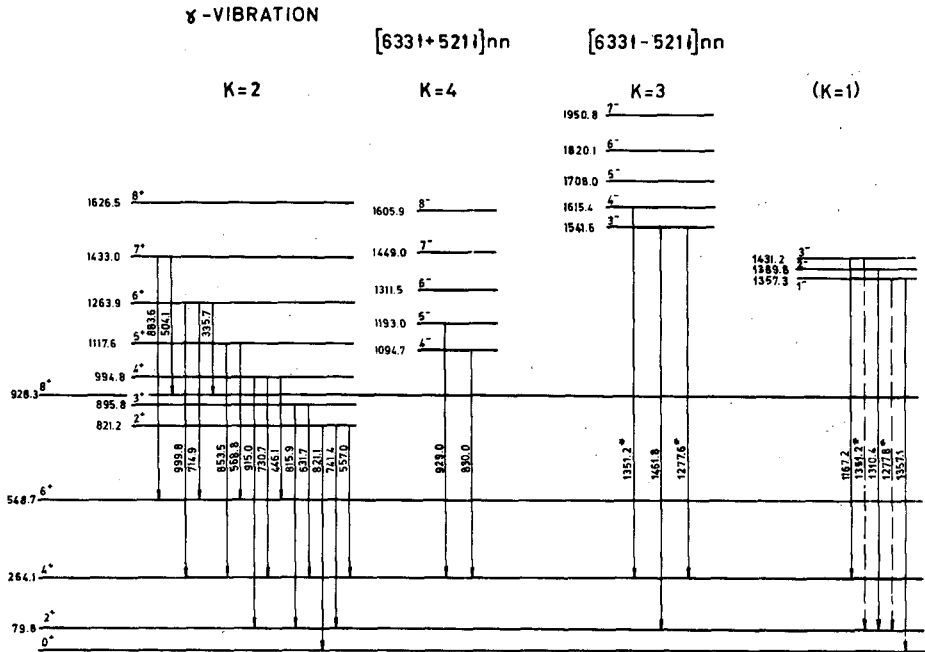


FIG. 3. Preliminary level scheme showing transitions from the proposed K=1 band to the groundstate band, together with the bands previously reported.

$10^6 \text{ n cm}^{-2} \text{ sec}^{-1}$ and the gamma-ray spectrum was registered in the usual way [8]. In the other arrangement the gamma rays were diffracted in a flat-crystal monochromator before entering the Ge(Li) detector. The principle of this arrangement is shown in Fig. 1. A flat Ge crystal utilizing the (400) plane is used. The diffraction peak is rather broad and allows an energy region of about 100 keV at 1 MeV to reach the Ge detector. Further details are given in Ref. [9]. The advantage of this combination method is the suppression of the Compton background caused by higher energies. The peak to background ratio is thus considerably improved over a direct spectrum which is illustrated in Fig. 2. A disadvantage is the complicated response function which depends on the intensity variation of the diffraction peak, the reflectivity and absorption in the Ge crystal as well as the efficiency of the Ge(Li) detector. Intensity calibration was made by using the strongest gamma lines in the direct spectrum, which were measured with an accurately calibrated 25-cm^3 Ge(Li) detector.

RESULTS AND DISCUSSION

About 80 gamma lines were observed in the energy region 0.6-2 MeV, most of which had not been observed earlier. The agreement with earlier data [1, 2] is in general good, except for intensities in the region 0.7-0.8 MeV where our values are systematically lower by a factor of 2.

Tjøm et al. [5] observe a strongly populated level at 1428 keV which they suggest to be the 3^- octopole vibration level. In the (d, p) reaction states at 1357, 1393 and 1427 keV are populated, which are suggested to be the 1^- , 2^- and 3^- members of a $K = 1^-$ band [4].

We find combinations of fairly strong lines with the levels of the ground-state band yielding level energies of 1357.3 ± 0.5 and 1431.2 ± 0.5 keV. Since the probability of finding such a combination by accident within ± 5 keV from a given energy is as small as 2% in this energy region, we may identify these levels with the 1^- and 3^- levels observed in the charged-particle reactions. The 2^- level is defined by the 1310.4-keV transition which appears quite isolated in the expected energy region. Its intensity also fits very well with regard to the population systematics of the states. The 1^- band is shown in Fig. 3 together with the bands previously established.

Since several of the transitions involved have alternative positions in the level scheme, no accurate ratios of $K = 1^- \rightarrow K = 0^+$ transitions can be obtained at the present stage.

Since some of our intensities for transitions from the gamma-vibrational band to the ground-state band differ from the earlier data [1], we have recalculated the z_2 mixing parameter to be 0.03.

REFERENCES

- [1] KOCH, H.R., Z. Phys. 192 (1966) 142.
- [2] GROSHEV, L.V., DEMIDOV, A.M., IVANOV, V.A., LUTSENKO, V.N., PELEKHOV, V.I., SHADIEV, N., Izv. Akad. Nauk SSSR, Ser. fiz. 29 (1965) 773.
- [3] BOLLINGER, L.M., THOMAS, G.E., Phys. Rev. Lett. 27 (1968) 233.
- [4] HARLAN, R.H., SHELINE, R.K., Phys. Rev. 160 (1967) 1005.
- [5] TJØM, P.O., ELBEK, B., Nucl. Phys. A107 (1968) 385.
- [6] KENEALY, P.F., FUNK, E.G., MIHELICH, J.W., Nucl. Phys. A110 (1968) 561.
- [7] KELLER, G.E., ZGANJAR, E.F., PINAJIAN, J.J., Nucl. Phys. A129 (1969) 481.
- [8] BÄCKLIN, A., BOLEU, R., FOGELBERG, B., Ark. Fys. 39 (1969) 221.
- [9] BROMAN, L., Nucl. Instrum. Meth. 50 (1967) 29.

LOW-LYING ROTATIONAL BANDS IN $^{153}\text{Sm}^*$

R. K. SMITHER

Argonne National Laboratory,
Argonne, Ill., United States of America
and

T. von EGIDY

Technische Hochschule,
Munich, Federal Republic of Germany

Abstract

LOW-LYING ROTATIONAL BANDS IN ^{153}Sm . A series of (n, γ) and (n, e^-) experiments were used to develop the level scheme of ^{153}Sm . Spin and parity assignments were made for 15 of the 25 levels below 700 keV. The ground state and nine of these levels below 300 keV are interpreted as members of three $K = 3/2$ rotational bands (two of negative parity and one of positive parity). The observed gamma-ray branching ratios were compared with the predictions of the Nilsson model for an odd neutron coupled to a deformed core. In most cases the experimental ratios agreed with the theoretical predictions to $\pm 10\%$. An attempt was made to extend this analysis to the higher levels but only limited success was achieved.

In our work a series of (n, γ) and (n, e^-) studies are combined to develop the level scheme of ^{153}Sm . The $^{152}\text{Sm}(n, \gamma)^{153}\text{Sm}$ spectrum was measured with the Argonne bent-crystal spectrometer and with a Ge(Li) detector at the in-pile facility at the Argonne CP-5 research reactor. The low-energy bent-crystal spectrum consisted of 251 gamma transitions associated with thermal-neutron capture in ^{152}Sm and with energies between 28 and 1041 keV. The gamma-ray intensities were normalized to the previously established intensity of the 103-keV line in ^{153}Eu from the beta decay of ^{153}Sm . The high-energy (n, γ) spectrum, consisting of 23 lines between 4.5 and 5.9 MeV, was obtained with a Ge(Li) detector. The very high resolution of the bent-crystal spectrometer at low gamma energies and of the Ge(Li) detector at high energies were essential to the unraveling of this very complicated level scheme. The full (n, γ) spectrum is plotted in Fig.1. It is one of the $\log I_\gamma$ versus $\log E_\gamma$ plots that take a little getting used to. Each gamma ray is represented as a point on the graph and, as we can see, the spectrum is typical of that obtained for neutron capture in even-Z even-N-nuclei. The large number of strong, low-energy gammas seen in the upper left are the transitions between the many low-lying states in the even-Z odd-N ^{153}Sm nucleus.

The conversion-electron spectrum was measured with the high-resolution magnetic spectrometer at Munich. The K and L conversion coefficients obtained by combining these data with the bent-crystal gamma intensities were used to obtain multipole assignments for 37 of the low-energy transitions.

* The full text of this paper will be published in The Physical Review under the title "Energy levels in ^{153}Sm based on (n, γ) (n, e^-) and beta decay studies" by R.K. Smither et al.

The low-energy level scheme of ^{153}Sm is given in Fig.2. The spin and parity assignments are based almost entirely on the present (n, γ) and (n, e^-) work.

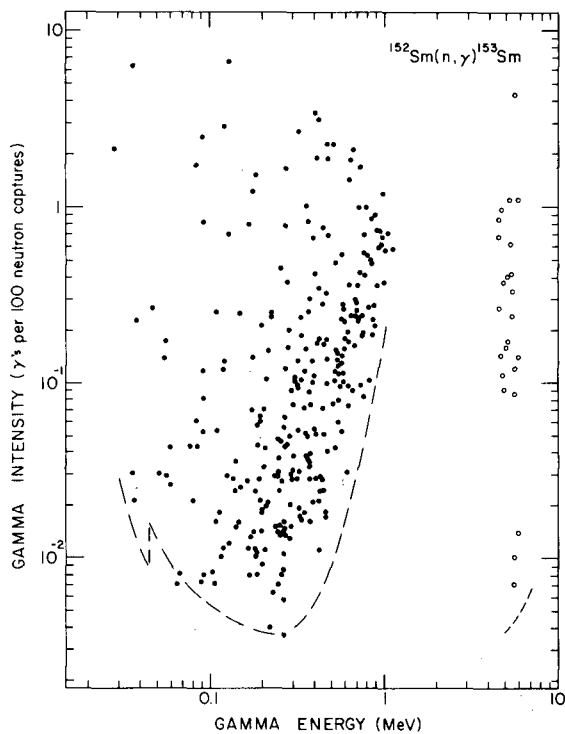


FIG.1. Log-log plot of I_γ versus E_γ for the gamma spectrum from $^{152}\text{Sm}(n, \gamma)^{153}\text{Sm}$. The filled circles are the bent-crystal data and the open circles are the Ge(Li) data; dashed line indicates the minimum sensitivity of the experiment.

R E F E R E N C E S

- [1] KENEFICK, R. A., SHELINE, R. K., Phys. Rev. 139 (1965) B 1479.
- [2] SHELINE, R. K., "Experimental decomposition of the wave-functions of deformed nuclear states into their components", Nuclear Structure (Proc. Symp. Dubna, 1968), IAEA, Vienna (1968) 71.

DIRECTIONAL ANISOTROPY OF CAPTURE GAMMA RAYS FROM ALIGNED ^{149}Sm NUCLEI

E.R. REDDINGIUS, H. POSTMA
Kamerlingh Onnes Lab.,
Leiden, The Netherlands

Abstract

DIRECTIONAL ANISOTROPY OF CAPTURE GAMMA RAYS FROM ALIGNED ^{149}Sm NUCLEI. Neutron capture gamma-ray experiments with aligned ^{149}Sm nuclei are reported. On the basis of these experiments spin values were assigned to many levels of ^{150}Sm .

Neutron capture gamma rays from aligned nuclei will in general have anisotropic directional distributions given by the expression:

$$W(\theta) = 1 + \sum_{k \text{ even}} f_k G_k A_k P_k(\cos \theta)$$

where f_k are orientation parameters of the capturing nucleus as originally defined by Tolhoek and Cox [1], the G_k 's are disorientation parameters related to the neutron capture and preceding gammas and the A_k 's are parameters which depend on the characteristics of the gamma transition. The values of A_k are often very much different for the various possible spins of the initial and final states. Consequently a measurement of the anisotropy of the gamma-ray emission from oriented nuclei may give conclusive information about spins of levels, provided that the multipolarity of the radiation is known. Usually it can be expected that the observed high-energy primary gamma rays have dipole character. In some cases this is known from electron conversion coefficients. In the case of dipole transitions only the term with $k = 2$ is different from zero. Several nuclei can be oriented to a sufficient degree to expect rather large anisotropies. Such experiments have been done in the past with the $^{143}\text{Nd}(n, \gamma)$ and $^{59}\text{Co}(n, \gamma)$ reactions, see Refs [2 - 4].

Recently we have finished experiments concerning the anisotropies of capture gamma rays from aligned ^{149}Sm nuclei. For this purpose single crystals of $\text{Ce}_2\text{Mg}_3(\text{NO}_3)_{12} \cdot 24\text{D}_2\text{O}$ with a total weight of 20 g, in which a small fraction of the cerium has been replaced by samarium, were used. These crystals were cooled to about 0.01 - 0.02°K by the method of adiabatic demagnetization starting from 1°K and an initial magnetic field of 12 kOe. It was not possible to keep the samples longer than about 10-15 min at a sufficiently low temperature because of the heat input due to radiation etc. and because of the very low specific heat of the bulk material. However, a fully automated system was developed which made it possible to repeat the demagnetizations and counting periods. Each cycle lasted about 35 min and contained a measurement of 11 min at 0.01 - 0.02°K and a measurement of the same length of time at 1°K; thus

TABLE I. ANISOTROPIES OF HIGH-ENERGY TRANSITIONS AND SPIN ASSIGNMENTS OF ¹⁵⁰Sm

E_γ	$W(0^\circ) - 1$	Final level	Spin assignment final level
7212.0 keV	-0.35 ± 0.01	773.4 keV	4 ⁺
6535.9 keV	-0.35 ± 0.03	1449.3 keV	4 ⁺
6479.9 keV	+0.18 ± 0.07	1504.7 keV	3 ⁺ (5) ⁺
6342.8 keV	-0.37 ± 0.08	1642.7 keV	4 ⁺
6158 keV	-0.20 ± 0.10	1822 keV	(3) ⁺ 4 ⁺
6016.3 keV	-0.36 ± 0.09	1971.9 keV	4
5961.7 keV	-0.36 ± 0.03	2021.5 keV	4 ⁺
5923.6 keV	+0.23 ± 0.07	2062.9 keV	3 ⁺ (5) ⁺
5891.8 keV	+0.02 ± 0.07	2093 keV	5 ⁺
5833 keV	-0.30 ± 0.07	2153.3 keV	4 ⁺
5792 keV	-0.39 ± 0.15	2191.2 keV	4
5725 keV	-0.31 ± 0.07	2260 keV	4
5617.0 keV	+0.29 ± 0.09	2368 keV	3 ⁺
5532.5 keV	+0.245 ± 0.015	2453 keV	3 ⁺
5492 keV	+0.17 ± 0.09	2493 keV	3 ⁺ , 5 ⁺
5338 keV	+0.14 ± 0.08	2647 keV	3, 5

with the nuclei unoriented. The spectra were accumulated for one week at both temperatures. For the detection of the gamma rays two Ge(Li) detectors of 2 and 6 cm³ have been used.

Very large anisotropies of many primary transitions and also secondary transitions were found. In one of the samples nearly the maximum value of f_2 was achieved directly after demagnetization.

The experiment was carried out with 0.047-eV neutrons. The capture cross-section at this temperature is mainly due to a 4⁻ resonance at 0.0976 eV. According to other authors a small fraction of the thermal neutron capture is related to a 3⁻ bound state. It has been shown that primary gamma rays of the ¹⁴⁹Sm(n, γ) reaction with intensities larger than 0.03 gammas per 100 neutrons captured originate from the 4⁻ resonance.

It is impossible to show in the scope of this contribution all the measured anisotropies and the analysis of the data. However, the anisotropies of several high-energy primary transitions and the assignments of the final levels of ¹⁵⁰Sm are given in Table I.

The positive parity of many of these levels quoted is based on electron conversion coefficients [5], which also justify the assumed dipole character. The spin assignments in the table in parentheses could be rejected on the basis of anisotropies of secondary gamma rays. More assignments of several other low-energy levels of ¹⁵⁰Sm were derived on the basis of

anisotropies and electron conversion coefficients of low-energy gamma transitions. The final conclusions on assignments of many levels of ^{150}Sm are condensed into the decay scheme shown in Fig.1.

REFERENCES

- [1] TOLHOEK, H.A., COX, J.A.M., *Physica* 19 (1953) 101.
- [2] POSTMA, H., REDDINGIUS, E.R., *Physica* 34 (1967) 541.
- [3] REDDINGIUS, E.R., POTTERS, J.F.M., POSTMA, H., *Physica* 38 (1968) 48.
- [4] MELLEMA, J., POSTMA, H., *Nucl. Phys.* (1969).
- [5] ELZE, Th.W., *Z. Phys.* 194 (1966) 280.

INVESTIGATION OF THE ^{158}Gd LEVEL SCHEME BY THERMAL NEUTRON CAPTURE

H. A. BAADER, H. R. KOCH, D. BREITIG, O. W. B. SCHULTZ
Physics Department,
Technische Hochschule,
Munich, Federal Republic of Germany,
R. C. GREENWOOD, C. W. REICH
Nuclear Reactor Testing Station,
Idaho Nuclear Corporation,
Idaho Falls, Idaho, United States of America, and
A. BÄCKLIN, B. FOGELBERG
Institute of Physics,
Uppsala University,
Uppsala, and
The Swedish Research Council's Laboratory,
Studsvik, Nyköping, Sweden

Abstract

INVESTIGATION OF THE ^{158}Gd LEVEL SCHEME BY THERMAL NEUTRON CAPTURE. The ^{158}Gd level scheme has been investigated through the study of the $^{157}\text{Gd}(n, \gamma)$ reaction with a Ge(Li) detector and a curved-crystal spectrometer and by measurement of the $^{157}\text{Gd}(n, e^-)$ spectrum. Preliminary results on the ground-state band up to $I=6$ and the gamma-vibrational band up to $I=5$ are presented and discussed.

The investigation on the level scheme of ^{158}Gd was performed by three groups in co-operation: R. C. Greenwood and C. W. Reich measured the neutron capture gamma spectrum of ^{157}Gd with a Ge(Li) spectrometer, A. Bäcklin and B. Fogelberg contributed the conversion-electron spectrum and the Risø group investigated the low-energy part of the (n, γ) spectrum with an automated bent-crystal spectrometer [1].

MEASUREMENTS WITH THE Ge(Li) SPECTROMETER ¹

The experimental set-up and procedure have been described elsewhere [2].

The ^{157}Gd thermal neutron capture gamma spectrum has been measured in the energy range from 70 keV up to the compound-state energy. 106 transitions were observed with energies above 1.5 MeV. The error for stronger lines is ± 0.5 keV at 7 MeV and 0.16 keV at 1.5 MeV. These data provide considerably more information about the high-energy part of the level scheme than do previous data. Below 1.5 MeV mainly the results from the bent-crystal spectrometer will be used because of the higher resolution.

¹ Part of this work performed under the auspices of the US Atomic Energy Commission.

INTERNAL-CONVERSION ELECTRON MEASUREMENTS

Internal-conversion electrons from slow neutron capture in ^{157}Gd were measured with the beta spectrometer at Studsvik [3] under conditions similar to those described in Ref. [4]. Targets were prepared from 93.7% enriched ^{157}Gd .² A total of seven targets were used, with thicknesses ranging from 0.02 to 3.6 mg/cm². Energy calibration was made relative to the 1173.23 ± 0.04 keV transition in ^{60}Ni [5].

The region from 20 to 1630-keV electron energy was scanned. About 340 conversion lines belonging to about 250 transitions were detected. The spectrum was similar to that shown in Bäcklin's paper to this Symposium [6].

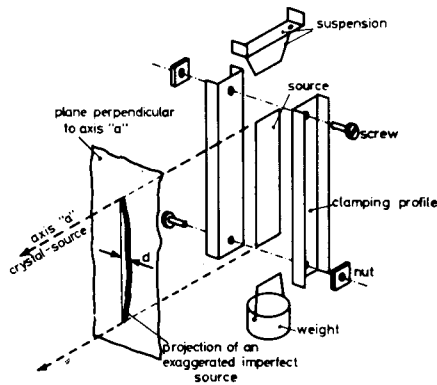


FIG. 1. Source used for measurements with diffracting spectrometer.

BENT-CRYSTAL SPECTROMETER MEASUREMENTS

The source used in this experiment contained 13 mg of $^{157}\text{Gd}_2\text{O}_3$ enriched to 98.6%.³ The source had the dimensions 26 × 4 × 0.045 mm. It was clamped between two plane ground aluminium U-profiles (Fig. 1) to keep the source flat because the line width (i. e. resolution) of the Risø spectrometer is mainly determined by the width d of the projection of the source. The line width obtained with the ^{157}Gd source was 1.7 - 2.0 seconds of arc, corresponding to an energy resolution of

$$\frac{\Delta E(\text{FWHM})}{\text{keV}} = \frac{3.3 \text{ to } 3.9}{n} \times \left(\frac{E}{\text{MeV}} \right)^2$$

in the n^{th} order of reflection (i. e. in the 5th order the FWHM is 0.66-0.78 keV at 1 MeV). The actual structure of the $^{157}\text{Gd}(n, \gamma)^{158}\text{Gd}$ spectrum below 1.5 MeV shows that this resolution is urgently required (Fig. 2). In some small energy regions an even better resolving power would be desirable and the remeasurement of these parts with a thinner

² Purchased from Union Carbide Nuclear Co., Oak Ridge.

³ Purchased from Austrian Atomic Research Center, Seibersdorf.

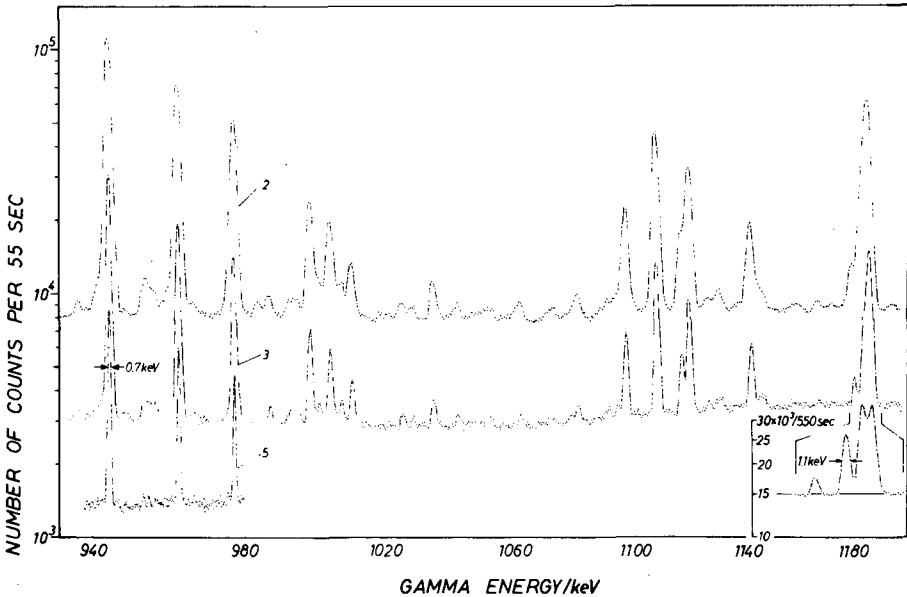


FIG. 2. Part of the ^{157}Gd thermal neutron capture gamma spectrum measured with a crystal spectrometer in the 2nd, 3rd and 5th order of reflection.

source has been planned. Improvement of the resolution by a factor of 1.4 seems to be possible [1].

Forty gamma transitions with a total of 139 different angular positions (different orders of reflection) were used to calculate the coefficients of a 4th degree polynomial for the correction of all reflection positions for non-linearities of the crystal drive [1]. The mean error of the reflection angles thus corrected is 0.15 seconds of arc for intense lines. Thus the lower limit of the energy error for strong lines after averaging of the information from different orders of reflection is

$$\frac{dE}{eV} = \pm 45 \times \left(\frac{E}{\text{MeV}} \right)^2$$

The high capture cross-section of 254 000 b for ^{157}Gd causes a reduction of the neutron flux to 1% of the incident intensity at a depth of 15 μm from the target surface. With a thickness of 45 μm the source was therefore completely black to neutrons at the beginning of the irradiation. Two thin active layers on both sides of the flat source emitted the gamma radiation. At the beginning of the experiment the line width was 2.0 seconds of arc. In the course of 10 days it decreased to 1.7 sec because the radiating layers moved towards the middle of the source foil due to burn-out of the ^{157}Gd .

This burn-out complicates the determination of intensities. In addition, small angular movements of the source around its vertical axis give rise to drastic alterations of the gamma self-absorption in the source at low energies. On the other hand, the high cross-section offers

a convenient method of overcoming these problems. A 23-mm long aluminium tube of 1 mm outer and 0.4 mm inner diameter was filled with the isotope powder, and 20 of the stronger lines were measured with this cylindrical source. The measurement was carried out in one day so that burn-out did not affect the intensities. The self-absorption in a source of this kind is insensitive to rotations and can be calculated with high accuracy. The intensities measured in this way were used as reference values for the measurements with the thin source.

The gamma spectrum was measured in 2 runs and a total of 540 gamma transitions below 1.7 MeV were found, most of which were unknown, owing to lack in resolution and sensitivity in earlier experiments.

^{158}Gd level scheme

The co-operative work on the level scheme of ^{158}Gd is still at an early stage. For this reason we will restrict ourselves to a presentation and discussion of preliminary results on the ground-state rotational band (gsb) and the gamma-vibrational band (γb).

Ground-state rotational band

The gsb presented in this work (Fig. 3) is in general agreement with the published data. The bent-crystal spectrometer data have disclosed the 277-keV reflection as a close doublet ($E_1 = 277.818$ keV, $E_2 = 277.540$ keV, $I_1/I_2 = 1/25$; see Fig. 4). An estimate of the population of the 6^+ gsb level in ^{158}Gd drawn from a comparison with other deformed nuclei [7, 8] regarding the spins of the capturing states allows only the assignment of the 277.540-keV line as the $6^+ \rightarrow 4^+$ gsb transition in ^{158}Gd . This is confirmed by energy combinations of transitions depopulating the 4^+ and 5^+ level of the γb .

Gamma vibrational band

Kern et al. [9] have established the $I = 2^+$ to $I = 5^+$ members of the γb using (d, p) data measured by Shelton and Sheline. Bloch et al. [10] have found a 2^+ level at 1187 keV and a 4^+ level at 1357 keV in the (d, d') reaction. The γb established in the present work (Fig. 3) agrees with both of the previous results within the experimental error.

1187.07-keV 2^+ state

The 1187.0-keV level follows directly from the 6750.0-keV primary transition observed with the Idaho Ge(Li) diode. It is obtained independently from the 1186.99, 1107.67 and 925.45-keV lines, the gsb and the energy combination principle.

The 1186.99-keV ground-state transition corresponds very closely in energy to the 1185.85-keV transition from the 3^+ state of the γb to the 2^+ level in the gsb. However, the two lines are clearly resolved in the 5th order spectrum recorded with the Risø spectrometer (right-hand lower corner of Fig. 2). The 4 lines around 1180 keV were measured in a special run with a 10-times longer counting time to obtain better statistics.

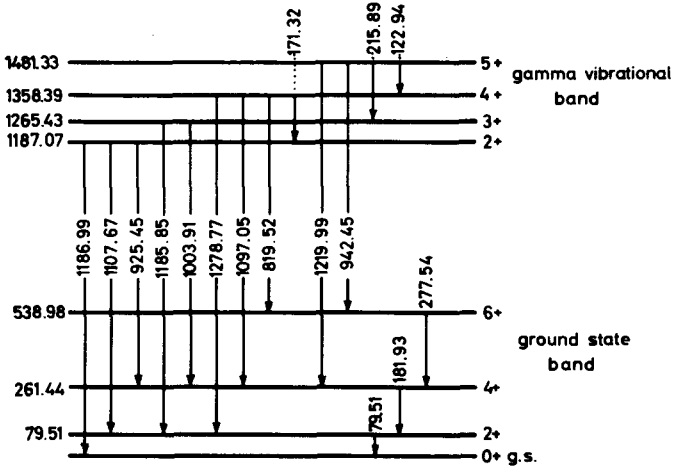


FIG. 3. ^{158}Gd level scheme.

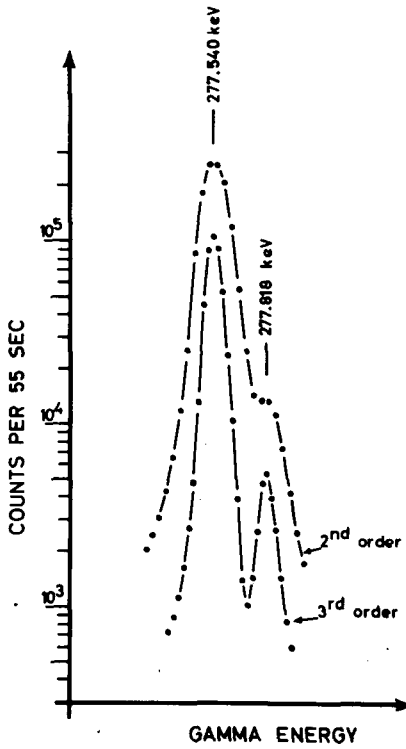


FIG. 4. The 277.5/277.8-keV doublet recorded in the 2nd and 3rd order of reflection.

TABLE I. ENERGIES AND MULTIPOLE ASSIGNMENTS OF THE TRANSITIONS FROM THE γ -VIBRATIONAL BAND TO THE LEVELS OF THE GROUND-STATE BAND

The conversion coefficients were normalized at the theoretical values [12, 13] of the strong 897 and 977-keV E1 transitions.

I_i	I_f	Transition energy	K-conversion coefficient $\times 10^3$			Assignment
			Exp.:	Theory:		
2	4	925.45	4.0 \pm 1.3	4.80	2.90	M1 or E2
	2	1107.67	1.97 \pm 0.14	3.12	2.01	E2 + < 10% M1
	0	1186.99	1.46 \pm 0.60	2.60	1.70	E2 + < 30% M1
3	4	1003.91	3.23 \pm 0.30	3.93	2.45	M1 + (47 \pm 20)% E2
	2	1185.85	1.56 \pm 0.60	2.60	1.70	E2 + < 50% M1
4	6	819.52	< 4	6.35	3.65	E2 + < 15% M1
	4	1097.05	2.12 \pm 0.14	3.12	2.01	E2 + < 25% M1
	2	1278.77	1.50 \pm 0.25	2.20	1.48	E2 + < 45% M1
5	6	942.45	2.5 \pm 1.3	4.50	2.75	E2 + < 65% M1
	4	1219.99	1.56 \pm 0.25	2.50	1.65	E2 + < 20% M1

1265.43-keV 3^+ state

This level is disclosed through the energy combination of the 1185.85 and 1003.91-keV lines leading to the 2^+ and 4^+ members of the gsb. It is directly fed from the compound state; the corresponding 6671.6-keV line was disclosed in the high-energy gamma data.

Bloch et al. [10] have observed a level at 1263 keV in their (d, d') data. They state that this level cannot be the 3^+ member of the γ_b , which should not be populated in the (d, d') reaction. Kern et al. [9] calculated the spectroscopic factors for (d, p) excitation of gamma-vibrational states in even deformed nuclei on the basis of the current microscopic description. They find good agreement between theory and experimental data for all states in the γ_b of ^{158}Gd with exception of the 3^+ level, where the experimental value is too high. Our data have revealed the 3^+ member of the γ_b at 1265.43 keV. This result and the (d, d') and (d, p) data strongly indicate the existence of close-lying states whose spins and parities explain the cross-section found in the (d, p) and (d, d') experiments.

1358.39-keV 4^+ state

This level was established by the energy combination of the 1278.77, 1097.05 and 819.52-keV transitions to the 2^+ , 4^+ and 6^+ states in the gsb.

In addition, the 171.32-keV intraband transition to the 2^+ level of the γb was found.

1481.33-keV 5^+ state

Transitions to the 4^+ and 6^+ level of the gsb and the intraband transitions to the 4^+ and 3^+ states were observed.

The 942.45-keV transition to the 6^+ level of the gsb was not resolved in the first crystal-spectrometer run, but is indicated in the low-energy tail of the strong 944-keV transition in the 3rd order (Fig.2). In the 5th order of the 2nd run, however, the line has been clearly resolved.

Further intraband transitions were not observed. This is consistent with the calculated transition probabilities, which give intensities below the sensitivity limit of the experiment. The experimental branching ratios of the gamma transitions from the γb to the gsb are in good agreement with theory. The z-parameter expressing the rotation-vibration interaction [11] is about 0.03. This value is based on the results of the first run at the Risø-spectrometer only, since the evaluation of the second run has not yet been finished.

The conversion coefficients for the transitions from the γb to the gsb are listed in Table I.

ACKNOWLEDGEMENTS

The Risø group wants to thank Professor Dr. H. Maier-Leibnitz for his constant support of this work. Furthermore, we are indebted to Professor Dr. O. Kofoed-Hansen, Professor Dr. T. Bjerger and the Danish Atomic Energy Commission for their hospitality during the measurements at the Risø Research Establishment.

REFERENCES

- [1] KOCH, H.R. et al., "The automation of the curved-crystal spectrometer at Risø", these Proceedings.
- [2] HELMER, R.G., GREENWOOD, R.C., REICH, C.W., "Levels in ^{182}Ta ", these Proceedings.
- [3] BÄCKLIN, A., Nucl. Instrum. Meth. 57 (1967) 261.
- [4] FOGELBERG, B., BÄCKLIN, A., "A $K=2^+$ band in ^{178}Hf ", these Proceedings.
- [5] MURRAY, G., GRAHAM, R.L., GEIGER, J.S., Nucl. Phys. 63 (1965) 353.
- [6] BÄCKLIN, A. et al., "Energy levels in ^{156}Gd ", these Proceedings.
- [7] SCHULT, O.W.B., GRUBER, U., MAIER, B.P.K., STANEK, F.W., Z. Phys. 180 (1964) 298.
- [8] KOCH, H.R., Z. Phys. 192 (1966) 142.
- [9] KERN, J., MIKOSHIBA, O., SHELIN, R.K., UDAGAWA, T., YOSHIDA, S., Nucl. Phys. A104 (1967) 642.
- [10] BLOCH, R., ELBEK, B., TJØM, P.O., Nuc. Phys. A91 (1967) 576.
- [11] HANSEN, P.G., NIELSEN, O.B., SHELIN, R.K., Nuc. Phys. 12 (1959) 389.
- [12] SLIV, L.A., BAND, I.M., Izv. Akad. Nauk SSSR (1956).
- [13] HAGER, R.S., SELTZER, E.C., Nuclear Data A4 1, 2 (1968).

ANGULAR CORRELATION MEASUREMENTS ON GAMMA-RAY CASCADES FOLLOWING THERMAL NEUTRON CAPTURE

H. SCHMIDT, D. HECK

Institut für angewandte Kernphysik,
Kernforschungszentrum Karlsruhe,
Karlsruhe, Federal Republic of Germany

Abstract

ANGULAR CORRELATION MEASUREMENTS ON GAMMA-RAY CASCADES FOLLOWING THERMAL NEUTRON CAPTURE. An experimental arrangement for angular correlation measurements on gamma-ray cascades following thermal neutron capture which is operated on-line to a computer is described. All of the interesting information can be accumulated simultaneously so that the determination of a large number of angular correlations is possible. Systematic errors arising from the coincident background under the peaks and from the complex structure of the capture spectrum can be eliminated either by a two-dimensional spectrum stripping procedure or, with sufficient accuracy, by application of the double-window technique. Practicable handling of data and comprehensive controls are thus possible. The extensive set of data obtained allows the results and their mutual consistency to be checked.

1. Introduction

Angular correlation measurements are of particular interest in experimental nuclear physics, because they supply information on characteristic properties of nuclear states that are necessary for the interpretation of nuclear level schemes and often constitute the basis for comparison with suggested nuclear models. Difficulties encountered in angular correlation measurements on γ -ray cascades following thermal neutron capture may arise mainly from the large number of γ rays usually present in the capture spectra and the high background coming from Compton scattered high-energy γ rays. In many cases, the capture cross sections are small and only small amounts of target material are available, thus requiring long measuring periods. Since the stability of the experimental equipment is limited, overly long measuring periods may also introduce errors, and one is forced to accumulate as much useful information as possible in a preset time. Another problem is the elimination of the coincident background underlying the peaks. This background is the main source of systematic errors in these measurements.

2. General Aspects

A difficulty common to all angular correlation measurements is the fact that the results can not always be explained unambiguously. In general, five unknowns are involved in a two-step cascade, namely the spins of the initial, intermediate and final levels and the multipole mixtures, δ , of the two γ -transitions. However, only the two coefficients A_2 and A_4 of the Legendre polynomials P_2 , P_4 in the correlation function

$$W(\theta) = 1 + A_2 P_2(\cos \theta) + A_4 P_4(\cos \theta) \quad (1)$$

can be determined. In eq. (1), $W(\theta)$ is normalized so that $A_0 = 1$. Octupole radiation is assumed to be negligible.

In many cases, the number of unknowns can be reduced either by using additional information from other experiments or by suitable choice of the experimental conditions. In neutron capture spectra primary transitions play a special role. If s-wave neutrons are captured in a target nucleus with spin I_t , the two spin states $I_p = I_t \pm 1/2$ are formed in the product nucleus. For even target nuclei one gets the unique capturing state spin $I_p = 1/2$ and the spins of lower levels may be determined from the angular correlation of two-step cascades involving primary transitions. If the spin of the ground state is known, it is useful to measure the correlation of cascades beginning in the capturing state and ending in the ground state and to apply the well known sum coincidence technique. For such measurements, however, only cascades with intense primary transitions can be used. These transitions are of pure dipole, mostly E1, character [1]. Hence, $A_4 = 0$ and only one measurable parameter remains. An unambiguous spin determination is possible if the final state has a parity different from that of the intermediate state and if it can be assumed from the radiation intensities that the second transition also has predominantly dipole character. With odd spin target nuclei this method can be applied if the thermal neutron capture is determined mainly by a single resonance or by resonances with the same spins. But, in general, both possible spin states participate in thermal neutron capture. The extent of their contribution to a certain primary transition cannot be stated in advance, since the resonance parameters and the partial radiation widths required for the calculation are not known accurately enough. In the theoretical expression of the angular correlation another unknown parameter then occurs which describes the branching of the intensity of the primary transition between the two spin states. This precludes an unambiguous interpretation in many cases. Therefore, in even product nuclei it is often more advantageous to investigate the angular correlation of γ rays in cascade with the intense ground state transitions from the first or second excited 2^+ levels. These transitions have pure quadrupole character and the remaining two unknown quantities can be determined, in principle, by the measurement of one correlation. The price for this advantage is the greater complexity of the spectra taken in coincidence with low-energy γ rays and the higher background compared to the simpler spectra coincident with high-energy primary transitions.

The ambiguity of the information can also be removed by the measurement of a larger number of correlations, which partially involve the same levels and transitions. If, for example, in a triple cascade (Fig. 1) the spin of the lowest level is known, the six unknown quantities $I_1, I_2, I_3, \delta_1, \delta_2, \delta_3$ can be determined from the three angular distributions:

$$W_{\gamma_1-\gamma_2}(\theta) = W(I_1, I_2, I_3, \delta_1, \delta_2, \theta)$$

$$W_{\gamma_2-\gamma_3}(\theta) = W(I_2, I_3, I_4, \delta_2, \delta_3, \theta)$$

$$W_{\gamma_1(\gamma_2)\gamma_3}(\theta) = W(I_1, I_2, I_3, I_4, \delta_1, \delta_2, \delta_3, \theta)$$

FIG. 1. Unknown quantities involved in a triple cascade.

The method applied to this simple example can easily be extended showing that as many cascades as possible should be investigated. Knowledge of their angular distribution also allows for valuable checks and permits accurate corrections for perturbing coincidences. Furthermore, a redundancy of the results is highly desirable in view of the many possible sources of error. Since the measurements require a long time to accumulate meaningful statistics, the maximum number of correlations of interest should be measured in one run. The best way to fulfil this requirement and overcome the difficulties is to perform a three parameter experiment with two parameters available for the energies of the γ rays in cascade and one parameter for the angle defined by the detector positions.

3. Experimental Details

There were some other factors that determined the arrangement of our equipment in the present form. One of these was the intention to avoid systematic errors as far as possible and another one was the need for the investigation of nuclei with small neutron capture cross sections.

The setup of the equipment has been described in detail in earlier work [2]. Only the main points will be repeated below. Fig. 2 is a schematic drawing of the arrangement installed at a horizontal core channel of the Karlsruhe research reactor FR-2. Thermal neutrons are diffracted from a lead single crystal in order to remove fast neutrons and γ -ray contamination present in the initial beam. Up to now

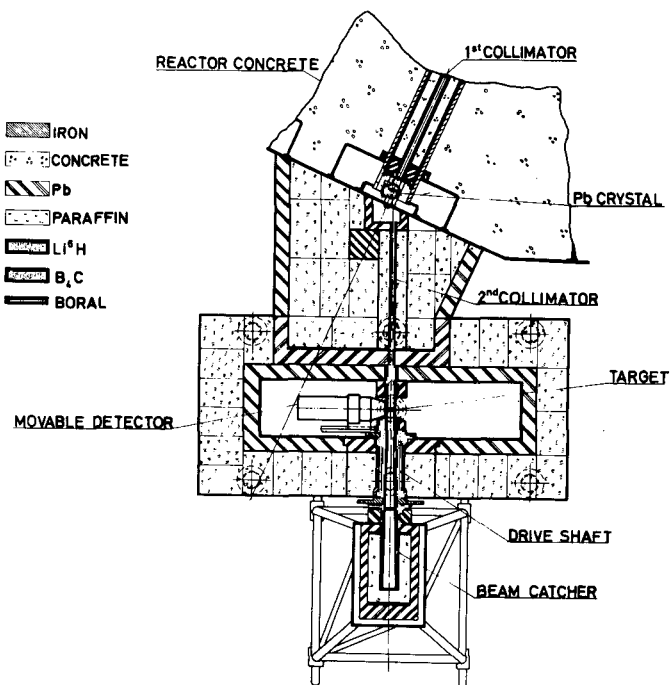


FIG. 2. Schematic drawing of experimental arrangement at the Karlsruhe research reactor FR-2.

the target was viewed by two gain-stabilized [3] scintillation spectrometers with 4" dia. x 5" long NaI(Tl) crystals mounted in a plane perpendicular to the neutron beam, one detector being fixed in the vertical direction. This detector can easily be replaced by a Ge(Li) diode. The other detector can be rotated around the axis of the beam for a range of angles from 60° to 360° with respect to the stationary detector. To avoid systematic errors due to incorrect adjustment of the source or of the beam and for purposes of control during the subsequent evaluation of data the movable detector is cycled through the angular range of two quadrants. The electronics include conventional coincidence circuits and sum coincidence circuits as well. The usual fast-slow technique is applied with an effective time resolution of $2\tau = 25$ nsec in the fast coincidence stage.

The entire system operates automatically. It is controlled by a neutron monitor located in front of the target in the deflected beam. A preselected number of neutron pulses determines the measuring time in one angular position. At the end of the interval the control counters are punched out, and the next angular position is set according to the selected program. The typical measuring time in one angular position is 30 minutes. Dead times of the equipment, especially those of the ADC, are taken into account automatically.

4. Data Acquisition

Recording of data is done with the dual ADC coupled to the Karlsruhe data acquisition system MIDAS (Multiple Input Data Acquisition System) [4, 5].

As shown in Fig. 3, the heart of this system consists of the coupled CDC 160 A and CDC 8090 computers, processor 1 and 2, respectively. A disk storage is used for on-line totalizing up to 256 K channels with a length of 21 bits. A total of 68 K channels is available for the angular correlation experiment and three subroutines are at the disposal of the experimenter. In the first subroutine the digital pulse height information is accumulated on the disk in a 256 x 256 channel matrix without any reduction. Whenever the angle between the detectors is changed, the data are read out automatically on magnetic tape and the disk area is cleared. Further data processing is carried out on a large off-line computer. Storage in full resolution allows for application of a two-dimensional spectrum stripping procedure which has been proved to be most suitable for off-line background elimination [6]. In most cases, a more direct processing is preferred which can be achieved by use of the double window technique [7]. This method is not as rigorous, but sufficiently accurate results are obtained faster and more easily. Fig. 4 demonstrates the application of the method. In order to systematically correct for the spectrum coincident with background underlying a peak of interest two or even three windows are needed. One window is centered on the peak, while the second and third windows, having in total the same width as the first one, select pulses of slightly higher or lower energy which might come from Compton scattering of higher-energy gamma rays or from interfering transitions (cf. below for more details). As shown in the figure the contributions of the individual primary γ rays to the coincidence spectra are clearly separated. For instance, in the coincidence spectrum with the 6.96 MeV transition none of the lines which are in coincidence with the strong 7.26 MeV transition appears while in the singles spectrum the 6.96 MeV transition is only a very small bump. The technique requires a second MIDAS subroutine which allows digital windows to be set on the energy axes. The coincident pulses are routed into subsections of the disk according to these

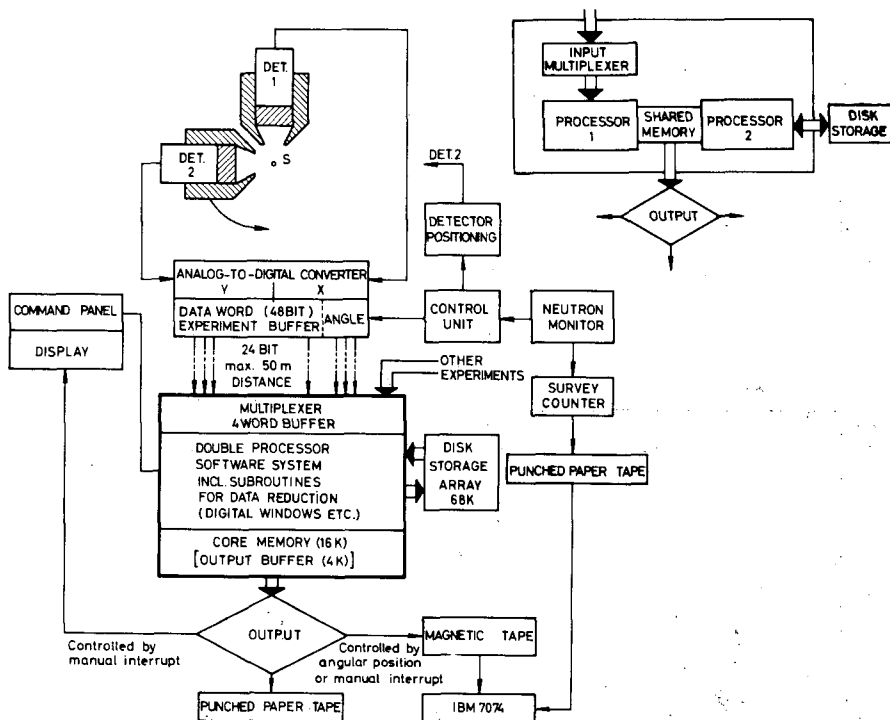


FIG. 3. Simplified block diagram of the data-acquisition system.

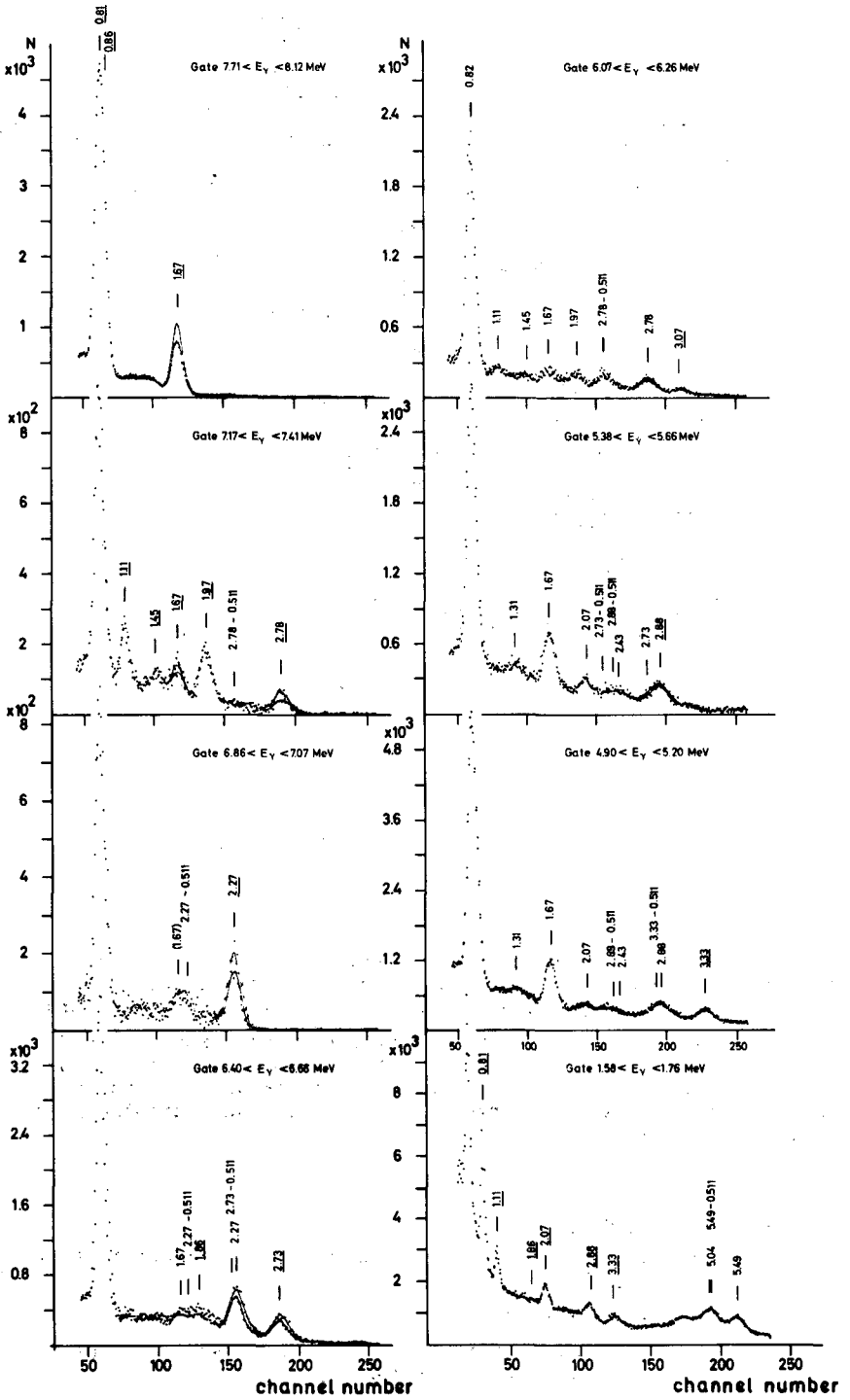
window settings and according to the angles defined by the detector positions. At present, a maximum of 32 windows can be set in each energy direction and 1024 channels are available for each spectrum.

Each section or group of sections of the disk can be displayed on the CRT, dumped on magnetic tape or punched out by manual interrupt so that a full evaluation of the state of the experiment is possible at any time. The presence of significant anisotropy is identified immediately (Fig. 5).

5. Off-line Data Processing

Off-line computer processing of the raw data consists of the following operations (Fig. 6):

- 1) Sorting out of faulty data.
- 2) Gain shift control (Corrections for small shifts in gain and base line are made if necessary).



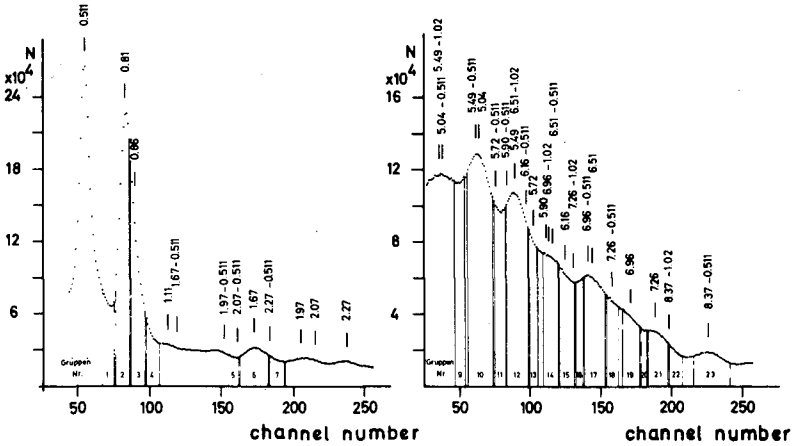


FIG. 4. ⁵⁷Fe(n, γ)⁵⁸Fe coincidence spectra at 90° and 180°. The coincident background is subtracted in each spectrum. Window settings in the spectrum of the fixed detector are shown above.

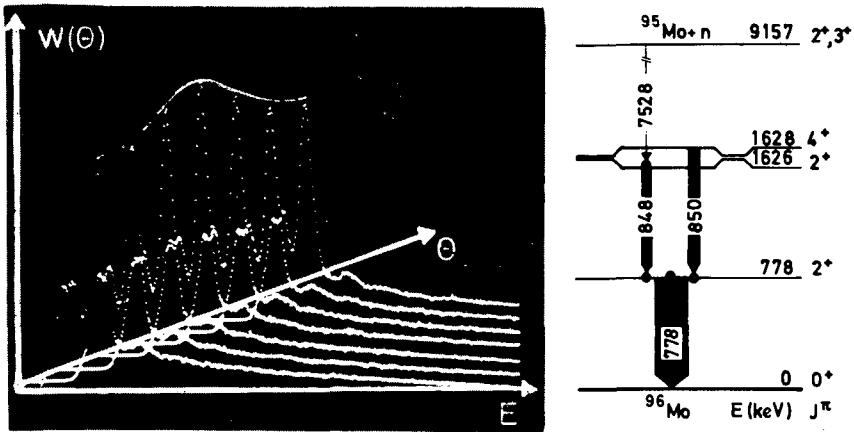
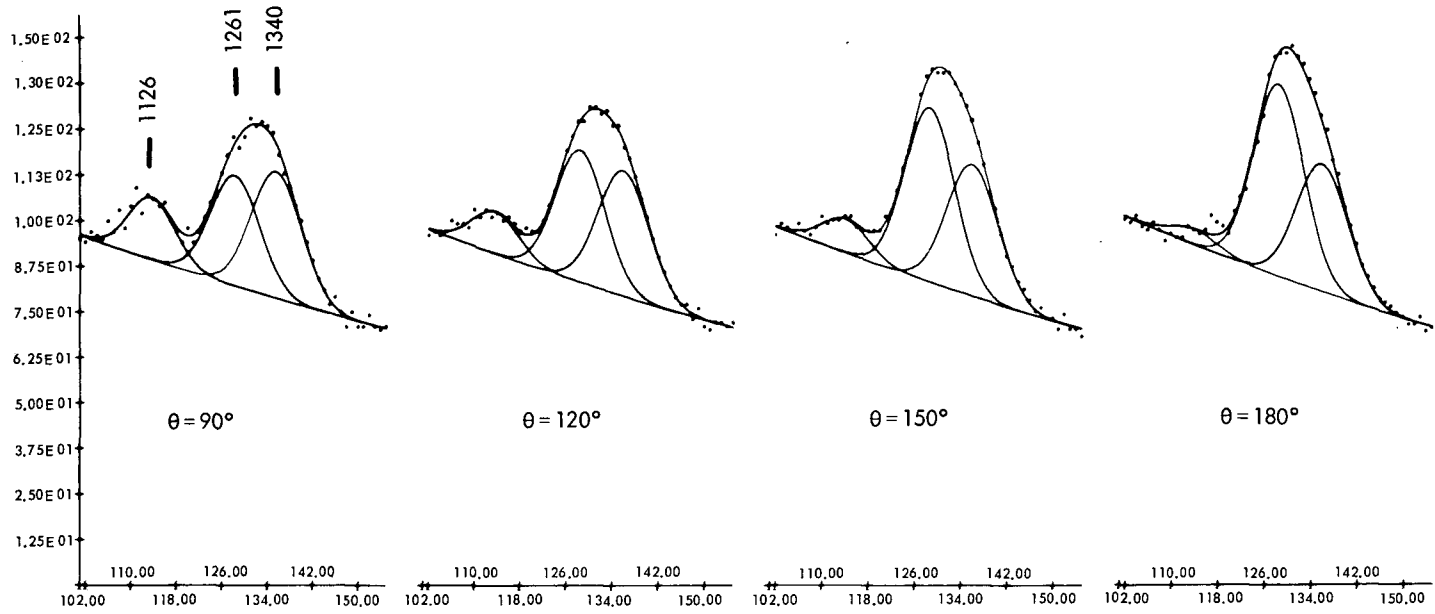


FIG. 5. Angular correlation of the (848 + 850) - 778 keV cascade from ⁹⁵Mo(n, γ)⁹⁶Mo displayed on CRT. NaI(Tl)-detector spectra taken at 90°, 120°, 150°, 180°, 210°, 240° and 270°. Digital window settings in the spectrum of the second detector at 850 keV. The relevant part of the ⁹⁶Mo decay scheme is shown.

- 3) Channel by channel summing up of all coincidence spectra pertaining to the same angles (not necessary if the data are totalized on the disk).
- 4) Normalization of the spectra to the individual counting rates of detectors 1 and 2.
- 5) Subtraction of accidental coincidences measured separately.
- 6) Two-dimensional spectrum stripping and determination of intensities, or correction for coincident background by application of double window technique.

from the spectrum shape. For further processing of the resulting spectra a computer program [8] is employed which allows the analysis of complex structures. An important factor in the analysis is the knowledge of the γ -ray energies and their relative intensities which is obtained from the singles spectra recorded with Ge(Li)-detectors. It is only in this way that complex peaks in the NaI-spectra can be decomposed unambiguously and correct estimates of the contributions of single lines to a measured angular distribution obtained. A measure of the intensities of the γ transitions is the area below the photopeaks. The calculation of this area with the computer program is based on the assumptions that the line shapes are Gaussian and the energy dependence of the background is a negative exponential function. The parameters of the approximation function are automatically determined by the program. Fig. 7 shows, as an example, the analysis of a doublet in ^{68}Zn . The intensity errors are compounded from the statistical errors of counting, contributions coming from errors in the goodness of fit and the uncertainties in determination of background underlying the measured peaks. In favourable cases the attainable accuracies are between 0.5 % and 1.0 %. As shown in the flow diagram (Fig. 6) data analysis is supervised by means of plots which are generated after each critical computer step. These plots are of great value, particularly for the intensity analysis since it may happen that the least squares fitting procedure of unfolding the spectra might fail to obtain the absolute minimum of χ^2 . In this case an iterative procedure is used to repeat the analysis with varied input parameters for line shapes and background. As usual the intensities are fitted with the angular correlation function $W(\theta)$ [eq.(1)] using the method of least squares [9]. Since the coincidence spectra are taken in at least four angular positions, it is possible to check the goodness of fit by a χ^2 -test. If there are indications of errors beyond the ordinary statistical uncertainties, the errors associated with the correlation coefficients A_k are increased according to the description given by Rose [9]. The uncertainty in the determination of the background is also taken into account. The correlation coefficients are corrected for the effects of the finite size of the source and the detectors, and the interaction processes of the gamma quanta and of the neutrons in the source, using the methods of Michaelis [10] and White [11]. If there are contributions of interfering lines, e.g. single or double escape peaks of higher-energy γ rays which can neither be resolved by the spectrometers nor be taken into account by application of the computer programs the correlation coefficients obtained have to be corrected for these contributions in a final step.

Spins and multipole mixtures are determined from the angular correlation coefficients by application of well-known analytical and graphical methods. For the analysis of correlations with one mixed transition the method recommended by Coleman [12] has proved to be most convenient. This method allows the representation of a larger number of results in one diagram thereby giving a good idea of the precision of the measurements. The method is also used for the analysis of correlations with two mixed transitions. With the aid of a computer and an incremental plotter it is easy to plot the necessary series of ellipses each of which represents the variation of one mixture while the other is fixed at a particular value. In other cases, a new procedure [2] is applied which is developed from the method described by Poletti and Warburton [13].



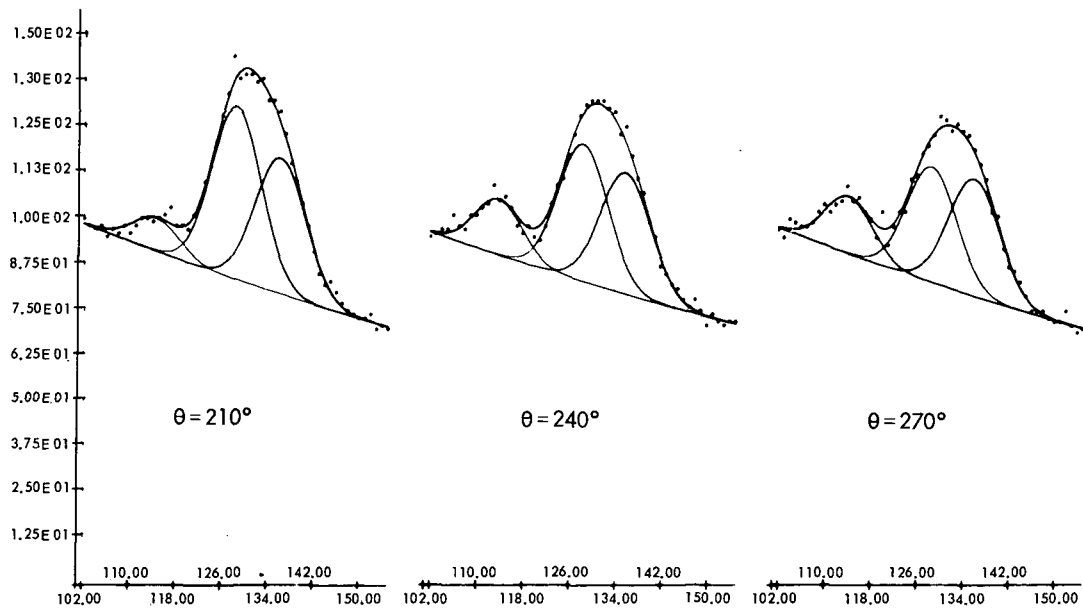


FIG. 7. $^{67}\text{Zn}(n, \gamma)^{68}\text{Zn}$ angular correlation analysis of the complex peak at 1300 keV [18].

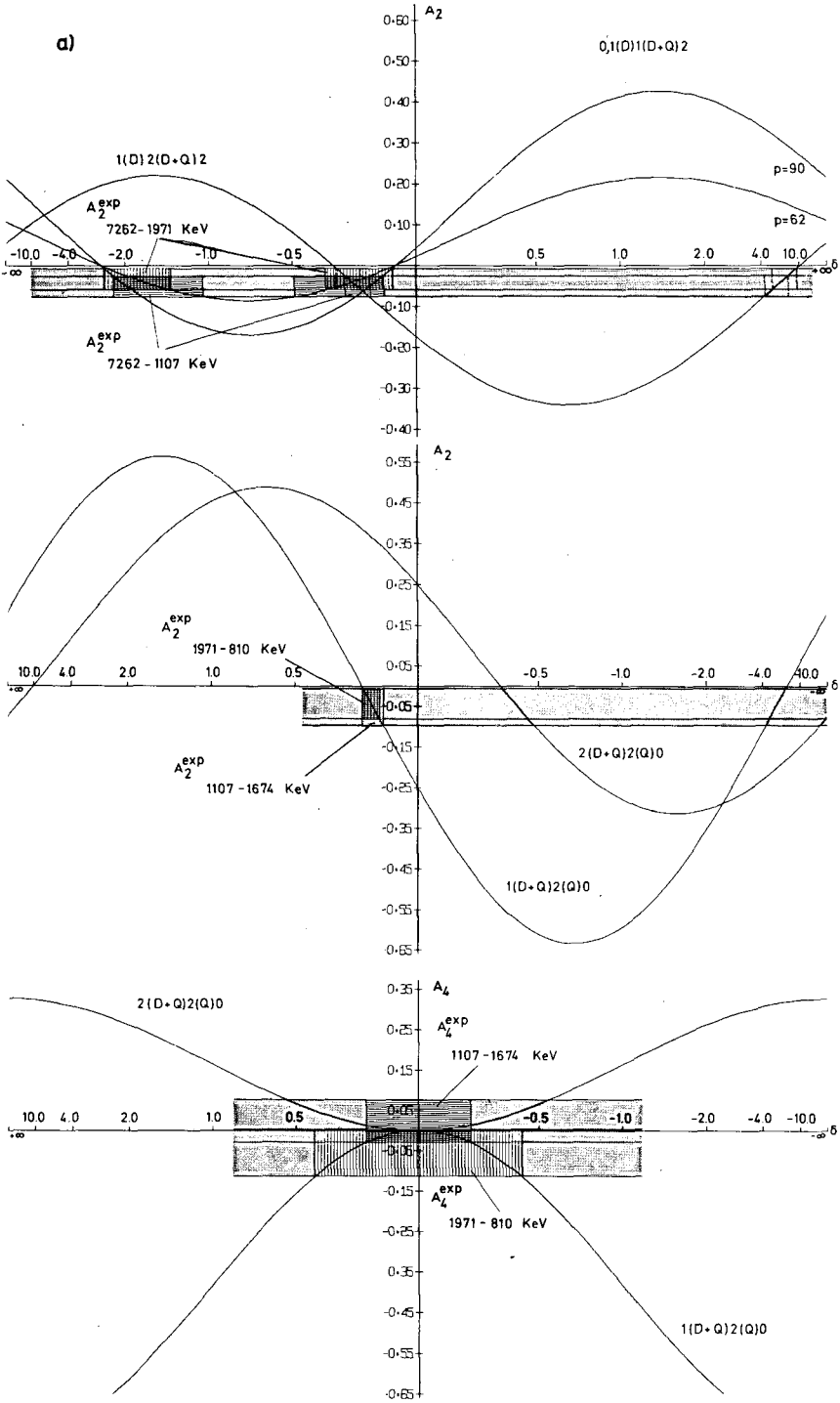
6. Test Measurements

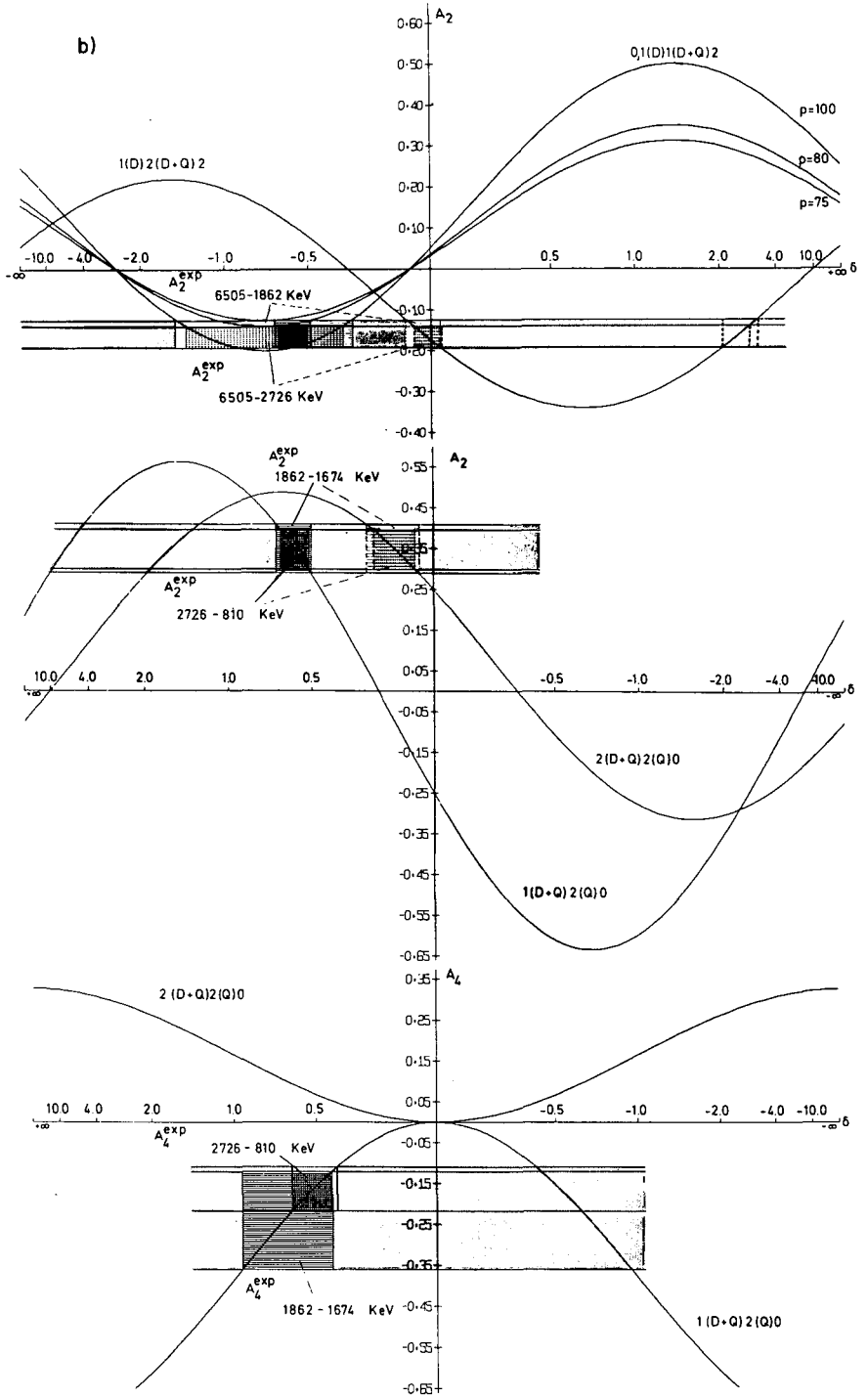
The equipment was carefully tested for mechanical asymmetries, e.g. eccentricity of the target position and eccentricity and inhomogeneity of the neutron beam. With various γ -ray sources the change in counting rate at the different angles was in general less than $\pm 0.5\%$. As a further test, the angular distribution of the 2.38 - 0.84 MeV cascade from the reaction $^{32}\text{S}(n,\gamma)^{33}\text{S}$ was investigated. This cascade goes through an intermediate state with spin $1/2$ and hence has an isotropic distribution. The correlation measured with a sample of 7.13 g of pure sulfur in a sample holder of 1.8 cm diameter and 1.9 cm length resulted in values of the corrected angular correlation coefficient of $A_2 = 0.002 \pm 0.004$ and $A_4 = 0.008 \pm 0.012$. Thus, the distortion of the angular distribution by mechanical asymmetries can generally be regarded as small relative to the other sources of error. The equipment was tested and the program checked in a further series of measurements using ^{60}Co sources of various diameters. The correlations observed gave the expected results for the correlation function which is known to be $W(\theta) = 1 + 0.102 P_2(\cos\theta) + 0.009 P_4(\cos\theta)$. With a source of 2.6 cm diameter and 2.7 cm length the correlation function obtained was $W(\theta) = 1 + (0.107 \pm 0.006) P_2(\cos\theta) + (0.009 \pm 0.015) P_4(\cos\theta)$ showing that proper corrections were applied by the program.

7. Results

Some of the results obtained from angular correlation measurements on γ -ray cascades following thermal neutron capture in ^{57}Fe , ^{61}Ni , ^{67}Zn , ^{95}Mo and ^{97}Mo are presented in these proceedings [17 - 20]. From the systematics of even mass nuclei between $A = 50$ and $A = 100$ it is expected that the low energy levels of these nuclei are adequately described by the vibrational model. Recently reported shell-model calculations [14 - 16] have also been very successful in predicting correct level energies. In order to clarify the level structure, knowledge of the multipole mixtures of the transitions is of great importance. Therefore, angular correlation measurements are particularly valuable in this mass region.

Our investigations [20] on γ -ray cascades following thermal neutron capture in ^{57}Fe have been selected as an example to demonstrate the efficiency of the method. In this case, more than 40 correlations have been measured, 33 of which have been evaluated. An extensive set of results was obtained which allowed the mutually consistent determination of a large number of level spins and multipole mixtures. Some of the results are shown in Fig. 8 (Part of the decay scheme relevant to the angular correlation measurements under discussion is shown in Fig. 9). The upper row in Fig. 8 represents the analysis of cascades involving a primary transition. The capturing state of ^{58}Fe is an unknown mixture of 0^- and 1^- states. P is the parameter indicating the relative contribution (in %) of the spin 0 states to a particular primary γ ray. The mixture parameter δ of the second member of these cascades is taken as the abscissa; the angular correlation coefficients are the ordinates. In all cases, the spin of the final state is 2. It can be concluded from the intensities that the primary transitions have an $E1$ character. Therefore, the following three alternative spin sequences are possible $0 - 1 - 2$, $1 - 1 - 2$, and $1 - 2 - 2$. The sequence $1 - 0 - 2$ was ruled out because of the nonzero anisotropies observed in these measurements. The middle and bottom rows of the diagrams refer to cascades with ground state transitions. The first member of each of these cascades is the same γ ray





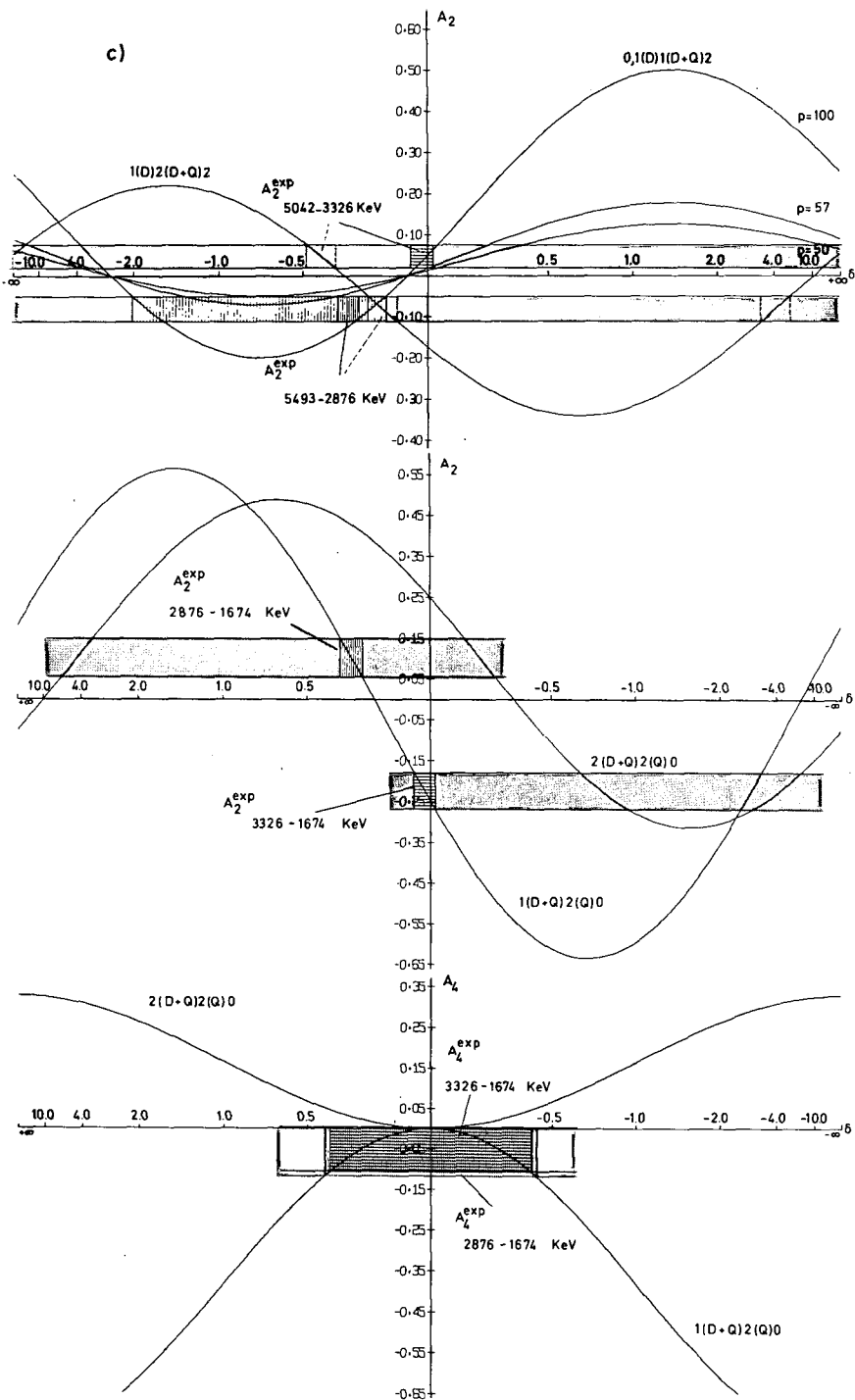


FIG. 8. $^{57}\text{Fe}(n, \gamma)^{56}\text{Fe}$ angular correlation measurements. Hatched bands represent the experimental results. Change in the sign of δ has been taken into account (cf. text).

as the second member of the cascades in which primary transitions are involved. With the definition adopted for δ [21] a change in sign of δ is necessary because of the different γ -ray order in these cascades. This has been taken into account by reversing the sign of the abscissa in the middle and the bottom rows. The observed γ -ray intensities and the neutron orbital momenta known from (d,p) reactions restrict the possible spin sequences in the low-energy cascades to 1 - 2 - 0 and 2 - 2 - 0. The spin 1 assignment of the 2782 keV level and the branching of the 7262 keV transition between the two capture state spins is determined from the angular correlation of the 7262-2782 keV two-step cascade to the ground state (Fig. 9). This branching ($p = 76 \pm 14$) and the spin assignment is adopted to determine the multipole mixtures of the 1971 keV and the 1107 keV transitions from the 7262-1971 keV and the 7262-1107 keV correlations, respectively. The results obtained are in excellent agreement with the values found from the analysis of the 1971-810 keV and 1107-1674 keV correlations (Fig. 8a).

It was not possible to determine the branching percentages of the 6505 keV, the 5493 keV and the 5042 keV transitions (Fig. 8b) and 8 c) directly through a two-step cascade to the ground state. These branchings were determined from the angular correlation measurements taking into account the mixture parameter δ of the second member of each cascade and the spin assignments of the intermediate states which are known from the analysis of the low-energy cascades to the ground state. In this way, for about 70 % of the observed intensity, the contributions of the two capture state spins (0^- , 1^-) to the intensities of the primary transitions have been accounted for.

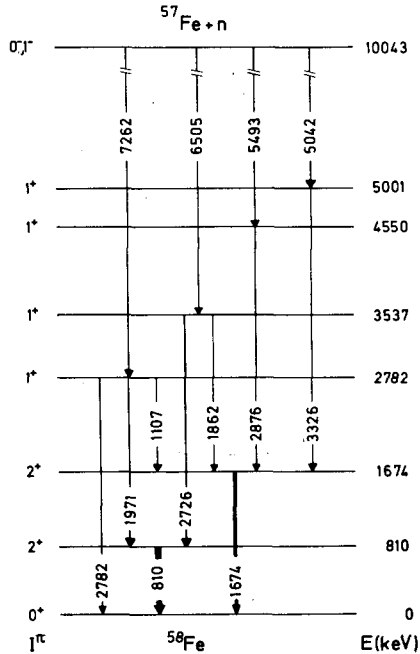


FIG. 9. Partial decay scheme relevant to the angular correlation measurements shown in Fig. 8.

References

- [1] G.A. Bartholomew and J.F. Vervier, Nucl. Phys. 50 (1964) 209
- [2] H. Schmidt, KFK 877
- [3] U. Tamm, Nucl. Instr. and Methods 40 (1966) 355
- [4] G. Krüger, G. Dimmler, G. Zipf, H. Hanak and R. Merkel, Kerntechnik 8 (1966) 273
- [5] G. Krüger, Proc. on Teilnehmer-Rechnesysteme, Oldenbourg, Verlag Munich and Vienna (1968) 135
- [6] T. Daniels, Nucl. Instr. 59 (1968) 214
- [7] D. White, Phys. Rev. 131 (1963) 777
- [8] V. Haase, KFK 730
- [9] M.E. Rose, Phys. Rev. 91 (1953) 610
- [10] W. Michaelis, KFK 135
- [11] D. White, Nucl. Instr. 21 (1963) 209
- [12] G.F. Coleman, Nucl. Phys. 5 (1958) 495
- [13] A.R. Poletti and E.K. Warburton, Phys. Rev. 137B (1965) 595
- [14] N. Auerbach, Phys. Rev. 163 (1967) 1203
- [15] S. Cohen, R.D. Lowson, M.H. Macfarlane, S.P. Pandya, and Michitoschi Soga, Phys. Rev. 160 (1967) 903
- [16] B. McGrory, Phys. Rev. 160 (1967) 915
- [17] U. Fanger, R. Gaeta, W. Michaelis, H. Ottmar, and H. Schmidt
Contribution to these Proceedings
- [18] H. Ottmar, N.M. Ahmed, U. Fanger, D. Heck, W. Michaelis,
and H. Schmidt; Contribution to these Proceedings
- [19] D. Heck, W. Michaelis, H. Ottmar and H. Schmidt
Contribution to these Proceedings
- [20] H. Schmidt, W. Michaelis, U. Fanger
to be published in Nucl. Phys.
- [21] L.C. Biedenharn, in Nuclear Spectroscopy, Part B, ed. by
F. Ajzenberg-Selove (Academic Press, New York, 1960)

LEVEL STRUCTURE OF LOW-LYING EXCITED STATES OF ^{187}W *

H. H. BOLOTIN, D. A. McCLURE**
Argonne National Laboratory,
Argonne, Ill., United States of America

Abstract

LEVEL STRUCTURE OF LOW-LYING EXCITED STATES OF ^{187}W . The low-lying excited states of ^{187}W populated by primary and secondary gamma-ray transitions from the $^{186}\text{W}(n, \gamma)^{187}\text{W}$ thermal neutron capture reaction were studied. Ge(Li) detectors were used exclusively in both singles and coincidence gamma-ray investigations. Coincidence investigations between high-energy ($\sim 4 - 5.5$ MeV) and low-energy (≤ 1200 keV) gamma rays, as well as among the low-energy transitions have allowed a total of 74 low-energy transitions to be assigned between states up to an excitation energy of 1217 keV. Several new levels have been inferred and the decay properties of all states observed have been established. The observed characteristics of these states are compared with the most recent (d, p) studies and a rotational model that included Coriolis band mixing.

I. Introduction

The odd-A deformed tungsten isotopes are close to the edge of the deformed region where rotational characteristics are not expected to be as strongly manifest as in nuclei close to the center of the deformed region. Nevertheless, the level structure of the low-lying excited states of W^{183} can be successfully interpreted in terms of a rotator-plus-odd nucleon model, when account is taken of Coriolis band mixing [1-3]. Although the low-lying levels of W^{185} and W^{187} also appear to display rotational-type structures [4] that have been described by this rotational model, fewer states at low excitation energy have been experimentally observed in these nuclides and, consequently, the degree of correspondence with this model is somewhat less certain. In contrast to W^{183} and W^{185} , the levels in W^{187} are not populated by beta decay and, as a result, less experimental information is available about the low-lying excited states and the characteristic radiative decay of the levels of this nuclide.

The low-lying excited states of W^{187} have been the subject of only a few previous experimental investigations [4]. The (d, p) work of Erskine [1] established the excitation energies of a number of levels up to ~ 1800 keV and resulted in orbital angular momentum assignments and Nilsson orbital specifications of five levels up to an excitation energy of 0.434 keV. The spectrum of the primary radiative transitions following thermal-neutron-capture in W^{186} was studied by Martin et al. [5] who succeeded in defining states in W^{187} up to an energy of ~ 1150 keV, some of which were not observed in the stripping study of Erskine. Finally,

* Work performed under the auspices of the US Atomic Energy Commission.

** Argonne Universities Association - Argonne National Laboratory predoctoral fellow.

Prokefev et al. [6] employed the thermal-neutron-capture reaction in a study of the internal-conversion electron spectrum of the secondary transitions in W^{187} and reported the energies of several low-energy γ -rays. Despite these efforts, many details of the level structure are still unknown or are poorly established.

The present experimental investigation of the levels in W^{187} was undertaken in an effort to provide additional detailed level structure information that might permit a more critical evaluation of the applicability of the simple rotational model to the low-lying states in this nuclide and/or point up any systematic behavior reflecting the approach of W^{187} to the edge of the deformed region.

This paper describes the results of a study of the low-lying states in W^{187} populated in the thermal-neutron-capture reaction $W^{186}(n, \gamma)W^{187}$. This investigation included studies of the primary and secondary transitions by means of singles and coincidence γ -ray techniques that made exclusive use of high-resolution Ge(Li) detectors. Coincidence data were recorded between the high-energy (~ 4 — 5.5 MeV) and the subsequently emitted low-energy transitions, as well as among the low-energy cascade γ rays.

II. Experimental Facilities and Techniques

An external-beam facility was employed to carry out these investigations. A highly collimated beam of thermal neutrons, effectively free of fast neutrons (Cd ratio ~ 570) and pile γ rays, was extracted from a modified thermal-column at the Argonne CP-5 reactor. An extremely well-defined beam (thermal flux $\approx 5 \times 10^7$ neutrons $\text{cm}^{-2} \text{sec}^{-1}$, height ≈ 2 cm, width ≈ 0.5 cm) was obtained by means of conventional collimators fitted with defining apertures of Li^6F disks enriched to 95.5% in Li^6 . The targets consisted of pressed cylindrical pellets of WO_3 enriched to 97.2% in W^{186} which were contained in thin-walled (4.5 mg/cm^2) aluminum holders.

Two coaxially drifted Ge(Li) detectors (active volumes ~ 20 and $\sim 30 \text{ cm}^3$) were mounted at 180° to each other and positioned 2.5 cm from the beam axis. Both detectors displayed an energy resolution of ~ 2.7 keV at 1.33 MeV deposited energy. The detectors were shielded by thin (0.25 cm thick) Li^6F disks to prevent scattered neutrons from entering the detectors or detector housings. The coincidence data were registered on a two-parameter magnetic tape storage unit in a 1024×1024 -channel pulse-height array. Digital gain and zero shift stabilization was employed in the ADC's of both arms of the coincidence system. A fast-slow coincidence resolving time of ~ 65 nsec was employed.

III. Results

Figure 1 displays a singles low-energy secondary γ -ray spectrum obtained for energies below ~ 1200 keV. Over 100 low-energy transitions were observed in this energy range. The energies and relative intensities of these γ rays are listed in Table I.

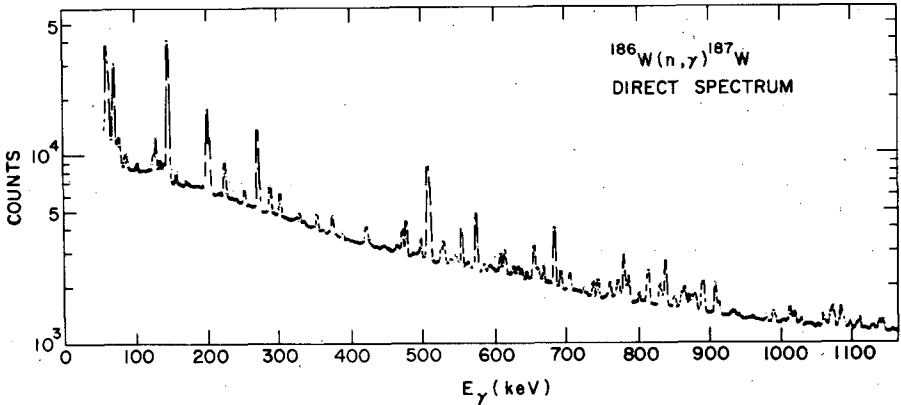


FIG. 1. Typical low-energy Ge(Li) singles pulse-height spectrum obtained for the reaction $^{186}\text{W}(n, \gamma)^{187}\text{W}$. Gamma-ray energies are listed above the appropriate peaks with lines indicating the position of the gamma ray in the case of unresolved multiple peaks. The energies and relative intensities are also listed in Table I.

Some typical high-low coincidence data are shown in Fig. 2. The upper portion of this figure displays the singles low-energy spectrum while the lower sections show various low-energy spectra in coincidence with the designated primary transitions. Representative low-low coincidence data are shown in Fig. 3 and are displayed in a similar format. The results of these coincidence studies are summarized in Tables II and III.

A proposed level scheme has been derived from the combined singles and coincidence γ -ray data and is shown in Fig. 4. The levels designated on the right by downward pointing flags are those previously observed in the (d,p) study of Erskine. With the exception of the state at 592 keV, all (d,p) levels up to ~ 1200 keV excitation energy were found to be populated by either primary or secondary γ -ray transitions in the (n, γ) reaction. In addition, a number of levels have been identified that were not seen in the (d,p) work. These coincidence data have also established several levels not observed to be populated by primary transitions, a number of which correspond to states populated in the (d,p) studies. The excitation energies of most states and the placement of the bulk of the transitions shown to proceed among them were dictated by the coincidence results. The remainder of the transitions were incorporated into the level scheme on the basis of their satisfaction of stringent energy and intensity criteria. All but the weakest transitions observed were found to be accommodated in this level scheme.

The necessity to include Coriolis band mixing in a comparison of the rotational model with experimental findings in the odd-A tungsten isotopes was previously demonstrated. Such a comparison was made by Erskine [1] who sought the best agreement with this model for the excitation energies and (d,p) strengths to those levels observed in his studies. The results of the present work have provided a great deal of new information

Table I. Energies and relative intensities of low-energy γ rays observed in W^{187}

Gamma-ray energy (keV)	Relative gamma-ray intensity ^a	Gamma-ray energy (keV)	Relative gamma-ray intensity ^a
101.8 ± 0.2	1.4	500.0 ± 0.2	8.6
124.3 ± 0.4	5.4	528.0 ± 0.3	5.7
127.7 ± 0.2	12.3	531.3 ± 0.3	9.2
139.8 ± 0.6	4.2	533.3 ± 0.6	3.5
145.7 ± 0.1	100	541.1 ± 0.4	3.5
149.0 ± 0.4	4.1	546.3 ± 0.7	2.8
157.4 ± 0.2	3.6	548.0 ± 0.8	3.8
171.6 ± 0.2	1.7	557.2 ± 0.1	23.4
175.1 ± 0.8	0.8	566.7 ± 0.6	2.2
198.2 ± 0.4	3.0	574.2 ± 0.9	2.3
201.4 ± 0.1	51.6	577.3 ± 0.1	36.8
204.9 ± 0.3	23.0	580.9 ± 0.8	1.9
219.0 ± 0.5	1.0	588.8 ± 0.4	3.3
225.9 ± 0.2	13.6	611.2 ± 0.2	8.6
227.4 ± 0.6	2.6	616.1 ± 0.3	9.0
250.7 ± 0.8	0.7	628.9 ± 0.2	3.0
253.4 ± 0.2	6.0	634.5 ± 0.4	2.0
273.0 ± 0.1	51.8	635.9 ± 0.4	2.7
276.3 ± 0.6	2.5	640.5 ± 0.3	3.2
287.0 ± 0.3	1.6	647.4 ± 0.3	2.7
289.9 ± 0.1	11.6	656.1 ± 0.3	8.4
294.3 ± 0.3	1.0	657.8 ± 0.5	12.2
303.3 ± 0.1	10.4	661.5 ± 0.5	4.3
330.7 ± 0.3	3.1	664.0 ± 0.5	3.0
337.7 ± 0.6	1.1	670.3 ± 0.2	6.9
354.8 ± 0.2	6.2	676.9 ± 0.4	1.0
376.7 ± 0.1	8.8	694.3 ± 0.3	7.3
390.6 ± 0.4	2.7	703.9 ± 0.8	1.4
423.9 ± 0.2	9.0	706.5 ± 0.3	6.2
428.1 ± 0.2	2.9	708.4 ± 0.9	1.3
466.0 ± 0.5	2.6	726.1 ± 0.3	2.5
469.0 ± 0.6	2.3	738.9 ± 0.2	5.7
474.0 ± 0.1	12.0	746.1 ± 0.3	6.9
489.4 ± 0.3	1.9	759.1 ± 0.7	1.5
495.0 ± 0.4	2.8	762.9 ± 0.3	7.1

Table I. (Cont'd.)

Gamma-ray energy (keV)	Relative gamma-ray intensity ^a	Gamma-ray energy (keV)	Relative gamma-ray intensity ^a
770.1 ± 0.9	2.1	934.4 ± 0.7	1.9
775.1 ± 0.7	6.2	936.7 ± 0.7	1.4
778.2 ± 0.9	1.7	941.3 ± 0.5	1.7
782.3 ± 0.2	23.2	979.2 ± 0.3	2.1
786.0 ± 0.5	5.2	988.8 ± 0.5	3.7
789.0 ± 0.3	11.1	990.4 ± 0.6	2.9
803.3 ± 0.2	4.4	1008.6 ± 0.9	1.2
808.8 ± 0.8	1.2	1012.3 ± 0.3	6.9
813.8 ± 0.4	6.6	1015.7 ± 1.0	1.3
816.1 ± 0.4	15.1	1018.3 ± 0.4	4.5
832.0 ± 0.4	10.0	1027.2 ± 0.4	2.3
835.4 ± 0.8	3.8	1034.1 ± 0.8	1.8
840.1 ± 0.2	23.5	1042.3 ± 0.8	1.7
852.3 ± 0.2	4.6	1050.5 ± 0.7	1.3
860.6 ± 0.5	3.4	1058.0 ± 0.3	5.5
863.0 ± 0.5	5.6	1061.7 ± 0.8	1.8
866.0 ± 0.3	10.5	1067.3 ± 0.3	6.9
872.7 ± 0.2	6.5	1071.2 ± 0.2	10.6
877.4 ± 0.2	6.3	1078.6 ± 0.5	2.3
881.5 ± 0.2	7.8	1082.3 ± 0.2	9.6
889.1 ± 0.3	3.8	1086.1 ± 0.4	3.4
891.8 ± 0.2	13.8	1094.3 ± 0.4	2.7
894.6 ± 0.4	2.4	1103.8 ± 0.8	1.6
909.0 ± 0.2	15.2	1107.4 ± 0.3	4.4
912.3 ± 0.5	3.1	1126.4 ± 2.0	0.9
914.7 ± 0.5	4.2	1134.8 ± 0.2	4.8
931.5 ± 0.7	1.9	1139.6 ± 0.2	4.8

^aThe listed intensities of the gamma-rays are relative to that of the 145.7-keV γ -ray taken as 100. The errors in the relative γ -ray intensities are 5—10% of the listed values for intensities > 10 , 10—20% for the weaker transitions.

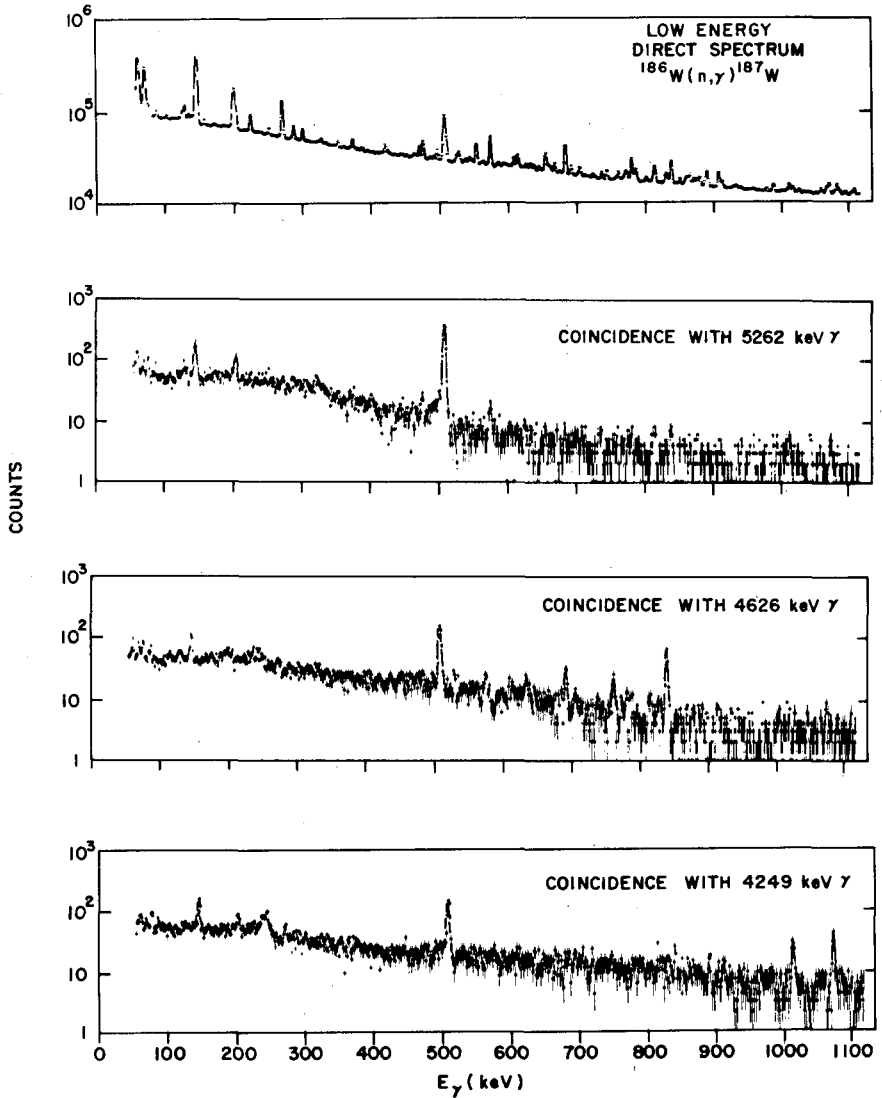


FIG. 2. Representative portions of the low-energy spectra in coincidence with the indicated high-energy gamma rays. The upper curve is the low-energy singles spectrum recorded under the same experimental conditions as the three lower coincidence spectra. In this figure no corrections have been made for chance coincidence events or events resulting from coincidences with higher-energy transitions whose continua underlie a particular high-energy coincidence gate. The contribution of chance events can be assessed by noting the relative heights of the 146, 201 and 273-keV transitions as compared to the direct spectrum in the upper curve whose shape is followed by the chance coincidence spectrum. In all cases the number of chance and underlying coincidence events were small compared to the number of real coincidence events.

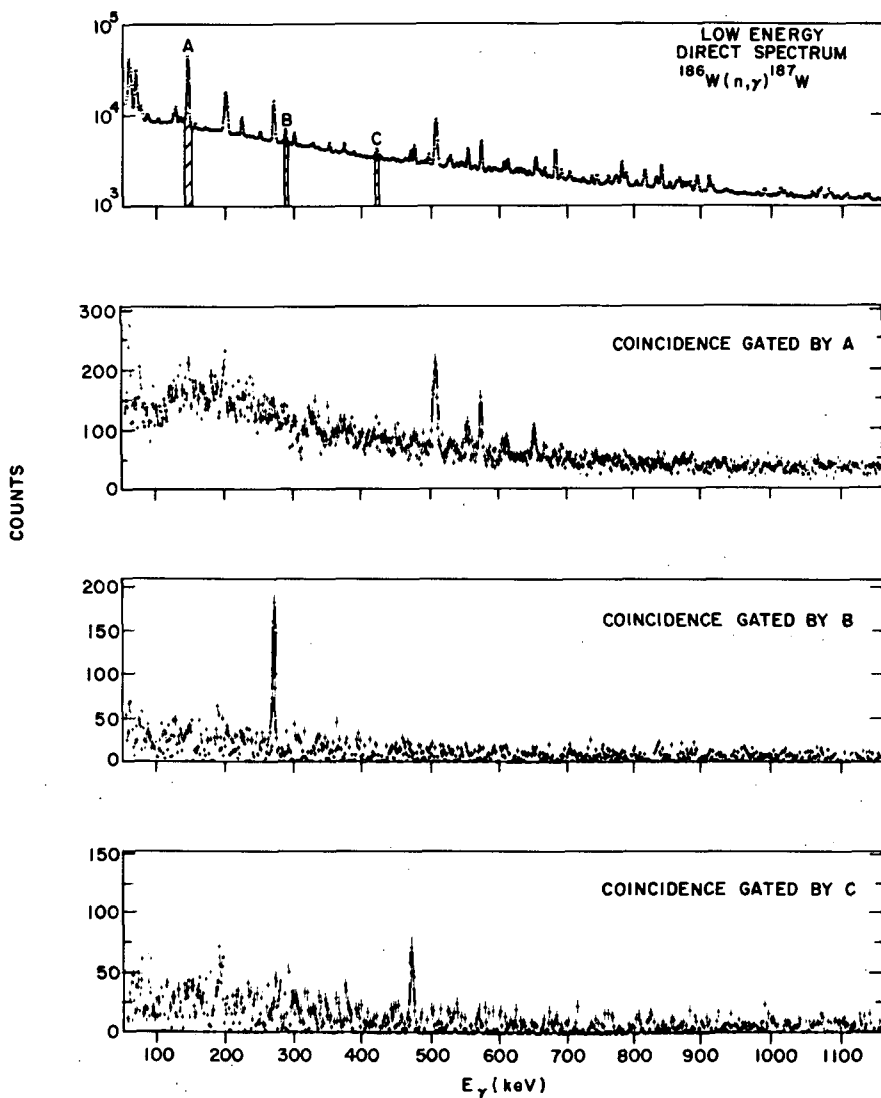


FIG. 3. Typical portions of the low-energy spectra in coincidence with the particular low-energy coincidence gates specified by the cross-hatched peaks of the singles spectrum shown in the upper portion of this figure. The three lower coincidence spectra shown have been corrected for chance coincidence events and for events due to those portions of the Compton distributions of higher energy transitions which underlie the respective coincidence gates employed. It should be noted that the direct spectrum (upper curve) is plotted on a semi-log scale while the coincidence spectra (three lower curves) are plotted on a linear scale.

Table II. Low-energy transitions observed to be in coincidence with high-energy primary γ rays in W^{187}

Gamma-ray energy (keV)	Coincidence Gamma-ray energies ^a (keV)
5321	146
5262	146, 205
4685	146, 205(?), 577, 782
4650	146, 205(?), 611, 670, 739, 816
4626	146, 694, 763, 840
4575	146, 746, 814, 892
4449	1018
4384	1082
4250	146, 205(?), 1012, 1071

^aThose γ -ray energies followed by (?) appear only faintly in the coincidence spectra and unambiguous establishment of their presence in these spectra is not claimed.

about the radiative decay characteristics of the low-lying excited states in W^{187} . The degree of band mixing imposed is expected to be more sensitive to electromagnetic transition rates and branching ratios than to (d,p) stripping strengths.

Of most significance is the identification of two main rotational band structures a low excitation; the ground state band, assigned to the $\frac{3}{2}^-$ [512] Nilsson orbital, and an excited state band built upon the $\frac{1}{2}^-$ [510] Nilsson orbital starting at an excitation energy of 145.7 keV. The information concerning each of these bands has been augmented in the present work by the establishment of one additional band member not observed in the previous (d,p) studies [1], as well as by the determination of the radiative decay branching ratios of all observed members of these rotational states. In analogy to the band mixing calculations [2,3] for W^{183} , Coriolis band mixing has been invoked [7], and the energies of the band members fit to the expression

$$E_K(I) = E_K^0 + A_K [I(I+1) + \delta_{K,\frac{1}{2}} a(-1)^I + \frac{1}{2}(I + \frac{1}{2})] + B_K [I(I+1) + \delta_{K,\frac{1}{2}} a(-1)^I + \frac{1}{2}(I + \frac{1}{2})]^2$$

Table III. Coincidence relationships observed among the low-energy transitions in W^{187}

Gamma-ray energy (keV)	Coincidence Gamma-ray energy ^a (keV)
57—60	146, 201, 273, 557(?), 577, 611
128	577
146	557, 577, 611(?), 616(?), 658
273	290
290	273
424	474
474	424
500	225
557	146
577	146, 205(?)
616	146
658	146

^a Those γ -ray energies followed by (?) appear only faintly in the coincidence spectra and unambiguous establishment of their presence in these spectra is not claimed. The coincidence relationships of these transitions are consistent with the proposed level scheme but their placements in the scheme were established on the basis of energy and intensity fits.

The energy spectrum was calculated using values for most of the parameters that were in close agreement with those found for the case of W^{183} . The radiative transition probabilities, corrected for pairing, were calculated, and the results compared with the present W^{187} findings. The values of the parameters were varied within reasonable limits until a "best fit" to the data was obtained. The results are presented in Tables IV and V.

As expected, the predicted energy spectrum and (d,p) strengths displayed very little sensitivity to the various choices of the parameter values. However, the calculated γ -ray branching ratios were far more sensitive to the parameterization and a comparison of these ratios to experimental data was used as the criterion of "best fit." None of the fits could be considered excellent. The parameters associated with the "most satisfactory" fit are presented in Table IV. These values are in good agreement with those obtained by Erskine [1] for fits to the (d,p) strengths, but obtained with the omission of the quadratic "stretching" energy term.

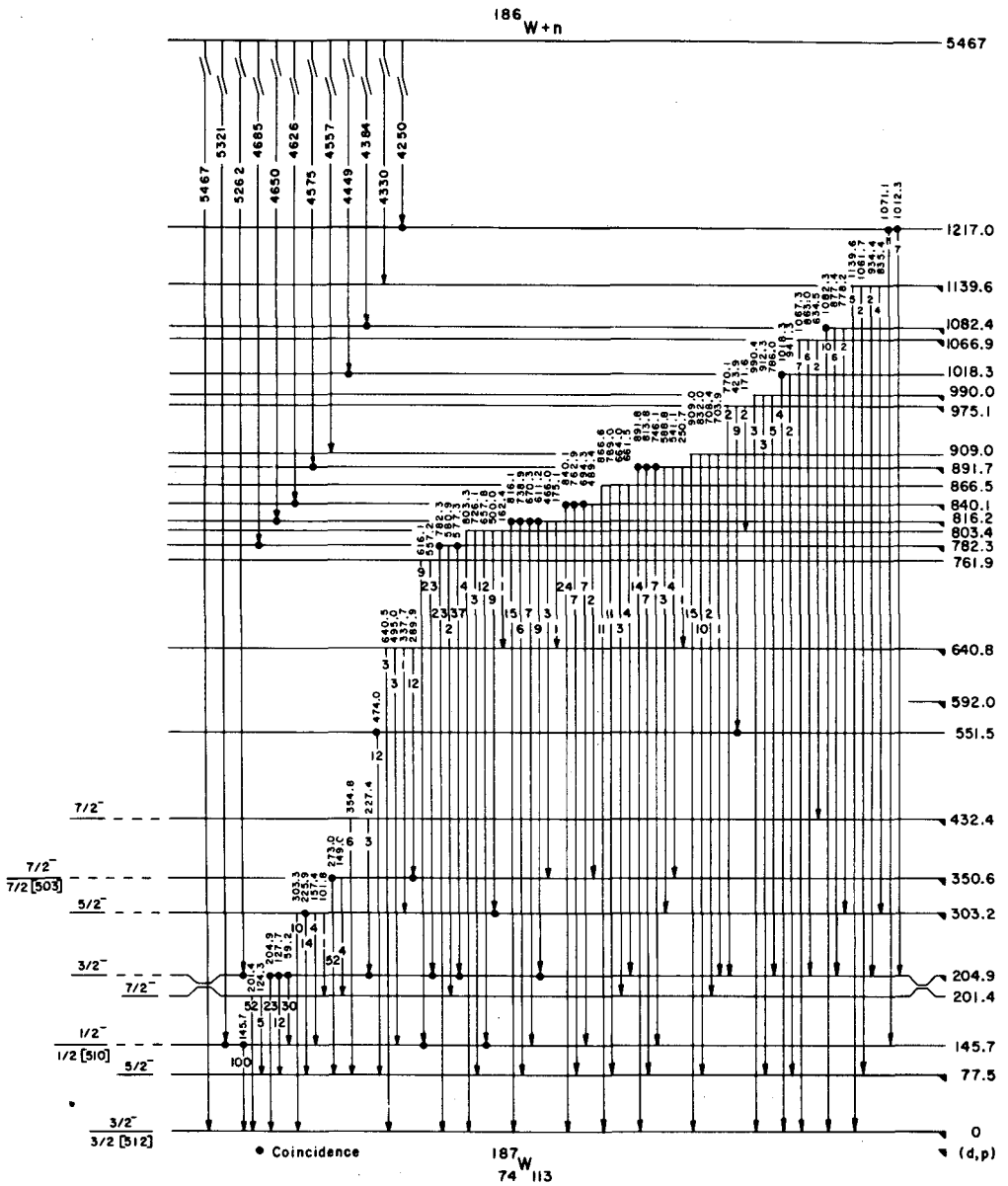


FIG. 4. Proposed level scheme of ^{187}W deduced from the various coincidence and singles gamma-ray investigations of the present work. The excitation energies are expressed in keV. Those levels marked on the right by downward-pointing flags are levels associated with reported (d, p) population. The dots at the beginning or ending of the arrow representing a gamma-ray transition indicate an observed coincidence between the gamma ray so marked and another gamma ray(s) proceeding to or from the same level. The levels observed to be populated in the present work are designated by full horizontal lines across the level scheme. The (d, p) state which has not been observed in this study is marked by a short horizontal line at the right of the

Despite the apparent satisfactory character of the agreement between experiment and calculation, the coefficient of the quadratic energy term, B , for the [512] band is disturbingly large and of sign opposite to that expected. The origin of the sizeable value of this coefficient stems from the rather large spacing between the $\frac{5}{2}^-$ and $\frac{7}{2}^-$ members of the ground state band. A vanishing value for B (expected for good rotators in the center of the deformed region) would imply an excitation energy of 185 keV for the $\frac{7}{2}^-$ member of the ground state band. There is no a priori reason to expect that a state at this energy would not be populated in either the (n, γ) or (d, p) reactions, but there exists no evidence that the data can accommodate this state despite repeated attempts to formulate such a level from the data obtained. A similar situation is also found for the same band in Os^{189} (an isotope of W^{187}) in which the $\frac{7}{2}^-$ member is also found to lie at an unexpectedly high excitation energy.

It is possible to enumerate several of the possible effects that individually, or in combination, may give rise to the observed discrepancies in the model descriptions of W^{187} and Os^{189} : (a) both nuclides are on the border of the deformed region and the pure rotator-plus-odd-nucleon model may not be expected to adequately describe their level structures, (b) some amount of $K + 2$ γ -vibrational mixing might be anticipated that affects these $\frac{7}{2}^-$ states, and is not taken into account in this simple model, and (c) the Nilsson wave-functions may not be sufficiently accurate to describe these "transitional" nuclides. None of these can be considered as sufficiently satisfactory causes at present, since a great deal of additional experimental information is still required to properly evaluate and assess their applicability. In any case, the level structure of the low-lying bands in W^{187} and Os^{189} do not display the well-behaved prescription of the simple rotator-plus-odd-nucleon model, found to be more satisfactorily applicable to W^{183} .

diagram. All levels which have been observed in the primary high-energy gamma-ray spectrum are indicated by a high-energy gamma-ray transition. States which are based solely upon the energy and intensity balance of low-energy transitions (indicated by the lack of coincidence indication and primary gamma-ray transition to the level) are not proposed as confidently as are the states assigned on the basis of coincidence results. The spins, parities, and rotational band configurations indicated to the left of the level diagram are those of Ref. [1].

TABLE IV. Parameters and excitation energies of Nilsson states in $^{187}_{74}\text{W}$

$$E_K = E_0 + A[J(J+1) + a(-)^{(J+\frac{1}{2})}(J+\frac{1}{2})\delta_{K,\frac{1}{2}}] + B[J(J+1) + a(-)^{J+\frac{1}{2}}(J+\frac{1}{2})\delta_{K,\frac{1}{2}}]^2$$

coupling constant
= 1.0928.

J	K	E_0 (keV)	A (keV)	B (keV)	a	E (theo) (keV) mixed	E (exp) (keV)
				[510]			
$\frac{1}{2}$	$\frac{1}{2}$	140.8	18.6	-57.0	-0.01566	145.7	145.7
$\frac{3}{2}$	$\frac{1}{2}$					204.8	204.9
$\frac{5}{2}$	$\frac{1}{2}$					303.0	303.2
$\frac{7}{2}$	$\frac{1}{2}$					432.6	432.4
				[512]			
$\frac{3}{2}$	$\frac{3}{2}$	0.0	14.7	182.0	0.0	0.0	0
$\frac{5}{2}$	$\frac{3}{2}$					77.6	77.5
$\frac{7}{2}$	$\frac{3}{2}$					200.5	201.4
				[503]			
$\frac{7}{2}$	$\frac{7}{2}$	345.6	17.0	0.0	0.0	350.6	350.6
$\frac{9}{2}$	$\frac{7}{2}$					503.5	not obs.

TABLE V. Branching ratios of the low-lying excited states in ^{187}W

Initial state (keV)	Final state (keV)	Branching Ratio ^a	
		(theory)	(exp.)
145	0	1.0	1.0
145	78	0.002	Not observed
201	0	1.0	1.0
201	78	0.12	0.10
205	0	1.0	1.0
205	78	0.0056	0.52
205	146	0.61	1.30 ^b
303	0	1.0	1.0
303	78	1.46	1.4
303	146	0.65	0.4
303	201	0.86	0.1
303	205	0.02	Not observed
351	0	22	Not observed
351	78	1.0	1.0
351	201	0.019	0.077
433	78	1.0	1.0
433	201	0.31	Not observed
433	205	0.34	0.50
433	303	0.61	Not observed

^aThe parameters used to generate the theoretical values are given in Table IV. The transition with branching ratio equal to 1.0 was used as the comparison state for each level.

^bThe 59 keV transition was not well resolved in the singles spectrum. The error associated with this value is therefore $\approx 50\%$.

References

- ¹J. R. Erskine, Phys. Rev. 138, B66 (1965) and references therein.
- ²A. K. Kerman, Kgl. Danske Videnskab. Selskab, Mat. Fys. Medd. 30, No. 15 (1956).
- ³R. T. Brockmeier, S. Wahlborn, E. J. Seppi, and F. Boehm, Nucl. Phys. 63, 102 (1965).
- ⁴Nuclear Data, B1-1-84, B1-2-24 (1966).
- ⁵M. J. Martin, J. A. Harvey, and G. G. Slaughter, Bull. Am. Phys. Soc. 11, 336 (1966) and private communication.
- ⁶P. R. Prokefev and L. I. Simonova, 16th All-Union Conf. Nucl. Spectroscopy and Structure of Atomic Nuclei, Moscow, p. 70 (1966).
- ⁷The authors are indebted to Merle E. Bunker of Los Alamos Scientific Laboratory who performed these band-mixing calculations at our request.

THERMAL NEUTRON CAPTURE INVESTIGATION OF THE ^{190}Os LEVEL STRUCTURE

E. BÖHM, K. STELZER
Institut für Kernphysik,
Johann Wolfgang Goethe Universität,
Frankfurt am Main,
Federal Republic of Germany

Abstract

THERMAL NEUTRON CAPTURE INVESTIGATION OF THE ^{190}Os LEVEL STRUCTURE. The level structure of ^{190}Os was investigated via the reaction $^{189}\text{Os}(n,\gamma)^{190}\text{Os}$. High-energy and low-energy singles spectra were measured with Ge(Li) detectors. Coincidence measurements were performed with a Ge(Li)-NaI combination. A level scheme is proposed. States at 912 and 1113 keV are discussed in terms of collective models.

INTRODUCTION

The even Os isotopes situated in a transition region between strongly deformed and spherical nuclei have been used to test models of nuclear collective motion. The main object of a comparison between experiment and theory [1] has been the ground-state rotational band and the one-phonon gamma-vibrational band, for which sufficient experimental material was available. For collective states of beta-vibrational or two-phonon gamma-vibrational character, which are expected to give more specific answers as to the applicability of existing collective models [2], the experimental information is still unsatisfactory.

We therefore investigated the nucleus ^{190}Os - the last in the sequence of Os nuclei expected to be appreciably deformed - via the reaction $^{189}\text{Os}(n,\gamma)^{190}\text{Os}$. For this reaction a direct population of 0^+ states from the capturing state can be expected. We have measured the high and low-energy gamma radiation with Ge(Li) detectors and determined the de-excitation of the populated levels by coincidence measurements.

During the course of our investigation we learnt that essentially equivalent experiments have been performed by Mariscotti, Kane and Emery [3] with similar experimental results and theoretical interpretations.

EXPERIMENTS

The experiments were performed at the Forschungsreaktor Frankfurt with an external target. The neutron beam was extracted from the central through hole by a Macrolon scatterer. A composite collimator system was used to ensure that only the scatterer was viewed by the target. The neutron beam diameter at the target was 10 mm, the neutron flux $3 \times 10^5 \text{ n cm}^{-2} \text{ sec}^{-1}$. The target consisted of $1.5 \text{ g } ^{189}\text{Os}$, enriched to 87.3%.

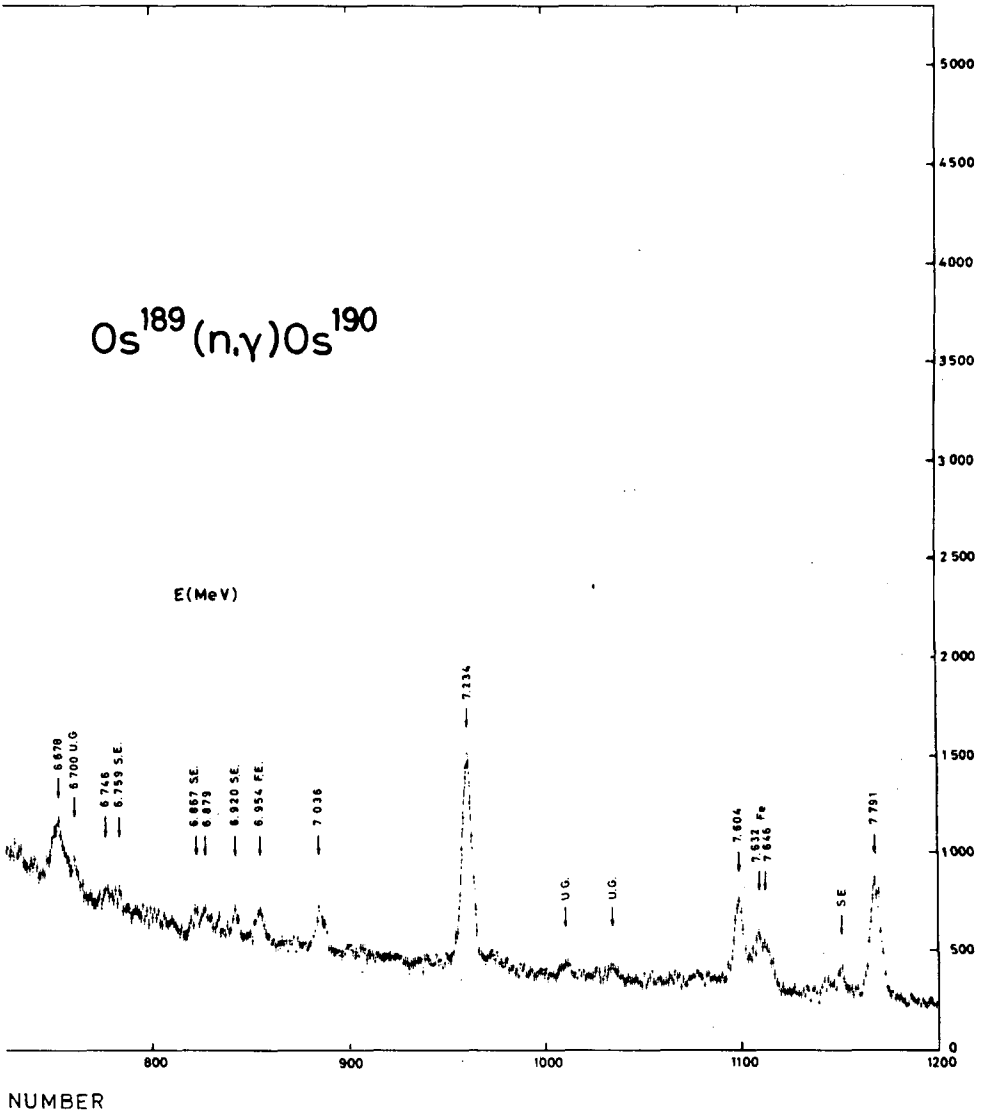


TABLE I. RESULTS OF COINCIDENCE EXPERIMENTS

Primary transition (MeV)	Relative intensity	Level and coincident transitions (keV)	Relative intensity of coincident transitions	Primary transition (MeV)	Relative intensity	Level and coincident transitions (keV)	Relative intensity of coincident transitions
7.791(3)	7.8	<u>ground state</u>				680	220(160)
						558	520(100)
7.604(3)	5.1	187				371	250(150)
		187				322	200(120)
						187	1700(300)
7.233(3)	14.1	558		6.246(3)	8.8	1545	(< 280)
		558	2600(180)			1358	570(290)
		371	1900(150)			986	2300(220)
		187	1200(100)			558	1400(250)
7.035	2.0	756				371	700(160)
		569	770(100)			187	1500(300)
		187	1100(150)	6.114(3)	7.0	1677	
6.879(3)	1.3	912	(< 70)			1677	750(500)
		725	300(100)			1488?	100(300)
		354	(< 120)			1119	800(310)
		187	400(100)			558	950(250)
						371	320(160)
6.678(3)	3.9	1113				187	1200(250)
		1113	290(170)	6.059(3)	5.2	1732	(< 220)
		926	470(100)			1546	850(480)
		725	100(75)			1174	930(330)
		558	530(270)			558	250(180)
		371	220(150)			371	310(120)
		187	550(130)			187	1500(300)
6.410(3)	9.1	1381	(< 200)	5.934(3)	30.5	1857	(< 500)
		1194	2600(360)			1670	3000(600)
		823	100(100)			1298	2600(600)
		187	1600(200)			1101	1300(550)
6.358(3)	5.8	1432				558	2200(300)
		1432	150 ± 250			371	1800(200)
		1247	390(250)			187	5100(450)
		874	550(210)				

High-energy and low-energy singles spectra were measured in the energy ranges of 5 - 8 MeV and of 100 - 2000 keV with planar Ge(Li) 6-cm³ detector with an energy resolution of 5 keV at 1300 keV and 14 keV at 8 MeV. The measurements delivered a level scheme up to 2.5 MeV.

To determine the decay pattern of the levels fed by the high-energy radiation, coincidence measurements were performed in which the high-energy radiation was recorded with the 6-cm³ Ge(Li) detector and the low-energy radiation with a 3 × 3-in. NaI crystal. The coincidence pulses were analysed in a two-dimensional pulse-height analyser of 10 000 channels in a 200 × 50 configuration. To cover a range up to 2 MeV of excitation energy, a series of successive runs with different energy settings were performed.

For the calibration of the high-energy spectra we used the reaction $^{199}\text{Hg}(n, \gamma)^{200}\text{Hg}$ and the energy values of Schult [4] and the $^{56}\text{Fe}(n, \gamma)^{57}\text{Fe}$ reaction with the data of Jackson et al. [5].

RESULTS AND DISCUSSION

Figure 1 shows a typical high-energy spectrum. 29 transitions in the energy range of 5 - 8 MeV were observed, of which 25 go to new levels. From the energy differences of the transitions four lines of highest energies can be identified to go to the ground state, the first 2⁺ state and the 2⁺ and 3⁺ levels of the gamma-vibrational excitation, which had previously been established [6]. The neutron binding energy is determined to be $B_n = 7791 \pm 3$ keV.

The results of the coincidence experiments are given in Table I. Because of the low number of coincident counts and the high and composite pulse background, the experimental errors for the intensities are high. In some cases upper limits for transitions that were not observed but were estimated from the pulse background are given in brackets.

The results of the coincidence measurements could be complemented by additional use of the low-energy transitions measured with the Ge detector.

Figure 2 shows the proposed level and decay scheme. Levels which had previously been established [6] are entered on the left-hand side of the figure. Because of the different population conditions, it is not unexpected that the levels of higher energy observed in this experiment do not coincide with those of previous investigations. The spin and parity of the capturing state is 1⁻, 2⁻. We assume that the high-energy transitions are of E1 character. With this assumption the low-energy levels populated by them can have spin 0, 1, 2 or 3 and positive parity.

We have tried to limit further the spin values of the levels, making use of their de-excitation to the lower levels of known spin and projection number K. The assignments depend on an approximate validity of the Alaga rules and must, therefore, be considered tentative.

The two levels at 912 and 1113 keV are of special interest. Their low energy suggests that they are of collective character. The coincidence measurements show that the 912-keV level decays to the first 2⁺ rotational state. No transition to the ground state was observed. The 1113-keV state decays to the ground state and the first 2⁺ level, and to

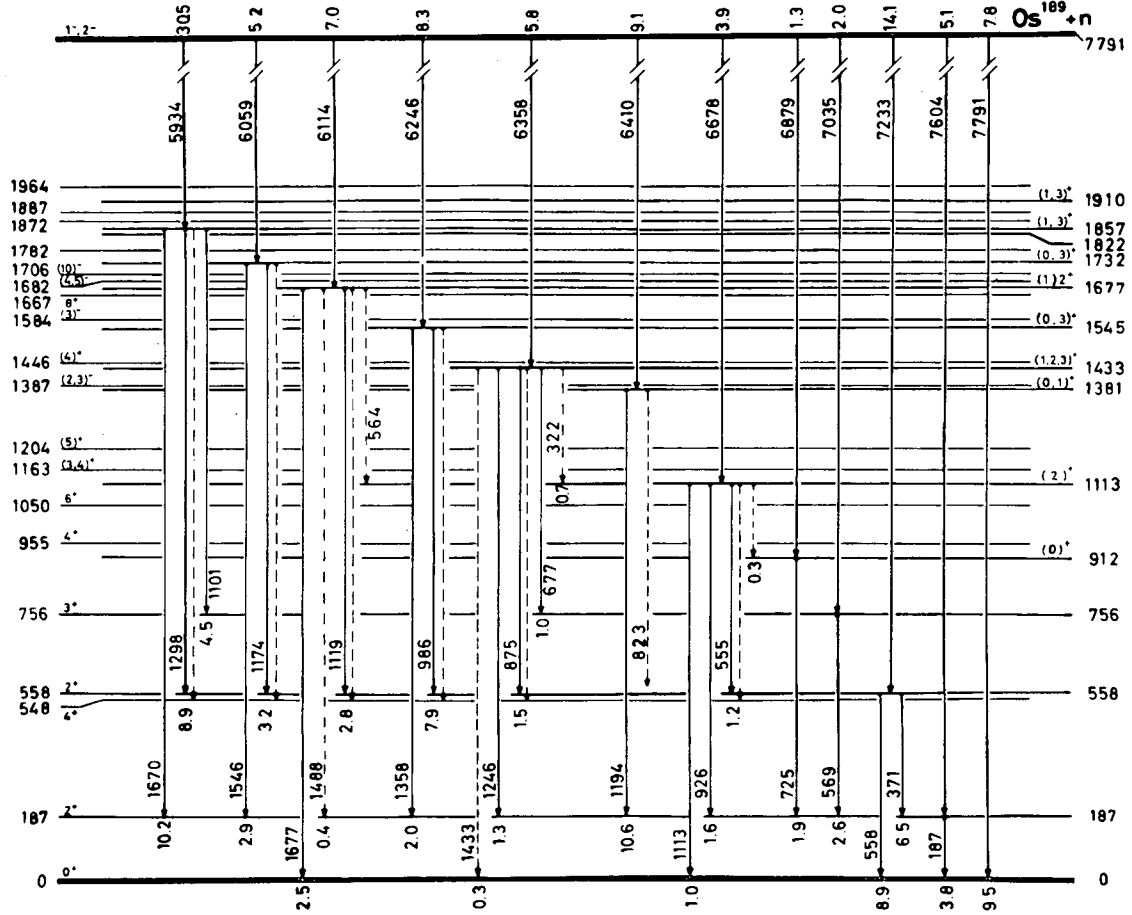


FIG. 2. Decay scheme of $^{189}\text{Os}(n, \gamma)^{190}\text{Os}$.

TABLE II. COMPARISON OF THEORETICAL B(E2) RATIOS AND EXPERIMENTAL RATIOS OF REDUCED TRANSITION PROBABILITIES FOR THE 912 AND 1113-keV STATES

	Theory [10]	Experiment
$\frac{B(E2, 0^+ (912) - 2^+)}{B(E2, 0^+ (912) - 2^+)}$	6.7	< 15
$\frac{B(E2, 2^+ (1113) - 0^+)}{B(E2, 2^+ (1113) - 2^+)}$	0.73	0.3 ± 0.2
$\frac{B(E2, 2^+ (1113) - 4^+)}{B(E2, 2^+ (1113) - 2^+)}$	15	14 ± 7 (1.5)
		or ^a
$\frac{B(E2, 2^+ (1113) - 2^+)}{B(E2, 2^+ (1113) - 2^+)}$	1	- 8 ± 4

^a Transitions are not resolved in the coincidence experiment.

levels at approximately 550 keV of excitation energy where the 4⁺ ground-state band-rotational level and the 2⁺ gamma-vibrational state are situated. The decay pattern and the energy difference of 200 keV suggest that the two levels are 0⁺ and 2⁺ members of a collective K = 0 excitation. Because the 912-keV level is situated at roughly twice the energy of the one-phonon gamma-vibrational energy, predicted by the rotation-vibration theory of Faessler, Greiner and Sheline [1] at about 480 keV, it is probable that the two states can be interpreted as members of a two-phonon gamma vibration. A 0⁺ level of this character has been observed in ¹⁸⁸Os at 1086 keV [7]. Other two-phonon gamma-vibrational states with different coupling of the phonons to K = 4 are believed to have been identified in ¹⁸⁶Os at 1352 keV [8] and in ¹⁹⁰Os at 1163 keV [9].

An alternative possibility is the interpretation as a beta vibration. Theoretically the decay pattern of a beta vibration is entirely different from that of a two-phonon gamma vibration if the excitations can be assumed to be pure. The decay of the beta-vibrational states should preferentially proceed by one-phonon transitions to the ground-state band, while a two-phonon level should proceed by one-phonon transitions to the one-phonon gamma-vibrational band.

The de-excitation of the 912 and 1113-keV levels as observed in our coincidence measurements indicates that, if the interpretation of these levels as belonging to a K = 0 band is correct, their character is intermediate between a two-phonon gamma vibration and a beta vibration. A similar situation has been reported for the 1086-keV level in ¹⁸⁸Os [7].

We have hitherto discussed the 912 and 1113-keV levels within the model of Bohr and Mottelson, which is valid for deformed nuclei of axial symmetry. Microscopic calculations [10, 11] have shown that the transition nuclei, even in the ground-state wave function will have prolate, oblate, asymmetric and spherical components. This indicates that the nucleus ¹⁹⁰Os cannot be adequately treated in terms of the Bohr-Mottelson model.

Recently Kumar and Baranger [10] have published data on ^{190}Os which have been obtained by a microscopic calculation of the collective functions and a numerical solution of the general Bohr Hamiltonian. They calculated the energies and wave functions of the ground-state band 0^+ , 2^+ and 4^+ levels, the 2^+ and 3^+ gamma-vibrational states and 0^+ and 2^+ levels next higher in energy which may be identified with the states which we discuss. The energies calculated are 877 and 1192 keV respectively. They also give the $B(E2)$ values for transitions which connect these levels with states of lower energy. In Table II we compare the theoretical $B(E2)$ ratios with the ratios of reduced transition probabilities estimated from our coincidence experiments. It is interesting to note that the theory predicts a strong favouring of the transition from the 2^+ state to the 4^+ 'rotational' state of the ground-state band, compared to the transition to the 2^+ gamma-vibrational level. Unfortunately, the two transitions (565 and 555 keV) and the radiation de-exciting the levels (361 and 558, 371 keV) could not be resolved in our coincidence measurements. Refined experiments should yield an interesting test for the calculations.

At the present stage of experimental information an attempt to assign properties to the new levels of higher energy would be very speculative. It is, however, to be expected that two-quasiparticle configurations become important. From states of low energy in neighbouring odd-A isotopes of Os and Re, which may be connected with the Nilsson neutron orbitals $3/2^-$ [512], $1/2^-$ [510] and $9/2^-$ [505] and the proton orbitals $5/2^+$ [402] and $7/2^+$ [404], two-neutron excitations with spin and parity 2^+ , 1^+ and 3^+ and a two-proton state 1^+ can be predicted.

REFERENCES

- [1] FAESSLER, A., GREINER, W., SHELINE, R.K., Nucl. Phys. 70 (1965) 33.
- [2] YAMAZAKI, T., Nucl. Phys. 49 (1963) 1.
- [3] MARISCOTTI, M.A., KANE, W.R., Bull. Am. phys. Soc. (1967) 597; EMERY, G.T., private communication; STELZER, K. et al., Verh. dt. phys. Ges. 5 (1967) 340; BÖHM, E., STELZER, K., Verh. dt. phys. Ges. 4 (1968) 345.
- [4] SCHULT, O.W.B. et al., Phys. Rev. 164 (1967) 1553.
- [5] JACKSON, H.E., NAMENSON, A., THOMAS, G., Physics Lett. 17 3 (1965) 324.
- [6] KANE, W.R. et al., Phys. Rev. 119 (1960) 1953; LEDERER, C.M., HOLLANDER, J., PERLMAN, I., Table of Isotopes (1967).
- [7] YAMAZAKI, T., Nucl. Phys. 44 (1963) 1.
- [8] HARMATZ, B., HANDLEY, T.H., Nucl. Phys. 56 (1964) 1.
- [9] KANE, W.R. et al., Phys. Rev. 119 (1960) 1953.
- [10] KUMAR, K., BARANGER, M., Nucl. Phys. A122 (1968) 273.
- [11] MOSEL, U., GREINER, W., Z. Phys. B217 (1968) 256.

NEUTRON CAPTURE INVESTIGATION OF THE ^{192}Ir AND ^{194}Ir LEVEL STRUCTURES

H. KRÜGER, K. STELZER, H. HANLE, M. KORIATH

Institut für Kernphysik,

Johann Wolfgang Goethe Universität,

Frankfurt am Main,

Federal Republic of Germany

Abstract

NEUTRON CAPTURE INVESTIGATION OF THE ^{192}Ir AND ^{194}Ir LEVEL STRUCTURES. The nuclei ^{192}Ir and ^{194}Ir have been investigated via the reactions $^{191}\text{Ir}(n, \gamma)^{192}\text{Ir}$ and $^{193}\text{Ir}(n, \gamma)^{194}\text{Ir}$. The high-energy spectra have been measured with a Ge(Li)-NaI pair spectrometer. 121 transitions in ^{192}Ir and 102 transitions in ^{194}Ir have been observed in an energy range corresponding to 1700-keV excitation energy. The neutron binding energy of ^{194}Ir is $B_n = 6066.1 \pm 1.5$ keV. The ^{192}Ir ground-state transition which would be M2 cannot be measured. It is assumed that the transition of highest energy observed goes to the 58-keV 1^+ excited state. The neutron binding energy is then $B_n = 6198.7 \pm 2.0$ keV. Level schemes are proposed.

Low-energy spectra up to 500 keV have been measured for both isotopes with Ge(Li) detectors. The ^{192}Ir high-energy spectrum has also been taken using a cadmium-filtered neutron beam. Large changes in intensity compared to the spectrum taken with thermal neutrons are observed.

INTRODUCTION

Doubly odd iridium isotopes have found interest in recent years in connection with the problem of proton-neutron coupling in the transition region between strongly deformed and spherical nuclei. Scharff-Goldhaber et al. [1] have pointed out that while the ground-state spins of the neighbouring odd-odd rhenium nuclei and of the most strongly deformed nuclei follow the asymptotic coupling rules of Gallagher and Moszkowski [2], those of the iridium isotopes, except ^{194}Ir , do not. Experimental information on excited states of the odd-odd iridium isotopes is scarce. Only for ^{188}Ir and for ^{194}Ir a few low-energy excited states could be investigated via electron capture [3] and beta decay [4]. Further information is limited to the study of the decay of isomeric states [5-11]. Previous neutron capture gamma and conversion electron data could not be used to extend the level schemes [12-17].

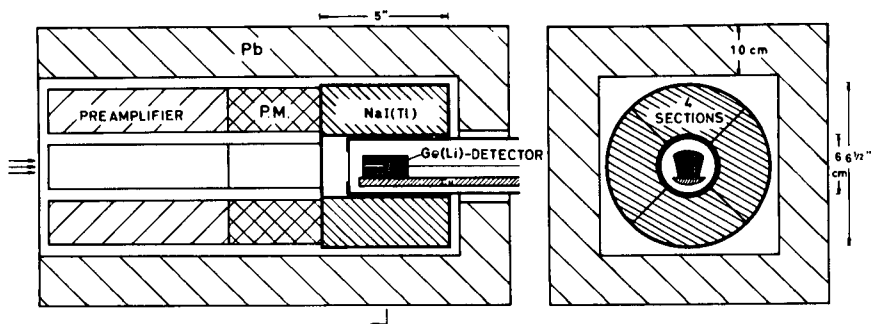
We have investigated the nuclei ^{192}Ir and ^{194}Ir via neutron capture in ^{191}Ir and ^{193}Ir using highly enriched samples. Both target nuclei have spin and parity $3/2^+$ leading to spin and parity 1^+ and 2^+ for the capturing states. Primary gamma transitions from the capturing state will preferentially proceed with E1 or M1 multipole order populating low-spin excited states. This is of special interest for ^{192}Ir where low spin states of negative parity are predicted, as for ^{194}Ir , by the Nilsson model and the spherical shell model but have not hitherto been observed.

EXPERIMENTAL TECHNIQUES AND DATA ANALYSIS

The high-energy gamma-ray spectra were measured with a pair spectrometer, consisting of a Ge(Li) central detector and a 4-sector NaI(Tl) annulus of 5 in. length and 6.5 in. diameter, with an inner bore of 6 cm diameter for the detector cryostat. The Ge(Li) detector was operated in triple coincidence with the 511-keV annihilation radiation recorded in opposite NaI sectors. Anticoincidence with a low-energy discriminator setting was required for adjacent sectors. This combination enhances the peak-to-background ratio for the double-escape-peak by a factor of 10-15 in the Ir spectra and completely removes single-escape and total-absorption peaks. The double-escape peak efficiency is reduced by a factor of 8. Two Ge(Li) detectors were used: a 4 cm long, 4-cm² trapezoidal coaxially drifted detector fabricated by the authors and especially well suited for the pair spectrometer geometry; and a planar detector of 7 cm² and 5 mm depletion depth of Princeton Gamma-Tech. The system resolution for both detectors was 7.5 keV at 6 MeV.

The measurements were performed with an internal target at the PD side of the through hole of the Munich research reactor (Fig.1). The target was placed near the core centre line at a neutron flux of about 8×10^{12} n cm⁻² sec⁻¹. A Pb collimator of 6 mm diameter and 20 cm length within the biological shield of the reactor ensured that only the target was viewed by the Ge detector. The beam diameter at the detector was 2.5 cm or less.

Highly enriched targets, supplied by Oak Ridge Nat. Lab., were used. This was especially important for the ¹⁹³Ir measurements, because the neutron capture cross-section is 950 b for ¹⁹¹Ir, as against 130 b for ¹⁹³Ir. The isotopic composition of the targets were:



SCHEMATIC DIAGRAM OF THE PAIR SPECTROMETER

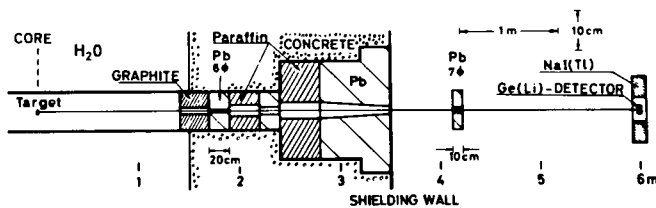


FIG.1. Experimental set-up at the FRM.

	p ₁ % ¹⁹¹ Ir	p ₂ % ¹⁹³ Ir	int. ratio p ₁ σ ₁ : p ₂ σ ₂
¹⁹¹ Ir sample	94.7	5.3	130 : 1
¹⁹³ Ir sample	1.3	98.7	1 : 10
Natural iridium	38.5	61.5	9 : 2

The ¹⁹⁴Ir spectra had to be corrected for ¹⁹²Ir background.

The target quantities used were 25 mg for ¹⁹³Ir and 6 mg for ¹⁹¹Ir. The energy calibration was performed by simultaneous measurements of the iridium and nitrogen spectra. To effect this, the normally evacuated through channel was filled with 1-2 atm of nitrogen.

Typical spectra for ¹⁹²Ir and ¹⁹⁴Ir are given in Fig.2. The residual background observed is mainly due to electron and bremsstrahlung-escape and the charge-collecting properties of the Ge detectors.

Measurements of the high-energy gamma radiation were also performed at the Forschungsreaktor Frankfurt (FRF) in an external beam geometry, with single Ge detectors of 0.4 and 5.6-cm² planar type (Solid State and RCA Canada). The neutron beam was extracted by a scatterer from the central through hole. An additional measurement with a cadmium-filtered neutron beam was made for ¹⁹²Ir.

We also measured the low-energy gamma spectra with the same apparatus at the FRF. The energy resolution was limited to 8 keV for ⁶⁰Co and the 5.6-cm² RCA detector and 4.5 keV for the 0.4-cm² Solid State detector. Spectra were taken for both isotopes in single mode and in coincidence with a 3 X 3-in. NaI(Tl) crystal which was set to register only radiation above 4.5 MeV. Energy and intensity calibrations were performed by various radioactive standards and additional lines originating from the decay of the Ir isotopes.

The high-energy gamma-ray spectra supplied by the pair spectrometer were analysed by a least-squares-fit computer program. Because of the complexity of the spectra, up to 7 overlapping lines were fitted simultaneously. The relative energy precision for isolated peaks with high intensity was about ± 200 eV. The absolute energy precision is estimated to be better than 1.5 keV. Errors are due to the calibration procedure and the reference energies of nitrogen used [18]. The energy precision of the low-energy lines is 0.5 to 1 keV, owing to the high pulse background and the bad energy resolution of the available detectors.

RESULTS AND DISCUSSION

121 high-energy lines leading to levels up to 1.7-MeV excitation energy in ¹⁹²Ir and 102 lines for the same energy range in ¹⁹⁴Ir were observed. Figures 3 and 4 give the proposed level schemes. On the left-hand side the previously known levels are indicated for comparison. It was assumed that the high-energy radiation precedes from the capturing state and that the multi-pole character is either E1 or M1. For some very strong transitions E1 character is very probable. In these cases we have assigned negative parity to the populated levels. The excitation energies are determined by the difference between the

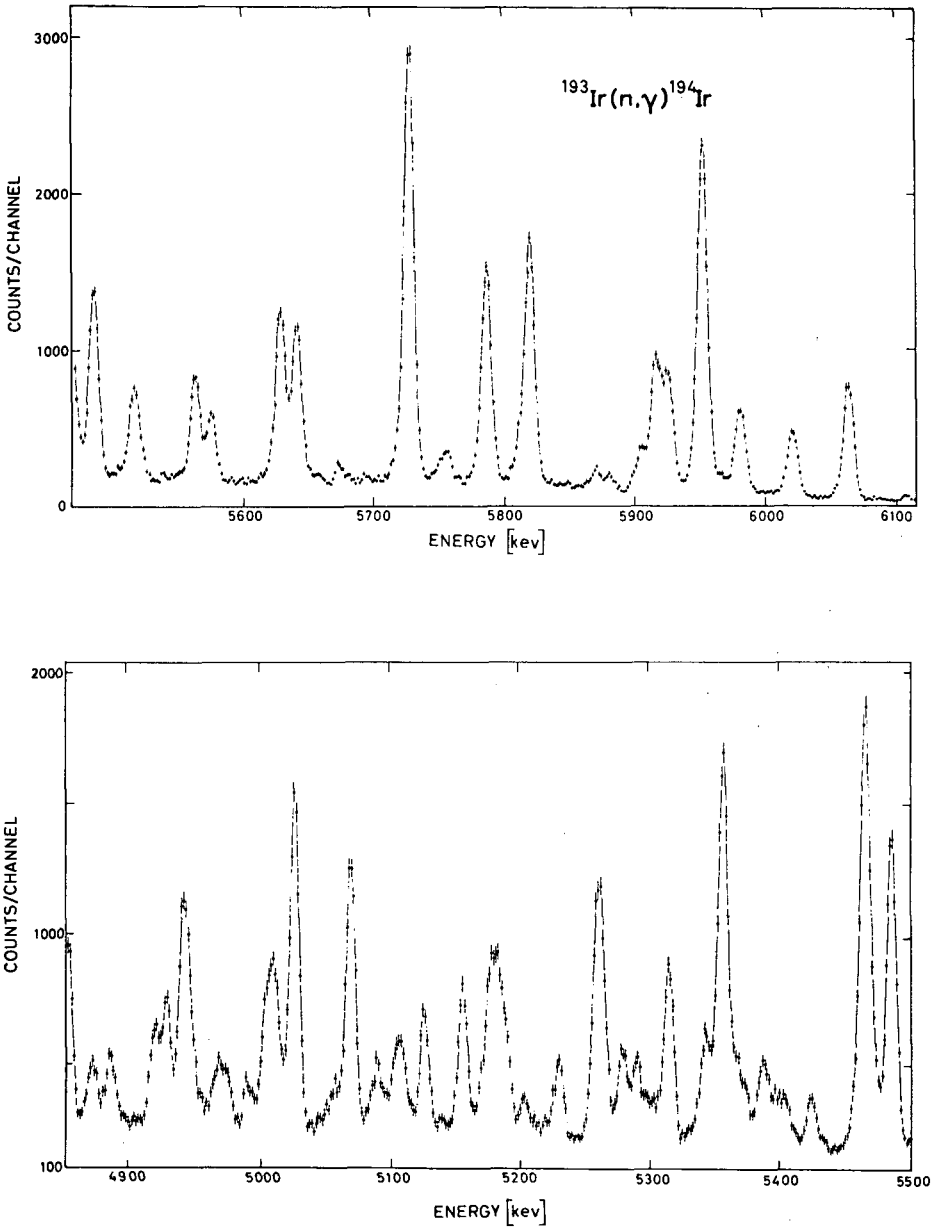


FIG. 2. High-energy part of the $^{193}\text{Ir}(n, \gamma)^{194}\text{Ir}$ spectrum corrected for $^{191}\text{Ir}(n, \gamma)^{192}\text{Ir}$.

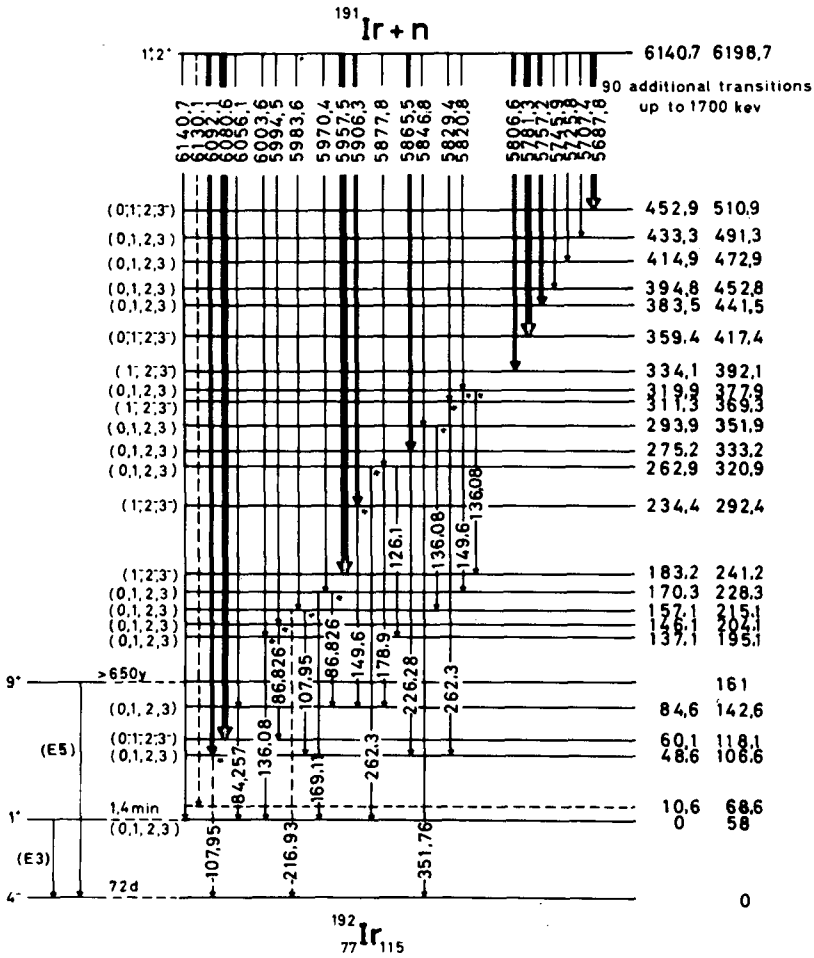
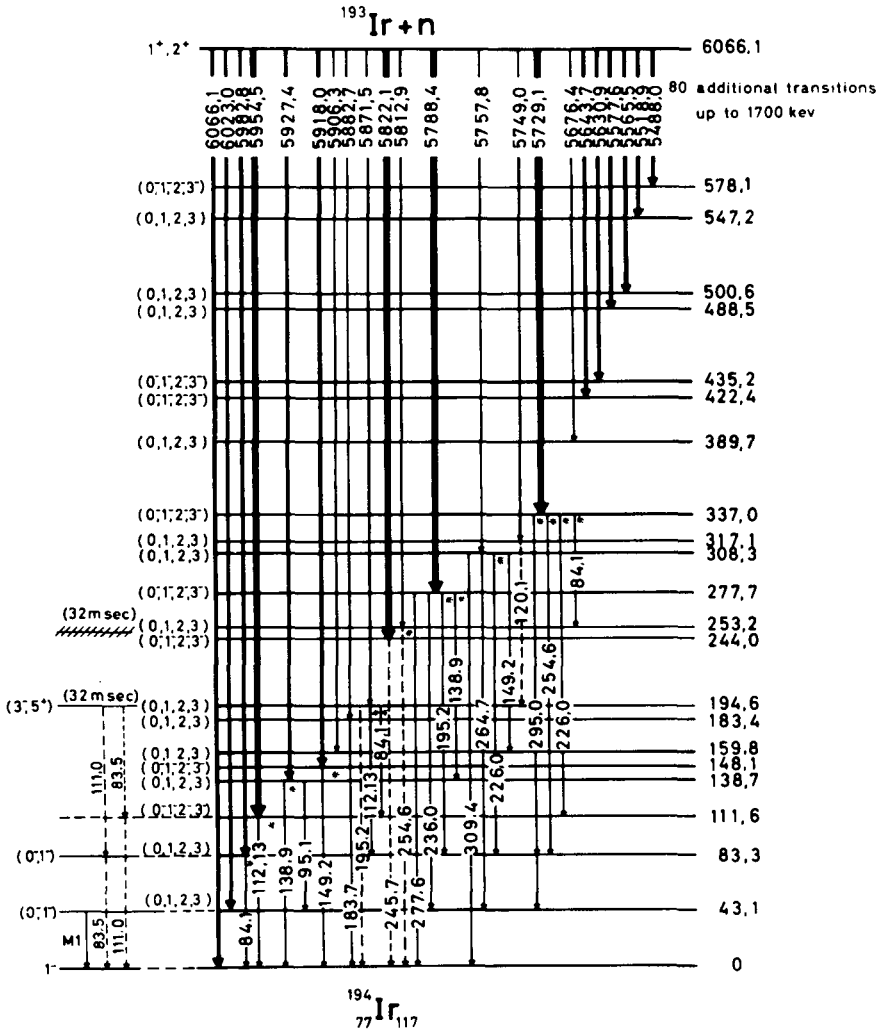


FIG. 3. ¹⁹²Ir level scheme.

transition energies and the highest transition energy observed. The standard errors of the excitation energies, which are determined by addition of the respective relative errors, lie between 0.4 and 1.0 keV, with only few exceptions.

For ¹⁹²Ir a transition of 6088 keV reported in Refs [13-15] has been assumed to go to the 58-keV isomeric level with spin 1 and then unknown positive parity [19]. Our spectra give two lines at 6080.6 and 6092.1 keV which could not be resolved in the previous experiments. Because of their high intensity, both lines are very probably E1 transitions, going to negative parity levels. At 6140.7 keV, however, a low-intensity line is observed which we conclude to be very probably the M1 transition to the 1⁺ isomeric state at 58 keV. With this assumption the neutron binding energy in ¹⁹²Ir is B_n = 6198.7 keV with an estimated error of 2 keV. It would be most desirable to confirm this value by coincidence measurements.

FIG. 4. ^{194}Ir level scheme.

In ^{194}Ir the 1^- ground state can be populated by a direct E1 transition from the capturing state. We assign the line of highest energy with 6066.1 ± 1.5 keV to be this transition and therefore the binding energy. This assignment is supported by other high-energy lines, the energy differences to 6066.1 keV of which agree with the excitation energies of known low-spin negative-parity levels. The energy precision obtained is insufficient to place the low-energy lines unambiguously in the level scheme. Therefore, we only tried to place the lines of higher intensity below 300-keV excitation energy as far as possible within the experimental errors. Transitions which fit in more than once are marked by an asterisk.

Because of a high probability for accidental placing and because it must be expected that at least some of the transitions connect levels which are not directly populated from the capturing state, we consider the placement as highly tentative. In the case of ^{192}Ir some of our low-energy lines could be identified with transitions measured by Rasmussen et al. [17] with much better energy resolution. For these lines we have used their energy values.

The 32-msec isomer of ^{194}Ir , first reported by Campbell and Fettweis [5], has recently been studied by Lundàn and Siivola [7] and by Heiser et al. [8]. While Lundàn and Siivola assumed a state of 194.5 keV to be isomeric and assigned it 5^+ , Heiser et al. gave strong arguments against this spin value and showed that it is probably a 3^- state. Our 5871.5-keV transition most probably leads to this state and supports the assumption of Heiser et al. The sequence of the transitions observed in the study of the isomeric decay could not be determined so that the intermediate (2^-) state had to be assumed to lie at 83.5 or 111.6 keV respectively. Unfortunately, our data cannot remove this ambiguity, because high-energy lines of 5982.8 and 5954.5 keV indicate the existence of levels at both energies. We think, however, that a decay to the 111.6-keV level is more probable because the 83.5-keV level should most probably be identified with the 82.1 ± 1 -keV (0^- , 1^-) state observed in the beta decay of ^{194}Os [4]. Additional 4 transitions leading to levels between 111.6 and 194.5-keV excitation energy indicate that the situation is much more complex than hitherto anticipated.

It is interesting to note that the gross structure of ^{192}Ir as revealed by the high-energy gamma data and that of ^{194}Ir are quite similar. Both nuclei have a high density of low spin excited states, with probably dominating negative parity. This is to be expected from the spherical shell model and the Nilsson model. In the language of the Nilsson model, proton levels $3/2^+$ [402] \downarrow and $1/2^+$ [400] \uparrow , observed as ground states and first low-lying excited states in the odd-A Ir isotopes, and neutron levels $3/2^-$ [512] \downarrow and $1/2^-$ [510] \uparrow , observed at low energy in neighbouring odd-A Os nuclei, are expected to couple to give states $3^-(0^-)$, $1^-(2^-)$, $1^-(2^-)$ and $1^-(0^-)$. Each first spin value corresponds to parallel coupling of asymptotic spins Σ and is the one expected to be lower in energy by the coupling rules of Gallagher and Moszkowski [2]. The values in parentheses correspond to antiparallel coupling of spins.

The apparent violation of the Gallagher-Moszkowski rule for the Ir isotopes is not surprising in view of the closeness of particle excitations in the neighbouring odd-A nuclei and the different deformations which are to be expected in odd-A and doubly odd nuclei. Thus the 4^- ground state of ^{192}Ir can easily be explained by the vicinity of the $9/2^-$ [615] \uparrow neutron orbital, coupling with the $1/2^+$ [400] \uparrow proton orbital. The 1^+ state in ^{192}Ir is probably built by a combination of the $11/2^-$ [505] \uparrow proton state and the $9/2^-$ [505] neutron state, both of which are observed as low-lying excited states in neighbouring odd-A nuclei. In both cases parallel coupling of spins applies.

Conclusions on the validity of the coupling rules can only be drawn when pairs of states of different coupling have been identified.

The high density of states observed makes it probable that collective quasi-rotational or vibrational excitations are present.

For ^{192}Ir we also measured the epithermal capture spectrum and observed very large intensity variations compared to thermal capture. This is probably caused by the statistical distribution of partial radiation widths. ^{191}Ir has neutron resonances at 0.65 and 5.36 eV with spin 2^+ . Their contribution to the thermal neutron cross-section is too low to explain the high value of the cross-section. It must, therefore, be assumed that a bound state contributes. Because of the low energy of the resonances, filter methods are sufficient to partially separate the contributions. We have measured the high-energy spectra in an external beam set-up with a reactor neutron beam and a beam filtered with cadmium. The results are demonstrated in Fig.5. The intensities of the two groups were separately normalized by the sum of intensities. Similar measurements, however with a much worse resolution are reported by Wasson and Draper [20].

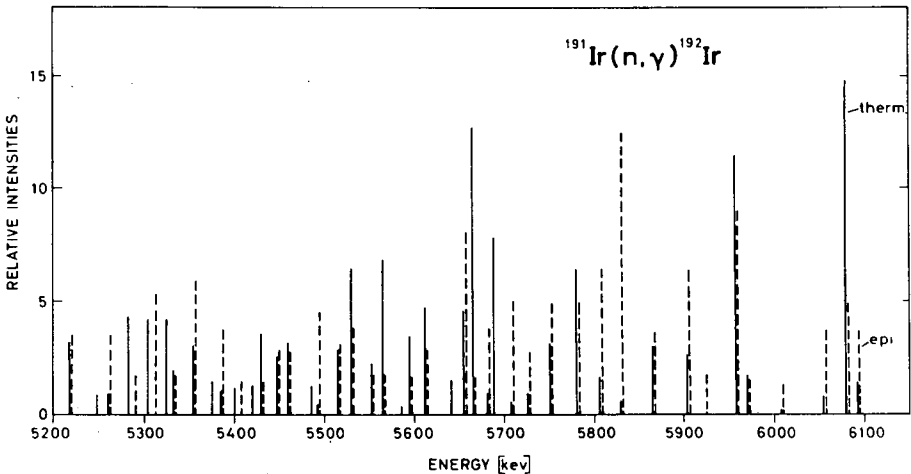


FIG.5. Comparison of thermal and epithermal intensities of the $^{191}\text{Ir}(n,\gamma)^{192}\text{Ir}$ spectrum. The broken bars give the intensities measurement with epicadmium neutrons, the filled-in bars the thermal neutron contribution determined by the difference of the reactor and epithermal spectra.

The measurements with epithermal neutrons give additional information which is useful to identify E1 transitions. Because the epithermal capture proceeds almost exclusively by the 2^+ resonance at 0.6 eV, the most intensive transitions - assumed to be E1 - can only populate states with 1^- , 2^- , 3^- .

The present investigations show that the structure of the isotopes ^{192}Ir and ^{194}Ir is very complicated. To get further insight into these nuclei additional data, especially from high-precision low-energy measurements, are needed.

ACKNOWLEDGEMENTS

The opportunity to do the experiments at the Forschungsreaktor in Munich is gratefully acknowledged. Our special thanks go to Dr. O.W.B. Schult.

REFERENCES

- [1] SCHARFF-GOLDHABER, G. et al., Proc. Congr. Int. Physique Nucléaire (Paris, 1964) 2, Centre National de la Recherche Scientifique, Paris (1964) 550.
- [2] GALLAGHER, C.J. Jr., MOSZKOWSKI, S.A., Phys. Rev. 111 (1956) 1282.
- [3] Table of Isotopes (LEDERER, C.M., HOLLANDER, J.M., PERLMAN, I., Eds), John Wiley (1967); Nuclear Data Sheets, Academic Press.
- [4] WILLIAMS, D.C., NAUMANN, R.A., Phys. Rev. 135 (1964) B289; HELMER, R.G., Phys. Rev. 137 (1965) B232; JOHNSON, N.R., BISHOP, W.N., Nucl. Phys. 69 (1965) 131; WILLIAMS, D.C., Phys. Rev. 143 (1966) 855.
- [5] CAMPBELL, E.C., FETTWEIS, P.F., Nucl. Phys. 13 (1959) 92; 33 (1962) 272.
- [6] ALEXANDER, K.F., BRINCKMANN, H.F., Z. Naturf., 16a (1961) 210.
- [7] LUNDÄN, A., SIIVOLA, A., Nucl. Phys. A106 (1968) 213.
- [8] HEISER, C., BRINCKMANN, H.F., FROMM, W.D., Nucl. Phys. A115 (1968) 213.
- [9] SUNYAR, A.W., SCHARFF-GOLDHABER, G., MCKOEWEN, M., Phys. Rev. Lett. 21 (1968) 237.
- [10] VONACH, H., MÜNZER, H., HILLE, P., Z. Phys. 195 (1966) 343.
- [11] Nucl. Data Sheets, 5-3-33 (May 1963).
- [12] PROKOFJEV, P.T. et al., Atlas Spektrov Conversionnich Elektronov, Riga (1967).
- [13] GROSHV, L.V., DEMIDOV, A.M., LUTSENKO, V.N., PELEKHOV, V.I., Atlas of Gamma-ray Spectra from Radiative Capture of Thermal Neutrons, Atomizdat, Moscow (1958); Pergamon Press, London (1959).
- [14] KNOEPFEL, H., SCHERRER, P., STOLL, P., Z. Phys. 156 (1959) 293.
- [15] TREADO, P.A., CHAGNON, P.R., Bull. Am. phys. Soc. 5 (1960) 369 T6.
- [16] DORCIOMAN, D.I., POPA, M.S., CHRISTU, M.I., Revue roum. Phys. 12 6 (1967) 561.
- [17] RASMUSSEN, N.C., THOMPSON, T.J., Rep. MITNE-70 (1966).
- [18] MARION, J.B., Gamma-ray calibration energies, Rep. ORO-2098-58 (1968).
- [19] BHATTACHERJEE, S.K. et al., Phys. Rev. 159 (1967) 1056.
- [20] WASSON, D.A., DRAPER, J.E., Nucl. Phys. 78 (1966) 576.

LOW-LYING EXCITED STATES OF ^{204}Tl AND ^{206}Tl POPULATED IN THERMAL NEUTRON CAPTURE*

C. WEITKAMP

Institut für angewandte Kerntechnik,
Kernforschungszentrum Karlsruhe,
Karlsruhe, Federal Republic of Germany
and

J. A. HARVEY, G. G. SLAUGHTER, E. C. CAMPBELL,
Oak Ridge National Laboratory,
Oak Ridge, Tenn., United States of America

(Presented by U. Fanger)

Abstract

LOW-LYING EXCITED STATES OF ^{204}Tl AND ^{206}Tl POPULATED IN THERMAL NEUTRON CAPTURE. New level diagrams of ^{204}Tl and ^{206}Tl are deduced from thermal neutron capture measurements on isotopically enriched samples. The agreement of the ^{206}Tl -level scheme with theory is poor. This is attributed to the attempt of all computations to reproduce a low-lying 1^- state for which no evidence could be found experimentally.

When capture of thermal neutrons was first used as a method to study the properties of particular nucleides, it proved a powerful means to obtain new and most valuable information on nuclear structure, and the first data on the odd-odd isotopes of thallium were obtained via this reaction almost twenty years ago [1].

Considerable improvement of these early data in both accuracy and completeness has been achieved during the past decade by the application of a series of other processes the most important of which are, for the case of ^{204}Tl , the reactions $^{203}\text{Tl}(d,p)^{204}\text{Tl}$ and $^{205}\text{Tl}(d,t)^{204}\text{Tl}$ [2] and, for the case of ^{206}Tl , the reactions $^{205}\text{Tl}(d,p)^{206}\text{Tl}$ [2...4], $^{208}\text{Pb}(d,\alpha)^{206}\text{Tl}$ [5] and the α and β^- decays [6...9, 10] of $^{210\text{m}}\text{Bi}$ and ^{206}Hg , respectively.

Despite these efforts, many details of the level structure of the two nucleides have remained either unknown or poorly established. For ^{204}Tl , a big step forward was achieved by Prestwich and collaborators [11] who used a Ge(Li) detector to observe the gamma spectrum from capture of thermal neutrons, but, because of the natural isotopic composition of the sample, attributed some γ rays to ^{204}Tl that did not arise from capture in ^{203}Tl .

For ^{206}Tl which, because of its simpler nucleonic structure, is of more direct use as a test case for different shell-model type calculations, a somewhat controversial situation had arisen whether or not a level with spin and parity 1^- existed a few keV above the ground state. This 1^- state, predicted by Sliv, Sogomonova and Kharitonov [12], was tentatively introduced into the measured level

* Research sponsored by the US Atomic Energy Commission under contract with the Union Carbide Corporation.

FIG. 1. High-energy part of the gamma spectrum from neutron capture in ^{203}Tl .

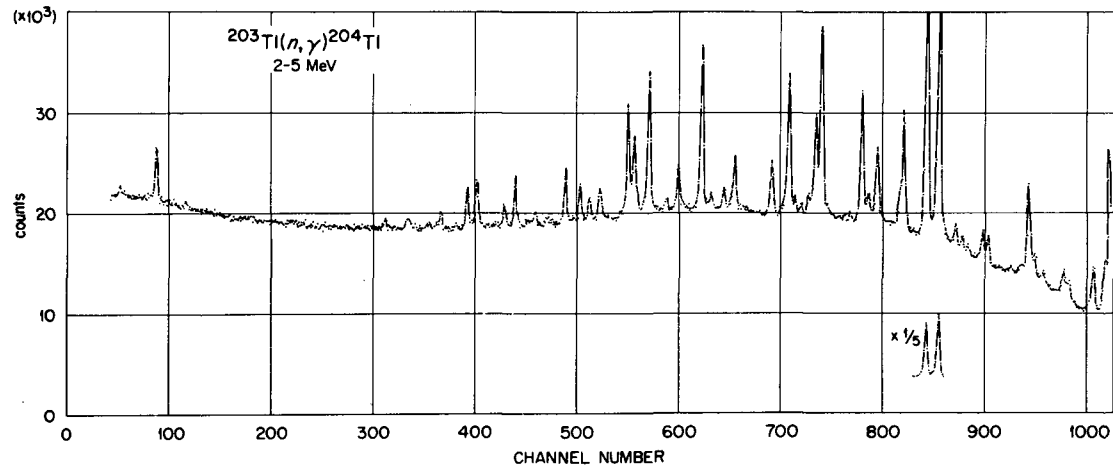


FIG. 2. High-energy part of the gamma spectrum from neutron capture in ^{205}Tl .

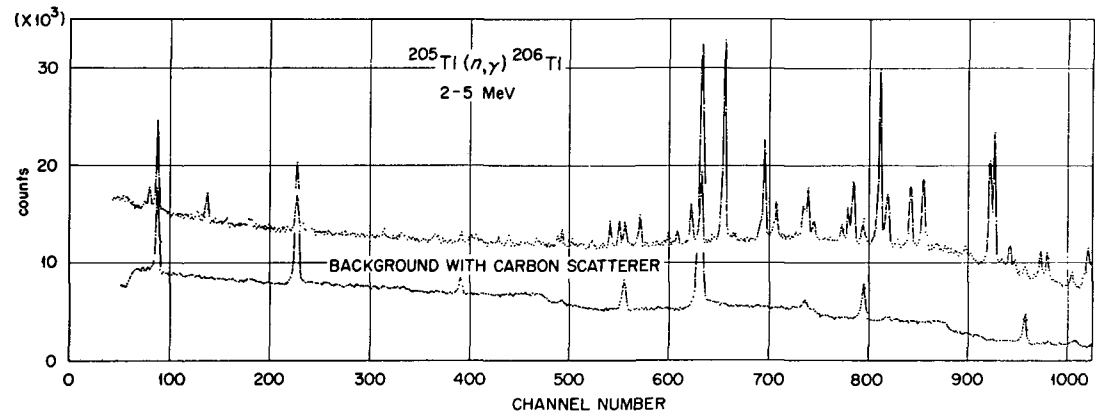


diagram of Rusinov et al. [7], and the authors of subsequent theoretical papers then tried to reproduce that level in their computations.

These calculations of systems with two nucleons outside a closed shell usually proceed in two steps. On account of the Pauli principle only the triplet-odd and singlet-even components of the residual nucleon-nucleon interaction contribute to the wave functions of those nuclei that are two like nucleons off a doubly magic "core" nucleus; so step 1 consists in an attempt to vary the magnitude of that half of the parameters until a best fit of the resulting level schemes with experiment is obtained. In step 2 the remaining parameters are fitted to the level diagrams of the nuclei that differ from the core nucleus by two different nucleons; to do this use is normally made of the unchanged parameters from step 1.

In the region of ^{208}Pb this procedure works well if the parameters determined for the even-even nuclei ^{210}Po , ^{210}Pb , ^{206}Pb , and ^{206}Hg are used to fit those of the odd-odd nuclei ^{210}Bi , ^{208}Bi , and ^{208}Tl . It fails, however, to give an adequate description of ^{206}Tl .

It was this failure that led us to a reexamination of the properties of the odd-odd isotopes of thallium, particularly ^{206}Tl . Our main interest centered on the following questions:

- 1) Is there a level in ^{206}Tl (presumably 1^-) 10 keV or less above the ground state, or is it possible to establish a smaller upper limit for such a hypothetical state?
- 2) Are there other levels observable in the energy range 0 to 800 keV in addition to the ones previously known?
- 3) What is the excitation spectrum of ^{206}Tl in the energy range between 0.8 and 2 MeV which is not accessible from decay measurements?
- 4) Are gamma transition probabilities and branching ratios from the (n,γ) reaction compatible with the known spin values of the levels?
- 5) Is the "anomalous bump", i.e. the unusually intense group of gamma rays around 5.5 MeV in the (n,γ) and $(d,p\gamma)$ spectra of nuclei with mass numbers between 180 and 208, observable for either of the two isotopes separately?

The experiment was done with Ge(Li) detectors of 6 and 30 cm³ and isotopically enriched samples of ^{203}Tl (96.69 %) and ^{205}Tl (99.46 %) in an external thermal neutron beam of the ORR reactor.

Let us first look at Fig. 1 and 2 to get the answer to question 5. Fig. 1 shows the high-energy portion of the γ -ray spectrum from capture in ^{203}Tl which is very similar to the spectrum from natural thallium and clearly exhibits the group of intense peaks around 4.5 MeV (corresponding to γ -ray energies around 5.5 MeV), with few γ rays present between 2 and 4 MeV. The spectrum from capture in ^{205}Tl is shown in Fig. 2. Despite the high enrichment of the sample, about 30 % of the counting rate of this spectrum is due to capture in ^{203}Tl , but an evaluation shows that the gross behaviour of ^{206}Tl does not differ appreciably from that of ^{204}Tl , in complete agreement with the conclusions from Bartholomew's recent explanation of the effect [13].

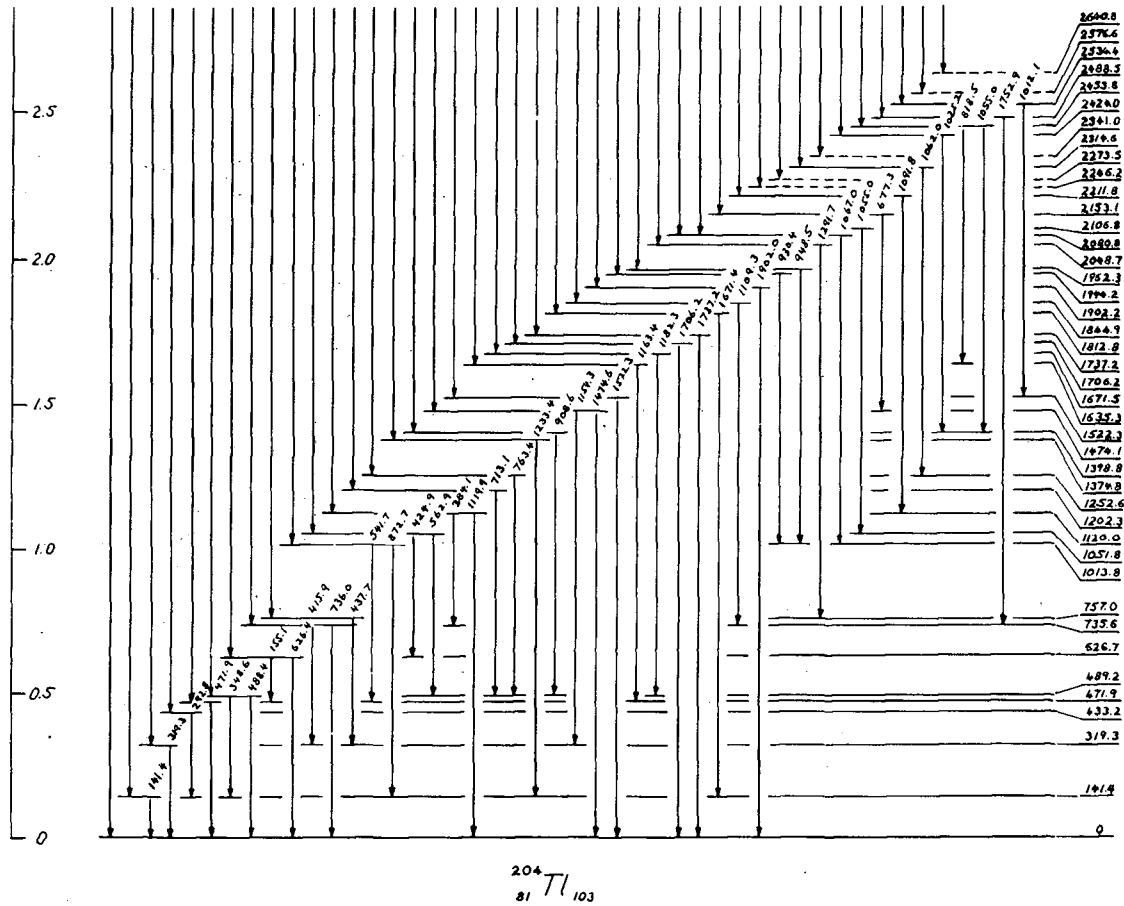


FIG.3. Transition diagram of ^{204}Tl .

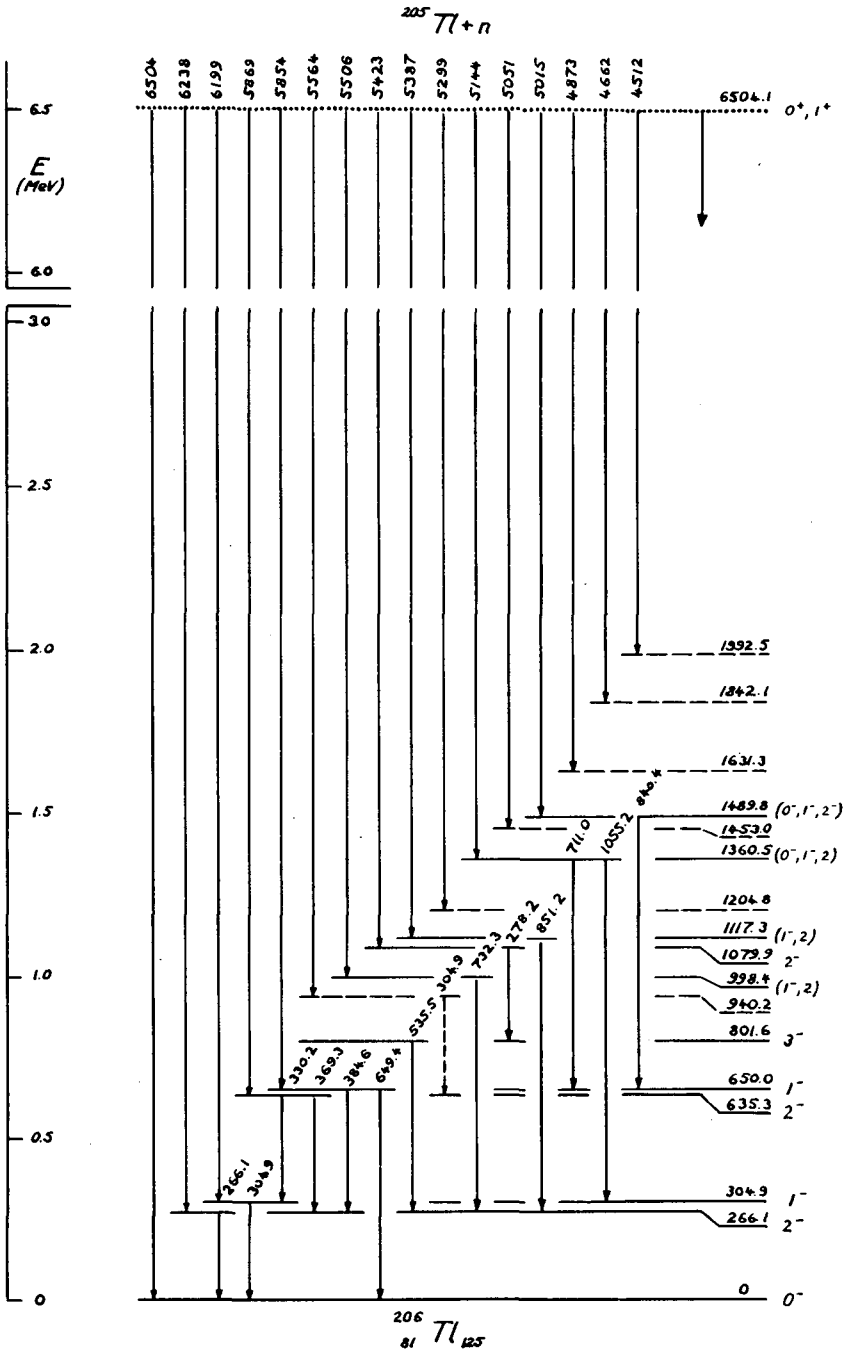


FIG. 4. Transition diagram of ^{206}Tl .

$^{206}\text{Thallium}$

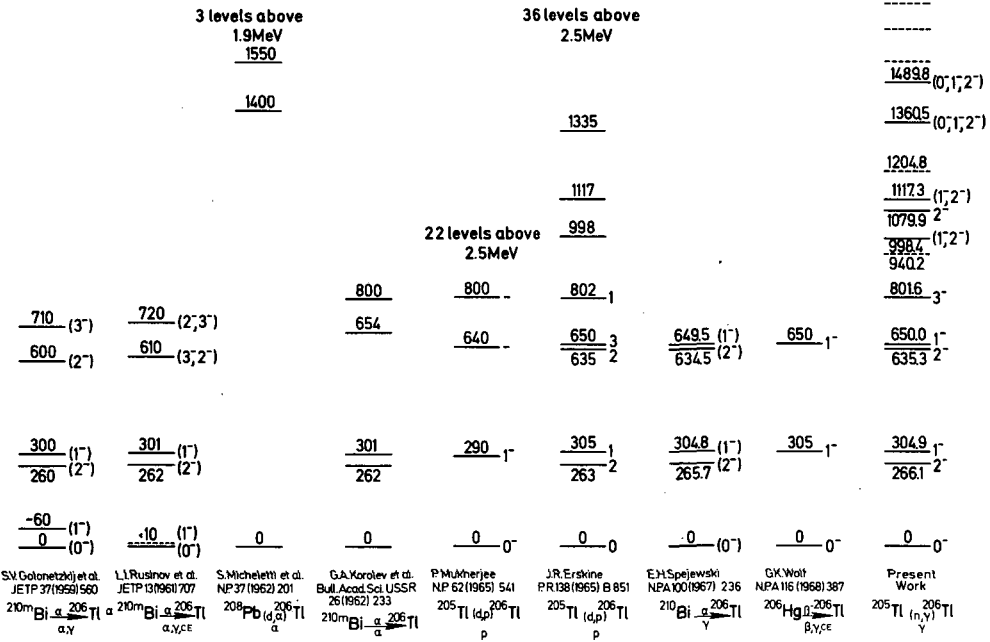


FIG. 5. Comparison of ^{206}Tl level diagrams as measured from different reactions.

The transition diagram of ^{204}Tl is given in Fig. 3. Except for a state at 553 keV which was not observed in our measurements the agreement with the level diagram of Prestwich et al. [11] is perfect. No evidence could be found for the existence of a long-lived metastable state in ^{204}Tl ; this is not amazing, however, because if such a state existed its excitation energy must be low, its spin high compared to the ^{204}Tl ground state spin (2), and the probability of feeding it via neutron capture by a spin 1/2 target nucleus would be small. Horrock's half life measurement [14] is therefore a stronger argument against the existence of a long-lived isomer in ^{204}Tl .

Fig. 4 shows the level diagram of ^{206}Tl . The presence of a low-lying 1^- level in ^{206}Tl should manifest itself by a splitting or broadening of at least some of the γ rays feeding the ground state. This broadening, if present, should be best visible for low-energy γ lines. To answer question 1 an analysis of the widths of the corresponding peaks was therefore done, and no evidence for a level = 2.3 keV above the ground state was found.

The answer to question 2 and 3 is given by Fig. 5 in which the ^{206}Tl level diagram as determined from the present work is compared to the results from other nuclear reactions. No new levels show up below 900 keV, but above, a series of previously unknown states could be found.

For question 4 let us once more look at the transition diagram of Fig. 4. As the energy dependence of the ^{205}Tl capture cross

²⁰⁶Thallium

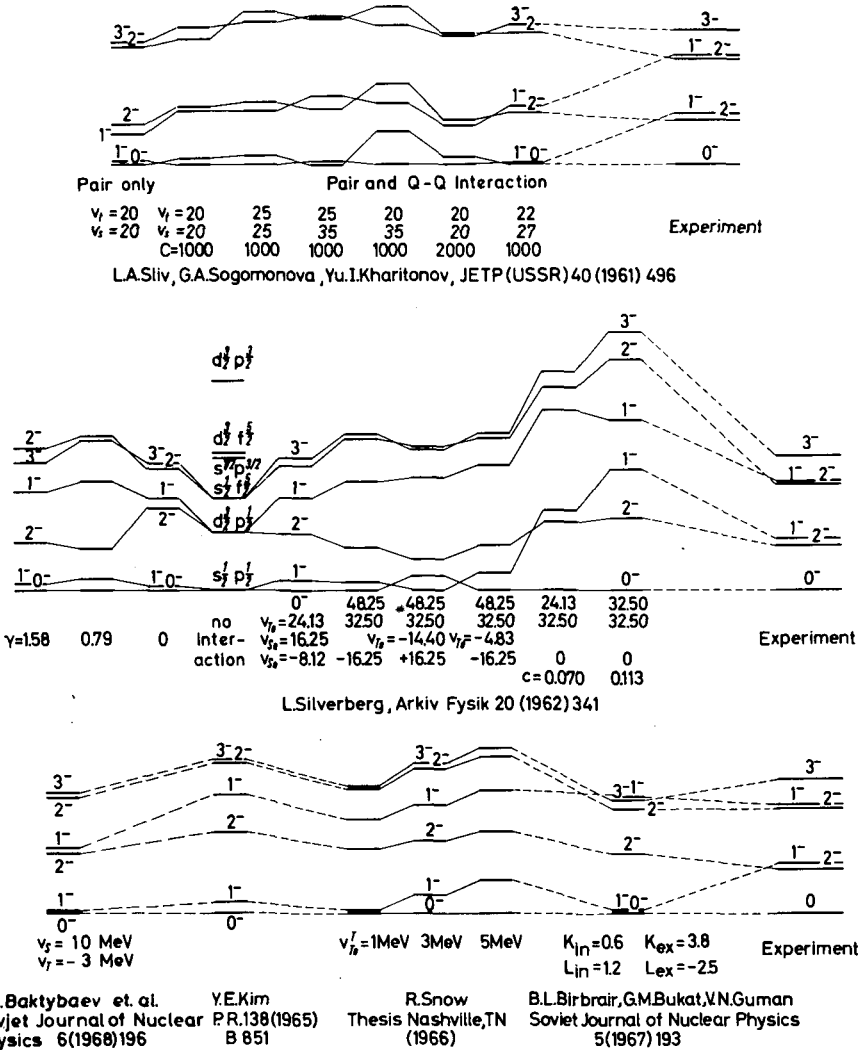


FIG. 6. Comparison of calculated level diagrams of ²⁰⁶Tl.

section is not well-known, both spin values of the capturing state must be admitted, and 0⁻, 1⁻ and 2⁻ states can be fed by primary electric dipole radiation. Both feeding and deexcitation of the ground and first three excited states is consistent with Erskine's assignment of spins. The 650 keV level, however, is strongly populated from the capturing state; as it feeds both the 0⁻ ground and 2⁻ 266 keV states the only possible spin value is 1 if dipole transitions are assumed. The absence of a primary transition to the 802 keV level, on the other hand, and the deexcitation of this state to the 2⁻ 266 keV

level only is strong evidence for the 802 keV state being the 3^- candidate that is expected in this region from theoretical considerations. This assignment of spins, although in contrast to Erskines interpretation, is but little outside the error bars of his data.

Fig. 6 shows a comparison of the results of different calculations [12, 16, ... 19] with experiment. For simplicity only the ground and lowest five excited states of ^{206}Tl are given which correspond to the proton-hole neutron-hole configurations ($s_{1/2} p_{1/2}$), ($d_{3/2} p_{1/2}$), and ($s_{1/2} p_{5/2}$). It follows from Fig. 6 that there has been no really good agreement so far although a great variety of shapes and of range and strength parameters were tried. This may be due to the fact that all calculations were biased by the endeavour to reproduce an almost degenerate $0^- - 1^-$ ground state doublet which till now was not established experimentally. It might be promising to try some of the approaches that worked so well in the case of other nuclei around ^{208}Pb with the newer experimental data now available for ^{206}Tl .

References

- [1] G.A. Bartholomew and B.B. Kinsey, Canadian Journal of Physics 31 (1953) 1025
- [2] P. Mukherjee, Physics Letters 13 (1964) 238
- [3] P. Mukherjee, Nuclear Physics 62 (1965) 541
- [4] J.R. Erskine, Physical Review 138 (1965) B 851
- [5] S. Micheletti and J.B. Mead, Nuclear Physics 37 (1962) 201
- [6] S.V. Golonetskii, L.I. Rusinow, and Yu.I. Filimonov; JETP (USSR) 37 (1959) 560; Soviet Physics JETP 10 (1960) 395
- [7] L.I. Rusinow, Yu. N. Andreev, S.V. Golonetskii, M.I. Kislov, and Yu.I. Filimonov; JETP (USSR) 40 (1961) 1007; Soviet Physics JETP 13 (1961) 707
- [8] G.A. Korolev and G.E. Kocharov, Izvest. Akad. Nauk SSSR, Ser. Fiz. 26 (1962) 235; Bull. Acad. Sci. USSR, Phys. Ser. 26 (1962) 233
- [9] E.H. Spejewski, Nuclear Physics A 100 (1967) 236
- [10] G.K. Wolf, Nuclear Physics A 116 (1968) 387
- [11] W.V. Prestwich, L.B. Hughes, T.J. Kennett, and H.J. Fiedler, Physical Review 140 (1965) B 1562
- [12] L.A. Sliv, G.A. Sogomonova, and Yu.I. Kharitonov, JETP (USSR) 40 (1961) 946; Soviet Physics JETP 13 (1961) 661

- [13] G.A. Bartholomew, Bull. Am. Phys. Soc. 13 (1968) 1416
- [14] D.L. Horrocks, Nuclear Physics A 110 (1968) 238
- [15] L. Silverberg, Arkiv Fysik 20 (1962) 341
- [16] B.L. Birbrair, G.M. Bukat, and V.N. Guman;
Yadernaja Fizika 5 (1967) 274;
Soviet Journal of Nuclear Physics 5 (1967) 193
- [17] Y.E. Kim, published by J.R. Erskine in Ref. [4]
- [18] R. Snow, Thesis, Vanderbilt University, Nashville,
Tennessee (1966)
- [19] K.B. Baktybaev, I.M. Band, L.A. Sliv, and Yu.I. Kharitonov,
Yadernaja Fizika 6 (1967) 270; Soviet Journal of Nuclear
Physics 6 (1968) 196

EXCITATION OF LEVELS IN ^{235}U BY THE $^{234}\text{U}(n, \gamma)^{235}\text{U}$ REACTION*

E. T. JURNEY

University of California,
Los Alamos Scientific Laboratory,
Los Alamos, N. Mex.,
United States of America

Abstract

EXCITATION OF LEVELS IN ^{235}U BY THE $^{234}\text{U}(n, \gamma)^{235}\text{U}$ REACTION. The high and low-energy gamma-ray spectrum from the thermal neutron capture reaction $^{234}\text{U}(n, \gamma)^{235}\text{U}$ has been studied with Ge(Li) and Si(Li) spectrometers. This work is part of an experiment involving several reactions directed toward the investigation of low-lying levels in ^{235}U . Twenty-three rotational bands have been proposed. The (n, γ) data were especially helpful in distinguishing low-spin levels.

The low-lying levels of ^{235}U have previously been studied by the alpha decay of ^{241}Pu [1], by the (d, p) stripping reaction on ^{234}U [2] and by Coulomb excitation [3]. Recent experiments [4] have been completed at Los Alamos in which targets were chosen so that the levels in ^{235}U could be studied through the (d, p) , (d, t) , (t, p) , (d, d') and thermal (n, γ) reactions. This combination of experiments, each with its own selective excitation characteristics, has been able to add considerably to the knowledge of the low-lying level structure of ^{235}U . This paper will be concerned with the (n, γ) contribution to the experiments.

Capture of an S-wave neutron by ^{234}U leads to a compound $J^\pi = 1/2^+$ state in ^{235}U . We therefore expect that the high-energy (n, γ) spectrum will largely be made up of transitions to states with $J^\pi = 1/2^+$ and $3/2^+$ in ^{235}U , since dipole transitions should generally predominate over higher multi-polarities. The low-energy part of the spectrum ($E < 2$ MeV) is important to the construction of the decay scheme of the low-lying levels and can, in some cases, be helpful in inferring spin and parity for a given level.

The capture gamma-ray spectra were obtained at the internal target facility built into the thermal column of the Omega West Reactor at Los Alamos [5]. The collimated external gamma-ray beam was viewed by a 6-cm³ coaxial Ge(Li) detector operated inside a divided NaI annulus. At high energies the system is used as a triple-coincidence pair spectrometer. At low energies the system operates as an anticoincidence Compton-suppression spectrometer by combining the signals from the two halves of the NaI annulus. That part of the spectrum in the lowest energy region ($11 \text{ keV} < E_\gamma < 130 \text{ keV}$) was obtained with a high-resolution Si(Li) detector placed in the external gamma-ray beam. Standard techniques were used throughout for energy calibration. Intensities were determined by a comparison with the known intensities [5] of transitions

* Work supported by the US Atomic Energy Commission.

in the $^{14}\text{N}(n, \gamma)^{15}\text{N}$ spectrum (high energy), and with the intensity of the 411-keV radioactive decay line of ^{198}Hg following neutron capture [6] by ^{197}Au (low energy).

The target was 17 mg of 99.7% enriched ^{234}U as UO_2 powder held in a graphite container. Larger amounts of well-separated target material were not available. Because of the relatively high capture cross-section of ^{234}U (~ 90 b), no contaminating lines from radioactive fission products could be detected in the prompt spectrum. Confirmation of this was made by inspecting the spectrum from the target both immediately (15 sec to 10 min) and for a relatively long period (15 sec to 1000 min) after reducing the neutron flux by a factor of 1/700.

Figure 1 shows the high-energy spectrum. Computer least-squares fits were made to 140 gamma rays between 2.2 and 5.3 MeV. Between 2.2 and 4.0 MeV the average observed spacing between lines is 9.6 keV or about 2.1 times the average detector FWHM response. Under these circumstances it is likely that only the stronger transitions are identified. Gamma-ray intensities vary from 0.95 to 0.02 $\gamma/100$ n, corresponding to source strengths of from 6.4×10^{-2} to 1.2×10^{-3} mb-mol for the target size used.

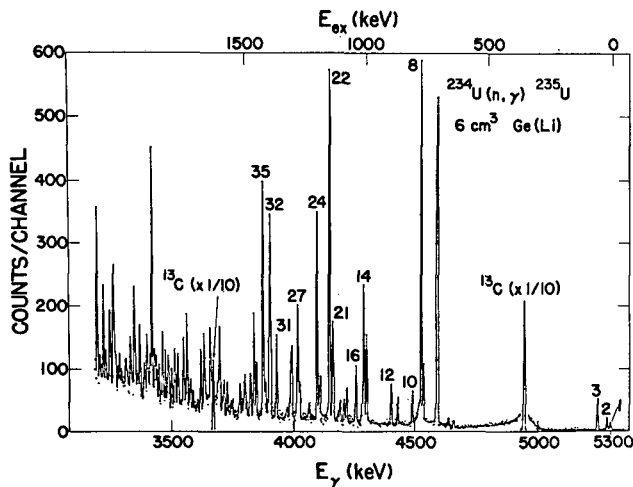


FIG. 1. Double-escape gamma-ray spectrum from $^{234}\text{U}(n, \gamma)^{235}\text{U}$. Peak numbers correspond to those in Table I. The two strong lines from $^{12}\text{C}(n, \gamma)^{13}\text{C}$ are from the graphite target holder. Time of run was 2800 minutes.

Table I is a list of the primary gamma rays corresponding to levels up to 1.5 MeV in ^{235}U . Transitions 1, 2 and 3 excite the $1/2^+$, $3/2^+$ and $5/2^+$ members of the $1/2^+$ [631] band at 80 eV, 13.0 and 51.7 keV, respectively.

Table II is a preliminary list of the gamma rays up to 1.5 MeV. Those up to 129.3 keV were measured with the Si(Li) spectrometer; the remainder were obtained with the Ge(Li) - NaI system. Figure 2 shows

TABLE I. HIGH-ENERGY GAMMA RAYS FROM $^{234}\text{U}(n, \gamma)^{235}\text{U}$
 CORRESPONDING TO EXCITATIONS UP TO 1500 keV IN ^{235}U ^a

No.	E_{γ} (keV)	E_{exc} (keV) ^b	I_{γ} ($\gamma/10^2$ n)
1	5297.7	0 ± 0.7	0.02 ± 0.006
2	5284.4	13.0 ± 0.4	0.03 ± 0.01
3	5245.7	51.7 ± 0.3	0.08 ± 0.02
4	4658.3	639.1 ± 0.8	0.02 ± 0.006
5	4639.0	658.4 ± 0.7	0.03 ± 0.008
6	4593.6	703.8 ± 0.3	0.77 ± 0.15
7	4536.5	760.9 ± 0.3	0.11 ± 0.03
8	4527.4	770.0 ± 0.3	0.89 ± 0.18
9	4519.3	778.1 ± 1.0	0.04 ± 0.01
10	4492.0	805.4 ± 0.4	0.09 ± 0.02
11	4432.2	865.2 ± 0.4	0.07 ± 0.02
12	4405.2	892.2 ± 0.3	0.10 ± 0.02
13	4305.0	992.4 ± 0.4	0.21 ± 0.05
14	4294.4	1003.0 ± 0.5	0.37 ± 0.08
15	4288.1	1009.3 ± 1.0	0.10 ± 0.04
16	4261.7	1035.7 ± 0.5	0.15 ± 0.04
17	4223.0	1074.4 ± 0.5	0.10 ± 0.02
18	4213.8	1083.6 ± 0.6	0.03 ± 0.01
19	4197.0	1100.4 ± 0.5	0.05 ± 0.02
20	4190.7	1106.7 ± 1.1	0.02 ± 0.01
21	4167.1	1130.3 ± 0.4	0.33 ± 0.08
22	4154.0	1143.4 ± 0.4	0.95 ± 0.20
23	4111.3	1186.1 ± 0.4	0.09 ± 0.03
24	4102.4	1195.0 ± 0.4	0.58 ± 0.12
25	4070.0	1227.0 ± 0.6	0.05 ± 0.02
26	4030.9	1266.5 ± 0.6	0.11 ± 0.03
27	4023.7	1273.7 ± 0.5	0.31 ± 0.08
28	3999.4	1298.0 ± 0.5	0.16 ± 0.04
29	3994.3	1303.1 ± 0.6	0.16 ± 0.04
30	3980.1	1317.3 ± 1.5	0.02 ± 0.01
31	3937.9	1359.5 ± 0.4	0.21 ± 0.05
32	3913.9	1383.5 ± 0.4	0.55 ± 0.11

TABLE I (cont.)

No.	E_γ (keV)	E_{exc} (keV) ^b	I_γ ($\gamma/10^2$ n)
33	3907.5	1390.0 ± 0.4	0.21 ± 0.05
34	3891.9	1405.5 ± 0.6	0.10 ± 0.03
35	3883.5	1413.9 ± 0.4	0.64 ± 0.13
36	3857.0	1440.4 ± 0.5	0.11 ± 0.03
37	3847.4	1450.0 ± 0.4	0.31 ± 0.07
38	3833.7	1463.7 ± 0.4	0.12 ± 0.03
39	3812.8	1484.6 ± 0.9	0.09 ± 0.03
40	3808.6	1488.8 ± 0.9	0.08 ± 0.03
41	3801.1	1496.3 ± 1.2	0.04 ± 0.02

^a Preliminary results.

^b Based on the deduced value of the neutron separation energy $B_n = 5297.4$ keV.

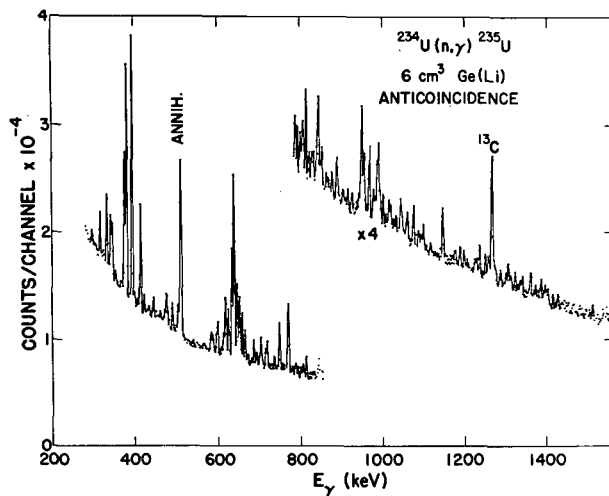


FIG.2. Gamma-ray spectrum from $^{234}\text{U}(n,\gamma)^{235}\text{U}$ between 300 and 1500 keV, with the system used as a Compton-suppression spectrometer.

TABLE II. LOW-ENERGY GAMMA RAYS FROM THE REACTION $^{234}\text{U}(n, \gamma)^{235}\text{U}$ ^a

E_γ (keV) ^b	I_γ ($\gamma/10^2$ n)	E_γ (keV)	I_γ ($\gamma/10^2$ n)
16.1 ± 0.2 ^c	0.5 ± 0.2	323.3 ± 0.7	0.05 ± 0.02
21.6 ± 0.2	0.09 ± 0.03	332.6 ± 0.3	0.50 ± 0.1
38.8 ± 0.2	0.02 ± 0.007	341.5 ± 0.3	0.40 ± 0.1
42.2 ± 0.1	0.07 ± 0.03	344.9 ± 0.3	0.35 ± 0.1
46.3 ± 0.2	0.02 ± 0.006	352.8 ± 0.5	0.07 ± 0.03
47.6 ± 0.2	0.04 ± 0.01	367.6 ± 0.5	0.08 ± 0.03
51.7 ± 0.1	0.06 ± 0.02	374.8 ± 0.3	0.79 ± 0.2
68.9 ± 0.2	0.07 ± 0.02	376.3 ± 0.3	0.55 ± 0.2
77.3 ± 0.1	0.52 ± 0.2	380.2 ± 0.2	1.8 ± 0.4
113.7 ± 0.2	0.11 ± 0.04	393.1 ± 0.2	2.2 ± 0.5
115.4 ± 0.2	0.07 ± 0.02	399.4 ± 0.7	0.11 ± 0.04
116.4 ± 0.2	0.23 ± 0.06	408.0 ± 0.5	0.08 ± 0.03
129.3 ± 0.2	3.0 ± 0.7	411.6 ± 0.5	0.12 ± 0.05
140.1 ± 0.2	0.14 ± 0.05	413.7 ± 0.3	0.96 ± 0.2
158.6 ± 0.7	0.02 ± 0.01	422.6 ± 0.3	0.17 ± 0.04
161.4 ± 0.3	0.12 ± 0.04	431.3 ± 0.8	0.03 ± 0.02
167.7 ± 0.6	0.04 ± 0.02	434.6 ± 0.5	0.10 ± 0.03
171.8 ± 0.3	0.10 ± 0.03	445.5 ± 0.3	0.17 ± 0.04
174.9 ± 0.4	0.14 ± 0.04	478.4 ± 0.3	0.43 ± 0.1
177.5 ± 0.6	0.07 ± 0.03	491.3 ± 0.2	0.32 ± 0.08
181.5 ± 0.6	0.05 ± 0.02	505.1 ± 0.2	0.35 ± 0.08
195.9 ± 0.3	0.10 ± 0.03	540.3 ± 0.8	0.07 ± 0.03
198.4 ± 0.3	0.13 ± 0.04	564.8 ± 0.6	0.09 ± 0.04
203.5 ± 0.2	0.51 ± 0.2	582.4 ± 0.3	0.26 ± 0.07
211.6 ± 0.3	0.05 ± 0.02	586.5 ± 0.3	0.28 ± 0.07
218.7 ± 0.5	0.03 ± 0.02	599.3 ± 0.3	0.45 ± 0.1
243.8 ± 0.4	0.06 ± 0.02	608.0 ± 0.6	0.14 ± 0.08
264.0 ± 0.3	0.15 ± 0.04	613.1 ± 0.3	0.43 ± 0.1
297.6 ± 0.4	0.09 ± 0.03	618.0 ± 0.2	1.1 ± 0.3
316.2 ± 0.3	0.26 ± 0.07	624.9 ± 0.2	0.89 ± 0.2

TABLE II (cont.)

E_{γ} (keV)	I_{γ} ($\gamma/10^2$ n)	E_{γ} (keV)	I_{γ} ($\gamma/10^2$ n)
633.1 ± 0.2	1.9 ± 0.4	821.9 ± 0.8	0.15 ± 0.07
638.0 ± 0.2	3.4 ± 0.8	829.3 ± 1.0	0.17 ± 0.08
642.2 ± 1.0	0.2 ± 0.1	832.6 ± 1.0	0.17 ± 0.08
646.2 ± 0.3	1.4 ± 0.3	840.3 ± 0.5	0.21 ± 0.07
652.0 ± 0.3	1.4 ± 0.3	844.0 ± 0.3	0.57 ± 0.2
659.0 ± 0.3	0.86 ± 0.2	849.6 ± 0.8	0.15 ± 0.07
664.6 ± 0.4	0.64 ± 0.2	852.5 ± 0.5	0.29 ± 0.08
670.9 ± 1.0	0.16 ± 0.07	864.6 ± 1.2	0.14 ± 0.06
680.2 ± 0.7	0.12 ± 0.06	871.0 ± 1.8	0.10 ± 0.05
685.9 ± 0.3	0.46 ± 0.1	878.9 ± 0.4	0.28 ± 0.1
691.1 ± 0.6	0.24 ± 0.1	889.6 ± 0.6	0.26 ± 0.1
693.8 ± 0.6	0.19 ± 0.1	892.2 ± 0.8	0.18 ± 0.08
699.1 ± 0.6	0.21 ± 0.08	904.8 ± 0.6	0.13 ± 0.05
703.7 ± 0.3	0.70 ± 0.2	917.5 ± 0.6	0.11 ± 0.05
714.5 ± 0.3	0.40 ± 0.1	927.6 ± 0.5	0.14 ± 0.06
718.5 ± 0.3	0.53 ± 0.1	944.4 ± 1.0	0.15 ± 0.06
724.0 ± 1.5	0.03 ± 0.02	948.9 ± 0.5	0.72 ± 0.2
728.2 ± 1.0	0.04 ± 0.03	951.2 ± 0.4	0.60 ± 0.2
735.7 ± 0.4	0.27 ± 0.07	955.8 ± 0.4	0.54 ± 0.1
748.2 ± 0.2	1.1 ± 0.3	969.1 ± 0.3	0.59 ± 0.2
756.6 ± 0.6	0.15 ± 0.05	978.9 ± 0.6	0.26 ± 0.1
762.6 ± 0.6	0.17 ± 0.06	982.9 ± 0.7	0.18 ± 0.07
769.8 ± 0.2	1.8 ± 0.4	987.5 ± 0.5	0.46 ± 0.1
779.3 ± 0.6	0.18 ± 0.06	990.9 ± 0.5	0.67 ± 0.2
787.2 ± 0.5	0.29 ± 0.1	995.0 ± 0.6	0.32 ± 0.1
792.6 ± 0.5	0.26 ± 0.1	1002.4 ± 0.4	0.28 ± 0.1
799.7 ± 0.7	0.22 ± 0.07	1028.4 ± 1.1	0.07 ± 0.04
804.6 ± 1.0	0.26 ± 0.1	1033.4 ± 0.7	0.13 ± 0.06
807.3 ± 1.2	0.23 ± 0.1	1046.3 ± 0.5	0.42 ± 0.1
813.7 ± 0.4	0.57 ± 0.2	1057.7 ± 0.5	0.25 ± 0.07

TABLE II (cont.)

E_γ (keV)	I_γ ($\gamma/10^2$ n)	E_γ (keV)	I_γ ($\gamma/10^2$ n)
1072.9 ± 0.4	0.34 ± 0.1	1302.2 ± 0.3	0.34 ± 0.08
1085.2 ± 0.6	0.14 ± 0.06	1308.1 ± 0.4	0.22 ± 0.05
1090.6 ± 1.0	0.13 ± 0.06	1318.8 ± 0.3	0.20 ± 0.05
1096.9 ± 0.5	0.23 ± 0.07	1325.6 ± 0.9	0.11 ± 0.03
1112.0 ± 0.7	0.07 ± 0.02	1331.8 ± 0.5	0.21 ± 0.05
1142.7 ± 0.3	0.54 ± 0.1	1337.0 ± 0.4	0.25 ± 0.07
1173.2 ± 0.5	0.14 ± 0.05	1345.9 ± 1.0	0.06 ± 0.03
1185.4 ± 0.4	0.21 ± 0.05	1355.1 ± 0.7	0.13 ± 0.06
1194.8 ± 0.4	0.17 ± 0.05	1358.0 ± 0.4	0.34 ± 0.1
1202.3 ± 0.7	0.07 ± 0.03	1369.5 ± 0.5	0.14 ± 0.05
1221.4 ± 0.8	0.15 ± 0.06	1383.5 ± 0.4	0.32 ± 0.09
1225.5 ± 1.0	0.14 ± 0.06	1392.6 ± 0.5	0.25 ± 0.07
1233.2 ± 0.4	0.32 ± 0.08	1396.8 ± 0.9	0.17 ± 0.07
1246.4 ± 0.5	0.28 ± 0.1	1400.8 ± 0.5	0.21 ± 0.07
1252.6 ± 0.6	0.27 ± 0.1	1413.6 ± 0.4	0.18 ± 0.05
1256.7 ± 0.5	0.29 ± 0.1	1419.7 ± 1.0	0.06 ± 0.03
1265.3 ± 0.6	0.43 ± 0.1	1425.2 ± 0.4	0.23 ± 0.07
1269.9 ± 0.9	0.24 ± 0.08	1438.6 ± 0.6	0.20 ± 0.07
1283.4 ± 0.5	0.18 ± 0.05	1449.9 ± 0.9	0.15 ± 0.05
1297.2 ± 0.4	0.18 ± 0.05	1462.6 ± 0.8	0.11 ± 0.05
		1465.4 ± 0.8	0.11 ± 0.05
		1478.8 ± 0.6	0.15 ± 0.05
		1495.4 ± 0.5	0.13 ± 0.05
		1503.6 ± 0.7	0.10 ± 0.03
		1511.7 ± 0.4	0.20 ± 0.05

^a Preliminary results.

^b Gamma rays from 16.1 through 129.3 keV were measured with the Si(Li) spectrometer.

^c Questionable line.

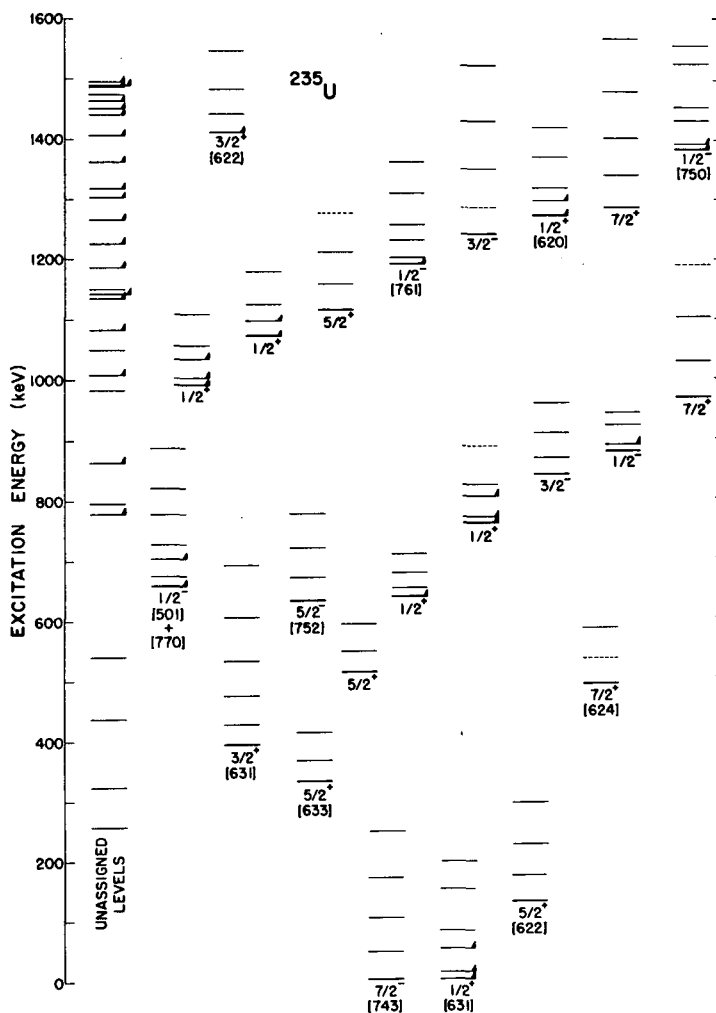


FIG. 3. Levels in ^{235}U determined from the several reactions of the experiment. Small flags indicate those levels excited by primary high-energy transitions in the (n, γ) reaction.

the gamma-ray spectrum over the 300-1500 keV interval. A significant part of the background continuum, particularly at lower energies, arises from scattering of degraded thermal column gamma rays by the graphite target holder. An improvement in the ratio of line height to background could be obtained by the use of more target material, or, possibly, by better packaging.

Figure 3 shows the levels in ^{235}U as determined by all the reactions used in this work. Those states which are excited by direct primary transition in the thermal (n, γ) reaction, mostly with $J^\pi = 1/2^\pm, 3/2^\pm$, are indicated by small flags.

Although transitions between levels have been omitted from Fig. 3 for the sake of clarity, much of the low-energy intensity represented by the gamma rays of Table II has been placed in the level scheme.

The experimentally determined levels have been organized into rotational bands. Twenty-three sets of levels have been determined to have rotational character; twelve of these have been identified with particular Nilsson orbitals, generally on the basis of intensity patterns in the charged particle reactions. The $J^\pi = 1/2^-$ band beginning at 659 keV is of particular interest. The existence of the $13/2^-$ member suggests $\Delta N = 2$ mixing, as do the observed spectroscopic intensities when they are compared with a Rost coupled-channel calculation in a Woods-Saxon well. The decoupling parameter of +2.3 is not of the sign expected for the $1/2^- [501] + 1/2^- [770]$ mixture, however, and the evidence for the assignment is by no means self-consistent.

Fourteen of the bands have $J = 1/2$ or $3/2$, with others likely, from the unassigned group of levels, as evidenced by their excitation with primary capture gamma rays. This large density of low-spin states is not explainable in terms of available Nilsson orbitals and vibrations of a known character built on them. The data suggest that other mechanisms for fragmentation may play a role in explaining the observed levels.

REFERENCES

- [1] LEDERER, C.M., HOLLANDER, J.M., PERLMAN, I., Table of Isotopes, 6th ed., John Wiley and Sons, New York (1967).
- [2] BRAID, T.H., CHASMAN, R.R., ERSKINE, J.R., FRIEDMAN, A.M., Physics Lett. 18 (1965) 149.
- [3] STEPHENS, F.S., HOLTZ, M.D., DIAMOND, R.M., NEWTON, J.D., Nucl. Phys. A115 (1968) 129.
- [4] RICKEY, F.A., Jr., BRITT, H.C., Jr., JURNEY, E.T., to be published.
- [5] JURNEY, E.T., MOTZ, H.T., VEGORS, S.H., Jr., Nucl. Phys. A94 (1967) 351.
- [6] Neutron Cross Sections, Rep. BNL-325, 2nd ed., Suppl.2 (1966).

COLLECTIVE DESCRIPTION OF NUCLEAR STATES

Chairman: S.E. ARNELL

Invited talk

ANALYSIS AND DESCRIPTION OF NUCLEAR ROTATIONAL SPECTRA

B. ELBEK
The Niels Bohr Institute,
Copenhagen, Denmark

Abstract

ANALYSIS AND DESCRIPTION OF NUCLEAR ROTATIONAL SPECTRA. The general properties of nuclear rotational spectra are discussed, first for a single nucleon in a static deformed potential, then for a real nucleus with a real rotational degree of freedom and definite total angular momentum, and finally as modified by nuclear pairing effects, Coriolis coupling and the crossing of levels of the same spin and parity ($\Delta N = 2$). Experimental illustrations of the predicted effects are given and compared to theory.

The subject of the nuclear rotational spectra of which I am speaking today is not a new one. Such spectra have now been known for almost twenty years and many nuclear physicists, including myself, have during this period been held fascinated by the simple beauty of the rotational spectra.

To forestall possible criticism of the narrowness of my subject, I shall hurry and relate the following story: An old man was sitting in a public park playing the violin. But all the time he was playing just a single note. When somebody asked him why he didn't try any of the other possibilities of the instrument, he answered: "Other people are still searching for the right tone, but I have found it." That is the way I feel about rotational spectra.

In my talk I shall first recapitulate a few simple facts about rotational motion and then I shall proceed to show how a number of effects cause deviations from the simplest picture. The main motive shall, however, be the great progress which in the last two years has been made in the experimental and theoretical analysis of the coupling of rotational bands. The result being that we today have more faith than ever in the basic soundness of the rotational description for the large group of nuclei (about 30% of all) which are classified as deformed.

In the presentation of the subject I shall try to follow a scheme where the general ideas are first described in elementary terms and then illustrated by experimental data. Most of the latter have been obtained from studies of single nucleon transfer reactions of (d, p) or (d, t), but I hope it will be clear that the nuclei studied that way really are identical to those studied by neutron capture techniques.

The simple structure of a rotational band is well known to us all. For any rotor, the angular momentum D and energy E are determined by

$$D = J\omega \quad \text{and} \quad E = \frac{1}{2}J\omega^2$$

from which elimination of the frequency of rotation ω yields

$$E = \frac{D^2}{2J} \quad \text{or quantized} \quad E = \frac{\hbar^2}{2J} I(I+1)$$

Pure rotational spectra occur if the frequency of rotation is small compared to other, e. g. vibrational, frequencies of the nucleus. For a rotating nucleus one has $J \sim MR^2$ and thus

$$\omega_{\text{rot}} \sim \frac{\hbar}{MR^2}$$

For a vibrating nucleus $\hbar\omega = \frac{1}{2}M\omega^2\Delta R^2$, that is

$$\omega_{\text{vib}} = \frac{\hbar}{M\Delta R^2}$$

The adiabatic condition $\omega_{\text{rot}} \ll \omega_{\text{vib}}$ therefore implies a vibrational amplitude small compared to the nuclear radius.

The rotational $I(I+1)$ formula is in many cases followed to surprising accuracy. I shall show a single example (^{152}Sm , Fig. 1) where the rotational structure is perhaps not so perfect because of the occurrence of low-lying vibrational excitations. It is a great challenge to the ingenuity of experimenters and theorists to analyse such border-line cases to rescue the rotational description.

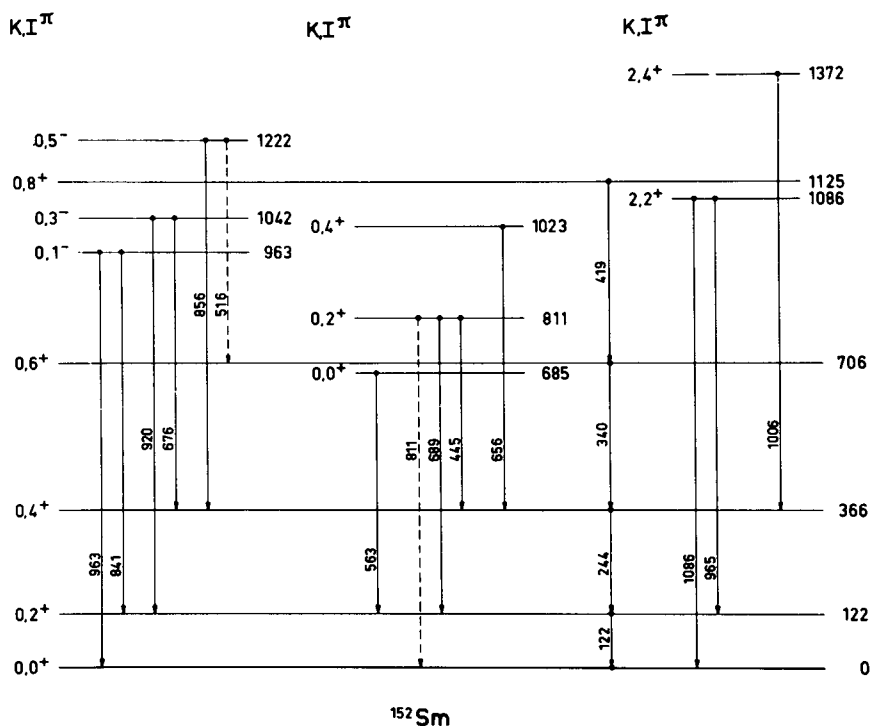


FIG. 1. ^{152}Sm levels.

Many of the tools for such a rescue operation have already been tested in odd nuclei which in some ways are easier to treat because the quantum state of the odd nucleon in a characteristic way affects the rotational spectra. The improved experimental methods for the study of the single nucleon quantum states is therefore the background for the successes in the analysis of the rotational bands.

For a description of the single nucleon states in a deformed potential, it is convenient to expand the deformed wave functions on spherical wave functions $\phi_{Nj\ell m}$. The deformation introduces a symmetry axis in the nucleus. Because of the axial symmetry, the projection Ω of j on this axis is a constant of motion.

The deformation of the nuclear surface will lift the degeneracy of the degenerate spherical shell model state. Thus, if the nucleus is a prolate spheroid (cigar), the orbitals with low Ω -values are energetically favoured as the nucleon motion is then mostly in the long direction of the spheroid where the oscillator quantum, $\hbar\omega$, is smallest. Conversely, orbitals with $\Omega \approx j$ correspond to motions in the directions where the oscillator quantum is large and the energy levels are lifted compared to the spherical values. Thus, the $2j+1$ fold degenerate shell model state is split into a total of $j+1/2$ states in the deformed nucleus having Ω -values $1/2, 3/2, \dots, j$. Each of these states are doubly degenerate and can contain two nucleons corresponding to the two possible directions of the angular momentum with respect to the nuclear symmetry axis. The general character of the splitting of the shell model states is illustrated in Fig. 2.

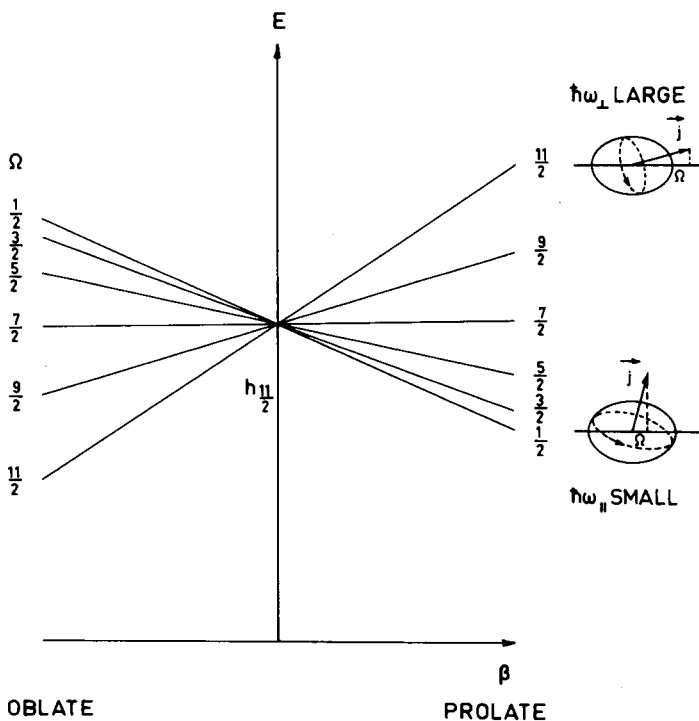


FIG. 2. Simple Nilsson scheme.

For large deformations, the total angular momentum j is frequently not even approximately a good quantum number. In the extreme of very large deformations the number of oscillator quanta, n_z , along the symmetry axis and the component of the orbital angular momentum A in this direction become constants of motion. The individual orbitals are therefore labelled by their asymptotic quantum numbers $[Nn_z\Lambda]$ together with the total angular momentum projection Ω and the parity π .

As already mentioned, it is convenient to expand the deformed wave functions on the spherical wave functions $\phi_{Nj\ell\Omega}$. The expansion is of the form

$$\chi_{N\Omega} = \sum_j C_{j\ell} (N\Omega) \phi_{Nj\ell\Omega}$$

where the deformed wave function χ is labelled by the oscillator quantum number N and the total angular momentum projection Ω . Under certain circumstances, states differing by two units in N can be mixed as will be discussed later. The structure of the wave function is simplified because the parity of ℓ must be that of N . For each ℓ , the j assumes values $\ell \pm 1/2$ subject to the condition $N + 1/2 \geq j \geq \Omega$. Thus, e. g., for $N=6$, $\Omega=5/2$ only terms with $(j, \ell) = (5/2, 2)$, $(7/2, 4)$, $(9/2, 4)$, $(11/2, 6)$ and $(13/2, 6)$ occur. The expansion coefficients $C_{j\ell}$ have been tabulated for different values of the deformation parameter.

The square of the expansion coefficient expresses the probability that the particle in a given Nilsson orbital has total angular momentum j . Therefore, the sum over j of the squares of the expansion coefficients for a given Nilsson state is unity:

$$\sum_j C_{j\ell}^2 (N\Omega) = 1$$

For a given (N, ℓ, j) value, the $C_{j\ell}^2$'s express how the shell model strength has been distributed on the various deformed states. Thus the sum of the squares times 2 (because of the Ω -degeneracy) for all Nilsson orbitals equals the degeneracy, $2j+1$, of the shell model state:

$$2 \sum_{\Omega, \alpha} C_{j\ell}^2 (N\Omega\alpha) = 2j+1$$

where the summation is extended over all states, here labelled by Ω and other quantum numbers α , to which the shell model state $\phi_{Nj\ell}$ contributes.

It is interesting to note how widely the shell model strength is spread by the deformation. Figure 3 shows as an example how the $N=5$, $j=11/2$ strength is distributed for a deformation of $\delta=0.3$. In this case the six deformed states which originate in the $h_{11/2}$ state itself get the largest contributions (about 87% of the total). The rest of the strength is spread on the remaining 15 states. Frequently, however, the different j -values are completely intermixed. An example is shown in Fig. 4. which illustrates the composition of a nuclear wave function for different deformations.

The wave functions discussed up to now refer to a single nucleon moving in a static deformed potential. These states do not possess a definite j and thus not a definite total angular momentum ($=j$). The real nucleus in addition has a rotational degree of freedom and of course possesses a definite total angular momentum. The total wave function therefore describes a situation

as illustrated in Fig. 5 where Ω is the projection of I on the nuclear symmetry axis. As the nucleus does not rotate around the symmetry axis, the rotational angular momentum \vec{R} is perpendicular to the symmetry axis. The \vec{j} is not a constant of motion, but fluctuates in direction so as to keep the projection Ω constant in the way specified by the expansion coefficients $C_{j\ell}^2$. At the same time, the rotational angular momentum \vec{R} fluctuates so that $\vec{R} + \vec{j}$ is constant ($=\vec{I}$). The time average of \vec{j} is $\vec{\Omega}$ (considered as a vector) and the time average $\langle \vec{R} \rangle$ is such as to make $\langle \vec{R} \rangle + \vec{\Omega} = \vec{I}$ (cf. Fig. 5). The special usefulness of the transfer reactions is connected to the fact that their cross-sections are proportional to the $C_{j\ell}^2$. For transfers leading to an odd nucleus, each j corresponds to a rotational state with $I=j$ and the $C_{j\ell}^2$'s are thus separately displayed, thanks to the energy differences between the rotational levels. This 'fingerprint' method therefore gives a direct determination of nuclear wave functions.

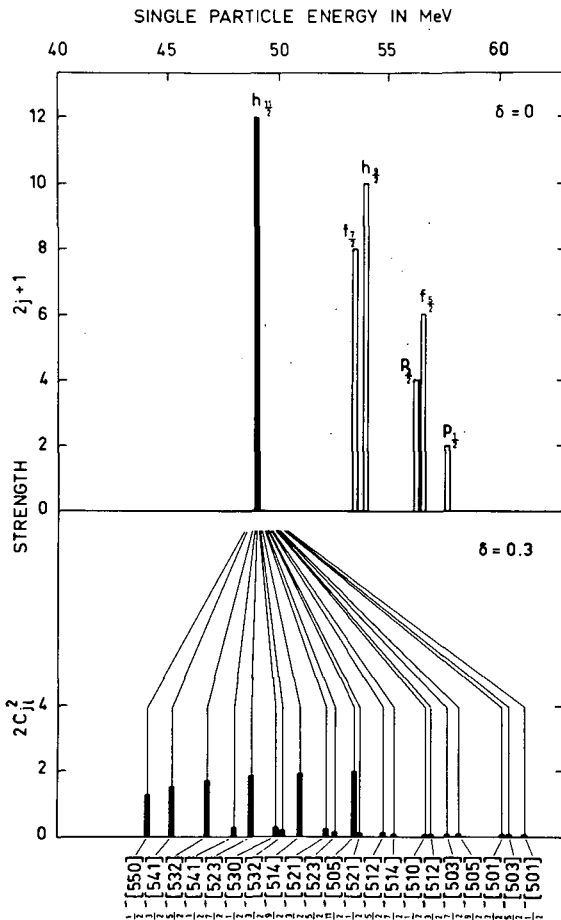
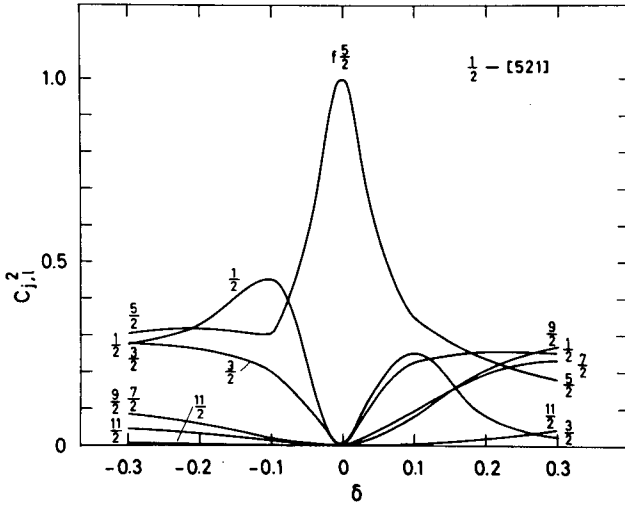
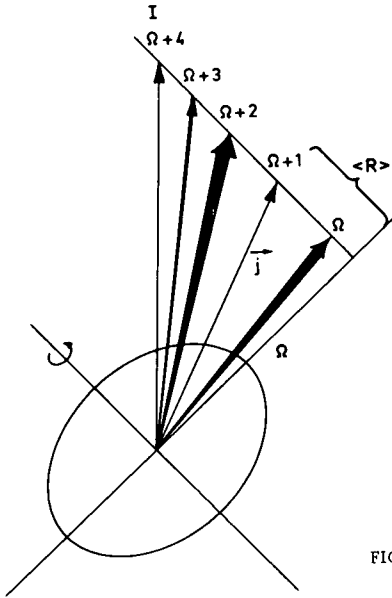


FIG. 3. Splitting of $h_{11/2}$ in deformed nuclei.

FIG. 4. j -components in $1/2$ -[521].FIG. 5. Meaning of $C_{j,l}^2$ coefficients.

Now let us look at the data. The nucleus ^{159}Gd can be taken as an example of the degree of completeness by which low-lying states in a deformed nucleus can be studied in a favourable case. Before the transfer reaction studies essentially nothing was known about the states in ^{159}Gd . Figure 6 shows an example of a (d, t) spectrum which can be analysed by the fingerprint method and Fig. 7 shows the resulting level scheme where a total of 14 Nilsson states have been rather definitely assigned.

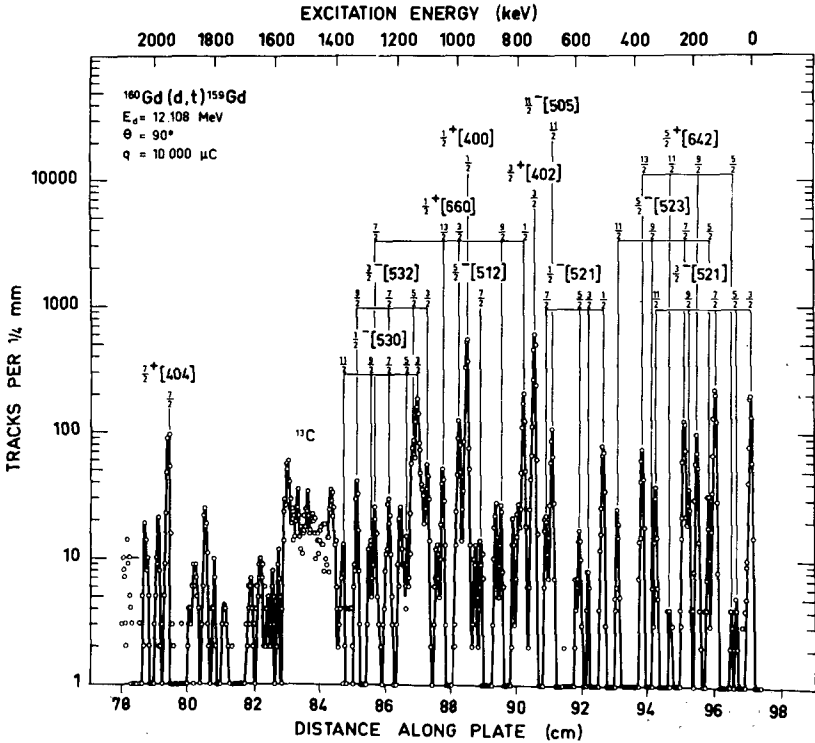
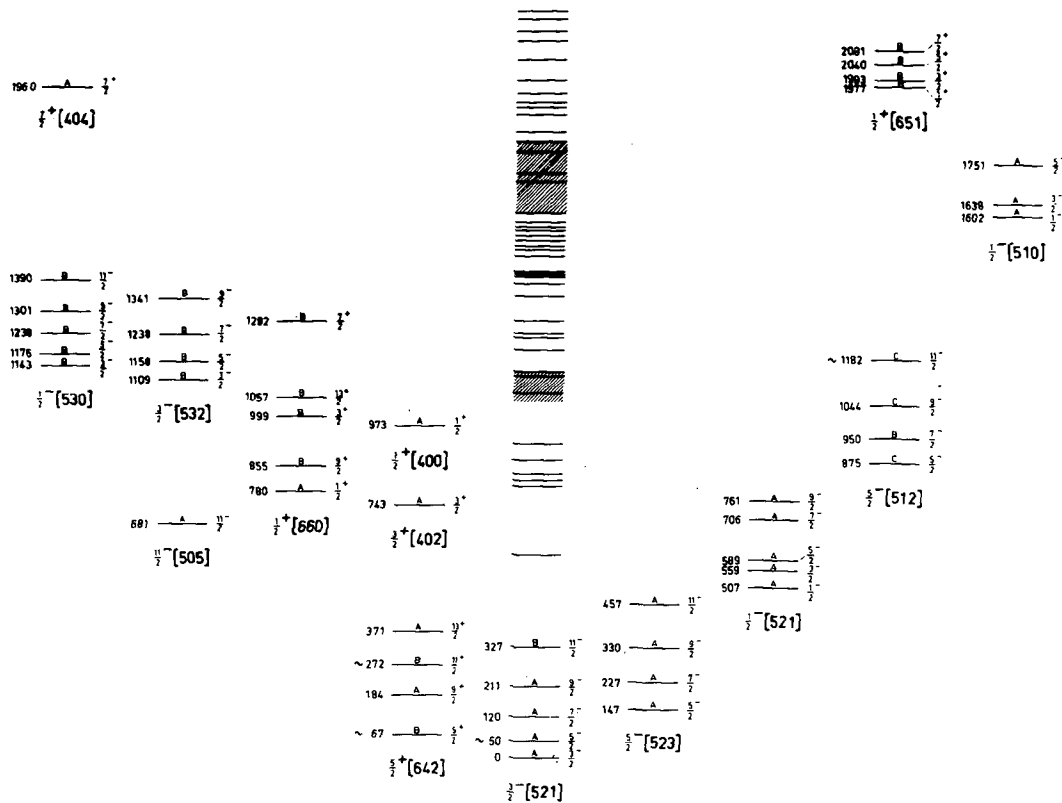


FIG. 6. ^{159}Gd triton spectrum.

The energy span is approximately 4 MeV between the deepest hole state, $7/2^+[404]$, and the highest particle state, $1/2^+[651]$, identified in ^{159}Gd . The main components of these states stem from the $1g7/2$ and the $2g9/2$ shell model states which can be estimated to be separated by approximately 15 MeV in a spherical nucleus. This illustrates clearly the tremendous change in the single-particle levels caused by the deformation. Figure 8 shows a comparison of the theoretical Nilsson states for a deformation of $\beta=0.3$ and $\hbar\omega_0 = 8.8 \text{ MeV}$ compared with those observed in ^{159}Gd . It is first of all noted that the observed level order by and large is in good agreement with the theoretical one. The only noticeable difference is for the $11/2^-$ -[505] state which occurs considerably lower than expected. Another example is ^{175}Yb (Fig. 9).

Let us now turn to the first complication, namely the pairing phenomenon which modifies in several ways the simple picture of independent nucleon motion in a deformed potential.

The deepest lying states in an even deformed nucleus are filled with nucleons which pairwise occupy the Ω -degenerate orbitals. Near the Fermi level, however, the orbitals are only partially occupied by pairs so that a diffuse Fermi surface is created. The partial filling of the states near the Fermi level is expressed by means of the quantities V_ν^2 , which gives the probability for state ν being occupied by a pair, and U_ν^2 which gives the

 ^{159}Gd FIG. 7. ^{159}Gd levels.

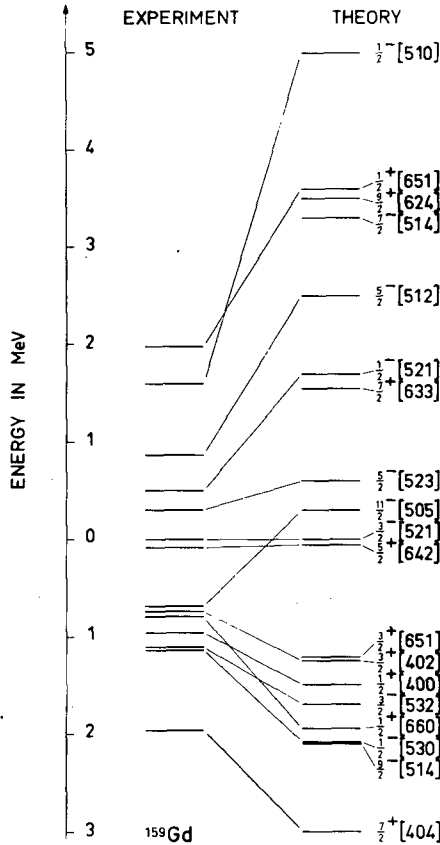


FIG. 8. ¹⁵⁹Gd levels, theory and experiment.

probability for state ν being empty (Fig. 10). Thus $U_{\nu}^2 + V_{\nu}^2 = 1$. The stripping and pick-up cross-sections for even target nuclei are proportional to U^2 and V^2 , respectively, and provide the most direct method for their determination.

In an odd nucleus, the odd nucleon occupies a definite orbital ν' . Relative to the even nucleus, this particle has the properties of a hole to the extent $V_{\nu'}^2$, and those of a particle to the extent $U_{\nu'}^2$. The term 'quasiparticle' has been introduced to describe this dual character. Far from the Fermi surface, the quasiparticle has the properties of a normal particle or hole.

The observed single-particle excitation energy in an odd nucleus is the difference between the ground-state quasiparticle energy and the quasiparticle energy of the excited nucleon. The quasiparticle energy is given by

$$E_{\nu} = \sqrt{(\epsilon_{\nu} - \lambda)^2 + \Delta^2}$$

where ϵ_{ν} is the single-particle energy, λ the Fermi energy and 2Δ the energy gap. Thus, the excitation energy of a quasiparticle, ϵ_{ν} , above the ground state, ν , is:

$$E = \sqrt{(\epsilon_{\nu'} - \lambda)^2 + \Delta^2} - \sqrt{(\epsilon_{\nu} - \lambda)^2 + \Delta^2}$$

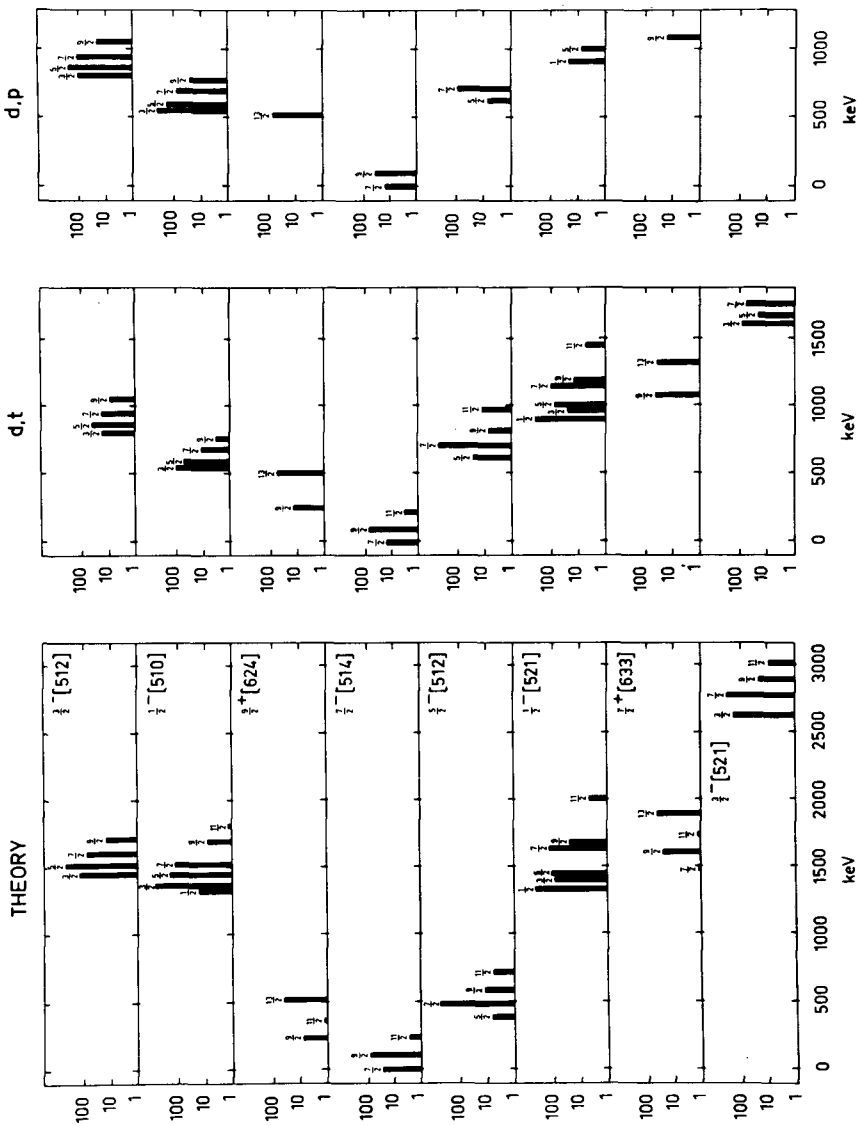


FIG. 9. ^{176}Yb fingerprints.

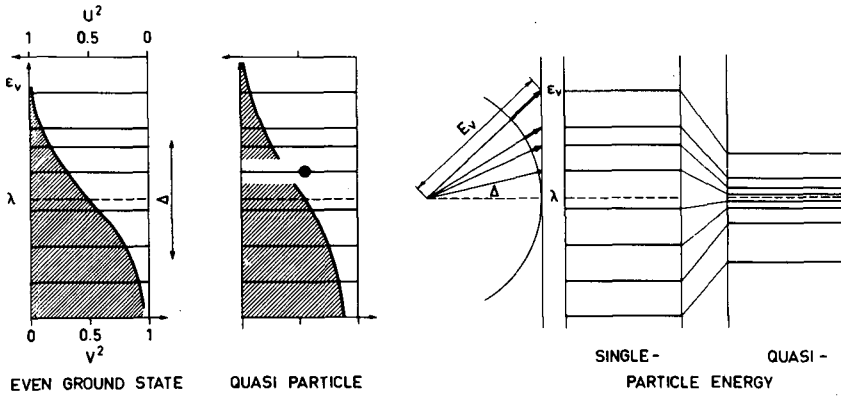


FIG. 10. Pairing U^2, V^2 .

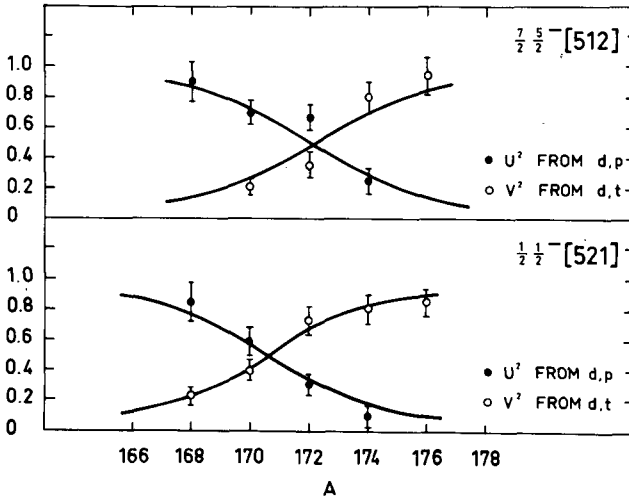


FIG. 11. Experimental U^2, V^2 .

As $\epsilon_v - \lambda \ll \Delta$, the last term is approximately equal to Δ . The general effect of the pairing is a compression of the energy levels around the ground state, the high-lying states being lowered by approximately Δ .

If we now return to the data, we note that the compression of the experimental energy scale of Fig. 8 relative to the theoretical scale is about 2Δ (~ 2 MeV) if the $1/2^- [510]$ state is excluded. (This latter state is partly a gamma vibration.) This compression is an illustration of the importance of the inclusion of pairing effects in the analysis. A second illustration is given in Fig. 11 which, by means of transfer reaction cross-sections, directly illustrates the diffuseness of the Fermi surface in nuclei.

Let us then discuss the Coriolis coupling which probably is the most important and best understood phenomenon which gives rise to intermixing of the one-particle wave functions. The motion of the individual nucleons in the rotating nucleus is affected by a force similar to the classical Coriolis force, $-2m\vec{\omega} \times \vec{v}$, acting on a particle with mass m moving with velocity \vec{v} in a co-ordinate system rotating with angular velocity $\vec{\omega}$.

If we substitute $v \rightarrow \hbar/mR$ and $\omega = \hbar/J$ and turn into a potential by multiplication with R , the Coriolis interaction becomes of the form $\hbar^2/2J I \cdot j$, which is close to the correct expression

$$H_{\text{PRC}} = - \frac{\hbar^2}{2J} (I_+ j_- + I_- j_+)$$

where the operators $I_{\pm} = I_1 \pm iI_2$ and $j_{\pm} = j_1 \pm ij_2$ are defined as usual in terms of the angular momentum projections on the plane perpendicular to the nuclear symmetry axis. These operators have non-vanishing matrix elements only between rotational bands differing by $\Delta K = \pm 1$.

If the expansion on spherical wave functions is introduced, the coupling term becomes

$$\langle IK | H_{\text{PRC}} | IK+1 \rangle = A_K \sqrt{(I-K)(I+K+1)}$$

where A_K , with the inclusion of pairing, is given by

$$A_K = - \frac{\hbar^2}{2J} \langle \chi_K | j_- | \chi_{K+1} \rangle (U_K U_{K+1} + V_K V_{K+1})$$

$$\langle \chi_K | j_+ | \chi_{-(K+1)} \rangle = - \sum_j C_{j\ell}^K C_{j\ell}^{K+1} \sqrt{(j-K)(j+K+1)}$$

If several bands are coupled, the perturbed energies and mixing amplitudes are determined by diagonalization of the energy matrix. Computer programs have been written for a direct evaluation of the stripping and pick-up cross-sections for mixed bands.

The Coriolis coupling is probably responsible for a large fraction of the observed departures from the simple theoretical intensity distributions. Only in a few cases has the experimental material available been analysed for such effects.

Figure 12 shows an example of a two-band coupling (Kleinheinz, Casten) which has been considered in some detail and where the introduction of the coupling drastically improves the agreement between theory and experiment.

The size of the coupling matrix element, of course, depends on the quantum states K and $K+1$. In general large matrix elements are expected between Nilsson states having an overweight of high angular momentum components. Nilsson states originating in high angular momentum shell model states often show reminiscences of their parentage in their $C_{j\ell}$ values. Thus, e. g., in the rare earth nuclei the $N=6$ states originating in the $li_{13/2}$ state are being filled as neutron states. These states all have coefficients $C_{13/2,6} \sim 1$ and are consequently quite strongly coupled to each other. Inserting $\hbar^2/2J \sim 10$ keV, the coupling matrix element A_K for $I = 13/2$ is seen to be of the order of 300 keV. As the single neutron states in question are often found considerably closer than this energy, very strong coupling effects are expected which can completely alter the rotational band structures and thus the distribution of cross-sections. In the limit of strong coupling, that is

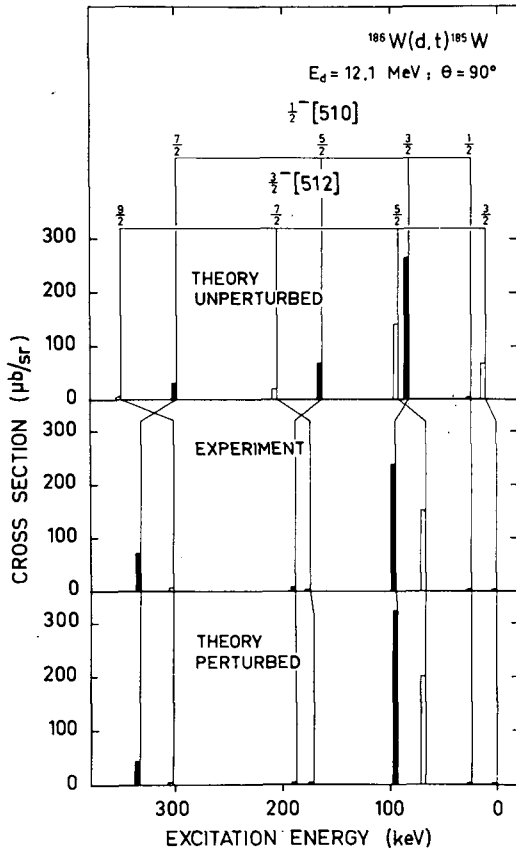


FIG. 12. ^{185}W Coriolis coupling.

when the coupling matrix element is much larger than the energy separation of the bands, the amplitudes a_n in a two-band case approach $1/\sqrt{2}$. This has the interesting consequence that the lower band gets approximately twice the unmixed intensity in a stripping process, the upper band almost nothing.

An example of the strong coupling type is found for the $3/2^+[651]$ and $5/2^+[642]$ orbitals which in the lighter rare-earth nuclei are found as low-lying states. As a consequence of the near disappearance of the cross-section for the upper band, it has been impossible directly to locate this band which only makes itself felt through its effect on the lower band. The violent changes in the rotational energies brought about by strong Coriolis coupling can be seen in Fig. 13.

The Coriolis force represents a reaction of the nucleon orbitals against being dragged around by the rotation. Therefore, in a certain sense, the Coriolis coupling tends to change conditions in the direction of the spherical situation. The gathering of $1/2$ strength in the lowest rotational band referred to here can be considered as an example of this effect.

Let us finally consider another type of coupling effect. The simple Nilsson diagram shows several examples of the crossing of levels with the same spin and parity, but belonging to different oscillator shells. If the interaction between states of different N is taken into account, such crossings do

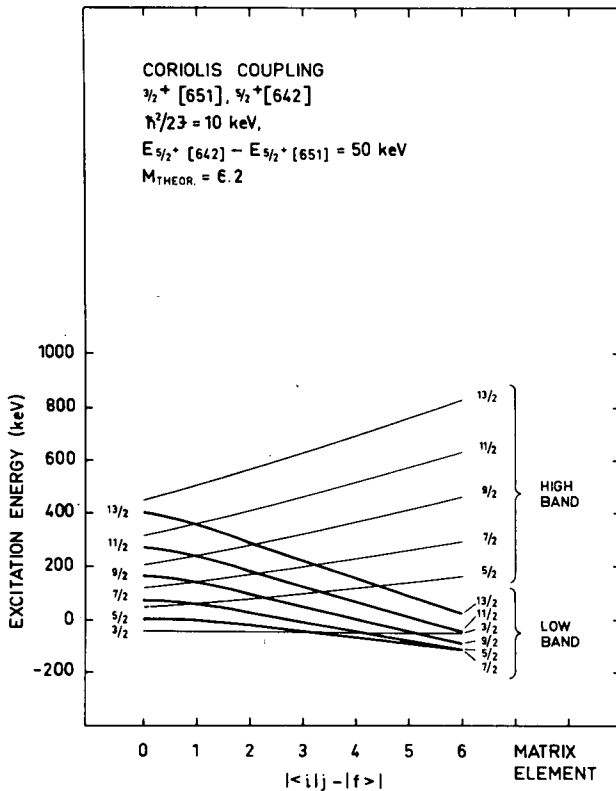


FIG. 13. $3/2^+ | 651 |, 5/2^+ | 642 |$ coupling.

not occur, but the levels in the Nilsson diagram will be deflected and change asymptotic quantum numbers (Fig. 14). The best studied examples are the crossings of the $N=4$ and $N=6$ states in the beginning of the rare-earth region. These crossings are especially easy to study by neutron transfer because they give rise to a splitting of the large $\ell=0$ and $\ell=2$ transfer cross-sections. Examples of this coupling are illustrated in Fig. 15 for the $3/2^+ | 402 |$ and $3/2^+ | 651 |$ bands. By the use of the two-band mixing expressions, one finds

$$\Delta E = \sqrt{\Delta H^2 + 4V^2}$$

and if $\alpha(N=6)/\beta(N=4)$ refers to the ratio of amplitudes,

$$\left| \frac{\alpha}{\beta} \right| = \left| \frac{2V}{\Delta H - (\Delta H^2 + 4V^2)^{1/2}} \right|$$

where ΔH is the unperturbed energy difference and V the unknown interaction. Solutions of ΔH of these equations are illustrated in Fig. 16. The interaction V is 60 keV, considerably stronger than obtained from the Nilsson wave functions (Grotdal, Nybo).

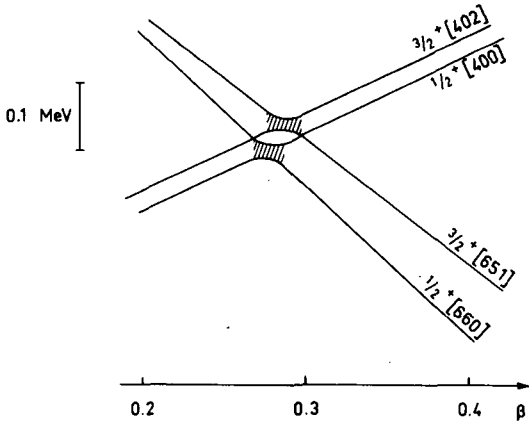


FIG. 14. $\Delta N=2$ coupling.

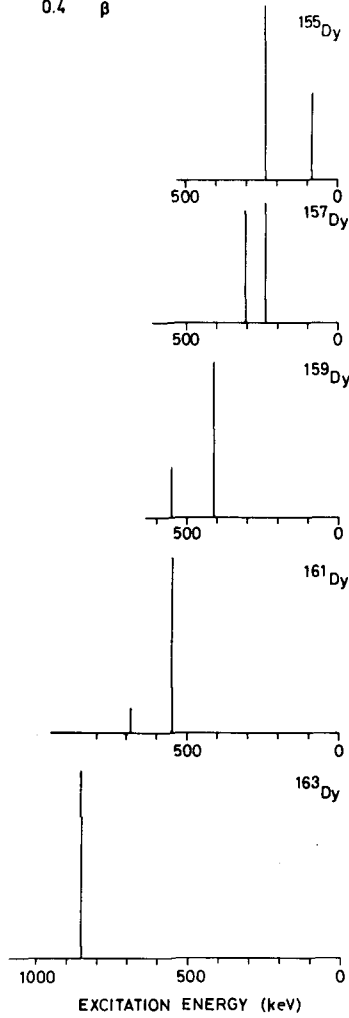
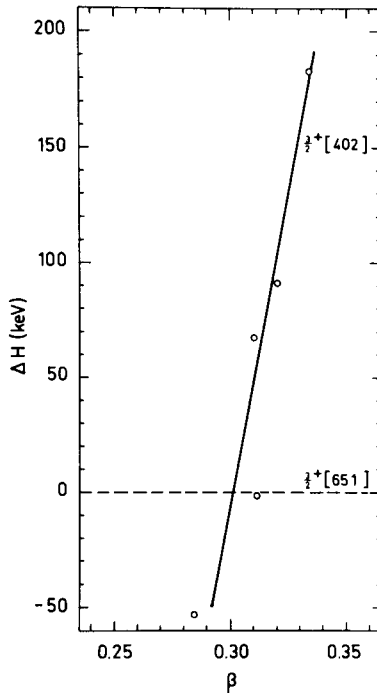


FIG. 15. $\Delta N=2$ coupling $3/2^+ [402]$.

FIG. 16. $\Delta N=2$ energy separation.

It has been shown that the use of a Saxon-Woods type deformed potential in the calculation of the matrix elements yields an interaction of the same magnitude as observed.

We have now mentioned and demonstrated the importance of three types of complications in the rotational spectra: Pairing, Coriolis coupling and $\Delta N=2$. In addition, there are examples of coupling of single-particle states to vibrational states, but they are less easy to discuss without the introduction of a good deal of microscopic description. The presence of such couplings is, of course, a familiar situation in nuclear physics, but perhaps the deformed nuclei separate themselves out from the majority of nuclei because it has been possible in many cases to identify and calculate the couplings responsible for the breakdown of the simplest patterns.

Let me therefore conclude by showing as an example the ^{155}Gd spectrum in which the simultaneous operation of all three types of coupling has been observed. The analysis of the spectrum of even-parity states (Fig. 17) is based on the simple Nilsson model, but with the inclusion of the above-mentioned effects. By means of extensive computer calculations (Borggreen, Løvnhøiden and Waddington), it has been possible to ascribe all the low-lying states to 5 orbitals. The energy fits are excellent, but the important fact is that the wave functions obtained from the energy fits in a convincing manner reproduce the observed (d, t) cross-sections (Fig. 18).

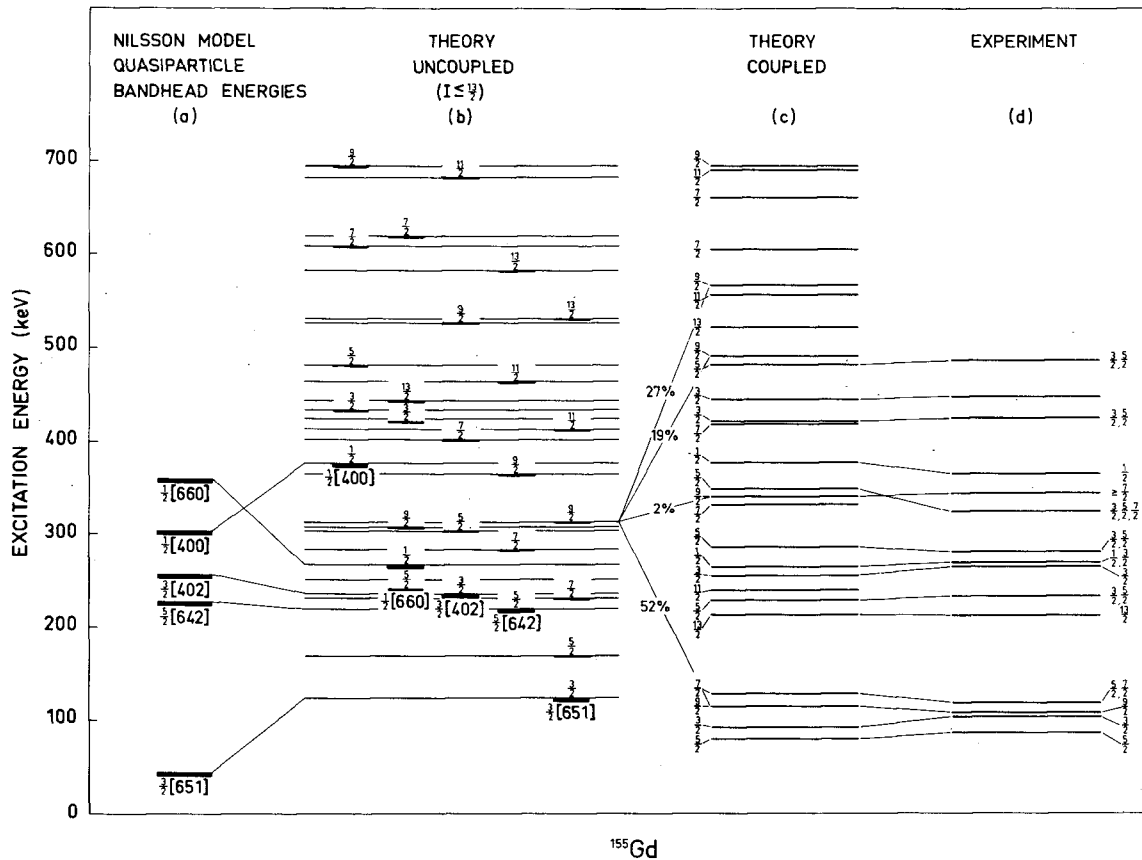


FIG. 17. ^{155}Gd levels.

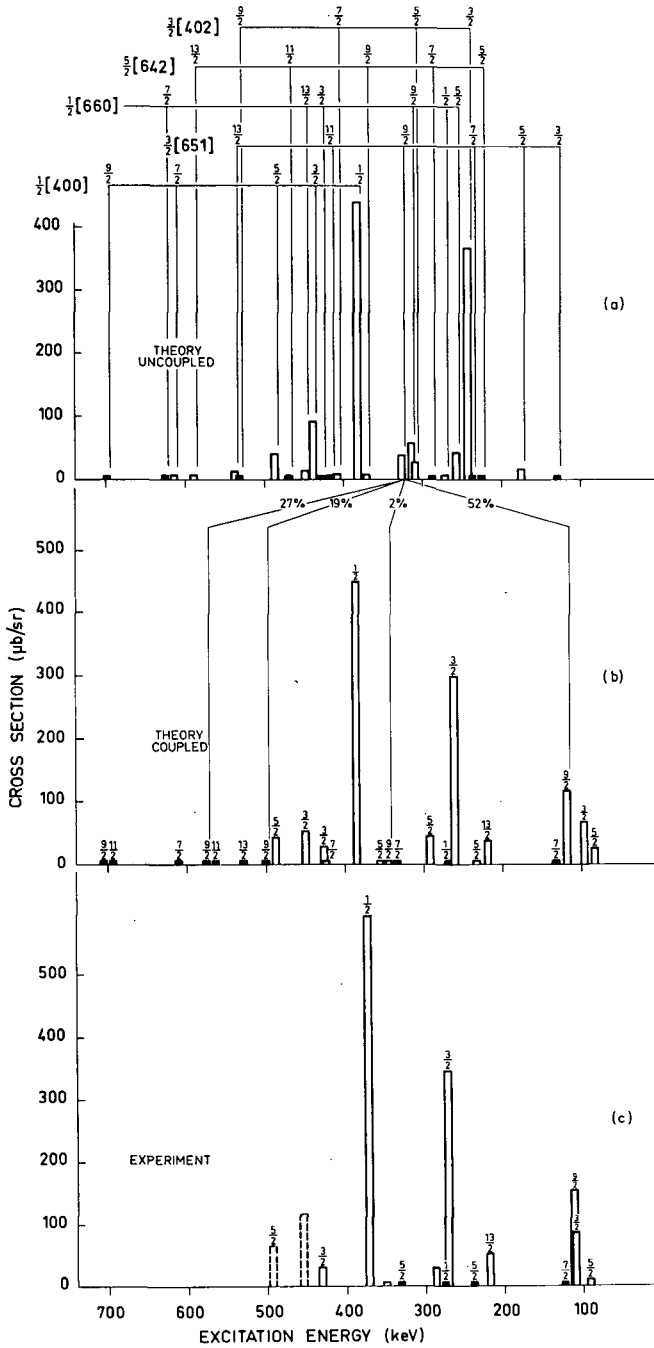


FIG. 18. ^{156}Gd (d, t) intensities.

Less than a year ago, I thought that this nucleus was an example of the breakdown of the Nilsson model. Now it is one of the most perfect examples of the strength of the underlying very simple principles which do not go beyond any introductory course in quantum mechanics. Nevertheless, the successes of the description can easily be matched with those of much more refined theories.

A C K N O W L E D G E M E N T S

This talk is to a large extent based on a review written in collaboration with Dr. P.O. Tjøm.

CALCULATION OF ROTATIONAL STATES IN DEFORMED NUCLEI

P. HOLMBERG
Department of Physics,
University of Helsinki,
Finland

Abstract

CALCULATION OF ROTATIONAL STATES IN DEFORMED NUCLEI. We consider the nucleus as a non-rigid rotator. When the stretching is taken into account we arrive at the formula $E = a \{ [1 + bI(I+1)]^{\frac{1}{2}} - 1 \}$ for the rotational energy. The formula can be obtained both from level systematics and from nuclear hydrodynamic considerations. A comparison of experimental and calculated values is performed for even-even ($K = 0$ bands) and odd-A ($K \geq 5/2$ bands) nuclei in the mass region $165 \leq A \leq 190$.

As rotational states with high I -values in even-even nuclei are reached, mainly from heavy-ion reactions, it is obvious that the moment of inertia J in the simple rotational formula

$$E = \frac{\hbar^2}{2J} I(I+1) \quad (1)$$

is only approximately a constant. An improvement is obtained when a rotation-vibration interaction is taken into account [1, 2] or stretching of the nucleus is allowed [3]. The improved formula now reads

$$E = AI(I+1) + BI^2(I+1)^2 \quad (2)$$

However, not even Eq. (2) is enough to reproduce rotational states with high I -values. Models taking into account stretching of the nucleus were later further developed [4-7]. A consequence of the stretching is that the moment of inertia changes as the excitation energy increases. We therefore plot J -values calculated according to Eq. (1) as a function of E for some even-even nuclei. This is illustrated in Fig. 1. We observe that, beyond the first few levels, J increases linearly with E . Thus we can write

$$J = c_1 + c_2 E \quad (3)$$

where c_1 and c_2 are constants. A substitution of Eq. (3) into Eq. (1) yields

$$E = a \{ [1 + bI(I+1)]^{\frac{1}{2}} - 1 \} \quad (4)$$

This is our energy formula. The constants a and b are positive and can be calculated from a least-squares fit to experimental data. Equation (4) can also be derived from nuclear hydrodynamic considerations [7].

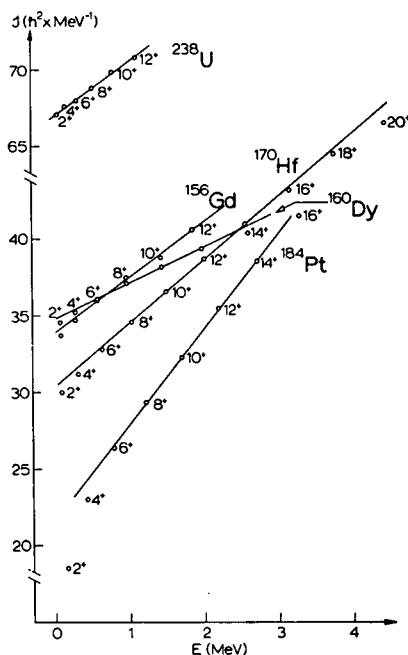


FIG. 1. Moment of inertia as a function of excitation energy according to Eq.(1).

In Table I we present results for a representative sample of even-even nuclei and compare them to experimental data.

Rotational states in odd-A nuclei are described by the formula [8]

$$E = E_K + \frac{\hbar^2}{2J} I(I+1) + \delta_{K,1/2} a(-)^{I+1/2} (I+1/2) + \delta_{K,3/2} b(-)^{I+3/2} (I-1/2)(I+1/2)(I+3/2) \dots \quad (5)$$

which indicates that the energies of rotational states are a sum of an intrinsic energy E_K , the simple rotational energy $\frac{\hbar^2}{2J} I(I+1)$ and the subsequent decoupling terms. To obtain a better agreement between experiment and theory, the rotational part of Eq. (5) is continued as a series in $I(I+1)$. However, the many parameters now occurring are a disadvantage.

The decoupling terms of Eq. (5) will be of greatest influence for the $K=1/2$ and $K=3/2$ bands. For rotational bands with $K \geq 5/2$ the correction terms will be of still higher order and hence their influence can be neglected in the present work.

As in the case of even-even nuclei, we calculate the moment of inertia. From Eq. (5) we drop the decoupling terms, according to our assumption, and assume different E_K -values and solve for J . For each I -value we have a corresponding experimental value for E and we plot J versus $E - E_K$.

TABLE I. CALCULATED ENERGIES OF ROTATIONAL STATES COMPARED TO EXPERIMENTAL DATA FOR SOME EVEN-EVEN NUCLEI

¹⁶⁰ Dy	Exp.	86.7	284	582	972	1437	1977	2602	
	Calc.	84.7	279	577	968	1442	1987	2595	
¹⁷⁰ Yb	Exp.	84.2	278	572	962	1439	1986		
	Calc.	83.4	277	573	963	1438	1986		
¹⁷⁰ Hf	Exp.	100.0	321	641	1041	1503	2013	2564	3147
	Calc.	96.4	313	632	1034	1501	2017	2570	3152
¹⁸⁰ W	Exp.	102.0	336	690	1147	1667	2252		
	Calc.	104.0	339	690	1139	1666	2256		

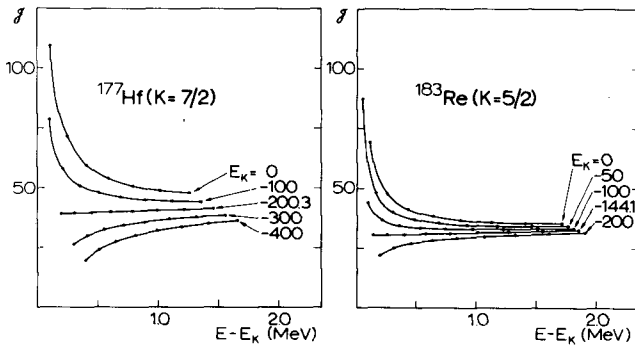


FIG. 2. Moment of inertia as a function of $(E - E_K)$ according to Eq. (5) for ¹⁷⁷Hf and ¹⁸³Re. J is given in units of $\hbar^2 \times \text{MeV}^{-1}$ and E_K is given in units of keV.

TABLE II. PARAMETERS E_K , a AND b FOR SOME ODD-A NUCLEI CALCULATED ACCORDING TO Eq. (7)

Nucleus	K	E_K	$a \times 10^3$	$b \times 10^{-3}$
¹⁸³ Re	5/2	-144.1	11.8	2.8
¹⁸¹ Re	5/2	-153.9	4.86	7.3
¹⁷⁷ Hf	7/2	-200.3	12.2	2.1
¹⁶⁵ Ho	7/2	-167.3	15.3	1.4

TABLE III. CALCULATED ENERGIES OF ROTATIONAL STATES COMPARED TO EXPERIMENTAL DATA FOR SOME ODD-A NUCLEI

¹⁸³ Re	Exp.	0.0	114.3	259.5	434.5	638.1	869.3	1126.0	1408.0	1712.3
	Calc.	0.1	114.2	259.3	434.4	638.1	869.3	1126.3	1407.7	1712.0
¹⁸¹ Re	Exp.	0.0	117.9	266.2	443.3	645.7	871.8	1114.8	1375.3	
	Calc.	-1.0	118.1	267.3	444.0	645.8	870.1	1114.4	1376.3	
¹⁷⁷ Hf	Exp.	0.0	113.0	249.7	409.4	591.3	794.4	1017.7	1260.3	
	Calc.	0.0	113.0	249.7	409.5	591.3	794.4	1017.8	1260.4	
¹⁶⁵ Ho	Exp.	0.0	94.7	209.8	345	499	672			
	Calc.	0.0	94.8	209.9	344.9	499.1	672.2			

This is illustrated in Fig. 2 which shows the J-dependence of $E-E_K$ for the nuclei ¹⁷⁷Hf and ¹⁸³Re. For a certain value of E_K we observe that a straight line can be fitted to the calculated J-values. This means that the expression

$$J = c_3 + c_4(E - E_K) \quad (6)$$

can be used for the moment of inertia. When we substitute Eq. (6) into Eq. (5) we obtain a quadratic equation in $(E - E_K)$ which gives

$$E = E_K + a \{ [1 + bI(I+1)]^{\frac{1}{2}} - 1 \} \quad (7)$$

The parameters appearing in Eq. (7) are calculated from a least-squares fit to experimental data. In Table II we present the values of E_K , a and b giving the best fit to experimental data for some nuclei with rotational bands of $K \geq 5/2$. In Table III we give the energies as calculated with the parameters of Table II. The agreement between experimental and calculated values is good. In most cases the deviation is less than ± 1 keV. The good agreement also justifies the assumption that the decoupling terms can be neglected for bands with $K \geq 5/2$.

ACKNOWLEDGEMENT

Discussions with P.O. Lipas are acknowledged.

REFERENCES

- [1] NIELSEN, O.B., Proc. Rutherford Jubilee Int. Conf., Manchester 1961 (BIRKS, J., Ed.), Heywood and Co., London (1961) 317.
- [2] LIPAS, P.O., Nucl. Phys. 39 (1962) 468.
- [3] MOSZKOWSKI, S.A., Handbuch der Physik (FLÜGGE, S., Ed.) 39, Springer-Verlag, Berlin (1957) 411.
- [4] SOOD, P.C., Phys. Rev. 161 (1967) 1063.
- [5] SCHARFF-GOLDHABER, G., Proc. Int. Conf. Nuclear Structure, Tokyo, 1967 (SANADA, J., Ed.), Suppl. to J. phys. Soc. Japan 24 (1968) 150.
- [6] DRAPER, J.E., McCAULEY, D.G., SMITH, G.L., to be published.
- [7] HOLMBERG, P., LIPAS, P.O., Nucl. Phys. A117 (1968) 552.
- [8] NATHAN, O., NILSSON, S.G., Alpha-, Beta- and Gamma-Ray Spectroscopy (SIEGBAHN, K., Ed.), North-Holland Publishing Company, Amsterdam (1965) 601.

BAND MIXING IN DEFORMED ODD-MASS NUCLEI

W. MICHAELIS, F. WELLER, H. OTTMAR,
U. FANGER, R. GAETA*, H. SCHMIDT
Institut für angewandte Kernphysik,
Kernforschungszentrum Karlsruhe,
Karlsruhe, Federal Republic of Germany

Abstract

BAND MIXING IN DEFORMED ODD-MASS NUCLEI. The level structure of several deformed odd-mass nuclei has been studied at the Karlsruhe research reactor FR-2 using radiative capture of thermal neutrons. High-resolution measurements of the gamma-ray spectrum have been performed with a Ge(Li) anti-Compton spectrometer and a Ge(Li) pair spectrometer. The high accuracy of the data allows the application of Ritz' combination principle up to energies above 1.5 MeV. Coincidence relationships have been obtained by means of a Ge(Li)-NaI(Tl) coincidence system. Detailed data are given for the transition diagram of ^{167}Er . The experiments reveal the occurrence of considerable band mixing. A theoretical treatment is presented within the framework of the unified model. The calculations take into account pair correlation, quasiparticle-phonon interaction, Coriolis coupling and rotation-vibration interaction. Various properties of the deexcitation mechanism are determined to a large extent by band mixing. Examples are given for branching ratios and partial gamma-ray half-lives both in ^{167}Er and ^{169}Yb .

1. Introduction

The rapid development of experimental techniques in gamma-ray spectroscopy has made feasible detailed investigations of nuclear structure by means of the radiative neutron capture process. In a recent paper on thermal neutron capture in ^{168}Yb we have pointed out the occurrence of considerable band mixing effects in ^{169}Yb [1]. Similar results have also been published on ^{165}Dy [2]. The purpose of this presentation is to provide a brief summary of experimental and theoretical data obtained for the isotonic nucleus ^{167}Er and to discuss some obvious consequences of band mixing on branching ratios and partial gamma-ray halflives both in ^{167}Er and ^{169}Yb .

2. Experimental Procedure

High-resolution measurements of the gamma-ray spectrum have been performed using a Ge(Li) anti-Compton spectrometer in the low-energy region [3, 4] and a Ge(Li) five-crystal pair spectrometer for the high-energy transitions [2]. Coincidence relationships have been studied by means of a Ge(Li)-NaI(Tl) coincidence system [5] coupled to an on-line computer [6]. The energy calibration is based on the decay lines of ^{192}Ir , ^{137}Cs , ^{60}Co and ^{88}Y and on capture lines from the product nuclei ^2H and ^{14}N . The procedures applied in spectrum stabilization, spectrum analysis, calibration and nonlinearity correction are described in detail in Ref. [4]. A brief discussion of the technique used for analysing complex coincidence spectra may be found in Ref. [7].

The measurements on ^{167}Er have been performed with a sample of Er_2O_3 enriched to 95.6 % in ^{166}Er . In spite of this relatively

* Visiting scientist from Junta de Energía Nuclear, Ciudad Universitaria, Madrid.

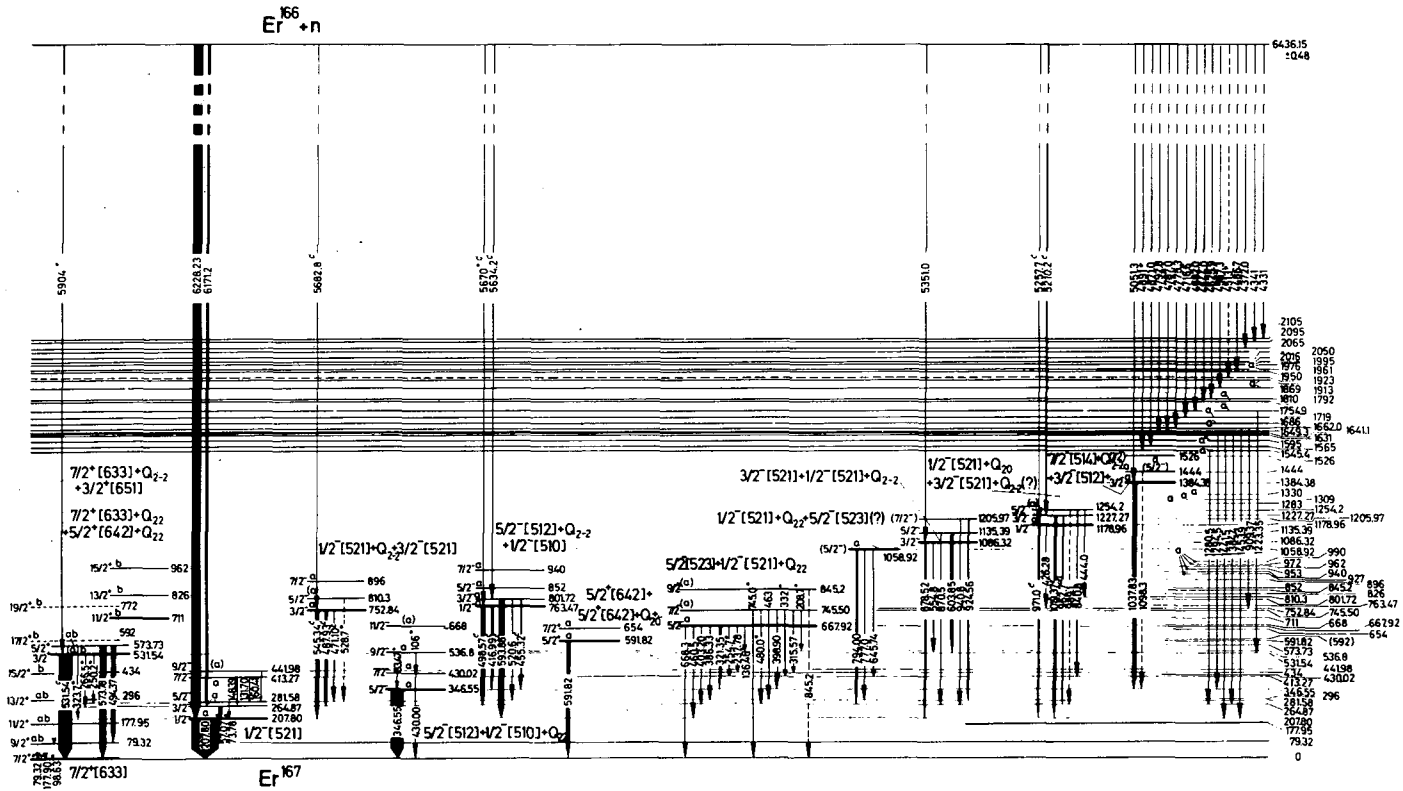


FIG. 1. Transitions of ^{167}Er .

high enrichment care had to be taken in the isotope assignment of the gamma-ray lines. Due to the unfavourable cross section, the capture contribution of ^{160}Er was only 68.8 %. The main interference resulted from the target nucleus ^{167}Er which contributed with 31.1 % to the total capture cross section. Neutron capture in other erbium isotopes was negligible. In order to obtain a reliable isotope assignment each run was repeated with a target of natural erbium. More than 350 gamma-ray lines have been observed from the enriched sample.

The data were also examined for the possibility of contributions from likely chemical contaminants and, in fact, several lines were identified as arising from Sm and Gd.

3. Transition Diagram of ^{167}Er

As yet no exhaustive investigation of the ^{167}Er neutron capture transition diagram has been performed and thus the information about the deexcitation mechanism was still limited. Most of the available data have come from studies with the Risø bent crystal spectrometer [8] and with a Ge(Li) pulse-height spectrometer [9]. In the first study 47 lines of the low-energy spectrum were assigned to ^{167}Er and 24 transitions were fitted into a level scheme. The second work examined the high-energy spectrum using a sample of very high enrichment (99.97 %). The most recent investigations of ^{167}Er levels by means of charged-particle reactions are those in Refs. [10] and [11]. The decay of ^{167}Ho (3 h) and ^{167}Tm (9.6 d) to ^{167}Er has recently been studied with Ge(Li) and scintillation counters both in single and coincidence mode [12].

The present research suggests a considerably extended transition diagram as represented in Fig. 1. The intensities of the gamma rays are expressed by the arrow width. Most of the lines were fitted into the diagram using the Ritz combination principle. Transitions marked with the letter "c" have been clearly observed in coincidence measurements and their position in the decay scheme is well established. Dashed arrows mean that the available data suggest the existence of these gamma rays and the position shown, but the assignment is considered to be somewhat tentative. Transitions labelled with an asterisk have been adopted from previous investigations provided that the assignment is consistent with the present study. For the sake of completeness the results obtained from charged-particle reactions have also been included in the decay scheme. Levels labelled with the letter "a" have also been observed in (d,p) reactions [10]. Letter "b" indicates excited states detected in inelastic scattering of deuterons [11].

Analysis of the experimental data and results of theoretical calculations described in section 4 suggest the following spectroscopic interpretation (bandhead energies and dominant structure):

0 keV	$7/2^+$ [633]	90 %	$7/2^+$ [633] + Q_{20}	6 %
208 keV	$1/2^-$ [521]	92 %		
347 keV	$5/2^-$ [512]	86 %	$1/2^-$ [510] + Q_{22}	11 %
532 keV	$7/2^+$ [633] + Q_{2-2}	81 %	$3/2^+$ [651]	15 %
592 keV	$5/2^+$ [642]	79 %	$5/2^+$ [642] + Q_{20}	12 %
	$3/2^+$ [651]	7.5 %		

668 keV	$5/2^-$ $[\bar{5}23]$	81 %	$1/2^-$ $[\bar{5}21]$ + Q_{22}	16 %
711 keV	$7/2^+$ $[\bar{6}33]$ + Q_{22}	94 %	$5/2^+$ $[\bar{6}42]$ + Q_{22}	5 %
753 keV	$1/2^-$ $[\bar{5}21]$ + Q_{2-2}	61 %	$3/2^-$ $[\bar{5}21]$	37 %
763 keV	$5/2^-$ $[\bar{5}12]$ + Q_{2-2}	56 %	$1/2^-$ $[\bar{5}10]$	38 %
1059 keV	$1/2^-$ $[\bar{5}21]$ + Q_{22}	80 %	$5/2^-$ $[\bar{5}23]$	15 % (?)
1086 keV	$3/2^-$ $[\bar{5}21]$	60 %	$1/2^-$ $[\bar{5}21]$ + Q_{2-2}	37 %
1179 keV	$1/2^-$ $[\bar{5}21]$ + Q_{20}	93 %	$3/2^-$ $[\bar{5}21]$ + Q_{2-2}	4 % (?)
1384 keV	$3/2^-$ $[\bar{5}12]$	41 %	$7/2^-$ $[\bar{5}14]$ + Q_{2-2}	38 %
	$1/2^-$ $[\bar{5}10]$ + Q_{2-2}	16 %		

A detailed analysis and discussion of the level structure will be given elsewhere [13].

4. Theoretical Considerations

In order to arrive at a better understanding of the level structure, theoretical calculations have been performed which take into account pair correlation, quasiparticle-phonon interaction, rotation-vibration interaction and Coriolis coupling. Since a solution with the exact Hamiltonian is beyond the possibilities of present theoretical nuclear physics, it is convenient to use a phenomenological approach. Such a procedure is justified, if only few additional parameters are introduced and an extensive set of data is predicted which can be examined experimentally. The calculations that will be outlined here very briefly reveal the energy and structure of individual levels, absolute transition rates and partial gamma-ray half-lives, multipolarity admixtures and branching ratios. They use a generally valid set of single-particle energies. The BCS treatment is performed with the constant $G_n = 0.021 \hbar \omega_0 = 26/A$ MeV ($\hbar \omega_0 = 41 A^{-1/3}$ MeV = 7.445 MeV). The parameter $\epsilon = \hbar^2/J_0$ is fitted where J_0 is the undisturbed moment of inertia. Excitation energies for the β and γ quadrupole vibrations are taken from the neighbouring even nuclei.

The Hamiltonian is written as [14, 15]

$$H = H_0 + H'$$

with

$$H_0 = H_N + H_{OC}$$

Here H_N is the Nilsson Hamiltonian [16] and H_{OC} describes the undisturbed collective motion, i.e. the rotation of the nucleus and the β and γ vibrations. The interactions between the various modes of motion are taken into account by H' . This term includes the Coriolis coupling, the particle-phonon interaction and the rotation-vibration interaction.

Neglect of pair correlations leads to unreasonable matrix elements and serious disagreement with experimental results. Therefore

$$H_N = \sum_{\nu} \epsilon_{\nu} a_{\nu}^{\dagger} a_{\nu}$$

has to be replaced by

$$H_{QP} = \sum_{\nu} E_{\nu} \alpha_{\nu}^{\dagger} \alpha_{\nu}$$

with the usual notation

$$E_{\nu} = \left[(\epsilon'_{\nu} - \lambda)^2 + \Delta_{\nu}^2 \right]^{1/2}$$

and

$$\epsilon'_{\nu} = \epsilon_{\nu} - G V_{\nu}^2$$

ϵ_{ν} and E_{ν} denote the particle and quasiparticle energies, respectively. The operators a and α are correlated via the Bogolyubov-Valatin transformation. The coefficients V_{ν} and U_{ν} ($V_{\nu}^2 + U_{\nu}^2 = 1$) are determined separately for each state from the well-known variational problem. Thus the blocking effect is fully taken into account. All quasiparticle matrix elements can be reduced to particle matrix elements. In many cases the pairing factors reduce the matrix elements considerably.

For calculating the structure of ^{167}Er and ^{169}Yb eleven Nilsson orbits near the Fermi level together with their γ^+ , γ^- and β vibrational bands have been taken as a basis. The contribution of each of these configurations to the structure of the individual levels results from the diagonalization. More details of the theoretical treatment may be found in Refs. [11] and [13].

In Fig. 2 the calculated excitation energies for ^{167}Er are compared with the experimental level scheme. In general, the agreement is surprisingly good. Some obvious consequences of band mixing on other nuclear properties are discussed in the following sections.

5. Branching Ratios.

The occurrence of strong band mixing is responsible for various phenomena which cannot be explained within the framework of simple models. It is beyond the scope of this presentation to give a detailed discussion here. As an example let us select the deexcitation of the $1/2^-$ rotational band observed at 763 keV in ^{167}Er (cf. Fig. 1). The only Nilsson state with spin and parity $1/2^-$ near the Fermi level is the orbit $1/2^- [521]$. This state, however, is well established to occur at 208 keV excitation energy. Thus it is reasonable to assume that the band at 763 keV corresponds to the γ^- vibrational band based upon the configuration $5/2^- [512]$ and, in fact, a collective E2 transition leaving the bandhead is observed. In other respects, however, the deexcitation shows clear anomalies. From both the first and second member of the band transitions proceed to the $1/2^- [521]$ Nilsson band which in intensity considerably exceed the E2 transitions to the "own" intrinsic configuration. In addition, the branching ratio to the $3/2^-$ and $1/2^-$ levels is exceptional. A reasonable explanation for these anomalies is provided by assuming a strong admixture of the $1/2^- [510]$ Nilsson state in the $5/2^- [512] + Q_{2-2}$ excitation. It is true that the $1/2^- [510]$ orbit is expected at much higher energies, but it is connected with the $5/2^- [512]$ orbit by a strong E2 matrix element. As mentioned above an admixture of 38 % is predicted by the calculations described in section 4. On the other hand, the rotational band at 208 keV consists only to 92 % of the Nilsson state $1/2^- [521]$.

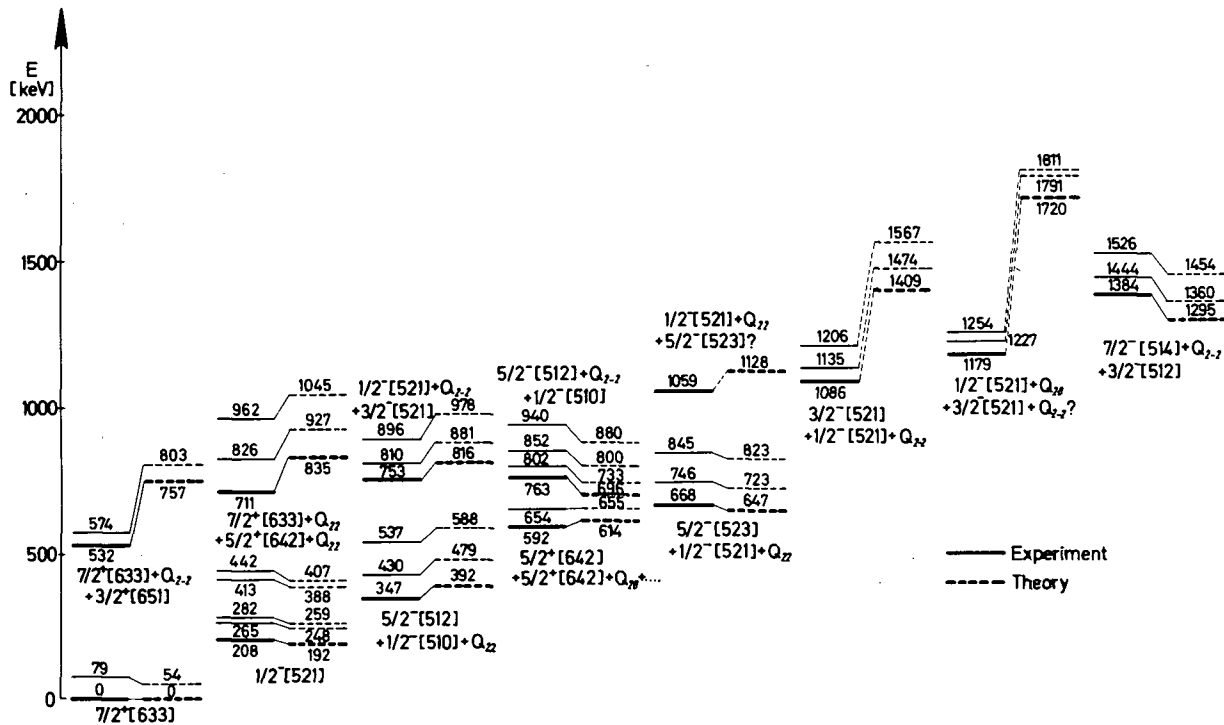
FIG. 2. Comparisons of experimental and theoretical excitation energies in ^{167}Er .

Table I

Transitions from the band
 $5/2^- [512] + Q_{2-2} + 1/2^- [510]$
 ^{167}Er

Intensity ratio	Assuming a pure Nilsson band	Assuming a collective nature		Exp.
		H' = 0	H' ≠ 0	
$\frac{I(1/2\ 1/2 \rightarrow 3/2\ 1/2)}{I(1/2\ 1/2 \rightarrow 1/2\ 1/2)}$	7.0	-	1570	> 15
$\frac{I(1/2\ 1/2 \rightarrow 3/2\ 1/2)}{I(1/2\ 1/2 \rightarrow 5/2\ 5/2)}$	-	0	6.1	3.6 ± 0.4

Table II

Partial gamma-ray halflives $T_{1/2\ \gamma}$

Nucleus	Initial con-figuration	Final con-figuration	Multi-polar-ity	$\sigma_{\text{theor.}}$	$T_{1/2\ \gamma} [\text{nsec}]$		
					H' = 0	H' ≠ 0	Exp.
^{167}Er	$1/2^- 1/2 [521]$	$7/2^+ 7/2 [633]$	E3	-	3.6 sec	4.3 sec	5.5 sec ^b
	$3/2^- 1/2 [521]$	$1/2^- 1/2 [521]$	M1+E2	0.74	13.5	23.5	39.4 ^a
	$5/2^- 5/2 [512]$	$7/2^+ 7/2 [633]$	E1	-	0.07	0.1	1.4 ^c
^{169}Yb	$5/2^- 5/2 [512]$	$7/2^+ 7/2 [633]$	E1	-	0.1	0.3	1.3 ^a 4.2 ^b
		$1/2^- 1/2 [521]$	E2	∞	21 000	630	102 ^a 320 ^b
		$3/2^- 1/2 [521]$	M1+E2	0.055	190 000 (M1: K-forb.)	135	103 ^a 260 ^b
		$5/2^- 1/2 [521]$	M1+E2	0.009	630 000 (M1: K-forb.)	110	84 ^a 220 ^b

^a Ref. [17] ^b Ref. [18] ^c Ref. [12]

The influence of the interaction term H' in the Hamiltonian is demonstrated in Table I. Both the assumption of a pure Nilsson state and a pure vibrational wave function reveal disagreement with the experimental data while the band mixing resulting from H' provides a reasonable explanation for the observed anomalies. Obviously, the transition to the $1/2^-$ state is strongly retarded compared to that reaching the $3/2^-$ level and, in fact, in none of the hitherto existing investigations of the nuclei ^{165}Dy , ^{167}Er and ^{169}Yb such a transition has been detected. When judging the theoretical branching ratio in the second line of Table I, one should notice that we are not dealing with a simple procedure such as that applied in the Alaga rule, but that the nuclear wave functions of three states directly enter into the result.

6. Partial Gamma-Ray Halflives

In general, the low-lying excited states are expected to be essentially characterized by pure wave functions and, in fact, only small admixtures are predicted for these states by the calculations described in section 4. Nevertheless such small admixtures may have a decisive influence on the partial gamma-ray halflives. This is demonstrated in Table II where the theoretical values both for $H' = 0$ and $H' \neq 0$ are compared with experimental data. In all cases the inclusion of band mixing yields an improvement of the theoretical predictions. This is particularly conspicuous for K-forbidden M1 transitions.

7. Conclusions

Considerable band mixing effects occur in deformed odd-mass nuclei. Experimentally these phenomena can thoroughly be studied by means of the radiative neutron capture process. A better understanding can be obtained within the framework of the unified model, if the interaction between all possible modes of nuclear motion is taken into account. The inclusion of pair correlations is essential for achieving agreement with experimental data. Various properties of the deexcitation mechanism are determined to a large extent by band mixing, even for low-lying states where the admixtures are small.

References

- [1] W. Michaelis, F. Weller, H. Schmidt, G. Markus, and U. Fanger, Nuclear Physics A119 (1968) 609
- [2] G. Markus, W. Michaelis, H. Schmidt, and C. Weitkamp, Z. Phys. 206 (1967) 84
- [3] W. Michaelis and H. K pfer, Nuclear Instr. and Meth. 56 (1967) 181
- [4] W. Michaelis and F. Horsch, contribution to this conference
- [5] U. Fanger, KFK 887 (1969)
- [6] G. Kr ger and G. Zipf, KFK 371 (1965)
- [7] U. Fanger, R. Gaeta, W. Michaelis, H. Ottmar, and H. Schmidt, contribution to this conference
- [8] H.R. Koch, Zeitschrift f r Physik 187 (1965) 450

- [9] W.V. Prestwich and R.E. Coté,
Phys. Rev. 162 (1967) 1112
- [10] R.A. Harlan and R.K. Sheline, Phys. Rev. 168 (1968) 1373
- [11] M. Rozkos, F. Sterba, J. Sterbova, B. Elbek, and P.O. Tjøm;
Int. Symp. on Nuclear Structure, Dubna, USSR, July 1968
- [12] L. Funke, W. Andrejtscheff, H. Graber, U. Hagemann,
K.-H. Kaun, P. Kemnitz, W. Meiling, H. Sodan, F. Stary,
and G. Winter, Nuclear Physics A 118 (1968) 97
- [13] W. Michaelis, F. Weller, H. Ottmar, U. Fanger, R. Gaeta,
G. Markus, and H. Schmidt, Nuclear Physics, to be published
- [14] A. Faessler, Nuclear Physics 59 (1964) 177
- [15] A. Faessler, Nuclear Physics 85 (1966) 679
- [16] S.G. Nilsson, Mat. Fys. Medd. Dan. Vid. Selsk. 29, No. 16 (1955)
- [17] H. Nabelek, SGAE PH-78/1968
- [18] K.E.G. Löbner and S.G. Malmkog, Nuclear Physics 80 (1966) 505

SCATTERING OF GAMMA RAYS FROM (n, γ) REACTIONS

Chairman: R.E. CHRIEN

THE USE OF A NEW HIGH-RESOLUTION GAMMA MONOCHROMATOR

(Abstract only)

R. MOREH, A. WOLF
Nuclear Research Centre-Negev,
Beer-Sheva, Israel

Abstract

THE USE OF A NEW HIGH-RESOLUTION GAMMA MONOCHROMATOR. A lead target which resonantly scatters the 7.28-MeV line of neutron capture gamma rays of iron was used as a source of variable-energy gamma radiation with an energy resolution of $4.8 \sin \theta$ eV/deg, where θ is the scattering angle of the incident photon. This amounts to a resolution of less than one part per million. These variable-energy scattered photons were used to search for highly excited bound nuclear levels in several elements. In this method the element to be studied is placed in front of a detector which measures the scattered radiation intensity as a function of θ . Any dip in such an absorption curve corresponds to an energy level being excited in the absorber nuclei. The validity of this method was first established by McIntyre and Randall who measured the forward angle resonance absorption in lead, which is itself a resonant scatterer.

In the present work the photon source consisted of about 10 kg of iron discs placed near the reactor core along a tangential beam tube. The intensity of the resulting beam is about 10^8 monoenergetic photons/cm² sec on the target position. A system of Soller slits was placed between the absorber and the 5×5 -in. NaI detector to reduce the effective angular divergence of the scattered radiation to about 1.6 deg. The number of counts of the detector as a function of angle was recorded automatically on a multichannel analyser operating in a multiscalar mode. The detector count rate was of the order of 50 counts/sec. Using this experimental arrangement, the angular interval between 90° and 150° corresponding to an energy width of about 220 eV at 7.28 MeV excitation was scanned in about 15 elements. Only cadmium seemed to yield one absorption dip at $\theta \approx 128^\circ$. The absorber thickness used was 35 g/cm² and the dip was about 3.5% at its minimum point. Assuming: (1) that the resonance isotope in Cd is of 25% abundance with a zero ground-state spin, (2) that the resonance excitation is by dipole absorption, then the ground-state radiation width Γ_0 may be found to be $\Gamma_0 = 0.06$ eV.

The usefulness of this method as a tool for studying the widths of dipole resonance levels and their spacings was found to be severely limited by the relatively low count rate. It was thus very difficult to detect weak resonances which are believed to exist at this excitation energy.

GAMMA-RAY INTENSITY ANOMALY IN THE (γ, γ') REACTION

R. MOREH, A. WOLF

Nuclear Research Centre-Negev.
Beer-Sheva, Israel

Abstract

GAMMA-RAY INTENSITY ANOMALY IN THE (γ, γ') REACTION. Anomalous intensity radiation was found near $E_\gamma = 5$ MeV in the resonantly scattered gamma-ray spectra in the mass region $180 < A < 208$. The origin of this intensity anomaly seems to be the same as that suggested for the well-known analogue of this effect in (n, γ) and ($d, p\gamma$) spectra.

Anomalous intensity radiation is known to occur in the gamma spectra of (n, γ) and ($d, p\gamma$) reactions [1, 2] on nuclei in the mass region $180 < A < 208$ and $110 < A < 140$. This anomaly was also observed in the gamma spectra of fast neutron capture [3] in Au. In the present work, some evidence is presented for the existence of a similar gamma-intensity anomaly in the (γ, γ') reaction on ^{205}Tl , ^{203}Tl , ^{186}W and ^{184}W . The gamma beam was obtained from neutron capture radiation on Fe and Ti.

The experimental assembly (Fig. 1) consisted of an (n, γ) source containing several kilograms of iron or titanium discs, placed along a tangential beam tube of the IRR-2 research reactor at a thermal neutron flux of $2 \times 10^{13} \text{ n cm}^{-2} \text{ sec}^{-1}$. The resulting gamma-ray beam was collimated, neutron filtered and allowed to hit 8-cm metallic targets 10 g/cm^2 thick. The detecting system consisted of a 20-cm^3 Ge(Li) detector in conjunction with a 1024-channel TMC analyser.

It may be noted that the choice of the target in the present technique suffers from a severe limitation: it is conditioned by the fact that a random overlap should exist between the incident capture gamma ray and a level in the particular isotope to be studied. It was therefore impossible to study the (γ, γ') reaction on each element in the region of heavy nuclei. Furthermore, because of cross-section and beam intensity limitations, large quantities of the targets ($\geq 100 \text{ g}$) were required for each measurement. It was thus impossible to make any detailed study of the scattered spectrum using small quantities of separated isotopes.

The present study was made feasible by the fact that chance resonance scattering events [4] were found to occur in the interesting mass region when gamma sources from Fe(n, γ) and Ti(n, γ) reactions were used. It was found that the iron capture gamma rays photoexcite a 7.646-MeV level in ^{205}Tl , the titanium capture gamma rays photoexcite a 6.418-MeV level in ^{203}Tl , a 6.418-MeV level in ^{186}W and two levels at 6.760 and 6.556 MeV in ^{184}W . Figure 2 shows the resonantly scattered spectra from ^{205}Tl , ^{203}Tl , ^{186}W , ^{184}W and ^{209}Bi . Besides the elastically scattered peaks, the anomalous intensity radiation is clearly evident near 5 MeV irrespective of the initial excitation energies involved. It may also be seen that the intensity of the bump is smaller in the tungsten isotopes than that of the thallium

isotopes. One should also note that three resonance levels contribute independently to the 5-MeV region in the tungsten target which explains the relatively stronger bump for this case. These spectra should be compared with that scattered from ^{150}Sm (not shown) by an incident $\text{Ni}(n, \gamma)$ gamma source [5], where very weak gamma transitions were observed in the 5-MeV range. As another example of a bumpless spectrum, the scattered radiation from ^{209}Bi is also shown in Fig. 2 where one resonance at 7.168 MeV was excited.

In the case of ^{205}Tl a detailed study [6] of the scattered radiation was made; the bump is believed to correspond to primary transitions from the resonance state. The character of the scattered radiation is thought to be mainly E1 as inferred from a measurement of the radiative width of the resonance level.

In the case of ^{203}Tl , ^{186}W and ^{184}W almost all transitions were found to decay to known low-lying levels in these isotopes. This certainly indicates that the transitions forming the bump in these isotopes are primary transitions.

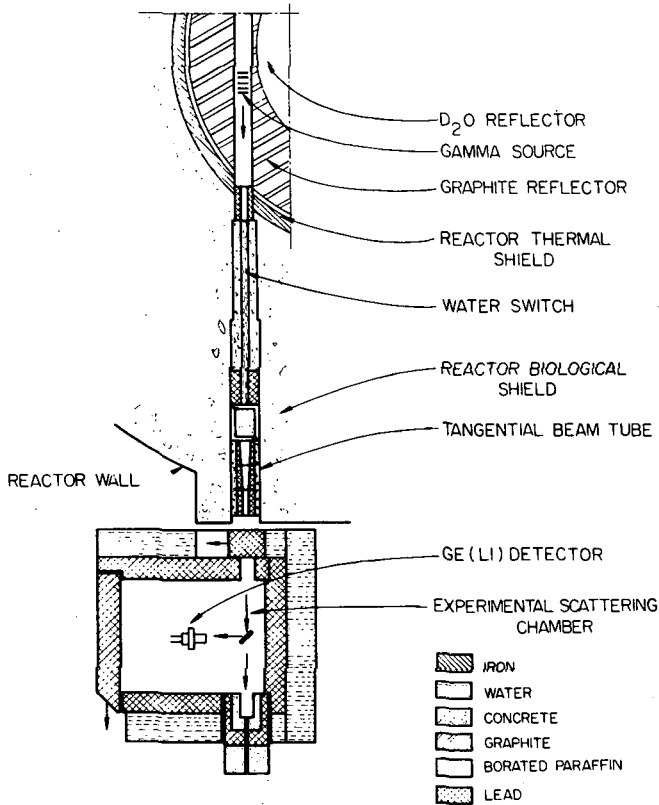


FIG. 1. Horizontal section of the experimental arrangement.

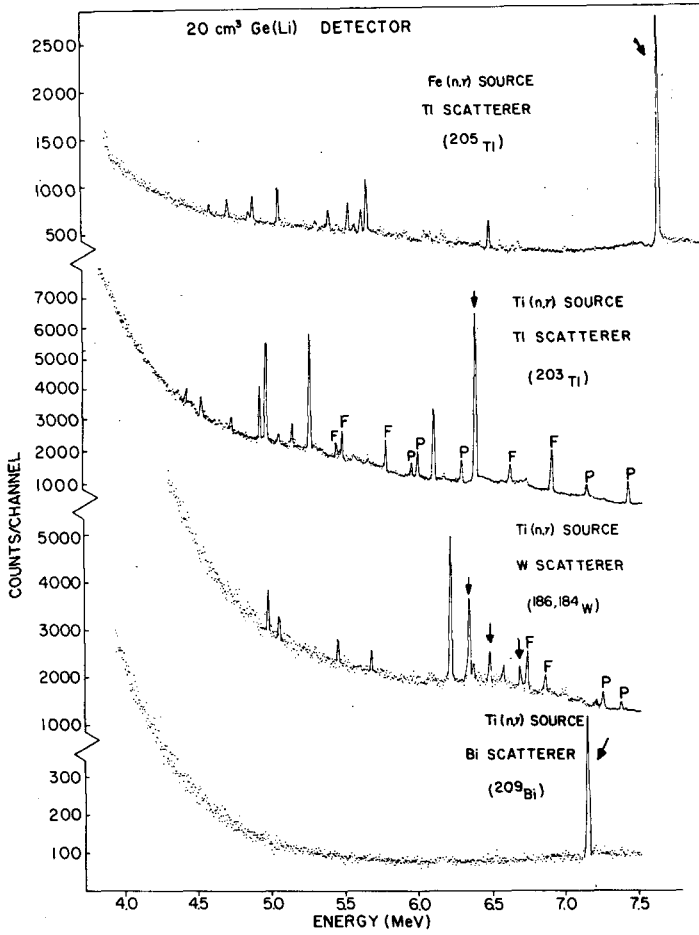


FIG. 2. Resonantly scattered gamma spectra from Tl, W and Bi targets at an angle of 135° . The energy scale refers to the energy of the double-escape peaks. Lines denoted P, F correspond to photopeaks and first-escape peaks. Other lines correspond to double-escape peaks where the arrows indicate independent resonance lines.

The anomalous bumps in (n, γ) and $(d, p\gamma)$ are believed [2] to be due to E_1 energy differences of the single-particle energies across the shell model orbits. It was suggested [2] that these bumps are obtained by the decay of doorway states of the final nucleus. The corresponding configurations are formed in the (n, γ) and $(d, p\gamma)$ reactions through a semi-direct process. It is very likely that the bump in the present case is also due to E_1 energy differences across the shell model orbits.

R E F E R E N C E S

- [1] KINSEY, B.B., BARTHOLOMEW, G.A., Phys. Rev. 93 (1954) 1260.
- [2] BARTHOLOMEW, G.A., EARLE, E.D., FERGUSON, A.J., BERGQVIST, I., Physics Lett. 24B (1967) 47.
- [3] LUNDBERG, B., STARFELT, N., Nucl. Phys. 67 (1965) 321.
- [4] BEN-DAVID, G., ARAD, B., BALDERMAN, J., SCHLESINGER, Y., Phys. Rev. 146 (1966) 852.
- [5] HASS, M., private communication.
- [6] MOREH, R., WOLF, A., to be published in Phys. Rev.

STUDY OF THE ENERGY LEVELS OF ^{139}La USING NUCLEAR PHOTOEXCITATION

R. MOREH, A. NOF
Nuclear Research Centre-Negev,
Beer-Sheva, Israel

Abstract

STUDY OF THE ENERGY LEVELS OF ^{139}La USING NUCLEAR PHOTOEXCITATION. Inelastic resonance scattering of neutron capture gamma radiation from iron was used for studying high and low-energy levels in ^{139}La . The spin and parity of the 6018-keV level was found to be $\frac{1}{2}^+$, corresponding to elastic M1 radiation. Possible spin values for four excited low-lying levels were obtained. The level parameters of the 6018-keV level in ^{139}La were measured and found to be $\Gamma = 0.08 \pm 0.02$ eV, $\Gamma_0/\Gamma = 0.52$.

The technique of using neutron capture gamma radiation for studying low-lying levels by inelastic scattering is relatively new. The energy levels of only few isotopes were investigated using the (γ, γ') reaction [1, 2]. In the present work the ^{139}La energy levels were studied; the gamma beam was obtained from neutron capture radiation on Fe. It should be realized that the choice of the target by the present technique is conditioned by the fact that a random overlap should exist between at least one of the incident capture gamma lines and at least one level in ^{139}La . It turned out that more than one iron capture gamma line happened to overlap levels in ^{139}La , of which only the 6018-keV level was strongly excited. It was thus possible to establish the spin of the 6018-keV resonance state and some low-lying levels populated by its de-excitation. The total width of the 6018-keV level was determined using self-absorption and temperature radiation measurements.

The experimental assembly consisted of a (n, γ) source containing several kg of iron discs placed along a tangential beam tube of the IRR-2 research reactor at a thermal neutron flux of 2×10^{13} n cm $^{-2}$ sec $^{-1}$. The resulting gamma beam was collimated, neutron filtered and allowed to hit a 10-cm diameter La target, 11 g/cm 2 thick. Angular distribution measurements of the scattered spectrum was performed by mounting a 30-cm 3 Ge(Li) detector on a rotating arm at a distance of 50 cm from the target.

Figure 1 shows the high-energy part of the spectrum where 3 independent resonance lines, namely 6018, 7279 and 7632 keV, which appear in the Fe(n, γ) spectrum [3] were excited. Another line at 7158 keV does not seem to correspond to an inelastic transition to any known level [4] in ^{139}La and is believed to be an independent resonance. However, this line was not reported in the Fe(n, γ) spectrum. Figure 2 shows another part of the scattered spectrum from which a decay scheme (Fig. 3) was constructed by assuming that high-energy gamma rays are emitted in primary transitions. The angular distribution at 7 angles between 90° and 155° of the 6018-keV resonance line and 5 strong inelastic transitions were measured.

The polarization of elastically scattered radiation was also measured using a Compton polarimeter [5] and found to be M1. Therefore,

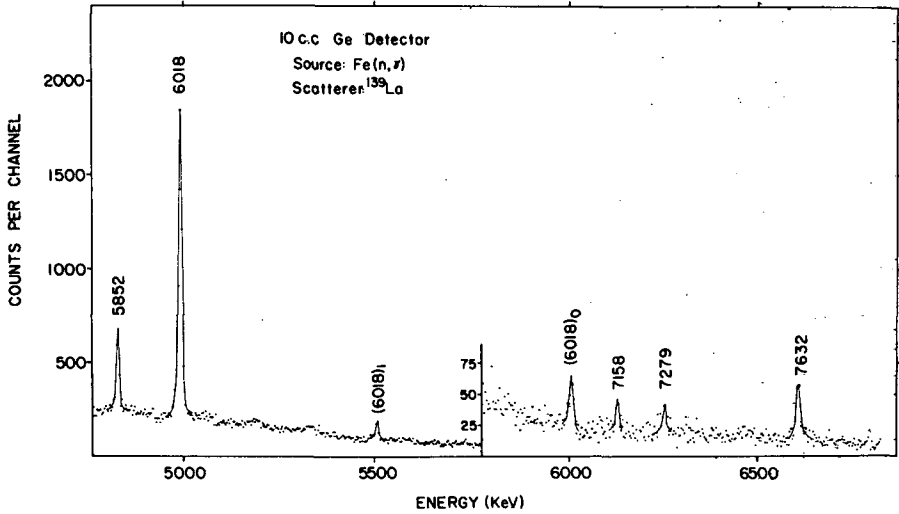


FIG.1. High-energy part of the resonantly scattered gamma spectrum from a La target. Energies with subscripts 0 and 1 refer to the photopeak and first-escape peak respectively; other energies refer to double-escape peaks.

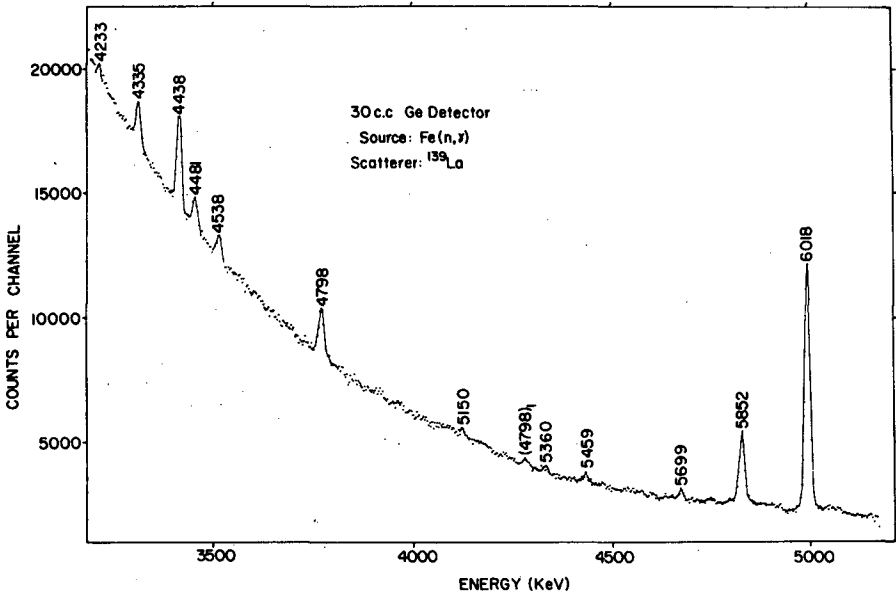


FIG.2. Lower energy part of the resonantly scattered gamma spectrum from a La target. Energies refer to double-escape peaks.

E2 admixtures are expected to contribute to the transitions; the amount of these admixtures could be detected from the angular distributions only for cases where the spins of the final states were known. Thus it was found that the E2 admixture is less than 4% in the elastic transition. Using this value and the measured angular distribution, it was possible to obtain the

E2 admixture of the inelastic transition leading to the first excited state. Again this was found to be less than 4%. Regarding the remaining inelastic transitions, it was not possible to make any conclusions about the E2 admixtures. However, assuming reasonable amounts of E2 mixing and using the results of Schlesinger [6] regarding ^{139}La levels, it was possible to obtain probable spin values of these levels (Fig. 3).

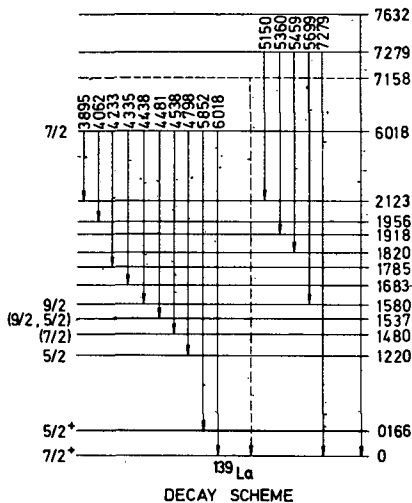


FIG. 3. Decay scheme of the resonant levels in ^{139}La showing level energies constructed by fitting line energy differences to known ^{139}La energy levels [4]. Spin values of the excited states were assigned in the present experiment where values in parentheses indicate an uncertain determination.

The level parameters of the 6018-keV level were determined by carrying out temperature variation and self-absorption measurements [2]. The results indicate that $\Gamma = 0.08 \pm 0.03$ eV and $I_0/\Gamma = 0.52 \pm 0.05$.

The present results regarding ^{139}La seem to be in much better agreement with shell model predictions [7] than those obtained from calculations using the unified model [8].

REFERENCES

- [1] SHIKAZONO, N., KAWARASAKI, Y., Nucl.Phys. **A118** (1968) 114.
- [2] MOREH, R., NOF, A., Phys.Rev. **178** (1969).
- [3] RASMUSSEN, N.C., HUKAI, Y., INOUE, T., ORPHAN, V.J., private communication.
- [4] HILL, J.C., WIEDENBECK, M.L., Nucl.Phys. **A119** (1968) 53; MALAN, J.G., McMURRAY, W.R., Van der MERWE, P., Van HEERDEN, I.J., Nucl.Phys. **A124** (1969) 111.
- [5] MOREH, R., FRIEDMAN, M., Physics Lett., **26B** (1968) 579.
- [6] SCHLESINGER, Y., private communication.
- [7] WILDENTHAL, H., private communication.
- [8] FREED, N., MILES, W., to be published in Nuovo Cim.

RECENT RESULTS ON (γ, γ) AND (γ, γ') REACTIONS FROM NEUTRON CAPTURE GAMMA RAYS

R. CESAREO, M. GIANNINI, P. OLIVA,
D. PROSPERI, M. C. RAMORINO
Laboratorio di Fisica Nucleare Applicata,
Centro di Studi Nucleari della Casaccia,
Comitato Nazionale per l'Energia Nucleare,
Rome, Italy

Abstract

RECENT RESULTS ON (γ, γ) AND (γ, γ') REACTIONS FROM NEUTRON CAPTURE GAMMA RAYS. The analysis of the elastic and inelastic photons following the resonance absorption of neutron capture gamma-rays has been successfully applied to the study of highly excited levels and low-energy level schemes. Results on the (γ, γ) and (γ, γ') reactions on ^{112}Cd , ^{205}Tl and ^{65}Cu are reported.

In the last few years the nuclear resonance scattering of neutron capture gamma rays has been successfully applied in studies of both the highly excited levels near the neutron binding energy and their de-excitation photons [1]. The gamma-ray source consists of monochromatic lines, the width being determined by the thermal Doppler broadening (a few eV at normal temperature). Resonance scattering occurs when the energy of one of the incident gamma lines (after correction for target recoil) happens to overlap, however partially, an individual nuclear level in the target nucleus. In this way it is possible to investigate individual levels, while nuclear scattering performed with continuous gamma-ray spectra allows one to determine only the average strength functions.

From cross-section measurements the partial radiation width to the ground state ($\Gamma_{\gamma 0}$) and the total radiation width (Γ_{γ}) can be determined. Both scattering and absorption effective cross-sections depend on $\Gamma_{\gamma 0}$, $\Gamma_{\gamma 0}/\Gamma_{\gamma}$ and δ (separation energy between the incident photon and the resonance level) for which the determination of the resonance scattering cross-section, as a function of both temperature and thickness of the scatterer, and the determination of the self-absorption ratio [2] are required. By measuring the radiative width of resonance levels it is possible to obtain useful information about absolute values of transition probabilities, such as those given by resonance neutron capture gamma rays.

Furthermore, by directional correlation measurements between incident and scattered gamma rays the spin of the resonance level can be determined. Polarization studies of elastically scattered gamma rays have also been performed [3] and it has been deduced that the radiation multipolarity is either E1 or M1.

Evidence of inelastic gamma rays leading to the low-lying nuclear levels was pointed out by our group in 1965 [4]. Estes and Min [5],

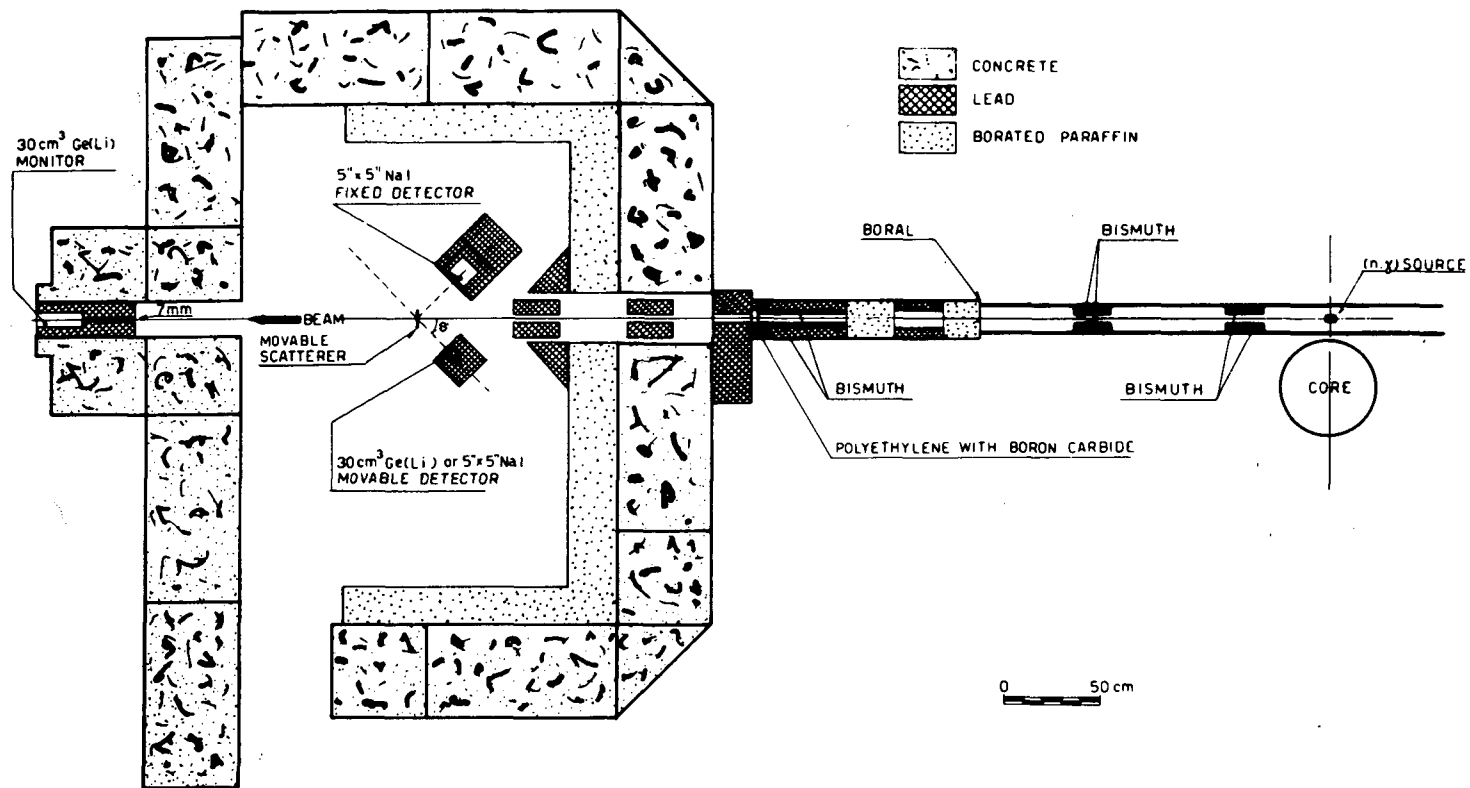


FIG.1. Horizontal section of the experimental arrangement.

following such a suggestion, observed low-energy gamma rays in ^{112}Cd and ^{62}Ni in coincidence with the inelastic transitions.

More recently, with the increasing use of Ge(Li) detectors, the resonance scattering technique has been applied to spectroscopy studies by relating the inelastically scattered gamma rays to the level structure of the resonant nucleus [6]. Such measurements give information similar to that obtainable with (n, γ) reactions, but with some advantages. The low-lying level spins can, in fact, be determined by measuring the directional correlations of the primary inelastic gamma rays, provided that the spin of the resonant level is known. It is also worth noting that (γ, γ') reactions are the most suitable for the study of those stable isotopes which may not be reached by (n, γ) or charged-particle reactions.

However, some disadvantages are present in this method. For instance, the choice of the target is conditioned by the fact that a random overlap should exist between the incident capture gamma ray and a level in the particular isotope to be studied. Even though such a probability might seem small, about 50 cases of nuclear fluorescence have been observed [7]. It is interesting to note that almost all these cases have been observed near the closed-shell nuclei. A further great problem is caused by the noticeable pile-up of small amplitude pulses which make it difficult to detect gamma transitions below 3 MeV. In several cases these latter difficulties could be overcome by coincidence techniques [5].

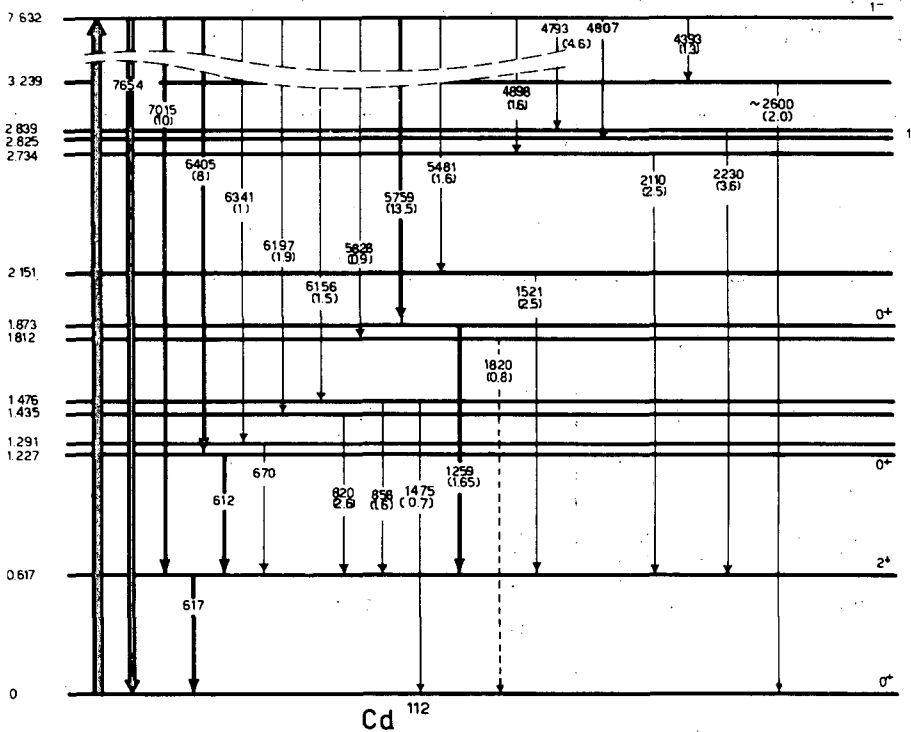
The results of the (γ, γ') reaction in ^{112}Cd (studied independently by our group [8] and by Moreh and Nof [9]) could be regarded as both an example and a test of the method, considering that the level scheme of ^{112}Cd has also been studied by different methods. Our source was the gamma rays from the 7632-keV iron capture. Our experimental assembly, set up at the tangential beam hole of the 1-MW RC-1 reactor of the CSN della Casaccia, has already been described [8] and is shown in Fig. 1. The scattered spectra were detected by means of a 30-cm³ Ge(Li) (or a 12.7×12.7 cm NaI) detector. For the angular distribution measurements the same detector was mounted on a platform pivoting on an axis passing through the centre of the scatterer. The beam monitor consisted of a 30-cm³ Ge(Li) detector arranged in such a way as to select a convenient line of the incident photons. The gamma spectra were recorded with a 1024 or a 4096-channel analyser.

Table I summarizes our results on ^{112}Cd . Those obtained with completely different experimental methods are also reported for comparison purposes [10-13]. It is clear that this method selects levels with spins 0, 1 or 2, as can be seen in Fig. 2 where the deduced decay scheme is shown. The secondary transitions shown in this figure were detected by means of coincidence measurements, while the spin values were deduced from the analysis of the angular distribution of primary inelastic gamma rays. The parity of the resonant level was determined by Moreh and Friedman [3].

With the same experimental arrangement the resonance scattering of the 7646-keV gamma rays (produced by the Fe(n, γ) reaction) in a natural Tl target was studied [14], the resonant isotope being identified as ^{205}Tl . At the same time a similar isotope was being studied by Moreh and Wolf [15], yielding results in very good agreement. More than 20 gamma-ray lines were detected in the energy range from 4 to

TABLE I. SUMMARY OF THE EXPERIMENTAL RESULTS ON THE ^{112}Cd LEVEL SCHEME

(x, γ') reaction [9] [10]		(d, p) [12]	(p, p') [14]	(d, d') [13]	Disintegration data [11]	
0	0	0	0	0	0	0 ⁺
617 \pm 2	2 616	619	619	620	616.8	2 ⁺
1227 \pm 2	0 1224	1228	1190	1220	1222.9	0 ⁺
1291 \pm 6			1270	1300	1311.3	2 ⁺
			1380	1420	1414.2	4 ⁺
1435 \pm 4	1439	1436			1431.7	0 ⁺
1476 \pm 4	1472	1474		1470	1468.1	2 ⁺
1812 \pm 8						
1873 \pm 3	0 1877	1876			1869.5	0 ⁺
			1964		1973.9	3-
		2009		2010-	2003.3	(2, 3, 4)
		2087				
		2123		2100+		
2151 \pm 8	2161	2159			2154.5	(2, 3) ⁺
	2237	2235			2229.2	2 ⁺
		2302	2335			
		2374				
		2424	2464	2420-	2414.6	(1, 2) ⁻
		2507		2520+	2505.9	2 ⁺
		2573	2570			
		2637				
		2657			2667.3	(1, 2)
		2678			2673.2	2 ⁺
					2686.1	(2) ⁺
2734 \pm 8	2720	2725	2723		2722.8	2 ⁺
	2768	2770		2760		
2825 \pm 8	2828	2822		2830+	2828.1	1 ⁺
2839 \pm 8	2844	2840	2854			
		2875				
		2901		2910-		
		2936				
		2965				
		2988				
		3071	3069		3066.9	(2, 3, 4)
	3115	3113			3130.2	2 ⁺
		3184			3168.8	2 ⁺
3239 \pm 8	3239	3240				
		3304				
	3348	3344				
			3411		3367.8	(2) ⁺
					3469.1	(1, 2)
					3477.7	(1, 2, 3)

FIG. 2. Level scheme of ^{112}Cd .

8 MeV. They have all been explained in terms of de-excitation of the 7646-keV resonant level.

The justification of this assumption is extensively discussed in Ref. [14]. Energies and intensities of all gamma lines are reported in Table II. The energies of the levels are compared with those obtained by different experimental methods [16-18]. The transitions de-exciting the first and second levels were detected by means of coincidence measurements.

Analysis of the angular distribution of the most intense lines gives $j = \frac{1}{2}$ for the resonant level spin. All the inelastic lines corresponding to the primary transitions are consequently isotropic and it is thus impossible to measure the spin of the intermediate levels.

The decay scheme is shown in Fig. 3 where the secondary gamma rays were deduced by coincidence measurements.

Information about the multipolarity of the primary gamma transitions can be obtained from the study of the reduced radiative widths for E1 and M1 transitions:

$$K_{\sigma 1} = \Gamma_{\gamma 1} E_{\gamma}^{-\alpha} D^{-1} \quad (1)$$

TABLE II. ENERGIES AND INTENSITIES OF ELASTIC AND INELASTIC GAMMA RAYS SCATTERED FROM A Tl TARGET

E_γ (keV)	I_γ (rel) (%)	Energy levels			
		Present work (keV)	[16] ^a (MeV)	[17] ^b (MeV)	[18] (keV)
7646	61.7 9.2	0	0	0	0
-	-	211 5	-	-	205 2
-	-	623 6	-	-	615 5
6505 3	3.60 0.55	1141 3	1.14	-	-
-	-	-	1.21	-	-
6309 3	0.80 0.15	1337 3	1.34	-	-
6213 3	1.75 0.30	1433 3	1.43	-	-
-	-	-	1.48	-	-
6080 3	1.25 0.20	1557 3	-	-	-
6071 5 ^c	0.75 0.15	1575 5	1.58	-	-
5772 4 ^c	0.50 0.15	1874 4	1.86	-	-
5681 2	7.70 1.20	1965 2	1.96	-	-
5645 3	3.35 0.50	2001 3	-	-	-
-	-	-	2.04	-	-
5556 3	2.90 0.45	2090 3	-	-	-
-	-	-	2.12	-	-
5483 3	1.00 0.20	2163 3	-	-	-
5436 5 ^c	0.45 0.15	2210 5	-	-	-
5424 3	2.00 0.30	2222 3	-	-	-
5346 3	0.65 0.15	2300 3	-	-	-
5331 3	0.75 0.15	2315 3	-	-	-
-	-	-	2.43	-	-
-	-	-	2.49	-	-
5088 3	3.40 0.50	2558 3	-	-	-
-	-	-	-	2.61	-
4977 4	0.30 0.10	2669 4	-	-	-
-	-	-	-	2.69	-
4941 5	0.25 0.10	2705 5	-	-	-
4923 3	2.05 0.30	2723 3	-	-	-
4895 3	1.05 0.20	2751 3	2.74	-	-
4750 3	1.75 0.30	2896 3	-	-	-
4625 3	0.85 0.15	3021 3	-	-	-
4470 5	0.50 0.15	3176 5	-	-	-
4357 3	0.65 0.15	3289 3	-	-	-

^a $^{206}\text{Pb}(t, \alpha)^{205}\text{Tl}$ reaction. The errors are ± 20 keV.

^b No error is given.

^c The evidence for this γ -transition is regarded as uncertain.

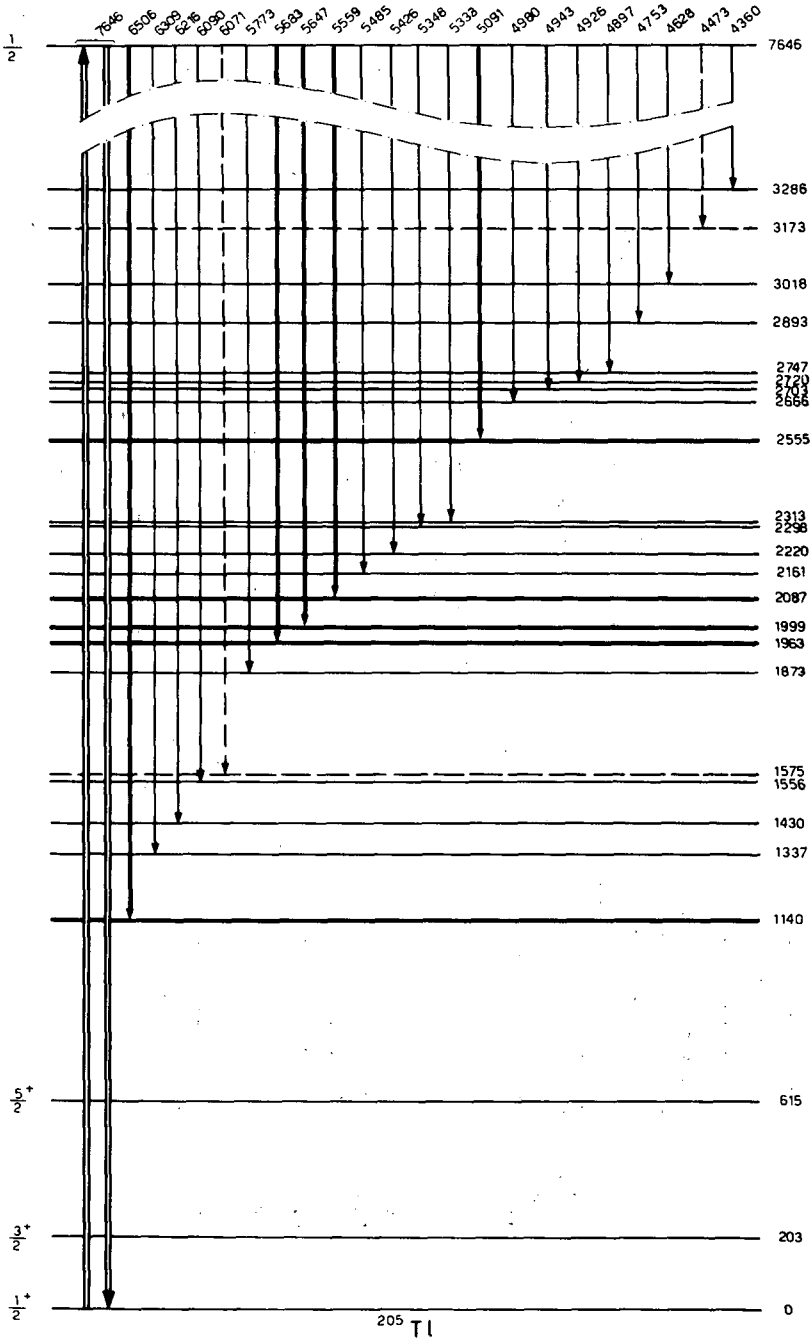
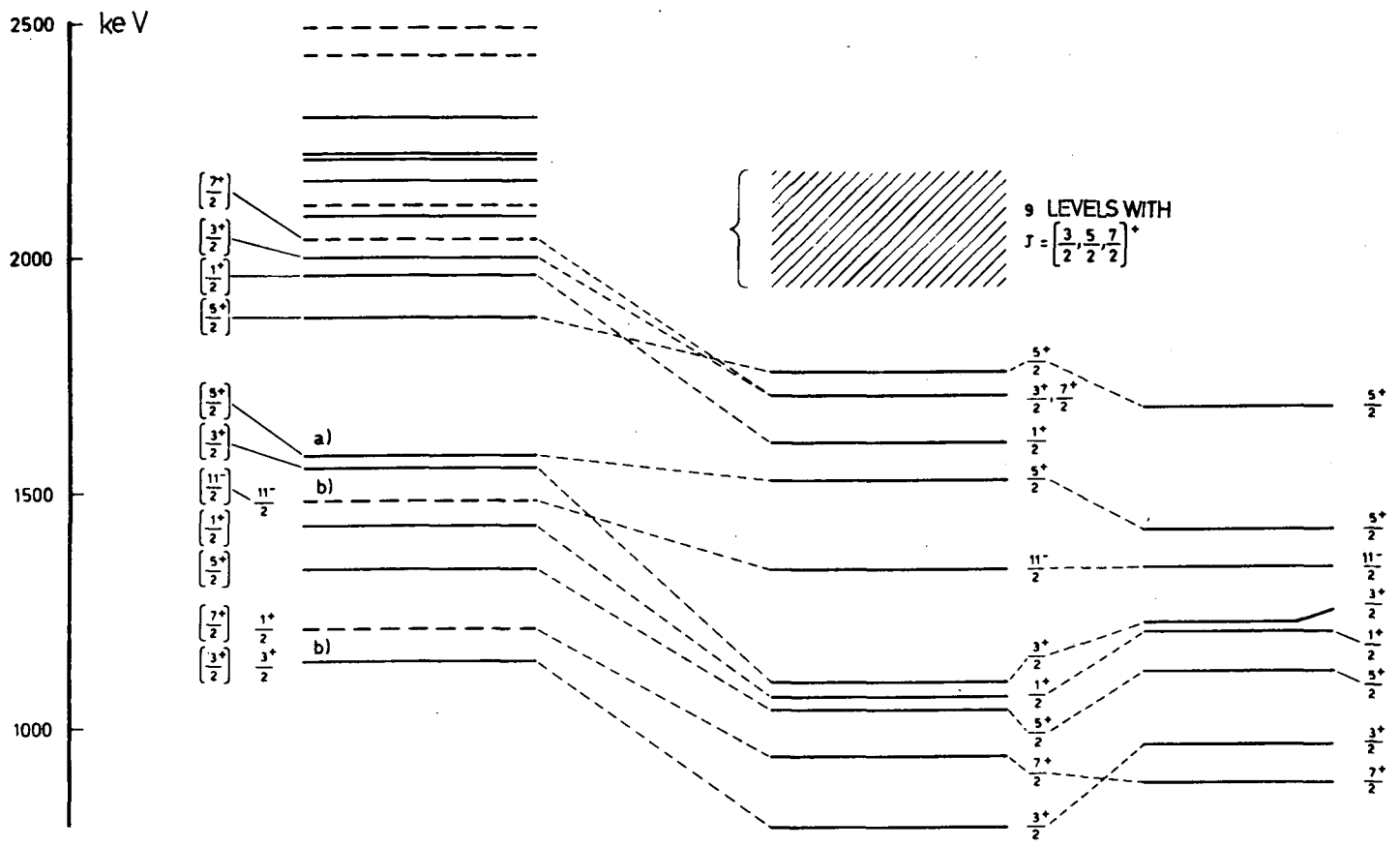


FIG.3. Level scheme of ^{205}Tl . Dashed lines represent levels or transitions whose existence is questionable.



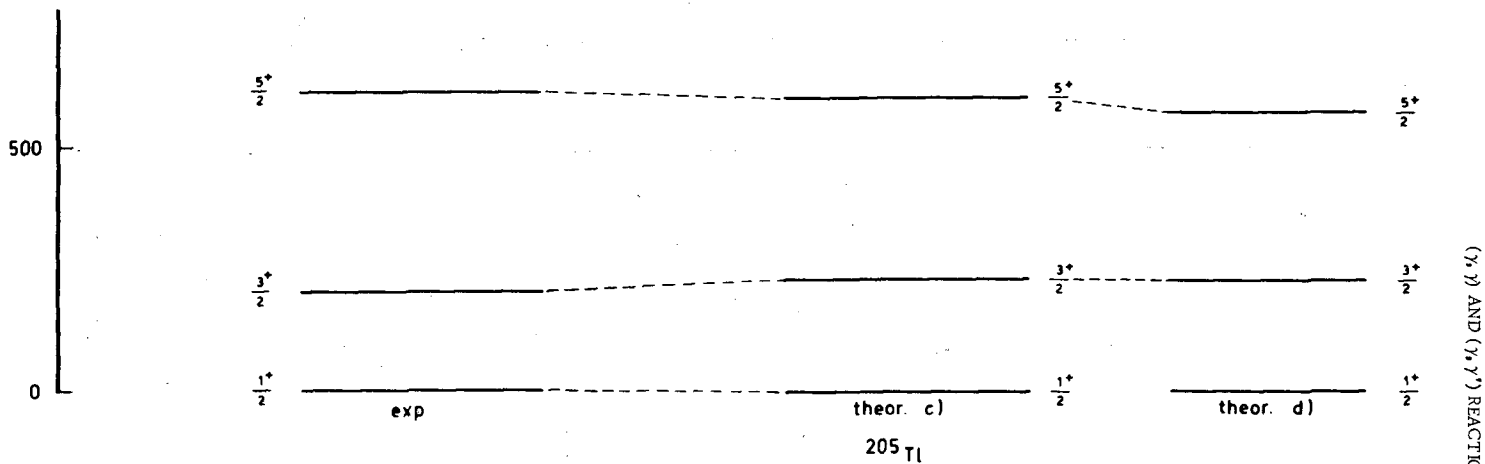


FIG. 4. Comparison of the ^{205}Tl level scheme as determined by the experimental data and by the theoretical predictions [20].

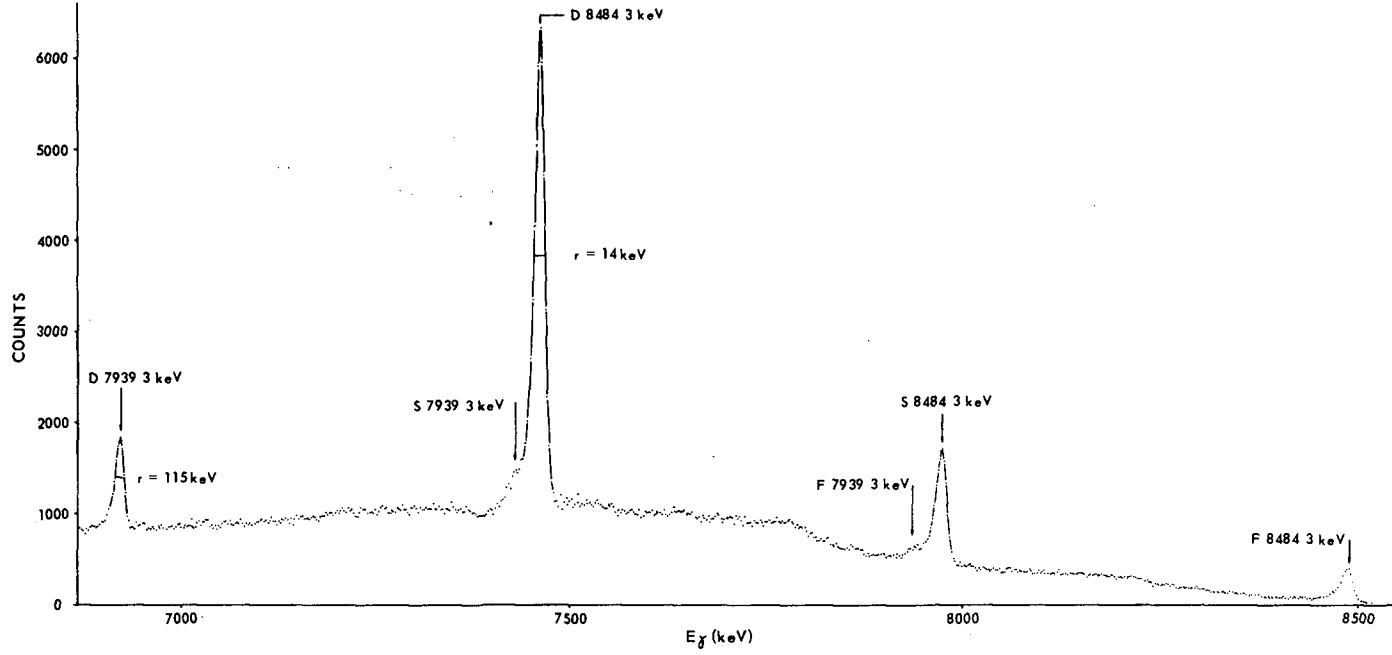


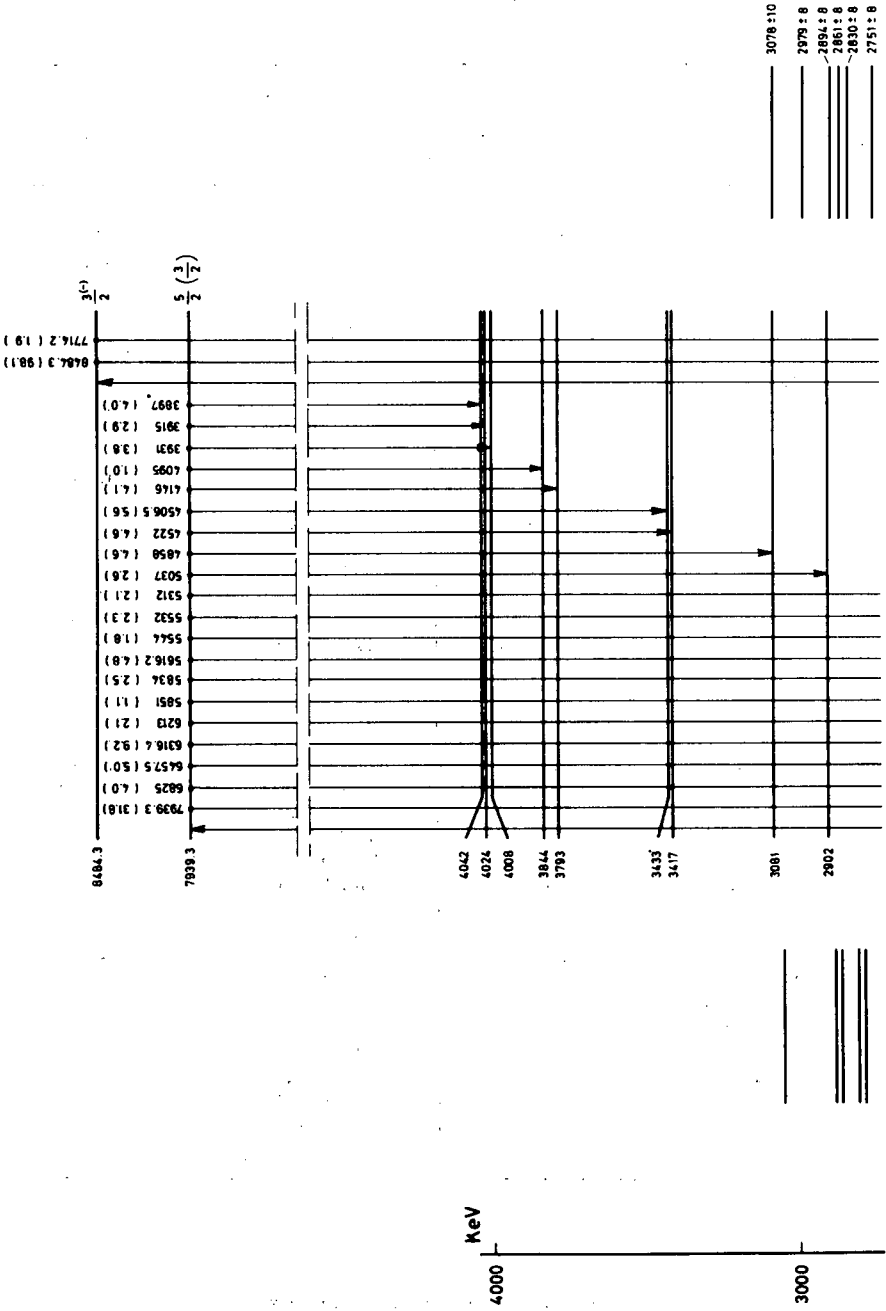
FIG. 5. Spectrum of gamma rays scattered from a Cu resonant target. The source was provided by the $Cu(n, \gamma)$ reaction.

TABLE III. ENERGIES AND INTENSITIES OF ELASTIC AND INELASTIC GAMMA RAYS SCATTERED FROM A Cu TARGET

E_γ (keV)	I_γ (rel) (%)	Energy levels (keV)	
		Present work	[22] ^a
8484.3 ± 1.0 ^a	98 ± 10	0	0
7714.0 ± 2.0	2 ± 0.2	770 ± 2	770 ± 4
7939.3 ± 1.0 ^a	31.8 ± 4.5	0	0
6827.0 ± 3.0	4.0 ± 0.8	1114.5 ± 0.5	1114 ± 4
6457.5 ± 2.0	5.0 ± 0.8	1481.8 ± 0.7	1482 ± 4
6316.4 ± 1.5	9.2 ± 1.4	1622.7 ± 1.1	1623 ± 4
6213.0 ± 2.0	2.1 ± 0.3	1724.6 ± 1.5	1725 ± 6
5851.0 ± 5.0	1.2 ± 0.2	2088.0 ± 5.0	2093 ± 8
5834.0 ± 4.0	2.5 ± 0.4	2105.0 ± 4.0	2105 ± 8
-	-	-	2213 ± 8
-	-	-	2280 ± 8
5616.2 ± 2.0	4.8 ± 0.7	2323.0 ± 2.0	2329 ± 8
5544.0 ± 3.0	1.8 ± 0.3	2395.0 ± 3.0	2404 ± 8 ^b
5532.0 ± 3.0	2.3 ± 0.4	2407.0 ± 3.0	
-	-	-	
-	-	-	2531 ± 8
-	-	-	2594 ± 8
5312.0 ± 5.0	2.1 ± 0.3	2627.0 ± 5.0	-
-	-	-	2648 ± 8 ^b
-	-	-	2751 ± 8
-	-	-	2830 ± 8
-	-	-	2861 ± 8 ^b
5037.0 ± 3.0	2.6 ± 0.4	2902.0 ± 3.0	2874 ± 8 ^b
-	-	-	2979 ± 8 ^b
4858.0 ± 2.0	4.6 ± 0.7	3081.0 ± 2.0	3078 ± 10
4522.0 ± 3.0	4.6 ± 0.7	3417.0 ± 3.0	-
4506.5 ± 2.5	5.6 ± 0.8	3433.5 ± 2.5	-
4146.0 ± 3.0	4.1 ± 0.6	3793.0 ± 3.0	-
4095.0 ± 3.0	1.0 ± 0.2	3844.0 ± 3.0	-
3931.0 ± 3.0	3.8 ± 0.8	4008.0 ± 3.0	-
3915.0 ± 3.0	2.9 ± 0.5	4024.0 ± 3.0	-
3897.0 ± 3.0	4.0 ± 0.6	4042.0 ± 3.0	-
2095.0 ± 4.0	-	2088.0	-
1724.1 ± 1.5	-	2105.0	-
1622.7 ± 1.1	-	1724.6 ± 1.5	-
1481.8 ± 0.7	-	1622.7 ± 1.1	-
1114.5 ± 0.5	-	1481.8 ± 0.7	-
-	-	1114.5 ± 0.5	-

^a The elastic gamma rays were employed for the energy calibration.

^b Perhaps a doublet.



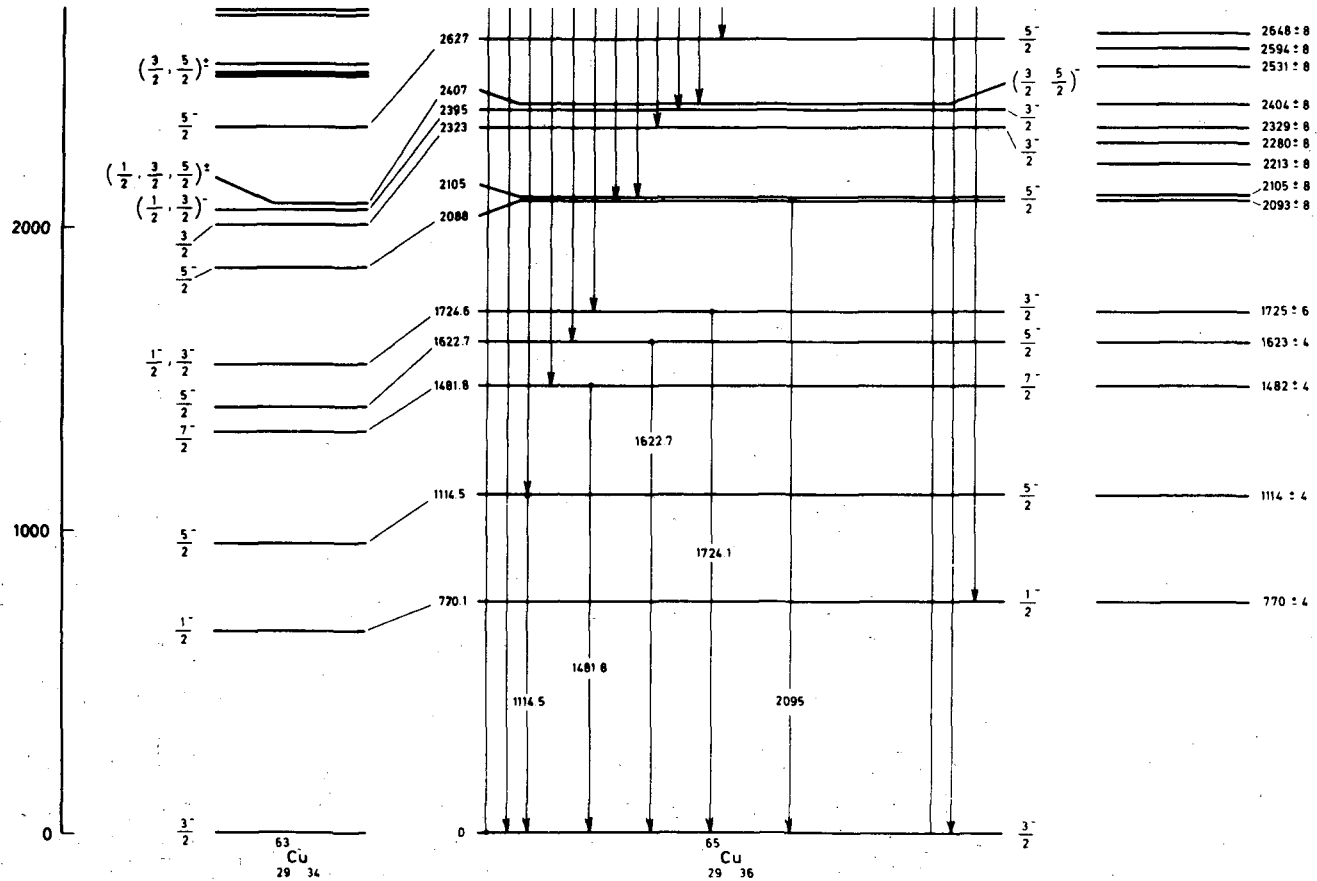


FIG. 6. Comparison of the ^{65}Cu level schemes as determined by the authors, Mazari et al. [22] and Borchert [23].

Here $\Gamma_{\gamma i}$ is the partial radiation width to the i^{th} level, E_{γ} is the energy of the transition and D is the average spacing, at the initial state energy, of the levels having the same spin and parity as the radiative state.

The best fit of Eq.(1) to our data on Tl yields a value of $\alpha \approx 5.3$.

The average reduced width for E1 transitions can be estimated by an extrapolation of the giant resonance [19], giving an E^{-5} dependence for the average radiative width.

The following approximate relationship can be deduced for the ^{205}Tl isotope

$$K_{\text{E1}} = \langle \Gamma_{\gamma i} E_{\gamma}^{-5} D^{-1} \rangle \approx 9 \times 10^{-9} \quad (2)$$

where $\Gamma_{\gamma i}$ and D are in the same units and E_{γ} is in MeV.

Using the numerical values $\alpha = 5$ and $D = 1$ keV, the average of Eq.(1) on all the gamma transitions observed in the present work turns out to be $K_{\text{E1}} = 6 \times 10^{-9}$, which is in very satisfactory agreement with Eq.(2).

It seems clear that the transitions observed are prevalently E1. The parity of the resonant level is consequently negative and the spin and parity of the most intensely populated levels are $1/2^+$ or $3/2^+$, whereas levels having spin $5/2$ are probably weakly populated. However, there is a large spread of the reduced widths around the average value. Groups of transitions, characterized by large reduced widths, are observed at about 5.5 and 4.5 MeV, corresponding to excitation energies at about 2 and 3 MeV. This phenomenon is probably connected with the bump observed at about 5 MeV in the gamma-ray spectra following neutron capture in nuclei near the closed shell, which is known to be prevalently E1.

An attempt to assign the spin to the observed energy levels can be based on a comparison with theoretical predictions [20, 21]. This comparison is shown in Fig. 4 and seems to be reasonable up to about 2 MeV. The spin value of $j = 7/2$ for the 1.21-MeV level, as measured by Hinds et al. [16] in (t, α) reactions, is in disagreement with the theoretical calculations and with our results.

Another case where the preliminary results seem to be of some interest is given by the nuclear resonance scattering in Cu of gamma rays from the $\text{Cr}(n, \gamma)$ reaction. Figure 5 shows the scattered spectrum, detected by means of a 30-cm³ Ge(Li) detector and recorded by a 4096-channel analyser. The energy resolution was about 13 keV at about 8.5 MeV. In the energy range from 1 to 8.5 MeV more than 25 gamma lines were clearly observed. Both the 8.484 and 7.939-MeV gamma rays, which were also present in the direct beam, can be explained as elastic transitions, de-exciting two different resonant levels of ^{65}Cu . Energies and intensities of all gamma rays detected are reported in Table III. The corresponding energy levels are also shown and compared with those previously known [22]. Assuming that intense high-energy gamma rays are primary transitions, the decay scheme of both resonant levels was deduced (Fig. 6).

From the analysis of the directional correlation of the 8.484-MeV elastic gamma line, a mixture of M1 and E2 ($\delta^2 = 0.1$) multipolarities was deduced and the level spin turns out to be $3/2^-$. The measurement of the angular distribution of the 7.939-MeV gamma ray gives an ambiguous

result resulting in a spin value of $5/2$ or $3/2$. However, the fact that the level at 1.48 MeV, which should have spin $7/2$, is intensely populated leads to the conclusion that the probable spin value of the 7.939-MeV resonant level is $5/2$. In the same figure the level scheme of ^{63}Cu , as obtained by Borchert [23], is also shown for comparison. The similarity between the two level schemes is very remarkable and, by extension, we can tentatively foresee the spin values up to about 2.5 MeV.

REFERENCES

- [1] A complete list of references can be found in Ref. [8].
- [2] METZGER, F.R., *Progr. nucl. Phys.* **7** (1959) 53; ARAD, B., BEN-DAVID, G., PELAH, I., SCHLESINGER, Y., *Phys. Rev.* **133** (1964) 684; GIANNINI, M., OLIVA, P., PROSPERI, D., TOUMBEV, G., *Nucl. Phys.* **A101** (1967) 145; RAMCHANDRAN, S., MCINTYRE, J.A., to be published in *Phys. Rev.*
- [3] MOREH, R., FRIEDMAN, M., *Physics Lett.* **26B** (1968) 579.
- [4] GIANNINI, M., OLIVA, P., PROSPERI, D., SCIUTI, S., *Nucl. Phys.* **65** (1965) 344.
- [5] MIN, K., *Phys. Rev.* **152** (1966) 1062; ESTES, G.P., MIN, K., *Phys. Rev.* **154** (1967) 1104.
- [6] SHIKAZONO, N., KAWARASAKI, Y., *Nucl. Phys.* **A118** (1968) 114; MICHALK, V.E., MCINTYRE, J.A., private communication; MOREH, R., NOF, A., to be published in *Phys. Rev.*
- [7] BEN-DAVID, G., ARAD, B., BALDERMAN, J., SCHLESINGER, Y., *Phys. Rev.* **146** (1966) 852.
- [8] CESAREO, R., GIANNINI, M., OLIVA, P., PROSPERI, D., RAMORINO, M.C., to be published in *Nucl. Phys.*
- [9] MOREH, R., NOF, A., *Bull. Am. phys. Soc.* **13** (1968) 1451.
- [10] LINGEMAN, E.W.A., KONIJN, J., MATHOT, L.G.R., *Nucl. Phys.* **A122** (1968) 557.
- [11] BARNES, P.D., COMFORT, J.R., BOCKELMAN, C.K., *Phys. Rev.* **155** (1967) 1319.
- [12] KIM, Y.S., COHEN, B.L., *Phys. Rev.* **142** (1966) 788.
- [13] KOIKE, M., *Nucl. Phys.* **A98** (1967) 209.
- [14] CESAREO, R., GIANNINI, M., OLIVA, P., PROSPERI, D., RAMORINO, M.C., submitted to *Nucl. Phys.*
- [15] MOREH, R., WOLF, A., private communication.
- [16] HINDS, S., MIDDLETON, R., BJERREGARD, J.H., HANSEN, O., NATHAN, O., *Nucl. Phys.* **83** (1966) 17.
- [17] WURM, J.P., GROSSE, E., *Physics Lett.* **28B** (1969) 413.
- [18] LEDERER, C., HOLLANDER, J.H., PERLMAN, I., *Table of Isotopes*, J. Wiley and Sons Inc., New York (1967) 394.
- [19] AXEL, P., *Phys. Rev.* **126** (1962) 671; OLIVA, P., PROSPERI, D., *Nuovo Cim.* **49** (1967) 161.
- [20] LO IUDICE, N., PROSPERI, D., SALUSTI, E., *Nucl. Phys.* **A127** (1969) 221.
- [21] AZZIZ, N., COVELLO, A., *Nucl. Phys.* **A123** (1969) 681.
- [22] MAZARI, M., BUECHNER, W.W., de FIGUEREDEO, R.P., *Phys. Rev.* **108** (1957) 373.
- [23] BORCHERT, I., *Z. Phys.* **223** (1969) 473.

(γ, γ') SPECTROSCOPY OF EVEN-EVEN NUCLEI USING THE (n, γ) REACTION

Y. SCHLESINGER*, H. SZICHMAN, M. HASS,
G. BEN-DAVID*

Israel Atomic Energy Commission, and
Bar-Ilan University,
Ramat-Gan, Israel

Abstract

(γ, γ') SPECTROSCOPY OF EVEN-EVEN NUCLEI USING THE (n, γ) REACTION. Monoenergetic gamma rays obtained in the (n, γ) reaction are used for photoexcitation of highly excited single nuclear levels in even-even nuclei. The de-excitation of these levels permits a study of nuclear levels in stable nuclei. The results obtained for the nuclei ^{66}Zn , ^{80}Se , ^{86}Sr , ^{120}Sn , ^{126}Te , ^{128}Te and ^{130}Te are presented and discussed.

Photoexcitation of nuclei by thermal neutron capture gamma rays has been applied by several groups [1-3] to the study of the nuclear levels of stable nuclei. This method gives results analogous to those obtained by neutron resonance reactions above the neutron binding energy but extends the field of research below the neutron threshold. Information regarding the low-lying levels in stable nuclei is also obtained, supplementing the data obtained by the (n, γ) reaction for those stable nuclei which cannot be reached by thermal neutron capture.

This paper reports recent photoexcitation studies on even-even nuclei. As the photoexcitation process is assumed to be of a pure dipole nature, it permits selective excitation of spin 1 levels only, making the analysis of the results much simpler than for nuclei having ground-state spin different from zero. The dipole character of the excitation was unambiguously established in those cases where the intensity of the resonantly scattered radiation permitted measurement of the angular distribution.

The nuclei studied were ^{66}Zn , ^{80}Se , ^{86}Sr , ^{120}Sn , ^{126}Te , ^{128}Te and ^{130}Te . The reactions were carried out using as (n, γ) sources targets of nickel, copper, aluminium and chlorine. Owing to the large mass of the scattering targets required for this type of experiment, natural abundance samples were used. The identification of the particular isotope excited was established through the inelastic de-excitation of the resonant state to known low-lying levels.

The results are summarized in Table I. In each case the ground-state branching ratio was calculated, and calculation of the total radiation widths Γ is in progress. In most cases the intensity of the inelastic transitions was too weak to permit angular distribution measurements for direct determination of the level spins. However, assuming that for such high-energy transitions dipole transitions are the most probable, the spins of the low-lying states may be taken as either 0, 1 or 2.

Our results are in good agreement with the published values. In addition, hitherto unknown levels were observed.

Bollinger et al. [4], using radiative capture of neutrons in unbound resonance levels, found that the distribution of partial radiative widths

follows the Porter-Thomas distribution law. As the photoexcitation mechanism is selective and biased to levels having large ground-state widths, in the present work we could check the distribution only for the inelastic transitions. Since in most nuclei only one or two resonant levels have so far been studied, no systematic study of one particular nucleus can be performed. Hence we analysed the photoexcitation of resonance levels in the groups of even-even nuclei having similar low-energy vibrational states and derived the distribution of the ratio of intensities of the transitions to the first two 2^+ levels. If the assumption of a Porter-Thomas distribution for this group of nuclei is valid, this ratio should follow a truncated β -distribution, known as a Fisher-z distribution, with the parameter ν giving the number of degrees of freedom. For the Porter-Thomas distribution $\nu = 1$. An analysis of ten nuclei, including published

TABLE I. GAMMA TRANSITIONS OBSERVED

Nucleus	Resonant level energy (keV) and spin	Gamma transitions energy (keV)	Excited states	Spin and parity	$\frac{\Gamma_0}{\Gamma}$
^{66}Zn	7696 (1)	7696	0	0^+	0.360 ± 0.048
		6657	1039	2^+	
		5829	1867	2^+	
		5309	2387	(0, 1, 2)	
		4910	2786	(0, 1, 2)	
		4742	2954	(0, 1, 2)	
		4579	3117	(0, 1, 2)	
		4467	3229	(0, 1, 2)	
		4253	3443	(0, 1, 2)	
		^{80}Se	7820 (1)	7820	
6344	1476			0^+	
5863	1957			(0, 1, 2)	
5312	2508			(0, 1, 2)	
4999	2821			(0, 1, 2)	
4801	3019			(0, 1, 2)	
4697	3123			(0, 1, 2)	
4576	3244			(0, 1, 2)	
4481	3339			(0, 1, 2)	
3610	4210			(0, 1, 2)	
3491	4329			(0, 1, 2)	
3417	4403			(0, 1, 2)	
3363	4457			(0, 1, 2)	

TABLE I. (contd.)

Nucleus	Resonant level energy (keV) and spin	Gamma transitions energy (keV)	Excited states	Spin and parity	$\frac{\Gamma_0}{\Gamma}$			
⁸⁶ Sr	7820 (1)	7820	0	0 ⁺	0.292 ± 0.033			
		6744	1076	2 ⁺				
		5969	1851	2 ⁺				
		5716	2104	(0, 1, 2)				
		5619	2201	(0, 1, 2)				
		5323	2497	(0, 1, 2)				
		5180	2640	(0, 1, 2)				
		5034	2786	(0, 1, 2)				
		4775	3045	(0, 1, 2)				
		4718	3102	(0, 1, 2)				
¹²⁰ Sn	8998 (1)	8998	0	0 ⁺	0.096 + 0.020 - 0.045			
		7823	1175	2 ⁺				
		7287	1711	(0, 1, 2)				
		6890	2108	(0, 1, 2)				
		6833	2165	(0, 1, 2)				
		6675	2323	(0, 1, 2)				
		6634	2364	(0, 1, 2)				
		6264	2734	(0, 1, 2)				
		5993	3005	(0, 1, 2)				
		5443	3555	(0, 1, 2)				
		4846	4152	(0, 1, 2)				
			7696 (1)	7696		0	0 ⁺	0.595 + 0.043 - 0.102
				6521		1175	2 ⁺	
				5985		1711	(0, 1, 2)	
5332	2364			(0, 1, 2)				
5095	2601			(0, 1, 2)				
4846	2850			(0, 1, 2)				
4059	3637			(0, 1, 2)				
¹²⁶ Te	7791 (1)			7791	0	0 ⁺	0.75 ± 0.09	
		6369	1422	(0, 2)				

TABLE I. (cont.)

Nucleus	Resonant level energy (keV) and spin	Gamma transitions energy (keV)	Excited states	Spin and parity	$\frac{\Gamma_0}{\Gamma}$
^{128}Te	7724 (1)	7724	0	0	0.51 \pm 0.07
		6207	1523	(0, 2)	
		5750	1974	(0, 1, 2)	
^{130}Te	7637 (1)	7637	0	0 ⁺	0.41 \pm 0.07
		6797	840	2 ⁺	
		6049	1588	1 ⁺	
		6012	1625	(0, 2)	
		5749	1888	(0, 1, 2)	

data by other groups, indicates that ν is indeed close to 1, in good agreement with Bollinger's value.

It is expected that further research on (γ, γ') resonance levels should provide more detailed information on the distribution of the partial radiation widths.

REFERENCES

- [1] SHIKAZONO, N., KAWARASAKI, Y., Nucl.Phys. A118 (1968) 114.
- [2] GIANNINI, M., OLIVA, P., PROSPERI, D., TOUMBEV, G., Nucl.Phys. A101 (1967) 145.
- [3] SCHLESINGER, Y., HASS, M., ARAD, B., BEN-DAVID, G., Phys.Rev. 178 (1969) 2013.
- [4] BOLLINGER, L.M., COTÉ, R.E., CARPENTER, R.T., MARION, J.P., Phys.Rev. 132 (1963) 1640.

THEORY OF CAPTURE

Chairman: R. MORINAGA

Invited talk

THE PRESENT THEORY OF CAPTURE

A.M. LANE

Atomic Energy Research Establishment,
Harwell, Didcot, Berks.,
United Kingdom

Abstract

THE PRESENT THEORY OF CAPTURE. Present channel capture theory, based on electric dipole operators, suggests, but does not necessarily establish, the existence of some of the correlations observed between parameters occurring in thermal and resonance capture. The correlation relationships implicit in this theory are discussed, along with possible theoretical generalizations which might improve the agreement with difficult data. The question of direct capture in the resonance region is examined and the theoretical implications of the anomalous high-energy bump which is found in the photon spectrum of neutron capture in several elements is discussed.

1. CORRELATIONS BETWEEN PARAMETERS OCCURRING IN THERMAL AND RESONANCE CAPTURE

This has been an exciting area experimentally, due particularly to the work at Brookhaven. In ^{169}Tm , correlations have been found between neutron resonance widths and partial gamma widths and it is a challenge to understand these. Equally, there is the problem of understanding the many observed correlations between gamma widths and neutron widths of the final states observed in (d, p) work.

Let us begin the theory by using the ideas of Lane and Lynn [1] who pointed out that such correlations may be expected from 'channel capture'. However, as we will see, these ideas are not fully in accord with the data on ^{169}Tm , and so must be improved. Nevertheless, they give a useful orientation. For other nuclei, 'channel capture' seems to be qualitatively correct.

Channel capture theory

The essence of the theory is very simple. The cross-section for capture $c_0(n, \gamma)f$ has the form:

$$\sigma_{nc_0, \gamma f} \sim |\langle \Psi_f | D | \Psi_{c_0} \rangle|^2$$

c_0 represents the target ground state. Excited target states will be labelled c , which can also be used as the neutron channel label. f is the final bound state. The channel $\gamma+f$ can be denoted simply by f . (We will suppress

reference to spins in future except at one point where it is vital to mention them.) Ψ_f is the normalized final state:

$$\int_{\text{all space}} |\Psi_f|^2 d\tau = 1$$

Ψ_{c_0} is the initial state, corresponding to unit flux in the channel c_0 . The operator D is the usual dipole operator and can be written as:

$$D = d + D_{\text{target}}$$

where

$$\left\{ \begin{array}{l} d = \left(-\frac{Z}{A} e \right) z_n \\ D_{\text{target}} = \sum_{\substack{i = \text{target} \\ \text{neutrons}}} \left(\frac{-Z}{A} e \right) z_i + \sum_{\substack{j = \text{target} \\ \text{protons}}} \left(\frac{N}{A} e \right) z_j \end{array} \right.$$

The operator z_n does not vanish outside the nuclear region $r > R$ so there are contributions to $\langle \Psi_f | D | \Psi_{c_0} \rangle$ from the channels. In the entrance channel:

$$\Psi_{c_0} \sim e^{-ik_n^r} - U e^{ik_n^r}$$

Using standard resonance theory for U :

$$U = e^{-2ik_n a} + ie^{-2ik_n a} \sum_{\lambda} \frac{\Gamma_{\lambda n}}{E_{\lambda} - E - \frac{i}{2} \Gamma_{\lambda}}$$

where λ labels resonances and total width $\Gamma_{\lambda} = \text{sum of neutron and gamma widths} = \Gamma_{\gamma n} + \sum_f \Gamma_{\lambda f}$

We obtain $\sigma_{c_0 f}$ in the form:

$$\sigma_{c_0 f} = \sigma_{c_0 f} (\text{hard sphere capture}) + \sigma_{c_0 f} (\text{resonances})$$

where

$$\left\{ \begin{array}{l} \sigma_{c_0 f} (\text{hard sphere capture}) \sim |\gamma_{fc_0} \langle e^{-k_f r} | d | \text{sink}_n(r-a) \rangle|^2 \\ \sigma_{c_0 f} (\text{resonances}) = \sum_{\lambda} \frac{\Gamma_{\lambda n} \Gamma_{\lambda f}}{E_{\lambda} - E - \frac{i}{2} \Gamma_{\lambda}} \end{array} \right.$$

$\gamma_{\lambda f}^2$ is the neutron width of the final state f for channel c_0 . The quantity $\Gamma_{\lambda f}^{fc_0}$ contains contributions from the external (channel) region as well as the internal (compound nucleus) region I:

$$\Gamma_{\lambda f} = |M_{\lambda f}|^2$$

$$M_{\lambda f} = M_{\lambda f}^I + \sum_c M_{\lambda f}^c \quad (A)$$

where

$$\left\{ \begin{array}{l} M_{\lambda f}^c \sim \gamma_{\lambda c} \gamma_{fc} I_c \\ I_c = \langle e^{-k_f r} | d | e^{-k_c r} \rangle_{r>R} \end{array} \right.$$

(Note that the channel integral I_c decreases rapidly as the excitation energy E_c^* of target state in channel c increases. For $E_c^* = 1.2$ MeV, I_c falls by 13.30 for $a = 7f$, $E_f = -6.5$ MeV. Thus only a few channels c in the sum on c are important.)

Correlations from the channel capture theory

The above form of $\Gamma_{\lambda f}$ implies joint correlations of a very special kind between the 3 observed quantities

$$\left\{ \begin{array}{l} \Gamma_{\lambda f} \quad - \gamma \text{ partial width} \\ \gamma_{\lambda c_0}^2 \quad - n \text{ resonance width} \\ \gamma_{fc_0}^2 \quad - n \text{ final state width (as observed by (dp) studies)} \end{array} \right.$$

It implies that the correlations $(\Gamma_{\lambda f}, \gamma_{\lambda c_0}^2)_{\text{fixed } f}$ and $(\Gamma_{\lambda f}, \gamma_{fc_0}^2)_{\text{fixed } \lambda}$ are of the same general magnitude, i. e. both are large together, or small together. We can display this explicitly.

On defining the correlation function:

$$c(a_i, b_i) \equiv \frac{\sum_i (a_i - a)(b_i - b)}{\left[\sum_i (a_i - a)^2 \sum_i (b_i - b)^2 \right]^{1/2}}$$

where

$$\left\{ \begin{array}{l} a \equiv \text{average of } a_i = \frac{1}{N} \sum_i a_i \\ b \equiv \text{average of } b_i = \frac{1}{N} \sum_i b_i \end{array} \right.$$

we find, using the above form of $\Gamma_{\lambda f}$:

$$c(\Gamma_{\lambda f}, \gamma_{\lambda c_0}^2)_{\text{fixed } f} = \frac{\langle \delta \Gamma_{\lambda f} c \rangle_{\text{av. over } \lambda}}{\langle \Gamma_{\lambda f} \rangle_{\text{av. over } \lambda}}$$

$$c(\Gamma_{\lambda f}, \gamma_{f c_0}^2)_{\text{fixed } \lambda} = \frac{\langle \delta \Gamma_{\lambda f} c \rangle_{\text{av. over } f}}{\langle \Gamma_{\lambda f} \rangle_{\text{av. over } f}}$$

where we have assumed that $(\gamma_{\lambda c}^2, \gamma_{\lambda c}^2)$ are uncorrelated, $(\gamma_{\lambda c}^2, M_{\lambda f}^2)$ are uncorrelated and $\gamma_{\lambda c}, M_{\lambda f}^1$ have random signs and where we define

$$\delta \Gamma_{\lambda f}^c \equiv |M_{\lambda f}^c|^2$$

The assumption of random signs implies

$$\langle \Gamma_{\lambda f} \rangle = \langle (M_{\lambda f}^1)^2 \rangle + \sum_c \langle \delta \Gamma_{\lambda f}^c \rangle$$

where the average is over either λ or f .

Note the following features of the above special correlation type (A)

(1) $c(\Gamma_{\lambda f}, \gamma_{\lambda c_0}^2)_{\text{fixed } f}$ depends on f through the factor $\gamma_{f c_0}^2$. Thus the correlation is stronger for a final state f with large $\gamma_{f c_0}^2$ (i. e. large (dp) intensity). Since the most probable value of $\gamma_{f c_0}^2$ is zero if the Porter-Thomas distribution applies, we expect that a randomly chosen f will give small correlation. Averaging over a set of f should increase it. (All these remarks also apply if f, λ are exchanged.)

(2) The average values of the two correlations are equal:

$$\langle c(\Gamma_{\lambda f}, \gamma_{\lambda c_0}^2)_{\text{fixed } f} \rangle_{\text{av. on } f} = \langle c(\Gamma_{\lambda f}, \gamma_{f c_0}^2)_{\text{fixed } \lambda} \rangle_{\text{av. on } \lambda}$$

(3) If we sum c over all final states f sharing out a single-particle state, then we may use the fact that $\sum_f \gamma_{f c_0}^2 \approx \hbar^2 / m a^2$ to predict

$\sum_f c(\Gamma_{\lambda f}, \gamma_{\lambda c_0}^2)$. Note also the following features of a rather general class of correlations. Averaging the distributions of $\Gamma_{\lambda f}$ before taking the correlation should increase the correlation. This prediction is not specific to the above form (A) but applies generally if $\Gamma_{\lambda f}$ is a sum of a random and a correlated part. In $c(\sum_f \Gamma_{\lambda f}, \gamma_{\lambda c_0}^2)_{\text{fixed set of } f}$, the numeration is just the sum on f of the numerations of $c(\Gamma_{\lambda f}, \gamma_{\lambda c_0}^2)$. However, the denominator quantity

$$\left[\sum_{\lambda} \left(\sum_f \Gamma_{\lambda f} - \sum_f \langle \Gamma_{\lambda f} \rangle_{\text{av. on } \lambda} \right)^2 \right]^{\frac{1}{2}}$$

is more complicated. If the random part of $\sum_f \Gamma_{\lambda f}$ dominates the mean and rms value, then this is $N_f^{\frac{1}{2}}$ times the denominator quantity in $c(\Gamma_{\lambda f}, \gamma_{\lambda c_0}^2)$ with the result that

$$c \left(\sum_f \Gamma_{\lambda f}, \gamma_{\lambda c_0}^2 \right)_{\text{fixed set of } f} = \frac{1}{N_f^{\frac{1}{2}}} \sum_f c \left(\Gamma_{\lambda f}, \gamma_{\lambda c_0}^2 \right)_{\text{fixed } f}$$

$$= N_f^{\frac{1}{2}} \langle c \left(\Gamma_{\lambda f}, \gamma_{\lambda c_0}^2 \right)_{\text{fixed } f} \rangle_{\text{av. on } f}$$

i. e. the correlation is increased by $\sqrt{N_f}$ where N_f is the number of states f that are averaged. In the opposite extreme when the correlated part of $\sum \Gamma_{\lambda f}$ dominates, the correlation is unchanged. In the intermediate situation the correlation is increased but by less than $\sqrt{N_f}$.

(4) In an odd target, the question of correlations between $(\Gamma_{\lambda f}, \gamma_{f c_0}^2)$ is slightly more complicated. Clement has exposed the position in terms of reduced widths $\gamma_{f c_0}^2$ in the representation with neutron spin coupled to orbital spin $\ell = 1$ to give $j = \ell + \frac{1}{2} = \frac{3}{2}$ on $\frac{3}{2}$. We may also present this, somewhat more simply, in terms of a channel spin representation. In the neutral state λ there is only one channel spin $S = I \pm \frac{1}{2}$ viz. $S = J$, so that $\delta \Gamma_{\lambda f}^{c_0}$ contains the factor $\gamma_{f c_0 S = J}$. In contrast, the (ap) cross-section contains: $\gamma_{f c_0 S = J}^2 + \gamma_{f c_0 S \neq J}^2$.

If the two quantities are of equal average value, then, since only the former is correlated with $\delta \Gamma_{\lambda f}^{c_0}$, it is easily shown that the correlation $c(\Gamma_{\lambda f}, \sigma(d, pf))$ is reduced by a factor $\sqrt{2}$ relative to the case of a spin-zero target.

General comment on correlations from channel capture theory

It must be said that this theory only suggests certain correlations but does not prove them. The point is that the use of the E1 operator D , with the consequent contribution to $\Gamma_{\lambda f}$ from the channel region, is arbitrary. In other, equally valid, approaches such contributions do not occur. For example, we can make a transformation of $\langle D \rangle_{if}$ to replace it by $\langle \text{grad } V \rangle_{if} (\epsilon_i - \epsilon_f)^2$, where V is the potential. (This displays explicitly the fact that radiation occurs only in the presence of forces, i. e. of acceleration.) This operation is zero outside the nucleus so has no channel contributions. (Incidentally, this shows that it is quite wrong to speak of 'channel capture' as if it were a direct physical process. It is not, but merely a result of the mathematical approach that is used.)

Theoretical prediction of correlation using the channel capture theory

We can calculate $\delta \Gamma_{\lambda f}^c / \Gamma_{\lambda f}$ by using observed values of $\Gamma_{\lambda f}$, and computed values of $\delta \Gamma_{\lambda f}^c$.

	$\langle \Gamma_{\lambda f} \text{ (observed)} \rangle$	$\langle \Gamma_{\lambda c_0} \text{ (1 eV)} \rangle$	$\delta \Gamma_{\lambda f}^c \text{ (calc.)}$	$\delta \Gamma_{\lambda f}^c / \Gamma_{\lambda f}$
^{55}Mn	15 meV	4 eV	$2400 \theta_{f c_0}^2$	$160 \theta_{f c_0}^2$
^{169}Tm	0.07 meV	1 meV	$0.1 \theta_{f c_0}^2$	$1.5 \theta_{f c_0}^2$
^{197}Au	1 meV	1 meV	$0.1 \theta_{f c_0}^2$	$0.1 \theta_{f c_0}^2$

where

$$\theta_{fc_0}^2 \equiv \gamma_{fc_0}^2 / \frac{\hbar^2}{ma^2}$$

$\theta_{fc_0}^2$ is probably in the range 0.1-1 for states in ^{55}Mn , but < 0.1 for ^{169}Tm , ^{197}Au . Thus we predict appreciable correlation in ^{55}Mn , but very little ($c \lesssim 0.01$) in Au.

Observed facts on correlations in resonance data

Let us consider ^{169}Tm where the most complete analysis has been made [2]: 13 levels λ , 15 final states f .

$c(\Gamma_{\lambda f}, \gamma_{\lambda c_0}^2)_{\text{fixed } f}$ varies from -0.24 to +0.79 for different f . The average value is 0.27. The sum is $\sum_f c \approx 4$.

This sum is rather larger than the channel capture theory products, but is in the right area. However, there are serious difficulties with more detailed features:

(1) Contrary to the prediction that states f with strongest (dp) groups should have the strongest correlation, c is weaker for states f with strong (d,p). (If the strong (dp) groups arose from the wrong channel spin, this might remove this objection, but this is unlikely.)

(2) Inspection of the data suggests $c(\Gamma_{\lambda f}, \gamma_{\lambda c_0}^2)_{\text{fixed } \lambda} \ll 0.27$, even at the 2 states (3.9, 34.8 eV) with very large $\gamma_{\lambda c_0}^2$. This conflicts with the prediction that $c(\Gamma_{\lambda f}, \gamma_{\lambda c_0}^2) \sim c(\Gamma_{\lambda f}, \gamma_{\lambda c_0}^2)$.

Finally, we note that the result of summing over the distributions before taking the correlation is to increase it from 0.27 to 0.68, an increase of 2.5. As we saw above, such an increase is expected rather generally, and is not therefore evidence for the channel capture theory.

^{238}U has been studied and no correlations found (Brookhaven)

^{181}W , ^{185}W have been studied and no correlations found (Harwell)

^{55}Mn has 3 resonances (at 336, 1098 and 2355 eV) and 11 states f .

The correlations $c(\Gamma_{\lambda f}, \gamma_{\lambda c_0}^2)$ are +0.06, 0.73 and 0.78. Average value 0.50. Value from superposing distributions: 0.87.

The values of $\gamma_{\lambda c_0}^2$ are 1.2, 0.4 and 8.3 eV. As expected, the strongest level has the largest c , but the weaker two are reversed. The fact that (d,p) data include two channel spins because of the target spin may help to explain this.

On balance, it looks as if ^{55}Mn may agree with the channel capture theory, both in general magnitude and detailed character of the correlations, but more data are needed.

Observed correlation between (d,p) and thermal (n, γ) intensities

A positive correlation has been found in many nuclei:

odd ^{45}Sc , ^{55}Mn , ^{165}Ho

even ^{24}Mg , $^{50,52}\text{Cr}$, ^{54}Fe , ^{58}Ni , ^{138}Ba , ^{140}Ce , ^{142}Nd , ^{42}Ca

The best case is $^{42}\text{Ca}(n, \gamma)$ where a very strong correlation has been found [3].

In one case, ^{56}Fe , a negative correlation appears which has been the subject of some theoretical speculation [4]. ^{59}Co and ^{115}In also show similar effects (but note that the channel spin effect above may be partly responsible). It is an open question whether the relevant thermal capture is mostly due to resonances or direct capture. The case of ^{55}Mn shows that resonances can be responsible even in lighter nuclei.

The correlation in ^{165}Ho , if thermal capture is due to resonances, is in disagreement with the Lane-Lynn model. In lighter nuclei, the model may be consistent with the data.

Generalization of channel capture model (needed for, e.g., ^{169}Tm)

A way to generalize the above model is suggested by first considering a special form of state f . After that we shall consider the general case.

Special case (a)

Consider expanding the states λ and f into product eigenstates of the uncoupled Hamiltonian $H_{\text{target}} + H_{\text{particle}}$ and suppose that f is a single product state of the ground state X_c of the target and an $\ell=1$ particle orbital u_1 . (This was considered by Clement.) $f = u_1 X_{c_0}$.

$$\Gamma_{\lambda f} = |M_{\lambda f}|^2$$

$$M_{\lambda f} = \gamma_{fc_0} \gamma_{\lambda c_0} \langle u_1 | d | u_0 \rangle + \gamma_{fc_0} \gamma_{\lambda c_D} M_D$$

with $\gamma_{fc_0}^2 = \hbar^2 / ma^2$. M_D is the total dipole matrix element of the target: $M_D = \langle X_{c_0} | D_{\text{target}} | X_{c_0} \rangle^{\frac{1}{2}}$ and $\gamma_{\lambda c_D}$ is the amplitude for the dipole state X_D ($\propto D_{\text{target}} X_{c_0}$) and u_1 in λ . The first term gives correlations ($\Gamma_{\lambda f}, \gamma_{\lambda c_D}^2$), while the second does not unless $\gamma_{\lambda c_D}, \gamma_{\lambda c_0}$ are correlated.

Special case (b)

We may argue that the second term does in fact contain a part proportional to $\gamma_{\lambda c_0}$ and so contributes to the correlation. This may be exposed by invoking the collective dipole coupling between target and particle. The modified approximate Hamiltonian is

$$H_0 = H_{\text{target}} + H_{\text{particle}} + H_{\text{dip. coupling}}$$

This has eigenstates like:

$$\begin{aligned} u_0 X_{c_0} + \alpha_0 u_1 X_D \\ u_1 X_{c_0} + \alpha_1 u_0 X_D \end{aligned} \quad \text{with } \alpha_0, \alpha_1 \ll 1$$

Let us suppose that f is a state of the latter type. We then have

$$\begin{aligned} M_{\lambda f} = \gamma_{fc_0} \gamma_{\lambda c_0} \langle u_1 | d | u_0 \rangle + \gamma_{fc_0} \gamma_{\lambda c_D} M_D + \alpha_1 \gamma_{fc_0} \gamma_{\lambda c_D} \langle u_0 | d | u_1 \rangle \\ + \alpha_1 \gamma_{fc_0} \gamma_{\lambda c_0} M_D \end{aligned}$$

The first and last terms give a correlation between $\Gamma_{\lambda f}$ and $\gamma_{\lambda c_0}^2$. If $(\alpha_1 M_D) > \langle u_1 | d | u_0 \rangle$, then the last term dominates. (This ratio of these quantities determines the relative value of collective and direct capture; estimates for $A \sim 190$ suggest that the former may dominate.) On considering the expansion of λ into the collective eigenstates above, $\gamma_{\lambda c_D}$ may be split into a part proportional to $\gamma_{\lambda c_0}$ and a random part.

$$\gamma_{\lambda c_D} = \alpha_0 \gamma_{\lambda c_0} + \gamma_{\lambda c_D}^1 \quad \text{say}$$

thus:

$$M_{\lambda f} = \gamma_{fc_0} \gamma_{\lambda c_0} (\alpha_1 M_D + \alpha_0 M_D + (1 + \alpha_0 \alpha_1) \langle u_0 | d | u_1 \rangle) \\ + \gamma_{fc_0} \gamma_{\lambda c_D}^1 (M_D + \alpha_1 \langle u_0 | d | u_1 \rangle)$$

The first part gives the correlation ($\Gamma_{\lambda f}$, $\gamma_{\lambda c_0}^2$) while the second does not. The importance of the two is determined by $\alpha_0 \gamma_{\lambda c_0} / \gamma_{\lambda c_D}^1$, i.e. by the extent to which the admixture of state $u_1 X_D$ in λ can be accounted for by the collective coupling acting on the component $u_0 X_0$ of λ . For the region $A \sim 190$, we can estimate $\langle \lambda | u_1 X_D \rangle^2$ as $(1/2\pi) \Gamma D / (E - E_r)^2$ where Γ is the dipole state width (~ 4 MeV) and $(E - E_r)$ is the energy separation of λ and $u_1 X_D \sim 8$ MeV so: $\langle \lambda | u_1 X_D \rangle^2 \sim 0.01 D$. The collective mixing gives $0.06 \alpha_0^2 D$. Since $\alpha_0^2 \ll 1$, the collective mixing is probably not the dominant part of $\langle \lambda | u_1 X_D \rangle^2$, so the correlated term in $M_{\lambda f}$ is probably not dominant. Nevertheless reasonable values like $\alpha_0^2 \sim 0.05$ would give a significant correlation ($c \sim 1/3$).

General case

We may regard a general final state f as containing a part $(u_1 X_0 + \alpha u_0 X_D)$ plus the rest. The rest will contribute an extra part to the above $M_{\lambda f}$, from which we can extract a part containing $\gamma_{\lambda c_0} \gamma_{fc_D}$ so the final structure of $M_{\lambda f}$ is:

$$M_{\lambda f} = \gamma_{fc_0} \gamma_{\lambda c_0} A + \gamma_{fc_0} \gamma_{\lambda c_D}^1 B \\ \gamma_{\lambda c_0} \gamma_{fc_D}^1 c + M_{\lambda f}^1$$

A , B are given by the above form: $c = M_D + \alpha_0 \langle u_0 | d | u_1 \rangle$; $\gamma_{\lambda c_D}^1$, $\gamma_{fc_D}^1$ and $M_{\lambda f}^1$ are random. The first term correlates (Γ_f , $\gamma_{fc_0}^2$) and ($\Gamma_{\lambda f}$, $\gamma_{\lambda c_0}^2$) the second correlates ($\Gamma_{\lambda f}$, $\gamma_{fc_0}^2$) but not ($\Gamma_{\lambda f}$, $\gamma_{\lambda c_0}^2$). The third correlates ($\Gamma_{\lambda f}$, $\gamma_{\lambda c_0}^2$) but not ($\Gamma_{\lambda f}$, $\gamma_{fc_0}^2$) and the last gives no correlations.

We may regard this form of $M_{\lambda f}$ as a reasonable practical form for the analysis of the data. Once it has been shown that it is consistent with the data, then more attention can be given to the expected magnitudes of A , B , C to see if these agree with observed values. For example, the data on Tm suggest that the term in C dominates those in A , B for this nucleus.

On forming the mean width (over λ) with the above form:

$$\langle \Gamma_{\lambda f} \rangle_{\text{av. on } \lambda} = \gamma_{fc_0}^2 \langle \gamma_{\lambda c_D}^1 \rangle^2 B^2 + (A \gamma_{fc_0} + c \gamma_{fc_D}^1)^2 \langle \gamma_{\lambda c_0}^2 \rangle + \langle M_{\lambda f}^1 \rangle^2$$

If this fluctuates with f , this will be direct evidence for the correlation effects (similarly if $\langle \Gamma_{\lambda f} \rangle_{\text{av. on } f}$ fluctuates with λ). If such fluctuations are strongly correlated with $\gamma_{f c_0}^2$, this is evidence for $C \ll A, B$. On averaging over f :

$$\langle\langle \Gamma_{\lambda f} \rangle\rangle = [\Gamma_{\lambda f}]_{\text{corr}} + [\Gamma_{\lambda f}]_{\text{uncorr}}$$

where

$$[\Gamma_{\lambda f}]_{\text{corr}} = \langle \gamma_{f c_0}^2 \rangle \langle \gamma_{\lambda c_D}^2 \rangle B^2 + \langle \gamma_{f c_0}^2 \rangle \langle \gamma_{\lambda c_0}^2 \rangle A^2 + \langle \gamma_{f c_D}^2 \rangle \langle \gamma_{\lambda c_0}^2 \rangle c^2$$

$$[\Gamma_{\lambda f}]_{\text{uncorr}} = \langle\langle M_{\lambda f}^2 \rangle\rangle$$

In the ^{169}Tm analysis, evidence was found for a correlation $c(\Gamma_{\lambda f}, \Gamma'_{\lambda f})$ of ~ 0.09 . On the present picture this correlation appears as:

$$c(\Gamma_{\lambda f}, \Gamma'_{\lambda f}) \sim \frac{[\Gamma_{\lambda f}]_{\text{corr}} [\Gamma'_{\lambda f}]_{\text{corr}}}{\langle\langle \Gamma_{\lambda f} \rangle\rangle \langle\langle \Gamma'_{\lambda f} \rangle\rangle}$$

so the observed value implies: $[\Gamma_{\lambda f}]_{\text{corr}} \sim \frac{1}{3} \langle\langle \Gamma_{\lambda f} \rangle\rangle$ in general agreement with $c(\Gamma_{\lambda f}, \gamma_{\lambda c}^2) \approx 0.27$.

General comment on theoretical position about correlations

At first sight it seems very unlikely that there should be correlations between $\Gamma_{\lambda f}$ and $\gamma_{\lambda c_0}^2$ in a nucleus like ^{170}Tm . The observed values of $\gamma_{\lambda c_0}^2$ show that only about one 10^{-5} part of a resonance λ consists of the entrance channel component. It follows that, for an arbitrary final state f (where the fraction of entrance channel component is also very small, say 10^{-3}), there cannot be any significant correlation between $\Gamma_{\lambda f}$ and $\gamma_{\lambda c_0}^2$. If such were observed, it could only mean that the non-entrance channel components in $\Gamma_{\lambda f}$ interfere in a systematically destructive fashion to give a contribution to $\Gamma_{\lambda f}$ which is much less than expected from random signs (which implies $\Gamma_{\lambda f} / \Gamma_{\lambda f(c_0)} \propto$ the number of channels involved). This would be hard to understand since it means that the entrance channel is "special" for no obvious reason.

When f is a single product state involving the target state, then, as we have seen, it is easy to see that a strong correlation is implied (since this structure of the state f means that the entrance channel is indeed special). For actual final states f , where the entrance channel fraction is usually $\lesssim 0.1$, it is rather surprising that observed correlations are so large. To put this in another way, when $\theta_{f c_0}^2$ is ~ 0.1 , this means that about 10 channel states play a comparable role in the states f . Thus the above form of $M_{\lambda f}$ should replace c_0 by these states c , and sum over them. For correlations like $(\Gamma_{\lambda f}, \gamma_{\lambda c_0}^2)$ involving c_0 quantities, these new elements are effectively random, which means in c that they do not contribute to the numerator, but they increase the denominator by ~ 10 , making $c \lesssim 0.1$.

2. EXISTENCE OF DIRECT CAPTURE IN THE RESONANCE REGION

This is difficult to isolate in practice because of interference between levels (including possible negative energy levels) which can give similar effects. The standard method is to look at

$$\frac{\sigma(n, f\gamma)}{\text{total } \sigma(n, \gamma)}$$

as a function of neutron energy (e.g. Brookhaven work [5] and Saclay work [6]). Near a truly isolated resonance without background this will be constant. In practice, on normalizing at the resonance centre deviations of up to 50% are sometimes observed in the wings.

Target	E_γ (keV)	Observed range of deviation	Observed direct capture (at 1 eV) (mb)
^{59}Co	7490	$E_n = 0 - 100 \text{ eV}$	10
^{197}Au	6245	$E_n = 0 - 4 \text{ eV}$	1
^{207}Pb	7.3 MeV	near 43 keV res.	40
^{238}U	4059	10 - 20 eV	1.6

The channel capture theory predicts typically $40\theta_{fc_0}^2$ mb for $\sigma(1 \text{ eV})$. Potential capture with the Saxon-Woods well gives values $20 - 300\theta_f^2$ mb. The observed values agree with these estimates using reasonable values of $\theta_{fc_0}^2$. As an example of uncertainty arising from negative energy resonances, a fit can be obtained to the Au with zero direct capture if such resonances are invoked [7].

The channel capture theory predicts that direct capture should be larger (and so more evident) in cross-sections for final dates f with large values of $\theta_{fc_0}^2$. It would be nice to see this in the data, but this is rather too sophisticated a matter at the present stage. In future it may be possible to reveal this effect.

3. THE ANOMALOUS BUMP IN THE PHOTON SPECTRUM

This is the excess of photons of energy 5-6 MeV observed in nuclei $A \sim 100 - 140$, $180 - 200$, but especially for $A \sim 195 - 200$, where it is a strong bump or group on the background.

While the data were only thermal capture, it remained an open question whether the bump came from resonance capture or from a direct capture process. It was shown that direct capture could not explain the observed magnitude [1] by a factor of $0.1 - 0.001$. $\sigma(n, \gamma)$ fluctuated violently with A in a manner suggesting that resonance effects are dominant. Recently direct observation of resonance capture (e.g. ^{197}Au) shows that resonances do indeed show the anomalous bump. One can then ask whether the channel resonance term could explain this.

Lane and Lynn [1] found that the observed magnitudes were too large (by a factor of 5-10). Further, as we have seen above, this channel capture cannot explain the large ($\Gamma_{\lambda f}$, $\gamma_{\lambda c_0}^2$) correlations which shows that the entrance channel role in $\Gamma_{\lambda f}$ is more important than channel resonance capture can explain. Thus the basic question is: "Is the bump associated with the entrance channel part of λ (i. e. with the correlated part of $\Gamma_{\lambda f}$) or not?"

At first sight the answer is yes because capture due to the entrance channel component would predict a group at about the correct energy $E_\gamma = 5-6$ MeV, since the single particle $3p_{\frac{1}{2}}$ state occurs at such a binding energy. (Note that the $4S_{\frac{1}{2}}$ state occurs just below zero energy in this mass region. However this fact does not affect the energy of the bump; it may contribute to its size in that $\gamma_{\lambda c_0}$ is larger than usual, and possibly the dipole integral is larger.)

Having seen that the entrance channel part of λ predicts the correct energy of the anomaly in thermal capture, let us now consider whether it is sufficiently large, i. e. whether $\Gamma_{\lambda f}^c$ is the larger fraction of $\Gamma_{\lambda f}$. In ^{169}Tm , we know directly from the observed correlation that $\delta\Gamma_{\lambda f}^c \sim 0.27 \Gamma_{\lambda f}$ on the average. This fraction would be rather too small. However, we may now argue that there will be other channel states in λ corresponding to low-lying excited target states which predict the correct energy of the anomaly and have $\delta\Gamma_{\lambda f}^c$ of comparable magnitude. Actually no anomaly is found in Tm, or nuclei of $A < 180$, except possibly in broadened form. This is what might be expected qualitatively from the large deformation which spreads out the final $3p$ state. We could apply the same argument above to Au, where a strong anomaly is observed, but we have no observed value of c to guide us. It seems likely that c is small so it remains unsettled whether the entrance and low-excited parts of λ are sufficient to dominate $\Gamma_{\lambda f}$.

This question seems to be clinched by the observed fact [8] that the anomaly persists when the neutron energy is raised to 3 MeV and also that its position remains at $E_\gamma = 5-6$ MeV. It would be hard to explain this in terms of entrance and low-lying channel components. At 3 MeV $\ell = 0, 1, 2$ waves are important. It would seem a remarkable coincidence if the 3 MeV $\ell = 1, 2$ capture occurred in just such a way as to give an anomaly like the thermal $\ell = 0$ capture. (In any case, there is no final $\ell = 1$ or 3 state at an energy to cause a 5-6 MeV group in $\ell = 2$ capture.)

Thus we must reluctantly dismiss the fact that entrance channel capture gives a group at the right energy as coincidence, and regard the anomaly as arising from the anomalous behaviour of $\langle \Gamma_{\lambda f} \rangle$ as a function of f , without any special reference to the low-lying channel components. The observed lack of dependence of the anomaly on neutron energy suggests that not only does $\langle \Gamma_{\lambda f} \rangle / D$, for fixed f , have a bump at $(E_\lambda - E_f) = 5-6$ MeV, but that this is the same for all f over the first 5 MeV of excitation energy. (The latter is an aspect of the Brink hypothesis, that the photon strength function is independent of the target state.)

Another coincidence seems to be the verdict on another hypothesis, viz. that the anomaly is due to an M1 giant resonance [9]. If the M1 resonance energy is taken as the spin-orbit splitting of the large j orbits, then 5-6 MeV seems reasonable. However, the M1 sum-rule predicts a maximum strength of about $\frac{1}{2}\%$ of the E1 sum, while the observed strength in Au is $\sim 2\%$. Further, according to recent theoretical results of W. Hay,

there is an upward collective repulsion effect that puts most of the M1 strength about 1 MeV above the spin-orbit splitting, so that the predicted energy is not quite right. The final clinching datum is that direct measurement shows some strong lines in the anomaly to be E1 [10].

'Pygmy' E1 resonance hypothesis

This is now the accepted interpretation. Theoretically it is not unexpected to find a slight excess of strength in the 5-6 MeV region. For example in a 1p-1h diagonalization, Pal, Soper and Stamp (Harwell Report) found that a few per cent of the dipole strength in ^{208}Pb remained in the region of the strong unmixed 1p-1h transitions at around 6 MeV. (This agreed with data by Axel from the (γ, γ) reaction.) It is not unreasonable to expect this situation to persist over a range of A.

When a level or group occurs systematically over a range of nuclei, it is nice to be able to pin a collective label on it. In this case, the only possible candidate is the spin dipole resonance associated with the operator $\sum_i z_i \sigma_i$. In light nuclei like ^{40}Ca , this is expected at an energy roughly equal to the usual dipole energy (since S and T are symmetrical features of such nuclei). For heavy nuclei this symmetry fails in view of the large T of nuclei and S-mixing due to spin orbit forces. A calculation for ^{90}Zr finds the spin-dipole strength at 11, 13, 17 and 21 MeV, with the usual dipole at 16 MeV and the mean 1p-1h energy at 11 MeV. It is interesting to see that an increase in normal dipole strength occurs at each of the spin-dipole groups.

This suggests that the mixing of the normal dipole state into the multiplicity of 1p-1h states occurs mainly through the other collective modes. Thus it is quite possible that the pygmy resonance at 6 MeV in ^{208}Pb can be identified as a branch of the spin-dipole collective state. This is being studied at present.

Problem with the anomalous bump

The bump is observed in the gamma spectra of (d, p γ) reactions where E_d and E_p are fixed [11]. When these energies correspond to $E_n \sim 1$ MeV, the bump is rather weaker (in contrast to the (n, γ) results, where it remains strong). Except for this, the (d, p γ) and (n, γ) spectra agree.

No bump is observed in the spectrum of photons from the An (n, n' γ) reaction with $E_n = 7.5$ MeV [12]. The Au (n, n') data agree well with the statistical model, and suggest that most n reaction events lead to the emission of low-energy neutrons leaving the target nucleus just above its neutron threshold. Thus one expects the photon spectrum to display the anomaly, but it does not. This is extremely strange at first sight. However the explanation may be simple. Bergquist et al. [12] assume (as most of us would) that photons from (n, γ) are negligible in number compared to those from (n, n' γ) when $E_n \sim 7.5$ MeV. However, in a rough calculation, without stretching any numbers, I estimate that the two sources of photons could be comparable for photons of energy ~ 4 MeV. The main 'input' of the calculation is the photon absorption cross-section on any nuclear state as a function of photon energy and the level densities. I have taken observed values of the latter (essentially $\rho(U) \propto \exp 2\sqrt{a}U$, where $a \approx 19$ for Au). For the former, I have used the E1 sum-rule for

the integral value, and have tried various reasonable models for the actual energy dependence (e.g. (1) resonance form centred at the dipole peak $E_\gamma = 14$ MeV; (2) constant over an energy range of 20 MeV).

Accepting that the two sources of photons may be comparable, one more assumption is needed before we can say that there is no problem over the absence of an anomaly, viz. that the (n, γ) spectrum at $E_n = 7.5$ MeV has no anomaly in it. Since the anomaly has been seen over the range $E_n = 0 - 4$ MeV, such an assumption is not trivial.

Finally, we note that the possibility of the two sources of photons being comparable means that $\sigma(n, \gamma)$ is comparable with $\sigma(n, n')$. This flies in the face of traditional belief and could lead to some very startling implications. The reason for the new result is essentially that the large ratio of final state densities for (n, γ) and (n, n') can compensate the small ratio of the intrinsic γ and n widths.

REFERENCES

- [1] LANE, A.M., LYNN, J.E., Nucl. Phys. 17 (1960) 563.
- [2] LONE, M.A. et al., Phys. Rev. 174 (1968) 1512.
- [3] GRUPPELAAR, H. et al., Nucl. Phys. 131 (1969) 180.
- [4] IKEGAMI, H., EMERY, G.T., Phys. Rev. Lett. 13 (1964) 26.
- [5] PRICE, D.L. et al., Nucl. Phys. 121 (1968) 630.
- [6] SAMOUR, C. et al., Nucl. Phys. 130 (1969) 353.
- [7] WASSON, O.A. et al., Phys. Rev. 173 (1968) 1170.
- [8] LUNDBERG, B., STARFELT, N., Nucl. Phys. 67 (1965) 321.
- [9] STARFELT, N., Nucl. Phys. 53 (1964) 397.
- [10] BARTHOLOMEW, G.A. et al., Can. J. Phys. 45 (1967) 2063.
- [11] BARTHOLOMEW, G.A. et al., Physics Lett. 24B (1967) 47.
- [12] BERGQVIST, I. et al., Nucl. Phys. 80 (1966) 198.

SEARCH FOR SIMPLE CONFIGURATIONS IN THE CAPTURE STATE OF (n, γ) REACTIONS

H. -U. GERSCH, W. RUDOLPH
Zentralinstitut für Kernforschung,
Rossendorf bei Dresden,
Democratic Republic of Germany

Abstract

SEARCH FOR SIMPLE CONFIGURATIONS IN THE CAPTURE STATE OF (n, γ) REACTIONS. The influence of simple configurations contained in the capture state of various (n, γ) reactions is investigated. A detailed comparison of the primary transition probabilities in (d, p) and (n, γ) reactions to the low-lying levels of the final nuclei shows in a few cases a dominant influence of the entrance channel on the primary gamma radiation (channel capture). However, in the most cases the gamma-ray transitions cannot be explained by the contribution of the entrance channel to the capture state. In cases where a dominant channel capture is to be expected the influence of potential capture and resonant channel capture is investigated. For this purpose estimations for both terms of the channel capture performed earlier are used. In the remaining cases a qualitative interpretation of the gamma-spectra is attempted by means of other simple configurations (perhaps doorway states) in the capture state.

1. INTRODUCTION

The anomalous behaviour of spectra following the capture of thermal neutrons was the first hint of the influence of simple configurations in the capture state on the primary gamma-ray transition probabilities [1]. The presence of such contributions was confirmed in many cases by the observation of considerable correlations between the reduced primary transition probabilities in the (n, γ) reaction and the $(2I+1)S$ values in the (d, p) reaction for levels with $l_n = 1$. This phenomenon is often called 'direct capture'. Such a notation is in a way misleading because usually we use this term only in connection with reactions showing giant resonance structure. However, neutron capture is a typical compound reaction.

The wave function of the capture state can be expanded in terms of basic functions and contains the entrance channel and basic states which arise from the entrance channel by a single two-particle interaction (doorway states) and also more complicated basic states. Correlations between the primary transition probabilities in both reactions can indicate only an essential contribution of the entrance channel to the primary gamma-ray intensities. Therefore, the term 'channel capture' introduced by Lane and Lynn [2] is a better notation for this phenomenon. On the other hand, strong primary gamma-ray transitions were found also to levels with no or with only relative small $l_n = 1$ strength. This behaviour cannot be interpreted by channel capture, however, it can be explained by the influence of other simple configurations contained in the capture state.

The present paper shows a few possibilities to deduce indications for such simple configurations from the experimental results of neutron capture.

2. THE CONTRIBUTION OF THE ENTRANCE CHANNEL

The channel part caused by the configuration 'target ground state + $s_{\frac{1}{2}}$ neutron' in the capture state has been investigated in several papers [2-4] with the limitation on E1 transitions¹ to the low-lying levels of the product nuclei in the mass regions $40 \leq A \leq 65$ and $180 \leq A \leq 210$. These investigations demonstrate that at least in the s-giant resonances the channel capture originates mainly from the 'external' region of the nucleus [4, 6]. From this follows a direct relation between the channel and the scattering cross-sections. Consequently, the channel cross-section has a smooth part (potential capture) and a part following the compound resonances (resonant channel capture) both of which interfere with each other.

Estimations of the channel cross-section in the region of the 3s-giant resonance ($40 \leq A \leq 65$) give for the potential cross-section [4]

$$\sigma_{\text{pot}} \approx \frac{80 \text{ mb}}{(E/\text{eV})^{\frac{1}{2}}} \quad (1a)$$

that is for thermal neutrons

$$\sigma_{\text{pot}} (\text{therm}) \approx 0.5 \text{ b} \quad (1b)$$

For the ratio of the resonant channel cross-section to the compound cross-section we obtain roughly (for $l = 0$ resonances)

$$\frac{\sigma_{\text{ch}}}{\sigma_{\text{cap}}} \approx 0.15 \frac{\Gamma_n^0}{\Gamma_\gamma} \quad (2)$$

This shows that a predominant channel capture can be expected only in those resonances where the scattering strongly prevails.

Similar values were obtained for the mass region $180 \leq A \leq 210$. However, in this case the assumption of the main contribution to the channel part coming from the external region of the nucleus is doubtful because there is no influence of a s-giant resonance.

3. EXPERIMENTAL EVIDENCE FOR CHANNEL CAPTURE

Neutron capture gamma-ray spectra are mostly known only for thermal neutron capture. In general, both capture states with the spins $I_i = J_0 \pm 1/2$ arise ($J_0 =$ target spin; $l = 0$ capture is supposed). For even-even target nuclei the spin is well defined as $I_i = 1/2$. In these cases proportionality is to be expected between the reduced probabilities of the primary E1 transitions B(E1) and the $(2I+1)S$ values of the (d, p) reaction to $l_n = 1$ levels. This strong correlation is used frequently as a criterion for channel capture.

¹ The M1 channel capture has not been investigated in detail so far. Estimations are given by Lynn [5].

Table I gives a survey of the correlation coefficients found in the mass region considered together with the proposed interpretations.

Generally, for odd target nuclei proportionality between (n, γ) and (d, p) strengths cannot be expected even in the case of channel capture. This can be easily seen by analysing the transition probability from the entrance channel with spin I_i to a final level I_f with the amplitude $C_{jI}(J_0 I_f)$ of the basic function 'target ground state + j neutron' ($l = 1; j = 3/2, 1/2; J_0 = \text{target spin}$)

$$B(E1; I_i \rightarrow I_f) \sim (2I_f + 1) \left[\sum_j \sqrt{2j+1} C_{jI}(J_0 I_f) \begin{Bmatrix} 1 & j & \frac{1}{2} \\ J_0 & I_i & I_f \end{Bmatrix} \right]^2 \quad (3)$$

Here the coupling scheme $|s \ 1; j\rangle$ is used.

If both capture states $I_i = J_0 \pm 1/2$ contribute (mixing coefficients $b(I_i)$) it follows that

$$B(E1; \rightarrow I_f) = \sum_{I_i} b(I_i) \cdot B(E1; I_i \rightarrow I_f) \quad (4)$$

The amplitudes $C_{jI}(J_0 I_f)$ are directly related to the spectroscopic factors of the (d, p) reaction (n denotes the number of active particles)

$$S(l) = n \cdot \sum_j C_{jI}^2(J_0 I_f) \quad (5)$$

Comparison of $(2I_f + 1)S$, where $S = S(l)$ is given by Eq.(5), with Eq.(3) shows that the proportionality is disturbed by the $6j$ -symbol and the statistical factors and also by the interference of the $j = 1/2$ and $j = 3/2$ contributions. For odd target nuclei the primary transition probabilities in both reactions are proportional to each other only in the special case where both possible capture states are statistically distributed and the following condition holds

$$C_{jI}(J_0, I_i = J_0 + 1/2) = C_{jI}(J_0, I_i = J_0 - 1/2)$$

Here, $C_{jI}(J_0, I_i)$ is the amplitude of the entrance channel. Therefore, in such nuclei deviations from proportionality cannot be used as an argument against channel capture unless the primary gamma-ray intensities are much greater than that expected according to the $l_n = 1$ strength [23-27]. Evidence for channel capture can be obtained if calculation with Eq.(3) agrees with the experimental primary transition probabilities. To do this a knowledge of the wave functions of the final states is necessary.

In this way, information on the capture mechanism of the $^{51}\text{V}(n, \gamma)^{52}\text{V}$ reaction could be obtained [28]. Here the primary transitions to the low-lying levels in ^{52}V could be explained by channel capture, taking into account a small contribution (10%) from the simplest doorway configuration $|f_{7/2}^3(5/2) s_{1/2}; I_i = 3\rangle$.

TABLE I. INDICATIONS OF CHANNEL CAPTURE OF THERMAL NEUTRONS IN THE MASS REGION $40 \leq A \leq 65$ (EVEN-EVEN TARGET NUCLEI)

Target nucleus	Number of levels used with $l_n = 1$	Correlation coefficient	References	σ_{th} (b)	Interpretation
^{40}Ar	8	≈ 0.7	[8,9]	0.53	Potential capture is probable
^{40}Ca	5	0.60	[10,11]	0.22	Potential capture, positive resonances have no influence on σ_{th}
^{44}Ca	12	0.91	[12]	0.67	Potential capture, the positive resonances contribute 10% to σ_{th}
^{48}Ti	7	0.88	[13,14]	8.3	Resonance at 17.34 keV with dominant channel capture contributes only 10% to σ_{th} ; potential capture is not probable
^{50}Cr	9	0.90	[15,16]	13.5	Resonance at 5.5 keV with dominant channel capture contributes only 20% to σ_{th} ; potential capture is not probable
^{52}Cr	8	0.96	[17,18]	0.7	Potential capture, positive resonances have no influence on σ_{th}
^{54}Fe	10	0.97	[19,20]	2.5	Channel capture due to the resonances at 7.25 and 8.0 keV which are responsible for σ_{th}
^{56}Fe		anti-correlations	[21]	2.6	A negative resonance with dominant channel capture generates σ_{th} , anticorrelations can be explained only by additional doorway configurations [21]
^{58}Ni	6	0.99	[22]	4.4	Known resonances contribute only 10% to σ_{th} ; potential capture to low-lying levels is possible
^{60}Ni	7	0.98	[22]	2.5	Resonance at 12.5 keV with dominant channel capture contributes only 30% to σ_{th} ; potential capture to low-lying levels is probable
^{62}Ni	4	-0.14	[22]	15	Resonance at 4.6 keV with dominant channel capture contributes only 20% to σ_{th} ; potential capture is not probable

However, in the case of odd target nuclei evidence for a dominant channel capture can also be obtained without knowledge of wave functions. If the comparison with (d, p) strengths is limited to final levels with the same spins $I_f = J_0 + 3/2$ or $I_f = J_0 - 3/2$, the proportionality is preserved (Eq.(3)). In the case of $^{51}\text{V}(n, \gamma)^{52}\text{V}$ a comparison of the transitions to two levels with $I_f = 2$ is possible. No correlation has been observed.

Contrary to the general behaviour of the odd target nuclei the gamma spectra of $^{55}\text{Mn}(n, \gamma)$ and $^{65}\text{Cu}(n, \gamma)$ show a reliable correlation to (d, p) strengths for low-lying levels [7, 27]. For ^{65}Cu this could be explained by a potential capture to levels with noticeable amplitudes of the configuration 'target ground state + p_j neutron' [27] because the partial capture cross-section of 0.5 barn to these levels agrees with the estimated potential cross-section. In the case of potential capture the distribution of the initial spins in the capture state corresponds approximately to the statistical factors $(2I_i + 1)$ and Eq.(4) is reduced using the orthogonality relation of the 6j-symbols to

$$B(E1; \rightarrow I_f) \sim (2I_i + 1) \cdot S(l) \quad (6)$$

This leads to proportionality between (n, γ) and (d, p) transition probabilities.

The capture mechanism of $^{55}\text{Mn}(n, \gamma)$ has not yet been clarified. Thermal neutron capture is caused only by the known neutron resonances which have no dominant channel part with the exception of the 2,375-keV resonance. Potential capture can be neglected. Therefore, the correlation to (d, p) strengths is an open question.

Frequently, the interpretation of thermal neutron capture spectra is complicated by the influence of bound levels. A distinction between potential and resonant channel capture is difficult even in cases where a channel capture is suggested. These difficulties can be overcome by measurements near the corresponding neutron resonances.

In principle, the potential cross-section can be proved with great sensitivity in the vicinity of resonances by means of interference effects of the partial capture cross-sections for final levels with $l_n = 1$. However, the mutual phases between potential capture and interfering resonances permit, in general, several interpretations. Reliable identifications for a potential capture have been found for the target nuclei ^{59}Co , ^{207}Pb and ^{238}U [29]. The partial potential cross-section observed for the ground-state transition in ^{60}Co (≈ 10 mb at 1 eV) agrees reasonably with the estimated value (≈ 20 mb at 1 eV) for a pure single-particle level [2, 4] taking into account the single-particle strength of this level. On the other hand, the dependence of the partial cross-sections of $^{55}\text{Mn}(n, \gamma)$ and $^{197}\text{Au}(n, \gamma)$ in the neighbourhood of the lowest neutron resonances could be explained by the influences of the neighbouring resonances, i.e. without a potential capture [30].

We wish to refer to the fact that a dominant resonant channel capture can be expected in some resonances in the keV region [4]. According to Eq.(2) these are resonances with reduced scattering widths at least one order of magnitude larger than their gamma widths. The resonances for nuclei of masses $40 \leq A \leq 65$ are compiled in Table II. The last column shows that beside ^{51}V and ^{54}Fe an influence of these resonances on the channel part of the thermal capture cannot be expected.

The experimental identification of a dominant channel capture expected for these resonances is possible for even target nuclei by comparison with (d, p) results, whereas in odd target nuclei a calculation of the primary gamma transitions by means of known wave functions for the initial and final states must be performed.

Until now neutron capture gamma spectra are very difficult to investigate in the keV resonances, because the capture cross-sections in the scattering resonances listed in Table II are very small. However, the example of $^{55}\text{Mn}(n, \gamma)$ [31] shows that such experiments can be carried out. (In the special case of $^{55}\text{Mn}(n, \gamma)$ the two resonances at 1 and 2 keV are not yet sufficiently separated to permit an interpretation of the capture mechanism.)

TABLE II. NEUTRON $s_{1/2}$ RESONANCES FOR WHICH A DOMINANT CHANNEL CAPTURE IS TO BE EXPECTED
The resonance parameters are taken from Ref. [32]

Target nucleus	E_{res} (keV)	I_i	Γ_n^0 (eV)	Γ_γ (eV) ^a	Influence on σ_{th}
^{48}Ti	17.34		57		0.1
^{51}V	4.16	4	7.9		0.25
	6.84	3	15.5		0.2
	11.75	3	51	2.3	0.5
^{50}Cr	5.5		21		0.2
^{53}Cr	4.2		7		0.3
^{55}Mn	2.37	3	8.2		0.2
^{54}Fe	7.25		13	3	0.55
	8.0		11		0.35
^{57}Fe	3.9	0	3.2	1	0.1
	6.1	1	5.3	1.7	0.2
^{59}Co	5.01	3	9.2	1	0.03
^{58}Ni	15.5		12		0.05
^{60}Ni	12.5		23		0.3
^{62}Ni	4.6		19		0.2

^a If not measured then $\Gamma_\gamma \approx 1$ eV can be used.

4. CONTRIBUTIONS OF FURTHER CONFIGURATIONS IN THE CAPTURE STATE

The description of the primary transition probabilities by channel capture is possible only in a few special cases. In general several configurations in the compound state contribute to the primary gamma transitions. Consequently, further configurations in the final levels can play an essential role.

It is necessary to confine ourself to relative simple configurations in the capture state because the number of configurations rises very quickly with their complexity and generates immense difficulties in interpretation. This limitation is approximately valid if only primary transitions to low-lying levels of the product nucleus are considered. In general, these levels contain only a few important simple configurations and E1 transitions can take place only from similar simple configurations in the capture state.

In several cases the influence of such configurations on the primary gamma spectra could be verified. As in the preceding discussions the most important method is the comparison of (n, γ) and (d, p) reactions for the same target nucleus. For the description of the transition probabilities in both reactions we expand the final states in terms of parent states of $(N-1)$ nucleons coupled with a nucleon $|s \ j_f; j_f\rangle$ [23, 33]

$$|(\alpha_f) I_f\rangle_a = \sum_{\beta_f J_f j_f} C_{\gamma I_f}(\beta_f J_f \alpha_f I_f) \{ \beta_f J_f \}_a j_f; \alpha_f I_f \rangle \quad (7)$$

where \rangle_a denotes total antisymmetrization, and α and β are additional quantum numbers omitted in the following. The coefficients $C_{\beta} (J, I_f)$ contain cfp's, statistical factors and 6j-symbols caused by the change of the coupling scheme. The components in Eq.(7) which have the target ground state as parent state contribute to the spectroscopic factors of the (d, p) reaction and were already used in Eq.(5). If the capture state is expanded in the same way as the final states, the reduced probabilities of the primary transitions are given by

$$B(E1; I_i \rightarrow I_f) \sim (2I_f + 1) \cdot \left| \sum_{J_i j_i} C_{j_i I_f} C_{j_i I_i} (-1)^{J_i + j_i + I_f} \begin{Bmatrix} j_f & j_i & 1 \\ I_i & I_f & J \end{Bmatrix} \langle j_f || \mathcal{M}_N(E1) || j_i \rangle \right|^2 \quad (8)$$

with the conditions $\beta_f = \beta_i = \beta$ and $J_f = J_i \pm J$; ($\mathcal{M}_N(E1)$ operates only on the particle with number N).

Contrary to the (d, p) reaction all configurations with common parent states in the initial and in the final state and with allowed E1 transitions between j_i and j_f contribute to the (n, γ) reaction. In Eq.(7) neutrons and protons are not distinguished. Thus neutrons as well as protons contribute to the primary gamma transitions. Further, the influence of configuration mixing in the capture state as well as in the final state is visible. Hence it follows, that for each gamma transition several single-particle states can contribute. So, for instance, besides the configuration of the entrance channel $|\{\beta_0 J_0\}_a j; I_i\rangle$ with $j = s_{1/2}$ also the configurations with $j = d_{3/2}$ and $d_{5/2}$ (if contained in the capture state) can contribute to the primary gamma

TABLE III. COMPARISON OF SPECIAL PRIMARY TRANSITION PROBABILITIES FOR EVEN-EVEN TARGET NUCLEI

Final nucleus	Level E_x (MeV)	I_n	$(I_\gamma/E_\gamma^3)_{rel.}$	$\left(\frac{I_\gamma/E_\gamma^3}{(2I+1)S}\right)_{rel.}$	References
^{41}Ca	1.95	1	1	1	[11,12]
	3.95	1	1.2	2.9	
	4.76	1	0.8	7	
^{49}Ti	1.38	1	1	1	[13,14,35]
	1.72	1	0.85	3.5	
	4.66	1	0.35	3	
	5.12		0.70		
^{53}Cr	0	1	1	1	[17, 36]
	2.32	1	1.1	2	
	2.70	1	0.55	>15	
	3.61	1	0.75	2	
^{55}Fe	0	1	1	1	[19,37]
	3.02	1	0.2	8	
	3.91	1	0.1	4	
	4.49	1	0.4	≈ 20	
	4.71	1	0.35	4	
^{57}Fe	0.014	1	1	1	[21,38-40]
	0	1	1	6	
	1.62	1	0.8	≈ 20	
	1.73	1	0.8	≈ 10	
	3.42	1	0.9	≈ 10	
	2.38		0.4		
	3.18		0.15		
	3.24		0.35		
	3.79		0.45		
	4.20		1.1		
	4.36		1		
	4.45		0.65		
	4.68		0.55		

TABLE IV. COMPARISON OF SPECIAL PRIMARY TRANSITION PROBABILITIES FOR ODD TARGET NUCLEI

Final nucleus	Level E_x (MeV)	l_n	$(I_\gamma/E_\gamma^3)_{\text{rel.}}$	$\left(\frac{I_\gamma/E_\gamma^3}{(2I+1)S}\right)_{\text{rel.}}$	References
^{40}K	2.04	1	} = 3	1	[4, 23, 41]
	2.07	1			
	2.10	1			
	2.29	(1)	0.85	> 50	
	2.41	1	2.2	> 50	
	2.80	1	0.9	> 50	
	3.59	1	0.7	> 40	
	2.34		0.35		
	2.36		0.3		
	2.72		0.7		
	2.98		0.3		
	3.12		0.35		
	3.43		1.8		
	3.66		1.9		
	0.03	3	0.4	0.35	
	0.80	3	0.55	0.4	
^{46}Sc	2.86	1	} = 3	1	[4, 23]
	2.70	1			
	2.44	1			
	1.92	1	1.5	> 30	
	2.41	1	0.9	> 5	
	0.58		1.4		
	0.63		0.4		
	2.20		0.7		
	2.41		0.75		
	0.23	3	0.7	0.25	
	0.44	3	0.35	0.23	

transitions. Such $l_n = 2$ contributions in the capture state can decay to low lying p-states ($l_n = 1$) as well as to f-states ($l_n = 3$). Consequently, one can find evidence for the components 'target ground state + d-particle' in the capture state from primary transitions to final levels with $l_n = 3$. Because we consider only E1 transitions, the method is limited to target nuclei with $J_0 \neq 0$, generally, that means to odd-odd and even-even final nuclei. However, in the same way other configurations leading by E1 transitions to the same final configurations are conceivable but the present methods are not yet able to examine their contributions in the capture state.

5. EVIDENCE FOR CONFIGURATIONS BESIDE THE ENTRANCE CHANNEL

Until now, we considered such configurations in the capture state which can populate low-lying levels (with simple structure) by E1 transitions. Guided by the resonance structure of doorway states, we can expect that only a few of these configurations play an essential role in the capture mechanism.

In section 3 we mentioned an attempt to regard the simplest doorway configuration in the $^{51}\text{V}(n, \gamma)^{52}\text{V}$ reaction. However, this method fails, if several doorway states are responsible for the gamma transitions because of the increasing number of free parameters. In spite of this, qualitative hints to special doorway configurations in the capture state can be obtained by strong primary gamma transitions to $l_n = 3$ levels and also to levels which are not or only weakly populated in the (d, p) reaction. In Tables III and IV a few examples are given for such cases. For even target nuclei (Table III) the values I_γ/E_γ^3 and $(I_\gamma/E_\gamma^3)/(2I+1)S$ are given relatively to a level with $l_n = 1$ excited strongly in both reactions. For odd target nuclei these values are related to $\Sigma(I_\gamma/E_\gamma^3)/\Sigma(2I+1)S$ for the levels marked }.

Strong primary gamma transitions to $l_n = 3$ levels have been observed in the odd-odd product nuclei ^{40}K , ^{46}Sc and ^{60}Co [23, 24, 26]. In ^{40}K the $f_{7/2}$ -strength of the neutron group is concentrated mainly within the ground-state multiplet with the spins $I_f = 2^-$ up to 5^- . The levels with $I_f = 2^-$ and 3^- can be reached by E1 radiation from the capture states ($I_i = 1^+$, 2^+) and they will be populated by strong primary gamma-ray transitions. In ^{46}Sc also strong primary gamma transitions to the $l_n = 3$ levels at 228 and 444 keV have been observed, and weaker transitions to the levels at 0 and 838 keV. The $l_n = 1$ strengths for the considered levels in ^{40}K and ^{46}Sc are too small and not able to explain the gamma transitions. Possibly these transitions are caused by configurations 'target ground state + f-neutron' in the final states and 'target ground state + d-neutron' in the capture state. Further strong transitions to levels with $l_n = 3$ have been found in ^{56}Mn and ^{60}Co . In these cases the interpretation is more difficult because of the strong configuration mixing between $f_{5/2}$ and $p_{1/2, 3/2}$ single-particle states.

For even target nuclei the variation of $(I_\gamma/E_\gamma^3)/(2I+1)S$ for states with $l_n = 1$ shows directly the influence of configurations different from the entrance channel. In many cases variations of a factor of 2...3 have been found (Table III). Here it should be expected that these 'other' configurations contribute with about the same strength to these primary transitions

as the entrance channel. On the other hand, strong primary transitions have been observed also to levels excited very weakly in the (d, p) reaction, for instance in the cases of $^{41}\text{Ca}(4.76 \text{ MeV})$, $^{53}\text{Cr}(2.70 \text{ MeV})$, $^{55}\text{Fe}(4.49 \text{ MeV})$ and $^{57}\text{Fe}(1.62; 1.73; 3.42 \text{ MeV})$. Here the primary gamma-ray transitions must be caused completely by configurations different from the entrance channel. The same should be true also in some cases where the l_n values are not known.

For odd target nuclei the situation is much more complicated because generally two initial states contribute and strong mixings of $p_{1/2}$ and $p_{3/2}$ single-particle states are possible. But in these cases such extreme variations of $(I_\gamma/E_\gamma^3)/(2I+1)S$ also occur. As examples we refer to the levels in ^{40}K with $l_n = 1$ and $E_x > 2.2 \text{ MeV}$ and also to the level at 1.92 MeV in ^{46}Sc (Table IV). The primary transitions to these states must originate also from configurations in the capture state which are different from the entrance channel.

Qualitative hints to the special configurations in the capture state giving rise to these 'anticorrelations' may be obtained from the structure of the final states, but in most cases such information is not available. Only for ^{46}Sc information about the level structure of low-lying states exists from the $^{47}\text{Ti}(d, ^3\text{He})^{46}\text{Sc}$ reaction [42]. Here a strong transition with $l_p = 2$ has been found to $E_x \approx 0.6 \text{ MeV}$. In the (d, p) reaction two states at $E_x = 0.58$ and 0.62 MeV are populated weakly, their l_n -values are not known [43]. Both levels are excited strongly by primary transitions in the (n, γ) reaction. If in all three reactions the same levels are populated, then the gamma transitions could be caused by the proton-hole configuration $(d_{3/2}^{-1}f_{7/2}^2)$ in the final states. But here it should be noted that in this case the primary transitions have M1 character.

Finally it should be emphasized that doorway configurations also exist that show a similar behaviour for gamma transitions to low-lying levels as the case of channel capture. As an example the reaction $^{54}\text{Fe}(n, \gamma)^{55}\text{Fe}$ will be used. The ground state of the target nucleus and the low-lying levels of the final nucleus can be described by the configurations $|f_{7/2}^{-2}; 0\rangle$ and $|f_{7/2}^{-2}(J) j; I_f\rangle$, respectively, where $J = 0, 2, 4, 6$ and $j = p_{3/2}, p_{1/2}, f_{5/2}$ [44]. It is easy to show that doorway states in the configuration space $|(f_{7/2})_0^{-2} (j_1^{-1} j_2) j; I_1\rangle$ with $j = p_{3/2}$ and $p_{1/2}$ (neutron) and a particle-hole excitation $(j_1^{-1} j_2)$ (proton or neutron) lead to the same relations for the transition probabilities as in the case of the entrance channel $|(f_{7/2})_0^{-2} j = s_{1/2}; I_1\rangle$ if we consider only transitions to final levels with the same spin. Because E1 transitions can excite levels with the two spins 1/2 and 3/2, differences in the relations between these two groups of final levels are expected. Of course, the distinction of various configurations in the capture state should be visible at higher final levels, but here an interpretation is more difficult.

6. CONCLUSIONS

Investigations of thermal neutron capture refer to the fact that in some cases only the entrance channel and a few doorway states play an essential role. The situation for the channel part of the reaction is relatively simple. However, the methods of interpreting thermal neutron capture gamma spectra are, in general, not able to decide between potential and resonant channel capture. Additional criteria, e.g. the value of the capture cross-

section or the influence of the neighbouring resonances, are used to get information about these details (Table I).

Contrary to this, investigations in the neutron resonances seem to be more suitable. In addition to the method of the search for a potential capture by asymmetries in the resonance cross-sections it is proposed to prove some special $l=0$ resonances in the keV region for a dominant channel capture (Table II).

Indications of other simple configurations in the capture states (perhaps doorway states) cannot be easily interpreted. While spectroscopic evidence for certain doorway states in some cases have been obtained, in general, a calculation fails because phases and amplitudes of such configurations in the capture state and also the structure of the final states are unknown.

REFERENCES

- [1] GROSHEV, L. V., DEMIDOV, A. M., *Atomn. Energ.* 3 (1957) 91; BARTHOLOMEW, G. A., CAMPION, P. J., KNOWLES, J. W., MANNING, G., *Proc. Conf. Neutron Interactions with the Nucleus*, New York (1957) 252.
- [2] LANE, A. M., LYNN, J. E., *Nucl. Phys.* 17 (1960) 563, 586.
- [3] BOCKELMAN, C. K., *Nucl. Phys.* 13 (1959) 205.
- [4] GERSCH, H. U., *Rep. ZfK-136* (1968); *Fortschr. Phys.* 17 (1969) 313.
- [5] LYNN, J. E., *Proc. Conf. Direct Interactions and Nuclear Reaction Mechanisms*, Padua (1962).
- [6] MORINAGA, H., ISHII, C., *Progr. theor. Phys.* 23 (1960) 161.
- [7] HUGHES, L. B., KENNETT, T. J., PRESTWICH, W. V., *Nucl. Phys.* 80 (1966) 131.
- [8] SKEPPSTEDT, Ö., HARDELL, R., ARNELL, S. E., *Chalmers University, Göteborg* (1967).
- [9] LYCKLAMA, H., ARCHER, N. P., KENNETT, T. J., *Nucl. Phys.* A100 (1967) 33.
- [10] GRUPPELAAR, H., SPILLING, P., *Rep. FOM 23607*, Utrecht (1967).
- [11] BELOTE, F. A., SPERDUTO, A., BUECHNER, W. W., *Phys. Rev.* 139 (1965) B80.
- [12] GRUPPELAAR, H., SPILLING, P., SPITS, A. M. J., *Nucl. Phys.* A114 (1968) 463.
- [13] BARNES, P. D., COMFORT, J. R., BOCKELMAN, C. K., HANSEN, O., SPERDUTO, A., *Phys. Rev.* 159 (1967) 920.
- [14] KLEINWÄCHTER, P., in preparation.
- [15] DAVID, P., *Thesis*, Bonn (1967).
- [16] BARTHOLOMEW, G. A., EARLE, E. D., GUNYE, M. R., *Can. J. Phys.* 44 (1966) 2111.
- [17] BOCK, R., DUHM, H. H., MARTIN, S., RÜDEL, R., STOCK, R., *Max-Planck-Institut für Kernphysik*, Heidelberg, 1965/V/5.
- [18] BARTHOLOMEW, G. A., GUNYE, M. R., *Can. J. Phys.* 43 (1965) 1128.
- [19] FULMER, R. H., MCCARTHY, A. L., *Phys. Rev.* 131 (1963) 2133.
- [20] ARNELL, S. E., HARDELL, R., HASSELGREN, A., JONSSON, L., SKEPPSTEDT, Ö., private communication.
- [21] GROSHEV, L. V., DEMIDOV, A. M., KOTELNIKOV, G. A., LUTSENKO, V. N., *Nucl. Phys.* 58 (1964) 465; *Izv. Akad. Nauk SSSR, Ser. fiz.* 28 (1964) 1234.
- [22] GROSHEV, L. V., DEMIDOV, A. M., SHADIEV, N., *Jaderná Fiz.* 3 (1966) 444.
- [23] RUDOLPH, W., *Rep. ZfK-PhA 24* (1967).
- [24] ALEXANDER, K. F., GERSCH, H. -U., RUDOLPH, W., *Congrès International de Physique Nucléaire (Proc. Congr. Paris, 1964) 2*, Paris (1964) 415.
- [25] HARVEY, J. A., WEITKAMP, C. C., CAMPBELL, E. C., SLAUGHTER, G. C., *Proc. Conf. Nuclear Physics*, Tokyo (1967).
- [26] GERSCH, H. U., RUDOLPH, W., ALEXANDER, K. F., *Nucl. Phys.* 54 (1964) 405.
- [27] GIPPNER, P., GERSCH, H. -U., RUDOLPH, W., *Int. Symp. Nuclear Structure, Dubna, 1968*, Dubna publication D-3893 (1968) 103.
- [28] GERSCH, H. -U., RUDOLPH, W., *Int. Symp. Nuclear Structure, Dubna, 1968*, Dubna publication D-3893 (1968) 104.

- [29] WASSON, O.A., BHAT, M.R., CHRIEN, R.E., LONE, M.A., BEER, M., Phys. Rev. Lett. 17 (1966) 1220; BROOMHALL, G.J., BIRD, J.R., Nucl. Phys. A121 (1968) 329; CHRIEN, R.E., PRICE, D.L., WASSON, O.A., BHAT, M.R., LONE, M.A., BEER, M., Physics Lett. 25B (1967) 195.
- [30] WASSON, O.A., DRAPER, J.E., Nucl. Phys. 73 (1965) 499; WASSON, O.A., CHRIEN, R.E., BHAT, M.R., LONE, M.A., BEER, M., Phys. Rev. 173 (1968) 1170.
- [31] PRESTWICH, W.V., COTÉ, R.E., Phys. Rev. 155 (1967) 1223.
- [32] GORDEEV, I.V., KARDASHEV, D.A., MALYSHEV, A.V., Jaderno-fizičeskie Konstanty, Moskva (1963); STEHN, J.R., GOLDBERG, M.D., MAGURNO, B.A., WIENER-CHASMAN, R., Rep. BNL 325 (1964).
- [33] LANE, A.M., WILKINSON, D.H., Phys. Rev. 97 (1955) 1199.
- [34] BARTHOLOMEW, G.A. et al., Compendium of Thermal-Neutron-Capture Gamma-Ray Measurements. Part I. $Z \leq 46$ Nuclear Data A3 (1967).
- [35] RASMUSSEN, N.C., HUKAI, Y., INOUE, T., ORPHAN, V.J., Prepublication copy of MITNE-85.
- [36] RUDAK, E.A., FIRSOV, E.I., Nuclear Data A3 (1967) 482.
- [37] ARNELL, S.E., Nuclear Data A3 (1967) 505.
- [38] IKEGAMI, H., EMERY, G.T., Phys. Rev. Lett. 13 (1964) 26.
- [39] COHEN, B.L., FULMER, R.H., MCCARTHY, A.L., Phys. Rev. 126 (1962) 698.
- [40] BJERREGAARD, J.H., DAHL, P.F., HANSEN, O., SIDENIUS, G., Nucl. Phys. 51 (1964) 641; SPERDUTO, A., BUECHNER, W.W., Phys. Rev. 134 (1964) B142.
- [41] KENNETT, T.J., HUGHES, L.B., PRESTWICH, W.V., Nuclear Data A3 (1967) 444.
- [42] YNTEMA, J.L., SATCHLER, G.R., Phys. Rev. 134 (1964) B976.
- [43] RAPAPORT, J., SPERDUTO, A., BUECHNER, W.W., Phys. Rev. 151 (1966) 939.
- [44] MAXWELL, J.R., PARKINSON, W.C., Phys. Rev. 135 (1964) B82; VERVIER, J., Nucl. Phys. 78 (1966) 497; OHNUMA, H., Nucl. Phys. 88 (1966) 273; RUDOLPH, W., GERSCH, H.-U., GIPPER, P., Rep. ZfK-150 (1968).

STATISTICAL CALCULATIONS OF NEUTRON CAPTURE RADIATION*

T. von EGIDY

Physics Department,
Technische Hochschule,
Munich, Federal Republic of Germany

Abstract

STATISTICAL CALCULATIONS OF NEUTRON CAPTURE RADIATION. The capture gamma-ray spectrum, the multiplicity, the population of the levels (isomer ratio) and the line density is calculated with a computer program using formulas for the level density and transition probability. With parameters for the level density and for the transition probability from other experiments good agreement is achieved in many cases. The number of detected lines in a spectrometer is expected to increase with about the square root of the sensitivity of a spectrometer.

1. INTRODUCTION

Measurement of thermal neutron capture radiation is used in most cases to develop the lower part of the level scheme of the final nucleus. But more information can be gained from neutron capture radiation. The numerous lines from the capture state to the intermediate levels and from the intermediate levels to the discrete low levels depend on the level density and transition probability. I would like to discuss the difficulties and some results of calculations which relate the level density and the transition probability to the whole measured capture radiation.

There are several thousand levels between the compound state and the ground state in heavier nuclei. Since most of these levels, their spins and parities or even the respective transition probabilities are not known, statistical assumptions on level density, spin distribution and transition probability must be used to calculate the neutron capture spectrum. It is obvious that the formulas for level density and transition probability, which are also not so well known, are a rough simplification. All special relations between levels are neglected, such as exist, for instance, in rotational bands. The K quantum number is not used. Anomalies in the capture spectrum cannot be explained by statistical calculations such as the 'gold bump' at 5 to 6 MeV, discussed by Bartholomew [1], or the strong transitions from the capture state in ^{114}Cd [2] and ^{165}Dy [3] to levels near 3 MeV. But it should be possible to get some information on the usefulness of a statistical model.

The publications on a statistical model for neutron capture radiation discuss two questions: (1) isomer ratios and (2) calculation of the neutron capture gamma spectrum, especially of the unresolved part above 2 MeV.

Huizenga and Vandenbosch [4, 5] describe a simple model to calculate isomer ratios. This model has been used and improved by many authors [6-9]. Pönitz [10] suggests a cascade model for the calculation of isomer ratios. Several publications apply this or similar models [10-15].

* Part of a Habilitationsschrift, Technische Hochschule, Munich, 1968.

Neutron capture gamma spectra were first calculated by Blatt and Weisskopf [16] and later dealt with in many papers [17-21]. All these calculations use integrals over line density times transition probability. They consider only dipole transitions in most cases. By this method of integrals the property that the spectrum consists of discrete lines gets lost. All these calculations for isomer ratios and gamma spectra provide arguments for level density formulas, spin cut-off factor and transition probabilities.

2. CALCULATIONS

A computer program similar to the cascade model of Pönitz [10] was developed to calculate all values which have a relation to a statistical model. The program requires a knowledge of the spin and the parity of the ground state, of the known levels and of the compound state and formulas for the level density and for the transition probability. Known low levels are treated individually, but the unknown levels are put together in groups with same spin J , same parity π and similar energy $E \pm dE/2$. The program calculates step by step the transitions from the compound state to all groups and to the discrete levels. Transitions within one group are neglected. All multiplicities are possible, but the program considers only the smallest ones given by spin and parity difference. Only 0-0 transitions are not allowed. Conversion electrons are not especially considered because they are relevant only at small energies.

The transition probability $S(\Delta E, \Delta J, \Delta \pi)$ depends on energy, spin and parity differences. The Weisskopf estimate [22] was used. Since this is only an approximation, hindrance factors from the publication of Löbner [23] were added. These hindrance factors may have different values for low-energy and high-energy transitions and are interpolated. Table I lists the hindrance factors used.

The level density $\rho(E, J, \pi)$ is a function of the excitation energy, the spin and the parity. There are two formulas for the energy dependence: $\rho \propto e^{2\sqrt{a}E}$ and $\rho \propto e^{E/T}$. According to Gilbert and Cameron [24] the second formula fits better for energies below 5 MeV. Adding the spin distribution formula [24] we get the level density formula:

$$\rho(E, J, \pi) = \frac{1}{T(\pi)} e^{\frac{E-E_0(\pi)}{T(\pi)}} \frac{2J+1}{2\sigma^2} e^{-\frac{(J+\frac{1}{2})^2}{2\sigma^2}}$$

The parity dependence of the level density is not well known at high energies but is assumed to be the same for both parities at the neutron capture energy [25]. At low energy the parity dependence is evident by counting the known levels. The known level density at low energies and at neutron capture energies (from neutron resonances [25]) was used to determine the parameters T and E_0 . Considering several publications [7, 11, 26, 27] a spin cut-off factor $\sigma = 3$ (in some cases for comparison 4) was taken. It should be pointed out that the computer program does not fit parameters, but uses parameters from other experiments so that the

TABLE I. HINDRANCE FACTORS

ΔJ	1	2	3	≥ 4	
E {	ground state	5000	1	1	1
	compound state	1000	100	1	1
M {	ground state	200	10	100	1
	compound state	100	10	100	1

result can be compared with the neutron capture radiation. The parameters used in the calculations for ^{152}Eu , ^{165}Dy and ^{200}Hg are listed in Table II. The level groups in the calculation have a distance of 100 keV.

The partial population probability dW of a level (E, J, π) by a level (E', J', π') which has the population $W(E', J', \pi')$ is given by:

$$dW(E', J', \pi' \rightarrow E, J, \pi) = \frac{S(E' - E, |J' - J|, \pi' \cdot \pi) W(E', J', \pi')}{B(E', J', \pi')}$$

$B(E', J', \pi')$ is the total decay probability of a level:

$$B(E', J', \pi') = \sum_{\substack{E < E', J, \pi \\ \text{sum over level groups}}} \{S(E' - E, |J' - J|, \pi' \cdot \pi) \cdot \rho(E, J, \pi)\} + \sum_{\substack{E < E' \\ \text{sum over discrete levels}}} S(E' - E, |J' - J|, \pi' \cdot \pi)$$

The total population of a level $W(E, J, \pi)$ is:

$$W(E, J, \pi) = \sum_{\substack{E' > E, J, \pi \\ \text{sum over level groups}}} dW(E', J', \pi' \rightarrow E, J, \pi) \rho(E', J', \pi) + \sum_{\substack{E' > E \\ \text{sum over discrete levels}}} dW(E', J', \pi' \rightarrow E, J, \pi)$$

The total population $W(E, J, \pi)$ corresponds to the isomer ratio. The computer program calculates the population for all levels. The number of lines between two level groups is $\rho(E', J', \pi') \rho(E, J, \pi)$. The intensity of these lines is $dW(E', J', \pi' \rightarrow E, J, \pi)$. One can calculate the density of gamma lines as a function of the energy and the intensity $D(E, I)$ (number of lines per energy interval and per intensity interval). The sum over all intensities with the same energies gives the gamma spectrum $G(E)$:

$$G(E) = \sum_I I D(E, I) dI$$

TABLE II. PARAMETERS USED FOR CALCULATION

Nucleus Parity	¹⁵² Eu		¹⁶⁵ Dy		²⁰⁰ Hg	
	+	-	+	-	+	-
Low-energy level density per MeV	100	100	6	18	12	1
Resonance level density per MeV	1.3×10^6	-	10^4	-	-	1.4×10^4
Total level density at compound state for $\sigma = 3$	2.7×10^6	2.7×10^6	10^5	10^5	7×10^4	7×10^4
E_0 (MeV)	-2.24	-2.24	-0.43	-1.29	0.17	1.81
T (MeV)	0.598	0.598	0.561	0.633	0.756	0.588

This sum can be taken only over intensities less than the sensitivity limit of a spectrometer. Then only that part of the gamma spectrum is calculated which cannot be resolved by the spectrometer.

The multiplicity ν (average number of gamma rays emitted per neutron capture) is given by the formula:

$$\nu = \int_E G(E) dE$$

3. LINE DENSITY AND INTENSITY DISTRIBUTION

With increasing sensitivity and resolution of spectrometers the question arises how many more lines these new spectrometers can find. If the line density increases faster than the resolution of the spectrometer, one cannot use the improved sensitivity of the spectrometer since it is no longer possible to separate the lines. It is one of the purposes of this paper to give an answer to this question.

Many low-energy capture gamma-ray spectra have been measured with the crystal spectrometers in Argonne and in Risø. The number of lines per 100 keV and per half intensity decade ($\Delta \log I = \Delta I/I = 0.5$) were counted in 18 spectra. It is obvious that nuclei with different level density have different line density. The spectra were separated into even-even nuclei, even-odd and odd-even nuclei and odd-odd nuclei and averaged. The result is shown in Fig. 1 which gives in a double logarithmic scale the number of lines per intensity interval. This graph demonstrates that

FIG.1. Average line density between 100 and 700 keV.

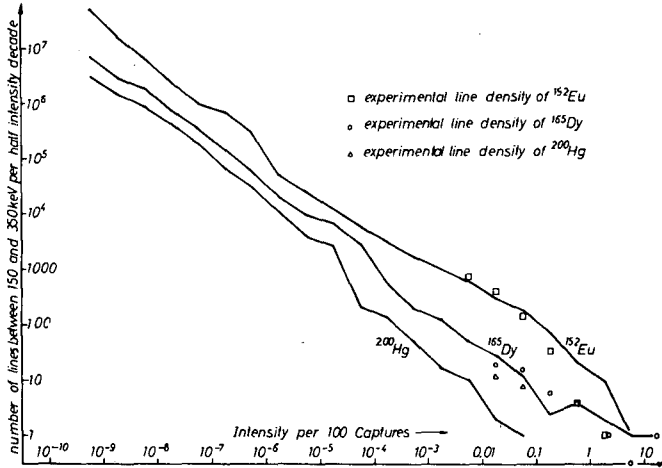
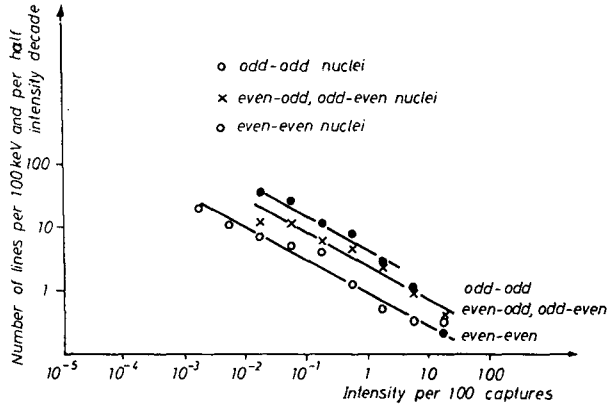


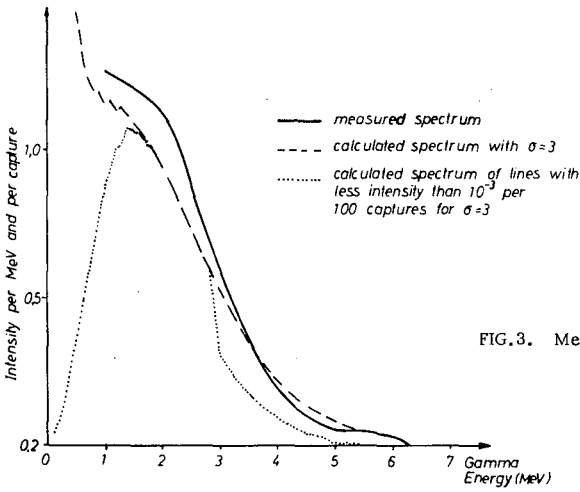
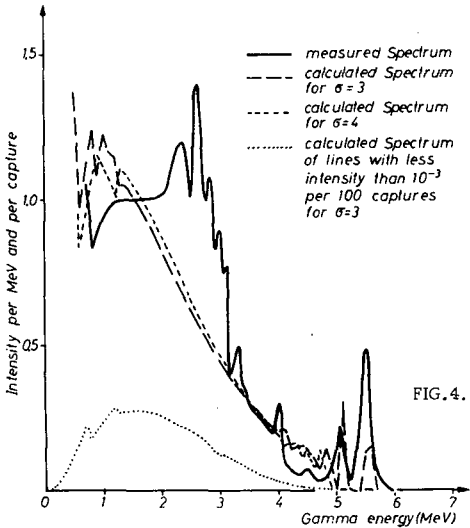
FIG.2. Calculated and measured line density of ²⁰⁰Hg, ¹⁶⁵Dy and ¹⁵²Eu between 150 and 350 keV.

the line density increases with about the same rate independently of the level density. There is a nearly linear relation in a double logarithmic scale. Only odd-odd nuclei have too few intense lines as is easy to understand.

One sees in a similar presentation in Fig.2 the measured line densities of ¹⁵²Eu [28], ¹⁶⁵Dy [29] and ²⁰⁰Hg [30] together with calculated values. Except for ²⁰⁰Hg, the agreement between the experimental values and the calculation is good. The line density shows a similar behaviour as in Fig.1. Therefore we conclude for the checked nuclei the following approximate relation between line density D and intensity I:

$$D(E, I) = C(E) \cdot (I_0/I)^a$$

with $a = 0.6 \pm 0.2$. C(E) depends on the energy region and level density; I₀ is a constant. This means that when the sensitivity of a spectrometer is increased by a factor of 10, the number of lines increases by a factor of 4 ± 2 . The line density grows at about the square root of the sensitivity.

FIG. 3. Measured and calculated spectrum of ^{152}Eu .FIG. 4. Measured and calculated capture spectrum of ^{165}Dy .

The low-energy line density gives an indication for the low-energy level density. The very high line density in ^{152}Eu (2600 lines between 30 and 700 keV [28]) can only be reproduced by a level density of 200 per MeV at low energies. This is reasonable since the high-energy capture gamma-ray data [31] already indicate 50 levels below 600 keV.

The line density changes only slightly when the spin cut-off factor in the level density formula is changed from 3 to 4.

4. GAMMA SPECTRUM

The gamma spectra of ^{152}Eu , ^{165}Dy and ^{200}Hg were calculated and compared with measured spectra of Groshev et al. [32] and of Bartholomew [33] (Figs 3-5). The general feature of the spectra is well reproduced,

FIG. 5. Measured and calculated capture spectrum of ^{200}Hg .

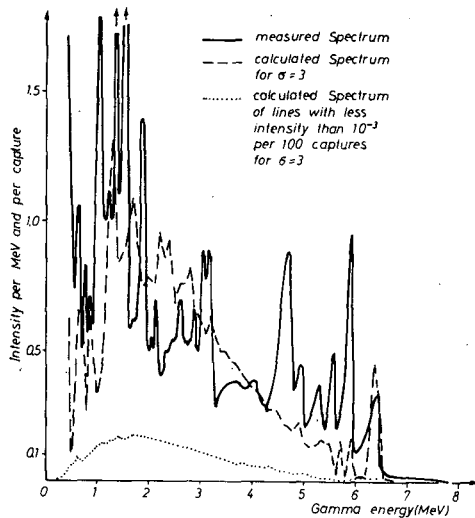
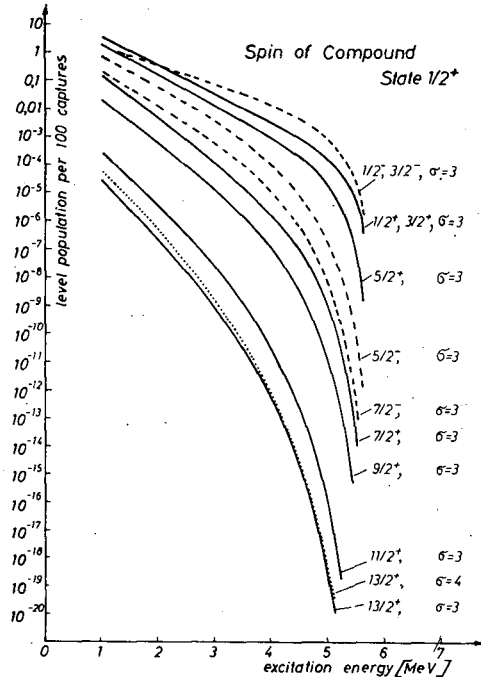


FIG. 6. Population of single levels in ^{165}Dy spin compound state $\frac{1}{2}^+$.



although some strong lines in ^{165}Dy and ^{200}Hg do not appear in the calculated spectrum. The spectrum of ^{165}Dy (Fig. 4) shows that the spin cut-off factor does not influence the calculated gamma spectrum very much.

The dotted spectra consist only of lines with an intensity less than 10^{-3} per 100 captures. This is the part of the spectrum that cannot be resolved. This is a small fraction in ^{165}Dy and ^{200}Hg . Nearly all lines around 2 MeV of ^{152}Eu are expected from this calculation to have too low intensity to be detectable.

TABLE III. MULTIPLICITIES

	Muehlhause [34]	Groshev et al. [20]	This work
^{152}Eu	3.8	3.5	4.9
^{165}Dy	3.7	3.9	4.2
^{200}Hg	3.3	3.3	3.6

The measured and calculated multiplicities of ^{152}Eu , ^{165}Dy and ^{200}Hg are listed in Table III.

The calculated values for ^{152}Eu and ^{165}Dy are too large because the conversion electron intensity is not included in the measurements but it is implicitly included in the calculations. There are no strong conversion lines in ^{200}Hg .

5. POPULATION OF LEVELS AND ISOMER RATIO

Following the decay of the compound state the levels are populated according to their energy, spin and parity. This is demonstrated by the calculated curves in Fig.6 for ^{165}Dy . It is interesting to see that the positive and negative parity levels are populated differently because of the positive parity of the compound state and the difference in transition probability for E1 and M1 transitions. A different spin cut-off factor of 4 does not change the population of single higher energy levels very much even if the spin is higher. The intensity of lines depopulating levels with certain energy, spin and parity can be estimated from this graph.

The calculated isomer ratio of ^{165}Dy is 0.66, the measured value is 0.654 ± 0.017 [35].

Figure 7 illustrates the total population of known levels with the same spin in a similar graph as in the publication of Schult et al. [7]. The agreement of calculation and measurement [3, 29] is very good. The small influence of the spin cut-off factor in this case is demonstrated.

The population of levels in ^{200}Hg is listed in Table IV. The agreement is not so good for all levels, but reasonable in many cases. This table gives an indication that one can guess the spin of a level from the population of a level.

The influence of the spin cut-off factor is seen only for very high spin states. The 8^- state in ^{152}Eu is populated according to Takahashi et al. [36] with 0.02 per 100 captures. At $\sigma = 4$ the population is calculated to 0.4, while at $\sigma = 3$ one gets 0.06.

6. CONCLUSION

The statistical calculations show that without fitting a parameter good agreement between the calculation and the experiment is achieved in many cases. The discrepancies illustrate the shortcomings of a statistical model. It is evident that the parameters in the level density

TABLE IV. POPULATION OF LEVELS IN ^{200}Hg

Energy	Spin	Measured population [30]	Calculated population	
			$\sigma = 3$	$\sigma = 4$
368	2	70	52	52
947	4	2.1	2.8	3.1
1029	0	6.0	6.6	6.5
1254	2	5.4	7.1	7.1
1570	1	11.2	6.9	7.4
1574	2	3.5	4.0	4.2
1594	(2)	2.9	4.0	4.2
1631	1	4.3	6.0	6.5
1642	(1)	2.9	6.0	6.5
1718	1	2.9	5.3	5.8
1731	(2)	2.3	2.8	3.0
1776	3	0.5	1.8	2.0
1846	(3)	0.3	1.5	1.7
1883	(2)	1.5	2.4	2.6

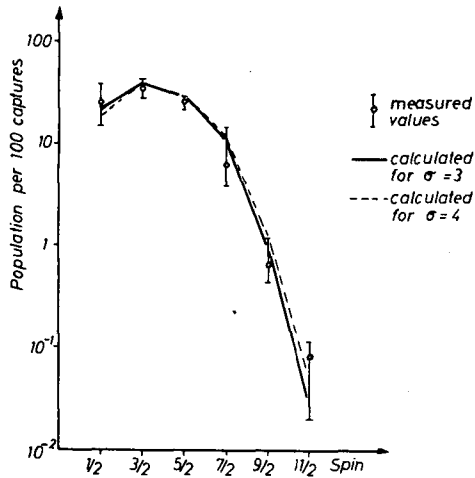


FIG. 7. Total population of levels in ^{165}Dy below 750 keV.

formula and transition probability formula can be checked more efficiently if not only the isomer ratio but also the gamma spectrum, the multiplicity, the line density and the population of all lower states are compared.

ACKNOWLEDGEMENTS

I should like to thank Prof. H. Maier-Leibnitz and Prof. H. Daniel for support and Dr. H. Vonach, Dr. O. Schult and Dr. G. Löbner for discussions.

REFERENCES

- [1] BARTHOLOMEW, G.A., "The 5.5-MeV gamma-ray anomaly, recent studies", these Proceedings.
- [2] von EGIDY, T., KAISER, W., Z. Phys. 201 (1967) 378.
- [3] DUTTA, B.C., von EGIDY, T., ELZE, Th.W., KAISER, W., Z. Phys. 207 (1967) 153.
- [4] HUIZENGA, J.R., VANDENBOSCH, R., Phys. Rev. 120 (1960) 1305.
- [5] VANDENBOSCH, R., HUIZENGA, J.R., Phys. Rev. 120 (1960) 1313.
- [6] VONACH, H.K., VANDENBOSCH, R., HUIZENGA, J.R., Nucl. Phys. 60 (1964) 70.
- [7] SCHULT, O.W.B., MAIER, B.P.K., GRUBER, U., KOCH, R., Z. Phys. 185 (1965) 295.
- [8] BISHOP, C.T., VONACH, H.K., HUIZENGA, J.R., Nucl. Phys. 60 (1964) 241.
- [9] MANNHART, W., VONACH, H.K., Z. Phys. 210 (1968) 13.
- [10] PÖNITZ, W.P., Z. Phys. 197 (1966) 262.
- [11] PAULSEN, A., Z. Phys. 205 (1967) 226.
- [12] SPERBER, D., Nucl. Phys. A90 (1966) 665.
- [13] SPERBER, D., MANDLER, J.W., Nucl. Phys. A113 (1968) 689.
- [14] SARANTITES, D.G., Nucl. Phys. A93 (1967) 576.
- [15] MALYSHEV, A.V., Sov. J. nucl. Phys. 6 (1967) 853.
- [16] BLATT, J.M., WEISSKOPF, V.F., Theoretical Nuclear Physics, J. Wiley and Sons, New York (1952) Chap. XII, 7. D.
- [17] STRUTINSKI, V.M., GROSHV, L.V., AKIMOVA, M.K., Nucl. Phys. 16 (1960) 657.
- [18] TROUBETZKOY, E.S., Phys. Rev. 122 (1961) 212.
- [19] BERGQUIST, I., STARFELT, N., Nucl. Phys. 39 (1962) 353.
- [20] GROSHV, L.V., DEMIDOV, A.M., LUTSENKO, V.N., PELEKHOV, V.I., Int. Conf. peaceful Uses atom. Energy (Proc. Conf. Geneva, 1958) 15, UN, New York (1958) 138.
- [21] STARFELT, N., Nucl. Phys. 53 (1964) 397.
- [22] BLATT, J.M., WEISSKOPF, V.F., Theoretical Nuclear Physics, J. Wiley and Sons, New York (1952) Chap. XII, 6. A.
- [23] LÖBNER, K.E.G., Physics Lett. 26B (1968) 369.
- [24] GILBERT, A., CAMERON, A.G.W., Can. J. Phys. 43 (1965) 1446.
- [25] LYNN, J.E., The Theory of Neutron Resonance Reactions, Clarendon Press, Oxford (1968) 114; 148.
- [26] BORMANN, A., Habilitationsschrift, Hamburg University (1965).
- [27] CHRIEN, R.E., MUGHABGHAB, S.F., BHAT, M.R., JAIN, A.P., Physics Lett. 24B (1967) 573.
- [28] MÜHLBAUER, K., Dissertation, Technische Hochschule München (1969).
- [29] SCHULT, O.W.B., MAIER, B.P., GRUBER, U., Z. Phys. 182 (1964) 171.
- [30] MAIER, B.P., GRUBER, U., KOCH, H.R., SCHULT, O.W.B., Z. Phys. 185 (1965) 478.
- [31] SHERA, E.B., Los Alamos, private communication (1969).
- [32] GROSHV, L.V., DEMIDOV, A.M., LUTSENKO, V.N., PELEKHOV, V.I., Atlas of Gamma Ray Spectra from Radiative Capture of Thermal Neutrons, Pergamon Press, London (1959).
- [33] BARTHOLOMEW, G.A., HIGGS, L.A., Rep. AECL 669 (1958).
- [34] MUEHLHAUSE, C.O., Phys. Rev. 79 (1950) 277.
- [35] TORNAU, R., Z. Phys. 159 (1960) 101.
- [36] TAKAHASHI, K., MCKEOWN, M., SCHARFF-GOLDHABER, G., Phys. Rev. 137 (1965) B763.

FAST NEUTRON CAPTURE

Chairmen: R. MORINAGA
W. MICHAELIS

Invited talk

THE 5.5-MeV GAMMA-RAY ANOMALY, RECENT STUDIES

G. A. BARTHOLOMEW
Atomic Energy of Canada Ltd.,
Chalk River, Ontario,
Canada

Abstract

THE 5.5-MeV GAMMA-RAY ANOMALY, RECENT STUDIES. The explanation of the 5.5-MeV gamma-ray anomaly as radiation from the decay of 3-quasiparticle configurations is consistent with gamma-ray strength function determinations and with experiments to excite those configurations selectively in the $^{207}\text{Pb}(p, p'\gamma)^{207}\text{Pb}$ reaction. Related experiments are reviewed.

This paper will go somewhat beyond the (n, γ) reaction, which is the main interest at this Symposium, but this departure is necessary to gain a full perspective on the anomalous radiation. We shall discuss mainly recent studies at Chalk River by E. D. Earle, A. J. Ferguson and myself in collaboration with I. Bergqvist of the University of Lund. In recent work we have been joined also by M. A. Lone.

By the anomalous radiation or 'anomalous bump' we refer to an increased intensity centred at 5.5 MeV in the spectral distribution of certain heavy elements. The effect is strongest in elements near Pb and decreases with A to disappear near Ta. This is illustrated in Fig. 1 which shows early Chalk River results. A weaker effect is found near the 82 neutron shell. The bump is a gross structure or statistical effect involving many gamma rays.

The spectral distribution $\nu_{E_x}^1(E_\gamma)$ for the primary gamma rays emitted from E_x is given in Fig. 2. It is proportional to the average partial radiation width $\bar{\Gamma}_{E_\gamma}$ divided by the spacing, $D'(E_x - E_\gamma)$, of levels at $(E_x - E_\gamma)$ that can be fed from E_x . This distribution takes the form of the full curve, ν^1 , if $\bar{\Gamma}_{E_\gamma}$ follows a power-law energy dependence and $D'(E_x - E_\gamma)$ an exponential energy dependence. The curve, ν_T , is the total spectral distribution including secondary cascade radiation. The primary spectrum can be rewritten in terms of a strength function $S(E_x, E_\gamma)$ as shown on the right in Fig. 2. Here $D(E_x)$ is the spacing of states of the same spin and parity. Converting spacing D' to D introduces the factor 3 and the proportionality constant becomes the total radiation width $\Gamma_\gamma(E_x)$ when the expression is normalized to unit population for level E_x .

The anomalous bump appears at 5.5 MeV as indicated by the broken curve in Fig. 2. It clearly represents a failure of the power law for $\bar{\Gamma}_{E_\gamma}$ or the exponential law for D , or both. The figure also shows that if we can unfold $\nu_{E_x}^1(E_\gamma)$ from the observed spectrum, ν_T , and if we adopt a realistic level-spacing formula, we can solve for $S/\Gamma_\gamma(E_x)$; and for S , itself, if we know the total radiation width.

TABLE I. PROPERTIES OF 5.5-MeV GAMMA-RAY ANOMALY

Reaction	Heavy targets	Properties	Ref.
Thermal (n, γ) spectra	Pb, Tl, Hg, Au, Pt, Ir, Re, W, Ta Cs, I, Sb, Ag, In	Amplitude decreases with A Weaker anomaly near N=82	[1] [1]
Thermal (n, γ) coincidences and $\gamma\gamma\theta$	Hg	\cong 45% primary	[2]
Thermal (n, γ) polarization correlation	Hg	\cong 85% E1	[3]
Resonance (n, γ)	Hg, Au, Pt	Present in resonances	[4, 5]
Resonance (n, γ)	U, Pb, Er, Ba, Sn, Pd	Individual strong M1 γ -rays	[6-11]
Resonance (n, γ)	Au	Primary, E1	[5]
Fast (n, γ)	Au, Ta, Cs, I, Sn, Ag	Energy invariant for $6.5 < E_x < 10.7$ MeV	[12, 13]
(d, γ)	Bi, Pb, Tl, Au, Pt, Ir, Re, Ta Cs, I, Sb, Ag, In	Similar to (n, γ), energy invariant, primary	[14]
(γ , n)	Pb	Individual strong M1 γ -rays	[15]
(n, n' γ)	Bi, Pb, Hg, Au, W, Ta, I, Ag	Not present	[16, 17]

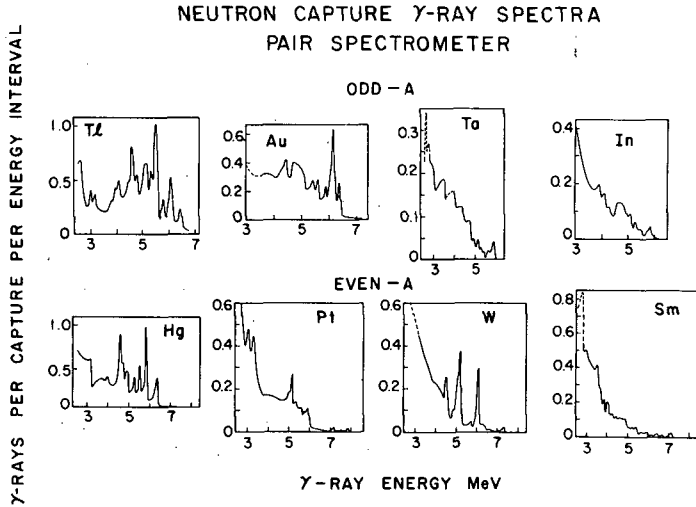


FIG. 1. Spectral distributions of elements near lead (Kinsey, B.B., Bartholomew, G.A., *Can. J. Phys.* **31** (1953) 927; 1025). The anomalous radiation is strongest in Tl and Hg and decreases with A until it disappears below Ta. The spectra of In and Sm are examples of essentially normal spectra.

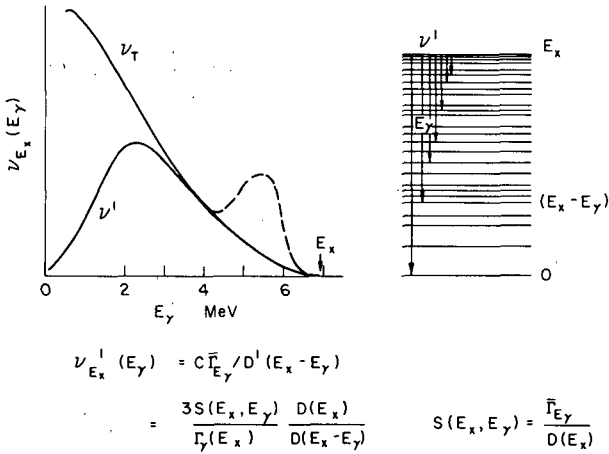


FIG. 2. Statistical spectral distribution.

The anomalous bump has been a matter of curiosity for many years. In Table I we attempt to summarize the main properties as determined in various experiments. To this we should now add the evidence from gamma-ray scattering presented by Moreh at this Symposium. The first item records the elements in which the effect is seen in thermal capture. The second and third items refer to coincidence, angular correlation, and polarization correlation measurements on ^{200}Hg at Chalk River which set lower limits for the amount of the bump that is primary radiation and the amount that is E1 in this particular nucleus. The fourth item records

that the bump is a resonance effect. We will return to this point later. The fifth entry records several experiments in which individual strong M1 gamma rays were detected near the high-energy end of the spectrum; the second last entry records the same conclusion from threshold photo-nuclear experiments on Pb. This list of M1 data is not exhaustive; a more complete summary is given by Bollinger [18]. The sixth item records the conclusion of Allen and Bird that bump gamma rays in Au are mostly primary and E1. The next item refers to the important observation of Lundberg and Starfelt and of Bergqvist and Starfelt that the bump remains at 5.5 MeV for all excitation energies up to that reached by 4.2-MeV neutron bombarding energy, which for gold is about 10.7 MeV. The next entry refers to the (d, p γ) work by Bergqvist, Earle, Ferguson and myself in which it was shown that the bump has very nearly the same energy, width, and A-dependence as in the (n, γ) reaction, that it is independent of excitation energy, and that it is mostly primary radiation. The last item calls attention to the observation of Perkin and Starfelt and of Bergqvist et al. that there is little, if any, evidence for the 5.5-MeV bump in the (n, n' γ) reaction.

Let me make the point now that, since the bump is independent of excitation energy and since it is mostly primary radiation as shown by several experiments listed in this table, it cannot be accounted for as

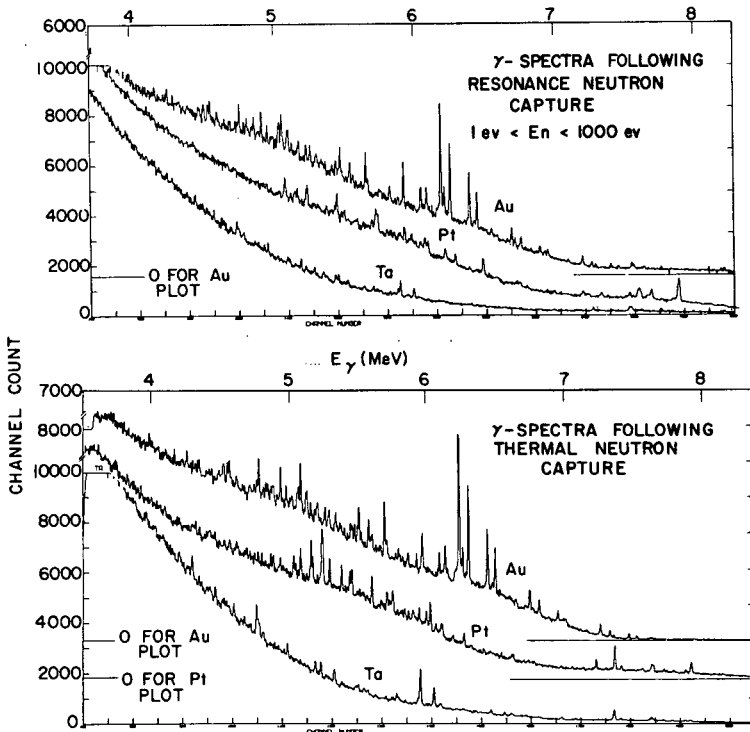


FIG.3. Comparison of spectra of Ta, Pt, and Au in the region of the bump [4]; thermal capture (lower) and summing over the resonance range 1-1000 eV (upper).

a peculiarity of the decay of certain favoured levels at a particular energy or as an effect of local departures from the exponential level spacing rule. It must therefore be caused by irregularities in the energy dependence of the partial radiation width or strength function [12].

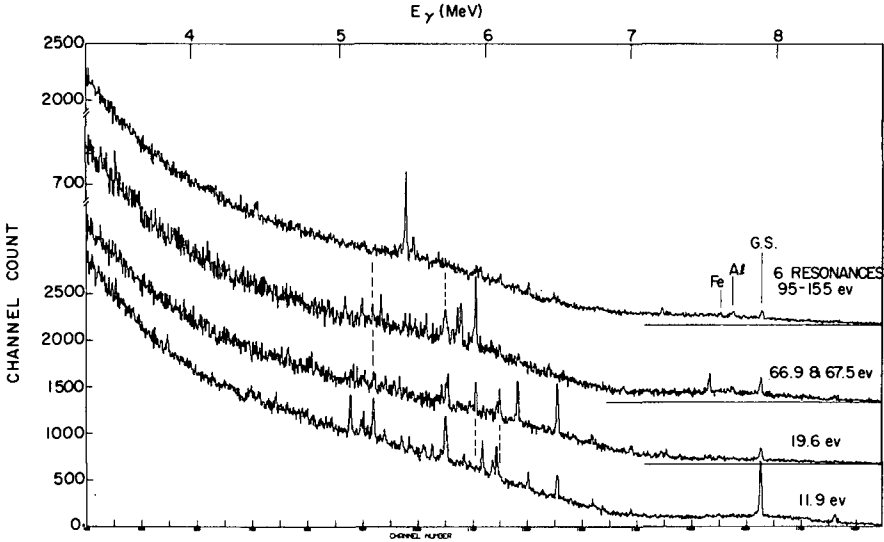


FIG. 4. Comparison of spectra in the region of the bump [4] for individual resonances in $^{195}\text{Pt}(n,\gamma)^{196}\text{Pt}$.

That the bump is a property of individual resonances, was brought out in recent measurements by Earle, Lone and myself [4]. In Fig. 3 the lower curves are spectra of Ta, Pt and Au from thermal capture and the upper curves are spectra of the same elements integrated between 1 and 1000 eV neutron energy. The two sets of spectra are much alike in gross shape although there are differences in detail. In Ta the bump is essentially absent while Pt and Au show the effect strongly. The spectra of several Pt resonances are shown separately in Fig. 4. Again, individual lines show Porter-Thomas fluctuations but the gross shapes are very much alike from resonance to resonance. There are exceptions to this uniformity in the recently reported results of Thomas et al. [19] in ^{198}Hg . Their data show strong gamma rays above 6 MeV and less intensity near 5.5 MeV in spectra from the 90 and 302-eV resonances while other resonances appear more normal. Nevertheless the bump, when it occurs, is present in individual resonances.

Now in interpreting these results we shall concentrate on the $180 < A < 208$ region where the effect is strongest. We have been led to favour a mechanism in which the 5.5-MeV radiation is emitted in particle-hole E1 transitions across the 126-neutron shell [14]. The unperturbed energies for such transitions tend to cluster near 5.5 MeV. The unperturbed energies for proton particle-hole E1 transitions, however, are spread over the range 7-12 MeV approximately so that in the approximation where residual interactions are ignored these configurations would

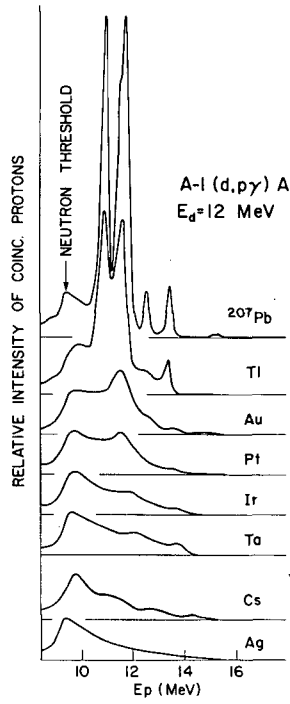


FIG. 5. Comparisons of particle spectra obtained in coincidence with gamma rays in (d, p γ) reaction [14]. The curves are normalized to equal amplitude at the neutron threshold.

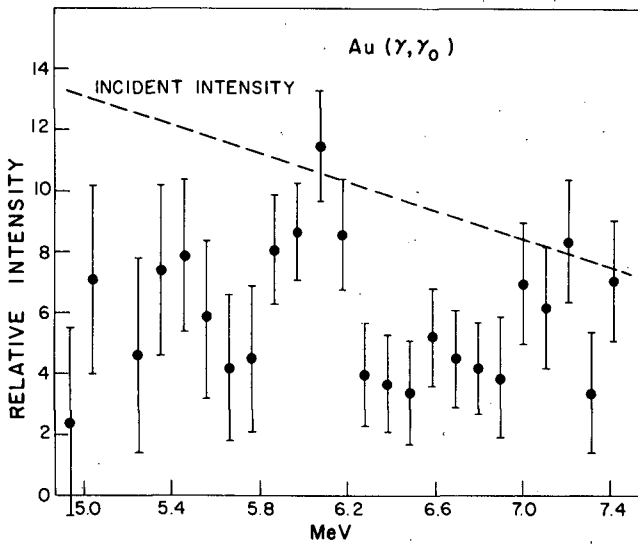


FIG. 6. Elastic photoexcitation relative yield for gold [26]. The data points have been corrected for the variation of incident intensity shown by the broken curve.

be expected to play only a small part at 5.5 MeV and not to give rise to a localized bump at higher energies. There is also the possibility [12] of M1 spin-flip transitions which, for both neutrons and protons, have about the same unperturbed energy of 5.5 MeV for large angular momentum orbits. These will give rise to enhanced M1 effects [20, 21]. While taking note of this fact we shall, to simplify discussion, concentrate on the E1 contributions which appear to dominate the effect at least in ^{198}Au and ^{200}Hg . The crucial observation from the fast neutron capture work [12, 13], backed up by the $(d, p\gamma)$ results [4], that the 5.5-MeV radiation is emitted from states over a wide range of excitation energy means that we cannot have simply a particle-hole excitation, but this particle-hole must be coupled to other excitations, i. e. to another quasiparticle or to a collective vibration, for example. For simplicity, we shall assume three-quasiparticle excitations, bearing in mind, however, that the weak coupling collective model [22] has been used with much success in this mass region [23]. In this spirit we might think of the bump gamma emission as a semidirect process or gamma decay from a doorway state [24, 25]. This is an attractive picture because it allocates the bump to a capture process between direct capture and compound nucleus capture. It remains to be demonstrated (a) that these 3-quasiparticle excitations are really the types of configuration responsible for the bump and (b) how the concentration of strength at 5.5 MeV fits with the E1 giant dipole theory. The experimental results to be described will be concerned mainly with our attempts to shed light on these questions.

A third question is: why is this radiation not evident at other mass numbers? A contributory reason would appear to be that the radiation does not remain localized near 5.5 MeV because shell spacings are not well-preserved far from closed shells. A measure of the range where shell effects are preserved is provided by the behaviour of 'single-particle' proton groups in the (d, p) reaction as one moves away from Pb toward the distorted nuclei [14]. This is demonstrated in Fig. 5 which shows that the strong single-particle groups (associated with transitions to $d_{5/2}$, $s_{1/2}$ and $d_{3/2}$ states in ^{207}Pb) become weaker and finally disappear below Ta, precisely where the gamma-ray bump disappears.

Let us now turn to the question of relating the 5.5-MeV radiation to the giant dipole resonance. From the particle-hole picture we would expect to see a peaking of the photoexcitation cross-section at 5.5 MeV and indeed, if one could do photonuclear reactions on excited states as targets, one would expect to see a peaking at 5.5 MeV in that cross-section also. The gamma-ray elastic scattering excitation function in Au recently obtained by Knowles [26] is shown in Fig. 6. Although the counting statistics are low, there is an unmistakable resonance near the expected energy. It must be remembered that this effect is not a precise parallel of the bump effect in the (n, γ) and $(d, p\gamma)$ reactions because, for example, different nuclei are involved and different angular momentum changes may, in general, be involved.

An important bridge to the photonuclear reaction was made by Starfelt [27] who demonstrated that the (n, γ) spectra can be fitted with an empirical strength function to reproduce the 5.5-MeV gamma-ray bump and, following a suggestion of Axel [28], this strength function can be related to the giant dipole resonance by making the assumption that excited states have associated with them giant resonances similar to that built on the ground

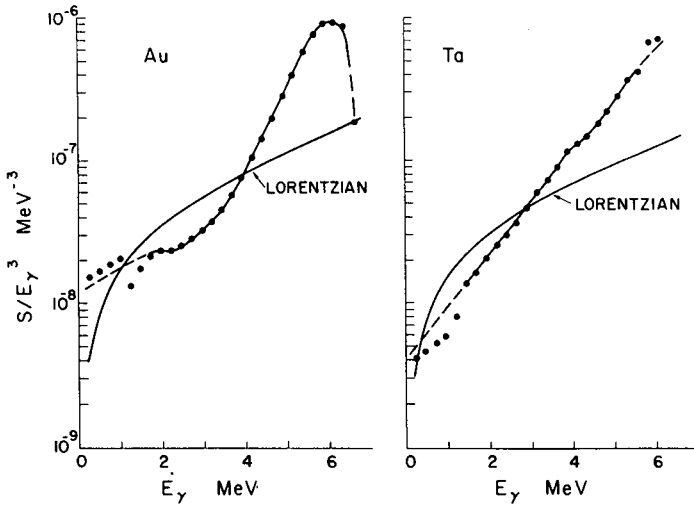


FIG. 7. Strength functions deduced from $(d, p\gamma)$ reaction [14] by procedure of Ferguson [29] (full circles) compared with that deduced from the Lorentzian line shape.

state. The net effect near 5.5 MeV is a giant resonance tail with a smaller resonance superimposed on it with, in the case of Au, an integrated photo-nuclear cross-section of 1% of that of the E1 giant resonance.

An analysis of the Chalk River $(d, p\gamma)$ gamma-ray spectra from a series of adjacent intervals of excitation energy in the product nucleus was carried out by Ferguson [29]. He was able to extract the primary spectra, $\nu_{E_x}^1(E_\gamma)$ by an unfolding procedure and hence deduce a strength function with the aid of the expression in Fig. 2. For this purpose Gilbert and Cameron [30] level spacings were adopted. A basic assumption of that analysis was that the population of levels reached by the (d, p) reaction in any interval of excitation energy was, on the average, the same as that reached by gamma cascade from higher intervals. This is supported by parentage overlap considerations [31] in so far as the ground state of the target is the chief common parent of states formed in stripping and it seems plausible to assume that this parentage overlap would tend to be preserved in gamma decay at least for one or two cascade steps. The strength functions found in this way for Au and Ta, evaluated at the neutron separation energy, are shown in Fig. 7. It was found that the primary spectra from all intervals of excitation in a given element followed the same overall energy distribution and hence obeyed the same strength function to within a constant multiplier. This result is consistent with the idea that excited states have built on them giant resonances similar to the ground state. The latter concept was invoked to calculate a strength function from the Lorentzian line shape for comparison with the curves deduced from the $(d, p\gamma)$ data (Fig. 7). The agreement is only fair. This may be because the Lorentzian is a poor approximation to the giant resonance in the tail region or because the families of states picked out from the sea of all states by the $(d, p\gamma)$ and photo-nuclear reactions are not identical, although they no doubt have common members.

It is important to note that the energy dependence, smoothed through the resonance in Au (Fig. 7) is similar to that in Ta and, between 5 and 6 MeV, the curves have about the same strength. This confirms the observation [32, 33] from inspection of the reduced radiation widths of individual lines in the (n, γ) reaction that the strengths of gamma rays in the bump are little, if anything, stronger on the average than the neighbouring elements without the bump. Thus it is not exceptional strength, but the shape of the strength function that gives rise to the bump.

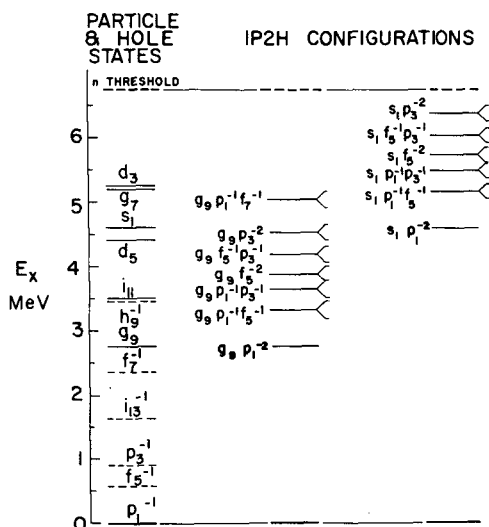
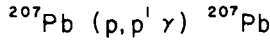


FIG. 8. Energy diagram showing unperturbed energies of one-particle two-hole configurations in ^{207}Pb .

The foregoing has reviewed the evidence for a peak in the gamma-ray strength function governing decay in (n, γ) and $(d, p\gamma)$ reactions. Recent calculations of Kuo and Brown [34] are not inconsistent with this requirement.

We shall now turn our attention to attempts at Chalk River [35] to show that a description in terms of 3-quasiparticle excitations has a certain validity. A good nucleus to study in this regard is ^{207}Pb because it exhibits a strong bump effect and yet is close enough to the closed shell to permit a strict shell model description. The 3-quasiparticle neutron configurations at low energies are one-particle two-hole states (1P2H) with respect to the ^{208}Pb closed shell, those of lowest energy are simply particle-hole excitations of ^{207}Pb . Two families of 1P2H configurations, one based on an excited $g_{9/2}$ neutron and the other an excited $s_{1/2}$ neutron, are shown in Fig. 8. These are shown at their unperturbed energy values calculated from the energies of the states of ^{207}Pb containing the major part of the single-particle and hole strength, shown on the left of the figure. Each configuration but the lowest represents many states of different J . The lowest configuration in each series, which acts as a sort of band head, is just the particle state, $g_{9/2}$ or $s_{1/2}$ as the case may be. These configurations (other than the single-particle states which are little fragmented) will be mixed into the real states of ^{207}Pb in the neighbourhood



NOMENCLATURE:

$g_9 p_1^{-1} = g_{9/2} p_{1/2}^{-1}$

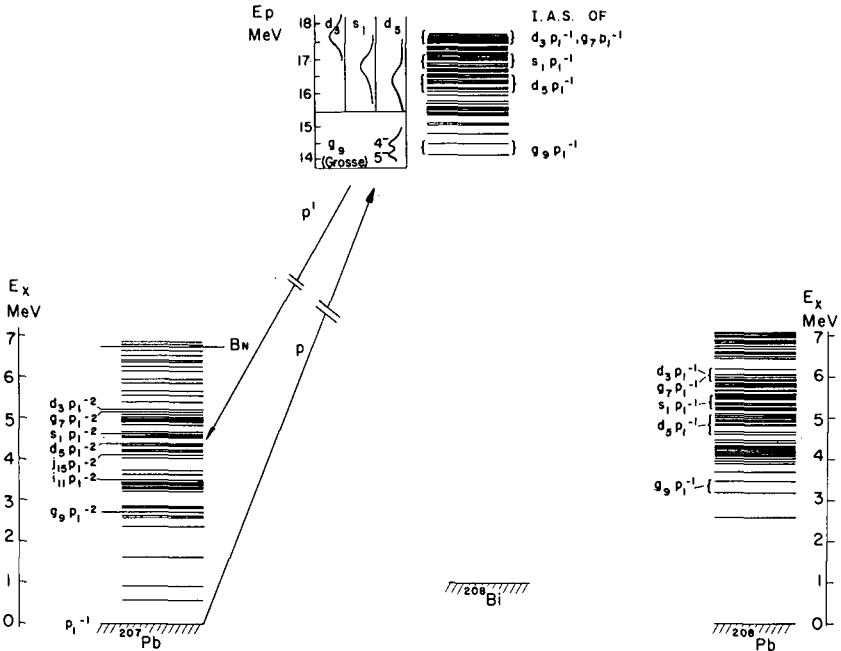


FIG. 9. Selective excitation of one-particle two-hole configurations in ^{207}Pb by means of the $(p, p^1 \gamma)$ reaction at appropriate isobaric analogue resonances in ^{208}Bi of known neutron particle-hole states of ^{208}Pb .

$^{208}\text{Pb} \quad 5^- \quad \text{LEVEL} \quad 3.19 \text{ MeV}$

$\psi_{5^-} = 0.79 \begin{matrix} \uparrow \\ \downarrow \end{matrix} \begin{matrix} \uparrow \\ \downarrow \end{matrix} + 0.20 \begin{matrix} \uparrow \\ \downarrow \end{matrix} \begin{matrix} \uparrow \\ \downarrow \end{matrix} - 0.19 \begin{matrix} \uparrow \\ \downarrow \end{matrix} \begin{matrix} \uparrow \\ \downarrow \end{matrix} + \dots - 0.32 \begin{matrix} \uparrow \\ \downarrow \end{matrix} \begin{matrix} \uparrow \\ \downarrow \end{matrix} - 0.19 \begin{matrix} \uparrow \\ \downarrow \end{matrix} \begin{matrix} \uparrow \\ \downarrow \end{matrix} + \dots$

(GILLET)

$\psi_{\text{IAR}} = \frac{1}{\sqrt{44}} \left\{ \begin{array}{l} 0.79 \left(\begin{matrix} \uparrow \\ \downarrow \end{matrix} \begin{matrix} \uparrow \\ \downarrow \end{matrix} + \sqrt{2} \begin{matrix} \uparrow \\ \downarrow \end{matrix} \begin{matrix} \uparrow \\ \downarrow \end{matrix} + \sqrt{6} \begin{matrix} \uparrow \\ \downarrow \end{matrix} \begin{matrix} \uparrow \\ \downarrow \end{matrix} + 2 \begin{matrix} \uparrow \\ \downarrow \end{matrix} \begin{matrix} \uparrow \\ \downarrow \end{matrix} + \dots \right) \\ 0.20 \left(\begin{matrix} \uparrow \\ \downarrow \end{matrix} \begin{matrix} \uparrow \\ \downarrow \end{matrix} + \sqrt{2} \begin{matrix} \uparrow \\ \downarrow \end{matrix} \begin{matrix} \uparrow \\ \downarrow \end{matrix} + \sqrt{6} \begin{matrix} \uparrow \\ \downarrow \end{matrix} \begin{matrix} \uparrow \\ \downarrow \end{matrix} + 2 \begin{matrix} \uparrow \\ \downarrow \end{matrix} \begin{matrix} \uparrow \\ \downarrow \end{matrix} + \dots \right) \\ + \\ -0.32 \left(\begin{matrix} \uparrow \\ \downarrow \end{matrix} \begin{matrix} \uparrow \\ \downarrow \end{matrix} + \sqrt{2} \begin{matrix} \uparrow \\ \downarrow \end{matrix} \begin{matrix} \uparrow \\ \downarrow \end{matrix} + \sqrt{6} \begin{matrix} \uparrow \\ \downarrow \end{matrix} \begin{matrix} \uparrow \\ \downarrow \end{matrix} + 2 \begin{matrix} \uparrow \\ \downarrow \end{matrix} \begin{matrix} \uparrow \\ \downarrow \end{matrix} + \dots \right) \\ + \end{array} \right\}$

FIG. 10. Schematic representation of the wave functions for the $[g_{9/2} p_{1/2}^{-1}] 5^-$ state of ^{208}Pb from Gillet et al. [40] and for the corresponding isobaric analogue resonances.

of their unperturbed energies. These series are arbitrarily cut off (there are higher members) and there are many other series based on other excited neutrons.

For most states in the $g_{9/2}$ series E1 transitions are forbidden because the angular momentum change for the jumping neutron is too large. An exception is the topmost configuration shown, where the $g_{9/2}$ neutron can jump into the $f_{7/2}$ hole leaving the nucleus in the $p_{1/2}^{-1}$ ground

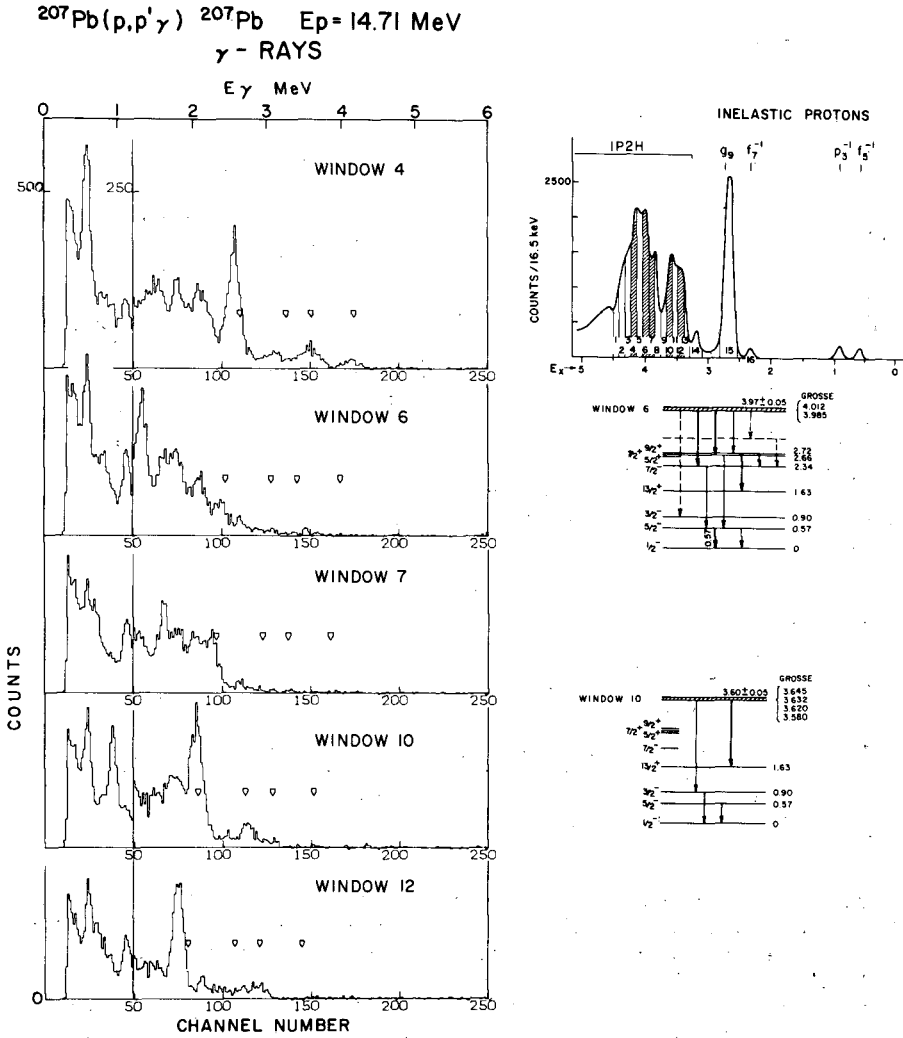


FIG. 11. Typical gamma-ray spectra in coincidence with windows on the inelastic proton spectrum (shown in the upper right) from $^{207}\text{Pb}(p,p'\gamma)^{207}\text{Pb}$ at the $[g_{9/2} p_{1/2}^{-1}] 5^-$ isobaric analogue resonance. Expected positions of gamma rays emitted in transitions to low-lying hole states are indicated by open arrow heads. Examples of detailed decay schemes are shown.

state. If we can selectively excite this series we would expect to find transitions to the low-lying low-spin hole states weak or absent. On the other hand, in the $s_{1/2}$ series many E1 transitions to low-lying hole states are possible. These will all have energies near 5.5 MeV. There are other series for which the same is true, notably the $d_{3/2}$ series. Since these configurations will be mixed into the nuclear states over a wide

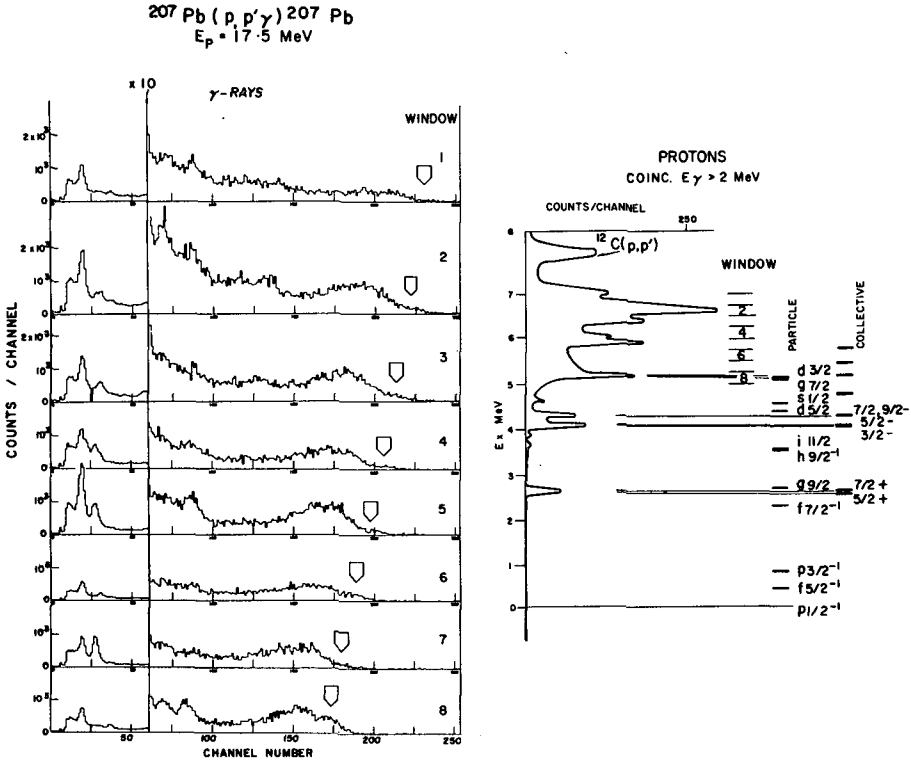


FIG. 12. Gamma-ray spectra in coincidence with eight-proton windows at bombarding energy exciting the $d_{2/2}^- p_{1/2}^-$ isobaric analogue resonance in $^{207}\text{Pb}(p,p'\gamma)^{207}\text{Pb}$. The windows are identified on the proton spectrum on the right wherein the energies of several groups feeding particle and collective-type states are marked. The open arrow heads indicate positions of ground-state gamma rays.

range one can expect to see 5.5 MeV a favoured energy over a wide range of excitation energies. At higher excitations one can form configurations in which the particle-hole is coupled to higher excited states. These would be 2P3H configurations in this notation. These would extend the region over which 5.5-MeV transitions are possible to still higher excitation energies. These various configurations including the 2P3H type can, in general, be reached by a single two-body (doorway) interaction following neutron capture or (d,p) reactions on the ground state of ^{206}Pb which is a mixture of several two-neutron-hole configurations $p_{1/2}^-$, $f_{5/2}^-$, $p_{3/2}^-$, etc.

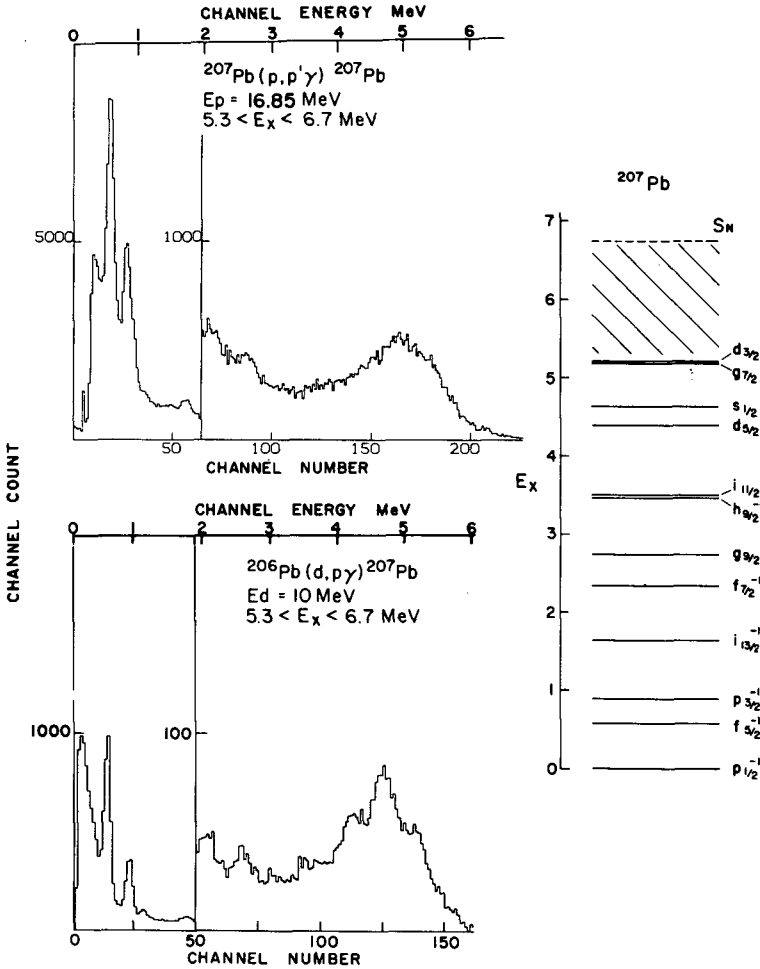


FIG. 13. Gamma rays in coincidence with protons from the $s_{1/2}p_{1/2}^{-1}$ isobaric analogue resonance in the $^{207}\text{Pb}(p, p'\gamma)^{207}\text{Pb}$ reaction (top) and from the $^{206}\text{Pb}(d, p\gamma)^{207}\text{Pb}$ reaction (bottom) for identical proton window energy intervals as indicated. The window interval is also shown cross hatched on the level scheme.

Many of the 1P2H configurations of interest can be excited selectively in the $^{207}\text{Pb}(p, p'\gamma)^{207}\text{Pb}$ reaction. The procedure, illustrated in Fig. 9, is to form isobaric analogue resonances in ^{208}Bi of neutron particle-hole states identified in ^{208}Pb in published (d, p) [36] and (p', p) [37] work. The 4^- and 5^- members of the $g_{9/2}p_{1/2}^{-1}$ isobaric analogue resonance have already been reported by Grosse et al. [38, 39]. In our experiment we located the $d_{5/2}p_{1/2}^{-1}$, $s_{1/2}p_{1/2}^{-1}$ and $d_{3/2}p_{1/2}^{-1}$ isobaric analogue resonances at 16.6, 16.85 and 17.5 MeV respectively. Inelastic decay of these resonances feeds states of the respective 1P2H series as suggested in Fig. 9; the locations of only the 'band heads' are marked on the ^{207}Pb level scheme. The mechanism can be understood from Fig. 10 which presents schematically

the wave function of the $[g_{9/2}p_{1/2}^{-1}]5^{-}$ state in ^{208}Pb from the theory of Gillet, Green and Sanderson [40] at the top and the wave function of the corresponding isobaric analogue resonance at the bottom. The first term of the parent-state wave function is the $g_{9/2}p_{1/2}^{-1}$ term. This is the predominant term but there are many others including excited proton configurations. One can see from the isobaric analogue wave function that inelastic proton scattering will leave the ^{207}Pb nucleus in excited $g_{9/2}$ neutron configurations of precisely the required 1P2H type.

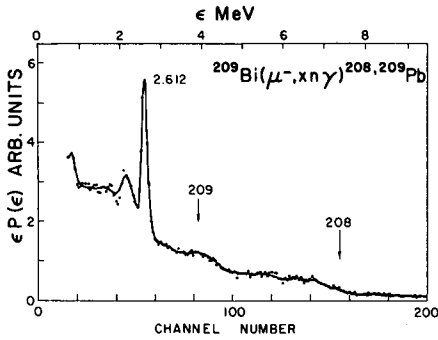
The gamma-ray spectra in coincidence with several windows on the inelastic proton spectrum from the $g_{9/2}p_{1/2}^{-1}$ isobaric analogue resonance are illustrated by five typical examples in Fig. 11. The plot at top right shows the inelastic proton spectrum plotted as a function of the excitation energy, E_x , in ^{207}Pb and identifies the windows used with reference to the region of the unperturbed 1P2H states energies. The g_9 single particle group and several weakly-fed hole-state groups are also shown. The gamma rays feeding the low-energy hole states should appear at positions indicated by the open arrow heads on the gamma-ray spectra. Since there are many levels in the 1P2H region [39] and a number of these should have low spin, the absence of strong transitions to the low-lying low-spin hole-states is confirmation of the inhibition predicted on the simple shell theory. It is possible to make detailed gamma-ray assignments as exemplified by two decay schemes on the right and much analysis of that sort remains to be done on these data.

The gamma-ray spectra in coincidence with the $d_{3/2}$ isobaric analogue resonance are shown in Fig. 12. Here a strong bump is found near the high-energy end of each spectrum. A spectrum unfolding analysis shows that at low excitations, e.g. near 5 MeV (window 8), the ground-state transition is prominent in the bump while at higher excitations, 5.5 MeV (window 6) and above, bump gamma rays feed the first and second excited states strongly, the bump energy remaining near 5.5 MeV. This tendency is in accord with expectations of the model discussed earlier and demonstrates the pattern of 5.5-MeV gamma decay that persists to much higher excitation energies in the (n, γ) reaction.

A similar pattern is followed at the $s_{1/2}$ isobaric analogue resonance as shown in the top part of Fig. 13. Here only one broad window extending from just above the $d_{3/2}$ particle state to the neutron separation energy was used. The bump radiation closely resembles that from the $(d, p\gamma)$ reaction for the same region of excitation energy shown in the lower part of the figure.

All of the above is consistent with our picture of the anomalous radiation as E1 gamma decay of 3-quasiparticle configurations. These may play the part of doorways in the (n, γ) and $(d, p\gamma)$ reactions. The M1 spin flip transitions can be excited in the same way and the picture can no doubt be generalized to include coupling of the particle-hole to vibrations or other motions. As one moves away from the closed shell the single-particle states get increasingly mixed over wider ranges of excitation energy and the characteristic transition energy no longer remains concentrated near 5.5 MeV.

In closing I would like to mention that recent experiments [41] with μ^{-} -meson capture have been carried out to confirm the implication of the $(n, n'\gamma)$ reaction that there are families of states in the region of the neutron threshold that do not in general decay with intense 5.5-MeV radia-



RANDOM BKGND. SUBTRACTED
 POST μ^- -STOP DELAY 120 n SEC.
 TIME WINDOW 100 n SEC.
 RANDOM DELAY 600 n SEC.

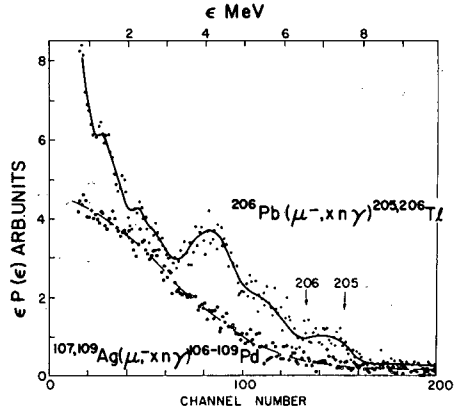
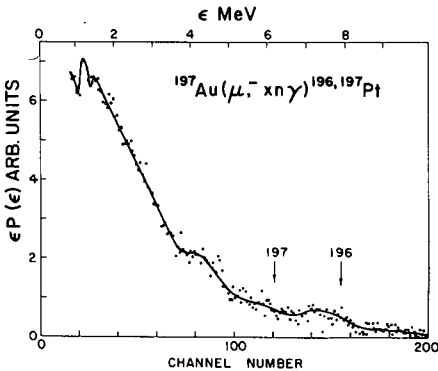


FIG. 14. Gamma spectra observed with NaI detector following μ^- -capture in elements indicated. The arrows indicate neutron separation energies of the product nuclei. Product nuclei corresponding to emission of 0 or 1 neutron only are represented for simplicity. The ordinate is counts per channel times channel energy.

tion. The capture of a μ^- -meson converts a proton into a neutron leaving a hole in the proton shell. The probability of subsequent emission of x neutrons is 37, 45, 12 and 6% respectively for $x=0, 1, 2$, and >2 [42]. The final nucleus may be excited to any energy up to (or slightly beyond) the neutron threshold prior to gamma emission. The gamma-ray spectra from targets near Pb, Fig. 14, show abrupt onset of radiation as the neutron binding energy is approached from above. There is some evidence of structure near 4 MeV, but no prominent radiation at 5.5 MeV. Thus these states, presumably involving proton-hole configurations, are further examples showing that 5.5-MeV decay is not the general rule. The meaning of the 4-MeV bump is currently under study [41].

REFERENCES

- [1] GROSHEV, L.V. et al., Nuclear Data A 5 (1969) 1; 243.
- [2] BARTHOLOMEW, G.A. et al., Can. J. Phys. 45 (1967) 1517.
- [3] BARTHOLOMEW, G.A. et al., Can. J. Phys. 45 (1967) 2063.
- [4] EARLE, E.D. et al., Bull. Am. phys. Soc. 14 (1969) 515.

- [5] ALLEN, B.J., BIRD, J.R., *Physics Lett.* **27B** (1968) 494.
- [6] BERGQVIST, I., *Nucl. Phys.* **74** (1965) 15.
- [7] BOLLINGER, L.M., THOMAS, G.E., *Rep. ANL-7405* (1967) 1.
- [8] BEČVAR, F. et al., *JINR Dubna preprint P3-3696* (1968).
- [9] SLAUGHTER, G.G. et al., *Rep. ANL-7282* (1968) 290.
- [10] THOMAS, G.E., BOLLINGER, L.M., *Bull. Am. phys. Soc.* **13** (1968) 721.
- [11] BIGGERSTAFF, J.A. et al., *Phys. Rev.* **154** (1967) 1136.
- [12] LUNDBERG, B., STARFELT, N., *Nucl. Phys.* **67** (1965) 321.
- [13] BERGQVIST, I., STARFELT, N., *Nucl. Phys.* **39** (1962) 529.
- [14] BARTHOLOMEW, G.A. et al., *Physics Lett.* **24B** (1967) 47; *Can. J. Phys.* (to be published).
- [15] BOWMAN, C.D. et al., *Rep. UCRL-71260* (1968).
- [16] PERKIN, J.L., STARFELT, N., *Nucl. Phys.* **63** (1965) 526.
- [17] BERGQVIST, I. et al., *Nucl. Phys.* **80** (1966) 198.
- [18] BOLLINGER, L.M., "Radiative transitions from highly excited nuclear states", *Nuclear Structure (Proc. Symp. Dubna, 1968), IAEA, Vienna (1968)* 317.
- [19] THOMAS, B.W., MURRAY, J., RAE, E.R., UTTLEY, C.A., *AERE-PR/NP 15* (1969) 18.
- [20] MOTTELSON, B.R., *Proc. Int. Conf. Nuclear Structure, Kingston, University of Toronto Press (1960)* 525.
- [21] SHAPIRO, C.S., EMERY, G.T., private communication.
- [22] DE-SHALIT, A., *Phys. Rev.* **122** (1961) 1530.
- [23] See, for example, AUERBACH, N., STEIN, N., *Physics Lett.* **27B** (1968) 122.
- [24] BLOCK, B., FESHBACH, H., *Ann. Phys.* **23** (1963) 47.
- [25] KERMAN, A.K., RODBERG, L.S., YOUNG, J.E., *Phys. Rev. Lett.* **11** (1963) 422.
- [26] KNOWLES, J.W., private communication.
- [27] STARFELT, N., *Nucl. Phys.* **53** (1964) 397.
- [28] AXEL, P., *Phys. Rev.* **126** (1962) 671.
- [29] FERGUSON, A.J., *Bull. Am. phys. Soc.* **12** (1967) 106.
- [30] GILBERT, A., CAMERON, A.G.W., *Can. J. Phys.* **43** (1965) 1446.
- [31] LANE, A.M., WILKINSON, D.H., *Phys. Rev.* **97** (1955) 1199.
- [32] BARTHOLOMEW, G.A., *Proc. Conf. Electro-magnetic Lifetimes and Properties of Nuclear States, Gatlinburg, 1961, Pub. 974, National Academy of Sciences - National Research Council, Washington, D.C. (1962)* 209.
- [33] PRESTWICH, W.V., BOLLINGER, L.M., private communication.
- [34] KUO, T.T.S., BROWN, G.E., 1968 (private communication to I. Bergqvist).
- [35] BARTHOLOMEW, G.A., EARLE, E.D., FERGUSON, A.J., LONE, M.A., *Bull. Am. phys. Soc.* **14** (1969) 590.
- [36] BARDWICK, J., TICKLE, R., *Phys. Rev.* **161** (1967) 1217.
- [37] MOORE, C.F., KULLECK, J.G., von BRENTANO, P., *Phys. Rev.* **164** (1967) 1559.
- [38] GROSSE, E., MOORE, C.F., SOLF, J., HERING, W.R., von BRENTANO, P., *Z. Phys.* **218** (1969) 213.
- [39] GROSSE, E., *Thesis, Heidelberg (1968)*.
- [40] GILLET, V., GREEN, A.M., SANDERSON, E.A., *Nucl. Phys.* **88** (1966) 321.
- [41] BARTHOLOMEW, G.A., EARLE, E.D., *Rep. AECL 3333* (1969) 56; and to be published.
- [42] WEISENBERG, A.O., *Muons, North-Holland, Amsterdam (1967)* 126.

HIGH-ENERGY GAMMA-RAY TRANSITIONS FROM MeV NEUTRON CAPTURE IN ^{206}Pb

I. BERGQVIST, B. LUNDBERG

Research Institute of National Defence,
Stockholm

and

L. NILSSON

AB ATOMENERGI,
STUDSVIK, NYKÖPING,
SWEDEN

Abstract

HIGH-ENERGY GAMMA-RAY TRANSITIONS FROM MeV NEUTRON CAPTURE IN ^{206}Pb . Gamma-ray spectra from neutron capture in ^{206}Pb (radiogenic lead) in the energy range 1.5 to 8.5 MeV were recorded using time-of-flight techniques. The gamma-ray spectrometer was a NaI(Tl) crystal, 20.8 cm long and 22.6 cm in diameter. The energy variation of the cross-section for high-energy gamma-ray transitions from the capturing state to low-lying states in the residual nucleus was determined. Comparisons with calculations based on semi-direct and direct capture theories show that these processes are not sufficient to explain the magnitude of the cross-section in the region of the giant dipole resonance.

Introduction

A semi-direct reaction process was proposed several years ago by Brown [1], by Clement et al. [2] and by Lushnikov and Zaretskii [3] to explain the results of nucleon capture experiments in the MeV region. The capture cross sections for heavy nuclei are much larger than can be accounted for by either the compound-nucleus or the direct reaction theories as discussed in connection with experiments by Daly and Shaw [4], Csikai et al. [5] and Menlove et al. [6]. The gamma-ray spectra following the capture of MeV neutrons show strong intensity of high-energy gamma rays to low-lying levels with large single-particle strength. These experiments have been carried out by Cvelbar et al. [7] using 14 MeV neutrons and by our group [8,9] with neutrons in the range 1.0 to 8.5 MeV.

In the semi-direct theory the nucleon capture is proposed to proceed via an intermediate stage involving the excitation of the giant electric dipole resonance and the cross section enhancement is due to the collective nature of this excitation. The intermediate excitation of the giant dipole resonance favours gamma-ray deexcitation directly to low-lying levels - in qualitative agreement with experimental results.

In the present work preliminary results on neutron capture in ^{206}Pb are given. Cross sections for (n,γ) transitions to individual single-particle orbits of the residual nucleus as functions of the neutron energy are compared with predictions from the direct and semi-direct capture theories.

Experimental procedure

Since most of the experimental details have been published elsewhere [9], only a brief outline of the experiment will be given together with a description of modifications introduced in connection with the $^{206}\text{Pb}(n,\gamma)$ experiment.

The measurements were performed at the 5.5 MeV van de Graaff accelerator at Studsvik using time-of-flight techniques and a large (22.6 cm diameter and 20.8 cm long) NaI scintillation crystal. Neutrons were produced in gas targets by means of the $^3\text{H}(p,n)^3\text{He}$ and $^2\text{H}(d,n)^3\text{He}$ reactions. The same target-sample-detector arrangement as in ref. [9] was used except that the sample-to-detector distance was reduced to 0.9 m, in order to improve the detection efficiency (fig. 1).

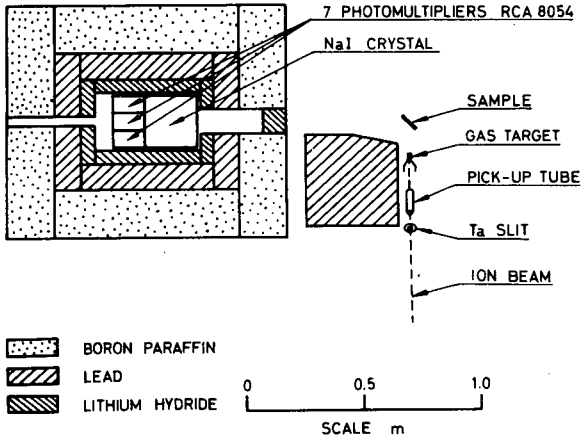


FIG. 1. Lay-out of experimental target-sample-detector arrangement.

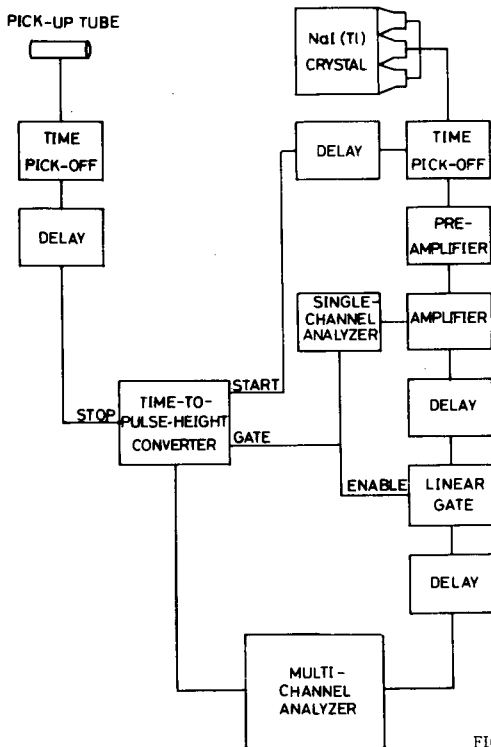


FIG. 2. Block diagram of the electronic equipment.

A two-parameter multi-channel analyser was used throughout the experiment. One parameter, the flight time, was divided into 16 equal groups. The other, the gamma-ray energy was ranged over 256 channels. A block diagram of the electronic equipment is shown in fig. 2. The long counter monitor used in earlier measurements was exchanged for a time-of-flight monitor using a plastic scintillation detector placed at 140° to the incident ion beam. This monitor was calibrated against a polythene counter of Los Alamos design [10].

It was found convenient to use a Bi sample of the same size as the ^{206}Pb sample to obtain a suitable background in the upper part of the $^{206}\text{Pb}(n,\gamma)$ spectra. The neutron binding energy in ^{207}Pb exceeds the ^{210}Bi value by more than 2 MeV, whereas the scattering properties of the two samples should be about the same. The results from the runs at $E_n = 6.5$ MeV are shown in fig. 3.

The measurements at the same energy for each sample were compared to check the internal consistency. The background was subtracted and the resulting spectra grouped into 0.2 MeV intervals. The pulse-height spectra were unfolded by means of the detector response functions which were determined as described in ref. [9]. In this way it is possible to obtain (n,γ) cross sections to single low-lying levels or groups of levels in the residual nucleus.

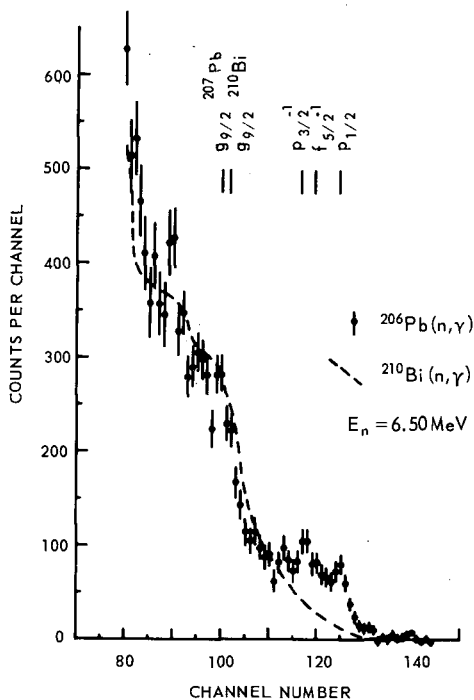


FIG. 3. High-energy part of the gamma-ray spectrum of the $^{206}\text{Pb}(n,\gamma)$ reaction at 6.5 MeV (closed circles). Statistical uncertainties are given by error bars through the data points. The corresponding spectrum from the $\text{Bi}(n,\gamma)$ reaction is represented by the dashed curve. Pulse heights corresponding to gamma-ray transitions directly from the capturing level to low-lying levels are indicated by vertical bars and the dominant single-particle configurations of the low-lying levels.

Theoretical calculations

Cross sections based on semi-direct capture theories by Brown [1] and Clement et al. [2] were calculated. Also direct capture cross sections according to a theory of Lane [11] were evaluated. The scattering wave functions and bound state wave functions necessary to calculate the matrix elements were obtained using the ABACUS code [12]. For the optical potential Rosen parameters [13] including spin-orbit interaction were used. In the calculations of the bound state wave functions the potential depth was adjusted to match the binding energy of the bound particle. Also here spin-orbit interaction was included. The potential shape parameters were chosen in accordance with "normal Oak Ridge procedure" [14].

Results and discussion

The $^{206}\text{Pb}(n,\gamma)$ reaction is suitable for investigating the semi-direct capture process in the neutron energy range easily achievable by the $^2\text{H}(d,n)^3\text{He}$ reaction at a 5.5 MeV van de Graaff accelerator. The neutron binding energy of ^{207}Pb is 6.7 MeV, which gives with the maximum neutron energy 8.5 MeV a maximum gamma-ray energy of about 15 MeV, i.e. well above the peak of the giant dipole resonance at 13.5 MeV. Preliminary experimental cross sections for $^{206}\text{Pb}(n,\gamma_0)$ at various energies are given in fig. 4 together with predictions of the semi-direct capture theories. The experimental cross section decreases smoothly with increasing neutron energy.

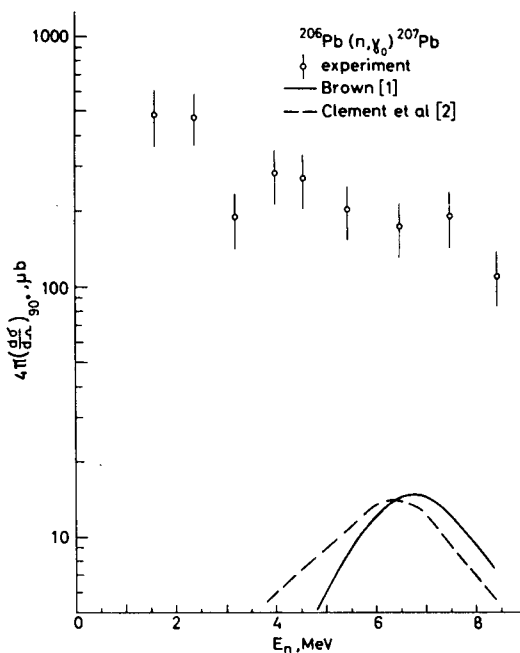


FIG. 4. Preliminary cross-sections for the $^{206}\text{Pb}(n,\gamma)$ reaction (open circles) with estimated errors. The full and dashed curves are based on the semi-direct capture theories of Brown [1] and Clement et al. [2] respectively.

The semi-direct process, however, accounts for only about 10 % of the cross section at the peak of the giant dipole resonance (see fig. 4). The direct capture theory gives cross sections which are about a factor of 10 smaller than the predictions of the semi-direct theory.

From fig. 3 it can be seen that also the first and second excited states in ^{207}Pb are populated in $^{206}\text{Pb}(n,\gamma)$. These states have been found to be fairly pure neutron hole states $(f_{5/2})^{-1}$ and $(p_{3/2})^{-1}$, respectively, and are therefore not expected to be populated in the direct or semi-direct neutron capture process within a pure single-particle framework. However, experimental and theoretical evidence shows that there is configuration mixing in the ^{206}Pb ground state and its wave function may be written

$$\psi(^{206}\text{Pb}) = (0.65 \pm 0.13) p_{1/2}^{-2} + (0.25 \pm 0.07) f_{5/2}^{-2} \\ + (0.20 \pm 0.08) p_{3/2}^{-2}$$

The coefficients given here are those obtained by Richard et al. [15] from proton elastic and inelastic scattering from the isobaric analogues of low-lying ^{207}Pb states. Coefficients of similar magnitude have been obtained by True [16] in shell-model calculations based on two interacting neutron holes. Also studies of the $^{206}\text{Pb}(d,p)$ reaction [17] and the $^{207}\text{Pb}(d,t)$ reaction [18] have given coefficients of this magnitude. One purpose of this paper is to investigate if the three lowest states in ^{207}Pb are populated in the $^{206}\text{Pb}(n,\gamma)$ process in proportions which are in agreement with the configuration mixing of the ^{206}Pb ground state given above. Another purpose of the paper is to evaluate cross sections to the $g_{9/2}$ state at 2.7 MeV and make comparisons with cross sections to the corresponding state in ^{210}Bi . The background subtraction in this case is somewhat more complicated and has not yet been performed.

At the present preliminary stage of the data analysis, it seems as if neither direct capture nor semi-direct capture are responsible for the major part of the $^{206}\text{Pb}(n,\gamma_0)$ cross section in the region of the giant dipole resonance. Further treatment of the data will show if this conclusion is applicable also to other final levels. The shape of the gamma-ray spectrum (fig. 3) shows that the process responsible for the cross section selects low-lying levels with large single-particle strength. Such a selection is not expected for processes involving the formation of a compound nucleus.

References

- [1] G.E. Brown, Nucl. Phys. 57 (1964) 339
- [2] C.F. Clement, A.M. Lane and J.R. Rook, Nucl. Phys. 66 (1965) 273, 293
- [3] A.A. Lushnikov and D.F. Zaretskii, Nucl. Phys. 66 (1965) 35
- [4] P.J. Daly and P.F.D. Shaw, Nucl. Phys. 56 (1964) 322
- [5] J. Csikai et al., Nucl. Phys. A95 (1967) 229
- [6] H.O. Menlove et al., Phys. Rev. 163 (1967) 1299

- [7] F. Cvelbar et al., Phys. Lett. 3 (1963) 364 and private communication
- [8] I. Bergqvist et al., Phys. Lett. 19 (1966) 670
- [9] I. Bergqvist et al., Nucl. Phys. A120 (1968) 161
- [10] S.J. Bame Jr. et al., Rev. Sci. Instr. 28 (1957) 997
S.J. Bame Jr. et al., Rev. Sci. Instr. 31 (1960) 911
- [11] A.M. Lane, Nucl. Phys. 11 (1959) 625
- [12] E.H. Auerbach, KAPL-M-EHA-1 (1960)
W. Hauser and H. Feshbach, Phys. Rev. 87 (1952) 366
- [13] L. Rosen et al., Ann. Phys. 34 (1965) 96
- [14] R.H. Bassel, R.M. Drisko and G.R. Satchler, ORNL-3240, unpublished
- [15] P. Richard et al., Phys. Rev. 171 (1968) 1308
- [16] W.W. True, Phys. Rev. 168 (1968) 1388
- [17] P. Mukherjee and B.L. Cohen, Phys. Rev. 127 (1962) 1284
- [18] R. Tickle and J. Bardwick, Phys. Rev. 166 (1968) 1167.

RADIATIVE CAPTURE OF NUCLEONS IN THE GIANT RESONANCE REGION

G. LONGO, F. SAPORETTI

Comitato Nazionale Energia Nucleare,

Centro di Calcolo,

Bologna, Italy

Abstract

RADIATIVE CAPTURE OF NUCLEONS IN THE GIANT RESONANCE REGION. Suggestions are made for measurements to throw light on the trend of nucleon radiative capture cross-sections in the giant resonance region. The difference between the relative contribution of direct and collective mechanisms for (p, γ) and (n, γ) reactions is brought out.

An analysis of the radiative capture data for 10-20-MeV energy neutrons has shown that the "direct" and "collective" capture mechanisms can reasonably explain the experimental (n, γ) cross sections of the heavy nuclei ($A > 40$) with magic or near-magic neutron number [1]. On the other hand, these models do not appear to account for the large increase (about one order of magnitude) in cross sections between closed shells. In the paper mentioned, calculations were carried out for nuclei with far-from-magic neutron numbers, as for example ${}^{165}_{67}\text{Ho}_{98}$. For these nuclei the neutron capture cross section was calculated by using wave functions of particles in a spherical potential. The (n, γ) cross sections thus calculated were about a factor 10 lower than the experimental ones, and it is not clear why the use of wave functions of particles in a deformed potential should give systematically different results from the spherical case. Work is in progress to evaluate the difference between the radial integrals calculated in these two ways.

Since many (n, γ) data (available especially at 14-15 MeV) have not yet been explained theoretically, an attempt was made to find regularities, which might lead to an empirical expression relating the (n, γ) cross section to some fundamental nuclear characteristic [2]. Unfortunately, there are few experimental data available, but an examination of these seems to indicate some regular behaviour, which may suggest new indicative measurements. This behaviour can be seen in fig. 1, where the experimental data at 14±15 MeV for nuclei with proton numbers $Z > 28$ (for which the neutron excess becomes appreciable) are plotted versus the nuclear parameter $(N-Z)^2/A$. Nuclei with neutrons in the same shells are indicated with the same symbol. The family of straight lines $\ln \sigma = -(N-Z)^2/A$, drawn in the figure, seems to suggest that for a given neutron shell the (n, γ) cross sections decrease exponentially with the increase of the parameter $(N-Z)^2/A$.

Experimental cross sections for the radiative capture of 10-20 MeV protons by nuclei with $Z > 28$ are available for only a few nuclei [3] and it is impossible to detect any particular trend from such limited data. The measurements give peak values of (p, γ) cross sections in the giant resonance region equal to $(1 \pm 0.3) \text{mb}$, both for near-magic target proton numbers ($Z=52, 83$) and for nuclei with far-from-magic proton numbers ($Z=34, 42, 58$). Calculations [3,4], carried out with direct and collective models, are in satisfactory agreement with the proton experimental data, regardless of the target proton or neutron number.

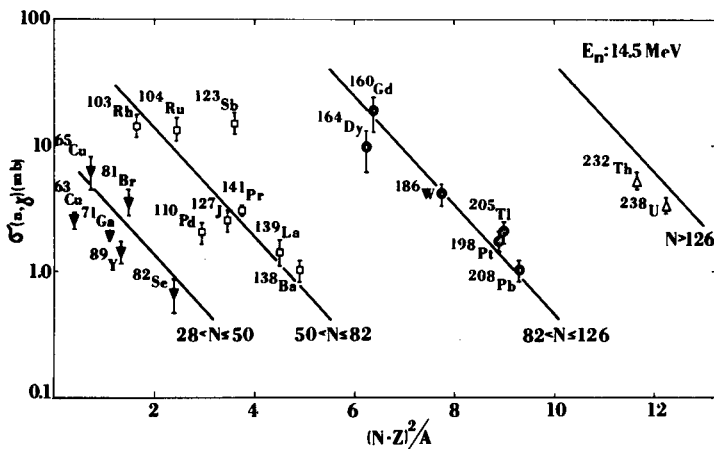


FIG. 1. Experimental (n, γ) cross-sections plotted against $(N-Z)^2/A$.

It is worth while noting that the relative contributions of direct and collective capture are different for (p, γ) and (n, γ) reactions (see calculations for Pb in ref. [4]). This is mainly due to the different behaviour of the proton and neutron continuum wave functions in the external and internal regions of the nucleus. As can be seen in figs. 2a) and 3a), the relative amplitude of the real part of the proton continuum wave function diminishes in the interior of the nucleus, while for the neutron the difference is less pronounced. So the exterior contribution to the real part of the direct radial integral is usually greater for proton capture than for neutron capture, as can be seen from the example shown in figs. 2b) and 3b). The opposite is true for the collective matrix element, which is mainly determined by the particle-vibration coupling operating on the wave functions in a thin shell around the nuclear radius. A more detailed analysis [5] shows that the difference between proton and neutron capture is reduced by the fact that the imaginary parts of the wave functions behave similarly in each case. The different contribution of the real part is probably a reflection of the Coulomb barrier influence. In the case of the proton, this barrier opposes the penetration of the nucleon into the nucleus, thus increasing the contribution from the exterior of the nucleus to direct capture; moreover this reduces the collective excitations of the nuclear surface, thus decreasing the collective capture.

In spite of the difference between the relative contributions of direct and collective capture for (p, γ) and (n, γ) reactions, these models taken together can account for cross section values of the order of 1 millibarn, in agreement with the proton experimental data available and with part of the neutron data. For neutron radiative capture cross sections between closed shells (~ 10 mbarns) new theoretical developments are probably required. An examination of fig. 1 suggests that we might regard the $(N-Z)$ "excess" neutrons, which affect the fraction $(N-Z)/A$ of the nuclear volume, as active participants in the capture process. On this hypothesis, it seems that the $(N-Z)$ neutrons, which occupy the highest energy states, influence the (n, γ) reaction more directly in some way.

Clearly, further data are needed to enable us to check the $\sigma(n, \gamma)$ trend indicated in fig. 1, and to investigate the possibility of relating (p, γ)

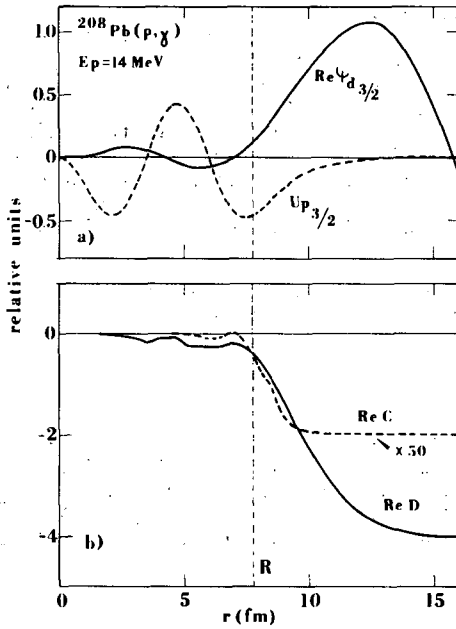


FIG. 2. (a) The $3p_{3/2}$ proton bound-state wave function and the real part of the $d_{3/2}$ continuum function. (b) Real part of the direct (D) and collective (C) integrals as function of the radius for the $d_{3/2} \rightarrow p_{3/2}$ proton transition.

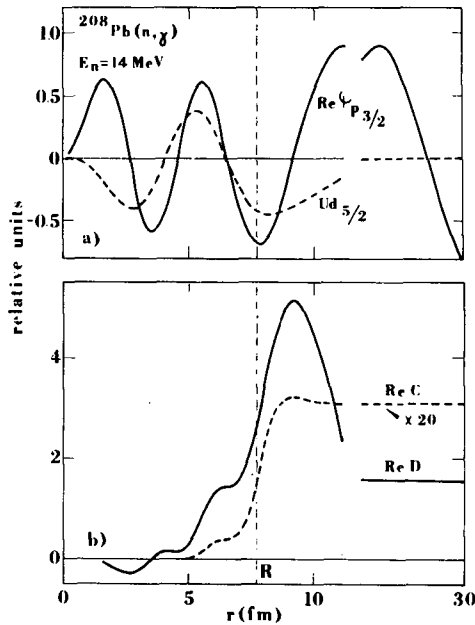


FIG. 3. (a) The $3d_{5/2}$ neutron bound-state wave function and the real part of the $p_{3/2}$ continuum function. (b) Real part of the direct (D) and collective (C) integrals as function of the radius for the $p_{3/2} \rightarrow d_{5/2}$ neutron transition.

cross sections to nuclear characteristics. Hence, it would be interesting to have measurements, made under the same experimental conditions, for neutron capture by nuclei with neutron numbers slightly greater than magic numbers. The experimental cross sections for different isotopes of the same element would also be indicative for studying the influence of the parameter $(N-Z)^2/A$ on the probability of neutron and proton radiative capture at this energy. A knowledge of (p,γ) cross sections for nuclei with the corresponding (n,γ) cross sections of the order of 10 mbarn would make it possible to establish whether there is a difference between the dependence on N, Z, A in neutron and proton radiative capture cross sections.

Thanks are due to prof. V. Benzi for valuable discussions and to dr. F. Fabbri for performing the required calculations.

References

- [1] G. Longo and F. Saporetti: Nucl. Phys. A127 (1969) 503.
- [2] G. Longo and F. Saporetti: CNEN Report RT/FI (1968) 42.
- [3] P.J. Daly, B.M. Seppelt and P.F.D. Shaw: Nucl. Phys. A119 (1968) 673.
- [4] G. Longo and F. Saporetti: Nuovo Cimento 56B(1968) 264.
- [5] G. Longo and F. Saporetti: to be submitted for publication.

SOME STATISTICAL PROPERTIES OF PARTIAL RADIATION WIDTHS IN TUNGSTEN

J. MURRAY, B. W. THOMAS, E. R. RAE
Atomic Energy Research Establishment,
Harwell, Didcot,
Berks., United Kingdom

Abstract

SOME STATISTICAL PROPERTIES OF PARTIAL RADIATION WIDTHS IN TUNGSTEN. High-resolution gamma-ray spectra from six resonances in ^{182}W , three resonances in ^{184}W and five resonances in ^{186}W have been obtained. By using the method of maximum likelihood, the properties of the reduced widths have been compared with those expected from a random distribution. There is no convincing discrepancy between the data and that expected from a random distribution.

It has been suggested [1] that thermal capture spectra in the mass region $A \approx 180$ have systematic features. This disagrees with the statistical model for neutron capture. In an experiment to test the validity of the statistical model as a description of resonant capture in tungsten, the booster target of the 45-MeV Linac at Harwell was used as a neutron source. The gamma rays emitted from a natural tungsten target were studied with a 30-cm³ germanium detector. A 32-channel time selector was used to select specific resonances.

The time-of-flight spectrum and the time gates used are shown in Fig. 1, while Fig. 2 shows the spectra obtained for ^{186}W .

Tables I, II and III list the relative intensities of the primary gamma rays. The intensities were normalized by dividing by the total count of events depositing more than 1.5 MeV in the crystal. The errors quoted are the statistical errors and do not include errors of normalization (< 10%) and errors in the efficiency curve for the detector (< 3%).

All the transitions with an energy within 2 MeV of the binding energy of the product nucleus were assumed to be primary transitions and E1 in character.

The method of maximum likelihood was used to compare the distribution of the reduced radiation widths with that obtained from samples drawn at random from a chi-squared distribution for various values of ν , where ν is the number of degrees of freedom. For each isotope the maximum likelihood estimator E , defined as

$$E = \left(\sum_{k=1}^{N_r} \sum_{i=1}^{N_\ell} \ln \Gamma_{\gamma ki} - N \ln \left(\sum_{k=1}^{N_r} \sum_{i=1}^{N_\ell} \Gamma_{\gamma ki} / N \right) \right) / N$$

where N_r is the number of resonances studied, N_ℓ is the number of final states excited, $N = N_r \times N_\ell$ and $\Gamma_{\gamma ki}$ is the reduced radiation width from resonance k to final state i , was obtained.

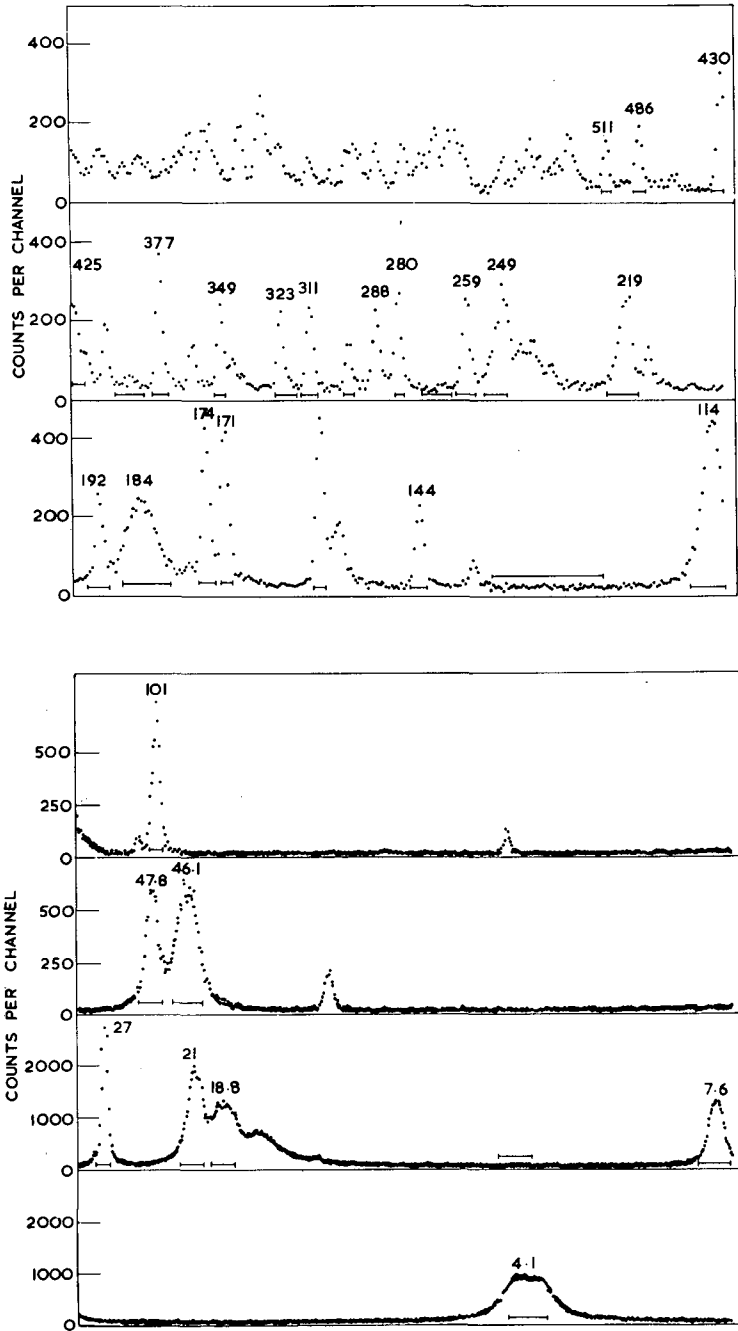


FIG. 1. Time-of-flight for capture in natural tungsten.

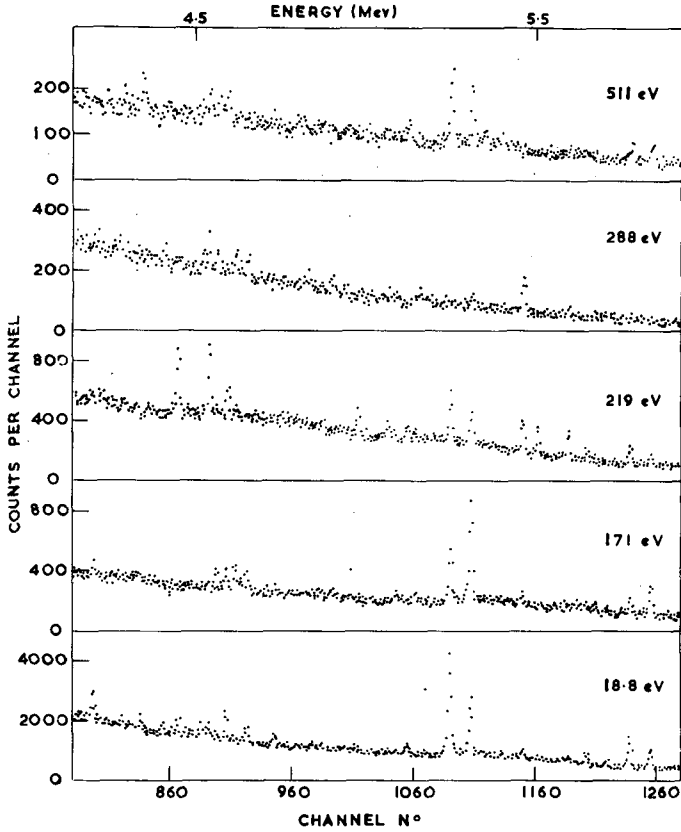


FIG. 2. Capture spectra for 511, 288, 219, 171, 18.8-eV resonances in ^{186}W .

The negative of $\Gamma_{\gamma ki}$, which result from the statistical errors of the intensity measurements, were removed by a cut-off procedure similar to that of Price et al. [2]. In the sample simulation the errors of the $\Gamma_{\gamma ki}$ and the possibility of missed levels was taken into account. The results of the analysis are shown in Table IV. In the giant-dipole resonance model the reduced widths have an E^2 dependence [3]. Therefore the distribution of the $\Gamma_{\gamma ki}/E_{\gamma i}^2$ was analysed in the same way. Table IV also includes the results of a similar analysis of $\Gamma_{\gamma i}$, the sum of the widths, to given final states. The expected value of ν in this case is equal to the number of resonances studied. In the sample simulation ν could only be an integer and the values quoted were obtained by interpolation.

The possibility of a correlation between the radiation widths and the reduced neutron widths as seen for capture by thulium [4] or between the radiative widths themselves was investigated. The results are shown in Tables V, VI and VII. The correlation coefficient t between widths to final states i and j is defined as

$$t_{ij} = \frac{N \sum_k \Gamma_{\gamma ki} \Gamma_{\gamma kj} - \sum_k \Gamma_{\nu ki} \sum_k \Gamma_{\gamma kj}}{\left(\left(N \sum_k \Gamma_{\gamma ki}^2 - \left(\sum_k \Gamma_{\gamma ki} \right)^2 \right) \left(N \sum_k \Gamma_{\gamma kj}^2 - \left(\sum_k \Gamma_{\gamma kj} \right)^2 \right) \right)^{\frac{1}{2}}}$$

and the correlation coefficient r between the reduced neutron widths and the widths to final state i is similarly given by

$$r_i = \frac{N \sum_k \Gamma_{\gamma ki} \Gamma_{nk} - \sum_k \Gamma_{\gamma ki} \sum_k \Gamma_{nk}}{\left(\left(N \sum_k \Gamma_{\gamma ki}^2 - \left(\sum_k \Gamma_{\gamma ki} \right)^2 \right) \left(N \sum_k \Gamma_{nk}^2 - \left(\sum_k \Gamma_{nk} \right)^2 \right) \right)^{\frac{1}{2}}}$$

TABLE I. TRANSITIONS PER 100 NEUTRON CAPTURES IN ^{182}W

E_n E_γ	486	377	249	114	21.2	4.1
3.866	-0.3(1.5)	-0.8(1.0)	0.4(0.5)	0.0(0.5)	0.0(0.3)	1.0(0.3)
4.014	0.5(1.5)	-1.1(0.9)	-0.4(0.5)	0.6(0.3)	1.7(0.2)	0.5(0.3)
4.063	0.8(1.5)	0.6(0.9)	0.2(0.5)	0.1(0.3)	0.9(0.2)	0.4(0.2)
4.094	-1.0(1.5)	1.3(0.9)	0.6(0.5)	1.1(0.3)	-0.2(0.2)	0.9(0.3)
4.197	-0.9(1.4)	2.5(0.9)	0.0(0.5)	-0.2(0.3)	0.9(0.2)	-0.4(0.2)
4.211	1.6(1.4)	0.2(0.9)	-0.5(0.5)	-0.7(0.3)	0.6(0.2)	0.0(0.2)
4.246	-0.6(1.4)	-0.7(0.9)	1.2(0.5)	-0.4(0.3)	0.1(0.2)	2.8(0.2)
4.273	-0.9(1.4)	3.0(0.9)	0.4(0.5)	3.6(0.3)	0.4(0.2)	0.1(0.2)
4.304	-0.9(1.4)	1.3(0.9)	0.6(0.4)	0.7(0.3)	3.0(0.2)	3.0(0.2)
4.325	-0.1(1.4)	4.0(0.9)	0.8(0.4)	1.3(0.3)	1.5(0.2)	0.6(0.2)
4.353	0.5(1.4)	-0.4(0.8)	0.2(0.4)	1.4(0.3)	0.2(0.2)	0.4(0.2)
4.391	-0.8(1.3)	0.8(0.8)	0.4(0.4)	3.4(0.3)	0.4(0.2)	-0.2(0.2)
4.463	1.8(1.3)	1.4(0.8)	3.5(0.4)	-0.5(0.3)	0.5(0.2)	0.0(0.2)
4.519	5.8(1.3)	1.1(0.9)	3.4(0.4)	3.4(0.3)	1.3(0.2)	1.9(0.2)
4.557	2.3(1.3)	0.2(0.8)	0.0(0.4)	1.1(0.3)	0.1(0.1)	0.8(0.2)
4.633	2.2(1.2)	0.0(0.8)	3.6(0.4)	3.6(0.3)	5.0(0.2)	0.0(0.2)
4.719	1.9(1.2)	2.4(0.8)	1.9(0.4)	2.1(0.3)	0.9(0.1)	-0.5(0.2)
4.898	-0.5(1.0)	-0.4(0.7)	0.3(0.4)	2.5(0.2)	0.1(0.1)	-0.1(0.2)
5.164	5.6(1.1)	0.6(0.6)	1.8(0.3)	2.5(0.2)	0.6(0.1)	19.4(0.2)
5.230	1.6(1.0)	0.4(0.6)	0.5(0.3)	0.0(0.2)	0.3(0.1)	0.1(0.1)
5.258	8.1(1.0)	0.8(0.5)	0.2(0.3)	2.6(0.2)	1.1(0.4)	0.9(0.2)
5.320	1.1(0.9)	0.2(0.6)	0.0(0.3)	-0.2(0.2)	0.8(0.3)	0.0(0.2)
5.658	-0.2(0.7)	0.0(0.5)	2.1(0.3)	0.0(0.2)	-0.1(0.1)	0.3(0.1)
5.983	0.7(0.6)	0.8(0.4)	1.3(0.2)	9.5(0.2)	1.9(0.08)	0.5(0.1)
6.145	3.6(0.6)	3.0(0.4)	2.2(0.2)	0.5(0.1)	6.9(0.1)	3.1(0.1)
6.190	1.5(0.6)	11.1(0.6)	0.5(0.2)	8.3(0.2)	4.4(0.1)	9.7(0.5)

TABLE II. TRANSITIONS PER 100 NEUTRON CAPTURES IN ^{184}W

E_j / E_D	425	311	184
3.914	-0.8(0.7)	2.8(1.1)	3.6(0.5)
4.218	-0.2(0.7)	-0.8(0.9)	1.4(0.4)
4.256	0.7(0.7)	4.8(0.9)	1.2(0.4)
4.536	-0.6(0.6)	0.5(0.8)	3.3(0.4)
4.608	0.6(0.6)	0.1(0.7)	3.1(0.4)
4.653	1.5(0.5)	1.1(0.7)	7.3(0.4)
4.750	0.3(0.5)	3.1(0.7)	0.5(0.3)
4.784	0.1(0.6)	0.4(0.7)	1.3(0.3)
4.930	7.5(0.5)	5.0(0.8)	6.7(0.5)
4.988	1.1(0.5)	5.0(0.7)	0.5(0.3)
5.092	1.8(0.4)	-0.5(0.6)	1.4(0.3)
5.662	3.9(0.4)	1.2(0.5)	0.5(0.2)
5.755	0.6(0.3)	1.5(0.4)	11.8(0.3)

Table V gives the values obtained for the average t_{ij} ,

$$T = 2 \sum_i \sum_{j>i} t_{ij} / N(N-1)$$

the average η_i , $R = \sum_i r_i / N$ and the probability, P , that their values will be exceeded in a random sample drawn from a population with one degree of freedom. The primed parameters are those obtained when only those final states seen in (d, p) studies [5] are considered.

The data disagree with the predictions of the statistical model for several of the parameters. The value of ν for the $\Gamma_{\gamma_{ki}}$ for ^{186}W has only a probability of 3% of being 1. The value of ν for the Γ_{γ_i} for ^{182}W has a probability of much less than 0.1% of being 6. This is due to the presence of four large values of Γ_{γ_i} and seven small values of Γ_{γ_i} . Since the possibility of M1 transitions in the sample cannot be ruled out, this is not convincing evidence for the presence of non-statistical effects. The four strongly excited levels seem to have no nuclear structure characteristics in common. While none of the averaged correlation coefficients in Table V are significant, several of the individual coefficients are. In particular

TABLE III. TRANSITIONS PER 100 NEUTRON CAPTURES IN ^{186}W

E_γ (MeV) \ E_n (eV)	511	288	219	171	18.8
4.083	2.1(1.4)	2.4(0.5)	2.8(0.6)	0.8(0.6)	0.4(0.3)
4.121	5.7(1.4)	0.5(0.7)	3.8(0.5)	0.2(0.6)	0.4(0.2)
4.156	4.2(1.4)	2.6(0.7)	0.4(0.5)	0.1(0.6)	0.5(0.2)
4.249	0.32(1.3)	0.9(0.7)	0.5(0.5)	2.1(0.6)	3.9(0.2)
4.332	3.1(1.3)	-0.1(0.7)	0.4(0.5)	0.1(0.5)	1.0(0.2)
4.384	7.2(1.3)	0.4(0.7)	-1.3(0.5)	1.5(0.5)	0.9(0.2)
4.449	0.7(1.2)	2.6(0.6)	-0.8(0.5)	-0.2(0.5)	0.6(0.2)
4.487	0.36(1.2)	0.5(0.6)	8.3(0.5)	-0.3(0.5)	0.3(0.3)
4.574	5.5(1.3)	4.2(0.6)	8.9(0.5)	1.3(0.5)	1.8(0.2)
4.598	3.7(1.2)	2.7(0.6)	0.3(0.5)	3.7(0.5)	0.6(0.2)
4.626	4.7(1.3)	0.9(0.6)	3.3(0.5)	2.8(0.6)	4.0(0.2)
4.650	0.6(1.2)	3.9(0.6)	1.5(0.5)	5.3(0.5)	0.2(0.2)
4.684	1.2(1.1)	2.8(0.6)	0.5(0.4)	3.5(0.5)	2.2(0.2)
5.261	15.1(1.2)	0.5(0.4)	6.8(0.4)	9.7(0.5)	15.2(0.2)
5.320	11.8(1.1)	1.5(0.4)	5.0(0.4)	19.2(0.6)	9.1(0.2)
5.468	0.14(0.9)	3.9(0.5)	4.6(0.4)	1.9(0.4)	0.8(0.2)

TABLE IV. VALUES FOR ν

	$\Gamma_{\gamma ki}$	$\Gamma_{\gamma ki}/E_{\gamma i}^2$	$\Gamma_{\gamma i}$	$\Gamma_{\gamma i}/E_{\gamma i}^2$	N_{Γ}
^{182}W	0.8(0.4)	0.9(0.3)	2.0(1.0)	2.5(1.0)	6
^{184}W	1.3(0.5)	0.9(0.5)	2.5(1.0)	2.5(1.0)	3
^{186}W	1.5(0.3)	1.7(0.3)	6.5(2.0)	5(2)	5

TABLE V. AVERAGE VALUES OF THE CORRELATION COEFFICIENTS

	T	P(T) (%)	T'	P(T') (%)	R	P(R) (%)	R'	P(R') (%)
^{182}W	-0.027	20	-0.054	40	-0.024	40	-0.075	9
^{184}W	0.081	6	0.089	16	0.385	2.2	-0.454	2.6
^{186}W	-0.004	13	0.039	10	-0.138	75	-0.164	75

TABLE VI. VALUES OF CORRELATION COEFFICIENTS USING THE NILSSON MODEL

	i	j	t_{ij}	P(t_{ij}) (%)
^{182}W	$\frac{3}{2}^- [510]$	$\frac{1}{2}^- [510]$	-0.218	65
	$\frac{3}{2}^- [510]$	$\frac{3}{2}^- [512]$	-0.548	90
	$\frac{1}{2}^- [510]$	$\frac{3}{2}^- [512]$	0.203	30
^{186}W	$\frac{3}{2}^- [510]$	$\frac{1}{2}^- [510]$	0.580	17
	$\frac{3}{2}^- [510]$	$\frac{3}{2}^- [512]$	-0.868	98
	$\frac{1}{2}^- [510]$	$\frac{3}{2}^- [512]$	-0.612	90

TABLE VII. CORRELATION WITH THE REDUCED NEUTRON WIDTH

	i	r_i	P(r_i) (%)
^{182}W	$\frac{3}{2}^- [510]$	-0.397	80
	$\frac{1}{2}^- [510]$	-0.696	97
	$\frac{3}{2}^- [512]$	+0.124	35
^{186}W	$\frac{3}{2}^- [510]$	0.417	23
	$\frac{1}{2}^- [510]$	-0.183	55
	$\frac{3}{2}^- [512]$	-0.096	50

Table VI gives the correlation coefficients involving the levels which have been interpreted using the Nilsson model [5]. It can be seen that there is a large anti-correlation between the $3/2^- [512]$ and the $3/2^- [510]$ for ^{186}W and that there is a marked anti-correlation for the same levels in ^{182}W .

Prestwich and Coté [6] have proposed that transitions to the [512] band should be hindered by a selection rule on Λ . Even when averaged over only six resonances in ^{182}W and five resonances in ^{186}W , the sum of the transitions to the $3/2^- [512]$ is not anomalously low. The effect of selection rules of this nature could, however, be giving the anti-correlation between transitions to the two bands. They would also be likely to give a positive correlation for transitions going to the same band but this correlation is not observed.

Table VII gives the correlation with the reduced neutron width, r_i , for the above levels.

We have started from the assumption that we are in each nucleus dealing with a single population of reduced radiation widths, whose distribution belongs to the χ^2 family (with a possible systematic E^2 energy dependence). We have found a number of parameters where the predictions of the statistical model are significantly violated, but the number of violations is not unreasonable in view of the large number of statistics obtained. Even for similar nuclei like ^{182}W and ^{186}W there is no parameter which is significantly at variance with the statistical model for both nuclei. Given that our initial assumptions are valid, we are forced to conclude that the statistical model gives an acceptable explanation of the data.

REFERENCES

- [1] NAMENSON, A. I., BOLOTIN, H. H., Phys. Rev. 158 (1967) 1206.
- [2] PRICE, D. L., CHRIEN, R. E., WASSON, O. A., BHAT, M. R., BEER, M., LONE, M. A., GRAVES, R., Nuc. Phys. A121 (1968) 630.
- [3] AXEL, P., Phys. Rev. 126 (1962) 671.
- [4] BEER, M., LONE, M. A., CHRIEN, R. E., WASSON, O. A., BHAT, M. R., MUETHER, H. R., Phys. Rev. Lett. 20 (1968) 340.
- [5] Nuclear Data B1 1, 2 (1966).
- [6] PRESTWICH, W. V., COTÉ, R. E., Phys. Rev. 160 (1967) 1038.

keV NEUTRON CAPTURE IN THE MASS REGION $A = 40-70$

J.R. BIRD, B.J. ALLEN, M.J. KENNY
AEEC Research Establishment,
Lucas Heights,
New South Wales, Australia

Abstract

keV NEUTRON CAPTURE IN THE MASS REGION $A = 40-70$. Data are presented from kilovolt neutron capture measurements on elements in the mass region $A = 40$ to 70 . Targets with even Z show individual resonances and transitions to high spin states are observed showing the importance of p- or d-wave capture. A probable interpretation is given in terms of d-wave capture but further experimental work is required.

INTRODUCTION

The dependence of both s and p wave neutron strength functions on mass number has been widely studied both with experimental measurements and with optical model calculations. The s-wave strength function peaks in the regions of mass near 60 and 160 so that neutron resonances in these regions are dominated by s-wave effects. Similarly, p-wave effects are important in the regions of mass number near 30, 100 and 230. Much less is known about the d-wave strength function but peaks are expected in the mass regions near 55 and 160. In this paper we present results for the mass region $A = 40 - 70$ and these are used to study these effects.

The differences in binding energy of neutrons in, for example, the 2p and 3s or the 3p and 4s shells are such as to be approximately equal to the neutron separation energy. Thus capture gamma ray spectra for nuclei in the regions near 60 and 160 are dominated by electric dipole transitions which take place between p and s states. This effect is illustrated schematically in Figure 1 in which the change in single neutron energies with mass number is used to show the regions of importance of s - p transitions. It is also now clear that when p-wave resonances are important at relatively low neutron energies, resonance neutron capture is dominated by electric dipole transitions from p to s states. These facts have made the measurement of resonance capture spectra a useful technique for l-wave assignments of resonances.

The positions of other single neutron states are shown in Figure 1 and it can be seen that electric dipole transitions are possible between d-wave resonances and either p or f states for nuclei in the mass regions near 55 and 160. By analogy with s and p wave effects, these transitions may be expected to dominate d-wave capture spectra.

keV CAPTURE RESULTS

Techniques have been developed for using a Ge(Li) detector to measure gamma ray spectra from the capture of neutrons in the energy range from approximately 10 to 100 keV¹). A schematic diagram of the experiment is shown in Figure 2. Simultaneous measurements of neutron time of flight and gamma ray pulse height allow capture spectra to be determined

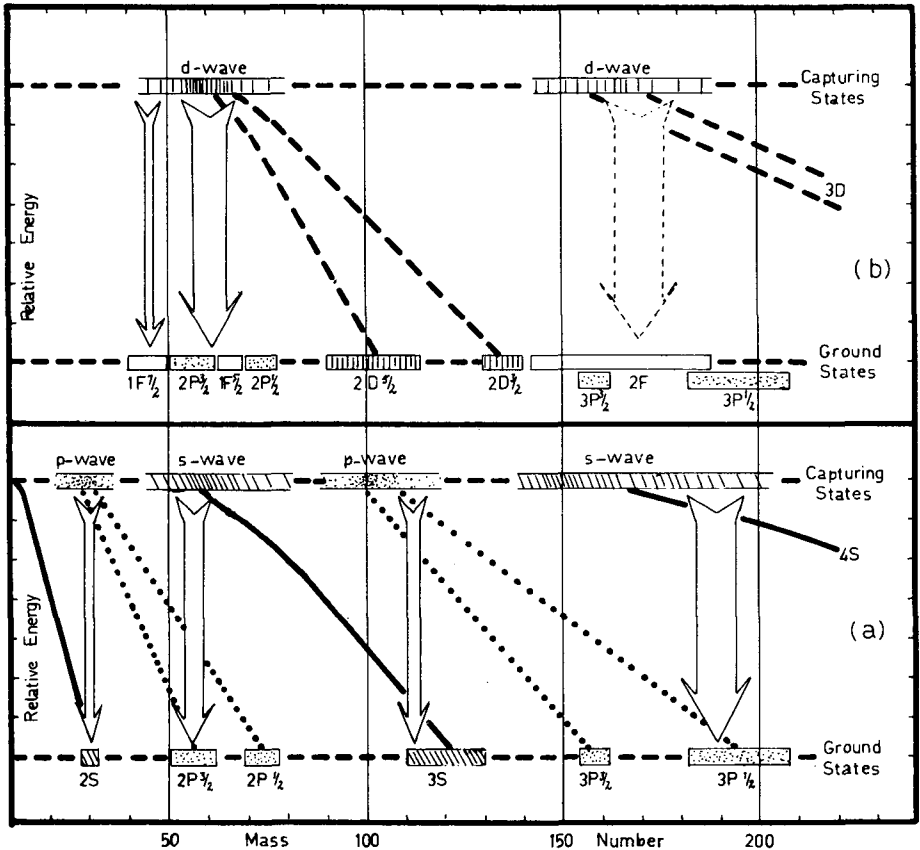


FIG.1. Schematic illustration of dependence of single neutron level energies on mass number (a) s and p states, (b) d states. Ground-state shell model assignments and strength function peaks are joined by lines representing the change in energy of particular shell model states. Arrows represent electric dipole transitions.

either for individual, well-spaced resonances or as an average over a number of resonances. In all cases the gamma ray energy for a transition to a particular final state increases with neutron energy and provides an additional measurement of the dependence of gamma ray intensity on neutron energy.

Measurements have been made for all elements from calcium to zinc using targets varying in mass from a few kilograms to 30 kilograms. Count rates were very low, requiring run times of from 40 to 100 hours. Nevertheless a great deal of information was obtained on transitions with intensities greater than approximately 10 per 100 captures and on their variation with neutron energy.

The results can be divided into two groups according to whether the target nuclei had either odd or even atomic number. For odd Z targets both initial and final states are relatively closely spaced and a considerable range of spin values is involved. For even Z targets, and particularly for even-even target nuclei, the gamma ray spectra and their interpretation are much simpler.

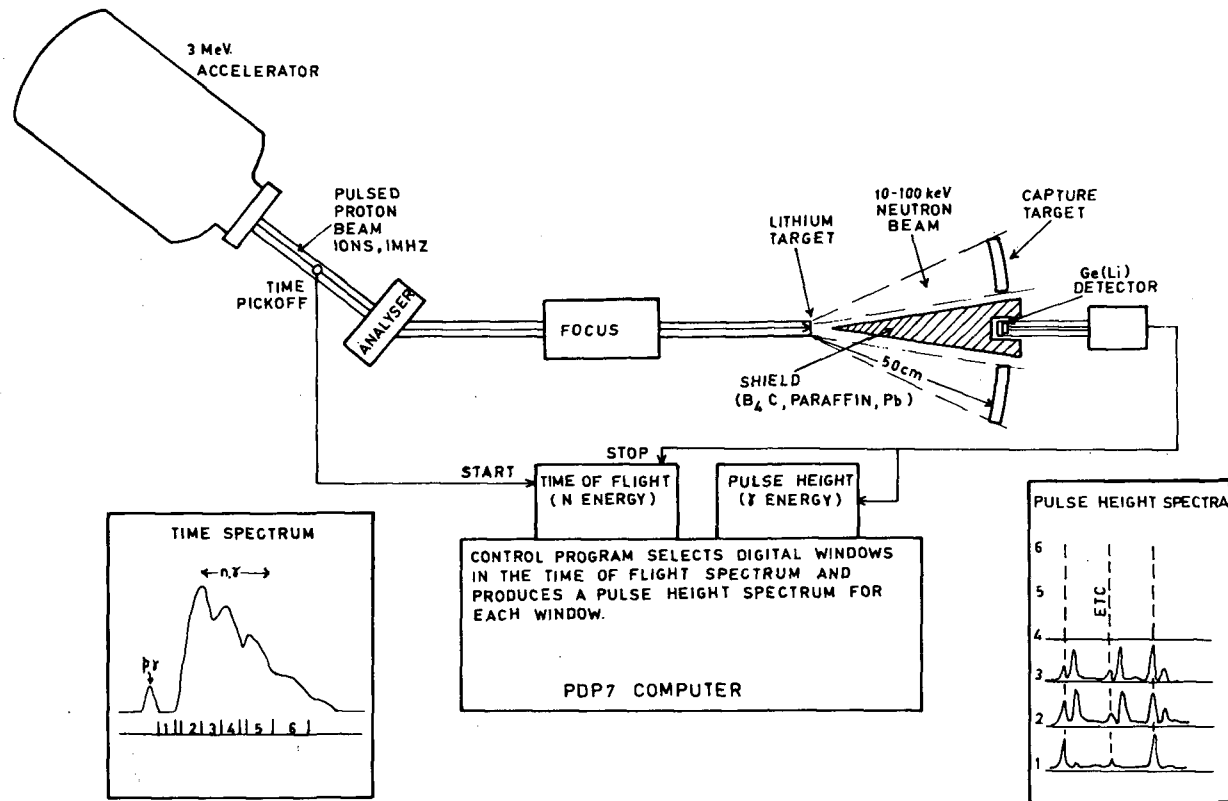


FIG.2. Dual-parameter system for the study of keV neutron capture. Gamma-ray and time-of-flight pulses are analysed in coincidence and proposed by an on-line computer.

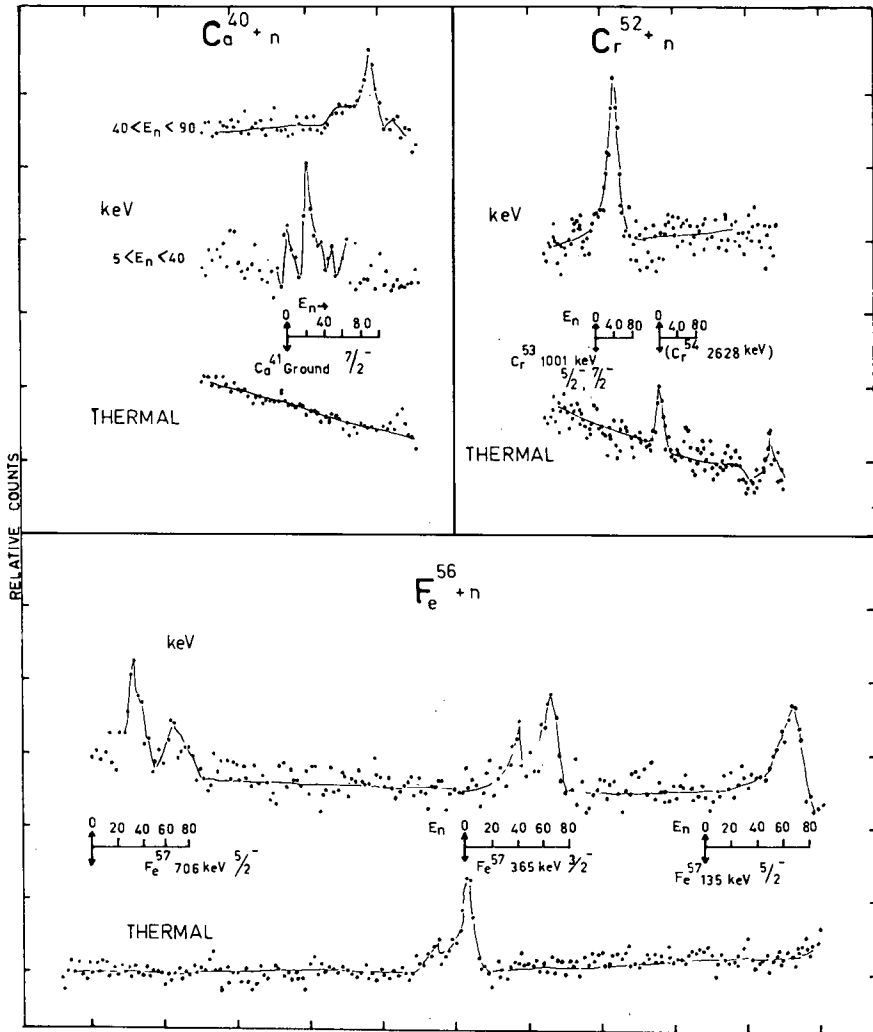


FIG.3. Partial gamma-ray spectra for keV capture in ^{40}Ca , ^{52}Cr and ^{56}Fe showing transitions to final states with spins $5/2^-$ and $7/2^-$. The corresponding thermal spectra are included.

A common feature, not observed in thermal capture, is the occurrence of transitions proceeding to final states with spins of $5/2^-$ and $7/2^-$. Some typical examples are shown in Figure 3. In each case the appropriate region of a thermal capture spectrum is shown with the calculated positions of possible 'high spin state transitions'. Also shown are the keV capture spectra in which these high spin state transitions appear, shifted by an amount equal to the neutron energy. In most cases particular neutron energies are important - indicating the role of individual resonances, even though these are not always completely resolved.

A list of the high spin state transitions that have been observed is given in Table I. The keV intensities are given as 'per cent captures' but the normalisation used depends on the rather crude assumption that the sum of all gamma rays observed is equal to that in the same energy region for thermal capture. The normalisation factors are unlikely to be in error by more than 30%. However, most of the measurements, especially those labelled average in Table I have an s-wave contribution to the capture spectrum. The measured intensities of the high spin state transitions are therefore lower limits to the intensities which they must have for the particular resonances in which they occur.

TABLE I

HIGH SPIN STATE TRANSITIONS IN EVEN-ODD MEDIUM WEIGHT NUCLEI

Compound Nucleus	$\langle D_1 \rangle$ keV	$\bar{\Gamma}_\gamma$ eV	E_n keV	I_i %	E_f keV	ℓ_n	J_F^π	$k(E1)$ $\times 10^{-3}$	$k(M1)$ $\times 10^{-3}$
$^{41}_{20}\text{Ca}$	49	1.0	Av	1.1	0	3	$7/2^-$	0.1	
$^{43}_{20}\text{Ca}$	29	1.0	Av	2.9	0	3	$7/2^-$	0.5	
				4.5	373	3	$5/2^-$	0.9	7.2
$^{45}_{20}\text{Ca}$	50	1.0	Av	3.2	0	3	$5/2^-$, $7/2^-$	0.4	3.1
$^{49}_{22}\text{Ti}$	17	1.0	44	6.4	0	3	$7/2^-$	1.5	
$^{53}_{24}\text{Cr}$	33	1.0	30	18	1007	3	$5/2^-$, $7/2^-$	3.6	34
$^{55}_{26}\text{Fe}$	20	0.3	Av	9	933	3	$5/2^-$	0.5	4.6
				4	1322	(3)		0.2	2.4
				2	1413	ISO	$7/2^-$	0.1	1.2
$^{57}_{26}\text{Fe}$	17	0.6 (1.3)	1.15	7	706	3	$5/2^-$		15
			26	3.3	706		$5/2^-$	1.6	15
		1.0	36	7.7	706		$5/2^-$	2.8	27
		1.0	52	8.4	135	3	$5/2^-$	2.4	23
				5.4	706		$5/2^-$	2.0	19
		1.0	72	12.6	135	3	$5/2^-$	3.6	35
				3.3	706		$5/2^-$	1.2	12
$^{59}_{28}\text{Ni}$	33	0.6	Av	4	341	3		0.2	2.0
$^{61}_{28}\text{Ni}$	14	0.4	Av	12	69	3	$5/2^-$	1.4	14
$^{65}_{30}\text{Zn}$	2.5	0.3	Av	2	0	3	$5/2^-$	0.9	9.4
$^{67}_{30}\text{Zn}$	4.5	0.2	Av	1.1	0	3	$5/2^-$	0.3	2.6

TABLE II
MULTIPOLARITY OF GAMMA RAY TRANSITIONS

ℓ Wave	Capture Resonance	$\langle D_J \rangle$	Final States			
			$1/2^-$	$3/2^-$	$5/2^-$	$7/2^-$
0	$1/2^+$	$D_{1/2}$	E1	E1	M2	E3
1	$1/2^-$	$D_{1/2}$	M1	M1	E2	M3
	$3/2^-$	$D_{1/2/2}$	M1	M1	M1	E2
2	$3/2^+$	$D_{1/2/2}$	E1	E1	E1	M2
	$5/2^+$	$D_{1/2/3}$	M2	E1	E1	E1

DISCUSSION

Estimated values of gamma ray reduced widths are included in Table I assuming that either E1 or M1 transitions are involved. The total radiative widths and average level spacings used in deriving these estimates are also given. The types of transitions that would be involved for s, p or d wave neutron capture in even-even target nuclei are listed in Table II.

It is usually assumed that only dipole transitions play a significant role in the high energy gamma ray spectra from neutron capture. This assumption would rule out s-wave capture as a possible source of high spin state transitions and would also rule out p-wave capture as a possible source of transitions to $7/2^-$ states. The evidence available concerning the possibility that p or d wave capture is responsible for the observed high spin state transitions can be summarized as follows :

(a) If all the transitions listed in Table I are assumed to arise from d-wave resonances, an average $k(E1)$ of 1.3×10^{-3} is obtained. This will be a lower limit and is close to the value (3×10^{-3}) given by Bartholomew²⁾ in his survey of thermal capture gamma rays.

(b) If we exclude the possibility of M3 transitions from $1/2^-$ resonances to $7/2^-$ final states, the value of E2 reduced widths obtained assuming $3/2^-$ resonances are of the order of 100 times the Weisskopf estimates. Since the observed results are effectively lower limits, they could only be explained by a major enhancement of E2 transitions.

(c) The transitions to $5/2^-$ states are even stronger than to $7/2^-$ states. If we exclude E2 transitions the average value of M1 reduced widths is 14×10^{-3} . This is comparable with the result reported by Bollinger³⁾ and others. However, two factors must be taken into account

in this comparison. Firstly, the particular resonances which give rise to $5/2^-$ transitions may also account for most of the observed strength to $1/2^-$ and $3/2^-$ states. If this is the case the latter transitions, being also M1, will raise the average reduced width considerably.

Alternatively, if the resonances under consideration have weaker transitions to $1/2^-$ and $3/2^-$ states (e.g. comparable to the $5/2^-$ transitions) then because of the overlap with s-wave resonances the values of I_γ and hence $k(M1)$ given in Table I are underestimated. In either case, if p-wave resonances are responsible for the $5/2^-$ transitions, the number of cases and the strengths observed require that strong M1 transitions be important in this mass region. There is no simple shell model explanation for such an effect.

(d) Positive parity states are known in some of the nuclei studied and some evidence is found in the experimental data from calcium and zinc for transitions to these states. However these transitions do not dominate the capture spectra as they do in the mass regions near 30 and 100 where p-wave resonances are known to be important.

(e) The resonance at 1.15 keV in ^{56}Fe target nucleus has been assigned as p-wave on the basis of the measured neutron width⁴⁾ and the measurement of interference in differential scattering cross sections⁵⁾. The estimate of transition strength to a $5/2^-$ state used in Table I is that given by Moore, Palevsky and Chrien⁶⁾. The value of $k(M1)$ is close to the average value given by Bollinger and hence is consistent with the p-wave assignment. This result is subject to considerable uncertainty since the NaI spectrum shows only broad features. Nevertheless it emphasizes the need for more detailed information on specific resonance assignments for high spin state transitions and the measurement of parameters for these resonances.

CONCLUSION

The most satisfactory explanation of the results reported here is both p and d-wave capture play an important role for neutron energies below 100 keV and for nuclei in the mass region 40 - 70. It is difficult to explain the stronger transitions solely in terms of p-wave capture. The appearance of many d-wave resonances would undoubtedly give rise to high values of the d-wave strength function and this is found in a more detailed analysis of results for zinc⁷⁾. Further measurements are needed of both neutron widths and partial radiation widths in order to clarify the respective roles of p and d wave resonances.

ACKNOWLEDGEMENTS

We wish to acknowledge the assistance of members of the 3 MeV Accelerator Group at Lucas Heights. Some of the data was supplied by D. Chan and G. J. Broomhall of the University of Melbourne from unpublished results.

REFERENCES

- 1) B.J. Allen, M.J. Kenny, R.J. Sparks. Nuclear Physics, A122 (1968) 220.
- 2) G. Bartholomew. Ann. Rev. Nuclear Science, 11 (1961) 259.
- 3) L.M. Bollinger. Proc. Int. Symp. on Nuc. Structure, Dubna, 1968.
- 4) R.C. Block. Physics Letters, 13 (1964) 234.
- 5) A. Asami, M.C. Moxon, W.E. Stein. Physics Letters, 28B (1969) 656.
- 6) J.A. Moore, H. Palevsky, R.E. Chrien. Phys. Rev., 132 (1963) 801.
- 7) B.J. Allen et al. (to be published).

GAMMA DECAY, INCLUDING INTENSE M1'S, IN $^{115}\text{In}(n, \gamma)^{116}\text{In}$

E. D. EARLE, M. A. LONE, G. A. BARTHOLOMEW
Atomic Energy of Canada, Ltd.,
Chalk River, Ontario,
Canada

Abstract

GAMMA DECAY, INCLUDING INTENSE M1'S, IN $^{115}\text{In}(n, \gamma)^{116}\text{In}$. The gamma-ray spectra above 4.5 MeV following resonance neutron capture in six ^{115}In resonances are reported. The correlation coefficient between gamma-ray intensities and (d, p) spectroscopic factors is zero. M1 transitions are prominent and an average value for K_{M1} of 1.5×10^{-2} eV/MeV² is found. Several levels strongly populated in the (n, γ) reaction were not seen in the (d, p) experiment.

Enhanced M1 transitions have been observed following neutron capture in several Sn isotopes by Harvey et al. [1] and Bhat et al. [2]. Strong M1 transitions have been predicted [3, 4] to occur at an energy somewhat higher than the spin-orbit splitting energy which, for $g_{3/2} - g_{7/2}$ in Sn, is about 5.3 MeV [5]. It is of interest to ascertain if nuclei adjacent to Sn also exhibit strong M1 transitions.

Recently Moorhead et al. [6] have done high-resolution (d, p) studies on ^{115}In and have been able to resolve many of the ^{116}In levels below 1.6 MeV. Their angular distribution data have enabled them to measure ℓ -values and hence to assign parities to these levels. Thus the multipolarity of gamma rays populating these levels following S-wave neutron capture in ^{115}In can be determined. In addition, a comparison of the (n, γ) and (d, p) reduced widths can provide information on the importance of the direct capture mechanism in the (n, γ) reaction.

The gamma-ray spectra following resonance neutron capture in a natural In target were studied with the Chalk River chopper facility. The chopper wheel is identical to that in use at the High Flux Beam Reactor at Brookhaven [7]. The neutron source is a D₂O-filled scattering can situated in a through tube of the NRU reactor and provides an epithermal beam largely free of reactor gamma rays and fast neutrons. The wheel is designed to rotate at 15 000 rev/min. At this speed the chopper resolution is 0.25 $\mu\text{sec}/\text{m}$ at our 20-m detector station and yields an intensity of about $2 \times 10^3/E^n \text{ cm}^{-2} \text{ sec}^{-1} \text{ eV}^{-1}$.

Figure 1 shows the In time spectrum of neutrons in coincidence with gamma rays greater than 3 MeV. These data were obtained at a time-of-flight resolution of 0.65 $\mu\text{sec}/\text{m}$. Not all of the neutron resonances seen here are in ^{115}In . The three resonances at 4.71, 14.7 and 31 eV are in ^{113}In . Properties of the gamma rays from ^{115}In resonances only will be discussed. By placing suitable gates on the resonance peaks, the gamma-ray spectra associated with each resonance were extracted. Examples of these spectra are shown in Fig. 2. Only the energy range from 4.3 to 7.5 MeV is shown and contains all the data used in the present analysis. Figure 2 shows gamma-ray spectra from three ^{115}In resonances and from thermal neutron

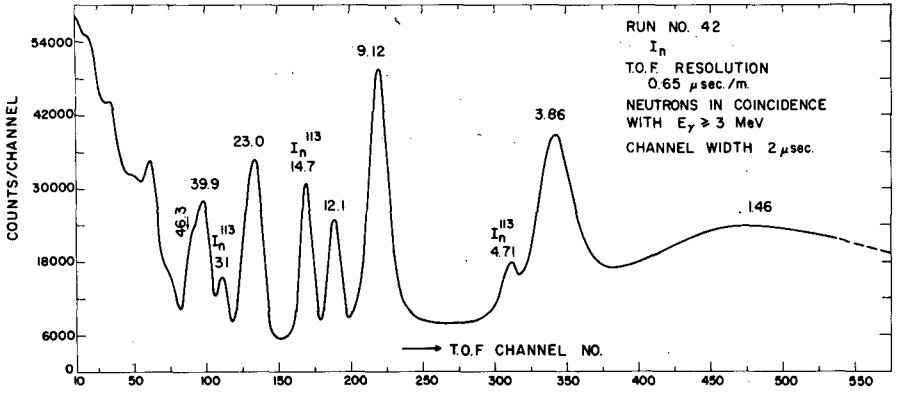


FIG. 1. Block diagram of the data collection system.

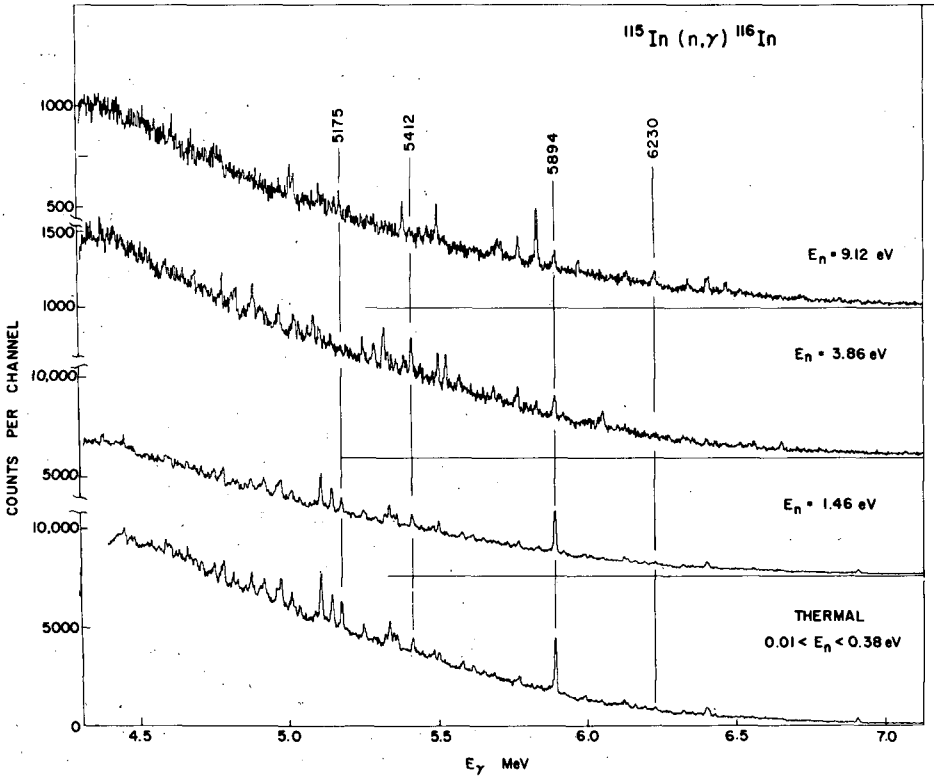


FIG. 2. Gamma-ray pulse height spectra from ^{115}In resonances and the thermal region.

TABLE I. CORRECTED RELATIVE INTENSITIES OF GAMMA-RAYS FROM RESONANCES IN ^{115}In

E_γ	E_x	π	I_γ Thermal	I_γ 1.48 eV	I_γ 3.86 eV	I_γ 9.12 eV	I_γ 12.1 eV	I_γ 23 eV	I_γ 40 eV
6503(2)	272	+		0.3(.2)	0.4(.3)				
6471(5)	304			0.2(.1)	0.5(.3)				
6411(7)	364	-	2.5(.3)	1.4(.2)		2.5(.4)			
6326(4)	449		2.2(.2)	1.3(.2)	1.6(.3)	4.8(.6)		2.6(.8)	5.4(1.3)
6230(3)	545		1.5(.2)	1.1(.2)	0.6(.4)	1.1(.4)	3.8(.9)	.8(.6)	
6136(4)	639		1.0(.3)	1.3(.2)	1.5(.4)	4.0(.5)	9.4(1.0)	1.4(.6)	16.1(1.2)
6048(2)	727	(-)	0.7(.4)	1.0(.3)	7.1(.6)	2.3(.5)		6.2(1.5)	2.6(1.0)
6013(7)	762	(+)		0.4(.2)	0.7(.4)		1.3(1.0)	1.8(.7)	
5981(5)	794	+				2.0(.6)			
5984(1)	881		24.7(.4)	15.1(.3)	4.2(.5)	4.0(.6)	2.4(1.1)	5.3(.8)	16.6(1.3)
5836(3)	939		0.5(.4)	1.0(.2)	0.9(.5)	13.3(.7)	9.0(1.3)	0.8(.8)	8.0(1.3)
5771(2)	1004	(-)	3.6(.4)	1.5(.3)	3.8(.6)	5.0(.7)	2.4(1.2)		3.8(1.3)
5716(5)	1059	(-)			0.9(.6)	4.4(.7)	4.1(1.3)	3.2(.9)	3.6(1.3)
5703(5)	1072					4.7(.7)	3.7(1.3)	1.3(.9)	1.4(1.3)
5687(5)	1088				2.7(.6)	1.8(.7)	1.4(1.3)	1.8(.9)	
5582(2)	1193	+	2.3(.5)		0.6(.5)				
5575(2)	1200		1.5(.4)	1.1(.3)	2.0(.6)				1.9(1.3)
5502(2)	1273		4.0(.5)	3.7(.3)	6.0(.7)	7.7(.8)	1.4(1.4)	1.9(1.0)	4.8(1.4)
5485(2)	1290	+	2.6(.5)	1.1(.3)		2.2(.8)	3.4(1.5)		
5445(4)	1330		2.4(.5)	1.0(.3)	2.0(.7)	2.3(.8)	2.3(1.5)	1.0(1.0)	1.3(1.4)
5412(2)	1363	+	9.9(.7)	6.1(.5)	8.0(1.0)	1.7(1.1)	7.2(2.1)	5.5(1.5)	3.6(2.0)
5387(2)	1388					2.6(.7)	1.8(1.5)	2.2(1.1)	
5361(2)	1414		6.9(.5)	3.4(.3)	1.4(.7)		1.7(1.5)	1.9(1.1)	1.8(1.5)
5349(2)	1426		6.6(.5)	3.6(.3)	1.1(.6)	1.2(.7)	2.5(1.4)	2.8(1.0)	2.1(1.3)
5336(2)	1439	+	12.5(.5)	7.1(.3)	1.2(.7)	1.2(.8)		4.0(1.1)	1.8(1.5)
5321(2)	1454	(-)	3.6(.5)	2.4(.3)	7.5(.8)		4.2(1.6)	2.2(1.1)	2.6(1.5)
5283(2)	1492	(+)			3.4(.8)		8.4(1.7)		
5249(2)	1526		5.0(.5)	2.9(.4)	3.1(.8)		1.6(1.6)	2.1(1.2)	3.0(1.5)
5175(2)	1600	+	13.1(.6)	4.9(.4)		3.8(.9)	4.5(1.7)	1.7(1.2)	4.5(1.6)
5143(2)	1632		16.8(.6)	8.9(.4)	2.0(.8)	1.5(.9)	1.9(1.7)	3.4(1.2)	2.7(1.6)
5120(2)	1655		4.7(.6)	2.3(.4)		2.2(1.0)		8.0(1.3)	2.9(1.6)
5106(2)	1669		22.5(.6)	11.8(.4)	2.9(.8)	3.4(1.0)		4.6(1.3)	2.1(1.6)
5087(2)	1688		6.0(.6)	2.8(.4)	6.0(.9)	1.2(1.0)	3.2(1.7)	2.7(1.3)	2.6(1.7)
5035(2)	1740		4.4(.6)	2.2(.4)	5.5(1.2)		4.7(1.8)	1.9(1.3)	6.2(1.7)
5017(4)	1758		3.3(.8)		5.4(1.3)	5.2(1.4)	6.9(2.0)	2.1(1.7)	
5008(4)	1767		9.8(.8)	6.6(.5)		5.2(1.4)		2.1(1.7)	
4972(4)	1803		16.7(1.0)	8.6(.6)	4.2(1.2)	1.3(1.2)		4.9(1.9)	
4959(4)	1816		9.6(1.0)	5.3(.6)	2.1(.5)	1.0(1.0)			4.3(2.5)
4915(2)	1860		11.9(.7)	8.0(.4)	3.2(.9)	1.6(1.1)	4.2(1.9)	2.6(1.4)	2.1(1.8)
4902(2)	1873		6.2(.7)	4.2(.4)	4.0(.9)			4.3(1.4)	

capture. The latter spectrum was obtained in a separate run at a time-of-flight resolution of $3.25 \mu\text{sec/m}$. All of these gamma-ray spectra were taken with a $23\text{-cm}^3 \text{Ge(Li)}$ detector and with a resolution of 7.5keV at 6MeV .

The relative intensities of all observed gamma rays were determined by obtaining the areas of the second-escape peaks, correcting for any first-escape or full-energy peaks superimposed on the second-escape peaks, and correcting for detector efficiency.

The information obtained from this analysis is summarized in Table I. The gamma-ray energies are listed in the first column. These energies were determined from calibration curves obtained from thermal capture gamma-ray spectra of chromium and cobalt oxide targets. The energies and relative intensities of the gamma rays seen in thermal capture compare well with the thermal capture work of Rasmussen et al. [8]. The energies of levels populated by these gamma rays (assuming they are primary) are given in the second column. These were derived by adopting the ^{116}In neutron separation energy of 6775keV determined in the (d, p) work of Moorhead et al. (B. L. Cohen, private communication). Levels observed in the present experiment which overlap to within 5-keV levels observed by Moorhead et al. were assumed to be the same level. Parity assignments

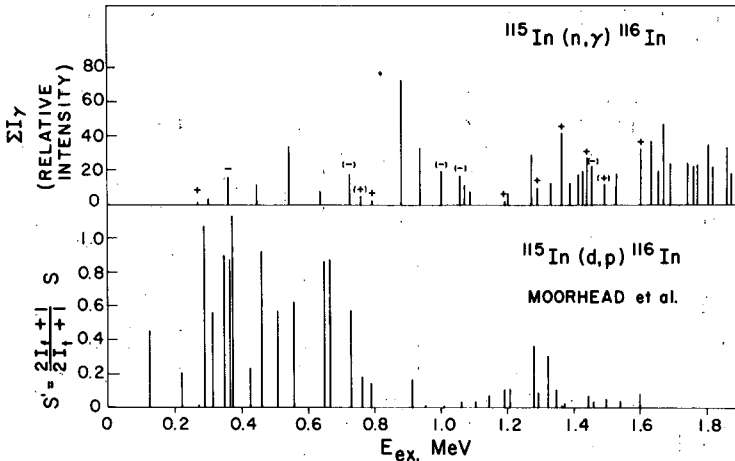


FIG. 3. Comparison between the averaged relative intensities and the (d, p) spectroscopic factors.

were made to these levels from the (d, p) angular distribution data and these are listed in the third column of this table. The parentheses indicate levels about which Moorhead et al. expressed some uncertainty.

The remaining columns of the table list the relative intensities of the gamma rays for each of the neutron energies indicated. The normalization of peak areas to obtain relative intensities involved correcting for the detector efficiency and dividing by the relative areas of the neutron resonances or, in other words, the total number of counts in the relevant gamma-ray spectrum. The errors are due to the statistical errors in the peak and background counts.

I shall not discuss detailed aspects of these intensities but merely show a comparison of the average intensities of the gamma rays and the (d, p) spectroscopic factors [6]. The average relative intensities of each gamma ray obtained by summing over the seven spectra listed here are shown in Fig. 3 where they are compared with the (d, p) spectroscopic factors. Here S' is the most useful quantity to plot because of the uncertainty in the spin of the final state, I_f . The abscissa is excitation energy in ^{116}In from 0 to 1.9 MeV. The (d, p) data do not extend beyond 1.6 MeV.

The (d, p) reaction favours levels between 0.3 and 0.7 MeV over levels between 1.2 and 1.6 MeV, whereas in the (n, γ) reaction the reverse is true. This anticorrelation is obvious from this figure. However, we need not attach a great significance to it because the (d, p) groups include many with large ℓ_n -values and the spin change to reach these levels in the (n, γ) reaction may be too large. The correlation coefficient, when the levels populated in the (n, γ) reaction only are considered, is zero which suggests that direct capture is not important in the $\text{In}(n, \gamma)$ reaction.

Levels for which parity signs are shown in Fig. 3 are populated in both the (n, γ) and (d, p) reactions. As mentioned earlier, these are the levels which overlap to within 5 keV. Fifty per cent of the levels seen in the (n, γ) reaction were not observed in (d, p) and several of these are strongly populated in the (n, γ) reaction, for example, the 881 and 939 keV states. A possible explanation for these levels is that they have large admixtures

of proton quasiparticle states which are not excited in the (d, p) reaction. Similar levels have been observed in thulium by Lone et al. at Brookhaven [9, 10].

A final observation from Fig. 3 is the prominence of M1 (E2) transitions. Since the capturing state in ^{116}In has positive parity the negative signs in this figure correspond to E1 transitions while the positive signs correspond to M1 (E2) transitions. The strength of the M1 transitions relative to the E1's is immediately obvious from this figure which shows three M1's to be stronger than any of the E1's observed in this experiment. The absolute intensities of these M1 lines, i.e. their reduced widths, determined by normalizing our thermal spectrum to the thermal spectrum of Rasmussen et al., are not exceptional when compared to those in other nuclei. An average value for K_{M1} of 1.5×10^{-2} eV/MeV⁴ was calculated for these M1 gamma rays and is about a factor of 10 less than that calculated for the stronger M1 gamma rays observed in Sn but comparable to that calculated for Cd.

REFERENCES

- [1] HARVEY, J.A., SLAUGHTER, G.G., BIRD, J.R., CHAPMAN, G.T., Rep. ANL 6797 (1963) 230.
- [2] BHAT, M.R., CHRIEN, R.E., WASSON, O.A., BEER, M., LONE, M.A., Phys. Rev. 166 (1968) 1111.
- [3] MOTTELSON, B.R., Proc. Int. Conf. Nuclear Structure, Kingston (BROMLEY, D.A., VOGT, E.W., Eds), University of Toronto Press, Toronto (1960) 525.
- [4] SHAPIRO, C.S., EMERY, G.T., Bull. Am. phys. Soc. 13 (1968) 1384.
- [5] SHAKIN, C., Annls Phys. 1 (1963) 373.
- [6] MOORHEAD, J.B., COHEN, B.L., MOYER, R.A., Phys. Rev. 165 (1968) 1287.
- [7] CHRIEN, R.E., REICH, M., Nucl. Instrum. Meth. 53 (1967) 93.
- [8] RASMUSSEN, N.C., INOUE, Y.H.T., ORPHAN, V.J., Rep. MITNE-85 (Jan. 1969).
- [9] LONE, M.A., Thesis, State University of New York, Stony Brook, 1967.
- [10] LONE, M.A., CHRIEN, R.E., WASSON, O.A., BEER, M., BHAT, M.R., MUETHER, H.R., Phys. Rev. 174 (1968) 1512.

USE OF AVERAGE RESONANCE CAPTURE MEASUREMENTS FOR NUCLEAR SPECTROSCOPY

R. K. SMITHER, L. M. BOLLINGER
Argonne National Laboratory,
Argonne, Ill.,
United States of America

Abstract

USE OF AVERAGE RESONANCE CAPTURE MEASUREMENTS FOR NUCLEAR SPECTROSCOPY. The use of the average capture gamma-ray spectrum as a spectroscopic tool is discussed in the light of Argonne experience.

Average resonance capture measurements have proved to be a valuable way to study the statistical properties of the neutron capture process. They are also a powerful spectroscopic tool. In favourable cases it is possible to determine the parity and restrict the choice of the spin to two values for 20 to 30 levels of the nucleus. The basic approach is quite simple. The neutron capture process is spread out over many neutron resonances so that no one resonance contributes more than a few per cent of the radiative capture. This averages out the Porter-Thomas fluctuations of the radiation widths of individual gamma rays associated with a single resonance and allows one to identify the multipole of the transition by its characteristic gamma intensity.

Figure 1 illustrates this approach. On the left is shown the neutron capture into many levels followed by the emission of primary gamma rays. On the right is the predictions for the distribution of radiation widths based on the Porter-Thomas theory. When the gamma strength is averaged over many resonances, the average fractional deviation $\Delta\Gamma/\Gamma$ is given by the expression

$$\Delta\Gamma/\Gamma \approx \sqrt{2/\nu}$$

where ν is the number of resonances used in the average. In our experiments $\nu \approx 200$ so that $\Delta\Gamma/\Gamma \approx 0.10$, or 10% of the average value. The averaging process is done by surrounding the neutron capturing sample by enough boron (1/16 - 1/8 in.) to strongly absorb all the incident neutrons with energies below 100 eV. This eliminates the strong low-energy neutron resonance from the capture process and leaves only the neutron capture in the numerous weak resonances above 100 eV to be averaged. A typical sample is shown in Fig. 2. The sample is placed in the high-flux region of the Argonne research reactor in the centre of a 5-in. diameter through tube (shown in Fig. 3). The gamma rays are brought out through a set of collimators and detected by a Ge(Li) detector. The Ge(Li) detector is incorporated in a large pair spectrometer (split ring of NaI, 12-in. diam.) to suppress Compton, single escape and full energy peaks.

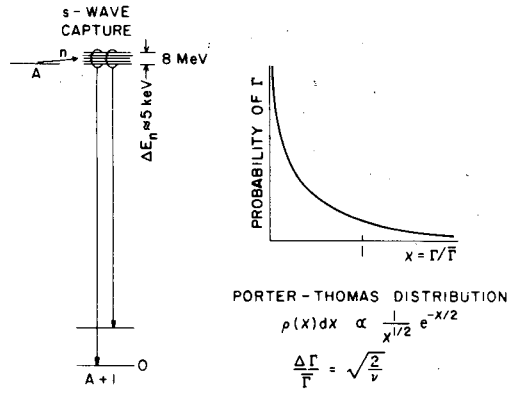


FIG. 1. (Left) Neutron capture into many levels followed by primary gamma rays. (Right) Predictions for the distribution of radiation widths.

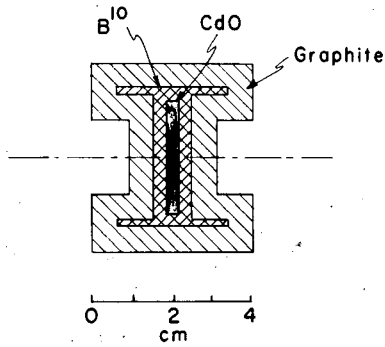


FIG. 2. Graphite holder with a typical sample.

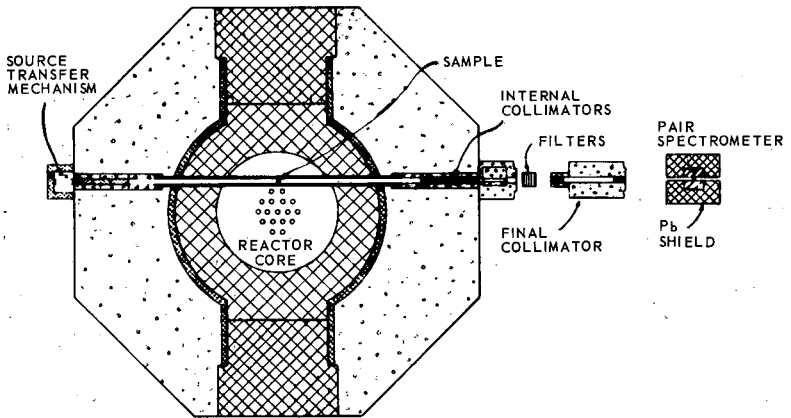


FIG. 3. The 5-in. diam. through tube.

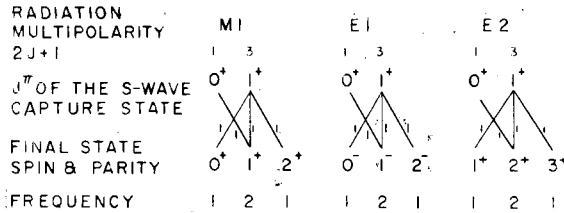


FIG. 4. Average intensities split into sub-groups.

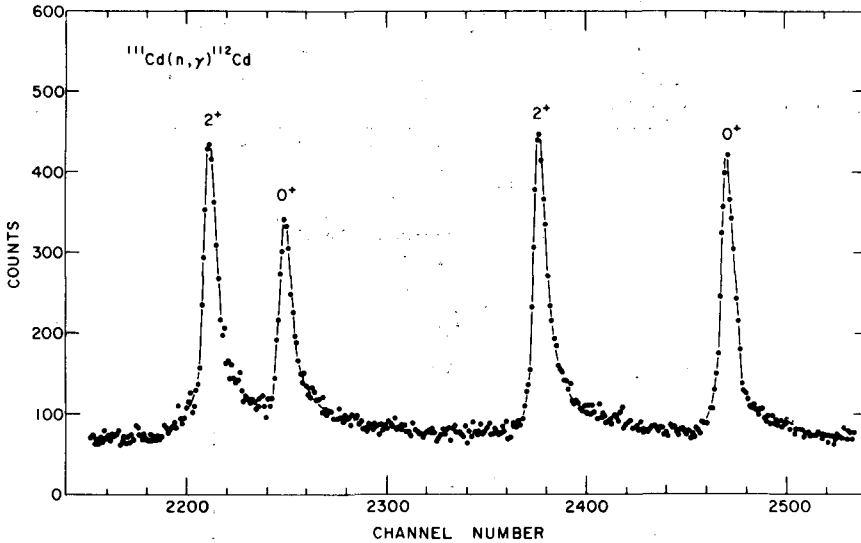


FIG. 5. Spectrum from an enriched cadmium sample showing the enhancement of 2^+ lines over 0^+ lines.

In general, the average E1 radiation is a factor of 8 to 12 stronger than the M1 radiation, which results in two easily separated groups. These average intensities are further split into subgroups according to the spin of the final state. This is shown in Fig. 4, where we consider the case of neutron capture in ^{111}Cd and ^{113}Cd , where the capturing state is $\frac{1}{2}^+$. For dipole radiation the strength to the $J=1$ levels is twice as strong as it is for the $J=0$ or $J=2$ ones. Furthermore, the presence of E2 radiation enhances the strength to the 1^+ and 2^+ states over that to the 0^+ states and generates some transition strength to the 3^+ states. p-wave capture, followed by E1 transitions, results in much the same type of enhancements and in the region of $A=85-135$ the p-wave contributions will often be stronger than the E2 component.

Figure 5 is an example of the data taken by Smither and Buss with an enriched sample of ^{111}Cd . The predicted enhancement of the 2^+ lines over the 0^+ lines is quite obvious.

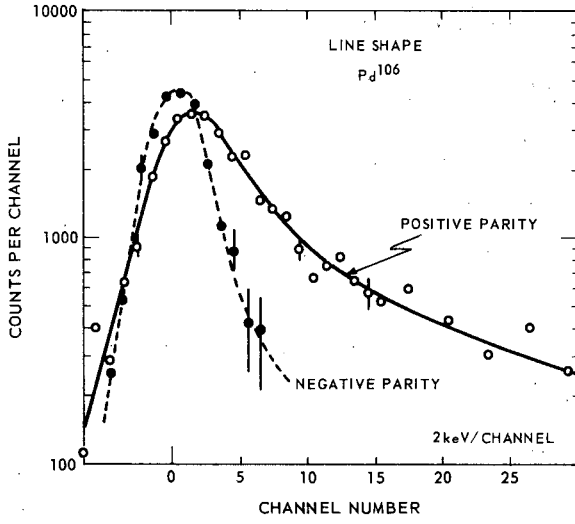
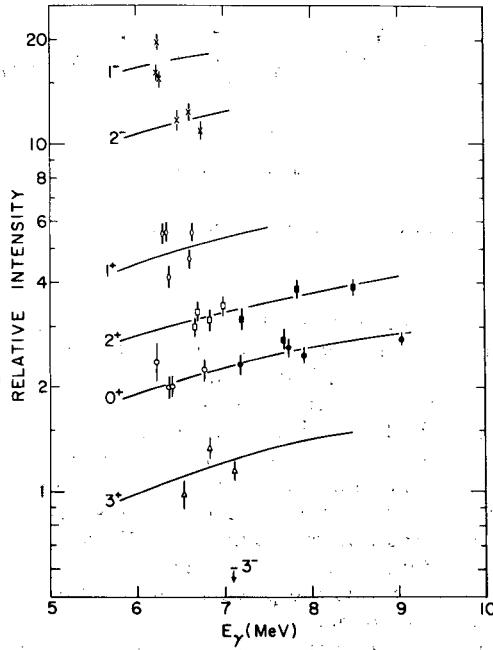


FIG. 6. Change in line shape of the peak.

FIG. 7. Experimental results for the $^{113}\text{Cd}(n, \gamma)^{114}\text{Cd}$ reaction:

When the p-wave strength is appreciable, it will of course be present in all the transitions where it is possible and can be detected by the change in the line shape of the peak in the Ge-Li detector. This is illustrated in Fig.6. This difference in shape can be used to distinguish E1 transitions from M1 or E2 transitions and is used as a check on the multipole assignments of the lines.

The experimental results for the $^{113}\text{Cd}(n, \gamma)^{114}\text{Cd}$ reaction are shown in Fig.7. The filled squares and circles are known 2^+ and 0^+ levels respectively. The relative intensity plotted is the observed gamma intensity divided by the cube of the gamma energy ($I_{\text{rel}} = I_{\gamma}/E^3$). The separation of the intensities into groups associated with a single spin value is due to the appreciable amounts of s-wave capture plus E2 and p-wave capture plus E1 components in the spectrum.

Table I gives a list of the isotopes studied to date. Of all the cases studied only ^{170}Tm did not follow the general pattern.

TABLE I. AVERAGE RESONANCE CAPTURE DATA RELATIONSHIP TO STATISTICAL MODEL

Agreement		Disagreement	Not analysed	
^{112}Cd	^{168}Er	^{170}Tm	^{74}Ge	^{136}Ba
^{114}Cd	^{178}Hf		^{92}Zr	^{138}B
^{126}Te	^{180}Hf		^{94}Nb	^{162}Dy
^{148}Sm	^{182}Ta		^{96}Mo	^{164}Dy
^{150}Sm	^{188}Os		^{98}Mo	^{172}Yb
^{156}Gd	^{190}Os		^{100}Ru	^{174}Yb
^{158}Gd	^{196}Pt		^{102}Ru	^{184}W
^{166}Ho			^{106}Pd	^{194}Au
			^{118}Sn	^{200}Hg
			^{120}Sn	^{202}Hg
			^{134}Cs	^{239}U

NEUTRON CAPTURE GAMMA-RAY MEASUREMENTS WITH A REACTOR-PRODUCED 2-keV NEUTRON BEAM*

R. C. GREENWOOD, R. A. HARLAN, R. G. HELMER, C. W. REICH
National Reactor Testing Station,
Idaho Nuclear Corporation,
Idaho Falls, Idaho,
United States of America

Abstract

NEUTRON CAPTURE GAMMA-RAY MEASUREMENTS WITH A REACTOR-PRODUCED 2-keV NEUTRON BEAM. Neutron capture gamma-ray measurements with a 2-keV neutron beam obtained from the Materials Testing Reactor are discussed. The utility of this beam for neutron capture gamma-ray spectroscopy is illustrated by considering the following three reactions: $^{181}\text{Ta}(n, \gamma)$, $^{180}\text{Hf}(n, \gamma)$ and $^{55}\text{Mn}(n, \gamma)$.

A beam of 2-keV neutrons has been extracted from the Materials Testing Reactor using a thick scandium filter. Scandium has the interesting property that its total neutron cross section approaches zero at 1.95 keV [1,2]. Because of this, 2-keV neutrons have excellent transmission through even a thick scandium filter. Actually, because of the exact shape of this "hole" in the total neutron cross section, the energy distribution of neutrons in a beam obtained through a thick scandium filter is approximately Gaussian, centered at 1.95 keV, with a full-width-at-half-maximum of about 700 eV. A detailed description of this beam facility is given by Simpson and Miller [2,3].

In this paper we will discuss the utility of this 2-keV neutron beam as a tool in neutron capture gamma-ray spectroscopy. In addition to the fact that this is an external beam and hence readily accessible, two features of the beam which make it attractive for neutron capture gamma-ray measurements are the following:

- the high flux of 2-keV neutrons obtained in the external beam. In this present facility a 2-keV neutron flux of approximately 2×10^6 neutrons/cm²/sec is obtained at the sample position using a 42-in. scandium filter.
- the low gamma-ray background which is present in this beam because of the thick filter (< 2 mR/hr).

In order to explore the utility of this 2-keV neutron beam facility for neutron capture gamma-ray spectroscopy we will discuss as illustrative examples the data obtained with the following three reactions: $^{181}\text{Ta}(n, \gamma)$, $^{180}\text{Hf}(n, \gamma)$ and $^{55}\text{Mn}(n, \gamma)$. These three reactions have been chosen because they include the following three types of neutron capture reaction: (1) with a high Z, odd-A target nucleus (where the neutron resonance spacing is a few eV), (2) with a high Z, even-even target nucleus (where the resonance spacing is not small, typically ranging from a few tens of eV upward), and (3) with a low-Z target nucleus (where the resonance spacing is typically a few keV).

* Work performed under the auspices of the US Atomic Energy Commission.

Before discussing these data we will briefly comment on the distribution of intensities (partial radiation widths) which are observed for primary capture gamma rays. Wide statistical fluctuations are expected in the distribution of partial radiation widths of transitions from individual neutron resonance states to a lower energy state. Porter and Thomas [4] have suggested that this distribution of partial radiation widths can be described by a chi-squared distribution with one degree of freedom. That is, the distribution function is of the form

$$P(x) dx = \frac{1}{2} \Gamma\left(\frac{1}{2}\right)^{-1} \left(\frac{x}{2}\right)^{-\frac{1}{2}} e^{-\frac{x}{2}} dx$$

where $P(x)$ is the probability at amplitude x , $\Gamma\left(\frac{1}{2}\right)$ is the gamma function, and where x is defined as

$$x = \frac{\Gamma_{\gamma i}}{\langle \Gamma_{\gamma i} \rangle_{Av}}$$

This distribution is illustrated in Fig. 1. Experimental data on the distributions of partial radiation widths tend to support this hypothesis [5], although Chrien [6] has suggested that the distribution of partial radiation widths for at least some nuclei is better fitted with a chi-squared distribution with greater than one degree of freedom. In the following discussion we will assume for simplicity that the distribution of partial radiation widths is described by a chi-squared distribution with one degree of freedom. (The conclusions we will reach, however, are not critically dependent on this assumption.) Then, if the neutron capture is an average over ν

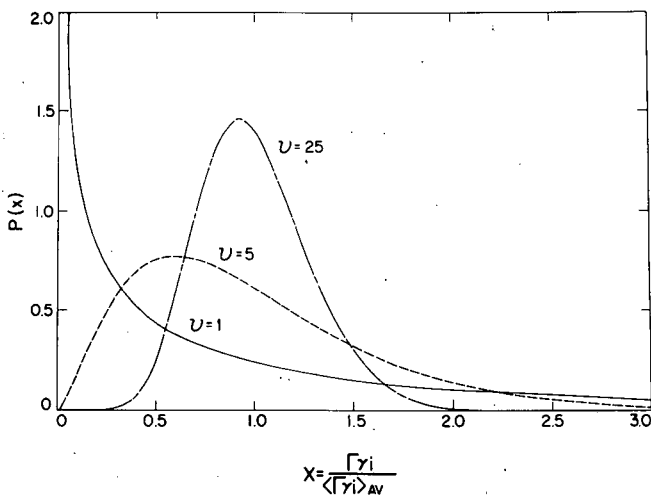


FIG. 1. Chi-squared probability distributions with 1, 5 and 25 degrees of freedom.

resonances, instead of merely resulting from one resonance, the total partial radiation width to a particular final state is given by

$$\Gamma_{\gamma i} = \sum_{j=1}^{\nu} \Gamma_{\nu ij}$$

For this case it is reasonable to suggest that this averaged partial radiation width has a chi-squared distribution with ν degrees of freedom [4]. That is a distribution with the following form:

$$P(x) dx = \Gamma \left(\frac{\nu}{2}\right)^{-1} \left(\frac{\nu x}{2}\right)^{\frac{\nu}{2}-1} e^{-\frac{\nu x}{2}} \left(\frac{\nu}{2}\right) dx$$

Additional chi-squared distributions with 5 and 25 degrees of freedom are illustrated for purposes of comparison in Fig. 1.

We now consider the three specific cases mentioned above.

$^{181}\text{Ta}(n,\gamma)$

The $^{181}\text{Ta}(n,\gamma)$ spectrum obtained using the 2-keV neutron beam provides an example of a capture gamma-ray spectrum which is averaged over many resonances. This spectrum is shown in Fig. 2. For comparison, the corresponding portion of the thermal-neutron capture gamma-ray spectrum is included in Fig. 2. Figure 3 shows a plot of $I_{\gamma} E_{\gamma}^{-3}$ versus the energy, E_{γ} , of the primary capture gamma-rays observed from 2-keV neutron capture in tantalum. It is seen from Fig. 3 that values of $I_{\gamma} E_{\gamma}^{-3}$ are significantly different for E1 and M1 transitions. Also, as expected [7], there is approximately a factor of two between the intensities of primary transitions to spin 3 or 4 and spin 2 or 5 states. (If only s-wave neutron capture is considered, the compound states in ^{182}Ta will have spins of 3 or 4.) The $J = 2,5$ lines in Fig. 3 are drawn in at one-half the intensity of the $J = 3,4$ lines. Each of these lines is drawn with an E_{γ}^{-5} energy dependence. As noted by Bollinger [5,8] this E_{γ}^{-5} energy dependence often seems to represent a better fit to the averaged intensity data than does the E_{γ}^{-3} function. This also appears to be the case for $^{181}\text{Ta}(n,\gamma)$, at least for the E1 transitions.

If we assume an average resonance spacing of 5 eV for the $^{181}\text{Ta}(n,\gamma)$ reaction [9] we would estimate that the 2-keV neutron capture gamma-ray spectrum is an average over approximately 170 resonances (with both $J = 3$ and 4). An estimate of the number of resonances that this spectrum is an average over can also be obtained from the distribution of primary capture gamma-ray intensities. Figure 4 shows a plot of the experimental distribution of the E1 transitions, grouped into intervals $\Delta x = 0.1$, plotted against x . The parallel lines drawn for $J = 3,4$ and $J = 2,5$ in Fig. 3 are used to define $x = 1.0$ and $x = 0.5$, respectively. For comparison, the expected probability distributions for a spectrum averaged over 50, 100 and 200 total (both $J = 3$ and 4 resonances) are also shown in Fig. 4. The variance computed from the transition intensities to final states assigned as 3- or 4- suggests that we are averaging over approximately 140 resonances. This is in rather good agreement with the approximately 170 resonances which we would expect to average over. The transition intensities to final states assigned as 2- or 5- show considerably more statistical

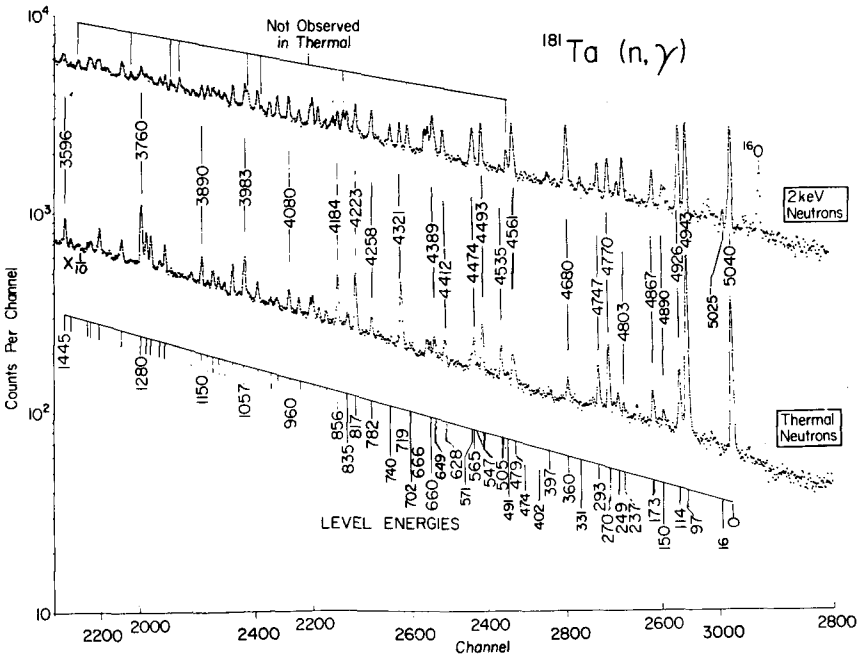


FIG. 2. Comparison of the high-energy portions of the prompt gamma-ray spectra resulting from 2-keV and thermal neutron capture in tantalum. The energies associated with the peaks are the double-escape peak energies measured for thermal neutron capture. The 2-keV capture gamma-ray spectrum was obtained with an 80-h run using a 15-g tantalum sample.

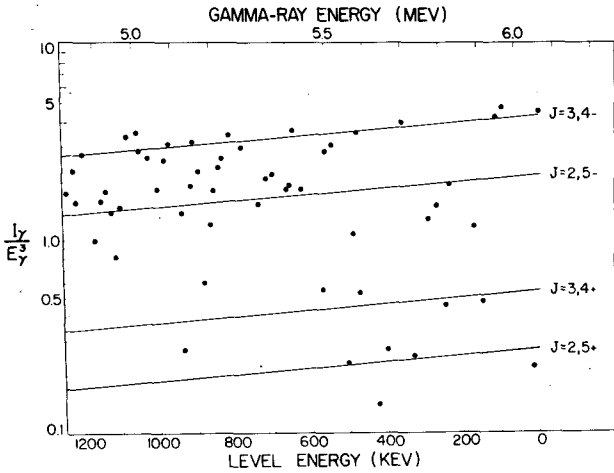


FIG. 3. A plot of I_γ/E_γ^3 against the energy of the prompt gamma-ray transitions observed from 2-keV neutron capture in tantalum. The I_γ represents the relative intensity of the prompt gamma-ray transitions.

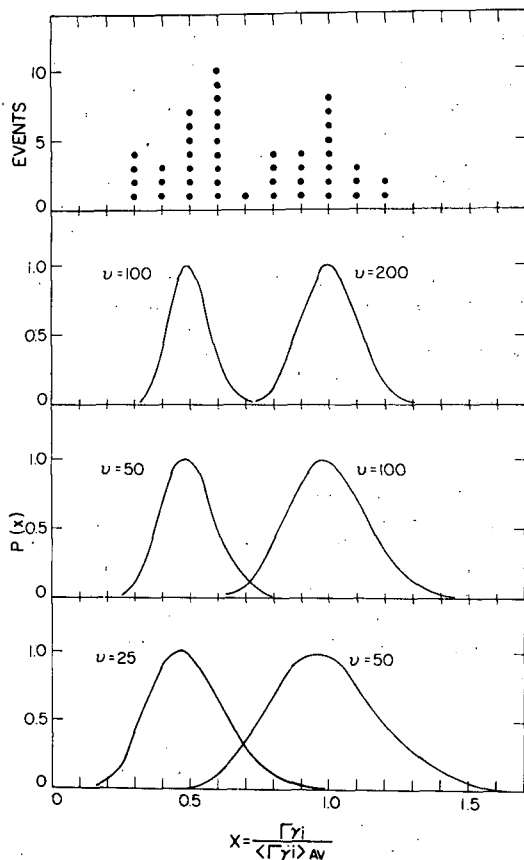


FIG.4. The observed distribution of the E1 transition intensities from 2-keV neutron capture in tantalum. For comparison, expected probability distributions for a spectrum averaged over 50, 100 and 200 total neutron resonances are also shown.

spread, and the computed variance in these experimental data suggests that we are only averaging over approximately 40 resonances, compared to an expected 85 resonances. However, it should be noted that the transition intensities to 2- or 5- final states, being weaker, would be affected proportionately more by unresolved M1 transitions within these peaks. Also, a pair of unresolved M1 transitions could be incorrectly assigned as an E1 transition to a final 2- or 5- state. Thus it is not surprising that we have an apparently poorer averaging of the E1 transition intensities to final states with spins 2- or 5-.

Actually, because the density of states in ^{182}Ta is becoming so high, any spin assignments based solely on the 2-keV neutron capture data must be considered as tentative above about 700 keV.

$^{180}\text{Hf}(n,\gamma)$

The $^{180}\text{Hf}(n,\gamma)$ spectrum obtained with the 2-keV neutron beam contains features of interest to this discussion. In this spectrum we observe

strong transitions to the $1/2^-$ and $3/2^-$ members of the $1/2^-$ -[510] ground-state band of ^{181}Hf but the primary transition intensity to the $3/2^-$ -[512] state at 255 keV is very weak. This fluctuation in primary E1 transition intensities may be explained by the wide resonance spacing for the $^{180}\text{Hf}(n,\gamma)$ reaction. Resonances in the $^{180}\text{Hf}(n,\gamma)$ reaction have spacings > 100 eV [9] so that our 2-keV neutron capture spectrum represents an average over about 5 resonances. As we note from Fig. 1, wide fluctuations in primary gamma-ray transition intensities are to be expected if the averaging is over so few resonances. In fact, in such a case it will be impossible to reliably distinguish primary E1 transitions from primary M1 transitions. This example perhaps serves to point up a limitation on an averaging technique using the 2-keV neutrons; namely that, even for the deformed rare-earth nuclei, many of the even-even stable isotopes will not have a sufficiently small neutron resonance spacing to permit good averaging. In these cases then the best that can be hoped for is that one gets a spectrum which is somewhat different than the thermal neutron capture spectrum, and which reveals some added features of the level scheme.

$^{55}\text{Mn}(n,\gamma)$

For the low-Z nuclei, the neutron resonance spacing is generally too wide to permit any kind of an averaging. In some cases though the 2-keV neutron capture spectrum is dominated by a different resonance than that which dominates the thermal neutron capture. Such is the case for $^{55}\text{Mn}(n,\gamma)$. The prompt gamma-ray spectra resulting from thermal and 2-keV neutron capture in manganese are shown in Fig. 5. Here the 2-keV neutron capture spectrum is principally contributed by the 2.375-keV resonance in the $^{55}\text{Mn}(n,\gamma)$ reaction.

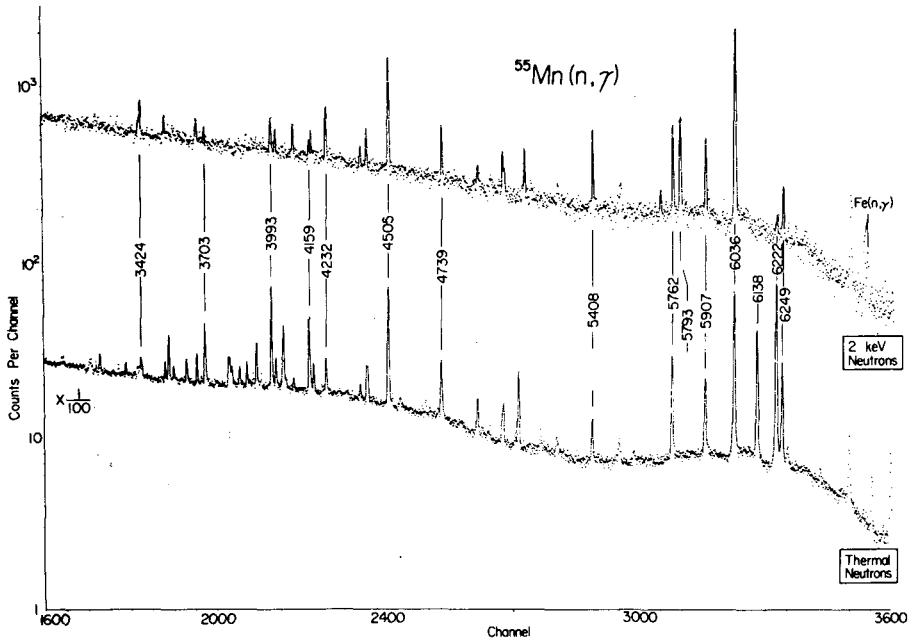


FIG. 5. Comparison of the high-energy portions of the prompt gamma-ray spectra resulting from 2-keV and thermal neutron capture in manganese. The 2-keV neutron capture gamma-ray spectrum was obtained with a 15-h run using a 25-g manganese sample.

However, a more important use of a 2-keV neutron capture gamma-ray spectrum obtained from a low-Z target nucleus should be that, when used in conjunction with the corresponding thermal neutron capture gamma-ray spectrum, it should allow primary capture gamma rays (those decaying from the capturing state) to be unambiguously distinguished from secondary capture gamma rays (which are emitted in the de-excitation of the lower energy states). This is because the primary capture gamma rays will have energies which are 2 keV greater than those measured from the corresponding thermal neutron capture spectrum, while the energies of the secondary prompt gamma rays will remain unchanged. We have demonstrated this effect with the $^{181}\text{Ta}(n,\gamma)$ spectra shown in Fig. 1. The 2-keV neutron capture gamma-ray line energies were measured relative to the 160 line (which resulted from the decay of 7-sec ^{16}N) and were found to have energies of 1.8 ± 0.3 keV greater than the corresponding line energies in the thermal spectrum.

REFERENCES

1. W. L. Wilson, M.S. Thesis, University of Idaho, 1966 (unpublished).
2. O. D. Simpson and L. G. Miller, Nuclear Instr. and Methods 61, 245 (1968).
3. O. D. Simpson and L. G. Miller, USAEC Report IN-1218 (1968).
4. C. E. Porter and R. G. Thomas, Phys. Rev. 104, 483 (1956).
5. L. M. Bollinger, "Nuclear Structure, Dubna Symposium 1968" (IAEA, Vienna, 1968) p. 317.
6. R. E. Chrien, "Nuclear Structure, Dubna Symposium 1968" (IAEA, Vienna, 1968) p. 342.
7. L. M. Bollinger and G. E. Thomas, Bull. Am. Phys. Soc. 12, 1200 (1967).
8. L. M. Bollinger and G. E. Thomas, Phys. Rev. Letters 18, 1143 (1967).
9. M. D. Goldberg, S. F. Mughabghab, S. N. Purohit, B. A. Magurno and V. M. May, USAEC Report BNL-325 (Second Edition, Supplement No. 2, Vol. II C, Z = 61 to 87) (1966).

LEVELS IN $^{182}\text{Ta}^*$

R. G. HELMER, R. C. GREENWOOD, C. W. REICH
 National Reactor Testing Station,
 Idaho Nuclear Corporation,
 Idaho Falls, Idaho,
 United States of America

Abstract

LEVELS IN ^{182}Ta . The level structure of ^{182}Ta has been studied from measurements of the prompt gamma rays following neutron capture in ^{181}Ta , from the beta decay of ^{182}Hf , and from the decay of the 16-min isomeric state in ^{182}Ta . The capture gamma-ray measurements were made using both thermal and 2-keV neutron beams obtained from the Materials Testing Reactor. A consistent level scheme has been constructed for ^{182}Ta using these data and configuration and band assignments have been made.

In this paper we wish to discuss the level structure of the odd-odd deformed nuclide ^{182}Ta which we have deduced from a study of the ^{182}Hf decay scheme, the decay scheme of the 16-min isomeric state of ^{182}Ta and the prompt gamma rays emitted as a result of neutron capture in ^{181}Ta .

The decay schemes which have been obtained for ^{182}Hf and ^{182m}Ta are shown in Fig. 1. These data have been reported previously [1] and will not be discussed further in this paper, except to note that the energy we have

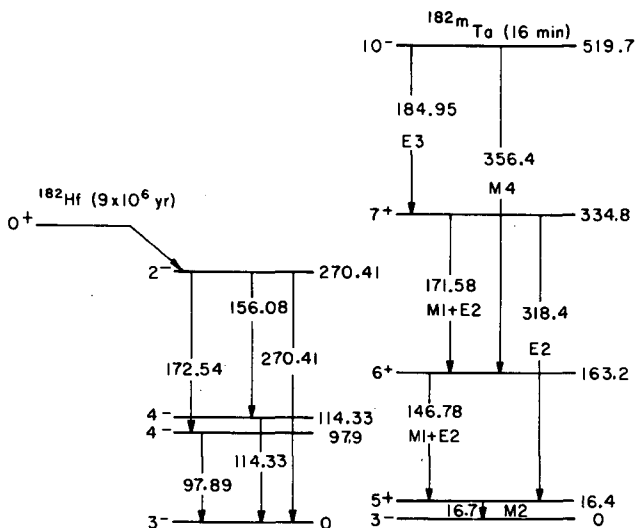


FIG. 1. Levels populated in ^{182}Ta from the beta decay of ^{182}Hf and the 16-min isomeric state of ^{182}Ta .

* Work performed under the auspices of the US Atomic Energy Commission.

assigned to the 5+ state is based on our study of the neutron capture gamma-ray data. The existence of this state, together with the fact that transition from it to the ground state is M2, was established by Clark and Stabenau [2] in studies of the $^{182\text{m}}\text{Ta}$ decay scheme. These authors, however, were unable to obtain a value for the energy of the state but merely placed a limit of 11.7 to 18 keV on it.

Extensive measurements of both low and high-energy neutron capture gamma rays were made in this present work. The low-energy portion (below 1.5 MeV) of the capture gamma-ray spectra was measured principally using a $6\text{ cm}^2 \times 8\text{ mm}$ planar Ge(Li) detector. This detector has an energy resolution of 0.9 keV (FWHM) at 100 keV and 1.7 keV at 1 MeV. Figure 2 shows a typical spectrum of tantalum capture gamma rays obtained with this system. Some measurements were also made using a smaller thin-window Ge(Li) detector to provide improved sensitivity below 100 keV. Energy calibration of these spectra was accomplished by simultaneously recording capture gamma-ray spectra and selected energy calibration lines obtained from radioactive decay sources. Gain scales ranging from 0.1 to 0.7 keV per channel were used in these measurements. A more complete discussion of the gamma-ray lines which are available for use as energy standards and the techniques which can be used to obtain the high precision with Ge(Li) detectors is given by Greenwood et al. [3]. Energies and intensities (relative) of the prompt gamma rays (below 1 MeV) from the $^{161}\text{Ta}(n, \gamma)$ reaction are given in Table I.

Spectra of the primary gamma rays resulting from neutron capture in tantalum were obtained using both an external thermal neutron beam and an external 2-keV neutron beam from the Materials Testing Reactor. These spectra are shown in Fig. 2 of Ref. [4]. Energy calibration of the thermal-neutron capture spectrum was accomplished using the mixed-source technique, with capture gamma-ray lines from hydrogen and sodium used as energy standards. The prompt gamma-ray data obtained from the $^{181}\text{Ta}(n, \gamma)$ reaction using the 2-keV neutron beam is discussed extensively in a separate contribution to this Symposium [4]. Since the neutron energy distribution in the 2-keV beam is approximately Gaussian with 700-eV FWHM, the resultant capture gamma-ray spectrum of tantalum is an average over many neutron resonances with spins and parities of 3+ and 4+ (the ground state of ^{181}Ta being 7/2+). The statistical fluctuations in the partial radiation widths are thus averaged out. The primary E1 transitions in this spectrum are observed to be about a factor of 8 stronger than the corresponding M1 transitions. Furthermore, transitions to final states with spins of 3 or 4 are approximately twice as strong as transitions to those with spins of 2 or 3. Figure 3 of the other paper [4] allows a differentiation between primary capture gamma-ray transitions which populate final states with spins and parities of 3- or 4-, 2- or 5-, 3+ or 4+, and 2+ or 5+.

The low-energy capture gamma-ray data have been combined with the primary capture gamma-ray data to form a consistent level scheme for ^{182}Ta . A preliminary version of this level scheme is shown schematically in Fig. 3. Thus far we have been able to arrange 24 levels into 11 rotational bands. Unassigned ^{182}Ta levels are shown on the right-hand side of Fig. 3. For clarity of presentation, transitions between levels in this scheme are omitted from this figure. Instead, these transition assignments are noted in column 3 of Table I. The most consistent set of excitation energies obtained from these data for ^{182}Ta is shown in Table II.

TABLE I. $^{181}\text{Ta}(n, \gamma)$ - GAMMA-RAY ENERGIES AND INTENSITIES

Gamma-ray energy (keV)	Intensity (relative)	Transition assignment
47.816 (30)	9.9	
74.136 (45)	3.7	
79.425 (80)	0.5	
90.104 (40)	0.9	360 → 270
92.420 (35)	0.9	
94.200 (20)	2.5	
95.117 (70)	1.0	
97.791 (10)	9.4	97 → 0
99.881 (10)	9.3	250 → 150
104.028 (15)	2.1	
105.868 (30)	0.9	
107.867 (10)	2.7	
114.396 (10) ^a	24	114 → 0
117.000 (40)	0.7	
118.888 (20)	5.3	479 → 360
119.594 (40)	1.4	292 → 173
122.742 (15)	4.7	(237 → 114), (360 → 237)
125.070 (25)	1.7	
133.871 (10)	33	150 → 16
139.474 (10)	4.0	237 → 97
141.222 (15)	3.2	
142.259 (20)	2.3	(292 → 150)
143.255 (15)	2.4	
146.770 (10)	6.7	163 → 16
154.082 (10)	3.1	
156.100 (10)	11.0	270 → 114
159.047 (10)	2.8	
171.681 (40)	3.0	334 → 163
173.193 (15)	53	
177.223 (60)	1.3	
178.665 (15)	3.3	292 → 114
180.825 (80)	1.1	331 → 150
182.783 (15)	1.4	
190.318 (15)	7.8	
193.135 (60)	0.6	
195.138 (15)	2.8	292 → 97
204.004 ^a (50)	1.1	
210.490 (15)	3.3	
214.185 (15)	2.2	
222.151 (30)	1.7	
228.777 (20)	1.3	
231.447 (170)	0.3	
233.747 (15)	2.5	250 → 16
237.268 (40)	1.9	237 → 0
242.368 (55)	1.0	479 → 237

^a doublet

TABLE I (cont.)

Gamma-ray energy (keV)	Intensity (relative)	Transition assignment
244.790 (50)	1.5	
246.162 (35)	1.2	360 → 114
251.069 (85)	1.3	
252.605 (85)	1.3	
258.927 (40)	1.5	
259.808 (180)	1.6	
268.569 (200)	1.9	
270.409 (15)	100	270 → 0
274.800 (40)	0.9	
276.791 (70)	1.1	(292 → 16)
284.103 (60)	0.8	
286.935 (30)	1.9	
297.131 (20)	23	
308.450 (40)	1.0	
315.139 (160)	0.3	331 → 16
317.560 (120)	0.5	
322.438 (70)	1.4	
325.535 (20)	1.0	
346.448 (20)	3.4	
349.887 (60)	1.0	
360.539 (20)	6.4	360 → 0
373.917 (30)	1.7	
377.240 (20)	4.1	
382.137 (20)	2.4	479 → 97
390.616 (110)	0.7	
396.910 (25)	1.9	
399.068 (180)	0.4	
402.645 (20)	40	402 → 0
406.308 (30)	2.3	
416.84 (13)	0.7	
420.36 (6)	1.2	
423.34 (7)	1.5	
443.45 (12)	1.2	
449.00 (13)	0.8	
473.65 (9)	1.0	
477.89 (9)	1.9	
479.86 (6)	2.7	479 → 0
489.43 (14)	1.2	
499.38 (15)	1.5	
501.43 (8)	1.3	
523.96 (14)	0.6	
530.48 (7)	1.1	
553.36 (20)	0.8	
567.47 (13)	1.1	
583.78 (14)	1.0	
602.86 (11)	1.0	
629.69 (10)	1.5	
646.36 (18)	1.1	
651.12 (20)	0.8	
675.51 (18)	1.2	
759.60 (30)	2.4	
870.95 (35)	2.8	
887.48 (22)	2.1	

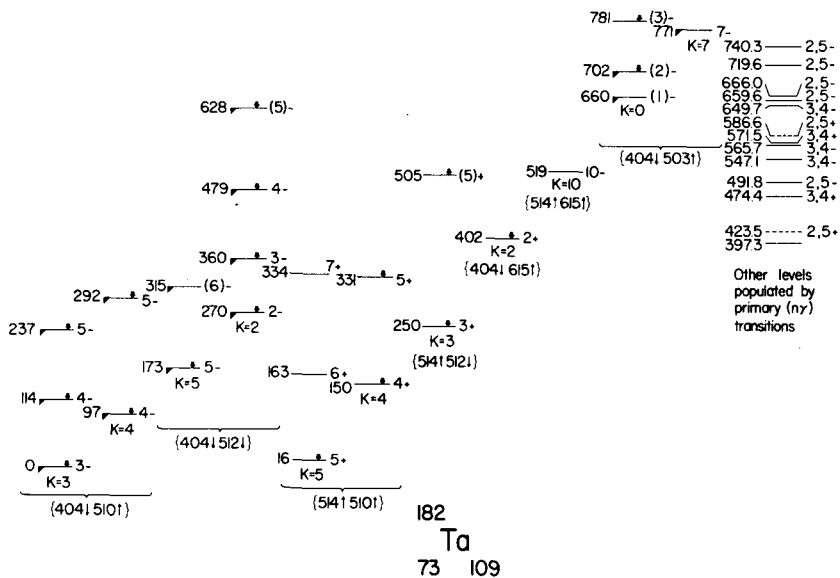


FIG. 3. Level scheme of ^{182}Ta . Heavy arrows into a level indicate that the level is populated by primary neutron capture gamma-ray transitions while an inverted triangle below and on the left-hand side of a level indicates that it is populated in the $^{181}\text{Ta}(d, p)$ reaction.

TABLE II. ENERGIES OF ^{182}Ta LEVELS

Levels in ^{182}Ta (keV)
16.4 \pm 0.4
97.80 \pm 0.02
114.33 \pm 0.02
150.7 \pm 0.4
163.2 \pm 0.4
173.3 \pm 0.2
237.27 \pm 0.10
250.5 \pm 0.3
270.41 \pm 0.01
292.97 \pm 0.03
331.2 \pm 0.4
334.8 \pm 0.4
360.52 \pm 0.02
402.65 \pm 0.02
479.70 \pm 0.20
505.4 \pm 0.2
519.7 \pm 0.4
628.5 \pm 0.2
659.6 \pm 0.4
702.0 \pm 0.2
782.0 \pm 0.2

We now consider possible configuration assignments for bands in ^{182}Ta . We first note that the lowest lying odd-proton states in ^{181}Ta are $7/2+[404]$ (the ground state), $9/2-[514]$ and $5/2+[402]$, and the lowest lying odd-neutron states in ^{183}W (which like ^{182}Ta has 109 neutrons) are $1/2-[510]$ (the ground state), $3/2-[512]$, $7/2-[503]$, $11/2+[615]$ and $9/2+[624]$. Combinations of these odd-proton and odd-neutron states are thus expected to constitute the lowest-energy states in ^{182}Ta . The $^{181}\text{Ta}(d,p)^{182}\text{Ta}$ data of Erskine and Buechner [5] have been of particular value in helping us make configuration assignments to states in ^{182}Ta because the only states which are expected to be excited directly in this (d,p) reaction are those containing the proton orbital $7/2+[404]$. Furthermore, the negative parity neutron orbitals noted above will be excited most strongly and the positive parity neutron orbitals will only be weakly excited. The odd proton-odd neutron configuration assignments to the bands shown in Fig. 3 are as follows:

{ $7/2+[404]$, $1/2-[510]$ } bands

Bands with $K^\pi = 3^-$ and $K^\pi = 4^-$ will be formed from the two possible couplings (that is, $K = |\Omega_p + \Omega_n|$ and $|\Omega_p - \Omega_n|$) of these orbitals. The ^{182}Ta ground state has $I^\pi = 3^-$ and corresponds to the band head of the $K^\pi = 3^-$ band. The ^{182}Hf decay scheme, together with the 2-keV neutron capture gamma-ray data, suggests that the two states at 97 and 114 keV have $I^\pi = 4^-$. (This is in contrast to the analysis of the $^{181}\text{Ta}(d,p)$ data by Erskine and Buechner [5] who suggested that the 97-keV state had $I^\pi = 5^-$.) It is reasonable to assume that these two 4- states are associated with the band head of the $K^\pi = 4^-$ band and the spin-4 member of the $K^\pi = 3^-$ band. The gamma branching ratios to these two states from the 270-keV state, as observed in the ^{182}Hf decay, strongly suggest that the 97-keV state carries most of the $K^\pi = 4^-$ strength. The states of 237 and 292 keV are the spin-5 members of these two bands.

{ $7/2+[404]$, $3/2-[512]$ } bands

The coupling of the $7/2+[404]$ proton and $3/2-[512]$ neutron gives rise to two bands having $K^\pi = 2^-$ and 5^- . The 2-keV neutron capture gamma-ray data require that the 173-keV state have $I^\pi = 2^-$ or 5^- . Since it is not populated in the ^{182}Hf decay, the 5- assignment is favoured. The most reasonable assignment for this level is as the band head of the $K^\pi = 5^-$ band. Although no information has been obtained in the present work about the 315-keV state, our analysis of the $^{181}\text{Ta}(d,p)$ data suggests that it is the spin-6 member of this band. The ^{182}Hf decay data when combined with the 2-keV neutron capture gamma-ray data require that the 270-keV state has a spin and parity of 2^- . This level is assigned here as the band head of the $K^\pi = 2^-$ band. Additional members of this band are observed at 360, 479 and 628 keV.

{ $9/2-[514]$, $1/2-[510]$ } bands

The coupling of the $9/2-[514]$ proton and $1/2-[510]$ neutron gives rise to two bands having $K^\pi = 5^+$ and 4^+ . Since the $7/2+[404]$ and $9/2-[514]$ bands are closely spaced in ^{181}Ta we expect this configuration to lie rather low in ^{182}Ta . The 2-keV neutron capture data suggest that the state at 16 keV has a spin

and parity of $2+$ or $5+$. Clark and Stabenau [2] have established the existence of a state in ^{182}Ta which has an energy of from 11.7 to 18 keV and which decays to the ground state of ^{182}Ta by an M2 transition. It seems reasonable then to suggest that these two states are the same and that the 16-keV state is $K^\pi = 5^+$ band head. Information about higher-spin members of this band, at 163 and 334 keV, is obtained from decay of the 16-min ^{182}Ta isomer. The 2-keV neutron capture gamma-ray data suggest that the 150-keV state has $I^\pi = 3^+$ or 4^+ . Furthermore, decay from this level is only to the 16-keV level, and when the $^{181}\text{Ta}(n, e^-)$ data of Goudsmit and Burson [6] are combined with our prompt gamma-ray data we conclude that the 133-keV transition is M1. Thus we conclude that the 150-keV state is the band head of the $K^\pi = 4^+$ band. The 331-keV level which we have assigned as the $5+$ member of this band must be considered tentative because of the small moment of inertia which is implied by this energy spacing.

{9/2-[514], 3/2-[512]} bands

Bands with $K^\pi = 3^+$ and 6^+ will be formed from the coupling of these two orbitals. The 2-keV neutron capture gamma-ray data suggest that the 250-keV level has $I^\pi = 3^+$ or 4^+ . Decay from this level occurs only to the 16- and 150-keV states. Thus assignment of this level as the band head of the $K^\pi = 3^+$ band seems reasonable. Since the 2-keV neutron capture gamma-ray data suggest that the 505-keV level is $2+$ or $5+$, we have tentatively assigned this state as the $5+$ member of this band.

Other band assignments

The 16-min isomeric state at 519 keV in ^{182}Ta has a spin and parity of 10^- . The only reasonable assignment for this state is that it is a band head of a $K^\pi = 10^-$ band. The configuration assignment, then, must be {9/2-[514], 11/2+[615]}, since no other combination of orbitals can give such a large K-value at this relatively low excitation energy.

The 2-keV neutron capture gamma-ray data suggest that the 402-keV state has $I^\pi = 2^+$ or 5^+ . The probable decay mode of this state is by a strong 402-keV transition directly to the ground state of ^{182}Ta . When the $^{181}\text{Ta}(n, e^-)$ data [6] are combined with our prompt gamma-ray data we conclude that the 402-keV transition is E1. These data then suggest that this 402-keV level is $2+$, and it seems reasonable to suggest that it is the band head of the $K^\pi = 2^+$ band {7/2+[404], 11/2+[615]}.

The state at 771 keV seen in the $^{181}\text{Ta}(d, p)$ reaction data is established as the band head of the $K^\pi = 7^-$ band with the configuration {7/2+[404], 7/2-[503]}. The band with $K^\pi = 0^-$, formed by the other coupling of these two orbitals should also be excited in the $^{181}\text{Ta}(d, p)$ reaction. By combining the (d, p) data with the 2-keV neutron capture data we can tentatively identify the 1-, 2- and 3- members of this band at 660, 702 and 781 keV.

While our analysis and interpretation of the properties of these levels in ^{182}Ta are only in an early stage, we feel that the following well-established features need to be pointed out.

(1) At the present time some question exists concerning the direct population of proton states (that is, states in which the odd proton does not have its ground-state configuration) by primary capture gamma-ray transitions. It has been suggested [7-9] that proton states are not populated by primary

neutron capture gamma-ray transitions in the $^{169}\text{Tm}(n, \gamma)$ and $^{165}\text{Ho}(n, \gamma)$ reactions. We find absolutely no evidence for such an effect. Here we find that the proton states which we have definitely identified are indeed populated by primary capture gamma-ray transitions. These proton states have positive parity. However, M1 transition intensities to these states are the same as the transition intensity to the one positive parity neutron state which we have identified. Furthermore, the M1 transition intensities are about one-eighth of the E1 transition intensities to neutron states. This M1 to E1 transition intensity ratio is quite similar to that observed for even-even nuclei in this region [9].

(2) In all cases where we have been able to identify the two bands which arise from the different relative couplings of a given pair of orbitals (that is, $K = \Omega_p + \Omega_n$ and $|\Omega_p - \Omega_n|$), that band corresponding to the parallel orientation ($\Sigma = 1$) of the intrinsic spins of the odd proton and odd neutron lies lower in energy. Table III shows the separation energy of the two possible bands for the various orbital pairs ($\Sigma = 1$ or 0) observed in ^{182}Ta .

TABLE III. ENERGY DIFFERENCES BETWEEN STATES OF THE SAME CONFIGURATION WHICH CORRESPOND TO PARALLEL ($\Sigma = 1$) AND ANTI-PARALLEL ($\Sigma = 0$) ORIENTATIONS OF THE ODD-PROTON AND ODD-NEUTRON ORBITALS

Odd proton-odd neutron configuration	$ \Omega_p + \Omega_n - \Omega_p - \Omega_n $ Level differences (keV)
{7/2+[404], 1/2-[510]}	97.8
{7/2+[404], 3/2-[512]}	97.1
{9/2-[514], 1/2-[510]}	134.3

(3) As pointed out by Erskine and Buechner [5] the $^{181}\text{Ta}(d, p)$ cross-sections for exciting the four bands arising from the configurations {7/2+[404], 1/2-[510]} and {7/2+[404], 3/2-[512]} require a band-mixing picture for their understanding. We are currently carrying out a detailed Coriolis-coupling analysis of these levels. This analysis is complicated by the fact that we are dealing here with the 1/2-[510] and 3/2-[512] orbitals. As is well known in the odd-A nuclei, Coriolis coupling of these orbitals is not well understood at the present time [10, 11]. These calculations are continuing, however, and promise to give information of a fundamental nature concerning the coupling of these bands.

R E F E R E N C E S

- [1] HELMER, R. G., GREENWOOD, R. C., McISAAC, L. D., USAEC Rep. IN-1218 (1968).
- [2] CLARK, D. D., STABENAU, W. F., Phys. Rev. Lett. 21 (1968) 925.
- [3] GREENWOOD, R. C., HELMER, R. G., GEHRKE, R. J., to be published.
- [4] GREENWOOD, R. C., HARLAN, R. A., HELMER, R. G., REICH, C. W., "Neutron capture gamma-ray measurements with a reactor-produced 2-keV neutron beam", these Proceedings.
- [5] ERSKINE, J. R., BUECHNER, W. W., Phys. Rev. 133 (1964) B370.

- [6] GOUDSMIT, P.F., BURSON, S.B., private communication.
- [7] SHELINE, R.K. et al., Phys. Rev. 143 (1966) 857.
- [8] MOTZ, H.T. et al., Phys. Rev. 155 (1967) 1265.
- [9] BOLLINGER, L.M., "Radiative transitions from highly excited nuclear states", Nuclear Structure (Proc. Symp. Dubna, 1968), IAEA, Vienna (1968) 317.
- [10] KERMAN, A.K., Mat. Fys. Medd. Dan. Vid. Selsk. 30 15 (1956).
- [11] BROCKMEIER, R.T., WAHLBORN, S., SEPPI, E.J., BOEHM, F., Nucl. Phys. 63 (1965) 102.

NEUTRON RESONANCE CAPTURE

Chairmen: W. MICHAELIS
J. URBANEC

Invited talk

EXPERIMENTAL STUDIES OF RESONANCE NEUTRON CAPTURE GAMMA RAYS *

R. E. CHRIEN

Brookhaven National Laboratory,
Upton, Long Island, N. Y.,
United States of America

Abstract

EXPERIMENTAL STUDIES OF RESONANCE NEUTRON CAPTURE GAMMA RAYS. The nature of the radiation following the capture of slow neutrons in resonances is discussed. The utility of resonance capture techniques in contributing to the knowledge of the parameters of both the initial and final states of the (n, γ) reaction is illustrated by examples drawn from the work of the Brookhaven fast chopper group. Deviations from the purely statistical decay of the highly excited neutron unbound states are reported and their relation to the nature of the capture reaction mechanism is explored.

Neutron capture gamma-ray spectroscopy has been a fruitful source of information relating to nuclear structure for about 35 years. The first direct observation of a capture gamma ray, the de-excitation following the capture of a neutron by a proton, was made by Lea [1] at Cambridge in the course of investigations of neutron scattering from hydrogenous materials. Lea identified the nature of this radiation by its appearance at backward angles in the laboratory reference frame and by its specific ionization in chambers filled with argon and hydrogen. By using lead absorbers, the energy of the hydrogen capture gamma ray was estimated to lie between 2 and 4 MeV. The technical progress which has been achieved in this field in the intervening years since this first crude measurement may be gauged from the fact that this same gamma ray has been measured [2] with an energy precision of 20 ppm, or 70 eV out of 2223.29 keV.

Up to now most neutron capture gamma-ray experiments have been carried out with thermalized neutrons from reactors and the widespread development of research reactors after the second World War led to a great increase of activity in this area [3,4]. Thermal neutron capture has inherent limitations, however. The excitation energy resulting from the capture of a relatively slowly moving neutron by a target nucleus does not, in general, coincide with any one of the metastable states of the compound system, hence thermal capture usually occurs in an indeterminate mixture of tails from nearby bound and unbound states.

The advantages of studying transitions from well-defined initial states are self-evident. Yet comparatively little effort has been expended on resonance capture studies because of the very severe limitations on the size of the available neutron flux. The first such measurements were carried out with the aid of photoneutrons produced by electron linear accelerators at Yale and at Harwell about thirteen years ago. The Yale

* Part of this work was supported by the US Atomic Energy Commission.

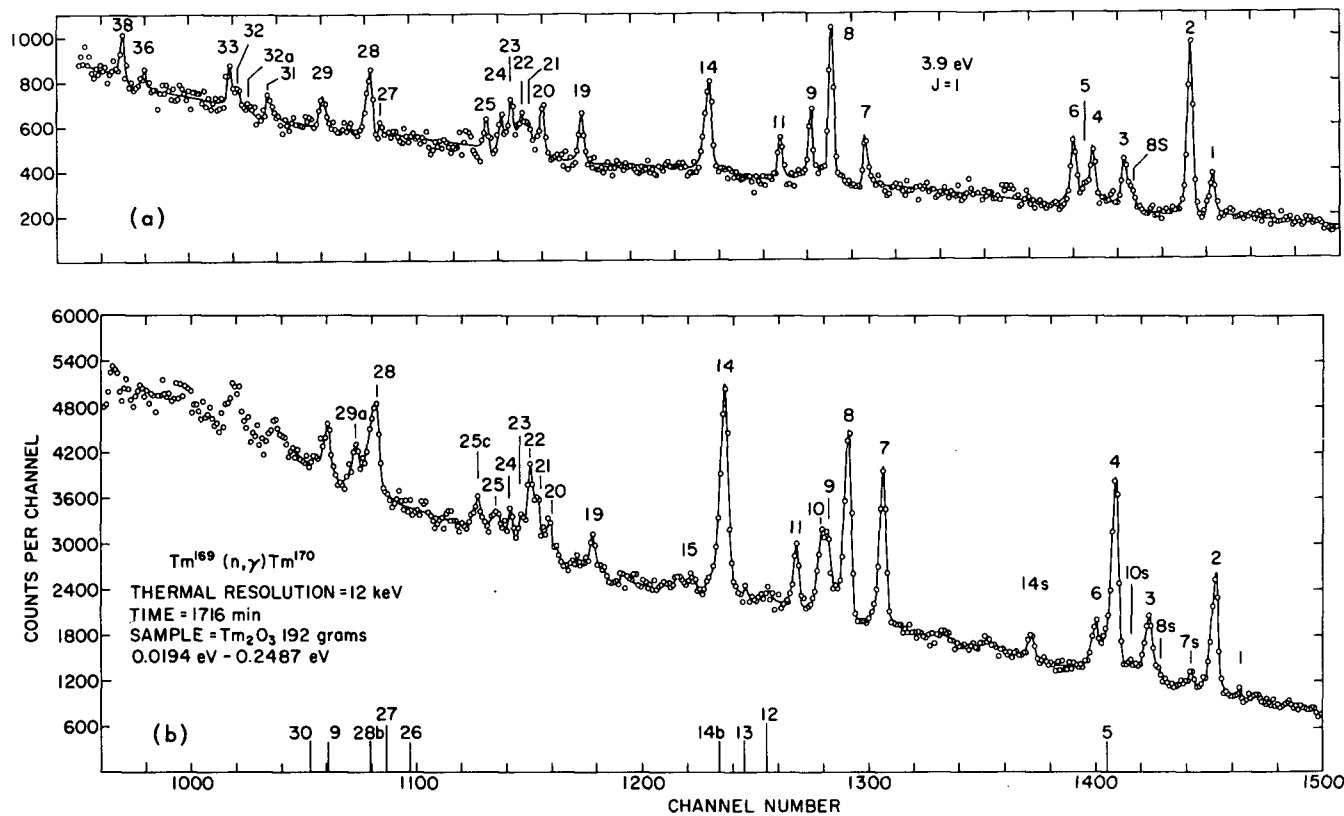


FIG. 1. (a) The spectrum from the 3.9-eV resonance from $^{169}\text{Tm}(n,\gamma)^{170}\text{Tm}$; peak 1 represents the transition to the 1^- ground state of ^{170}Tm ; (b) the thermal neutron capture gamma-ray spectrum. The ground-state gamma ray is extremely weak.

group [5] studied low-energy gamma rays, while at Harwell Landon and Rae [6] studied high-energy transitions in mercury. These authors pointed out the usefulness of resonance capture spectra in making isotopic assignments and in spin determinations of neutron resonant states. Since that time the development of stronger sources and particularly the creation of high-resolution high-efficiency detectors has made resonance spectral studies feasible for many nuclides over a fairly wide range of neutron energy.

Let us examine the usefulness of resonance gamma-ray spectroscopy from several points of view. From the standpoint of nuclear structure studies, resonance capture is useful as a way of populating low-lying states of the residual nucleus which cannot be reached from thermal capture. This may occur simply because of the selection rules which determine the multipole order of the emitted radiation. The observed neutron capture gamma rays are predominantly dipole in character, and mostly electric dipole. E2 radiation is rarely observed, and higher multipoles are too weak to be observable. The greater range of spin and parities available in resonance capture thus increases the number of final states populated over that observed for thermal capture. Capture into p-wave resonances is particularly effective in populating states not seen, or weakly seen, in thermal capture. Even if selection rules are favourable for thermal capture, the widely-varying distribution of transition probabilities may account for the absence of an allowed transition. Finally, since thermal capture is inherently non-resonant in character, it is sometimes strongly influenced by the interference terms between resonant radiative amplitudes. Since this effect is often neglected, it is perhaps useful to point to a specific example of this effect in $^{169}\text{Tm}(n, \gamma)^{170}\text{Tm}$ [7]. Figure 1 shows the gamma-ray spectrum at the 3.9-eV resonance, which accounts for about half of the thermal capture cross-section. The ground-state gamma ray, peak 1, is seen to have a sizeable strength, resulting from the 1^+ resonance decaying to the 1^- ground state. The thermal spectrum, however, shows little or no evidence of this transition in spite of the sizeable tail of the 3.9-eV resonance at thermal neutron energies. This can be understood in terms of destructive interference of the amplitude of the 3.9-eV resonance with that from a bound state about 8 eV away. A similar effect is seen in $^{238}\text{U}(n, \gamma)^{239}\text{U}$ [8]. Such effects should be considered carefully when, for example, one discusses (n, γ) -(d, p) correlations in thermal neutron capture. Resonance capture spectra can also play an important role in determining the parameters of the initial state, or neutron resonances, and can therefore be an important adjunct to total neutron cross-section, scattering and total capture measurements in the assignment of resonance spins and parities. Spin determinations can be based on several methods: the observation of primary transitions to low-lying states of known spin, on the differences in the population of low-lying states by cascades of gamma rays originating from the initial state, or by resonance-resonance interference analyses. In the case of p-wave capture, the angular distribution for dipole radiation is given by the expression

$$W(\theta) = a_0 + a_2 P_2(\cos \theta)$$

and observation of the relative size of the anisotropic component $P_2(\cos \theta)$ may be used to determine the parity of the resonance as well as the initial

and final state spins. Examples of these varied methods of spin determinations will be discussed. It is clear that these methods of gamma-ray spectroscopy very directly and easily determine parameters which are obtained indirectly, and with great difficulty, in the more conventional methods of total cross-section experiments.

While spectral measurements can be a useful tool in spectroscopic applications, even more interesting are the aspects which bear on the fundamental problems of the structure of highly excited nuclear states and on the nature of the neutron capture reaction mechanism. The gross shape of the primary gamma-ray spectrum and the statistical properties of the radiative widths may be examined to yield such fundamental information. The point of departure for these studies is usually taken to be the 'statistical nucleus', i. e. (1) one which exhibits a smooth primary decay spectrum of the form

$$\nu(E_\gamma) = \frac{S(E_B, E_\gamma)}{\Gamma_\gamma} \frac{D(E_B)}{D(E - E_\gamma)}$$

where S is the photon strength function; E_B is the neutron binding energy; Γ_γ is the total radiation width; and D is the applicable level spacing; (2) one which displays the so-called Porter-Thomas distribution for both neutron and radiative widths,

$$P(X) = \text{const.} (x/2)^{-1/2} e^{-x/2} dx$$

$$x = \Gamma_i / \langle \Gamma_i \rangle$$

and (3) one which exhibits no correlation among the various decay widths. Departures from these conditions may be interpreted as revealing structure in the initial or final states connected by the radiative transitions. We can hope to relate such structure to the reaction mechanism by a visualization of the compound nucleus wave function in terms of a succession of simple components, starting with a neutron single-particle motion, a two-particle one-hole or doorway state excitation, and continuing into higher order excitations involving more nucleons consistent with a statistical distribution of the excitation energy. The high-energy primary gamma rays connect these highly excited nuclear states with the relatively simple low-lying states of the residual nucleus, many of which can be described in terms of single-particle or collective motions. It may well be profitable then to interpret these high-energy transitions as originating in simple structural components of the capturing state, such as single-particle or two-particle one-hole excitations, or alternatively in terms of some collective motion such as described by the hydrodynamical model of the giant dipole resonance. Indeed, some of the experiments which I shall shortly describe seem to suggest the usefulness of this viewpoint.

These introductory remarks have served to indicate some of the interesting applications of resonance spectra. For reasons of convenience the topics will be illustrated largely by examples drawn from data accumulated by the Brookhaven High Flux Beam Reactor fast chopper group. Many groups have become active in this and related fields and it is appropriate

hence the 12.1-eV resonance must have spin and parity $3/2^-$, since the alternative possibilities $1/2^+$ or $1/2^-$ lead to isotropic distributions. Having established the 12.1-eV resonance as a P-wave resonance we can examine the ratios of intensities at 90° and 135° to identify spins for the low-lying state connected to the resonance by dipole transitions. Nine final states have been so identified and have been compared to (d, p) data of Moorhead and Moyer [10]. A similar experiment was carried out in the case of the 1167-eV resonance in ^{56}Fe ; the first resonance in iron. This resonance is a good example of the combination of various techniques for establishing level parameters. Total cross-section data taken some years ago indicated that this resonance was not an S-wave resonance on the basis of the lack of the characteristic asymmetry resulting from resonance-potential scattering interference. Recent work on the differential scattering cross-section at Harwell [11], however, indicates a shape asymmetry in the differential cross-section and the behaviour of this asymmetry establishes the state as possessing odd parity. The spectrum of this resonance is shown in Fig.3. Strong transitions to final $1/2^-$ and $3/2^-$ states are seen limiting the initial state spin to $3/2$ or less. A sizeable transition to $5/2^-$ level at 135 keV in ^{57}Fe is also seen. The angular distribution of the dipole transitions to the $1/2^-$ and $3/2^-$ final states is given in Fig.4. The relative population is identical at the two

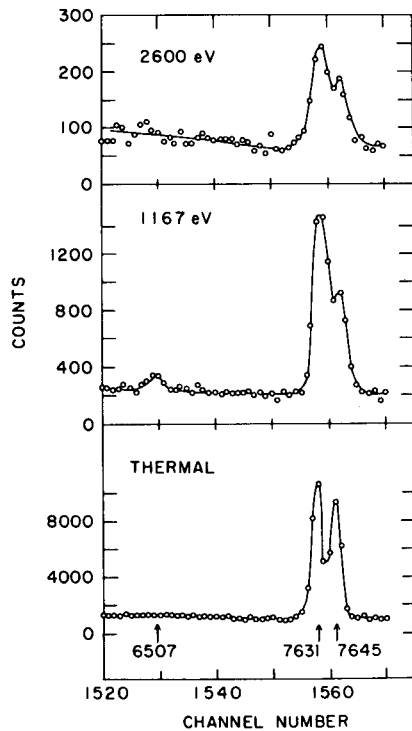


FIG.3. Gamma rays in ^{57}Fe after neutron capture at three energy regions. Note the appearance of the 6507-keV transition to the 135-keV $5/2^-$ state in the 1167-eV resonance spectrum.

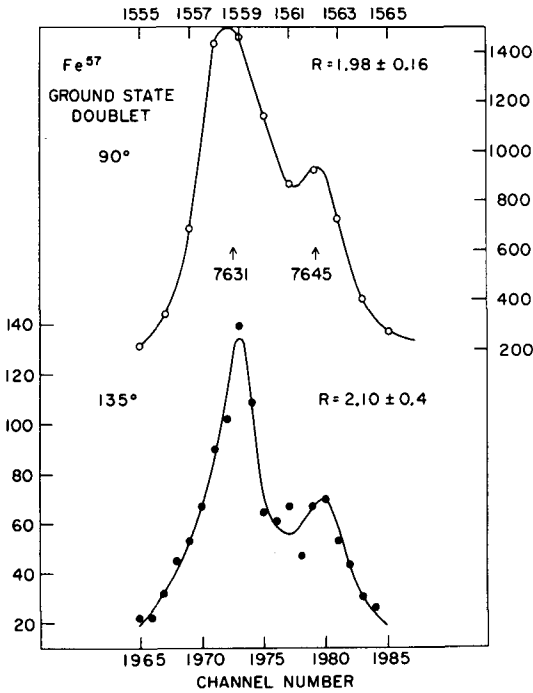


FIG.4. The $^{56}\text{Fe}(n,\gamma)^{57}\text{Fe}$ ground-state doublet at 90° and 135° in the resonance.

angles 135° and 90° , hence a $3/2^-$ assignment is ruled out and the resonance must be a $P_{1/2}$ state. The weak transition to the 135 keV $5/2^-$ level is therefore an E2 gamma ray. A consequence of this assignment is that most of the radiation depopulating this resonance must be magnetic dipole, and the strengths are within a factor of two of the E1 transition strengths observed in the thermal neutron spectrum. The E2 strength represents an enhancement of about 200 over the modified Weisskopf estimate quoted by Bartholomew [3].

$$\Gamma_\gamma(E2) = (1.2 \times 10^{-7}) A^{4/3} E_\gamma^5 D(E_B)/D_0$$

while the M1's are found to be a factor of 17 over the M1 estimate:

$$\Gamma_\gamma(M1) = (6 \times 10^{-2}) E_\gamma^3 D(E_B)/D_0$$

Low-energy gamma rays are also useful in establishing capturing state spins. It has long been known that the population of the low-lying levels by gamma cascades ought to be dependent on the initial spin value. About ten years ago Huizenga and Vandenbosch [12] pointed this out in connection with a study of isomeric cross-section ratios. States with spins closer to the initial value are expected to be more strongly populated

and a simple model of gamma-ray cascades, taking into account the spin cut-off factor σ in the level density formula:

$$P(J) \propto (2J + 1) \exp[-(J + \frac{1}{2})^2 / 2\sigma^2]$$

supports this expectation. Figure 5 illustrates the population of final states of spin 3 and 5 from two-step gamma cascades from capturing states of spin 3 and 4. This simple model has been refined by Pönitz [13] who includes the effects of higher multipoles, higher multiplicities and nuclear structure effects. Although the simple model predictions are only qualitatively successful, experiment confirms the predicted differences in level population in a rather convincing way. Figure 6 shows the low-energy capture spectrum from two resonances in thulium, the 0^+ 14-eV and the 1^+ 34.8-eV levels. Note first that the very large variations of transition intensities characteristic of high-energy spectra are lacking here. Each resonance has quite a similar spectrum, indicating a good average over many intermediate states in the multi-step gamma cascade. The de-excitation of the 3^+ state at 183.2 keV and the 0^- 149.7-keV state occurs with different intensities at the two resonances, however. Note that in the 0^+ resonance the 3^+ de-excitation is relatively weak. This is consistent with the simple motion that the 3^+ state cannot be reached in a simple two-step dipole cascade, while the 0^+ can. Figure 7 shows the effect in ^{165}Ho . Here the decay of a 5^- level (149.3-keV gamma ray) is compared to that of a 3^- state in resonances of spins 3^- and 4^- (116.8-keV gamma ray), and in accord with expectations, the 5^- final state is more strongly populated in the 4^- resonances. Figure 8 shows a summary of

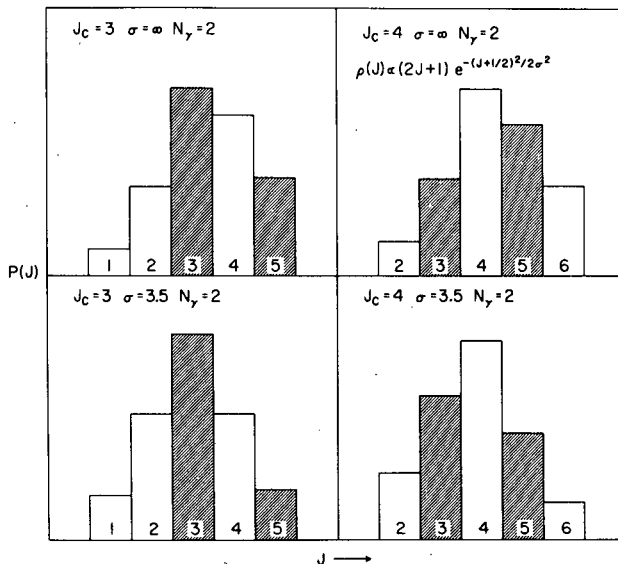


FIG. 5. A calculation of the relative population of low-lying states by two-step dipole cascades from $J = 3$ and $J = 4$ capturing states. At the top $\sigma = \infty$ ($D_j \propto 2j + 1$) is assumed and at the bottom $\sigma = 3.5$ is assumed.

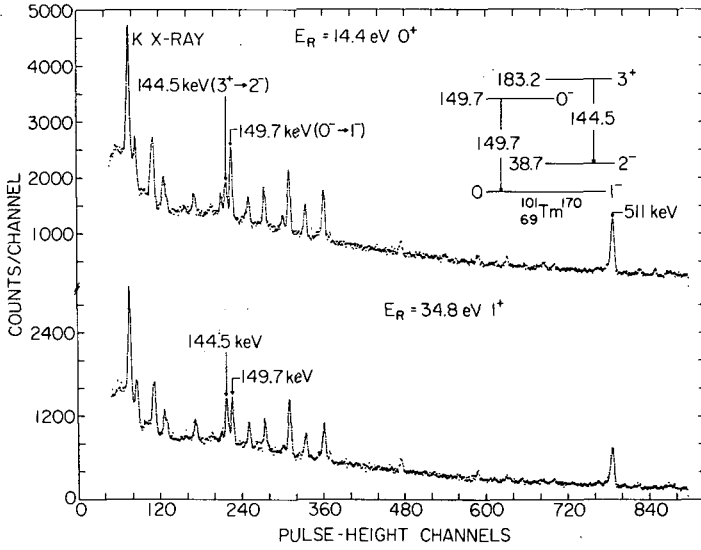


FIG. 6. A portion of the low-energy spectrum from $^{169}\text{Tm}(n, \gamma)^{170}\text{Tm}$. The relative strengths of the 3^+ and 0^- level de-excitations are seen to depend on the capturing state spin.

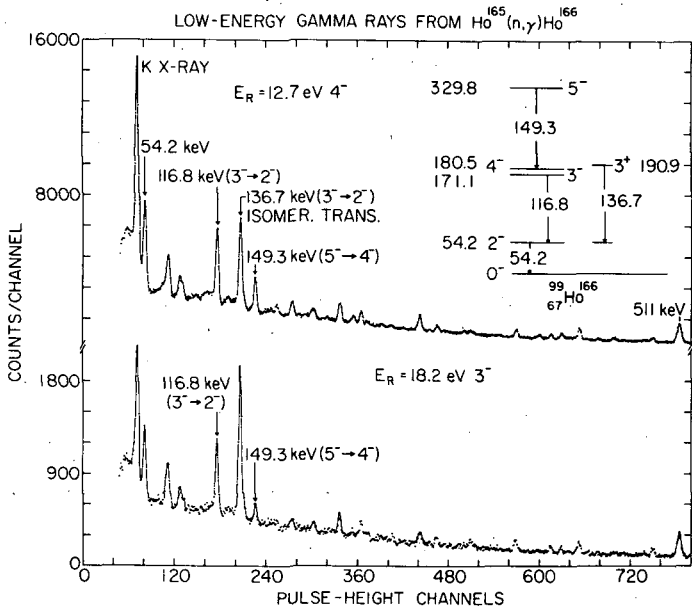


FIG. 7. A portion of the low-energy spectrum from $^{165}\text{Ho}(n, \gamma)^{166}\text{Ho}$. Again, the ratio (3^- decay to 5^- decay) depends on the resonance spin.

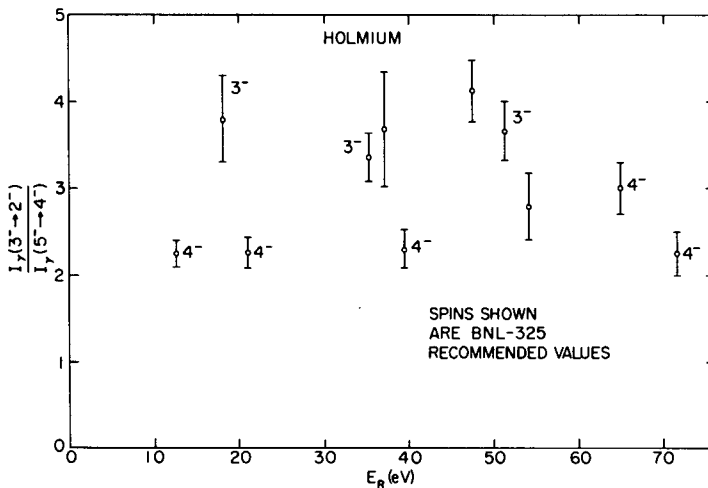


FIG. 8. A comparison of the 3^- to 5^- decay ratio for resonances in holmium. The assigned spin values are from BNL-325.

3^- to 5^- decay ratios, compared to spin assignments of BNL-325. The two groups of decay ratios are rather clearly seen and in good agreement with previous spin assignments. Weigmann [14] and his colleagues at Geel have applied this technique to the nucleus ^{235}U with convincing results.

Let us now turn to several topics concerned with the capture reaction mechanism. Lane and Lynn [15] have formulated the mechanism of slow neutron capture. They start by dividing the capture cross-section to a particular final state into a resonant and a non-resonant part; to be identified with the compound nucleus and direct reaction components, respectively:

$$\sigma(n, \gamma) = \pi \lambda_0 \lambda_g |A_0 + \sum_{\lambda} (\Gamma_{n\lambda}^0)^{\frac{1}{2}} (\Gamma_{\gamma\lambda})^{\frac{1}{2}} / (E - E_R) + i\Gamma/2|^2$$

This distinction is not quite so clear cut as it might superficially appear to be since 'local' resonance tails can contribute to the smoothly varying cross-section between resonances and must be subtracted out.

The most satisfying method of identifying the direct component is by evaluating the interference term between direct and resonance scattering. These interference effects can be quite noticeable in many nuclides, as is evident in the following set of figures drawn from an experiment in capture on ^{238}U [8]. There are two strong doublets in uranium near 4059 and 3990 MeV respectively, and the 4059-MeV transition shows an extremely pronounced interference maximum at thermal energies. The behaviour of the doublets is shown in Figs 9 and 10. The interference between the smoothly varying transition amplitude and the resonance term is destructive above the 6.7-eV resonance and constructive below it as shown. There is another feature of the resonance capture data in uranium that is perhaps worth remarking on in Fig. 10. The 4068 transition, quite

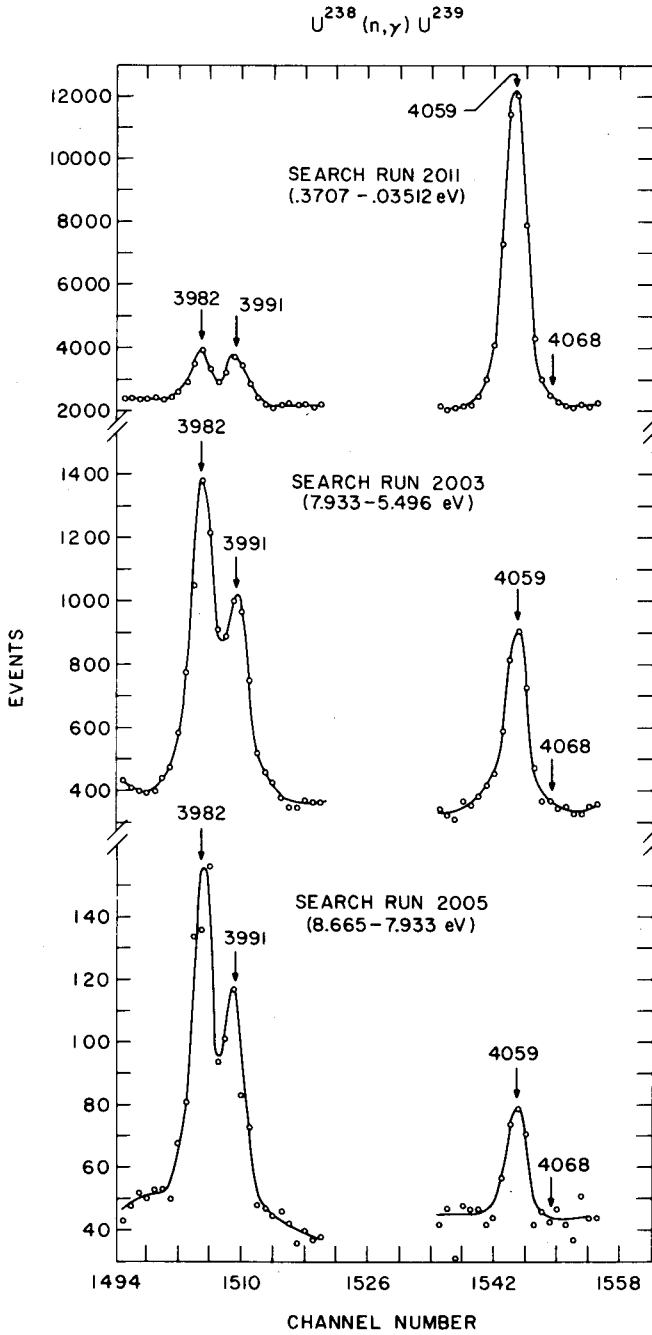


FIG. 9. Four closely spaced gamma rays in $^{238}\text{U}(n,\gamma)^{239}\text{U}$. The 4059-keV gamma ray is seen to display constructive interference with the background amplitude below the 6.7-eV resonance and destructive interference above.

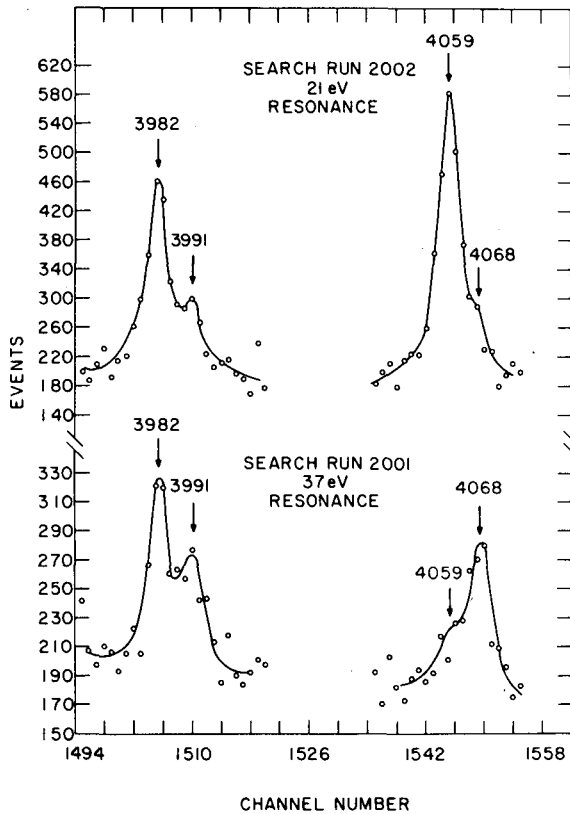
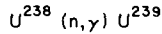


FIG. 10. The doublets of Fig. 9 in the 21 and 37-eV resonances. Note the appearance of the 4068-keV gamma-ray, not visible at thermal.

strong in the 37-eV resonance, is not seen at all in thermal. This can be interpreted in terms of destructive interference and illustrates as in the case of thulium that resonance capture can supplement information derived from thermal neutrons concerning the level scheme of the product nucleus.

A less obvious, but nonetheless quite identifiable, interference effect occurs in ^{59}Co [16], where a detailed comparison of the thermal and resonance capture spectrum at 130 eV shows some small but definite differences, especially in the strength of the ground-state transition (Fig. 11). The enhancement of the ground-state gamma is perhaps more striking if we remember that about 1/5 of thermal capture is accountable in terms of one or more bound levels with 3^- assignments, which are unable to contribute by E1 radiation to the ground state, with 5^+ spin and parity. Figure 12 shows the fit to the observed partial cross-section for this transition and the constructive interference can be seen raising the

cross-section above the value predicted from the resonance contribution above. The required direct amplitude corresponds to a cross-section of 9.2 mb at 1 eV, compared to a hard sphere scattering value of 12.6 mb for a pure single-particle final state. With currently available source strengths these detailed measurements in the off-resonance region can only be carried out at fairly low neutron energies, thus limiting their application to a few favourable nuclides.

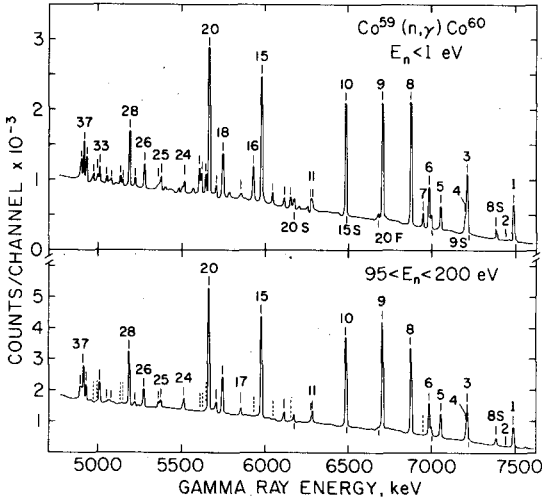


FIG. 11. Thermal capture and resonance capture in cobalt. The ground-state gamma ray, peak 1, is relatively stronger near thermal energy.

Lane and Lynn [15] have discussed in detail the resonance neutron capture mechanism and have shown that single-particle effects can be present in the resonance 'channel capture' region as well as in the off-resonance region. By making the usual, but somewhat artificial, distinction between the external and internal parts of the dipole integral, separated by the nuclear boundary at $r = R$, they show that in the channel region strong contributions to single-particle final states might arise. The observed 'channel capture' contributions may be written as the following:

$$\delta\Gamma^{1/2} = \frac{4}{\sqrt{3}} k_\gamma^{3/2} \exp\left(-\frac{\theta_i\theta_f}{k_f}\right) (-1)^{J_f - J_i - 1} (2J_f + 1)^{1/2} \delta_{si, sf} \left\{ \begin{matrix} 110 \\ J J J_f \end{matrix} \right\}$$

where θ_i , θ_f are dimensionless reduced width amplitudes for the initial and final states; k_γ , k_f are the wave numbers corresponding to the photon and bound neutron, respectively; J_i , J_f , S_i , S_f are the initial and final values of the total angular momentum and the channel spin; and $\left\{ \begin{matrix} \\ J J J_f \end{matrix} \right\}$ denotes the $6j$ coefficient.

The partial width is then written as

$$\Gamma_{\gamma ij} = (\Gamma_{\gamma \text{ internal } ij})^{1/2} + \delta\Gamma_{ij}^{1/2, 2}$$

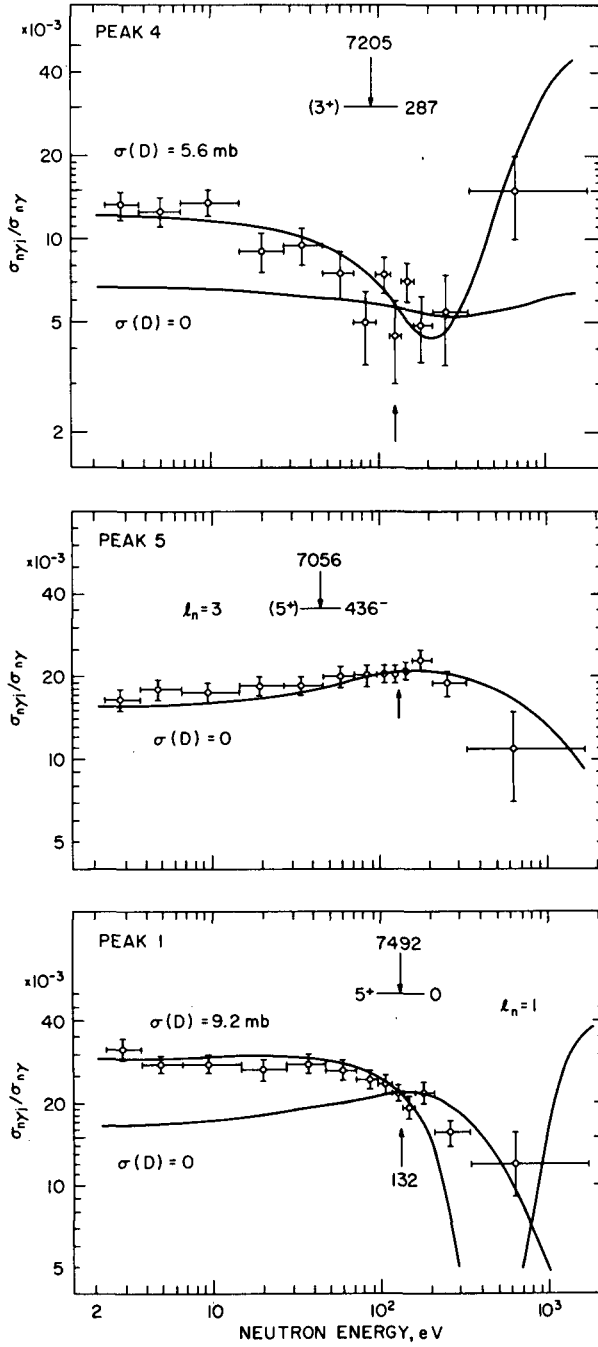


FIG. 12. Interference fits for cobalt. The ground-state gamma ray fit is consistent with a capture cross-section of 9.2 mb at 1 eV.

The channel capture contribution is proportional to the neutron reduced widths of both initial and final states, hence the expected strong transitions to single-particle final states. Such enhanced transitions have been reported for many years in the case of thermal capture, particularly by Groshev [17] and his collaborators, and have been identified as single-particle transitions. Evidence for this interpretation is based on the observed correlation of (n, γ) strengths with the (d, p) cross-sections, which depend on the spectroscopic factor, and therefore the single-particle nature of the final state. Since thermal capture represents an indeterminate mixture of resonance and direct contributions at thermal energies, it is not possible to separate channel capture and direct capture. In resonances, the channel capture could be recognized by studying the correlation between partial widths and the product of initial and final state reduced widths.

The Brookhaven group has made a systematic attempt to study width correlations in resonances. The distribution of correlation coefficients for a limited sample size is indeed a very broad one, and careful analysis is required to establish the significance of a sample correlation. To illustrate this point, the results of a Monte Carlo simulation of the sample correlation coefficient between two independent variables drawn from Porter-Thomas distributions are shown in Fig. 13. For a large sample size the distribution is approximately Gaussian in form centred approximately on zero. For such a sample size the usual 'distribution-free' statistical tests may be applied. Consider, however, Fig. 13, the distribution for $n = 5$. The nature of the Porter-Thomas distribution is such as to produce a skewed distribution of p with a sizeable tail to values near plus one. Thus, even highly positive correlation coefficients for small samples may not be significant.

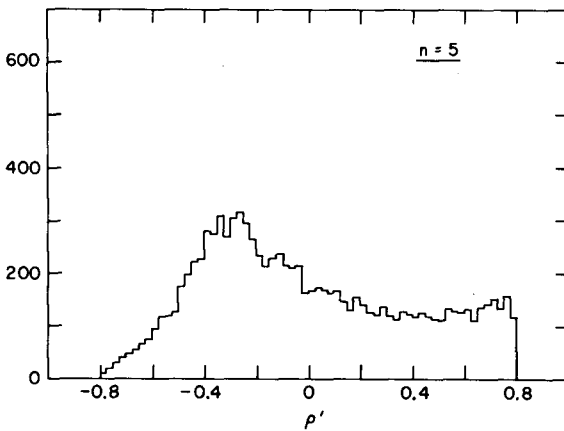


FIG. 13. The sample size is $n = 5$. Note the asymmetry and the long positive tail to the maximum value of ρ' , where

$$\rho' = \frac{\text{covar}(x, y)}{\sigma_x \sigma_y} \left(\frac{n-1}{n} \right)$$

Nevertheless it has definitely been established that correlations are present in resonance as well as in thermal capture. In thulium, for example, a significant positive correlation has been established between the average partial widths to low-lying states of the residual nucleus and the reduced neutron width of the resonance [18]. On the other hand, correlations between the average partial widths and the final state reduced neutron widths (or more properly the d, p reaction cross-sections) have been established for ^{165}Ho and ^{166}Er , and probably for several others (Table I). These correlations are, for the most part, small, but several are statistically significant. Recently the p-wave resonances in niobium have been analysed and show a significant correlation with final state widths, while the s-wave resonances show no significant effect [19].

TABLE I. SUMMARY OF (n, γ)-(d, p) CORRELATION COEFFICIENTS MEASURED AS OF JANUARY 1969

Target	No. final states	r	P ($x \leq r$)
Mn ⁵⁵	10	+0.364	0.846
Fe ⁵⁶ , thermal	20	+0.141	0.721
Fe ⁵⁶ , resonance	20	+0.461	0.980
Co ⁵⁹	12	+0.253	0.782
*La ¹³⁹	8	+0.493	0.889
*Ho ¹⁶⁵	18	+0.480	0.978
Tm ¹⁶⁹	13	+0.276	0.816
*Er ¹⁶⁶	25	+0.694	0.999
*Ta ¹⁸¹	22	+0.279	0.895
*W ¹⁸²	18	+0.100	0.652
*W ¹⁸⁶	17	-0.084	0.377
U ²³⁸	18	+0.363	0.930

An attempt has been made to interpret these correlations as a manifestation of channel capture of manganese, a nucleus showing a significant correlation between n, γ and d, p strengths for thermal capture. Many of the spins and spectroscopic factor for states in ^{56}Mn are known [20] and the spectra for four resonances in manganese have been measured. The channel capture widths have been evaluated and compared to the observed widths [21]. Some of the results are shown in Fig. 14. Exact correspondence between the predicted and measured widths is obscured by the presence of the internal portion of the width amplitude which may interfere with the channel portion to produce widely varying partial widths. Nevertheless, there is a significant correlation coefficient between the predicted channel widths and observed widths in the manganese resonances, its value being + 0.4. It is possible, by Monte Carlo techniques, to estimate the ratio

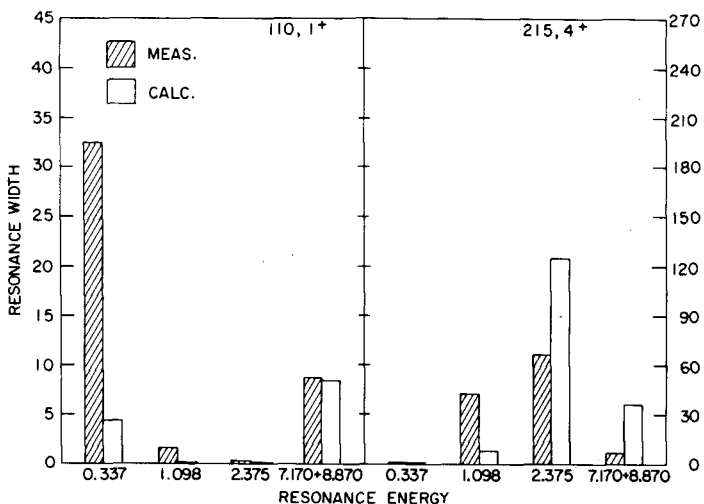


FIG. 14. Channel capture radiative widths $\delta\Gamma$ compared to measured partial widths for resonances in $^{55}\text{Mn}(n,\gamma)^{56}\text{Mn}$. (Note the different vertical scales.)

of internal/external capture in manganese by assuming that the former quantity is randomly distributed while the latter is calculated from Lynn's formula. The result is that internal capture is ~ 5 times larger than external capture for manganese; on the average

$$\langle \Gamma_{\text{int}} \rangle / \langle \delta\Gamma \rangle \approx 5$$

For heavier nuclei we have not been able to establish a channel capture effect, that is, no correlation has been observed with the product of initial and final state reduced width amplitudes. The observed correlations must therefore be ascribed to other effects. Bartholomew has suggested the importance of particle-hole states in the de-excitation following neutron capture [22]. The departure of the shape of the capture gamma-ray spectrum from the smooth form expected from the statistical model leads to speculation that the doorway states or two-particle one-hole states may play an important role in the neutron capture process, with strong dipole transitions resulting from the annihilation of the particle and the hole. The decay of a 2p-1h state to a single-particle state would presumably provide the observed correlation of transition strength with final-state reduced width, since the incoming neutron can be pictured as dropping into appropriate orbital upon producing the particle-hole excitation.

The low-lying configurations for states of ^{94}Nb have been assigned in some detail by Journey et al. [23] and the population of these states from S and P-wave capture in resonances of niobium provide us with some interesting results relevant to this discussion. Figure 15 shows some P-wave capture spectra from niobium - note particularly the highly intense transitions which proceed to low-lying positive parity states in ^{94}Nb . These states have configurations $\pi g_{9/2}(\nu d_{5/2})^3$ or $\pi g_{9/2}(\nu d_{5/2})^2 P_{1/2}$,

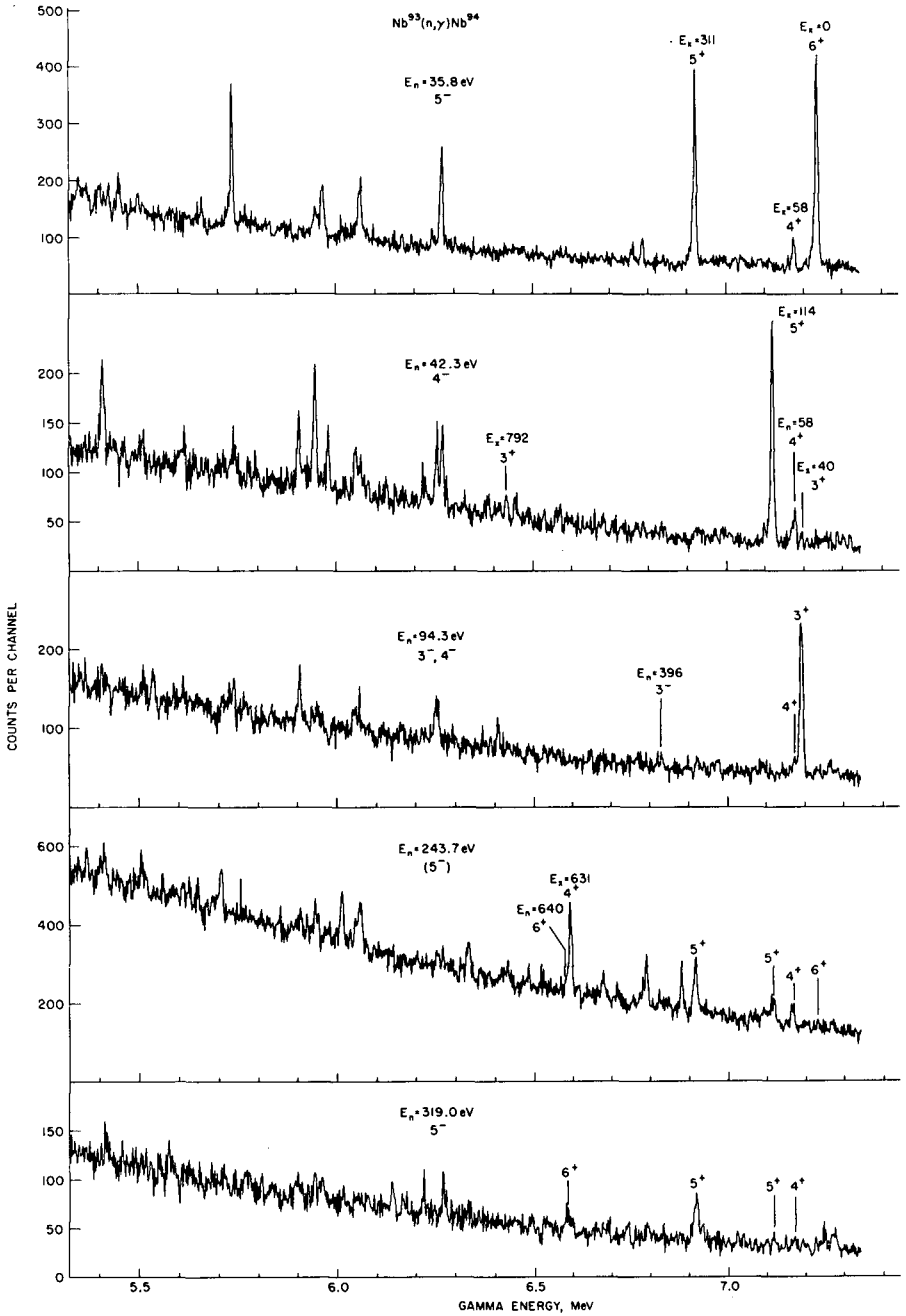


FIG. 15. P-wave capture spectra in $^{93}\text{Nb}(n,\gamma)^{94}\text{Nb}$. The transitions at high energies are extremely strong E1's.

and are strongly populated in the (d, p) reaction with $\ell = 2$ and $\ell = 0$ stripping patterns. It is significant to note that there are a number of negative parity states which are believed to be proton-excited states with $\pi p_{1/2}^{-1} (g_{9/2})^2 \nu(d_{5/2})_{5/2}^3$ and $\pi p_{1/2}^{-1} (g_{9/2})^2 \nu(d_{5/2})_{9/2}^3$. These are populated from the S-wave resonances with intensities of average strength. The reduced intensity plots of Fig. 16 illustrate the anomalous strengths of these E1 transitions in the P-wave resonances, and the non-statistical shape of the gross gamma-ray spectrum is clearly indicated. On the other hand, the S-wave resonances appear to contain no such enhancements.

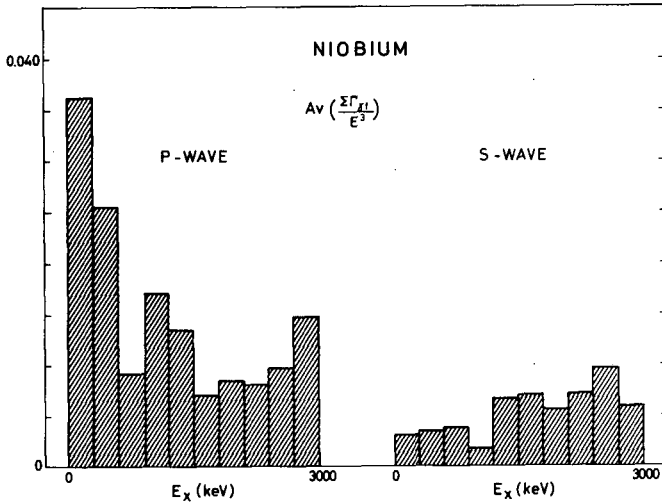


FIG. 16. The averaged gamma-ray spectra for P- and S-wave Nb resonances. All gamma-rays regardless of multipolarity are included, averaged over 300-keV intervals, and plotted against excitation energy.

The (n, γ) intensities have been averaged over resonances and the correlation coefficients between these (n, γ) and (d, p) strengths are -0.09 and $+0.58$ for S and P-wave resonances, respectively. These enhanced transitions from P-wave resonances are thus correlated with d, p cross-sections, while no such correlation occurs in S-wave capture. It is tempting to interpret this in terms of a single-particle neutron transition $P \rightarrow D$ or $P \rightarrow S$. There is, however, no significant correlation between the neutron reduced widths and the radiative width, as would be expected in that picture. On the other hand, there are in ^{94}Nb several possible particle-hole states whose annihilation would produce gamma rays of the appropriate energy [24]. These E1 transitions ($3s_{1/2} \rightarrow 2p_{1/2}$, $3s_{1/2} \rightarrow 2p_{3/2}$, $2d_{5/2} \rightarrow 2p_{3/2}$ and $2d_{5/2} \rightarrow 1f_{5/2}$) could result from the excitation of protons from the filled $p_{1/2}$, $p_{3/2}$ and $f_{5/2}$ shells, while the neutron drops down to d or s states. Such transitions can be initiated by neutrons, but not by S-wave neutrons, since no suitable shell model states exist of the appropriate parity. The enhanced E1 transitions produced by this mechanism are also evident in a comparison of the E1 to M1 strengths averaged over S-wave and P-wave resonances. For S-wave we find that $\langle (\Gamma_\gamma)_{E1} \rangle / \langle (\Gamma_\gamma)_{M1} \rangle \cong 3$, while for P-wave we find $\langle (\Gamma_\gamma)_{E1} \rangle / \langle (\Gamma_\gamma)_{M1} \rangle \cong 10.5$.

These marked differences occurring in the spectra of resonances of opposite parity in ^{94}Nb thus find a plausible interpretation in terms of the shell model structure of that nucleus and indicate the important role of doorway states in the capture process. A similar explanation may prevail for the (n, γ) - (d, p) correlations occurring for other nuclei.

Our final topic for discussion is the distribution function for partial radiative widths, a subject of intense study since the first measurements of resonance capture spectra.

The simple statistical assumptions of the complexity of the initial state leads to the expectation that these widths are distributed according to the chi-squared distribution of one degree of freedom - the Porter-Thomas [25] distribution. Indeed, most nuclei which have been investigated follow such a distribution. The most easily interpreted experimental situation involves the measurement of the resonance partial widths for decay to a single final state. Experimental limitations are forced in general to include several final states in the analysis and to cover only a limited region of incident neutron energy. Jackson et al. [26] have measured the partial widths for 3 final states in $^{195}\text{Pt}(n, \gamma)^{196}\text{Pt}$ and find ν satisfactorily near 1 for a sample of 66 widths (22 $J = 1$ resonances). Other measurements have been made involving fewer resonances but including more final states. Among these are the experiments of Rae et al. [27] in mercury and Price et al. [8] in ^{238}U . A considerable amount of preliminary data has been accumulated by the Brookhaven fast chopper group and several apparent deviations from the Porter-Thomas distribution have been noted. These results are given in Table II and have been analysed in terms of the chi-squared distribution with ν degrees of freedom. The most notable departures are those for ^{103}Rh , ^{142}Pr and ^{238}U . Each of these is very difficult to reconcile with $\nu = 1$. Recently Bečvář and co-workers [28] at Dubna have also reported the unusual behaviour for the 3^+ resonances of praeosodymium. On the other hand, the Harwell group of Murray et al. [29] report a value of ν consistent with one for ^{182}W and ^{186}W , a value considerably lower than the BNL preliminary value.

In view of the fact that all these data are drawn from a limited set of neutron resonances and include a large set of final states, the interpretation of the apparent departures from the Porter-Thomas distribution must be treated with caution. It is nevertheless interesting to speculate on the departure from the Porter-Thomas distribution due to some specific feature of nuclear structure. Both Rosenzweig [30] and more recently Beer [31] have proposed theories for treating the anomalous width distribution. Beer's theory is based on the decomposition of the initial state wave function into two components of widely different dimensionality. The departure from the Porter-Thomas distribution is dictated by the small number of basis states in the second component. This theory, however, does not provide a model for the nuclear structure effect involved. It may well be that these apparent discrepancies with the statistical picture of randomly distributed width amplitudes are indicative of structural effects. The resolution of this question depends on the continuing accumulation of accurately measured widths for each nuclide.

In closing, I would like to suggest that the next few years will see significant progress in the measurements or radiative transitions in fissile nuclides. The problem of separating fission and capture gamma rays, and performing high-resolution spectroscopy on the latter is being attacked in

TABLE II. SUMMARY OF RADIATIVE WIDTH DISTRIBUTIONS ANALYSED AT BROOKHAVEN AND INCLUDING DATA FROM BNL, SACLAY AND DUBNA

Residual Nucleus	+ 90% limit v - 10% limit	Comments
$^{104}_{45}\text{Rh}$	2.73 + 0.51 - 0.35	Mean value of spin 1^- and spin 0^- resonances (3 res. per spin)
$^{183}_{74}\text{W}$	2.38 + 0.72 - 0.63	28 final states - entire set
$^{184}_{74}\text{W}$	0.69 + 0.29 - 0.27	
$^{187}_{74}\text{W}$	2.20 + 1.65 - 0.85	
$^{196}_{78}\text{Pt}$	0.93 + 0.15 - 0.18	(Saclay Data) [†]
$^{170}_{69}\text{Tm}$	1.97 + 0.77 - 0.45	
$^{166}_{67}\text{Ho}$	0.73 + 0.37 - 0.25	
$^{167}_{68}\text{Er}$	1.68 + 0.58 - 0.45	
$^{233}_{90}\text{Th}$	1.32 + 0.44 - 0.34	
$^{239}_{92}\text{U}$	3.80 + 1.45 - 1.00	Data norm. to E^3 , 72 widths, 4 resonances
$^{198}_{79}\text{Au}$	1.40 + 0.48 - 0.35	57 final states
$^{182}_{73}\text{Ta}$	0.75 + 0.23 - 0.13	Res. spins 3 & 4 mixed, 0's added to math. samples according to selection rules
$^{94}_{41}\text{Nb}$	$\left\{ \begin{array}{l} 0.93 + 0.32(4^-) \\ 0.78 + 0.43(4^+) \\ 0.83 + 0.40(5^-) \end{array} \right\}$	E^3 normalization
$^{142}_{\text{Pr}}$	3.25 + 2.25 - 1.25	Spin 3 only, E^3 norm. ^{††}
$^{134}_{\text{Cs}}$	1.35 + 0.43 - 0.28	(Dubna Data) [*]
$^{92}_{\text{Zr}}$	0.98 + 0.35 - 0.20	E^3 norm.

several laboratories. The level schemes of the compound nuclei in these cases are very poorly known and the gamma spectra may also shed light on the nature of the double-peaked fission barrier [32, 33].

Further experiments on the correlations and statistical properties of radiative widths and on the shape of the gamma-ray energy spectrum will, it is hoped, clarify the role of single-particle and doorway states in neutron capture. Further and better determinations of the potential capture cross-section are needed to compare with the existing theory. Finally, the extension of resonance measurements to higher neutron energies to encompass more neutron resonances is needed to study width distributions and to uncover evidence for short-range intermediate structure. The range of problems and the technical challenges should provide the stimuli to make resonance capture spectroscopy a continually fruitful and interesting field for many years to come.

ACKNOWLEDGEMENTS

The author wishes to acknowledge the important contributions of several colleagues in providing the material presented in this review. The work mentioned here is due to the efforts of M. R. Bhat, O. A. Wasson, M. Beer, Karim Rimawi, R. Graves, S. F. Mughabghab, D. I. Garber, J. B. Garg, M. A. Lone and D. L. Price.

REFERENCES

- [1] LEA, D. E., *Nature, Lond.* 133 (1934) 24.
- [2] GREENWOOD, R. C., BLACK, W. W., *Phys. Lett.* 21 (1966) 702.
- [3] BARTHOLOMEW, G. A., "Neutron capture gamma rays", *Ann. Rev. nucl. Sci.* 11 (1961) 259.
- [4] MOTZ, H., BÄCKSTRÖM, G., *Neutron Capture Radiation Spectroscopy in Alpha-, Beta-, and Gamma-Ray Spectroscopy*, 1, North Holland Publishing Co., Amsterdam (1965).
- [5] BENNETT, R. G., WALTERS, A. E., FENSTERMACHER, C. A., ROSLER, L., *Bull. Am. phys. Soc.* II 1 (1956) 62.
- [6] LONDON, H. H., RAE, E. R., *Phys. Rev.* 107 (1957) 1333.
- [7] LONE, M. A., CHRIEN, R. E., WASSON, O. A., BEER, M., BHAT, M. R., MUETHER, H. R., *Phys. Rev.* 174 (1968) 1512.
- [8] PRICE, D. L., CHRIEN, R. E., WASSON, O. A., BHAT, M. R., BEER, M., LONE, M. A., GRAVES, R. G., *Nucl. Phys.* A121 (1968) 630.
- [9] BOLLINGER, L. M., THOMAS, G. E., *Phys. Rev. Lett.* 21 (1968) 233; BOLLINGER, L. M., *Nuclear Structure (Proc. Symp. Dubna, 1968)*, IAEA, Vienna (1968) 317.
- [10] MOORHEAD, J. B., MOYER, R. A., *Bull. Am. phys. Soc.* II 13 (1968) 119; private communication.
- [11] ASAMI, A., MOXON, M. C., STEIN, W. E., *Physics Lett.* 28B (1969) 656.
- [12] HUIZENGA, J. R., VANDENBOSCH, R., *Phys. Rev.* 120 (1960) 1305.
- [13] PÖNITZ, W. P., *Z. Phys.* 197 (1966) 262.
- [14] WEIGMANN, H., WINTER, J., "Measurements of prompt gamma rays from neutron interaction in ^{235}U resonances", these Proceedings.
- [15] LANE, A. M., LYNN, J. E., *Nucl. Phys.* 17 (1960) 563.
- [16] WASSON, O. A., BHAT, M. R., CHRIEN, R. E., LONE, M. A., BEER, M., *Phys. Rev. Lett.* 17 (1966) 1220; *Phys. Rev.* 176 (1968) 1314.
- [17] GROSHEV, L. V., DEMIDOV, A. M., LUTSENKO, V. N., PELEKHOV, V. I., *Int. Conf. peaceful Uses of atom. Energy (Proc. Conf. Geneva, 1958)* 15, UN, New York (1958) 138.
- [18] BEER, M., LONE, M. A., CHRIEN, R. E., WASSON, O. A., BHAT, M. R., MUETHER, H. R., *Phys. Rev. Lett.* 20 (1967) 340.

- [19] RIMAWI, K., Thesis, State University of New York (Albany); see also Bull. Am. phys. Soc. II 14 (1969) 104.
- [20] COMFORT, J. R., Phys. Rev. 177 (1969) 1573.
- [21] RIMAWI, K., WASSON, O. A., CHRIEN, R. E., GARBER, D. I., contribution to Int. Conf. Nuclear States, Montreal, 25-30 August 1969.
- [22] BARTHOLOMEW, G. A., invited talk, Miami American Physical Society Meeting, 25-27 November 1968.
- [23] JURNEY, E. T., MOTZ, H. T., SHELINE, R. K., SHERA, E. B., VERVIER, J., Nucl. Phys. A111 (1968) 105.
- [24] COHEN, B. L., FULMER, R. H., McCARTHY, A. L., MUKHERJEE, P., Rev. mod. Phys. 35 (1963) 332.
- [25] PORTER, C. E., THOMAS, R. G., Phys. Rev. 104 (1956) 483.
- [26] JACKSON, H. E., JULIEN, J., SAMOUR, C., BLOCK, A., LOPATA, C., MORGENSTERN, J., MANN, H., THOMAS, G. E., Phys. Rev. Lett. 17 (1966) 656.
- [27] RAE, E. R., MOYER, W. R., FULLWOOD, R. R., ANDREWS, J. L., Phys. Rev. 155 (1967) 1301.
- [28] URBANEC, J., VRZAL, J., UJV 2228.R; BEČVÁŘ, F. et al., "Fluctuation of partial widths from resonance neutron capture in the ^{141}Pr nucleus", these Proceedings.
- [29] MURRAY, J., THOMAS, B. W., RAE, E. R., "Some statistical properties of partial radiation widths in tungsten", these Proceedings.
- [30] ROSENZWEIG, N., Phys. Rev. Lett. 6 (1963) 123.
- [31] BEER, M., Phys. Rev. (in press).
- [32] STRUTINSKY, V. M., BJØRNHOLM, S., Nuclear Structure (Proc. Symp. Dubna, 1968), IAEA, Vienna (1968) 431.
- [33] LYNN, J. E., Nuclear Structure (Proc. Symp. Dubna, 1968), IAEA, Vienna (1968) 463.

FLUCTUATION OF PARTIAL WIDTHS FROM RESONANCE NEUTRON CAPTURE IN THE ^{141}Pr NUCLEUS

F. BEČVÁŘ, J. POSPÍŠIL, S. A. TELEZHNIKOV

Joint Institute of Nuclear Research,

Dubna, USSR

and

J. URBANEC, J. VRZAL

Nuclear Research Institute of the Czechoslovak Academy of Sciences,

Řež near Prague,

Czechoslovakia

Abstract

FLUCTUATION OF PARTIAL WIDTHS FROM RESONANCE NEUTRON CAPTURE IN THE ^{141}Pr NUCLEUS. Earlier experimental data obtained by us in Dubna from gamma-ray spectra studies on ^{142}Pr have been re-analysed. Unambiguous spin assignments for five neutron resonances in ^{141}Pr have been made. The analysis of 27 partial radiation widths has led to a value of $\nu = 3.56$ for 3^+ resonances and the value obtained for them in 2^+ resonances is compatible with the expected value of $\nu = 1$.

The preliminary results of our measurements of the gamma spectra in the transitions following neutron resonance capture on ^{141}Pr at the pulsed fast reactor of the Joint Institute for Nuclear Research, Dubna, have been given elsewhere [1]. As an example of the gamma spectra obtained, Fig. 1 shows the 84.8-eV resonance spectrum. In the same paper the relative intensities were determined of some primary high-energy transitions and low-lying transition energies and the first low-lying level scheme of ^{142}Pr was given.

Kern et al. [2] gave a more precise scheme of low-lying levels in ^{142}Pr and determined unambiguous spin and parity assignments of the levels up to ~ 200 keV based on precise measurements of low-energy transitions following thermal neutron capture and on an interpretation of the results of (d-p) experiments. The detailed knowledge of the energies, spins and parities of low-lying levels given in Ref. [2] made it possible to reinterpret the experimental data obtained in our work. The spins of some resonances in the ^{142}Pr nucleus could be checked or assigned and thus the basic conditions for a statistical analysis of the fluctuations of partial widths were obtained.

The spins of the levels in the Pr nucleus can have the values 2^+ , 3^+ in neutron capture. As the low-lying levels are predominantly formed by the configuration of states of the last odd neutron and the last odd proton (the ground state has the characteristics $f_{7/2}$, $d_{5/2}$), the parity of these states is negative and high-energy transitions can be E1, M2 etc. As M2 transitions cannot compete with E1 transitions as regards the observable intensity, only primary E1 transitions appear in the compound-state decay of ^{142}Pr .

On the basis of these considerations spins could be assigned to the states following capture in the resonances observed. The capture spin 2^+ may be recognized in the spectra by an intense primary transition to the 1^- 85.0-keV level. This transition would be M2 in the case of the 3^+ spin.

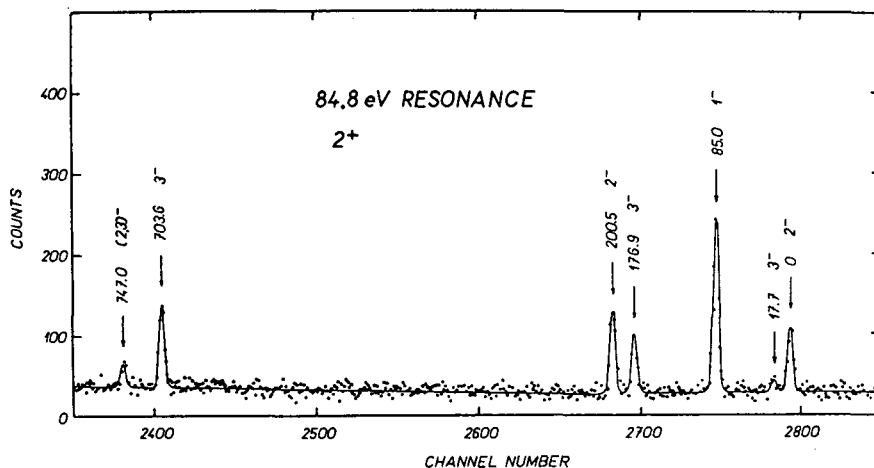


FIG. 1. Ge(Li) detector pulse height spectrum from neutron capture in ^{141}Pr . Energies and spin assignments given at different peaks belong to the final states of ^{142}Pr as given in Ref. [2].

The state with 3^+ spin and parity assignment is seen in transitions to the 4^- spin states (723, 144.8 and 637.2 keV). Transitions to low-lying 2^- and 3^- levels may appear in capture states with both possible spin values. It must be added that the 3^+ spin resonance gamma spectra suggest that the intensity of the ground-state transition and of the transition to the 17.7-keV level with spin 2^- or 3^- is probably suppressed by the structural effects.

In this way the 84.8-eV resonance spin was found for the first time and the spins of the 231.7, 215.6 eV (3^+), 231.7 eV (3^+), 519.2 eV (2^-) and 635.7 eV (3^+) resonances were determined unambiguously. The energy values were taken from Ref. [3]. The spin assignment for the 231.7-eV resonance agrees with Ref. [3] and that for 215.6, 519.2 and 835.7 eV agrees with the values given in the two latest papers [3, 4].

At the same time an unambiguous spin value for the low-lying 703.6-keV level could be determined. In Ref. [2] it was found that either 3^- or 4^- spin values could be assigned to this level. Our experiment, however, shows that only 3^- is possible because direct transition to this level is possible in resonances with both spins.

The spectra obtained by us were reanalysed recently, using a modified non-linear least-squares fitting program and thus more precise energy values and relative intensities were obtained for ten high-energy transitions in five resonances to which unambiguous spin values could be ascribed. Of these gamma-ray transitions 9 could be observed for 3^+ spin resonances and 7 for 2^+ spin resonances.

The partial widths were reduced to the energy dependence in E3 and to the relative level density spin dependence. The sum of 5 intense low-lying transitions was used to measure the capture process in individual resonances. To check these results the reduction for the dependence on the fifth power of energy was used, which showed that it exhibited only a small effect on the determination of the resultant range of Porter-Thomas distribution due to the narrow range of the gamma-ray energies concerned. The

relative partial reduced widths obtained by this procedure and the errors involved are given in Table I.

The number of degrees of freedom in the Porter-Thomas distribution was estimated for a statistical sample of experimental values of the relative partial reduced widths by the maximum-likelihood method. Since this method may yield a biased estimation due to considerable statistical errors in the experimental values, a more detailed analysis was carried out using the Monte Carlo method. A large number of samples of the same size as the experimental sample with fixed parameter ν_m of the Porter-Thomas distribution was generated by this method. A normal distribution with the dispersions corresponding to experimental errors was used to smooth the individual widths. For each sample obtained in this way the number ν_p of the degrees of freedom in the Porter-Thomas distribution was estimated by the maximum likelihood method. By comparing the distribution of the quantity ν_p with the values $\nu_p \text{ exp}$ for individual ν_m it was possible to estimate the degrees of freedom in the Porter-Thomas distribution and the confidence interval.

For the whole sample of 41 values an estimated value of $\nu = 1.65$ was obtained. As the 3^+ spin resonances have a high value of the reduced neutron width Γ_n^0 in the region up to 1 keV and show low fluctuations around this value, a sample of 27 values corresponding to 9 transitions in three 3^+ spin resonances was treated. This treatment yielded the resultant estimated value of $\nu = 3.60 \pm_{1.08}^{1.28}$. An independent analysis of 14 width values for the 2^+ spin resonance yielded the value $\nu = 1.25 \pm_{0.48}^{0.74}$. The dependence of the probability $P(\nu_p > \nu_p \text{ exp})$ that the generated sample yields a ν_p greater than $\nu_p \text{ exp}$ by a given value ν_m is shown in Fig. 2 for both spin cases and a comparison of the integral distribution of experimental widths with those from the Porter-Thomas for various ν_m values is given in Fig. 3 for both spins. A histogram of the distribution of ν_p generated by the Monte Carlo method for $\nu_m=1$ is shown in Fig. 4. In 5000 samples none was found with higher values than $\nu_p \text{ exp} = 3.31$ (for 3^+ resonances) (see Table I).

The high value of ν obtained for 3^+ resonances suggests that pronounced effects of nuclear structure appear in the ^{142}Pr nucleus and that the application of the statistical model is not fully correct in this case. It appears furthermore that the 3^+ spin resonance differs considerably in its behaviour from that with 2^+ spin, which may be due to a number of simple admixtures appearing in each resonance type. It is interesting that the mean value of $\langle \Gamma_{\gamma i} \rangle$ in the 3^+ spin resonances is substantially smaller than the mean value of $\langle \Gamma_{\gamma i} \rangle$ in the 2^+ spin resonances. The ratio of the two quantities yields $\langle \Gamma_{\gamma i} \rangle_{2^+} / \langle \Gamma_{\gamma i} \rangle_{3^+} = 3.56$.

The strong effects of structure in the ^{142}Pr nucleus with one extra neutron over the closed stable shell with 82 neutrons may be expected. The 58-proton subshell appears to be relatively stable in some cases and the odd proton and neutron in the ^{142}Pr nucleus, therefore, can probably form strong admixtures of simple structure even at relatively high excitation energies.

Both the value of ν in the Porter-Thomas distribution and the shape of the spectra of the primary gamma-rays differ considerably from the statistical model predictions. It will be possible to confirm the assumption of the influence of the structure effect definitely after an analysis of a larger number of resonances with both spin values following neutron capture in the ^{141}Pr nucleus.

TABLE I. RELATIVE REDUCED PARTIAL RADIATION WIDTHS

Values are reduced to E^3 . All values are normalized to the mean value of all relative widths of 3^+ resonances.

Final state energy ^a (keV)	Neutron resonance energy ^b (eV)				
	84.8 (2 ⁺)	519.2 (2 ⁺)	215.6 (3 ⁺)	231.7 (3 ⁺)	635.7 (3 ⁺)
0 (2 ⁻)	2.47 ± 0.17	17.90 ± 0.94	0.21 ± 0.15	0.16 ± 0.10	0.79 ± 0.21
17.7 (3 ⁻)	0.46 ± 0.12	5.16 ± 0.60	0.24 ± 0.15	0.17 ± 0.10	0.48 ± 0.19
72.3 (4 ⁻)	---	---	0.45 ± 0.17	1.95 ± 0.15	0.09 ± 0.18
85.0 (1 ⁻)	6.65 ± 0.25	5.20 ± 0.63	---	---	---
144.6 (4 ⁻)	---	---	0.98 ± 0.20	0.92 ± 0.13	0.53 ± 0.22
176.9 (3 ⁻)	2.35 ± 0.18	0.64 ± 0.45	1.23 ± 0.21	0.35 ± 0.11	3.78 ± 0.35
200.5 (2 ⁻)	3.30 ± 0.20	0.00 ± 0.40	2.12 ± 0.24	1.12 ± 0.14	0.90 ± 0.24
637.2 (4 ⁻)	---	---	1.01 ± 0.26	0.67 ± 0.16	1.13 ± 0.30
703.6 (3 ⁻)	3.91 ± 0.25	0.34 ± 0.56	1.07 ± 0.28	1.25 ± 0.19	2.05 ± 0.35
747.0 (2 ⁻ , 3 ⁻)	1.14 ± 0.19	0.66 ± 0.60	0.70 ± 0.28	1.17 ± 0.19	1.47 ± 0.34

^a Values are taken from Ref. [2]. For 3⁻ assignment of the 703.6-keV level see text.

^b Values of the energies are taken from Ref. [3]. For the spin assignments see text.

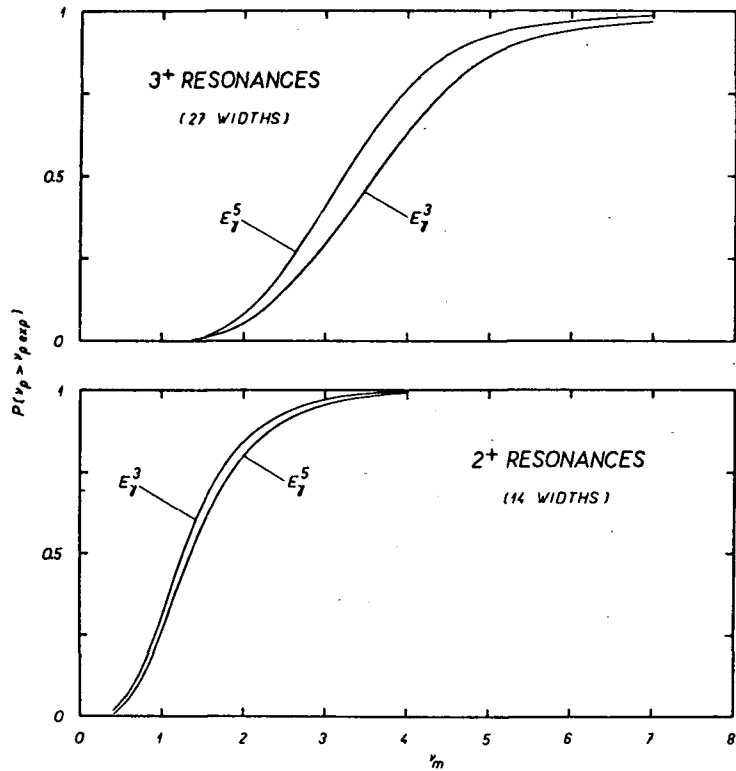


FIG. 2. Probability $P(\nu_p > \nu_{p \text{ exp}})$ expressing that the value of ν_p of generated widths by the Monte Carlo method is higher than $\nu_{p \text{ exp}}$ for both spin values and for both energy dependencies. Experimental errors are included.

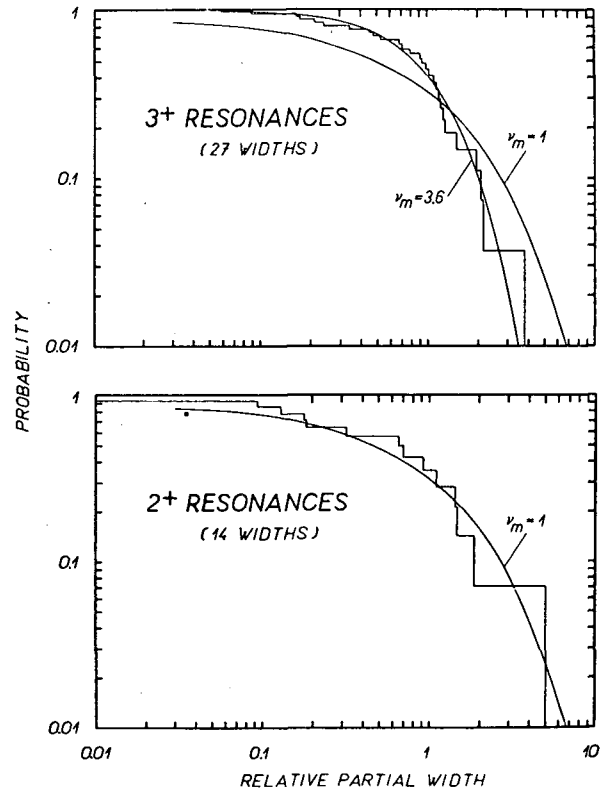


FIG. 3. Distribution of experimental values of relative partial radiation widths for 3+ and 2+ resonances. For comparison Porter-Thomas distributions for different ν_m values are shown.

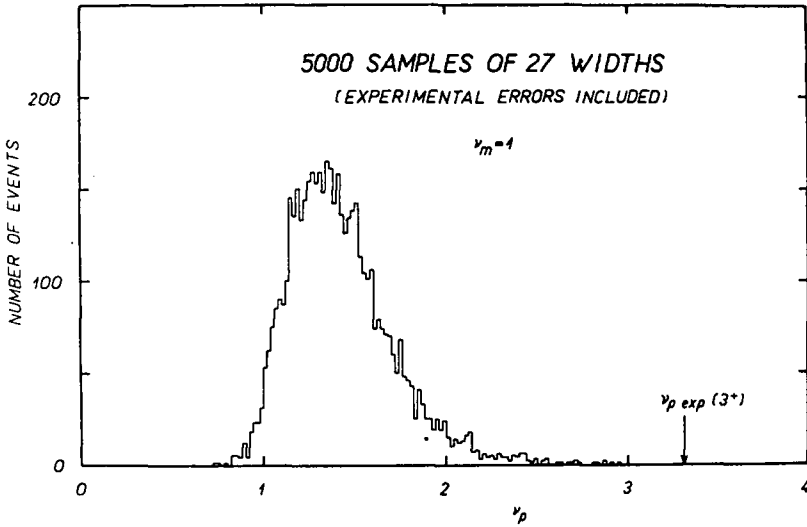


FIG. 4. Distribution ν_p for 5000 cases of 27 widths generated by the Monte Carlo method for $\nu_m = 1$.

With a higher number of observed resonances it will also be possible to check the correlations between the reduced neutron widths Γ_n^0 and partial radiation widths $\Gamma_{\gamma i}$.

ACKNOWLEDGEMENTS

We should like to express our thanks to I. M. Frank and F. L. Shapiro for their continuous interest in this work and to J. Hroník and Z. Pospíšilová for their help in handling the experimental data.

REFERENCES

- [1] BEČVÁŘ, F., VRZAL, J., LIPTÁK, J., URBANEC, J., Preprint JINR P3-3696 (1968).
- [2] KERN, J., STRUBLE, G. I., SHELINE, R. K., JURNEY, E. T., KOCH, M. R., MAIER, B. P. K., GRUBER, U., SCHULT, O. W. B., Phys. Rev. 173 (1968) 1133.
- [3] MORGENSTERN, J. et al., Nucl. Phys. A123 (1969) 561.
- [4] WYNCHANG, S. et al., Phys. Rev. 166 (1968) 1234.
- [5] BEČVÁŘ, F., TELEZHNIKOV, S. A., to be published.

GAMMA-RAY SPECTRA FROM RADIATIVE CAPTURE OF RESONANCE NEUTRONS IN ANTIMONY

D. PAYA, A. LOTTIN
Commissariat à l'Energie Atomique,
CEN de Saclay,
91 Gif-sur-Yvette, France

Abstract

GAMMA-RAY SPECTRA FROM RADIATIVE CAPTURE OF RESONANCE NEUTRONS IN ANTIMONY. Gamma-ray spectra from individual resonances in natural $Sb+n$ have been measured using a Ge(Li) detector and the 45-MeV Saclay linear accelerator as a pulsed neutron source. The intensities of the strongest lines which appear in the low-energy resonances are given.

INTRODUCTION

The availability of high-resolution gamma-ray spectrometers and intense neutron sources has made possible the study of the radiative de-excitation of states formed in resonance neutron capture. These states are pure spin states and due to Porter-Thomas fluctuations do not exhibit the intensity pattern found in the thermal spectrum.

EXPERIMENTAL METHOD

This work was done at the Saclay 45-MeV electron linear accelerator facility. A sample of 660 grams of metallic natural antimony $10 \times 10 \times 1$ cm, was placed at an angle of 45° to the neutron beam on a 13-m flight path. The flight tube itself made an angle of 45° with the moderator so that the time resolution was principally due to the uncertainty on the flight length.

To prevent overloading the amplifier during the accelerator burst which causes a big gamma flash in the uranium target used to produce the neutrons, a shadow shield was placed in the target room. This consisted of a 24-cm thick lead brick whose height was greater than that of the target which gives the gamma flash but smaller than that of the polyethylene slab which is the source of moderated neutrons. The loss in neutron flux was 30% but the gamma flash was reduced in such a way that the resolution of the gamma-ray spectrometer was not affected.

An 8-cm³ planar Ge(Li) detector with a resolution of 7 keV at 6 MeV was used for gamma detection in connection with standard low-noise pre-amplifier and amplifier. The crystal pulses were amplified and passed through 80 m of 50- Ω double-screened coaxial cable to the analyser system. Here the pulse-height and time-of-flight information were separately encoded and written on magnetic tape; 4096 pulse-height channels were used for each of the 4096 time-of-flight channels. By reading the tape afterwards it was possible to obtain the pulse-height spectrum corresponding

to any time-of-flight region or vice versa. During the accumulation time a gain control was used which ensured that pulses delivered by two pulsers were stored in preset pulse-height channels. The results presented in this paper were collected in a three-week run during which the linear accelerator was operated at 500 pulses/sec with a burst width of 50 nsec.

RESULTS

The background spectra between the resonances have been subtracted from the pulse-height spectra in the resonances. The background correction varied from 7 to 15%. The areas under the peaks were normalized to the total area above an energy of 2 MeV deposited in the detector, then corrected for detector efficiency as obtained from an independent experiment with thermal neutrons on a CCl_4 sample.

A flight time spectrum is shown in Fig. 1. Time resolution is good enough to separate resonances up to an energy of 300 eV. So far the analysis has been performed up to 170 eV which made it possible to obtain the pulse-height spectra of 12 resonances of ^{121}Sb and 4 resonances of ^{123}Sb . A part of the spectra, between 5500 and 7000 keV, is shown in Figs 2 and 3 for some resonances of ^{121}Sb and in Fig. 4 for the resonances of ^{123}Sb . The most striking differences between the spectra are the strong variations in individual gamma-ray intensities due to different spins of capturing states and large fluctuations in partial radiation widths. More

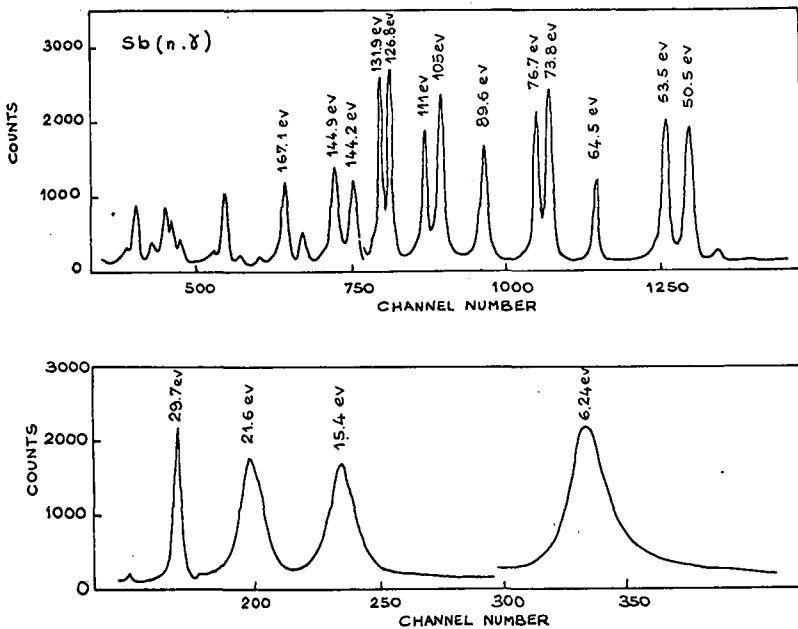


FIG. 1. Flight time spectrum for $E_d > 1$ MeV, where E_d represents the energy deposited in the Ge(Li) detector.

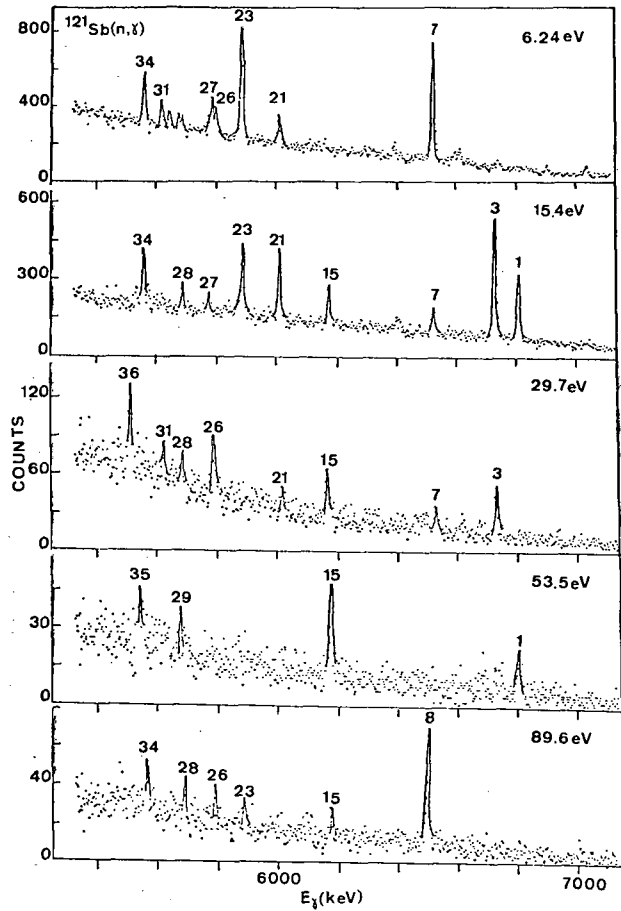


Fig. 2. Gamma-ray spectra for the indicated resonances of ^{121}Sb for $5.5 < E_\gamma < 7$ MeV.

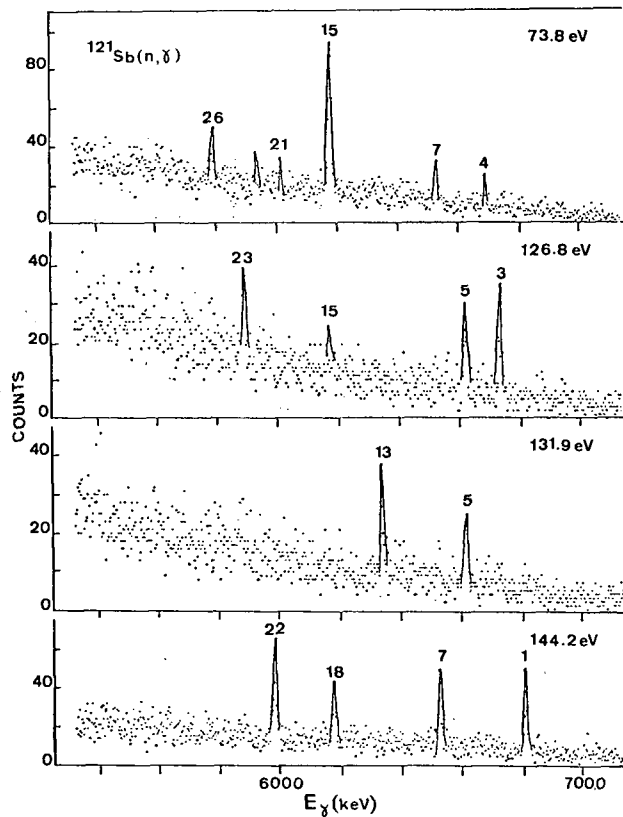


Fig. 3. Gamma-ray spectra for the indicated resonances of ^{121}Sb for $5.5 < E_\gamma < 7$ MeV.

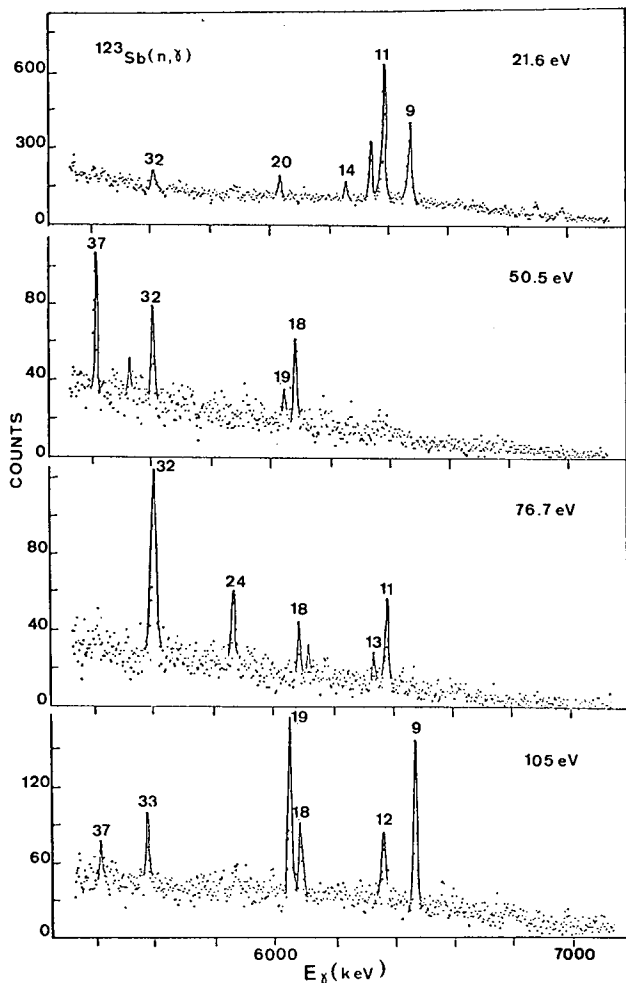


FIG. 4. Gamma-ray spectra for the indicated resonances of ^{123}Sb for $5.5 < E_n < 7$ MeV.

than 35 lines with a gamma energy higher than 4900 keV were detected in the de-excitation of ^{122}Sb against 9 in ^{124}Sb . Half of them have been observed by Rasmussen [1] in thermal capture. Of course the easiest information to obtain is the isotopic assignment of the line from a knowledge of the isotope responsible for the resonance. Some preliminary results on the intensities are given in Tables I and II. But the analysis is still in progress in order to obtain a better gamma-energy determination. Furthermore, some more data collected recently will give us better statistics and, possibly, some indication on the spins of the capturing states.

TABLE I. GAMMA-RAY ENERGIES AND INTENSITIES IN THE RESONANCES OF ^{121}Sb

Column 1 identifies the gamma ray. Column 2 lists the energy. The remaining columns list the observed gamma-ray intensities for three different resonances.

No.	E_γ (keV)	I (photons per 100 neutron captures)		
		6.24 eV	15.4 eV	29.7 eV
1	6808		3.43 ± 0.4	
2	6746	0.49 ± 0.1		
3	6731		7.72 ± 0.8	1.80 ± 0.3
5	6616	0.62 ± 0.1		0.48 ± 0.1
6	6599	0.46 ± 0.1		
7	6524	4.93 ± 0.6	2.75 ± 0.3	0.52 ± 0.1
10	6401		0.55 ± 0.1	
16	6164	0.26 ± 0.1		1.75 ± 0.3
17	6114	0.21 ± 0.1		
21	6012	1.05 ± 0.3	3.15 ± 0.4	0.53 ± 0.1
23	5889	4.56 ± 0.5	2.88 ± 0.4	
25	5802	0.86 ± 0.2		
26	5789	1.18 ± 0.2		1.60 ± 0.3
27	5779	0.40 ± 0.1	0.60 ± 0.1	
28	5689	0.33 ± 0.1	0.74 ± 0.2	
29	5679	0.41 ± 0.1		0.72 ± 0.2
30	5649	0.47 ± 0.1		
31	5621	0.63 ± 0.2	0.30 ± 0.1	1.01 ± 0.2
33	5576		0.76 ± 0.2	
34	5559	1.79 ± 1.3	2.45 ± 0.3	
35	5536		1.27 ± 0.3	
36	5511			0.84 ± 0.2
38	5349			0.37 ± 0.1
39	5253		0.69 ± 0.2	
40	5238			0.75 ± 0.2
41	5208	0.54 ± 0.1	1.13 ± 0.3	0.99 ± 0.2
42	5161	0.52 ± 0.1		
43	5128	0.35 ± 0.1		
44	5045		0.92 ± 0.3	
45	5025		0.95 ± 0.3	
46	5003	1.36 ± 0.3		0.35 ± 0.1
47	4973	0.42 ± 0.1		
48	4928	0.18 ± 0.1		

TABLE II. GAMMA-RAY ENERGIES AND INTENSITIES IN THE RESONANCES OF ^{123}Sb

Column 1 identifies the gamma ray. Column 2 lists the energy. The remaining columns list the observed gamma-ray intensities for three different resonances.

No.	E_γ (keV)	I		
		21.6 eV	50.5 eV	76.7 eV
9	6469	5.50 ± 0.6		
11	6381	8.65 ± 0.9		0.39 ± 0.1
13	6339	3.40 ± 0.4		
14	6256	0.86 ± 0.2		
18	6087		0.22 ± 0.1	0.21 ± 0.1
19	6054	0.08 ± 0.05	0.08 ± 0.05	
20	6032	0.77 ± 0.2		
24	5874			0.32 ± 0.1
32	5611	1.33 ± 0.3	0.28 ± 0.1	1.28 ± 0.3
37	5416		0.41 ± 0.1	

CONCLUSION

This first attempt made in our group to use a good resolution gamma-ray detector with neutron time-of-flight spectrometry looks very encouraging because it shows that a Linac is a good instrument for this kind of work and that it can compete with a chopper when good resolution is needed.

REFERENCE

- [1] Nuclear Data A 5 (1968) 61.

STUDY OF GAMMA-RAY SPECTRA FROM THE $^{163}\text{Dy}(n, \gamma)^{164}\text{Dy}$ REACTION ON NEUTRON RESONANCE CAPTURE

L. S. DANELYAN, B. V. EFIMOV, S. K. SOTNIKOV

I. V. Kurchatov Institute of Atomic Energy,
Moscow, USSR

and

B. KARDON, D. KISS, Z. SERES, L. SZABO

Central Research Institute for Physics,
Budapest, Hungary

Abstract

STUDY OF GAMMA-RAY SPECTRA FROM THE $^{163}\text{Dy}(n, \gamma)^{164}\text{Dy}$ REACTION ON NEUTRON RESONANCE CAPTURE. With the use of an anticoincidence scintillation gamma spectrometer the partial radiation transitions to the rotational band levels from the $^{163}\text{Dy}(n, \gamma)$ resonance energies up to 150 eV were determined. The spins of neutron levels and the average value of the partial transitions were evaluated.

Neutrons were produced by the linear electron accelerator of the Kurchatov Institute, Moscow. The gamma spectra of the neutron resonances were measured by the time-of-flight technique. The flight path from the accelerator target to the dysprosium sample was 7 m and the number of ^{163}Dy nuclei was equivalent to 100g.

The capture gamma rays were detected by an anticoincidence scintillation spectrometer with a central analysing, 70×100 mm NaI(Tl) crystal and a protecting annular, 200×380 mm crystal. Between the crystals of the spectrometer and the sample a 5-cm lead shield with an aperture in front of the analysing crystal and a full 3.5-cm ^6LiH shield were mounted. The gamma-ray spectra were recorded by a 2048-channel multi-dimensional analyser divided into 16 time intervals, each with 128 amplitude channels. The amplifier chain of the central analysing detector, including the input block of the multidimensional analyser, was covered by stabilization systems. An oxide sample enriched to 93% in ^{163}Dy was used. The gamma-ray spectra were measured in the energy interval $E_\gamma = 6-8.5$ MeV on ten ^{163}Dy resonances up to a neutron energy of 150 eV and also in the thermal range (0.08 eV). The other time intervals of the analyser were set between resonances to record the background spectra. The proper operation of the apparatus and the energy calibration were checked by the spectrum of the $\text{Fe}(n, \gamma)$ reaction. The background spectra measured in the intervals between the resonances were interpolated to the range of the resonances studied. The background spectrum was evaluated by normalization to the total number of captures recorded in the range of gamma-ray energies from 5 to 7 MeV. The absolute intensity values were obtained by comparison with known intensities in the capture spectrum of thermal neutrons [1] (with this type of calibration a systematic error may be introduced).

RESULTS

The relevant part of the ^{164}Dy level scheme is given in Fig. 1. The gamma transition intensities are shown in Table I. Assuming the E1 transition to be dominant in the observed transition to the 4^+ level ($K = 0$, $E_{\text{excit}} = 242.2$ keV), spin 3^- was assigned to the resonances at the energies of 16.18, 19.7, 35.0, 55.8, 65.8, 106, 126 and 142 eV. Spin 2^- can be assigned with a probability of 90% to the resonance at 78.8 eV and with a probability of 75% to that at 50.1 eV.

The comparison of the transition intensities to the rotational band levels at the resonances with spin 3^- shows that the average transition intensity to level 4^+ (7411 keV) is greater by a factor of 3 than the average intensity to level 2^+ (7580 keV). The total ^{163}Dy radiation width is 100 MeV, thus the average high-energy partial transition intensity is of the order of 1 MeV, which exceeds by several factors the predictions of different nuclear models of radiative transition [2]. The scintillation detector and processing method used did not permit a detailed evaluation of the transition intensities to the vibrational band levels. At present the $^{163}\text{Dy}(n, \gamma)$ spectra are measured with a Ge(Li) detector.

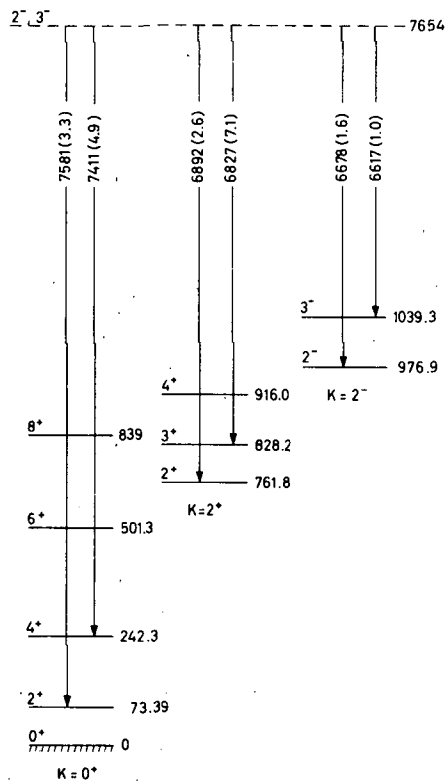
 ^{164}Dy FIG. 1. The level scheme of ^{164}Dy .

TABLE I. GAMMA TRANSITION INTENSITIES

No.	$^{163}\text{Dy} \left(I = \frac{5}{2}^- \right)$ resonance energy (eV)	Partial transition intensities (per 100 captures)			J of neutron resonance
		7580 keV	7411 keV	Sum of trans. 6892 keV 6826 keV 6737 keV	
1	therm. 0.08	0.45	0.49	0.95	
2	16.18	-0.07 ± 0.06	1.33 ± 0.08	1.45 ± 0.30	3^-
3	19.7	-0.04 ± 0.12	0.43 ± 0.15	1.8 ± 0.9	3^-
4	35.0	0.6 ± 0.1	0.73 ± 0.13	4.85 ± 0.5	3^-
5	50.1	0.3 ± 0.22	0.4 ± 0.3	1.8 ± 0.7	
6	55.8	0.02 ± 0.1	2.4 ± 0.2	4.1 ± 0.6	3^-
7	65.8	0.4 ± 0.22	1.6 ± 0.3	4.2 ± 0.6	3^-
8	78.8	0.38 ± 0.22	0.17 ± 0.25	2.3 ± 0.5	
9	106	-0.2 ± 0.1	3.5 ± 0.2	5.4 ± 0.7	3^-
10	126	0.9 ± 0.2	2.1 ± 0.3	3.1 ± 0.8	3^-
11	142	2.5 ± 0.2	2.5 ± 0.24	3.7 ± 0.7	3^-
	I_γ average only 3^- spin levels	0.5	1.55	1 (for one transition)	

REFERENCES

- [1] HAFEMEISTER, D. W. et al., Phys. Rev. 152 (1966) 1084.
 [2] LYNN, J. E., Theory of Neutron Resonance Reactions, Oxford (1968) Chap. VII.

GAMMA RAYS FROM NEUTRON RESONANCE CAPTURE IN Mg, Si, P AND S

B. LUNDBERG, G. NYSTRÖM, I. BERGQVIST

Research Institute of National Defence,

Stockholm, Sweden

Abstract

GAMMA RAYS FROM NEUTRON RESONANCE CAPTURE IN Mg, Si, P AND S. The gamma-ray spectra from neutron resonance capture in Mg, Si, P and S were measured using a NaI(Tl) scintillation spectrometer, 22.6 cm in diameter and 20.8 cm long. The resonances at 47 keV in ^{24}Mg and 30 keV in ^{32}S had previously been studied. A weak resonance in ^{32}S was observed at 42 keV which predominantly decays through the $3/2^-$ level at 3.22 MeV in ^{33}S . A new resonance was also found in ^{31}P at 27 keV and for Si complex resonance structure was observed in the neutron energy range 20-80 keV. The gamma-ray spectra were found to be dominated by a few intense gamma-ray lines through low-lying levels in agreement with previous observations.

INTRODUCTION

The aim of the experiment was to study gamma-ray spectra from resonance neutron capture in $2s\ 1d$ shell nuclei. This region represents the transition between single-particle-like capture of lighter nuclei and the much more complicated heavy nucleus case. The gamma-ray spectra from thermal neutron capture [1] are dominated by high-energy gamma-ray lines (E1 or M1) and experiments on resonance capture by Bird et al. [2, 3] and Bergqvist et al. [4, 5] also show prominent high-energy gamma-rays.

Nuclei in this mass range, $20 \leq A \leq 40$, have well-separated resonances in the energy range $E_n = 10 - 100$ keV, for which spins, parities and radiation widths are known or can be determined. Spins and parities of low-lying levels are also known, at least below an excitation energy of 3-4 MeV. Hence these nuclei are suitable to study in neutron resonance capture experiments.

The gamma-ray spectra emitted from resonance capture were measured for the following nuclei at the resonances indicated by their energies: ^{24}Mg at 47 keV, ^{28}Si at 68 keV, ^{31}P at 27 keV and ^{32}S at 30 keV. In an additional experiment the capture cross-sections were measured near these resonances.

RESULTS

The results of the measurements of the capture cross-sections are shown in Figs 1, 3, 5, 7 and the gamma-ray spectra are given in Figs 2, 4, 6, 8. The gamma-ray spectra are represented by the solid lines which are drawn through the experimental points. The spectra show intense gamma rays to low-lying levels in agreement with previous observations [1-4].

A first attempt to decompose the spectra into individual gamma-ray lines has been made and the results are indicated in Figs 2, 4, 6, 8 as dashed curves. More analysis is required to determine the decay schemes and to deduce partial radiation widths.

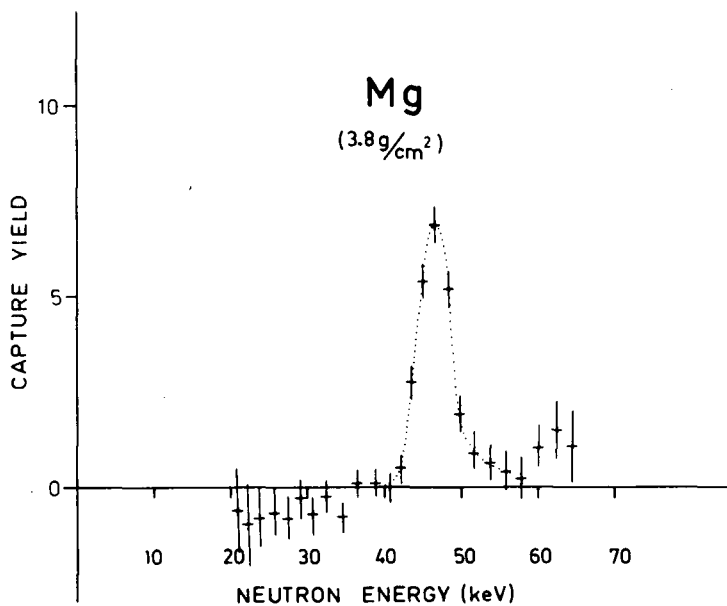
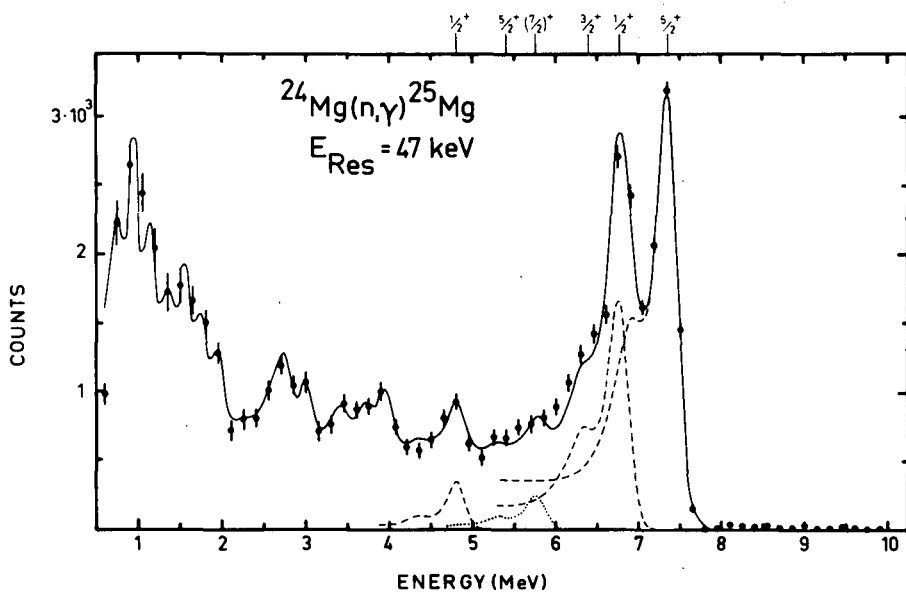


FIG.1. Gamma yield from neutron capture in Mg.

FIG.2. Gamma spectra from Mg (n, γ), $E_T = 47$ keV. The solid curve was calculated using the known detector response matrix. Some response line shapes are indicated as dashed curves.

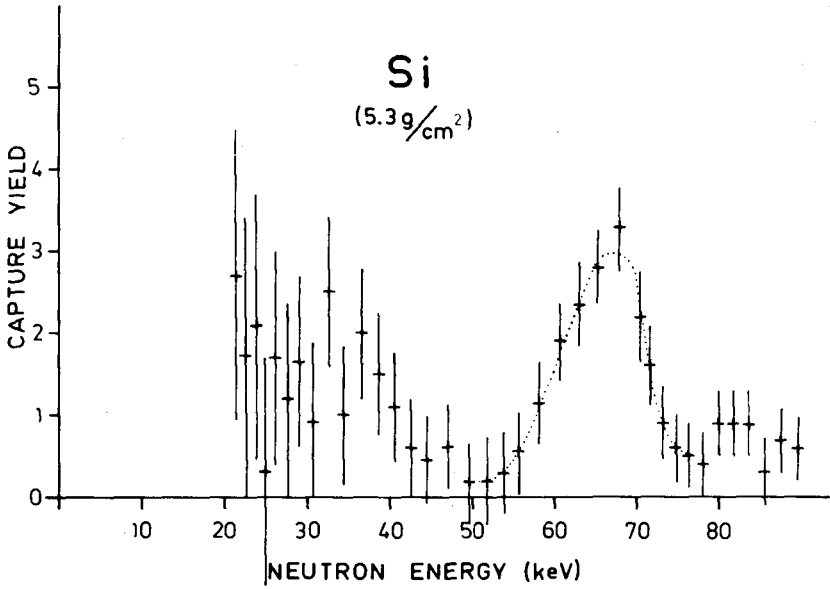


FIG. 3. Gamma yield from neutron capture in Si.

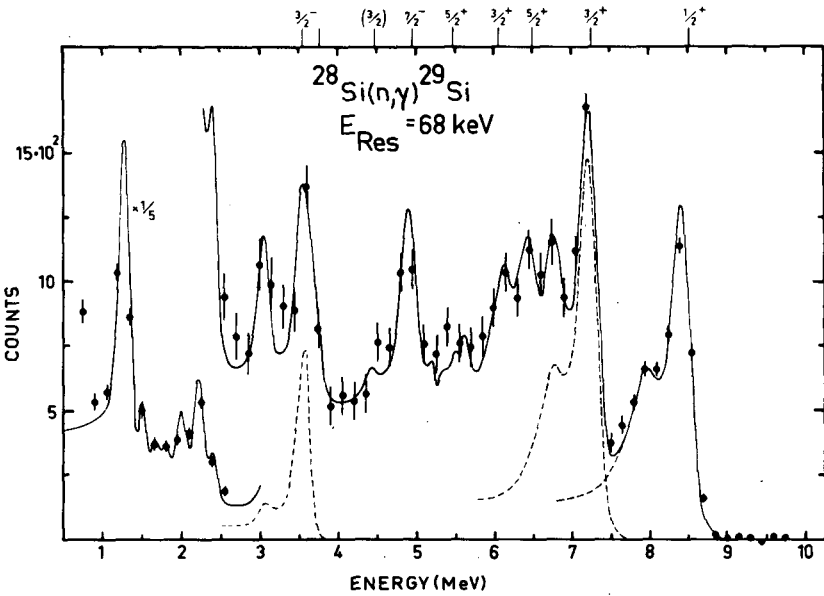


FIG. 4. Gamma spectra from Si (n, γ), $E_T = 68$ keV. The solid curve was calculated using the known detector response matrix. Some response line shapes are indicated as dashed curves.

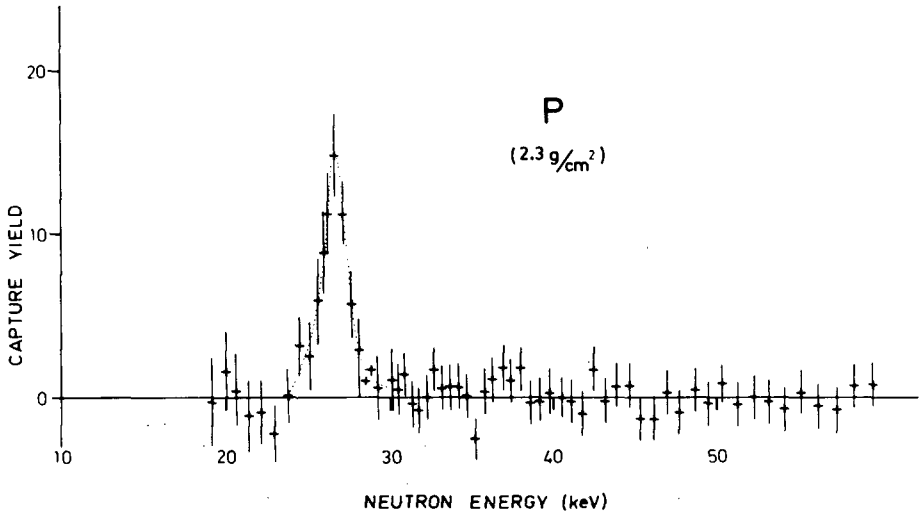


FIG. 5. Gamma yield from neutron capture in P.

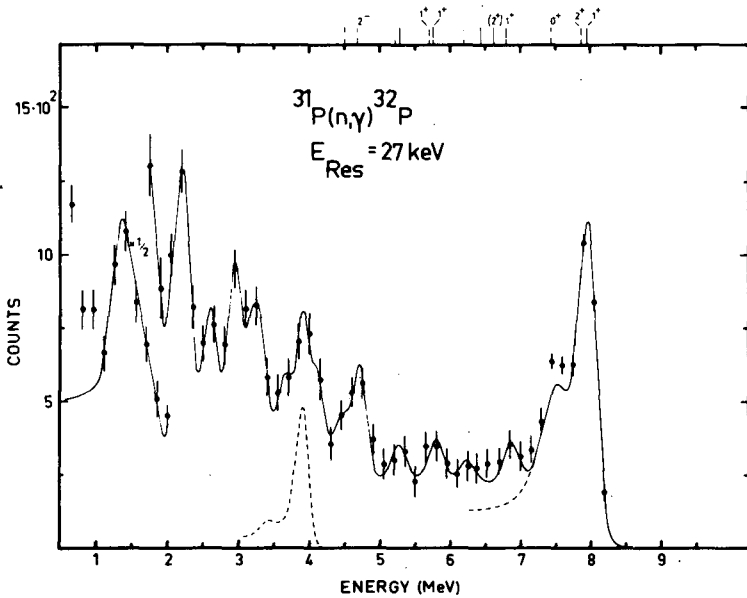


FIG. 6. Gamma spectra from $\text{P}(n,\gamma)$, $E_T = 27 \text{ keV}$. The solid curve was calculated using the known detector response matrix. Some response line shapes are indicated as dashed curves.

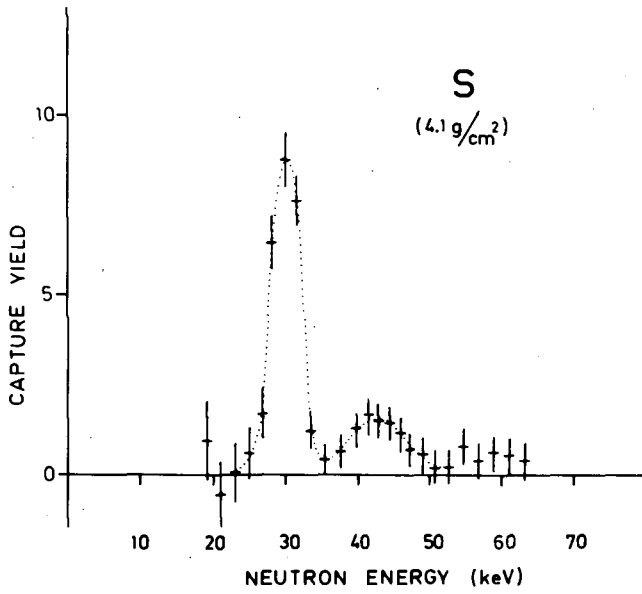
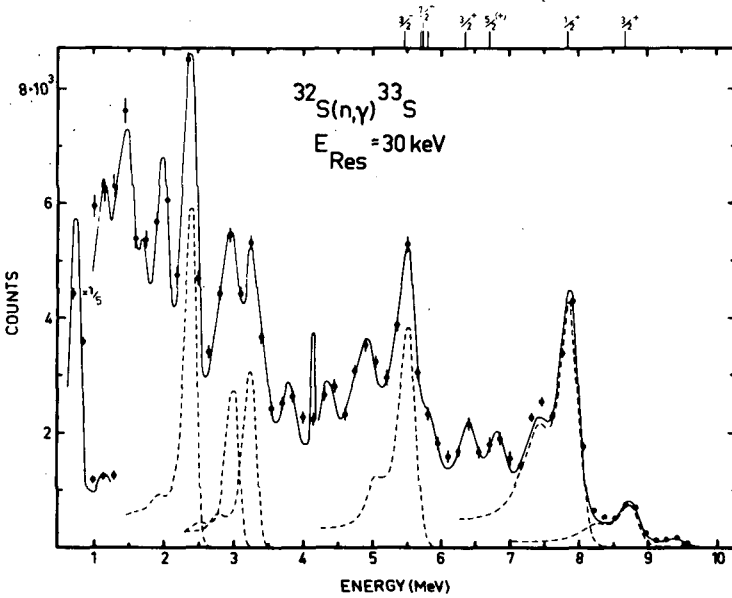


FIG. 7. Gamma yield from neutron capture in S.

FIG. 8. Gamma spectra from $S(n, \gamma)$, $E_n = 30$ keV. The solid curve was calculated using the known detector response matrix. Some response line shapes are indicated as dashed curves.

^{24}Mg , $E_r = 47 \text{ keV}$

In addition to the well-established resonance at 84 keV a relatively weak resonance around 50 keV had previously been observed [5]. The capture cross-section for this resonance is shown in Fig. 1. The gamma-ray spectrum from this resonance (Fig. 2) is dominated by the transitions to the ground state ($5/2^+$) and to the first excited state at 0.58 MeV ($1/2^+$), in agreement with previous experiments [5]. The intensities of other gamma-rays are low; some intensity can be assigned to the primary transition to the $3/2^-$ level at 3.41 MeV ($E_\gamma = 3.97 \text{ MeV}$).

The spin and parity of the resonance is not known. From (d, p) stripping angular distributions Middleton and Hinds [6] suggest $l_n = 2$ which would imply $3/2^+$ or $5/2^+$. Assuming dipole transitions the observed gamma-ray spectrum gives $J = 3/2$.

 ^{28}Si , $E_r = 68 \text{ keV}$

A narrow neutron resonance at 55 keV had previously been observed in a transmission experiment by Newson et al. [7]. It was interpreted as a weak *s*-wave resonance from area analysis. The present results (Fig. 3) show resonance structure at $E_n = 68 \text{ keV}$. The experimental points below 50 keV indicate the presence of several resonances in the range 20-40 keV. The gamma-rays to the ground state ($1/2^+$) and to the first excited level ($3/2^+$) have about the same intensity and these two transitions dominate the spectrum (Fig. 4). The gamma-ray line at 3.6 MeV is identified as a primary transition to the $3/2^-$ level at 4.9 MeV which is strongly fed in thermal neutron capture. The level is known to decay predominantly to the ground state and the line at 4.9 MeV has roughly the same intensity as the line at 3.6 MeV. Based on the assumption that the capture state has $J^\pi = 1/2^+$, the transition to the ground state and the first excited state are M1 and transition to the 4.9-MeV level ($3/2^-$) is E1. The strength (I_γ/E_γ^3) of the E1 transition is found to be 3-4 times larger than that of M1.

 ^{31}P , $E_r = 27 \text{ keV}$

The cross-section curve, Fig. 5, shows a resonance at 27 keV which has not previously been reported. The prominent gamma-ray line near 8.0 in the gamma-ray spectrum (Fig. 6) MeV represents transitions to the ground state (1^+) and to the 78-keV level (2^+). Unresolved structure is observed between 5 and 7 MeV, implying the presence of several weak lines. The peak at 4.7 MeV might be assigned to the decay of the 2^- level at 4.66 MeV fed by 3.3-MeV gamma-rays from the capturing state. Further analysis, in particular of the low-energy part of the spectrum, is necessary to be able to construct a detailed decay scheme.

 ^{32}S , $E_r = 30 \text{ keV}$

Previous experiments [5, 8] suggest $J^\pi = 3/2^-$ for the resonance at 30 keV. Using a thick sample a second, previously unreported, resonance at 42 keV is observed (Fig. 7). By studying the gamma-ray spectra at

different time channels (corresponding to different neutron energies) it appears that the 5.5, 3.2 and 2.4-MeV peaks (Fig. 8) resonate with the 42-keV resonance and the 7.9-MeV peak with the 30-keV resonance. The 5.5-MeV line is assigned to the transition from the capturing state to the $3/2^-$ level at 3.22 MeV and the 3.2 and 2.4-MeV lines are from the decay of this level. The gamma-ray transitions from the 30-keV resonance to the ground state ($3/2^+$) and the first excited level ($1/2^+$) at 0.84 MeV are E1, provided the $3/2^-$ assignment of the resonance is correct. We would suggest that the gamma-ray transition from the 42-keV resonance to the $3/2^-$ level at 3.22 MeV also is E1, in which case this resonance has $J^\pi = 1/2^+, 3/2^+$ or $5/2^+$.

REFERENCES

- [1] BARTHOLOMEW, G. A., DOVECKA, A., EASTWOOD, K. M., MONARO, S., GROSHEV, L. V., DEMIDOV, A. M., PELEKHOV, V. I., SOKOLOVSKII, L. L., Nuclear Data 3 A (1967).
- [2] BIRD, J. R., BIGGERSTAFF, J. A., GIBBONS, J. H., GOOD, W. M., Phys. Rev. 138 (1965) B20.
- [3] BIRD, J. R., GIBBONS, J. H., GOOD, W. M., Physics Lett. 1 (1962) 262.
- [4] BERGQVIST, I., BIGGERSTAFF, J. A., GIBBONS, J. H., GOOD, W. M., Physics Lett. 18 (1965) 323.
- [5] BERGQVIST, I., BIGGERSTAFF, J. A., GIBBONS, J. H., GOOD, W. M., Phys. Rev. 158 (1967) 1049.
- [6] MIDDLETON, R., HINDS, S., Nucl. Phys. 34 (1962) 404.
- [7] NEWSON, H. W., BLOCK, R. C., NICHOLS, P. F., TAYLOR, A., FURR, A. K., MERZBACHER, E., Annls Phys. 8 (1959) 211.
- [8] MACKLIN, R. L., PASMA, P. J., GIBBONS, J. H., Phys. Rev. 136 (1964) B695.

RADIATIVE TRANSITIONS FROM NEUTRON RESONANCES OF ^{105}Pd

C. COCEVA*, F. CORVI*, P. GIACOBBE*,
M. STEFANON*, G. CARRARO**

Central Bureau for Nuclear Measurements,
EURATOM,
Geel, Belgium,
and
CNEN, Centro di Calcolo,
Bologna, Italy

Abstract

RADIATIVE TRANSITIONS FROM NEUTRON RESONANCES OF ^{105}Pd . The intensities of high-energy gamma rays following neutron capture in ^{105}Pd were determined for 15 s-wave resonances selected by time-of-flight. Eighteen transitions to low-lying levels of ^{106}Pd were observed up to an excitation energy of 3.15 MeV. Knowledge of spin and parity of all the initial states and of many final states allowed the identification of E1 and M1 transitions. The values of electric and magnetic dipole transition probabilities are deduced. Useful information is obtained about spin and parity of several final states.

1. INTRODUCTION

^{105}Pd was chosen for the measurement of resonance neutron capture gamma rays because the s-wave neutron resonance spins had already been determined [1] and the low-lying states has been investigated in many studies, in particular by radioactive decay methods [2 - 8], by spectroscopy of gamma rays from capture of thermal neutrons [9 - 14], and from resonance averaged neutrons [15]. The gamma-ray spectra obtained here were in most cases interpreted making use of the results of these previous studies. Thus, the estimates of the average E1 and M1 radiation widths, which is the major achievement of this work, depend on the available information about the energies of the involved states and their spin and parity. This experiment also contributes to the nuclear spectroscopy of ^{106}Pd ; in fact our results restrict the choice of the spins of many levels. In addition, two new levels of ^{106}Pd with excitations above 2.5 MeV were observed.

2. EXPERIMENT

The measurements were performed at the pulsed 90-MeV Linac of CBNM Euratom, Geel (Belgium). The experimental set-up is shown in Fig.1. Neutrons produced by bremsstrahlung radiation in a uranium target and moderated by a 2-cm-thick polyethylene slab strike a 4-mm thick palladium sample placed at about 13 m from the neutron source.

* CNEN, Ispra, Italy.

** CBNM, EURATOM, Geel, Belgium.

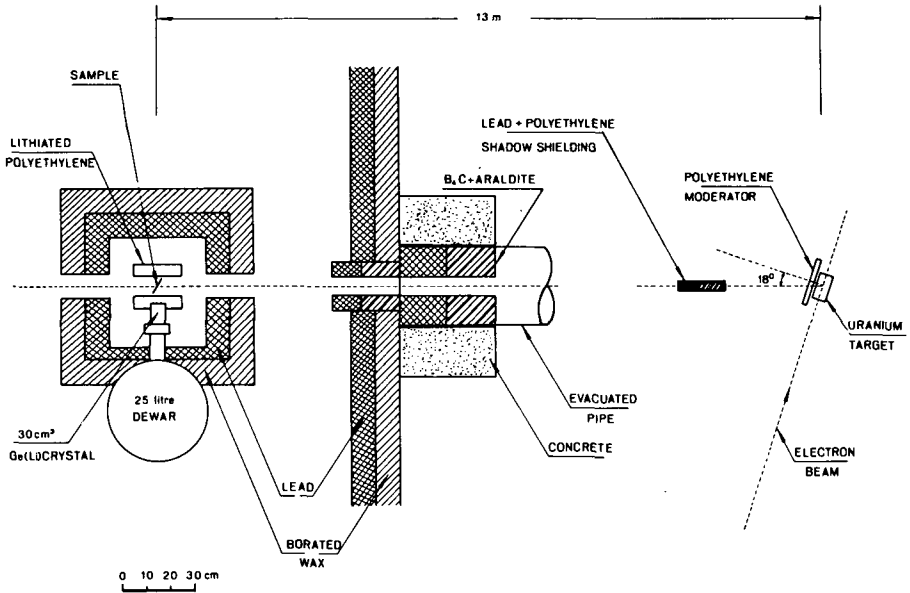


FIG.1. Experimental set-up.

The neutron beam at the sample is 7×10 cm. Capture gamma rays are detected by a 30-cm^3 active volume Ge(Li) crystal. To reduce the gamma flash due to bremsstrahlung in the target and the fast neutron flux viewed by the detector, a lead and polyethylene shadow shielding with 4×4 cm cross-section was placed on the axis of the neutron beam in order to partially shield the uranium target. Moreover, a 2.5 cm slab of lithiated polyethylene and a 1-mm thick lead foil were inserted between sample and detector. In this way the pulse due to the gamma flash in the crystal was equivalent to about 50-MeV gamma-ray energy and the fast neutron dose was reduced by a factor 15, while the reduction of the epithermal neutron flux was only 20%.

The following Linac parameters were used in the measurement:

Electron energy 60 MeV
 Peak current 2.3 A
 Neutron burst FWHM 50 nsec
 Repetition frequency 600 pulses/sec
 Average beam power 4.1 kW.

The spectra were registered in a 4096-channel Laben analyser whose memory was divided into 16 groups of 512 channels with 999 maximum capacity. In this way it was possible to register 16 amplitude spectra of 512 channels, relating to 16 different time-of-flight intervals. Such intervals were chosen to correspond to ^{15}Pd resonances and one background region through the use of a time programmer. The total measuring time was 360 hours.

The energy resolution of the detector was about 15 keV for gamma rays of 6-7 MeV energy; the effective resolution of the measurement was at least 50% larger due to instability of the electronic chain. To limit this effect, data were punched out every 24 hours and the partial spectra were added together with an appropriate shift in order to compensate for gain variation.

Gamma-ray spectra in the energy range from 6.30 to 9.16 MeV were measured for 15 ^{105}Pd resonances of known spin (seven with $J = 2$ and eight with $J = 3$) below 360-eV neutron energy. Double-escape peaks corresponding to 18 gamma-energies were unambiguously identified. It was assumed that gamma lines belonging to different resonances correspond to the same transition when their peaks coincide within \pm one channel (\pm 5.6 keV). Energy calibration of gamma rays was performed in a separate run in which a sample of NaCl was added to Pd and the Cl gamma rays from thermal neutron capture were compared to the main transitions in the 13.21-eV resonance of ^{105}Pd . A precision pulse generator was used to interpolate in between. The error in the given energies is estimated to be \pm 8 keV. The relative intensity of gamma transitions in each resonance was obtained by evaluating the areas of the double escape peaks. These intensities were normalized to the same number of captures by dividing the areas by the total capture yield of the corresponding resonance. Such yields were assumed to be proportional to the total counts, in the same time-of-flight interval, obtained in an independent measurement with a threshold set at 2-MeV gamma energy.

To obtain the transition probability from the measured intensities the following calibration procedure was carried out. Thermal neutron capture gamma rays were measured for samples of NaCl, HgO and Cr in the same geometry as for palladium. Knowing the behaviour of the neutron flux against energy and calculating from the known cross-sections the capture rates of Cl and Hg in the thermal region and of Pd in the resonance at 13.21 eV, it was possible to compare the transition intensities in such a resonance with the known transition intensities in Cl and Hg.

As intensity standards we used 22.1 photons per 100 captures for the 6.115-MeV transition in Cl [10] and 13.4 photons per 100 captures for the 5.95-MeV line in Hg [11]. The agreement between the two calibrations was excellent and their average was taken as a standard. The Cl and Cr data also allowed the relative detector efficiency against energy to be determined: a linear fit of the data gave for the relative efficiency, ϵ_{rel} , normalized to unity at 6 MeV, the expression:

$$\epsilon_{\text{rel}} = 1.88 - 0.148 E_{\gamma} \text{ (MeV)}$$

The efficiency drops about a factor two from 6 to 9 MeV and therefore the correction involved is by no means negligible in our case.

3. DATA REDUCTION AND RESULTS

Absolute intensities, given as the number of photons per 10^4 neutron captures, are listed in Tables I and II, where column entry is the energy E_n of the resonances and row entry the energy E_{γ} of gamma transitions.

TABLE I. GAMMA-RAY INTENSITIES I_{ij} IN REACTION $^{105}\text{Pd} (n, \gamma) ^{106}\text{Pd}$ (photons per 10^4 captures)

678

E_n (eV) E_γ (keV)	J = 2 resonances						
	13.2	77.7	141.2	150.1	202.6	260.1	305.4
9042	< 2	13 ± 2	< 6	37 ± 3	< 7	18 ± 5	5 ± 2
8426	26 ± 2	49 ± 3	< 9	< 6	< 10	8 ± 3	20 ± 5
8325	< 4	< 6	< 10	< 5	< 10	< 7	< 7
7994	17 ± 3	13 ± 2	< 10	35 ± 4	50 ± 9	< 10	14 ± 4
7622	< 4	9 ± 4	20 ± 7	22 ± 6	60 ± 18	17 ± 10	< 12
7477	< 4	15 ± 4	20 ± 6	24 ± 3	< 18	< 13	< 14
7313	< 6	9 ± 5	< 15	10 ± 2	< 20	< 14	< 31
7249	< 6	< 9	< 13	< 9	36 ± 9	< 14	< 15
7160	34 ± 3	< 9	86 ± 15	11 ± 3	< 35	93 ± 9	< 17
7060	76 ± 3	54 ± 4	< 17	13 ± 3	51 ± 10	< 15	133 ± 7
6979	< 6	< 10	18 ± 5	< 10	< 24	< 16	< 18
6810	19 ± 6	< 10	< 17	12 ± 4	43 ± 9	43 ± 8	30 ± 6
6699	< 6	< 11	< 16	< 12	< 25	< 18	< 21
6662	49 ± 3	< 11	< 17	8 ± 3	236 ± 24	48 ± 12	38 ± 6
6594	57 ± 4	32 ± 5	16 ± 7	9 ± 4	< 30	< 18	< 22
6490	78 ± 5	< 14	< 18	< 13	157 ± 17	86 ± 14	98 ± 10
6432	< 8	59 ± 12	35 ± 7	21 ± 4	< 31	16 ± 6	< 25
6395	7 ± 5	15 ± 5	19 ± 6	70 ± 4	< 31	< 20	< 25

COCEVA et al.

TABLE II. GAMMA-RAY INTENSITIES I_{ij} IN REACTION $^{105}\text{Pd}(n, \gamma)^{106}\text{Pd}$ (photons per 10^4 captures)

E_n (eV) E_γ (keV)	J = 3 resonances							
	11.8	25.3	55.2	68.3	86.7	126.3	227.0	354.4
9042	< 7	< 3	9 ± 2	< 6	< 3	< 8	< 11	50 ± 6
8426	14 ± 2	6 ± 3	14 ± 2	12 ± 4	< 5	< 11	< 15	< 11
8325	8 ± 2	14 ± 1	< 4	36 ± 6	< 5	< 11	< 17	< 11
7994	< 9	23 ± 2	12 ± 3	22 ± 7	< 12	17 ± 6	72 ± 14	19 ± 9
7622	72 ± 7	3 ± 2	21 ± 6	< 14	46 ± 8	48 ± 13	56 ± 18	± 15
7477	38 ± 4	< 7	36 ± 3	< 14	33 ± 6	59 ± 11	< 24	18 ± 10
7313	< 23	29 ± 3	< 8	< 14	< 9	< 20	< 26	< 17
7249	29 ± 5	< 6	29 ± 6	42 ± 7	31 ± 5	< 20	< 26	22 ± 8
7160	23 ± 5	< 11	24 ± 8	23 ± 9	< 13	< 20	< 28	< 18
7060	13 ± 4	< 8	13 ± 3	24 ± 6	< 9	< 22	< 29	< 20
6979	24 ± 5	< 8	43 ± 8	< 18	145 ± 5	< 22	< 30	34 ± 10
6810	< 12	9 ± 3	10 ± 3	36 ± 12	< 10	< 24	75 ± 12	< 19
6699	77 ± 7	30 ± 7	< 10	79 ± 11	< 14	< 26	< 36	< 20
6662	25 ± 6	106 ± 12	24 ± 4	35 ± 11	135 ± 13	< 26	< 36	93 ± 13
6594	14 ± 6	50 ± 7	43 ± 7	22 ± 11	23 ± 7	22 ± 11	< 31	< 22
6490	50 ± 11	29 ± 6	59 ± 7	20 ± 8	19 ± 5	< 28	< 37	32 ± 7
6432	< 14	< 10	11 ± 4	21 ± 8	22 ± 5	37 ± 10	< 41	< 23
6395	18 ± 4	< 10	< 14	< 21	< 13	< 30	< 42	< 23

NEUTRON RESONANCES OF ^{105}Pd

The errors quoted include the statistical error and the uncertainty in the evaluation of the base-line of the peaks; no systematic error due to the intensity calibration is included. In general, not all the peaks are observed in all resonances since the intensities often fall below the threshold of observability. The values of such thresholds quoted in Tables I and II are three times the error evaluated at the transition energies.

For each transition the intensities averaged over the initial states were estimated separately for the two groups of resonances with spin 2 and 3. In the evaluation of these averages we took into account the information coming from unobserved peaks by means of the estimated observability thresholds.

It was assumed that the intensities of those transitions which can be assigned to a single final state follow a Porter-Thomas distribution. Where we knew from other sources that the observed peaks were the superposition of two or three unresolved transitions of the same multiplicity, we assumed a χ^2 -distribution with two or three degrees of freedom, respectively. The maximum-likelihood estimate T_i of the intensity of a single transition corresponding to the gamma line labelled with the index i , is found to satisfy the following equation:

$$T_i = \frac{\sum_{M+1}^N I_{ij}}{\sum_{M+1}^N \nu_j + \sum_1^M \nu_j \beta\left(\frac{\eta_j}{T_i}, \nu_j\right)} \quad (1)$$

where N is the total number of resonances; in the first M resonances the intensities fall below the threshold η_j . I_{ij} are the intensities observed in the remaining $N-M$ resonances, ν_j are the multiplicities of the transitions and the function $\beta(x, \nu)$ is

$$\beta(x, \nu) = \frac{2}{\nu} \frac{x^{\nu/2} e^{-x/2}}{\int_0^x dt t^{\nu/2} e^{-t/2}} \quad (2)$$

The function $\beta(\eta/T, \nu)$ decreases from 1 to 0 when the threshold η goes from 0 to ∞ ; it has the meaning of a weight connected with the reduced content of information when one has an upper limit instead of an actual value. Having tabulated $\beta(x, \nu)$, Eq. (1) was easily solved by iteration. The errors are roughly estimated by calculating 67.4% confidence limits with the assumption that the obtained averages follow a χ^2 -distribution with

$$\nu \approx \sum_{M+1}^N \nu_j + \sum_1^M \nu_j \beta\left(\frac{\eta_j}{T_i}, \nu_j\right)$$

degrees of freedom.

Knowledge of the excited states of ^{106}Pd from the literature [2 - 9, 14, 15] allowed us to establish that of the eighteen gamma lines observed one is a triplet, seven are doublets and eight are singlets. Of the two remaining transitions that at $E_\gamma = 6490$ keV was also observed by Rasmussen [14], but we interpreted it as a doublet on the basis of its intensity; the other at $E_\gamma = 6395$ keV corresponds to a level not previously observed.

In our measurement a doublet or a triplet corresponds to the sum of two or three transitions which are less than about 20 keV apart; in fact this was our effective resolution.

From the work of Thomas and Bollinger [15], which gives the most complete picture of the excited states of ^{106}Pd , we see that below 7.51 MeV we begin to miss the weakest M1 transitions and below 6.94 MeV no M1 transition is visible any longer. In fact our limit of observability is a decreasing function of the gamma-ray energy.

In Table III we list the average intensity I_i of each observed gamma line, in units of photons per 10^4 captures, i.e. the I_i are the T_i of Eq. (1) multiplied by the number of transitions adding up in the gamma line. Separate averages for spin 2 and spin 3 resonances are given in columns 2 and 3 respectively. For those gamma lines which are given in have the same number of transitions of the same kind in either initial spin, a common value is given in column 4. This common value is calculated in the same way, but starting from the quantities

$$\frac{2J + 1}{2I + 1} I_{ij}$$

where J is the spin ($I + \frac{1}{2}$ or $I - \frac{1}{2}$) of the resonance corresponding to the index j . The factor $(2J + 1)/(2I + 1)$ was introduced to eliminate the dependence of the intensities on the spacing of the resonances. This spacing is assumed to be inversely proportional to the factor $2J + 1$.

Columns 5 and 6 of Table III show, for each initial spin state, the character of the transitions and their number in the unresolved peaks. Most of this information has been taken from Ref. [15].

In the case of gamma lines with pure E1 or M1 transitions, the average reduced strengths, listed in columns 7 and 8 of Table III, were deduced from the expression

$$S_i = \frac{10^{-4} T_i r_\gamma}{E_\gamma^3 D} = \frac{\Gamma_{\gamma i}}{E_\gamma^3 D}$$

where T_i are the transition intensities obtained by inserting in Eq. (1) the I_{ij} of Tables I and II and the ν_j according to columns 5 and 6 of Table III; $\Gamma_{\gamma i}$ and Γ_γ are the partial and total radiation widths respectively and D the average spacing of the resonances of the appropriate spin.

$\Gamma_\gamma = 0.155$ eV, $D = 28.2$ eV were taken for spin 2 resonances and $D = 20.2$ eV for spin 3 resonances, in agreement with the $(2J + 1)$ dependence of the level densities. When a gamma line is a doublet or a triplet, this procedure yields the reduced strength averaged over the multiplet.

TABLE III. AVERAGE INTENSITIES AND STRENGTHS OF E1 AND M1 TRANSITIONS IN ^{105}Pd (n, γ)

E_γ (keV)	Average intensities I_j (photons per 10^4 captures)			Number and character of dipole transitions		$\overline{F}(D \times E_\gamma^2)$ (10^{-8} MeV $^{-2}$)		Final states	
	J = 2	J = 3	both spins	from J = 2	from J = 3	E1	M1	E_{exc} (keV)	J
9042	11.1 7 ²³	8.8 6 ¹⁸	9.9 7 ¹⁶	1 × M1	1 × M1		8.8 6 ¹⁴	512	2 ⁺
8426	15.8 10 ³⁵	7.2 4 ¹⁶	10.7 7 ¹⁷	1 × M1	1 × M1		11.7 8 ¹⁹	1128	2 ⁺
8325	4.4	8.9 6 ¹⁸		-	1 × M1		11.9 8 ²⁴	1229	4 ⁺
7994	19.3 13 ³⁹	21.8 16 ³⁴		1 × M1	2 × M1		17.8 14 ²⁵	1557 1562	(3 ⁺) ₄ ⁺ 2 ⁺
7622	19.4 14 ³²	32.4 23 ⁵²	27.7 22 ³⁸	2 × M1	2 × M1		20.6 16 ²⁸	1910 ^a 1932	(2,3) ⁺ 3 ⁺
7477	10.3 6 ²³	24.8 17 ⁴⁸		1 × E1	E1 + M1	22.5 16 ³⁶		2077 2084	4 ⁺ 3 ⁻
7313	5.2 3 ¹⁵	7.0 4 ²⁰	6.4 4 ¹²	1 × M1	1 × M1		10.8 14 ²¹	2241	(2,3) ⁺
7249	7.9 5 ¹⁹	21.0 14 ⁴³		1 × M1	1 × E1	42.4 28 ⁸⁷	11.4 7 ²⁸	2305 2309	4 ⁻ (1,2) ⁺
7160	34.7 22 ⁷⁷	11.6 7 ²⁶	20.9 15 ³⁴	1 × E1	1 × E1	37.5 27 ⁶¹		2394	(2,3) ⁻
7060	49.0 35 ⁸⁰	9.1 6 ²⁰		2 × E1	1 × E1	32.4 25 ⁴⁷		2485 ^a 2500 ^a	1 ⁻ (2,3) ⁻
6979	4.8 3 ¹³	33.6 22 ⁶⁹		1 × M1	E1 + M1	61.1 40 ¹²⁵		2579 ^a 2590 ^a	4 ⁻ (1,2,3) ⁺
6810	22.2 14 ⁴⁵	18.6 12 ³⁸	20.2 14 ³²	1 × E1	1 × E1	42.2 31 ⁶⁷		2744	(2,3) ⁻
6699	9.0	27.2 18 ⁵⁶		-	E1 + M1	54.6 36 ¹¹¹		2848 ^a 2861 ^a	(1,2,3,4) ⁺ 4 ⁻
6662	56.2 40 ⁹¹	56.4 43 ⁸⁰		2 × E1	3 × E1	50.1 40 ⁶⁵		2886 ^a 2899 ^a 2908 ^a	
6594	19.1 12 ⁴²	23.7 15 ⁴⁹	22.2 16 ³⁶	1 × E1	1 × E1	51.1 37 ⁸³		2961	(2,3) ⁻
6490	63.2 45 ¹⁰²	29.4 21 ⁴⁷	43.0 34 ⁵⁹	2 × E1	2 × E1	51.8 41 ⁷¹		3060 3070	(2,3) ⁻ (2,3) ⁻
6432	18.9 12 ⁴²	14.1 9 ³¹	17.1 12 ²⁸	1 × E1	1 × E1	42.3 30 ⁶⁹		3122	(2,3) ⁻
6395	18.9 12 ⁴²	5.6 3 ²⁰		1 × E1		39.7 26 ⁸⁷		3159	(1,2,3) ⁻

^a Values from Ref. [15]

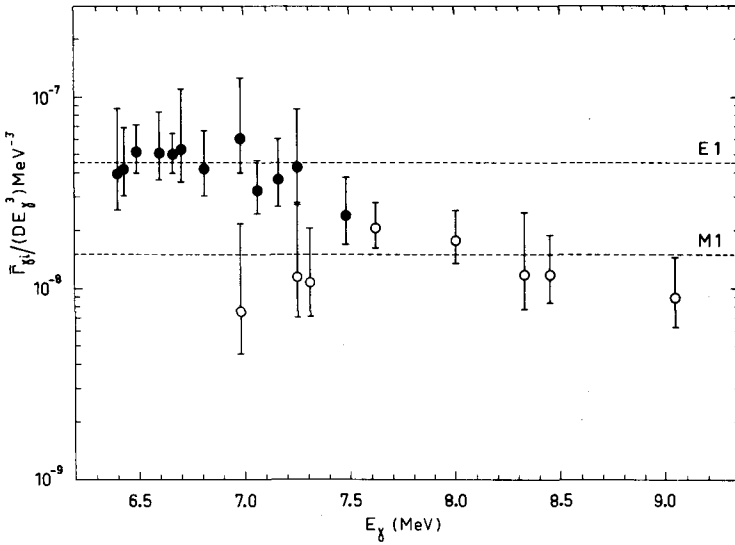


FIG.2. Reduced strengths of the observed transitions.

The average reduced strengths \$S_i\$ in units of \$10^{-9} \text{ MeV}^{-3}\$ are plotted against energy in Fig.2. Full circles refer to E1 and open circles to M1 transitions. The error bars correspond to the 67.4% probability of encompassing the true values. The data plotted in Fig.2 are consistent with the statistical assumption that the average reduced M1 and E1 strengths do not depend on the final states.

Averaging over all the pure E1 and M1 transitions, we obtained the average reduced strengths:

$$S(E1) = \left\langle \frac{\Gamma_{\gamma i}}{E_{\gamma}^3 D} \right\rangle_{E1} = 44.8 \begin{matrix} 50.4 \\ 40.1 \end{matrix} \times 10^{-9} \text{ MeV}^{-3}$$

$$S(M1) = \left\langle \frac{\Gamma_{\gamma i}}{E_{\gamma}^3 D} \right\rangle_{M1} = 14.9 \begin{matrix} 17.2 \\ 13.0 \end{matrix} \times 10^{-9} \text{ MeV}^{-3}$$

Such values are shown by dotted lines in Fig.2. The ratio between the two strengths is \$3.0 \pm 0.6\$, in agreement with the value 3.5 found by Bollinger [16] with the average resonance capture method.

The errors quoted above and in Table III refer only to the statistics of the limited samples used in the averages. However, a reliable estimate of the absolute strengths should take into account also the systematic errors inherent in the intensity calibration.

We estimate that the overall error associated with the intensity calibration should not exceed 20%.

It is interesting to compare our direct measurements of E1 and M1 transition strengths with those previously given in the literature. For

this purpose we introduce our experimental estimates of Bartholomew's [12] reduced widths, which assume the classical single-particle treatment [17]

$$k_{E1} = \frac{1}{A^{2/3}} \left\langle \frac{\Gamma_{\gamma i}}{E_{\gamma}^3 D} \right\rangle_{E1} = (2.0 \pm 0.6) \times 10^{-9} \text{ MeV}^{-3}$$

$$k_{M1} = \left\langle \frac{\Gamma_{\gamma i}}{E_{\gamma}^3 D} \right\rangle_{M1} = (15 \pm 5) \times 10^{-9} \text{ MeV}^{-3}$$

The quoted errors include both statistical and systematic uncertainties.

The average value given by Bartholomew [12] from a review of the intensities of gamma rays emitted in both resonance and thermal neutron capture is: $k_{E1} \approx 3 \times 10^{-9}$; the value deduced by Carpenter [13] from resonance neutron capture measurements in 12 nuclides, is $k_{E1} = 4.0 \times 10^{-9}$.

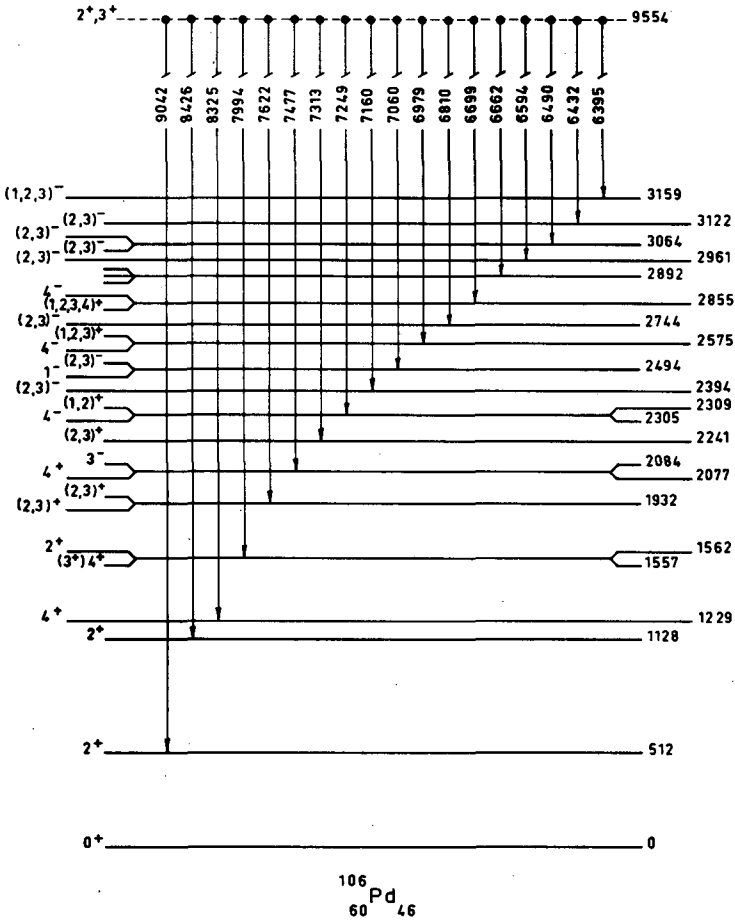


FIG. 3. ^{106}Pd level scheme deduced from this study.

When interpreted in terms of the electric dipole giant-resonance model [18], our data give

$$\frac{1}{A^{8/3}} \left\langle \frac{\Gamma_{\gamma i}}{E_{\gamma}^5 D_{E1}} \right\rangle = (4.0 \pm 1.2) \times 10^{-15} \text{MeV}^{-5}$$

This value is to be compared with the value of 3.2×10^{-15} obtained by Carpenter. Clearly the agreement between the two sets of data is much more satisfactory in the framework of this model than when using the single-particle model. Therefore the results of our work are in favour of the giant-dipole resonance assumption.

Our value of K_{M1} is in good agreement with the values of $k_{M1} = 17 \times 10^{-9}$ and $k_{M1} = 18 \times 10^{-9}$ deduced by Bollinger [16] from Groshev's thermal capture and from average resonance experiments.

In the last but one column of Table III we quote the energies of the excited states populated by the corresponding primary transitions. With the exception of the two levels at 1910 and 2241 keV, the values E_{exc} quoted up to 2309 keV excitation energy are taken from radioactive decay studies [2 - 8]. Such values, together with the energies of the corresponding gamma lines, can be used to determine the neutron separation energy: a fit to the data gives a value of 9554 ± 8 keV. The values not taken from Ref. [15] were obtained from the expression $E_{\text{exc}} = 9554 - E_{\gamma}$.

The nature of our data allow in most cases a choice of three spin assignments: $J = 2$, $J = (2, 3)$, $J = 4$. This selection was applied to the previous spin information contained in Refs [2 - 8, 15] and the results are listed in the last column of Table III. These results are entirely consistent with the previous spin assignments.

In Fig.3 we give the scheme of the excited states and the associated primary gamma lines involved in the present measurement.

REFERENCES

- [1] COCEVA, C., CORVI, F., GIACOBBE, P., CARRARO, G., Nucl. Phys. A117 (1968) 586;
BOLLINGER, L.M., COTÉ, R.E., JACKSON, H.E., Congrès International de Physique Nucléaire, Paris, 1964, 2, Centre National de la Recherche Scientifique (1964) 673.
- [2] SMITH, W.G., Phys. Rev. 131 (1963) 351.
- [3] de AISENBERG, E.Y., SUAREZ, J.F., Nucl. Phys. 83 (1966) 289.
- [4] RAO, P.V., FINK, R.W., Nucl. Phys. A103 (1967) 385.
- [5] VRZAL, Ya. et al., Izv. Akad. Nauk SSSR, Ser. fiz. 31 (1967) 1656.
- [6] TAYLOR, H.W., NEFF, N., KING, J.D., Nucl. Phys. A106 (1968) 49.
- [7] MORAGUES, J.A., REYES-SUTER, P., SUTER, T., PÉREZ, M., Nucl. Phys. A106 (1968) 289.
- [8] HATTULA, J., LIUKKONEN, L., Ann. Acad. Sci. Fenn. Ser. A, VI (1968) 274.
- [9] GROSHEV, L.V., DEMIDOV, A.M., SHADIEV, N., Izv. Akad. Nauk SSSR, Ser. fiz. 29 (1965) 760.
- [10] BARTHOLOMEW, G.A. et al., Nucl. Data A3 (1967) 434.
- [11] GROSHEV, L.V. et al., Bull. Acad. Sci. USSR Phys. Ser. 27 (1964) 1353.
- [12] BARTHOLOMEW, G.A., Ann. Rev. nucl. Sci. 11 (1961) 259.
- [13] CARPENTER, R.T., Rep. ANL-6589 (1962).
- [14] RASMUSSEN, N.C., ORPHAN, V.J., HUKAI, Y., INOUE, T., private communication in:
BARTHOLOMEW, G.A. et al., Nucl. Data A3 (1967) 625.
- [15] THOMAS, G.E., BOLLINGER, L.M., Bull. Am. phys. Soc. II 14 (1969) 515.

- [16] BOLLINGER, L.M., Nuclear Structure (Proc. Symp. Dubna, 1968) IAEA, Vienna (1968) 317; private communication.
- [17] BLATT, J.M., WEISSKOPF, V.F., Theoretical Nuclear Physics, J. Wiley and Sons, New York (1952).
- [18] AXEL, P., Phys. Rev. 126 (1962) 671.

MEASUREMENTS OF PROMPT GAMMA RAYS FROM NEUTRON INTERACTION IN ^{235}U RESONANCES

H. WEIGMANN, J. WINTER
Central Bureau for Nuclear Measurements,
EURATOM,
Geel, Belgium

Abstract

MEASUREMENTS OF PROMPT GAMMA RAYS FROM NEUTRON INTERACTION IN ^{235}U RESONANCES. A two-parameter system for measurements of capture gamma-ray spectra from individual neutron resonances has been set up at the CBNM linear accelerator. As an example, measurements of prompt gamma-ray spectra from neutron interaction (capture as well as fission) in ^{235}U resonances are discussed. A resonance spin classification is attempted on the basis of the capture data.

1. EXPERIMENTAL LAY-OUT

A two-parameter system for measurements of gamma-ray spectra from neutron capture in individual resonances has been installed at the CBNM linear accelerator. The details of the electronic system have been described elsewhere [1] and will only be summarized here.

The bursts of neutrons delivered by the linear accelerator bombard a sample which is placed 8.5 m from the accelerator target. The resulting gamma spectra are measured by means of a Ge(Li) detector. The signals of the detector are analysed for their times of occurrence and amplitude, thus yielding simultaneous information on neutron energy and gamma spectra. Time-of-flight analysis is performed by means of a time coder with 256 channels, while amplitudes are analysed by an analog-to-digital converter with 4096 channels. Special care has been taken to obtain rapid recovery of the system after the very strong gamma flash of the linear accelerator. The information obtained from the time and amplitude coders is stored, event by event, on magnetic tape. To obtain the gamma-ray spectrum of a definite neutron resonance the amplitude information is played back from the tape into a 4096-channel memory with an appropriate condition imposed on the time-of-flight with the aid of a digital window comparator.

Up to now measurements have been performed on gamma-ray spectra from neutron interaction in individual resonances of ^{98}Mo and ^{235}U .

2. RESULTS ON ^{235}U

The spectra observed show very little structure, especially at high (> 1.5 MeV) gamma-ray energies. In particular, when searching for a possible direct transition from the capturing state to the 2^+ -member (at 45.3-keV excitation energy) of the ground-state rotational band in ^{235}U (this transition would be E1 for 3^- resonances), a slight evidence of its existence was found only for the 7.1-eV resonance.

TABLE I. RELATIVE INTENSITIES OF GAMMA RAYS PER NEUTRON CAPTURE EVENT IN THE 6.4-eV RESONANCE OF ^{235}U

E_γ (keV)	$I_\gamma (10^{-2})$	E_γ (keV)	$I_\gamma (10^{-2})$
401	1.2 ± 0.3	909	1.15 ± 0.4
423	1.1 ± 0.3	941	1.1 ± 0.4
642	6.5 ± 1.0	955	1.75 ± 0.45
687	1.8 ± 0.4		

TABLE II. RELATIVE INTENSITIES OF FISSION GAMMA RAYS PER FISSION EVENT IN THE 8.8-eV RESONANCE OF ^{235}U

E_γ (keV)	$I_\gamma (10^{-2})$	E_γ (keV)	$I_\gamma (10^{-2})$
297	1.1 ± 0.35	706	3.4 ± 0.65
330	1.25 ± 0.25	769	1.15 ± 0.3
353*	1.75 ± 0.35	814	1.05 ± 0.25
457	0.6 ± 0.2	835	2.4 ± 0.45
483	2.25 ± 0.45	951	1.05 ± 0.25
495	1.15 ± 0.25	974	1.25 ± 0.3
571*	0.95 ± 0.25	1178	0.9 ± 0.35
586*	1.55 ± 0.35	1217	1.75 ± 0.4
615	1.75 ± 0.35	1278	1.9 ± 0.4
693	5.5 ± 1.0		

* See text.

However, at lower gamma-ray energies, i. e. between 250 keV and 1.5 MeV (below 250 keV no measurements were possible due to the strong natural activity of the sample), a number of individual gamma-ray lines are observed, the spectra depending mainly on the capture-to-fission ratio, α , of the resonance in question. By suitable handling of the spectra obtained from resonances which differ strongly in α (i. e. by subtracting one from another after application of an appropriate normalization factor), it is possible to obtain gamma-ray spectra which represent 'capture only' and 'fission only', i. e. to decide whether a certain gamma-ray line occurs in the capture cascade or is associated with fission.

Energies and intensities of several 'capture' and 'fission' gamma rays are shown in Tables I and II, respectively. More precisely, the numbers listed represent the percentage with which the gamma ray in question occurs per capture event in the 6.4-eV resonance and per fission event in the 8.8-eV resonance. The uncertainties given in the tables include the common error on absolute values of detector efficiency, solid angle, neutron flux, etc. Some of the gamma-ray energies listed in Table II (marked *) coincide with energies of prompt gamma rays from spontaneous fission of ^{252}Cf reported by Bowman et al. [2].

In the 'capture' gamma-ray spectrum the strongest lines are those with 642 and 687-keV energy. They correspond to the deexcitation of the 2⁻ level at 687 keV in ²³⁶U to the first excited state (2⁺, 45-keV excitation energy) and to the ground state. In Fig.1 is plotted the relative intensity per capture event, R, of the 642-keV gamma ray as a function of resonance energy. R has been determined as the ratio of the area under the 642-keV line to the integral

$$A = \int_{E_0}^{\infty} n(E) dE$$

over the observed gamma-ray spectrum n(E) above a threshold E₀, where A still has to be corrected for the fission gamma-ray contribution which is known from the above-mentioned determination of 'capture only' and 'fission only' spectra (in fact, three different threshold energies E₀ have been used which gave the same results).

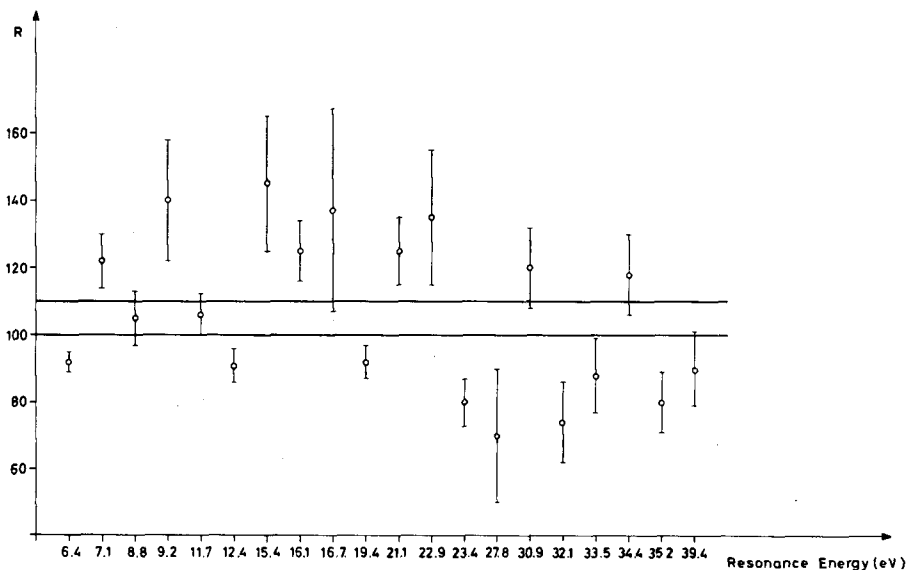


FIG. 1. Relative intensity of 642-keV gamma ray as a function of resonance energy.

From Fig.1 it is seen that, with the exception of the resonances at 8.8 and 11.65-eV neutron energy, the values of R fall into two groups. One may suspect that it is the spin of the capturing resonance which causes this grouping. In fact calculations on the basis of the gamma-ray cascade model of Pönitz [3] have shown that the relative population of the 2⁻ (687-keV) level should be about 40% larger for 3⁻ resonances than for 4⁻ ones, although one has to be careful with this result for two reasons: (1) the gamma-ray cascade model is a rather crude approximation in that it is not capable of treating, e.g. k-selection rules; (2) the properties

of the 2^- (687-keV) level in ^{236}U are not fully understood, especially as regards its very slow E1 decay to the 2^+ (45-keV) state [4]. This could suggest that it might be fed in also from 3^- and eventually 4^- rotational states [5].

If, despite these uncertainties, the grouping of the quantity R of Fig. 1 is attributed to the resonance spin, the spin values quoted in Table III together with values obtained by Asghar et al. [6], Weinstein et al. [7], Cowan et al. [8] and Melkonian and Mehta [9] may be inferred. In general, the agreement is satisfactory.

TABLE III. COMPARISON OF ($^{235}\text{U}+n$) RESONANCE SPINS AS OBTAINED BY SEVERAL AUTHORS

Res. energy (eV)	Present data	[6]	[7]	[8]	[9]
6.39	4	4	4		
7.08	3	3	3		
8.79		3	3	(A)	L
9.29	3	3			
10.20		3			
11.65		4	4		
12.39	4	4	4		
15.40	3	3	(4)	A	H
16.08	3	(4)	4	A	H
16.69	3	3	4	A	
18.07		3	4	(A)	
19.31	4	4	4	A	H
21.08	3		3	A	H
22.94	3	3	3	A	
23.42	4		(4)	A	H
27.82	4	3		(A)	H
30.86	3				
32.07	4	(4)		(A)	H
33.53	4	4		(A)	L
34.39	3	4		(S)	L
35.20	4	4		S	L
39.41	4	4		S	L

S = increased symmetric fission; A = decreased symmetric fission;

L = lower average kinetic energy of fragments; H = higher average kinetic energy of fragments.

REFERENCES

- [1] WINTER, J., Proc. Int. Symp. Nuclear Electronics, Versailles, 1968.
- [2] BOWMAN, H.R., THOMPSON, S.G., WATSON, R.L., KAPOOR, S.S., RASMUSSEN, J.O., Physics and Chemistry of Fission (Proc. Symp. Salzburg, 1965) 2, IAEA, Vienna (1965) 125.
- [3] PÖNITZ, W.P., Z. Phys. 197 (1966) 262.
- [4] LEDERER, C.M., Rep. UCRL 11028.
- [5] BJORNHOLM, S., private communication.
- [6] ASGHAR, M., MICHAUDON, A., PAYA, D., Physics Lett. 26B (1968) 664.
- [7] WEINSTEIN, S., REED, R., BLOCK, R.C., Second Symposium on the Physics and Chemistry of Fission (Proc. Symp. Vienna, 1969), IAEA, Vienna (in press).
- [8] COWAN, G.A., BAYHURST, B.P., PRESTWOOD, R.J., Phys. Rev. 130 (1963) 238.
- [9] MELKONIAN, E., MEHTA, G.K., Physics and Chemistry of Fission (Proc. Symp. Salzburg, 1965) 2, IAEA, Vienna (1965) 355.

OFFICERS OF THE SYMPOSIUM

Chairman of the Symposium
President of the Symposium

N. RYDE
H. MAIER-LEIBNITZ

CHAIRMEN OF SESSIONS

Introductory session	H. MAIER-LEIBNITZ	Federal Republic of Germany
Experimental techniques I and II	G. A. BARTHOLOMEW	Canada
Conversion electron studies of (n, γ) reactions	O. W. B. SCHULT	Federal Republic of Germany
Experimental techniques III	J. VERVIER	France
Thermal neutron capture I	L. V. GROSHEV	USSR
Thermal neutron capture II	H. H. BOLOTIN	United States of America
Collective description of nuclear states	S. E. ARNELL	Sweden
Thermal neutron capture III	B. ELBEK	Denmark
Thermal neutron capture IV	R. E. CHRIEN	United States of America
Scattering of gamma rays from (n, γ) reactions	R. E. CHRIEN	United States of America
Theory of capture	R. MORINAGA	Japan
Fast neutron capture I	R. MORINAGA	Japan
Fast neutron capture II	W. MICHAELIS	Federal Republic of Germany
Neutron resonance capture I	W. MICHAELIS	Federal Republic of Germany
Neutron resonance capture II	J. URBANEC	Czechoslovakia

SECRETARIAT

Scientific Secretary:	L. JONSSON	Department of Physics, Chalmers University of Technology
Assistant Scientific Secretary:	Ö. SKEPPSTEDT	Department of Physics, Chalmers University of Technology
IAEA Scientific Representative:	G.A. GRAVES	Division of Research and Laboratories, IAEA
Administrative Secretary:	Mrs. A. WALL	Department of Physics, Chalmers University of Technology
Editor:	C.N. WELSH	Division of Publications, IAEA

LIST OF PARTICIPANTS

NAME	ADDRESS
Abrahams, K.	Reactor Centrum Nederland, Petten (N. H.), The Netherlands
Ahmed, N.M.	Institut für angewandte Kernphysik, Gesellschaft für Kernforschung mbH, Postfach 3640, 75 Karlsruhe, Federal Republic of Germany
Albinsson, H.	AB Atomenergi, Studsвик, S-611 01 Nyköping 1, Sweden
Arnell, S.E.	Department of Physics, Chalmers University of Technology, Fack, S-402 20 Göteborg 5, Sweden
Asghar, M.	F11D, Residence Compostelle, Route de Bayonne, 33 - Pessac, France
Baader, H. A.	Atomic Energy Commission, Risø Research Establishment, Roskilde, Denmark
Bäcklin, A.	The Swedish Research Council's Laboratory, Studsвик, S-611 01 Nyköping 1, Sweden
Barthel, F.	Institut für Kernphysik, Universität Frankfurt, August-Euler-Str. 6, 6 Frankfurt, Federal Republic of Germany
Bartholomew, G.A.	Neutron Physics Branch, Atomic Energy of Canada Ltd., Chalk River, Ontario, Canada
Bečvář, F.	Joint Institute for Nuclear Research, Head Post Office, P. O. Box 79, Moscow, USSR

NAME	ADDRESS
Ben-David, G.	Nuclear Physics Department, Soreq Nuclear Research Center, Yavne, Israel
Bergqvist, I.	Institutionen för Kärnfysik, Tekniska Högskolan i Lund, S-220 07 Lund, Sweden
Bergström, I.	Forskningsinstitut för atomfysik, Roslagsvägen 100, 104 50 Stockholm 50, Sweden
Blichert-Toft, P.	AB Atomenergi, Studsvik, S-611 01 Nyköping 1, Sweden
Böhm, E.	Institut für Kernphysik, Universität Frankfurt, August-Euler-Str. 6, 6 Frankfurt, Federal Republic of Germany
Bohr, A.	Niels Bohr Institutet, Blegdamsvej 17, Copenhagen, Denmark
Bolotin, H. H.	Physics Department, Argonne National Laboratory, Argonne, Illinois 60439, United States of America
Broman, L.	Department of Physics, Chalmers University of Technology, Fack, S-402 20 Göteborg 5, Sweden
Chrien, R. E.	Brookhaven National Laboratory, Upton, Long Island, New York 11973, United States of America
Coceva, C.	Gruppo CNEN - c/o BCMN EURATOM, Steenweg naar Retie, Geel, Belgium
Condé, H.	Försvarets Forskningsanstalt, Avd. 4, 104 50 Stockholm 80, Sweden

NAME	ADDRESS
Delang, W.	Institut für Festkörper u. Neutronenphysik, 517 Jülich 1, Postfach 365, Federal Republic of Germany
Earle, E. D.	Chalk River National Laboratory, Chalk River, Ontario, Canada
von Egidy, T.	Physik-Department der Technischen Hochschule, Arcisstrasse 21, 8 Munich 2, Federal Republic of Germany
Elbek, B.	Tandem Accelerator Laboratoriet Risø, Roskilde, Denmark
Falkström-Lund, Eva	AB Atomenergi, Studsвик, S-611 01 Nyköping 1, Sweden
Fanger, U.	Institut für angewandte Kernphysik, Gesellschaft für Kernforschung mbH, Postfach 3640, 75 Karlsruhe, Federal Republic of Germany
Fettweis, P.	GEN-SCK, Boeretang 200, Mol, Belgium
Fogelberg, B.	AB Atomenergi, Studsвик, S-611 01 Nyköping 1, Sweden
Forsblom, I.	Helsingfors University, Acceleratorlaboratoriet, Brobergsterrassen 20 e, Helsinki 17, Finland
Gersch, H. -U.	Zentral Institut für Kernforschung, Rossendorf bei Dresden, Democratic Republic of Germany
Göttel, P.	Institut für Festkörper u. Neutronenphysik, 517 Jülich 1, Postfach 365, Federal Republic of Germany
Graves, G. A.	International Atomic Energy Agency, Kärntner Ring 11, A-1010 Vienna, Austria

NAME	ADDRESS
Greenwood, R. C.	National Reactor Testing Station, Idaho Nuclear Corp., P.O. Box 1845, Idaho Falls, Idaho 83401, United States of America
Groshev, I. V.	I. V. Kurchatov Institute of Atomic Energy, Moscow, USSR
Hanle, H.	Institut für Kernphysik, Universität Frankfurt, August-Euler-Str. 6, 6 Frankfurt, Federal Republic of Germany
Haouat, G.	CEA, B. P. 511-15, Paris 15 ^e , France
Hardell, R.	AB Atomenergi, Drottning Kristinasväg 47, S-114 28 Stockholm, Sweden
Hasselgren, A.	Department of Physics, Chalmers University of Technology, Fack, S-402 20 Göteborg 5, Sweden
Heck, D.	Institut für angewandte Kernphysik, Gesellschaft für Kernforschung mbH, Postfach 3640, Karlsruhe, Federal Republic of Germany
Hofmeyr, C.	Atomic Energy Board, Private Bag 256, Pretoria, South Africa
Holmberg, P.	University of Helsinki, Department of Physics, Siltavuorenpenger 20 c, Helsinki 17, Finland
Holmqvist, B.	AB Atomenergi, Studsvik, S-611 01 Nyköping 1, Sweden
Holte, G.	AB Atomenergi, Studsvik, S-611 01 Nyköping 1, Sweden

NAME	ADDRESS
Irigaray, J. L.	CEN de Bordeaux-Gradignan, Le Haut-Vigneau, 33 - Gradignan, France
Jafar, J. D.	Physics Division, Nuclear Research Institute, Atomic Energy Commission, Tuwaitha, Baghdad, Iraq
Jonsson, L.	Department of Physics, Chalmers University of Technology, Fack, S-402 20 Göteborg 5, Sweden
Jurney, E. T.	Los Alamos Scientific Laboratory, Los Alamos, N. Mex., United States of America
Kalebin	I. V. Kurchatov Institute of Atomic Energy, Moscow, USSR
Kane, W. R.	Physics Department, Brookhaven National Laboratory, Upton, Long Island, New York 11973, United States of America
Kardon, B.	Hungarian Academy of Sciences, Central Research Institute for Physics, P. O. B. 49, Budapest 114, Hungary
Kenny, M. J.	AAEC Research Establishment, Private Mail Bag, Sutherland, NSW 2232, Australia
Kiss, D.	Hungarian Academy of Sciences, Central Research Institute for Physics, P. O. B. 49, Budapest 114, Hungary
Koch, H. R.	Atomic Energy Commission, Risø Research Establishment, Roskilde Denmark
Konečný, K.	Nuclear Research Institute of the Czechoslovak Academy of Sciences, Řež near Prague, Czechoslovakia

LIST OF PARTICIPANTS

NAME	ADDRESS
Kopecný, J.	Reactor Centrum Nederland, Petten (N. H.), The Netherlands
Krüger, E.	Physikalisch-Technische Bundesanstalt, Bundesallee 100, 33 Brunswick, Federal Republic of Germany
Krüger, H.	Institut für Kernphysik, Universität Frankfurt, August-Euler-Str. 6, 6 Frankfurt, Federal Republic of Germany
Lachkar, J.	CEA, B. P. 511 - 15, Paris 15 ^e , France
Lalovic, B.	Boris Kidrič Institute of Nuclear Sciences, P. O. Box 522, Belgrade, Yugoslavia
Lane, A. M.	Atomic Energy Research Establishment, Harwell, Didcot, Berks., England
Lundberg, B.	Försvarets Forskningsanstalt, Avd. 4, 104 50 Stockholm 80, Sweden
Maier, B.	Institut Max von Laue-Paul Langevin, CEDEX 156, 38 Grenoble - Gare, France
Maier-Leibnitz, H.	Institut Max von Laue-Paul Langevin, CEDEX 156, 38 Grenoble - Gare, France
Malmskog, S.	AB Atomenergi, Studsvik, S-611 01 Nyköping 1, Sweden
Mampe, W.	Physik Department der T. H. M., Teilinstitut E 14, 8046 Garching, Freisinger Landstr., Federal Republic of Germany
Manfrass, P.	Central Institute for Nuclear Research, Rossendorf near Dresden, Democratic Republic of Germany

NAME	ADDRESS
Martinot, M.	3, rue Pierre Curie, 94 Brevannes, France
Mattsson, C.G.	Department of Physics, Chalmers University of Technology, Fack, S-402 20 Göteborg 5, Sweden
Michaelis, W.	Institut für angewandte Kernphysik, Gesellschaft für Kernforschung mbH, Postfach 3640, 75 Karlsruhe, Federal Republic of Germany
Moreh, R.	Nuclear Research Centre-Negev, Beer-Sheva, P. O. B. 9001, Israel
Morinaga, R.	Physics Department, Technische Hochschule München, 8046 Garching bei München, Federal Republic of Germany
Murray, J.	Atomic Energy Research Establishment, Harwell, Didcot, Berks., England
Nilsson, L.	AB Atomenergi, Studsvik, S-611 01 Nyköping 1, Sweden
Nyström, G.	Department of Physics, Sölvegatan 14, S-223 62 Lund, Sweden
Oliva, P.	Laboratorio Fisica Nucleare Applicata, Centro Studi Nucleari della Casaccia, Casella Postale 2400, 00100 Rome A. D., Italy
Op den Kamp, A.M.F.	Jan van Goyenstraat 142, Alkmaar, The Netherlands
Orphan, V.J.	Gulf General Atomic Inc., P.O. Box 608, San Diego, Calif. 92112, United States of America
Ottmar, H.	Institut für angewandte Kernphysik, Gesellschaft für Kernforschung mbH, 75 Karlsruhe, Federal Republic of Germany

NAME	ADDRESS
Pauli, R.	AB Atomenergi, Studsvik, S-611 01 Nyköping 1, Sweden
Paya, D.	CEN de Saclay, B. P. 2, 91 Gif-sur-Yvette, France
Perchereau, J.	CEA, B. P. 511-15, Paris 15 ^e , France
Prosperi, D.	Laboratorio Fisica Nucleare Applicata, Centro Studi Nucleari della Casaccia, Casella Postale 2400, 00100 Rome A. D. , Italy
Rabenstein, D.	Reaktorstation, 8046 Garching bei München, Federal Republic of Germany
Reddingius, E. R.	Reactor Centrum Nederland, Petten (N. H.), The Netherlands
Rumpold, K.	Reaktorzentrum der Österreichischen Studiengesellschaft für Atomenergie, A-2444 Seibersdorf, Austria
Ryde, N.	Department of Physics, Chalmers University of Technology, Fack, S-402 20 Göteborg 5, Sweden
Samama, R.	DRP/SMPNF, CEN de Saclay, B. P. No. 2, 91 Gif-sur-Yvette, France
Saporetti, F.	c/o Centro di Calcolo del CNEN, Via Mazzini, 2, 40138 Bologna, Italy
Schmidt, H.	Institut für angewandte Kernphysik, Gesellschaft für Kernforschung mbH, Postfach 3640, 75 Karlsruhe, Federal Republic of Germany

NAME	ADDRESS
Schult, O. W. B.	Physics Department, Technische Hochschule München, 8046 Garching bei München, Federal Republic of Germany
Selin, Eva	Department of Physics, Chalmers University of Technology, Fack, S-402 20 Göteborg 5, Sweden
Seres, Z.	Hungarian Academy of Sciences, Central Research Institute for Physics, P. O. B. 49, Budapest 114, Hungary
Seyfarth, H.	Institut für Festkörper und Neutronenphysik, 517 Jülich 1, Postfach 365, Federal Republic of Germany
Simić, J.	Boris Kidrič Institute of Nuclear Sciences, Belgrade, Yugoslavia
Simons, L.	Helsingfors Universitet, Acceleratorlaboratoriet, Brobergsterrassen 20 e, Helsinki 17, Finland
Skeppstedt, Ö.	Department of Physics, Chalmers University of Technology, Fack, S-402 20 Göteborg 5, Sweden
Skřivánek, J.	Nuclear Research Institute of the Czechoslovak Academy of Sciences, Řež near Prague, Czechoslovakia
Slavić, I. A.	Boris Kidrič Institute of Nuclear Sciences, Belgrade, Yugoslavia
Smither, R. K.	Argonne National Laboratory, Argonne, Illinois 60439, United States of America
Spits, A. M. J.	Reactor Centrum Nederland, Petten, (N. H.), The Netherlands
Starfelt, N.	Atlas Copco, Fack, S-101 01 Stockholm 1, Sweden

NAME	ADDRESS
Stecher-Rasmussen, F.	Reactor Centrum Nederland, Petten (N. H.), The Netherlands
Stelzer, K.	Institut für Kernphysik, Universität Frankfurt, August-Euler-Str. 6, 6 Frankfurt, Federal Republic of Germany
Sundius, T.	Accelerator Laboratory, Physics Department, University of Helsinki, Helsinki 17, Finland
Takekoshi, E.	Nuclear Physics Laboratory, Japan Atomic Energy Research Institute, Tokai-mura, Naka-gun, Ibaraki-ken, Japan
Tripathi, K.	AB Atomenergi, Studsvik, S-611 01 Nyköping 1, Sweden
Urbanec, J.	Nuclear Research Institute of the Czechoslovak Academy of Sciences, Rež near Prague, Czechoslovakia
Vervier, J.	Centre d'Etude de l'Energie Nucléaire, Mol-Donk, Belgium
Viitasalo, M.	Accelerator Laboratory, University of Helsinki, Siltavuoren pengeri 20e, Helsinki 17, Finland
Vonach, H.	Physik-Department, Technische Hochschule, Arcisstrasse 21, 8 Munich 2, Federal Republic of Germany
Waldschmidt, M.	Hessenstrasse 14, 6231 Schwalbach, Federal Republic of Germany
Wallander, E.	Department of Physics, Chalmers University of Technology, Fack, S-402 20 Göteborg 5, Sweden

LIST OF PARTICIPANTS

705

NAME	ADDRESS
Wallin, Marie	AB Atomenergi, Drottning Kristinasväg 47, S-114 28 Stockholm, Sweden
Weigmann, H.	CBNM-EURATOM, Steenweg op Retie, Geel, Belgium
Weise, K.	Physikalisch-Technische Bundesanstalt, Bundesallee 100, 33 Brunswick, Federal Republic of Germany
Wiedling, T.	AB Atomenergi, Studsvik, S-611 01 Nyköping 1, Sweden

AUTHOR INDEX

(Literature references are not indexed)

- Abdulla, A.A.: 115
Abrahams, K.: 261
Ahmed, N.M.: 289
Ajdačić, V.: 349
Allen, B.J.: 587
Al-Quraishi, N.H.: 115
Alwash, M.S.: 115
Arnell, S.E.: 231
Asghar, M.: 337
Assche, P.H.M.van: 165
Audias, A.: 267, 337
Baader, H.A.: 65, 147, 363
Babinet, R.: 267
Bäcklin, A.: 141, 147, 155, 351,
363
Bartholomew, G.A.: 553, 595
Bečvář, F.: 651
Beitins, M.: 161
Ben-David, G.: 507
Bergqvist, I.: 569, 667
Beyster, J.R.: 117
Bird, J.R.: 587
Blichert-Toft, P.H.: 173, 183
Böhm, E.: 403
Bohr, A.: 3
Bollinger, L.M.: 601
Bolotin, H.H.: 15, 389
Boreving, S.: 183
Breitig, D.: 65, 147, 363
Brown, T.: 105
Buss, D.J.: 55
Campbell, E.C.: 421
Carlson, A.D.: 117
Carraro, G.: 675
Cesareo, R.: 491
Chrien, R.E.: 627
Coceva, C.: 675
Corvi, F.: 675
Danelyan, L.S.: 663
der Mateosian, E.: 105
Earle, E.D.: 595
Efimov, B.V.: 663
Egidy, T. von: 127, 355, 541
Eichholz, J.J.: 113
Elbek, B.: 443
Emery, G.T.: 105
Falkström-Lund, Eva: 141, 351
Fanger, U.: 273, 289, 469
Fettweis, P.: 259
Fogelberg, B.: 141, 147, 155, 363
Fubini, A.: 317
Gaeta, R.: 273, 469
Gardien, J.J.: 267
Gardner, D.: 105
Gelletly, W.: 105
Gersch, H.-U.: 527
Giacobbe, P.: 675
Giannini, M.: 317, 491
Girard, J.: 267, 337
Greenwood, R.C.: 147, 363, 607,
615
Gruber, U.: 65
Gruppelaar, H.: 171, 257
Gryska, P.: 307
Hanle, H.: 411
Haouat, G.: 119
Hardell, R.: 199, 209, 231
Harlan, R.A.: 607
Harvey, J.A.: 421
Hass, M.: 507
Heck, D.: 289, 309, 371
Hedin, G.: 147
Helmer, R.G.: 607, 615
Hofmeyr, C.: 301
Holmberg, P.: 463
Hoot, C.G.: 117
Horsch, F.: 35
Irigaray, J.L.: 337
Ivanov, E.: 317
Jafar, J.D.: 115
John, J.: 117
Jonsson, L.: 199

- Journey, E.T.: 431
 Kajfosz, J.: 115
 Kane, W.: 105
 Kardon, B.: 663
 Kenny, M.J.: 587
 Kevey, A.: 105
 Khadduri, I.Y.: 115
 Khalil, M.A.: 115
 Kiss, D.: 663
 Koch, H.R.: 65, 89, 147, 363
 Kopecký, J.: 261
 Koriath, M.: 411
 Kosina, Z.: 115
 Kramer, N.: 161
 Krüger, H.: 411
 Lachkar, J.: 119
 Lalović, B.: 349
 Lane, A.M.: 513
 Lange, D.: 75
 Lenkszus, F.R.: 113
 Leuschner, H.: 51
 Lone, M.A.: 595
 Longo, G.: 575
 Lottin, A.: 657
 Lundberg, B.: 569, 667
 McClure, D.A.: 389
 Maier, B.P.K.: 65, 89
 Maier-Leibnitz, H.: 93
 Malan, J.G.: 301
 Manfrass, P.: 161
 Mariscotti, M.A.J.: 105
 Matussek, P.: 51
 Michaelis, W.: 35, 51, 75, 273,
 289, 309, 469
 Moreh, R.: 481, 483, 487
 Mottelson, B.R.: 3
 Mühlbauer, K.: 65
 Murray, J.: 579
 Nilsson, L.: 569
 Nof, A.: 487
 Nyström, G.: 667
 Oliva, P.: 491
 Op den Kamp, A.M.F.: 171, 257
 Orphan, V.J.: 117
 Ottmar, H.: 273, 289, 309, 469
 Patin, Y.: 119
 Paya, D.: 657
 Petit, G.Y.: 337
 Popa, M.: 317
 Pospíšil, J.: 651
 Postma, H.: 359
 Prade, H.: 161
 Prokoviev, P.: 161
 Prosperi, D.: 317, 491
 Rado, V.: 317
 Rae, E.R.: 579
 Ramorino, M.C.: 491
 Reddingius, E.R.: 359
 Reich, C.W.: 147, 363, 607, 615
 Riehs, P.: 307
 Rudolph, W.: 527
 Rumpold, K.: 307
 Saidane, M.: 259
 Samama, R.: 267, 337
 Saporetti, F.: 575
 Saraceno, M.: 147
 Schlesinger, Y.: 507
 Schmidt, H.: 273, 289, 309, 371,
 469
 Schröder, I.: 105
 Schult, O.W.B.: 65, 89, 147, 363
 Seres, Z.: 663
 Sigaud, J.: 119
 Simić, J.: 349
 Skeppstadt, Ö.: 217, 231
 Slaughter, G.G.: 421
 Slavić, I.A.: 123, 349
 Smither, R.K.: 55, 355, 601
 Sotnikov, S.K.: 663
 Spits, A.M.J.: 171, 257
 Stary, F.: 161
 Stecher-Rasmussen, F.: 261
 Stefanon, M.: 675
 Stelzer, K.: 403, 411
 Strauss, M.G.: 113
 Szabo, L.: 663
 Szichman, H.: 507
 Telezhnikov, S.A.: 651
 Tepel, J.W.: 301
 Thomas, B.W.: 579
 Tripathi, K.C.: 173, 183
 Urbanec, J.: 651
 Villiers, J.A.M. de: 301
 Vrzal, J.: 651
 Wallander, E.: 231
 Weigmann, H.: 687
 Weitkamp, C.: 421
 Weller, F.: 469
 Wilhelmi, G.: 75
 Winkler, B.C.: 301
 Winter, J.: 687
 Wolf, A.: 481, 483

IAEA SALES AGENTS AND BOOKSELLERS

Orders for Agency publications can be placed with your bookseller or any of the addresses listed below:

ARGENTINA

Comisión Nacional de
Energía Atómica
Avenida del Libertador 8250
Buenos Aires

AUSTRALIA

Hunter Publications
23 McKillop Street
Melbourne, C.1

AUSTRIA

Publishing Section
International Atomic Energy Agency
Kärntner Ring 11
P.O. Box 590
A-1011 Vienna

BELGIUM

Office International
de Librairie
30, Avenue Marnix
Brussels 5

CANADA

Canadian Government Printing Bureau,
International Publications Main Stores,
Room 2738, Second Floor,
Sacred Heart Boulevard,
Hull, Québec

C. S. S. R.

S. N. T. L.
Spolena 51
Nové Mesto
Prague 1

DENMARK

Ejnar Munksgaard Ltd.
6 Norregade
DK-1165 Copenhagen K

FRANCE

Office International de
Documentation et Librairie
48, Rue Gay-Lussac
F-75 Paris 5e

GERMANY, Fed. Rep.

R. Oldenbourg Verlag
Rosenheimer Strasse 145
D-8 Munich 80

HUNGARY

Kultura
Hungarian Trading Company
for Books and Newspapers
P.O. Box 149
Budapest 62

ISRAEL

Heiliger & Co.
3, Nathan Strauss Str.
Jerusalem

ITALY

Agenzia Editoriale Commissionaria
A. E. I. O. U.
Via Meravigli 16
I-20123 Milan

JAPAN

Maruzen Company, Ltd.
P.O. Box 5050,
100-31 Tokyo International

MEXICO

Librería Internacional, S. A.
Av. Sonora 206
México 11, D. F.

NETHERLANDS

Martinus Nijhoff N. V.
Lange Voorhout 9
P.O. Box 269
The Hague

PAKISTAN

Mirza Book Agency
65, Shahrah Quaid-E-Azam
P.O. Box 729
Lahore - 3

POLAND

Ars Polona
Centrala Handlu Zagranicznego
Krakowskie Przedmieście 7
Warsaw

ROMANIA

Cartimex
3-5 13 Decembrie Street
P.O. Box 134-135
Bucarest

SPAIN

Librería Bosch
Ronda Universidad 11
Barcelona - 7

SWEDEN

C. E. Fritzes Kungl. Hovbokhandel
Fredsgatan 2
Stockholm 16

SWITZERLAND

Librairie Payot
Rue Grenus 6
CH-1211 Geneva 11

U. S. S. R.

Mezhdunarodnaya Kniga
Smolenskaya-Sennaya 32-34
Moscow G-200

U. K.

Her Majesty's Stationery Office
P.O. Box 569
London S. E. 1

U. S. A.

UNIPUB, Inc.
P.O. Box 433
New York, N. Y. 10016

YUGOSLAVIA

Jugoslovenska Knjiga
Terazije 27
Belgrade

IAEA Publications can also be purchased retail at the United Nations Bookshop at United Nations Headquarters, New York, from the news-stand at the Agency's Headquarters, Vienna, and at most conferences, symposia and seminars organized by the Agency.

In order to facilitate the distribution of its publications, the Agency is prepared to accept payment in UNESCO coupons or in local currencies.

Orders and inquiries from countries not listed above may be sent to:

Publishing Section
International Atomic Energy Agency
Kärntner Ring 11
P.O. Box 590
A-1011 Vienna, Austria

INTERNATIONAL
ATOMIC ENERGY AGENCY
VIENNA, 1969

PRICE: US \$20.00
Austrian Schillings 517,-
(££ 6.8, F.Fr. 111,-; DM 73.20)

SUBJECT GROUP: III
Physics / Nuclear Physics,
Reactor Physics, Fission